Optical Fiber Telecommunications V

B: Systems and Networks

Ivan P. Kaminow
Tingye Li
Alan E. Willner

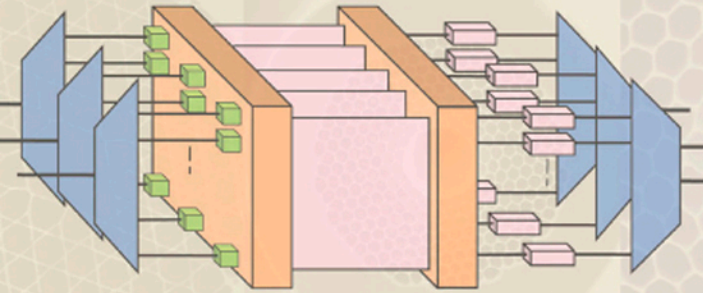

INCLUDES CD-ROM

AP

Optical Fiber Telecommunications V B

About the Editors

Ivan P. Kaminow retired from Bell Labs in 1996 after a 42-year career. He conducted seminal studies on electrooptic modulators and materials, Raman scattering in ferroelectrics, integrated optics, semiconductor lasers (DBR, ridge-waveguide InGaAsP, and multi-frequency), birefringent optical fibers, and WDM networks. Later, he led research on WDM components (EDFAs, AWGs, and fiber Fabry-Perot Filters), and on WDM local and wide area networks. He is a member of the National Academy of Engineering and a recipient of the IEEE/OSA John Tyndall, OSA Charles Townes, and IEEE/LEOS Quantum Electronics Awards. Since 2004, he has been Adjunct Professor of Electrical Engineering at the University of California, Berkeley.

Tingye Li retired from AT&T in 1998 after a 41-year career at Bell Labs and AT&T Labs. His seminal work on laser resonator modes is considered a classic. Since the late 1960s, he and his groups have conducted pioneering studies on lightwave technologies and systems. He led the work on amplified WDM transmission systems and championed their deployment for upgrading network capacity. He is a member of the National Academy of Engineering and a foreign member of the Chinese Academy of Engineering. He is also a recipient of the IEEE David Sarnoff Award, IEEE/OSA John Tyndall Award, OSA Ives Medal/Quinn Endowment, AT&T Science and Technology Medal, and IEEE Photonics Award.

Alan E. Willner has worked at AT&T Bell Labs and Bellcore, and he is Professor of Electrical Engineering at the University of Southern California. He received the NSF Presidential Faculty Fellows Award from the White House, Packard Foundation Fellowship, NSF National Young Investigator Award, Fulbright Foundation Senior Scholar, IEEE LEOS Distinguished Lecturer, and USC University-Wide Award for Excellence in Teaching. He is a Fellow of IEEE and OSA, and he has been President of the IEEE LEOS, Editor-in-Chief of the IEEE/OSA J. of Lightwave Technology, Editor-in-Chief of Optics Letters, Co-Chair of the OSA Science & Engineering Council, and General Co-Chair of the Conference on Lasers and Electro-Optics.

Optical Fiber Telecommunications V B

Systems and Networks

Edited by

Ivan P. Kaminow
Tingye Li
Alan E. Willner

ELSEVIER

AMSTERDAM • BOSTON • HEIDELBERG • LONDON
NEW YORK • OXFORD • PARIS • SAN DIEGO
SAN FRANCISCO • SINGAPORE • SYDNEY • TOKYO

Academic Press is an imprint of Elsevier

Academic Press is an imprint of Elsevier
30 Corporate Drive, Suite 400, Burlington, MA 01803, USA
525 B Street, Suite 1900, San Diego, California 92101 4495, USA
84 Theobald's Road, London WC1X 8RR, UK

This book is printed on acid free paper. ♾

Library of Congress Cataloging-in-Publication Data
Application submitted

British Library Cataloguing-in-Publication Data
A catalogue record for this book is available from the British Library.

ISBN: 978 0 12 374172 1

Printed in the United States of America
08 09 10 11 12 8 7 6 5 4 3 2 1

For Florence, Paula, Leonard, and Ellen with Love IPK
For Edith, Debbie, and Kathy with Love TL
For Michelle, our Children (Moshe, Asher, Ari, Jacob), and my Parents with Love AEW

This page intentionally left blank

Contents

Contributors

Keren Bergman, Department of Electrical Engineering, Columbia University, 1312 S.W. Mudd, 500 West 120th Street, New York, NY 10027, USA, bergman@ee.columbia.edu

Sébastien Bigo, Alcatel-Lucent Bell Labs, Centre de Villarceaux, Route de Villejust, 91620, Nozay, France, Sebastien.Bigo@alcatel-lucent.fr

Sethumadhavan Chandrasekhar, Bell Laboratories, Alcatel-Lucent, Holmdel, NJ, USA, sc@alcatel-lucent.com

Robert Doverspike, Transport Network Evolution Research AT&T Labs Research Room A5-1G12, 200 S. Laurel Ave, Middletown, NJ, USA, rdd@research.att.com

René-Jean Essiambre, Bell Laboratories, Alcatel-Lucent, 791 Holmdel-Keyport Road, Holmdel, NJ 07733, USA, rjessiam@alcatel-lucent.com

Mark D. Feuer, Optical Systems Research, AT&T Labs, 200 S. Laurel Ave, Middletown, NJ, USA, mdfeuer@research.att.com

Michael Y. Frankel, CTO Office, Ciena, 920 Elkridge Landing Rd, Linthicum, MD, USA, mfrankel@ciena.com

Ori Gerstel, Cisco Systems, 170 West Tasman Drive, San Jose, CA 95134, USA, ogerstel@cisco.com

Ivan P. Kaminow, University of California, Berkeley, CA, USA, Kaminow@eecs.berkeley.edu

Kazuro Kikuchi, Department of Frontier Informatics, University of Tokyo, 5-1-5 Kashiwanoha, Kashiwa, Chiba 277-8561, Japan, kikuchi@ginjo.k.u-tokyo.ac.jp

Daniel C. Kilper, Bell Laboratories, Alcatel-Lucent, 791 Holmdel-Keyport Road, L-137, Holmdel, NJ, USA, dkilper@alcatel-lucent.com

Eugen Lach, Alcatel-Lucent Deutschland AG, Bell Labs Germany, Lorenzstrasse 10, D-70435 Stuttgart, Germany, eugen.lach@alcatel-lucent.de

Cedric F. Lam, OpVista, 870 N. McCarthy Blvd, Milpitas, CA, USA, cflam@ieee.org

Andreas Leven, Bell Laboratories, Alcatel-Lucent, Holmdel, NJ, USA, aleven@alcatel-lucent.com

Tingye Li, Boulder, CO, USA, tingyeli@aol.com

Xiang Liu, Bell Laboratories, Alcatel-Lucent, Department of Optical Networks, Holmdel, NJ, USA, xliu20@alcatel-lucent.com

Reinhold Ludwig, Fraunhofer Institute for Telecommunications, Heinrich-Hertz-Institut, Einsteinufer 37, D-10587 Berlin, Germany, ludwig@hhi.de

Richard Mack, KMI Research, CRU Group, Mount Pleasant, London, UK, Richard.Mack@crugroup.com

Peter Magill, Optical Systems Research, AT&T Labs, 200 S. Laurel Ave; Middletown, NJ, USA, pete@research.att.com

Michael O'Mahony, Department of Electronic System Engineering, University of Essex, Colchester, CO43SQ, UK, mikej@essex.ac.uk

Zhongqi Pan, Department of Electrical and Computer Engineering, University of Louisiana at Lafayette, USA, zpan@louisiana.edu

Loukas Paraschis, Cisco Systems, 170 West Tasman Drive, San Jose, CA 95134, USA, loukas@cisco.com

Robert Scarmozzino, RSoft Design Group, 400 Executive Blvd., Ossining, NY 10562, USA, rob@rsoftdesign.com

Karsten Schuh, Alcatel-Lucent Deutschland AG, Bell Labs Germany, Lorenzstrasse 10, D-70435 Stuttgart, Germany, karsten.schuh@alcatel-lucent.de

Alwyn J. Seeds, Department of Electronic and Electrical Engineering, University College London, Torrington Place, London WC1E 7JE, England, a.seeds@ee.ucl.ac.uk

Rodney S. Tucker, Department of Electrical and Electronic Engineering, University of Melbourne, Vic., 3010, Australia, r.tucker@ee.unimelb.edu.au

Richard E. Wagner, Corning International, Corning, New York, USA, wagnerre@corning.com

Winston I. Way, OpVista, 870 N. McCarthy Blvd, Milpitas, CA, USA, wway@opvista.com

Hans-Georg Weber, Fraunhofer Institute for Telecommunications, Heinrich-Hertz-Institut, Einsteinufer 37, D-10587 Berlin, Germany, hans-georg.weber@gmx.de

Alan E. Willner, University of Southern California, Los Angeles, CA, USA, willner@usc.edu

Peter J. Winzer, Bell Laboratories, Alcatel-Lucent, 791 Holmdel-Keyport Road, Holmdel, NJ 07733, USA, peter.winzer@ieee.org

Sheryl L. Woodward, Optical Systems Research, AT&T Labs, 200 S. Laurel Ave, Middletown, NJ, USA, sheri@research.att.com

S. J. Ben Yoo, Department of Electrical and Computer Engineering, University of California, Davis, CA, USA, yoo@ece.ucdavis.edu

Changyuan Yu, Department of Electrical and Computer Engineering, National University of Singapore, Singapore, eleyc@nus.edu.sg

This page intentionally left blank

1

Overview of OFT V volumes A & B

Ivan P. Kaminow[*], Tingye Li[†], and Alan E. Willner[‡]

[*]*University of California, Berkeley, CA, USA*
[†]*Boulder, CO, USA*
[‡]*University of Southern California, Los Angeles, CA, USA*

Optical Fiber Telecommunications V (OFT V) is the fifth installment of the *OFT* series. Now 29 years old, the series is a compilation by the research and development community of progress in optical fiber communications. Each edition reflects the current state-of-the-art at the time. As Editors, we started with a clean slate of chapters and authors. Our goal was to update topics from *OFT IV* that are still relevant as well as to elucidate topics that have emerged since the last edition.

1.1 FIVE EDITIONS

Installments of the series have been published roughly every 6 8 years and chronicle the natural evolution of the field:

- In the late 1970s, the original *OFT* (Chenoweth and Miller, 1979) was concerned with enabling a simple optical link, in which reliable fibers, connectors, lasers, and detectors played the major roles.
- In the late 1980s, *OFT II* (Miller and Kaminow, 1988) was published after the first field trials and deployments of simple optical links. By this time, the advantages of multiuser optical networking had captured the imagination of the community and were highlighted in the book.
- *OFT III* (Kaminow and Koch, 1997) explored the explosion in transmission capacity in the early-to-mid 1990s, made possible by the erbium-doped fiber amplifier (EDFA), wavelength division multiplexing (WDM), and dispersion management.

Optical Fiber Telecommunications V B: Systems and Networks

ISBN: 978 0 12 374172 1

- By 2002, *OFT IV* (Kaminow and Li, 2002) dealt with extending the distance and capacity envelope of transmission systems. Subtle nonlinear and dispersive effects, requiring mitigation or compensation in the optical and electrical domains, were explored.
- The present edition of *OFT, V,* (Kaminow, Li, and Willner, 2008) moves the series into the realm of network management and services, as well as employing optical communications for ever-shorter distances. Using the high bandwidth capacity in a cost-effective manner for customer applications takes center stage. In addition, many of the topics from earlier volumes are brought up to date; and new areas of research which show promise of impact are featured.

Although each edition has added new topics, it is also true that new challenges emerge as they relate to older topics. Typically, certain devices may have adequately solved transmission problems for the systems of that era. However, as systems become more complex, critical device technologies that might have been considered a "solved problem" previously have new requirements placed upon them and need a fresh technical treatment. For this reason, each edition has grown in sheer size, i.e., adding the new and, if necessary, reexamining the old.

An example of this circular feedback mechanism relates to the fiber itself. At first, systems simply required low-loss fiber. However, long-distance transmission enabled by EDFAs drove research on low-dispersion fiber. Further, advances in WDM and the problems of nonlinear effects necessitated development of nonzero dispersion fiber. Cost considerations and ultra-high-performance systems, respectively, are driving research in plastic fibers and ultra-low-polarization-dependent fibers. We believe that these cycles will continue. Each volume includes a CD-ROM with all the figures from that volume. Select figures are in color. The volume B CD-ROM also has some supplementary Powerpoint slides to accompany Chapter 19 of that volume.

1.2 PERSPECTIVE OF THE PAST 6 YEARS

Our field has experienced an unprecedented upheaval since 2002. The *irrational* exuberance and despair of the technology "bubble-and-bust" had poured untold sums of money into development and supply of optical technologies, which was followed by a depression-like period of over supply. We are happy to say that, by nearly all accounts, the field is gaining strength again and appears to be entering a stage of *rational* growth.

What caused this upheaval? A basis seems to be related to a fundamental discontinuity in economic drivers. Around 2001, worldwide telecom traffic ceased being dominated by the slow-growing voice traffic and was overtaken by the rapidly growing Internet traffic. The business community over-estimated the

growth rate, which generated enthusiasm and demand, leading to unsustainable expectations. Could such a discontinuity happen again? Perhaps, but chastened investors now seem to be following a more gradual and sensible path. Throughout the "bubble-and-bust" until the present, the actual demand for bandwidth has grown at a very healthy ~80% per year globally; thus, real traffic demand experienced no bubble at all. The growth and capacity needs are real, and should continue in the future.

As a final comment, we note that optical fiber communications is firmly entrenched as part of the global information infrastructure. The only question is how deeply will it penetrate and complement other forms of communications, e.g., wireless, access, and on-premises networks, interconnects, satellites, etc. This prospect is in stark contrast to the voice-based future seen by *OFT,* published in 1979, before the first commercial intercontinental or transatlantic cable systems were deployed in the 1980s. We now have Tb/s systems for metro and long-haul networks. It is interesting to contemplate what topics and concerns might appear in *OFT VI*.

1.3 OFT V VOLUME A: COMPONENTS AND SUBSYSTEMS

1.3.1 Chapter 1. Overview of OFT V volumes A & B (*Ivan P. Kaminow, Tingye Li, and Alan E. Willner*)

This chapter briefly reviews herewith all the chapters contained in both volumes of OFT V.

1.3.2 Chapter 2. Semiconductor quantum dots: Genesis—The Excitonic Zoo—novel devices for future applications (*Dieter Bimberg*)

The ultimate class of semiconductor nanostructures, i.e., "quantum dots" (QDs), is based on "dots" smaller than the de Broglie wavelength in all three dimensions. They constitute nanometer-sized clusters that are embedded in the dielectric matrix of another semiconductor. They are often self-similar and can be formed by self-organized growth on surfaces. Single or few quantum dots enable novel devices for quantum information processing, and billions of them enable active centers in optoelectronic devices like QD lasers or QD optical amplifiers. This chapter covers the area of quantum dots from growth via various band structures to optoelectronic device applications. In addition, high-speed laser and amplifier operations are described.

1.3.3 Chapter 3. High-speed low-chirp semiconductor lasers (*Shun Lien Chuang, Guobin Liu, and Piotr Konrad Kondratko*)

One advantage of using quantum wells and quantum dots for the active region of lasers is the lower induced chirp when such lasers are directly modulated, permitting direct laser modulation that can save on the cost of separate external modulators. This chapter provides a comparison of InAlGaAs with InGaAsP long-wavelength quantum-well lasers in terms of high-speed performance, and extracts the important parameters such as gain, differential gain, photon lifetime, temperature dependence, and chirp. Both DC characteristics and high-speed direct modulation of quantum-well lasers are presented, and a comparison with theoretical models is made. The chapter also provides insights into novel quantum-dot lasers for high-speed operation, including the ideas of p-type doping vs tunneling injection for broadband operation.

1.3.4 Chapter 4. Recent advances in surface-emitting lasers (*Fumio Koyama*)

Vertical cavity surface-emitting lasers (VCSELs) have a number of special properties (compared with the more familiar edge-emitting lasers) that permit some novel applications. This chapter begins with an introduction which briefly surveys recent advances in VCSELs, several of that are then treated in detail. These include techniques for realizing long-wavelength operation (as earlier VCSELs were limited to operation near 850 nm), the performance of dense VCSEL arrays that emit a range of discrete wavelengths (as large as 110 in number), and MEMS-based athermal VCSELs. Also, plasmonic VCSELs that produce subwavelength spots for high-density data storage and detection are examined. Finally, work on all-optical signal processing and slow light is presented.

1.3.5 Chapter 5. Pump diode lasers (*Christoph Harder*)

Erbium-doped fiber amplifiers (EDFAs) pumped by bulky argon lasers were known for several years before telecom system designers took them seriously; the key development was a compact, high-power semiconductor pump laser. Considerable effort and investment have gone into today's practical pump lasers, driven by the importance of EDFAs in realizing dense wavelength division multiplexed (DWDM) systems. The emphasis has been on high power, efficiency, and reliability. The two main wavelength ranges are in the neighborhood of 980 nm for low noise and 1400 nm for remote pumping of EDFAs. The 1400-nm band is also suitable for Raman amplifiers, for which very high power is needed.

This chapter details the many lessons learned in the design for manufacture of commercial pump lasers in the two bands. Based on the performance developed for telecom, numerous other commercial applications for high-power lasers have emerged in manufacturing and printing; these applications are also discussed.

1.3.6 Chapter 6. Ultrahigh-speed laser modulation by injection locking (*Connie J. Chang-Hasnain and Xiaoxue Zhao*)

It has been known for decades that one oscillator (the slave) can be locked in frequency and phase to an external oscillator (the master) coupled to it. Current studies of injection-locked lasers show that the dynamic characteristics of the directly modulated slave are much improved over the same laser when freely running. Substantial improvements are found in modulation bandwidth for analog and digital modulation, in linearity, in chirp reduction and in noise performance.

In this chapter, theoretical and experimental aspects of injection locking in all lasers are reviewed with emphasis on the authors' research on VCSELs (vertical cavity surface-emitting lasers). A recent promising application in passive optical networks for fiber to the home (FTTH) is also discussed.

1.3.7 Chapter 7. Recent developments in high-speed optical modulators (*Lars Thylén, Urban Westergren, Petter Holmström, Richard Schatz, and Peter Jänes*)

Current high-speed lightwave systems make use of electro-optic modulators based on lithium niobate or electroabsorption modulators based on semiconductor materials. In commercial systems, the very high-speed lithium niobate devices often require a traveling wave structure, while the semiconductor devices are usually lumped.

This chapter reviews the theory of high-speed modulators (at rates of 100 Gb/s) and then considers practical design approaches, including comparison of lumped and traveling-wave designs. The main emphasis is on electroabsorption devices based on Franz Keldysh effect, quantum-confined Stark effect and intersubband absorption. A number of novel designs are described and experimental results given.

1.3.8 Chapter 8. Advances in photodetectors (*Joe Charles Campbell*)

As a key element in optical fiber communications systems, photodetectors belong to a well developed sector of photonics technology. Silicon p i n and avalanche photodiodes deployed in first-generation lightwave transmission systems operating at 0.82-μm wavelength performed very close to theory. In the 1980s, InP photodiodes

were developed and commercialized for systems that operated at 1.3- and 1.5-μm wavelengths, albeit the avalanche photodiodes (APDs) were expensive and nonideal. Introduction of erbium-doped fiber amplifiers and WDM technology in the 1990s relegated APDs to the background, as p i n photoreceivers performed well in amplified systems, whereas APDs were plagued by the amplified spontaneous emission noise. Future advanced systems and special applications will require sophisticated devices involving deep understanding of device physics and technology. This chapter focuses on three primary topics: high-speed waveguide photodiodes for systems that operate at 100 Gb/s and beyond, photodiodes with high saturation current for high-power applications, and recent advances of APDs for applications in telecommunications.

1.3.9 Chapter 9. Planar lightwave circuits in fiber-optic communications (*Christopher R. Doerr and Katsunari Okamoto*)

The realization of one or more optical waveguide components on a planar substrate has been under study for over 35 years. Today, individual components such as splitters and arrayed waveguide grating routers (AWGRs) are in widespread commercial use. Sophisticated functions, such as reconfigurable add drop multiplexers (ROADMs) and high-performance filters, have been demonstrated by integrating elaborate combinations of such components on a single chip. For the most part, these photonic integrated circuits (PICs), or planar lightwave circuits (PLCs), are based on passive waveguides in lower index materials, such as silica.

This chapter deals with the theory and design of such PICs. The following two chapters (Chapters 11 and 12) also deal with PICs; however, they are designed to be integrated with silicon electronic ICs, either in hybrid fashion by short wire bonds to an InP PIC or directly to a silicon PIC.

1.3.10 Chapter 10. III–V photonic integrated circuits and their impact on optical network architectures (*Dave Welch, Chuck Joyner, Damien Lambert, Peter W. Evans, and Maura Raburn*)

InP-based semiconductors are unique in their capability to support all the photonic components required for wavelength division multiplexed (WDM) transmitters and receivers in the telecom band at 1550 nm. Present subsystems have connected these individual components by fibers or lenses to form hybrid transmitters and receivers for each channel.

Recently, integrated InP WDM transmitter and receiver chips that provide 10 channels, each operating at 10 Gb/s, have been shown to be technically and

economically viable for deployment in commercial WDM systems. The photonic integrated circuits are wire-bonded to adjacent silicon ICs. Thus a single board provides optoelectronic regeneration for 10 channels, dramatically reducing interconnection complexity and equipment space. In addition, as in legacy single-channel systems, the "digital" approach for transmission (as compared to "all-optical") offers ease of network monitoring and management. This chapter covers the technology of InP photonic integrated circuits (PICs) and their commercial application. The impact on optical network architecture and operation is discussed and technology advances for future systems are presented.

1.3.11 Chapter 11. Silicon photonics (*Cary Gunn and Thomas L. Koch*)

Huge amounts of money have been invested in silicon processing technology, thanks to a steady stream of applications that justified the next stage of processing development. In addition to investment, innovative design, process discipline and large-volume runs made for economic success. The InP PICs described in the previous chapter owe their success to lessons learned in silicon IC processing.

Many people have been attracted by the prospects of fabricating PICs using silicon alone to capitalize on the investment and success of silicon ICs. To succeed one requires a large-volume application and a design that can be made in an operating silicon IC foundry facility. A further potential advantage is the opportunity to incorporate on the same photonic chip electronic signal processing. The application to interconnects for high-performance computers is a foremost motivation for this work.

While silicon has proven to be the ideal material for electronic ICs, it is far from ideal for PICs. The main shortcoming is the inability so far to make a good light source or photodetector in silicon. This chapter discusses the successes and challenges encountered in realizing silicon PICs to date.

1.3.12 Chapter 12. Photonic crystal theory: Temporal coupled-mode formalism (*Shanhui Fan*)

Photonic crystal structures have an artificially created optical bandgap that is introduced by a periodic array of perturbations, and different types of waveguides and cavities can be fabricated that uniquely use the band gap-based confinement. These artificially created materials have been of great interest for potential optical information processing applications, in part because they provide a common platform to miniaturize a large number of optical components on-chip down to single wavelength scale. For this purpose, many devices can be

designed using such a material with a photonic bandgap and, subsequently, introducing line and point defect states into the gap. Various functional devices, such as filters, switches, modulators and delay lines, can be created by controlling the coupling between these defect states. This chapter reviews the temporal coupled-mode theory formalism that provides the theoretical foundation of many of these devices.

1.3.13 Chapter 13. Photonic crystal technologies: Experiment (*Susumu Noda*)

Photonic crystals belong to a class of optical nanostructures characterized by the formation of band structures with respect to photon energy. In 3D photonic crystals, a complete photonic band gap is formed; the presence of light with frequencies lying in the band gap is not allowed. This chapter describes the application of various types of materials engineering to photonic crystals, with particular focus on the band gap/defect, the band edge, and the transmission band within each band structure. The manipulation of photons in a variety of ways becomes possible. Moreover, this chapter discusses the recent introduction of "photonic heterostructures" as well as recent developments concerning two- and three-dimensional photonic crystals.

1.3.14 Chapter 14. Photonic crystal fibers: Basics and applications (*Philip St John Russell*)

Photonic crystal fibers (PCFs) fibers with a periodic transverse microstructure first emerged as practical low-loss waveguides in early 1996. The initial demonstration took 4 years of technological development, and since then the fabrication techniques have become more and more sophisticated. It is now possible to manufacture the microstructure in air glass PCFs to accuracies of 10 nm on the scale of 1 μm, which allows remarkable control of key optical properties such as dispersion, birefringence, nonlinearity and the position and width of the photonic band gaps (PBGs) in the periodic "photonic crystal" cladding. PCF has in this way extended the range of possibilities in optical fibers, both by improving well-established properties and introducing new features such as low-loss guidance in a hollow core.

In this chapter, the properties of the various types of PCFs are introduced, followed by a detailed discussion of their established or emerging applications. The chapter describes in detail the fabrication, theory, numerical modeling, optical properties, and guiding mechanisms of PCFs. Applications of photonic crystal fibers include lasers, amplifiers, dispersion compensators, and nonlinear processing.

1.3.15 Chapter 15. Specialty fibers for optical communication systems (*Ming-Jun Li, Xin Chen, Daniel A. Nolan, Ji Wang, James A. West, and Karl W. Koch*)

Specialty fibers are designed by changing fiber glass composition, refractive index profile, or coating to achieve certain unique properties and functionalities. Some of the common specialty fibers include active fibers, polarization control fibers, dispersion compensation fibers, highly nonlinear fibers, coupling or bridge fibers, high-numerical-aperture fibers, fiber Bragg gratings, and special single mode fibers. In this chapter, the design and performance of various specialty fibers are discussed. Special attention is paid to dispersion compensation fibers, polarization-maintaining and single-polarization fibers, highly nonlinear fibers, double clad fiber for high-power lasers and amplifiers, and photonic crystal fibers. Moreover, there is a brief discussion of the applications of these specialty fibers.

1.3.16 Chapter 16. Plastic optical fibers: Technologies and communication links (*Yasuhiro Koike and Satoshi Takahashi*)

Plastic optical fiber (POF) consists of a plastic core that is surrounded by a plastic cladding of a refractive index lower than that of the core. POFs have very large core diameters compared to glass optical fibers, and yet they are quite flexible. These features enable easy installation and safe handling. Moreover, the large-core fibers can be connected without high-precision accuracy and with low cost. POFs have been used extensively in short-distance datacom applications, such as in digital audio interfaces. POFs are also used for data transmission within equipment and for control signal transmission in machine tools. During the late 1990s, POFs were used as the transmission medium in the data bus within automobiles. As we move into the future, high-speed communication will be required in the home, and POFs are a promising candidate for home network wiring. This chapter describes the POF design and fabrication, the specific fiber properties of attenuation, bandwidth and thermal stability, and various communications applications, concluding with a discussion of recent developments in graded-index POFs.

1.3.17 Chapter 17. Polarization mode dispersion (*Misha Brodsky, Nicholas J. Frigo, and Moshe Tur*)

Polarization-mode dispersion (PMD) has been well recognized for sometime as an impairment factor that limits the transmission speed and distance in high-speed lightwave systems. The complex properties of PMD have enjoyed scrutiny by

theorists, experimentalists, network designers, field engineers and, during the "bubble" years, entrepreneurial technologists. A comprehensive treatment of the subject up to year 2002 is given in a chapter bearing the same title in *Optical Fiber Telecommunications IVB, System and Impairments*. The present chapter is an overview of PMD with special emphasis on the knowledge accumulated in the past 5 years. It begins with a review of PMD concepts, and proceeds to consider the "hinge" model used to describe field test results, which are presented and analyzed. The important subject of system penalties and outages due to first-order PMD is then examined, followed by deliberations of higher-order PMD, and interaction between fiber nonlinear effects and PMD.

1.3.18 Chapter 18. Electronic signal processing for dispersion compensation and error mitigation in optical transmission networks (*Abhijit Shanbhag, Qian Yu, and John Choma*)

Dispersion equalization has its origin in the early days of analog transmission of voice over copper wires where loading coils (filters) were distributed in the network to equalize the frequency response of the transmission line. Digital transmission over twisted pairs was enabled by the invention of the transversal equalizer which extended greatly the bandwidth and reach. Sophisticated signal processing and modulation techniques have now made mobile telephones ubiquitous. However, it was not until the mid 1990s that wide deployment of Gigabit Ethernet rendered silicon CMOS ICs economical for application in high-speed lightwave transmission. Most, if not all lightwave transmission systems deployed today, use electronic forward error correction and dispersion compensation to alleviate signal degradation due to noise and fiber dispersive effects.

This chapter presents an overview of various electronic equalization and adaptation techniques, and discusses their high-speed implementation, specifically addressing 10-Gb/s applications for local-area, metro, and long-haul networks. It comprises a comprehensive survey of the role, scope, limitations, trends, and challenges of this very important and compelling technology.

1.3.19 Chapter 19. Microelectromechanical systems for lightwave communication (*Ming C. Wu, Olav Solgaard, and Joseph E. Ford*)

The earliest commercial applications of microelectromechanical systems (MEMS) were in digital displays employing arrays of tiny mirrors and in accelerometers for airbag sensors. This technology has now found a host of applications in lightwave communications. These applications usually require movable components, such as mirrors, with response times in the neighborhood of 10^{-6} s, although fixed

elements may be called for in some applications. Either a free-space or integrated layout may be used.

This chapter describes the recent lightwave system applications of MEMS. In telecommunications, MEMS switches can provide cross-connects with large numbers of ports. A variety of wavelength selective devices, such as reconfigurable optical add drop multiplexers (ROADM) employ MEMS. More recent devices include tunable lasers and microdisk resonators.

1.3.20 Chapter 20. Nonlinear optics in communications: from crippling impairment to ultrafast tools (*Stojan Radic, David J. Moss, and Benjamin J. Eggleton*)

It is perhaps somewhat paradoxical that optical nonlinearities, whilst having posed significant limitations for long-haul WDM systems, also offer the promise of addressing the bandwidth bottleneck for signal processing for future optical networks as they evolve beyond 40 Gb/s. In particular, all-optical devices based on the 3rd order $\chi^{(3)}$ optical nonlinearity offer a significant promise in this regard, not only because the intrinsic nonresonant $\chi^{(3)}$ is nearly instantaneous, but also because $\chi^{(3)}$ is responsible for a wide range of phenomena, including 3rd harmonic generation, stimulated Raman gain, four-wave mixing, optical phase conjugation, two-photon absorption, and the nonlinear refractive index. This plethora of physical processes has been the basis for a wide range of activity on all-optical signal processing devices.

This chapter focuses on breakthroughs in the past few years on approaches based on highly nonlinear silica fiber as well as chalcogenide-glass-based fiber and waveguide devices. The chapter contrasts two qualitatively different approaches to all-optical signal processing based on nonphase-matched and phase-matched processes. All-optical applications of 2R and 3R regeneration, wavelength conversion, parametric amplification, phase conjugation, delay, performance monitoring, and switching are reviewed.

1.3.21 Chapter 21. Fiber-optic quantum information technologies (*Prem Kumar, Jun Chen, Paul L. Voss, Xiaoying Li, Kim Fook Lee, and Jay E. Sharping*)

Quantum-mechanical (QM) rules are surprisingly simple: linear algebra and first-order partial differential equations. Yet, QM predictions are unimaginably precise and accurate when compared with experimental data. A "mysterious" feature of QM is the superposition principle and the ensuing quantum entanglement. The fundamental difference between quantum entanglement and classical correlation lies in the fact that particles are quantum-mechanical objects which can exist not only in states $|0>$ and $|1>$ but also in states described by $\alpha|0>+\beta|1>$, while classical objects

can only exist in one of two deterministic states (i.e., "heads" or "tails"), and not something in between. In other words, the individual particle in quantum entanglement does not have a well-defined pure state before measurement.

Since the beginning of the 1990s, the field of quantum information and communication has expanded rapidly, with quantum entanglement being a critical aspect. Entanglement is still an unresolved "mystery," but a new world of "quantum ideas" has been ignited and is actively being pursued. The focus of this chapter is the generation of correlated and entangled photons in the telecom band using the Kerr nonlinearity in dispersion-shifted fiber. Of particular interest are microstructure fibers, in which tailorable dispersion properties have allowed phase-matching and entanglement to be obtained over a wide range of wavelengths.

1.4 OFT V VOLUME B: SYSTEMS AND NETWORKS

1.4.1 Chapter 1. Overview of OFT V volumes A & B (*Ivan P. Kaminow, Tingye Li, and Alan E. Willner*)

This chapter briefly reviews herewith all the chapters contained in both volumes of OFT V.

1.4.2 Chapter 2. Advanced optical modulation formats (*Peter J. Winzer and René-Jean Essiambre*)

Today, digital radio-frequency (rf) communication equipment employs sophisticated signal processing and communication theory technology to realize amazing performance; wireless telephones are a prime example. These implementations are made possible by the capabilities and low cost of silicon integrated circuits in high-volume consumer applications. Some of these techniques, such as forward error correction (FEC) and electronic dispersion compensation (EDC) are currently in use in lightwave communications to enhance signal-to-noise ratio and mitigate signal degradation. (See the chapter on "Electronic Signal Processing for Dispersion Compensation and Error Mitigation in Optical Transmission Networks" by Abhijit Shanbhag, Qian Yu, and John Choma.) Advanced modulation formats that are robust to transmission impairments or able to improve spectral efficiency are being considered for next-generation lightwave systems.

This chapter provides a taxonomy of optical modulation formats, along with experimental techniques for realizing them. The discussion makes clear the substantial distinctions between design conditions for optical and rf applications. Demodulation concepts for coherent and delay demodulation are also covered analytically.

1.4.3 Chapter 3. Coherent optical communication systems (*Kazuro Kikuchi*)

The first generation of single-channel fiber optic networks used on-off keying and direct detection. Later, coherent systems, employing homodyne and heterodyne detection, were intensely researched with the aim of taking advantage of their improved sensitivity and WDM frequency selectivity. However, the quick success of EDFAs in the 1990s cut short the prospects for coherent systems.

Now, interest in coherent is being renewed as the need for greater spectral efficiency in achieving greater bandwidth per fiber has become apparent. This chapter reviews the theory of multilevel modulation formats that permit multiple bits/s of data per Hz of bandwidth. (See the chapter on "Advanced Modulation Formats" by Winzer and Essiambre.) The growing capabilities of silicon data signal processing (DSP) can be combined with digital coherent detection to provide dramatic improvements in spectral efficiency. Experimental results for such receivers are presented.

1.4.4 Chapter 4. Self-coherent optical transport systems (*Xiang Liu, Sethumadhavan Chandrasekhar, and Andreas Leven*)

As stated above, coherent detection transmission systems were investigated in the 1980s for their improved receiver sensitivity and selectivity, and for the promise of possible postdetection dispersion compensation. However, the emergence of EDFAs and amplified WDM systems relegated the technically difficult coherent technology to the background. Now, as high-speed signal processing technology becomes technically and economically feasible, there is renewed interest in studying coherent and self-coherent systems, especially for their capability to increase spectral efficiency through the use of advanced multilevel modulation techniques and, more important, for the possibility of implementing postdetection equalization functionalities.

Self-coherent systems utilize differential direct detection that does not require a local oscillator. With high-speed analog-to-digital conversion and digital signal processing, both phase and amplitude of the received optical field can be reconstructed, thus offering unprecedented capability for implementing adaptive equalization of transmission impairments. This chapter is a comprehensive and in-depth treatment of self-coherent transmission systems, including theoretical considerations, receiver technologies, modulation formats, adaptive equalization techniques, and applications for capacity upgrades and cost reduction in future optical networks.

1.4.5 Chapter 5. High-bit-rate ETDM transmission systems (*Karsten Schuh and Eugen Lach*)

Historically, it has been observed that the first cost of a (single-channel) transmission system tended to increase as the square root of its bandwidth or bit rate. This

observation has prompted the telecom industry to develop higher-speed systems for upgrading transport capacity. Indeed, there is a relentless drive to explore higher speed for multichannel amplified WDM transmission where, for a given speed of operation, the total system cost is roughly proportional to the number of channels plus a fixed cost. It is important to note that the cost of equalizing for signal impairment at higher speeds must be taken into account.

This chapter is an up-to-date review of high-speed transmission using electronic time division multiplexing (ETDM), a time-honored approach for upgrading system capacity. The emphasis is on 100-Gb/s bit rate and beyond, as 40-Gb/s systems are already being deployed and 100-Gb/s Ethernet (100 GE) is expected to be the next dominant transport technology. The chapter includes a basic treatment of ETDM technology, followed by a description of the concepts of high-speed ETDM systems. Requirements of optical and electronic components and the state-of-the-art technologies are then examined in detail, and an up-to-date overview of ultra-high-speed systems experiments is presented. Finally, prospects of the various approaches for rendering cost-effective 100 GE are contemplated.

1.4.6 Chapter 6. Ultra-high-speed OTDM transmission technology (*Hans-Georg Weber and Reinhold Ludwig*)

The expected increase of transmission capacity in optical fiber networks will involve an optimized combination of WDM and TDM. TDM may be realized by electrical multiplexing (ETDM) or by optical multiplexing (OTDM). Dispersion impairment notwithstanding, OTDM offers a means to increase the single-channel bit rate beyond the capability of ETDM. Thus OTDM transmission technology is often considered to be a research means with which to investigate the feasibility of ultra-high-speed transmission. Historically, the highest speed commercial systems have been ETDM systems. Latest examples are 40 G systems being deployed at present and (serial) 100 G systems expected to be commercially available in a few years. In the past 10 years, OTDM transmission technology has made considerable progress towards much higher bit rates and much longer transmission links.

This chapter discusses ultra-high-speed data transmission in optical fibers based on OTDM technology. The chapter gives a general description of an OTDM system, the OTDM transmitter, the OTDM receiver, and the fiber transmission line. WDM/OTDM transmission experiments are also described.

1.4.7 Chapter 7. Optical performance monitoring (*Alan E. Willner, Zhongqi Pan, and Changyuan Yu*)

Today's optical networks function in a fairly static fashion and are built to operate within well-defined specifications. This scenario is quite challenging for

higher-capacity systems, since network paths are not static and channel-degrading effects can change with temperature, component drift, aging and fiber plant maintenance. In order to enable robust and cost-effective automated operation, the network should be able to: (i) intelligently monitor the physical state of the network as well as the quality of propagating data signals, (ii) automatically diagnose and repair the network, and (iii) redirect traffic. To achieve this, optical performance monitoring should isolate the specific cause of the problem. Furthermore, it can be quite advantageous to determine when a data signal is beginning to degrade, so that the network can take action to correct the problem or to route the traffic around the degraded area.

This chapter explores optical performance monitoring and its potential for enabling higher stability, reconfigurability, and flexibility in an optical network. Moreover, this chapter describes the specific parameters that a network might want to monitor, such as chromatic dispersion, polarization-mode dispersion, and optical SNR. Promising monitoring techniques are reviewed.

1.4.8 Chapter 8. ROADMs and their system applications (*Mark D. Feuer, Daniel C. Kilper, and Sheryl L. Woodward*)

As service providers begin to offer IPTV services in addition to data and voice, the need for fast and flexible provisioning of mixed services and for meeting unpredictable traffic demand becomes compelling. Reconfigurable optical add/drop multiplexers (ROADMs) have emerged as the network element that can satisfy this need. Indeed, subsystem and system vendors are rapidly developing and producing ROADMs, and carriers are installing and deploying them in their networks.

This chapter is a comprehensive treatment of ROADMs and their application in WDM transmission systems and networks, comprising a review of various ROADM technologies and architectures; analyses of their routing functionalities and economic advantages; considerations of design features and other requirements; and discussions of the design of ROADM transmission systems and the interplay between the ROADM and transmission performance. The chapter ends with some thoughts on the remaining challenges to enable ROADMs to achieve their potential.

1.4.9 Chapter 9. Optical Ethernet: Protocols, management, and 1–100 G technologies (*Cedric F. Lam and Winston I. Way*)

As the Internet becomes the de facto platform for the delivery of voice, data, and video services, Ethernet has become the technology of choice for access and metro

networks, and for next-generation long-haul networks. As stated concisely by the authors, "The success of Ethernet is attributed to its simplicity, low cost, standard implementation, and interoperability guarantee," attributes that helped the "networking community it serves to prosper, hence producing the economy of scale."

This chapter is an in-depth review of the evolution and development of Ethernet technology for application in optical fiber telecommunications networks. Topics covered include: point-to-point Ethernet development, Layer-2 functions, Carrier Ethernet, Ethernet in access PONs, Ethernet OAM (Operation, Administration, Maintenance), development of 10 GE for PON and 100 GE for core applications, and examples of high-speed Ethernet.

1.4.10 Chapter 10. Fiber-based broadband access technology and deployment (*Richard E. Wagner*)

One of the earliest long-haul commercial optical fiber telecom systems was the AT&T Northeast Corridor link from Boston to New York to Washington in 1983. In this application, the large capital investment could be amortized among many users. The prospect of economically bringing fiber all the way to a large number of end users, where cost sharing is not available, has continuously appealed to and challenged the telecom industry. Presently, technology advances and volume manufacture are reducing costs/user, fabulous broadband applications are luring subscribers, and government legislation and subsidies are encouraging growth worldwide. This chapter tracks the history of broadband access, compares the competing access technologies, and projects the roadmap to future deployment in the US, Asia, Europe and the rest of the world. The economic driver for widespread deployment is the explosive growth of Internet traffic, which doubles annually in developed countries and grows even faster in developing countries, such as China. In developed countries, growth is due to new broadband applications; in developing countries, both new users and new applications drive traffic growth.

This chapter focuses on the fiber-based approaches to broadband access worldwide, including some of the drivers for deployment, the architectural options, the capital and operational costs, the technological advances, and the future potential of these systems. Three variants of fiber-based broadband access, collectively called FTTx in this chapter, have emerged as particularly important. They are: hybrid-fiber-coax (HFC) systems, fiber-to-the-cabinet (FTTC) systems, and fiber-to-the-home (FTTH) systems.

1.4.11 Chapter 11. Global landscape in broadband: Politics, economics, and applications (*Richard Mack*)

The technology of choice that predominates in a specific telecom arena depends ultimately upon the competitive economics: the normalized capital and

operational costs in dollars per unit bandwidth (per unit distance). For metro, regional, and long-haul arenas, lightwave technology is indisputably the king. However, in the access arena, the competitive unit cost of lightwave technology has not favored rational deployment. Indeed, the history of FTTH has followed a tortuous path; the early trials in the 1980s and 1990s did not lead to massive deployment. Globally, Japanese and Korean telecom companies have been leading the installation of FTTH (with as yet unknown economic consequences). In the meantime, the cost of FTTH equipment has been decreasing steadily. Recently, relief from "unbundling" (exemption from requirement for incumbent carriers to share facilities with competitive carriers, as ruled by FCC) and competition from cable TV companies have prompted incumbent carriers in the US to install FTTH with competitive (triple-play) service offerings. As the demand for broadband services grows and revenue improves, the return from the vast investment in FTTH may be realized in the not-to-distant future.

This chapter is a fascinating, data-laden account of the history of deployment of optical fiber telecommunications, with emphasis on economics, growth landscape, and broadband services in the access arena. The discussion includes historical highlights, demographics, costs and revenues, fiber installations, services scenarios, competition and growth, regulatory policies, applications and bandwidth requirements, technology and network architecture choices, market scenarios, etc. The interplay of these issues is discussed and summarized in the concluding section.

1.4.12 Chapter 12. Metro networks: Services and technologies (*Loukas Paraschis, Ori Gerstel, and Michael Y. Frankel*)

Metropolitan networks operate in the environs of a major city, transporting and managing traffic to meet the diverse service needs of enterprise and residential applications. Typically, metro networks have a reach below a few hundred kilometers with node traffic capacities and traffic granularity that require amplified dense WDM technology with optical add/drop, although the more economical coarse WDM technology has also been deployed. At present, convergence of IP services and traditional time-division multiplexed (TDM) traffic with low operational cost is an important issue.

This chapter reviews the architecture and optical transport of metro networks, which have evolved to meet the demand of various applications and services, including discussions of the evolution of network architecture, physical building blocks of the WDM network layer, requirements of network automation, and convergence of packetized IP with traditional TDM traffic, and ending with a brief perspective on the future outlook.

1.4.13 Chapter 13. Commercial optical networks, overlay networks, and services (*Robert Doverspike and Peter Magill*)

As service providers are the ultimate users of novel technologies and systems in their networks, it is important that the innovators have a sound understanding of the structure and workings of the carriers' networks: the architecture and layers, traffic and capacity demands, management of reliability and services, etc. Commercial networks are continuously upgraded to provide more capacity, new services and reduced capital and operational cost; seamless network evolution is essential for obvious economic reasons. Even when "disruptive" technologies and platforms are introduced, smooth integration within the existing infrastructure is imperative.

This chapter reviews the important aspects of current commercial optical networks in all three segments or layers: access, metro, and core. Topics include 1. relationship of services to layers, covering service requirements, layer technology, quality of service, Service Level Agreements, network availability, and network restoration; and 2. network and services evolution, covering demand and capacity, and applications and technologies in all three segments of the network. In the summary section, the authors point out that while much of the "industry focuses on advanced optical technologies for the long-distance network, most of the investment and opportunity for growth resides in the metro/access [sector]."

1.4.14 Chapter 14. Technologies for global telecommunications using undersea cables (*Sébastien Bigo*)

The introduction of WDM has enabled a tremendous capacity growth in undersea systems, both by the increase in the number of carrier wavelengths and by the increase in the channel bit rate. Starting from 2.5 Gbit/s in the mid-1990s, the bit rate was upgraded in commercial products to 10 Gbit/s at the end of the last century. The next generation of undersea systems will likely be based on 40-Gbit/s bit-rate channels. However, transmission at 40 Gbit/s is significantly more challenging than at 10 Gbit/s.

This chapter gives an overview of the specificities of submarine links with respect to terrestrial links and provides a few examples of recently deployed undersea systems. Moreover, it describes the key technologies involved in undersea systems, explaining particular implementations of early optical systems, today's 10-Gbit/s systems, and future 40-Gbit/s links. The key technologies are related to fiber selection and arrangement, to amplifier design, to modulation formats, to detection techniques, and to advanced impairment-mitigation solutions.

1.4.15 Chapter 15. Future optical networks (*Michael O'Mahony*)

In the past few years Internet traffic, doubling annually, has dominated the network capacity demand, which has been met by the advances in lightwave communications. The transformation from a circuit-switched, voice-centric to a packet-switched, IP-centric network is well underway; amplified WDM transmission systems with terabits-per-second capacity are being deployed; rapid reconfigurable networking and automatic service provisioning are being implemented. The drive to reduce cost and increase revenue has being inexorable. In the meantime, carriers are installing FTTH and offering IPTV services, which will undoubtedly change network traffic characteristics and boost the traffic growth rate. What will the future networks look like?

This chapter reviews the growth of the data traffic and evolution of the optical network, including user communities, global regional activities, and service requirements. Discussions cover the diversity of architectures, the evolution of switching, cross-connecting and routing technologies, and the transformation to carrier-grade (100 G) Ethernet. The author notes that device integration "will enable the realization of many of the key functionalities for optical networking."

1.4.16 Chapter 16. Optical burst and packet switching (*S. J. Ben Yoo*)

Optical switching has the potential of providing more-efficient and higher-throughput networking than its electronic counterpart. This chapter discusses optical burst and packet switching technologies and examines their roles in future optical networks. It covers the roles of optical circuit, burst, and packet switching systems in optical networks, as well as their respective benefits and trade-offs. A description is given of the networking architecture/protocols, systems, and technologies pertaining to optical burst and packet switching. Furthermore, this chapter introduces optical-label switching technology, which provides a unified platform for interoperating optical circuit, burst, and packet switching techniques. By exploiting contention resolution in wavelength, time, and space domains, the optical-label switching routers can achieve high-throughput without resorting to a store-and-forward method associated with large buffer requirements. Testbed demonstrations in support of multimedia and data communications applications are reviewed.

1.4.17 Chapter 17. Optical and electronic technologies for packet switching (*Rodney S. Tucker*)

The Internet provides most of the traffic and growth in lightwave systems today. Unlike the circuit-switched telephone network, the Internet is based on packet

switching, which provides statistical multiplexing of the many data streams that pass through a given switch node. A key element of any packet switch is the ability to buffer (or store) packets temporarily to avoid collisions. Since it is easy to store bits as electronic charge in silicon, commercial packet switches are electronic.

This chapter introduces the basics of practical packet routers, indicating the requirements of a switch based on either electronics or photonics. The author compares the physical limits on routers based on storing and switching electrons vs photons. While many in the optics field would like to see photonic switches dominate, it appears that the physical inability to provide a large optical random access buffer means that packet switches will continue to be optoelectronic rather than all-optical for some time.

1.4.18 Chapter 18. Microwave-over-fiber systems (*Alwyn J. Seeds*)

The low-loss, wide-bandwidth capability of optical transmission systems makes them attractive for the transmission and processing of microwave signals, while the development of high-capacity optical communication systems has required the import of microwave techniques in optical transmitters and receivers. These two strands have led to the development of the research area of microwave photonics. Following a summary of the historic development of the field and the development of microwave photonic devices, systems applications in telecommunications, and likely areas for future development are discussed. Among the applications reviewed are wireless-over-fiber access systems, broadband signal distribution and access systems, and communications antenna remoting systems.

1.4.19 Chapter 19. Optical interconnection networks in advanced computing systems (*Keren Bergman*)

High-performance computers today use multicore architectures involving multiple parallel processors interconnected to enhance the ultimate computational power. One of the current supercomputers contains over one hundred thousand individual PowerPC nodes. Thus the challenges of computer design have shifted from "computation-bound" to "communication-bound." Photonic technology offers the promise of drastically extending the communications bound by using the concepts and technologies of lightwave communications for interconnecting and networking the individual multi-processor chips and memory elements. Silicon photonics (see the chapter on "Silicon Photonics" by C. Gunn and T. L. Koch) looms as a possible subsystem technology having the cost-effectiveness of silicon CMOS manufacturing process.

This chapter is a review of the subject of interconnection networks for high-performance computers. Performance issues including latency, bandwidth and power consumption are first presented, followed by discussions of design considerations including technology, topology, packet switching nodes, message structure and formation, performance analysis, and evaluation. Network design implementation, architectures, and system demonstrations are then covered and thoughts are offered on future directions, including optical interconnection networks on a chip.

1.4.20 Chapter 20. Simulation tools for devices, systems, and networks (*Robert Scarmozzino*)

The ability of optical fiber telecommunications to satisfy the enormous demand for network capacity comes from thorough understanding of the physics and other disciplines underlying the technology, as well as the abilities to recognize sources for limitation, develop ideas for solution, and predict, test, and demonstrate those ideas. The field of numerical modeling has already been an important facilitator in this process, and its influence is expected to increase further as photonics matures.

This chapter discusses the broad scope of numerical modeling and specifically describes three overarching topics: (i) active and passive device/component-level modeling with emphasis on physical behavior, (ii) transmission-system-level modeling to evaluate data integrity, and (iii) network-level modeling for evaluating capacity planning and network protocols. The chapter offers an overview of selected numerical algorithms available to simulate photonic devices, communication systems, and networks. For each method, the mathematical formulation is presented along with application examples.

ACKNOWLEDGMENTS

We wish sincerely to thank Tim Pitts and Melanie Benson of Elsevier for their gracious and invaluable support throughout the publishing process. We are also deeply grateful to all the authors for their laudable efforts in submitting their scholarly works of distinction. Finally, we owe a debt of appreciation to the many people whose insightful suggestions were of great assistance.

We hope our readers learn and enjoy from all the exciting chapters.

This page intentionally left blank

2

Advanced optical modulation formats

Peter J. Winzer and René-Jean Essiambre

Bell Laboratories, Alcatel-Lucent, Holmdel, NJ, USA

2.1 INTRODUCTION

Since the publication of the fourth volume of the book series *Optical Fiber Telecommunications* in 2002, high-speed optical transmission systems have increasingly been building on techniques that are well established in radio-frequency (RF) communication systems, and in particular in wireless communication. Examples are advanced modulation formats, line coding, enhanced forward error correction (FEC), and digital signal processing at transmitter and receiver. The adoption and extension of these techniques from the Mb/s regime into the multi-Gb/s realm is driven by the desire to steadily lower the cost per end-to-end networked information bit in an environment of continuously increasing data traffic. This is being done by extending the regeneration-free reach of optical line systems at the highest possible per-fiber transmission capacities, while at the same time allowing for optical wavelength routing in optically transparent mesh networks. In this context, *communication engineering techniques* are now supplementing established methods from optical physics to increase transmission reach, system capacity, and network flexibility. Today, research and commercial implementation of digital optical communication techniques fall into two main areas, distinguished by the per-wavelength symbol rates they operate at:

- At per-channel symbol rates of 10 Gbaud, *electronic signal processing* ranging from simple feed-forward and decision-feedback equalizers (FFE, DFE) at the receiver all the way to maximum-likelihood sequence estimation (MLSE) is commercially available today [1 3], and FEC is found in most commercial 10-Gb/s transport products [4, 5]. Digital signal predistortion at the transmitter is being actively pursued [6], and coherent detection is

Optical Fiber Telecommunications V B: Systems and Networks

ISBN: 978 0 12 374172 1

experiencing renewed[1] interest [14 16]. In contrast to widely deployed direct detection, coherent detection allows electronic signal processing to make use of the full optical field (magnitude *and* phase), which can be exploited for more efficient mitigation of fiber transmission impairments such as chromatic dispersion (CD) or polarization mode dispersion (PMD). Coherent detection research is also aiming at increasing the bit rate through multilevel modulation and polarization multiplexing while keeping the signal bandwidth similar to that of a 10-Gb/s binary signal to reuse 10-Gb/s optical line infrastructure and to increase the system's spectral efficiency (SE). In general, narrow signal bandwidths are desired in high-SE optically routed networks to minimize excessive filtering penalties due to the concatenation of reconfigurable optical add/drop multiplexers (ROADMs) and to avoid excessive cross talk between adjacent wavelength-division multiplexed (WDM) channels.

- At per-channel symbol rates of 40 Gbaud, and up to 100 Gbaud, the capabilities of electronic equalization are still limited to low complexity electronic [17 21] and optical [22 24] FFE structures. In this area, *modulation formats* and *line coding* are at the center of interest. They are used to mitigate linear and nonlinear impairments of fiber-optic transmission, as well as to achieve high SEs in optically routed networks. At 40 Gb/s, FEC is a standard feature of commercially deployed optical transport systems [25].

Despite the many benefits brought by electronic signal processing and digital communication techniques, it should be noted that an optical fiber network differs substantially from an RF communication link, both *fundamentally* and *technologically*. Some key differences relevant to the discussions in this chapter are summarized in Table 2.1.

Fiber Nonlinearities

The most important fundamental difference between optical and RF communications is the presence of nonlinear distortions in the optical fiber communication channel. The high transversal confinement of the optical signal field in a fiber core with effective areas between 20 and 110 μm^2 causes light intensities to reach or exceed a megawatt/cm^2. At such high optical intensities, the fiber's index of refraction is affected by the presence of optical signals through the optical *Kerr effect* [26], and signal-induced refractive index changes translate into changes of the signals' optical phases. Over optically amplified distances of many hundred or even several thousand

[1] Coherent detection using advanced optical modulation formats was widely discussed in the context of *unamplified* lightwave systems in the 1980s [7 12], where attenuation limited single span transmis sion required utmost receiver sensitivities. With the advent of efficient optical amplifiers, allowing for comparable direct detection receiver sensitivities [9, 13], coherent systems research decayed in the early 1990s.

kilometers, these phase rotations, in conjunction with fiber dispersion, result in a host of different waveform distortions that increase with signal power. As a consequence, and in stark contrast to classical RF systems, the performance of an optical communication link exhibits a maximum at a certain signal power level, which represents the optimum trade-off between optical amplifier noise (amplified spontaneous emission, ASE) and fiber Kerr nonlinearity. As an example, Figure 2.1(a) [27] shows the

Table 2.1

Optical vs radio-frequency communication systems.

	Optical communications	RF communications
Fundamental		
Noise	Quantum noise	Thermal noise
Interference	Multipath, WDM crosstalk	Multipath, multiuser
Channel	Fiber nonlinearity + dispersion	Linear channel, fading
Channel dynamics	~kHz (const. for~10^7 bits)	~kHz (const. for ~10^1 10^3 bits)
Technological		
Electrical bandwidth	~60 GHz limited by technology (bandwidth/carrier~10^{-4} to 10^{-6})	Limited by spectral regulations (bandwidth/carrier~10^{-2} to 10^{-4})
Detection	Predominantly square law	Predominantly coherent (I/Q) demodulation
Digital processing	Fairly simple equalization and FEC	Extensively used, sophisticated
Processing power per information bit	Fairly low	Very high

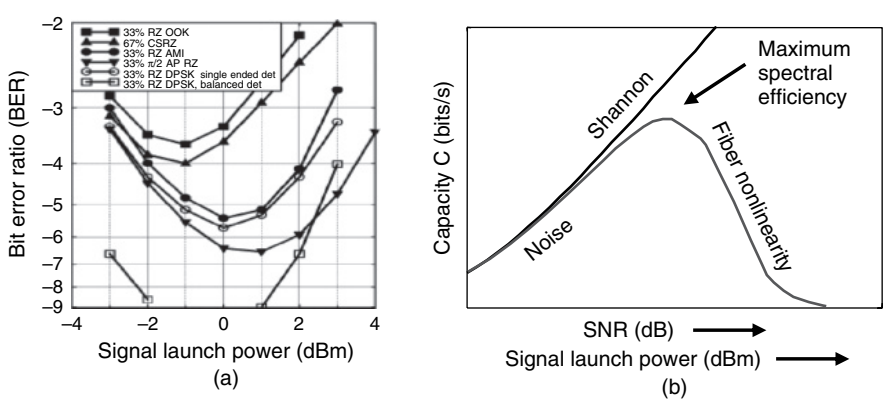

Figure 2.1 (a) Measured BER vs signal launch power for various optical modulation formats transmitted over 1980 km of SSMF [27]; (b) Schematic representation of fiber channel capacity vs received SNR. Both cases exhibit maximum performance at a specific signal power level, representing the optimum trade off between optical amplifier noise and fiber Kerr nonlinearity (this figure may be seen in color on the included CD ROM).

measured bit error ratio (BER) as a function of launched signal power for various optical modulation formats transmitted over 1980 km of standard single-mode fiber (SSMF). The figure reveals the trade-off between ASE-dominated performance at low signal launch powers and dominating fiber nonlinearity at high powers, indicating different performance optima at format-specific optimum launch powers. Figure 2.1(b) shows the schematic behavior of *fiber channel capacity* as a function of the received signal-to-noise ratio (SNR) [28]. Due to quantum-mechanical lower bounds on optical amplifier noise, the SNR can only be increased by launching higher signal power, which eventually leads to nonlinear signal distortions. Note that when operated at optimum performance, *every* fiber-optic communication system shows signs of nonlinear signal distortions.

Electronic Bandwidth Limitations

The second major difference between optical and RF communication systems, with both fundamental and technological consequences, is the high *absolute bandwidth* of optical communication signals. In general, and as evidenced by the historic evolution of lightwave systems [29], the highest possible per-channel bit rates have always yielded the lowest cost, footprint, and power consumption per end-to-end networked information bit, once the underlying technologies were sufficiently mature. Therefore, optical communication systems have always been pushing the limits of high-speed electronic and optoelectronic components, with 100-Gb/s binary transmission systems representing the current limit of electronic multiplexing and demultiplexing capabilities (see Refs [24, 30] and Chapter 5 of this book). The sheer per-channel bandwidth has left little room for the implementation of sophisticated signal processing algorithms, including coherent detection with digital phase locking ("intradyne" detection [14, 15, 31], cf. Sec. 2.4.1 and Chapter 3 of this book). The last 5 years, however, have seen a period of stagnation due to the burst of the telecom bubble, which has allowed electronic processing to catch up with 10-Gb/s line rates, still the most dominantly deployed per-channel bit rate. It remains to be seen whether future systems will be based on 10-Gbaud technology and its evolution to higher rates, with substantial digital processing complexity, or whether systems will continue to use the highest possible symbol rates in conjunction with direct detection and advanced optical technologies such as adaptive dispersion management or optical phase conjugation but with modest electronic processing. In any case, optical communication technologies will always be facing the limits of high-speed signal processing and modulation, which is an important factor to take into account when discussing advanced optical modulation formats.

In this chapter, we review, on an advanced level, important communication engineering techniques that have been discussed in the context of optical

networking over the past 5 years and that are likely to be the subject of further studies over the next 5 years. We also want to point the reader to additional reviews on the topic [27, 32 36]. On a more introductory level, optical modulation formats are discussed in, e.g., [37 39]. The communication engineering background is covered in textbooks such as [40 42], and the background in optical physics can be found in, e.g., [26, 43, 44]. A list of acronyms used in this chapter can be found on pages 80-81.

2.2 COMMUNICATION ENGINEERING AND OPTICAL COMMUNICATIONS

The broad field of communication engineering has developed a variety of techniques that can be used to beneficially impact digital data transmission and to approach the capacity [45, 28] of a given communication channel. Figure 2.2 visualizes those methods and ingredients that are relevant to the understanding of advanced optical communication systems, and in particular to the understanding of

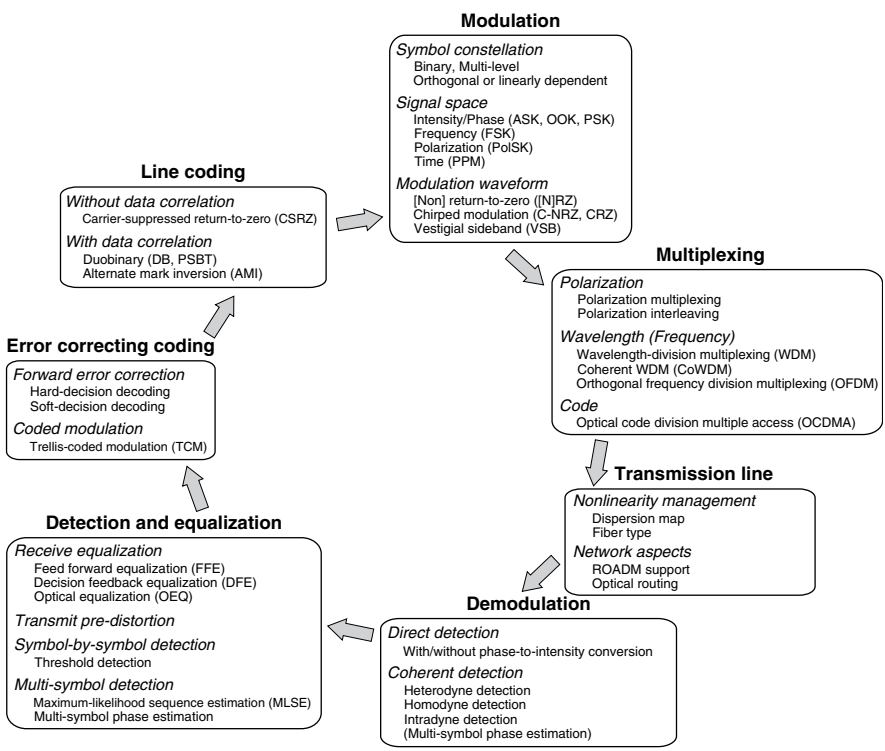

Figure 2.2 Overview of communication engineering techniques discussed in optical networks research today.

advanced modulation formats in the broader context of optical transport networks. The aspect of *modulation* comprises the choice of symbol constellations and signal spaces used to encode information onto an optical carrier. Of particular importance to the optical communication channel is also the appropriate choice of modulation waveforms. In addition to choosing a modulation scheme, *redundancy* may be introduced into the symbol sequence. This may either be done by *line coding*, which shapes the spectrum or avoids certain adverse bit patterns to beneficially impact a format's transmission performance, or by *error correcting coding*, which uses redundancy to correct symbol errors at the receiver. In either case, redundancy can be added in the *time domain* by increasing the signal's symbol rate (typically by 7% in FEC schemes employed in standardized terrestrial optical communications [46]) or in *signal space* by adding more points or even more dimensions to the symbol constellation. If used for error correcting purposes, the latter strategy is generally referred to as *coded modulation*. To exploit the vast bandwidth provided by a single optical fiber, *multiplexing* of many channels is typically performed, with wavelength-division multiplexing (WDM) being the most prominent technique. At the receiver, the optical signal is *demultiplexed*, and the channel of interest is *demodulated* from optical carrier frequencies to baseband. The majority of optical communication systems uses demodulation by direct (i.e., square-law) photodetection. Recently, coherent demodulation has also received renewed interest, fueled by advances in high-speed digital signal processing hardware. Along the same lines, signal processing at both transmitter and receiver as well as advanced detection techniques have become important fields of research and commercialization. All these communication engineering techniques, however, have to be seen in the bigger picture of established optical *line system design*, such as dispersion management, which effectively solves problems particular to the optical communication channel, most notably mitigating impairments brought by fiber nonlinearity. In this chapter, we will discuss several of the techniques shown in Figure 2.2. We will start by looking at *modulation waveforms* and their properties, which form the basis for classifying modulation formats as well as multiplexing techniques.

2.2.1 Signal Spaces for Modulation and Multiplexing

Any digital modulation format is composed of a discrete set $\{x_1(t), x_2(t), \ldots, x_M(t)\}$ of analog modulation waveforms that represent an *alphabet* of $M \geq 2$ *communication symbols*.[2] If $M = 2$ we speak of binary modulation, which is the prevailing

[2] This general concept is very similar to written text, which is based on an *alphabet of letters* (e.g., 26 discrete letters in the standard Roman alphabet). To convey information, each letter is represented by an analog "waveform". For example, the letter "A" can be represented by the "waveforms" A, *A*, $\mathcal{A}$, a, *a*, or even by ' ' in Morse code. As long as transmitter and receiver use the same alphabet *and* are able to correctly read the letters' analog waveform representations, communication may take place.

alphabet size used in commercially deployed optical communication systems. To convey digital information, the transmitter picks one symbol per symbol interval of duration T_S and transmits a string of symbols at the symbol rate $R_S = 1/T_S$. The symbol rate is measured in *Baud*, where 1 Baud = 1 symbol/s. If all symbols in the alphabet occur with equal probability and are all used to carry information, each symbol conveys $\log_2 M$ *bits of information*, and bit rate R_B and symbol rate R_S are related by

$$R_B = R_S \log_2 M. \tag{2.1}$$

For the analysis and classification of modulation formats and multiplexing schemes, it is convenient to express the set of modulation waveforms as "vectors" in a linear vector space. In analogy to the geometric vector space, where a vector is represented as a two- or three-dimensional "arrow", a signal may be thought of as an object in an N-dimensional space of continuous functions, called the *signal space*. The "inner product" between two (generally complex) signals is defined as [40]

$$\langle x_i(t)|x_k(t)\rangle = \int_{\infty}^{\infty} x_i(t)x_k^*(t)\mathrm{d}t. \tag{2.2}$$

In the context of optical communication signals, the modulation waveforms $x_{i,k}(t)$ are physically represented by *optical field vectors* $\vec{e}_{i,k}(t,\vec{r})$, where $\vec{r}$ denotes the transverse coordinate, and the definition of the inner product can be extended to

$$\langle \vec{e}_i(t,\vec{r})|\vec{e}_k(t,\vec{r})\rangle = \int_{\infty}^{\infty} \mathrm{d}t \int_{\mathcal{A}} \mathrm{d}\vec{r}\, \vec{e}_i(t,\vec{r}) \cdot \vec{e}_k^*(t,\vec{r}), \tag{2.3}$$

where "$\cdot$" is the inner product of two vectors in the geometric sense, and $\mathcal{A}$ denotes the transverse area covered by the two optical fields. This definition extends Eqn (2.2) into the modal $(\vec{r})$ and polarization $(\vec{e})$ domain.

The "*length*" (or "*norm*") of a signal vector equals the signal's energy

$$\|\vec{e}_k(t)\| = \langle \vec{e}_k(t,\vec{r})|\vec{e}_k(t,\vec{r})\rangle = E_k. \tag{2.4}$$

Importantly, two signals are *orthogonal* if their inner product is zero,[3]

$$\vec{e}_i(t) \perp \vec{e}_k(t) \Leftrightarrow \langle \vec{e}_i(t,\vec{r})|\vec{e}_k(t,\vec{r})\rangle = 0. \tag{2.5}$$

[3] Note that for two *real valued bandpass signals* (such as the optical field $||e||^2$) to be orthogonal, it suffices that the *real part* of the inner product of the two fields' complex envelopes is zero [40].

A *digital communication receiver* generally *projects* the received waveform into the signal space used for modulation by evaluating the inner product of the received waveform and the set of known modulation waveforms. By acknowledging the fact that the inner product, Eqn (2.2), can also be written as a convolution ($*$) sampled at $t = 0$ [40],

$$\langle x_i(t)|x_k(t)\rangle = \int_{\infty}^{\infty} x_i(\tau)x_k^*(-[t-\tau])\mathrm{d}\tau\Big|_{t=0} = x_i(t) * x_k^*(-t)\Big|_{t=0}, \qquad (2.6)$$

we see that this projection can be performed by a *matched filter* (or a *bank* of matched filters working in parallel for the case of multiple orthogonal modulation waveforms), followed by a sampling device [40 42]. The impulse response $h(t)$ of the respective matched filter is given by the complex conjugate of the temporally reversed modulation waveform, $h(t) = x_k^*(-t)$. Figure 2.3 shows a matched filter front-end for a three-dimensional signal space, together with its graphical representation. The input signal waveform is $y(t)$ and the three orthogonal modulation waveforms are $x_{1,2,3}(t)$.

A matched filter bank can be shown to be the theoretically optimum receiver front-end for a wide class of communication scenarios [40], including the detection of optical signals impaired by additive white Gaussian noise, properly modeling amplified spontaneous emission (ASE) of optical amplifiers. Note that in square-law (direct detection) receivers the *optical* filter (OFs) need to be matched to the modulation waveforms [10, 47]. In general, as many matched filters are needed as there are dimensions of the signal space underlying the modulation format. For example, binary optical intensity modulation (IM), also referred to as on/off keying (OOK), requires a single real-valued filter; quadrature modulation, i.e., separate modulation of the complex optical field's real and imaginary parts, requires two real-valued (or, equivalently, one complex-valued) filter; polarization shift keying (PolSK) asks for a polarization beam splitter that separates the two orthogonal polarization dimensions. By performing matched filtering, any *noise components* outside the signal space defined by the matched filter bank are filtered out and have no impact on detection. For example, by introducing a polarization filter, which is the filter that is matched to the signal's

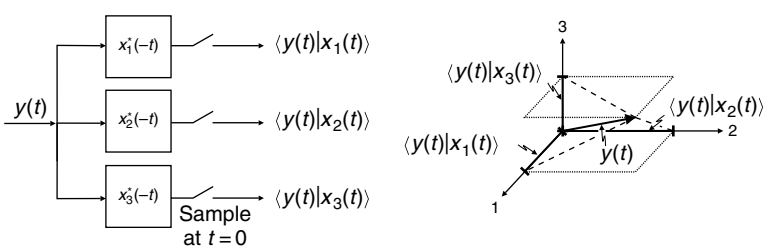

Figure 2.3 Matched filter front end and its graphical representation for a three dimensional signal space. The input signal waveform is $y(t)$ and the three orthogonal modulation symbols have waveforms $x_{1,2,3}(t)$.

polarization, the optical noise in the orthogonal polarization is filtered out, thereby improving detection performance. However, due to many practical reasons faced in high-speed optical communication systems, including the effects of frequency offsets, residual CD nonlinear signal distortions, the impact of non-negligible postdetection electronic filtering, the presence of intersymbol interference (ISI) together with the lack of sufficiently powerful equalization or sequence detection devices, or the sheer difficulties associated with the design of commercially attractive matched optical filters, matched filtering is generally *not* used in optical communications. One rather optimizes *manufacturable* optical filters for best overall receiver performance in the presence of all practical limitations and shortcomings [48 50]. Nevertheless, the general philosophy of matched filtering is still applicable in optics, even if it is used in a relaxed sense in practice, which we may refer to as "quasi-matched" filtering.

Since matched (or quasi-matched) filtering eliminates signal dimensions outside the signal space defined by the matched filter bank, these dimensions can be used for data streams belonging to *different users* of the same communication channel. The process of sharing a common channel by exploiting signal orthogonality is referred to as *multiplexing*. Orthogonality can also be used for other purposes, such as *optical label encoding*, where the payload of a data packet is encoded in one dimension and a packet overhead used for routing purposes is encoded in an orthogonal dimension [51]. Figure 2.4 summarizes the most

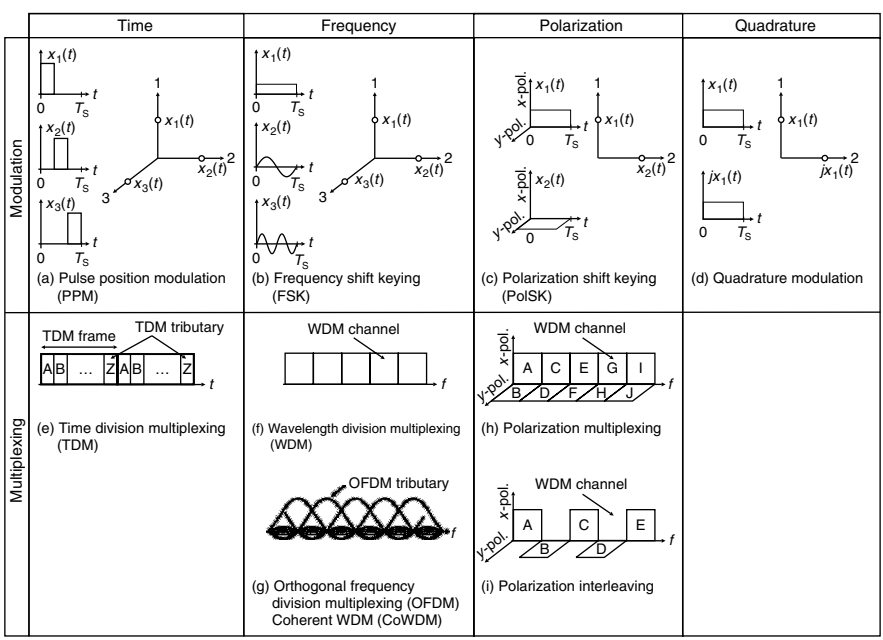

Figure 2.4 Signal orthogonality can be exploited to construct modulation formats (a d), or to multiplex signals onto a shared communication channel (e i).

important ways orthogonality is used in optical communications for *modulation* and *multiplexing* purposes:

Orthogonality in time is achieved by having disjoint time slots within the symbol period T_S represent different modulation symbols. The resulting modulation format is called *pulse position modulation* (PPM) [52, 53] and is depicted in Figure 2.4(a) for the case of a ternary modulation alphabet carrying $\log_2 3 \approx 1.6$ bits/symbol. By assigning non-overlapping time slots to different users of a common communication channel, one arrives at *time division multiplexing* (TDM) shown in Figure 2.4(e), where users A through Z share slots in a *TDM frame*. The synchronous optical transport network (SONET) as well as the synchronous digital hierarchy (SDH) are examples of TDM systems used in optical networking. If TDM tributaries are added and dropped to a TDM frame fully electronically, one speaks of *electronic* TDM (ETDM), and of *optical* TDM (OTDM) if these operations are performed through optical means. Historically, only ETDM systems have lent themselves to successful commercialization, but OTDM systems have proven to be valuable research tools to explore bit rates far beyond the capabilities of current electronic multiplexing technologies. Today, ETDM systems operate at bit rates up to 100 Gb/s (cf. Refs [24, 30, 54] and Chapter 5 of this book); OTDM systems with bit rates of 160 and 320 Gb/s have been reported [55, 56], with some demonstrations going up to 2.56 Tb/s on a single optical carrier wavelength [57, 58], as reviewed in Chapter 6 of this book.

Orthogonality in frequency can be achieved by choosing strictly disjoint frequency bands, which is used in WDM as shown in Figure 2.4(f). Dense WDM (DWDM) systems used in transport networks typically have 50- or 100-GHz wide frequency bands, while coarse WDM (CWDM) access systems have 20-nm (≈2.5 THz) wide wavelength bands [59]. Any residual spectral overlap between WDM channels degrades their orthogonality and manifests itself in coherent WDM crosstalk if adjacent channels are at least partially copolarized. The use of orthogonal polarizations of adjacent channels (*polarization interleaving*) can re-establish orthogonality using the polarization domain, as discussed below.

Alternatively to choosing completely disjoint frequency bands, one can also exploit the fact that two pulses of duration T_S are orthogonal if their carrier frequencies are separated by integer multiples of $1/T_S$, even if they are temporally fully overlapping[4] [40, 42]. Hence, different data signals may be modulated onto such orthogonal frequencies, which is at the heart of *orthogonal frequency division multiplexing* (OFDM) [60 62] or *coherent WDM* (CoWDM) [63] shown in Figure 2.4(g). In optical communications, the term "OFDM" is typically used whenever the orthogonal subcarriers are generated and modulated electronically, followed by a single electro-optic modulator to convert the frequency multiplex to the optical

[4] This is easily seen by evaluating the inner product, Eqn (2.2), for two rectangular pulses of duration T_S that have a carrier frequency difference of $1/T_S$.

domain. In contrast, the term "CoWDM" is used whenever a set of orthogonal optical subcarriers is generated from a single continuous-wave laser, followed by individual electro-optic modulation on each subcarrier. Both methods are presently being studied in optical communications research.

In the context of modulation, orthogonality in frequency may be exploited using *frequency shift keying* (FSK), as shown in Figure 2.4(b) for a ternary alphabet. Note in this context that the ternary alphabets for PPM and FSK are identical in Figure 2.4, but the analog modulation waveforms are very different. This underlines the fact that digital communication requires knowledge of both the symbol alphabet *and* the set of analog modulation waveforms. The generation and detection of binary optical FSK transmission at multi-Gb/s rates has been reported [8, 64, 65] but neither FSK nor its continuous-phase line-coded version, minimum shift keying (MSK) [40 42, 66, 67], has yet been studied in the context of high SE long-haul transport systems.

Orthogonality in polarization is achieved by choosing one of two orthogonal polarization states. When used for data modulation, one speaks of PolSK shown in Figure 2.4(c). Although PolSK has been studied for optical communications applications (see, e.g., [9, 68 70]) it has not been intensively pursued, primarily due to the need for active polarization management at the receiver, necessitated by random polarization changes in optical fiber [71]. The additional receiver complexity associated with polarization management could be acceptable if PolSK offered significant transmission advantages. As for receiver sensitivity, PolSK is equivalent to OOK [9, 68]. The polarization degree of freedom can also be used to improve the propagation properties of a non-PolSK format by line coding [72, 73] (see Section 2.3.3). With the increasing popularity of coherent detection, which is inherently polarization-sensitive and is therefore typically implemented with polarization diversity at the receiver (cf. Section 2.4.1), the polarization dimension may be further exploited for the construction of modulation formats in the future.

When applied to multiplexing, one may either transmit different data streams in the same WDM frequency band but in orthogonal polarizations [*polarization multiplexing*, Figure 2.4(h)], or one may alternate the polarization of adjacent WDM channels to avoid coherent WDM crosstalk, since coherent interference ("beating") only occurs if two optical fields have the same polarization [*polarization interleaving*, Figure 2.4(i)]. Both techniques are used in research experiments to increase SE, with a current experimental record of 3.2 b/s/Hz per wavelength using polarization multiplexed differential quadrature phase shift keying (DQPSK) [74, 75]. However, none of these methods is currently used in commercial direct detection systems due to the complexity associated with polarization maintaining system components and the wavelength-dependent random polarization rotations in transmission fiber [76]. However, due to its inherent need for polarization diversity, coherent detection allows for a straightforward implementation of polarization multiplexing (cf. Section 2.5.9). A significant amount of research is expected to take place in this area over the next 5 years.

Orthogonality of the two quadratures of a narrowband bandpass signal, i.e., the real and the imaginary parts of the signal's complex envelope, is the basis for the signal space most widely used in digital communications. The resulting formats are generally referred to as *quadrature modulation* formats and the resulting signal space is shown in Figure 2.4(d). The format uses an *arbitrary* complex-valued optical modulation waveform $x_1(t)$ which can, e.g., be pulsed or chirped (i.e., contain some analog, non data-bearing phase modulation). Within each symbol interval (i), the modulation waveform is multiplied by a symbol from an alphabet $\{a_k\}$ of complex numbers, leading to the complex communication signal

$$x(t) = \sum_{i=-\infty}^{\infty} a_{k(i)} x_1(t - iT_S). \tag{2.7}$$

Figure 2.5 shows three important examples for symbol constellations using quadrature modulation. If the alphabet $\{a_k\}$ modulates only along a single quadrature of the signal (e.g., only along the real part), we speak of *amplitude shift keying* (ASK), as visualized in Figure 2.5(a) for a 4-ary alphabet. In optical communications, the term "ASK" is sometimes used as a synonym for IM. However, M-ary IM only distinguishes between M optical intensity levels and not between M levels of the optical field amplitude.

If only the phase is modulated ($|a_k| = \text{const.}$), we speak of *phase shift keying* (PSK), shown for an 8-ary alphabet in Figure 2.5(b). If a_k can take on other sets of complex values, which are often chosen on a Cartesian grid, the modulation format is referred to as *quadrature amplitude modulation* (QAM), as shown for a 16-ary alphabet in Figure 2.5(c).

The average energy *per symbol* is related to the average energy *per bit* E_B by

$$E_B = \frac{E_S}{\log_2 M} \tag{2.8}$$

provided that all symbols are sent with equal probability of $1/M$. All constellations in Figure 2.5 are shown with the same energy per bit.

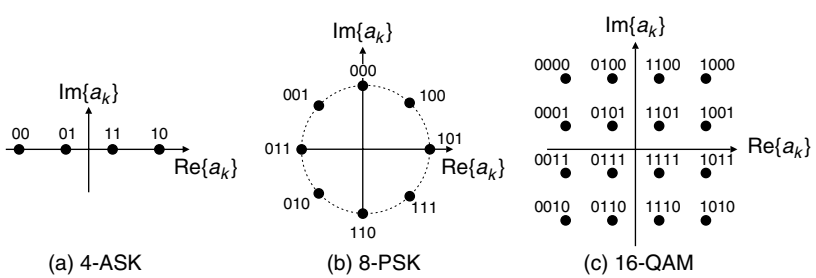

Figure 2.5 Three examples of frequently encountered symbol alphabets in a two dimensional complex signal space; (a) 4 ary amplitude shift keying (ASK); (b) 8 ary phase shift keying (PSK); (c) 16 ary quadrature amplitude modulation (QAM). Bit combinations are mapped to modulation symbols using Gray coding.

The assignment of bit combinations to modulation symbols in Figure 2.5 is not arbitrary but is chosen using *Gray coding* [40]. This coding method describes a mapping of bit combinations to modulation symbols in such a way that only a single bit is changed when transitioning from any symbol to an immediately adjacent symbol separated by the *minimum distance* in the symbol constellation. For example, the symbol "0101" in 16-QAM is surrounded by the nearest neighbors "0100," "0001," "0111," and "1101," which differ from the original symbol only in a single digit. Detecting one of these nearest-neighbor symbols is by far the most likely error event in the presence of circularly symmetric noise. Hence, Gray coding ensures that the prevailing class of symbol errors causes no more than a single bit error, which implies that the bit error probability is very similar to the symbol error probability. If Gray coding is not done, a single symbol error can produce as many as $\log_2 M$ bit errors.

In an alternative view of quadrature modulated signals, one can interpret the modulation symbols a_k as real and imaginary parts of the analog modulation waveform $x(t)$ *sampled at* T_S-spaced sampling instants. These sample values can then be plotted in the complex plane representing the complex optical field. Figure 2.6 visualizes this process for the simple example of OOK, where the sample values for a 0 and a 1 bit are transferred to the complex plane. Note that this representation of complex envelope signals is *not* a signal space representation in the strict sense, because the two orthogonal axes are only associated with *sampled symbol values* rather than with *entire symbol waveforms* that would form a signal space. Nevertheless, for ISI-free signals that can be written in the form of Eqn (2.7), the symbol constellations obtained this way are equivalent to the ones of the corresponding signal space. Displaying constellations in the complex plane of the sampled optical field offers several distinct advantages over the related signal space representation discussed above. First, it allows the representation of signals that cannot be easily written in the form of Eqn (2.7), which is the case for frequently encountered waveforms with pattern dependencies. For example, non-return-to-zero (NRZ) OOK with non rectangular pulses can only be written in the form of Eqn (2.7) if the optical power of several adjacent pulses adds up to a constant 1-bit level, which places severe restrictions on the allowed NRZ pulse shapes. Second, the complex plane representation captures a digital waveform at discrete points in time, separated by one symbol interval. In a natural extension, one can then visualize the

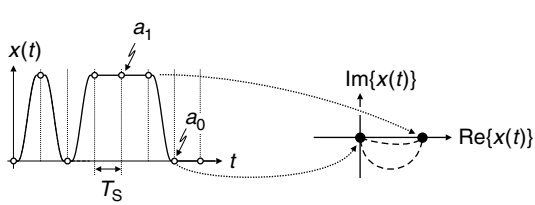

Figure 2.6 As an alternative to a strict signal space representation, one can visualize the complex amplitudes of T_S spaced signal samples (open circles) in the complex plane of the optical field (black dots). This representation can be extended by showing the continuous time transitions between symbols (dashed lines).

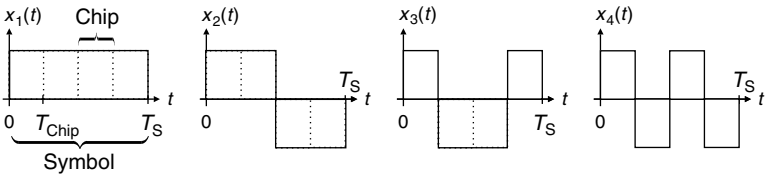

Figure 2.7 Orthogonality in code is established on a subsymbol (chip) granularity. Chips are shown as dotted lines. All four modulation waveforms $x_1(t)$ through $x_4(t)$, shown as solid lines, are orthogonal to each other.

complex amplitude of the signal *transitioning* between symbols, as indicated by the dashed curves joining the modulation symbols in Figure 2.6. The particular example in the figure applies to chirped OOK. Note, however, that this way of visualizing symbol transitions does not specify *dynamic aspects* of the signal, such as pulse rise and fall times or the duration of signal pulses.

Orthogonality in code captures the notion of temporally and spectrally fully overlapping signals that are made orthogonal by proper choices of their individual waveforms. Waveform orthogonality is established on a subsymbol granularity where a subsymbol is referred to as a *chip*. A simple example is visualized in Figure 2.7. The four modulation waveforms shown here are all mutually orthogonal, which is easily verified using Eqn (2.2). Orthogonal waveforms of this kind are also called *orthogonal codes* and can use other dimensions than the temporal as well. Oftentimes, orthogonal codes are constructed in the time/frequency plane [40, 42].

By assigning orthogonal codes to different users and letting each user perform modulation according to Eqn (2.7) with "his" waveform, we arrive at *code division multiple access* (CDMA), also called OCDMA in its optical implementation [77]. Note that OCDMA is not an optical modulation format but an optical multiplexing technique. OCDMA is studied in the optical research community for access networks, but has not yet found its way into commercial optical networks.

Orthogonality in space can be achieved by allowing no spatial overlap between copropagating signals, e.g., by placing them on separate fibers. This trivial multiplexing technique is sometimes referred to as *space division multiplexing* and is frequently encountered on short optical links, e.g., for optical interconnects between racks of equipment, where fiber ribbons can be used. Less trivially, different transverse modes propagating in a multimode optical fiber are all orthogonal [78, 79] and may be assigned to different users, which leads to the notion of *mode division multiplexing*. However, multimode fibers are prone to random mode coupling, and the recovery of any particular transverse fiber mode from a mixture of modes is not easily achieved [80, 81]. Modal multiplexing is an interesting research topic, including the study of multiple-input multiple-output (MIMO) communication techniques [82, 83].

2.2.2 Memory-Less Multilevel Modulation

Modulation formats whose symbol alphabets consist of more than the absolute minimum of two symbols are generally referred to as *multilevel* formats. If the assignment of symbols to bits or to groups of bits is *independent* of the symbols sent before or after, one speaks of *memory-less modulation*, discussed in this section. In contrast, if the assignment is made according to certain rules for the succession of different symbols, one speaks of *modulation with memory* [40], discussed in Section 2.2.3.

Introducing more symbols to a modulation alphabet can either be done by *expanding the dimensionality* of the signal space or by *placing more symbols* in an already existing signal space of given dimensionality [40 42, 84, 85]. The former approach typically increases the resilience to detection noise, which is the reason for the exploitation of PPM in deep-space optical links, where receiver sensitivity is of utmost concern [53]. However, an increased signal dimensionality comes at the expense of an increased signal bandwidth if dimensions are added in time or frequency. An important orthogonal dimension that does *not* increase the signal bandwidth is the polarization dimension. Its exploitation comes at the expense of an increased transmitter and receiver complexity as well as with a limited increase of orthogonal dimensions to be added.

The latter approach of placing more symbols in an already existing signal space[5] increases the bit rate at constant symbol rate, which has several important implications:

- The spectral extent of the multilevel modulated optical signal is less than that of a binary modulated signal at the same bit rate, which allows for stronger filtering in optically routed networks at higher SE.
- The reduced symbol rates compared to binary modulation increase the formats' robustness to some propagation impairments such as CD and PMD.
- The reduced symbol rates help to overcome potential limits of high-speed optoelectronic components. For example, the required components to build a 50-Gbaud DQPSK transponder [86 88] are more mature today than those needed to build a 100-Gb/s OOK system [24, 30, 54].
- The reduced symbol rates enable the use of digital electronic signal processing, albeit at the cost of multi-GSamples/s analog-to-digital and/or digital-to-analog conversion.
- As a downside, multilevel modulation is generally associated with a reduced tolerance to noise, since adding points to the symbol constellation reduces the minimum distance for a fixed average signal power.

[5] All symbol alphabets shown in Figure 2.5 are of this kind.

- As another downside, multilevel modulation generally leads to a reduced tolerance to fiber nonlinearity due to the reduced distance between the constellation points. Furthermore, for sufficiently high SE, the impact of fiber nonlinearity is generally more severe for the associated lower symbol rates.

In the context of multi-Gb/s optical communications, multilevel IM [32, 89], multilevel phase modulation [90 92], as well as hybrid multilevel intensity/phase and quadrature amplitude modulation [93 97] have been discussed and demonstrated. Multilevel IM has not proven beneficial for fiber-optic transport applications, mainly due to a substantial back-to-back receiver sensitivity penalty compared to binary OOK. For example, the four-level 4-ary IM format incurs a penalty of about 8 dB due to the unequal amplitude level spacings necessitated by signal-dependent noise arising from square-law detection [32, 89]. The multilevel modulation format that undoubtedly has received the most attention, including recent transponder commercializations, is (differential) quadrature phase shift keying (QPSK, DQPSK, see Sections 2.5.8 and 2.5.9).

2.2.3 Modulation with Memory and Coding

If redundancy is incorporated into a digital modulation signal, we generally speak of *coding*. As visualized in Figure 2.8, we distinguish between two forms of coding: *line coding* and *error correcting coding*.

Line coding denotes the introduction of redundancy with the aim to *prevent* detection errors and to mitigate transmission impairments, e.g., by shaping the modulation spectrum or by avoiding certain adverse symbol patterns.[6] This class of coding is also referred to as *modulation with memory* (i.e., the succession of symbols follows

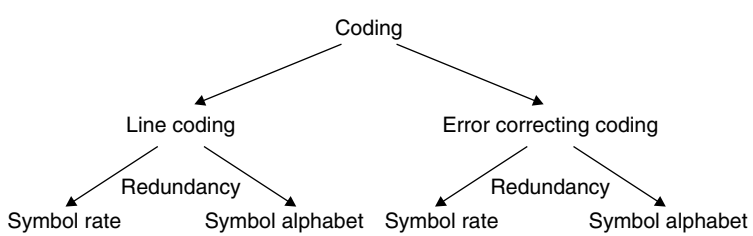

Figure 2.8 Introducing redundancy into a digital signal is referred to as *coding*. If coding is used to *prevent* errors, one speaks of line coding. If coding is used to *correct* for errors, one speaks of error correcting coding. In each case, redundancy can be introduced either in the time domain by increasing the symbol rate or in signal space by expanding the symbol alpabet.

[6] An example for line coding is the avoidance of certain words in English spoken by non native speakers. For example, people with a strong German accent may substitute words containing "th" by a suitable synonym; people with an Italian or French accent may avoid words starting with the letter "h"; and people with a Japanese accent may find themselves not understood when using words containing the letter "r".

specific rules dictated by the code) or *constrained coding* (i.e., the nature of the channel constrains the number of allowed symbol sequences). The required overhead to accommodate redundancy can either be added in the *time domain* by increasing the symbol rate or in *signal space* by increasing the symbol alphabet size [40, 98 102].

Alternatively, or in addition to line coding, *error correcting coding* can add redundancy at the transmitter in order for the receiver to be able to *correct* or at least to *detect* transmission errors.[7] Like in line coding, redundancy can be added in the time domain by increasing the symbol rate (by 7% when using FEC schemes employed in standardized terrestrial optical communication systems [46]) or in *signal space* by adding more points to the symbol constellation. The latter strategy is generally referred to as *coded modulation* [85, 103 105].

Modulation schemes with memory are conveniently characterized using the concept of a *finite state machine*, represented by *state diagrams* as shown in Figure 2.9. A state diagram captures the set of possible states of an abstract machine, called an "encoder" in our context, together with a set of inputs and a set of outputs for each state transition. A state machine is fully and uniquely defined if all possible inputs are represented on exactly one transition leaving each state.

As two simple yet highly relevant examples for optical modulation formats, consider the two finite state machines shown in Figure 2.9. Both encoders possess two states (A and B) and accept single bits {0, 1} as their input, i.e., they process the input information stream bit by bit. The output of both encoders is the ternary symbol alphabet {−1, 0, +1}, where one symbol is put out for

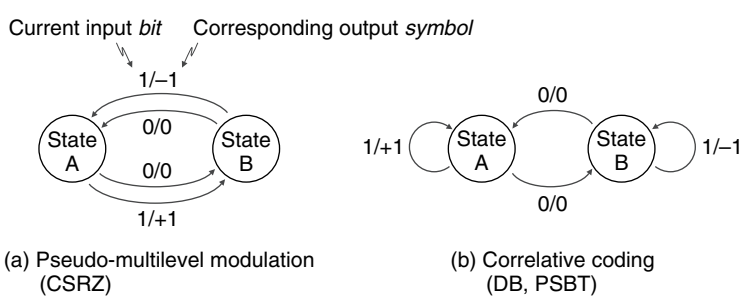

Data bits	0	0	1	0	1	1	1	0	0	1	0	1
Pseudo-multilevel symbols	0	0	+1	0	+1	−1	+1	0	0	−1	0	−1
Correlative coding symbols	0	0	+1	0	−1	−1	−1	0	0	−1	0	+1

Figure 2.9 Finite state machine representations of two examples of modulation with memory. In pseudo multilevel modulation (a), the state transitions are independent of the input bit stream, while in correlative coding (b) the value of the current input bit determines the encoder's new state.

[7] Most languages contain a high degree of redundancy, with the human brain acting as a powerful FEC decoder.

each input information bit, i.e., redundancy is introduced in the symbol domain without adding any temporal overhead. Both encoders represent a 0 bit by the symbol 0, whereas a 1 bit may be represented either by symbol $+1$ or by -1. The symbol set $\{-1, 0, +1\}$ is highly convenient for the dominant class of direct-detection (square-law) optical receivers, which only respond to the optical *power* $\mathrm{P} = |\vec{e}|^2$, the squared magnitude of the complex optical field $\vec{e}$. As a consequence, a direct-detection receiver is unable to distinguish between the two received symbols $\pm|\vec{e}|$, since they both have the same optical power, $P_1 = P_2 = |\pm\vec{e}|^2$. Therefore, the ternary symbol set $[\{+|\vec{e}|, 0, -|\vec{e}|\}$ is automatically mapped to the binary set $\{0, |\vec{e}|^2\}$ at the receiver, amenable to single-threshold detection.

The difference in the two encoders shown in Figure 2.9 lies in the set of rules that determine the next output symbol, and more specifically whether a 1 bit is represented by a $+1$ or a -1. If the new state after a state transition depends on the current input bit, we speak of *correlative* or *constrained coding*, while we speak of *pseudo-multilevel modulation* if the new state after a state transition does not depend on the current input bit.

Pseudo-Multilevel Modulation

The encoder in Figure 2.9(a) represents a *pseudo-multilevel* modulation format, since the new state does not depend on the input bit; starting at state A, we arrive at state B for both a 0 bit and a 1 bit at the input, and vice versa when starting at state B. As a result, the alternation between the symbols $+1$ and -1 is completely independent of the input data stream but only depends on whether the input bit falls in an "even" or an "odd" time slot. An example symbol sequence at the encoder output is shown in the table in Figure 2.9 for a given data sequence at the encoder input, assuming that the encoder is in state A initially. With a pulse-like modulation waveform carrying the amplitude-modulated symbols, the resulting format is known as *carrier-suppressed return-to-zero* (CSRZ, Section 2.5.5) in optical communications.

Although CSRZ is by far the best studied pseudo-multilevel modulation scheme in optical communications, other pseudo-multilevel formats have also been discussed, predominantly in the context of mitigating fiber nonlinearities. For example, Ref. 106 shows that an optimum choice of relative phases between adjacent pulses in a set of four consecutive bits can be either $\{0,\pi/2, 0,\pi/2\}$ or $\{0,0,\pi,\pi\}$ to suppress intrachannel four-wave mixing (IFWM). The mechanism for the reduction of IFWM using these coding schemes is by destructive interference of IFWM effects [106, 107]. The effectiveness of pseudo-level modulation has also been studied when implemented using a single phase modulator operating at a fraction of the symbol rate [108 111]. An advanced transmitter based on nonlinear polarization rotations coupled with polarizers is described in [112]. Another example of pseudo-multilevel coding is auxiliary polarization modulation [73] where the

polarization state is rotated back and forth by 90° every other symbol. This type of pseudo-multilevel modulation is particularly efficient to reduce the impact of IFWM [73]. We refer to these modulation schemes as *alternate phase* (AP) or *alternate polarization* (APol) modulation.

Correlative and Constrained Coding

The encoder in Figure 2.9(b) represents a *correlative coding* scheme, in which the new state depends on the input bit. For a 1 bit at the input, the encoder does not change state. Hence, a continuous string of 1 bits is represented by a continuous succession of $+1$ or -1 symbols, depending on the encoder's current state. Every 0 bit changes state, which implies that an odd number of 0 bits between any two 1 bits alternates the sign of the output symbol representing a 1 bit, while an even number of 0 bits between any two 1 bits does not have an effect. An example symbol sequence at the encoder output is shown in the table in Figure 2.9 for a given data sequence at the encoder input, assuming that the encoder is in state A initially. The resulting modulation format is known as *duobinary modulation* (DB) or *phase-shaped binary transmission* (PSBT), discussed further in Section 2.5.3.

Another easily generated (and hence fairly well studied) line coded modulation format in optical communications is *alternate mark inversion* (AMI), with the same symbol set as DB but with a different correlation rule: Each 1 bit is associated with a sign change, *irrespective* of the number of zeros in between. The example sequence listed in Figure 2.9 would read $\{0, 0, +1, 0, -1, +1, -1, 0, 0, +1, 0, -1\}$ for AMI. Interestingly, AMI can be generated by applying the pseudo-multilevel CSRZ correlation rule to a DB signal (cf. Figure 2.19). This fact has lead to the name *duobinary carrier suppressed* (DCS) as a sometimes encountered synonym for AMI [113 115]. Transmission of AMI has been investigated at 40 Gb/s [116 118], where its resistance to fiber nonlinearity has been found to be similar to OOK formats for nonzero dispersion fiber (NZDF) [117]. A moderate advantage has been found for nonlinear transmission over SSMF [116, 119, 118]. In recent literature, the term "modified duobinary" has also been used to denote AMI. Note, however, that modified duobinary is *not* equivalent to AMI but represents a distinctly different line coded modulation format [40, 84, 120, 121].

Line coding has also been studied in the context of pattern-dependent intrachannel fiber nonlinearities. Here, one can either introduce bit-correlated phase modulation to mitigate transmission impairments [116, 122, 123], or one can remove certain "bad" bit patterns that are responsible for a large part of the nonlinear signal distortions due to intrachannel nonlinearities, which is generally referred to as constrained coding. For example, the impact of IFWM depends on the transmitted data patterns [124] and the relative phases between symbols [125]. For binary OOK, the bit patterns impacting the BER most severely are generally the ones that include very isolated "0's." Removing such isolated "0's" can significantly improve the BER [124]. A variety of line codes have been devised

to minimize the impact of IFWM [100, 126 128] and significant improvements in transmission have been predicted. One should point out, however, that constrained coding generally requires an increase in symbol rate, which may offset the advantages brought by the code because of a higher required optical signal-to-noise ratio (OSNR) or, at high SEs, because of a broader signal spectrum.

2.3 ELECTRO-OPTIC MODULATOR TECHNOLOGIES

As data rates in optical communication systems have traditionally been limited by the speed of available opto-electronic components, it is of utmost importance to always consider practical aspects of modulation and detection hardware when designing optical modulation formats. Finding the most cost-effective modulation technique for a particular system application involves aspects of *modulation format* and *modulator technology*. Three basic modulator technologies are widely in use today: *directly modulated lasers* (DMLs), *electroabsorption modulators* (EAMs), and *Mach Zehnder modulators* (MZMs), together with their extension to *nested MZMs*.

2.3.1 Directly Modulated Lasers

Direct modulation of lasers is the easiest way to imprint data onto an optical carrier. Here, the transmit data is modulated onto the laser drive current, which then switches on and off the light emerging from the laser [129, 130]. The resulting modulation format is binary IM (OOK). Due to their compactness and low cost, DMLs ideally lend themselves to dense integration in small form factor pluggable transponders (SFPs at 2.5 Gb/s; XFPs at 10 Gb/s). Today, DMLs are widely available up to modulation speeds of 2.5 Gb/s, with some availability up to 10 Gb/s and research demonstrations up to 40 Gb/s [131, 132]. The main drawback of DMLs for high bit rate transmission beyond short-reach access applications is their inherent, highly component-specific *chirp*, i.e., a residual phase modulation accompanying the desired IM [26, 129, 130]; laser chirp broadens the optical spectrum, which impedes dense WDM channel packing and can lead to increased signal distortions caused by the interaction with fiber CD [129, 130] and fiber nonlinearity [133].

On the other hand, the residual frequency modulation of DMLs can be exploited for formats related to binary FSK, such as dispersion supported transmission (DST) [134], where a DML is used to predominantly modulate the frequency of the optical field, with the intent to have the correct amount of CD convert this frequency modulation into IM upon transmission. Transmission distances of 250 km at 10 Gb/s have been achieved using DST [135]. More recently, chirp-controlled DML designs, promoted under the name *chirp-managed laser* (CML), have achieved transmission distances in excess of 200 km at 10 Gb/s over SSMF [136].

2.3.2 Electroabsorption Modulators (EAMs, EMLs)

EAMs are *pin* semiconductor structures whose bandgap can be modulated by applying an external voltage, thus changing the device's *absorption* properties [130]. EAMs feature relatively low drive voltages (typ. 2V), and are cost-effective in volume production. They are available for modulation up to 40 Gb/s today, with research demonstrations up to 80 Gb/s [137]. However, similar to DMLs, they produce some residual *chirp*, which can be engineered to increase dispersion limited transmission distances. By carefully controlling the chirp, an EAM may also be used as an optical in-phase/quadrature (I/Q) modulator to generate an electronically predistorted optical field [138], or it can be embedded in an interferometric waveguide structure similar to a nested MZM (Section 2.3.4) [139].

As a downside, EAMs have wavelength-dependent absorption characteristics, dynamic extinction ratios (maximum-to-minimum-modulated light power) typically not exceeding 10 dB, and limited optical power-handling capabilities. Their fiber-to-fiber insertion loss is about 10 dB. "On-chip" integration with laser diodes avoids the high loss at the input fiber-to-chip interface, and leads to compact transmitter packages. The resulting *electroabsorption-modulated lasers* (EMLs), with output powers on the order of 0 dBm, are widely available today for modulation up to 10 Gb/s and integration into XFP transponders. Another way of eliminating the high insertion losses of EAMs is the integration with semiconductor optical amplifiers (SOAs), which can even yield some net fiber-to-fiber gain [140]. Figure 2.10(a) shows the typical exponential transmission characteristics of an EAM as a function of drive voltage.

2.3.3 Mach–Zehnder Modulators

Unlike EAMs, which work by the principle of *absorption*, MZMs work by the principle of *interference*, controlled by modulating the optical *phase*. The

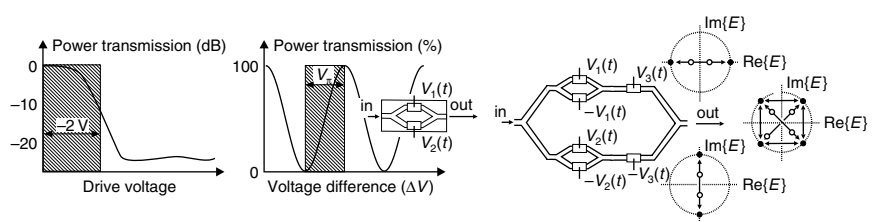

Figure 2.10 Overview of modulator technologies used for advanced optical modulation formats: (a) typical transmission function of an EAM; (b) sinusoidal power transmission function of a MZM, whose structure is shown in the inset; (c) structure of a quadrature modulator (or nested MZM), together with its main application as a modulator for QPSK signals. (Solid symbols: full drive voltage; open symbols: reduced drive voltage.)

modulator structure is shown in the inset to Figure 2.10(b): The incoming light is split into two paths at an input coupler. One (or both) paths are equipped with *phase modulators* that let the two optical fields acquire some phase difference relative to each other, controlled by the applied phase modulation voltages $V_{1,2}(t)$. Finally, the two fields interfere at an output coupler. Depending on the applied electrical voltage, the interference varies from destructive to constructive, thereby producing IM.

The optical field transfer function $T_E(V_1, V_2)$ of the MZM reads (see, e.g., [146, 32])

$$\begin{aligned} T_E(V_1, V_2) &= \frac{1}{2}\{e^{j\phi(V_1)} + e^{j\phi(V_2)+j\psi}\} \\ &= e^{j(\phi(V_1)+\phi(V_2)+\psi)/2}\cos[(\phi(V_1) - \phi(V_2))/2 - \psi/2], \end{aligned} \tag{2.9}$$

where $\Phi(V_{1,2})$ are the voltage-modulated optical phases of the two MZM arms, and ψ is an additional, temporally constant phase shift in one of the arms, referred to as the *modulator bias*. If the phase modulation depends linearly on the drive voltage ($\phi = \kappa V$), which is true for most materials used for MZMs, the MZM *power* transfer function depends only on the drive voltage difference ΔV: $T_P(V_1,V_2) = |T_E(V_1, V_2)|^2 = T_P(\Delta V) = \cos^2(\kappa\Delta V/2 + \kappa V_{\text{bias}}/2)$. The characteristic sinusoidal MZM power transfer function is shown in Figure 2.10(b). Its periodicity is fundamentally related to the 2π periodicity of the optical phase. The modulation voltage that is required to change the phase in one modulator arm by π, and thereby lets the MZM switch from full transmission to full extinction, is called *switching voltage* V_π.

For a given drive voltage difference ΔV according to the desired modulated intensity, the additional degree of freedom in choosing $V_\Sigma(t) = V_1(t) + V_2(t)$ can be exploited to imprint phase modulation on the signal. By separately controlling $V_\Sigma(t)$ and $\Delta V(t)$, one can operate a MZM as an I/Q modulator to independently modulate both quadratures of the optical field, e.g., to produce electronically predistorted optical waveforms [141]. One may also use $V_\Sigma(t)$ to imprint an analog phase modulation (*chirp*) onto a digital signal [142 145]. If chirp is not desired (which is often the case in digital optical modulation), the two modulator arms are driven by the same amount but in opposite directions [$V_1(t) = -V_2(t)$], which eliminates the phase term in Eqn (2.9). This driving condition is known as *balanced driving* or *push pull operation*. Some modulator structures, e.g., x-cut lithium niobate ($LiNbO_3$) use only a *single* drive signal which modulates both arms of the MZM simultaneously, having the condition $V_1(t) = -V_2(t)$ for chirp-free operation built in by appropriate drive electrode design.

MZMs are most conveniently implemented in $LiNbO_3$ [64, 146, 147], gallium arsenide (GaAs) [148], or indium phosphide (InP) [149 152]. $LiNbO_3$-based devices are bulkier than their semiconductor equivalents, but offer easier fiber-to-chip coupling, less wavelength dependence, and no residual IM accompanying the desired phase modulation. In contrast, semiconductor devices, and in

particular InP, lend themselves to much denser integration [151, 153]. MZMs, especially $LiNbO_3$-based devices, feature wavelength-independent modulation characteristics, excellent extinction performance (typ. 20 dB), and lower insertion losses (typ. 5 dB) than EAMs. The required (high-speed) switching voltages of up to 6 V, however, require broadband driver amplifiers, which can be challenging to build at data rates in excess of 10 Gb/s. Today, $LiNbO_3$-based MZMs are widely available for modulation up to 40 Gb/s. Using optical equalization or duobinary modulation, bit rates of 100 Gb/s have been achieved in research labs [24]. InP-based modulators, available for 10-Gb/s modulation today, feature lower switching voltages (typ. 2 3 V) but exhibit residual absorption in addition to phase modulation in the modulator arms which can lead to chirp unless counteracted by proper electrode design [152].

Due to their well controllable modulation performance and the possibility of independently modulating intensity and phase of the optical field, MZMs form the basis of many advanced optical modulation formats.

2.3.4 Nested MZMs—Quadrature Modulators

A single MZM is in principle capable of covering the full complex plane of the optical field, but this requires a drive voltage swing of $2V_\pi$ on each arm [141], which can be difficult to achieve in practice. Furthermore, according to Eqn (2.9), modulation of the two quadratures is not accomplished *independently* of each other which can complicate the generation of the required high-speed drive waveforms.

A solution to both problems is provided by a true quadrature modulator (QM) [64]. The structure of a QM, also referred to as a "nested MZM," a "double-nested MZM," "I/Q modulator," or "Cartesian modulator" and initially proposed for FSK and single-sideband (SSB) modulation [154, 155], is shown in Figure 2.10(c). The symbol diagrams (solid dots) illustrate its most prominent application as a QPSK modulator [90, 91]: first, the incoming light is split into two arms. The sub-MZMs in each arm imprint two independent bit streams on the lightwave, typically using chirp-free (push pull) modulation with voltages $\pm V_1(t)$ and $\pm V_2(t)$. In the case of QPSK modulation, these two signals are binary PSK signals. A third modulator in the outer MZM structure (V_3) introduces a temporally constant 90° phase shift between the two signals, which puts them in quadrature to each other. Upon combination in the output coupler, the four-phase states characteristic of QPSK modulation are obtained.

Being a true I/Q modulator, the nested MZM can be used for a variety of other applications [64]. By driving one sub-MZM with the data sequence and the quadrature sub-MZM with the sequence's Hilbert transform generates SSB modulation [155]. Allowing the third electrode [$V_3(t)$] to be RF-modulated as well, one can implement FSK and MSK, a line-coded version of FSK with continuous optical phase [40, 42, 66, 67]. Furthermore, a QM can be used to generate electronically predistorted optical waveforms [141] with independent control of real and imaginary parts of the optical field as well as with reduced drive amplitude requirements: the whole

complex plane can be covered by arbitrarily small modulation voltages, albeit at the expense of an increased insertion loss, as visualized by the open symbols in the constellation diagrams in Figure 2.10(c), showing the set of QPSK symbols obtained if only half the drive voltage is available.

QMs are commercially available in $LiNbO_3$ technology for modulation speeds of 20 Gb/s on each sub-MZM, allowing for the generation of 40-Gb/s QPSK signals. Research prototypes have been reported for QPSK modulation at data rates as high as 111 Gb/s [86 88].

2.4 OPTOELECTRONIC DEMODULATION CONCEPTS

The conversion process of an (optical) bandpass signal to an (electrical) baseband signal is called *demodulation* and relies on *photodetectors* as its key component. Photodetectors used in optical fiber communications are implemented as reverse-biased semiconductor *pin* diodes [43] with demonstrated bandwidths of 100 GHz and beyond [54, 156, 157]. Often, transimpedance amplifiers are copackaged with the photodiodes (PDs) to form a *photoreceiver* [158]. Diode structures with a built-in high-field carrier multiplication region to produce a larger output current while adding a minimum of extra noise are referred to as *avalanche photodiodes* (APDs) [43, 159, 160]. APDs are widely available for 10-Gb/s applications today. Across a wide range of optical input powers, photodetectors generate an electrical current that is linearly proportional to the optical intensity impinging on the diode, but is inherently independent of the optical phase and also independent of polarization. Hence, any modulation format that carries information by means of a physical quantity other than the optical intensity requires additional demodulation elements prior to photodetection [9]:

- PolSK requires demodulation by means of a *polarization beam splitter* that is aligned to the two orthogonal polarizations used as modulation waveforms.
- FSK requires an optical filter that either passes or rejects the symbol waveform depending on its frequency.
- PSK or, more generally, any modulation format in quadrature space that transports information using the optical phase, requires appropriate phase-to-intensity conversion prior to photodetection, which can either be based on a local oscillator (LO) laser (*coherent demodulation*) or on a delay interferometer (DI) (*delay demodulation* or *differentially coherent demodulation*).

2.4.1 Coherent Demodulation

Figure 2.11(a) shows the conceptual structure of a coherent receiver [9 12], and discussed in more detail in Chapter 3 of this book. A sufficiently phase-stable (coherent) LO laser acts as a phase reference for the received signal. If the received

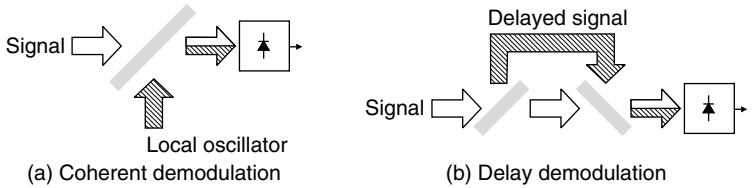

Figure 2.11 Demodulation of a phase modulated format can either be accomplished using a *local oscillator* laser as a phase reference (a) or differentially by comparing the phase of two different symbols of a symbol sequence (b).

signal is in-phase with the LO, the photodetector records constructive interference, while it records destructive interference if the two optical fields have opposite phase, thus converting phase modulation into IM amenable to photodetection. The resulting optical power $P(t)$ at the photodetector reads

$$\begin{aligned} P(t) &= |\vec{e}_{\mathrm{LO}}|^2 + \left|\vec{e}_{\mathrm{Sig}}(t)\right|^2 + 2\mathrm{Re}\left\{\vec{e}_{\mathrm{LO}} \cdot \vec{e}_{\mathrm{Sig}}(t)\right\} \\ &= P_{\mathrm{LO}} + P_{\mathrm{Sig}}(t) + \underbrace{2\eta\sqrt{P_{\mathrm{LO}} P_{\mathrm{Sig}}(t)}\cos(2\pi f_{\mathrm{IF}} t + \varphi_{\mathrm{Sig}}(t))}_{\text{Beat term}}, \end{aligned} \tag{2.10}$$

where $0 \le \eta \le 1$, the *heterodyne efficiency*, denotes the spatial, modal, and polarization alignment of signal and LO fields. In a single-mode fiber system, η captures the polarization mismatch between the signal optical field $\vec{e}_{\mathrm{Sig}}$ and the LO field $\vec{e}_{\mathrm{LO}}$. Phase modulation is included in the optical signal's phase $\varphi_{\mathrm{Sig}}(t)$. Typically, the first two terms on the right-hand side of Eqn (2.10) can be ignored in favor of the *beat term*, either because the temporally constant LO is chosen much stronger than the signal, or because the signal $P_{\mathrm{LO}} + P_{\mathrm{Sig}}(t) - 2\eta\sqrt{P_{\mathrm{LO}} P_{\mathrm{Sig}}(t)}\cos\left(2\pi f_{\mathrm{IF}} t + \varphi_{\mathrm{Sig}}(t)\right)$ from the second output port of the beam splitter is subtracted using *balanced detection*. Importantly, note that in contrast to delay demodulation, balanced detection does not impact the sensitivity of a coherent receiver in a fundamental way. Nevertheless, balanced detection is preferred in practice because it allows to suppress the first two terms on the right-hand side of Eqn (2.10), i.e., any LO relative intensity noise and the direct-detection signal component. Balanced detection also makes use of the entire available signal and LO power.

To make a coherent receiver polarization-independent, which is critical in a fiber-optic communication system with inherently randomly varying polarization, one either needs to track the signal polarization by the LO polarization at the receiver (*polarization control*), or one has to use two parallel coherent receiver setups, one for each of the two orthogonal polarizations (*polarization diversity*). The latter approach is the more practical one, even though it requires more hardware components. Furthermore, once polarization diversity is implemented, *polarization multiplexing* can be added without additional complexity in the optoelectronic receiver front-end [15, 161, 162].

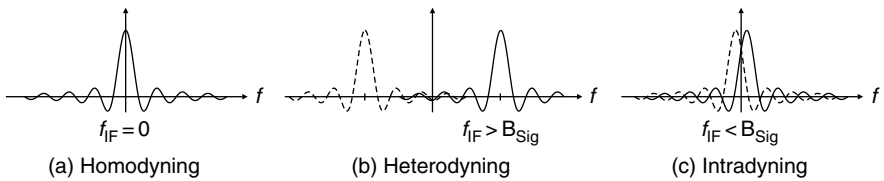

Figure 2.12 (a) Homodyning implies an intermediate frequency f_{IF} of exactly zero; (b) heterodyning uses an IF typically in excess of three times the signal bandwidth; (c) intradyning uses an IF that falls within the signal band, followed by digital phase locking. The positive frequency portions of the IF spectra are shown solid and the negative frequency portions are shown dashed.

Note from Eqn (2.10) and with reference to Figure 2.12(a) that stable interference across the symbol stream is only obtained if the optical frequencies of the LO and the signal carrier are precisely the same (*homodyne detection*), resulting in $f_{IF} = |f_{Sig} - f_{LO}| = 0$. Robust analog phase-locking of two optical signals is a nontrivial task, which is one of the main reasons why homodyne detection was never commercialized by the optical fiber telecommunications industry. If the two frequencies are offset, the detected photocurrent shows oscillations at the *intermediate frequency* f_{IF}. If the IF is chosen significantly higher than the signal bandwidth (typically at least by a factor of three), the entire optical signal spectrum (in magnitude and phase) is directly translated from its optical carrier of around 195 THz to an electrical bandpass signal centered at the IF for further electronic processing, as visualized in Figure 2.12(b). Alternatively, one may choose the IF to fall within the signal band by roughly aligning the LO frequency with the signal frequency (*intradyning,* Figure 2.12(c) [31]). In this case, one saves on optoelectronic front-end bandwidth and processing bandwidth compared to heterodyning, but due to the overlap of positive (solid) and negative (dashed) signal frequency components one has to use digital phase locking algorithms to recover the modulation signal from its sampled I and Q components, which requires high-speed analog-to-digital conversion and digital signal processing hardware [14 16, 161 163]. Note also that a second coherent receiver setup with a 90° phase-shifted LO is needed to access both I and Q components simultaneously. The resulting dual-output combination optics for signal and LO is generally referred to as a *90° hybrid.*

2.4.2 Delay Demodulation

Figure 2.11(b) shows the second method for phase-to-intensity conversion at the receiver. Here, a portion of the received signal is tapped off, delayed, and reinserted into the signal path. That way, the signal interferes with a delayed version of itself upon detection to produce constructive interference if the *phase difference* between the two interfering portions of the signal is zero, and destructive interference if it is π. Hence, the signal acts as a phase reference to itself and takes the role of the LO in a coherent receiver; this similarity is indicated by the hatched and white arrows in Figure 2.11. The demodulation delay is typically chosen to be an

integer multiple of the symbol duration to provide clean interference properties. Due to stability reasons, one almost exclusively chooses a demodulation delay of a single symbol period.[8] If *both* signal quadratures (I and Q) are to be detected, a second interferometer with 90° shifted interference properties is typically used, in analogy to a 90° hybrid in coherent detection.

If a phase modulation format is detected differentially, i.e., by delay demodulation, one generally speaks of *differential* phase shift keying (DPSK), although the word "differential" characterizes the detection technique and not the format itself. From a strict modulation format point of view, there is no difference between a PSK and a DPSK signal.

Finally, we note that one can also use delay demodulation in combination with signal processing to *estimate* the phase of the received signal by averaging the differential phases over many symbols (*multisymbol phase estimation*). This averaged phase estimate then takes the role of the LO in coherent detection [166, 167] and Chapter 4 of this book.

2.5 FREQUENTLY ENCOUNTERED OPTICAL MODULATION FORMATS

Figure 2.13 summarizes the wealth of possibilities in modulation and multiplexing in a single-mode optical fiber system, which supports a single transverse mode in two polarizations. While not yet extensively pursued, any combination of the orthogonal

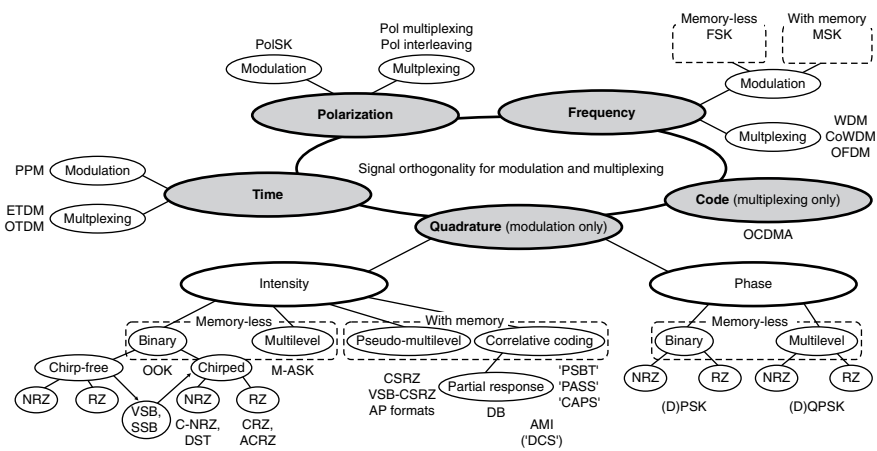

Figure 2.13 Classification of the most important modulation formats and multiplexing schemes discussed in optical communications today.

[8] For signals that undergo strong optical filtering, best receiver performance is obtained if the delay is chosen somewhat smaller than one symbol duration [164, 165].

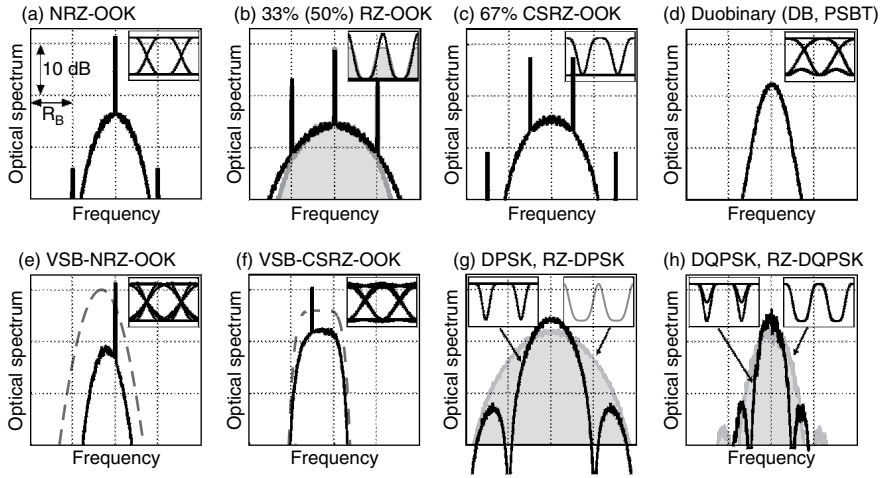

Figure 2.14 Optical spectra and optical intensity eye diagrams of important modulation formats.

signal spaces discussed above may be used for future advanced optical modulation schemes. For example, combining the quadrature space with the space of orthogonal polarizations yields a four-dimensional signal space with interesting properties.

In this section, we will limit ourselves to a discussion of the most frequently encountered modulation formats in the context of optical communications today, which are all based on the *quadrature signal space*. These and more formats are reviewed in more detail in, e.g., [27, 32 38, 64].

Optical spectra and intensity eye diagrams for the formats discussed here are shown in Figure 2.14. Some key performance characteristics are listed in Table 2.2.

2.5.1 Non-Return-to-Zero Modulation (NRZ and NRZ-OOK)

The simplest optical modulation format to generate is NRZ-OOK, often just referred to as "NRZ". Because of its simplicity, this is also the most widely deployed format in fiber-optic communication systems today. The name "NRZ" takes account of the fact that the optical power does *not return to zero* between two successive "1" bits. More generally, the term "NRZ" is employed as a qualifier for other than binary intensity modulated (i.e., OOK) formats if they do not use optical pulses as symbol waveforms. For example, "NRZ-DPSK" denotes differential phase shift keying (DPSK) where the optical intensity may stay constant over multiple bits. In contrast, return-to-zero DPSK (RZ-DPSK) denotes binary phase modulation of distinct optical pulses.

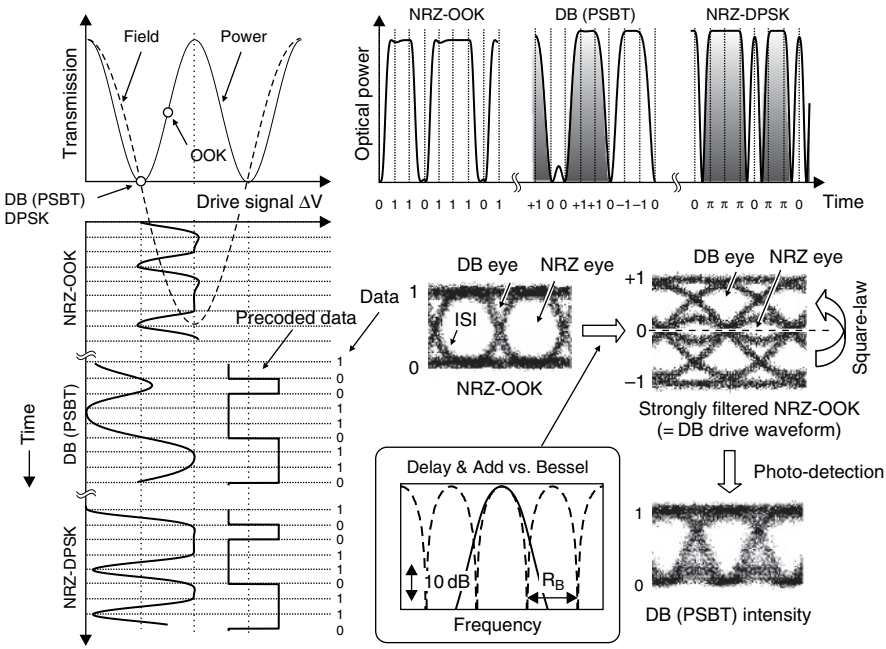

Figure 2.15 Overview of data modulation using a MZM for NRZ OOK, DB (PSBT), and NRZ DPSK. The electrical drive signals in the lower left are applied to the sinusoidal MZM transfer characteristic (upper left; solid: optical power; dashed: optical field) to yield the optical intensity waveforms in the upper right. The MZM bias points are indicated by open circles. Insets: Eye diagrams for NRZ (left) and DB (right) measured at 10.7 Gb/s; filter characteristics of delay and add filtering (dashed) and Bessel low pass filtering (solid), two common options for DB prefiltering.

At bit rates of 10 Gb/s and above, NRZ-OOK is most conveniently generated using DMLs or EAMs (for short-reach and intermediate reach transponders) or using chirp-free MZMs (for long-haul applications). When using a MZM, the modulator is biased at 50% transmission (often referred to as the *quadrature point*) and is driven from minimum to maximum transmission with a voltage swing of V_π, as visualized in Figure 2.15. The inset shows a typical measured NRZ eye diagram at 10.7 Gb/s. Note that when fully driven between its transmission minimum and maximum, the nonlinear (sinusoidal) compression of the MZM transfer function steepens the drive waveform and suppresses overshoots and ripple upon conversion to optical power. A controlled amount of chirp may be introduced to increase the dispersion-limited propagation distance, as discussed in Section 2.4.

Figure 2.14(a) shows the optical spectrum and the optical intensity eye diagram of an idealized NRZ signal. The NRZ optical spectrum is composed of a continuous portion, which reflects the shape of the individual NRZ data pulses, and a strong discrete tone at the carrier wavelength. The residual tones at multiples of the bit rate R_B are generally much weaker than the tone at the carrier frequency; their strength is determined by the spectrum of an individual NRZ data pulse.

As evident from Table 2.2, NRZ has a modest receiver sensitivity (fairly high required OSNR) and despite its low signal bandwidth exhibits a comparatively low tolerance to narrow-band optical filtering, which is mainly due to the *pronounced impact of ISI* on this format, arising whenever a symbol waveform spreads across symbol boundaries and affects detection of the neighboring symbols. The inset to Figure 2.15 shows the onset of ISI in a measured 10.7-Gb/s NRZ waveform, becoming more pronounced under additional optical or electrical filtering.

Regarding its robustness to fiber nonlinearity, NRZ generally performs well at 10 Gb/s as long as optimized dispersion maps are used [168]. The optimum dispersion map is largely determined by single-channel transmission, with cross-phase modulation (XPM) and four-wave mixing (FWM) forcing a reduction of the signal power by a few dB over single-channel transmission for most installed fibers. At 40 Gb/s and 100 Gb/s, advanced modulation formats have generally better nonlinear transmission properties [118]. It is important to note that the resistance to fiber nonlinearity depends greatly on the exact system parameters such as signal power, distance, dispersion map, fiber type, channel spacing, or on the level of copropagating noise (especially in the case of phase shift keyed formats). In this context, all comments made in this chapter on the nonlinear transmission performance of various formats should be interpreted as guidelines (or "rules of thumb") rather than having universal scope.

2.5.2 Vestigial Sideband and Single Sideband Modulation

When narrow-band optical filtering is desired, as is the case in optically routed networks at high SEs one can take advantage of the fact that *real-valued* baseband waveforms have *symmetric*[9] *spectra* around the carrier frequency [84]. Hence, one half of the spectrum can (at least in principle) be perfectly reconstructed from knowledge of the other half. As an important caveat, note that the vast majority of optical receivers still use *square-law* rather than coherent detection. To be a successful candidate for vestigial sideband (VSB) or single sideband (SSB) filtering, a real-valued modulation format should therefore maintain square-law detectability after conversion to VSB or SSB.

In SSB modulation [84], one sideband is suppressed by modulating one quadrature of the optical field with the data signal itself and the other with the signal's Hilbert transform. While the practical generation of high-quality SSB signals is difficult due to problems in implementing broadband Hilbert transformers [32, 64, 169, 170], VSB signals have been successfully realized in optical communications. A VSB signal is generated [84] by suppressing major parts of one sideband by the gradual roll-off of an optical VSB filter, offset by half its bandwidth from the

[9] Strictly speaking, the spectral magnitude is symmetric while the spectral phase is antisymmetric.

carrier frequency, while performing some filter action on the remaining sideband [cf. dashed filter characteristics in Figure 2.14(e, f)]. VSB-NRZ has been successfully transmitted at 40 Gb/s [33, 171 173] and 100 Gb/s [174, 175], and VSB-RZ [176] and VSB-CSRZ [177, 178] have been demonstrated at 40 Gb/s. Figure 2.14(e) and (f) shows optical spectra and intensity eye diagrams of VSB-NRZ and VSB-CSRZ.

In a WDM system, VSB filtering can either be done at the *transmitter* (i.e., before or in combination with multiplexing the WDM channels) [174, 177, 178] or at the *receiver* (i.e., after or in combination with demultiplexing) [33, 171 173]. Filtering at the transmitter allows for ultimate spectral compression and spectrally efficient transmission. The advantage from VSB when filtered at the *receiver* comes from reduced WDM crosstalk for the desired sideband if *unequal* WDM channel spacings are employed [33, 171, 172, 173], however, at a somewhat lower overall SE. Nonlinear transmission of VSB and SSB formats is similar to that of their double-sideband counterparts [33, 176] for 20 Gb/s and above. At 10 Gb/s and below, the missing sideband has been shown to partly reconstruct itself due to fiber nonlinearity [33], limiting the SE advantage of VSB.

2.5.3 Duobinary Modulation (DB, PSBT)

As an alternative to VSB filtering, the modulation spectrum of an optical signal can be compressed by correlative coding. Within the class of line-coded modulation, optical *duobinary* (DB) is the most frequently used format. It belongs to the subclass of *partial response* signaling [32, 40, 84, 121, 179, 180]. In optical communications, duobinary modulation [181, 182] is also referred to as *phase-shaped binary transmission* (PSBT) [101] and *phased amplitude-shift signaling* (PASS) [102]; although PSBT and PASS, like the combined amplitude phase shift signaling "CAPS" [99], are meant to comprise more general correlative coding rules between amplitude and phase, PSBT and PASS are mostly used as synonyms for DB. The state diagram of DB line coding is shown in Figure 2.9 together with example bit and symbol sequences.

The generation of an optical DB signal is visualized in Figure 2.15. The transmitter first uses a *differentially precoded* version of the data signal [84, 183] at the input. The precoded data stream exhibits a level change for every 0 bit contained in the original data sequence and is used to let the square-law detected DB signal represent the original data sequence. Precoding should be implemented at the transmitter to prevent error propagation at the receiver [84, 121]. The precoded sequence is converted into a three-level electrical DB signal by means of *severe electrical low-pass filtering*, which can be implemented, e.g., as a delay-and-add filter (dashed filter transfer function in the inset to Figure 2.15) or a Bessel filter (solid in the inset). The 3-dB bandwidth of the DB low-pass filter should be about 25% of the bit rate. Delay-and-add filters typically result in a better back-to-back sensitivity of the optical DB signal,

while carefully tailored low-pass characteristics yield higher tolerances to CD at the expense of a typically 1- to 2-dB back-to-back sensitivity penalty relative to NRZ-OOK [184] (cf. Table 2.2). A typical low-pass filtered electrical signal, measured at 10.7 Gb/s, is shown as an inset to Figure 2.15. This three-level signal is used to drive a chirp-free MZM between its transmission maxima, where the outer levels generate the ±1 symbols and the center level generates the 0 symbol. When detected by a square-law photodetector, the negative portion of the optical field is mapped on top of the positive portion, resulting in the *binary optical intensity eye diagram* shown as an inset to Figure 2.15 (measured at 10.7 Gb/s) and in Figure 2.14 (d, simulated).

DB and NRZ are intimately related to each other, as visualized along with the measured eyes in Figure 2.15. Any NRZ eye diagram simultaneously exhibits an "NRZ eye opening" as well as a "DB eye opening." Depending on whether detection takes place at the centers of the NRZ eye or at the $T_S/2$-shifted centers of the DB eye, the receiver detects NRZ or DB. By narrow-band (optical or electrical) filtering of the NRZ signal, the NRZ eye gradually closes in while the DB eye opens up.

Alternatively to using a separate LP filter preceding the MZM, a MZM designed for 1/4-th of the desired data rate may be used to combine the functionality of low-pass filtering and modulation [185 187], which has allowed MZM-based DB modulation up to 107 Gb/s [188]. Equivalently, low-pass filtering can be performed in the *optical* domain, with generally less ISI penalty introduced by amplitude and phase ripple of real-world, imperfect electrical prefiltering: passing a binary signal with levels $\{-1, +1\}$, i.e., a (D)PSK signal, through a narrow-band optical bandpass filter produces optical duobinary [189].

The main benefit of DB signals is their higher tolerance to CD and narrow-band optical filtering compared to binary signaling formats. This can be understood both in the time domain [102, 190] and in the frequency domain [32, 183, 184]. The *time-domain explanation* considers a "1 0 1" bit pattern, which for duobinary is encoded as "+1 0 −1". If, due to CD or optical filtering, the two 1-bit pulses spread into the 0 bit between them, duobinary encoding lets them interfere *destructively*, thus maintaining a low 0-bit level. Conventional OOK formats, in contrast, let the pulses interfere *constructively*, which raises the 0-bit level and closes the eye. The *frequency-domain explanation* is based on the narrower spectral extent of properly filtered DB signals [cf. Figure 2.14(e)], which reduces CD-induced signal distortions.[10] The spectral compression of DB results from the *smoother* "+1 0 −1" transitions of properly filtered duobinary as compared to the *sharper* "+1 0 +1" transitions of conventional OOK.

Regarding the impact of nonlinear transmission at 10 Gb/s, DB exhibits roughly the same properties as OOK as long as the dispersion maps are optimized for each

[10] Note that it is the *entire* spectral shape rather than just the 3 dB bandwidth that influences the robustness of a format to CD.

format. However, the large dispersion tolerance advantage of DB over other formats such as NRZ can be dramatically reduced after nonlinear transmission [191]. At 40 Gb/s, DB has a modestly better transmission performance compared to OOK [116, 118] but is inferior to some other line-coded formats such as AMI [116, 118] or other pseudo-multilevel formats [106].

2.5.4 Return-to-Zero Modulation (RZ and RZ-OOK)

Like NRZ modulation, return-to-zero (RZ) modulation can be used in connection with *almost any* digital modulation format by having the modulation waveform take on a pulse-like shape within the symbol duration. This is visualized by measured eye diagrams in Figure 2.16, showing NRZ-OOK and RZ-OOK at 10 Gb/s, NRZ-DPSK and RZ-DPSK at 40 Gb/s, as well as NRZ-DQPSK and RZ-DQPSK at 100 Gb/s. As evident from Table 2.2, RZ formats generally require 1 3 dB less OSNR for a given BER than their NRZ equivalents, even for identical

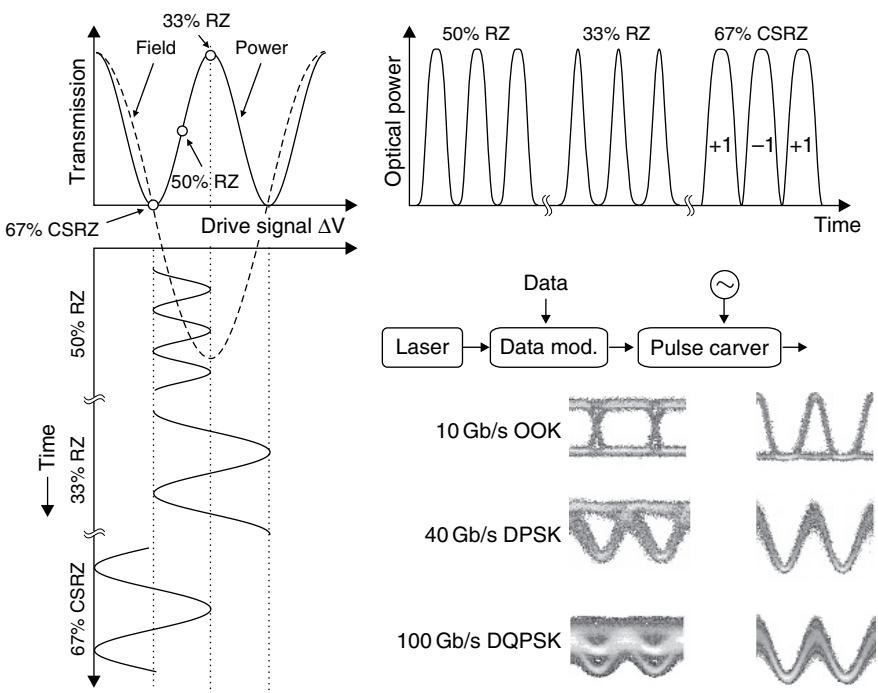

Figure 2.16 Sinusoidally driven MZM as pulse carver for 33% duty cycle RZ, 50% duty cycle RZ, and 67% duty cycle CSRZ. The MZM bias points are indicated by an open circle. Lower right: measured optical intensity eye diagrams for NRZ and RZ versions of OOK, DPSK, and DQPSK at various bit rates (this figure may be seen in color on the included CD ROM).

receiver bandwidths [48, 192 194]. For beat noise limited direct-detection receivers, this is mostly due to the reduced impact of ISI on RZ formats. As evident from Figure 2.14, the OSNR advantage of RZ waveforms comes at the expense of a broader optical spectrum. However, experiments at high SEs have shown [74, 75] that optical prefiltering can be advantageously used to convert an RZ signal back to NRZ while at the same time introducing much less ISI than would be found by passing an NRZ signal through the same narrow-band OF. This phenomenon is due to the fact that OFs generally possess smoother and better defined transfer characteristics than electrical filters across the same absolute bandwidth.

Using RZ symbol waveforms as the basis for a modulation format has important consequences on nonlinear transmission. The signal spectrum is broader than its NRZ equivalent, which generally favors nonlinear transmission, especially at high speeds of 10 Gb/s and above [125]. This fact is discussed further in the context of nonlinear transmission impairments (cf. Figure 2.21).

RZ transmitters can be implemented either by *electronically* generating RZ drive waveforms, which are then modulated onto an optical carrier, or by carving out pulses from an NRZ signal using an additional modulator, called *pulse carver*. While the first option [195] is feasible up to data rates of 10 Gb/s with today's technology [196, 197], a pulse carver has to be employed at 40 Gb/s and beyond. Typically, pulse carvers are implemented as *sinusoidally* driven EAMs or MZMs, since multi-GHz sinusoidal signals of appreciable drive amplitudes are easily generated.

Using sinusoidally driven EAMs, low duty cycle optical pulses can be realized. This makes EAM-based pulse carvers well suited for OTDM experiments [125, 198]. Due to the variable absorption characteristics and residual chirp of EAMs, advanced RZ modulation formats are typically implemented using MZM-based pulse carvers, where one of the following three carving methods is commonly employed (cf. Figure 2.16):

- Sinusoidally driving a MZM *at the data rate* between the minimum and the maximum transmission results in optical pulses with a full-width at half-maximum (FWHM) of 50% of the bit duration (a duty cycle of 50%). Decreasing the modulation swing while lowering the modulator bias to still reach good extinction between pulses, the duty cycle can in principle be reduced to 36%, however, with significant excess insertion loss, since the modulator is then no longer driven to its transmission maximum.
- Sinusoidally driving a MZM at *half the data rate* between its transmission minima produces a pulse whenever the drive voltage passes a transmission maximum. This way, duty cycles of 33% can be realized. The pulses may be broadened at the expense of a reduced extinction ratio between pulses by lowering the drive voltage.
- Sinusoidally driving a MZM at *half the data rate* between its transmission maxima results in pulses with 67% duty cycle and with alternating phase. The resulting format [199, 200] is called carrier-suppressed return-to-zero (CSRZ), cf. Section 2.5.5.

Spectra and intensity eye diagrams of 50% duty cycle RZ (gray) and 33% duty cycle RZ (black), as produced by a MZM in push pull operation, are shown in Figure 2.14(b).

2.5.5 Carrier-Suppressed Return-to-Zero

As introduced in Section 2.2.3, CSRZ [199, 200] is a modulation format with memory, more specifically a pseudo-multilevel format. It is characterized by reversing the sign of the optical field at each bit transition. In contrast to formats using correlative coding, the sign reversals occur at *every* bit transition, and are completely *independent* of the information-carrying part of the signal. CSRZ is most conveniently realized by sinusoidally driving a MZM pulse carver at half the data rate between its transmission maxima, as visualized in Figure 2.16. Since the optical *field* transfer function $T_E(\Delta V)$ (dashed) of the MZM changes its sign at the transmission minimum [cf. Eqn (2.9)], phase inversions between adjacent bits are produced. Thus, on average, the optical field of half the 1 bits has positive sign, while the other half has negative sign, resulting in a zero-mean optical field envelope. As a consequence, the carrier at the optical center frequency vanishes, giving the format its name. Since the optical phase in a CSRZ signal is periodic at half the data rate, the CSRZ spectrum exhibits characteristic tones at $\pm R_B/2$. Spectrum and eye diagram of 67% duty cycle CSRZ, as generated by a MZM in push pull configuration, are shown in Figure 2.14(c).

Using a MZM to generate CSRZ results in a duty cycle of 67%, which can be brought down to 50% at the expense of excess insertion loss by reducing the drive voltage swing. It is important to note that, due to its most widely used practical implementation with MZMs, the duty cycle of CSRZ signals usually differs from the ones of standard RZ. Thus, care has to be taken when comparing the two formats, since some performance differences result from the *carrier-suppressed* nature of CSRZ, while others simply arise from the *different duty cycles*. When used in conjunction with a priori carrier-free formats (such as (D)PSK) the carrier-suppressing effect of CSRZ does not come into play. A CSRZ pulse carver then merely generates 67% duty cycle versions of the underlying modulation formats, where the CSRZ phase flips only impact the data encoding onto the format. For example, applying a CSRZ pulse carver to a DPSK signal generates 67% RZ-DPSK with inverted data logic, sometimes still referred to as "CSRZ-DPSK."

Regarding its transmission performance, CSRZ generally provides increased resistance to fiber nonlinearity relative to plain OOK formats at 40 Gb/s [27, 201]. More advanced pseudo-multilevel formats, e.g., using the alternate $\pi/2$ modulation [106] formats discussed in Section 2.2.3, can show superior nonlinear transmission performance than CSRZ [107]. An advantage of CSRZ is that it can be strongly filtered [202] or even VSB-filtered [178] while largely preserving its good transmission properties [203, 204].

2.5.6 Chirped Return-to-Zero

If a symbol waveform contains a controlled amount of *analog phase modulation* rather than being purely real-valued, the qualifier *chirped* is added to describe the resulting modulation format. In the case of chirped return-to-zero (CRZ) [205, 206] or alternate-chirp return-to-zero (ACRZ) [145, 207], bit-synchronous periodic chirp spectrally broadens the signal bandwidth. Although this reduces the format's suitability for high SE WDM systems, it generally increases its robustness to fiber nonlinearity [208, 209]. CRZ is predominantly used in ultralong-haul point-to-point fiber communications, as found in transoceanic (submarine) systems [209 212], with a typical phase modulation amplitude around 1 rad [205]. Submarine systems typically use low-dispersion fibers with nearly full periodic dispersion compensation [212]. A significant value of uncompensated dispersion slope remains in these transmission lines [209]. As a result, the dispersion map varies widely across the amplification band. The ability to generate a *tunable* chirp at the transmitter by using CRZ accommodates the variations of dispersion maps across the amplification band and, at the same time, broadens the spectrum which improves nonlinear transmission (similarly to pseudo-linear transmission at higher bit rates or with shorter pulses). The format CRZ can generally outperform NRZ and RZ in the context of submarine systems [209, 212].

CRZ signals are typically generated by sinusoidally modulating the phase of a RZ signal at the symbol rate using a separate phase modulator. This leads to a complex, three-modulator transmitter architecture, which requires careful synchronization of the three drive signals. Integrated GaAs/AlGaAs modulators for CRZ, combining NRZ data modulator, RZ pulse carver, and CRZ phase modulator in one package, have been reported [213]. Alternative implementations that take advantage of the phase-modulation properties of dual-drive MZMs [cf. phase term in Eqn (2.9)] have also been demonstrated [145].

2.5.7 Binary Differential Phase Shift Keying (DBPSK or DPSK)

As introduced in connection with Figure 2.5, modulation formats that multiply a generally complex symbol waveform by an alphabet of complex numbers that all lie on the unit circle in the complex plane are referred to as *phase shift keying* (PSK) formats. Due to the dominance of square-law detection in optical communications today, the vast majority of phase modulated systems employs *delay demodulation* or *differential detection* (cf. Section 2.4), and the formats are thus referred to as *differential phase shift keying* (DPSK) [214].

Differential binary phase shift keying (DBPSK, or often just "DPSK") encodes information on the binary phase change between two adjacent bits: A 1 bit is encoded onto a π phase change, whereas a 0 bit is represented by the absence of a phase change. To avoid error propagation at the receiver, differential precoding is used at the transmitter, in analogy to a DB transmitter [84, 121]. Note that differential

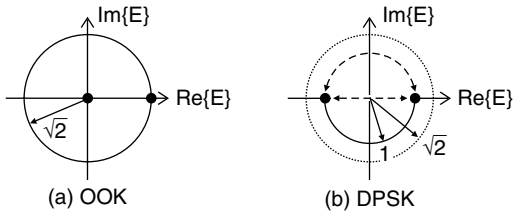

Figure 2.17 Symbol diagrams for (a) OOK and (b) DPSK. The 3 dB sensitivity advantage of DPSK is due to the $\sqrt{2}$ increased symbol spacing for equal average optical power. The dashed double arrows in (b) illustrate two possible phase modulator implementations.

precoding can be omitted in laboratory experiments using pseudo-random bit sequences (PRBS), since differential precoding does not change a PRBS [215].

The main advantage from using DPSK instead of OOK comes from a 3-dB receiver sensitivity improvement [9, 216], which can be intuitively understood from Figure 2.17, showing that the symbol spacing for DPSK is increased by $\sqrt{2}$ compared to OOK for fixed average optical power [214]. This increased symbol distance makes DPSK accept a $\sqrt{2}$ larger standard deviation of the optical field noise than OOK for equal BER, which translates into a 3-dB reduction in the required OSNR. Depending on modulation waveforms, extinction ratios, and optical as well as electrical filters, the gain of DPSK can also *exceed* 3 dB in practice (cf. NRZ-OOK and NRZ-DPSK in Table 2.2).

Like for OOK a pulse carver can be inserted to convert the NRZ-DPSK signal to RZ-DPSK (cf. Figure 2.16). However, special care has to be taken to avoid chirp from imperfect pulse carving, which impacts DPSK much more severely than OOK [217].

To perform optical phase modulation, one can either use a *straight-line phase modulator* or a *MZM* [214, 218]. The difference between the two phase modulation schemes is indicated by the dashed double arrows in Figure 2.17(b): a straight-line phase modulator modulates the phase *along the unit circle* in the complex plane, leaving constant the intensity of the phase-modulated light. However, since the optical phase directly follows the electrical drive signal in this modulation scheme, the speed of phase transitions is limited by the combined bandwidth of driver amplifier and phase modulator, and any overshoot or ringing in the drive waveform manifests itself in phase distortions. A MZM, symmetrically driven around zero transmission, modulates *along the real axis* through the origin of the complex optical field plane [cf. Figure 2.17(b)], which always produces *exact* π phase jumps at the expense of residual, pattern-dependent *optical intensity dips* at the locations of the phase transitions (cf. the NRZ-DPSK waveform in the upper right corner of Figure 2.15). These intensity dips get narrower with increasing modulation bandwidth.[11] Since exact phase modulation is more important for DPSK than

[11] Exploiting DPSK (or DQPSK) intensity dips for data modulation on top of a separately imposed phase modulation has also been studied, predominantly under the name *inverse RZ* [219 221].

a constant optical intensity, practical DPSK transmitters are most conveniently implemented using a MZM as a phase modulator [214]. Note, though, that the pattern-dependent intensity dips can have a negative impact on nonlinear transmission performance compared to modulation with a straight-line phase modulator, especially at low symbol rates such as at 10 Gbaud [222].

Figure 2.14(g) shows optical spectra and intensity eye diagrams for NRZ-DPSK generated by a MZM as a phase modulator (black) and 33% duty cycle RZ-DPSK (gray), respectively. Note the absence of a zero-intensity rail in the eye diagrams, which is characteristic of phase-modulated formats.

The nonlinear transmission properties of DPSK vary greatly with system parameters. At 10 Gb/s, nonlinear transmission is similar to OOK in terms of the optimum signal launch power levels [223]. Due to the substantially reduced pattern-dependent IM of DPSK, one expects a reduced impact of XPM, which should favor DPSK at high SEs (≥ 0.4 bits/s/Hz) where the impact of XPM typically increases. Note however that XPM-induced nonlinear phase noise (NPN) [224] may partially offset this advantage of DPSK. At 40 Gb/s, DPSK has nonlinear transmission thresholds similar or slightly better than CSRZ, as shown in Fig. 2.1(a) [27]. Note, though, that these results are obtained for widely differing BER values, from near the FEC threshold to a few decades below. The performance assessment may be somewhat different if two systems of different lengths but operating at the same BER would be compared. Further optimization of dispersion maps may also impact a performance comparison. Finally, one should note that at equal resistance to nonlinear distortion, the linear sensitivity advantage of DPSK allows improved overall system performance.

Figure 2.18(a) shows a balanced DPSK receiver. As discussed in Section 2.4.2, a DI is used to convert phase modulation into intensity modulation prior to photodetection. The delay is typically chosen equal to (or slightly shorter than) the bit duration, $T \lesssim T_B$ (25 ps at 40 Gb/s). In practice, the differential delay is implemented by different physical path lengths within the DI. In addition, the DI path length difference has to be *fine*-tuned with subwavelength accuracy (i.e., on

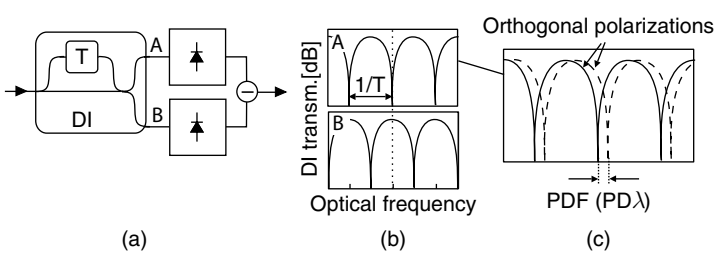

Figure 2.18 (a) Balanced DPSK receiver using an optical delay interferometer (DI) to convert phase modulation to intensity modulation. (b) Periodic DI power transmission characteristics for the destructive port ($\mathcal{A}$) and the constructive port ($\mathcal{B}$). (c) Polarization dependent interference conditions within the DI lead to a polarization dependent shift of the DI transfer characteristic (solid vs dashed), quantified by the parameters PDF or PDλ.

the order of 10 nm, corresponding to less than 0.1 fs, in the 1550-nm wavelength range) to control the interference conditions at the DI output [214, 225]. Maintaining good interference is the most critical aspect in the design of high-performance DPSK receivers, as discussed in more detail in the context of DQPSK receivers in Section 2.5.8. At the DI output port $\mathcal{A}$ (the "destructive port"), the two optical fields interfere destructively whenever there is *no* phase change, and constructively whenever there *is* a phase change between subsequent bits, in agreement with the differential precoding rule (cf. Figure 2.15). Due to energy conservation within the DI, the second DI output port $\mathcal{B}$ (the "constructive port") yields the *logically inverted* data pattern. In principle, one of the two DI output ports is sufficient to fully detect the DPSK signal ("*single-ended detection*"). However, the 3-dB sensitivity advantage of DPSK is *only* seen for *balanced detection* [214, 226, 227]; as shown in Figure 2.18(a), a balanced receiver forms the difference of ports $\mathcal{A}$ and $\mathcal{B}$ to obtain the electrical decision variable. The reason for the superior performance of balanced detection compared to single-ended detection is the non-Gaussian beat noise statistics in combination with the differential detection mechanism (as opposed to fixed threshold detection for OOK) [214, 226, 227].

Figure 2.18(b) shows, on a logarithmic scale, the sinusoidal transmission characteristics of ports $\mathcal{A}$ and $\mathcal{B}$ of a DI as a function of frequency. The laser carrier frequency is indicated by a dotted line. Both transmission spectra are periodic with period $1/T$. The destructive DI output port $\mathcal{A}$ acts as a delay-and-subtract filter (high-pass characteristics to first order), while the constructive port $\mathcal{B}$ is a delay-and-add filter (low-pass characteristics to first order) [189]. Therefore, the formats seen at ports $\mathcal{A}$ and $\mathcal{B}$ are AMI and DB, respectively. Figure 2.19 summarizes the interesting relationship between the modulation formats discussed so far, all starting from the same binary transmit data stream. The apparent lack of symmetry in Figure 2.19 (no arrow from NRZ to DB) is due to the fact that

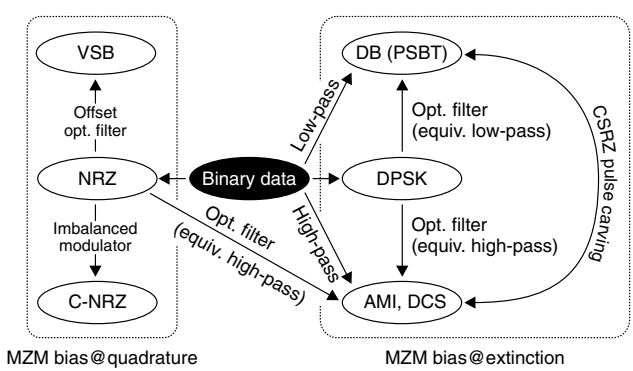

Figure 2.19 Relationship between NRZ (including C NRZ and VSB NRZ), DPSK, DB, and AMI. Arrows indicate how to transition from one format to another, starting from the same binary electrical data stream.

narrow-band optical filtering of NRZ-OOK results in an optical duobinary signal with three *intensity levels* [228], in analogy to the three-level electrical drive waveform shown in Figure 2.15. Such a signal cannot take advantage of the square-law detecting property of PD and requires special detection schemes [229 231].

2.5.8 Differential Quadrature Phase Shift Keying

Differential quadrature phase shift keying (DQPSK) is the only true multilevel modulation format (more than one bit per symbol) that has received appreciable attention in optical communications so far [86 88, 90 92, 222, 232 236]. It transmits the four phase shifts $\{0, +\pi/2, -\pi/2, \pi\}$ at a symbol rate of *half* the aggregate bit rate.

As in the case of DPSK, a DQPSK transmitter is most conveniently implemented by two nested MZMs operated as phase modulators, as shown in Figure 2.10(c) [91, 213]. The symbol constellations of the upper and lower modulator paths as well as at the modulator output are also shown, together with the symbol transitions. Using this transmitter structure, one first takes advantage of the exact π-phase shifts produced by MZMs, independent of drive signal overshoot and ringing. Second, this transmitter structure requires only *binary* electronic drive signals, which are much easier to generate at high speeds than multilevel drive waveforms. As in the case of NRZ-DPSK, the NRZ-DQPSK signal generated with a nested MZM exhibits pattern-dependent intensity dips at the bit transitions [cf. Figure 2.14(h)], where the deeper dip corresponds to a phase transition of both I and Q components and the shallower dip represents a phase transition in either I or Q. Optionally, a pulse carver can be added to the structure to produce RZ-DQPSK as shown in Figure 2.16.

Like at the transmitter, one also strives to work with *binary* electrical signals at the DQPSK receiver due to implementation benefits in high-speed electronics. At the receiver, the DQPSK signal is thus first split into two equal parts, and *two* balanced receivers of the form depicted in Figure 2.18(a), but with differently biased DIs, are used in parallel to simultaneously demodulate the two binary data streams contained in the DQPSK signal [90]. Note that the DI delay is in the order of the *symbol* duration for DQPSK demodulation, which is *twice* the bit duration.

The price for using DQPSK is a *six times* lower tolerance to frequency drifts between transmit laser and DI compared to DPSK [214, 237]. For example, at 40 Gb/s and for a 1-dB penalty, DPSK tolerates ±1.2 GHz of laser-to-DI frequency mismatch, whereas DQPSK only allows for ±200 MHz. At 10 Gb/s, the tolerances are tighter by a factor of four, and at 100 Gb/s the tolerances are relaxed by a factor of 2.5. Note in this context that the end-of-life stability of wavelength-locked distributed feedback (DFB) lasers used in commercial optical transmitters amounts to ±2.5 GHz, which requires feedback-controlled DI tuning within the receiver. Furthermore, any *polarization*-dependent frequency shift of the DI transfer characteristics ["PDF" or "PDλ," Figure 2.18(c)] has to be kept below the respective format's tolerance to frequency offsets [214, 225, 237]. An innovative DI design that simultaneously

demodulates both binary bit streams of a DQPSK signal mitigates the problem [238]. Also, digital signal processing can be used to circumvent the frequency stability issues, albeit at the expense of electronic processing hardware [239], as discussed in Chapter 4 of this book.

Optical spectrum and intensity eye diagram for NRZ-DQPSK and 50% duty cycle RZ-DQPSK are shown in Figure 2.17(h). Note that the *shape* of the DQPSK optical spectrum is identical to that of DPSK, but the DQPSK spectrum is compressed in frequency by a factor of two due to the halved symbol rate for transmission at fixed bit rate. The compressed spectrum is beneficial for achieving high SEs in WDM systems [74, 75, 85, 88, 90, 234], with a single-polarization record of 1.6 b/s/Hz reported today [74, 75], and optically routed networking with concatenated OADMs reported at 1.0 b/s/Hz [240]. As discussed along with Table 2.2, the spectral compactness of DQPSK also increases the format's tolerance to CD [90, 241], and the longer symbol duration compared to binary modulation formats makes DQPSK more robust to PMD [90, 241]. Furthermore, it is worth noting from Table 2.2 that DQPSK requires only 1 1.5 dB more OSNR than DPSK at *poor BER* (e.g., 10^{-3}). At *good BER* (e.g., 10^{-12}), the OSNR gap between DPSK and DQPSK increases, and DQPSK approaches the performance of OOK [40]. Despite the more complex transmitter and receiver, the good OSNR performance at FEC error ratios makes DQPSK an attractive candidate for optically routed networks that require narrow optical signal spectra.

In the nonlinear transmission regime, the performance of DQPSK depends on the specific system conditions of operation such as the presence of tight optical filtering [242], the dispersion map parameters [243] and the presence of neighboring WDM channels [222, 242, 244, 245]. In general, DQPSK suffers more than DPSK from NPN at the same bit rate due to the halved symbol rate and the doubled number of constellation points. More studies remain to be done to better understand all trade-offs associated with nonlinear DQPSK transmission.

2.5.9 Polarization-Multiplexed QPSK with Coherent Detection

As detailed in Section 2.4.1, intradyne detection naturally lends itself to polarization multiplexing, which makes polarization-multiplexed QPSK at 10 Gbaud an attractive modulation solution for 40-Gb/s traffic (or 25 Gbaud modulation for 100 Gb/s traffic). The advantage of this approach lies in the reduced signal bandwidth, which for 40-Gb/s polarization-multiplexed QPSK is comparable to that of a 10-Gb/s OOK signal; narrow signal spectra are important in the context of optically routed networks with dense WDM channel packing. Furthermore, the possibility of phase-sensitive digital signal processing enabled by intradyne detection opens up elegant ways for the mitigation of transmission impairments such as CD, PMD, and partially even fiber nonlinearity. Note, though, that the OSNR requirements for polarization-multiplexed modulation are identical to those for a

system at twice the symbol rate but without polarization multiplexing, which follows directly from the definition of the OSNR, Eqn (2.11). Note also that at equal OSNR the signal launch power in each polarization is lower by 3 dB compared to single-polarization transmission at twice the symbol rate. Compared to DQPSK with delay demodulation, coherently detected QPSK shows a theoretical sensitivity advantage of 1.5 2.4 dB [40]. From a nonlinear transmission point of view, polarization multiplexing may add nonlinear depolarization, which results from XPM for polarization multiplexed OOK [246, 247]. Using phase-modulated formats such as QPSK can significantly reduce nonlinear depolarization [247]. Using coherent detection in principle allows for efficient compensation of some nonlinear effects [162, 163, 248], but effects such as nonlinear depolarization in the presence of PMD may prove more difficult to compensate. Detailed studies are expected to determine the nonlinear performance of polarization multiplexed signals over the next few years.

From an implementation point of view, intradyne detection at multi-Gbaud rates relies on the availability of sufficiently fast analog-to-digital converters and digital signal processing engines. Recent research demonstrations at 10 Gbaud and up to 28 Gbaud have predominantly used real-time oscilloscopes instead of integrated A/D converters to sample a portion of the optical waveform for processing, performed off-line on personal computers [162, 163, 248]. Real-time demonstrations of intradyne detection have been performed at 4.4 Gbaud [15], with ASICs being currently developed for 10-Gbaud operation [163]. As a further trade-off aspect, we note that polarization-multiplexed QPSK with intradyne detection requires significantly more transponder hardware than direct detection, including an additional QPSK modulator at the transmitter to cover the second polarization as well as the coherent receiver optics (LO, 90° hybrids for signal-LO combination). Optoelectronic integration is expected to consolidate components and to allow for better integrated and hence more cost-effective systems in the future.

2.6 SYSTEM DESIGN AND ADVANCED MODULATION FORMATS

From a system perspective, the performance trade-offs entering into the choice of a modulation format include

- Receiver sensitivity
- Resistance to fiber nonlinearity
- Tolerance to dispersion accumulation and dispersion map
- Resistance to PMD
- Achievable SE
- Resistance to concatenated filtering in optically routed networks
- Complexity and cost of terminal equipment

The importance of each of these items varies widely between network types. Metropolitan area systems (reach of ~300 km or less) generally emphasize the dispersion tolerance since the impact of fiber nonlinearity is often small for such systems. One should point out however that that some metropolitan as well as regional networks (~300 to ~1000 km) are composed of very lossy spans and include many ROADMs. For such networks, increasing the signal powers and operating in the nonlinear regime may allow the network to remain optically transparent. In long-haul (~1000 to ~3000 km) and ultralong-haul ($\gtrsim$ 3000 km) communication systems the emphasis is almost always put on receiver sensitivity and resistance to fiber nonlinearity. At high speeds (40 Gb/s and above), SE becomes particularly important, enabled by state-of-the-art OF technologies and laser frequency stability. PMD can also be an important issue with high-speed systems, especially on older fiber plant.

To better understand the performance of optically amplified lightwave systems and how modulation formats impact system design, we now consider relevant performance criteria and transmission impairments. Many important impairments and modulation formats are summarized in Table 2.2 and discussed in the following sections. The implementation complexities of transmitter and receiver are summarized in the second and third column of the table.

2.6.1 Delivered and Required OSNR

The ultimate measure of system performance is the BER after FEC decoding at the receiver. Typical requirements for the post-FEC BER for carrier-grade telecommunication equipment are on the order of or better than 10^{-16}. Enhanced FEC for terrestrial applications has a correction threshold of around 10^{-3}, below which a post-FEC BER of better than 10^{-16} can be guaranteed as long as errors occur statistically independently of each other. Note that this prerequisite for achieving a theoretically expected FEC performance is often only *assumed* in experimental practice, either because FEC chips cannot be used and pre-FEC error ratios have to be measured, or because post-FEC error ratios cannot be measured over sufficiently long time intervals to reliably predict BERs on the order of 10^{-16}.

To link BER measurements to system design, in which the dominant random signal impairment is noise from in-line optical amplifiers (ASE), one typically uses the optical signal-to-noise ratio (OSNR). The OSNR is defined as

$$\mathrm{OSNR} = \frac{P}{2\,B_{\mathrm{Ref}}\,N_{\mathrm{ASE}}}, \tag{2.11}$$

where P is the average signal power (in both polarizations for polarization-multiplexed systems), B_{Ref} is an optical reference bandwidth (typically chosen as 0.1 nm, or 12.5 GHz at 1550 nm), and N_{ASE} is the power spectral density of the ASE in each polarization. Another quantity commonly used in digital communication is the SNR per bit [40]. It is defined as the ratio E_{b}/N_0, where E_{b} is the energy

Table 2.2

Overview of modulation formats and some performance values at 42.7 Gb/s, using direct detection (required OSNR at BER = 10^{-3}) [38].

Modulation format	TX complexity	RX complexity (direct detection)	$OSNR_{Req}$ (dB)			CD (ps/nm) (2 dB penalty)	DGD (ps) (1 dB penalty)
			Back to back	10 OADMs (0.4 b/s/Hz)	5 OADMs (0.8 b/s/Hz)		
NRZ OOK	1 MZM	1 PD	15.9	18.2	n/a	54	8
50% RZ OOK	1 2 MZMs	1 PD	14.4	15.8	n/a	48	10
67% CSRZ OOK	2 MZMs	1 PD	14.9	14.2	n/a	42	11
DB	1 MZM	1 PD	16.6	14.2	18.4	211 (152)	6
VSB NRZ OOK	1 MZM + 1 OF	1 PD	16.4	15.6	17.3	63 (155)	6
VSB CSRZ	2 MZMs + 1 OF	1 PD	14.8	14.7	16.7	51 (154)	11
NRZ DPSK	1 MZM	1 DI + 2 PDs	11.7	12.1	17.6	74 (161)	10
50% RZ DPSK	1 2 MZMs	1 DI + 2 PDs	11.1	11.5	17.0	50 (161)	10
NRZ DQPSK	2 QMs	2 DIs + 4 PDs	13.2	12.6	12.9	168 (176)	20
50% RZ DQPSK	2 QMs + 1 MZM	2 DIs + 4 PDs	12.2	12.0	12.0	161 (186)	21

per bit and N_0 is the noise power spectral density. The relation between the SNR and OSNR is given by

$$\mathrm{OSNR} = \frac{R_\mathrm{S}}{2\,B_\mathrm{Ref}}\,\mathrm{SNR}, \tag{2.12}$$

where is the R_S is the symbol rate.

To specify the tolerance of a modulation format to ASE, the *required OSNR* ($\mathrm{OSNR_{Req}}$) is introduced. It specifies the minimum necessary OSNR that is required to achieve a certain target BER. The fourth column of Table 2.2 lists the required OSNR, based on system simulations described in Ref. 38. The assumed rate of 42.7 Gb/s is representative of a 40-Gb/s per-channel bit rate, including a 7% FEC overhead. Since enhanced FEC schemes for multi-Gigabit/s optical communications are able to correct BER values of 10^{-3} to values below 10^{-16} [4], Table 2.2 is based on 10^{-3} as the target BER for stating $\mathrm{OSNR_{Req}}$. Actually measured values for $\mathrm{OSNR_{Req}}$ may differ somewhat from the numbers given in Table 2.2 due to various optical and electronic hardware implementation aspects at different bit rates, including drive waveforms, filter characteristics, and modulator extinction ratios. Nevertheless, the general trends and most of the quantitative differences predicted by simulation agree well with measurement. As evident from the table, differences in excess of 5 dB between various modulation formats can be observed. Note that in the context of system design, an improvement in the back-to-back sensitivity of a modulation format only leads to improved system performance if the improved back-to-back performance can be retained after transmission. Finally, note that the required OSNR, in contrast to the SNR (or E_b/N_0), scales linearly with bit rate, increasing by 3 dB for every doubling in bit rate. This is caused by the fixed reference noise bandwidth used in the definition of the OSNR. A bit rate independent performance parameter that is sometimes used in the context of optical communication systems is "photons/bit," which is numerically equivalent to E_b/N_0 in an optically preamplified receiver.

Knowing the required OSNR that guarantees satisfactory system performance, system design needs to ensure that the OSNR delivered to the receiver is sufficiently high. The *delivered OSNR* ($\mathrm{OSNR_{Del}}$) is the OSNR at the end of a transmission line and depends only on line parameters and on the launched signal power but not on the modulation format or on transmission impairments. Evaluating signal and noise at the end of a transmission line composed of N identical amplification sections ("spans"), the delivered OSNR can be expressed on a logarithmic scale in the useful form

$$\mathrm{OSNR_{Del}}\ (\mathrm{dB}) = \underbrace{10\,\log_{10}\left(\frac{1000}{h\nu\,B_\mathrm{Ref}}\right)}_{\approx 58 \text{ at } \lambda = 1550\,\mathrm{nm}} + P_\mathrm{in} - \mathrm{NF} - L_\mathrm{SP} - 10\,\log_{10} N, \tag{2.13}$$

where the factor 1000 captures the conversion of Watts to mW to have the signal power appear in "dBm." The parameters P_{in}, NF, and L_{SP} are the launch power (dBm), effective noise figure of a span (dB), and the span loss (dB).

2.6.2 System Penalties and System Margins

The transmission of signals over fibers can suffer from a variety of impairments, such as uncompensated CD, PMD, optical filtering from ROADMs, and fiber nonlinearity. The effect of these impairments on transmission performance can be captured by the difference between the required OSNR after transmission and the required OSNR in the absence of the respective impairment. This difference is referred to as the *OSNR penalty*. In most cases, once the OSNR penalty has reached a few dB for a given impairment, one finds a rapid increase in penalty with any further increase in the impairment. In some cases, a signal corrupted by one transmission impairment may also become more vulnerable to other transmission impairments. One therefore strives to operate a system at low individual impairments (typically less than 2 dB per impairment).

The *OSNR margin* is the ratio of delivered OSNR to required OSNR and accommodates various system penalties. In the early days of system design, the management of system penalties was performed with margin allocation tables [212, 249], similar to link budgets in RF communications, where a fixed penalty is associated with each transmission impairment as well as with a mismatch between system components and with component aging.

In a simple treatment, the total allocated system margin is calculated by adding the penalties due to individual impairments, in analogy to a classical RF link budget. However, this margin allocation captures the improbable case where all impairments *simultaneously* have their worst-case impact. Also, it treats penalties as strictly additive, which is not always the case. Therefore, it is often preferable to apply a statistical treatment to margin allocations. In a statistical approach, one calculates the probability that the OSNR margin falls below a predetermined value and guarantees a maximum system *outage probability*, i.e., one specifies a very low yet finite probability that the system will not meet the allocated OSNR margin.

Filter Concatenation

The fifth and sixth columns in Table 2.2 give, respectively, the required OSNR for the concatenation of 10 OADMs in a system suitable for 0.4 b/s/Hz SE, and 5 OADMs for 0.8 b/s/Hz SE [38]. Note that these simulation results represent the effect of *filter concatenation only*, as they were carried out for a *single* WDM channel. Strictly speaking, the values therefore apply to a WDM system using polarization interleaving, where coherent WDM crosstalk is negligible. Depending on the modulation format, coherent WDM crosstalk can lead to further penalties,

especially at 0.8 b/s/Hz SE; properly capturing coherent WDM crosstalk in numerical simulations for various modulation formats is still a topic of active research [250, 251]. Another aspect of filter narrowing that is *not* taken into account in Table 2.2 is closely related to nonlinear fiber propagation: since OADMs can be spaced by several hundred kilometers in optically routed networks, a modulation format suitable for high-SE networks has to simultaneously lend itself to multiple passes through OADMs *and* to nonlinear fiber propagation over appreciable distances. The impact of joint impairments incurred in this scenario has been experimentally studied for 40- and 100-Gb/s systems with SEs between 0.4 and 1.0 b/s/Hz using a variety of modulation formats [27, 162, 203, 204, 240, 252, 253].

Chromatic Dispersion

The seventh column in Table 2.2 quantifies the accumulated CD (ps/nm) that results in a 2-dB OSNR penalty at 42.7 Gb/s, assuming no OADMs and mux/demux bandwidths of 85 GHz. Most 40-Gb/s modulation formats exhibit dispersion tolerances on the order of 50 ps/nm, the exception being some *spectrally narrow* formats, which in general yield significantly better dispersion tolerance [32, 89]. Note that CD tolerance values, like back-to-back OSNR requirements, can depend to an appreciable extent on the waveforms and filters used in the system. Where applicable, the numbers in parentheses in the seventh column of Table 2.2 refer to the dispersion tolerance in a system with 5 OADMs at 0.8 b/s/Hz SE. Since filter narrowing curtails the signal spectrum, an *increase* in dispersion tolerance is typically observed. Only DB, tailored (by optimized electrical low-pass filtering at the receiver) for high dispersion tolerance in the *absence* of severe optical filtering, sees a reduction in dispersion tolerance (albeit an improvement in sensitivity) when tightly filtered. This discussion shows that the performance of a modulation format to various impairments cannot be taken in isolation, but has to be evaluated in the context of the system in which it is operating in. Another important example is the format-dependent shrinkage of dispersion tolerance in the presence of fiber nonlinearity, which, for example, is more pronounced for DB than for NRZ-OOK [38].

Advanced *digital signal processing* at the receiver can significantly increase the dispersion tolerance. For example, by using a MLSE at 10.7 Gb/s, an increase in dispersion tolerance by up to a factor of 2.6 has been demonstrated experimentally for NRZ-OOK [2, 254], with virtually unlimited tolerance if the MLSE complexity can be substantially increased [255]. Note, however, that the amount of increase in dispersion tolerance due to equalization depends on the equalization technique as well as on the modulation format [1, 2, 254, 256, 257]. For example, MLSE reception of DB improves the dispersion tolerance by a factor of $\sim$1.3 [254]. Furthermore, the use of coherent demodulation with subsequent digital signal processing can greatly improve dispersion tolerance, albeit at the expense of more complex digital signal processing hardware [163].

Finally, the CD values given in Table 2.2 apply for 42.7 Gb/s and scale *quadratically* with bit rate: a four-fold increase in bit rate is accompanied by a 16-fold reduction in dispersion tolerance. As a useful coincidence, and as an aid to remembering CD tolerances, the numerical value of the dispersion tolerance in ps/nm at 40 Gb/s is almost identical to the dispersion tolerance in km SSMF ($D = 17$ ps/nm) at 10 Gb/s. For example, if a signal tolerates 50 ps/nm at 42.7 Gb/s, it can propagate over roughly 50 km of SSMF at 10.7 Gb/s for the same OSNR penalty.

Polarization Mode Dispersion

The eighth column in Table 2.2 quantifies the tolerance of different modulation formats to first-order PMD [258]. It shows the differential group delay (DGD) (ps) that leads to a 1-dB OSNR penalty. For most modulation formats, a 1-dB penalty occurs at a DGD between 30% and 40% of the symbol duration, with RZ formats being in general more resilient to PMD than NRZ formats [258, 259]. Note that the resilience to PMD, in addition, depends to an appreciable extent on the waveforms [260, 261] and filters [260, 262], as well as on other residual distortions. The tolerance to first-order PMD scales linearly with symbol duration. Therefore, DQPSK has about twice the PMD tolerance of binary modulation formats at the same bit rate. The tolerance to first-order PMD shrinks linearly with bit rate.

The main problem with PMD in optical fiber systems is its stochastic nature, letting the principal state of polarization (PSP) and the DGD vary on timescales between milliseconds (acoustic vibrations) and months (temperature variations of buried fiber) [263]. The rare occurrence of exceedingly high DGD values prohibits worst-case system design by allocating a fixed OSNR margin to accommodate all possible PMD-induced signal distortions. Instead, systems are allocated some reasonable margin (e.g., 1 dB), and the rare occurrence of DGDs exceeding the margin results in *system outage*. Properly specifying the *outage probability* is an important interface between fiber manufacturers, systems integrators, and service providers [258, 263]. If outage requirements cannot be met, PMD has to be *compensated* on a per-channel basis at the receiver, or the PMD tolerance of the respective modulation format has to be increased using optical [22] or electronic [2, 256, 264, 265] *equalization* or *mitigation* [266, 267] techniques.

Fiber Nonlinearity

The instantaneous Kerr nonlinearity in optical fibers [26] can lead to a host of elementary nonlinear interactions. Knowing which fundamental nonlinear interaction dominates transmission is helpful to conceive techniques that improve transmission, including advanced modulation formats, digital signal processing, and distributed optical nonlinearity management.

Determining the fundamental nonlinear interactions distorting the signal in a specific system is an arduous task as it depends on a large number of *fiber, signal*, and *system* parameters. The most important fiber parameters impacting the nature

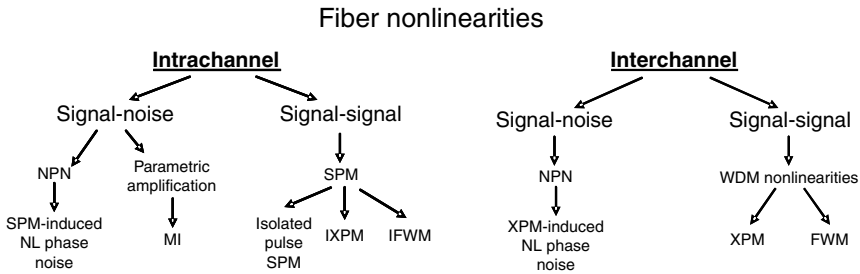

Figure 2.20 Classification of nonlinearities in optical fibers. Intrachannel and interchannel stand for nonlinearities occurring within or between WDM channels, respectively. SPM: self phase modulation, (I)XPM: (intrachannel) cross phase modulation, (I)FWM: (intrachannel) four wave mixing, MI: modulation instability, NPN: nonlinear phase noise.

of nonlinear transmission are the fiber dispersion, nonlinear coefficient, dispersion slope, and PMD. For the signal it is the symbol rate, the modulation format, and the WDM channel spacing. The predominant system parameters are signal power, transmission distance and amplification scheme (determining the noise level throughout the system, especially important for phase shift keying). As a result of the enormous parameter space impacting nonlinear fiber transmission, accurate predictions of nonlinear transmission penalties require a combination of extensive system modeling with careful experimental measurements.

Figure 2.20 summarizes the main fundamental nonlinear interactions in fiber-optic communication systems. Fiber nonlinearities that occur between different symbols of the *same* WDM channel or between a WDM channel and a spectrally overlapping second optical field (such as ASE or multipath interference, MPI) are referred to as *intrachannel* nonlinearities. When the nonlinear interactions occur between different WDM channels or between a WDM channel and a spectrally nonoverlapping second optical field, we speak of *interchannel* nonlinearities. The importance of each class of nonlinearities depends significantly on the per-channel symbol rate. As a "rule of thumb," for systems using conventional periodic optical dispersion compensation (ODC) as a powerful tool for nonlinearity management, interchannel effects affect WDM systems most strongly at per-channel rates of 10 Gbaud and below, i.e. dispersion-managed solitons [268] and quasi-linear transmission regime (see discussion in Ref. 38), while intrachannel nonlinearities affect systems most strongly at rates above 10 Gbaud (i.e., pseudo-linear transmission [125]). The impact of fiber nonlinearity also depends on the local fiber dispersion: in general, lower-dispersion fibers have stronger interchannel effects than fibers with high local dispersion. These statements are quantified in Figure 2.21, based on extensive sets of numerical simulations for NRZ-OOK and RZ-OOK. The figure indicates the dominant nonlinear impairment as a function of fiber dispersion (y-axis) and bit rate (lower x-axis). Because Figure 2.21 applies to OOK formats, signal signal nonlinear interactions are dominating transmission. For a given SE (upper x-axis) the figure reveals the bit rate per WDM channel (lower x-axis) that allows for the maximum transmitted energy per

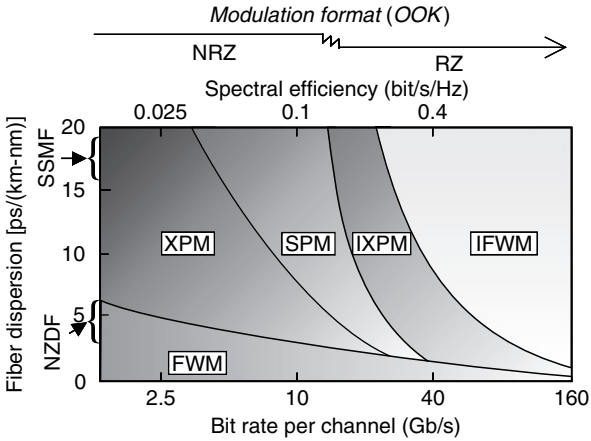

Figure 2.21 Significance of inter and intrachannel nonlinear impairments in WDM systems of different per channel bit rates and OOK modulation. For high speed TDM systems exceeding 10 Gb/s per channel, the dominant nonlinear interactions are IXPM and IFWM (this figure may be seen in color on the included CD ROM).

bit over a distance of 1000 2000 km. A transition from NRZ-OOK to RZ-OOK as the optimum OOK format occurs around 20 Gb/s.

In addition to the signal signal interactions, we also find nonlinear signal noise interactions in transmission. These interactions depend significantly on the noise level during propagation and become stronger if the OSNR is poor *during propagation*, which has become a common situation with the use of strong FEC [269]. The most important signal noise interaction found in currently discussed transmission systems is SPM-induced nonlinear phase noise (SPM-NPN) [270 272] and XPM-induced NPN (XPM-NPN) [224]. These NPN phenomena are most important for modulation formats that use the optical phase to carry information (e.g., DPSK, DQPSK) and of less importance for formats where the optical phase does not carry information but is used for line coding purposes (e.g., CSRZ, DB). In general, the effect of NPN is largest when the signal waveform evolution is slow during propagation (e.g., when the symbol rate is low) or when fibers with low values of CD are used. Formats with a large number of phase levels are also generally more sensitive to NPN. One should also point out that NPN depends on both the signal and noise powers. Therefore, systems with identical signal power evolution but different noise power evolution (and most likely different delivered OSNRs) will generally have different OSNR penalties if they are affected by NPN.

An example of the impact of SPM-NPN on transmission of DPSK at 42.7 Gb/s is shown in Figure 2.22. Each of the three plots shows the required OSNR as a function of input power to each of the 32×100-km spans of a nonzero dispersion shifted fiber that constitutes the link [273]. In Figure 2.22(a), a balanced detector is used while in Figure 2.22(b) and (c), single-ended detection is used.

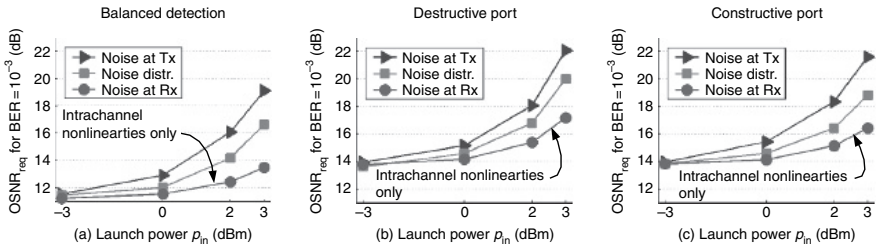

Figure 2.22 Required OSNR (10^{-3} BER) as a function of fiber launch power P_{in} for RZ DPSK using (a) balanced detection and (b, c) single ended detection: (b) destructive and (c) constructive port. The lower, middle, and upper curves of each graph, respectively, apply to the cases where noise is added just prior to the receiver, distributed along the line, and at the transmitter [273] (this figure may be seen in color on the included CD ROM).

The middle curves on each graph represent the case of distributed noise, i.e., the physically realistic case where ASE is generated by an optical amplifier placed after each span. The lower and upper curves of each graph represent the hypothetical cases where the same amount of ASE is added at the receiver only (lowest curves) or at the transmitter only (uppermost curves). The difference between the lowest curves and the middle curves represents the SPM-NPN penalty. Figure 2.22(b) and (c) shows that the benefit of balanced detection over single-ended detection is preserved even for strong intrachannel nonlinearities and nonlinear phase noise.

Figure 2.23 demonstrates how a system generally behaves in terms of nonlinearity, showing required and delivered OSNR at a target BER of 10^{-3} for signal power levels between -6 and 0 dBm. One can see that there is an optimum power (~ -4 dBm in this example) that maximizes system reach ($\sim$28 spans). At lower signal launch powers, the system is limited by ASE and hence by the delivered OSNR, while at higher powers it is limited by fiber nonlinearity. An example of an achievable distance ($\sim$16 spans) for a certain OSNR margin (4 dB) at the power level of -2 dBm is also shown (bold curves). The system parameters for Figure 2.23 are single-channel transmission of 33% RZ-OOK at 42.8 Gb/s. The fiber is NZDF and the amplifier spacing is 100 km. Note that Figure 2.23 applies for a given system configuration and a given signal. Changing the system configuration can change both the delivered and required OSNR. Most system designs use a fixed launch power per channel which may not be the optimum power for a given optical network infrastructure (e.g., average span loss or maximum span length).

An important difference between modulation formats is the required OSNR back-to-back. In the absence of nonlinear effects (sufficiently low powers or sufficiently short distance), the signal remains undistorted after transmission and the improvement of the required OSNR back-to-back by a certain factor translates directly into a proportional increase in reach by the same factor. This can be seen by considering that the delivered OSNR in Eqn (2.13) increases "dB for dB" with P_{in}. For instance, if the required OSNR back-to-back improves by 3 dB and does not degrade with

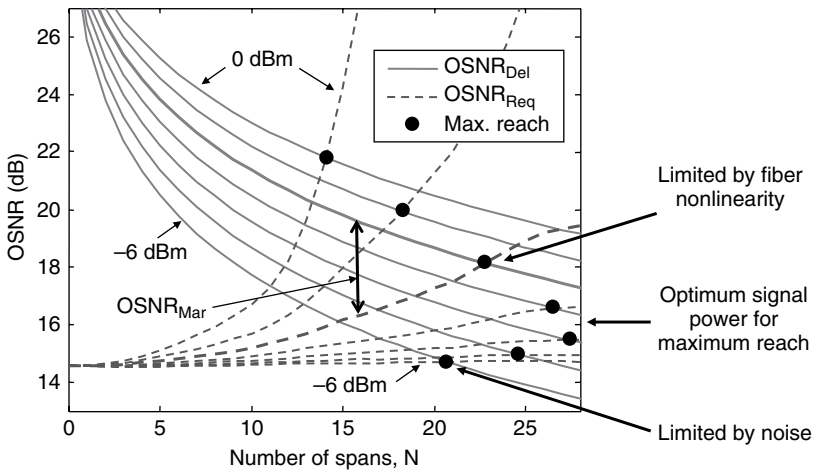

Figure 2.23 Required (lower curves) and delivered OSNR (upper curves) as a function of the number of spans for a range of per channel signal launch powers. At a given power, the maximum number of spans can be bridged at the point where the required OSNR crosses the delivered OSNR (full circles). In this example, a maximum distance of 28 spans is achieved using 4 dBm per channel. The OSNR margin at 16 spans for a power of 2 dBm per channel is also shown (double headed arrow) (this figure may be seen in color on the included CD ROM).

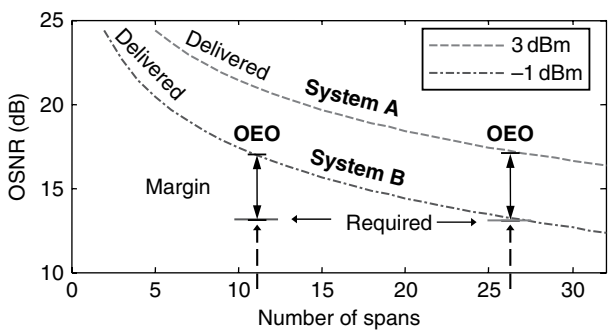

Figure 2.24 Delivered and required OSNR evolution for two systems, A and B, that have the same back to back required OSNR but different resistances to fiber nonlinearity. An increased distance is possible for system A. OEO: optical electronic optical (this figure may be seen in color on the included CD ROM).

distance (linear system), the same BER can be achieved with 3 dB worse OSNR. Therefore, twice the number of optical amplifiers can be tolerated, and hence twice the number of spans can be bridged. As a result, in a system where transmission suffers less from fiber nonlinearity, the reach can be extended considerably. Many techniques can be used to reduce the impact of fiber nonlinearity, including advanced modulation formats, new fiber designs and advanced dispersion mapping.

A comparison of two systems having identical back-to-back required OSNRs but different tolerances to fiber nonlinearity is represented in Figure 2.24. System B has a

lower tolerance to nonlinearity and is limited in power to −1 dBm for a certain distance that guarantees a certain OSNR margin. System A suffers less from nonlinear distortions and can operate at +4 dBm over a larger distance than system B at the same OSNR margin. In Figure 2.24, an improvement of 11 26 spans is brought by greater resistance to nonlinearity of system A, even though the required (back-to-back) OSNR is the same in both cases.

2.7 SYSTEM TECHNOLOGIES AND MODULATION FORMATS

In this section, we discuss the interplay between advanced modulation formats and optical and electronic system technologies. This topic is at the frontier of the understanding of systems and therefore is likely to evolve further over the next years.

2.7.1 Optical Dispersion Compensation (ODC)

ODC is used in transmission lines to reduce the accumulation of dispersion so as to minimize signal distortions at the receiver. Probably the most important role of ODC, as an all-optical impairment mitigation technique, is its ability to be inserted periodically in the optical path for optimum mitigation of fiber nonlinearity. The process of finding the best location of the ODC is referred to as optimization of the dispersion map [125, 168]. The *dispersion map* of a transmission line specifies the precise accumulation of dispersion with distance, as visualized in Figure 2.25(a).

A general principle of dispersion mapping relates to how various elementary nonlinear interactions (see Figure 2.20) are managed in the transmission line. For instance, one effect of dispersion mapping is to provide a partial cancelation of intrachannel nonlinearities (IXPM and IFWM) generated at different locations in a

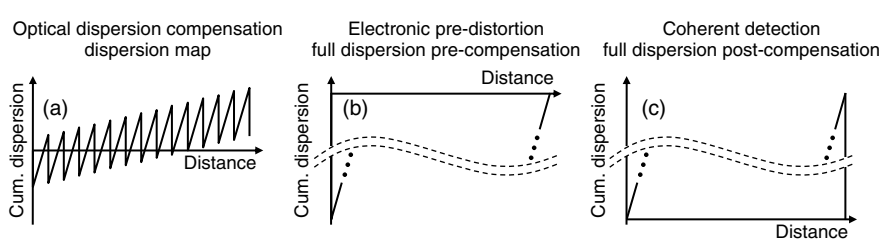

Figure 2.25 Three dispersion maps associated with different transponder technologies: (a) optical dispersion compensation with dispersion map optimized for the mitigation of fiber nonlinearity; (b) electronic predistortion with full precompensation of dispersion at the transmitter; and (c) coherent detection with full compensation of dispersion at the receiver.

fiber segment or in the transmission line [125]. As discussed along with Figure 2.21, the relative importance of each elementary nonlinear interaction depends on the modulation format as well as on other system parameters (symbol rate, channel spacing, power levels, distance, etc.), making dispersion mapping generally depend on the system specifications.

2.7.2 Electronic Predistortions (EPD)

Electronic predistortion (EPD) is a technique to generate arbitrary waveforms (amplitude and phase) at the transmitter [6, 274]. In combination with digital signal preprocessing, it allows the generation of a variety of modulation formats [275] and opens up the possibility of compensation of some propagation effects such as dispersion accumulation [276, 277] and fiber nonlinearity [276, 278]. Electronic predistortion enables the compensation of large amounts of fiber dispersion at the transmitter, which at a first glance could allow the design of transmission systems without ODC. The resulting "all-precompensation" dispersion map is shown in Figure 2.25(b). Similarly, an "all-postcompensation" dispersion map for coherent detection with digital signal processing is depicted in Figure 2.25(c).

The impact of fiber nonlinearity on single-channel transmission of advanced modulation formats using EPD with full precompensation of dispersion (but no compensation of fiber nonlinearity) is shown in Figure 2.26 [279]. The system is composed of 14 spans $\times$ 80 km of SSMF and operates at a bit rate of 10.7 Gb/s. The modulation formats considered are DB, 33% RZ-OOK, NRZ-DPSK, and 33% RZ-DPSK. Nonlinear phase noise is not taken into account here.

Duobinary, shown in Figure 2.26(a), exhibits the lowest threshold to fiber nonlinearity. Higher signal launch powers are permissible for RZ-OOK and NRZ-DPSK, and the highest power levels can be used for RZ-DPSK. The low resistance of DB to fiber nonlinearity is consistent with this format's slower waveform evolution during transmission compared to formats with broader spectra. In many cases, a faster waveform evolution helps to minimize signal distortions by distributing nonlinear distortions more uniformly across different bits [125].

Evaluating the impact of *WDM transmission* on nonlinear distortions for 10-Gb/s systems with large accumulated dispersion is more challenging than for systems with frequent ODC that limits the maximum excursion of dispersion. When using frequent ODC, and at symbol rates of $\sim$20 Gbaud and lower, variations in signal distortions between short and long pattern lengths and between different data patterns remain typically small. In contrast, when all the dispersion of the entire line is compensated at the transmitter, large variations in nonlinear distortions can be observed when changing the data patterns [276, 280]. This is represented in Figure 2.27 in the form of OSNR penalty histograms for the RZ-DPSK modulation format [279]. At low power per channel (2 dBm/ch), the average penalty is low ($\sim$1 dB) with a moderate spread in penalty ($\sim$1.5 dB). At

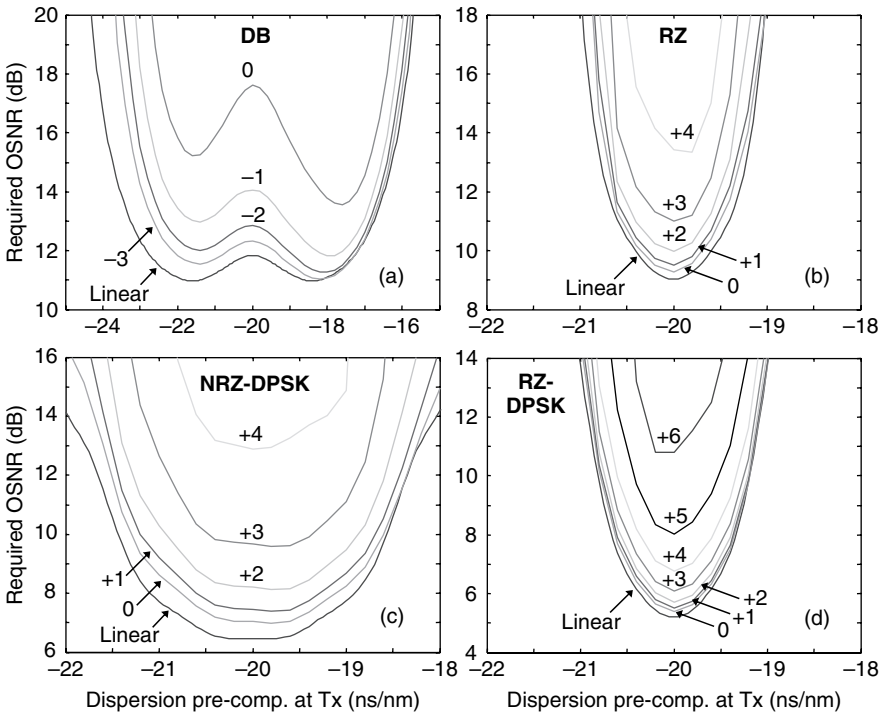

Figure 2.26 Required OSNR (10^{-3} BER) after transmission as a function of dispersion precompensation for single channel transmission: (a) duobinary (DB), (b) 33% RZ OOK, (c) NRZ DPSK and (d) RZ DPSK. The labels refer to the signal launch power (dBm). "Linear" means "in the absence of fiber nonlinearity." Nonlinear phase noise is not included (this figure may be seen in color on the included CD ROM).

higher powers (3 dBm/ch and higher), the average penalty rises and the penalty spread increases considerably with different data (or time delays) between neighboring channels. The spread in penalty slowly shrinks with increasing pattern length [280].

Finally, we note that the compensation of transmission impairments at the transmitter generally requires a feedback loop between transmitter and receiver. As CD is varying slowly (if at all) in a lightwave system, the respective feedback loop can be slow. Since transmission distances can be considerable in optical networks, the feedback time (i.e., the round trip time between transmitter and receiver) can be as large as 10 ms for a 1000-km transmission line. Rapidly varying impairments that change over the timescale of the feedback loop (including the required number of iterations for the predistortion algorithms to converge) can therefore not be handled by EPD. Examples for such impairments are PMD or nonlinear distortions caused by sudden power transients in a network.

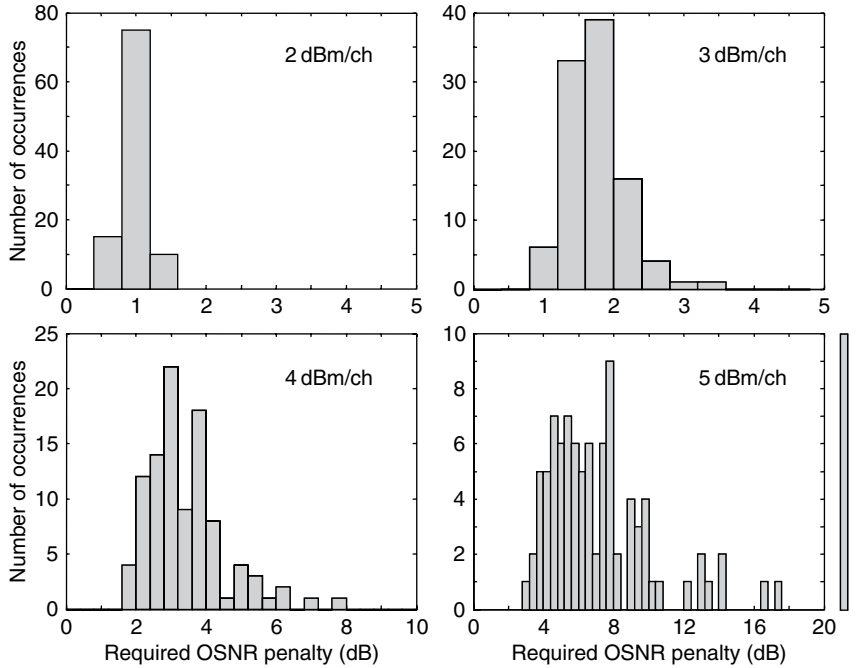

Figure 2.27 Histograms of required OSNR penalties (10^{-3} BER) of a channel in a 50 GHz spaced WDM system using RZ DPSK at 10.7 Gb/s. Histogram bins are 0.4 dB wide on all graphs. A large spread in penalties from XPM is observed. At 5 dBm per channel, 10 timing realizations had penalties exceeding 20 dB and are shown on the right side of 6 dBm histogram. Nonlinear phase noise is not included (this figure may be seen in color on the included CD ROM).

2.7.3 Coherent Detection and Digital Signal Processing at the Receiver

Coherent detection is a technique that is particularly efficient to detect advanced *multilevel* modulation formats in quadrature signal space, since the optical field is directly translated into the electrical domain. Furthermore, as outlined in Sections 2.4.1 and 2.5.9, polarization multiplexing is a natural consequence of using coherent detection, and the use of elegant equalization strategies based on the optical field information is made possible.

In contrast to conventional direct detection systems, both electronic predistortion and coherent detection use digital signal processing based on the optical field. This lets the compensation of transmission impairments exhibit some similarities between both techniques [141]. One notable difference however is that coherent detection does not require a transmitter-receiver feedback loop. Hence, rapidly varying impairments can also be handled by coherent detection.

In the case of signal distortions from nonlinear propagation, the behavior of a system based on coherent detection in the absence of ODC is very similar to the case of EPD discussed in previous section. As shown in Figure 2.25(c), a dispersion compensation free system using coherent detection implements an "all-postcompensation" dispersion map, whereas EPD implements an "all-precompensation" map, both of which are, in general, not optimum for nonlinear transmission. Nonlinearity compensation using digital signal processing at the receiver can be based on backward propagation of single-channel nonlinear transmission [278, 280]. Knowing the transmission line parameters and the signal power evolution along the link, reverse propagation can be computed using the signal field detected at the receiver. Note, though, that the detected channel at the receiver is generally corrupted by noise and can be distorted not only by fiber nonlinearity but also by PMD. The simultaneous presence of multiple sources of impairments may limit the efficient compensation of fiber nonlinearity. Moreover, as discussed in previous sections, it is not possible in the context of optically routed networks to perform full compensation of interchannel nonlinearities such as XPM [280] or of signal-noise nonlinearities such as NPN.

2.8 CONCLUSION

High-speed optical transmission systems are increasingly building on digital signal processing and digital communication techniques that are well established in RF communication systems, including efficient FEC, advanced modulation, line coding, polarization multiplexing, digital signal processing at both transmitter and receiver, and coherent detection. Nevertheless, an optically routed network exhibits important fundamental as well as technological differences from a radio-frequency system, and not all techniques that have proven successful in radio-frequency communication should be expected to work well for optical networks. Detailed studies over the next few years will screen digital communication techniques with respect to their applicability in high bit rate, high capacity, and inherently nonlinear optical networks, with the goal to lower the overall cost per end-to-end transmitted information bit in an environment of exponentially increasing needs for transport capacity.

ACKNOWLEDGMENTS

The authors thank S. Bigo, S. Chandrasekhar, G. Charlet, A.R. Chraplyvy, C.R. Doerr, F. Fidler, G.J. Foschini, A.H. Gnauck, R. Griffin, T. Kawanishi, H. Kogelnik, G. Kramer, J. Proakis, G. Raybon, and R.W. Tkach for valuable discussions.

LIST OF ACRONYMS

ACRZ	Alternate-chirp return-to-zero
AMI	Alternate mark inversion
AP	Alternate phase
APD	Avalanche photodiode
APol	Alternate polarization
ASE	Amplified spontaneous emission
ASK	Amplitude shift keying
BER	Bit error ratio
CAPS	Combined amplitude phase shift signaling
CD	Chromatic dispersion
C-NRZ	Chirped non-return-to-zero
CoWDM	Coherent wavelength division multiplexing
CRZ	Chirped return-to-zero
CSRZ	Carrier-suppressed return-to-zero
DB	Duobinary
DCS	Duobinary carrier suppressed
DFE	Decision-feedback equalizer
DGD	Differential group delay
DI	Delay interferometer
DML	Directly modulated laser
DPSK	Differential phase shift keying
DQPSK	Differential quadrature phase shift keying
DST	Dispersion supported transmission
DWDM	Dense wavelength-division multiplexing
EAM	Electroabsorption modulator
EML	Electroabsorption-modulated laser
EPD	Electronic predistortion
ETDM	Electronic time division multiplexing
FEC	Forward error correction
FFE	Feed-forward equalizer
FSK	Frequency shift keying
FWHM	Full-width at half-maximum
FWM	Four-wave mixing
IFWM	Intrachannel four-wave mixing
IM	Intensity modulation
I/Q	In-phase/quadrature
ISI	Intersymbol interference
IXPM	Intrachannel cross-phase modulation
LO	Local oscillator
MLSE	Maximum-likelihood sequence estimation
MSK	Minimum shift keying
MZM	Mach Zehnder modulator

NPN	Nonlinear phase noise
NRZ	Non-return-to-zero
NZDF	Nonzero dispersion fiber
OCDMA	Optical code division multiple access
ODC	Optical dispersion compensation
OEQ	Optical equalizer
OF	Optical filter
OFDM	Orthogonal frequency division multiplexing
OOK	On/off keying
OSNR	Optical signal-to-noise ratio
OTDM	Optical time division multiplexing
PASS	Phased amplitude-shift signaling
PD	Photodiode
PMD	Polarization mode dispersion
PolSK	Polarization shift keying
PPM	Pulse position modulation
PSBT	Phase-shaped binary transmission
PSK	Phase shift keying
QAM	Quadrature amplitude modulation
QM	Quadrature modulator
QPSK	Quadrature phase shift keying
RF	Radio frequency
(R)OADM	(Reconfigurable) optical add/drop multiplexer
RZ	Return-to-zero
SE	Spectral efficiency
SNR	Signal-to-noise ratio
SPM	Self-phase modulation
SSB	Single sideband
SSMF	Standard single-mode fiber
TCM	Trellis-coded modulation
TDM	Time division multiplexing
VSB	Vestigial sideband
WDM	Wavelength-division multiplexing
XFP	Small form factor pluggable transponder (10 Gb/s)
XPM	Cross-phase modulation

REFERENCES

[1] T. Nielsen and S. Chandrasekhar, "OFC 2004 workshop on optical and electronic mitigation of impairments," *J. Lightw. Technol.*, 23(1), 131 142, 2005.

[2] A. Färbert, S. Langenbach, N. Stojanovic et al., "Performance of a 10.7 Gb/s Receiver with Digital Equalizer using Maximum Likelihood Sequence Estimation," in Proc. *ECOC*, page Th4.1.5, 2004.

[3] Q. Yu and A. Shanbhag, "Electronic data processing for error and dispersion compensation," *J. Lightw. Technol.*, 24, 4514 4525, 2006.
[4] T. Mizuochi, K. Kubo, H. Yoshida et al., "Next Generation FEC for Optical Transmission Systems," in Proc. *OFC*, page ThN1, 2003.
[5] T. Mizuochi, "Recent progress in forward error correction and its interplay with transmission impairments," *IEEE J. Sel. Top. Quantum Electron.*, 12, 544 554, 2006.
[6] D. McGhan, C. Laperle, A. Savchenko et al., "5120 km RZ DPSK Transmission over G.652 Fiber at 10 Gb/s with no Optical Dispersion Compensation," in Proc. *OFC*, page PDP27, 2005.
[7] Y. Yamamoto, "Receiver performance evaluation of various digital optical modulation demodulation systems in the 0.5 10 μm wavelength region," *IEEE J. Quantum Electron.*, 16(11), 1251 1259, 1980.
[8] R. A. Linke and A. H. Gnauck, "High capacity coherent lightwave systems," *J. Lightw. Technol.*, 6(11), 1750 1769, 1988.
[9] G. Jacobsen, "*Noise in Digital Optical Transmission Systems*," Artech House, 1994.
[10] L. G. Kazovsky, S. Benedetto, and A. E. Willner, "*Optical Fiber Communication Systems,* Artech House, 1996.
[11] S. Betti, G. De Marchis, and E. Iannone, "*Coherent Optical Communications Systems*," 1995, John Wiley and Sons Inc.
[12] S. Ryu, "*Coherent Lightwave Communication Systems*," Artech House, 1995.
[13] O. K. Tonguz and R. E. Wagner, "Equivalence between preamplified direct detection and heterodyne receivers," *IEEE Photon. Technol. Lett.*, 3(9), 835 837, 1991.
[14] K. Kikuchi, "Coherent Detection of Phase Shift Keying Signals using Digital Carrier Phase Estimation," in Proc. *OFC*, page OTuI4, 2006.
[15] A. Leven, N. Kaneda, U. V. Koch, and Y. K. Chen, "Coherent Receivers for Practical Optical Communication Systems," in Proc. *OFC*, page OThK4, 2007.
[16] S. J. Savory, "Coherent Detection Why is it Back?" in Proc. *IEEE/LEOS Annual Meeting*, Paper TUH1, 2007.
[17] A. Hazneci and S. P. Voinigescu, "49 Gb/s, 7 tap transversal filter in 0.18 μm SiGe BiCMOS for backplane equalization," *IEEE CSICS*, 2004, pp. 101 104.
[18] H. Jiang and R. Saunders, "Advances in SiGe ICs for 40Gb/s Signal Equalization," in Proc. *OFC*, page OTuE1, 2006.
[19] B. Franz, D. Roesener, F. Buchali et al., "Adaptive Electronic Feed Forward Equaliser and Decision Feedback Equaliser for the Mitigation of Chromatic Dispersion and PMD in 43 Gbit/s Optical Transmission Systems," in Proc. *ECOC*, page We1.5.1, 2006.
[20] S. Wada, R. Ohhira, T. Ito et al., "Compensation for PMD Induced Time Variant Waveform Distortions in 43 Gbit/s NRZ Transmission by Ultra Wideband Electrical Equalizer Module," in Proc. *OFC*, page OWE2, 2006.
[21] M. Nakamura, K. Murata, and M. Tokumitsu, "Advances in 40 G Electronic Equalizers," in Proc. *OFC*, page OThN6, 2007.
[22] C. R. Doerr, S. Chandrasekhar, P. J. Winzer et al., "Simple Multi Channel Optical Equalizer Mitigating Intersymbol Interference for 40 Gb/s Non Return to Zero Signals," *J. Lightw. Tech nol.*, 22(1), 249 256, 2004.
[23] C. R. Doerr, P. J. Winzer, G. Raybon et al., "A Single Chip Optical Equalizer Enabling 107 Gb/s Optical Non Return to Zero Signal Generation," in Proc. *ECOC*, page Th4.2.1, 2005.
[24] P. J. Winzer, G. Raybon, C. R. Doerr et al., "107 Gb/s optical signal generation using electronic time division multiplexing," *J. Lightw. Technol.*, 24, 3107 3113, 2006.
[25] P. Hofmann, E. E. Basch, S. Gringeri et al., "DWDM Long Haul Network Deployment for the Verizon GNI Nationwide Network," in Proc. *OFC*, page OTuP5, 2005.
[26] Govind P. Agrawal, "*Nonlinear Fiber Optics,"* San Diego: Elsevier Science & Technology, 4th edition, 2006.
[27] A. H. Gnauck, "Advanced Amplitude and Phase Coded Formats for 40 Gb/s Fiber Transmission," in Proc. *IEEE/LEOS Annual Meeting*, page WR1, 2004.

[28] R. J. Essiambre et al., "Capacity Limits of Fiber Optic Communication Systems, in Proc. OFC, 2008.
[29] H. Kogelnik, "On Optical Communication: Reflections and Perspectives," in Proc. *ECOC*, page Mo1.1.1, 2004.
[30] K. Schuh and E. Lach, "Recent advances in ultrahigh bit rate ETDM transmission systems," *J. Lightw. Technol.*, 24, 4455 4467, 2006.
[31] F. Derr, "Optical QPSK transmission system with novel digital receiver concept," *IEE Electron. Lett.*, 27, 2177 2179, 1991.
[32] J. Conradi, "Bandwidth efficient modulation formats for digital fiber transmission systems," In *Optical Fiber Telecommunications IV B* (I. Kaminow and T. Li eds), 2002, Academic Press, pp. 862 901.
[33] S. Bigo, "Multiterabit DWDM terrestrial transmission with bandwidth limiting optical filtering," *IEEE J. Sel. Top. Quantum Electron.*, 10(2), 329 340, 2004.
[34] S. Bigo, G. Charlet, and E. Corbel, "What has Hybrid Phase/Intensity Encoding Brought to 40 Gbit/s Ultralong Haul Systems," in Proc. *ECOC*, page Th2.5.1, 2004.
[35] P. J. Winzer and R. J. Essiambre, "Advanced Optical Modulation Formats," in Proc. *ECOC*, page Th2.6.1, 2003.
[36] P. J. Winzer and R. J. Essiambre, "System Trade Offs and Optical Modulation Formats," in Proc. *OAA*, page OTuC4, 2004.
[37] P. J. Winzer, "Optical transmitters, receivers, and noise," in *Wiley Encyclopedia of Tele communications* (J. G. Proakis, ed), John Wiley & Sons, pp. 1824 1840. online: http:// www.mrw.interscience.wiley.com/eot/eot sample fs.html.
[38] P. J. Winzer and R. J. Essiambre, "Advanced optical modulation formats," in Proc. *IEEE*, 94, pp. 952 985, 2006.
[39] G. P. Agrawal, "*Lightwave Technology: Telecommunication Systems*," John Wiley and Sons, 2005.
[40] J. G. Proakis, "*Digital Communications*," Mc Graw Hill, 4th edition, 2001.
[41] E. A. Lee and D. G. Messerschmitt, "*Digital Communication*," Kluwer Academic Press, 1994.
[42] B. Sklar, "*Digital Communications*," Prentice Hall, 2th edition, 2001.
[43] B. A. E. Saleh and M. C. Teich, "*Fundamentals of Photonics*," John Wiley & Sons, 1991.
[44] G. P. Agrawal, "*Fiber Optic Communication Systems*," John Wiley & Sons, 3rd edition, 2002.
[45] C. E. Shannon, "A mathematical theory of communication," *The Bell System Technical Journal*, 27, 379 423 and 623 656, 1948.
[46] "Interfaces for the optical transport network (OTN)," *Standard ITU T G.709*, 2003.
[47] D. O. Caplan and W. A. Atia, "A Quantum Limited Optically Matched Communication Link," in Proc. *OFC*, page MM2, 2001.
[48] P. J. Winzer, M. Pfennigbauer, M. M. Strasser, and W. R. Leeb, "Optimum filter bandwidths for optically preamplified RZ and NRZ receivers" *J. Lightw. Technol.*, 19(9), 1263 1273, 2001.
[49] P. J. Winzer and R. J. Essiambre, "Optical Receiver Design Trade Offs," in Proc. *OFC*, page ThG1, 2003.
[50] M. Pfennigbauer, M. Pauer, M. M. Strasser, and P. J. Winzer, "Dependence of optically pre amplified receiver sensitivity on optical and electrical filter bandwidths measurement and simulation," *IEEE Photon. Technol. Lett.*, 14, 831 833, 2002.
[51] G. K. Chang, J. Yu, Y. K. Yeo et al., "Enabling technologies for next generation optical packet switching networks" in Proc. *IEEE*, 94, 2006, pp. 892 910.
[52] A. J. Phillips, R. A. Cryan, and J. M. Senior, "Novel Laser Intersatellite Communication System Employing Optically Preamplified PPM Receivers," *IEE Proc. Commun.,* 142, 1995, pp. 15 20.
[53] D. O. Caplan, B. S. Robinson, R. J. Murphy, and M. L. Stevens, "Demonstration of 2.5 Gslot/s Optically Preamplified M PPM with 4 Photons/Bit Receiver Sensitivity," in Proc. *OFC*, page PDP32, 2005.
[54] J. Sinsky, A. Adamiecki, L. Buhl et al., "107 Gbit/s Opto Electronic Receiver with Hybrid Integrated Photodetector and Demultiplexer," in Proc. *OFC*, page PDP30, 2007.

[55] B. Mikkelsen, G. Raybon, R. J. Essiambre et al., "320 Gb/s single channel pseudolinear transmis sion over 200 km of nonzero dispersion fiber," *IEEE Photon. Technol. Lett.*, 12, 1400 1402, 2000.
[56] A. H. Gnauck, G. Raybon, P. G. Bernasconi et al., "1 Tb/s (6×170.6 Gb/s) transmission over 2000 km NZDF using OTDM and RZ DPSK format," *IEEE Photon. Technol. Lett.*, 15, 1618 1620, 2003.
[57] M. Nakazawa, T. Yamamoto, and K. R. Tamura, "1.28 Tbit/s 70 km OTDM transmission using third and fourth order simultaneous dispersion compensation with a phase modulator," *IEE Electron. Lett.*, 36, 2027 2029, 2000.
[58] H. G. Weber, R. Ludwig, S. Ferber et al., "Ultrahigh speed OTDM transmission technology," *J. Lightw. Technol.*, 24, 4616 4627, 2006.
[59] H. J. Thiele and M. Nebeling editors, "*Coarse Wavelength Division Multiplexing*: Technologies and Applications," CRC Press, 2007.
[60] L. J. Cimini, "Analysis and simulation of a digital mobile channel using OFDM," *IEEE Trans. Commun.*, 33, 665 675, 1985.
[61] A. J. Lowery, L. B. Du, and J. Armstrong, "Performance of optical OFDM in ultralong haul WDM lightwave systems," *J. Lightw. Technol.*, 25, 131 138, 2007.
[62] W. Shieh and C. Athaudage, "Coherent optical orthogonal frequency division multiplexing," *IEE Electron. Lett.*, 42, 587 589, 2006.
[63] A. D. Ellis, F. G. C. Gunning, and T. Healy, "Coherent WDM: The Achievement of High Information Spectral Density Through Phase Control within the Transmitter," in Proc. *OFC*, page OThR4, 2006.
[64] T. Kawanishi, S. Sakamoto, and M. Izutsu, "High speed control of lightwave amplitude, phase, and frequency by use of electrooptic effect," *IEEE J. Sel. Top. Quantum Electron.*, 13, 79 91, 2007.
[65] T. Kawanishi, T. Sakamoto, S. Shinada et al., "$LiNbO_3$ high speed optical FSK modulator", *IEE Electron. Lett.,* 40, 691 692, 2004.
[66] T. Sakamoto, T. Kawanishi, and M. Izutsu, "Continuous phase frequency shift keying with external modulation," *IEEE J. Sel. Top. Quantum Electron.*, 12, 589 595, 2006.
[67] J. Mo, Y. J. Wen, Y. Dong et al., "Optical Minimum Shift Keying Format and its Dispersion Tolerance." in Proc. *OFC*, page JThB12, 2006.
[68] S. Betti, G. De Marchis, and E. Iannone, "Polarization modulated direct detection optical trans mission systems," *J. Lightw. Technol.*, 10(12), 1985 1997, 1992.
[69] A. S. Siddiqui, S. G. Edirisinghe, J. J. Lepley et al., "Dispersion tolerant transmission using a duobinary polarization shift keying transmission scheme," *IEEE Photon. Technol. Lett.*, 14(2), 158 160, 2002.
[70] S. Benedetto and P. Poggiolini, "Theory of polarization shift keying modulation," *IEEE Trans. Inf. Theory*, 40, 708 721, 1992.
[71] J. J. Lepley, J. G. Ellison, S. G. Edirisinghe et al., "Excess penalty impairments of polarization shift keying transmission format in presence of polarization mode dispersion," *IEE Electron. Lett.*, 36(8), 736 737, 2000.
[72] A. Hodzic, B. Konrad, and K. Petermann, "Improvement of system performance in $N \times 40$ Gb/s WDM transmission using alternate polarizations," *IEEE Photon. Technol. Lett.*, 15, 153 155, 2003.
[73] C. Xie, I. Kang, A. H. Gnauck et al., "Suppression of intrachannel nonlinear effects with alternate polarization formats," *J. Lightw. Technol.*, 22(3), 806 812, 2004.
[74] A. H. Gnauck, P. J. Winzer, L. L. Buhl et al., "12.3 Tb/s C Band DQPSK Transmission at 3.2 b/s/ Hz Spectral Efficiency," in Proc. *ECOC*, page Th4.1.2, 2006.
[75] A. H. Gnauck, G. Charlet, P. Tran et al., "25.6 Tb/s C+L band transmission of polarization multiplexed RZ DQPSK signals," in Proc. *OFC*, page PDP19, 2007.
[76] L. E. Nelson and H. Kogelnik, "Coherent crosstalk impairments in polarization multiplexed transmission due to polarization mode dispersion," *Opt. Express*, 7(10), 350 361, 2000.
[77] Paul R. Prucnal, editor, "*Optical Code Division Multiple Access: Fundamentals And Applications*," CRC Press, 2006.
[78] H. G. Unger, "*Planar Optical Waveguides and Fibers*," Clarendon Press: Oxford Engineering Science Series, 1977.

[79] J. A. Buck, "*Fundamentals of Optical Fibers*," John Wiley & Sons, 1995.
[80] X. Shen, J. M. Kahn, and M. A. Horowitz, "Compensation for multimode fiber dispersion by adaptive optics," *Opt. Lett.*, 30, 2985 2987, 2005.
[81] J. Kahn, "Compensating Multimode Fiber Dispersion using Adaptive Optics," in Proc. *OFC*, page OTuL1, 2007.
[82] H. R. Stuart, "Dispersive multiplexing in multimode optical fiber," *Science*, 289(5477), 281 283, 2000.
[83] S. Schoellmann, S. Soneff, and W. Rosenkranz, "10.7 Gb/s over 300 m GI MMF using a 2×2 MIMO System Based on Mode Group Diversity Multiplexing," in Proc. *OFC*, page OTuL2, 2007.
[84] R. Gitlin, J. F. Hayes, and S. B. Weinstein, "*Data Communications Principles*," Plenum Press, 1992.
[85] G. Kramer, A. Ashikhmin, A. J. van Wijngaarden, and X. Wei, "Spectral efficiency of coded phase shift keying for fiber optic communication," *J. Lightw. Technol.*, 21, 2438 2445, 2003.
[86] M. Daikoku, I. Morita, H. Taga et al., "100 Gbit/s DQPSK Transmission Experiment Without OTDM for 100 G Ethernet Transport," in Proc. *OFC*, page PDP36, 2006.
[87] P. J. Winzer, G. Raybon, C. R. Doerr et al., "2000 km WDM Transmission of 10×107 Gb/s RZ DQPSK," in Proc. *ECOC*, 2006.
[88] A. Sano, H. Masuda, Y. Kisaka, et al., "14 Tb/s (140×111 Gb/s PDM/WDM) CSRZ DQPSK Transmission over 160 km using 7 THz Bandwidth Extended L Band EDFA," in Proc. *ECOC*, page Th4.1.1, 2006.
[89] S. Walklin and J. Conradi, "Multilevel signaling for increasing the reach of 10 Gb/s lightwave systems," *J. Lightw. Technol.*, 17(11), 2235 2248, 1999.
[90] R. A. Griffin and A. C. Carter, "Optical Differential Quadrature Phase Shift Key (oDQPSK) for High Capacity Optical Transmission," in Proc. *OFC*, page WX6, 2002.
[91] R. A. Griffin, R. I. Johnstone, R. G. Walker et al., "10 Gb/s Optical Differential Quadrature Phase Shift Key (DQPSK) Transmission Using GaAs/AlGaAs Integration," in Proc. *OFC*, page FD6, 2002.
[92] M. Ohm, "Optical 8 DPSK and receiver with direct detection and multilevel electrical signals," *IEEE/LEOS Workshop on Advanced Modulation Formats*, 2004, pp. 45 46.
[93] M. Ohm and J. Speidel, "Quaternary optical ASK DPSK and receivers with direct detection," *IEEE Photon. Technol. Lett.*, 15(1), 159 161, 2003.
[94] S. Hayase, N. Kikuchi, K. Sekine, and S. Sasaki, "Proposal of 8 state per symbol (binary ASK and QPSK) 30 Gbit/s optical Modulation/Demodulation scheme," in Proc. *ECOC*, page Th2.6.4, 2003.
[95] K. Sekine, N. Kikuchi, S. Sasaki et al., "Proposal and Demonstration of 10 Gsymbol/s 16 ary (40 Gbit/s) Optical Modulation/Demodulation Scheme," in Proc. *ECOC*, page We3.4.5, 2004.
[96] T. Tokle, B. Zsigri, C. Peucheret, and P. Jeppesen, "Generation and transmission of 160 Gbit/s polarisation multiplexed RZ DBPSK ASK signal," *IEE Electron. Lett.*, 41, 433 435, 2005.
[97] J. Hongo, K. Kasai, M. Yoshida, and M. Nakazawa, "1 Gsymbol/s 64 QAM coherent optical transmission over 150 km," *IEEE Photon. Technol. Lett.*, 19, 638 640, 2007.
[98] K. A. S. Immink, "*Codes for Mass Data Storage Systems*," Shannon Foundation Publishers, 2nd edition, 2004.
[99] E. Forestieri and G. Prati, "Novel optical line codes tolerant to fiber chromatic dispersion," *J. Lightw. Technol.*, 19, 1675 1684, 2001.
[100] B. Vasic, V. S. Rao, I. B. Djordjevic et al., "Ghost pulse reduction in 40 Gb/s systems using line coding," *IEEE Photon. Technol. Lett.*, 16(7), 1784 1786, 2004.
[101] D. Penninckx, M. Chbat, L. Pierre, and J. P. Thiery, "The phase shaped binary transmission (PSBT): A new technique to transmit far beyond the chromatic dispersion limit," *IEEE Photon. Technol. Lett.*, 9(2), 259 261, 1997.
[102] J. B. Stark, J. E. Mazo, and R. Laroia, "Phased amplitude shift signaling (PASS) codes: Increas ing the spectral efficiency of DWDM transmission," in Proc. *ECOC*, 1998, pp. 373 374.
[103] C. N. Georghiades, "Modulation and coding for throughput efficient optical systems," *IEEE Trans. Inform. Theory*, 40, 1313 1326, 1994.

[104] S. Benedetto, G. Olmo, and P. Poggiolini, "Trellis coded polarization shift keying modulation for digital optical communications," *IEEE Trans. Inf. Theory*, 43, 1591 1602, 1995.
[105] H. Bulow, G. Thielecke, and F. Buchali, "Optical Trellis Coded Modulation (oTCM)," in Proc. *OFC*, page WM5, 2004.
[106] S. Randel, B. Konrad, A. Hodžić, and K. Petermann, "Influence of bitwise phase changes on the performance of 160 Gbit/s transmission systems," in Proc. *ECOC*, page P3.31, 2002.
[107] D. M. Gill A. H. Gnauck et al., "$\pi/2$ alternate phase On/Off keyed 42.7 Gb/s long haul transmission over 1980 km of standard single mode fiber," *IEEE Photon. Technol. Lett.*, 16, 906 908, 2004.
[108] J. Martensson, J. Li, A. Berntson et al., "Suppression of intra channel four wave mixing by phase modulation at one quarter of bit rate," *IEE Electron. Lett.*, 38, 1463 1465, 2002.
[109] M. Forzati, A. Berntson, and J. Martensson, "IFWM suppression using APRZ with optimized phase modulation parameters," *IEEE Photon. Technol. Lett.*, 16, 2368 2370, 2004.
[110] S. Appathurai, V. Mikhailov, R. I. Killey, and P. Bayvel, "Investigation of the optimum alternate phase RZ modulation format and its effectiveness in the suppression of intrachannel nonlinear distortion in 40 Gbit/s transmission over standard single mode fiber," *IEEE J. Select. Topics Quantum Electron.*, 10, 239 249, 2004.
[111] M. Forzati, A. Berntson, J. Martensson, and R. J. Davies, "Performance analysis of single MZM APRZ transmitters," *J. Lightw. Technol.*, 24, 2006 2014, 2006.
[112] Y. Su, L. Moller, C. Xie et al., "Ultra high speed data signals with alternating and pairwise alternating optical phases," *J. Lightw. Technol.*, 23, 26 31, 2005.
[113] Y. Miyamoto, K. Yonenaga, A. Hirano et al., "Duobinary Carrier Suppressed Return to Zero Format and its Application to 100 GHz Spaced 8×43 Gb/s DWDM Unrepeatered Transmission over 163 km," in Proc. *OFC*, page TuU4, 2001.
[114] Y. Miyamoto, A. Hirano, S. Kuwahara et al., "S band 3×120 km DSF Transmission of 8×42.7 Gbit/s DWDM Duobinary Carrier Suppressed RZ Signals Generated by Novel Wideband PM/AM Conversion," in Proc. *OAA*, page PD6, 2001.
[115] A. Hirano and Y. Miyamoto, "Novel Modulation Formats in Ultra High Speed Optical Transmission Systems and their Applications," in Proc. *OFC*, page ThM1, 2004.
[116] K. S. Cheng and J. Conradi, "Reduction of pulse to pulse interaction using alternative RZ formats in 40 Gb/s systems," *IEEE Photon. Technol. Lett.*, 14, 98 100, 2002.
[117] P. J. Winzer, A. H. Gnauck, G. Raybon et al., "40 Gb/s alternate mark inversion return to zero (RZ AMI) transmission over 2000 km," *IEEE Photon. Technol. Lett.*, 15(5), 766 768, 2003.
[118] A. H. Gnauck, X. Liu, X. Wei et al., "Comparison of modulation formats for 42.7 Gb/s single channel transmission through 1980 km of SSMF," *IEEE Photon. Technol. Lett.*, 16, 909 911, 2004.
[119] J. Martensson, A. Berntson, A. Djupsjobacka et al., "Phase Modulation Schemes for Improving Intra Channel Nonlinear Tolerance in 40 Gbit/s Transmission," in Proc. *OFC*, Paper FE5, 2003.
[120] A. Matsuura, K. Yonenaga, Y. Miyamoto, and H. Toba, "High speed transmission based on optical modified duobinary signals," *IEE Electron. Lett.*, 35(9), 736 737, 1999.
[121] P. Kabal and S. Pasupathy, "Partial response signaling," *IEEE Trans. Commun.*, 23(9), 921 934, 1975.
[122] X. Liu, X. Wei, A. H. Gnauck, C. Xu, and L. K. Wickham, "Suppression of intrachannel four wave mixing induced ghost pulses in high speed transmissions by phase inversion between adjacent marker blocks," *Opt. Lett*., 27, 1177 1179, 2002.
[123] N. Alić and Y. Fainman, "Data dependent phase coding for suppression of ghost pulses in optical fibers," *IEEE Photon. Technol. Lett.*, 16, 1212 1214, 2004.
[124] L. K. Wickham, R. J. Essiambre, A. H. Gnauck et al., "Bit pattern length dependence of intrachannel nonlinearities in pseudolinear transmission," *IEEE Photon. Technol. Lett.*, 16, 1591 1593, 2004.
[125] R. J. Essiambre, G. Raybon, and B. Mikkelsen, "Pseudo linear transmission of high speed TDM signals: 40 and 160 Gb/s." In *Optical Fiber Telecommunications IV*, (I. Kaminow and T. Li, eds), Academic Press, 2002, pp. 232 304.

[126] E. G. Shapiro, M. P. Fedoruk, S. K. Turitsyn, and A. Shafarenko, "Reduction of nonlinear intrachannel effects by channel asymmetry in transmission lines with strong bit overlapping," *IEEE Photon. Technol. Lett.*, 15, 1473 1475, 2003.

[127] I. B. Djordjevic, S. K. Chilappagari, and B. Vasic, "Suppression of intrachannel nonlinear effects using pseudoternary constrained codes," *J. Lightw. Technol.*, 24, 769 774, 2006.

[128] V. Pechenkin and F. R. Kschischang, "Constrained coding for quasi linear optical data transmis sion systems," *J. Lightw. Technol.*, 24, 4895 4902, 2006.

[129] T. L. Koch, "Laser sources for amplified and WDM lightwave systems." In *Optical Fiber Telecommunications III*, (I. P. Kaminow and T. L. Koch, eds), Academic Press, 1997, pp. 115 162.

[130] D. A. Ackermann, J. E. Johnson, L. J. P. Ketelsen et al., "Telecommunication lasers." In *Optical Fiber Telecommunications IV*, (I. Kaminow and T. Li, eds), Academic Press, 2002, pp. 587 665.

[131] K. Sato, S. Kuwahara, Y. Miyamoto, and N. Shimizu, "40 Gb/s direct modulation of distributed feedback laser for very short reach optical links." *IEE Electron. Lett.*, 38(15), 816 817, 2002.

[132] B. Wedding, W. Pohlmann, H. Gross, and O. Thalau, "43 Gbit/s transmission over 210 km SMF with a directly modulated laser diode," in Proc. *ECOC*, page Mo4.3.7, 2003.

[133] I. Tomkos, D. Chowdhury, J. Conradi et al., "Demonstration of negative dispersion fibers for DWDM metropolitan area networks" *IEEE J. Select. Topics Quantum Electron.*, 7, 439 460, 2001.

[134] B. Wedding, "New method for optical transmission beyond dispersion limit" *IEE Electron. Lett.*, 28(14), 1298 1300, 1992.

[135] B. Wedding, B. Franz, and B. Junginger, "10 Gb/s optical transmission up to 253 km via standard single mode fiber using the method of dispersion supported transmission," *J. Lightw. Technol.*, 12(10), 1720 1727, 1994.

[136] S. Chandrasekhar, C. R. Doerr, L. L. Buhl et al., "Flexible Transport at 10 Gb/s from 0 to 675 km (11500 ps/nm) using a Chirp Managed Laser and no DCF and a Dynamically Adjustable Dispersion Compensating Receiver," in Proc. *OFC*, page PDP30, 2005.

[137] Y. Yu, R. Lewen, S. Irmscher et al., "80 Gb/s ETDM Transmitter with a Traveling wave Electroabsorption Modulator," in Proc. *ECOC*, page OWE1, 2005.

[138] D. Walker, H. Sun, C. Laperle et al., "960 km transmission over G.652 fiber at 10 Gb/s with a laser/electroabsorption modulator and no optical dispersion compensation," *IEEE Photon. Technol. Lett.*, 17, 2751 2753, 2005.

[139] C. R. Doerr, L. Zhang, P. J. Winzer et al., "Compact high speed InP DQPSK modulator," *IEEE Photon. Technol. Lett.*, 19, 1184 1186, 2007.

[140] A. Ougazzaden, C. W. Lentz, T. G. B. Mason et al., "40 Gb/s Tandem Electro Absorption Modulator," in Proc. *OFC*, page PD14, 2001.

[141] D. McGhan, M. O'Sullivan, C. Bontu, and K. Roberts, "Electronic Dispersion Compensation," in Proc. *OFC*, page OWK1, 2006.

[142] S. K. Korotky, J. J. Veselka, C. T. Kemmerer et al., "High speed, Low Power Optical Modulator with Adjustable Chirp Parameter," *Topial Meeting on Integrated Photonics Research*, page TuG2, 1991.

[143] A. H. Gnauck, S. K. Korotky, J. J. Veselka et al., "Dispersion penalty reduction using an optical modulator with adjustable chirp," *IEEE Photon. Technol. Lett.*, 3(10), 916 918, 1991.

[144] H. Kim and A. H. Gnauck, "Chirp characteristics of dual drive Mach Zehnder modulator with a finite DC extinction ratio." *IEEE Photon. Technol. Lett.*, 14(3), 298 300, 2002.

[145] P. J. Winzer, C. Dorrer, R. J. Essiambre, and I. Kang, "Chirped return to zero modulation by imbalanced pulse carver driving signals," *IEEE Photon. Technol. Lett.*, 16(5), 1379 1381, 2004.

[146] F. Heismann, S. K. Korotky, and J. J. Veselka, "Lithium niobate integrated optics: Selected contemporary devices and system applications," In *Optical Fiber Telecommunications III*, (I. P. Kaminow and T. L. Koch, eds), Academic Press, 1997, pp. 377 462.

[147] A. Mahapatra and E. J. Murphy, "Electrooptic modulators," In *Optical Fiber Telecommunica tions IV*, (I. Kaminow and T. Li, eds), Academic Press, 2002, pp. 258 294.

[148] R. A. Griffin, R. G. Walker, and R. I. Johnstone, "Integrated devices for advanced modulation formats," *IEEE/LEOS Workshop on Advanced Modulation Formats*, 2004, pp. 39 40.
[149] M. Erman, P. Jarry, R. Gamonal et al., "Mach Zehnder modulators and optical switches on III V semiconductors" *J. Lightw. Technol.*, 6(6), 837 846, 1988.
[150] S. Akiyama, H. Itoh, T. Takeuch, et al., "Mach Zehnder modulator driven by 1.2 V single electrical signal," *IEE Electron. Lett.*, 41(1), 40 41, 2005.
[151] R. A. Griffin, B. Pugh, J. Fraser et al., "Compact, High Power, MQW InP Mach Zehnder Transmitters with Full Band Tunability for 10 Gb/s DWDM," in Proc. *ECOC*, page Th2.6.2, 2005.
[152] R. A. Griffin, A. Tipper, and I. Betty, "Performance of MQW InP Mach Zehnder Modulators for Advanced Modulation Formats," in Proc. *OFC*, page OTuL5, 2005.
[153] K. Tsuzuki, H. Kikuchi, E. Yamada et al., "1.3 Vpp push pull drive InP Mach Zehnder Mod ulator Module for 40 Gbit/s Operation," in Proc. *ECOC*, page Th2.6.3, 2005.
[154] B. Culshaw and M. F. G. Wilson, "Integrated optic frequency shifter modulator." *IEE Electron. Lett.*, 17, 135 136, 1981.
[155] M. Itsuzu, S. Shikama, and T. Sueta, "Integrated optical SSB modulator/frequency shifter." *IEE J. Quantum Electron.*, QE 17, 2225 2227, 1981.
[156] Y. Muramoto, K. Yoshino, S. Kodama et al., 100 and 160 Gbit/s operation of uni travelling carrier photodiode module. *IEE Electron. Lett.*, 40, 378 380, 2004.
[157] A. Beling, H. G. Bach, G. G. Mekonnen et al., "High speed miniaturized photodiode and parallel fed traveling wave photodetectors based on inp." *IEEE J. Select. Topics Quantum Electron.*, 13, 15 21, 2007.
[158] J. H. Sinsky, A. Adamiecki, C. A. Burrus et al., A "40 Gb/s integrated balanced optical front end and RZ DPSK performance," *IEEE Photon. Technol. Lett.*, 8, 1135 1137, 2003.
[159] K. Sato et al., "Record highest sensitivity of 28 dBm at 10 Gb/s achieved by newly developed extremely compact superlattice APD module with TIA IC," in Proc. *OFC*, page FB11, 2002.
[160] J. C. Campbell, "Recent advances in telecommunications avalanche photodiodes." *J. Lightw. Technol.*, 25, 109 121, 2006.
[161] C. R. S. Fludger, T. Duthel, T. Wuth, and C. Schulien, "Uncompensated transmission of 86 Gbit/s polarisation multiplexed RZ QPSK over 100 km of NDSF employing coherent equalisation," in Proc. *ECOC*, page Th4.3.3, 2006.
[162] C. R. S. Fludger, T. Duthel, D. van den Borne et al., "10 × 111 Gbit/s, 50 GHz spaced, POLMUX RZ DQPSK transmission over 2375 km employing coherent equalisation," in Proc. *OFC*, page PDP22, 2007.
[163] C. Laperle, B. Villeneuve, Z. Zhang et al., "Wave Length Division Multiplexing (WDM) and Polarization Mode Dispersion (PMD) Performance of a Coherent 40 Gbit/s Dual Polarization Quadrature Phase Shift Keying (DP QPSK) Transceiver," in Proc. *OFC*, page PDP16, 2007.
[164] B. Mikkelsen, C. Rasmussen, P. Mamysnev, and F. Liu, "Partial DPSK with excellent filter tolerance and OSNR sensitivity," *IEE Electron. Lett.*, 42, 1363 1364, 2006.
[165] C. Malouin, J. Bennike, and T. Schmidt, "DPSK receiver design optical filtering considerations," in Proc. *OFC*, page OThK1, 2007.
[166] S. Calabro, D. van den Borne, S. L. Jansen et al., "Improved Detection of Differential Phase Shift Keying Through Multi Symbol Phase estimation," in Proc. *ECOC*, page We4.P118, 2005.
[167] X. Liu, "Receiver Sensitivity Improvement in Optical DQPSK and DQPSK/ASK Through Data Aided Multi Symbol phase Estimation," in Proc. *ECOC*, page We2.5.6, 2006.
[168] S. Bigo, "Modelling of WDM Terrestrial and Submarine Links for the Design of WDM Networks.," in Proc. *OFC*, page OThD1, 2006.
[169] S. Shimotsu, S. Oikawa, T. Saitou et al., "Single side band modulation performance of a $LiNbO_3$ integrated modulator consisting of four phase modulator waveguides." *IEEE Photon. Technol. Lett.*, 13(4), 364 366, 2001.
[170] P. M. Watts, V. Mikhailov, M. Glick et al., "Single sideband optical signal generation and chromatic dispersion compensation using digital filters." *IEE Electron. Lett.*, 40(15), 958 960, 2004.
[171] W. Idler, S. Bigo, Y. Frignac et al., "Vestigial Side Band Demultiplexing for Ultra High Capacity (0.64 bit/s/Hz) Transmission of 128 × 40 Gb/s Channels," in Proc. *OFC*, page MM3, 2001.

[172] S. Bigo, Y. Frignac, G. Charlet et al., "10.2 Tbit/s (256 × 42.7 Gbit/s PDM/WDM) Transmission over 100 km Teralight™ Fiber with 1.28 bit/s/Hz Spectral Efficiency," in Proc, *OFC*, page PD25, 2001.

[173] Y. Frignac, G. Charlet, W. Idler et al., "Transmission of 256 Wavelength Division and Polarization Division Multiplexed Channels at 42.7 Gb/s (10.2 Tb/s capacity) over 3 × 100 km of TeraLight™ fiber," in Proc. *OFC*, page FC5, 2002.

[174] S. L. Jansen, R. H. Derksen, C. Schubert et al., "107 Gb/s Full ETDM Transmission over Field Installed Fiber using Vestigial Sideband Modulation," in Proc. *OFC*, page OWE3, 2007.

[175] K. Schuh, E. Lach, B. Junginger et al., "8 × 107 Gbit/s Serial Binary NRZ/VSB Transmission over 480 km SSMF with 1 bit/s/Hz Spectral Efficiency and without Optical Equalizer," in Proc. *ECOC*, Paper 2.3.1, 2007.

[176] T. Tsuritani, A. Agata, I. Morita et al., "Performance Comparison Between DSB and VSB Signals in 20 Gb/s based Ultra Long Haul WDM Systems," in Proc. *OFC*, page MM5, 2001.

[177] P. Mamyshev, B. Mikkelsen, F. Liu et al., "Spectrally Efficient Pseudo Duo Binary Modulation Formats for High Speed Optical Data Transmission," in Proc. *Conf. on Lasers and Electro optics*, 2002.

[178] A. Agarwal, S. Chandrasekhar, and R. J. Essiambre, "42.7 Gb/s CSRZ VSB for Spectrally Efficient Meshed Networks," in Proc. *ECOC*, page We3.4.4, 2004.

[179] A. Lender, "The duobinary technique for high speed data transmission," *IEEE Trans. Commun. Electron.*, 82, 214 218, 1963.

[180] A. Lender, "Correlative digital communication techniques," *IEEE Trans. Commun.*, 12(4), 128 135, 1964.

[181] A. J. Price and N. LeMercier, "Reduced bandwidth optical digital intensity modulation with improved chromatic dispersion tolerance," *IEE Electron. Lett.*, 31(1), 58 59, 1995.

[182] K. Yonenaga, S. Kuwano, S. Norimatsu, and N. Shibata, "Optical duobinary transmission system with no receiver sensitivity degradation," *IEE Electron. Lett.*, 31(4), 302 304, 1995.

[183] T. Ono, Y. Yano, K. Fukuchi et al., "Characteristics of optical duobinary signals in Terabit/s capacity, high spectral efficiency WDM systems," *J. Lightw. Technol.*, 16(5), 788 797, 1998.

[184] S. Walklin and J. Conradi, "On the relationship between chromatic dispersion and transmitter filter response in duobinary optical communication systems." *IEEE Photon. Technol. Lett.*, 9(7), 1005 1007, 1997. [see also: Comments by D. Penninckx, pp. 902 903, 1998].

[185] H. Kim, G. Lee, H. Lee et al., "On the use of 2.5 Gb/s Mach Zehnder modulators to generate 10 Gb/s optical duobinary signals." *IEEE Photon. Technol. Lett.*, 16(11), 2577 2579, 2004.

[186] D. M. Gill, A. H. Gnauck, X. Liu et al., "42.7 Gb/s cost effective duobinary optical transmitter using a commercial 10 Gb/s Mach Zehnder modulator with optical filtering." *IEEE Photon. Technol. Lett.*, 17(4), 917 919, 2005.

[187] P. J. Winzer, S. Chandrasekhar, C. R. Doerr et al., "42.7 Gb/s Modulation with a Compact InP Mach Zehnder Transmitter," in Proc. *ECOC*, page We1.6.1, 2006.

[188] P. J. Winzer, G. Raybon, and M. Duelk, "107 Gb/s optical ETDM Transmitter for 100 G Ethernet Transport," in Proc. *ECOC*, page Th4.1.1, 2005.

[189] D. Penninckx, H. Bissessur, P. Brindel et al., "Optical Differential Phase Shift Keying (DPSK) Direct Detection Considered as a Duobinary Signal," in Proc. *ECOC*, page We.P.40, 2001.

[190] D. Penninckx, L. Pierre, J. P. Thiery et al., "Relation between spectrum bandwidth and the effects of chromatic dispersion in optical transmissions," *IEE Electron. Lett.*, 32(11), 1023 1024, 1996.

[191] W. Kaiser, M. Wichers, T. Wuth et al., "SPM limit of duobinary transmission," in Proc. *ECOC*, page We7.2.2, 2000.

[192] L. Boivin and G. J. Pendock, "Receiver Sensitivity for Optically Amplified RZ Signals with Arbitrary Duty Cycle.," in Proc. *OAA*, page ThB4, 1999.

[193] P. J. Winzer and A. Kalmar, "Sensitivity enhancement of optical receivers by impulsive coding," *J. Lightw. Technol.*, 17(2), 171 177, 1999.

[194] W. Idler, A. Klekamp, R. Dischler et al., "System Performance and Tolerances of 43 Gb/s ASK and DPSK Modulation Formats," in Proc. *ECOC*, page Th2.6.3, 2003.

[195] N. M. Froberg, G. Raybon, U. Koren et al., "Generation of 2.5 Gbit/s soliton data stream with an integrated laser modulator transmitter," *IEE Electron. Lett.*, 30(22), 1880 1881, 1994.

[196] Y. Kao, A. Leven, Y. Baeyens et al., "10 Gb/s Soliton Generation for ULH Transmission using a Wideband GaAs pHemt Amplifier," in Proc. *OFC*, page FF6, 2003.

[197] X. Liu and Y. H. Kao, "Generation of RZ DPSK using a Single Mach Zehnder Modulator and Novel Driver Electronics," in Proc. *ECOC*, page We3.4.2, 2004.

[198] M. Suzuki, H. Tanaka, K. Utaka et al., "Transform limited 14 ps optical pulse generation with 15 GHz repetition rate by InGaAsP electroabsorption modulator," *IEE Electron. Lett.*, 28(11), 1007 1008, 1992.

[199] Y. Miyamoto, A. Hirano, K. Yonenaga et al., "320 Gbit/s (8 × 40 Gbit/s) WDM transmission over 367 km with 120 km repeater spacing using carrier suppressed return to zero format," *IEE Electron. Lett.*, 35(23), 2041 2042, 1999.

[200] A. Hirano, Y. Miyamoto, and K. Yonenaga, "40 Gbit/s L band transmission experiment using SPM tolerant carrier suppressed RZ format," *IEE Electron. Lett.*, 35(25), 2213 2215, 1999.

[201] A. Hodžić, B. Konrad, and K. Petermann, "Alternative modulation formats in n 40 Gb/s WDM standard fiber RZ transmission systems," *J. Lightw. Technol.*, 20, 598 607, 2002.

[202] A. Agarwal, S. Banerjee, D. F. Grosz et al., "Ultra high capacity long haul 40 Gb/s WDM transmission with 0.8 b/s/Hz spectral efficiency by means of strong optical filtering," *IEEE Photon. Technol. Lett.*, 15, 470 472, 2003.

[203] G. Raybon, A. Agarwal, S. Chandrasekhar, and R. J. Essiambre, "Transmission of 42.7 Gb/s VSB CSRZ over 1600 km and Four OADM Nodes with a Spectral Efficiency of 0.8 bit/s/Hz," in Proc. *ECOC*, page Mo3.2.7, 2005.

[204] G. Raybon, "Performance of Advanced Modulation Formats in Optically Routed Networks," in Proc. *OFC*, 2006.

[205] N. S. Bergano, "Undersea communication systems." In *Optical Fiber Telecommunications IV* (I. Kaminow and T. Li, eds), Academic Press, 2002, pp. 154 197.

[206] C. R. Menyuk, G. M. Carter, W. L. Kath, and R. M. Mu, "Dispersion managed solitons and chirped return to zero: What is the difference." In *Optical Fiber Telecommunications IV* (I. Kaminov and T. Li, eds), Academic Press, 2002, pp. 305 328.

[207] R. Ohhira, D. Ogasahara, and T. Ono, "Novel RZ Signal Format with alternate Chirp for Suppres sion of Nonlinear Degradation in 40 Gb/s based WDM," in Proc. *OFC*, page WM2, 2001.

[208] E. A. Golovchenko, N. S. Bergano, C. R. Davidson, and A. N. Pilipetskii, "Modeling vs Experiments of 1610 Gbit/s WDM Chirped RZ Pulse Transmission Over 7500 km," in Proc. *OFC*, page ThQ3, 1999.

[209] B. Bakhshi, M. Vaa, E. A. Golovchenko et al., "Comparison of CRZ, RZ and NRZ Modulation Formats in a 64 × 12.3 Gb/s WDM Transmission Experiment Over 9000 km," in Proc. *OFC*, page WF4, 2001.

[210] N. S. Bergano, C. R. Davidson, and F. Heismann, "Bit synchronous polarisation and phase modulation scheme for improving the performance of optical amplifier transmission systems," *IEE Electron. Lett.*, 32, 52 54, 1996.

[211] E. A. Golovchenko, A. N. Pilipetskii, N. S. Bergano et al., "Modeling of transoceanic fiber optic WDM communication systems." *IEEE J. Select. Topics Quantum Electron.*, 6, 337 347, 2000.

[212] N. S. Bergano, "Wavelength division multiplexing in long haul transoceanic transmission sys tems." *J. Lightw. Technol.*, 23, 4125 4139, 2005.

[213] R. A. Griffin, R. G. Walker, R. I. Johnstone et al., "Integrated 10 Gb/s Chirped Return to Zero Transmitter using GaAs AlGaAs Modulators," in Proc. *OFC*, page PD15, 2001.

[214] A. H. Gnauck and P. J. Winzer, "Optical phase shift keyed transmission." *J. Lightw. Technol.*, 23(1), 115 130, 2005.

[215] M. Rice, S. Tretter, and P. Mathys, "On differentially encoded m sequences." *IEEE Trans. Commun.*, 49, 421 424, 2001.

[216] P. A. Humblet and M. Azizoglu, "On the bit error rate of lightwave systems with optical amplifiers." *J. Lightw. Technol.*, 9, 1576 1582, 1991.

[217] P. J. Winzer, D. Stahl, and H. Kim, "Impact of Pulse Carver Chirp on RZ DPSK Receiver Performance," in Proc, *ECOC*, page We3.5.6, 2003.

[218] T. Chikama, S. Watanabe, T. Naito et al., "Modulation and demodulation techniques in optical heterodyne PSK transmission systems," *J. Lightw. Technol.*, 8, 309 321, 1990.

[219] T. Miyazaki and F. Kubota, "2 bit Per Symbol Modulation/Demodulation by DPSK over Inverse RZ Optical Pulses," in Proc. *IEEE/LEOS Annual Meeting*, page CThBB2, 2004.

[220] T. Miyazaki and F. Kubota, "Superposition of DQPSK over inverse RZ for 3 bit/symbol mod ulation demodulation." *IEEE Photon. Technol. Lett.*, 16, 2643 2645, 2004.

[221] M. Zitelli, "Optical phase and intensity modulation using dark pulses." *IEEE Photon. Technol. Lett.*, 16, 1972 1974, 2004.

[222] H. Kim and R. J. Essiambre, "Transmission of 8 × 20 Gb/s DQPSK signals over 310 km SMF with 0.8 b/s/Hz spectral efficiency," *IEEE Photon. Technol. Lett.*, 15(5), 769 771, 2003.

[223] J. X. Cai, D. G. Foursa, L. Liu et al., "RZ DPSK field trial over 13 100 km of installed non slope matched submarine fibers," *J. Lightw. Technol.*, 23, 95 103, 2005.

[224] H. Kim, "Cross phase modulation induced nonlinear phase noise in WDM direct detection DPSK systems," *J. Lightw. Technol.*, 21, 1770 1774, 2003.

[225] P. J. Winzer and H. Kim, "Degradations in balanced DPSK receivers," *IEEE Photon. Technol. Lett.*, 15(9), 1282 1284, 2003.

[226] P. J. Winzer, S. Chandrasekhar, and H. Kim, "Impact of filtering on RZ DPSK reception." *IEEE Photon. Technol. Lett.*, 15(6), 840 842, 2003.

[227] H. Kim and P. J. Winzer, "Nonlinear Phase Noise in Phase Coded Transmission," in Proc. *OFC*, page OThO3, 2005.

[228] X. Gu and L. C. Blank, "10 Gbit/s unrepeated three level optical transmission over 100 km of standard fibre." *IEEE Electron. Lett.*, 29, 2209 2211, 1993.

[229] G. May, A. Solheim, and J. Conradi, "Extended 10 Gb/s fiber transmission distance at 1538 nm using a duobinary receiver," *IEEE Photon. Technol. Lett.*, 6, 648 650, 1994.

[230] J. H. Sinsky, M. Duelk, and A. Adamiecki, "High speed electrical backplane transmission using duobinary signaling," *IEEE Trans. Micro. Theo. Techn.*, 53(1), 152 160, 2005.

[231] N. Alic, G. C. Papen, R. E. Saperstein et al., "Experimental demonstration of 10 gb/s NRZ Extended Dispersion Limited Reach over 600 km SMF Link Without Optical Dispersion Compensation," in Proc. *OFC*, page OWB7, 2006.

[232] T. Tokle, C. R. Davidson, M. Nissov et al., "6500 km transmission of RZ DQPSK WDM signals," *IEE Electron. Lett.*, 40(7), 444 445, 2004.

[233] M. Ohm and T. Freckmann, "Comparison of different DQPSK transmitters with NRZ and RZ impulse shaping," *IEEE/LEOS Workshop on Advanced Modulation Formats*, page ThB2, 2004.

[234] A. H. Gnauck, P. J. Winzer, S. Chandrasekhar, and C. Dorrer, "Spectrally Efficient (0.8 b/s/Hz) 1 Tb/s (25 × 42.7 Gb/s) RZ DQPSK Transmission over 28 100 km SSMF Spans with 7 Optical Add/Drops," in Proc." *OFC*, page Th4.4.1, 2004.

[235] M. Cavallari, C. S. R. Fludger, and P. J. Anslow, "Electronic Signal Processing for Differential Phase Modulation Formats," in Proc. *OFC*, page TuG2, 2004.

[236] N. Yoshikane and I. Morita, "1.14 b/s/Hz spectrally efficient 50 × 85.4 Gb/s transmission over 300 km using copolarized RZ DQPSK signals," *J. Lightw. Technol.*, 23(1), 108 114, 2005.

[237] H. Kim and P. J. Winzer, "Robustness to laser frequency offset in direct detection DPSK and DQPSK systems." *J. Lightwave Technol.*, 21(9), 1887 1891, 2003.

[238] C. R. Doerr, D. M. Gill, A. H. Gnauck et al., "Simultaneous reception of both quadratures of 40 Gb/s DQPSK using a simple monolithic demodulator," in Proc. *OFC*, page PDP12, 2005.

[239] X. Liu, S. Chandrasekhar, A. H. Gnauck et al., "DSP enabled compensation of demodulator phase error and sensitivity improvement in direct detection 40 Gb/s DQPSK," in Proc. *ECOC*, page Th4.4.5, 2006.

[240] P. J. Winzer, G. Raybon, S. Chandrasekhar et al., "10 × 107 Gb/s NRZ DQPSK transmission at 1.0 b/s/Hz over 12 × 100 km including 6 optical routing nodes," in Proc. *OFC*, page PDP24, 2007.

[241] J. Wang and J. M. Kahn, "Impact of chromatic and polarization mode dispersions on DPSK systems using interferometric demodulation and direct detection," *J. Lightw. Technol.*, 22(2), 362 371, 2004.

[242] A. H. Gnauck, J. Sinsky, P. J. Winzer, and S. Chandrasekhar, "Linear Microwave Domain Dispersion Compensation of 10 Gb/s Signals using Heterodyne Detection," in Proc. *OFC*, page PDP31, 2005.

[243] D. van den Borne, S. L. Jansen, G. D. Khoe et al., "A Comparison between Multi Level Modulation Formats: 21.4 Gbit/s RZ DQPSK and POLMUX RZ DPSK," in Proc." *OFC*, page OThR2, 2006.

[244] T. Tokle, C. R. Davidson, M. Nissov et al., "Transmission of RZ DQPSK over 6500 km with 0.66 bit/s/Hz Spectral Efficiency." *IEEE/LEOS Workshop on Advanced Modulation Formats*, page ThA2, 2004.

[245] G. Charlet, H. Mardoyan, P. Tran et al., "Nonlinear Interactions Between 10 Gb/s NRZ Channels and 40 Gb/s Channels with RZ DQPSK or PSBT format, over Low Dispersion Fiber," in Proc. *European Conf. on ECOC*, page Mo3.2.6, 2006.

[246] B. C. Collings and L. Boivin, "Nonlinear polarization evolution induced by cross phase modulation and its impact on transmission systems," *IEEE Photon. Technol. Lett.*, 12, 1582 1584, 2000.

[247] D. van den Borne, N. E. Hecker Denschlag, G. D. Khoe, and H. de Waard, "Cross Phase Modulation Induced Depolarization Penalties in 2 × 10 Gbit/s Polarization Multiplexed Trans mission," in Proc. *ECOC*, page Mo4.5.5, 2004.

[248] G. Charlet, J. Renaudier, M. Salsi et al., "Efficient Mitigation of Fiber Impairments in an Ultra Long Haul Transmission of 40 Gbit/s Polarization Multiplexed Data, by Digital Processing in a Coherent Receiver," in Proc. *OFC*, page PDP17, 2007.

[249] N. S. Bergano, "Undersea amplified lightwave systems design." In *Optical Fiber Telecommuni cations III A* (I. P. Kaminov and T. L. Koch eds), Chapter 10, Academic Press, 1997.

[250] P. J. Winzer, M. Pfennigbauer, and R. J. Essiambre, "Coherent crosstalk in ultra dense WDM systems." *J. Lightw. Technol.*, 23(4), 1734 1744, 2005.

[251] M. Pfennigbauer and P. J. Winzer, "Choice of MUX/DEMUX Filter Characteristics for NRZ, RZ, and CSRZ DWDM systems," *J. Lightw. Technol.*, 24, 1689 1696, 2005. submitted.

[252] G. Raybon, S. Chandrasekhar, A. H. Gnauck et al., "Experimental Investigation of Long Haul Transport at 42.7 Gb/s Through Concatenated Optical Add/Drop Nodes," in Proc. *OFC*, page ThE4, 2004.

[253] G. Raybon, S. Chandrasekhar, A. Agarwal et al., "Limitations of Optical Add/Drop Filtering on 42.7 Gb/s Transmission with 50 GHz Channel Spacing," in Proc. *ECOC*, page Mo4.5.1, 2004.

[254] S. Chandrasekhar, "Dispersion Tolerant Alternative 10 Gb/s Transmitters and Implications for WDM Optical Networking," in Proc. *OFC*, 2006.

[255] G. Bosco and P. Poggiolini, "Long distance effectiveness of MLSE IMDD receivers," *IEEE Photon. Technol. Lett.*, 18, 1037 1039, 2006.

[256] D. Castagnozzi, "Digital Signal Processing and Electronic Equalization (EE) of ISI," in Proc. *OFC*, page WM6, 2004.

[257] P. J. Winzer, R. J. Essiambre, and S. Chandrasekhar, "Dispersion Tolerant Optical Communica tion Systems," in Proc. *ECOC*, page We2.4.1, 2004.

[258] H. Kogelnik, R. M. Jopson, and L. E. Nelson, "Polarization mode dispersion" In *Optial Fiber Telecommunication* (I. Kaminow and T. Li eds), Academic Press, 2002, pp. 725 861.

[259] R. M. Jopson, L. E. Nelson, G. J. Pendock, and A. H. Gnauck, "Polarization Mode Dispersion Impairment in Return to zero and Non Return to zero Systems," in Proc. *OFC*, page WE3, 1999.

[260] P. J. Winzer, H. Kogelnik, C. H. Kim et al., "Receiver impact on first order PMD outage," *IEEE Photon. Technol. Lett.*, 15(10), 1482 1484, 2003.

[261] C. Xie, S. Shen, and L. Moller, "Effects of transmitter imperfection on polarization mode dispersion impairments," *IEEE Photon. Technol. Lett.*, 15(4), 614 616, 2003.

[262] C. H. Kim, H. Kim, R. M. Jopson, and P. J. Winzer, "Dependence of PMD Penalties on Decision Point and Receiver Bandwidth," in Proc. *OFC*, page TuI4, 2002.
[263] M. Brodsky, N. J. Frigo, M. Boroditsky, and M. Tur, "Polarization mode dispersion of installed fibers," *J. Lightw. Technol.*, 24, 4584 4599, 2006.
[264] H. F. Haunstein, W. Sauer Greff, A. Dittrich et al., "Principles for electronic equalization of polarization mode dispersion," *J. Lightw. Technol.*, 22(4), 1169 1182, 2004.
[265] F. Buchali and H. Bulow, "Adaptive PMD compensation by electrical and optical techniques," *J. Lightw. Technol.*, 22(4), 1116 1126, 2004.
[266] B. Wedding and C. N. Haslach, "Enhanced PMD Mitigation by Polarization Scrambling and Forward Error Correction," in Proc. *OFC*, page WAA1, 2001.
[267] X. Liu, "All channel Pmd Mitigation using Distributed Fast Polarization Scrambling in WDM Systems with FEC," in Proc. *OFC*, page OMH4, 2007.
[268] L. F. Mollenauer and J. P. Gordon, "*Solitons in Optical Fibers: Fundamentals and Applications,"* Academic Press, 2006, Section 3.3.
[269] T. Mizuochi, K. Ishida, T. Kobayashi et al., "A comparative study of DPSK and OOK WDM transmission over transoceanic distances and their performance degradations due to nonlinear phase noise," *J. Lightw. Technol.*, 21, 1933 1943, 2003.
[270] J. P. Gordon and L. F. Mollenauer, "Phase noise in photonic communications systems using linear amplifiers," *Opt. Lett.*, 15(23), 1351 1353, 1990.
[271] A. Mecozzi, "Limits to long haul coherent transmission set by the Kerr nonlinearity and noise of the in line amplifiers," *J. Lightw. Technol.*, 12, 1993 2000, 1994.
[272] H. Kim and A. H. Gnauck, "Experimental investigation of the performance limitation of DPSK Systems due to nonlinear phase noise," *IEEE Photon. Technol. Lett.*, 15, 320 322, 2003.
[273] M. Ohm, R. J. Essiambre, and P. J. Winzer, "Nonlinear Phase Noise and Distortion in 42.7 Gbit/s RZ DPSK Systems," in Proc. *ECOC*, page Tu1.2.1, 2005.
[274] M. M. El Said, J. Sitch, and M. I. Elmasry, "An electrically pre equalized 10 Gb/s duobinary transmission system," *J. Lightw. Technol.*, 23(1), 388 400, 2005.
[275] P. J. Winzer and R. J. Essiambre, "Electronic Pre Distortion for Advanced Modulation Formats," in Proc. *ECOC*, page Tu4.2.2, 2005.
[276] R. J. Essiambre and P. J. Winzer, "Fibre Nonlinearities in Electronicaly Pre Distorted Trans mission," in Proc. *ECOC*, page Tu3.2.2, 2005.
[277] R. I. Killey, P. M. Watts, V. Mikhailov et al., "Electronic dispersion compensation by signal predistortion using digital processing and a dual drive Mach Zehnder modulator," *IEEE Photon. Technol. Lett.*, 17, 714 716, 2005.
[278] K. Roberts, L. Strawczynski, C. Li et al., "Electronic precompensation of optical nonlinearity," *IEEE Photon. Technol. Lett.*, 18, 403 405, 2006.
[279] R. J. Essiambre and P. J. Winzer, "Impact of Fiber Nonlinearities on Advanced Modulation Formats using Electronic Pre Distortion," in Proc. *OFC*, page OWB1, 2006.
[280] R. J. Essiambre, P. J. Winzer, X. Q. Wang et al., "Electronic predistortion and fiber non linearity," *IEEE Photon. Technol. Lett.*, 18, 1804 1806, 2006.

This page intentionally left blank

3

Coherent optical communication systems

Kazuro Kikuchi

Department of Frontier Informatics, University of Tokyo, Kashiwa, Chiba, Japan

3.1 INTRODUCTION

3.1.1 Coherent Optical Communications Twenty Years Ago

The research and development in optical fiber communication systems started around the first half of the 1970s. Such systems used intensity modulation of semiconductor lasers, and the transmitted optical signal intensity was detected by a photodiode, which was regarded as a square-law detector. This combination of the transmitter and receiver is called the intensity modulation/direct detection (IMDD) scheme, which has been commonly employed in current optical communication systems.

However, coherent optical receivers were studied extensively in the 1980s [1]. Coherent receivers could linearly down-convert the whole optical signal to a baseband electrical signal by using heterodyne or homodyne detection, and had the following advantages against direct detection:

(1) The shot-noise limited receiver sensitivity can be achieved with a sufficient local oscillator (LO) power. The LO gives us a signal gain, whereas the LO shot noise overwhelms the thermal noise of the receiver; thus we can achieve the shot-noise limited receiver sensitivity.
(2) The frequency resolution at the intermediate frequency (IF) or baseband stage is so high that we can separate closely spaced wavelength-division multiplexed (WDM) channels at the electrical stage.
(3) The ability of phase detection can improve the receiver sensitivity compared with the IMDD system. This is due to the fact that the distance between symbols, which are expressed as phasors on the complex plane, is extended by the use of the phase information.

Optical Fiber Telecommunications V B: Systems and Networks

ISBN: 978 0 12 374172 1

(4) The multilevel modulation format such as quadrature phase-shift keying (QPSK) can be introduced into optical communications by using phase modulation.

A number of research groups challenged optical transmission experiments with coherent receivers. However, the invention of erbium-doped fiber amplifiers (EDFAs) made the shot-noise limited receiver sensitivity of the coherent receiver less significant. This is because the signal-to-noise ratio (SNR) of the signal transmitted through the amplifier chain is determined from the accumulated amplified spontaneous emission (ASE) rather than the shot noise. In addition, even in unrepeated transmission systems, the EDFA used as a low-noise preamplifier eliminated the need for the coherent receiver with superior sensitivity.

Technical difficulties inherent in coherent receivers could not also be disregarded. The heterodyne receiver requires an IF, which should be higher than the signal bit rate, and the maximum bit rate of the heterodyne receiver is always less than the half of that the square-law detector can achieve. In contrast, the homodyne receiver is essentially a baseband receiver; however, the complexity in stable locking of the carrier phase drift has prevented its practical applications.

From these reasons, further research and development activities in coherent optical communications have almost been interrupted for nearly 20 years. In contrast, rapid progress in EDFA technologies entirely changed the direction of R&D in optical communications. The EDFA-based system started to take benefit from WDM techniques to increase the transmission capacity of a single fiber. The hardware required for WDM networks became widely deployed owing to its relative simplicity and the relatively low cost associated with optical amplifier repeaters where multiple WDM channels could be amplified all at once. The WDM technique marked the beginning of a new era in the history of optical communication systems and brought forth 1000 times increase in the transmission capacity during the 1990s.

3.1.2 Rebirth of Coherent Optical Communications

With the transmission-capacity increase in WDM systems, coherent technologies have restarted to attract a large interest over the recent years. The motivation lies in finding methods of meeting the ever-increasing bandwidth demand with multilevel modulation formats based on coherent technologies [2].

The first step of the revival of coherent optical communications research was ignited with the QPSK modulation/demodulation experiment featuring optical in-phase and quadrature (IQ) modulation and optical delay detection [3]. In such a scheme, one symbol carries two bits by using the four-point constellation on the complex plane; therefore, we can double the bit rate, while keeping the symbol rate, or maintain the bit rate even with the halved spectral width.

The optical IQ modulation has been realized with Mach Zehnder type push pull modulators in parallel [4]. The IQ components of the optical carrier can be

modulated independently, enabling any kind of modulation formats. IQ modulators integrated on $LiNbO_3$ substrates are now commercially available.

The optical delay detector is composed of an optical one-bit delay line and a double-balanced photodiode. With such a receiver, we can compare the phase of the transmitted signal with that of the previous bit and restore the data, which is differentially precoded at the transmitter. Using two such receivers in parallel, we can demodulate the signal IQ components separately without the need for LO. A number of long-distance WDM QPSK transmission experiments have been reported recently, based on IQ modulation and differential IQ demodulation.

The next stage has opened with high-speed digital signal processing (DSP) [5]. The recent development of high-speed digital integrated circuits has offered the possibility of treating the electrical signal in a DSP core and retrieving the IQ components of the complex amplitude of the optical carrier in a very stable manner. The authors have demonstrated a phase-diversity homodyne receiver for demodulating the 20-Gbit/s QPSK signal. Since the carrier phase is recovered after homodyne detection by means of DSP, this type of receiver has now commonly been called the "digital coherent receiver." While an optical phase-locked loop (PLL) that locks the LO phase to the signal phase is still difficult to achieve, DSP circuits are becoming increasingly faster and provide us with simple and efficient means for estimating the carrier phase [6].

Any kind of multilevel modulation formats can be introduced by using the coherent receiver [7]. While the spectral efficiency of binary modulation formats is limited to 1 bit/s/Hz/polarization, which is called the Nyquist limit, modulation formats with M bits of information per symbol can achieve the spectral efficiency up to M bit/s/Hz/polarization. Although optical delay detection has been employed to demodulate the QPSK signal ($M = 2$) [3], further increase in multiplicity is hardly achieved with such a scheme.

Another and probably more important advantage of the digital coherent receiver is the post signal-processing function. The IQ demodulation by our receiver is the entirely linear process; therefore, all the information on the complex amplitude of the transmitted optical signal is preserved even after detection, and conventional signal processing functions acting on the optical carrier, such as optical filtering and dispersion compensation [8,9], can be performed at the electrical stage after detection. Post signal-processing based on DSP has been employed in direct detection systems for adaptive equalization and maximum likelihood estimation (MLE) of the distorted signal, and has become a new trend of optical communications [10]. In contrast, the digital coherent receiver enables more sophisticated signal processing on the homodyne-detected complex amplitude because the optical phase information is not lost even after detection.

For the moment, DSP at 10 Gsymbol/s in the digital coherent receiver has been performed still offline; however, the real-time operation has already been demonstrated at a few Gsymbol/s [11], and dedicated integrated circuits will make the real-time operation over 10 Gsymbol/s possible in the near future. The combination of coherent detection and DSP is thus expected to become a part of the next

generation of optical communication systems and provide new capabilities that were not possible without the detection of the phase of the optical signal.

3.1.3 Organization of this Chapter

This chapter reviews the results of recent developments on the digital coherent receiver. After historical perspective given in Section 3.1, Section 3.2 provides the principle of coherent detection. Section 3.3 discusses the concept of the digital coherent receiver, and the basic performance of the digital coherent receiver is evaluated in Section 3.4. Section 3.5 deals with postprocessing functions, which enable compensation for transmission impairments at the receiver. Finally, a summary is provided in Section 3.6.

3.2 PRINCIPLE OF COHERENT DETECTION

In this section, we describe the principle of operation of coherent detection. Especially, we show that with the homodyne receiver, which comprises phase and polarization diversities, we can restore the full information on the optical complex amplitude, namely the amplitude, the phase, and the state of polarization (SOP).

3.2.1 Coherent Detection

The fundamental concept behind coherent detection is to take the product of electric fields of the modulated signal light and the continuous-wave LO. The optical signal coming from the transmitter can be described by

$$E_s(t) = A_s(t)\exp(j\omega_s t), \tag{3.1}$$

where $A_s(t)$ is the complex amplitude and ω_s is the angular frequency. Similarly, the field of the LO can be described by

$$E_{LO}(t) = A_{LO}\exp(j\omega_{LO} t), \tag{3.2}$$

where A_{LO} is the complex amplitude and ω_{LO} is the angular frequency of the LO. We note here that the complex amplitudes A_s and A_{LO} are related to the power of the optical fields by $P_s = |A_s|^2/2$ and $P_{LO} = |A_{LO}|^2/2$, where P_s and P_{LO} are the power of the signal and LO, respectively.

Balanced detection is usually introduced into the coherent receiver as a mean to suppress the DC component and maximize the signal photocurrent. Figure 3.1 shows the block diagram of such a receiver. The concept resides in using a 3-dB

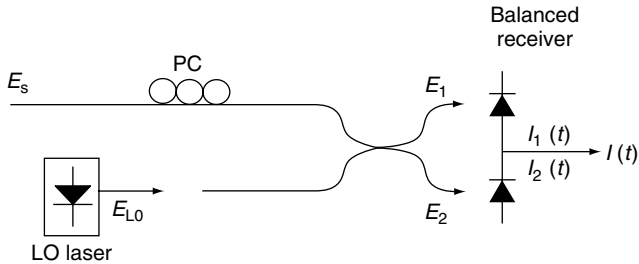

Figure 3.1 Configuration of the coherent receiver.

optical coupler that adds a 180° phase shift to either the signal field or the LO field between the two output ports. When the signal and LO are copolarized, the electric fields incident on the upper and lower photodiodes are given as

$$E_1 = \frac{1}{\sqrt{2}}(E_s + E_{LO}), \tag{3.3}$$

$$E_2 = \frac{1}{\sqrt{2}}(E_s - E_{LO}), \tag{3.4}$$

and the output photocurrents are written as

$$\begin{aligned} I_1(t) &= R\left[\mathrm{Re}\left\{\frac{A_s(t)\exp(j\omega_s t) + A_{LO}(t)\exp(j\omega_{LO}t)}{\sqrt{2}}\right\}\right]^{ms}, \\ &= \frac{R}{2}\left[P_s + P_{LO} + 2\sqrt{P_s P_{LO}}\ \cos\{\omega_{IF}t + \theta_{sig}(t) - \theta_{LO}(t)\}\right] \end{aligned} \tag{3.5}$$

$$\begin{aligned} I_2(t) &= R\left[\mathrm{Re}\left\{\frac{A_s(t)\exp(j\omega_s t) - A_{LO}(t)\exp(j\omega_{LO}t)}{\sqrt{2}}\right\}\right]^{ms}, \\ &= \frac{R}{2}\left[P_s + P_{LO} - 2\sqrt{P_s P_{LO}}\ \cos\{\omega_{IF}t + \theta_{sig}(t) - \theta_{LO}(t)\}\right] \end{aligned} \tag{3.6}$$

where ms represents the mean square with respect to the optical frequencies, Re the real part, ω_{IF} the IF given by $\omega_{IF} = \omega_s \quad \omega_{LO}$, and $\theta_{sig}(t)$ and $\theta_{LO}(t)$ are phases of the transmitted signal and LO, respectively. R is the responsitivity of the photodiode and is given as

$$R = \frac{e\eta}{h\omega_s}, \tag{3.7}$$

where h stands for the Planck's constant, e is the electron charge, and η is the quantum efficiency of the photodiode. We neglect the sum frequency component

since it will be averaged out to zero due to the limited bandwidth of the photodiode. The balanced detector output is then given as

$$I(t) = I_1(t) - I_2(t) = 2R\sqrt{P_s(t)P_{LO}}\cos\{\omega_{IF}t + \theta_{sig}(t) - \theta_{LO}(t)\}. \tag{3.8}$$

P_{LO} is always constant and $\theta_{LO}(t)$ includes only the phase noise that varies with time.

3.2.2 Heterodyne and Homodyne Receivers

Heterodyne detection refers to the case where $|\omega_{IF}| >> \omega_b/2$, with ω_b being the modulation bandwidth of the optical carrier determined by the bit rate. In such a case, Eqn (3.8) shows that the electric field of the signal light is down-converted to the IF signal including the amplitude information and the phase information.

If we consider the PSK modulation format, P_s is constant and $\theta_{sig}(t) = \theta_s(t) + \theta_{sn}(t)$, where $\theta_s(t)$ is the phase modulation and $\theta_{sn}(t)$ the phase noise. The receiver output is given as

$$I(t) = 2R\sqrt{P_s P_{LO}}\cos\{\omega_{IF}t + \theta_s(t) + \theta_n(t)\}, \tag{3.9}$$

and we can determine the complex amplitude on $\exp(j\omega_{IF}t)$ from Eqn (3.9) as

$$I_c(t) = 2R\sqrt{P_s P_{LO}}\exp j\{\theta_s(t) + \theta_n(t)\}, \tag{3.10}$$

which is equivalent to the complex amplitude of the optical signal except for the phase noise increase. In this case, although the total phase noise $\theta_n(t) = \theta_{sn}(t) \quad \theta_{LO}(t)$ might vary with time, electrical synchronous demodulation can be used to estimate the phase noise and decode the symbol $\theta_s(t)$.

Homodyne detection refers to the case where $\omega_{IF} = 0$. The photodiode current then becomes

$$I(t) = 2R\sqrt{P_s P_{LO}}\cos\{\theta_{sig}(t) - \theta_{LO}(t)\}. \tag{3.11}$$

The LO phase $\theta_{LO}(t)$ must track the transmitter phase noise $\theta_{sn}(t)$ such that $\theta_n(t) = 0$ to decode the symbol $\theta_s(t)$ correctly. This function is realized by the optical phase-locked loop (OPLL); however, in practice, the implementation of such a loop is not simple and adds to the complexity of homodyne detection. In addition, Eqn (3.11) only gives the cosine component (in other words, the in-phase component with respect to the LO phase), and the sine component (the quadrature component) cannot be detected. Therefore, this type of homodyne receivers is not able to extract the full information of the signal complex amplitude.

3.2.3 Phase-diversity Homodyne Receiver

If we prepare another LO, whose phase is shifted by 90°, in the homodyne receiver, we can detect both IQ components of the signal light. This function is achieved by a 90° optical hybrid (see Section 3.4 for the more detailed optical circuit configuration). As shown in Figure 3.2, using the 90° optical hybrid, we can obtain four outputs E_1, E_2, E_3, and E_4 from the two inputs E_s and E_{LO} as

$$E_1 = \frac{1}{2}(E_s + E_{LO}), \tag{3.12}$$

$$E_2 = \frac{1}{2}(E_s - E_{LO}), \tag{3.13}$$

$$E_3 = \frac{1}{2}(E_s + jE_{LO}), \tag{3.14}$$

$$E_4 = \frac{1}{2}(E_s - jE_{LO}). \tag{3.15}$$

Output photocurrents from balanced photodetectors are then given as

$$I_I(t) = I_{I1}(t) - I_{I2}(t) = R\sqrt{P_s P_{LO}}\ \cos\{\theta_{sig}(t) - \theta_{LO}(t)\}, \tag{3.16}$$

$$I_Q(t) = I_{Q1}(t) - I_{Q2}(t) = R\sqrt{P_s P_{LO}}\ \sin\{\theta_{sig}(t) - \theta_{LO}(t)\}. \tag{3.17}$$

In the case of PSK modulation, these are written as

$$I_I(t) = R\sqrt{P_s P_{LO}}\ \cos\{\theta_s(t) + \theta_n(t)\}, \tag{3.18}$$

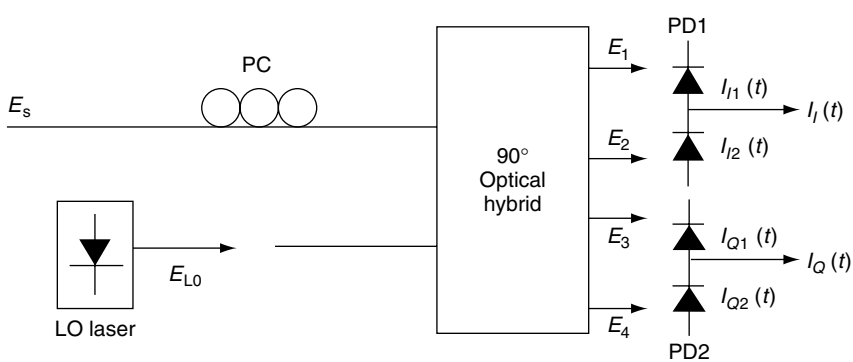

Figure 3.2 Configuration of the phase diversity homodyne receiver.

$$I_Q(t) = R\sqrt{P_s P_{LO}}\ \sin\{\theta_s(t) + \theta_n(t)\}. \tag{3.19}$$

Using Eqns (3.18) and (3.19), we can restore the complex amplitude as

$$I_c(t) = I_I(t) + jI_Q(t) = R\sqrt{P_s P_{LO}}\exp\{j\,(\theta_s(t) + \theta_n(t)\}, \tag{3.20}$$

which is equivalent to the complex amplitude of the optical signal except for the phase noise increase. The receiver thus leads to the recovery of both the sine and cosine components. It is possible to estimate the phase noise $\theta_n(t)$ varying with time and restore the phase information $\theta_s(t)$ through DSP on the homodyne detected signal given by Eqn (3.20). In addition, even the frequency offset can be allowed if $|\omega_{IF}| << \omega_b/2$ since it is also estimated after detection. These properties relax severe requirements for OPLL-type homodyne receivers. See Section 3.6 for details of the carrier phase-estimation method.

This type of receiver is commonly called the "phase-diversity homodyne receiver [12]." This is because the signal amplitude $|A_s|$ can always be determined independently of the phase noise from the measured sine and cosine components of the complex amplitude. It is also named the "intradyne receiver [13]," because the full information on the optical complex amplitude is restored in the baseband ($|\omega_{IF}| << \omega_b/2$) without frequency and phase locking.

Eventually, the phase-diversity homodyne receiver and the heterodyne receiver can similarly restore the full information on the optical complex amplitude, as shown by Eqns (3.10) and (3.20), respectively. However, since the phase-diversity homodyne receiver generates the baseband signal, it is more advantageous over the heterodyne receiver dealing with the rather high IF.

3.2.4 Homodyne Receiver Employing Phase and Polarization Diversities

It was assumed up to this point that the polarization of the incoming signal was always aligned to that of the LO. However, in practical systems the polarization of the incoming signal is unlikely to remain aligned to the SOP of the LO because of random changes on the birefringence of the transmission fiber. One of the most serious problems of the coherent receiver is that the receiver sensitivity is dependent on SOP of the incoming signal. In the worst case where the SOP of the incoming signal is orthogonal to that of the LO, we cannot have any output from the coherent receiver. In this section, we show the polarization-diversity receiver to cope with the polarization dependence of the coherent receiver.

The receiver employing polarization diversity is shown in Figure 3.3, where the two phase-diversity homodyne receivers are combined with the polarization diversity configuration (see Section 3.4 for the detailed optical circuit) [14]. The incoming signal having an arbitrary SOP is separated into two linear polarization

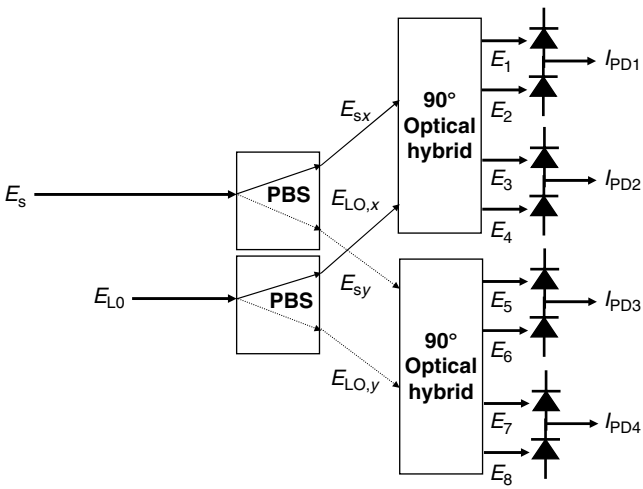

Figure 3.3 Configuration of the phase/polarization diversity receiver.

components with a polarization beam splitter (PBS). Let the *x*- and *y*-polarization components after PBS be written as

$$\begin{bmatrix} E_{sx} \\ E_{sy} \end{bmatrix} = \begin{bmatrix} \sqrt{\alpha} A_s e^{j\delta} \\ \sqrt{1-\alpha} A_s \end{bmatrix} \exp(j\omega_s t), \tag{3.21}$$

where α is the power ratio of the two polarization components and δ is the phase difference between them. These parameters are dependent of the birefringence of the transmission fiber and time varying. In contrast, the *x*- and *y*-polarization components equally separated from the linearly polarized LO are written as

$$\begin{bmatrix} E_{LO,x} \\ E_{LO,y} \end{bmatrix} = \frac{1}{\sqrt{2}} \begin{bmatrix} A_{LO} \\ A_{LO} \end{bmatrix} \exp(j\omega_{LO} t). \tag{3.22}$$

The 90° optical hybrids in Figure 3.3 generate electric fields $E_{1,\ldots,8}$ at the double-balanced photodiodes PD1 PD4:

$$E_{1,2} = \frac{1}{2}\left(E_{sx} \pm \frac{1}{\sqrt{2}} E_{LO}\right), \tag{3.23}$$

$$E_{3,4} = \frac{1}{2}\left(E_{sx} \pm \frac{j}{\sqrt{2}} E_{LO}\right), \tag{3.24}$$

$$E_{5,6} = \frac{1}{2}\left(E_{sy} \pm \frac{1}{\sqrt{2}} E_{LO}\right), \tag{3.25}$$

$$E_{7,8} = \frac{1}{2}\left(E_{sy} \pm \frac{j}{\sqrt{2}} E_{LO}\right), \tag{3.26}$$

where $E_{LO} = E_{LO,x} = E_{LO,y}$. Photocurrents from PD1 to PD4 are then given as

$$I_{PD1} = R\sqrt{\frac{\alpha P_s P_{LO}}{2}} \cos\{\theta_s(t) - \theta_{LO}(t) + \delta\}, \tag{3.27}$$

$$I_{PD2} = R\sqrt{\frac{\alpha P_s P_{LO}}{2}} \sin\{\theta_s(t) - \theta_{LO}(t) + \delta\}, \tag{3.28}$$

$$I_{PD3} = R\sqrt{\frac{(1-\alpha) P_s P_{LO}}{2}} \cos\{\theta_s(t) - \theta_{LO}(t)\}, \tag{3.29}$$

$$I_{PD4} = R\sqrt{\frac{(1-\alpha) P_s P_{LO}}{2}} \sin\{\theta_s(t) - \theta_{LO}(t)\}. \tag{3.30}$$

From Eqns (3.27) (3.30), we find that the polarization-diversity receiver can separately measure complex amplitudes of the two polarization components as

$$I_{xc}(t) = I_{PD1}(t) + jI_{PD2}(t), \tag{3.31}$$

$$I_{yc}(t) = I_{PD3}(t) + jI_{PD4}(t), \tag{3.32}$$

from which we can reconstruct the signal complex amplitude A_s in a polarization-independent manner.

3.2.5 Considerations on the Signal-to-Noise Ratio

From the complex amplitude at the IF stage given by Eqn (3.10), the SNR of the heterodyne signal is given as

$$\gamma_s = \frac{\overline{|I_c(t)|^2}/2}{2eRP_{LO}B} = \frac{\eta P_s}{hfB}, \tag{3.33}$$

where we assume that the shot noise from LO is dominant as the noise source, and B is the receiver bandwidth at the IF stage. Noting the Nyquist limit

$$B = \frac{1}{T}, \tag{3.34}$$

where T is the bit duration, we find

$$\gamma_s = \frac{\eta P_s T}{hf} = \eta N_s, \tag{3.35}$$

where $N_s = P_s T / hf$ means the number of photons per bit.

However, the homodyne phase-diversity receiver can generate the complex amplitude given by Eqn (3.20) at the baseband. Therefore, the mean square of the signal photocurrent is given as $\overline{|I_c(t)|^2} = R^2 P_s P_{LO}$. When reconstructing the complex amplitude, we need to add shot noises due to the LO powers of $P_{LO}/2$ from the two ports. The receiver bandwidth at the baseband is $B/2 = 1/2T$; therefore, the total noise current is given as $eP_{LO}B$. We can thus obtain the SNR $\gamma_s = \eta P_s / hfB = \eta N_s$, which is the same as the heterodyne receiver. Even when the polarization diversity is introduced, signal processing called "maximal-ratio combining" can maintain the SNR. Details will be discussed in Section 3.3.

Finally, we point out the role of an optical preamplifier in the homodyne phase-diversity receiver. In our experiment described in Section 3.4, we employ an optical preamplifier in front of the receiver. This is because the LO shot-noise-limited receiver sensitivity cannot always be achieved due to the insufficient LO power as well as a relatively large circuit noise. If we use the optical preamplifier with an enough gain, the receiver noise is dominated by the ASE LO beat noise, which is larger than the LO shot noise. In the case of direct detection, the SNR is degraded by the noise figure $NF = 2n_{sp}$, where n_{sp} is the spontaneous emission factor ≥ 1, compared with the shot-noise limit. However, since in the homodyne phase-diversity receiver, the signal light is separated into two branches after preamplification, the SNR degradation is as small as n_{sp}. Therefore, the SNR is given as

$$\gamma_s = \frac{P_s T}{hf n_{sp}} = \frac{N_s}{n_{sp}}. \tag{3.36}$$

It should be noted that if the amplifier has the ideal noise characteristics $n_{sp} = 1$, the SNR is the same as the shot-noise-limited value, and that the SNR is independent of the quantum efficiency of the photodiode; thus, we find that the use of optical preamplification in the homodyne phase-diversity receiver is not harmful for maintaining the receiver sensitivity.

3.3 CONCEPT OF DIGITAL COHERENT RECEIVER

Outputs from the homodyne phase/polarization diversity receiver are processed by DSP circuits, restoring the complex amplitude of the signal in a stable manner

despite of fluctuations of the carrier phase and signal SOP. Hereafter, we call such receiver the digital coherent receiver. This section describes details of DSP.

3.3.1 Basic Concept of the Digital Coherent Receiver

Figure 3.4 shows the basic concept of the digital coherent receiver. First, the incoming signal is detected linearly with the homodyne receiver, comprising phase and polarization diversities. Using this receiver, we can obtain full information on the optical carrier, namely the complex amplitude and the SOP. This receiver features the vector demodulation architecture based on linear homodyne detection. Second, such information on the amplitude and phase, and the SOP of the carrier is converted to digital data with analog-to-digital converters (ADCs) and processed by DSP circuits. It should be noted that this receiver realizes the software-defined optical communication similar to the software radio owing to flexible DSP on the received complex amplitude and SOP.

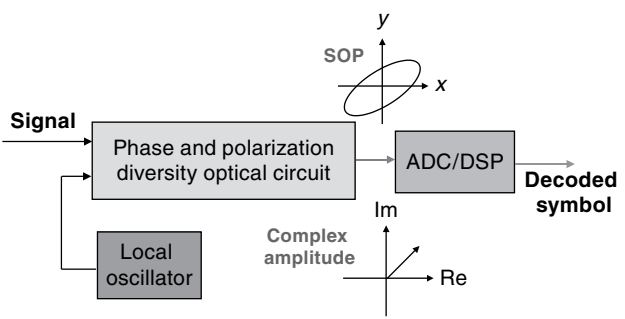

Figure 3.4 Basic concept of the digital coherent receiver (this figure may be seen in color on the included CD ROM).

3.3.2 Vector Modulation/Demodulation Architecture

The combination of the optical IQ modulator and the optical IQ demodulator realizes the linear optical communication system as shown in Figure 3.5. At the

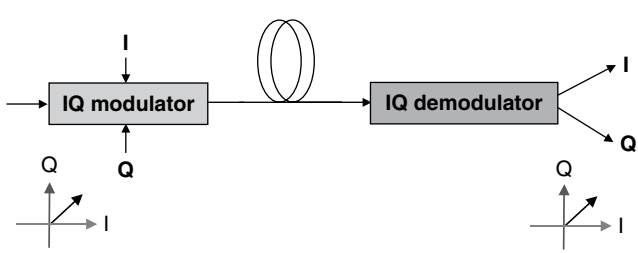

Figure 3.5 Linear optical communication systems based on vector modulation/demodulation scheme (this figure may be seen in color on the included CD ROM).

transmitter, we define a vector on the complex plane using two voltages driving the IQ modulator. This vector is mapped on the phasor of the optical carrier through the IQ modulator. Such optical IQ modulation is perfectly restored by IQ demodulation, which is performed by the digital coherent receiver. This is exactly the linear system, where IQ information is preserved even with E/O and O/E conversion processes.

3.3.3 Digital Signal Processing

The progress in the increased performance, speed, and reliability with reduction in size and cost of integrated circuits now makes DSP an attractive approach to recover the information from the baseband signal. The DSP circuit must operate the following sequence of operations to retrieve the information from the modulated signal as shown in Figure 3.6:

- Sampling and digitizing the analog signal by an ADC
- Clock extraction and resampling the digital signal
- Polarization alignment
- Equalization
- Estimation of the carrier phase
- Symbol discrimination.

The digital circuit optionally includes compensation functions to electronically equalize the received signal. Electronic equalization takes advantage of its fast adaptability and this advantage is inherent for future dynamic optical networks where new optical paths can be created or annihilated at any time. The adaptive equalization will be discussed in Section 3.5.

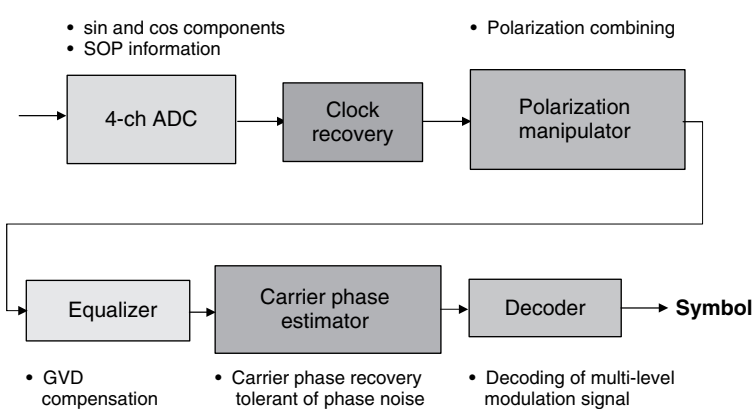

Figure 3.6 Concept of the digital signal processing (this figure may be seen in color on the included CD ROM).

3.3.4 Sampling of the Signal

When the PSK signal is coded on a RZ pulse train (return-to-zero phase-shift keying, RZ-PSK), we can realize accurate extraction of the clock from the transmitted signal, detecting the intensity of the received signal and using a standard clock recovery circuit. Photocurrents are then sampled and digitized by ADCs at the timing of the extracted clock. In this case, the digital circuit does not need to resample the data, so that it saves on the complexity of the digital circuit.

It is also possible to extract the clock from the sampled signal. The necessary conditions are that the sampling frequency must be equal or greater than twice the highest frequency. Once the samples are digitally converted, the digitized samples are interpolated in the time domain. When the PSK signal is on the RZ pulse train, we reconstruct the intensity waveform using

$$P(iT) = |I_{\mathrm{cx}}(iT)|^2 + \left|I_{\mathrm{cy}}(iT)\right|^2, \tag{3.37}$$

from which we can extract the clock. When the modulation format is non-return-to-zero phase-shift keying (NRZ-PSK), we need to differentiate $I_{cx,y}\,(iT)$ to detect edges of the NRZ waveform. After the clock is extracted, the interpolated data are resampled to keep one sample within a symbol interval.

3.3.5 Polarization Alignment

ADCs sample and digitize the four outputs $I_{\mathrm{PD1}}, \ldots, I_{\mathrm{PD4}}$ from the phase/polarization diversity receiver shown in Figure 3.3. The x- and y-polarization components of the complex amplitude of the signal are given from Eqns (3.29) and (3.30) as

$$\begin{aligned} I_{\mathrm{cx}}(iT) &= I_{\mathrm{PD1}}(iT) + jI_{\mathrm{PD2}}(iT) \\ &= R\sqrt{\frac{\alpha P_{\mathrm{s}}(iT)P_{\mathrm{LO}}}{2}}\exp j\{\theta_{\mathrm{s}}(iT) + \theta_{\mathrm{n}}(iT) + \delta\}, \end{aligned} \tag{3.38}$$

$$\begin{aligned} I_{\mathrm{cy}}(iT) &= I_{\mathrm{PD3}}(iT) + jI_{\mathrm{PD4}}(iT) \\ &= R\sqrt{\frac{(1-\alpha)P_{\mathrm{s}}(iT)P_{\mathrm{LO}}}{2}}\exp j\{\theta_{\mathrm{s}}(iT) + \theta_{\mathrm{n}}(iT)\}, \end{aligned} \tag{3.39}$$

where T denotes the sampling time interval and i the number of samples.

The left-hand side of Figure 3.7 shows the postprocessing circuit realizing the maximal-ratio polarization combining process [14]. We define the ratio $r(i)$ as

$$r(i) = I_{\mathrm{cx}}(iT)/I_{\mathrm{cy}}(iT). \tag{3.40}$$

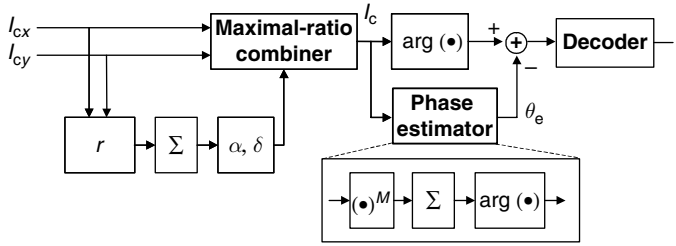

Figure 3.7 DSP circuit for polarization combiner and phase estimator.

Polarization parameters α and δ of the incoming signal vary much more slowly than the phase modulation. Therefore, by averaging $r(i)$ over many symbol intervals, it is possible to obtain accurate values of α and δ. The ratio $r(i)$ averaged over $2l+1$ samples is written as

$$r(i) = \frac{1}{2l+1} \sum_{j=-l}^{l} r(i+j), \tag{3.41}$$

and α and δ are calculated from

$$|r(i)| = \sqrt{\alpha}/\sqrt{\alpha - 1}, \tag{3.42}$$

$$\arg(r(i)) = \delta. \tag{3.43}$$

The signal complex amplitude, independent of SOP of the incoming signal, is then reconstructed by maximal-ratio combining as

$$\begin{aligned} I_c(iT) &= r^* I_{cx}(iT) + I_{cy}(iT) \\ &\propto \sqrt{\alpha} I_{cx}(iT) e^{\,j\delta} + \sqrt{1-\alpha} I_{cy}(iT) \\ &= E_s(iT). \end{aligned} \tag{3.44}$$

However, the above procedure is not effective when $\alpha \simeq 1$, because δ contains a large error and the term $r^* I_{cx}$ is not determined correctly. In such a case, we should use $I_c(iT) = I_{cx}(iT) + I_{cy}(iT)/r^*$ to reconstruct the signal complex amplitude more accurately. The term $|I_{cy}/r^*|$ is much smaller than $|I_{cx}|$, and hence the error in I_c is reduced. In summary, the reconstruction formula is given as

$$I_c(iT) = \begin{cases} r^* I_{cx}(iT) + I_{cy}(iT), & \alpha \le 0.5, \\ I_{cx}(iT) + \frac{I_{cy}(iT)}{r^*}, & \alpha > 0.5. \end{cases} \tag{3.45}$$

3.3.6 Phase Estimation

Since the linewidth of semiconductor distributed feedback (DFB) lasers used as the transmitter and LO typically ranges from 100 kHz to 10 MHz, the optical carrier phase $\theta_n(t)$ varies much more slowly than the phase modulation, whose symbol rate is 10 Gsymbol/s in the experiments described in Section 3.4. Therefore, by averaging the carrier phase over many symbol intervals, it is possible to obtain an accurate phase estimate. In the following, assuming the M-ary PSK modulation, we explain the phase-estimation procedure, but such procedure can easily be extended to quadrature amplitude modulation (QAM).

The phase of the complex amplitude obtained from Eqn (3.20) contains both the phase modulation $\theta_s(iT)$ and the phase noise $\theta_n(iT)$. The procedure to estimate θ_n is shown on the right-hand side of Figure 3.7. We take the Mth power of $I_c(iT)$, because the phase modulation is removed from $I_c(iT)^M$ in the M-ary PSK modulation format. Averaging $I_c(iT)^M$ over $2k+1$ samples constitutes a phase estimate as

$$\theta_e(iT) = \arg\left(\sum_{j=\ k}^{k} I_c((i+j)T)^M\right) \Big/ M. \tag{3.46}$$

The phase modulation $\theta_s(iT)$ is determined by subtracting $\theta_e(iT)$ from the measured phase of $\theta(iT)$. The phase modulation is then discriminated among M symbols.

The symbols thus obtained have the ambiguity because we cannot know the absolute phase. It is important to note that the data should be differentially precoded. By differentially decoding the discriminated symbol after symbol discrimination, we can solve the phase-ambiguity problem although the bit error rate is doubled by error multiplication.

The phase estimate $\theta_e(iT)$ ranges between π/M and $+\pi/M$. Therefore, if $|\theta_e(iT)|$ exceeds π/M, the phase jump of $2\pi/M$ occurs inevitably as shown in Figure 3.8. To cope with this problem, the correction for the phase jump is done as follows:

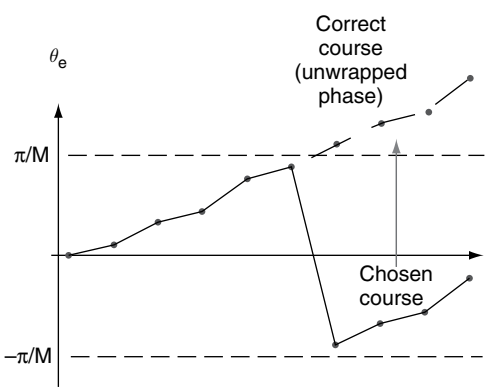

Figure 3.8 Phase jump during the phase estimation process (this figure may be seen in color on the included CD ROM).

$$\theta_e(iT) \leftarrow \theta_e(iT) + \frac{2\pi}{M} f(\theta_e(iT) - \theta_e((i-1)T)), \tag{3.47}$$

where $f(x)$ is defined as

$$f(x) = \begin{cases} +1 & \text{for} \quad x < -\frac{\pi}{M}, \\ 0 & \text{for} \quad |x| \le \frac{\pi}{M}, \\ -1 & \text{for} \quad x > \frac{\pi}{M}. \end{cases} \tag{3.48}$$

This adjustment ensures that the phase estimate follows the trajectory of the physical phase and cycle slips are avoided [15].

3.4 PERFORMANCE EVALUATION OF THE DIGITAL COHERENT RECEIVER

This section deals with evaluation of basic characteristics of the digital coherent receiver. After showing the optical circuit for the homodyne receiver comprising phase and polarization diversities, we discuss the receiver sensitivity limit, the polarization dependence of the receiver sensitivity, and the phase noise tolerance in M-ary PSK systems.

3.4.1 Optical Circuit for the Homodyne Receiver Comprising Phase and Polarization Diversities

The optical phase-diversity homodyne receiver that was used in our experiments is shown in Figure 3.9 [6]. The receiver uses free-space optical components packaged in a small metal case. Fiber pigtails are attached to input and output ports by using collimators (Coll.). Orthogonal states of polarization for the LO and the incoming signal create the 90° hybrid necessary for phase diversity. With the $\lambda/4$ waveplate

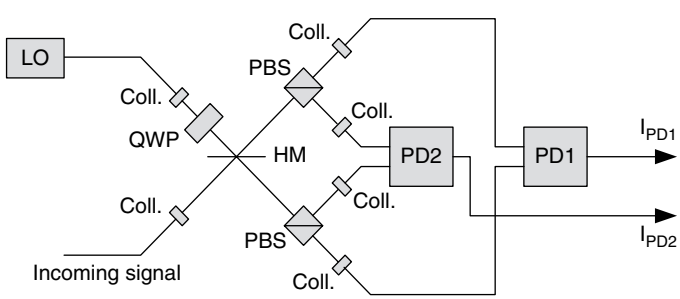

Figure 3.9 Optical circuit for the homodyne phase diversity receiver (this figure may be seen in color on the included CD ROM).

(QWP), the polarization of the LO becomes circular, while the signal remains linearly polarized and its polarization angle is 45° with respect to principal axes of the polarization beam splitters (PBSs). After passing through the half mirror (HM), the PBSs separate the two polarization components of the LO and signal while two balanced photodiodes PD1 and PD2 detect the beat between the LO and signal in each polarization. When the circularly polarized LO is split with a PBS, the phase difference between the split beams is 90°. In contrast, there is no phase difference between the split signal beams, because the signal is linearly polarized. Photocurrents from PD1 and PD2 are then given by Eqns (3.16) and (3.17).

The optical circuit for the homodyne phase/polarization diversity receiver is shown in Figure 3.10. In this receiver, two homodyne phase-diversity receivers are combined with the polarization diversity configuration. The receiver consists of a 2×8 free-space optical circuit packaged in a small metal case as shown by Figure 3.11 [14].

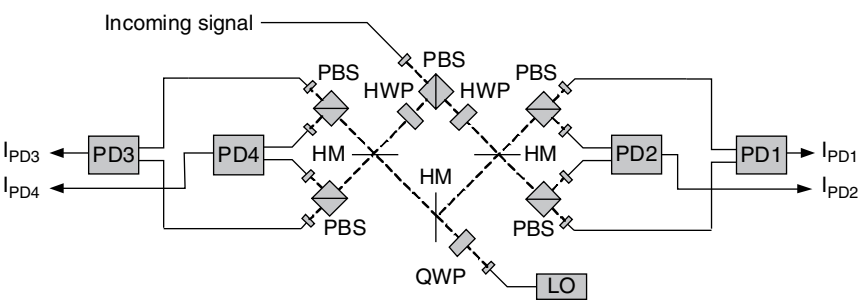

Figure 3.10 Optical circuit for the homodyne receiver employing phase and polarization diversities.

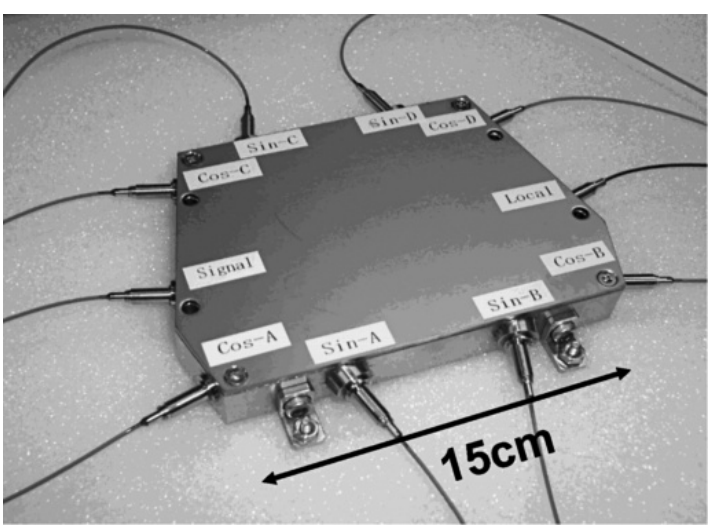

Figure 3.11 Photograph of the packaged receiver (this figure may be seen in color on the included CD ROM).

The incoming signal having an arbitrary SOP is separated into two polarization components with a PBS. We refer to the *x*- and *y*-polarizations with respect to the principal axes of the PBS. However, the LO is split into two paths with a HM, after its SOP is made circular by a QWP. Right- and left-hand sides of the receiver then constitute phase-diversity receivers for *x*- and *y*-polarizations, respectively. Photocurrents from PD1 PD4 are then given by Eqns (3.27) (3.30), respectively.

3.4.2 Receiver Sensitivity

The back-to-back bit error rate (BER) of the BPSK signal is measured to access the sensitivity of the homodyne phase-diversity receiver as follows. Data were precoded at the pulse pattern generator (PPG) such that differential decoding of the transmitted data resulted in a pseudo-random binary sequence (PRBS) (2^7 1). Lasers used as a transmitter and an LO were 1.55-μm DFB semiconductor lasers, whose linewidths were about 150 kHz. The laser temperature and bias current were carefully maintained via feedback control to keep frequency drifts of the lasers below 10 MHz. The transmitter laser output was modulated through a $LiNbO_3$ push pull modulator to generate a BPSK signal at a bit rate of 10 Gbit/s. The received power was adjusted with an attenuator and monitored with a power meter. The received signal was amplified with an EDFA to −10 dBm before it was detected with the coherent receiver. The maximum LO power was 10 dBm, which was determined from the allowable power of the photodiodes. The signals I_{PD1} and I_{PD2} were simultaneously sampled at a rate of 20 Gsample/s with ADCs. The 3-dB bandwidth of ADCs was 8 GHz. The BER measurement was performed offline. The collected samples were resampled to keep only one point per symbol and combined to form a 100-ksymbol-long stream. During phase estimation, we used the averaging span $k = 10$. The SOP of the signal was controlled manually so as to maximize the receiver sensitivity.

The number of errors was counted from these streams to determine the BER. Figure 3.12 shows BER measured as a function of the received power with and without optical preamplification. The power was measured before the preamplifier in the case with preamplification. The LO power is also changed when we do not use optical preamplification. The dotted curve is the theoretical one, which is calculated from the formula

$$P_e = \frac{1}{2}\mathrm{erfc}\left(\sqrt{\gamma_s}\right), \tag{3.49}$$

where erfc(*) means the complimentary error function and we assume the ideal SNR given as

$$\gamma_s = N_s = \frac{P_s T}{h\omega_s}. \tag{3.50}$$

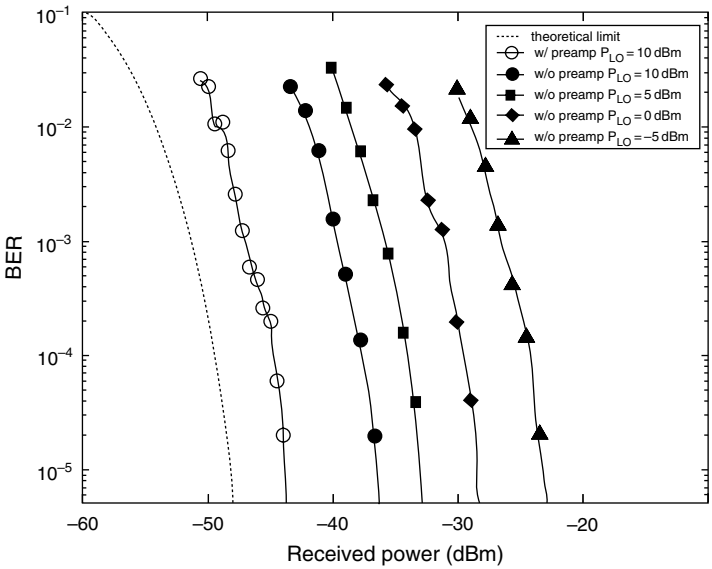

Figure 3.12 Bit error rates of BPSK signal measured by the digital coherent receiver with and without optical pre amplification.

Without optical preamplification, the increase in the LO power improves the receiver sensitivity; however, 10-dB power penalty still remains from the theoretical limit even at $P_{\mathrm{LO}} = 10$ dBm, because we cannot reach the shot-noise limit due to the relatively large circuit noise. On the other hand, with optical preamplification, power penalty is as small as 3 dB, which stems from the spontaneous emission factor larger than 1 and the 8-GHz receiver bandwidth larger than the Nyquist limit $1/2T = 5$ GHz.

3.4.3 Polarization Sensitivity

We evaluate the performance of our homodyne phase/polarization diversity receiver in the 10-Gbit/s binary PSK system. During DSP for polarization alignment and carrier phase estimation, we used $l = 10$ and $k = 10$, respectively.

We measured the BER offline from recorded 100-ksymbol data. Figure 3.13 shows BERs as a function of the received power before the preamplifier. While we change values of α ($= 0$, 0.25, 0.5, 0.75, 1), BER curves are almost independent of α. The power penalty is negligible compared with the case where we do not employ polarization diversity but align the signal SOP optimally ($\alpha = 0$, 1). Thus, we find that our receiver is insensitive to the polarization fluctuation of the incoming signal.

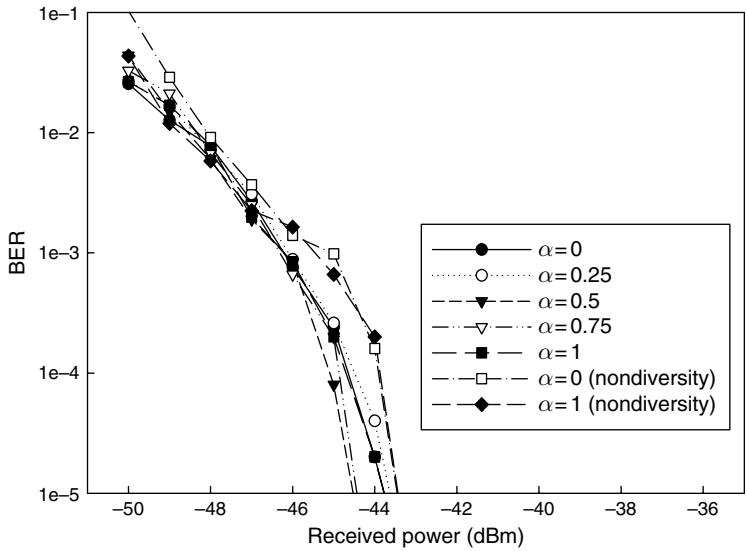

Figure 3.13 BER curves with and without polarization diversity.

3.4.4 Phase-noise Tolerance

The requirement for the laser linewidth in M-ary PSK systems becomes much more stringent as M increases. To evaluate the BER performance of the homodyne phase-diversity receiver for the 8-PSK case, we conduct a computer simulation where the phase-noise variance σ_p^2 and the phase-estimation span k are used as parameters [7]. We assume that the laser phase noise accumulated during a symbol interval T has a Gaussian distribution with the variance $\sigma_p^2 = 2\pi(\delta f_s + \delta f_{LO})T$, where δf_s and δf_{LO} denote 3-dB linewidths of the transmitter and LO, respectively, and that signals are contaminated by additive white Gaussian noise.

Figure 3.14 shows the simulated BER performance of 8-PSK systems calculated as a function of the SNR per bit when $\sigma_p = 0$, 1.4×10^{-2} and 4.3×10^{-2}, together with the ideal performance assuming perfect carrier recovery. For comparison, simulated BERs of the differential demodulation scheme are also shown in Figure 3.14. For 10-Gsymbol/s systems, σ_p of 1.4×10^{-2} gives a linewidth of $\delta f = 150$ kHz for either transmitter or LO laser, and σ_p of 4.3×10^{-2} does 1.5 MHz. Without phase noise, the BER performance of the phase-estimation method approaches the ideal performance when k becomes larger; therefore, our phase-estimation method is very effective for obtaining a noiseless accurate phase reference. In contrast, differential demodulation incurs a nearly 3-dB penalty in the SNR, because the reference phase has the same amount of noise as the target phase. As far as the carrier phase is relatively constant over the duration of $(2k + 1)T$, the phase estimation provides excellent performance. When $\sigma_p = 1.4 \times 10^{-2}$, the phase estimation is still efficient

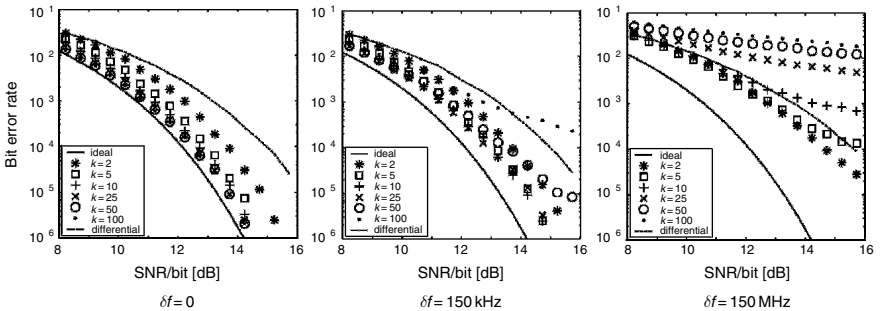

Figure 3.14 Simulation results on BER performance in 8 PSK systems for three cases, i.e., the ideal homodyne scheme without phase noise, the differential detection, and the homodyne detection with phase estimation (k 2, 5 10, 25, 100), as a function of the SN ratio per bit.

and the SNR penalty is less than 1 dB at BER $= 10^{-6}$ for $k = 5$, 10, and 25. However, the phase-noise increase gradually neutralizes the advantage of phase estimation compared to differential demodulation. This is because the phase difference between the first and last samples of $(2k + 1)$ samples becomes significant. For example, in the case of $\sigma_p = 4.3 \times 10^{-2}$, the error floor appears even when $k = 5$, and the merit of phase estimation is small. Also note that independently of σ_p, the BER performance when $k = 0$ is identical to that of differential detection. These results indicate that if the laser linewidth is as low as 150 kHz, the acceptable performance in 8-PSK systems is obtained by the optimal choice of $k = 10$. These parameter values are used in the experiment described in the next section.

3.4.5 Coherent Demodulation of Optical *M*-ary Phase-Shift Keying Signals

We demonstrate coherent demodulation of optical M-ary PSK signals [7]. Since the carrier phase is estimated accurately through DSP after phase-diversity homodyne detection, the system performance is highly tolerant to the carrier phase noise. By using DFB semiconductor lasers with linewidths of 150 kHz as a transmitter and a LO, BPSK ($M = 2$), QPSK ($M = 4$), and 8-PSK ($M = 8$) signals are successfully demodulated at the symbol rate of 10 Gsymbol/s.

Figure 3.15 shows experimental setup for demodulating optical 8-PSK signals. The optical 8-PSK signal was obtained with a $LiNbO_3$ IQ modulator and a phase modulator. The IQ modulator generated QPSK signals and the subsequent phase modulator gave an additional phase shift of either 0 or $\pi/4$ during the symbol interval that was synchronized to the QPSK modulation. The PPG was programmed to generate a set of three 10-Gbit/s precoded data streams such that three independent pseudo-random bit sequences were obtained after differential

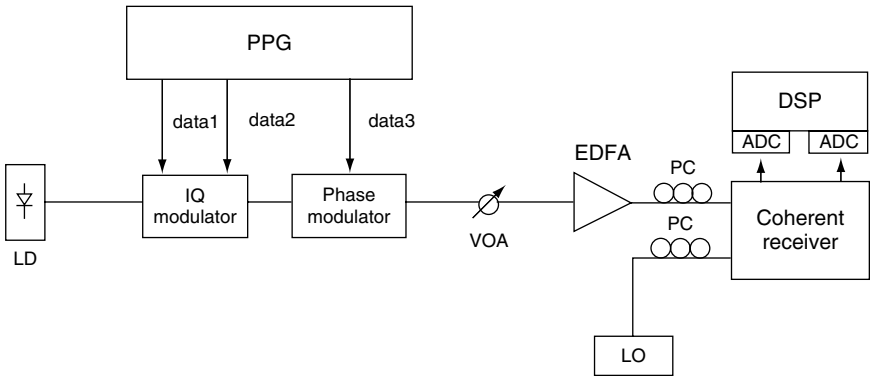

Figure 3.15 Experimental setup for 8 PSK modulation and demodulation.

decoding. Transmission loss was emulated by a variable optical attenuator. The received signal was optically preamplified and fed into the homodyne phase-diversity receiver shown in Figure 3.9. We measured the BERs offline from recorded 100-ksymbol data after carrier phase estimation, where $k = 10$, and symbol discrimination. For comparison, we measured BERs of BPSK and QPSK signals in a similar manner, where modulators were replaced with a single-phase modulator and a single IQ modulator, respectively.

Figure 3.16 shows the BERs measured as a function of the received power for 10-Gsymbol/s BPSK, QPSK and 8-PSK. In comparing the performance of QPSK

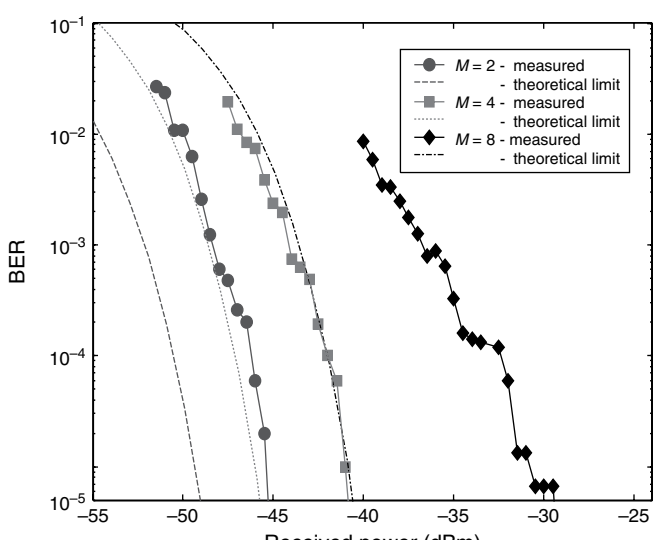

Figure 3.16 BER characteristics for BPSK, QPSK, and 8 PSK systems (this figure may be seen in color on the included CD ROM).

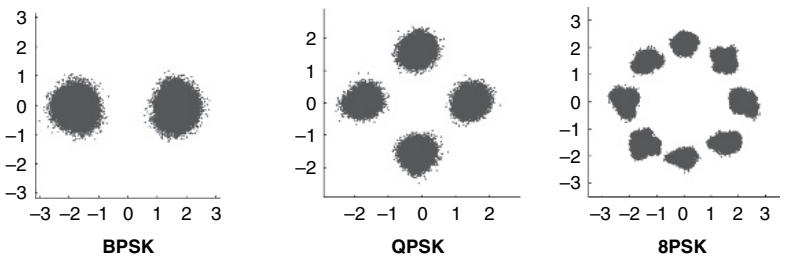

Figure 3.17 Constellation map for the *M* ary PSK signal (this figure may be seen in color on the included CD ROM).

and 8 PSK with BPSK, power penalties measured at BER $= 10^{-5}$ are 4 and 15 dB, respectively. When the phase noise is negligible and the symbol rate is kept constant, the theoretical power penalty of *M*-ary PSK relative to BPSK is given as $1/\sin^2(\pi/M)$, which are 3 and 8.3 dB for QPSK and 8-PSK, respectively. In the case of 8-PSK, considering the 1-dB penalty due to the phase noise, we find that our experiment still includes a 5.7-dB excess penalty. The distribution of the complex amplitude of the received signal in the error-free state is depicted in Figure 3.17. Compared to BPSK and QPSK, we find that the constellation map of 8-PSK is disordered due to imperfect 8-PSK modulation, which stems from the timing error and waveform difference between IQ modulation and subsequent phase modulation. Such imperfect 8 PSK modulation seems the main cause of the excess penalty.

3.5 POST-PROCESSING FUNCTIONS

Coherent detection can linearly recover the amplitude and phase information of optical signals. Therefore, any transfer functions acting on the optical complex amplitude can be realized at the baseband stage after detection. In this section, we discuss some examples of the postprocessing functions.

3.5.1 WDM Channel Demultiplexing

When the LO wavelength is set to the wavelength λ_n of a WDM channel, as shown in Figure 3.18, the channel at a wavelength $\lambda_{(n+1)}$ will overlap the channel at a wavelength $\lambda_{(n-1)}$ in the spectral domain, but the channel at the selected wavelength λ_n will not be overlapped by any other wavelength channel. Therefore, the two electrical signals I_{PD1} and I_{PD2} can be lowpass filtered to demultiplex the selected wavelength from the incoming signal. The system can benefit from the sharp cutoff characteristics of

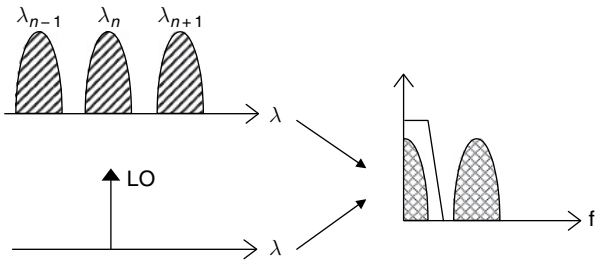

Figure 3.18 Optical spectra of WDM channels and electrical spectrum of the homodyne detected signal.

electrical filters, without the need for any optical filter to filter out the adjacent wavelength channels. Dense wavelength-division multiplexing (DWDM) QPSK transmission experiments are presented in Section 3.6.

3.5.2 OTDM Channel Demultiplexing

We next consider the optical time-division multiplexed (OTDM) system. Figure 3.19 shows the temporal relations between the base-clock pulse train and the OTDM signal, where IQ modulation is encoded on RZ pulses.

Spectra of the base-clock pulse and the OTDM signal must be overlapped so that the OTDM signal is homodyne-detected with the base-clock pulse train. In the time domain, on the other hand, the base-clock pulses are overlapped by one of the tributaries of the OTDM signal as shown in Figures 3.19 (a) and (b). Since

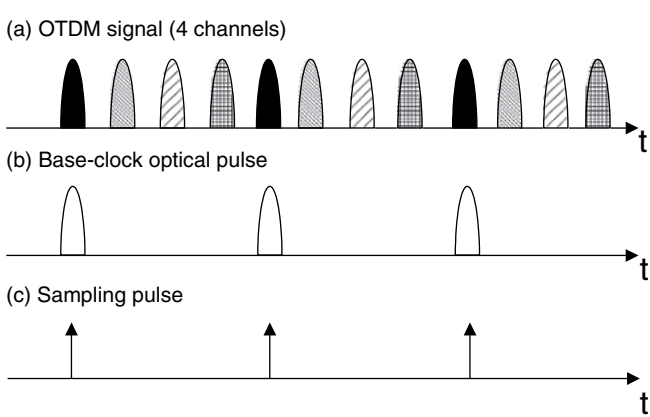

Figure 3.19 Temporal relation among (a) the OTDM signal, (b) base clock pulse train, and (c) sampling pulses, when our proposed receiver demultiplexes the OTDM signal.

the homodyne signals I_{PD1} and I_{PD2} contain only the beat between the OTDM signal and the base-clock pulse, we can demultiplex the OTDM signal. I_{PD1} and I_{PD2} are then sampled at the base-clock frequency [Figure 3.19 (c)], giving us the information on the complex amplitude of the demultiplexed tributary.

3.5.3 Group-Velocity Dispersion Compensation

Since the restored complex amplitude $E(t)$ contains the information on the amplitude and phase of the optical signal, the group-velocity dispersion (GVD) of the fiber for transmission can be compensated after detection. The transfer function of the fiber with GVD $= \beta_2$ is written as

$$T(\omega_m) = \exp\left(-\frac{j}{2}\beta_2 L\omega_m^2\right), \tag{3.51}$$

where ω_m stands for the modulation sideband frequency and L the transmission distance. Therefore, the transversal filter shown in Figure 3.20, which has the inverse transfer function of Eqn (3.51), can perform GVD compensation. The tap spacing is equal to the sampling interval $T/2$, where T denotes the symbol interval. We represent the received complex amplitude as $I_c(nT)$, where n is the number of the samples. The function of the transversal filter is given as

$$I_{eq}(nT) = \sum_{k=0}^{N\ 1} C_k I_c[(n-k)T], \tag{3.52}$$

where $I_{eq}(nT)$ is the complex amplitude of the output, C_k are complex tap weights, and N denotes the number of taps. Theoretically, with a sufficient number of taps, this filter can compensate for any amount of chromatic dispersion.

We performed the GVD compensation experiment using the digital coherent receiver [8]. The fiber for transmission was a 200-km standard single-mode fiber

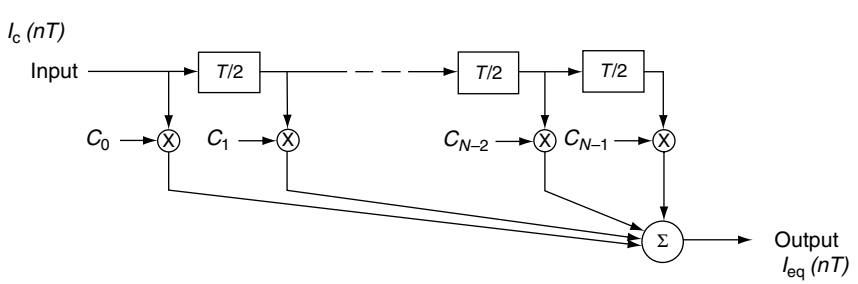

Figure 3.20 Configuration of the transversal filter for GVD compensation.

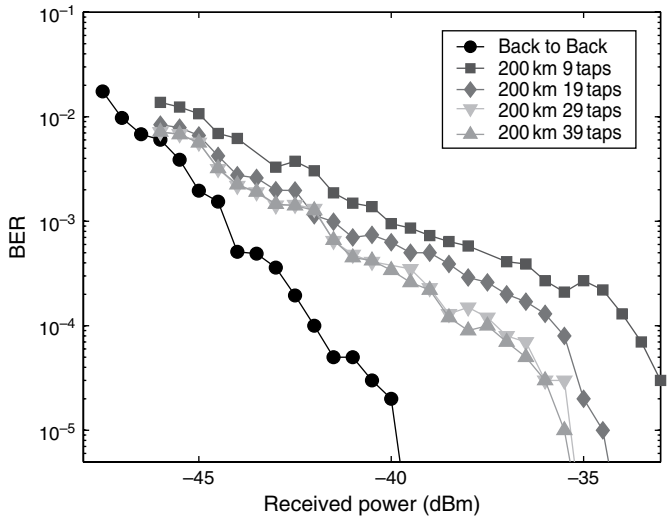

Figure 3.21 BERs measured as a function of the received power after transmission through a 200 km SMF (this figure may be seen in color on the included CD ROM).

(SMF) with the dispersion value of $D = 20$ ps/nm/km ($\beta_2 = -25$ ps^2/km). From the measured GVD value, we determined the tap coefficients of the transversal filter.

Figure 3.21 shows measured BER of the 20-Gbit/s QPSK signals, when the fiber dispersion is compensated with various filters. For comparison, the back-to-back BER is also shown in Figure 3.21. We find that 39 taps are sufficient to compensate for dispersion values of 4000 ps/nm. Although chromatic dispersion is thus compensated to significant degree, power penalties of about 5 dB still remain after transmission of 200-km distance. This penalty may stem from the nonlinear distortion due to the relatively large input power and nonideal filter coefficients.

Figure 3.22 shows the distribution of the complex amplitude of the received signal after 200-km transmission with and without dispersion compensation. The received power is -35.0 dBm in both the cases. Without dispersion compensation, the constellation diagram is heavily distorted and we cannot recover the information at all as shown in Figure 3.22 (a); however, Figure 3.22 (b) shows that we can obtain the constellation diagram clearly separated into four phase states using the filter with 39 taps.

From these experimental results, we confirm that even a simple transversal filter implemented in our coherent receiver can compensate for chromatic dispersion of up to 4000 ps/nm. By using coherent detection in conjunction with DSP, the QPSK transmission system has excellent tolerance toward the chromatic dispersion.

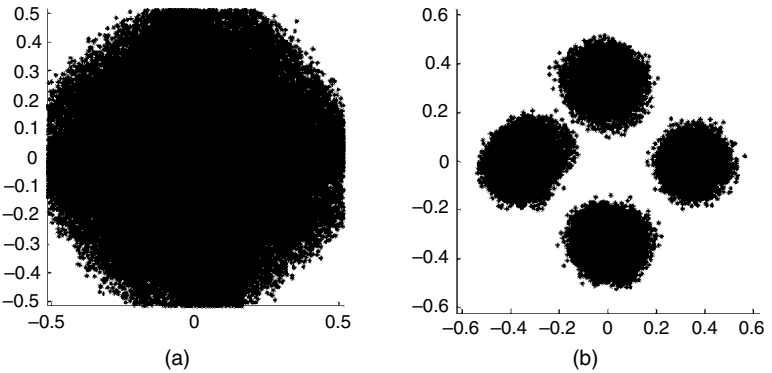

Figure 3.22 Complex amplitudes of the received signal after 200 km transmission: (a) without dispersion compensation and (b) with dispersion compensation (this figure may be seen in color on the included CD ROM).

3.5.4 Adaptive Equalization Techniques

Even if we do not know the origin of transmission impairments, it is possible to equalize the transmitted signal using adaptive filters. Figure 3.23 shows the basic construction of the adaptive equalization circuit [16]. Four transversal filters h_{xx}, h_{xy}, h_{yx}, h_{yy} with complex tap coefficients $C_{xx}(k)$, $C_{xy}(k)$, $C_{yx}(k)$, $C_{yy}(k)$, respectively, are implemented in the butterfly configuration behind the phase/polarization-diversity receiver. The output complex amplitudes $I'_{\mathrm{cx,cy}}$ are given as

$$\begin{aligned} I'_{\mathrm{cx}}(nT) &= \sum_{k=0}^{N-1} \left\{ C_{xx}(k) I_{\mathrm{cx}}[(n-k)T] + C_{xy}(k) I_{\mathrm{cy}}[(n-k)T] \right\} \\ I'_{\mathrm{cy}}(nT) &= \sum_{k=0}^{N-1} \left\{ C_{yx}(k) I_{\mathrm{cx}}[(n-k)T] + C_{yy}(k) I_{\mathrm{cy}}[(n-k)T] \right\} \end{aligned} \quad . \tag{3.53}$$

For the polarization-multiplexed QPSK signal, blind equalization is demonstrated by using the Godard algorithm [17], where the tap coefficients are modified

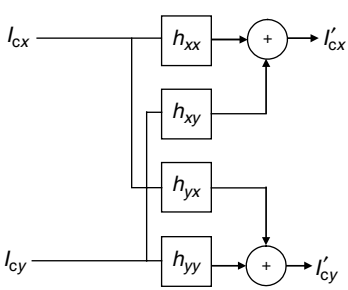

Figure 3.23 Schematic representation of adaptive transversal filters in the butterfly configuration.

iteratively so that normalized intensities of equalized outputs converge to unity. Using this algorithm, we can compensate for chromatic dispersion and polarization-mode dispersion simultaneously. This method is very effective for compensating for time-varying dispersion values.

3.6 WAVELENGTH-DIVISION MULTIPLEXED QUADRATURE PHASE-SHIFT KEYING TRANSMISSION EXPERIMENTS

We report 1000-km transmission of DWDM copolarized 20-Gbit/s NRZ-QPSK signals with high spectral efficiency of 1.05 bit/s/Hz, using a digital homodyne receiver that has sharp cutoff characteristics relying on electrical filters for wavelength-channel demultiplexing [18]. The use of this receiver also enables us to investigate transmission impairments caused by self-phase modulation (SPM) and cross-phase modulation (XPM) on the optical complex amplitude. We find that spectral efficiency for the long-haul DWDM system is mainly limited by the XPM between the DWDM channels.

3.6.1 Advantages of Digital Coherent Receiver for DWDM Transmission

Recently, multilevel coding based on IQ modulation such as optical QPSK, QAM, and amplitude-phase-shift keying has attracted increased attention for spectral efficiency beyond 1 bit/s/Hz, which is the limit of conventional on-off keying. With polarization multiplexing and optical prefiltering, improved results of spectral efficiency above 3 bit/s/Hz have been obtained for transmission length of several hundred kilometers covering metro systems [19].

DWDM has become a suitable technique for taking full advantages of the increased spectral efficiency of the multilevel coding. Optical demultiplexers consisting of cascaded optical filters followed by optical delay detectors have been commonly employed for IQ demodulation of DWDM signals [20]; however, cascaded filters inevitably introduce demultiplexing impairments because these filters usually have insufficient cutoff characteristics and GVD. In contrast, the digital coherent receiver relies on sharp cutoff characteristics of electrical filters for channel demultiplexing [5], and will be the best solution to cope with the filtering impairments.

In long-haul ($>$1000 km) DWDM systems, the transmission performance is ultimately limited by inter-symbol interference due to tight filtering of each channel, crosstalk between adjacent channels due to the narrow channel spacing, XPM between the closely spaced channels through fiber nonlinearity, and phase fluctuation induced by SPM in each channel. Compared to the existing delay-line

receiver, the digital homodyne receiver enables us to analyze conveniently transmission impairments mentioned above because phase and intensity information of the received signal is linearly mapped on the IQ vector space.

We introduce the digital homodyne receiver with a 3-dB bandwidth of 8 GHz to demultiplex 20-Gbit/s QPSK DWDM channels. By using this receiver, transmission impairments caused by SPM and XPM are diagnosed and the appropriate system parameters are determined. On the basis of this result, we elucidate the channel spacing limit in a dispersion-managed 1000-km link, and achieve the spectral efficiency as high as 1.05 bit/s/Hz.

3.6.2 Experimental Setup

The experimental setup is shown in Figure 3.24. At the transmitter, six distributed-feedback laser diodes (DFB-LD) were separated to even and odd channels, multiplexed with a fiber coupler, and modulated by a $LiNbO_3$ optical IQ modulator. The IQ modulator was used to form each 20-Gbit/s QPSK signal from pre-coded two 10-Gsymbol/s data streams with $2^7 - 1$ PRBS. 10-Gsymbol/s electrical signals

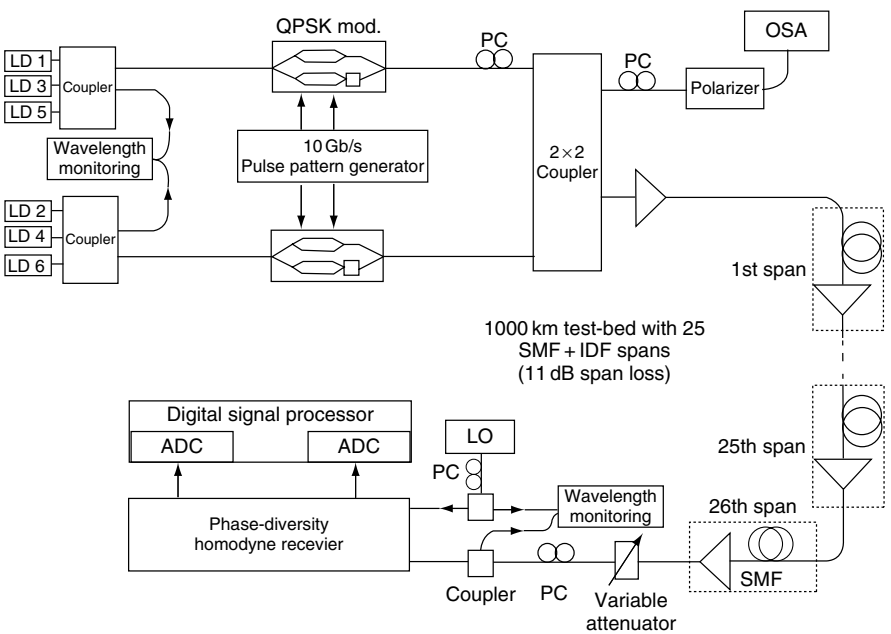

Figure 3.24 Experimental setup for 1000 km DWDM QPSK transmission. LD: laser diode, PC: polarization controller, SMF: single mode fiber, IDF: inverse dispersion fiber, LO: local oscillator, ADC: analog to digital converter.

were band limited by 7.5-GHz electrical filters for pre-filtering, generating a 15-GHz optical spectrum of each channel. Then even and odd channels were launched on the link with a 2×2 optical coupler. All the channels were made co-polarized by a polarization controller (PC). The transmission line consisted of 26 spans with a total length of 1074 km and 980-nm pumped EDFAs. Each span was composed of a 28-km-long large effective area fiber with dispersion of 21 ps/nm/km and a 12-km-long inverse dispersion fiber (IDF) with dispersion of -54 ps/nm/km, resulting in a span loss of 11 dB. In the final span, a 74-km-long SMF was used to compensate for the residual dispersion.

We employed a digital coherent receiver for demultiplexing WDM channels and decoding symbols [5]. Since the 3-dB bandwidth of the receiver was 8 GHz, the QPSK DWDM channels with 15-GHz bandwidths were almost ideally demultiplexed without any power penalty. The restored IQ data were sampled and digitized by 8-bit AD converters. The linewidth of the transmitters and the LO was about 150 kHz. Channel frequencies were stabilized below 3 MHz by monitoring the beat frequencies between the transmitters and the LO. The BER was measured offline. The receiver sensitivity was evaluated at BER $= 10^{-4}$ by assuming the use of forward error correction (FEC).

3.6.3 Single-channel Transmission

Figure 3.25 shows the receiver sensitivity at BER $= 10^{-4}$ and OSNR degradation as a function of the launched power for single-channel transmission. Sensitivity measurements were made on the fourth channel at 1551.71 nm. OSNR was measured in 0.07-nm OSA resolution.

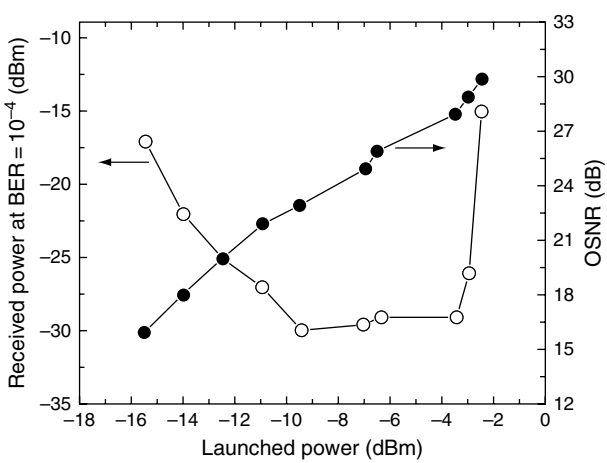

Figure 3.25 Receiver sensitivity at BER 10^{-4} and OSNR for single channel transmission as a function of the launched power.

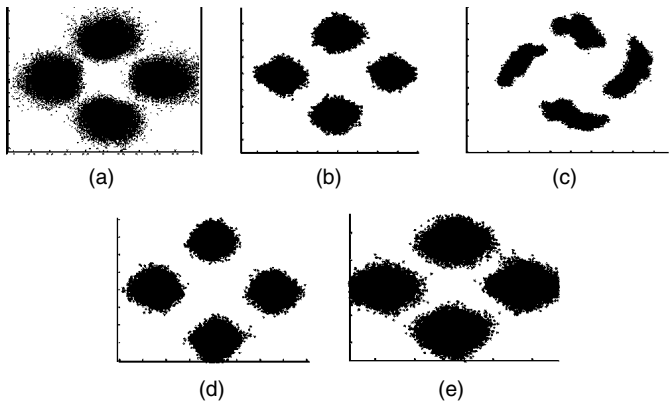

Figure 3.26 Constellation maps. Launched power of (a) 15.5 dBm, (b) 9.5 dBm, and (c) 2.5 dBm for single channel transmission. Channel spacing of (d) 43 GHz and (e) 19 GHz at 9.5 dBm/ch for six channel transmission.

In the lower power side, transmission performance is affected by OSNR degradation. In contrast, receiver sensitivity rapidly decreases above a launched power of −3 dBm. This is due to the SPM-induced phase shift converted from amplitude fluctuations, which originate from the IQ modulation process. For NRZ-QPSK signals produced by a Mach Zehnder modulator, amplitude dips occur only at π-phase transitions. Therefore, GVD-induced amplitude fluctuation caused by the pattern effect raises the nonlinear phase shift.

Figure 3.26 (a) (c) shows the constellation maps when launched powers are −15.5, −9.5, and −2.5 dBm, respectively. We can clearly see the OSNR degradation in (a), the nonlinear phase shift in (c), and the most compact distribution in (b).

3.6.4 DWDM Transmission

In DWDM transmission experiments, the power launched on the fiber was set to −9.5 dBm per channel (OSNR: 22 dB) to minimize the power penalty for single-channel transmission.

Figure 3.27 shows the receiver sensitivity against channel spacing for the six-channel transmission. In back-to-back measurements, almost no performance degradation is observed when channel spacing is larger than about 21 GHz. At narrower channel spacing, the performance is degraded by crosstalk between adjacent channels.

In the long-haul DWDM system, GVD-induced amplitude fluctuations of the adjacent channels contribute significantly to phase fluctuations through XPM and limit the minimum channel spacing. When six channels are transmitted over 1074 km, we obtain the channel spacing limit as narrow as 19 GHz, which is

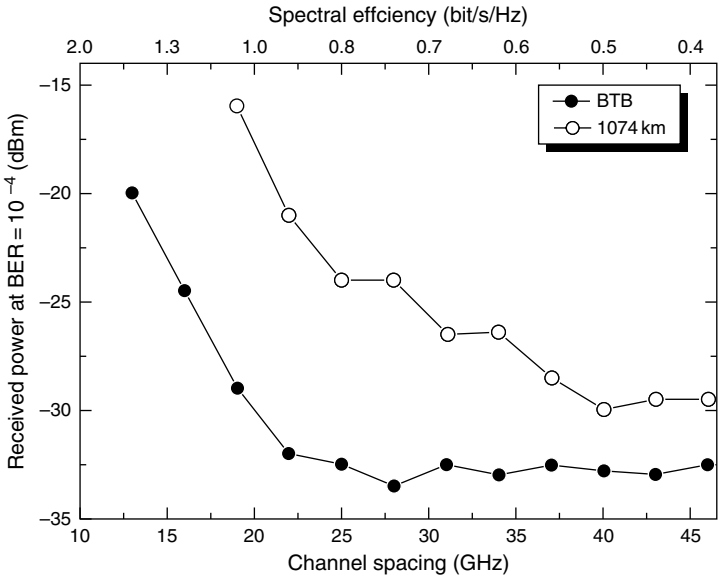

Figure 3.27 Receiver sensitivity at BER 10^{-4} for six channel transmission as a function of the channel spacing.

determined from XPM-induced phase fluctuations. The spectral efficiency reaches 1.05 bit/s/Hz in this case. Such nonlinear phase fluctuations due to the XPM effect impose a serious transmission penalty as channel spacing is decreased. This is because of the reduction of the walk-off parameter, which is defined as the difference in the group delay per length between DWDM channels.

Figures 3.26 (d) and (e) show the constellation maps, when channel spacing is 43 and 19 GHz, respectively, measured at the launched power of −9.5 dBm/ch. We find that the symbol distribution is seriously broadened through XPM as channel spacing decreases.

3.7 CONCLUSION

We have investigated the digital coherent receiver, where the carrier phase is estimated with DSP, alleviating locking the phase of the LO to the carrier phase in the conventional homodyne receiver. We have found that the phase noise of state-of-the-art semiconductor DFB lasers is substantially small such that an accurate phase estimate can be obtained from the sampled signal in order to demodulate *M*-ary PSK signals up to eight phase states at the symbol rate of 10 Gsymbol/s. Using our receiver, we have experimentally demonstrated WDM QPSK transmission. GVD of fibers for transmission is also compensated for by the postprocessing function of the receiver.

The next step is to develop dedicated integrated circuits for real-time operation of the receiver. The real-time operation has already been demonstrated at a few

Gsymbol/s, and 10-Gsymbol/s operations will appear very soon. The born again digital coherent technology seems to have enormous potential for innovating future optical communication systems.

REFERENCES

[1] T. Okoshi and K. Kikuchi, "*Coherent Optical Fiber Communications,*" Boston, Kluwer Academic Publishers, 1988.

[2] J. Kahn and K. P. Ho, "Spectral efficiency limits and modulation/detection techniques for DWDM systems," *IEEE J. Sel. Top. Quantum Electron.*, 10(2), 259 272, 2004.

[3] R. Griffin and A. Carter, "Optical Differential Quadrature Phase Shift Key (oDQPSK) for High Capacity Optical Transmission," in Proc. *OFC 2002*, paper WX6, Anaheim, CA, USA, March 17 22, 2002.

[4] S. Shimotsu, S. Oikawa, T. Saitou et al., "Single side band modulation performance of a $LiNbO_3$ integrated modulator consisting of four phase modulator waveguides," *IEEE Photonics Technol. Lett.*, 13(4), 364 366, 2001.

[5] S. Tsukamoto, D. S. Ly Gagnon, K. Katoh, and K. Kikuchi, "Coherent Demodulation of 40 Gbit/s Polarization Multiplexed QPSK signals with 16 GHz Spacing after 200 km Transmission," in Proc. *OFC 2005*, paper PDP29, Anaheim, CA, March 7 12, 2005.

[6] K. Kikuchi, "Phase diversity homodyne detection of multi level optical modulation with digital carrier phase estimation," *IEEE J. Sel. Top. Quantum Electron.*, 12(4), 563 570, 2006.

[7] S. Tsukamoto, K. Katoh and K. Kikuchi, "Coherent demodulation of optical multilevel phase shift keying signals using homodyne detection and digital signal processing," *IEEE Photon. Technol. Lett.*, 18(10), 1131 1133, 2006.

[8] S. Tsukamoto, K. Katoh and K. Kikuchi, "Unrepeated transmission of 20 Gbit/s optical quadrature phase shift keying signal over 200 km standard single mode fiber based on digital processing of homodyne detected signal for group velocity dispersion compensation," *IEEE Photon. Technol. Lett.*, 18(9), 1016 1018, 2006.

[9] M. Taylor, "Coherent detection method using DSP for demodulation of signal and subsequent equalization of propagation impairments," *IEEE Photon. Technol. Lett.*, 16(2), 674 676, 2004.

[10] H. Bülow, "Electronic Dispersion compensation," in Proc. *OFC 2007*, paper OMG5, Anaheim, CA, March 25 29, 2007.

[11] A. Leven, N. Kaneda, U. V. Koc, and Y. K. Chen, "Coherent Receiver for Practical Optical Communication Systems," in Proc. *OFC 2007*, paper OThK4, Anaheim, CA, March 25 29, 2007.

[12] H. Hodgikinson, R. A. Harmon, and D. W. Smith, "Demodulation of optical DPSK using in phase and quadrature detection," *Electron Lett.*, 21, 867 868, 1985.

[13] F. Derr, "Optical QPSK Transmission system with novel digital receiver concept," *Electron Lett.*, 23(23), 2177 2179, 1991.

[14] S. Tsukamoto, Y. Ishikawa, and K. Kikuchi, "Optical Homodyne Receiver Comprising Phase and Polarization Diversities with Digital Signal Processing," in Proc. *ECOC 2006*, paper Mo4.2.1, Cannes, France, September 24 28, 2006.

[15] R. Noé, "Phase Noise Tolerant Synchronous QPSK Receiver Concept with Digital I&Q Baseband Processing," in Proc. *OECC 2004*, Paper 16C2 5, Yokohama, Japan, July 12 16, 2004.

[16] S. J. Savoy, G. Gavioli, R. I. Killey, and P. Bayvel, "Transmission of 42.8 Gbit/s Polarization Multiplexed NRZ QPSK over 6400 km of Standard Fiber with no Optical Dispersion Compensation," in Proc. *OFC 2007*, paper OTuA1, Anaheim, CA, March 25 29, 2007.

[17] D. N. Godard, "Self recovering equalization and carrier tracking in two dimensional data com munication systems," *IEEE Trans. on Commun.*, COM 28(11), 18671875, 1980.

[18] S. Y. Kim and K. Kikuchi, "1000 km Transmission of 20 Gbit/s QPSK NRZ Co Polarized DWDM Signals with Spectral Efficiency of 1 bit/s/Hz using Coherent Detection," in Proc. *OFC 2007*, paper OThS4, Anaheim, CA, March 25 29, 2007.

[19] A. H. Gnauck, P. J. Winzer, L. L. Buhl et al., "12.3 Tb/s C band DQPSK Transmission at 3.2 b/s/Hz Spectral Efficiency," in Proc. *ECOC 2006*, paper Th4.1.2, Cannes, France, September 24 28, 2006.

[20] C. Wree, M. Serbay, and W. Rosenkranz, "Towards 1.6 b/s/Hz Spectral Efficiency by Strong Optical Filtering of RZ DQPSK," in Proc. *ECOC 2003*, paper We4.P.126, Rimini, Italy, Septem ber 21 25, 2003.

This page intentionally left blank

4

Self-coherent optical transport systems

Xiang Liu, Sethumadhavan Chandrasekhar, and Andreas Leven

Bell Laboratories, Alcatel-Lucent, Holmdel, NJ, USA

4.1 INTRODUCTION

Self-coherent optical transmission based on differential phase-shift keying (DPSK) and direct detection [1–4] has emerged as an attractive vehicle for supporting high-speed optical transport networks by offering lower requirements on optical signal-to-noise ratio (OSNR) and higher tolerance to system impairments such as fiber nonlinear effects and coherent crosstalk, as compared to traditional on-off keying (OOK)-based transmission. Multilevel DPSK formats such as differential quadrature phase-shift keying (DQPSK) additionally offer high spectral efficiency and high tolerance to chromatic dispersion (CD), polarization mode dispersion (PMD), and optical filtering, particularly when polarization-division multiplexing (PMUX) is also applied.

Self-coherent signals are commonly received by differential direct detection that does not need an optical local oscillator as required in coherent detection. With the help of high-speed analog-to-digital conversion (ADC) and digital signal processing (DSP) following the differential direct detection, the phase and even the field of a received optical signal can be digitally reconstructed in such a digital *self-coherent* optical receiver (DSCOR). Digital *coherent* optical receivers are covered in depth in Chapter 3 "Coherent Optical Communication Systems" by K. Kikuchi. Adaptive equalization of transmission impairments such as nonlinear phase noise, CD, and PMD could then be subsequently performed. These new capabilities bring opportunities to make transport systems more versatile, flexible, and ultimately cost-effective. With advances in high-speed electronic circuits, self-coherent optical transport systems are expected to find a wide range of applications to meet the ever-increasing demand of capacity upgrade and cost reduction in future optical networks.

This chapter is organized as follows. In Section 4.2, we briefly discuss historical perspectives and current demand in optical transport systems, and review

Optical Fiber Telecommunications V B: Systems and Networks

ISBN: 978 0 12 374172 1

self-coherent optical modulation formats such as binary DPSK (DBPSK), DQPSK, and DPSK in combination with amplitude shift keying (ASK) and polarization multiplexing. Section 4.3 describes the principle of differential direct-detection, particularly orthogonal differential direct detection for multilevel DPSK. Section 4.4 presents the principle and implementation of digital self-coherent receiver that couples orthogonal differential direct-detection with ADC and DSP. Digital field reconstruction and data-aided multisymbol phase estimation (MSPE) will be discussed. Section 4.5 introduces adaptive equalization techniques that can be commonly used in digital self-coherent receiver as well as digital coherent receiver to compensate or mitigate transmission impairments. Section 4.6 briefly reviews the start-of-the-art applications of self-coherent transport systems in high-capacity optical networks. Section 4.7 concludes this chapter with a summary.

4.2 SELF-COHERENT OPTICAL MODULATION FORMATS

4.2.1 Evolution of Optical Transport Networks

Optical transport networks are evolving quickly to adapt to the ever-increasing demands of telecommunication needs, most noticeably witnessed by the explosive growth in transmission capacity demand. The channel data rate in modern optical transport networks is migrating from 2.5- to 10-Gb/s. 40-Gb/s per-channel data rate is on the horizon for commercial deployment, and 100-Gb/s per-channel data rate is under consideration by standard bodies for next-generation Ethernet. In addition to increases in data rate per channel, the number of channels per fiber is also increased through wavelength-division multiplexing (WDM) or dense WDM (DWDM) to further improve overall transmission capacity. Besides the demand for high capacity, optical transport networks desire long un-regenerated optical transmission distance to effectively support metropolitan, regional, and national network applications. Moreover, flexible wavelength management, enabled by elements such as reconfigurable optical add/drop multiplexers (ROADM), is often utilized to make optical networks transparent and scalable. Optical transport networks are expected to continue to evolve to offer higher capacity, longer reach, and more flexible wavelength management, and do so with minimal operational expenditure and capital expenditure.

The evolution of optical transport networks is empowered by technological innovation in several key elements of an optical communication system, one of which is the optical transponder. An optical transponder consists of a transmitter that encodes information on a lightwave through optical modulation and a receiver that recovers the information. An essential part of an optical transponder is its modulation format, which defines how the information is encoded at the transmitter and how it is recovered at the receiver. Furthermore, the modulation format has strong system-level implications since the transmission performance of an optical

signal in an optical network is related to how the signal is modulated. Different modulation formats have different receiver sensitivities or required optical signal-to-noise ratios for a given bit error rate (BER), different spectral efficiencies, and different tolerances to transmission impairments such as CD, PMD, optical filtering, and fiber nonlinearity [5].

4.2.2 Overview of Optical Modulation Formats

Generally, there are three basic physical attributes of a lightwave that can be used, through optical modulation, to carry information: its amplitude, phase and its time derivative frequency, and polarization. The most common optical modulation format is OOK, in which the light intensity is turned on and off to represent the "1" and "0" states of a digital signal. OOK is widely used in optical fiber communication due to its simple transmitter and receiver configuration, but its receiver sensitivity is quite limited as compared to most other modulation formats. Another common type of optical modulation format is phase-shift keying, which utilizes the phase of a lightwave to carry information. To recover the information, a PSK receiver requires a phase reference, which might be provided by an optical local oscillator (OLO). Phase coherence between the OLO and the PSK signal is required. A special type of PSK is DPSK, in which information is encoded onto a lightwave by the phase difference between adjacent symbols. For DBPSK, the modulated information can be recovered without resorting to an OLO by the so-called *self-homodyne detection* [1], where an optical delay interferometer (ODI) is used to compare the signal with a delayed copy of itself and convert the phase modulation into intensity modulation that can be directly detected by square-law detectors. This detection scheme can be generalized to any *differentially coherent* or *self-coherent* signals, including multilevel DPSK signals, by using *orthogonal* differential detection, where both the *in-phase* and *quadrature* components of a product of the signal field and the complex conjugate of a delayed copy of the field are obtained. A digital precoder is needed to ensure that the recovered data is the original data. Optical frequency-shift keying (FSK) and polarization-shift keying are less commonly used, mainly because appropriate transmitters and receivers are less readily available and often exhibit poorer transmission performance. More than one of the three physical attributes may be simultaneously modulated to either carry more information bits per symbol or mitigate a certain transmission penalty. For example, PMUX can be combined with DPSK to offer halved symbol rate for a given bit rate.

Constellation diagrams are often used to illustrate different modulation formats. In a constellation diagram, the real and imaginary parts of the complex fields of a modulated optical signal at the centers of bit periods are plotted. Figure 4.1 shows the constellation diagrams of OOK, duobinary [6], DBPSK [1 4], DQPSK [7 9], 8-ary DPSK [10 12], and a hybrid DQPSK and 2-level pulse-amplitude modulation (PAM2) [13,14]. By creating more states in the symbol constellation, one can transmit the same information bit rate with lowered symbol rate, which leads to higher achievable spectral efficiency,

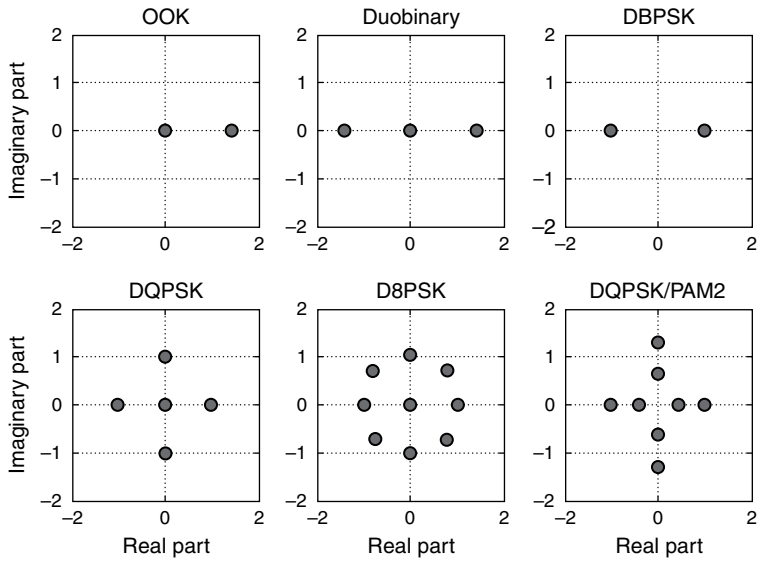

Figure 4.1 Constellation diagrams of OOK, duobinary, DBPSK, DQPSK, 8 ary DPSK, and hybrid DQPSK/PAM2. The average signal power is normalized to unity (this figure may be seen in color on the included CD ROM).

higher tolerance to CD and PMD, and lower transmitter and receiver bandwidth requirements. However, modulation formats carrying more bits per symbol also tend to require higher OSNR for a given BER due to reduced separations among symbols. More detailed descriptions on various optical modulation formats can be found in Chapter 2 "Advanced Optical Modulation Formats" by P. J. Winzer and R.-J. Essiambre.

4.2.3 Common Self-Coherent Optical Modulation Formats

Differential Binary Phase-Shift Keying

As discussed in Section 4.2.2, self-coherent modulation formats generally refer to any formats containing DPSK. The most basic one is DBPSK, which can be generated by a single-waveguide phase modulator or a Mach-Zehnder Modulator (MZM) configured for phase modulation. There are two common types of modulators to effectively realize phase modulation. The single-waveguide phase modulator has the advantage of low loss, no need for bias control, and absence of modulator bandwidth-limitation-induced signal amplitude fluctuations. However, it has the drawback of the presence of modulator bandwidth-limitation-induced phase fluctuations and stringent drive voltage requirement for realizing the exact π phase shift. In contrast, the MZM has the advantage that the exact π phase shift can be obtained even with nonexact drive voltages and limited modulator bandwidth. However, the use of the MZM requires an accurate bias control (at extinction or null) and causes some signal

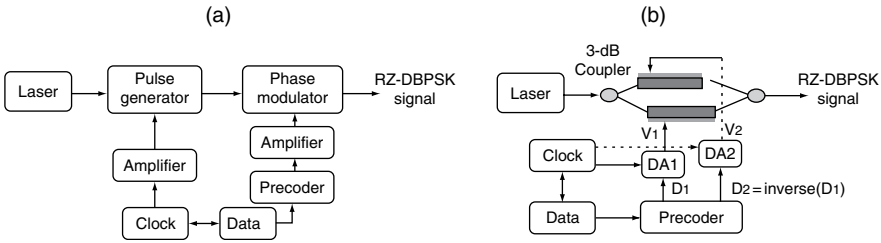

Figure 4.2 (a) Schematic of a RZ DBPSK transmitter based on two modulators; (b) schematic of a RZ DBPSK transmitter based on a single dual drive Mach Zehnder modulator (MZM) (this figure may be seen in color on the included CD ROM).

amplitude fluctuations due to limited modulator bandwidth which can be suppressed by operating the modulator in the saturation range of its intensity transfer function. Typically, the bias needs to be controlled near the null point to avoid noticeable penalty. Overall, MZMs configured for phase modulation are preferred over single-waveguide phase modulators in high-speed DBPSK transmission.

Return-to-zero (RZ) pulse formatting is usually used in association with DBPSK to improve its transmission performance [2 4]. Unlike non-return-to-zero (NRZ) pulse formatting, RZ pulse formatting minimizes the optical intensity between any adjacent bits, and offers higher receiver sensitivity and a higher degree of immunity to intersymbol interference (ISI), which may result from linear and nonlinear transmission effects. RZ-DBPSK has become the modulation format of choice for many record-setting high-capacity, long-haul transmission experiments [2 4]. The generation of an RZ-DBPSK signal usually requires one modulator for pulse generation and another modulator for phase modulation, as shown in Figure 4.2 (a). For RZ-DPSK, it is needed to align the centers of the bits with the peaks of the RZ pulse train. Typically, the alignment accuracy needs to be within 20% of the pulse duration to avoid noticeable penalty. To reduce the complexity of a RZ-DPSK transmitter, a single MZM has been used to simultaneously perform the RZ pulse formatting and phase modulation functions based on different methods [15]. Both chirp-free and chirped RZ-DBPSK signals have been generated. Figure 4.2 (b) shows the schematic of a single modulator-based chirped RZ-DBPSK transmitter. The original data is first differentially encoded to form two complementary NRZ signal streams, D1 and D2, which are later converted to RZ format by two differential amplifiers, DA1 and DA2, with two clock signals whose frequency equals the bit rate [15]. The two RZ drive signals provide voltages V_1 and V_2 that are synchronously applied to the two arms of the MZM which is biased at null, to modulate the light from the CW laser to generate the chirped RZ-DPSK signal.

Differential Quadrature Phase-Shift Keying

DQPSK is a promising modulation format [7 9] that offers doubled spectral efficiency as compared to DBPSK and suffers only slightly in terms of receiver

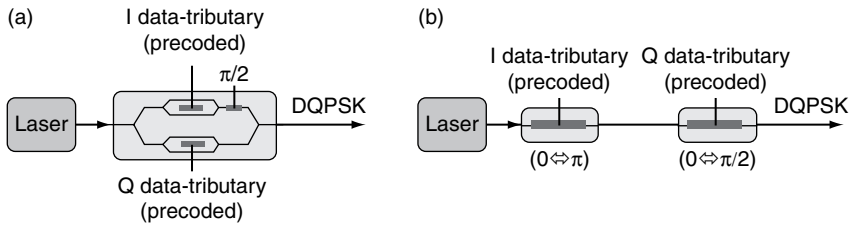

Figure 4.3 Schematic of a DQPSK transmitter based a nested Mach Zehnder phase modulator (a) and cascaded phase modulators (b) (this figure may be seen in color on the included CD ROM).

sensitivity. The transmitter for DQPSK needs to generate four differential-phase states [0, 0.5π, π, and 1.5π]. This four-phase levels can be generated by using a nested MZM or using of a MZM together with a single-waveguide phase modulator that encodes a 0 or $\pi/2$ phase modulation. A nested MZM is usually preferred since exact phase levels are more readily achievable. Figure 4.3 shows the schematic of a DQPSK transmitter based on a nested MZM and cascaded phase modulators. A precoder whose operation depends on the transmitter and receiver configurations [4] is needed to ensure that the received signal is the original signal.

M-ary DPSK

Higher spectral efficiency can be obtained by using *m*-ary DPSK formats having more phase states. Optical 8-ary DPSK has been proposed and demonstrated [10 12]. Generally, for a *m*-ary DPSK transmitter, $\log_2(m)$ binary phase modulators are needed to encode the *m*-phase states. As *m* increases, signal immunity to noise decreases. There is a trade-off between spectral efficiency and receiver sensitivity or OSNR requirement when choosing the number of phase states *m*. *m*-ary DPSK formats with $m > 4$ are expected to find very limited applications only where sufficiently high OSNR can be obtained.

Hybrid DPSK and PAM

Another way to carry more bits per symbol is by combining DPSK with PAM. The simplest such format is the combination of DBPSK and a 2-level PAM [13]. DQPSK/PAM2, a 3-bit/symbol format, was also demonstrated [16]. A 5-bit/symbol format based on 8-ary DPSK and PAM4 was recently demonstrated at 50-Gb/s [17]. DPSK/PAM formats generally have high OSNR requirement, and are also more susceptible to transmitter bandwidth-limitation-induced ISI [18]. In addition, self-phase modulation (SPM)-induced phase offsets between symbols with different intensities reduce the nonlinear tolerance of these DPSK/PAM formats.

Polarization-Multiplexed DPSK

A commonly used means to double the spectral efficiency is via PMUX, with a trade-off of increased complexity at both the transmitter and the receiver. At the transmitter, two sets of modulators are usually needed to individually modulate the two polarization states of a polarization-multiplexed DPSK signal. Since the polarization of a signal after fiber transmission is uncertain and time-varying, adaptive polarization demultiplexing is needed, either through optical means or electronic means. Furthermore, in WDM transmission, interchannel cross-phase modulation (XPM) may lead to nonlinear polarization scattering, which causes signal polarization to vary on a bit-by-bit basis and degrade the performance of adaptive polarization demultiplexing. DPSK, by having nearly identical intensity profiles in all the bit slots, exhibits smaller XPM effects and smaller nonlinear polarization scattering than OOK [19]. A special case of polarization multiplexing is polarization bit interleaving [20], which is more robust against fiber nonlinear effects [19 21] but requires RZ pulse formatting and likely more spectral bandwidth.

A particularly interesting format is polarization-multiplexed DQPSK that carries 4 bits/symbol [21 23]. A 40-Gb/s polarization-multiplexed DQPSK signal has similar spectral bandwidth and CD and PMD tolerance as a conventional 10-Gb/s OOK signal, and is a promising candidate for upgrading DWDM networks with 10-Gb/s channels.

4.3 DIRECT-DETECTION OF SELF-COHERENT SIGNALS

One attractive feature of a self-coherent signal is that it can be directly detected without resorting to coherent detection that requires an OLO. For direct detection of self-coherent signals, optical demodulation that convert differential phase modulation to intensity modulation needs to be performed prior to the square-law detection. In this section, we describe common differential direct-detection schemes for self-coherent signals. The upper limits of the receiver sensitivities for some of these signals will also be given. In optical noise limited (or optically pre-amplified) receivers, there are three commonly used receiver sensitivity indicators, namely, signal-to-noise ratio per bit (SNR_b), OSNR, and number of photons per bit (PPB) that are required for a given BER. SNR_b is defined as

$$SNR_b = \varepsilon_b / N_0 = P_s / (N_0 B), \tag{4.1}$$

where ε_b is the signal energy per bit, N_0 is the noise spectral density, P_s is the signal power, and B is the bit rate of the signal. In amplified spontaneous emission (ASE) noise limited case, N_0 is the ASE noise spectral density per polarization. The physical meaning of the SNR_b is the ratio between the signal power and the power of the single polarized optical noise within a bandwidth of the signal bit rate.

OSNR is conventionally defined as the ratio between the signal power and the power of optical noise of two polarization states within a fixed bandwidth of

0.1 nm (or 12.5 GHz at a signal wavelength of about 1550 nm). If the optical noise is the dominant noise source in the receiver and information is coded in one optical polarization state only, OSNR relates to SNR_b as

$$\mathrm{OSNR} = (\mathrm{SNR_b} \times B)/(2 \times 12.5\,\mathrm{GHz}). \tag{4.2}$$

As an example, at bite rates of 10 Gb/s and 40 Gb/s, the OSNR values are approximately 4 dB and 2 dB higher than the SNR_b values, respectively.

The PPB of the signal inputted to the optical pre-amplifier is related to the SNR_b of the amplified signal as

$$\mathrm{PPB} = n_{sp} \times \mathrm{SNR_b}, \tag{4.3}$$

where n_{sp} is the spontaneous emission factor of the optical amplifier. For an ideal optical pre-amplifier that has a noise figure of 3 dB, $n_{sp} = 1$ [4], and SNR_b and PPB happen to be equal.

4.3.1 Direct-detection DBPSK

Receiver Configuration of Direct-Detection DBPSK

A direct-detection DBPSK receiver generally consists of three components, an ODI, a balanced detector, and a clock and data recovery (CDR) unit with a binary decision circuitry, as shown in Figure 4.4. The ODI is used for demodulating the DBPSK signal into two complementary OOK signals that can be directly detected by intensity detectors. The signal is first split into two paths that have a certain path difference so that the signal at the end of one path is delayed by approximately one bit period, denoted as T, with respect to that of the other path. This effectively causes two adjacent bits to interfere with each other, and depending on their phase difference of 0 or π, they interfere constructively or destructively. The constructively and destructively interfered signal components exit the ODI through its constructive and destructive output ports, respectively, and are detected by a balanced detector which consists of two matched photodiodes. The photocurrents generated by the two matched photodiodes are subtracted and the current difference is then converted to a

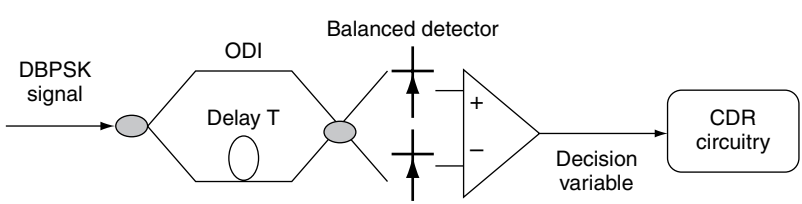

Figure 4.4 Schematic of a DBPSK receiver. CDR: clock data recovery.

voltage difference before it is used for CDR with a nominal decision threshold at about zero. The CDR circuitry can be similar to those conventionally used for OOK detection. Mathematically, the decision variable can be expressed as

$$u_{\mathrm{DBPSK}}(t) = \mathrm{Re}[E_{\mathrm{RX}}(t) \times E^{*}_{\mathrm{RX}}(t - T)], \tag{4.4}$$

where E_{RX} is the normalized optical field of the DBPSK signal entering the receiver, Re[X] is the real part of a complex variable x, and "*" denotes the complex conjugate.

The ODIs are commonly made with optical fiber [24], planar lightwave circuit [25], free-space optics [26], or $LiNbO_3$ waveguide [23]. Note that a precise phase control of the phase difference between the two optical paths of the ODI is required. The penalty associated with a nonexact phase difference will be discussed later. Since the phase difference may be changed by environmental temperature, accurate temperature control and stabilization of the ODI are usually required. Athermal ODIs have been demonstrated by using a free-space optics design [26]. In addition to temperature changes, laser frequency drift also affects the phase difference, so adaptive control of the ODI to adjust the phase difference depending on laser frequency drift may be needed.

Balanced detectors are usually used for DBPSK to take the advantage of the higher receiver sensitivity offered by DBPSK over OOK. With a loss in receiver sensitivity, a DBPSK signal may be received by a single detector that detects the signal component from either the constructive port or the destructive port of the ODI. Effectively, the signal components from the constructive and destructive ports are of the optical duobinary format and the alternating mark-inversion format [27, 28], which exhibit unique spectral characteristics. Figure 4.5 shows simulated optical spectra of an DBPSK signal, and its filtered components from the constructive and destructive ports of a 1-bit ODI.

Optimal Receiver Sensitivity of Direct-Detection DBPSK

It may be useful to compare the optimal receiver sensitivity of DBPSK, obtained when a matched optical filter is assumed [4, 29], with those of BPSK and OOK. For homodyne or heterodyne BPSK, we have the following dependence of BER on $\mathrm{SNR_b}$:

$$\mathrm{BER_{BPSK}} = \frac{1}{2}\mathrm{erfc}(\sqrt{\mathrm{SNR_b}}). \tag{4.5}$$

For direct-detection DBPSK with polarization filtering at the receiver so that only the noise component whose polarization is aligned with that of the signal is detected with the signal, we have

$$\mathrm{BER_{DBPSK\_1p}} = \frac{\exp(-\mathrm{SNR_b})}{2}. \tag{4.6}$$

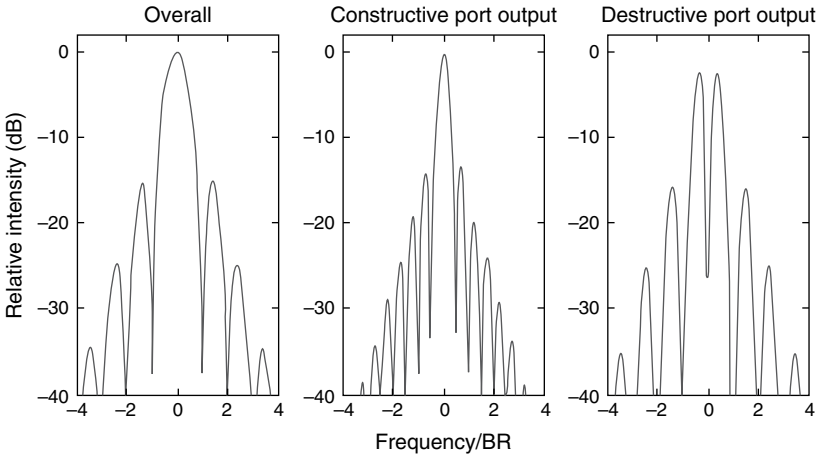

Figure 4.5 Spectra of a DBPSK signal and its filtered components from the constructive and destructive ports of a 1 bit ODI. The spectral resolution is 5% of the bit rate (this figure may be seen in color on the included CD ROM).

For direct-detection DBPSK without polarization filtering at the receiver, we have

$$\mathrm{BER}_{\mathrm{DBPSK\_2p}} = \frac{\exp(-\mathrm{SNR_b})}{2}\left(1 + \frac{\mathrm{SNR_b}}{4}\right). \tag{4.7}$$

For direct-detection OOK with polarization filtering at the receiver, we have

$$\begin{aligned}\mathrm{BER}_{\mathrm{OOK\_1p}} = &\frac{1}{2}\left[1 - Q\left(2\sqrt{\mathrm{SNR_b}}, 2\sqrt{\mathrm{SNR_b} \times \mathrm{V_{th}}}\right)\right] \\ &+ \frac{1}{2}\exp(-2\mathrm{SNR_b} \times \mathrm{V_{th}}),\end{aligned} \tag{4.8}$$

where V_{th} is the decision threshold normalized to the signal peak power, and $Q(a, b)$ is the first-order Marcum Q-function [30]

$$\begin{aligned}Q(a,b) &= \mathrm{e}^{-(a^2+b^2)/2} \times \sum_{m=0}^{\infty}\left(\frac{a}{b}\right)^m I_m(ab), \qquad a \le b \\ &= 1 + \mathrm{e}^{-(a^2+b^2)/2} I_0(ab) - \mathrm{e}^{-(a^2+b^2)/2} \times \sum_{m=0}^{\infty}\left(\frac{b}{a}\right)^m I_m(ab), \qquad a > b\end{aligned} \tag{4.9}$$

where $I_{\mathrm{m}}(x)$ is the mth-order modified Bessel function of the first kind. The optimal decision threshold satisfies

$$I_0(4\mathrm{SNR_b} \times \sqrt{V_{\mathrm{th}}})\exp(-2\mathrm{SNR_b}) = 1 \tag{4.10}$$

The optimal BER for direct-detection OOK can thus be numerically calculated by solving Eqns (4.8 4.10).

For direct-detection OOK without polarization filtering, we have [4]

$$\mathrm{BER}_{\mathrm{OOK\_2p}} = \frac{1}{2}\left[1 - Q_2\left(2\sqrt{\mathrm{SNR_b}}, 2\sqrt{\mathrm{SNR_b} \times V_{\mathrm{th}}}\right)\right] + \frac{1}{2}\exp(-2\mathrm{SNR_b} \times \mathrm{V_{th}}) \times (1 + 2\mathrm{SNR_b} \times \mathrm{V_{th}}), \quad (4.11)$$

where $Q_2(a,b) = Q(a,b) + \frac{b}{a}\mathrm{e}^{-(a^2+b^2)/2} \times I_1(ab)$, and the optimal decision threshold can be numerically calculated.

Figure 4.6 shows the BER performances of BPSK, DBPSK, and OOK with and without polarization filtering. Table 4.1 summarizes the receivers sensitivities at $\mathrm{BER} = 10^{-3}$ and 10^{-9} for the above signal formats. With polarization filtering at the receiver, the receiver sensitivity of DBPSK is slightly worse than that of the OBPSK: about 0.45 dB at $\mathrm{BER} = 10^{-9}$. This penalty is often referred to as *the differential-detection penalty*. The differential-detection penalty increases for DPSK formats having more than 2 symbols per bit, as will be discussed later. Without polarization filtering, the receiver sensitivity of DBPSK is further degraded by approximately 0.4 dB at $\mathrm{BER} = 10^{-9}$. Two commonly used modulation/detection configurations are direct-detection DBPSK and OOK that do not have the polarization filtering. The DBPSK outperforms the OOK by about 2.7 dB at $\mathrm{BER} = 10^{-9}$: this is commonly referred to as *the 3-dB advantage of DBPSK over OOK* in optical receiver sensitivity. DBPSK with balanced detection is also found to have 6 dB higher tolerance to coherent crosstalk than OOK [31].

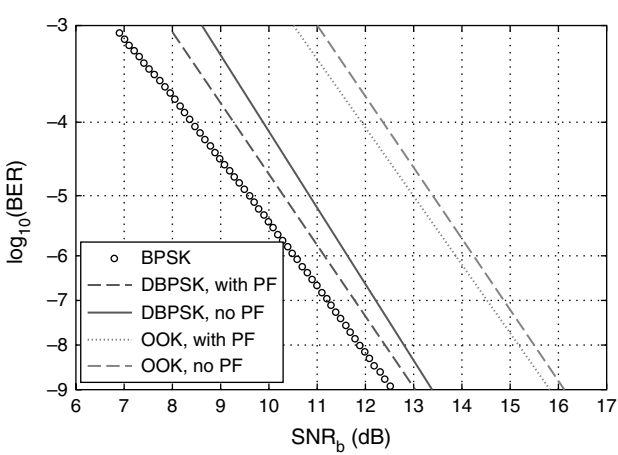

Figure 4.6 The optimal BER performances of BPSK, DBPSK, and OOK with and without polarization filtering (PF) (this figure may be seen in color on the included CD ROM).

Table 4.1
Receiver sensitivity comparison among different binary signal formats*.

				DBPSK		OOK	
			BPSK	With PF	No PF	With PF	No PF
BER	10^{-9}	PPB	18	20	22	38.3	40.7
		SNR_b	12.5 dB	13 dB	13.4 dB	15.8 dB	16.1 dB
		OSNR(10 G)	8.5 dB	9 dB	9.4 dB	11.8 dB	12.1 dB
BER	10^{-3}	PPB	4.8	6.2	7.2	11.2	12.7
		SNR_b	6.8 dB	8 dB	8.6 dB	10.5 dB	11 dB
		OSNR(10 G)	2.8 dB	4 dB	4.6 dB	6.5 dB	7 dB

* Ideal Optical preamplifier with NF 3 dB is assumed. OSNR(10 G) is the required OSNR values for a 10 Gb/s signal. PF: polarization filtering.

Receiver Impairments in Direct-Detection DBPSK

One significant impairment in DBPSK receiver performance is the phase error due to nonexact phase matching between the two arms of the ODI. The phase error usually comes from temperature-induced phase mismatch or laser frequency offset from the passband center of the ODI. With the consideration of the phase error, we have for direct-detection DBPSK with polarization filtering [4]

$$\mathrm{BER}_{\mathrm{DBPSK\_1p}} = Q(a,b) - \frac{1}{2}\mathrm{e}^{-(a^2+b^2)/2} \times I_0(ab),$$
$$a = \sqrt{2\mathrm{SNR}_\mathrm{b}}|\sin(\phi_\mathrm{e}/2)|, \qquad b = \sqrt{2\mathrm{SNR}_\mathrm{b}}|\cos(\phi_\mathrm{e}/2)|, \tag{4.12}$$

where ϕ_e is the phase error, and $I_0(x)$ is the zeroth-order modified Bessel function of the first kind, and $Q(a, b)$ is the first-order Marcum Q-function.

For direct-detection DBPSK without polarization filtering at the receiver, we have

$$\mathrm{BER}_{\mathrm{DBPSK\_2p}} = Q(a,b) - \frac{1}{2}\mathrm{e}^{-(a^2+b^2)/2} \times I_0(ab) + \frac{1}{8}\mathrm{e}^{-(a^2+b^2)/2\left(\frac{b}{a}-\frac{a}{b}\right)} \times I_1(ab), \tag{4.13}$$

where the last term on the right-hand side of the equation represents the error contribution from the noise component whose polarization is orthogonal to that of the signal. When the phase error becomes zero, Eqns (4.12) and (4.13) reduces to Eqns (4.6) and (4.7), respectively. Figure 4.7 shows the OSNR penalty as a function of the phase error for direct-detection DBPSK.

The phase error due to laser frequency offset, f_e, can be expressed as

$$\phi_\mathrm{e} = 2\pi\frac{f_\mathrm{e}}{\mathrm{FSR}}, \tag{4.14}$$

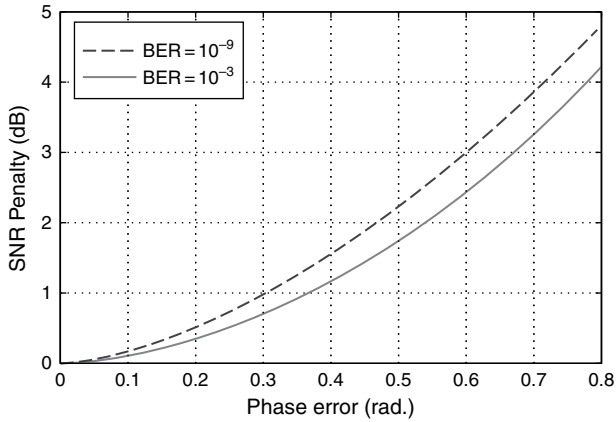

Figure 4.7 The OSNR penalty as a function of the phase error for direct detection DBPSK without polarization filtering at BER 10^{-9} and BER 10^{-3} (this figure may be seen in color on the included CD ROM).

where FSR is the free spectral range of the ODI. Usually, the FSR of the ODI equals the bit rate of the DBPSK signal, and thus the phase error resulting from a same laser frequency offset or uncertainty decreases as the bit rate of the DBPSK signal increases. Note that any laser has a finite linewidth or frequency jitter, which causes random phase errors with a given distribution, e.g., Lorentzian distribution, and degrades the performance of DPSK. The linewidth of commonly used DFB lasers is on the order of a few MHz, which causes negligible penalty for DPSK signals with multi-gigabits-per-second bit rate. However, laser frequency drift due to temperature and aging may cause sufficiently large frequency offset (e.g., >1 GHz) to cause severe degradation of the DPSK performance. In addition, the phase error due to a certain temperature change of the ODI is proportional to the length difference between the two arms of the ODI, which is inversely proportional to the signal bit rate. So the higher the signal rate, the higher the tolerance of the direct-detection DBPSK to laser frequency uncertainties and temperature changes at the receiver. This makes DBPSK particularly suitable for high-speed optical transmissions.

Another receiver imperfection is the nonexact 1-bit delay of the ODI. DBPSK is quite tolerant to the delay mismatch. Negligible OSNR penalty was observed when an ODI with a FSR of 50 GHz (or a delay of 20 ps) was used for demodulating a 42.7 Gb/s DBPSK signal (with 23.4 ps bit period) [26]. Under severe optical filtering, partial-bit delay may actually provide better overall signal performance [32].

Other receiver imperfections such as the arrival time mismatch and amplitude mismatch between the two electrical signals detected by the balanced detector and receiver also contribute to the degradation of the DBPSK receiver sensitivity. Generally, the associated penalties become negligible when the time and amplitude mismatches are less than 5% of the bit period and the nominal amplitude,

respectively [3]. Since the amplitude mismatch is related to the finite common-mode rejection of the balanced detector, so the required common-mode rejection ratio is desired to be higher than about 13 dB.

4.3.2 Direct-Detection DQPSK

Receiver Configuration of Direct-Detection DQPSK

Figure 4.8 shows the schematic of a direct-detection DQPSK receiver, consisting of two *orthogonal* ODIs that demodulate the in-phase (I) and quadrature (Q) tributaries of the signal, two balanced detectors, and a CDR unit with a binary decision circuitry. The I and Q decision variables can be expressed as

$$\begin{aligned} u_I(t) &= \mathrm{Re}[\mathrm{e}^{j\frac{\pi}{4}} E_{\mathrm{RX}}(t) \times E^*_{\mathrm{RX}}(t-T)], \\ u_Q(t) &= \mathrm{Im}[\mathrm{e}^{j\frac{\pi}{4}} E_{\mathrm{RX}}(t) \times E^*_{\mathrm{RX}}(t-T)], \end{aligned} \tag{4.15}$$

where E_{RX} is the normalized optical field of the DQPSK signal entering the receiver, and Re[x] and Im[x] are, respectively, the real and imaginary parts of complex variable x. Note that the DQPSK demodulator can be simplified by using a single optical delay interferometer followed by an optical hybrid [23] or star coupler [33].

For the optical encoding and detection configurations shown in Figure 4.3(a) and Figure 4.8, the relations among the precoder outputs and the original data are summarized in Table 4.2 [4]. The precoder outputs at the kth bit, p_k and q_k, can be obtained by performing the following logic operations on the original data at the kth bit, a_k and b_k, and the previous outputs of the precoder, p_{k-1} and q_{k-1}, according to the following equation:

$$\begin{aligned} p_k &= \overline{a}_k \overline{b}_k \overline{p}_{k-1} + \overline{a}_k b_k q_{k-1} + a_k \overline{b}_k \overline{q}_{k-1} + a_k b_k p_{k-1} \\ q_k &= \overline{a}_k \overline{b}_k \overline{q}_{k-1} + \overline{a}_k b_k \overline{p}_{k-1} + a_k \overline{b}_k p_{k-1} + a_k b_k q_{k-1} \end{aligned} \tag{4.16}$$

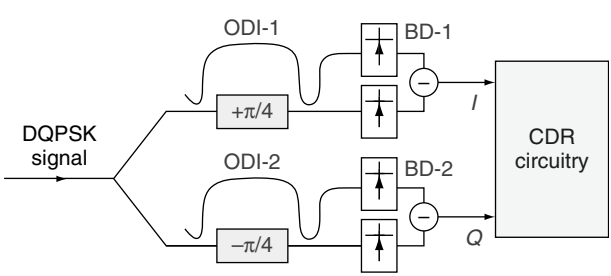

Figure 4.8 Schematic of a direct detection DQPSK receiver (this figure may be seen in color on the included CD ROM).

Table 4.2

The relations among the precoder outputs and the original data for a typical DQPSK transmitter and receiver configuration [4].

Original data ($a_k b_k$)	Optical phase difference	First precoder output, p_k	Second precoder output, q_k
(00)	π	$\bar{p}_{k-1}$	$\bar{q}_{k-1}$
(01)	$\pi/2$	$\bar{q}_{k-1}$	$\bar{p}_{k-1}$
(10)	1.5π	$\bar{q}_{k-1}$	$\bar{p}_{k-1}$
(11)	0	$\bar{p}_{k-1}$	$\bar{q}_{k-1}$

Optimal Receiver Sensitivity of Direct-Detection DQPSK

Under the matched optical filer assumption, the optimal BER performance of direct-detection DQPSK with polarization filtering can be written as [4].

$$\begin{aligned} &\mathrm{BER}_{\mathrm{DQPSK\_1p}} = Q(a,b) - \frac{1}{2}\mathrm{e}^{-(a^2+b^2)/2} I_0(ab), \\ &\text{with } a = \sqrt{2\mathrm{SNR}_\mathrm{b}(1-1/\sqrt{2})} \quad \text{and} \quad b = \sqrt{2\mathrm{SNR}_\mathrm{b}(1+1/\sqrt{2})}. \end{aligned} \tag{4.17}$$

For direct-detection DQPSK without polarization filtering, we have

$$\begin{aligned} \mathrm{BER}_{\mathrm{DQPSK\_2p}} = Q(a,b) &- \frac{1}{2}\mathrm{e}^{-(a^2+b^2)/2} \times I_0(ab) \\ &+ \frac{1}{8}\mathrm{e}^{-(a^2+b^2)/2\left(\frac{b}{a}-\frac{a}{b}\right)} \times I_1(ab), \end{aligned} \tag{4.18}$$

where a and b are the same as those given in Eqn. (4.17).

As a comparison, the optimal BER performance of coherent detection (homodyne or heterodyne) QPSK is [29]

$$\mathrm{BER}_{\mathrm{QPSK}} = \frac{1}{2}\mathrm{erfc}\left(\sqrt{\mathrm{SNR}_\mathrm{b}}\right). \tag{4.19}$$

Figure 4.9 shows the BER performances of QPSK and DQPSK without polarization filtering, as compared to those of BPSK and DBPSK. QPSK performs the same as the BPSK, while the DQPSK (without polarization filtering) exhibits a differential-detection penalty of $\sim$2.4 dB over the BER range from 10^{-3} to 10^{-9}. Comparing DQPSK with DBPSK, the relative sensitivity penalty of DQPSK is $\sim$1.5 dB at $\mathrm{BER} = 10^{-9}$ and $\sim$0.8 dB at $\mathrm{BER} = 10^{-3}$. These performance differences were confirmed experimentally [34]. In optical transmission systems with modern forward error correction (FEC) codes, the raw BER of interest

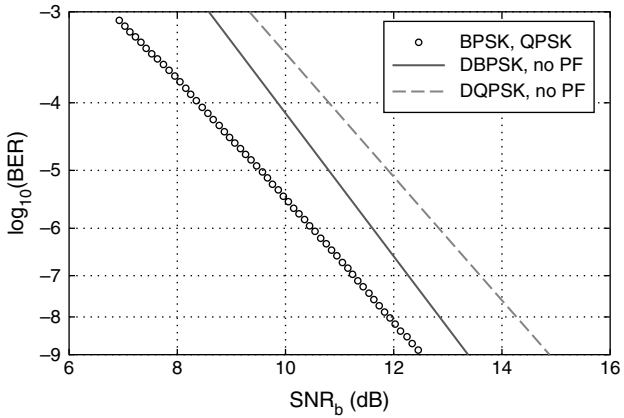

Figure 4.9 Optimal BER performances of QPSK and DQPSK without polarization filtering, as compared to those of BPSK and DBPSK (this figure may be seen in color on the included CD ROM).

is in the range around 10^{-3}, and the receiver sensitivity disadvantage of the direct-detection DQPSK as compared to the DBPSK is about 1 dB.

Receiver Impairments in Direct-Detection DQPSK

Similar to DBPSK, DQPSK also suffers from implementation imperfections. Particularly, DQPSK is very sensitive to phase errors. The BER of an DQPSK signal in the presence of a phase error, ϕ_e , is

$$\begin{aligned} \mathrm{BER}_{\mathrm{DQPSK}-\phi_e} &= \tfrac{1}{2}\left[\mathrm{BER}_{\mathrm{DQPSK}}(a_+, b_+) + \mathrm{BER}_{\mathrm{DQPSK}}(a_-, b_-)\right], \\ \text{with } a_\pm &= \sqrt{2\mathrm{SNR}_b\left[1 - \cos\left(\tfrac{\pi}{4} \pm \phi_e\right)\right]}, \quad \text{and} \\ b_\pm &= \sqrt{2\mathrm{SNR}_b\left[1 + \cos\left(\tfrac{\pi}{4} \pm \phi_e\right)\right]}, \end{aligned} \tag{4.20}$$

where $\mathrm{BER}_{\mathrm{DQSPK}}$ can be obtained from Eqn (4.17) or Eqn (4.18) depending on whether polarization filtering is applied. Figure 4.10 shows the OSNR penalty (at $\mathrm{BER} = 10^{-9}$) of a 40-Gb/s DQPSK as a function of the laser frequency offset, as compared to that of a 40-Gb/s DBPSK signal. DQPSK requires approximately 5.5 times tighter laser frequency accuracy [35].

4.3.3 Direct-Detection *m*-ary DPSK

Higher spectral efficiency can be obtained by using *m*-ary DPSK formats with more phase levels. For direct detection of *m*-ary DPSK, a straightforward but

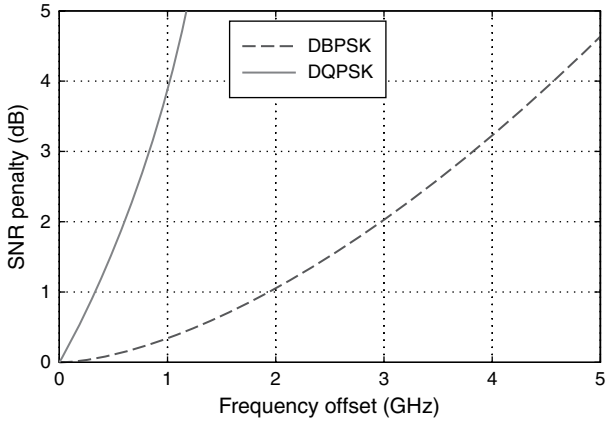

Figure 4.10 The OSNR penalty (at BER 1E 9) as a function of the laser frequency offset in 40 Gb/s DQPSK and DBPSK systems using 1 bit ODIs. No polarization filtering is used (this figure may be seen in color on the included CD ROM).

cumbersome demodulation scheme is to use $m/2$ ODIs with the following different phase offsets (between the two arms of each ODI).

$$\Delta\phi_{\mathrm{ODI}}(n) = \frac{[1-2(n-1)]\pi}{m}, \quad n = 1, 2, \ldots, m/2. \tag{4.21}$$

For example, the demodulation of an 8-ary DPSK signal thus requires four ODIs with phase offsets of $\pi/8$, $\pi/8$, $3\pi/8$, and $5\pi/8$ between the interfering arms. Following the demodulation, $m/2$ pairs of balanced detectors are needed to obtain $m/2$ decision variables, $u[\Delta\phi_{\mathrm{ODI}}(n)]$, where $n = 1, 2, \ldots, m/2$. Generalizing the analysis on 8-ary DPSK to m-ary DPSK, we can recover the $\log_2(m)$ data tributaries of an m-ary DPSK signal by [36]

$$\begin{aligned}
&c_1 = c_I = \left[u\left(\frac{\pi}{m}\right) > 0\right], \quad c_2 = c_Q = \left[u\left(\frac{\pi}{m} - \frac{\pi}{2}\right) > 0\right], \\
&c_3 = \left[u\left(\frac{\pi}{m} + \frac{\pi}{4}\right) > 0\right] \oplus \left[u\left(\frac{\pi}{m} - \frac{\pi}{4}\right) > 0\right], \ldots \\
&c_{\log_2(\mathrm{m})} = \left[u\left(\frac{3}{m}\pi\right) > 0\right] \oplus \left[u\left(\frac{7}{m}\pi\right) > 0\right], \ldots \oplus \left[u\left(\frac{m/2-1}{m}\pi\right) > 0\right] \\
&\quad \oplus \left[u\left(\frac{3}{m}\pi - \frac{\pi}{2}\right) > 0\right] \oplus \left[u\left(\frac{7}{m} - \frac{\pi}{2}\right) > 0\right] \ldots \oplus \left[u\left(\frac{m/2-1}{m}\pi - \frac{\pi}{2}\right) > 0\right].
\end{aligned} \tag{4.22}$$

Since there are correlations among the decision variables obtained by the $m/2$ ODIs, the first two decision variables are sufficient to derive all the other decision variables with the help of analog signal processing [37] or DSP [36] that will be discussed in detail in a later section on digital self-coherent receivers. Note that an

appropriate precoder is needed to ensure the recovered data tributaries are the original ones.

The receiver sensitivity of an m-ary PSK signal can be straightforwardly estimated from the minimum Euclidean distance between the two closest symbols in its constellation diagram (with a normalized average signal power). The receiver sensitivity penalty (in dB) of m-ary PSK with respect to coherent-detection BPSK can be approximated as [4]

$$\Delta \mathrm{SNR_b}^{\mathrm{PSK}}(\mathrm{m}) \approx -20\log_{10}\left[\sin\left(\frac{\pi}{m}\right) \times \sqrt{\log_2(m)}\right] \tag{4.23}$$

For m-ary DPSK signals, the errors are dominated by differential phase noise. We define a minimum *differential phase distance* for m-ary DPSK as

$$d_{\Delta\phi}{}^{\mathrm{DPSK}}(\mathrm{m}) = \frac{2\pi}{m} \times \frac{1}{\sqrt{2}} = \frac{\sqrt{2}\pi}{m}, \tag{4.24}$$

where the factor of $\sqrt{2}$ comes from the fact that the differential-phase deviation is $\sqrt{2}$ times as large as the absolute phase deviation, assuming that the optical noise induced phase fluctuations in adjacent signal symbols are independent Gaussian random variables. Under the assumption of low BER where the minimum differential-phase distance determines the BER performance, we can then approximate the receiver sensitivity penalty (in dB) of m-ary DPSK with respect to coherent-detection BPSK as

$$\begin{aligned}\Delta \mathrm{SNR_b}^{\mathrm{DPSK}}(m) &\approx -20\log_{10}\left[\frac{d_{\Delta\phi}{}^{\mathrm{DPSK}}(m)}{2} \times \sqrt{\log_2(m)}\right] \\ &= -20\log_{10}\left[\frac{\pi}{\sqrt{2}m} \times \sqrt{\log_2(m)}\right].\end{aligned} \tag{4.25}$$

Figure 4.11 shows the receiver sensitivity penalties of m-ary PSK and DPSK as compared to BPSK as a function of the number of phase states. The sensitivity penalties become ≥ 3 dB for $m \geq 8$. In addition, the differential-detection penalty approaches 3 dB as m increases. This suggests that m-ary DPSK formats with $m \geq 8$ are only viable in systems with sufficiently high OSNR.

4.3.4 Direct-Detection of Hybrid DPSK and PAM

Combining DPSK with PAM provides another means to carry more bits per symbol. Since DPSK acts on signal phase and PAM acts on signal amplitude, they can be independently received. The DPSK portion of a DPSK/PAM signal

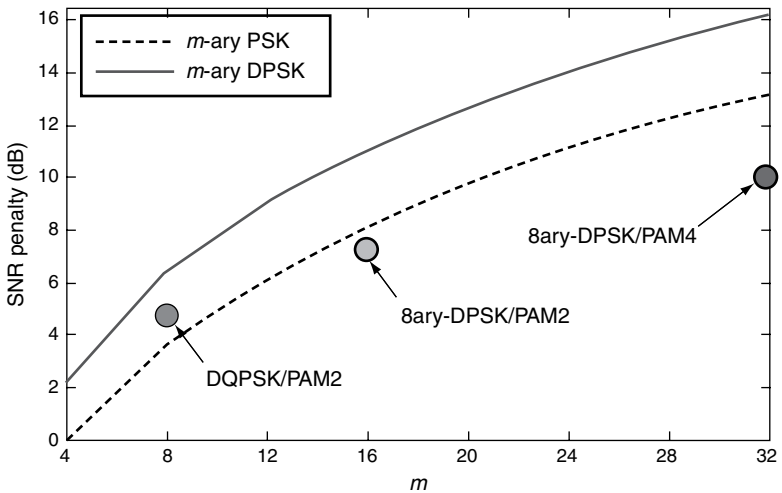

Figure 4.11 Receiver sensitivity penalties of m ary PSK and DPSK as compared to BPSK as a function of the number of phase states. The symbols are for DPSK/PAM formats (this figure may be seen in color on the included CD ROM).

can be received by the direct-detection schemes described previously, and the PAM portion can be received by a binary [16] or multilevel decision circuitry [18] depending the number of the PAM levels.

For direct-detection DPSK/PAM, the ideal receiver sensitivity is optimized when the Euclidean distances between two adjacent PAM levels in its constellation diagram are equal, and they are also equal to the minimum differential-phase distance in the DPSK modulation. The optimal locations of the $m \times p$ symbols of a DPSK/PAM signal with m DPSK phase states and p PAM levels are thus

$$s(n,q) = c \times \exp\left(j\frac{2\pi n}{m}\right) \times \left(1 + \frac{\sqrt{2\pi}q}{m}\right),$$
$$n = 0, 1, \ldots, m-1, \quad q = 0, 1, \ldots, p-1, \tag{4.26}$$

where c is a normalization constant. The receiver sensitivity penalty of direct-detection DPSK/PAM as compared to coherent-detection BPSK can be estimated as

$$\begin{aligned}\Delta\mathrm{SNR}_{\mathrm{b}}^{\mathrm{DPSK/PAM}}(m,p) \\ \approx \quad & 10\log_{10}\left\{\left(\frac{d_{\Delta\phi}{}^{\mathrm{DPSK}}(m)}{2}\right)^2 \times \left[\sum_{q\ 0}^{p-1}\left(1 + q \times d_{\Delta\phi}{}^{\mathrm{DPSK}}(m)\right)^2\right]^{-1} \times \log_2(m \times p)\right\} \\ & 10\log_{10}\left\{\frac{\pi^2}{2m^2} \times \left[1 + (p \quad 1)\frac{\sqrt{2\pi}}{m} + (p \quad 1)(2p \quad 1)\frac{\pi^2}{3m^2}\right]^{-1} \times \log_2(m \times p)\right\}.\end{aligned} \tag{4.27}$$

For DQPSK/PAM2 [14], the theoretical receiver sensitivity penalty as compared to BPSK with the same bit rate) is 4.7 dB, about 1.7 dB smaller than 8-ary DPSK which is also a 3-bit/symbol format. At 4-bit/symbol and 5-bit/symbol, the hybrid DPSK/PAM offers higher optimal receiver sensitivities than *m*-ary DPSK, as shown in Figure 4.11. However, DPSK/PAM usually suffers more transmitter/receiver bandwidth limitation induced ISI and nonlinear penalty than *m*-ary DPSK which may be regarded as a *constant-amplitude* format. Note that in principle, one can improve the receiver sensitivity of hybrid formats based on DPSK and PAM (or ASK) by arranging the signal constellation such that more DPSK phase states are assigned at high power regime than at low power regime, similar to conventional quadrature amplitude modulation (QAM) schemes commonly used in digital communication [29]. However, sophisticated transmitter and receiver designs are needed.

4.4 DIGITAL SELF-COHERENT OPTICAL RECEIVER

With recent advances in high-speed electronic circuits and DSP, optical receiver technologies are evolving to provide unprecedented capabilities that may substantially impact optical transport systems. Combining square-law detection with ADC and DSP, maximum likelihood sequence estimation (MLSE) was used to improve receiver tolerance to chromatic dispersion [38]. However, square-law detection loses optical signal phase information, and limits the dispersion equalization capability. A coherent optical receiver is capable of recovering signal phase and amplitude, but traditionally requires a sophisticated optical phase-locked loop for its OLO. Recently, sampled coherent optical receivers [39 42] based on ADC and DSP have been proposed to omit the OLO and allow advanced signal processing for optical field reconstruction and subsequent electronic compensation of dispersion (EDC) [42 45] and polarization mode dispersion (EPMDC) [43, 44]. Real-time demonstration of sampled coherent receiver has also been reported [46 48]. As described in the Section 4.3, signals modulated with DPSK, such as DBPSK and DQPSK, can be received with direct-detection that does not require an OLO. Enhancing differential direct-detection with ADC and DSP, a new type of optical receiver, referred to as *DSCOR* in which a digital representation of received signal phase waveform is obtained, has recently emerged [49 51]. A phase reference approaching the accuracy of an ideal OLO can be digitally extracted in a DSCOR via data-aided MSPE [49] to improve its sensitivity to approach that of a sampled coherent receiver. The received signal optical field can also be digitally reconstructed in a DSCOR with the additional recovery of the signal amplitude, making digital compensation of dispersion possible [50, 51]. DSCOR is also naturally suitable for receiving high spectral-efficiency *m*-ary DPSK signals [17]. In this section, we present the concept and principle of DSCOR. Particularly, we describe data-aided MSPE for sensitivity improvement, electronic demodulator error compensation (EDEC), simplification in multilevel DPSK detection, and reconstruction of signal optical field, with

which digital compensation of transmission impairments such as dispersion and nonlinear phase noise dispersion could be realized. A polarization-diversity version of the DSCOR allowing the reception of polarization-multiplexed self-coherent signals will also be discussed.

4.4.1 Receiver Architecture of DSCOR

The schematic of DSCOR is shown in Figure 4.12. The optical complexity of the DSCOR is similar to that of a conventional direct-detection DQPSK receiver. The received signal, $r(t) = |r(t)|\exp[j \times \phi(t)]$, is first split into two branches that are connected to a pair of ODIs with *orthogonal* phase offsets θ and $\theta \quad \pi/2$, where θ is an arbitrary phase value. Note that the phase orthogonality is assumed to be guaranteed, e.g., via the design reported in Ref. [33]. This simplifies the control of the pair of ODIs to a single phase control. The delay in each of the ODI, τ, is set to be approximately T/sps, where T is the signal symbol period and sps is the number of samples per symbol of the ADCs that convert the two detected analog signal waveforms, referred to as the I and Q components, to digitized waveforms $u_I(t)$ and $u_Q(t)$, which follow

$$u(t) = u_I(t) + j \times u_Q(t) = \mathrm{e}^{j\cdot\theta} r(t) \times r^*(t - \tau). \tag{4.28}$$

The optical phase difference between adjacent sampling locations can be obtained from

$$e^{j\times[\phi(t) \quad \phi(t \quad \tau)]} = u(t)\mathrm{e}^{\ j\cdot\theta} \Big/ \left|u(t)\mathrm{e}^{\ j\cdot\theta}\right|. \tag{4.29}$$

With the differential phase information being available, a digital representation of the received signal field can be obtained by

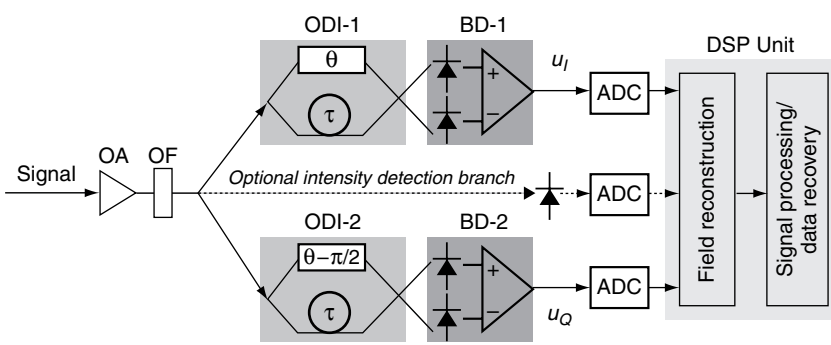

Figure 4.12 Schematic of DSCOR architecture based on orthogonal differential direct detection and DSP. OA: optical preamplifier; OF: optical filter; ODI: optical delay interferometer; BD: balanced detector; ADC: analog to digital converter (this figure may be seen in color on the included CD ROM).

$$r(t_0 + n \times \tau) = |r(t_0 + n \times \tau)| e^{j \cdot \phi(t_0)} \prod_{m=1}^{n} e^{j \times \Delta\phi(t_0 + m \times \tau)}, \tag{4.30}$$

where t_0 is an arbitrary reference time, $\phi(t_0)$ is a reference phase that can be set to 0, and the amplitude of the receiver signal can be obtained by an additional intensity detection branch [50] or approximated as below [51]

$$|r(t_0 + n \times \tau)| \approx |u(t_0 + n \cdot \tau) \times u(t_0 + n \times \tau + \tau)|^{1/4}. \tag{4.31}$$

When the ISI caused by distortions such as dispersion and PMD is reasonably small, synchronous sampling with sps = 1 may be used and the signal amplitude may be approximated as a constant. Note that DSCOR can be designed to be polarization-independent to readily receive a single-polarization signal, while sampled coherent receiver requires polarization alignment between the signal and the OLO or polarization diversity. Once the received optical signal field is digitally available, advanced signal processing techniques, similar to those used in sampled coherent receivers, may be applied in DSCOR to mitigate transmission impairments, as to be discussed in Section 4.5.

In the special case with sps = 1, the delay in the orthogonal ODI pair equals to the symbol period, and the I and Q decision variables for an m-ary DPSK signal can be directly obtained by setting $\theta = \pi/m$ (as discussed earlier). Any demodulator phase error $\phi_e = \theta - \pi/m$ can be compensated by using the following simple EDEC process:

$$u(t) \rightarrow e^{\ j \cdot \phi_e} u(t). \tag{4.32}$$

Figure 4.13 shows the eye diagrams for the detected I and Q components of a 40-Gb/s DQPSK signal at different demodulator phase errors [49]. With $\phi_e = \pi/8$, the eyes are heavily distorted. With $\phi_e = \pi/2$, the eye of the I component is completely inverted, corresponding to a BER of 0.5. Figure 4.14 shows the measured BER

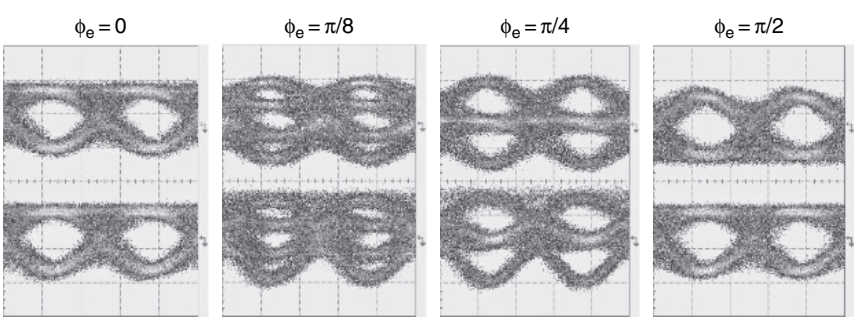

Figure 4.13 Measured I (upper) and Q (lower) eye diagrams of a 40 Gb/s DPQSK signal at different demodulator phase errors. Timescale is 20 ps/div [49] (this figure may be seen in color on the included CD ROM).

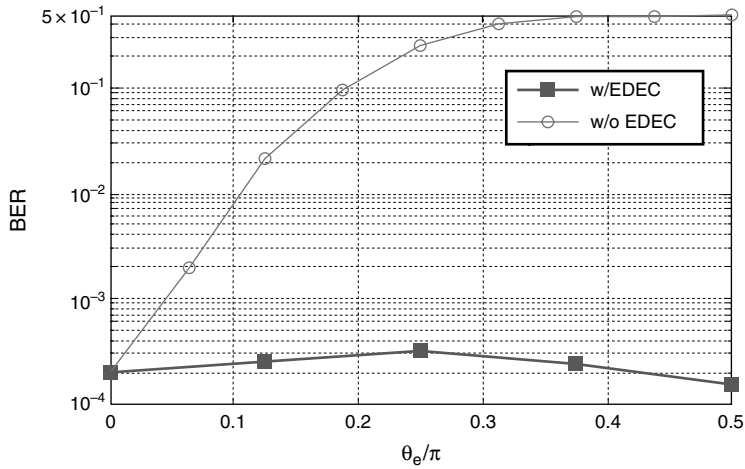

Figure 4.14 Measured BER of the 40 Gb/s DQPSK signal as a function of demodulator phase error. The optical power before the preamplifier is 38.5 dBm, corresponding to an OSNR of 16 dB [49] (this figure may be seen in color on the included CD ROM).

as a function of the demodulator phase error with the EDEC. The open symbols show the calculated BERs without the EDEC. The EDEC effectively compensates for these demodulator errors with <0.3 dB penalty. It is also confirmed that the EDEC remains effective for any arbitrary demodulator phase error. Note that the EDEC process can be automated, e.g., with the help of the error information provided by FEC.

4.4.2 Receiver Sensitivity Enhancement Via MSPE

We know from previous sections that there is a differential-detection penalty in receiver sensitivity for DPSK as compared to PSK. This penalty can be substantially reduced by using a data-aided MSPE that utilizes the previously recovered data symbols to recursively extract a new phase reference that is more accurate than that provided by the immediate past symbol alone [52], and its *analog* implementations have been proposed for optical DQPSK [53 55], DQPSK/ASK [54], and *m*-ary DPSK [56]. The MSPE concept was recently extended to the *digital* domain in Refs [49] and [36]. An improved complex decision variable for *m*-ary DPSK can be written as [36]

$$x(n) = u(n) + \sum_{p=1}^{N} \left\{ w^p \mathrm{e}^{\ jp\pi/m} u(n) \prod_{q=1}^{p} \left[u(n-q) \times \mathrm{e}^{\ j\Delta\phi(n\ \ q)} \right] \right\}, \qquad (4.33)$$

where $u(n)$ is the directly detected complex decision variable for the nth symbol, m is the number of phase states of the m-ary DPSK signal, N is the number of past

decisions used in the MSPE process, w is a forgetting factor, and $\Delta\phi\ (n \quad q) = \phi\ (n \quad q) \quad \phi\ (n \quad q \quad 1)$ is the optical phase difference between the $(n \quad q)$th and the $(n \quad q \quad 1)$th symbols, which can be estimated based on the past decisions. One advantage of the digital implementation is that w can be conveniently set at 1, and N can be small (e.g., <5) to obtain most of the sensitivity enhancement [36]. The computational complexity of the data-aided MSPE, in terms of the number of complex multiplications and additions, increases roughly linearly with N.

In a recent 40-Gb/s DQPSK experiment with offline DSP, the benefits of the MSPE and EDEC were confirmed. Figure 4.15 shows the BER performance with the data-aided MSPE activated in both back-to-back and nonlinear transmission configurations [49]. At BER = 10 ^{3}, the MSPE improves the back-to-back receiver sensitivity by 0.5 dB and 1 dB with $N = 1$ and $N = 3$, respectively. The forgetting factor w was set to 1. The performance difference between $2^{15} \quad 1$ and $2^{7} \quad 1$ patterns is negligible. The achieved back-to-back sensitivity is $\quad 41.5$ dBm for BER = 10^{-3}, which is close to that obtained with coherent-detection QPSK ($\quad 42$ dBm for BER = 10 ^{3}) [42]. After transmission over the 320-km fiber link, the signal performance was severely degraded by nonlinear phase noise and polarization-dependent frequency shift of the demodulator. Remarkably, with the combined use of EDEC and MSPE, the required OSNR for BER = 10 ^{3} is reduced by 3.2 dB, indicating the improved performance of DSCOR over conventional direct-detection receivers with binary decision circuitries.

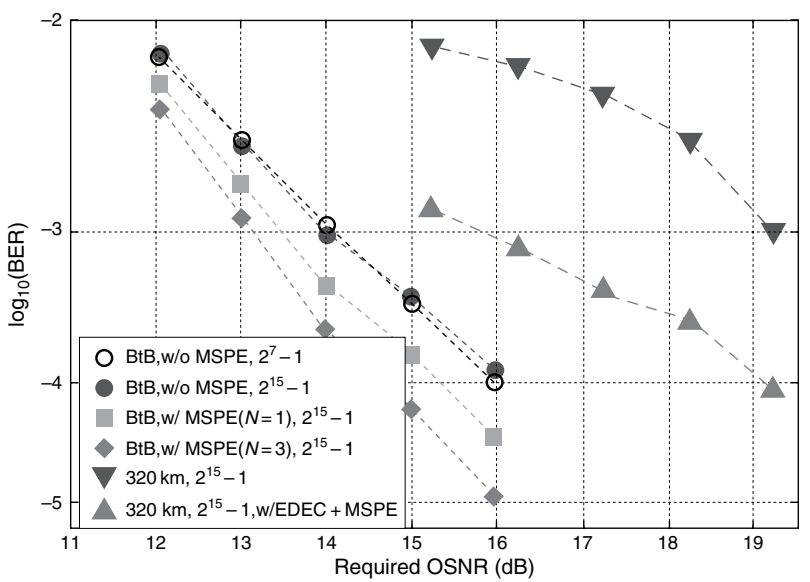

Figure 4.15 Measured BER performance of the 40 Gb/s DQPSK signal received with and without the MSPE [49] (this figure may be seen in color on the included CD ROM).

4.4.3 Detection of *m*-ary DPSK

The DSCOR can be used to receive high spectral-efficiency *m*-ary DPSK signals [17, 36]. As described previously, the $\log_2(m)$ data tributaries of an *m*-ary DPSK signal are usually obtained from *m*/2 decision variables associated with *m*/4 ODI pairs having the following orthogonal phase offsets, $\left(\frac{\pi}{m}, \frac{\pi}{m} - \frac{\pi}{2}\right)$, $\left(\frac{3\pi}{m}, \frac{3\pi}{m} - \frac{\pi}{2}\right)$, …, $\left(\frac{(m/2\ \ 1)\pi}{m}, -\frac{\pi}{m}\right)$. With the assistance of DSP, we show below that the last (*m*/2 2) decision variables can be derived by linear combinations of the first two decision variables, u_I and u_Q. This dramatically reduces the optical complexity associated with the detection of *m*-ary DPSK. The decision variables associated with phase offset $\pi p/m$ ($p = 3, 5, \ldots, m/2\ \ 1$) can be expressed as

$$\nu(\pi p/m) = \cos\left(\frac{p-1}{m}\pi\right)u_I - \sin\left(\frac{p-1}{m}\pi\right)u_Q. \tag{4.34}$$

Similarly, we can express their orthogonal counterparts as

$$\nu(\pi p/m - \pi/2) = \sin\left(\frac{p-1}{m}\pi\right)u_I + \cos\left(\frac{p-1}{m}\pi\right)u_Q. \tag{4.35}$$

The data tributaries of an *m*-ary DPSK signal can then be retrieved by Eqn (4.22). When the data-aided MSPE is applied, u_I and u_Q in the above two equations need to be replaced with their corresponding improved decision variables. In effect, the complex decision variable $u(n)$ or $x(n)$ contains complete information on the differential phase between adjacent symbols, and is sufficient for deriving all the needed decision variables. The above formulas form the basis of a simple yet universal DSCOR receiver platform for *m*-ary DPSK using only one pair of orthogonal demodulators as shown in Figure 4.12.

Figure 4.16 shows the BER performances of a 30-Gb/s 8-ary DPSK signal as a function of OSNR (defined with 0.1-nm noise bandwidth) in linear and nonlinear transmissions. In the nonlinear transmission, the mean nonlinear phase shift increases with the signal power and consequently the received OSNR, and it reaches 1 rad when the OSNR is 19 dB. With $N = 8$, the data-aided MSPE improves the signal performance by 2.14 and 2.3 dB, respectively, in the linear and nonlinear regimes, substantially eliminating the differential-detection penalty.

4.4.4 Polarization-Diversity DSCOR

PMUX provides a straightforward way to double spectral efficiency, relax transmitter/receiver bandwidth requirement, and increase signal tolerance to CD and PMD. To receive a polarization-multiplexed self-coherent signal, polarization diversity is needed for DSCOR. Figure 4.17 shows the schematic of a polarization-diversity

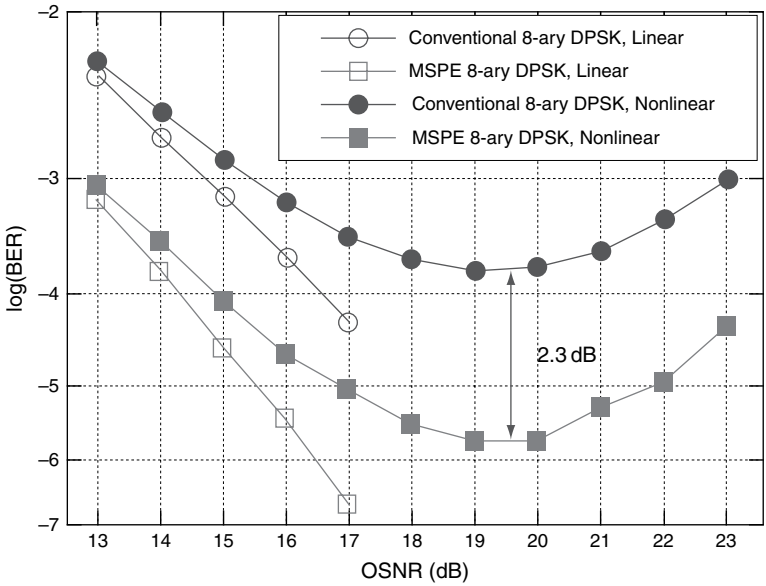

Figure 4.16 Simulated BER performances of a 30 Gb/s 8 ary DPSK signal received with the data aided MSPE (N 8 and w 1) as compared to those without (this figure may be seen in color on the included CD ROM).

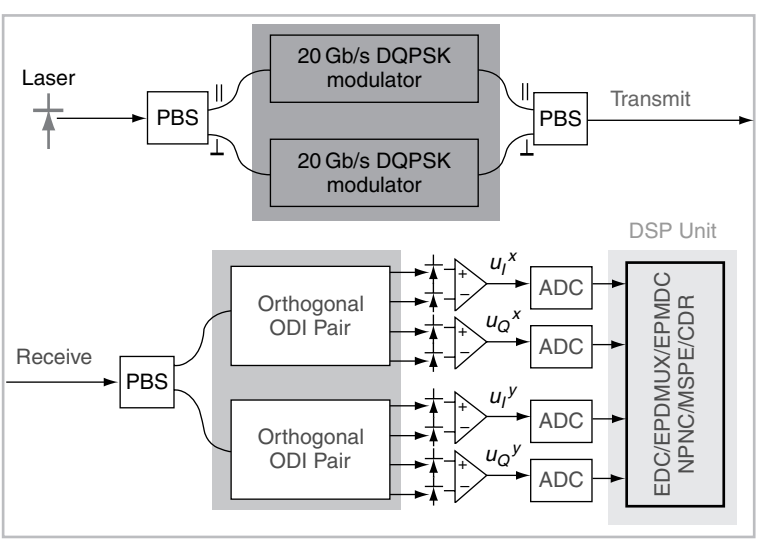

Figure 4.17 Schematic of a polarization diversity DSCOR with EPDMUX for receiving a polarization multiplexed DQPSK signal. PBS: polarization beam splitter (this figure may be seen in color on the included CD ROM).

DSCOR. The upper plot shows the transmitter setup for a polarization-multiplexed DQPSK signal. The output from a laser is equally split by a polarization beam splitter (PBS) into two orthogonally polarized components, each of which is modulated by DQPSK at 20 Gb/s. A second PBS combines the two generic DQPSK signals into a 40-Gb/s polarization-multiplexed DQPSK signal. For better signal performance, RZ pulse formatting can be used, in which case polarization bit-interleaving may be optionally used to improve signal tolerance to nonlinearity. The received optical signal is first split by a PBS into two orthogonally polarized components, each of which is differentially detected and sampled according to the single-polarization DSCOR architecture described previously. The complexity of the optical front end may be reduced through integration. The optical fields of these two polarization components are then reconstructed, and used to recover the fields of the original polarization components through an electronic polarization demultiplexing (EPDMUX) process. Since the signal polarization after fiber transmission is arbitrary, adaptive EPDMUX is needed. With the access to the optical fields of two orthogonal polarization components of the signal, electronic PMD compensation (EPMDC) may be performed. Detailed discussions on various digital equalization or compensation algorithms will be given in Section 4.5.

4.5 ADAPTIVE EQUALIZATION TECHNIQUES IN DIGITAL COHERENT/SELF-COHERENT OPTICAL RECEIVERS

With the reconstruction of signal optical field, digital equalization or compensation of transmission impairments can be applied, offering system-level benefits not possible with traditional direct detection receivers. Figure 4.18 shows the block diagram of possible signal processes that can be implemented in the DSP unit of a polarization-diversity DSCOR. The inputs to the DSP unit are four digitized waveforms, e.g., sampled by four ADCs as shown in Figure 4.17, that represent the I and Q components of each of two (arbitrary) orthogonal polarization states of the received signal. The outputs from the DSP unit are digital representations of the recovered I and Q components of each of the two *original* polarization states of the signal. If the self-coherent signal is based on m-ary DPSK with $m > 4$, further signal processing, as described in Section 4.4.3, is needed to recover the other data tributaries in addition to the I and Q tributaries. The outputs can also be of a multilevel format (rather than a binary format) so that soft FEC [57, 58] can be applied to further improve the receiver performance. Feedbacks from FEC may be needed for the EDEC and nonlinear phase noise compensation (NPNC) processes. As a comparison, Figure 4.19 shows a similar block diagram for a digital coherent optical receiver. In principle, DSCOR offers similar impairment equalization capabilities as digital coherent optical receiver. In this section, we will discuss algorithms for processes such as EDC, EPDMUX, EPMDC, and NPNC that are common to both coherent and self-coherent receivers. Signal processes that are unique to digital coherent optical receivers such as carrier

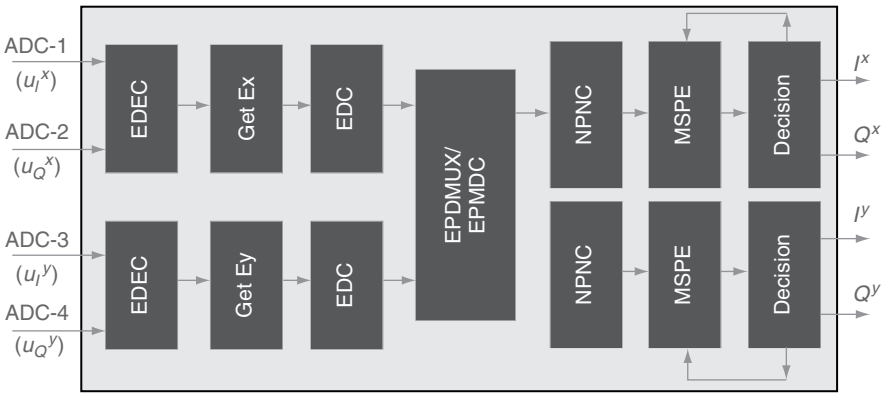

Figure 4.18 Block diagram of possible signal processes implemented in the DSP unit of a polarization diversity DSCOR. EDEC: electronic demodulator error compensation; EDC: electronic dispersion compensation; Get *E*: optical e field reconstruction; EPDMUX: electronic polarization de multiplexing; EPMDC: electronic PMD compensation; MSPE: data aided multisymbol phase estimation; NPNC: nonlinear phase noise compensation (this figure may be seen in color on the included CD ROM).

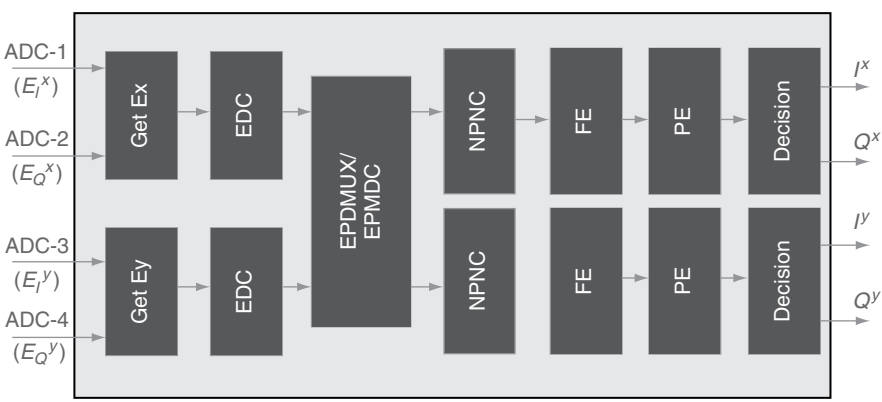

Figure 4.19 Block diagram of signal processes implemented in the DSP unit of a polarization diversity digital coherent optical receiver. FS: frequency estimation; PE: phase estimation (this figure may be seen in color on the included CD ROM).

frequency estimation (FE) and phase estimation (PE) will also be discussed. Implementation complexity of these algorithms will be briefly mentioned. More detailed descriptions on digital coherent optical receivers can be found in Chapter 3 "Coherent Optical Communication Systems" by K. Kikuchi.

4.5.1 Electronic Dispersion Compensation

As shown previously, the signal field can be digitally reconstructed in the DSCOR. EDC can be performed to restore the original signal via, e.g., a multistage digital

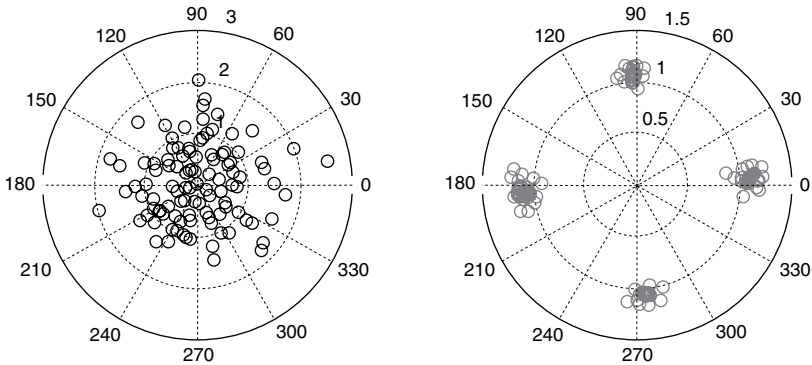

Figure 4.20 Constellation diagrams of a 20 Gb/s DQPSK signal after experiencing 34,000 ps/nm dispersion without EDC (left) and with EDC (right) (this figure may be seen in color on the included CD ROM).

finite impulse response (FIR) filter that approximates the inverse function of the dispersion experienced by the signal during fiber transmission. Figure 4.20 shows simulated constellation diagrams of a 20-Gb/s DQPSK signal after experiencing 34,000 ps/nm dispersion without EDC and with EDC using sps = 4 and approximated signal amplitude [51]. Large sps helps to capture more details in the signal waveform to allow more effective EDC, but at the expense of higher requirement in electronics. Without EDC, the signal constellation is completely destroyed, while with the EDC, signal constellation is almost fully restored. The effectiveness of the field reconstruction and EDC in DSCOR was also confirmed, both experimentally [50] and numerically [51], in typical optically repeated transmission links with the consideration of optical amplified spontaneous noise (ASE) and fiber nonlinearity. We note, however, that care needs to be taken at sampling locations where the signal amplitude is close to zero, particularly when the sampling resolution is limited [50, 51].

4.5.2 Electronic Polarization Demultiplexing

In a polarization multiplexed transmission system, two signals x_1 and x_2 are launched into two orthogonal polarization states which are typically linearly oriented. If nonlinear effects are ignored, the transmission over fiber can be modeled by dividing up the transmission channel (e.g., the fiber) in multiple sections. In each section, the optical field is modified by a random polarization transformation, which can be described by a lossless Jones matrix. This transformation is followed by a differential delay for modeling polarization mode dispersion and a loss term in one mode, which describes elements with

polarization-dependent loss. The received field (y_1, y_2) is then the result of a cascade of multiple of these operations:

$$\begin{pmatrix} y_1 \\ y_2 \end{pmatrix} \begin{pmatrix} \cos\phi_n + j\sin\phi_n\cos\varphi_n & j\sin\phi_n\sin\varphi_n(\exp j\eta_n) \\ j\sin\phi_n\sin\varphi_n\exp(\ j\eta_n)\exp(\ \alpha_n\ j\omega\tau_n) & (\cos\phi_n\ j\sin\phi_n\cos\varphi_n)\exp(\ \alpha_n\ j\omega\tau_n) \end{pmatrix}$$
$$\bullet$$
$$\bullet$$
$$\bullet$$
$$\begin{pmatrix} \cos\phi_1 + j\sin\phi_1\cos\varphi_1 & j\sin\phi_1\sin\varphi_1(\exp j\eta_1) \\ j\sin\phi_1\sin\varphi_1\exp(\ j\eta_1)\exp(\ \alpha_1\ j\omega\tau_1) & (\cos\phi_1\ j\sin\phi_1\cos\varphi_1)\exp(\ \alpha_1\ j\omega\tau_1) \end{pmatrix} \begin{pmatrix} x_1 \\ x_2 \end{pmatrix}. \tag{4.36}$$

In Eqn (4.36), we assume that n sections are sufficient to describe the linear polarization effects in the fiber channel. ϕ_k, φ_k, η_k denote the phase parameters of the Jones matrix transformation, α_k denotes the polarization-dependent loss, and τ_k denotes the differential group delay of the kth transformation. ω is the angular frequency of the optical system.

Neglecting polarization mode dispersion, Eqn (4.36) can be simplified to a simple matrix transformation

$$\begin{pmatrix} y_1 \\ y_2 \end{pmatrix} = \begin{pmatrix} g_{11} & g_{12} \\ g_{21} & g_{22} \end{pmatrix} \begin{pmatrix} x_1 \\ x_2 \end{pmatrix} = \mathbf{G} \begin{pmatrix} x_1 \\ x_2 \end{pmatrix} \tag{4.37}$$

with g_{ij} complex numbers slowly varying in time. Purpose of the adaptive polarization demultiplexer is to find a matrix transformation $\mathbf{H}$ that transforms the received symbols y_1, y_2 in estimates z_1, z_2 for the transmitted symbols x_1, x_2:

$$\begin{pmatrix} z_1 \\ z_2 \end{pmatrix} = \mathbf{H} \begin{pmatrix} y_1 \\ y_2 \end{pmatrix} \approx \begin{pmatrix} x_1 \\ x_2 \end{pmatrix}. \tag{4.38}$$

Inserting Eqn (4.37) into Eqn (4.38) yields that the matrix product $\mathbf{HG}$ should be the unity matrix.

As mentioned before, in this calculation we omitted the effects of polarization mode dispersion.

There are several options for determining the coefficients of the equalization filters $h_{ij}(l)$. One possibility is to transmit a known symbol sequence, called training sequence, calculating the coefficients of the matrix $\mathbf{G}$ and then inverting $\mathbf{G}$ to calculate $\mathbf{H}$. There are two problems with this method: First, matrix inversion in a signal processor, albeit possible, e.g., with the QR algorithm, requires a large amount of processing resources. Second, as the g_{ij} are varying in time, the training sequence has to be retransmitted every time there had been a significant change of the parameters g_{ij}.

More desirable would be a method that can adaptively estimate the coefficients $h_{ij}(l)$ without the need of training sequences. Such an estimation algorithm is called a blind estimator. One commonly used algorithm for this purpose is the so-called

Goddard or constant modulus algorithm (CMA). Originally proposed in Ref. [59] and independently in Ref. [60], this algorithm, in its original form, provides as criterion to reduce ISI for channels with impulse responses longer than the sampling time. It is designed to operate for modulation formats having a constant modulus, i.e., a constant amplitude, as phase-shift keyed modulation formats do. It has been shown though that the same algorithm is even applicable for some nonconstant modulus modulation formats, e.g., QAM. Already in Ref. [61], this algorithm was proposed for source separation in a multiple-in multiple-out communication (MIMO) system. A polarization multiplexed transmission system is essentially a MIMO system as well, or more precisely a two-in, two-out system. A comprehensive review of the constant modulus algorithm can be found, e.g., in Refs [62, 63].

The CMA tries to penalize deviations from a constant modulus of the equalized signals and adapt the equalization filter coefficients to minimize a cost function

$$\begin{aligned} \varepsilon_1 &= E\left\{\left(1-|y_1|^2\right)^2\right\}, \\ \varepsilon_2 &= E\left\{\left(1-|y_2|^2\right)^2\right\}, \end{aligned} \tag{4.39}$$

$E\{\cdot\}$ denotes the expectation operator. Using an iterative gradient-type optimization algorithm, coefficients $h_{ij}(l)$ can be found that minimize Eqn (4.39) for instance as follows:

$$\begin{aligned} h_{11}(k+1,l) &= h_{11}(k,l) + \mu\,\delta\varepsilon_1\, z_1(k) y_1^*(k+l), \\ h_{12}(k+1,l) &= h_{12}(k,l) + \mu\,\delta\varepsilon_1\, z_1(k) y_2^*(k+l), \\ h_{21}(k+1,l) &= h_{21}(k,l) + \mu\,\delta\varepsilon_2\, z_2(k) y_1^*(k+l), \\ h_{22}(k+1,l) &= h_{22}(k,l) + \mu\,\delta\varepsilon_2\, z_2(k) y_2^*(k+l) \end{aligned} \tag{4.40}$$

with constant μ being the step size of the algorithm. The parameters $\delta\varepsilon_1$ and $\delta\varepsilon_2$ are derivatives of the cost functions expressed in Eqn (4.39), which can be estimated by replacing the expectation values by their respective instantaneous values:

$$\begin{aligned} \delta\varepsilon_1 &= 2\left(1-|y_1|^2\right), \\ \delta\varepsilon_2 &= 2\left(1-|y_2|^2\right). \end{aligned} \tag{4.41}$$

4.5.3 Electronic PMD Compensation

PMD is a major impairment for some high-speed transmission systems. With the access to the optical fields of two orthogonal polarization components of a signal, electronic PMD compensation (EPMDC) has been recently demonstrated in

sampled coherent receivers [43, 44] through off-line DSP. It is expected that polarization-diversity DSCOR can similarly provide the EPMDC function. To compensate for PMD, we can rewrite Eqn (4.38) so that the coefficients h_{ij} of the matrix **H** are replaced by FIR filters:

$$\begin{pmatrix} z_1(k) \\ z_2(k) \end{pmatrix} = \sum_{l=-B/2}^{B/2} \begin{pmatrix} h_{11}(l) & h_{12}(l) \\ h_{21}(l) & h_{22}(l) \end{pmatrix} \begin{pmatrix} y_1(k+l) \\ y_2(k+l) \end{pmatrix}, \tag{4.42}$$

k is the sampling time index. To effectively compensate for PMD, the FIR filter length $B+1$ of the equalization filters h_{ij} (l) should be longer than the maximum differential group delay divided by the sampling time T_s.

The constant modulus algorithm using an unrestricted full FIR filter in place of each of the matrix coefficients can be potentially simplified by accepting certain performance restrictions, such as compensation of the first-order PMD only. Up to now, only limited work has been reported on the study of the convergence characteristics of such algorithms.

4.5.4 Nonlinear Phase Noise Compensation

In optical fiber transmission, phase-modulated signals are susceptible to the Gordon-Mollenauer phase noise [64] resulting form the interaction between SPM and ASE noise. It is possible to partially compensate for the nonlinear phase noise at receiver [43, 65, 66]. This can be achieved by replacing the directly measured complex decision variable, $u(n)$, with the following compensated complex variable:

$$u^{\mathrm{NPNC}}(n) = u(n) \times \exp\{-j \times c_{\mathrm{NL}}[P(n) - P(n-1)]/2\}, \tag{4.43}$$

where c_{NL} is the average nonlinear phase shift experienced by the signal over the fiber transmission, and $P(n)$ is the normalized signal power of the nth symbol. Partial NPNC in a 40-Gb/s QPSK signal was recently demonstrated in a sampled coherent receiver using offline DSP [43]. XPM between different WDM channels is another nonlinear effect that causes nonlinear phase noise. Without knowing the signal fields of other WDM channels, it is not possible to compensate for XPM-induced nonlinear phase noise in either digital coherent receiver or DSCOR. Note that in DSCOR, the data-aided MSPE can help extracting a more stable phase reference, and thus mitigate the XPM-induced penalty.

4.5.5 Frequency Estimation

In digital coherent (or intradyne) optical receivers, there is no phase locking between the OLO and the received optical signal. Typical phase estimation algorithms, which will be discussed below, can only tolerate small amount of frequency difference

between the OLO and the transmit laser. Therefore, either a frequency-locked loop has to be incorporated in the receiver to keep the OLO frequency close enough to the transmit laser or a frequency offset compensation has to be incorporated into the digital signal processor [67]. Either way, frequency offset estimation has to be performed in the DSP.

Frequency offset compensation can be performed by estimating the phase shift $\Delta\varphi = 2\ \pi\Delta\nu\ T_s$ between two consecutive samples a_k, a_{k+1} that is caused by a frequency offset $\Delta\nu$ between the OLO and the transmit laser frequency, with T_s sampling time. The operation is as follows. First, the received symbol is multiplied with the complex conjugate of the previous symbol. This results in a complex number whose phase is equal to the difference in phase of the two symbols. Then, any information that is encoded in the signal phase has to be removed. This can easily be performed for *m*-ary PSK signals by taking the *m*th power of the complex symbol, e.g., for QPSK, the fourth power has to be taken. Taking the *m*th power of a complex number is equivalent to taking the, *m*th power of its magnitude and multiplying its phase by m. With proper phase wrapping, for a PSK-modulated signal, this operation will yield in a constellation where all constellation points lie on top of each other.

The result is then summed up over a large number of samples. This summation essentially performs a *long-range* averaging operation to find the mean frequency difference between the OLO and the signal in the presence of the laser noise. The phase then has to be divided by four to correct for the earlier power-of-four operation.

The result is an estimate for the phase difference $\Delta\varphi$ between consecutive samples. To correct for the frequency offset, an accumulated phase offset $\varphi_k = k\ \Delta\varphi$ has to be subtracted from the phase of each symbol a_k with k being a running symbol index, to obtain a corrected symbol. Figure 4.21 shows a block diagram of a frequency estimator for QPSK modulation. Further processing utilizing proper phase estimation techniques will remove any residual phase error from frequency offset that has not been fully compensated by the frequency estimator.

4.5.6 Phase Estimation

The main task of the phase estimation is to establish a phase reference to decode the phase-encoded data of a PSK or DPSK modulated signal. The phase difference

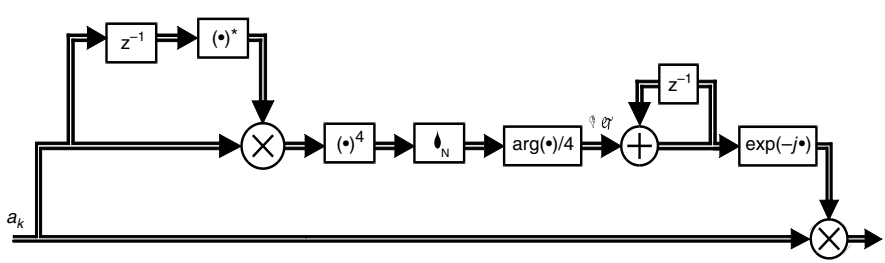

Figure 4.21 Block diagram of a phase estimator for QPSK modulation.

between the local oscillator laser and the transmit laser is changing slowly with respect to the signal baud rate due to the aggregate linewidth of the two lasers, which is typically about three orders of magnitude smaller than the baud rate, as well as optical noise from ASE and nonlinear phase noise. The simplest estimate that can be made is to assume that the phase difference between the two lasers actually did not change between two consecutive symbol slots. The phase of the previous received symbol is simply taken as phase reference. This is equivalent to the differential detection scheme. The drawback of this method is that a noisy received symbol phase is compared with a noisy reference, which leads to higher symbol errors.

To improve on the performance over the differential detection scheme, one has to establish a phase reference with improved noise performance. This can be done by taking more than one symbol into account, e.g., by averaging the phase over a number of consecutive symbols. One method to realize this is to use decision feedback to remove the data content and extract the phase reference from multiple past symbols [29, 68], in a similar way as the data-aided MSPE scheme described previously. Another method is based on a feed-forward scheme in which the phase modulation of a *m*-ary PSK signal is removed by raising the received signal field to its *m*th power [29, 39 42]. Note that differential coding is needed to solve the phase ambiguity issue even when the differential detection is not used. A commonly used phase estimator is based on the Viterbi and Viterbi algorithm [69]. Figure 4.22 shows a block diagram of a phase estimator for QPSK modulation. Originally proposed in Ref. [69] for phase estimation in burst mode digital transmission, e.g., for satellite communications, this simple feed-forward algorithm has been very popular for optical intradyne receivers as well. The operation of the phase estimator is as follows. In a first step, any coded information of the PSK-modulated signal has to be removed by the same *m*th power operation as discussed for the frequency estimator. After phase modulation removal, the symbols can be passed through a digital low-pass filter as discussed before to establish a phase reference. In case of the Viterbi and Viterbi algorithm, filtering is performed by summing the complex symbols over a short sequence of symbols. The sequence length is called block length. The appropriate block length is determined by the amount of phase noise and nonlinear phase noise in the received signal and the laser linewidth [70]. More detailed descriptions on the phase estimation process for digital coherent receivers can be found in Chapter 3 “Coherent Optical Communication Systems” by K. Kikuchi.

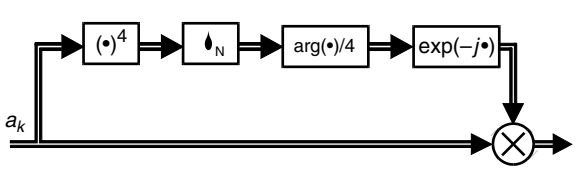

Figure 4.22 Block diagram of the phase estimator for QPSK.

4.5.7 Receiver Implementation

For practical implementation of digital coherent receivers or DSCORs, it is important to assess the required DSP resources. As current generation signal processor are not capable of processing data at rates commonly used in fiber-optic communication, data processing is typically performed in a parallel manner, with about 20 64 parallel processing paths per polarization orientation.

The most complex operation in the signal processor is the CD compensation and the polarization demultiplexing operation. As discussed in Section 4.5.1, CD compensation is typically performed using an all-pass FIR filter that inverts the frequency-dependent phase shift introduced by the fiber dispersion. The number of taps required is proportional to the amount of dispersion that has to be compensated. Each tap requires one complex multiplier, i.e., four real multipliers and one adder. On the receiver side, the FIR filter has to operate on the complex sampled symbols with a typical resolution in the order of 6 bits, while a transmitter-side precompensation filter can operate on binary data. Therefore, receiver-side dispersion compensation requires much more signal processing resources than required in a transmitter-side predistortion compensator.

From Eqn (4.38), it can be seen that the polarization demultiplexing algorithm needs four complex multipliers per filter tap. The FIR filters used in the polarization demultiplexer are typically much shorter, in the order of 3 10 taps. Additional resources are required for the adaptation of this filter according to Eqn (4.40). If the rate of polarization change is slow in comparison to the symbol rate, updating of the coefficients can be performed at a reduced rate so that the resources required for coefficient updating are negligible in comparison to the matrix operation.

Frequency and phase estimation can be implemented with a small amount of signal processing resources, as there is no need to preserve the amplitude information anymore. Multiplication operations shown in Figures 4.21 and 4.22 can be efficiently replaced by summation of the phases.

The signal processing tasks discussed in this chapter can be implemented in high-performance field programmable gate arrays (FPGA) or in latest generation application-specific integrated circuits (ASIC). While FPGAs have limitations in the amount of available processing resources, the capability of reprogramming these devices make them ideal tools for investigating the performance of the various algorithms in a more realistic setting than scope measurements coupled with offline processing. Even with the limited resources, the development of an intradyne receiver based on synchronous sampling comprising a digital polarization demultiplexer and frequency and phase estimation seems feasible in today's or next-generation FPGA technology. Early demonstrations of real-time implementation based on FPGA have been reported in Refs [46 48]. An implementation in FPGAs using oversampling and dispersion compensation at a Baud rate higher than 10 GBaud requires a significant advance in FPGA technology.

An implementation in semi-custom or even full-custom ASIC offers sufficient processing power even for an oversampling receiver with CD compensation. The required development resources as well as access cost to ASCI foundries require a much higher commitment, though. In Ref. [44], it has been reported that a full intradyne receiver comprising CD compensation and polarization demultiplexing should fit in an ASIC with 20 million gates, which can be considered a mid-size ASCI design.

Besides the signal processor, the ADCs are components that have not been used in conventional optical receivers, but in receivers using MLSE. For MLSE, typically a resolution in the order of 3 bits is sufficient [38]. For intradyne or self-coherent receivers, ADCs with an effective resolution of about 5 bits are necessary. If dispersion compensation has to be performed in the signal processor, the effective ADC resolution should be about 6 bits. A reduction of the ADC resolution by 1 bit results in an OSNR penalty of about 1 dB.

There are different options for the implementation of ADCs for Baud rates typically used for intradyne or self-coherent receivers: Direct conversion ADCs, also called flash ADCs, perform all operations, as comparison and code conversion, at sampling rate. Because of the rather high sampling rate required, typically advanced semiconductor technologies have to be used as silicon germanium (SiGe) bipolar [71] or Bi-CMOS (complementary metal-oxide semiconductor) processes [72]. Another option is to use a parallel structure, called "pipelined," were a large number of parallel slices are sampling the analog signal at a much lower rate. Small phase offsets in the clock of each slice produce time-interleaved samples. This architecture can be advantageously implemented in CMOS technology [73] and therefore lends itself to a monolithic integration of ADC and signal processor.

4.6 APPLICATIONS OF SELF-COHERENT OPTICAL TRANSPORT SYSTEMS

In optical transport systems, optical signal quality generally degrades due to transmission impairments such as optical noise, chromatic dispersion, PMD, optical filtering, and fiber nonlinearity. Compared to traditional OOK, self-coherent optical modulation and detection schemes offer higher signal immunity to one or more of these impairments, and are being used for many start-of-the-art optical transport systems. In this section, we review some of the applications for DBPSK and DQPSK for high-capacity, long-haul, transparent optical transport systems.

4.6.1 40-Gb/s DBPSK for Long-haul WDM Transmission

Nonlinear effects in WDM optical transmissions can be categorized into intrachannel nonlinear effects and interchannel effects [5, 74]. Interchannel effects include XPM and four-wave mixing (FWM) among different wavelength

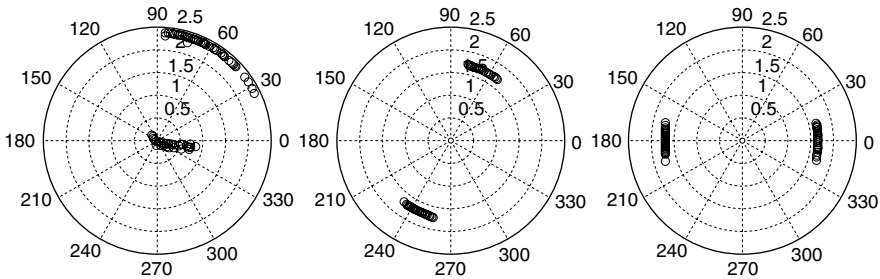

Figure 4.23 Simulated phasor diagrams showing the amplitude and phase at the centers of signal bits in RZ OOK (left) and RZ DBPSK (center), and the differential phase between adjacent bits in RZ DBPSK (right) after a typical 40 Gb/s nonlinear transmission [75].

channels, and intra-channel effects include SPM, intrachannel XPM (IXPM), and intrachannel FWM (IFWM). For DPSK, the signal quality is also degraded by the Gordon Mollenauer nonlinear phase noise [64], which is converted from the ASE noise-induced signal amplitude fluctuations through the SPM and/or the XPM. The importance of each nonlinear effect in a particular optical transmission system depends on the system parameters. In modern dispersion-managed 40-Gb/s WDM transmissions, the IFWM is a major nonlinear impairment. DBPSK is found to be much more tolerant to the IFWM than OOK with the same average power [75, 76]. This is attributed to the fact that signal peak power is lower in DBPSK than OOK with the same average power, and there exists a correlation between the IFWM induced nonlinear phase shifts of any two adjacent bits [76]. Figure 4.23 shows the simulated phasor diagrams of a 40-Gb/s RZ-OOK signal and a 40-Gb/s RZ-DPSK signal that have the same average power after transmission over a symmetrically dispersion-managed link. The simulated signal pattern is a pseudo-random binary sequence (PRBS) of length 2^9 1, which is sufficient for capture most of the intra-channel nonlinear interactions in the dispersion-managed transmission. Evidently, there is a severe eye-closure penalty in the OOK signal due to the generation of ghost pulses while DBPSK suffers relatively smaller eye closure in the phase domain (see the center subplot). Interestingly, the variance of differential phase, as shown in the right subplot, is almost the same as (instead of twice as large as) that of the absolute phase, showing a strong correlation between the IFWM-induced phase noises of two adjacent bits.

Experimentally, DBPSK is also found to offer higher tolerance to nonlinear effects than OOK in most pulse-overlapped 40-Gb/s transmissions [3, 25, 77], and is considered for implementation in a nationwide optical transport network [78].

PMD is another obstacle in 40-Gb/s long-haul transmissions. DBPSK is found to have a slightly higher PMD tolerance than OOK [79]. Due to the stochastic nature of PMD and its wavelength dependence, PMD mitigation is normally done on a per-channel basis through PMD compensation (PMDC). From a system perspective, cost-effective PMD mitigation is essential. While forward error correction (FEC) is effective in correcting random errors, it is ineffective in the

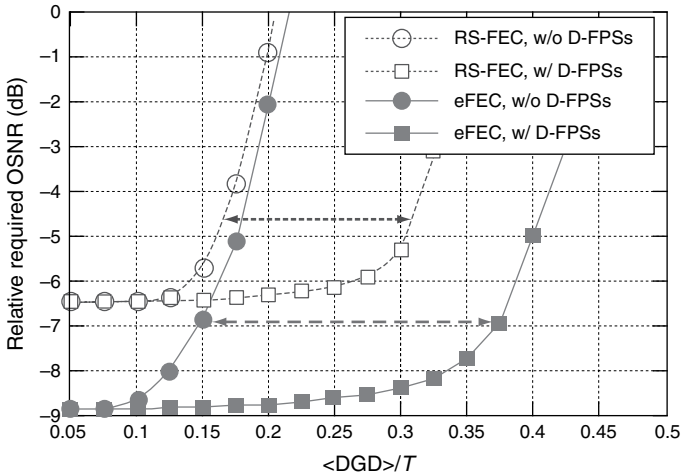

Figure 4.24 Simulated relative required OSNR at BER 10^{-15} vs $\langle DGD \rangle$ in NRZ DPSK systems that use Reed Solomon FEC (empty) or the enhanced FEC (solid) [81] (this figure may be seen in color on the included CD ROM).

presence of PMD-induced burst errors. It is found that substantial improvement in PMD tolerance can be achieved for all WDM channels by using distributed fast polarization scramblers and FEC [80 82]. It is also shown that this PMD mitigation scheme is even more effective for DBPSK with balanced detection than for OOK. Over 140% improvement in PMD tolerance was achieved in a DBPSK system that uses an enhanced FEC code with a 7% overhead [81]. Figure 4.24 shows simulated relative required OSNR as a function of the mean DGD divided by the bit period T. The effectiveness of the PMD mitigation technique has also been demonstrated in a straight-line experiment with 40-Gb/s DBPSK [83]. Note that with the use of this PMD mitigation scheme, the PMD tolerance of 40-Gb/s DQPSK channels can be as large as 15 ps, which is larger the PMD tolerance specified in typical 10-Gb/s systems that do not adopt PMD mitigation or compensation.

4.6.2 Mixed 40-Gb/s DBPSK and DQPSK for High Spectral-Efficiency DWDM

Hybrid DWDM transmission with 10-Gb/s OOK and 40-Gb/s DBPSK channels has been demonstrated in nationwide optical transport network [78]. The network incorporates a novel ROADM architecture [84] that incorporates 50-GHz-spaced asymmetric-bandwidth interleavers to allocate wider bandwidth for 40-Gb/s channels and narrower bandwidth for 10-Gb/s channels, without sacrificing the performance of 10-Gb/s channels. To further increase the capacity of such a deployed

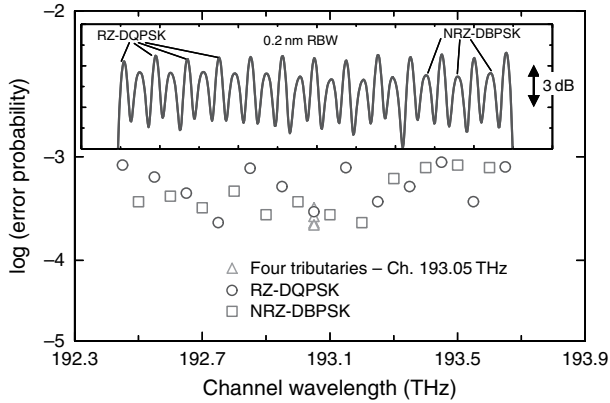

Figure 4.25 Received BER for each of the 25 channels after transmission over a 1280 km SSMF link having four ROADMs [85] (this figure may be seen in color on the included CD ROM).

network, it is desirable to upgrade the 10-Gb/s channels with bandwidth-efficient 40-Gb/s formats such as DQPSK. Recently, hybrid transmission of 40-Gb/s DBPSK and DQPSK channels with a spectral efficiency of 0.8-bit/s/Hz was demonstrated [85] in such a DWDM system. 25 DWDM channels carrying an overall capacity of 1 Tb/s were transmitted over 16×80-km standard single mode fiber (SSMF) spans with EDFA-only amplification and four passes through bandwidth-managed ROADMs. Figure 4.25 shows the transmission performance in terms of the received BER for each of the 25 channels after the 1280-km transmission. The BER of each of these channels is lower than 8×10^{-4}, which is well below the threshold of a typical enhanced FEC of 2×10^{-3}, at which the corrected BER is expected to be below 10^{-15}. The inset shows the channel spectra, with alternating 40-Gb/s DQPSK and 40-Gb/s DBPSK channels. The nonlinear crosstalk among the WDM channels was found to be acceptably small.

4.6.3 100-Gb/s Transmissions

100-Gb/s Ethernet is currently under consideration for next-generation Ethernet transport systems [86]. While a parallel approach that supports 100-Gb/s by using multiple low data-rate wavelength channels (e.g., 10-Gb/s channels) may be more readily adopted, it would not offer as high spectral efficiency and system cost-saving as those would be offered by a serial approach based on a single wavelength channel. 100-Gb/s per channel data rate, however, puts a set of stringent requirements on transmitter/receiver bandwidth, system OSNR performance, and system tolerance to CD and PMD. Multilevel self-coherent modulation formats DQPSK and polarization-multiplexed DQPSK lower the signal baud rates by two and four times, respectively, and are promising candidates for 100-Gb/s. WDM

transmission of 10×107-Gb/s RZ-DQPSK channels over 2000 km has recently been demonstrated [87]. More recently, WDM transmission with 204×111-Gb/s polarization-multiplexed RZ-DQPSK channels over 240 km was demonstrated [88]. Transparent optical transmission of 10×107-Gb/s NRZ-DQPSK channels over a 1200-km link having six ROADM nodes was also reported [89]. To improve the system tolerance to CD and PMD, a 111 Gb/s digital coherent optical receiver for polarization-multiplexed RZ-DQPSK signals has been demonstrated with four 50-Gsamples/s 6-bit ADCs (embedded in a digital storage oscilloscope) and an offline DSP unit [45]. The throughout of the DSP unit is on the order of 1 Tb/s. It remains to be seen if the real-time implementation of such 100-Gb/s digital coherent receivers is technologically feasible and economically viable.

4.6.4 Forward-Looking Topics

There are other promising applications of self-coherent transmission systems. We briefly mention a few in this section. With the availability of optical phase as a means to carry information, self-coherent optical systems may also find interesting applications in secured communications [90, 91]. A new physical layer optical encryption approach based on quantum noise limited optical signals and *m*-ary DPSK that operates at high data rates was demonstrated. Keyed *m*-ary DPSK was used to encrypt quantum noise limited mesoscopic signals with about 50 k photons/bit that are compatible with current directions in optical networking, allowing the physically encrypted signals to be optically amplified, routed through optical switches, and transmitted over long distances approaching 1000 km [91].

With its high tolerance to coherent crosstalk [31], DBPSK is finding applications in optical code-division multiple access system [92]. Semiconductor optical amplifiers (SOAs) have promising applications in systems such as integrated communication circuits. RZ-DPSK is found to exhibit small ISI after amplification in SOAs [93, 94], and is well suited for SOA-based communication systems. Optical packet switching (OPS) and optical burst switching (OBS) are regarded as promising transport technologies. In OPS and OBS systems, a challenging issue is the need of burst-mode receivers capable of fast resynchronization to different data packets or bursts with different amplitudes and timings. Direct-detection DPSK with balanced detectors has a fixed optimal decision threshold at about zero, and may allow burst-mode detection be more easily implemented than in the OOK case.

While the XPM among DPSK signals may not be a major issue in most optical transport systems, the XPM from neighboring 10-Gb/s OOK channels to 40-Gb/s DBPSK or DQPSK is found to cause severe nonlinear impairments [95 98] in various fiber types. Since most optical transport system upgrades are expected to take place in systems already carrying 10-Gb/s OOK channels, the XPM penalty needs to be carefully managed. Given the strong dependence of XPM on system designs such as dispersion map and channel occupancy, it is needed to systematically investigate the XPM penalty in a WDM system mixed with high-speed

(40 and 100 Gb/s, etc.) self-coherent channels and 10-Gb/s OOK channels. Mitigation strategies for the XPM penalty are also desired.

4.7 CONCLUSION

We have reviewed the principle and progress of self-coherent optical transport systems. Various self-coherent modulation formats and their detection schemes are presented. Particularly, digital self-coherent receiver and its potential capabilities in mitigating transmission impairments are discussed. Self-coherent optical transport systems, promising many benefits not possible with traditional OOK-based systems are expected to find a wide range of applications to meet the ever-increasing demand of capacity upgrade and cost reduction in future optical networks.

LIST OF ACRONYMS

ADC	Analog-to-digital conversion (converter)
ASIC	Application specific integrated circuit
BER	Bit error rate
CD	Chromatic dispersion
CMA	Constant modulus algorithm
DBPSK	Differential binary phase-shift keying
DQPSK	Differential quadrature phase-shift keying
DPSK	Differential phase-shift keying
DSCOR	Digital self-coherent receiver
DSP	Digital signal processing
EDC	Electronic dispersion compensation
EPDMUX	Electronic polarization demultiplexing
EPMDC	Electronic PMD compensation
FEC	Forward error correction
FIR	Finite impulse response
FPGA	Field programmable gate array
FS	Frequency estimation
IFWM	Intrachannel four-wave mixing
ISI	Intersymbol interference
MLSE	Maximum likelihood sequence estimation
MSPE	Multisymbol phase estimation
MZM	Mach Zehnder modulator
NPNC	Nonlinear phase noise compensation
NRZ	Non-return-to-zero
OBS	Optical burst switching
ODI	Optical delay interferometer

OLO	Optical local oscillator
OOK	On-off keying
OPS	Optical packet switching
OSNR	Optimal signal-to-noise ratio
PAM	Pulse amplitude modulation
PE	Phase estimation
PMD	Polarization-mode dispersion
PMUX	Polarization-division multiplexing
PPB	Photons per bit
PSK	Phase-shift keying
QAM	Quadrature amplitude modulation
ROADM	Optical add/drop multiplexer
RZ	Return-to-zero
SPM	Self phase modulation
SSMF	Standard single mode fiber
WDM	Wavelength-division multiplexing
DWDM	Dense wavelength-division multiplexing
XPM	Cross-phase modulation

ACKNOWLEDGMENTS

The progress on self-coherent optical transport systems summarized in this chapter implicitly represents the works of many researchers and developers around the world, and in this limited space the authors were unable to include all the contributions. The authors are especially grateful to their colleagues working in this field in Bell Laboratories, Alcatel-Lucent, for fruitful collaborations and valuable discussions. Among them are C. R. Doerr, R. Essiambre, D. A. Fishman, D. M. Gill, A. H. Gnauck, I. Kang, Y.-H. Kao, N. Kaneda, D. Kilper, Ut-Va Koc, S. K. Korotky, G. Kramer, J. Leuthold, C. J. McKinstrie, L. F. Mollenauer, L. Möller, Y. Su, A. J. van Wijngaarden, X. Wei, S. Weisser, P. J. Winzer, C. Xie, C. Xu, and A. Zottmann. The authors also wish to thank Y. K. Chen, A. R. Chraplyvy, C. R. Giles, and R. W. Tkach for their support.

REFERENCES

[1] R. C. Giles and K. C. Reichmann, "Optical self homodyne DPSK transmission at 1 Gbit/s and 2 Gbit/s over 86 km of fiber," *Electron. Lett.*, 23, 1180 1181, 1987.

[2] C. Xu, X. Liu, and X. Wei, "Modulation formats for high spectral efficiency fiber optic commu nications," *IEEE J. Sel. Top. in Quantum Electron.*, 10, 281 293, 2004.

[3] A. H. Gnauck and P. J. Winzer, "Optical phase shift keyed transmission," *J. Lightw. Technol.*, 23, 115 130, 2005.

[4] K. P. Ho, "*Phase Modulated Optical Communication Systems,"* New York, Springer, 2005.

[5] F. Forghieri, R. W. Tkach, and A. R. Chraplyvy "Fiber nonlinearities and their impact on transmission systems," in *Optical Fiber Telecommunications III A*, (I. P. Kaminov and T.L. Koch eds), San Diego, Calif., Academic, 1997.
[6] A. J. Price and N. Le Mercier, "Reduced bandwidth optical digital intensity modulation with improved chromatic dispersion tolerance," *Electron. Lett.*, 31, 58 59, 1995.
[7] R. A. Griffin, R. I. Johnstone, R. G. Walker et al., "10 Gb/s Optical Differential Quadrature Phase Shift Key (DQPSK) Transmission using GaAs/AlGaAs Integration," in Proc. *OFC'02*, paper FD6 , 2002.
[8] H. Kim and R. J. Essiambre, "Transmission of 8 × 20 Gb/s DQPSK signals over 310 km SMF with 0.8 b/s/Hz spectral efficiency," *IEEE Photon. Technol. Lett.*, 15(5), 769 771, 2003.
[9] P. S. Cho, V. S. Grigoryan, Y. A. Godin et al., "Transmission of 25 Gb/s RZ DQPSK signals with 25 GHz channel spacing over 1000 km of SMF 28 fiber," *IEEE Photon. Technol. Lett.*, 15, 473 475, 2003.
[10] C. Kim and G. Li, "Direct detection optical differential 8 level phase shift keying (OD8PSK) for spectrally efficient transmission," *Opt. Express*, 12, 3415 3421, 2004, http://www.opticsexpress.org/abstract.cfm?URI OPEX 12 15 3415.
[11] H. Yoon, D. Lee, and N. Park, "Performance comparison of optical 8 ary differential phase shift keying systems with different electrical decision schemes," *Opt. Express*, 13, 371 376, 2005, http://www.opticsinfobase.org/abstract.cfm?URI oe 13 2 371.
[12] M. Serbay, C. Wree, and W. Rosenkranz, "Experimental Investigation of RZ 8 DPSK at 3 × 10.7 Gb/s," 2005 IEEE *LEOS'05*, paper WE3, 2005.
[13] X. Liu, X. Wei, Y. H. Kao et al., "Quaternary Differential Phase Amplitude Shift Keying for DWDM Transmission," in Proc. *ECOC'03*, paper Th26.5, 2003.
[14] X. Liu, X. Wei, Y. Kao et al., "Quaternary differential phase amplitude shift keying for DWDM transmission," *ECOC'2003,* Rimini, Italy, 2003.
[15] X. Liu and Y. H. Kao, "Chirped RZ DPSK based on single Mach Zehnder modulator and its nonlinear transmission performance," *IEEE Photon. Tech. Lett.*, 17, 1531 1533, 2005.
[16] S. Hayase, N. Kikuchi, K. Sekine, and S. Sasaki, "Chromatic Dispersion and SPM Tolerance of 8 state/Symbol (Binary ASK and QPSK) Modulated Signal," in Proc. *OFC'04*, paper ThM3, 2004.
[17] N. Kikuchi, K. Mandai, K. Sekine, and S. Sasaki, "First Experimental Demonstration of Single Polarization 50 Gbit/s 32 level (QASK and 8 DPSK) incoherent Optical Multilevel Trans mission," in Proc. *OFC'07*, Post deadline paper PDP21, 2007.
[18] N. Kikuchi, K. Sekine, and S. Sasaki, "Modulation/Demodulation Schemes for Optical Multi Level Transmission," in Proc. *OFC'07*, paper OThL3, 2007.
[19] X. Liu, C. Xu, and X. Wei, "Performance analysis of time/polarization multiplexed 40 Gb/s RZ DPSK DWDM transmission," *IEEE Photon. Technol. Lett.*, 16, 302 304, 2004.
[20] S. G. Evangelides, L. F. Mollenauer, J. P. Gordon, and N. S. Bergano, "Polarization multiplexing with solitons," *J. Lightw. Technol.*, 10, 28 35, 1992.
[21] D. van den Borne, S. L. Jansen, E. Gottwald et al., "1.6 b/s/Hz Spectrally Efficient Transmission Over 1700 km of SSMF Using 40 × 85.6 Gb/s POLMUX RZ DQPSK," *J. Lightw. Technol.*, 25, 222 232, 2007.
[22] C. Wree, N. Hecker Denschlag, E. Gottwald et al., "High spectral efficiency 1.6 b/s/Hz transmis sion (8 × 40 Gb/s with a 25 GHz grid) over 200 km SSMF using RZ DQPSK and polarization multiplexing," *IEEE Photon. Technol. Lett.*, 15, 1303 1305, 2003.
[23] P. S. Cho, G. Harston, C. Kerr et al., "Investigation of 2 bit/s/Hz 40 Gb/s DWDM transmission over 4 × 100 km SMF 28 fiber using RZ DQPSK and polarization multiplexing," *IEEE Photon. Technol. Lett.*, 16, 656 658, 2004.
[24] F. Seguin and F. Gonthier, "Tuneable All Fiber Delay Line Interferometer for DPSK Demodulation," in Proc. *OFC'05*, paper OFL5, 2005.
[25] A. H. Gnauck, G. Raybon, S. Chandrasekhar et al., "2.5 Tb/s (64 × 42.7 Gb/s) Transmission over 40 × 100 km NZDSF using RZ DPSK Format and all Raman Amplified Spans," in Proc. *OFC'02*, Post deadline paper FC2, 2002.
[26] X. Liu, A. H. Gnauck, X. Wei et al., "Athermal optical demodulator for OC 768 DPSK and RZ DPSK signals," *IEEE Photon. Technol. Lett.*, 17, 2610 2612, 2005.

[27] X. Wei, X. Liu, S. Chandrasekhar et al., "40 Gb/s Duobinary and Modified Duobinary Transmitter Based on an Optical Delay Interferometer," in Proc. *ECOC 2002*, paper 9.6.3, 2002.
[28] A. H. Gnauck, X. Liu, S. Chandrasekhar, and X. Wei, "Optical duobinary format from demodula tion of DPSK using athermal delay interferometer," *IEEE Photon. Technol. Lett.*, 18, 637 639, 2006.
[29] J. G. Proakis, "*Digital Communications,"* fourth edition, New York, McGraw Hill, 2000.
[30] Weisstein E.W (2005)"Marcum Q Function" From *MathWorld* A Wolfram Web Resource. http://mathworld.wolfram.com/MarcumQ Function.html
[31] X. Liu, Y. H. Kao, M. Movassaghi, and R. C. Giles, "Tolerance to in band coherent crosstalk of differential phase shift keyed signal with balanced detection and FEC," *IEEE Photon. Technol. Lett.*, 16, 1209 1211, 2004.
[32] B. Mikkelsen, C. Rasmussen, P. Mamyshev, and F. Liu, "Partial DPSK with excellent filter tolerance and OSNR sensitivity," *Electron. Lett*, 42, 1363 1364, November 2006.
[33] C. R. Doerr, D. M. Gill, A. H. Gnauck et al., "Simultaneous Reception of both Quadratures of 40 Gb/s DQPSK using a Simple Monolithic Demodulator," in Proc. *OFC'05*, Post deadline paper PDP12, 2005.
[34] A. H. Gnauck, P. J. Winzer, C. R. Dorrer, and S. Chandrasekhar, "Linear and nonlinear perfor mance of 42.7 Gb/s single polarization RZ DQPSK format," *IEEE Photon. Technol. Lett.*, 18, 883 885, 2006.
[35] H. Kim and P. J. Winzer, "Robustness to laser frequency offset in direct detection DPSK and DQPSK systems," *J. Lightw. Technol.*, 21, 1887 1891, 2003.
[36] X. Liu, "Generalized data aided multi symbol phase estimation for improving receiver sensitivity in direct detection optical *m* ary DPSK," *Opt. Express*, 15, 2927 2939. http://www.opticsinfoba se.org/abstract.cfm?URI oe 15 6 2927.
[37] Y. Han, C. Kim, and G. Li, "Simplified receiver implementation for optical differential 8 level phase shift keying," *Electron. Lett*, 40, 1372 1373, 2004.
[38] J. P. Elbers, H. Wernz, H. Griesser et al., "Measurement of the dispersion Tolerance of Optical Duobinary with an MLSE Receiver at 10.7 Gbit/s," in Proc. *OFC'05*, paper OThJ4, 2005.
[39] F. Derr, "Coherent optical QPSK intradyne system: Concept and digital receiver realization," *J. Lightw. Technol.*, 10, 1290 1296, 1992.
[40] M. Taylor, "Coherent detection method using DSP for demodulation of signal and subsequent equalization of propagation impairments," *IEEE Photon. Technol. Lett.*, 16, 674 676, 2004.
[41] R. Noe, "PLL free synchronous QPSK polarization multiplex/diversity receiver concept with digital I&Q baseband processing," *IEEE Photon. Technol. Lett.*, 17, 887 889, 2005.
[42] K. Kikuchi, "Phase diversity homodyne detection of multilevel optical modulation with digital carrier phase estimation," *IEEE J. Sel. Top. Quantum Electron.*, 11, 563 570, July August 2006.
[43] G. Charlet, J. Renaudier, M. Salsi et al., "Efficient Mitigation of fiber Impairments in an Ultra Long Haul Transmission of 40 Gbit/s Polarization Multiplexed Data, by Digital Processing in a Coherent Receiver," in Proc. *OFC'07*, Post deadline paper PDP17, 2007.
[44] C. Laperle, B. Villeneuve, Z. Zhang et al., "Wavelength Division Multiplexing (WDM) and Polarization Mode Dispersion (PMD) Performance of a Coherent 40 Gbit/s Dual Polarization Quadrature Phase Shift Keying (DP QPSK) Transceiver," in Proc. *OFC'07*, Post deadline paper PDP16, 2007.
[45] C. R. S. Fludger, T. Duthel, D. van den Borne et al., "10 × 111 Gbit/s, 50 GHz Spaced, POLMUX RZ DQPSK Transmission over 2375 km Employing Coherent Equalisation," in Proc. *OFC'07*, Post deadline paper PDP22, 2007.
[46] T. Pfau, S. Hoffmann, R. Peveling et al., "First real time data recovery for synchronous QPSK transmission with standard DFB lasers," *IEEE Photon. Technol. Lett*, 18, 1907 1909, 2006.
[47] A. Leven, N. Kaneda, A. Klein, U. V. Koc, and Y. K. Chen, "Real time implementation of 4.4 Gbit/s QPSK intradyne receiver using field programmable gate array," *Electron. Lett.*, 42, 1421 1422, 2006.
[48] A. Leven, N. Kaneda1, U. V. Koc, and Y. K. Chen, "Coherent Receivers for Practical Optical Communication Systems," in Proc. *OFC'07*, paper OThK4.

[49] X. Liu, S. Chandrasekhar, A. H. Gnauck, et al., "DSP Enabled Compensation of Demodulator Phase Error and Sensitivity Improvement in Direct Detection 40 Gb/s DQPSK," in Proc. *ECOC'06*, Post deadline paper Th4.4.5.

[50] N. Kikuchi, K. Mandai, S. Sasaki, and K. Sekine, "Proposal and First Experimental Demonstration of Digital Incoherent Optical Field Detector for Chromatic Dispersion Compensation," in Proc. *ECOC'06*, Post deadline paper Th4.4.4.

[51] X. Liu and X. Wei, "Electronic Dispersion Compensation Based on Optical Field Reconstruction with Orthogonal Differential Direct Detection and Digital Signal Processing," in Proc. *OFC'07*, paper OTuA6, 2007.

[52] H. Leib, "Data aided noncoherent demodulation of DPSK," *IEEE Trans. Commun*, 43, 722 725, 1995.

[53] D. van den Borne, S. Jansen, G. Khoe et al., "Differential Quadrature Phase Shift Keying with Close to Homodyne Performance Based on Multi Symbol Phase Estimation," *IEE Seminar on Optical Fiber Comm. and Electronic Signal Processing*, ref. No. 2005 11310, 2005.

[54] X. Liu, "Receiver Sensitivity Improvement in Optical DQPSK and DQPSK/ASK Through Data Aided Multi Symbol Phase Estimation," in Proc. *ECOC'06*, paper We2.5.6, 2006.

[55] M. Nazarathy, X. Liu, L. Christen et al., "Self coherent decision feedback directed 40 Gb/s DQPSK receiver," *IEEE Photon. Technol. Lett.*, 19, 828 830, 2007.

[56] M. Nazarathy, Y. Yadin, M. Orenstein et al., "Enhanced Self Coherent Optical Decision Feed back Aided Detection of Multi Symbol m DPSK/PolSK in Particular 8 DPSK/BPolSK at 40 Gbps," in Proc. *OFC'07*, paper JWA43, 2007.

[57] T. Mizuochi, "Recent progress in forward error correction and its interplay with transmission impairments," *J. Sel. Top. Quantum Electron*, 12, 544 554, 2006.

[58] G. Kramer, A. Ashikhmin, A. J. van Wijngaarden, and X. Wei, "Spectral efficiency of coded phase shift keying for fiber optic communication," *J. of Lightw. Technol*, 21, 2438 2445, 2003.

[59] D. N. Godard, "Self recovering equalization and carrier tracking in two dimensional data com munication systems," *IEEE Trans. Commun.*, COM 28, 1867 1875, 1980.

[60] J. R. Treichler and B. G. Agee, "A new approach to multipath correction of constant modulus signals," *IEEE T. Acoust. Speech*, ASSP 31, 459 472, 1983.

[61] J. R. Treichler and M. G. Larimore, "New processing techniques based on the constant modulus adaptive algorithm," *IEEE T. Acoust. Speech*, ASSP 33 420 431, 1985.

[62] R. Johnson, Jr., P. Schniter, T. J. Endres et al., "Blind Equalization using the Constant Modulus Criterion: A Review," in Proc. *IEEE*, 86, 1998, pp. 1927 1950.

[63] C. Y. Chi, C. Y. Chen, C. H. Chen, and C. C. Feng, "Batch processing algorithms for blind equalization using higher order statistics," *IEEE Signal Proc. Mag.*, 20, 25 49, 2003.

[64] J. P. Gordon and L. F. Mollenauer, "Phase noise in photonics communications systems using linear amplifier," *Opt. Lett.*, 15, 1351 1355, 1990.

[65] X. Liu, X. Wei, R. E. Slusher, and C. J. McKinstrie, "Improving transmission performance in differential phase shift keyed systems by use of lumped nonlinear phase shift compensation," *Opt. Lett.*, 27, 1616 1618, 2002.

[66] K. P. Ho and J. M. Kahn, "Electronic compensation technique to mitigate nonlinear phase noise," *J. Lightw. Technol.*, 22, 779 783, 2004.

[67] A. Leven, N. Kaneda, U. V. Koc, and Y. K. Chen, "Frequency estimation in intradyne reception," *IEEE Photon. Technol. Lett.*, 19, 366 368, 2007.

[68] Y. Cai and A. N. Pilipetskii, "Comparison of Two Carrier Phase Estimation Schemes in Optical Coherent Detection Systems," in Proc. *OFC'07*, paper OMP5, 2007.

[69] A. J. Viterbi and A. M. Viterbi, "Nonlinear esitimation of PSK modulated charier phase with application to burst digital transmission," *IEEE Trans. Inform. Theory*, IT 29, 543 551, 1983.

[70] G. Goldfarb and G. Li, "BER estimation of QPSK homodyne detection with carrier phase estimation using digital signal processing," *Opt. Express* 14, 8043 8053 (2006) http://www.op ticsinfobase.org/abstract.cfm?URI oe 14 18 8043

[71] J. Lee, P. Roux, U. V. Koc et al., "A 5 b 10 GS/s A/D converter for 10 Gb/s optical receivers," *IEEE J. Solid St. Circ.*, 39, 1671 1679, October 2004.

[72] P. Schvan, D. Pollex, S. C. Wang, C. Falt, and N. Ben Hamida, "A 22 GS/s 5 b ADC in 0.13 um SiGe BiCMOS," *ISSCC*, Dig. Tech. Papers, 572 573, Feburary 2006.
[73] K. Poulton, R. Neff, B. Setterberg et al., "20 GS/s 8 Bit ADC with a 1 MB Memory in 0.18 um CMOS," *ISSCC*, Dig. Tech. Papers, 318 319 , Feburary 2003.
[74] R. J. Essiambre, G. Raybon, and B. Mikkelsen , "Pseudo linear transmission of high speed TDM signals: 40 and 160 Gb/s," in *Optical Fiber Telecommunications IV B*, (I. P. Kaminov and T. Li, eds), San Diego, Calif., Academic, 2002.
[75] X. Liu, "Nonlinear Effects in Phase Shift Keyed Transmissions," in Proc. *OFC'04*, paper ThM4 , 2004.
[76] X. Wei and X. Liu, "Analysis of intrachannel four wave mixing in differential phase shift keyed transmission with large dispersion," *Opt. Lett.*, 28, 2300 2302, 2003.
[77] A. H. Gnauck, X. Liu, X. Wei, D. M. Gill, and E. C. Burrows, "Comparison of modulation formats for 42.7 Gb/s single channel transmission through 1980 km of SSMF," *IEEE Photon. Technol. Lett.*, 16, 852 854, 2004.
[78] P. Hofmann, E. E. Basch, S. Gringeri et al., "DWDM Long Haul Network Deployment for the Verizon Nationwide GNI Network," Proc. *OFC'05*, paper OTUP5, 2005.
[79] C. Xie, L. Möller, H. Haunstein, and S. Hunsche, "Comparison of system tolerance to polarization mode dispersion between different modulation format systems," *IEEE Photon. Technol. Lett.*, 15, 1168 1170, 2003.
[80] X. Liu, C. R. Giles, X. Wei et al., "Demonstration of broad band PMD mitigation in the presence of PDL through distributed fast polarization scrambling and forward error correction," *IEEE Photon. Tech. Lett.*, 17, 1109 1111, 2005.
[81] X. Liu, C. R. Giles, X. Wei et al., "Experimental Demonstration of Broadband PMD Mitigation Through Distributed Fast Polarization Scrambling and FEC," in Proc. *ECOC'04*, Post deadline paper Th4.1.4, 2004.
[82] X. Liu, "All Channel PMD Mitigation Using Distributed Fast Polarization Scrambling in WDM Systems with FEC," in Proc. *OFC'07*, paper OMH4, 2007.
[83] A. Klekamp, B. Junginger, and H. Bülow, "Experimental PMD Mitigation for 43 Gb/s DPSK by Distributed Polarization Scrambling over 4 spans SMF Fibre," in Proc. *ECOC'06*, Post deadline paper Th4.3.6, 2006.
[84] D. Fishman, J. Ying, X. Liu, S. Chandrasekhar, and A. H. Gnauck, "Optical Add/Drop Multiplexer with Asymmetric Bandwidth Allocation and Dispersion Compensation for Hybrid 10 Gb/s and 40 Gb/s DWDM Transmission," in Proc. *OFC'06*, paper OWI64, 2006.
[85] S. Chandrasekhar, X. Liu, D. Kilper et al., "0.8 bit/s/Hz Terabit Transmission at 42.7 Gb/s Using Hybrid RZ DQPSK and NRZ DBPSK Formats over 16 $\times$ 80 km SSMF Spans and 4 Bandwidth Managed ROADMs," in Proc. *OFC'07*, Post deadline paper PDP28, 2007.
[86] IEEE 802.3 Higher Speed Study Group http://grouper.ieee.org/groups/802/3/hssg/
[87] P. J. Winzer, G. Raybon, C. R. Doerr et al., "2000 km WDM Transmission of 10 $\times$ 107 Gb/s RZ DQPSK," in Proc. *ECOC'06*, Post deadline paper Th 4.1.3, 2006.
[88] H. Masuda, A. Sano, T. Kobayashi et al., "0.4 Tb/s (204 $\times$ 111 Gb/s) Transmission over 240 km Using Hybrid Raman/EDFAs," in Proc. *OFC'07*, Post deadline paper PDP20, 2007.
[89] P. J. Winzer, G. Raybon, S. Chandrasekhar et al., "10 $\times$ 107 Gb/s NRZ DQPSK Transmission over 12 $\times$ 100 km Including 6 Routing Nodes," in Proc. *OFC'07*, paper PDP24, 2007.
[90] P. Kumar, "Practical Quantum Communications for Telecom Networks," 2006 *LEOS Summer Topical Meetings*, paper WB1.2.
[91] T. Banwell, P. Toliver, J. C. Young et al., "High Data Rate Quantum Noise Protected Encryption Over Long Distances," Digest of 2005 IEEE *MILCOM'05*, 1, 2005, pp. 398 404.
[92] X. Wang, N. Wada, T. Miyazaki, and K. Kitayama, "Coherent OCDMA system using DPSK data format with balanced detection," *IEEE Photon. Tech. Lett.*, 18, 826 828, 2006.
[93] P. S. Cho and J. B. Khurgin, "Suppression of cross gain modulation in SOA using RZ DPSK modulation format," *IEEE Photon. Technol. Lett.*, 15, 162 164, 2003.
[94] X. Wei, Y. Su, X. Liu, J. Leuthold, and S. Chandrasekhar, "10 Gb/s RZ DPSK transmitter using a saturated SOA as a power booster and limiting amplifier," *IEEE Photon. Technol. Lett.*, 16, 1582 1584, June 2004.

[95] M. Daikoku, I. Morita, and H. Tanaka, "Study of 40 Gbit/s Modulation Format to Upgrade 10 Gbit/s Long Haul Transmission Systems with 50 GHz Channel Spacings," in Proc. *ECOC'06*, paper Tu.4.2.3, 2006.

[96] G. Charlet, H. Mardoyan, P. Tran et al., "Nonlinear interactions between 10 Gb/s NRZ channels and 40 Gb/s channels with RZ DQPSK or PSBT format, over low dispersion fiber," in Proc. *ECOC'06*, paper Mo3.2.6, 2006.

[97] M. LeFrancois, F. Houndonoughbo, T. Fauconnier, G. Charlet, and S. Bigo, "Cross Comparison of the Nonlinear Impairments caused by 10 Gbit/s Neighboring Channels on a 40 Gbit/s Channel Modulated with Various Formats, and over Various Fiber Types," in Proc. *OFC'07*, paper JThA44, 2007.

[98] S. Chandrasekar and X. Liu, "Impact of channel plan and dispersion map on hybrid DWDM transmission of 42.7 Gb/s DQPSK and 10.7 Gb/s OOK on 50 GHz Grid," *IEEE Photon. Technol. Lett.,* 19, 1801 1803, 2007.

This page intentionally left blank

5

High-bit-rate ETDM transmission systems

Karsten Schuh and Eugen Lach

Alcatel-Lucent Deutschland AG, Bell Labs Germany, Stuttgart, Germany

5.1 INTRODUCTION

As 40-Gbit/s transmission systems based on electrical time-division multiplexing (ETDM) have reached product status, the research has moved toward higher bit rates. An 85-Gbit/s receiver [1] was reported in 2004 on the basis of advanced 40-Gbit/s optoelectronic devices and the latest generation of high-speed electronics (SiGe heterojunction bipolar transistor (HBT)) as a first ETDM subsystem operating at higher speeds. A year later the first full 85-Gbit/s ETDM transmission system [2] was realized.

At that time, a new trend evolved in research, which was the 100-Gbit/s Ethernet transport technology. Ethernet is expected to be the dominant transport technology of future metro/core networks. Today Ethernet has reached a bit rate of 10 Gbit/s and the next bit rate in that hierarchy is expected to be 100 Gbit/s. Early standardization activities toward 100-Gbit/s Ethernet (100 GE) have been started by the IEEE Higher Speed Study Group (HSSG) [3], with the goal to define first 100 GbE standards around the year 2010. An early analysis for technical and economical implementation of 100 GE was already presented in Ref. [4].

This chapter deals with the aspects of high channel data rate transmission at 100 Gbit/s and the status of the required components for realizing the transmission systems.

It starts with a description of the basics of ETDM technology, the concepts for realization of high-speed ETDM systems and subsystems, an overview on the reported transmission experiments to date, and finally gives an outlook toward applications and networking aspects of the different approaches.

Optical Fiber Telecommunications V B: Systems and Networks

ISBN: 978 0 12 374172 1

5.2 THE BASICS OF ETDM TRANSMISSION

An optical transmission system consists of a transmitter and a receiver (Figure 5.1) and between both of them an optical fiber is used as a transmission medium. All deployed optical transmission systems are based on ETDM, which means purely electronic signal processing up to the final bit rate in the transmitter as well as in the receiver, in contrast to optical time-division multiplexing (OTDM) where signal processing, especially multiplexing and demultiplexing, involves optical components or subsystems.

At its input, an ETDM transmitter has an interface for connecting several lower speed data signals. These data signals undergo electrical signal processing like framing, encoding by a forward error correction (FEC) and multiplexing to the output line rate. The FEC is based on block coding and mainly concatenated Reed Solomon codes are used. It adds an overhead of 7% to the signal, e.g. a 10-Gbit/s signal rate is converted to 10.7 Gbit/s after FEC encoding and has the capability to reduce a raw bit error rate (BER) of 10^{-3} down to a BER of better 10^{-13} after FEC decoding in the receiver. After FEC coding the data signal is amplified and modulated onto a continuous wave (CW) light, and a pulse carver can be placed in the light path to generate either a return-to-zero (RZ) or a carrier suppressed return-to-zero (CS-RZ) signal.

At the input of the receiver, the optical signal is first amplified and optically filtered to eliminate the wideband noise, then fed to a photodiode. Data and clock are extracted from the received electrical signal, afterward the data is FEC-decoded and demultiplexed.

For transmission of optical data signals, mainly standard single mode fiber (ITU G.652 SSMF) is deployed in the optical networks. The key parameters of that fiber are a power loss of $\sim$0.2 dB/km, a chromatic dispersion of $+17$ ps/(nm km), and a polarization mode dispersion (PMD) of 0.15 ps/km$^{1/2}$.

The optical loss means that the light can be transmitted only over a limited distance before optical amplification is needed. Therefore, in optical transmission networks, an erbium-doped fibre amplifier (EDFA) is placed after each segment of fiber. As each amplifier adds noise to a signal, the transmission reach of an optical

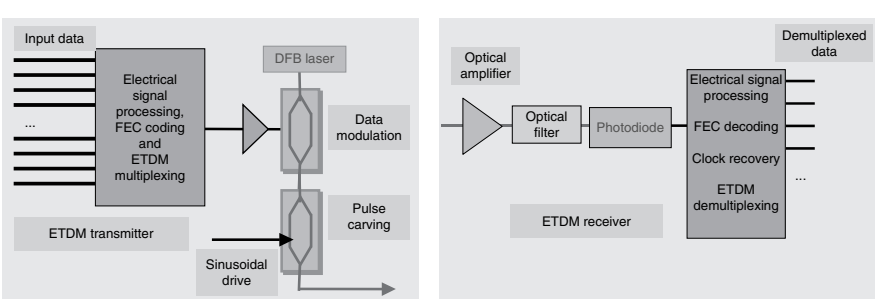

Figure 5.1 Schematic setup of an ETDM transmitter and receiver (this figure may be seen in color on the included CD ROM).

signal can be determined by the minimum optical signal-to-noise ratio (OSNR), which is needed at the receiver for achieving error free transmission.

The chromatic dispersion characterizes the wavelength-dependent propagation velocity of a fiber. This means that different wavelengths are propagating at slightly different speeds through the fiber. In the time domain, this means that optical pulses are spreading during propagation. On the one hand, this effect is advantageous because the fibre exhibits peak-power-dependent nonlinear effects during transmission, which are reduced when the pulses spread. On the other hand, the chromatic dispersion has to be compensated for, which is usually done by placing dispersion compensating fiber modules (DCM) in the link, to recover the initial signal shape and enable signal detection at the receiver. A key parameter for optical transmission systems is their chromatic dispersion tolerance, which means the amount of residual chromatic dispersion leading to a 1-dB OSNR sensitivity penalty, which is highly dependent upon the modulation format. When the bit rate is doubled, the chromatic dispersion tolerance is reduced by a factor of 4.

A static dispersion compensation using DCMs alone is not sufficient for long-haul transmission at bit rates above 10 Gbit/s because the fiber dispersion is temperature dependent to some degree. Buried links are only slightly affected as the temperature variations are slow and comparatively small. But especially the DCMs, which are typically located in amplifier sites above the ground, can undergo significant temperature variations during the time of a day.

The dispersion variation with temperature of standard DCMs [5] of ultra-long-haul transmission links [6] and the associated system outage probability [7] have been well studied. For practical application of 100 Gbit/s in long-haul transmission networks, dynamic chromatic dispersion compensation is required to counter the impact of temporal variations in the fibers to avoid system outage.

For such compensation, thermally tuneable chirped fiber Bragg gratings (CFBGs), which are now commercially available, can be applied. At high bit rates, CFBGs were successfully applied in a single-channel 107-Gbit/s ETDM transmission experiment [8] for tuneable chromatic dispersion compensation.

Multichannel compensation and its limitations were shown for 40-Gbit/s wavelength division multiplexing (WDM) signals [9, 10].

A different method for residual chromatic dispersion compensation are lattice filters based on planar lightwave circuits (PLCs). Their application has been demonstrated for 40-Gbit/s systems [11]. Such optical equalizers and their applications in 100-Gbit/s systems will be explained later.

PMD in fibers is caused by imperfections, which lead to different propagation speeds for different polarizations. As PMD shows a temporally statistical behavior, a static compensation scheme is not effective. As a rule of thumb, a differential group delay, which is the instantaneous value of the PMD at a certain wavelength, of 30% of the bit duration results in an OSNR penalty of 1 dB. For long-haul high-speed transmission systems, compensation of the PMD is necessary.

Optical PMD compensation with double-stage polarization maintaining fiber-based compensators is a well-known concept. Using a feedback signal, input

polarizations of the two polarization maintaining fibers are adaptively adjusted by the polarization controllers for optimum system performance. This was already examined in numerous experiments with data rates up to 170 Gbit/s (160 Gbit/s + 7% FEC overhead), e.g., in Ref. [12]. Such a compensation scheme will work also in high-speed ETDM systems, but it has the disadvantage that it has to be applied on a per-channel basis.

The distributed fast polarization scrambling together with FEC is a concept which forces errors due to PMD, but as high scrambling speeds are used, the error distribution in the FEC frames allows the FEC to fully correct them. This concept has been demonstrated in single-channel experiments at 10.7 Gbit/s in Ref. [13] and 43 Gbit/s in Ref. [14], but also the simultaneous compensation of multiple channels was demonstrated in a 42×43-Gbit/s transmission experiment [15].

Electronic compensation for distortions in high-speed ETDM systems is only possible for bit rates up to 43 Gbit/s presently. The compensators that have been applied are the electronic equivalent of PLC-based optical equalizers. These electronic transversal filter devices are relatively simple structures and their applicability for high data rate systems is dependent on the electrical bandwidth of these circuits. Promising results with a linear equalizer for distortion mitigation at 43 Gbit/s were published recently [16], showing that the dispersion tolerance of a receiver can be improved by 50% and the PMD tolerance by 60%.

The higher speed of SiGe electronics also allows for improving transmission systems at lower speeds. Two concepts have been successfully realized for 10-Gbit/s operation. The first is a maximum-likelihood sequence estimator (MLSE) which is a digital equalizer circuit. It calculates the most likely symbol sequence applying a Viterbi algorithm based on channel histograms. Such an equalizer can compensate for more than 2000 ps/nm residual chromatic dispersion [17].

Dispersion can also be compensated for by electronic precompensation [18]. This approach is based on the knowledge of the link dispersion and calculates the signal shape having the same amount of dispersion with inverse sign at the transmitter. That signal is converted from digital-to-analog form and modulated by an I/Q modulator.

To meet the demand of more capacity in an optical transport network three main measures can be taken:

- Use more fibers
- Use more wavelengths per fiber
- Use higher channel data rates

Using more fibers is only practical when fiber loss and dispersion are not the limiting factors. This means the transmission reach is limited and transmission bit rate is low. Otherwise, dispersion-compensating fiber modules and optical amplifiers have to be deployed for each new fiber.

The use of several wavelengths per fiber, the so-called WDM, is a very common approach to increase the capacity of a fiber. The advantage is that

dispersion-compensating fiber modules and optical amplifiers are shared by all channels simultaneously. As WDM channels are usually transmitted on a fixed frequency grid, adding more and more channels at low speeds has the disadvantage that the spectral efficiency, measured in bit/s/Hz, is limiting the overall transmission capacity. For example, 10-Gbit/s WDM transmission systems reach a spectral efficiency of 0.1 0.2 bit/s/Hz, depending on the used channel grid, e.g., 100 or 50 GHz.

The use of higher channel data rates, achieved by applying ETDM technique, offers a way to upgrade optical connections with high spectral efficiency, reduced efforts regarding wavelength management, and a reduction of port counts. Another advantage is the reduction of space and power consumption. However, some additional effort has to be spent for maintaining the signal integrity during transmission, which will be discussed later.

5.3 CONCEPTS FOR HIGH-SPEED ETDM SYSTEMS

The principle setup for ETDM transmitters and receivers is shown in Figure 5.1. For upgrading a transmitter subsystem to higher bit rates, here we chose a line rate of 100 Gbit/s for simplicity, one has three different possibilities:

(1) Polarization multiplexing.
(2) Applying a modulation format with several bits/symbol.
(3) Increasing the bit rate by an additional multiplexing stage.

These three possibilities are schematically depicted in Figures 5.2 5.4.

Polarization multiplexing as shown in Figure 5.2 is in principle not ETDM, as it uses two parallel sets of driver amplifiers and modulators and the combination of their output signals with orthogonal polarization.

At the receiver, a polarization demultiplexer consisting of a tuneable polarization controller and a polarization beam splitter are used for dividing the two polarizations. (The polarization controller is adjusted by means of a feedback signal.) Two parallel 50-Gbit/s ETDM receivers detect the signals and demultiplex the data. Compared

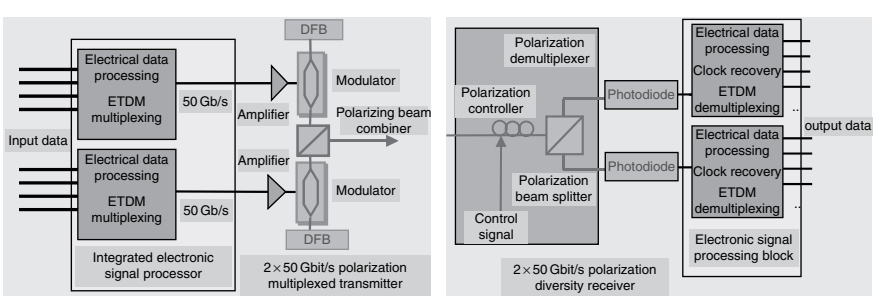

Figure 5.2 TX and RX for 2 × 50 Gbit/s polarization multiplexing (this figure may be seen in color on the included CD ROM).

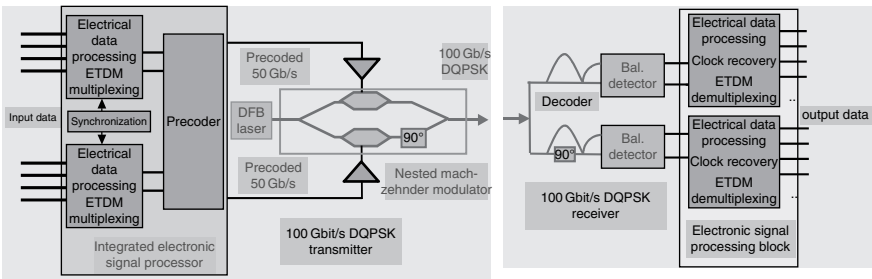

Figure 5.3 TX and RX for 100 Gbit/s DQPSK (this figure may be seen in color on the included CD ROM).

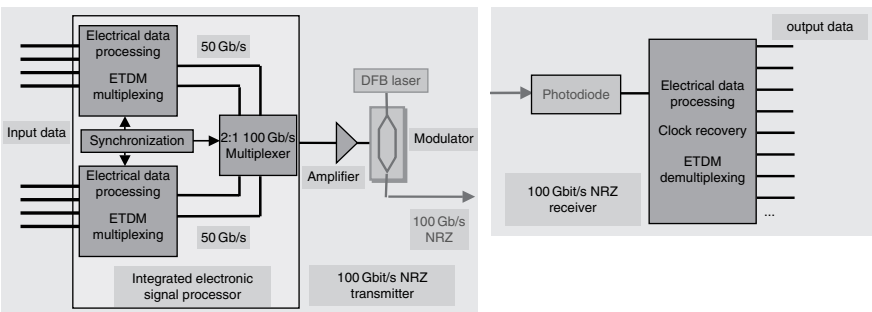

Figure 5.4 TX and RX for 100 Gbit/s NRZ (this figure may be seen in color on the included CD ROM).

with WDM approach, the spectral efficiency is doubled. The price for this is the additional hardware needed for polarization multiplexing and demultiplexing. This approach is somewhat sensitive to polarization-dependent loss which can occur in optical components throughout the transmission link and the higher-order PMD. An endless polarization controller is required in front of the polarization demultiplexer.

Applying a modulation format with several bits/symbol is a method which is mainly used in phase modulation such as DQPSK (differential quadrature phase-shift keying). A DQPSK transmitter requires synchronization between the two parallel electronic multiplexers followed by a precoder and a nested Mach Zehnder modulator (MZM) (see Figure 5.3).

At the receiver, an optical demodulator is required for converting the phase modulation to amplitude modulation. A pair of balanced photodiodes is used for converting the signals into the electrical domain for electronic signal processing in the two parallel receivers. The principle of DQPSK modulation and the required specific nested MZMs needed are covered in other chapters, so here we will focus on the high-speed transmission experiments employing DQPSK.

Both of the above approaches require some more components than the straight-forward Serial (non-return-to-zero, NRZ) approach; however, these components require only half the bandwidth.

The third technique is the binary modulation at 100 Gbit/s as depicted in Figure 5.4. It is the one with the highest demands on the hardware. At the transmitter, the two parallel electronic 50-Gbit/s multiplexers are followed by another electronic multiplexing stage which aggregates the data to an electrical 100-Gbit/s signal. The signal is amplified by a modulator driver amplifier which drives the optical data modulator.

At the receiver a high-speed photodiode is used for O/E conversion followed by electronic signal processing, e.g., clock extraction, decision, and electronic demultiplexing.

All of the transmitter subsystems in Figures 5.2 5.4 have, in common, two parallel electronic multiplexers which aggregate the incoming lower speed data streams to two 50-Gbit/s data streams. Table 5.1 summarizes the required components for a 100 Gbit/s ETDM system and compares their typical specifications; for simplicity, we assumed the required bandwidth equals the bit rate.

The DQPSK system and the polarization multiplexed system maintain the symbol rate at 50 Gbit/s and transfer the additional effort partly into the optical domain, but lower speed components are used, whereas the NRZ minimizes the number of components by using high-speed devices.

Which approach is the most cost-effective is not entirely clear today. The price of a 100-Gbit/s NRZ system, for example, will highly depend on the degree of integration that can be achieved. In the past, however, the binary modulation at the highest symbol rate has always been the most cost-effective solution when the mass fabrication of the required components can be done.

Table 5.1

Component specifications for the different approaches.

Transmitter	Polarization multiplex	DQPSK	NRZ (binary OOK)
2×50 to 100 Gbit/s data combination	Polarizing beam combiner	Precoder	Electronic multiplexer
Amplifier bandwidth	50 GHz	50 GHz	100 GHz
No. of amplifiers	2	2	1
Modulator bandwidth	50 GHz	50 GHz	100 GHz
No. of modulators	Two	One nested type	One
Receiver			
Demultiplex	Polarization demultiplexer with adaptive polarization controller	Optical demodulator, maybe temperature controlled by feedback	All electrical
O/E conversion	Two photodiodes, 50 GHz bandwidth	Two balanced photodiodes, 50 GHz bandwidth	One photodiode, 100 GHz bandwidth

In the next section we will give an overview on the currently available components for experimental demonstration of ETDM NRZ systems at 100 Gbit/s and comment on the potential of higher speeds beyond.

5.4 COMPONENTS FOR 100-GBIT/S ETDM NRZ AND BEYOND

In the research laboratories, commonly hybrid transmitter and receiver setups are assembled. These hybrid setups allow for the evaluation of each electronic or optoelectronic component individually to optimize the configuration for best performance. At data rates of 100 Gbit/s, good system performance is not easy to achieve with hybrid setups, as the high-speed electronic interfaces are critical. The hybrid setups include cables for connection of different high-speed modules, which will act as low-pass filters and thus limit system performance. Hybrid setups also include many electrical connectors, which implies either a very high cost for high performance (like the 1-mm connector), or reduced performance for a reasonable price (in case of a V-connector). Thus it is clear that integration is essential for cost reduction and performance improvement.

For realizing high-speed electronic circuits two competing material platforms can be used, namely Indium-Phosphide (InP) and Silicon-Germanium (SiGe).

Using advanced processing technology, a transit frequency f_T of 225 GHz and an f_{max} of 300 GHz for SiGe-based transistors can be obtained. For InP transistors, an f_T of 400 GHz and an f_{max} of 400 GHz have been attained.

Both material platforms have advantages and disadvantages. Using SiGe, it is possible to integrate all the signal processing functions required in a transmitter or receiver in one compact chip. However, in the transmitter, the output voltage swing of a SiGe multiplexer is not sufficient for driving modulators available today. This means that either a high-speed interface at the full line rate is required to connect the driver amplifier or a hybrid integration of the SiGe chip with a driver amplifier chip is necessary, but still a high-speed interface to the modulator will be needed. First silicon modulators have been demonstrated for lower speeds [19] and if the speed can be increased, the size of a transmitter could be reduced greatly, because then only the laser is left as additional discrete component.

The use of InP for the last 2×50:100 Gbit/s multiplexing stage could be advantageous, as the speed of the interface could then be reduced. InP is also suitable for fabricating broadband driver amplifiers; of course, all lasers and electroabsorption modulators (EAMs) deployed in the field are InP-based. InP-based PICs have been demonstrated and commercialized as described in several chapters in this book. However, it is not very likely that such an all-inclusive chip containing 2:1 multiplexer, modulator driver, laser, and modulator can be realized for 100-Gbit/s NRZ in the near future and one problem to solve could be the power consumption, which is in general higher than for SiGe circuits.

The critical components for a 100-Gbit/s NRZ ETDM transmitter are the electronic 100-Gbit/s multiplexer, the driver amplifier, and the modulator. We will now give an overview on the status of these components.

Due to their circuit layout a single multiplexer circuit can only deal with two electrical input signals, which are aggregated to one signal at double speed. A 4:1 multiplexer circuit therefore is more complex, as it contains three multiplexer circuits and the clock distribution circuits (frequency dividers or doublers) to drive them. Several high-speed multiplexer ICs operating at 100 Gbit/s or above have been reported in the literature [20 26].

The currently realized InP multiplexer ICs allow for higher speed operation than SiGe ICs. The highest operation speed reported is 165 Gbit/s achieved with a 4:1 InP multiplexer [20]. 2:1 InP multiplexers capable of an output data rate of 144 Gbit/s were also realized [21]. A 100-Gbit/s 2:1 multiplexer chip with a high output swing of more than 1 V was reported [22]. Such a high output swing could be sufficient to directly drive an advanced differential drive modulator.

For SiGe electronic circuits, record operating speeds of up to 132 Gbit/s were reported for 4:1 multiplexer circuits [23]. Several other modules are reported capable of operating at speeds above 100 Gbit/s, but without explicitly giving the speed limits. Those 2:1 SiGe multiplexer modules are included in all 100/107 Gbit/s ETDM transmitter subsystems reported to date [24 26].

In a standard ETDM transmitter, the electrical data signal is amplified after electronic multiplexing to drive the data modulator. When discussing the requirements for a driver amplifier, the properties of the modulator have to be taken into account. So we describe the possible modulators first and then discuss the driver amplifiers.

For the data modulation in 100-Gbit/s ETDM systems, only external optical modulators are applicable. Those modulators are based either on interferometric effects, like the MZM, or on electro-absorption, like the EAM. MZMs can be fabricated in lithium-niobate ($LiNbO_3$), GaAs, polymers, silicon, and InP, whereas EAMs are usually based on InP.

The EAMs are small size and have a steep modulation characteristic for which 20 dB/V have been reported [27]. A 40 Gbit/s operation of an EAM was reported with only 1.1 V modulation swing [28].

One further advantage of EAMs is the possibility of monolithic integration together with laser and driver amplifier. For achieving high modulation efficiency together with high modulation bandwidth, a travelling wave approach is applied, which benefits from partial synchronization of propagating electrical and optical waves within the device. Such kind of segmented EAM design has been realized and applied for 80-Gbit/s modulation [29]. Recently a special parallel EAM structure has been realized for 80-Gbit/s DQPSK modulation [30].

Commercially available EAMs target only the 40-Gbit/s market and their modulation bandwidth has a steep decrease toward higher frequencies making them unusable for operation at 100 Gbit/s.

Recently, a lot of effort is put on the development of optoelectronic components in silicon. It can be expected that silicon electronics and optoelectronic components can be integrated using standard Si-CMOS fabrication processes for low-cost applications. But silicon-on-insulator modulators are still in an early research phase. Prototype devices have reached bandwidths of more than 20 GHz, while requiring a V_{pi} of 8 V for single or 4 V for differential drive. Operation up to 30 Gbit/s was shown [19]. In the future, these devices could be an attractive option for high-speed transmitters with all components except the laser integrated in silicon. (Chapter 11, in Volume A of this book is devoted to the topic of "Silicon Photonics.")

The research on polymer materials for fabricating MZMs has progressed further compared to the silicon modulators and the first prototype devices have been realized some years ago [31]. Polymers can have a large electrooptic coefficient, leading to lower modulator drive voltages compared to $LiNbO_3$-based MZMs. However, polymer modulators with a V_{pi} of 4.5 V have been realized if only one electrode is driven [31], which is in range of the V_{pi} of $LiNbO_3$ modulators. To our knowledge, no polymer MZM has been applied in high-speed ETDM experiments to date.

In research labs recently InP-based MZMs have been realized; they could also be integrated with laser and modulator driver amplifier. Up to now, only the latter has been demonstrated for 40-Gbit/s application thus reducing the input voltage to 0.3 V_{pp} [32]. Application of InP MZMs for 40-Gbit/s operation has been reported with low required differential driving voltages of 2×1.3 V [33] and also with 2.6-V single-ended drive voltage [34].

Although the above described different modulators are promising devices for future high-speed transmission systems, up to now only advanced $LiNbO_3$ MZMs have been used for 100-Gbit/s system experiments. High-speed $LiNbO_3$ MZMs require a relatively large voltage swing of several volts (typically 5 V). Even though their optoelectronic bandwidth of roughly 35 GHz is lower than e.g., 45 GHz for InP MZMs, they benefit from a very smooth roll-off compared to the latter.

To summarize, the modulators that are commercially available now and in the near future will probably require a drive voltage of 4 5 V; from today's perspective, this can only be lower for InP modulators, which are still in research and prototyping phase. For modulator driver amplifiers, the requirements are therefore 5 V output voltage and the bandwidth should be as high as possible to maintain the excellent signal quality that can be achieved by the latest generation of electronic multiplexers. For avoiding a pattern-dependent performance, the frequency response of the driver has to be very flat across the complete frequency range.

A lot of publications on high-speed broadband amplifier chips can be found in the literature and, in Figure 5.5, an overview on achieved gain and 3-dB bandwidth is given [35 39], unfortunately, the saturated output power is seldom given in these publications. Most of these driver amplifiers are realized as distributed amplifiers based on InP. For most of them, only the frequency characteristic is given and only a few are tested with high-speed data signals. To our knowledge, none of the amplifiers described here was used in conjunction with a modulator to generate an optical signal.

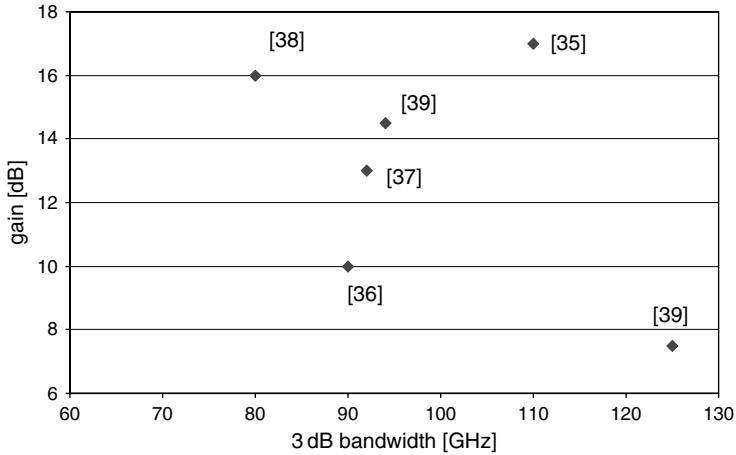

Figure 5.5 Gain vs 3 dB bandwidth for amplifier ICs reported in the literature [35 39] (this figure may be seen in color on the included CD ROM).

In Ref. [39] two amplifier chips designed for flip-chip bonding are presented. The first amplifier chip has a gain of 14.5 dB and a bandwidth of 94 GHz, the second amplifier chip has a gain of 7.5 dB and a bandwidth of 125 GHz, respectively. Both amplifier chips have a flat gain characteristic. After flip-chip bonding the second amplifier had a reduced bandwidth of roughly 85 GHz and a smooth roll-off.

In Ref. [40] distributed amplifier circuits showing a gain of 14.5 dB were tested with an 80-Gbit/s data signal; a good eye opening was achieved by using gain peaking, a technique which leads to a gain peak at high frequencies and thus a high-pass-like characteristic. The frequency characteristic of existing modulators is several dB down if the frequency exceeds 50 GHz and thus the overall performance at high frequencies could be improved. Another broadband driver amplifier tested at 80 Gbit/s having an output voltage of 2.7 V_{pp} was reported in Ref. [41].

As reported for the flip-chip bonded amplifier, the electrical bandwidth usually decreases after packaging. For amplifier modules additionally, the microwave input and output lines as well as the connectors will have losses. Therefore, for the near future, we do not expect driver amplifier modules with sufficient gain to deliver the 5 V_{pp} output to drive a modulator.

However, if we assume an output voltage swing of 400 mV_{pp} of the multiplexer and a V_{pi} of 5 V for the modulator, thus the driver amplifier should have a gain of more than 20 dB or a dual drive configuration has to be used.

Up to now three different realizations of 100-Gbit/s ETDM NRZ transmitter subsystems have been demonstrated, as depicted in Figure 5.6. They differ in the way the MZM is driven.

The first realization of a 107-Gbit/s transmitter was based on a dual electrode MZM differentially driven by the two output signals of an electronic multiplexer,

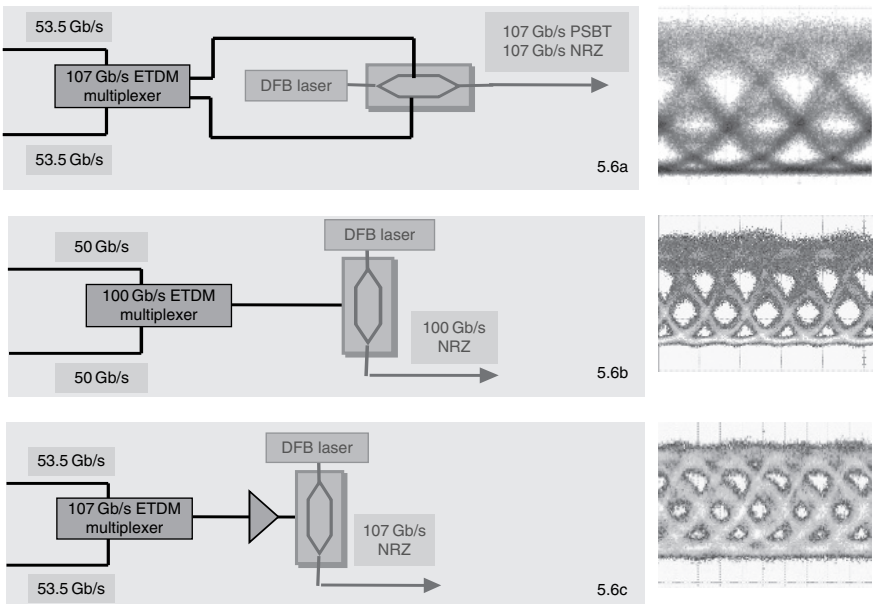

Figure 5.6 Demonstrated transmitter configurations and their optical eye diagrams (this figure may be seen in color on the included CD ROM).

as shown in Figure 5.6a [42]. It exploits the modulator characteristic for low-pass filtering to generate a phase shaped binary transmission (PSBT) signal. In general, for PSBT signal generation a drive voltage of $2 \times V_{\mathrm{pi}}$ is required and the modulator is biased at the minimum transmission point. Having only the output of the multiplexer available results in low optical output power, which means that the OSNR is already degraded by the booster amplifier of the transmitter.

By applying an optical equalizer, a 107-Gbit/s NRZ signal could be generated [43] by changing the modulator bias point. The change of the bias point results in considerably higher optical output power.

For a 100-Gbit/s NRZ transmitter, a single drive modulator driven with the multiplexer output signal was reported, as shown in Figure 5.6b [25]. This realization has the advantage of having no cables between the multiplexer and modulator, thus avoiding low-pass filtering effects of the cables and reducing the number of RF connectors.

Driving the modulator directly with the output signal of the multiplexer has in principle the advantage that no bandwidth is lost due to limitations of a driver amplifier; however, it results in low optical output power.

Therefore, in Ref. [44] a driver amplifier in conjunction with a single-drive modulator was used, as shown in Figure 5.6c. This results in a good optical output power, but an optical equalizer is required to compensate for the bandwidth limitation of the driver amplifier.

To summarize, all of the above-described transmitter configurations suffer mainly from limitations of driver amplifier and modulator. The realized electronic multiplexers have excellent performance, which is a clear indication that all the required signal processing in a transmitter can be realized with today's advanced IC processing technology. The bottlenecks are the bandwidth and output power of the driver amplifiers and/or bandwidth and required V_{pi} of the commercially available modulators.

As the research on 100-Gbit/s transmission systems has just started and a first 100-Gbit/s subsystem has been demonstrated at ECOC 2005 we can expect that the maturity of the required components could be achieved within few years.

Up to now, only a limited number of research groups have published results for high-speed photodiodes for application in high-speed ETDM receivers. Mainly uni-travelling carrier (UTC) and waveguide photodiodes are suited for o/e conversion of high speed optical signals. (See Chapter 10, Volume A of this book on "III-IV Photonic Integrated Circuits and their Impact on Optical Network Archirtectures.")

Uni-travelling-carrier photodiodes feature high saturation electrical output power and high bandwidth. A disadvantage of the UTC photodiode is that its electro-optical bandwidth depends on the optical input power. For optimum operation at 100 Gbit/s, up to $+14$ dBm have been used [45].

Operation of UTC photodiodes has been reported at 100 and 160 Gbit/s with OTDM signals with very short pulse width [45]. At 100 Gbit/s, the electrical output signal had an amplitude of 0.5 V, while the signal still had a clear RZ characteristic on an electrical sampling oscilloscope. The responsivity of that device was only 0.21 A/W. The responsivity can be improved by evanescent edge coupling [46] to 0.65 A/W, while maintaining high electro-optical bandwidth.

Using waveguide photodiodes with 3-dB bandwidth of 100 GHz and responsivity of 0.66 A/W, eye diagrams of a 160-Gbit/s OTDM signal were also measured [47]. A waveguide photodiode with an improved 3-dB bandwidth of 120 GHz and a reduced responsivity of 0.5 A/W was also reported [48]. For increasing the speed of the photodiodes, the size has to be reduced, which results in a decrease of the responsivity and saturation current. In Ref. [49], the low saturation current due to the smaller size of a single photodiode was compensated for by using a travelling wave structure with four parallel photodiodes, resulting in a bandwidth of 125 GHz and a responsivity of 0.24 A/W.

For operation at low optical input power, a photoreceiver comprising a photodiode monolithically integrated with a travelling-wave amplifier. Such a photoreceiver has been reported with a bandwidth of 72 GHz and a conversion gain of 45 V/W [47]. The bandwidth of these devices is determined by the electrical amplifier bandwidth, which has to be improved further for operation at 100 Gbit/s.

In the receiver, electronic demultiplexers are applied for converting the serial high-speed data stream into several parallel data streams at lower speed. In principle, a 1:2 demultiplexer consists of two parallel decision flip-flops (DFFs) each performing at half the sampling rate of the incoming data signal. The clock

signals of the DFFs have a phase difference of 180° for addressing both the data tributaries. These DFFs are used in half-rate operation in that case, which means that the clock frequency is only half the speed of the bitrate, so that only every second the bit is decided. This is in contrast to full-rate decision where the clock frequency equals the bit rate and every bit is decided and electronically regenerated. The quality of a DFF is usually determined by the clock-phase margin, the sensitivity and the maximum operation speed. The clock-phase margin is defined by the allowed phase mismatch between the clock and the data signal at a given error rate. The sensitivity means the minimum input voltage swing needed to obtain certain BER, e.g., 10^{-10}. The sensitivity is often measured with low-noise electrical output signals of an electronic multiplexer, which are attenuated. However, if an optical signal is transmitted over large distances, it accumulates noise due to optical amplification. In that case, the measured sensitivity after O/E conversion is worse.

In research, often discrete setups comprising a cascade of DFFs operated with half of the speed of the input signal are used for demultiplexing; after the last DFF the BER is measured. As with a cascade of half-rate DFFs, only one of the tributaries is available, electrical phase shifters are necessary to address the other tributaries. In contrast to electronic multiplexers where InP has a clear lead in operating speed, the speed of reported DFFs for demultiplexing is roughly the same for InP and SiGe ICs.

The fastest InP electronic DFF IC was tested for half-rate decision of an electrical 110-Gbit/s signal and full-rate decision of 70 Gbit/s [50]. Full-rate decision was demonstrated up to 90 Gbit/s [51]; however, the required input voltage swing was roughly 1 V, which is very difficult to obtain using a photoreceiver. For SiGe, a DFF module was used for half-rate decision of an optical 107-Gbit/s signal in conjunction with a photodiode [44].

In ETDM receivers, a synchronous electrical clock signal is required for signal processing and electronic demultiplexing. It has to be recovered from the incoming data signal. In general, two different types of clock recovery, namely phase-locked loop (PLL) and filter clock recovery, can be used in ETDM systems. For PLLs, manifold designs can be found in the literature and all of them have in common that the frequency and phase of a local oscillator is locked onto an incoming signal. As the local oscillator is often working on a subrate of the system clock rate this approach requires frequency doublers. In contrast, a filter clock recovery works at the system clock rate and thus frequency dividers are required to generate appropriate electronic clock signals to drive the electronic demultiplexer circuits.

The first clock recovery demonstrated at 100 Gbit/s was a classical discrete electronic PLL setup consisting of a high-speed photodiode, harmonic mixer, voltage-controlled oscillator, and loop filter [52].

So far on the receiver side, only an integrated clock data recovery and a hybrid integrated photodiode, clock amplifier, and demultiplexer combination for 100-Gbit/s operation have been demonstrated.

The above-mentioned clock data recovery incorporates a PLL-based clock recovery with a voltage-controlled oscillator and a 1:2 demultiplexer [53]. The device was originally designed for 86-Gbit/s operation and thus an external voltage-controlled oscillator has been applied; its control circuit has to be provided externally for higher speed operation. The device was operated at 107 Gbit/s using an OTDM-based transmitter, which eliminates bandwidth limitations by modulating the data at a lower bit rate on a stream of short pulses and subsequent optical multiplexing [54]. Applying a 107-Gbit/s ETDM transmitter, the operation of this receiver was limited to a PRBS length of 2^7 1 [26]. A clock data recovery circuit with the same functionality as described above has also been realized in InP and its operation was demonstrated at 80 Gbit/s [55].

The hybrid integrated InP photodiode and 1:2 SiGe demultiplexer module was demonstrated to work at 107 Gbit/s [56]. In that demonstration, the electrical clock was obtained from the synthesizer. The optical input signal was generated by the ETDM transmitter reported in Ref. [24] and additionally CS-RZ pulse carving was applied.

Up to now, only one hybrid ETDM receiver was demonstrated for the 107-Gbit/s operation [44]. It also contained a photodiode and a clock data recovery, but the clock data recovery device was used only as phase comparator for clock recovery. A second photodiode was used for data reception. The signals were demultiplexed by a high-speed SiGe DFF and a following 1:4 demultiplexer.

5.5 OPTICAL EQUALIZATION OF HIGH-SPEED ETDM SIGNALS

When describing the 100-Gbit/s ETDM transmitter technology, we already discussed the problem of the bandwidth limitations of driver amplifiers and modulators. The optical eye diagrams of those transmitters are mostly closed (see Figure 5.6), and for achieving a useful transmission distance that bandwidth limitations have to be counteracted.

In almost all 100-Gbit/s ETDM transmission experiments reported so far, an optical equalizer had to be included. Such optical equalizers are integrated PLC-based cascades of Mach Zehnder interferometers as shown in Figure 5.7, where τ denotes the delays.

These devices include sequences of wavelength-selective couplers followed by a delay interferometer. The properties of the individual wavelength-selective

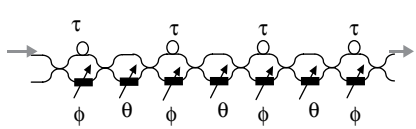

Figure 5.7 Optical equalizer structure (this figure may be seen in color on the included CD ROM).

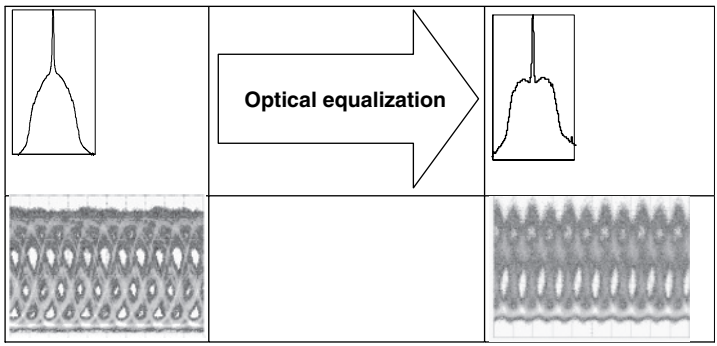

Figure 5.8 Optical spectrum and eye diagram of an NRZ modulated 107 Gbit/s signal (left) and optical spectrum and eye diagram of 107 Gbit/s NRZ signal after optical equalizer (right) (this figure may be seen in color on the included CD ROM).

couplers and delay interferometers can be controlled by heaters, which heat one Mach Zehnder branch. The devices are periodical filters and their free spectral range (FSR) depends on the amount of delay in the delay interferometers. Such devices have been designed and applied some years ago for dispersion compensation [11]. Due to their periodicity, they can be used for simultaneous multichannel equalization if the FSR matches the WDM channel grid, but the WDM grid could also be adapted to the FSR of the device as shown in Ref. [58].

In the left part of Figure 5.8, the optical spectrum and eye diagram of a 107-Gbit/s NRZ modulated signal are shown. One can see that the sidebands are very weak indicating limited bandwidth of the optical signal and the carrier contains most of the signal power. After applying an optical equalizer on that signal, the resulting eye diagram opens and the sidebands in the optical spectrum are lifted up, as shown in the right part of Figure 5.8. This effect is based on the Mach Zehnder characteristic, the dip is used for suppression of the carrier while the power of the sidebands is increased relative to the carrier by the high-pass characteristics of the Mach Zehnder lobes.

5.6 ETDM TRANSMISSION EXPERIMENTS

The reported publications on transmission experiments cover, to date, several high-speed ETDM subsystems at data rates of 100 Gbit/s. We will now give an overview on these high-speed system experiments which include at least one ETDM subsystem. We group the experiments by the applied modulation formats, NRZ and DQPSK.

The first 107-Gbit/s subsystem reported was the PSBT transmitter [42] shown in Figure 5.7a. It was operated in conjunction with an OTDM receiver and a clock obtained electrically from the transmitter. At the same time, that transmitter was applied with NRZ modulation enabled by an optical equalizer placed after the transmitter as described in the preceding section [43]. In a WDM transmission

experiment over 400-km non zero dispersion shifted fiber (NZDSF), the WDM channel spacing was equal to the 144-GHz FSR of the optical equalizer, which was operated for multichannel equalization [57]. In that experiment, the clock was transmitted on a separate optical channel. The same setup was used for exploring the possible fiber transmission reach, which was found to be 1000-km NZDSF [58].

The integrated clock data recovery was applied at 100 Gbit/s in conjunction with an OTDM transmitter [59] in a transmission experiment over 480 km of dispersion managed fiber. A modified OTDM transmitter was used to demonstrate transmission over the same 480 km link using the integrated clock data recovery in the ETDM receiver [54]. A field experiment was also conducted over 160-km NZDSF using an 107-Gbit/s ETDM NRZ transmitter as shown in Figure 5.7a. In that experiment, an optical equalizer and a vestigial sideband filter were used after the transmitter [26].

The first 100-Gbit/s experiment using electronic signal processing not only in the NRZ transmitter (see Figure 5.7b) and receiver, but also with clock handed over electrically from the transmitter to the receiver was reported in Ref. [25]. That transmission system was upgraded to 107-Gbit/s NRZ including an integrated clock data recovery as phase comparator for a PLL and a driver amplifier in the transmitter (see Figure 5.7c). Applying an optical equalizer in front of the receiver, transmission over 320 km was achieved [44]. The same setup was used for demonstrating 107-Gbit/s application of a chirped Bragg-grating-based tuneable dispersion compensator [8]. With improved components, the first 107-Gbit/s WDM experiment with full ETDM equipment and 10 decorrelated DWDM channels on a 200 GHz grid over 480-km SMF was demonstrated [60]. Recently, the transmission of 8×107 Gbit/s on a 100-GHz grid was achieved over 480-km SMF by applying vestigial sideband filtering at the transmitter, which is the first transmission experiment at 107-Gbit/s NRZ without optical equalizer [61].

The first transmission experiment applying the DQPSK modulation format at 100 Gbit/s was performed over 50-km SMF [62]. In another experiment, transmission over 2-km SMF without dispersion compensation was shown.

In [63] the transmission of 140×111 Gb/s WDM CSRZ-DQPSK with polarization multiplexing over 160 km was demonstrated. At that time, it was a new transmission capacity record; it used the C- and L-band with special extended L-band EDFAs [63]. The spectral efficiency was 2 bit/s/Hz. With a hybrid Raman and EDFA amplification scheme, this experiment was upgraded to 204×111 Gbit/s transmission over 240 km [64].

The longest transmission distance was a 2000-km NZDSF transmission of 10×107 Gbit/s RZ-DQPSK [65] on a 150-GHz grid applying a hybrid Raman/EDFA amplification. In another 10×107-Gbit/s NRZ-DQPSK transmission on a 100-GHz grid was demonstrated over a 1200-km NZDSF link, which included six optical routing nodes [66]. The optical filtering effects in the optical routing nodes were combated by an optical equalizer.

The latest trend is to use the DQPSK format at 27.75 GBaud/s in conjunction with polarization multiplexing and coherent detection [67]. This allows for WDM

transmission within a 50-GHz grid, and coherent detection would enable digital postprocessing with digital signal processors (DSPs) for impairment mitigation once the required DSPs are realized. In a first demonstration, a 10×111 Gbit/s signal based on RZ-DQPSK and polarization multiplexing were transmitted over 2375 km of SMF and, after coherent detection, the signals were sampled by a digital sampling oscilloscope and postprocessed on a personal computer.

5.7 OUTLOOK

The throughput in optical networks is increasing inexorably, the backhauling traffic generated by triple-play and video-on-demand services being the main drivers. Therefore, the first application for 100-Gbit/s systems for Ethernet transport is expected in metro networks and storage-area networks [68]. A serial transmission approach is advantageous in the case of large capacities that require WDM transmission, because of the reduced efforts for wavelength management.

However, at the time of this writing it is uncertain which exact line-rate will be standardized for the 100-Gbit/s Ethernet (100 GbE), as this is still under discussion. The way 100 GbE transponders will be realized depends on the network environment. The requirements for 100 GbE transport are different for point-to-point connections, meshed networks, or meshed networks with ROADMs. For meshed networks, the transmission reach is critical due to the PMD of the fibres forming that network. In meshed networks with ROADMs, the signal in addition must have a high robustness against narrowband filtering caused by cascaded ROADMs.

In a WDM network the commonly used frequency grid is either 50 or 100 GHz, which will have a major impact on which of the above-described approaches can be applied. Also a mixed bit rate operation with 10- or 40-Gbit/s channels and 100-Gbit/s channels will have to be studied.

Of course, 100-Gbit/s Ethernet can always be realized with a WDM approach (e.g., 10×10 Gbit/s), but this will not increase the actual throughput. Such a WDM approach could be attractive for low-cost application, but for networks with dimensions of a MAN or WAN the wavelength management effort can be complex. For example, if we assume a MAN with ROADMs in case of a WDM approach several channels have to be dropped at a time instead of a single channel.

We agree with [69] that the serial approaches for realizing a 100 GbE will mainly be suitable for MAN and WAN. In that case such 100 GbE transmission systems have to fulfil several other requirements of carriers. These are described in [70] dealing with the so-called carrier-grade Ethernet. (See also Chapter 9, Volume B of this book on "Optical Ethernet: Management, Protocols, and 1 100 G Technologies".) In [71] the possible configuration of 100 GbE metro networks are discussed.

Ethernet has in principle the reputation of being a low-cost technology. Besides the advantages of a serial approach, the serial approaches will have to compete

with WDM approaches regarding the cost for the terminal equipment. This is possible only if components are matured and integration is progressing like indicated in the chapter on components for 100 Gbit/s systems.

REFERENCES

[1] K. Schuh, B. Junginger, E. Lach et al., "85.4 Gbit/s ETDM Receiver with Full Rate Electronic Clock Recovery Circuit," in Proc. *ECOC 2004*, Post deadline paper Th4.1.1, 2004.

[2] K. Schuh, B. Junginger, H. Rempp et al., "85.4 Gbit/s ETDM Transmission over 401 km SSMF Applying UFEC," in Proc. *ECOC 2005*, Post deadline paper Th4.1.4, 2004.

[3] IEEE 802, High speed study group (HSSG): http://grouper.ieee.org/groups/802/3/hssg/public/index.html

[4] A. Schmid Egger and A. Kirstädter, "Ethernet in Core Networks: A Technical and Economical Analysis," HPSR2006 2006 IEEE Workshop on High Performance Switching and Routing, Ponzan, Poland, June 7 9, 2006.

[5] T. Kato, Y. Koyano, and N. Nishimura, "Temperature dependence of chromatic dispersion in various types of optical fiber," *Opt. Lett.*, 25(16), 1156 1158, August 2000.

[6] A. Walter and G. Schaefer, "Chromatic Dispersion Variations in Ultra Long Haul Transmission Systems Arising from Seasonal Soil Temperature Variations," in Proc. *OFC 2002*, Paper WU4, 2007.

[7] H. C. Ji, J. H. Lee, and Y. C. Chung, "Evaluation on system outage probability due to temperature variation and statistically distributed chromatic dispersion of optical fiber," *J. of Lightw. Technol.*, 22(8), 1893 1898, August 2004.

[8] E. Lach, K. Schuh, B. Junginger et al., "Serial 107 Gbaud ETDM Transmission and System Aspects," in Proc. *Fotonica 2007*, Mantua, Italy, Paper A3.6, 2007.

[9] Y. Li, B. Zhu, C. Soccolich et al., "Multi Channel High Performance Tunable Dispersion Compensator for 40 Gb/s Transmission Systems," in Proc. *OFC 2003*, Paper ThL4, 2003.

[10] S. Bhandare, D. Sandel, A. Hidayat et al., "1.6 Tb/s (40×40 Gb/s) Transmission over 44,. . ., 94 km of SSMF with Adaptive Chromatic Dispersion Compensation," *IEEE Photon. Technol. Lett.*, 17(12), 2748 2750, December 2005.

[11] J. Gehler, R. Wessel, F. Buchali et al., "Dynamic Adaptation of a PLC Residual Chromatic Dispersion Compensator at 40 Gb/s," in Proc. *OFC 2003*, Paper FN7, 2003.

[12] M. Schmidt, M. Witte, F. Buchali et al., "8×170 Gbit/s DWDM Field Transmission Experiment over 430 km SSMF Using Adaptive PMD Compensation," in Proc. *ECOC 2004*, Stockholm, Post deadline paper Th4.1.2, 2004.

[13] X. Liu, C. R. Giles, X. Wei et al., "Experimental Demonstration of Broadband PMD Mitigation through Distributed Fast Polarization Scrambling and FEC," in Proc. *ECOC 2004,* Post deadline paper Th4.14, 2004.

[14] A. Klekamp, B. Junginger, and H. Bülow, "Experimental PMD Mitigation for 43 Gb/s DPSK by Distributed Polarisation Scrambling over 4 Spans SMF Fibre," in Proc. *ECOC 2006*, Post deadline paper Th4.3.6, 2006.

[15] A. Klekamp, S. Dupont, P. Plantady et al., "PMD Mitigation for 42×43 Gb/s DPSK (NRZ and RZ) by Distributed Polarisation Scrambling over 4820 km Long NZDSF Fibre," in Proc. *ECOC 2007*, Paper We.P075, 2007.

[16] B. Franz, D. Rösener, R. Dischler et al., "43 Gbit/s SiGe Based Electronic Equalizer for PMD and Chromatic Dispersion Mitigation," in Proc. *ECOC 2005*, Paper We1.3.1, 2005.

[17] A. Färbert, S. Langenbach, N. Stojanovic et al., "Performance of a 10.7 Gb/s Receiver with Digital Equaliser using Maximum Likelihood Sequence Estimation," in Proc. *ECOC 2004*, Post deadline paper Th4.1.5, 2004.

[18] J. McNicol, M. O'Sullivan, K. Roberts et al., "Electrical Domain Compensation of Optical Dispersion," in Proc. *OFC 2005*, Paper OthJ3, 2005.

[19] A. Liu, L. Liao, D. Rubin et al., "High speed optical modulation based on carrier depletion in a silicon waveguide," *Opt. Express*, 15(2), 660, 2007.
[20] J. Hallin, T. Kjellberg, and T. Swahn, "A 165 Gb/s 4:1 Multiplexer in InP DHBT Technology," *in IEEE Journal of solid state circuits*, 41(10), 2209, October 2006.
[21] T. Suzuki, Y. Nakasha, T. Takahashi et al., "144 Gbit/s Selector and 100 Gbit/s 4:1 Multiplexer using InP HEMTs" in *IEEE MTT S Int. Microw. Symp. Dig.*, 1, 2004, pp. 117 120.
[22] K. Murata, T. Enoki, H. Sugahara, and M. Tokumitsu, "ICs for 100 Gbit/s Data Transmission," in Proc. *11th GaAs Symposium Munich 2003*, 2003, pp. 457 460.
[23] M. Meghelli, "A 132 Gb/s 4:1 multiplexer in 0.13 µm SiGe bipolar technology," *IEEE J. Solid St. Cir.*, 39(12), 2403 2407, December 2004.
[24] P. J. Winzer, G. Raybon, C. R. Doerr et al., "107 Gb/s optical signal generation using electronic time division multiplexing," *J. lightw. technol.*, 24(8), 3107 3103, 2006.
[25] K. Schuh, E. Lach, and B. Junginger, "100 Gbit/s ETDM Transmission System Based on Electronic Multiplexing Transmitter and Demultiplexing Receiver," in Proc. *ECOC 2006*, Paper We3.P. 124, 2006.
[26] S. L. Jansen, R. H. Derksen, C. Schubert et al., "107 Gb/s full ETDM Transmission Over Field Installed Fiber using Vestigial Sideband Modulation," in Proc. *OFC 2007*, Paper OWE3, 2007.
[27] T. Yamanaka, K. Tsuzuki, N. Kikuchi et al., "High Performance InP based Optical Modulators," in Proc. *OFC 2006*, Paper OWC1, 2006.
[28] H. Fukano, M. Tamura, T. Yamanaka et al., "Low Driving Voltage (1.1 Vpp) Electroabsorption Modulators Operating at 40 Gbit/s," in Proc. *16th IPRM 2004*, 2004, pp. 573 576.
[29] Y. Yu, R. Lewen, S. Irmscher et al., "80 Gb/s Transmitter with a Travelling Wave Electroabsorp tion Modulator," in Proc. *OFC 2005*, Paper OWE1, 2005.
[30] C. R. Doerr, L. Zhang, A. L. Adamiecki et al., "Compact EAM Based InP DQPSK Modulator and Demonstration at 80 Gb/s," in Proc. *OFC 2007*, Post deadline paper PDP33, 2007.
[31] H. R. Fetterman, Seong Ku Kim, K. Geary et al., "Novel Configurations and Approaches for Polymer Electrooptic Devices," in Proc. *SPIE 2004*, 5351, 2004, pp. 16 27.
[32] K. Tsuzuki, K. Sano, N. Kikuchi et al., "0.3 Vpp Single Drive Push Pull InP Mach Zehnder Modulator Module for 43 Gbit/s Systems," in Proc *OFC 2006*, Paper OWC2, 2006.
[33] K. Tsuzuki, H. Kikuchi, E. Yamada et al., "1.3 Vpp Push Pull Drive InP Mach Zehnder Modulator Module for 40 Gbit/s Operation," in Proc. *ECOC 2005*, Paper Th2.6.3, 2005.
[34] H. N. Klein, H. Chen, D. Hoffmann et al., "1.55 µm Mach Zehnder Modulators on InP for Optical 40/80 Gbit/s Transmission Networks," in in Proc. *IPRM 2006*Paper TuA2.4, 2006.
[35] Y. Baeyens, N. Weimann, V. Houtsma et al., "Submicron InP D HBT Single Stage Distributed Amplifier with 17 dB Gain and over 110 GHz Bandwidth," in *Microwave Symposium Digest* 2006. IEEE MIT S International, http://ieeexplore.ieee.org/xp1/RecentCon.jsp?punumber 4014788, 11 16 June 2006, pp. 818 821.
[36] S. Kimura, Y. Imai, Y. Umeda, and T. Enoki, "Loss Compensated Distributed Baseband Amplifier ICs for Optical Transmission Systems," *IEEE Trans. Microw Theory Tech.*, 44(10), 1688 1693, October 1996.
[37] C. Meliani, G. Post, J. Decobert et al., "92 GHz Cut Off Frequency InP Double Channel HEMT Based Coplanar Distributed Amplifier for 40 Gbit/s Applications and Beyond," in Proc. *ESSCIRC 2002*, 2002, pp. 615 617.
[38] Y. Arayashiki, Y. Ohkubo, Y. Amano et al., "16 dB 80 GHz InGaP/GaAs HBT Distributed Amplifier," *IEE Electron. Lett.*, 40(4), 244 245, February 2004.
[39] S. Masuda, T. Hirose, T. Takahashi et al., "An over 110 GHz InP HEMT Flip Chip Distributed Baseband Amplifier with Inverted Microstrip Line Structure for Optical Transmission Systems," *2002 IEEE GaAs Digest*, 2002, pp. 99 102.
[40] K. Schneider, R. Driad, R. E. Makon et al., "Comparison of InP/InGaAs DHBT distributed amplifiers as modulator drivers for 80 Gbit/s operation," *IEEE T. Microw. Theory*, 53(11), November 2005.
[41] Y. Suzuki, Z. Yamazaki, and H. Hida, "An 80 Gb/s 2.7 V_{pp} River IC Based on Functional Distributed Circuits for Optical Transmission Systems," in *Digest of Papers Radio Frequency Integrated Circuits (RFIC) Symposium 2005*, 2005, pp. 325 328.

[42] P. J. Winzer, G. Raybon, and M. Duelk, "107 Gb/s Optical ETDM Transmitter for 100 G Ethernet Transport," in Proc. *ECOC 2005*, Post deadline paper Th4.1.1, 2005.
[43] C. R. Doerr, P. J. Winzer, G. Raybon et al., "A Single Chip Optical Equalizer Enabling 107 Gb/s Optical Non Return to Zero Signal Generation," in Proc. *ECOC 2005*, Post deadline paper Th4.2.1, 2005.
[44] K. Schuh, B. Junginger, E. Lach et al., "107 Gbit/s ETDM NRZ Transmission over 320 km SSMF," in Proc. *OFC 2007*, Paper OWE2, 2007.
[45] Y. Muramoto, K. Yoshino, S. Kodama et al., "100 and 160 Gbit/s operation of uni travelling carrier photodiode module," *IEE Electron. Lett.*, 40(6), 378 380, March 2004.
[46] M. Achouche, F. Blache, J. G. Provost et al., "High Speed and High Responsivity UTC Photo diode Module for >40 Gb/s Optical Receivers," in Proc. *OFC 2004*, Paper TuM4.
[47] H. G. Bach, A. Beling, R. Kunkel et al., "Ultra high Bandwidth Optical Detectors (100 GHz) and Monolithic Photoreceivers for 80 Gbit/s NRZ/RZ Transmission Systems," in Proc. *ECOC 2004*, Paper Tu3.1.2, 2004.
[48] A. Beling, H. G. Bach, G. G. Mekonnen et al., "Miniaturized waveguide integrated p i n photo detector with 120 GHz bandwidth and high responsivity," *IEEE Photon. Technol. Lett.*, 17(10), 2152 2154, October 2005.
[49] A. Beling, J. C. Campbell, H. G. Bach et al., "High Power Parallel Fed Travelling Wave Photo detector Module for >100 GHz Applications," in Proc. *OFC 2007*, Post deadline paper PDP29, 2007.
[50] Y. Suzuki, Z. Yamazaki, Y. Amamiya et al., "120 Gb/s Multiplexing and 110 Gb/s Demultiplex ing ICs," *IEEE J. Solid St. Cir.*, 39(12), 2397 2401, December 2004.
[51] K. Ishii, H. Nosaka, K. Sano et al., "High bit rate low power decision circuit using InP InGaAs HBT technology," *IEEE J. Solid St. Circ.*, 40(7), 1583 1588, July 2005.
[52] I. D. Phillips, A. D. Ellis, T. Widdowson et al., "100 Gbit/s optical clock recovery using an electrical phase locked loop consisting of commercially available components," *IEE Electron. Lett.*, 36(7), 650 652, March 2000.
[53] U. Dümler, M. Möller, A. Bielik et al., "86 Gbit/s SiGe receiver module with high sensitivity for 160×86 Gbit/s DWDM system," *IEE Electron. Lett.*, 42(1), 21 22, January 2006.
[54] C. Schubert, R. H. Derksen, M. Möller et al., "107 Gbit/s Transmission Using An Integrated ETDM Receiver," in Proc. *ECOC 2006*, Paper Tu1.5.5, 2006.
[55] R. E. Makon, R. Driad, K. Schneider et al., "80 Gbit/s Monolithically Integrated Clock and Data Recovery Circuit With 1:2 DEMUX using InP based DHBTs," in *CISC 2005* digest, 2005, pp. 268 271.
[56] J. H. Sinsky, A. L. Adamiecki, L. Buhl et al., "107 Gbit/s Opto Electronic Receiver with Hybrid Integrated Photodetector and Demultiplexer," in Proc. *OFC 2007*, Post deadline paper PDP30, 2007.
[57] G. Raybon, P. J. Winzer, and C. R. Doerr, "10×107 Gbit/s Electronically Multiplexed and Optically Equalized NRZ Transmission over 400 km," in Proc. *OFC 2006*, Post deadline paper PDP32, 2006.
[58] P. J. Winzer, G. Raybon, and C. R. Doerr, "10×107 Gb/s Electronically Multiplexed NRZ Transmission at 0.7 bits/s/Hz over 1000 km Non Zero Dispersion Fiber," in Proc. *ECOC 2006*, Invited paper Tu1.5.3, 2006.
[59] R. H. Derksen, G. Lehmann, C. J. Weiske et al., "Integrated 100 Gbit/s ETDM Receiver in a Transmission Experiment over 480 km DMF," in Proc. *OFC 2006*, Post deadline paper PDP37, 2006.
[60] K. Schuh, B. Junginger, E. Lach, and G. Veith, "1 Tbit/s (10×107 Gbit/s ETDM) Serial NRZ Transmission over 480 km SSMF," in Proc. *OFC 2007*, Post deadline paper PDP23, 2007.
[61] K. Schuh, E. Lach, B. Junginger et al., "8×107 Gbit/s Serial Binary NRZ/VSB Transmission over 480 km SSMF with 1 bit/s/Hz Spectral Efficiency and without Optical Equalizer," in Proc. *ECOC 2007*, Invited paper Mo2.3.1, 2007.
[62] M. Daikoku, I. Morita, H. Taga et al., "100 Gbit/s DQPSK Transmission Experiment without OTDM for 100 G Ethernet Transport," in Proc. *OFC 2006*, Post deadline paper PDP36, 2006.

[63] A. Sano, H. Masuda, Y. Kisaka et al., "14 Tb/s (140 × 111 Gb/s PDM/WDM) CSRZ DQPSK Transmission over 160 km using 7 THz Bandwidth Extended L band EDFAs," in Proc. *ECOC 2006*, Post deadline paper Th4.1.1, 2006.

[64] H. Masuda, A. Sano, T. Kobayashi et al., "20.4 Tb/s (204 × 111 Gb/s) Transmission over 240 km," in Proc. *OFC 2007*, Post deadline paper PDP20, 2007.

[65] P. J. Winzer, G. Raybon, C. R. Doerr et al., "2000km WDM Transmission of 10 × 107 Gb/s RZ DQPSK," in Proc. *ECOC 2006*, Post deadline paper Th4.1.3, 2006.

[66] P. J. Winzer, G. Raybon, S. Chandrasehkar et al., "10 × 107 Gb/s NRZ DQPSK Transmission at 1.0 b/s/Hz over 12 × 100 km Including 6 Optical Routing Nodes," in Proc. *OFC 2007*, Post deadline paper PDP24, 2007.

[67] C. R. S. Fludger, T. Duthel, D. van den Borne et al., "10 × 111 Gb/s, 50 GHz Spaced, POLMUX RZ DQPSK Transmission over 2375 km Employing Coherent Equalization," in Proc. *OFC 2007*, Post deadline paper PDP22, 2007.

[68] M. Duelk and M. Zirngibl, "100 Gigabit Ethernet Applications, Features," *High Speed Network ing Workshop: The Terabits Challenge* in conjunction with Infocom 2006.

[69] M. Duelk, "Next Generation 100 G Ethernet," in Proc. *ECOC 2005*, Invited paper Tu3.1.2, 2005.

[70] A. Kirstädter, "Carrier Grade Ethernet for Core Networks," in Proc. *OFC 2007*, Paper OWK4, 2007.

[71] J. Spencer, M. Düser, A. Zapata et al., "Design Considerations for 100 GIGABIT Metro Ethernet (100 GbME)," in Proc. *ECOC 2003*, Th1.4.3, 2003.

6

Ultra-high-speed OTDM transmission technology

Hans-Georg Weber and Reinhold Ludwig

Fraunhofer Institute for Telecommunications, Heinrich-Hertz-Institut, Einsteinufer 37, Berlin, Germany

6.1 INTRODUCTION

The expected increase of transmission capacity in optical fiber networks presents us with many technology challenges [1]. One of these challenges is an optimized combination of wavelength-division multiplexing (WDM) and time-division multiplexing (TDM). TDM may be realized by electrical multiplexing (ETDM) or by optical multiplexing (OTDM) to a high-speed data signal, i.e., by electrical signal processing or optical signal processing. Presently, the first 40 Gb/s systems based on ETDM have been installed and in laboratories the first 100 Gb/s ETDM-experiments have been performed, e.g., Ref. [2]. In contrast, at the same data rates, OTDM transmission experiments have been carried out more than 10 years earlier. For instance, the first 100 Gb/s OTDM transmission experiment over a 36 km fiber link was reported already in 1993 [3]. Since then, OTDM transmission technology has been made a lot of progress towards much higher bit rates and much longer transmission links, as has been described in several review articles [4 6] and will be discussed in this chapter with special emphasis on the most recent developments. Recently, OTDM transmission technology succeeded in the transmission of a TDM data rate of 160 Gb/s over a record fiber length of 4320 km [7] and of a TDM data rate of 2.4 Tb/s over a fiber link length of 160 km [8].

The past has seen that OTDM will be replaced by ETDM as soon as electrical signal processing becomes available at the required TDM data rate. Therefore, OTDM transmission technology is often considered to be an interim technique with which to investigate the feasibility of ultra-high-speed data transmission in fibers. Today, the ultimate limits of ETDM technology are not known. An ETDM data rate of 160 Gb/s is very likely in the future. However, the performance of the ETDM terminal equipment may eventually be worse than the OTDM terminal

Optical Fiber Telecommunications V B: Systems and Networks

ISBN: 978 0 12 374172 1

equipment. OTDM receivers perform better than ETDM receivers already at data rates of 80 Gb/s. In this chapter we will show that the OTDM terminal equipment for 160 Gb/s TDM data transmission provides already very stable operation conditions. These results suggest that 160 Gb/s OTDM transmission systems can be used in deployed systems and can be operated error-free for years. ETDM technology must work hard to compete with these systems for instance as regards receiver sensitivity. Moreover, it is not sure that ETDM terminal equipment for 160 Gb/s will be less expensive and less energy consuming than the corresponding OTDM terminal equipment.

The ultimate limits of OTDM transmission technology are not given by the terminal equipment but by the transmission properties of the fiber link including all repeater or amplifier stages. With higher TDM bit rate data transmission in fiber is stronger affected by chromatic dispersion (CD), polarization-mode dispersion (PMD), fiber nonlinearity, and the limited bandwidth of repeaters or amplifiers in the transmission link. This is independent of the signal processing in the terminal equipment whether it is based on ETDM or OTDM technology. At present therefore, a main task of OTDM technology is to explore the ultimate capacity for fiber transmission in a single wavelength channel. The most challenging view as regards OTDM technology is that optical networks will evolve into "photonic networks," in which ultra-fast optical signals of any bit rate and modulation format will be transmitted and processed from end to end without optical electrical optical (O/E/O) conversion. This "photonic network" is a target for the distant future, and it presents us with the present challenge of investigating and developing high-speed optical signal processing and exploring the ultimate capacity for fiber transmission in a single wavelength channel.

OTDM transmission technology is described in this chapter as follows: Section 6.2 gives a general description of an OTDM system, followed by a discussion of the OTDM transmitter in Section 6.3, of the OTDM receiver in Section 6.4 and of the fiber transmission line in Section 6.5. Transmission experiments are described in Section 6.6 starting with a review on 160 Gb/s transmission experiments in Section 6.6.1, on transmission at data rates beyond 160 Gb/s in Section 6.6.2, and on OTDM/WDM transmission experiments in Section 6.6.3. Then follows a detailed description of two 160 Gb/s transmission experiments: transmission with long-term stability in Section 6.6.4 and transmission over a record fiber length of 4320 km in Section 6.6.5. In Section 6.6.6 we report on transmission experiments at the TDM data rates of 1.28 and 2.56 Tb/s. Finally, Section 6.7 summarizes our conclusions on the present state of OTDM technology.

6.2 OTDM TRANSMISSION SYSTEM

Figure 6.1 (upper part) is a schematic depiction of a 160 Gb/s OTDM transmission system as an example. On the transmitter side, the essential component is an optical pulse source. The repetition frequency of the generated pulse train is

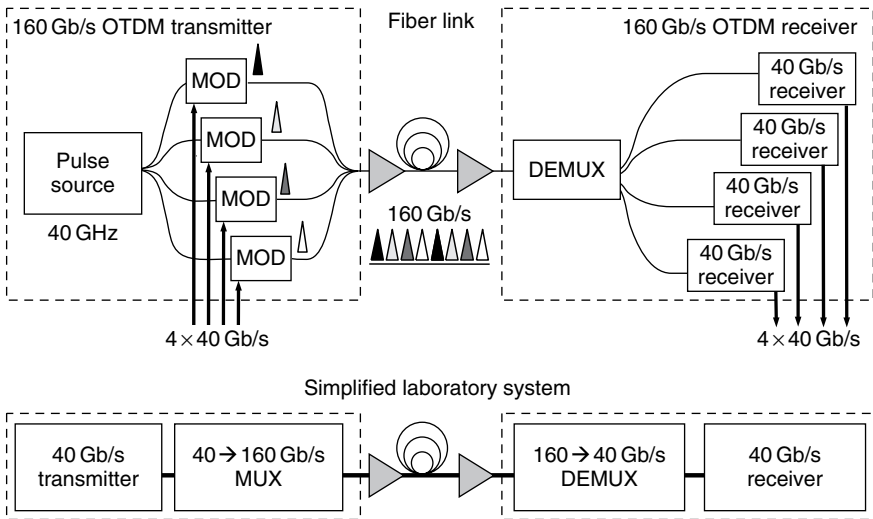

Figure 6.1 Schematic view of a 160 Gb/s OTDM transmission system (upper part of figure) and of a simplified laboratory system (lower part of figure).

assumed to be 40 GHz. In general, the repetition frequency depends on the base data rate (or on the symbol rate, see Section 6.3.2), at which the subsequent modulators (MOD) are driven by an electrical data signal (base rate signal). The 40 GHz optical pulse train is coupled into four optical branches, in which four 40 Gb/s non-return-to-zero (NRZ) electrical data signals drive four modulators (MOD) and generate four 40 Gb/s optical return-to-zero (RZ) data signals. The modulation formats include on off keying (OOK) and differential phase shift keying (DPSK). The setup in Figure 6.1 can also be used for the modulation format differential quadrature phase shift keying (DQPSK). However, in this case one has to take into account that the bit rate (expressed in bit per second, b/s) is twice the symbol rate (expressed in baud, for details see Section 6.3.2). The four optical data signals (TDM channels) are combined to a multiplexed 160 Gb/s optical data signal by bit-interleaving with use of an appropriate delay in the four optical branches. Multiplexing (MUX) can be such that all bits of the multiplexed data signal have the same polarization (single polarization (SP) signal, SP multiplexing) or adjacent bits have alternating (orthogonal) polarization (AP multiplexing, AP-signal). On the receiver side, the essential component is an optical demultiplexer (DEMUX), which separates the four base rate data signals (TDM channels) again for subsequent detection and electrical signal processing. The transmission link requires in general compensation for CD and PMD, which both depend on the type of single-mode fiber (SMF) used in the transmission system.

The DEMUX shown in Figure 6.1 comprises two parts, an optical gate and a clock recovery device. The optical gate is a fast switch with a switching time that is shorter than the bit period (6.25 ps for 160 Gb/s) of the multiplexed data signal.

The clock recovery device provides the timing signal for the optical gate. In Sections 6.3, 6.4, and 6.5 we discuss the OTDM transmitter, the OTDM receiver, and the fiber transmission line in more detail.

Laboratory systems are frequently simplified as follows (Figure 6.1, lower part): on the transmitter side, only one modulator is used and combined with the pulse source for a 40 Gb/s optical transmitter. The generated optical data signal is then multiplexed by a fiber delay line multiplexer (MUX) to a 160 Gb/s data signal using either SP or AP multiplexing. On the receiver side, the DEMUX selects only one 40 Gb/s TDM channel, which is detected by one 40 Gb/s optoelectronic receiver at a given time. In a proper experiment all TDM channels are measured successively in this way.

In this chapter we discuss point-to-point transmission as shown in Figure 6.1. We do not consider network components and subsystems such as add drop multiplexers, e.g., Refs [9 12], wavelength converters, e.g., Refs [13 16], modulation format converters, e.g., Ref. [17], optical regenerators, e.g., Ref. [18] and optical sampling systems, e.g., Refs [19, 20].

6.3 OTDM TRANSMITTER

6.3.1 Pulse Sources

The pulse source is a key component in an OTDM transmitter. The pulse source must provide a well-controlled repetition frequency and wavelength, a pulse width significantly shorter than the bit period of the multiplexed data signal, a timing jitter much less than the pulse width, low-amplitude noise, and a high extinction ratio. For instance, typical values for stable 160 Gb/s (bit period 6.25 ps) OOK transmission are RMS jitter <300 fs, pulse width (FWHM, full-width at half-maximum) <2 ps for SP multiplexing and <4 ps for AP multiplexing, extinction ratio ≈ 30 dB, amplitude noise $<3\%$. Moreover, if some sort of phase modulation format such as DPSK or DQPSK is used, there are further pulse source requirements, namely the pulse source must be highly stable in terms of carrier phase and wavelength.

The optical pulses have preferably a sech^2 pulse shape and an optical spectrum with the spectral width (FWHM) $\Delta\nu$ leading to a time-bandwidth product close to the theoretical minimum of $\Delta\nu \bullet \Delta t = 0.3148$. The sech^2 shape is especially attractive as solitons are advantageous for optical signal processing, e.g., for pulse compression.

Pulse sources used for high-bit-rate transmission experiments include mode-locked laser diodes (MLLD) either external cavity devices, e.g., Refs [21 23] or monolithically integrated devices, e.g., Refs [24, 25], mode-locked fiber lasers (MLFL), e.g., Refs [26 28], mode-locked solid-state lasers (MLSL) [29], and CW lasers externally modulated (pulse carving), e.g., by an electroabsorption modulator (EAM), e.g., Refs [30, 31]. For WDM/OTDM applications, a multi-wavelength pulse source is of particular interest. Such a pulse source is obtained by

supercontinuum generation (SC pulses), e.g., Ref. [32]. High-power pulses can generate a supercontinuum spectrum. Spectral slicing provides the multiwavelength pulse source.

These pulse sources provide in general a 10 GHz (10.7 GHz) or 40 GHz (43 GHz) pulse train with a pulse width of a few picoseconds. The numbers in brackets are valid if standard FEC (forward error correction assuming a 7% overhead) is used. If the pulse width is not sufficient narrow for the considered bit rate, some sort of subsequent pulse compression and optical regeneration, e.g., Refs [33 36] is used.

The characterization of the generated pulse train is essential for a successful transmission experiment at high data rates. A convenient technique to characterize the pulses in the time domain is a photodiode and a electrical sampling oscilloscope. An optical pulse with a pulse width of $\Delta t = 1$ ps requires a detector bandwidth of more than 500 GHz for exact recovery of the pulse shape. Today, the fastest photodiodes and electrical sampling systems available do not provide this bandwidth. An alternative is the application of the optical sampling technique. Here a fast optical gate samples the signal directly in the optical domain. This technique enables a bandwidth of 500 GHz and beyond [19]. Autocorrelation measurements provide a convenient technique to estimate the pulse width if the pulse shape is known. FROG measurements provide additionally the chirp of the optical pulses. Next to measurements in the time domain, there are also measurements in the frequency domain. Figure 6.2 shows the optical spectrum (mode comb spectrum) of a 40 GHz pulse train generated by a monolithically integrated MLLD. A small linewidth and a large contrast ratio of the mode combs indicate a pulse train with low phase and amplitude noise. If phase modulation formats such

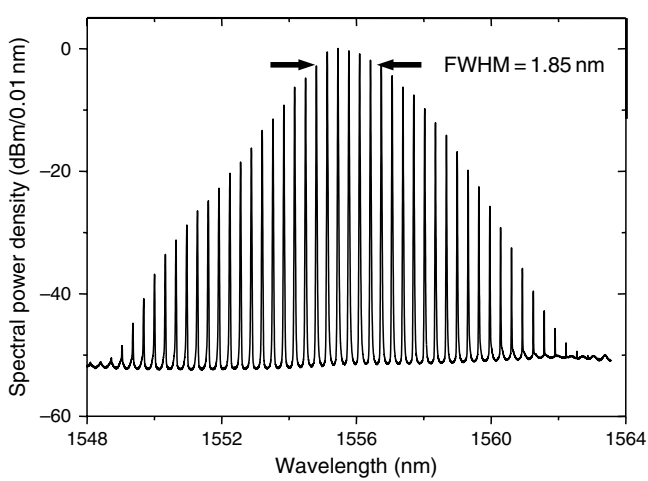

Figure 6.2 Pulse spectrum of mode locked laser diode, which was successfully operated in 160 Gb/s DPSK transmission experiments.

as DPSK or DQPSK are used, this spectrum needs to have in addition a long-term stability in the wavelength position appropriate for the phase-demodulator in the receiver (see Section 6.4.3). This is often a problem for the MLFL. This laser needs harmonic mode locking and long-term stability is a critical issue.

The noise of the pulse train comprises amplitude noise and phase noise. An often used method to estimate the timing jitter is the measurement of the single sideband (SSB) phase noise. The SSB phase noise level per 1 Hz bandwidth relative to the carrier, $L(f)$, can be measured using a photodetector and an RF-spectrum analyzer. From $L(f)$, the RMS timing jitter of the pulse source can be calculated [37].

6.3.2 Modulator

In OTDM experiments, lithium-niobate ($LiNbO_3$) modulators are most frequently used to modulate the generated pulse train. Some OTDM experiments applied EAMs. The modulation characteristics of $LiNbO_3$ modulators are very broad band (up to 80 GHz) and little dependent on the wavelength in the 1.3 1.6 μm range.

$LiNbO_3$ modulators were operated for OOK, DPSK, and DQPSK modulation formats. In a DPSK system, each pulse is modulated in the phase with $n \times \pi$, $n \in \{0,1\}$. A nearly perfect π phase shift is obtained in DPSK systems by use of a push pull-operated $LiNbO_3$ Mach Zehnder-modulator (MZM), which is biased at zero transmission and driven by two times the "π" switching voltage [38, 39]. This modulator may show some residual amplitude modulations. Those, however, are less detrimental than deviations from the desired phase shift [40].

In a DQPSK system, each pulse is modulated in the phase with $n \times \pi/2$, $n \in \{0,1,2,3\}$. Consequently, in a DQPSK-modulated signal, each symbol (optical pulse) carries 1 out of 4 logical states instead of 1 out of 2 logical states as in an OOK or a DPSK system. We will often use the symbol rate, which is expressed in "baud." For OOK and DPSK, the data rate is equal to the symbol rate, whereas for DQPSK the data rate is twice the symbol rate. For example, a 160 Gbaud DQPSK data signal carries a data rate of 320 Gb/s. There are several ways to realize a DQPSK modulator. A very attractive solution is to place two push pull-operated $LiNbO_3$ MZM in a "super" Mach Zehnder interferometer (MZI) with one MZM in each branch and with a constant phase difference of $\pi/2$ between both branches [41].

6.3.3 Multiplexer

In real OTDM systems different data signals are combined with a delay (see upper part of Figure 6.1) to provide a multiplexed data signal. An example of such a "real multiplexer" is reported in Refs [42, 43]. This multiplexer enables the multiplexing of eight different 20 Gb/s OOK data signals to one multiplexed 160 Gb/s OOK data signal by using an integrated planar lightwave circuit. Yet another "real multiplexer"

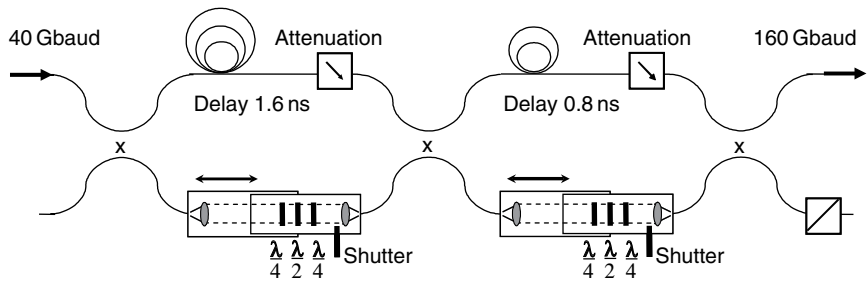

Figure 6.3 Setup of 40 to 160 Gbaud "test multiplexer" for laboratory experiments.

is reported in Ref. [44]. It provides independent modulation of all TDM channels and optical phase alignment between adjacent bits. We have to note here that in these "real" systems multiplexer and modulators constitute in general one unit.

Most laboratory experiments are performed using "test multiplexers," which combine several replicas of one data signal with different relative delays to a high-bit-rate test signal. Figure 6.3 shows schematically the setup of a "test multiplexer" (MUX) for multiplexing the symbol rate from 40 to 160 Gbaud. The MUX comprises two stages with a multiplexing factor of 2 for each stage. Multiplexing the symbol rate from 40 to 640 Gbaud requires four stages. Each stage has the configuration of an MZI with a relative delay of an odd multiple of ½ T_B where T_B is the period of the symbol rate of the signal at the input of the stage.

The MUX is realized by using 2×2 optical couplers and optical delay lines either as fiber device or as planar lightwave circuit. The setup depicted in Figure 6.3 is a fiber-based device. The lower branch of the interferometer configuration includes an adjustable free space optical delay line ($\approx$200 ps), a polarization controller (PC) ($\lambda/4$, $\lambda/2$, $\lambda/4$ plates), and a shutter. These tools enable a precise adjustment of the relative delay and of the polarization of the output signal, i.e., the adjustment for an SP signal or an alternating polarization signal. There is an additional attenuator in the upper branch to compensate for the loss in the free beam optics in the lower branch to provide constant amplitude for all pulses.

An important requirement for these "test multiplexers" is that there is strong decorrelation between adjacent bits of the multiplexed data signal. This is obtained by employing a delay time, which is long compared with the period of the symbol rate of the input signal. Laboratory experiments are usually performed using PRBS (pseudo-random bit stream) data signals at the base rate. The PRBS structure is preserved if the relative delay in one stage equals half the word length of the PRBS word at the input of this stage. For a PRBS word with $2^7 \quad 1 = 127$ bit, this gives a delay time of (127/2) $T_B = 1.595$ ns for an input STM-rate of 39.813 Gbaud. This delay corresponds to about 32 cm fiber in the first stage and 16 cm in the second stage in Figure 6.3. A PRBS word length of 2^{15} 1 corresponds already to a delay length of 82 m. Consequently, the use of longer PRBS word lengths is not reasonable.

In constructing a fiber-based "test multiplexer" for very high symbol rates, e.g., 640 Gbaud, the effect of CD has to be taken into account. The following consideration shows this as regards CD. The optical pulses at the output of the "test multiplexer" have passed different fiber lengths. Thus they suffer different pulse broadening due to CD. The generation of data signals having a symbol rate of 640 Gbaud from a base symbol rate of 10 Gbaud requires a 10 640 Gbaud "test multiplexer." Using a delay as determined by a PRBS word length with 2^7 1 bit gives delays with the fiber lengths of 1.28 m, 0.64 m, 0.32 m, 0.16 m, 0.08 m, and 0.04 m. The maximum difference of fiber length passed by the pulses in the six stages of the "test multiplexer" adds up to 2.52 m. An optical pulse with a pulse width of 0.4 ps is broadened to 0.58 ps over a fiber length of 2.52 m assuming a CD of $D = 17$ ps/nm/km. Such a "test multiplexer" requires already some sort of dispersion compensation in the first stages. In contrast, a MUX starting at the first stage with 40 Gbaud requires in general no additional dispersion compensation in the first stages.

In general, the delay line multiplexer provides an arbitrary relative phase of adjacent pulses in the multiplexed data signal, because usually no effort is made in these experiments to adjust and stabilize the delay line multiplexer for a well-defined relative phase of the adjacent pulses. The effect of a well-defined relative phase of adjacent data pulses in the multiplexed data signal is expected to increase the tolerance of the transmission system with respect to CD and fiber nonlinearity and it will increase the spectral efficiency [45]. Therefore, the controllability of the optical phase alignment between adjacent pulses in the multiplexed data signal is an important feature of a transmission system. Techniques for realizing optical phase alignment have been introduced [46, 47] and several OTDM and OTDM/WDM transmission experiments have been performed using such formats as "carrier-suppressed return-to-zero (CS-RZ)," in which the optical pulses in adjacent bit slots have a relative phase shift of π [44, 48 51]. In contrast, the improvement for the transmission system is not as significant as to justify the effort of adjustment and stabilization of a "test multiplexer," even not for phase modulated data signals. In DPSK and DQPSK transmission systems the well-defined phase of adjacent pulses is only required behind the demultiplexer (i.e., within the base rate-channel) and is independent of the adjustment of the delay line "test multiplexer."

6.4 OTDM RECEIVER

Figure 6.4 shows schematically a particular 160 Gbaud OTDM receiver, which was used in several transmission experiments as described in Section 6.6. The receiver comprises the three subsystems, the optical gate and the timing extraction device (clock recovery) for demultiplexing (DEMUX), and the optoelectronic receiver for the base symbol rate (40 Gbaud receiver in the example shown in Figure 6.4). The key device for optical signal processing in this setup is the EAM. In this chapter, we will come to the conclusion that an OTDM receiver based on EAMs for optical signal processing is presently the best choice for a 160 Gbaud

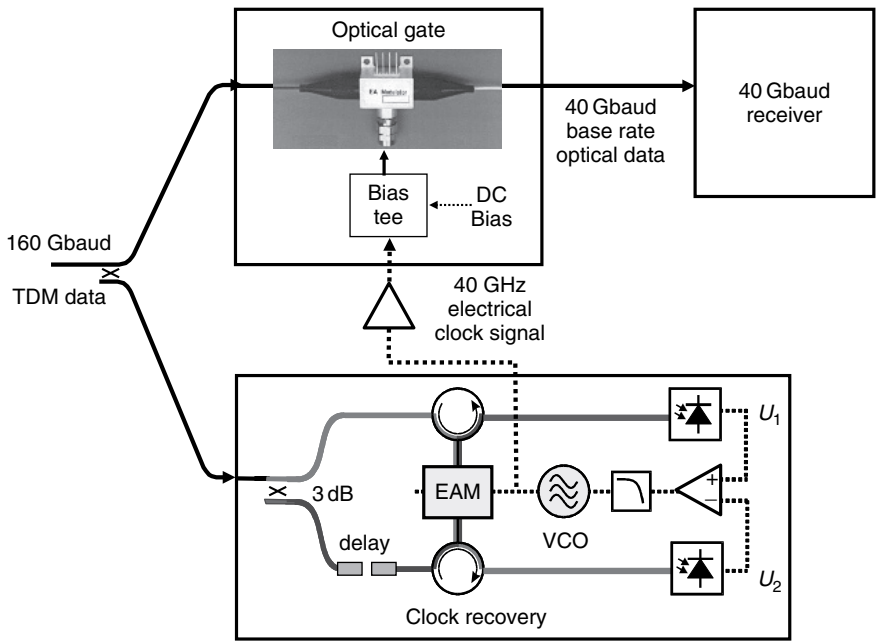

Figure 6.4 Schematic of 160 Gbaud receiver comprising the subsystems optical gate and clock recovery for demultiplexing as well as the 40 Gbaud base rate receiver (this figure may be seen in color on the included CD ROM).

transmission system. However, there are also many other configurations for the three subsystems as we will discuss in the following.

6.4.1 Optical Gates for the OTDM Demultiplexer

Various optical gates have been used for demultiplexing. At symbol rates beyond 160 Gbaud, the optical gates are mostly fiber based using cross-phase modulation (XPM) or four-wave mixing (FWM) in fibers [4 6]. A well-known example is the nonlinear optical loop mirror (NOLM) [52], which was applied as a DEMUX for symbol rates up to 640 Gbaud, the fastest DEMUX reported so far [8, 53 56]. Another class of optical gates is based on XPM and FWM in a semiconductor optical amplifier (SOA) [57]. Examples of XPM-based optical gates include the SOA in a Mach Zehnder interferometer (SOA-MZI) [58, 59], the SOA in a polarization discriminating switch (SOA-UNI) [60, 61], and the SOA in a Sagnac interferometer [62]. In general, the SOA-based optical gates operate well at symbol rates up to 160 Gbaud [57] although operation at symbol rates up to 320 Gbaud was also reported [58, 59].

SOA- and fiber-based optical gates use all-optical switching. An optical signal controls the gate, which switches an optical data signal. Thus, these optical gates

require also an appropriate optical pulse source. In contrast, in an optical gate based on an EAM as depicted in Figure 6.4, an electrical control signal controls the gate that switches the optical data signal. This is an enormous simplification of the DEMUX, because appropriate optical pulse sources are expensive and difficult to handle. The EAM-based optical gate has been used as DEMUX in many transmission experiments as described in Section 6.6.

The EAM is a commercially available device. In the application as optical gate it is characterized by the switching window, which has typically a width (FWHM) of about 5 ps and a switching contrast of about 20 dB both for a DC-bias voltage of about 3.5 V and for a 40 GHz clock signal with an RF power of about 26 dBm. The width of the switching window depends on the frequency of the clock signal. Demultiplexing of 160 Gbaud to 10 Gbaud with a 10 GHz clock signal requires in general a cascade of two EAMs. The EAM is a polarization independent gate. More details on EAM-based 160 Gbaud demultiplexing are described in Refs [31, 63]. Recently, an EAM was monolithically integrated with a photodiode and an electrical signal from the photodiode drove the EAM directly [64, 65]. Demultiplexing up to a symbol rate of 500 Gbaud was reported. However, this gate needs an optical control signal.

The demultiplexers described above are capable of selecting only one TDM channel (base rate channel) of the multiplexed data signal (single-channel output operation). Multiple channel output operation can be achieved by a serial-parallel configuration of several of these switches. Examples for multichannel output operation using only one device are reported in Refs [5, 6, 66].

6.4.2 Timing Extraction Devices

The clock recovery depicted in Figure 6.4 is a prescaled optoelectronic timing extraction device using a phase-locked loop (PLL) configuration. The optical data signal with a symbol rate of 160 Gbaud is split into two branches and fed into the EAM via two circulators. The switched output signals of the EAM are detected by two low bandwidth (100 MHz) photodetectors. The two electrical signals U_1 and U_2 are subtracted from each other by a difference amplifier to generate the bipolar feedback signal $U_1 \quad U_2$ for the 40 GHz voltage-controlled oscillator (VCO). The PLL comprises a low-pass filter with a bandwidth of 50 kHz. The electrical 40 GHz VCO signal is finally fed into the electrical input of the EAM to close the loop of the PLL. This electrical 40 GHz signal controls also the optical gate.

In this setup, the EAM acts as an ultra-fast electro-optical phase comparator. The optical power transmitted through the EAM to both sides is determined by the phase difference between the data signal and the 40 GHz RF signal driving the EAM. Thus the two electrical signals U_1 and U_2 depend on this phase difference. Figure 6.5 (upper traces) shows both signals vs the relative phase of the data signal and the 40 GHz RF signal taken while the PLL was not closed. There is a shift between U_1 and U_2, because of the optical delay in one of the two signal

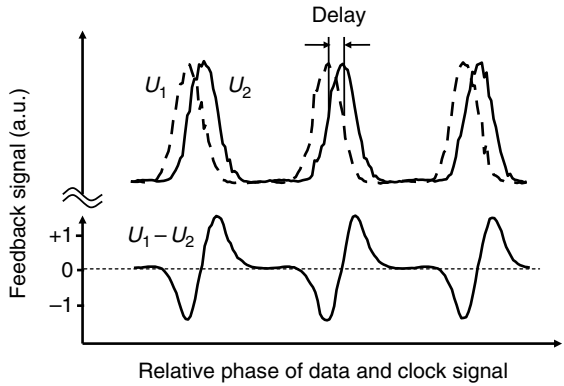

Figure 6.5 Principle of operation of clock recovery where signals were taken when PLL was not closed.

branches at the input of the EAM. The bipolar feedback signal $U_1 \quad U_2$ (Figure 6.5, lower trace) is within the locking-range proportional to the relative phase of the data signal and the 40 GHz RF signal. This clock recovery was successfully operated at symbol rates up to 320 Gbaud [67].

Optoelectronic clock recovery was also achieved by using PLL configurations with optical phase comparators based on FWM or XPM in an SOA and operation up to symbol rates of 400 Gbaud was reported [113]. Many transmission experiments were also performed without recovering the clock signal from the multiplexed data signal, because an appropriate clock recovery device was unavailable. Two alternative approaches were used. A clock signal was generated at the transmitter and transmitted together with the data signal over the fiber at a separate wavelength ("clock transmitted," e.g., Ref. [61]), or the multiplexer at the transmitter end was adjusted for slightly different pulse amplitudes ("clock modulation," e.g., Ref. [53]) such that a simple photodetector was able to detect the clock signal at the receiver end.

6.4.3 The Optoelectronic Base Rate Receiver

In OOK transmission experiments the optoelectronic base rate receiver comprises in general an optical amplifier, an optical filter, a fast photo detector and subsequently the equipment for electrical signal processing at the base rate, e.g., at 40 Gb/s. DPSK and DQPSK OTDM receiver require additionally a demodulator before the photodetector. The demodulator converts the phase-modulated data signal into two complementary amplitude-modulated data signals. In the DPSK receiver, the demodulator is an MZI, as shown in Figure 6.6, with a delay between both interferometer arms of one period at the symbol base rate, for instance, 25 ps for a symbol base rate of 40 Gbaud. Adjacent pulses with zero phase difference, which carry the logical

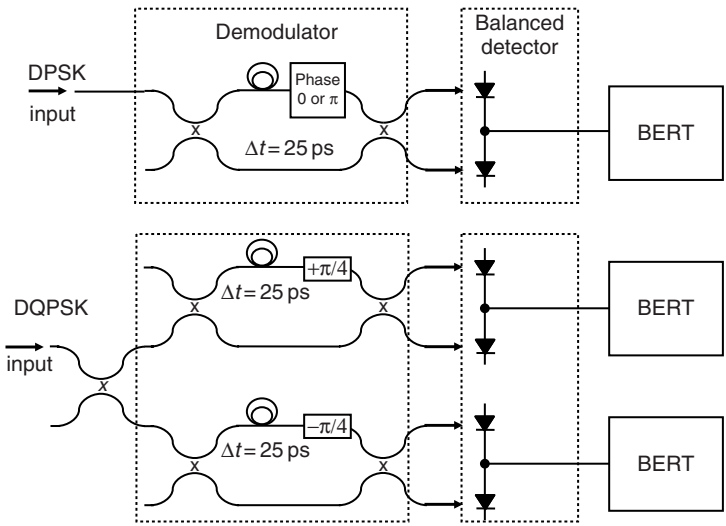

Figure 6.6 Schematic of phase demodulators for DPSK and DQPSK transmission systems at 40 Gbaud base symbol rate.

information equivalent to a "space" in OOK, interfere constructively at one port (e.g., upper port in Figure 6.6) and destructively at the other port (lower port in Figure 6.6) of the interferometer, whereas adjacent pulses with π phase difference, which carry the logical information equivalent to a "mark" in OOK, interfere constructively at the lower port and destructively at the upper port. If the two complementary signals are detected by a balanced photodetector, an improvement in receiver sensitivity of 3 dB as compared with OOK is obtained [40].

The demodulator for a DQPSK signal is also shown in Figure 6.6. It comprises two MZIs each with a differential delay (in the interferometer arms) of one period at the symbol base rate (i.e., 25 ps for 40 Gbaud or 80 Gb/s) plus an additional phase shift of $+\pi/4$ or $-\pi/4$ to detect the in-phase or quadrature component, respectively. The DPSK (or DQPSK) demodulator needs to be actively matched to the transmitter wavelength for proper operation. This requires a control loop for the demodulator and also a pulse source in the transmitter, which is highly stable in terms of the carrier wavelength.

6.5 FIBER TRANSMISSION LINE

6.5.1 Compensation of Chromatic Dispersion

For application in commercial systems, a fiber link length on the order of 1000 km is desirable. For these fiber lengths, compensation of CD and of PMD is essential for high-speed data transmission. Already for a system with a symbol rate of

160 Gbaud, it is necessary to compensate for both the path-averaged CD ($D = 0$) at the center wavelength of the pulse and for the path-averaged CD slope ($dD/d\lambda = 0$), because the dispersion slope produces oscillations near the trailing edge of the data pulse even if $D(\lambda) = 0$ for the center wavelength λ of the pulse. Currently, the most mature dispersion compensation technique is based on dispersion compensating fiber (DCF) which compensates simultaneously for both D and $dD/d\lambda$. Generally, the DCF is localized as module in the repeaters and does not contribute to the transmission length. In contrast, DCF has further evolved into inline dispersion-managed fiber (DMF) transmission lines. The DMF represents a pair of transmission fibers, which together compensate for the path-averaged D and $dD/d\lambda$ over a wide wavelength range.

Various types of transmission fiber in combination with their associated DCF have been investigated for high-speed data transmission near 1550 nm. Examples are standard SMF ($D \approx 17$ ps/nm/km), dispersion-shifted fiber (DSF, $D \approx 0.1$ ps/nm/km), and various types of non-zero dispersion-shifted fiber (NZDSF, $D \approx 2$ 8 ps/nm/km). Additionally, there are several types of DMF such as SMF/RDF (SMF/reverse dispersion fiber) or SLA/IDF. The latter comprises "super large area fiber" (SLA, $D \approx 20$ ps/nm/km) and "inverse dispersion fiber" (IDF, $D \approx$ 40 ps/nm/km), which together compensate for D and $dD/d\lambda$.

Fibers with low CD are not favorable for high-speed data transmission because of the fiber nonlinearity. High-speed transmission experiments are commonly performed in the quasi-linear (pseudo-linear) transmission regime, where the nonlinear length is much greater than the dispersion length, e.g., Ref. [47]. A high local dispersion is advantageous for this transmission regime, provided that the path-averaged dispersion and dispersion slope are close to zero. The short pulses of the data signal disperse very quickly in the fiber, spreading into many adjacent timeslots before the original pulse sequence is restored by dispersion compensation. Therefore, the peak power of the pulses is low for most of the path along the fiber. Consequently, fibers with high dispersion D are favorable for high-speed transmission. For example, 160 Gb/s DPSK data transmission was successful with transmission distances of up to 2000 km using NZDSF [68]. In contrast, 160 Gb/s DPSK data transmission over the SLA/IDF fiber with its high local dispersion and low nonlinearity (large effective area) achieved a transmission distance of more than 4000 km [7].

The tolerances as regards residual dispersion or residual SMF or DCF length are particularly crucial for high-speed systems. For instance, for an SP signal at the symbol rate of 160 Gbaud (pulse width 1.5 ps), simulations yield a tolerance (eye opening penalty of 1 dB for BER = 10^{-9}) of $\pm$ 2.5 ps/nm, which corresponds to an SMF length of $\pm$ 150 m [69]. However, in experiments a fine tuning of $\pm$ 50 m is appropriate. To maintain such tolerances over a large environmental temperature range requires automatic dispersion compensation in addition to the DCF. Various tunable dispersion compensators have been proposed [70 73].

For symbol rates of 640 Gbaud and beyond, higher order dispersion terms ($d^2D/d\lambda^2$) cause substantial pulse broadening in most fibers also in transmission links

with exact compensation of the dispersion D and the dispersion slope ($dD/d\lambda$). Simultaneous compensation of D, $dD/d\lambda$, and of $d^2D/d\lambda^2$ is obtained by applying a phase modulation to the pulse [74 76]. This dispersion compensation technique was successfully realized in a 1.28 Tb/s OOK transmission experiment over a 70 km DMF link comprising SMF-RDF [55, 56]. On the contrary, modern fibers like the SLA/IDF fiber are more suitable for high-speed data transmission. A 2.56 Tb/s DQPSK data signal, corresponding to a symbol rate of 1.28 Tbaud, was transmitted over 160 km SLA/IDF fiber without application of an additional sophisticated compensation scheme [8].

6.5.2 Compensation of Polarization Mode Dispersion

PMD is a severe limitation for high-speed data transmission. PMD is caused by a slight birefringence of the fiber and of other components in the transmission line. It results in broadening and depolarization of optical pulses. Unlike CD, PMD is much more difficult to compensate for because it changes with time and wavelength in a nondeterministic way. Even for fiber links with low PMD, i.e., sufficiently low mean differential group delay (DGD), instantaneous DGD values can exceed the tolerable margin and cause system outages if the PMD value of the fiber link is higher than approximately 0.1 T_B [77]. Here $1/T_B$ is the symbol rate of the transmitted (multiplexed) data signal. This shows that PMD becomes a serious impairment at high data rates.

Since PMD is influenced by environmental conditions and varies on different timescales, an automatic and dynamic approach for PMD compensation is necessary. Electrical signal processing, e.g., transversal filters and decision feedback equalizers [78], can mitigate the distortions after detection, requiring fast electronics, where necessary processing speed increases with bit rate. A second approach is based on optical devices, which compensate for optical properties of the PMD impaired fiber link itself. Such PMD compensators usually consist of one or more stages of PCs and birefringent elements. The latter have either a fixed [79] or variable differential group delay [80], and a feedback loop based on a monitor signal as, for instance, the degree of polarization (DOP) [80 82].

In most ultra-high-speed transmission experiments, PMD (first order) was compensated for by manually adjusting the polarization of the data signal at the transmission link input ("principal state transmission"). Automatic and dynamic PMD compensation has been demonstrated in some transmission experiments with the symbol rate 160 Gbaud [51, 83 86]. For example, Ref. [86] reports on PMD-compensated DPSK transmission at 160 Gb/s over an installed standard SMF of 46 km (total transmission distance: 75 km). The mean DGD of the fiber link was 2.1 ps (i.e., 0.34 T_B), which leads to severe penalty values for arbitrary input polarizations in the absence of PMD compensation. The transmission system comprised a 160 Gb/s DPSK transmitter (MLLD pulse source) and the 160 Gb/s DPSK receiver based on EAMs for optical signal processing as described in

Section 6.4. The polarization of the data signal was scrambled for the transmission and "descrambled" before detection. BER measurements confirmed the performance of the PMD compensator, which decreased the penalty by more than 8 dB and thus enabled error-free 160 Gb/s transmission over this fiber link with only 1.3 dB penalty compared to back-to-back performance. All settings related to polarization and PMD were found in an automatic adaptation process.

6.6 TRANSMISSION EXPERIMENTS

6.6.1 Review on 160 Gb/s Transmission Experiments

In 1995, the first 160 Gb/s OOK transmission experiment was performed in the NTT laboratories based on soliton transmission over 200 km DSF using AP-multiplexing [87]. The pulse source was an MLFL followed by an optical pulse compressor, and the demultiplexer comprised a polarizer and an NOLM. EDFAs were used as inline amplifiers. Using essentially fiber-based optical signal processing technology for the terminal equipment and OOK modulation format, the NTT groups increased the OTDM bit rate in a number of spectacular experiments [53 56, 88 91] within 5 years up to 1.28 Tb/s (AP multiplexing). The 1.28 Tb/s transmission experiment will be described in Section 6.6.6. The NTT groups made also significant contributions to the OTDM/WDM-technology, which combined, e.g., the technologies of 160 Gb/s OTDM and ultra-wideband WDM [91]. We report on this experiment in Section 6.6.3.

The employment of semiconductor devices for optical signal processing in the transmitter and receiver of the OTDM system is an alternative to fiber-based optical signal processing. In particular, the SOA has long been considered a key device for optical signal processing, such as optical gates and optical clock recovery devices [57]. There are many transmission experiments resting upon SOA-based optical signal processing in the terminal equipment [11, 43, 58 62, 92 94]. Examples of single wavelength channel OOK transmission experiments are the first 160 Gb/s field trial involving unrepeatered transmission over 116 km field-installed SMF using an MLLD as pulse source and an SOA-UNI as optical gate for DEMUX [61], and another 160 Gb/s field trial over various link lengths of installed fiber of up to 275 km SMF using a DEMUX based on FWM in an SOA [11]. The latter field experiment is of particular interest because it also includes a 160 Gb/s add-drop node based on gain-transparent operation of an SOA. This is the first OTDM networking experiment using deployed fiber. A hybrid-integrated SOA-MZI DEMUX was used in the two OTDM/WDM transmission experiments: 1.28 Tb/s (160 Gb/s $\times$ 8 λ-channel) unrepeatered OOK transmission over 140 km SMF [94] and 3.2 Tb/s (320 Gb/s $\times$ 10 λ-channel) OOK transmission over 40 km SMF [58]. Also of particular importance is the first 160 Gb/s OOK transmission experiment with all-channel independent modulation and all-channel simultaneous demultiplexing achieved by using a multiplexer and a demultiplexer based

on periodically poled $LiNbO_3$ and SOA hybrid integrated planar lightwave circuits [43].

For OTDM systems with a symbol rate of 160 Gbaud, the SOA-based optical gate is probably the better choice for demultiplexing applications as compared to fiber-based optical gates, because of its compactness and the possibility of integration with other components. However, another semiconductor device, the EAM, has been developed into a very effective component for optical signal processing (demultiplexing) [95, 96]. In 1999, the first 160 Gb/s OOK transmission experiment was reported, which used the EAM as an optical gate in the demultiplexer, as a basic element in the clock recovery circuit and as a device for optical pulse generation (CW + Mod) [97]. This investigation also stimulated similar experiments in many laboratories [98 106] because the EAM-based 160 Gb/s OTDM technology does not require such sophisticated devices as interferometric optical gates or FWM configurations for demultiplexing applications. Moreover, the EAM-based demultiplexer is polarization insensitive, which is difficult to achieve with the fiber-based and SOA-based demultiplexers. Also, the EAM-based demultiplexer does not need an optical pulse source to operate the optical gate. The simpler technology of the EAM-based OTDM-system stimulated also several $N \times 160$ Gb/s OTDM/WDM transmission experiments [48 51, 107, 108] as we will report in Section 6.6.3.

At present, the EAM-based optical gate is to our knowledge the best choice for demultiplexing applications and clock recovery devices in OTDM transmission systems at the symbol rate 160 Gbaud. On the contrary, the EAM is probably not the best choice for optical pulse generation (CW + Mod), because it requires in general some sort of subsequent pulse compression. In Sections 6.6.4 and 6.6.5, we describe two 160 Gb/s OTDM transmission experiments in detail, which use EAM-based terminal equipment in the receiver, an MLLD in the transmitter and the modulation format DPSK.

6.6.2 Beyond 160 Gb/s Transmission

OTDM data transmission beyond 160 Gb/s was first performed in the NTT laboratories. Examples of this work are the following single wavelength channel, SP transmission experiments: 200 Gb/s over 100 km DSF [88], 400 Gb/s over 40 km SMF [89], 640 Gb/s over 60 km, and 92 km SMF [53, 54], and the OTDM/WDM experiment: 1.4 Tb/s (200 Gb/s $\times$ 7 λ-channel) over 50 km DSF [90]. In these experiments, OOK modulation format was used and the terminal equipment mainly comprised fiber devices. The pulse source in the transmitter was either an MLFL or a pulse source based on supercontinuum generation (SC pulse source). The demultiplexer in the OTDM receiver was an optical gate based either on an NOLM or on FWM in fiber. An exception was the optical clock recovery device, which comprised a PLL with a phase comparator based on FWM in an SOA. EDFAs were used as in-line amplifiers. Of particular importance is the

1.28 Tb/s, AP multiplexing, single λ-channel transmission experiment over 70 km SMF + RDF [55], which is discussed in more detail in Section 6.6.6.

Recently, 1.28 and 2.56 Tb/s single λ-channel transmission was also realized using DQPSK modulation format and AP multiplexing [8]. These experiments are also described in detail in Section 6.6.6.

There are a few transmission experiments at data rates beyond 160 Gb/s, which do not use fiber-based optical signal processing in the terminal equipment in particular for the optical gate in the demultiplexer. Based on EAMs for optical signal processing, some 320 Gb/s OOK transmission experiments used AP multiplexing and a polarizer either before or behind the demultiplexer [102, 103]. These experiments require essentially 160 Gb/s optical signal processing in the terminal equipment. The 160 Gb/s OTDM technology (MLLD, EAM, for DEMUX and clock recovery) was even upgraded to 640 Gb/s by applying the modulation format DQPSK and AP multiplexing [109]. The 640 Gb/s DQPSK data signal was transmitted over 480 km SLA/IDF (Ultrawave^{TM}) fiber error-free (BER $\leq 10^{-9}$). In an OTDM/WDM experiment 10 λ-channels (spectral efficiency 0.8 bit/s/Hz), each carrying a 320 Gb/s OOK, SP signal, were transmitted over 40 km SMF [58]. In this experiment, the optical gate comprised a hybrid-integrated SOA-MZI DEMUX and an SC pulse source was used.

6.6.3 OTDM/WDM Transmission Experiments

Large-capacity OTDM/WDM transmission experiments combining OTDM and ultra-wideband WDM technologies have been demonstrated by NTT already since 1995 [114]. In 1997 and 1999 NTT reported 1.4 Tb/s (200 Gb/s $\times$ 7 λ-channel, OOK, SP multiplexing) and 3 Tb/s (160 Gb/s $\times$ 19 λ-channel, OOK, SP multiplexing) transmission over 50 and 40 km DSF respectively [90, 91]. The 3 Tb/s transmission experiment is described here in more detail. The 19 λ-channel signal was generated by two SC pulse sources. Each comprising a 10 GHz MLFL, an optical modulator, an optical amplifier, and an SC fiber. The 19 λ-channel signal combined from both SC spectra ranged from 1540 to 1609 nm with a channel spacing of 480 GHz. Each 10 Gb/s λ-channel was time-division multiplexed (TDM) to 160 Gb/s using a planar lightwave circuit OTDM multiplexer. Subsequently, all λ-channels were WDM multiplexed by AWG filters to produce the 3 Tb/s WDM signal, which was transmitted over the 40 km DSF fiber link. In the OTDM receiver, all λ-channels were WDM and TDM demultiplexed successively. TDM demultiplexing of the 160 Gb/s signal into a 10 Gb/s signal was performed by an optical gate based on FWM in fiber and a prescaled PLL timing extraction circuit based on FWM in an SOA. The demultiplexed 10 Gb/s signal was detected by an optical receiver. BER performance was measured and error-free operation was confirmed for all 19 λ-channels.

In 2001 the first OTDM/WDM transmission experiment was reported using EAMs as OTDM demultiplexer [107]. Error-free 160 10 Gb/s demultiplexing of

six 160 Gb/s OOK wavelength channels has been achieved using two cascaded EAMs as demultiplexer. Similar experiments were performed by many other groups [48 51, 108]. OTDM/WDM transmission experiments were also performed based on the 40 Gb/s ETDM technology, which simplifies the design of the 160 Gb/s OTDM receiver. For instance, only one EAM is required for demultiplexing. This was demonstrated in a 640 Gb/s (160 Gb/s × 4 λ-channel, OOK) 3 × 80 km transmission experiment [108], in a 1.28 Tb/s (160 Gb/s × 8 λ-channel, OOK, AP multiplexing) 85 km transmission experiment [48], and in a 1.12 Tb/s (160 Gb/s + 7% FEC × 7λ-channels, OOK, AP multiplexing) 600 km transmission experiment performed in a recirculating loop [49]. In the two latter experiments, the channel spacing was 300 GHz corresponding to a spectral efficiency of 0.53 bit/s/Hz, and the transmitters were DFB-lasers modulated by EAMs (pulse carving). The 1.12 Tb/s transmission experiment was extended to a 1.28 Tb/s (160 Gb/s + 7% FEC × 8 λ-channels, AP multiplexing) 430 km field transmission experiment using nearly the same terminal equipment [51].

OTDM/WDM transmission experiments were also performed using a hybrid-integrated SOA-MZI DEMUX as optical gate in the OTDM receiver. Examples are 1.28 Tb/s (160 Gb/s × 8 λ-channel, OOK, AP multiplexing) unrepeatered transmission over 140 km SMF [94] and 3.2 Tb/s (320 Gb/s × 10 λ-channel, OOK, AP multiplexing) transmission over 40 km SMF [58]. In these experiments, the spectral efficiencies were 0.4 and 0.8 bit/s/Hz, respectively.

DQPSK transmission provides a bit rate that is twice the symbol bit rate. Based on 40 Gb/s ETDM technology, the application of DQPSK provides 80 Gb/s data transmission. In Refs [110, 111] this was further combined with polarization-division multiplexing (AP multiplexing) to generate a 160 Gb/s data signal. In this experiment, 40 WDM channels, each carrying a 160 Gb/s data signal generated in this way, were transmitted over a 324 km SMF fiber link. The system was operated above the FEC limit. This corresponds to a 5.94 Tb/s error-free transmission conditional on the use of FEC. A spectral efficiency of 1.6 bit/s/Hz was obtained.

6.6.4 160 Gb/s Transmission With Long-Term Stability

The system performance for 160 Gb/s DPSK transmission in combination with balanced detection is at least 3 dB better than the system performance for OOK transmission [40, 104]. The increased system margin was used to demonstrate long-term stability of the DPSK transmission system [105, 106].

Figure 6.7 shows schematically the experimental setup. The 160 Gb/s transmitter comprised a 40 GHz optical pulse source, a push pull-operated $LiNbO_3$ Mach Zehnder DPSK phase modulator driven by a pattern generator and a fiber delay line MUX providing a SP multiplexed 160 Gb/s PRBS data signal ($sech^2$ pulses, FWHM 1.4 ps, jitter <250 fs, almost transform limited $\Delta\nu^*\Delta t = 0.32$) at the input of the fiber link. The optical pulse source was a 10 GHz MLLD followed by a compact and temperature-stabilized 10 40 GHz fiber delay line pulse multiplier.

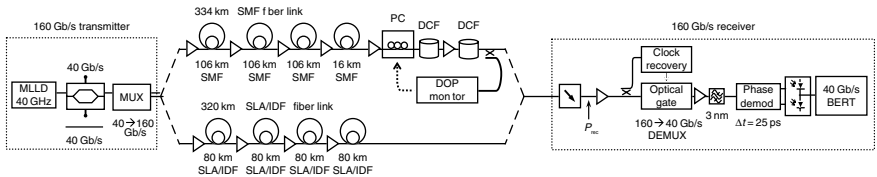

Figure 6.7 Experimental setup of 160 Gb/s DPSK transmission over either a 334 km SMF fiber link or a 320 km SLA/IDF fiber link.

The 160 Gb/s receiver comprised an automatic PC, the EAM-based 160 40 Gb/s DEMUX consisting of the optical clock recovery [67] and the optical gate, a 3 nm optical bandpass filter, a DPSK demodulator (see Section 6.4.3), a balanced photodetector, and a 40 Gb/s bit error ratio tester (BERT).

Two transmission experiments were performed, one experiment using a 334 km SMF fiber link (upper link in Figure 6.7) and the other experiment using a 320 km SLA/IDF fiber link (lower link in Figure 6.7). The PRBS word lengths were 2^7 1 and 2^{31} 1 bits in the experiments. The results showed that the penalty due to the longer pattern is negligible. Using PRBS sequences, a DPSK precoder or decoder could be avoided. The dispersion was carefully compensated for in both transmission links to provide a pulse width below 1.7 ps at the receiver. The reamplification was realized by EDFAs and the average power to the spans was set to 10 dBm in both experiments.

The mean DGD of the SLA/IDF fiber link (including EDFAs) was 0.7 ps, and PMD mitigation was not required. In the SMF experiment, the mean DGD was 0.8 ps for the SMF link and 1.4 ps for the two DCF modules including the EDFAs. Because of the high DGD of the DCF, a PMD mitigation scheme was used in the SMF experiment as shown in Figure 6.7. It consisted of an automatic PC before the DCF modules and a polarimeter after the DCF modules. The polarization was controlled such that the degree of polarization after the dispersion compensation was maximum. This is a feasible concept because the dispersion compensation was realized as postcompensation and thus was located altogether in front of the receiver. The described scheme avoided an adjustment to the principal states of polarization. This scheme was dynamic but not adaptive. Hence it was a PMD mitigation, but not a full PMD compensation scheme. A complete PMD compensation scheme is described in Refs [82, 86].

The BER measurements vs the received power P_{rec} resulted in a back-to-back sensitivity of 28.4 dBm, a penalty of almost 3 dB for transmission using the SMF link and a penalty below 1.5 dB for transmission using the SLA/IDF fiber link. More details of these measurements are reported in Refs [105, 106]. For the SMF experiment, Figure 6.8 shows the BER over the decision threshold of the receiver. The corresponding eye diagrams are shown as insets. A wide error-free range was obtained for both fiber links. The curves also confirm the good balance of the receiver as the optimum threshold is at about 0 mV. Degradations narrow the

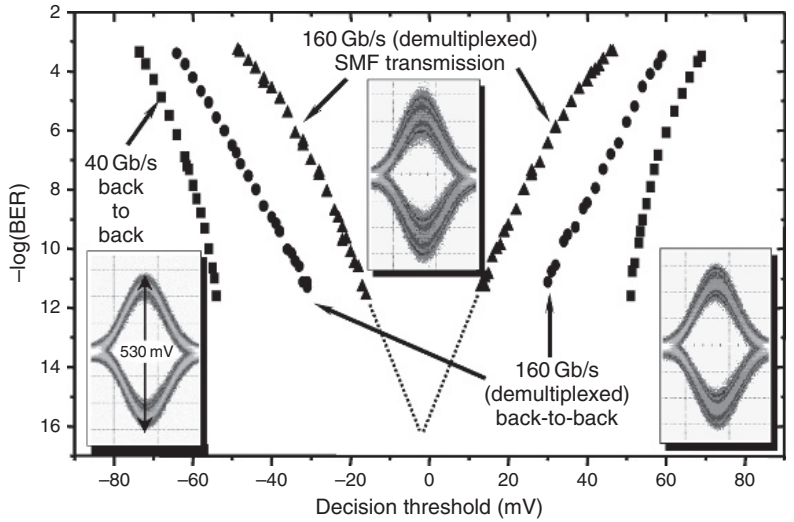

Figure 6.8 BER measurements vs decision threshold, back to back and after 334 km SMF transmission, and corresponding eye diagrams [112].

curve, but do not change the decision threshold. This enabled stable operation without realignment or active control of the decision threshold and is the main cause of the long-term stability of the DPSK transmission system in combination with the increased system margin. A BER in the order $<10^{-15}$ is expected from these measurements and was confirmed in the long-term measurements.

Figure 6.9 depicts the results of the long-term measurements without any manual readjustment for the transmission over both fiber links. For the SMF experiment, the polarization to the DCF was tracked and aligned by an automatic computer control. The plot shows the absolute number of bit errors which happened

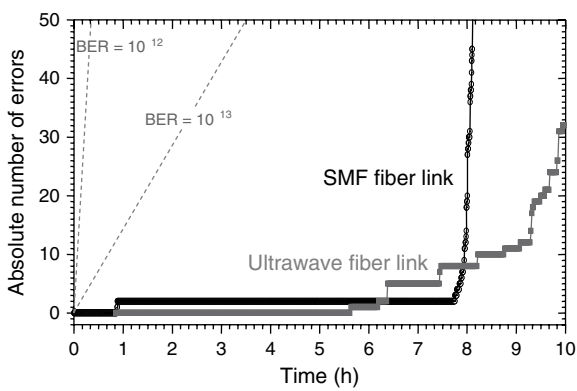

Figure 6.9 Measurements of absolute number of errors vs time (this figure may be seen in color on the included CD ROM).

during the time interval of 10 h. For a period of more than 5 h, the system was running without any bit error for both fiber links. This indicates a bit error floor due to intrinsic transmission impairments in the order of 10^{-15}, which confirms the results in Figure 6.8. Since the laboratory system did not include any automatic feedback (in contrast to a commercial system), a slight drift of the system started after some time. However, even the steep increase still corresponds to a bit error ratio of 10^{-12} (plotted as dotted line on the left-hand side). As the system can be adjusted by using power monitors (mainly the input and output powers of the EDFAs), the adjustment can be easily automated. These results suggest that this 160 Gb/s DPSK transmission system can be used in deployed systems and can be operated error-free for years if some feedback for compensating the slow drifts and FEC is implemented.

6.6.5 160 Gb/s Ultra-Long-Haul Transmission

Figure 6.10 shows schematically the experimental setup of a 170 Gb/s (160 Gb/s + 7% FEC) DPSK transmission experiment using a recirculating loop arrangement [7]. Transmission was investigated using SP signals and AP signals. The 170 Gb/s transmitter and receiver were similar to those of the long-term stability experiment in Section 6.6.4. The loop comprised six 80 km DMF spans (480 km) of SLA/IDF (Ultrawave^{TM}) fiber (see Section 6.5.1). Using commercial Raman pump modules (RPM1 RPM6) with pump lasers operating around 1444 and

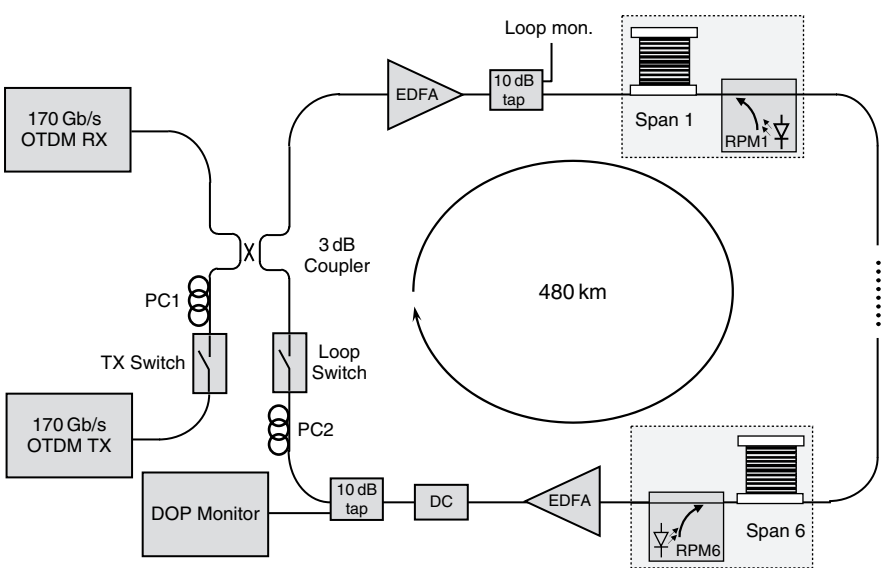

Figure 6.10 Schematic view of setup in 160 Gb/s DPSK long haul transmission [112].

1456 nm, the span losses including Raman couplers were fully compensated. The average span loss including couplers was 19.3 dB and the average span noise figure was 16.6 dB. The dispersion slope at the operating wavelength of 1551.5 nm was only 0.1 ps/nm^2, and the residual dispersion was minimized by inserting short SMF fiber pieces in the loop (DC in Figure 6.10). The 2 ps (FWHM) data pulses were broadened to 2.6 ps after 4320 km propagation.

The average DGD of the 480 km setup was 0.9 ps. Transmission of 170 Gb/s data signals significantly beyond this distance requires PMD compensation or suitable polarization adjustment in the loop. In this experiment, we used the latter technique, which was called "principal state transmission" in Section 6.5.2. To mitigate PMD effects, the SP signal must propagate in one of the principal states of polarization of the transmission link for each round trip in the loop. We obtained this by maximizing the DOP using the PCs, PC1 and PC2, and a polarization analyzer with high temporal resolution (μs range). For the AP signal, PC2 was adjusted for minimum BER after the ninth roundtrip. In this case, the slow and fast DGD axis seem to interchange after each round trip. Otherwise, the accumulated DGD would cause a shift of the relative temporal position of adjacent orthogonally polarized OTDM tributaries, yielding a degradation of the transmission performance, because no polarization demultiplexing was used in the receiver.

The BER was measured for SP and AP signals using a PRBS 2^{31} 1 sequence. In both cases, no polarizing filter was used at the receiver. For the SP signal, BER values of 5×10^{9} and 1.6×10^{4} were obtained after 960 and 2880 km, respectively. For the AP signal, the optimum launched power was consistently 2 3 dB higher than for the SP signal due to smaller nonlinear degradations. This enabled longer transmission distances. For a distance of 1920 km (four round trips), a BER of 2×10^{9} was obtained. At 4320 km transmission distance, a minimum BER value of 5×10^{5} was achieved. Using advanced FEC, the BER values for transmission distances up to 4320 km can be corrected to values below 10^{12}.

6.6.6 1.2 and 2.5 Tb/s OTDM Transmission Experiments

In 2000, the first 1.28 Tb/s, AP multiplexing, single λ-channel transmission experiment over a fiber link of 70 km SMF + RDF was reported [55, 56]. This experiment combined all achievements in high-speed data transmission technology using the modulation format OOK. A regeneratively MLFL generated a 10 GHz, 3 ps pulse train. The optical pulse train was modulated at 10 Gb/s by a $LiNbO_3$ intensity modulator. Then the signal pulses were coupled into an adiabatic soliton compression stage comprising amplification in an EDFA and compression in 1100-m-long dispersion-flattened dispersion-decreasing fiber (DF-DDF). After the pulse was compressed to less than 200 fs, the signal was coupled into a dispersion imbalanced nonlinear optical loop mirror (DI-NOLM) to reduce the pedestal of the signal pulse. The pulse width at the output of the DI-NOLM was

200 fs and the peak-to-pedestal ratio was larger than 30 dB. For the 1.28 Tb/s OTDM transmission, the signal pulse width was broadened to an optimized value of 380 fs by using an optical filter with a bandwidth of 15 nm. CD compensation was applied taking into account not only D and $dD/d\lambda$ but also $d^2D/d\lambda^2$ by cosine phase modulation to the pulses [74, 75]. Then the 10 Gb/s signal was optically multiplexed up to 640 Gb/s using a planar lightwave circuit OTDM multiplexer. Subsequently, the signal was polarization multiplexed up to 1.28 Tb/s using two polarization beam splitters (PBSD) and an optical delay. After amplification by an EDFA, the 1.28 Tb/s signal was coupled into the 70 km transmission line. At the receiver, the 1.28 Tb/s signal was polarization demultiplexed to 640 Gb/s using a PBS. Then, the signal was demultiplexed to 10 Gb/s using a walk-off reduced NOLM. A second MLFL generated the 10 GHz control pulse train for the NOLM. This MLFL was synchronized with the data signal with use of a transmitted clock signal. Error-free operation was confirmed for all 128 TDM channels.

Recently, 1.28 and 2.56 Tb/s, AP multiplexing, single λ-channel transmission was also realized using DQPSK modulation format [8]. Figure 6.11 shows the experimental setup of these transmission experiments. In the transmitter, a 10 GHz MLSL (1550 nm, 2.1 ps) and a pulse compression unit (DF-DDF followed by a DI-NOLM) provided a 10 GHz optical pulse train with a pulse width of 0.42 ps. An optical bandpass filter centered at 1556 nm defined the final pulse width for transmission. An important requirement for the pulse compression unit was to preserve the phase coherence of the pulse train as required for a DQPSK-modulated data signal. Data generation based on a symbol rate of 10 Gbaud was used to improve the pulse compression and data modulation. This pulse train was modulated and multiplexed to generate an 80 Gb/s DQPSK signal (symbol rate 40 Gbaud, see Section 6.3.2). Finally, the 80 Gb/s DQPSK signal was multiplexed by a delay-line multiplexer (OTDM-MUX) to an AP-signal with the data rate 1.28 or 2.56 Tb/s.

The data signal was transmitted over two or three 80 km DMF spans of SLA/IDF (Ultrawave^{TM}) fiber (see Section 6.5.1). The dispersion was precisely matched by the insertion of short SMF pieces, while the dispersion slope was compensated for by the SLA/IDF combination and combining different spans with opposite residual slope. The span input power was set to 12 dBm. The average DGD of the link was

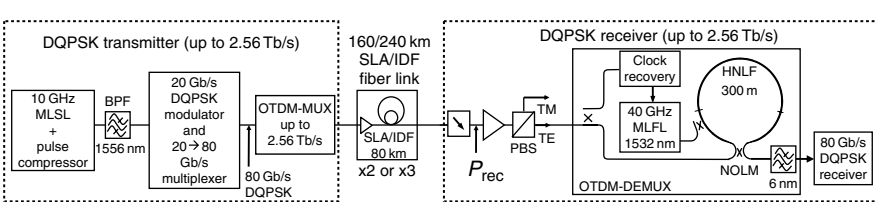

Figure 6.11 Schematic view of the experimental setup for 1.28 and 2.58 Tb/s DQPSK transmission over a 160 or 240 km SLA/IDF fiber link [112].

below 0.7 ps for three spans. To mitigate the detrimental effects of PMD, the input polarization was adjusted to the principal states of polarization of the fiber.

In the receiver, a polarization demultiplexer (PBS) was followed by an NOLM (300 m highly nonlinear fiber, HNLF) as optical gate. An MLFL (40 GHz, FWHM 1.0 ps) provided the control pulses for the NOLM. This laser was synchronized to the data signal by a clock recovery unit, which operated well up to a symbol rate of 320 Gbaud [67]. In the 2.56 Tb/s experiment, this clock recovery could also be operated at the symbol rate of 640 Gbaud. We attributed this to small imperfections of the optically multiplexed data signal (clock modulation). At the output of the NOLM, the signal passed a 6 nm filter to separate the data signal from the control pulses. The 80 Gb/s DQPSK receiver comprised a delay-line interferometer as phase demodulator, a balanced photodetector, a 40 10 Gb/s ETDM demultiplexer and a BER.

Figure 6.12 shows the results of BER measurements of the 2.56 and the 1.28 Tb/s AP signals vs the received signal power at the input of the receiver (as indicated in Figure 6.11) after transmission over 160 km SLA/IDF (Ultrawave^{TM}) fiber (two spans) and in back-to-back measurements. This figure shows also the results of back-to-back measurements of 80 and 640 Gb/s SP signals for comparison. The results for 2.56 Tb/s cover the dashed area in Figure 6.12, because the overlapping pulse tails caused coherence cross talk resulting in variations of the performance. The pulse width was 0.65 ps at the output of the transmitter. The pulse width after

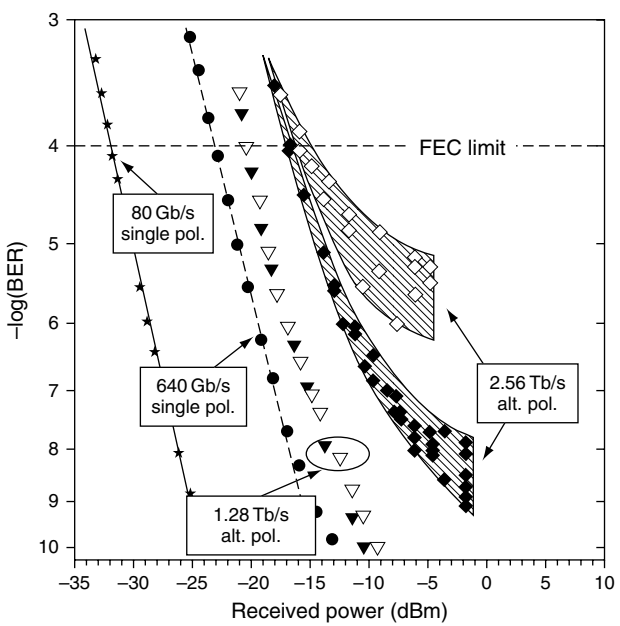

Figure 6.12 BER measurements for 2.56 and 1.28 Tb/s back to back (solid symbols) and 160 km fiber transmission (hollow symbols) experiment [112].

160 km transmission was 0.75 ps. For the 2.56 Tb/s transmission, shorter pulses are desirable. However, the reduction of the pulse width in the present set up was limited by the bandwidth of the cascaded non-gain-flattened EDFAs, fourth-order CD and higher order PMD.

For 2.56 Tb/s transmission, the system performed nearly error-free (BER $\approx 10^{-9}$) in the back-to-back configuration and revealed BER values $\leq 10^{-5}$ after 160 km transmission. BER values $< 10^{-4}$ result in an effective BER $< 10^{-12}$ if standard FEC (assuming a 7% overhead) is used. This FEC would reduce the payload to 2.4 Tb/s. For 1.28 Tb/s, error-free (BER $< 10^{-9}$) transmission was obtained. At this data rate, error-free transmission was also possible over a fiber link of 240 km Ultrawave^{TM} fiber (three spans) for all tributaries of the 1.28 Tb/s data signal (not shown in Figure 6.12).

6.7 CONCLUSIONS

For 160 Gb/s TDM transmission, there are several optical signal processing technologies available. Presently, the optimum terminal equipment includes an optical gate and a clock recovery device in the receiver both based on EAMs and an MLLD as pulse source in the transmitter. These components are commercially available today.

Based on this terminal equipment, 160 Gb/s OTDM point-to-point transmission technology seems to be nearly a mature technology. Combined with the modulation format DPSK and balanced detection, it provides very stable operation. This transmission technology seems to be already appropriate for deployed systems if well-established techniques like FEC and Raman amplification will be implemented to further increase the system margin.

Today, commercial systems use ETDM and not OTDM. The present research work on ETDM technology focuses on 100 Gb/s Ethernet rather than on the next bit rate in the STM hierarchy, which would be 160 Gb/s, e.g., Ref. [2]. We think that ETDM technology will have to work hard to compete with OTDM technology as regards receiver sensitivity and power consumption at 160 Gb/s. Even if electrical signal processing at 160 Gb/s would be available, it will be difficult to provide terminal equipment, which is cheaper and less energy consuming than the terminal equipment based on optical signal processing at 160 Gb/s. OTDM receivers perform better than ETDM receivers already at data rates of 80 Gb/s.

This chapter was restricted to point-to-point OTDM transmission technology. However, an optical network comprises also networking components, like add-drop multiplexers, 3R-regenerators, etc. The principal operation of these networking components has been shown based on OTDM technology at 160 Gb/s. However, up to now, the reported solutions for these networking components are not very promising. A weakness of optical signal processing is the lacking of appropriate optical buffers, which are required to realize practical solutions for all-optical networking components. In contrast, logical operations and data

buffering are a strength of electrical signal processing. Consequently, a possible scenario for future communication networks with TDM data rate of 160 Gb/s is that these networks use a hybrid technology based on a mixture of OTDM and ETDM technologies. OTDM subsystems or components, such as transmitter pulse sources based on monolithically integrated MLLDs or the OTDM multiplexing and demultiplexing components, will very likely find applications in this hybrid communication network. OTDM components, such as pulse sources, optical gates and clock recovery devices are already being employed in optical sampling systems for waveform and signal quality measurements.

160 Gb/s OTDM transmission experiments revealed also some limitations for data transmission over deployed fiber links. The standard SMF is well suited for high-bit-rate transmission, as a high local dispersion is in favor for high-speed transmission. However, many old fiber links have very high PMD values, which make 160 Gb/s data transmission impractical even if PMD compensators are available.

Moreover, upgrading existing systems to higher data rates has also to take into account that today's transmission systems are essentially WDM systems equipped with components like WDM multiplexers and demultiplexers, and with a channel spacing of 100 or 200 GHz. This restricts the bandwidth of each channel. Upgrading the data rate per channel requires data signals with high spectral efficiency. The installment of high-bit-rate data signals with high spectral efficiency requires techniques like phase stable multiplexing, multilevel modulation formats, or polarization multiplexing. In contrast to upgrading an existing transmission system, installing a new transmission system based on 160 Gb/s data rate imposes no limitations on the design.

As already pointed out in the Introduction, the most challenging view as regards OTDM technology is that optical networks will evolve into "photonic networks," in which ultra-fast optical signals of any bit rate and modulation format will be transmitted and processed from end to end without O/E/O conversion. With this view as target, transmission experiments at data rates beyond 160 Gb/s investigate the feasibility of ultra-high-speed data transmission in communication networks in the far future. Transmission at data rates beyond 160 Gb/s will require not only appropriate terminal equipment but also improved transmission fibers and improved in-line amplifiers. This is in particular true for data transmission at 1.2 and 2.5 Tb/s, which seems to be strongly limited by the properties of the transmission line and the amount of work required to combat all fiber impairments. However, the view of a "photonic networks" presents us also with a guide line of finding innovative solutions in the near future.

ACKNOWLEDGMENTS

The authors dedicate this chapter in love to Gudrun, Ingeborg, Julia and Michael.

REFERENCES

[1] E. B. Desurvire, "Capacity demand and technology challenges for lightwave systems in the next two decades," *J. Lightw. Technol.*, 34(12), 4697 4710, 2006.

[2] C. Schubert, R. H. Derksen, M. Möller et al., "Integrated 100 Gb/s ETDM receiver," *J. Lightw. Technol.*, 25(1), 122 130, 2007.

[3] S. Kawanishi, H. Takara, K. Uchiyama et al., "Single Polarization Completely Time Division Multiplexed 100 Gbit/s Optical Transmission Experiment," in *Proc. ECOC'93*, 3, 1993, pp. 53 56.

[4] S. Kawanishi, "Ultrahigh speed optical time division multiplexed transmission technology based on optical signal processing," *IEEE J. Quant. Electron.*, 34, 2064 2079, 1998.

[5] M. Saruwatari, "All optical signal processing for Tera bit/s optical transmission," *IEEE J. Sel. Top. Quant. Electron.*, 6, 1363 1374, 2000.

[6] M. Saruwatari "All optical time division multiplexing technology," in *Fiber Optic Communica tion Devices* (N. Grote and H. Venghaus, eds), Berlin: Springer Verlag, 2001.

[7] S. Weisser, S. Ferber, L. Raddatz et al., "Single and alternating polarization 170 Gbit/s transmis sion up to 4000 km using dispersion managed fiber and all Raman amplification," *Photon. Technol. Lett.*, 18(6), 1320 1322, 2006.

[8] H. G. Weber, S. Ferber, M. Kroh et al., "Single channel 1.28 Tbit/s and 2.56 Tbit/s DQPSK transmission," *Electron. Lett.*, 42, 178 179, 2006.

[9] O. Kamatani and S. Kawanishi, "Add/drop operation for 100 Gbit/s optical signal based on optical wavelength conversion by four wave mixing," *Electron. Lett.*, 32, 911 913, 1996.

[10] C. Schubert, C. Schmidt, S. Ferber et al., "Error free all optical add drop multiplexing at 160 Gbit/ s," *Electron. Lett.*, 39, 1074 1076, 2003.

[11] J. P. Turkiewicz, E. Tangdiongga, G. Lehmann et al., "160 Gbit/s OTDM networking using deployed fiber," *J. Lightw. Technol.*, 23, 225 235, 2005.

[12] H. F. Chou, J. E. Bowers, and D. J. Blumenthal, "Compact 160 Gb/s Add Drop Multiplexing with a 40 Gb/s Base Rate," in *Proc. OFC 2004*, PDP28, 2004.

[13] S. Nakamura, Y. Ueno, and K. Tajima, "168 Gb/s all optical wavelength conversion with a symmetric Mach Zehnder type switch," *Photon. Technol. Lett.*, 13, 1091 1093, 2001.

[14] J. Leuthold, C. Joyner, B. Mikkelsen et al., "100 Gbit/s all optical wavelength conversion with integrated SOA delayed interference configuration," *Electron. Lett.*, 36, 1129 1130, 2000.

[15] J. Hansryd, P. A. Andrekson, M. Westlund et al., "Fiber based optical parametric amplifiers and their applications," *IEEE J. Sel. Top. Quant. Electron.*, 8, 506 520, 2002.

[16] F. Futami, R. Okabe, Y. Takita, and S. Watanabe, "Transparent Wavelength Conversion at up to 160 Gb/s by using Supercontinuum Generation in a Nonlinear Fiber," in *Proc. OAA 2003*, Paper MD07, Otaru, Japan, 2003.

[17] S. Ferber, R. Ludwig, F. Futami et al., "160 Gbit/s Regenerating Conversion Node," in *Proc. OFC 2004*, Los Angeles, CA, USA, paper ThT2, 2004.

[18] S. Watanabe, R. Ludwig, F. Futami et al., "Ultrafast all optical 3R regeneration," *IEICE Trans. Electron.*, E87 C(7), 1114 1118, 2004.

[19] C. Schmidt Langhorst, and H. G. Weber "Optical sampling techniques" in *Optical and Fiber Communication Reports 3*, "Ultrahigh speed optical transmission technology", (H. G. Weber and M. Nakazawa eds), New York: Springer Science + Business Media, LLC, ISBN 13: 978 3 540 23878 2, pp. 453 481, 2007.

[20] M. Westlund, P. A. Andrekson, H. Sunnerud et al., "High performance optical fiber nonlinearity based optical waveform monitoring," *J. Lightw. Technol.*, 23(6), 2012 2022, 2006.

[21] R. Ludwig, S. Diez, A. Ehrhardt et al., "A tunable femtosecond modelocked semiconductor laser for applications in OTDM systems," *IEICE Trans. Electron.*, E81 C, 140 145, 1998.

[22] H. Yokoyama, "Highly reliable mode locked semiconductor lasers," *IEICE Trans. Electron.*, E85 C, 27 36, 2002.

[23] Leaf A. Jiang, Erich P. Ippen, and Hiroyuki Yokoyama "Semiconductor mode locked lasers as pulse sources for high bit rate data transmission," in *Optical and Fiber Communication Reports 3*,

"Ultrahigh speed optical transmission technology"(H. G. Weber and M. Nakazawa, eds), New York: Springer Science + Business Media, LLC, ISBN 13: 978 3 540 23878 2, pp. 21 51, 2007.

[24] S. Arahira, and Y. Ogawa, "40 GHz Actively Mode Locked Distributed Bragg Reflector laser diode module with an impedance matching circuit for efficient RF signal injection," *Jpn. J. Appl. Phys.*, 43, 1960 1964, 2004.

[25] H. Heidrich, B. Huettl, R. Kaiser et al., "Optical 40 GHz pulse source module based on a monolithically integrated mode locked DBR laser," in *SPIE Proc.* of *APOC 2005*, Session 12b, paper 6020 6079, 2005.

[26] K. Tamura, H. A. Haus, and E. P. Ippen, "Self starting additive pulse mode locked erbium fibre ring laser," *Electron. Lett.*, 28, 2226 2228, 1992.

[27] M. Nakazawa, E. Yoshida, and Y. Kimura, "Ultrastable harmonically and regeneratively modelocked polarisation maintaining erbium fibre laser," *Electron. Lett.*, 30, 1603 1604, 1994.

[28] Masataka Nakazawa "Ultrafast mode locked fiber lasers for high speed OTDM transmission and related topics," in *Optical and Fiber Communication Reports 3*, "Ultrahigh Speed Optical Trans mission Technology" (H. G. Weber and M. Nakazawa, eds), New York: Springer Science + Busi ness Media, LLC, ISBN 13: 978 3 540 23878 2, pp. 53 87, 2007.

[29] S. C. Zeller, L. Krainer, G. J. Spühler et al., "Passively mode locked 40 GHz Er:Yb:glass laser," *Appl. Phys.*, B 76, 787 788, 2003.

[30] M. D. Pelusi, Y. Matsui, and A. Suzuki, "Femtosecond Optical Pulse Generation from an Electro Absorption Modulator with Repetition Rate and Wavelength Tuning," in *Proc. ECOC 99*, Nice, Volume II, 1999, pp. 26 27.

[31] Eugen Lach, Karsten Schuh, and Michael Schmidt, "Application of electroabsorption modulators for high speed transmission systems," in *Optical and Fiber Communication Reports 3*, "Ultrahigh speed optical transmission technology" (H. G. Weber and M. Nakazawa, eds), New York, Springer Science + Business Media, LLC, ISBN 13: 978 3 540 23878 2, pp. 347 377, 2007.

[32] T. Morioka, K. Uchiyama, S. Kawanishi et al., "Multiwavelength picosecond pulse source with low jitter and high optical frequency stability based on 200 nm supercontinuum filtering," *Elec tron. Lett.*, 31, 1064 1066, 1995.

[33] M. Nakazawa, E. Yoshida, K. Kubota, and Y. Kimura, "Generation of a 170 fs, 10 GHz transform limited pulse train at 1.55 μm using a dispersion decreasing, erbium doped active soliton compressor," *Electron. Lett.*, 30, 2038 2039, 1994.

[34] K. R. Tamura, and M. Nakazawa, "54 fs, 10 GHz soliton generation from a polarization maintaining dispersion flattened dispersion decreasing fiber compressor," *Opt. Lett.*, 26, 762 764, 2001.

[35] W. S. Wong, S. Namiki, M. Margalit et al., "Self switching of optical pulses in dispersion imbalanced nonlinear loop mirrors," *Opt. Lett.*, 22, 1150, 1997.

[36] I. Y. Khrushchev, I. D. Phillips, A. D. Ellis et al., "Dispersion Imbalanced Fiber Loop Mirror for High Bit Rate OTDM," in *Proc. ECOC 99*, Nice, II, 24 25, 1999.

[37] D. von der Linde, "Characterization of the noise in continuously operating mode locked lasers," *Appl. Phys.*, B 39, 201 217, 1986.

[38] A. H. Gnauck, S. Chandrasekhar, J. Leuthold, and L. Stulz, "Demonstration of 42.7 Gb/s DPSK receiver with 45 Photons/Bit sensitivity," *IEEE Photon. Technol. Lett.*, 15(1), 99 101, 2003.

[39] T. Chikama, S. Watanabe, T. Naito et al., "Modulation and demodulation techniques in optical heterodyne PSK transmission systems," *J. Lightw. Technol.*, 8(3), 309 321, 1990.

[40] A. H. Gnauck, and P. J. Winzer, "Optical phase shift keyed transmission," *J. Lightw. Technol.*, 23(1), 115 130, 2005.

[41] R. Griffin and A. Carter, "Optical Differential Quadrature Phase Shift Key (oDQPSK) for High Capacity Optical Transmission," in Techn. Dig. 27th *OFC'02*, Annaheim, CA (USA), paper WX6, March 2002, pp. 367 368.

[42] T. Ohara, H. Takara, I. Shake et al., "160 Gbit/s optical time division multiplexing with PPLN hybrid integrated planar lightwave circuit," *IEEE Photon. Technol. Lett.*, 15, 302 304, 2003.

[43] T. Ohara, H. Takara, I. Shake et al., "160 Gb/s OTDM transmission using integrated all optical MUX/DEMUX with all channel modulation and demultiplexing," *IEEE Photon. Technol. Lett.*, 16, 650 652, 2004.

[44] H. Murai, M. Kagawa, H. Tsuji, and K. Fujii, "Single Channel 160 Gbit/s Carrier Suppressed RZ Transmission over 640 km with EA Modulator based OTDM Module," in *Proc. ECOC 2003*, paper Mo.3.6.4, Rimini, 2003.

[45] S. Randel, B. Konrad, A. Hodzic, and K. Petermann, "Influence of Bitwise Phase Changes on the Performance of 160 Gbit/s transmission systems," in *Proc. ECOC 2002*, Copenhagen proceedings, 3, paper P3.31, 2002.

[46] M. Kagawa, H. Murai, H. Tsuji, and K. Fujii, "Performance Comparison of Bitwise Phase Controlled 160 Gbit/s Signal Transmission using an OTDM Multiplexer with Phase Correlation Monitor," in *Proc. ECOC 2004*, paper We 4.P.109, 2004.

[47] Y. Su, L. Moller, C. Xie et al., "Ultra high speed data signals with alternating and pairwise alternating optical phases," *J. Lightw. Technol.*, 23(1), 26 31, 2005.

[48] M. Schmidt, K. Schuh, E. Lach et al., "8 × 160 Gbit/s (1.28 Tbit/s) DWDM Transmission with 0.53 bit/s/Hz Spectral Efficiency using Single EA Modulator Based RZ Pulse Source and Demux," in *Proc. ECOC 2003*, paper Mo3.6.5, Rimini, 2003.

[49] E. Lach, K. Schuh, M. Schmidt et al., "7 × 170 Gbit/s (160 Gbit/s + FEC Overhead) DWDM Transmission with 0.53 bit/s/Hz Spectral Efficiency over Long Haul Distance of Standard SMF," in *Proc. ECOC 2003*, paper PD Th4.3.5, 2003.

[50] M. Daikoku, T. Otani, and M. Suzuki, "160 Gb/s Four WDM Quasi Linear Transmission over 225 km NZ DSF with 75 km Spacing," *IEEE Photon. Technol. Lett.*, 15(8), 1165 1167, 2003.

[51] M. Schmidt, M. Witte, F. Buchali et al., "8 × 170 Gbit/s DWDM Field Transmission Experiment over 430 km SSMF Using Adaptive PMD Compensation," in *Proc. ECOC 2004*, Stockholm, PDP Th4.1.2, 2004.

[52] K. J. Blow, N. J. Doran, and B. P. Nelson, "Demonstration of the nonlinear fibre loop mirror as an ultrafast all optical demultiplexer," *Electron. Lett.*, 26, 962 963, 1990.

[53] M. Nakazawa, E. Yoshida, T. Yamamoto et al., "TDM single channel 640 Gbit/s transmission experiment over 60 km using 400 fs pulse train and walk off free, dispersion flattened nonlinear optical loop mirror," *Electron. Lett.*, 34, 907 908, 1998.

[54] T. Yamamoto, E. Yoshida, and K. R. Tamura et al., "640 Gbit/s optical TDM transmission over 92 km through a dispersion managed fiber consisting of single mode fiber and reverse dispersion fibre," *IEEE Photon. Technol. Lett.*, 12, 353 355, 2000.

[55] M. Nakazawa, T. Yamamoto, and K. R. Tamura, "1.28 Tbit/s 70 km OTDM transmission using third and fourth order simultaneous dispersion compensation with a phase modulator," *Electron. Lett.*, 36, 2027 2029, 2000.

[56] T. Yamamoto and M. Nakazawa, "Ultrafast OTDM transmission using novel fiber devices for pulse compression, shaping, and demultiplexing," in *Optical and Fiber Communication Reports 3*, "Ultrahigh speed optical transmission technology," (H. G. Weber and M. Nakazawa eds), New York: Springer Science + Business Media, LLC, ISBN 13: 978 3 540 23878 2, 2007, pp. 379 395.

[57] C. Schubert, R. Ludwig, and H.G. Weber "High speed optical signal processing using semicon ductor optical amplifiers," in *Optical and Fiber Communication Reports 3*, "Ultrahigh speed optical transmission technology" (H. G. Weber and M. Nakazawa, eds), New York: Springer Science + Business Media, LLC, ISBN 13: 978 3 540 23878 2, 2007, pp. 103 140.

[58] A. Suzuki, X. Wang, Y. Ogawa, and S. Nakamura, "10 × 320 Gbit/s (3.2 Tbit/s) DWDM/OTDM Transmission by Semiconductor Based Devices," in *Proc. ECOC 2004*, paper Th4.1.7, 2004.

[59] K. Tajima, S. Nakamura, and A. Furukawa, "Hybrid integrated symmetric Mach Zehnder all optical switches and ultrafast signal processing," *IEICE Trans. Electron.*, E87 C (7) 1119 1125, 2004.

[60] C. Schubert, S. Diez, J. Berger et al., "160 Gbit/s all optical demultiplexing using a gain transparent ultrafast nonlinear interferometer (GT UNI)," *IEEE Photon. Technol. Lett.*, 13, 475 477, 2001.

[61] U. Feiste, R. Ludwig, C. Schubert et al., "160 Gbit/s transmission over 116 km field installed fibre using 160 Gbit/s OTDM and 40 Gbit/s ETDM," *Electron. Lett.*, 37, 443 445, 2001.

[62] K. Suzuki, K. Iwatsuki, S. Nishi, and M. Saruwatari, "Error free demultiplexing of 160 Gbit/s pulse signal using optical loop mirror including semiconductor laser amplifier," *Electron. Lett.*, 30, 1501 1503, 1994.

[63] H. Murai, M. Kagawa, H. Tsuji, and K. Fuji: "EA modulator based optical multiplexing/demulti plexing techniques for 160 Gbit/s OTDM signal transmission," *IEICE Trans. Electron.*, E88 C(3), 309 318, 2005.

[64] S. Kodama, T. Yoshimatsu, and H. Ito, "320 Gbit/s error free demultiplexing using ultrafast optical gate monolithically integrating a photodiode and electroabsorption modulator," *Electron. Lett.*, 39(17), 1269 1270, 2003.

[65] S. Kodama, T. Yoshimatsu, and H. Ito, "500 Gbit/s Demultiplexing Operation of Monolithic PD EAM Gate," in *Proc. ECOC 2003*, Postdeadline paper Th4.2.8, Rimini, 2003.

[66] I. Shake, H. Takara, K. Uchiyama et al., "160 Gbit/s full optical time division demultiplexing using FWM of SOA array integrated on PLC," *Electron. Lett.*, 38, 37 38, 2002.

[67] C. Boerner, V. Marembert, S. Ferber et al., "320 Gbit/s Clock Recovery with Electro Optical PLL using a Bidirectionally Operated Electroabsorption Modulator as Phase Comparator," in *Proc. OFC 2005*, paper OTuO3, 2005.

[68] A. H. Gnauck, G. Raybon, P. G. Bernasconi et al., "(1 Tb/s 6×170.6 Gb/s) transmission over 2000 km NZDF using OTDM and RZ DPSK," *IEEE Photon. Technol. Lett.*, 15(11), 1618 1620, 2003.

[69] S. Vorbeck and R. Leppla, "Dispersion and dispersion slope tolerance of 160 Gb/s systems, considering the temperature dependence of chromatic dispersion," *IEEE Photon. Technol. Lett.*, 15(10), 1470 1472, 2003.

[70] B. J. Eggleton, B. Mikkelsen, G. Raybon et al., "Tunable dispersion compensation in a 160 Gb/s TDM system by voltage controlled chirped fiber Bragg grating," *IEEE Photon. Technol. Lett.*, 12, 1022 1024, 2000.

[71] C. K. Madsen, "Integrated Waveguide Allpass Filter Tunable Dispersion Compensator," in *Proc. OFC'2002*, paper TuT1, 2002.

[72] T. Inui, T. Komukai, M. Nakazawa et al., "Adaptive dispersion slope equalizer using a nonlinearly chirped fiber Bragg grating pair with a novel dispersion detection technique," *IEEE Photon. Technol. Lett.*, 14, 549 551, 2002.

[73] S. Wakabayashi, A. Baba, H. Moriya et al., "Tunable dispersion and dispersion slope compensator based on two twin chirped FBGs with temperature gradient for 160 Gbit/s transmission," *IEICE Trans. Electron*, E87 C, 1100 1105, 2004.

[74] M. D. Pelusi, X. Wang, F. Futami et al., "Fourth order dispersion compensation for 250 fs pulse transmission over 139 km optical fiber," *IEEE Photon. Tech. Lett.*, 12, 795 798, 2000.

[75] Mark D. Pelusi, and Akira Suzuki, "Higher order dispersion compensation using phase mod ulators," in *Optical and Fiber Communication Reports 3*, "Ultrahigh speed optical transmission technology," (H. G. Weber and M. Nakazawa, eds), New York: Springer Science + Business Media, LLC, ISBN 13: 978 3 540 23878 2, pp. 307 321, 2007.

[76] T. Yamamoto and M. Nakazawa, "Third and fourth order active dispersion compensation with a phase modulator in a terabit per second optical time division multiplexed transmission," *Opt. Lett.*, 26, 647, 2001.

[77] L. E. Nelson and R. M. Jopson "Introduction to polarization mode dispersion in optical systems," in *Polarization Mode Dispersion* (A. Galtarossa and C. R. Menyuk, eds), Optical and Fiber Communication Reports (OFCR) Springer Science + Business Media, Inc., 2005.

[78] H. Bülow, F. Buchali, and W. Baumert et al., "PMD mitigation at 10 Gbit/s using linear and nonlinear integrated equaliser circuits," *Electron Lett.*, 36(2), 163 164, 2000.

[79] F. Buchali, W. Baumert, M. Schmidt, and H. Bülow, "Dynamic distortion compensation in a 160 Gbit/s RZ OTDM system: Adaptive 2 stage PMD compensation," in *Proc. OFC 2003*. Atlanta, paper ThY1, 2003.

[80] H. Rosenfeldt, Ch. Knothe, R. Ulrich et al., "Automatic PMD Compensation at 40 Gbit/s and 80 Gbit/s using a 3 Dimensional DOP Evaluation for Feedback," in *Proc. OFC 2001*. Anaheim, Postdeadline paper PD27, 2001.

[81] C. Francia, F. Bruyère, J. P. Thiéry, and D. Penninckx, "Simple dynamic polarization mode dispersion compensator," *Electron. Lett.*, 35(5), 414 415, 1999.

[82] Harald Rosenfeldt and Ernst Brinkmeyer: "PMD compensation techniques," in *Optical and Fiber Communication Reports 3*, "Ultrahigh Speed Optical Transmission Technology" (H. G. Weber and M. Nakazawa, eds), New York: Springer Science + Business Media, LLC, ISBN 13: 978 3 540 23878 2, pp. 323 346, 2007.

[83] M. Westlund, H. Sunnerud, J. Li et al., "Long term automatic PMD compensation for 160 Gbit/s RZ transmission," *Electron. Lett.*, 38, 982 983, 2002.

[84] T. Miyazaki, M. Daikoku, I. Morita et al., "Stable 160 Gbit/s DPSK Transmission using a Simple PMD Compensator on the Field Photonic Network Test Bed of JGN II," in *Proc. OECC 2004*. PD 1 3, 2004.

[85] F. Buchali, W. Baumert, M. Schmidt, and H. Buelow, "Dynamic Distortion Compensation in a 160 Gb/s RZ OTDM System: Adaptive 2 Stage PMD Compensation," in *Proc. OFC* 589 590, 2003.

[86] S. Kieckbusch, S. Ferber, H. Rosenfeldt et al., "Automatic PMD compensator in a single channel 160 Gb/s transmission over deployed fiber using RZ DPSK modulation format," *J. Lightw. Technol.*, 23(1), 165 171, 2005.

[87] M. Nakazawa, K. Suzuki, E. Yoshida et al., "160 Gbit/s soliton data transmission over 200 km," *Electron. Lett.*, 31, 565 566, 1995.

[88] S. Kawanishi, H. Takara, T. Morioka et al., "200 Gbit/s, 100 km time division multiplexed optical transmission using supercontinuum pulses with prescaled PLL timing extraction and all optical demultiplexing," *Electron. Lett.*, 31, 816 817, 1995.

[89] S. Kawanishi, H. Takara, T. Morioka et al., "Single channel 400 Gbit/s time division multiplexed transmission of 0.98 ps pulses over 40 km employing dispersion slope compensation," *Electron. Lett.*, 32, 916 917, 1996.

[90] S. Kawanishi, H. Takara, K. Uchiyama et al., "1.4 Tbit/s (200 Gbit/s $\times$ 7 ch) 50 km optical transmission experiment," *Electron. Lett.*, 33, 1716 1717, 1997.

[91] S. Kawanishi, H. Takara, K. Uchiyama et al., "3 Tbit/s (160 Gbit/s $\times$ 19 channel) optical TDM and WDM transmission experiment," *Electron. Lett.*, 35(10), 826 827, 1999.

[92] R. Ludwig, U. Feiste, S. Diez et al., "Unrepeatered 160 Gbit/s RZ single channel transmission over 160 km of standard fibre at 1.55 um with hybrid MZI optical DEMUX," *Electron. Lett.*, 36, 1405 1406, 2000.

[93] T. Yamamoto, U. Feiste, J. Berger et al., "160 Gbit/s Demultiplexer with Clock Recovery using SOA Based Interferometric Switches and its Application to 120 km fiber transmission," in *Proc. ECOC'01*, Amsterdam, Tu.L.2.6, 2001.

[94] A. Suzuki, X. Wang, T. Hasegawa et al., "8 $\times$ 160 Gb/s (1.28 Tb/s) DWDM/OTDM Unrepeate dred Transmission over 140 km Standard Fiber by Semiconductor Based Devices," in *Proc. ECOC 2003*, Rimini, paper Mo3.6.1, 2003.

[95] D. D. Marcenac, A. D. Ellis, and D. G. Moodie, "80 Gbit/s OTDM using electroabsorption modulators," *Electron. Lett.*, 34(1), 101 103, 1998.

[96] A. D. Ellis, J. K. Lucek, D. Pitcher et al., "Full 10 $\times$ 10 Gbit/s OTDM data generation and demultiplexing using electroabsorption modulators," *Electron. Lett.*, 34, 1766 1767, 1998.

[97] B. Mikkelsen, G. Raybon, R. J. Essiambre et al., "160 Gbit/s Single Channel Transmission over 300 km Nonzero Dispersion Fiber with Semiconductor Based Transmitter and Demultiplexer," in *Proc. ECOC 1999*, postdeadline paper 2 3, Nice, 1999.

[98] J. Yu, K. Kojima, N. Chand et al., "160 Gb/s Single Channel Unrepeatered Transmission over 200 km of Non Zero Dispersion Shifted Fiber," in *Proc. ECOC 2001*, paper PD M.1.10, 2001.

[99] J. L. Augé, M. Cavallari, M. Jones et al., "Single Channel 160 Gbit/s OTDM Propagation over 480 km of Standard Fiber using a 40 GHz Semiconductor Mode Locked Laser Pulse Source," in *Proc. OFC 2002*, paper TuA3, Anaheim, 2002.

[100] E. Lach, M. Schmidt, K. Schuh et al., "Advanced 160 Gb/s OTDM System based on Wavelength Transparent 4 × 40 Gb/s ETDM Transmitters and Receivers," in *Proc. OFC 2002*, Anaheim, paper TuA2, 2002.

[101] H. Murai, M. Kagawa, H. Tsuji et al., "Single Channel 160 Gbit/s (40 Gbit/s × 4) 300 km Transmission Using EA Modulator based OTDM Module and 40 GHz External Cavity Mode locked LD," in *Proc. ECOC 2002*, paper 2.1.4, Copenhagen, 2002.

[102] M. Schmidt, E. Lach, K. Schuh et al., "Unrepeatered 320 Gbit/s (8 × 40 Gbit/s) OTDM Trans mission over 80 km TeraLightTM Reverse TeraLightTM Fiber Link," in *Proc. ECOC 2003*, We.4.P.117, Rimini, 2003.

[103] B. Mikkelsen, G. Raybon, R. J. Essiambre et al., "320 Gbit/s single channel pseudolinear transmission over 200 km nonzero dispersion fiber," *IEEE Photon. Technol. Lett.*, 12, 1400 1402, 2000.

[104] S. Ferber, R. Ludwig, C. Boerner et al., "Comparison of DPSK and OOK modulation format in 160 Gbit/s transmission system," *Electron. Lett.*, 39(20), 1458 1459, 2003.

[105] S. Ferber, R. Ludwig, C. Boerner et al., "160 Gbit/s DPSK transmission over 320 km fibre link with high long term stability," *Electron. Lett.*, 41, 200 202, 2005.

[106] S. Ferber, C. Schmidt Langhorst, R. Ludwig et al., "160 Gbit/s OTDM long haul transmission with long term stability using RZ DPSK modulation format," *IEICE Trans. Commun.*, E88 B (5), 1947 1954, 2005.

[107] B. Mikkelsen, G. Raybon, B. Zhu et al., "High Spectral Efficiency (0.53 bit/s/Hz) WDM Transmission of 160 Gb/s per Wavelength over 400 km of Fiber," in *Proc. OFC 2001*, paper ThF2 1, Anaheim, 2001.

[108] K. Schuh, M. Schmidt, E. Lach et al., "4 × 160 Gbit/s DWDM/OTDM Transmission over 3 × 80 km TeraLightTM Reverse TeraLightTM fibre," in *Proc. ECOC 2002*, paper 2.1.2, Copenhagen, 2002.

[109] S. Ferber, C. Schubert, R. Ludwig et al., "640 Gbit/s DQPSK single channel transmission over 480 km fibre link," *Electron. Lett.*, 41(22), 1234 1235, 2005.

[110] A. Fauzi Abas Ismail, D. Sandel, A. Hidayat et al., "2.56 Tbit/s, 1.6 bit/s/Hz, 40 Gbaud RZ DQPSK polarization division multiplex transmission over 273 km of fiber," in *Proc. OECC 2004*, PD paper PD1 4, Yokohama, Japan, 2004.

[111] B. Milivojevic, A. F. Abas, A. Hidayat et al. "1.6 bit/s/Hz, 160 Gbits/s, 230 km RZ DQPSK Polarization Multiplex Transmission with Tunable Dispersion compensation," *IEEE Photon. Technol. Lett.*, 17(2), 495 497, 2005.

[112] H. G. Weber, R. Ludwig, S. Ferber et al., "Ultrahigh speed OTDM transmission technology," *IEEE J. Lightw. Technol.*, 24(12), 4616 4627, 2006.

[113] O. Kamatani and S. Kawanishi, "Prescaled Timing extraction from 400 Gbit/s optical signal using a phase lock loop based on four wave mixing," *IEEE Photon. Technol. Lett.*, 8, 1094 1096, 1996.

[114] Toshio Morioka "Ultrafast optical technologies for large capacity TDM/WDM photonic networks," in *Optical and Fiber Communication Reports 3,* "Ultrahigh Speed Optical Transmission Technology" (H. G. Weber and M. Nakazawa, eds) New York: Springer Science + Business Media, LLC, ISBN 13: 978 3 540 23878 2, pp. 397 423, 2007.

7

Optical performance monitoring

Alan E. Willner[*], Zhongqi Pan[†], and Changyuan Yu[‡]

[*]*University of Southern California, Los Angeles, CA, USA*
[†]*Department of Electrical and Computer Engineering, University of Louisiana at Lafayette, USA*
[‡]*Department of Electrical and Computer Engineering, National University of Singapore, Singapore*

7.1 INTRODUCTION

Today's optical networks function in a fairly static fashion and are built to operate within well-defined specifications. This scenario is quite challenging for higher-capacity systems, since network paths are not static and channel-degrading effects can change with temperature, component drift, aging, and fiber plant maintenance. Moreover, we are far from being able to simply "plug-and-play" an optical node into an existing network in such a way that the network itself can allocate resources to ensure error-free transport. This chapter explores optical performance monitoring (OPM) and its potential for enabling higher stability, reconfigurability, and flexibility in a self-managed optical network.

To enable robust and cost-effective automated operation, the network should probably be able to: (i) intelligently monitor the physical state of the network as well as the quality of propagating data signals, (ii) automatically diagnose and repair the network, (iii) allocate resources, and (iv) redirect traffic. To achieve this, OPM should isolate the specific cause and location of the problem rather than simply sound an alarm. This chapter describes the specific parameters that a network might want to monitor as well as promising techniques.

7.1.1 Window of Operability

The bit rate of a transmitted channel is limited by many physical considerations, which can be described by the notion of a "window of operability" for a transmission system [1]. For example, as the number of network channels and bit-rate-per-channel

Optical Fiber Telecommunications V B: Systems and Networks

ISBN: 978 0 12 374172 1

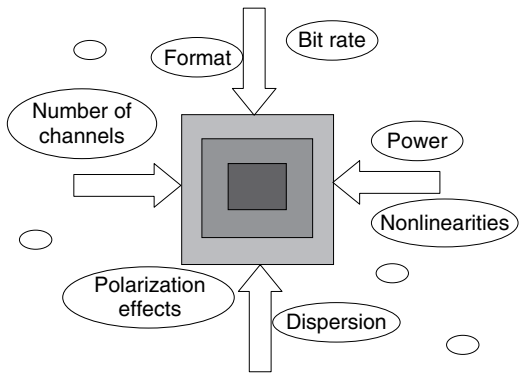

Figure 7.1 Window of operability is shrinking as systems become more complex (this figure may be seen in color on the included CD ROM).

increase, effects such as fiber impairments reduce this window (see Figure 7.1). The evolution to transparent mesh networks further threatens to close the window of operability due to the complexity of managing the degrading effects. The introduction of $\geq$40-Gbit/s transmission links increases the deleterious impact on data channels due to fiber impairments, such as chromatic dispersion (CD), polarization mode dispersion (PMD), and nonlinearities. OPM is one potential means of either widening this window or helping to maintain channel operation within a small window, such that rapid growth of high-performance optical networks is enabled.

7.1.2 Nonstatic Nature of Optical Networks

High spectral efficiencies, narrow channel spacing, long transmission distances, high bit rates, and transparent switching all create new challenges in network management. Basic changes, such as temperature changes, component aging, and plant maintenance, will all have an effect on the physical properties that impact the integrity of data channels. Moreover, the ability to reconfigure a network to provide dynamic services causes many traditionally static network properties to become dynamic quantities. Troubleshooting faults becomes more difficult as distances between end terminals increases and more complex components are used, such as intelligent routers and dispersion compensation modules. For brief illustrative purposes, let us consider changes in CD, PMD, nonlinearities, and optical signal-to-noise ratio (OSNR)[2]:

(a) CD: The effect of CD increases as the square of the bit-rate increase, thus making CD significantly more important for $\geq$40-Gbit/s systems than for lower-rate systems. Any slight inaccuracies in dispersion compensation will result in severe power penalties, and changes in dispersion accumulation on a channel should be monitored. For instance, due to repair and maintenance, the link length or fiber type itself may change. Moreover, CD has a temperature dependence that causes

a change in net link dispersion. In addition, future networks may perform restoration and protection in the optical domain, and CD should be monitored and compensated after each reconfiguration. Furthermore, any wavelength drifts could result in a chirp of a signal through an optical filter, such that the ps/nm chirp will interact with the fiber dispersion. Additionally, since tunable electrical or optical modules might be used for managing accumulated CD for next-generation $\geq$40-Gbit/s telecommunication networks, it might be valuable to implement some method of dynamic monitoring to drive the compensator.

(b) PMD: PMD is an important impairment in high-speed reconfigurable optical networks. PMD is based on the fact that a given signal spectral component of the optical data propagates along two identifiable principle states of polarization (PSPs) within a noncircularly symmetric fiber core, and these two spectral copies travel down the fiber at slightly different speeds. PMD accumulates due to fiber and any slight birefringence of many in-line components. By its inherent nature, deleterious PMD effects are stochastic, time varying, vibration dependent, and temperature dependent. Moreover, these effects include first-order and higher order components. These degradations may require the monitoring of signal quality to either dynamically tune a compensator or simply to determine the network location that must be diagnosed and repaired.

(c) Nonlinearities: Since nonlinearities are so destructive to data channels, they are typically designed out of the network. Key techniques for decreasing the effects of nonlinearities are maintaining fairly low channel powers and using carefully designed CD maps, such that dispersion will destroy the phase matching necessary for some nonlinear effects to accumulate. Any changes in channel powers or CD (as noted in (a) above) can dramatically affect the integrity of the data channels.

(d) OSNR: Channel power relative to the erbium-doped fiber amplifier (EDFA) generated amplified spontaneous emission (ASE) noise must be maintained at a fairly high level throughout the transmission link to ensure error-free data recovery. Much of the noise accumulation depends on the balance of input power and gain of the amplifier, such that a certain amount of EDFA saturation is desired for an optimum OSNR. Any simple change can dramatically impact the OSNR, and these changes can include laser power decrease, connector degradation, MUX/DEMUX wavelength drift, and EDFA pump power decrease. Monitors can help isolate and diagnose such problems.

We will discuss these and other parameters in greater detail later in the chapter.

7.1.3 Monitoring for a Self-Managed Network

Today's optical networks function in a fairly static fashion and are built to operate within well-defined specifications. Since these parameters can change over time, operating and managing an existing optical network requires a fair amount of person

time. Importantly, enormous amounts of time, money, and upkeep are required to deploy new nodes or upgrade existing links for these networks. Deployment is an onerous, labor-intensive task due to the numerous system variables that must be balanced. The required steps generally include making extensive initial measurements of the existing fiber plant; building terminal and in-line equipment to a narrow range of specifications that is "customized" to each specific deployment; fine tuning upon deployment in the field; and hoping that nothing changes over time. This scenario may no longer be suitable for higher-capacity future systems, since network paths are not static and channel-degrading effects can change dynamically with environments such as temperature, component drift, aging and fiber plant maintenance.

Compared to wireless Wi-Fi local area networks (LANs), optical networking is in a relatively primitive stage of development. When a laptop is opened, for example, consider how almost like magic available frequencies are allocated, the maximum transmission rate is found for that user's signal-to-noise ratio (SNR), and path-routing hand offs are achieved seamlessly.

Figure 7.2 shows a scenario that might enable "plug-and-play" operation of an optical node into an existing network and "self-managed" automated operation. For this to happen, the network should intelligently monitor the state of the network so that it can: (i) automatically diagnose and repair the network, (ii) redirect traffic, and (iii) dynamically allocate resources such as amplifier gain, signal wavelength, tunable dispersion compensation, electronic equalization, data coding, path determination, and channel bandwidth. Therefore, OPM might be essential for ensuring the high-quality operation for future intelligent optical networks [2].

To facilitate widespread adoption, OPM should be easily deployable, compact, inexpensive, accurate, stable and reliable. The specific parameters that a network might want to monitor range from the most basic to the highly complex. We note that some issues, such as channel power, channel wavelength, and fiber breaks, are already being monitored in many networks.

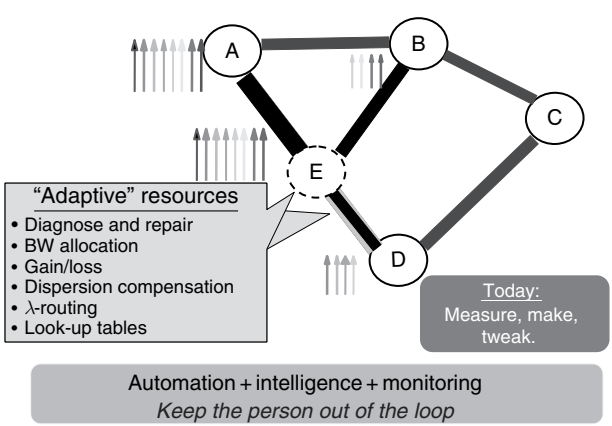

Figure 7.2 Intelligent self managed networks might require optical performance monitoring. (After Ref. [2]. © 2006 OSA.) (This figure may be seen in color on the included CD ROM).

7.2 NETWORK FUNCTIONALITY USING PERFORMANCE MONITORING

OPM plays an important role for maintenance and management of high-speed intelligent, reconfigurable optical networks. In this section, we give a brief introduction of network functionality that can be enabled by using OPM.

7.2.1 Robust and Stable Operation

Many impairments on optical signals are time-varying due to a changing environment, drift of components, and rapid reconfiguration of network paths. Moreover, the fiber impairments depend on complex interactions of linear and nonlinear fiber effects, which in turn are a function of the signal power, data rate, and data modulation format. These properties imply that the OPM should provide real-time information about the quality of these transmitted signals and also isolate the specific cause and location of the problem.

To enable robust and stable operation, the monitoring information corresponding to the accumulated impairment due to each specific degrading effect should probably be deployed ubiquitously around the network. Furthermore, it can be quite advantageous to determine when a data signal is *beginning* to degrade, so that the network can take action to correct the problem (i.e., change a laser wavelength, tune a compensator) or to route the traffic around the degraded area [2].

7.2.2 Accommodate Transparency

A network feature that might be desirable is for the monitor to be independent of the data format to accommodate a convergence of different traffic types. This is because the future network will possibly be used for many applications, and it seems inefficient to build a separate optical network to accommodate each one; rather, one network would accommodate a wide variety of traffic. Since each application might have a different set of optimal requirements, one can envision that one network might be required to transmit different modulation formats, a wide range in data rates, commercial and military traffic, and variable quality of service (QoS), as shown in Figure 7.3. Therefore, OPM should accommodate transparency [2, 3].

7.2.3 Impairment-Aware Routing

In existing networks, routing is typically based either on a shortest path calculation or on paths that satisfy certain network QoS constraints (e.g., data rate, delay, jitter, or packet loss). However, it might be quite advantageous for the network controller to also take

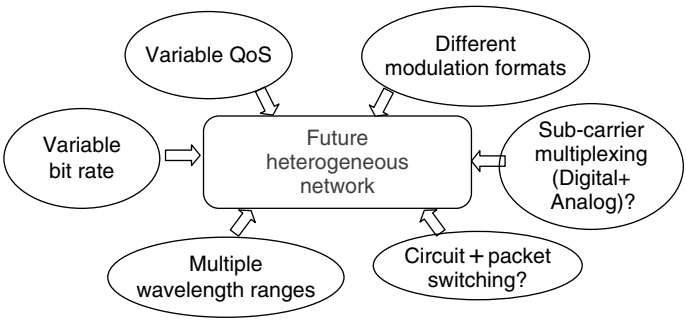

Figure 7.3 One network might accommodate many different types of traffic, and the hardware should be reconfigurable and transparent. An intelligent network could use the optimal channel characteristics for each application/user (this figure may be seen in color on the included CD ROM).

into account the variable *physical* state of the network, especially given that transparency domains are growing, data rates are increasing, and channel spacing is denser. It might be valuable for the network controller and routing algorithms to consider the optical layer impairments that degrade the bit error rate (BER) of the signal [4].

Figure 7.4 shows a diagram of multiple variable routing. Each link and optically transparent node has a set of parameters such as fiber length, signal degradation, amplification, and transients. The network must interpret the "cost function" for routing table and determine ranges of these parameters for inclusion into network model. Therefore, OPM might be required to provide valuable information such that routing tables themselves can dynamically reflect the state of the physical links, the fidelity of the channels, and the addition/deletion of nodes. This "impairment-aware" routing would enable routing tables to be modified based on physical changes in the links, instead of routing decisions being based simply on of the fewest hops and shortest links between source and destination. This results in severe challenges in terms of algorithm complexity and interpreting monitor output for any protocol.

In general, links today are assigned either a "1" or "0", depending on whether the link is considered working or malfunctioning. However, a link might be functional

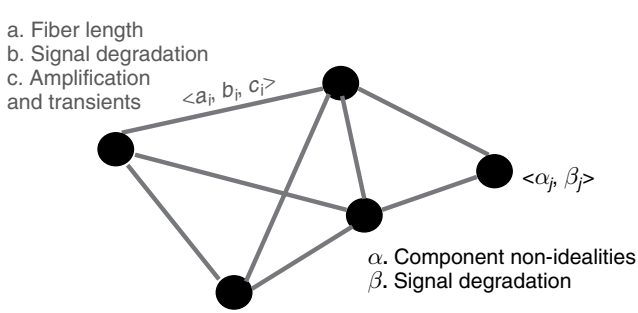

Figure 7.4 Multivariable routing (this figure may be seen in color on the included CD ROM).

well for some traffic but not sufficiently well for all traffic. Therefore, we emphasize that the network could assign "weights" to each link, such that a partially functioning link can still be used for some traffic, while rerouting other traffic. This is analogous to closing down only two lanes of a four-lane highway, which is significantly more preferable for traffic management than shutting down the entire highway.

The backbone network will likely be a transparent wavelength-division multiplexed (WDM) system. The key benefits of all-optical transport networks are the transparency to bit rate, protocol, and modulation format of all the various wavelength channels propagating in the system. However, key challenges exist when determining an optimum path through the network, since an optical wavelength might accumulate different physical impairments as it is switched through the network. These nonidealities will be imposed by both the transmission links and the optical switching nodes. The performance penalty due to the different optical impairments will depend on many factors, including the bit rate, modulation format, and electronic processing within the receiver [5 8]. Without physical impairment awareness, a network-layer routing, and wavelength assignment (RWA) algorithm might rapidly provision a lightpath that cannot meet the signal-quality requirement. Therefore, the control plane of an optical transparent network should incorporate the characteristics of the physical layer in establishing a lightpath for a new connection. To greatly simplify the network management, some margin in BER fluctuation could be considered to mitigate the effects of traffic distribution on a lightpath's quality. Figure 7.5 shows an impairment-aware RWA algorithm that requires some form of OPM [5].

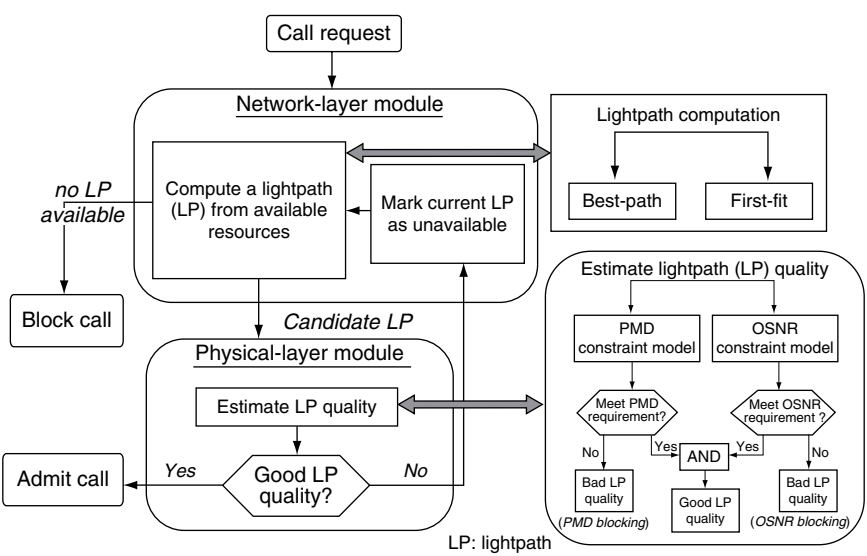

Figure 7.5 An example of an integrated model of an impairment aware algorithm. (After Ref. [6]. © 2005 IEEE/OSA.)

The results of Figure 7.6 show that: (1) impairment-unaware algorithms (i.e., traditional best-path algorithm (TBP) and the traditional first-fit algorithm (TFF)) have higher blocking probability in a realistic network than in an ideal network due to the effects of transmission impairments; and (2) significant improvement in blocking can be achieved by the proposed algorithms (i.e., impairment-aware routing and wavelength assignment algorithms (IABP) and the impairment-aware first-fit algorithm (IAFF)). With a load of 220 Erlangs,

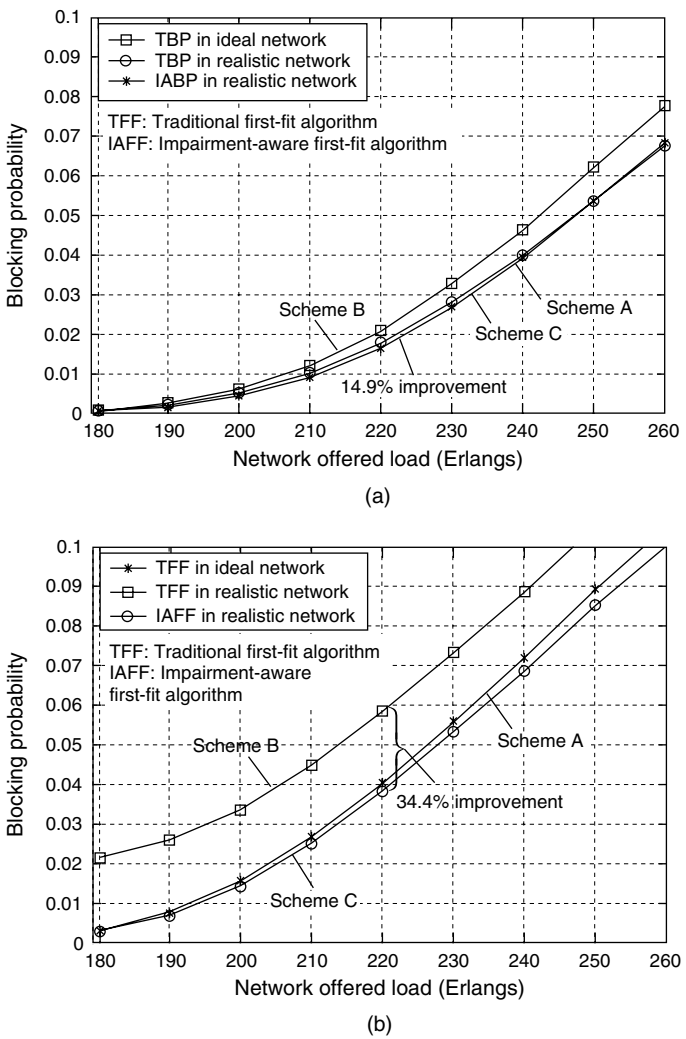

Figure 7.6 Connection blocking probability vs network offered load: (a) best path algorithms; (b) first fit algorithms. (After Ref. [6]. © 2005 IEEE/OSA.)

a 14.9% and 34.4% improvement in blocking probability is achieved by using IABP and IAFF, respectively.

7.2.4 Secure Links to Denial-of-Service

Complex WDM networks have dramatically higher performance, but they also pose new security vulnerabilities that go beyond severing a fiber or detecting the evanescent tail of the fiber core.

Monitoring might provide enhanced security to initiate preventive measures against denial-of-service, either through human error or malicious attack [9, 10]. As a simple example, as shown in Figure 7.7, an unwelcome high-power wavelength that is added and dropped somewhere in the middle of a long-distance link could cause severely degrading nonlinear effects (e.g., four-wave mixing (FWM) and cross-phase modulation (XPM)) on all of the existing WDM data channels. Furthermore, an intense unwanted wavelength can saturate and reduce the gain of an optical amplifier for all existing channels. Additionally, simple crosstalk can also destroy the data on the channels. If this wavelength disappears, the network returns to normal without any lasting trace of the "culprit".

In addition, this new wavelength could generate optical FWM nonlinear mixing products that would contain the data information of the existing channels, such that only mixing products that contain the original data bits need be recovered by an eavesdropper. In general, the network should be able to find the spatial and spectral locations of all wanted and unwanted wavelength channels and detect the generation of any nonlinear mixing products.

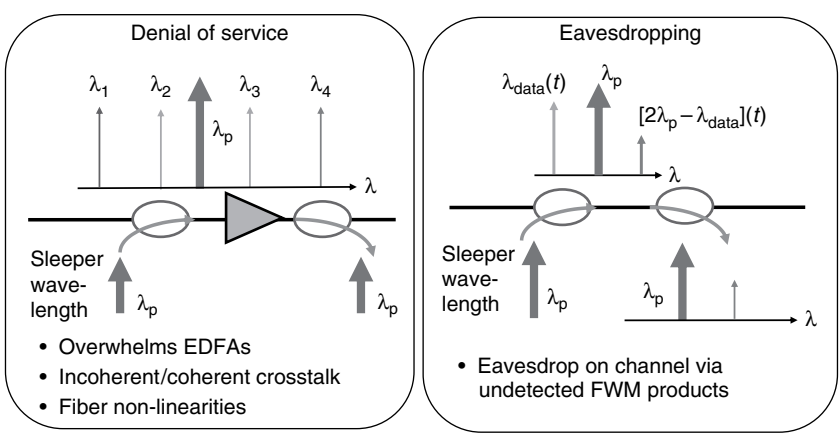

Figure 7.7 Denial of service and eavesdropping in the optical domain due to the insertion of an unwanted, intense optical wavelength. (After Ref. [2]. © 2006 OSA.) (This figure may be seen in color on the included CD ROM).

7.2.5 Optical Supervisory Channel

In some optical networks, a separate wavelength may be allocated to carry management and control information. Unlike the service-bearing data channels which might travel transparently through a node, an optical supervisory channel (OSC) might be electro-optically terminated, processed, and regenerated at each adjacent node [11 13]. Figure 7.8 shows an example of a wavelength-selective crossconnect (XC) and the processing of an OSC [11]. Since the OSC wavelength may not fall within the amplifier gain bandwidth, OSC signals might be demultiplexed and detected without propagation through an optical amplifier. After processing of the incoming management data, the outgoing OSC signal is generated and added to the appropriate output port. Some bit-oriented data such as alarm indication signal and remote defect indication signal are specific to a particular service-bearing data wavelength and are forwarded to the correct output port after processing.

Some commercial optical systems include OSC, such as CIENA's CN 4200 OSC module [14]. Built around a dedicated 1510-nm laser and receiver, the OSC provides an out-of-band, full-duplex communication channel for remote node management, monitoring and control. The OSC optically segregates network management and control from user data, so even if the OSC is lost, data forwarding continues uninterrupted. Equipped with 1510-nm MUX/DEMUX filter, the OSC travels the same fiber as the dense WDM stream and always terminates on neighboring nodes. Because it has a dedicated wavelength, the OSC data is entirely

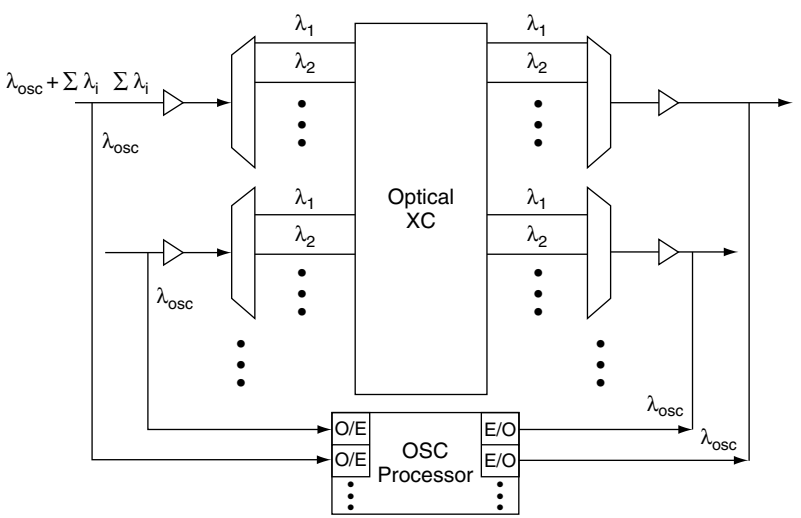

Figure 7.8 Wavelength selective crossconnect (XC) node that supports an optical supervisory channel (OSC). (After Ref. [11]. © 1998 IEEE.)

independent of the user data. The OSC carries a 100 Mb/s Ethernet-over-IP management channel used for inter-nodal management and control. Additionally, the module's built-in controller CPU allows it to assume the added role of system controller. The OSC can help determine major changes in the system, but it tends not to accurately determine subtle-yet-destructive fiber-based impairments on the data channels (i.e., CD, PMD, nonlinearities, and OSNR).

7.2.6 Introduction of Performance Monitoring Techniques

Fundamentally, OPM is a potential mechanism to improve control of transmission- and physical-layer fault management, which is essential for the operation of complex WDM transmission and switching systems. Examples of functions that require OPM include amplifier control, channel identification, and signal quality assessment. OPM can be broken down into three layers [15], as shown in Figure 7.9. Firstly, the WDM channel management layer monitoring involves a determination of the optical domain characteristics essential for transport and channel management at the WDM layer, such as real-time measurements of channel presence, power levels, and the OSNR. Secondly, optical signal quality monitoring involves a single wavelength and performs signal transition sensitive measurements such as eye diagram statistics, *Q*-factor, electronic SNR, and distortions that occur within the eye diagram, due to dispersion and nonlinear effects. Finally, the data protocol monitoring involves measuring the protocol performance information, such as the BER.

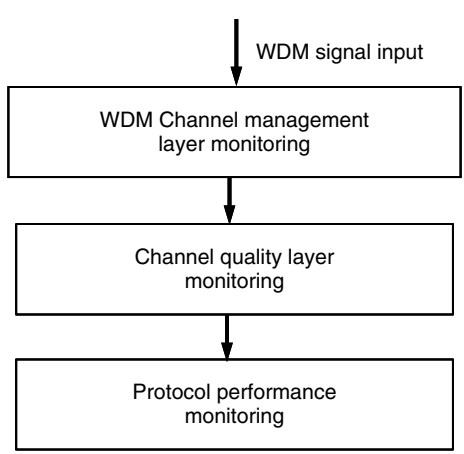

Figure 7.9 Three layers of optical performance monitoring: transport monitoring, signal quality monitoring, and protocol monitoring. (After Ref. [15]. © 2004 IEEE/OSA).

Another issue related to OPM is the troubleshooting that is often a trial-and-error process, and the cost is likely to scale rapidly with the number of sites visited and components tested. Troubleshooting will be especially difficult if the maintenance teams cannot obtain accurate information concerning the signal routes and channel configurations. This reality of managing a large network places a greater premium on accurate and automated performance information about a network.

We note that an effective monitor should be able to detect outages for network fault management, i.e., to the identification, diagnosis, resolution, and tracking of faults in a network. The fault is recognized when a component or monitor alarm is triggered or a customer report is filed. The monitors should have equal or better sensitivity than the end terminal receiver, where sensitivity is defined relative to a particular impairment. For example, noise might accumulate throughout the network and waveform distortion might follow the dispersion map. The combination of both noise and distortion at a given location will determine the sensitivity requirements for that location.

In general, optical impairments can be classified into catastrophic and noncatastrophic problems. Catastrophic problems tend to decrease the optical power and include individual or multiple component malfunctions, improperly installed or configured equipment, fiber breaks, and damage or intrusion to the network. Impairments due to such faults are as diverse as the components and network designs deployed in the field. In addition to faulty outages, there are many other well-known effects that are always present and must be minimized or controlled [15]. These might be classified as "noncatastrophic" problems, in which there is sufficient optical signal power but that the data bits themselves are unrecoverable due to various linear and nonlinear dispersive effects.

Laudable characteristics of an OPM also include being in-line, in-service, fast, sensitive, and relatively low cost. High-performance OPM should be ubiquitous around the network to enable proper diagnosis, such that the monitor should isolate the specific cause and location of the problem, not just simply sound an alarm. It should be noted that high-data-rate optical networks are quite susceptible to noncatastrophic problems. Exhaustive monitoring might be possible with an unlimited budget, and the value of monitoring increases with the increase of transparency.

As mentioned previously, OPM might be used to realize new methods of managing traffic. For instance, routing decisions based upon performance monitoring is one possibility. By monitoring the channel quality and link security and updating the routing look-up tables continually, high capacity and priority traffic can be dynamically tuned to high-performance optical channels [16], thus ensuring that the data channels achieve acceptable BER and the whole network achieves sufficient transmission and protection capacity.

In general, physical layer monitoring depends strongly on the physical network design. Different OPM parameters often require different monitors; therefore,

OPM is highly constrained by the available optical monitoring technology. The many possible physical layer measurement parameters might include:

(1) average and peak power (per wavelength or aggregate)
(2) pulse/bit shape
(3) timing jitter
(4) intensity/field autocorrelation (including higher order)
(5) amplitude power spectrum (RF spectrum)
(6) optical spectrum (i.e., channel wavelength and spectral shape)
(7) amplifier noise, gain and distortion
(8) pump laser relative intensity noise transfer
(9) amplitude histogram (synchronous and asynchronous)
(10) *Q*-factor/eye diagram/BER (i.e., V-curve measurements)
(11) crosstalk and interference effects
(12) CD
(13) polarization state and polarization-dependent effects
(14) PMD (first and higher order)
(15) optical filter distortion
(16) signal chirp and phase characteristics
(17) OSNR
(18) fiber nonlinearity-induced distortion and crosstalk

The monitoring techniques can either be analog or digital. Digital techniques use high-speed electronic logic to process digital information encoded on the optical waveform. Measurements on the digital signal are used to infer the characteristics of the optical signal. Digital methods have the strongest correlation with the BER, but are usually less effective at *isolating* the effects of individual impairments. Analog measurement techniques treat the optical signal as an analog waveform and attempt to measure specific characteristics of this waveform. These measurements are typically protocol independent and can be subdivided further into either time-domain methods or spectral methods. Time domain monitoring includes eye diagram measurements and auto- or cross-correlation measurements. Spectral methods must be broken down into optical spectrum and amplitude power spectrum (RF spectrum) measurements. The optical spectrum is conveniently measured using highly sensitive optical techniques and can provide optical noise information. The amplitude power spectrum is a better measure of signal quality because it measures the spectrum of the signal that is encoded on the optical carrier. Noise and distortion on the amplitude power spectrum will usually directly translate to impairments on the signal.

In Sections 7.3 7.5 of this chapter, we will give a review of OPM analog techniques in the optical domain for monitoring physical-layer impairments, including power/wavelength, OSNR, CD, PMD, and fiber nonlinearities. In Section 7.6, we will discuss electronic digital monitoring techniques based on analyzing the signals after optical-to-electrical (O/E) conversion.

7.3 POWER-RELATED IMPAIRMENTS MONITORING

7.3.1 Fiber Attenuation and Optical Power Loss

The most basic characteristic of a link is the power loss that is caused by fiber attenuation and connections [17]. Attenuation, defined as the ratio of the input power to the output power, is the loss of optical power as light travels along the fiber. Attenuation in an optical fiber is caused by absorption, scattering, and bending losses. The fundamental physical limits imposed on the fiber attenuation are due to scattering off the silica atoms at shorter wavelengths and the material absorption at longer wavelengths. There are two minima in the loss curve, one near 1.3 μm and an even lower one near 1.55 μm. Fiber bending can also induce power loss because radiation escapes through its bends. The bending loss is inversely proportional to the bend radius and is wavelength dependent.

Power loss is also present at fiber connections, such as connectors, splices, and couplers. Coupling of light into and out of a small-core fiber is much more difficult to achieve than coupling electrical signals in copper wires since: (i) photons are weakly confined to the waveguide whereas electrons are tightly bound to the wire, and (ii) the core of a fiber is typically much smaller than the core of an electrical wire. First, light must be coupled into the fiber from a diverging laser beam, and two fibers must be connected to each other. Second, connecting two different fibers in a system must be performed with great care due to the small size of the cores. One wishes to achieve connections exhibiting: (i) low loss, (ii) low back reflection, (iii) repeatability, and (iv) reliability. Two popular methods of connectorizing fibers are the permanent splice and the mechanical connector. The permanent "fusion" splice can be accomplished by placing two fiber ends near each other, generating a high-voltage electric arc which melts the fiber ends, and "fusing" the fibers together. Losses and back reflections tend to be extremely low, being <0.1 dB and <-60 dB, respectively. Disadvantages of these fusion splices include (i) the splice is delicate and must be protected, and (ii) the splice is permanent. Alternatively, there are several types of mechanical connectors, such as ST and FC/PC. Losses and back reflection are still fairly good, and are typically <0.3 dB and <-45 dB, respectively.

Low loss is extremely important since a light pulse must contain a certain minimum amount of power to unambiguously detect a "0" or "1" data bit. Therefore, an optical power measurement (or fiber link loss measurement) is the most basic testing in any optical fiber network. Note that optical return loss (ORL) characterization is related to optical power measurement, and is required for many digital and analog fiber systems, such as passive optical networks (PONs). ORL along a fiber span is a combination of Rayleigh scattering and Fresnel reflections, and can reduce fiber system performance and increase BER by degrading transmitter stability.

7.3.2 Wavelength/Frequency Drift

Another potential source of attenuation and penalty in spectrally efficiency WDM systems is the wavelength drift that results in a relative offset between the center frequencies of the laser and any in-line filter. The frequency drift and the resulting misalignment of lasers and filters in the network cause significant optical power loss and crosstalk between channels, as shown in Figure 7.10. More importantly, frequency drift induced power loss/penalty is time varying and dynamically fluctuating due to environmental changing and component aging that cause the center frequency of optical components (e.g., filters, MUX, DEMUX, and lasers) to drift in wavelength. Note that relative frequency drift between optical carriers and filters will also induce chirp, which will interact with fiber CD.

To pack more channels within the given fiber bandwidth, one obvious solution is using closer channel spacing in DWDM systems. For example, the channel spacing has been decreased from 100 s of GHz to 10 s of GHz over the last decade (from 1990s to present) to support ultra-high-capacity transmission. As the spectral range between optical channels decreases, the requirements for frequency/wavelength drift of optical components increases. This trend requires more sophisticated monitoring of optical power and related control techniques.

Note that incorporation of forward error correction (FEC) would increase the signal bandwidth and hence impose even tighter tolerances on wavelength/frequency stability and accuracy.

7.3.3 Amplifier Noise, Distortion, and Power Transients

The optical amplifier is ideally a transparent module that provides gain to overcome any losses within a fiber link (fiber loss, connector loss, etc.). Beyond gain, it

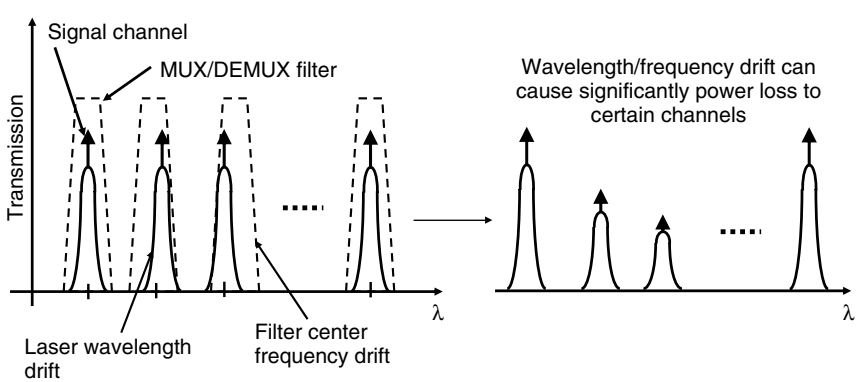

Figure 7.10 Uniform input channels to a MUX/DEMUX may result in unequal output power due to wavelength/frequency drift of lasers or filters. This problem becomes more serious as channel spacing decreases and spectral efficiency increases in DWDM systems.

is of paramount importance to understand the effects of amplifier noise on the optical communication systems. The noise in an amplifier is inherently due to the random incoherent spontaneous emission events of excited carriers. The spontaneously emitted light that gets coupled into the beam propagation path is subsequently amplified and in total is called the ASE. This ASE is quite broadband, occurring over the entire gain bandwidth. In the optically amplified systems, the main source of SNR degradation is the accumulated ASE of many cascaded optical amplifiers. If the losses were too large in a fiber link, then optical amplification would be required somewhere in the system. In addition to the optical power budget, the system must exceed the minimum required OSNR. The OSNR is a critical system design parameter for optically amplified systems, and is defined as the ratio of signal power to ASE power in a fixed bandwidth (optically and electrically). It directly affects the ultimate system performance that is quantitatively measured by the BER or Q-factor.

In addition to added ASE noise, an optical amplifier may induce other degradations to the channels. One notable degradation example involves channel power transients in reconfigurable WDM networks. When channels are added or dropped from a partially saturated EDFA, the power of the remaining channels will increase on a rapid time scale, resulting in gain and power transient effects. The EDFAs could be critically affected by the adding/dropping of WDM channels, network reconfiguration, or link failures. The transients can be very fast in EDFA cascades. These fast power transients in chain-amplifier systems should be controlled dynamically, and the response time required scales with the size of the network. To maintain the QoS, the surviving channels must be protected when channel add/drop or network reconfiguration occurs to avoid fiber nonlinearity induced by too much channel power and small SNR induced by too little remaining power. Another example is the intermodulation distortion and saturation-induced crosstalk that occurs in a semiconductor optical amplifier (SOA). These two effects are both nonlinear, and these are manifested more prominently from SOAs as opposed to EDFAs due to the vastly different carrier lifetimes. These effects have been troublesome in WDM multichannel systems.

7.3.4 Power/Wavelength Monitoring Techniques

Optical power at a given wavelength is the most basic parameter in any fiber network. Other parameter or impairment monitoring will depend upon the optical power measurement. Therefore, power monitoring is the basic requirement for any optical network. We actually can categorize the power and wavelength monitoring to optical channel monitoring that is becoming more common in WDM systems and may be well adapted to standardization. Frequently suggested OPM parameters include optical power, wavelength and wavelength range/spacing, and OSNR [15, 18] in optical layer. In a point-to-point WDM system, power/wavelength monitoring is fairly straightforward. For example, one optical performance

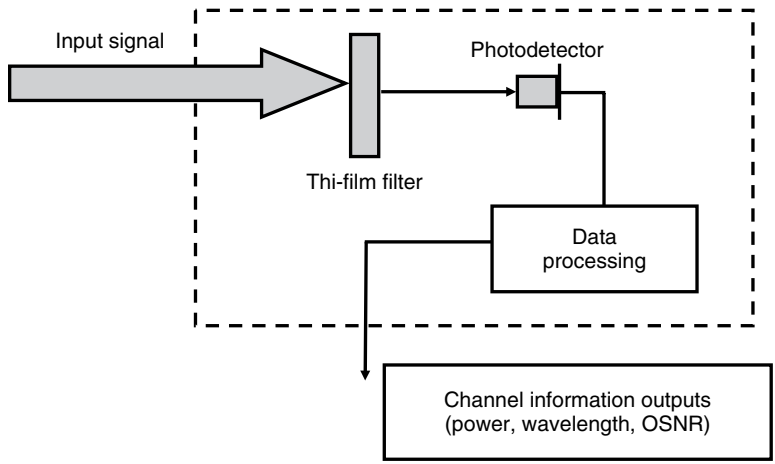

Figure 7.11 The scheme of Optoplex's optical channel monitor [18].

monitor uses proprietary thin-film filter (TFF) technology combined with a micro-actuator and high-speed electronics [18]. Figure 7.11 shows the scheme of the monitor. It is used to measure critical information data on optical transmission signals in DWDM networks for monitoring signal dynamics, determining system functionality, identifying performance change, and providing feedback for controlling network elements so as to optimize operational performance. It can also automatically scan the C-, L-, and/or C + L-band wavelength range and precisely measure channel wavelength, power, and OSNR.

Operating through a continuous wavelength scan and built-in wavelength reference with optical-tunable filter technology, the optical channel monitor (OCM) produced by Optolex has a high wavelength accuracy and resolution with a low channel crosstalk. Built with Optoplex's high-isolation and wide passband thin-film filter and assembled together with a high-grade single detector, Optoplex's OCM increases channel power measurement accuracy and dynamic range. Using an innovative optical design and high-grade single-element InGaAs detector, channel OSNR measurement range is increased to >30 dB. Other commercially available OCMs also have similar performance, such as volume phase gratings [19, 20], microelectro mechanical systems (MEMS)-tunable filter [21], and OCM based on fiber gratings [22].

Channel power monitoring is a challenge for a PON due to the nature of its point-to-multipoint and bidirectional structure. To meet the challenge of remote monitoring and diagnosis in a PON, the monitoring tool generally should be based on reflectometry that can send a signal out while detecting its reflected echoes, such as an optical time-domain reflectometer (OTDR). The use of an OTDR for detecting and locating degradations is more valuable on live fibers than on dark ones because one can measure, pinpoint, and eventually correlate problems raised

by other systems dedicated to measuring signal quality such as BER, *Q*-factor, or other more sophisticated parameters.

Recently, one demonstration shows the detection and localization of the fiber failures in WDM-PON by monitoring the status of the upstream signals [23]. Figure 7.12 shows the proposed experimental setup. When a failure occurred in the feeder fiber, the optical powers of every upstream channel were reduced. In this case, the control unit randomly selected one of the downstream light sources and used it to transmit OTDR pulses instead of data for the localization of fiber fault. When the failures occurred in several drop fibers simultaneously, the control unit identified the failed channels and then analyzed the locations of fiber failures channel by channel according to the predetermined priorities. Figure 7.13 shows the measured dynamic range of the proposed technique using various light sources and the output of the downstream light source when the fiber failure occurs. The advantage of this technique is the failures in drop fibers and the feeder fiber can be located without using the wavelength-tunable OTDR. Since this technique reuses the downstream light source of the failed channel to transmit the OTDR pulse, it does not require additional light sources for the localization of fiber failure. Moreover, the proposed approach can detect and localize the fiber failure of the failed channel without affecting the operation of other channels.

Since a PON using optical power splitter mixes many almost identical paths together, OTDR analysis can sometimes be erroneous. To differentiate among 32 or more optical paths, an optical wavelength domain reflectometry (OWDR) method has been recently proposed [24]. The idea is to embed a permanent passive component at each optical network terminal (ONT). The embedded component was called a wavelength coded tag (WCT) that has the following features: (1) having unique

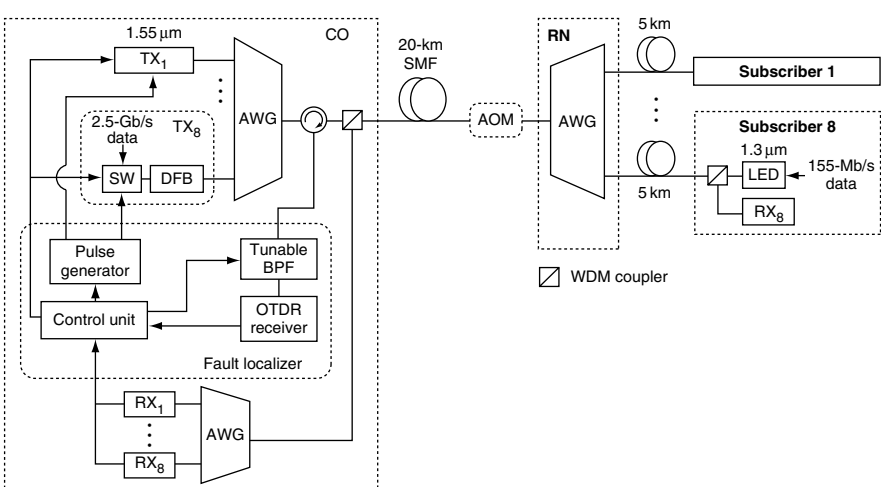

Figure 7.12 Example on the detection and localization of fiber failures in a bidirectional WDM PON. (After Ref. [23]. © 2005 IEEE.)

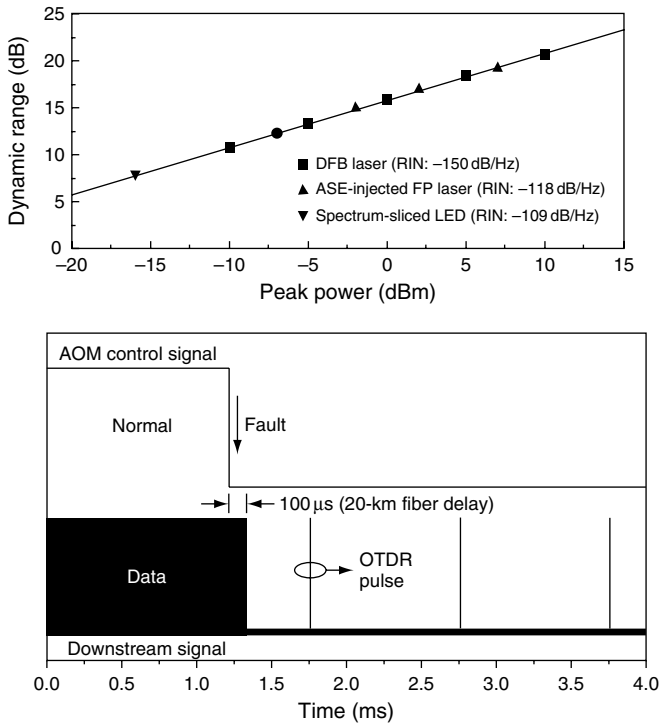

Figure 7.13 Measured dynamic range of the proposed technique using various light sources (upper). Measured output of the downstream light source when the fiber failure occurs (below). (After Ref. [23]. © 2005 IEEE.)

wavelength characteristics that can be distinguished by a spectrum analysis remotely, (2) transparent to the entire signal traffics that share the network, (3) wavelength and optical-loss stable over a severe environmental condition, and (4) low-cost structure and manufacturing process to justify the fiber to the home (FTTH) vast deployment.

Figure 7.14 depicts a schematic diagram of an OWDR-embedded FTTH optical network from optical line terminal (OLT) to ONT. As an example to illustrate functionality, a 1575- to 1600-nm band could be used for the fiber diagnostic band. Each end user is assigned a unique wavelength code through a WDM tag or WCT inside the OLT. One can even embed additional WCT's into different sections of the network, given that each embedded WCT has a unique wavelength code. To make the OWDR work, an additional filter wavelength division multiplexer (FWDM) device, a single TFF-based band separator, which is shown in Figure 7.15, is inserted to serve as a MUX for the downstream to combine monitoring band with FTTH bands, and as a DeMUX for upstream signals. The monitoring band can be fed from a tunable laser or a SLED-based broadband light source covering wavelength from 1260 to 1600 nm. Each WCT can retro-reflect a unique narrowband WDM signal within the monitoring band of 1575 1600 nm. All other wavelengths

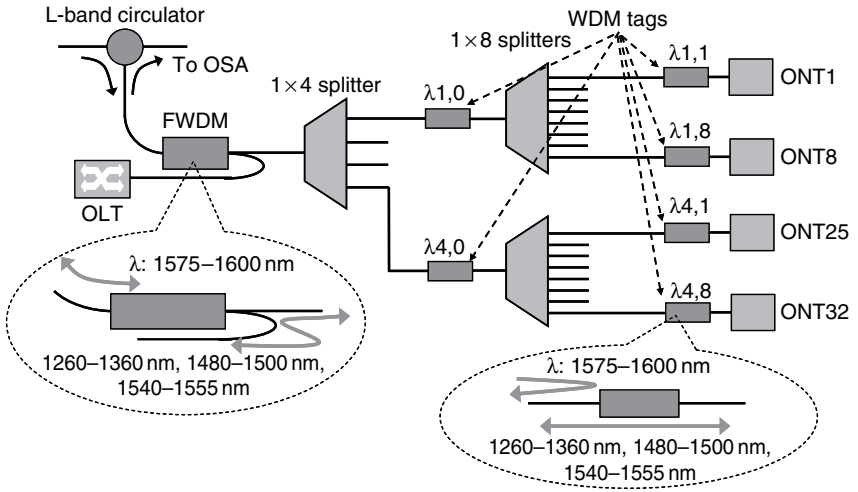

Figure 7.14 Schematic of an OWDR embedded FTTH network from OLT to ONT. (After Ref. [24]. © 2006 IEEE/OSA.)

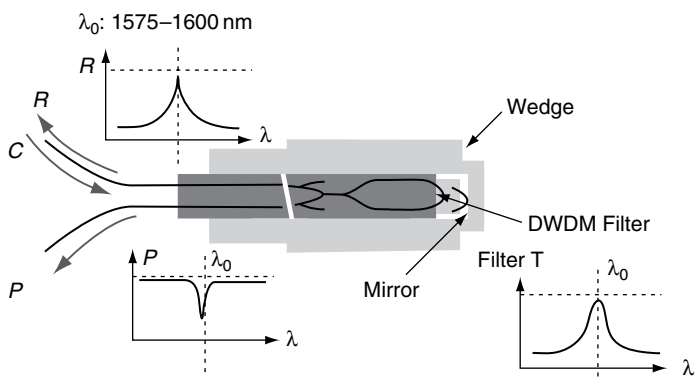

Figure 7.15 A TFF based WCT using double transmission of the TFF filter followed by a mirror reflector aligning to reflect signal back to the input port. (After Ref. [24]. © 2006 IEEE/OSA.)

should pass this WCT with minimum power loss. Thus, any fiber cut can be remotely detected through sending a probe signal while analyzing its echoes generated from all the WCT's. Any missing WCT wavelength tags indicates something happened to that section of fibers, and an additional OTDR can pinpoint the exact location of the fiber fault.

In WDM networks, channel power needs to be equalized dynamically to ensure stable system performance. To obtain feedback for control purposes, a channel power monitoring scheme is very important. A simple way to accomplish this is to demultiplex all the channels and detect the power in each channel using different

photodetectors or detector arrays. To avoid the high cost of many discrete components in WDM systems with large numbers of channels, other monitoring techniques that take advantage of wavelength-to-time mapping have also been proposed including the use of concatenated fiber Bragg gratings or swept acousto-optic tunable filters.

To maintain the QoS, the surviving channels must be protected when channel add/drop or network reconfiguration occurs. The techniques include (a) optical attenuation, by adjusting optical attenuators between the gain stages in the amplifier to control the amplifier gain, (b) pump power control, by adjusting the drive current of the pump lasers to control the amplifier gain [25], (c) link control, using a power-variable control channel propagating with the signal channels to balance the amplifier gain [26], and (d) EDFA gain clamping, by an automatic optical feedback control scheme to achieve all-optical gain clamping [27].

Various techniques have been proposed for dynamic channel power equalization, including parallel loss elements [28], individual bulk devices (e.g., acousto-optic tunable filters) [29], serial filters [30], micro-opto-mechanics (MEMS) [31], and integrated devices [32].Using the power monitoring and feedback control, an automatic channel-by-channel equalizer based on the silica planar lightwave circuits equalized 40 laser peaks with an initial deviation of up to 9 dB [33, 34].

7.3.5 OSNR Monitoring Techniques

A common technology for channel OSNR monitoring is the optical spectrum analyzer method based on analyzing the optical spectrum of the detected signal [18]. The wavelength-tunable devices for channel OSNR monitoring are fiber Fabry Perot filters, fiber Bragg grating filters, free space and MEMS diffractive optics, and dielectric thin-film filters. Several techniques have been developed that do not directly measure the optical spectrum or focus on wavelength monitoring [35 38]. Modulation tone techniques have also been used as a low-cost alternative to spectral measurements. In principle, the techniques that measure signal power can also be used to obtain the optical noise power, which is extrapolated from the power level adjacent to the channel. This approach works well if the optical noise can in fact be obtained from the power level adjacent to the channel. This condition is not true for many important types of optical noise including multipath interference effects, amplifier pump laser RIN transfer noise, and FWM.

Conventional OSNR measurements use out-of-band techniques, i.e., the noise measured in the spectrum located midway between the optical channels. However, this method may misestimate noise and affect by channel crosstalk, filters, or MUX/DEMUX along the optical path. For example, measuring noise in a spectral region that does not overlap with the channel becomes increasingly complicated as DWDM channels are more tightly spaced. Precise measurements on grid spacing of $\leq$50 GHz are quite challenging. Another challenge arises when channels pass through a different number of amplifier nodes in long-haul network with optical add/drop multiplexers (OADMs). In this scenario, even adjacent channels may

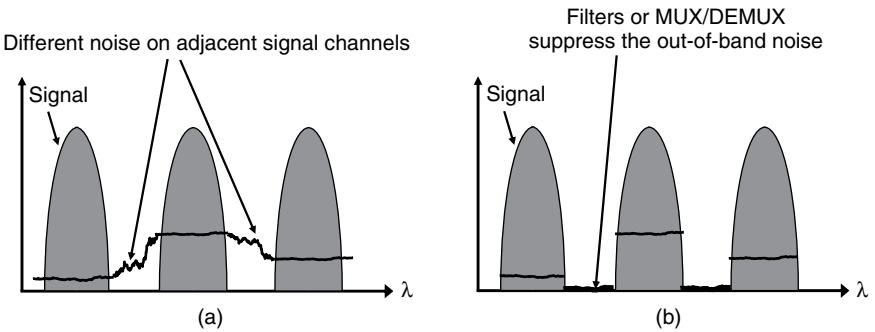

Figure 7.16 (a) Undermined noise level: different noise on adjacent signal channels; (b) "missing" noise between channels: optical filters or MUX/DEMUX may remove the out of band noise.

experience a significantly different noise level as shown in Figure 7.16(a). Moreover, when channels pass through filters or MUX/DEMUX that suppress the spectral regions beside channels, very low noise may be measured out-of-band (between channels) regardless of the true OSNR level, as shown in Figure 7.16(b) [39].

Polarization nulling method may overcome this limitation [40, 41]. In principle, an optical signal will have a well-defined polarization, whereas optical noise will be unpolarized, as shown in Figure 7.17. Therefore, the polarization extinction ratio is a measure of the optical SNR. In this technique, the received signal (together with noise) is split into two orthogonal polarization components in which one component consists of signal and polarized noise, while the other has

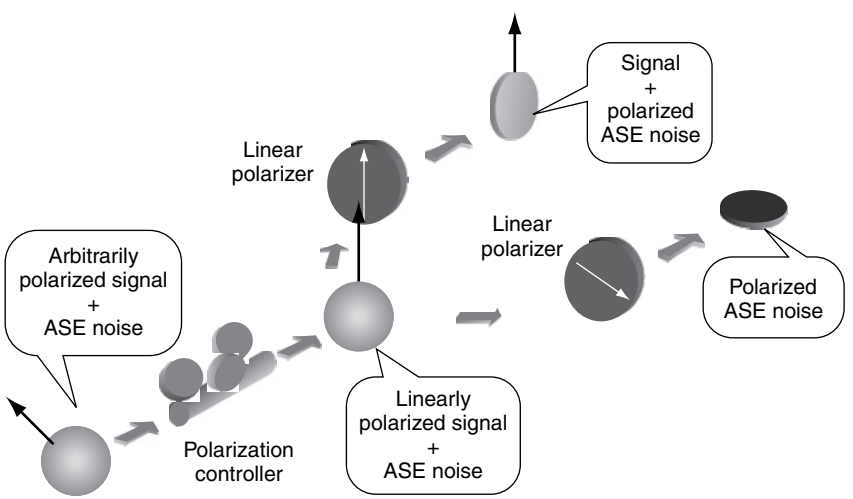

Figure 7.17 Operating principle of the polarization technique: the polarized noise (i.e., half of the total noises) can be measured by using the second linear polarizer, which is aligned to be orthogonal from the signal's polarization. (After Ref. [42]. © 2006 IEEE/OSA.)

polarized noise only (assuming that the signal is highly polarized, and the noise is completely unpolarized). Thus, it is possible to measure the signal and noise powers right at the signal's wavelength since the powers of the polarized noises measured in these polarization components should be the same (i.e., one half of total noise power) [42]. The performance of this technique could be affected by various polarization effects in the transmission link. For example, the accuracy of this technique could be degraded significantly if the signal is depolarized by PMD and nonlinear birefringence, and/or the ASE noise is partially polarized due to polarization-dependent loss (PDL).

Figure 7.18 shows the measured OSNR by using the polarization nulling technique. The monitoring error was maintained to be less than 0.6 dB for the 2.5-Gb/s 640-km single-mode fiber (SMF) link. The maximum errors were increased up to about 4 and 6 dB for a nonzero dispersion-shifted fiber (NZDSF) link or an SMF plus dispersion compensation fiber (DCF) link, respectively. When the bit rate was increased to 10 Gb/s, the maximum errors were decreased to 1.2 and 3.7 dB for the 640-km-long NZDSF link and SMF + DCF link, respectively, as shown in Figure 7.18(b). The errors could be attributed to PMD and nonlinear birefringence. The polarization nulling technique could overestimate the ASE noise power due to the depolarized signal component and become erroneous.

Another method for in-channel OSNR monitoring is to use the amplitude power spectrum of the data and monitor at spectral locations at which the signal is not present. This can involve monitoring at low frequencies, high frequencies, or at special null locations within the spectrum [43]. Optical subcarrier monitoring has been used to directly measure the OSNR and correlate the optical measured value to the electrical SNR seen by the receiver [44]. This method has an advantage in

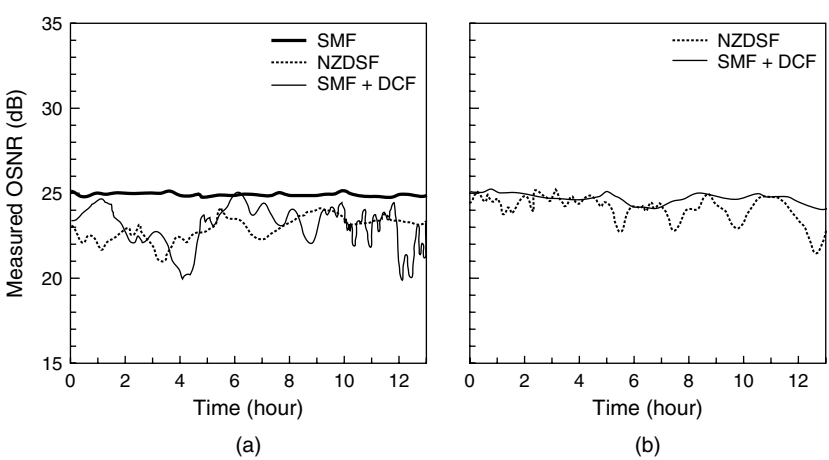

Figure 7.18 Measured OSNR in various types of fiber links: (a) 2.5 Gb/s and (b) 10 Gb/s. (After Ref. [42]. © 2006 IEEE/OSA.)

that it involves monitoring on the actual data signal as it has propagated along the impairment path of the signal itself.

In fact, the pilot-tone-based monitoring technique can monitor many other physical parameters cost-effectively in the optical domain. This technique typically utilizes a small amplitude-modulated pilot tone dedicated to each WDM channel, as shown in Figure 7.19. Because the tone is at a single, low frequency, it is easy to generate and process using conventional electronics. In addition, it can monitor the optical parameters without using the expensive demultiplexing filters such as tunable optical filter and diffraction grating. A common RF tone monitoring method is to assign each WDM channel to a different RF frequency tone. The average power in these tones will be proportional to the average optical power in the channel. Thus, the aggregate WDM optical signal on the line can be detected and the tones of all the channels will appear in the RF power spectrum in much the same way they would appear in the optical spectrum [45 49]. Moreover, the monitoring of RF tones can be used for measuring the accumulation of CD and PMD on a digital signal [50 54]. The RF spectral techniques have the advantage that they can be implemented with narrowband electronics. Even though high frequencies might be used, the narrow bandwidths will reduce the cost of the electronics. Furthermore, if the detection bandwidth can be narrowed as well, then the sensitivity can be increased. It is worth to mention that one of the major drawbacks of this technique is that the AM tone and data could interfere with each other and cause deleterious effects. Thus, the amplitude of the pilot tone should be large enough to discern the tone signals from the noise-like random data, but small enough not to induce a significant degradation in the receiver sensitivity for data.

For non-return-to-zero on-off keying (NRZ-OOK) systems, a simple OSNR monitoring technique has been demonstrated by using a one-bit delay Mach Zehnder interferometer (MZI) [55]. A step forward was the demonstration of a monitoring solution with a ¼-bit delay MZI for different modulation formats including OOK, differential-phase-shifted-keying (DPSK) and duobinary [56]. In the ¼-bit delay method, one output port gives constructive (P_{const}) while the other port provides destructive interference (P_{dest}). The constant phase relationship in a single bit translates MZI into constant constructive interference over

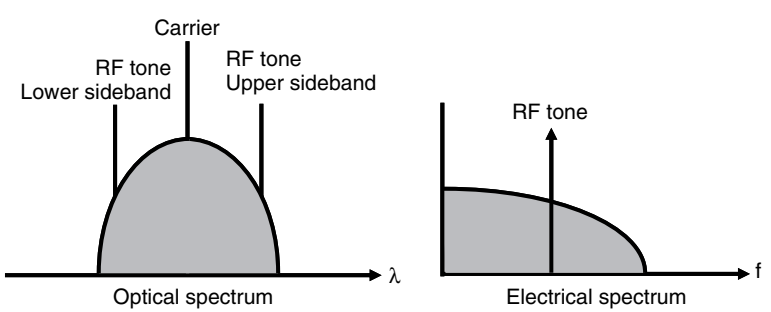

Figure 7.19 RF pilot tone added to the channel bandwidth as the signal quality/degradation monitor.

¾ of the bit period at the output of a ¼-bit delay. With increasing ASE power (i.e., decreasing ONSR) P_{dest} increases faster than P_{const} because of the random phase of the noise. The OSNR is proportional to the ratio P_{const}/P_{dest}. Since the phase relationship between successive bits is not important, the method is applicable to multiple modulation formats. This principle can also be explained in the spectral domain as illustrated in Figure 7.20. Since a ¼-bit delay MZI has a free spectral range (FSR) equal to four times the bit rate, most of the signal power goes to the constructive port. The noise then evenly distributes between the two ports. Figure 7.21 shows the measurement results. The interferometer-assisted clock tone monitoring using the same device [57] was shown to provide measurements of CD and PMD but the method is ONSR sensitive. With the OSNR values known, the CD and PMD measurement can be normalized in postprocessing by multiplying by a fit factor.

Uncorrelated beat noise can also be used for OSNR monitoring [58]. Figure 7.22 shows the principle and the experimental setup of the OSNR monitoring method. Within the OSNR monitoring module, the modulated signal with ASE noise is split into two branches by a 50:50 coupler. Subsequently, the two parts pass through the tunable optical bandpass filters (BPF 1 and BPF 2), which have identical optical bandwidths but different center frequencies. BPF 1 and BPF 2 select the channel of interest and obtain the optical signal and ASE noise for OSNR monitoring. Following BPF 1 and BPF 2 are a variable optical attenuator

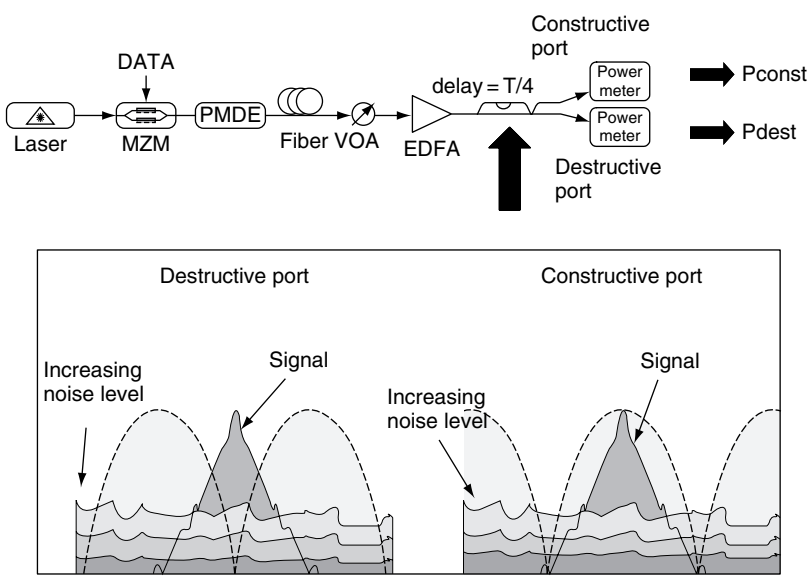

Figure 7.20 Concept of ¼ bit delay in the spectral domain. Most of the signal is notched out in the destructive port. The power ratio between the two arms is directly related to the OSNR. (After Ref. [56]. © 2007 IEEE/OSA.)

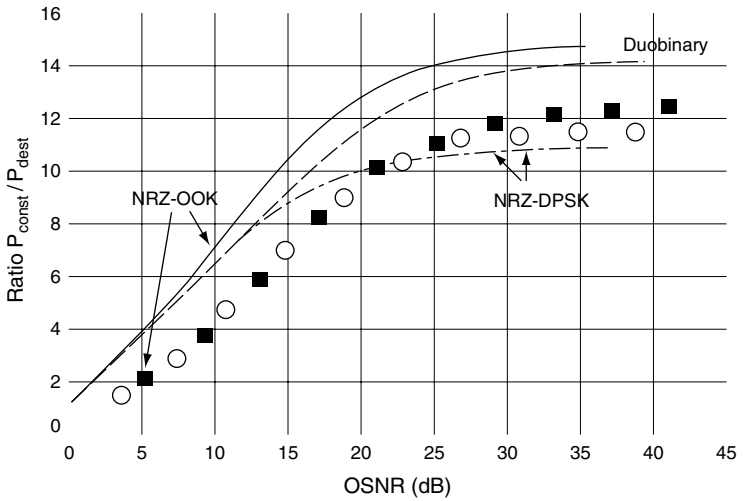

Figure 7.21 Simulated (lines) and measured (symbols) P_{const}/P_{dest} vs OSNR for 10 Gbit/s NRZ OOK, NRZ DPSK, and duobinary. (After Ref. [56]. © 2007 IEEE/OSA.)

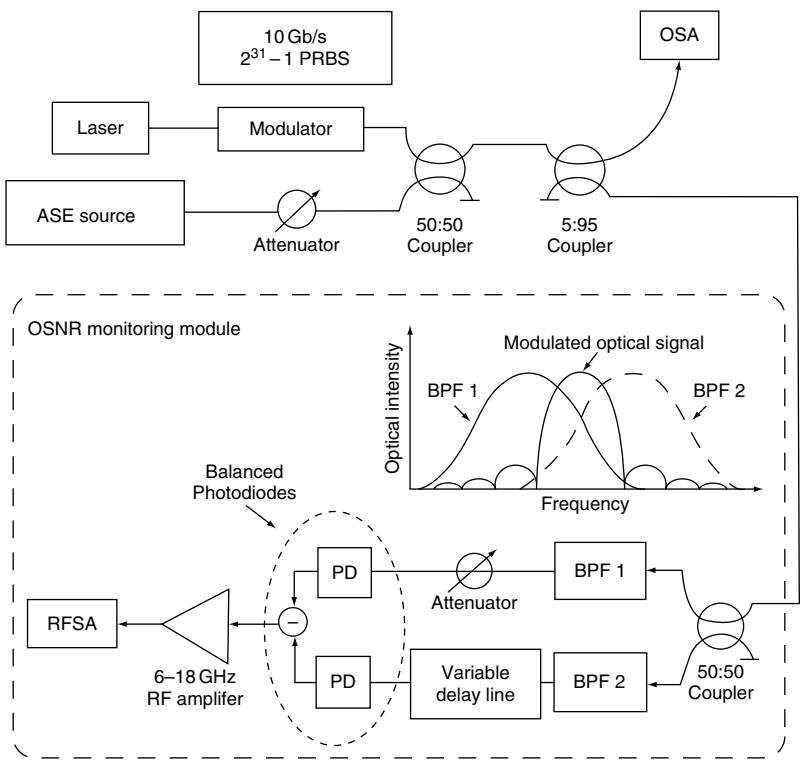

Figure 7.22 Experimental setup and principle of OSNR monitoring based on uncorrelated beat noise. (After Ref. [58]. © 2005 IEEE.)

and a variable optical delay line used to match the power and the delay of the two paths, respectively. The outputs of the two paths are sent to a pair of balanced photodiodes, in which detection and RF subtraction are performed. An RF amplifier and RF spectrum analyzer are used to measure the uncorrelated beat noise. The signal of each path is correlated while the ASE noise in different frequency bandwidths is uncorrelated, as the ASE noise can be modeled as additive white Gaussian noise. Subsequently, beating between signal and the ASE noise within different bandwidths is uncorrelated. The optical signals pass through these two identical filters with passbands that symmetrically cover different halves of the optical data spectrum. Where the filters overlap, the ASE noise is correlated; while in the other parts, the ASE noise is uncorrelated. Therefore, after balanced RF subtraction, the uncorrelated beat noise can be measured in the RF domain and OSNR can be extracted. The method is compatible with different modulation formats, independent of the pattern length and insensitive to PMD.

Figure 7.23 shows the experiment results for a 10-Gbit/s system. In the OSNR range from 10 to 30 dB, this OSNR monitoring scheme produces errors of less than 0.5 dB.

Recently, an interesting OSNR monitoring technique based on orthogonal-polarization heterodyne mixing of two spectral components of the signal was demonstrated [59], which is insensitive to polarization-mode dispersion but also robust to nonlinear polarization scattering. And a narrow-band off-center optical

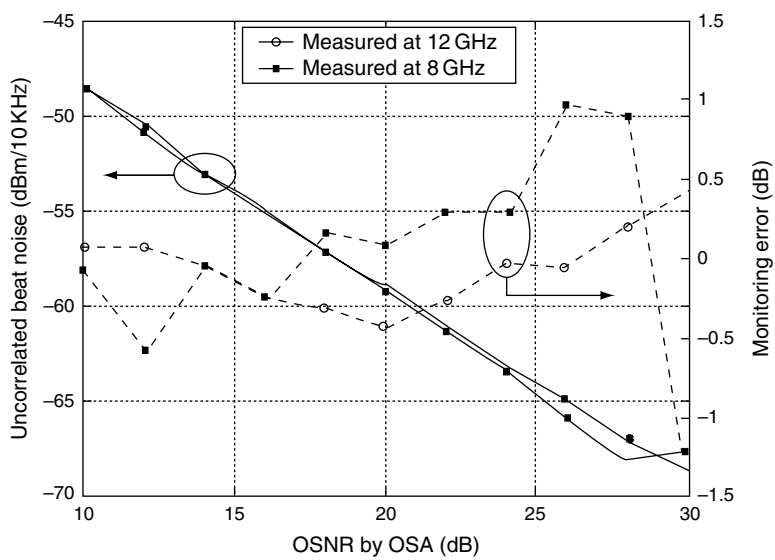

Figure 7.23 Measured uncorrelated beat noise power density and the monitoring error vs the OSNR measured by the OSA. (After Ref. [58]. © 2005 IEEE.)

filtering technique was used to enhance the monitoring sensitivity of degree-of-polarization-based OSNR monitors [60]. Fiber nonlinear effects such as FWM and optical parametric amplification (OPA) have also been employed to monitor OSNR [61 64]. The techniques based on fiber nonlinearities are all-optical and fast, though they generally require high power light or special fiber as nonlinear medium.

Electronic techniques such as histogram analysis are also powerful tools for OSNR monitoring, which will be discussed in more details in Section 7.6.

Note that OSNR monitoring is an excellent measure of optical amplifier performance and is frequently used for troubleshooting optical power induced or amplifier induced network faults.

7.4 DISPERSIVE IMPAIRMENTS MONITORING

7.4.1 Chromatic Dispersion

In any medium other than vacuum and in any waveguide structure (other than ideal infinite free space), different electromagnetic frequencies travel at different speeds. This is the essence of CD. The velocity in fiber of a single monochromatic wavelength is constant. However, data modulation causes a broadening of the spectrum of even the most monochromatic laser pulse. Thus, all modulated data has a nonzero spectral width that spans several wavelengths, and the different spectral components of the modulated data travel at different speeds. In particular, for digital data intensity modulated on an optical carrier, CD leads to pulse broadening which limits the maximum data rate that can be transmitted through optical fiber. The units of CD are (ps/nm)/km; thus, shorter time pulses, wider frequency spread due to data modulation, and longer fiber lengths will each contribute to temporal dispersion.

The data rate and the data modulation format can significantly affect the sensitivity of a system to CD. For a given system, a pulse will disperse more in time for a wider frequency distribution of the light and for a longer length of fiber. Higher data rates inherently have both shorter pulses and wider frequency spreads. Therefore, as network speed increases, the impact of CD rises precipitously as the square of the increase in data rate. The quadratic increase with the data rate is a result of two effects, each with a linear contribution. Firstly, a doubling of the data rate makes the spectrum twice as wide, doubling the effect of dispersion. Secondly, the same doubling of the data rate makes the data pulses only half as long, thus making it twice as sensitive to dispersion. The combination of a wider signal spectrum and a shorter pulse width is what leads to the overall quadratic impact when the bit rate increases by a factor of 4, the effects of CD increase by a factor of 16 [50].

A rule for the maximum distance over which data can be transmitted is to consider a broadening of the pulse equal to the bit period. For a bit period B, a

dispersion value D and a spectral width $\Delta\lambda$, the dispersion-limited distance is given by

$$L_D = \frac{1}{D \cdot B \cdot \Delta\lambda} = \frac{1}{D \cdot B \cdot (cB)} \propto \frac{1}{B^2} \tag{7.1}$$

For example, for single mode fiber, $D = 17$ ps/nm/km, so for 10 Gbit/s data the distance is $L_D = 52$ km. In fact, a more exact calculation shows that for 60 km, the dispersion induced power penalty is less than 1 dB [65]. The power penalty for uncompensated dispersion rises exponentially with transmission distance. 40-Gbit/s signals are 16 times more sensitive to CD than 10-Gbit/s signals. Therefore, CD is one of the main impairments that limit the performance of optical fiber systems. For robust high-bit-rate systems, it is essential that dispersion be compensated to within tight tolerances. Static and fixed dispersion compensation is inadequate when system conditions can change in the following scenarios: (i) reconfigurable optical networks for which a given channel's accumulated dispersion will change when the network routing path is reconfigured, and (ii) $\geq$40-Gbit/s long-distance links for which CD and signal degradation may change substantially due to normal changes in temperature, as shown in Figure 7.24. In almost all 40-Gbit/s systems, highly accurate dispersion management must be implemented, potentially requiring tunable dispersion compensators that are accompanied by dynamic monitoring of the accumulated CD.

7.4.2 Polarization Mode Dispersion

SMFs actually support two perpendicular polarizations of the original transmitted signal (fundamental mode). In an ideal fiber (perfect), these two modes are

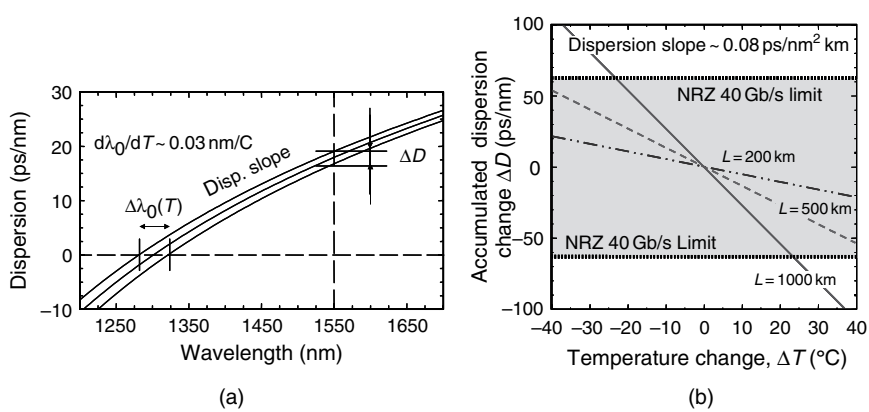

Figure 7.24 (a) The zero dispersion wavelength shifts due to temperature change, thus dispersion itself changes at a fixed wavelength. (b) For a 40 Gb/s, 1000 km fiber link, 30°C temperature change causes the dispersion beyond the system limit.

indistinguishable, and have the same propagation constants owing to the cylindrical symmetry of the waveguide. However, the core of an optical fiber may not be perfectly circular, and the resultant ellipse has two orthogonal axes. The index-of-refraction of a waveguide, which determines the speed of light, depends on the shape of the waveguide as well as the glass material itself. Therefore, light splits on two orthogonal states of polarization (i.e., PSPs), and the component of the light polarized along one PSP travels at a different speed than does the component polarized along the orthogonal PSP, which is termed as PMD. Fiber asymmetry may be inherent in the fiber from the manufacturing process, or it may be a result of mechanical stress on the deployed fiber. The inherent asymmetries of the fiber are fairly constant over time, while the mechanical stress due to movement of the fiber can vary, resulting in a dynamic aspect to PMD. Since the light in the two orthogonal axes travel with different group velocities, to first order, this differential light speed will cause a temporal spreading of signals, which is termed the differential group delay (DGD).

Because of random variations in the perturbations along a fiber span, PMD in long fiber spans accumulates in a random walk-like process that leads to a square root of transmission length dependence [66]. Moreover, PMD does not have a single value for a given span of fiber. Rather, it is described in terms of average DGD, and a fiber has a distribution of DGD values over time. The probability of the DGD of a fiber section being a certain value at any particular time follows a Maxwellian distribution (see Figure 7.25). The probability of DGD $= \Delta\tau$ is given by

$$\text{prob}(\Delta\tau) = \sqrt{\frac{2}{\pi}}\frac{\Delta\tau^2}{\alpha^3}\exp\left(-\frac{\Delta\tau^2}{2\alpha^2}\right) \tag{7.2}$$

with mean value $<\Delta\tau> = \sqrt{8/\pi}\alpha$. PMD is usually expressed in ps/km$^{1/2}$ in long fiber spans, and the typical PMD parameter (D_p) is 0.1 to 10 ps/km$^{1/2}$ [67, 68].

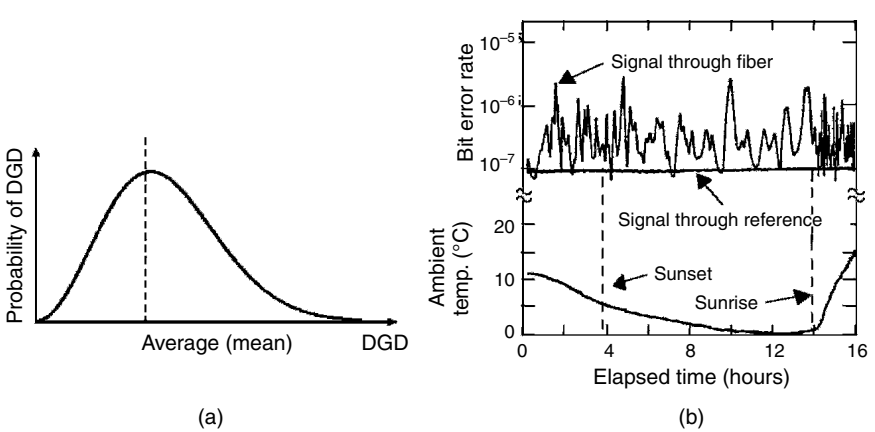

Figure 7.25 (a) Probability distribution of DGD in a typical fiber. (b) System performance (BER) fluctuations due to changes in temperature caused by PMD. (After Ref. [69]. © 1991 IEEE.)

As shown in Figure 7.25, PMD, by its nature, is a stochastic, dynamically varying process [69]; the compensation of the channel degradation induced by PMD must be dynamic and thus requires constant monitoring.

PDL, expressed as the ratio of the maximum to minimum transmission on a log scale as the launch polarization is rotated through all possible states, has been recognized as another critical polarization-related impairment. Due to non-negligible PDL in various in-line optical components, such as switches, isolators, couplers, filters, and circulators, when the optical pulse passes through these optical components, it splits between two orthogonal polarization modes that attenuate each optical pulse replica differently. PDL can cause deleterious effects in a fiber transmission link, such as optical power fluctuations resulting in random OSNR variations due to polarization state wandering during propagation, and limited PMD compensator performance.

Another polarization effect, polarization-dependent gain (PDG), is due to anisotropic gain saturation in fiber amplifiers and appears in amplified fiber links. The source of PDG in EDFAs has been identified as polarization hole burning (PHB): signals with orthogonal states of polarization can utilize different subsets of gain producing ions [70]. PDG can randomly degrade the OSNR, inducing significant fluctuations in the BER over time. Although the PDG from a single amplifier is quite small and negligible, the PDG effects from cascaded amplifiers in the overall optical link can result in a several-dB fluctuation in the received Q-factor.

Note that the interaction between PMD and PDL/PDG may lead to significant overall performance degradation, which dramatically surpasses the result of adding the degradations induced by the two impairments independently [71 75]. When PDL exists in a fiber link also impaired by PMD, the PSPs of the fiber are no longer orthogonal to each other; the probability distribution of the DGD degenerates from its Maxwellian shape; and the PDL seen by the WDM channels may become uncorrelated.

7.4.3 Chromatic Dispersion Monitoring Techniques

Measurement of RF Tone

Several techniques have been demonstrated for real-time CD monitoring to enable dynamic dispersion compensation and may be applied more generally as OPM techniques. One method is to detect the conversion of a phase-modulated signal into an amplitude-modulated signal due to CD [76]. A second method is inserting a subcarrier (RF tone) at the transmitter. The subcarrier approach measures the resulting delay of the subcarrier sidebands relative to the baseband and can be used to measure the accumulated dispersion with fine and medium accuracy without knowledge of the signal transport history [44, 46, 51, 77 82]. These two methods are simple and applicable to WDM systems, but require modification of

the transmitter. Based on the dispersion-induced RF power fading effect, an alterative technique is to extract the bit-rate frequency component (clock) from photodetected data and monitor its RF power [83, 84]. This technique does not require modification of the transmitter, but is bit rate and modulation format dependent. Although this approach cannot isolate CD, like other tone-fading techniques it is sensitive to a variety of distortion effects including PMD and pulse carver misalignment, which is advantageous for fault localization.

The CD monitoring techniques based on RF tone measurement are relatively simple but PMD and the chirp of the external modulator may influence the CD monitoring. It is well known that when an RF modulated light travels along an optical path, both CD and PMD will result in the RF power fading at the photodetector. As shown in Figure 7.26, CD causes a phase difference between the two sidebands, and PMD induces the DGD between the two PSPs. Both of these two effects will introduce RF power fading in electrical domain after photodetection.

Considering the phase difference between the two RF sidebands and the PMD and chirp effects, the detected RF power with double sideband (DSB) at the photodetector is given by [85 87]:

$$P_{\mathrm{DSB}} = P_0[1 - 4\gamma(1-\gamma)\sin^2(\pi f_{\mathrm{RF}}\Delta\tau)] \times (1+\alpha^2)\cos^2(\pi D_{\mathrm{total}}\lambda^2 f_{\mathrm{RF}}^2/c + \arctan\alpha) \tag{7.3}$$

where P_0 is the RF power without CD and PMD effects, which depends on the loss or gain that the signal experiences; γ and $\Delta\tau$ are PMD-related factors: the power splitting ratio and DGD between the two PSPs; α is a parameter that relates the instantaneous intensity-induced phase variation of the modulated light, also known as chirp parameter [86]; D_{total} is the total CD induced by fibers and other optical components; f_{RF} is the RF frequency; λ is the carrier wavelength; and c is the speed of light in vacuum. This equation indicates that the faded RF power could be

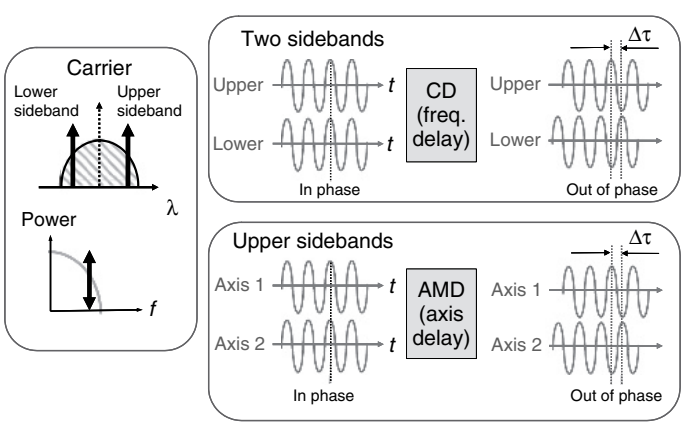

Figure 7.26 RF tone fading due to CD and PMD.

employed in CD monitoring, but the DGD (first-order PMD) may considerably influence the RF power, which leads to monitoring errors for the RF tone-based CD monitoring techniques.

An interesting technique is proposed to suppress the effects of PMD and chirp [87]. By inserting a filter to remove one of the transmitted sideband tones just before the detector, the detected RF power of the single sideband (SSB) signal is given by [assuming the lower sideband (LSB) tone is removed]:

$$P_{\mathrm{SSB}} = P_0(1+\alpha^2)|H(f_0)|^2|H(f_0+f_{\mathrm{RF}})|^2/4 \times \left[1-4\gamma(1-\gamma)\sin^2(\pi f_{\mathrm{RF}}\Delta\tau)\right], \tag{7.4}$$

where H is the electrical field transfer function of the optical filter and f_0 is the optical carrier frequency. By taking the ratio of the RF power with DSB to that with SSB, the power variation related term P_0 and PMD-related term $1-4\gamma(1-\gamma)\sin^2(\pi f\Delta\tau)$ are cancelled. The RF power ratio is then given by

$$R = \frac{4\cos^2(\pi D_{\mathrm{total}}\lambda^2 f_{\mathrm{RF}}^2/c + \arctan\alpha)}{|H(f_0)|^2|H(f_0+f_{\mathrm{RF}})|^2}, \tag{7.5}$$

where $|H|$ is fixed and can be easily measured. Therefore, CD can be monitored by this RF power ratio without the influence of PMD. Furthermore, the monitoring error induced by the small chirp fluctuation can be suppressed using two RF tones and a CD offset. Figure 7.27 shows the experimental setup. Experimental results in Figure 7.28 show that this technique could accurately monitor the accumulated CD without being affected by the PMD and small chirp fluctuation.

Recently, Lize et al. [57] demonstrated another technique that simultaneously monitors and isolates CD and PMD or NRZ OOK and DPSK signals. The RF clock-tone power is monitored at the output ports of an unbalanced Mach Zehnder delay line interferometer (DLI) with a quarter bit delay in one arm. It

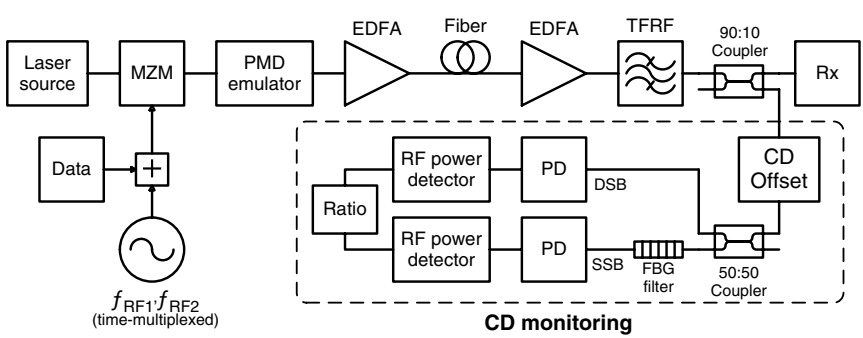

Figure 7.27 System setup of the CD monitoring scheme suppressing PMD and chirp effects. (After Ref. [87]. © 2006 IEEE.)

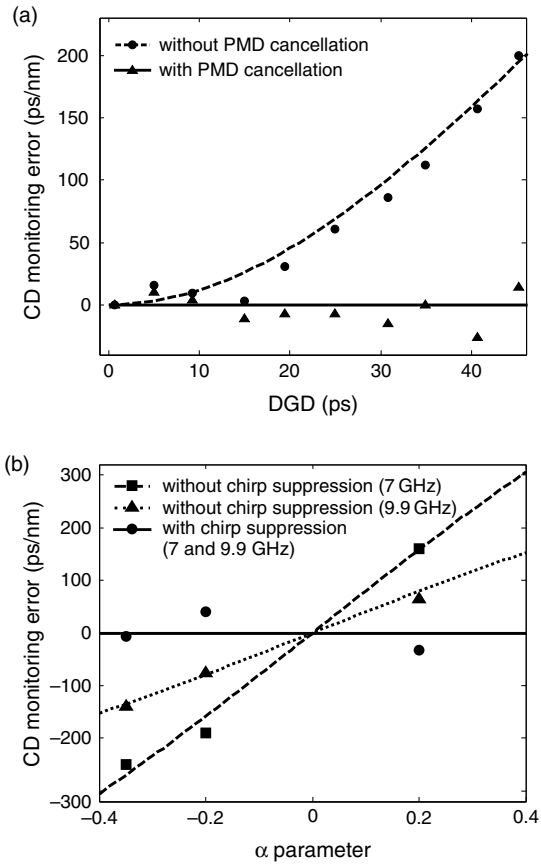

Figure 7.28 CD monitoring error (a) vs DGD without and with PMD cancellation; and (b) vs α parameter without and with chirp suppression. (After Ref. [87]. © 2006 IEEE.)

is observed that the clock power from the constructive port of the DLI grows with an increase in CD and with a decrease in PMD, whereas the clock power from the destructive port grows with a decrease in both CD and PMD. By appropriately adding and subtracting the constructive and destructive clock powers, the individual contributions of CD and PMD can be derived simultaneously while the sensitivity is also increased. The same setup can be used for OSNR monitoring at the same time [56].

Measurement of Relative Group Delay Between VSB Signals

Another powerful technique is detecting the relative group delay between the upper and lower vestigial sideband (VSB) signals in transmitted data [88]: the lower and

upper vestigial sidebands are obtained by tuning an optical filter away from the optical spectrum center of the double sideband data, as shown in Figure 7.29. Since the two optical sidebands occupy different wavelength ranges, fiber CD induces a relative group delay between the lower and upper VSB signals. This group delay can be measured through clock recovery and phase-sensitive detection. Figure 7.30 shows both simulation and experimental results. This technique requires no modification at

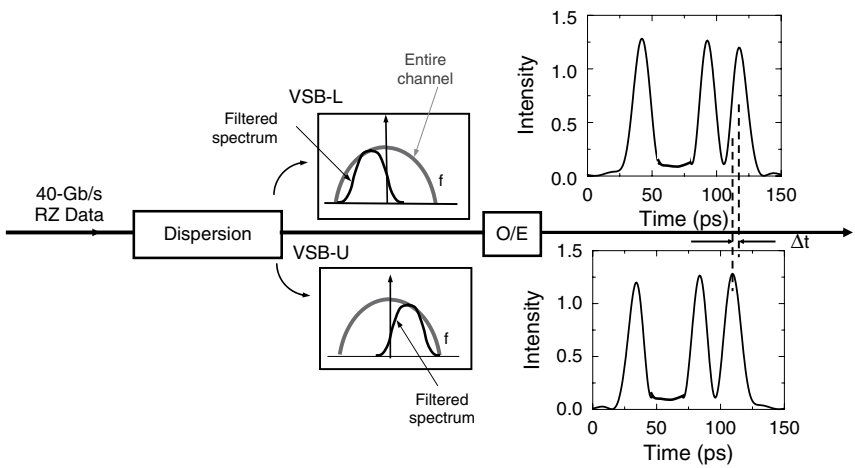

Figure 7.29 Conceptual diagram for monitoring CD using optical vestigial sideband (VSB) filtering: the recovered bits from either part of the spectrum arrive at slightly different times depending on the CD. (After Ref. [88]. © 2002 IEEE/OSA.)

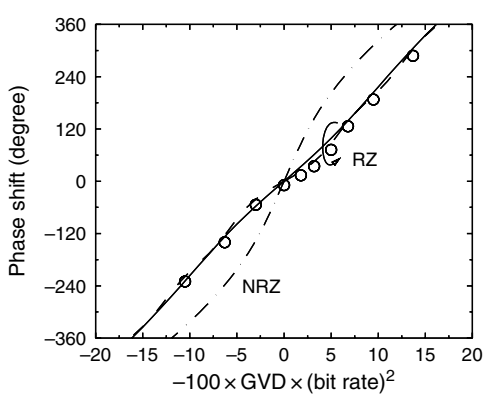

Figure 7.30 Phase shift between the two VSB signals vs the normalized. The three lines are simulation results for (i) NRZ data, Gaussian filter (dash dot), (ii) RZ data, Gaussian filter (solid), and (iii) RZ data, fiber Fabry Perot filter (dash). The scatter points are experimental results for 10 Gbit/s RZ data using a fiber Fabry Perot filter. (After Ref. [88]. © 2002 IEEE/OSA.)

the transmitter, is highly sensitive, is unaffected by PMD, fiber nonlinearities and transmitter chirp, and can be applied to WDM signals by sweeping the optical filter.

Other Chromatic Dispersion Techniques

Other techniques of CD monitoring include utilizing nonlinear effects in fiber or SOA [89 95]; coherent detection [96, 97]; two-photon absorption in a semiconductor microcavity [98]; data stream intensity autocorrelation [89, 100]; and FIR filters and spectrum monitoring [101]. Some of these techniques can also be used for PMD monitoring [91, 96, 101].

7.4.4 Polarization Mode Dispersion Monitoring Techniques

Deleterious PMD effects are stochastic, time-varying, temperature-dependent, and worsen as the bit rate rises. Moreover, the instantaneous first-order PMD (i.e., DGD) follows a Maxwellian probability distribution, always with some finite possibility of a network outage. Therefore, it requires real-time monitoring.

Measurement of RF Tone

A number of monitoring techniques have been demonstrated to provide appropriate control signals for PMD mitigation. Several techniques are based on spectral analysis such as RF tones [52, 53, 102 105]. A given optical frequency component splits on two orthogonal PSPs and each replica travels down the fiber with a different speed that dephases these replicas. This effect reduces the corresponding spectral component in the detected RF power spectrum through destructive interference. Therefore, the RF power is a function of PMD according to Eqn (7.3).

For RZ data, its strong RF clock tone can be used as a monitoring signal. Unfortunately, according to Eqn (7.4), CD will also affect the power in the RF tone, since dispersion causes a relative time delay between the upper and lower frequency optical clocks. After power detection, the RF clock will fade when these two optical clocks are out of phase due to CD. Therefore, CD will cause ambiguity in PMD monitoring using the recovered RF tone. According to Eqn (7.3), a potential solution to chromatic-dispersion-insensitive PMD monitoring is to use a narrowband optical filter centered at either the upper or the lower optical clock tones before a photodetector [106], which is shown in Figure 7.31. Since only one optical clock tone frequency is detected, any CD effects are negated. The RF clock power is then due solely to the beating of one optical clock tone and the carrier. Because the first-order PMD effect still causes power fading for single sideband signals, this technique can be used to monitor PMD. For a 10-Gb/s system, a narrow filter is centered at the upper 10-GHz optical clock tone and the power of the 10-GHz RF clock is measured to monitor the PMD. As shown in Figure 7.32, the RF tone power gives accurate DGD values and is insensitive to CD up to 640 ps/nm.

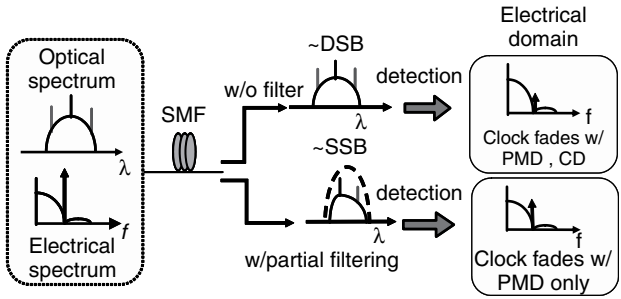

Figure 7.31 Concept of CD insensitive RF power fading using optical bandpass filtering. (After Ref. [106]. © 2004 IEEE.)

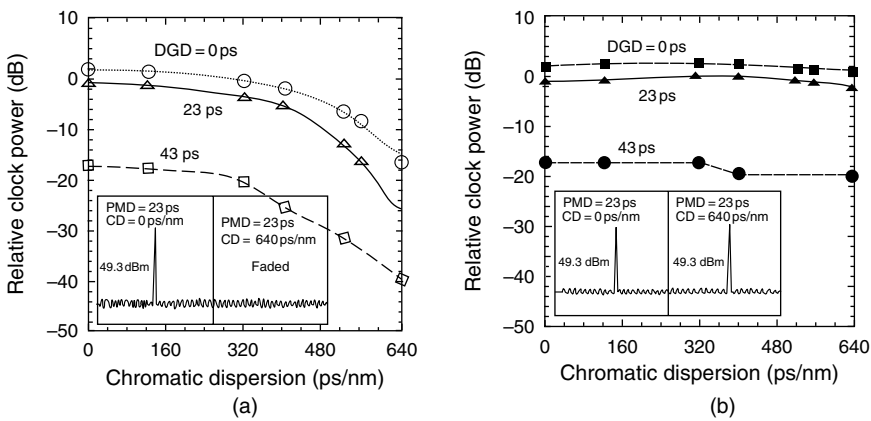

Figure 7.32 CD induced RF clock power fading under different DGD values (a) without bandpass filtering; (b) with bandpass filtering. The insets are RF clocks when PMD is 23 ps and CD is 0, 640 ps/nm, respectively. (After Ref. [106]. © 2004 IEEE.)

The clock tone does not appear at the receiver for NRZ data. Using a narrowband FBG notch filter to filter off one of the optical clock sidebands, the RF clock tone can be recovered from the beating between the carrier and the remaining optical clock sideband. Again, the recovered RF clock power depends on the relative polarization state of the carrier to the optical clock sideband, which is determined by PMD of the transmission link. CD only affects the phase of the recovered RF clock tone but not the amplitude. Therefore, the recovered RF clock power can be used as a PMD monitoring signal, and is insensitive to CD [107].

An interesting CD-insensitive PMD monitor has been demonstrated for differential phase-shift keying (DPSK) and differential quadrature phase-shift keying (DQPSK) [108]. As shown in Figure 7.33, DGD causes walk-off in time between the two PSPs. After passing through a polarization beam splitter (PBS), the two polarizations are beating together, resulting in a periodic filter response. The

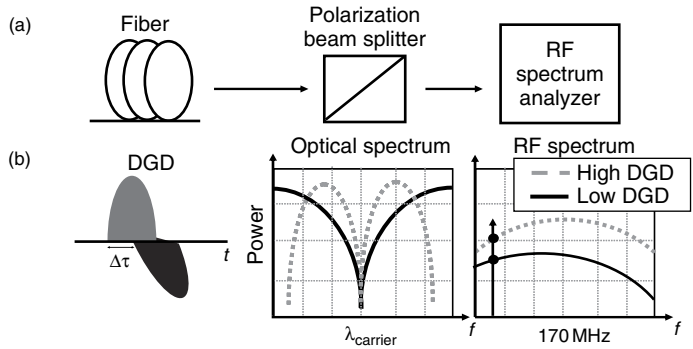

Figure 7.33 (a) Conceptual diagram of the PMD monitoring technique for DPSK/DQPSK. (b) The RF power increases with the decreasing FSR of the polarization based interferometer filter (i.e., with the increasing DGD values). (After Ref. [108]. © 2007 IEEE/OSA.)

resulting FSR is equal to $1/\Delta\tau$, where $\Delta\tau$ is the DGD experienced throughout the link. As a result of this filtering effect, the spectral content of the transmitted RF spectrum changes with DGD. As the DGD of the link increases, the RF power also increases. Therefore, it is possible to measure variations in power level of the RF spectrum and correlate these variations to the first-order PMD of the link. Because the RF content is not impacted much by CD at lower RF frequencies, this monitoring technique is relatively insensitive to CD. Besides the dispersion insensitivity, this monitoring scheme operates on very low frequencies, for example, 170 MHz in the experiment, and therefore does not require any high-speed components, such as a high-speed photodiode.

The proposed PMD monitoring technique was demonstrated in both the 20 Gb/s NRZ-DQPSK and the 10 Gb/s NRZ-DPSK systems. Figure 7.34(a) illustrates that

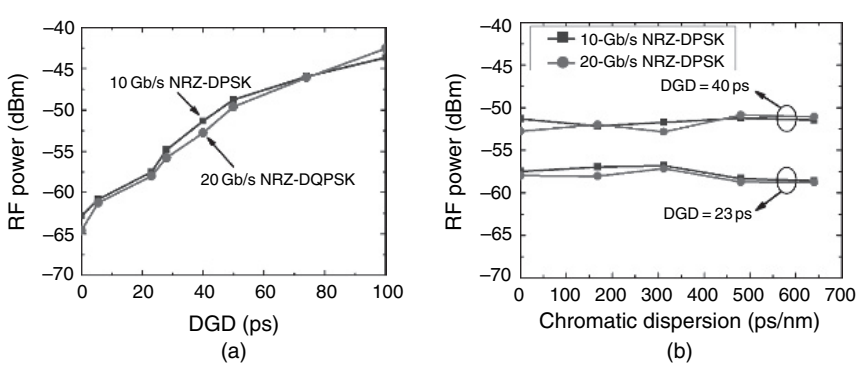

Figure 7.34 Experimental results of (a) RF Power measured at 170 MHz for PMD monitoring of NRZ DQPSK and NRZ DPSK; (b) the CD dependence for PMD monitoring with DGD 23 and 40 ps, respectively. (After Ref. [108]. © 2007 IEEE/OSA.) (This figure may be seen in color on the included CD ROM.)

the RF power at 170 MHz increases by ~20 dB in the presence of 0 to 100 ps of DGD, for both NRZ-DQPSK and DPSK. Figure 7.34(b) illustrates the sensitivity of the proposed scheme to CD. The measured RF powers at 170 MHz with 23 and 40 ps DGD vary within ±1 dB in the presence of 0 650 ps/nm CD.

Measurement of Degree of Polarization

The degree of polarization (DOP) is given by the ratio of the power of the polarized part of the light to the total power of the light. By measuring the DOP of the received signal light, one can evaluate the signal affected by PMD [109, 110]. This DOP measurement requires no high-speed circuit and is insensitive to the other degrading effects [111]. The mechanism of DOP degradation of the signal via PMD is illustrated in Figure 7.35. Without PMD, the optical signal is pure polarized light with a single state of polarization (SOP) as in Figure 7.35(a). With PMD, the SOP at the edge (SOP B and SOP C) and at the mid-point (SOP A) of "1's" of NRZ signal become different due to the PMD-induced pulse shift as in Figure 7.35(b). The amount of DOP of the signal decrease corresponds to the amount of signal pulse distortion caused by PMD.

Note that the DOP is pulse-width dependent [103]. DOP-based techniques may suffer from the following disadvantages: (i) a small DGD monitoring range for short pulse RZ signals, (ii) a lack of sensitivity for NRZ signals, as shown in Figure 7.36, and (iii) they are affected by higher order PMD. As shown in Figure 7.37, the maximum DOP equals to 1 when the state of polarization of the input signal aligns

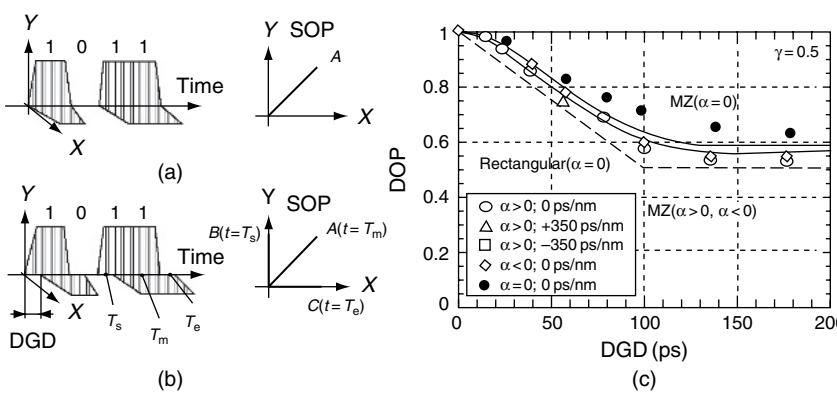

Figure 7.35 Schematic illustration of DOP degradation of the signal by PMD: (a) optical waveform and SOP of the signal without PMD; (b) optical waveform and SOP of the signal with PMD. The *X* and *Y* axis correspond to the two principal states of polarization (PSP) of the transmission media; (c) DOP as a function of DGD for 10 Gb/s LN MZ NRZ modulation (plots: experiment, dashed line: rectangular waveform approximation derived in the appendix, thin lines: numerical simulation. All the simulated DOP curves are relatively unaffected by α and by the fiber dispersion of 350 ps/nm). (After Ref. [111]. © 2001 IEEE/OSA.)

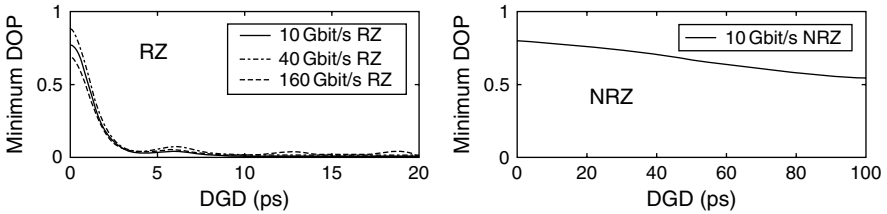

Figure 7.36 Sensitivity of the DOP reduction as a function of DGD (first order PMD). (After Ref. [112]. © 2001 IEEE/OSA.)

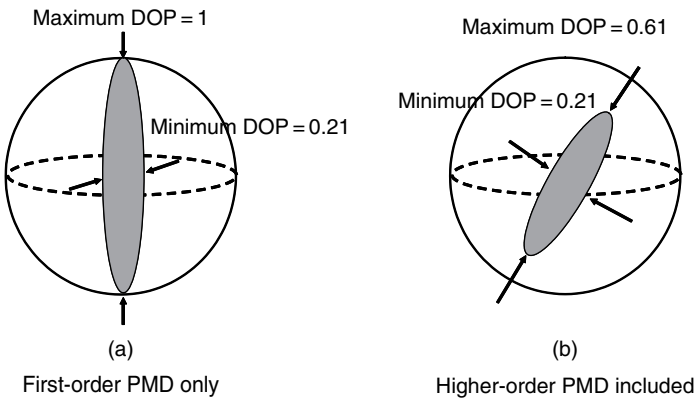

Figure 7.37 Measured DOP reduction with scrambled input polarization of a 40 Gbit/s RZ signal: (a) first order PMD of 1.25 ps and (b) second order PMD, concatenation of two unaligned birefringent sections (6 and 4 ps DGD). (After Ref. [112]. © 2001 IEEE/OSA.)

with the fiber's PSP (first order only). The minimum DOP depends upon the data rate, modulation format and so on. While higher order PMD is included, it decreases the signal's maximum DOP at the receiver to less than unity [112]. These limitations can potentially be overcome by centering a narrowband optical filter at either the optical central frequency or one of the signal's sidebands [113].

Other Polarization Mode Dispersion Techniques

A straightforward technique involves measuring the phase difference between the two optical frequency components for the two orthogonal PSPs [114]. This technique requires polarization tracking at the receiver to be able to find the PSPs so the phase can be measured. Other techniques of PMD monitoring include using nonlinear effects [91, 115, 116]; coherent detection [96, 117]; real-time optical Fourier transformation [118]; FIR-filters and spectrum monitoring [101]; and measurement of "string" length [119].

7.5 FIBER NONLINEARITIES MONITORING

7.5.1 Fiber Nonlinearities

The index of refraction of optical fiber is slightly dependent on optical power, according to the relationship [17]:

$$\tilde{n}(\omega, P) = n_0(\omega) + n_2 I = n_0(\omega) + n_2 \frac{P}{A_{\text{eff}}}, \tag{7.6}$$

where $n_0(\omega)$ is the linear refractive index of silica, n_2 is the intensity-dependent refractive index coefficient, and $I = P/A_{\text{eff}}$ is the effective intensity in the medium. The typical value of n_2 is 2.6×10^{-20} m^2/W. This number takes into account the averaging of the polarization states of the light as it travels in the fiber.

The intensity dependence of the refractive index gives rise to three major effects which tend to degrade the signal integrity significantly: (i) self-phase modulation (SPM) occurs because the intensity profile of an optical pulse on a single channel causes an index-of-refraction profile and, thus, the higher intensity center of a pulse travels slower than the lower intensity pulse wings. (ii) When considering many WDM channels co-propagating in a fiber, photons from channels 2 through N can distort the index profile that is experienced by channel 1. This XPM index distortion translates into a lightwave speed distortion. (iii) The optical intensity propagating through the fiber is the square of the electric field. When squaring the sum of different fields, products emerge that are beat terms at various sum and difference frequencies to the original signals. If a WDM channel exists at one of the FWM beat-term frequencies, the beat term will interfere coherently with this other WDM channel and potentially destroy the data. Nonlinearities can be controlled by carefully introducing and balancing CD, perhaps with fixed and/or tunable compensation.

The nonlinear effects described above are governed by the power dependence of refractive index, and are elastic in the sense that no energy is exchanged between the electromagnetic field and the dielectric medium. A second class of nonlinear effects results from stimulated inelastic scattering in which the optical field transfers part of its energy to the nonlinear medium. Two important nonlinear effects fall in this category [17]: (i) stimulated Raman scattering (SRS) and (ii) stimulated Brillouin scattering (SBS). The main difference between the two is that optical phonons participate in SRS, while acoustic phonons participate in SBS. In a simple quantum-mechanical picture applicable to both SRS and SBS, a photon of the incident field is annihilated to create a photon at a downshifted frequency. The downshifted frequency range where new photons can be generated is $\sim$30 THz in SRS and only $\sim$30 MHz in SBS.

The fiber nonlinearities including SPM, XPM, and FWM as well as stimulated scattering will start to degrade the optical signals when the optical power in fiber becomes high. An important parameter when setting up spans in optical systems is

the launch power to the fiber. The power must be large enough to provide an acceptable OSNR at the output of the span but below the limit where excited fiber nonlinearities distort the signal. The specific limit depends on several different factors such as the type of fiber used, the bit rate, amplifier spacing, and the applied dispersion map. In dense WDM systems, the trade-off relationship between OSNR degradation by accumulation of ASE noise from optical amplifiers and nonlinear waveform distortion in transmission fibers determines the optimum transmission power and together they limit the regenerative repeater spacing [120]. Compared to traditional OOK, Phase-shift keying (PSK) such as DPSK has significant OSNR advantage when balanced receivers are employed. However, nonlinear phase noise caused by amplitude fluctuations and SPM still poses limitations on any PSK systems. Since SPM and XPM depend on the intensity, amplitude fluctuations caused by ASE or nonlinear interactions will translate into phase noise through both the SPM and the XPM. Therefore, fiber nonlinearities need to be monitored and carefully managed for high-speed WDM systems [121 123].

7.5.2 Nonlinear Phase Noise

The nonlinear refractive index increases with optical intensity to slow down the propagation speed, thus inducing intensity-dependent nonlinear phase shift. In an optical amplified WDM system, a number of sources, such as the optical intensity noise from optical amplifiers and intensity modulated signal from other channels (through XPM effect), can induce random nonlinear phase shift, called nonlinear phase noise, in a given data channel. By its nature, nonlinear phase noise is statistical effect [124 126] and is the limiting factor of phase modulated systems.

One report showed a simulated distribution of the received electric field for a binary PSK (BPSK) system at different mean nonlinear phase levels [125]. As shown in Figure 7.38(a), the mean nonlinear phase is 1 rad, corresponding to the case when the variance of nonlinear phase noise approximately equals the variance of linear phase noise. Figure 7.38(b) illustrates the case of 2 rad. The helical-shaped distributions arise because the nonlinear phase rotation is correlated with the received intensity.

Another study compared various nonlinear effects for different data modulation formats [126]. Figure 7.39 shows the phasor diagrams of RZ-OOK and RZ-DPSK (with the same average power) 40-Gb/s nonlinear transmission with a maximum accumulated dispersion of 850 ps/nm. The intrachannel FWM- and XPM-induced ghost pulse generation on “zeros” is a major nonlinear penalty source in OOK transmission. The major nonlinear penalty in 40-Gb/s DPSK is intrachannel FWM-induced nonlinear phase noise. Note that DPSK suffers less penalty from intrachannel FWM than OOK with the same average power due to the lower peak power of DPSK and a correlation between the nonlinear phase shifts experienced by any two adjacent bits [127].

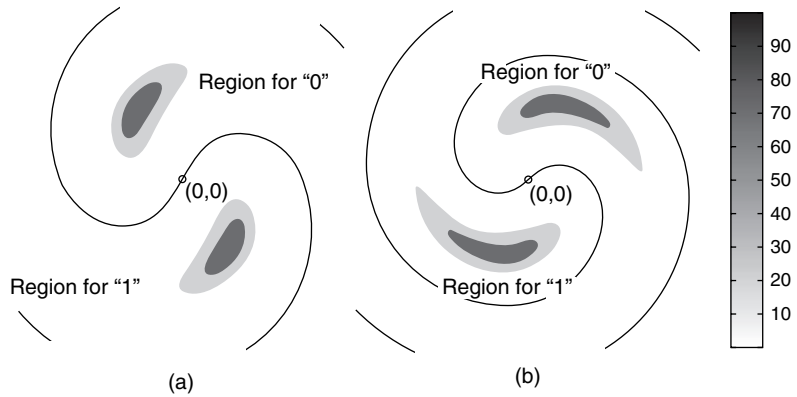

Figure 7.38 Simulated distribution of received signal with nonlinear phase noise for various mean nonlinear phase shifts: (a) 1 rad and (b) 2 rad. (After Ref. [125]. © 2004 IEEE/OSA.)

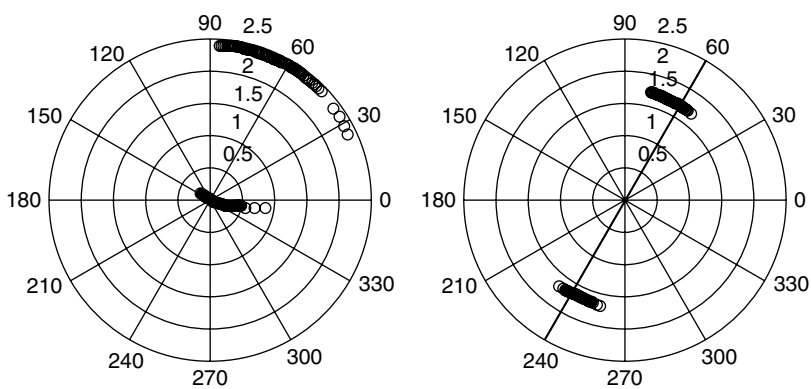

Figure 7.39 Simulated phasor diagrams showing the amplitude and phase at the centers of signal bits in 40 Gb/s RZ OOK (left) and RZ DPSK (right). (After Ref. [126]. © 2004 IEEE/OSA.)

To summarize, fiber nonlinearities represent the fundamental limits to the amount of data that can be transmitted in a single fiber. Since fiber nonlinearities-induced noise is power dependent, it is a random noise by its nature and will induce system performance or QoS fluctuating. Therefore, in long-haul DWDM systems, it is necessary to monitor the fiber's nonlinearity and its effects to ensure satisfactory system performance.

7.5.3 Fiber Nonlinearities Monitoring Techniques

As described in CD monitoring section, the accumulated CD can be monitored by adding a subcarrier to the baseband of the signal. However, Eqn (7.3) is only valid when

nonlinear effects are ignored. When dispersion is assumed constant, the subcarrier can also be used to monitor fiber nonlinearities, as the detected power of the RF tone will fade according to the level of excited nonlinearities in the system [123]. A subcarrier tone at 5.1 GHz is added electrically to the 10-Gbit/s data signal using a power combiner, and then subsequently modulated onto the optical carrier, and transmitted through the 80 km postdispersion compensated span. The subcarrier modulation index is 5%, which by itself gives negligible power penalty to the data. After transmission the composite signal is detected and the subcarrier power is observed using an electrical spectrum analyzer.

Figure 7.40 illustrates both the added subcarrier power and receiver sensitivity vs the launch power for the compensated 80-km span. We can see the correlation between the BER performance and the detected power of the added subcarrier. Therefore, the power of the added subcarrier can be used as a signal for fiber nonlinearities monitoring.

Another proposed nonlinear monitoring approach is simply a data power monitor as shown in Figure 7.41 [121]. In front of the receiver, the received signal is used to drive a phase modulator to partially compensate for the nonlinear phase noise. The magnitude of the phase modulation is proportional to the detected pulse intensity, and the sign is opposite to that of the nonlinear phase shift caused by self-phase modulation, thus to partially cancel nonlinear phase fluctuation. Figure 7.42 shows the phasor diagram of the E-field and eye diagram of a DPSK transmission system at a transmission distance of 6000 km after compensation. The fluctuations in the phase are dramatically reduced, and the eye opening is significantly improved.

Another interesting method related to fiber nonlinearities monitoring is based on Broadband Asynchronous Histogram [128]. Tunable narrowband filtering is

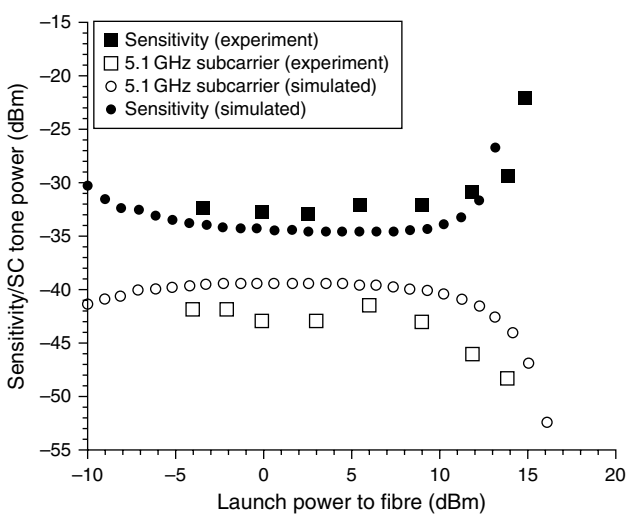

Figure 7.40 Subcarrier (SC) power and receiver sensitivity against launch power for postdispersion compensated 80 km span. (After Ref. [123]. © 2005 IEE.)

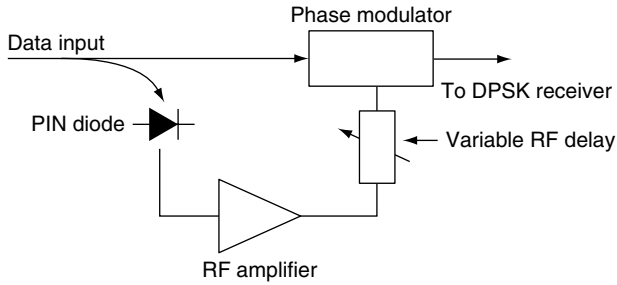

Figure 7.41 Schematic of a DPSK system with postnonlinearity compensation. (After Ref. [121]. © 2002 OSA.)

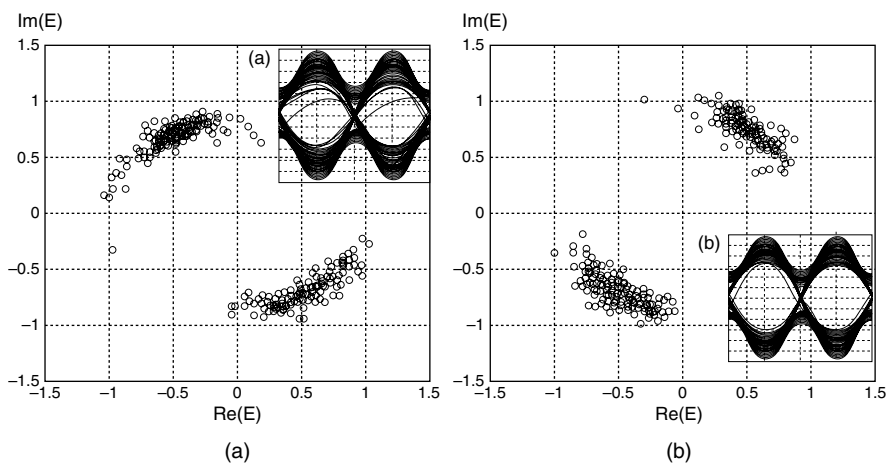

Figure 7.42 Phase shift keying transmission: phasor diagrams of the E field at a transmission distance of 6000 km (a) without and (b) with post nonlinearity compensation (PNC). Re(E), real part of the E field; Im(E), imaginary part of the E field. The insets are corresponding eye diagrams. (After Ref. [121]. © 2002 OSA.)

combined with asynchronous sampling to produce broadband histograms that measure frequency-resolved signal distortion. This distortion can be used as a monitor of transmitter chirp, filter detuning, dispersion and SPM. Section 7.7 will have further discussion of monitoring different impairments using histogram techniques.

7.6 ELECTRONIC MONITORING TECHNIQUES

Electronic monitoring techniques are based on the analysis of the electrical signal after the O/E conversion at the receiver, such as Q/BER measurement, eye diagram analysis, and histogram analysis. The error correlation information from FEC and

the coefficients obtained from an electrical equalizer at the receiver can also be used for OPM to identify and quantify optical distortions and perform network monitoring without additional expensive optical equipment. By comparing the coefficients of an adaptive electrical equalizer to precomputed coefficient vectors, it is possible to identify and quantify the most common distortions of an optical link [129].

7.6.1 *Q*/Bit Error Rate Monitoring Techniques

BER is the ultimate measurement of system performance, and it is the preferred parameter to use for fault management. In fact, this is precisely the parameter used in electronic networks. However, one difficulty for BER monitoring in optical networks is that the signal is typically error free within the network. For monitoring at an amplifier site, the signal is amplified only and not regenerated. Therefore, noise will pass through and continue to accumulate. Measurement of the BER at the location of the fault would result in an error-free measurement. When the signal reaches the end terminal, however, due to accumulated noise it is not error free and the performance degradation on the BER is observed. To detect the degradation within the network, one solution is to use noise loading. In this case, noise is intentionally added to the signal to bring the BER to a measurable level and then the additional noise caused by the impairment can be detected.

The common method to the low sensitivity of BER monitoring is to use *Q*-factor monitoring [130, 131]. The *Q*-factor is obtained by adjusting the decision threshold voltage of the monitor receiver away from the optimum level so that errors are recorded. Figure 7.43(a) shows typical measured data for the logarithm of the BER vs the decision threshold in the decision circuit. Once an error rate is generated, changes to that rate can be monitored and small degradations become visible. Several such techniques have been developed for measuring the *Q*-factor [132, 133]. Note that the *Q*-factor is essentially the SNR. Figure 7.43(b) shows the BER as a function of the received optical power [134]. If *Q*-factor is measured using a receiver, then it is precisely the electronic SNR. If measured by other means such as optical sampling, then it is the in-band optical SNR. It is defined as the difference between the average value of the marks (ones) and of the spaces (zeros) divided by the sum of the standard deviations of the noise distributions around each.

Due to the strong correlation between *Q*-factor and BER, the *Q*-factor measurement is highly effective for fault management. *Q*-factor is sensitive to the same impairments that impact the end terminal receiver with the appropriate sensitivity. Although the cost of this approach may be high for many embedded network-monitoring applications, a portable unit can be a valuable tool in troubleshooting faults particularly to target the rare complication that is not identified by embedded OCMs.

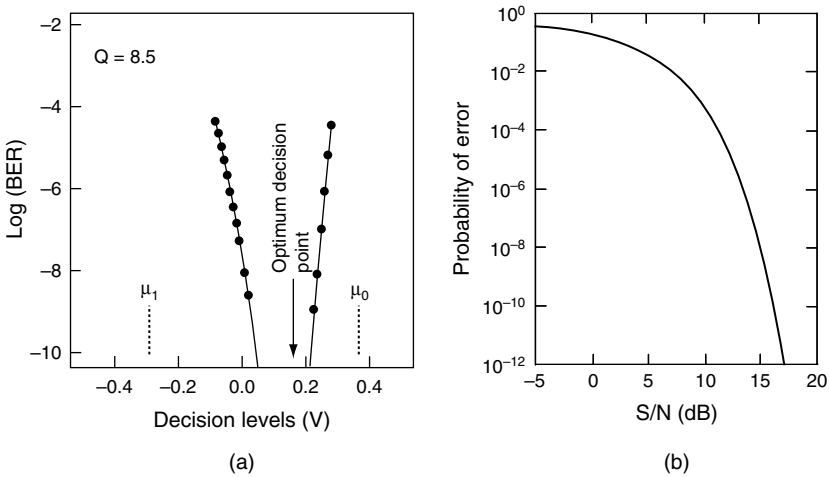

Figure 7.43 (a) Typical measured data for the logarithm of the BER vs the decision threshold. (After Ref. [130]. © 1993 IEEE.) (b) the BER as a function of the received optical SNR [134]. (After Ref. [134]. © 1988 Holt, Rinehart, and Winston.)

7.6.2 Eye Monitoring Techniques

Eye diagram is a common used tool to analyze the quality of signals, which can be used for OPM. Figure 7.44(a) exhibits excellent correlation between BER and eye opening down to 10^{-10} of BER [135]. Using the eye opening monitor, a PMD compensator was tested with 1045 independent PMD conditions at 10 Gb/s. The correlation between the

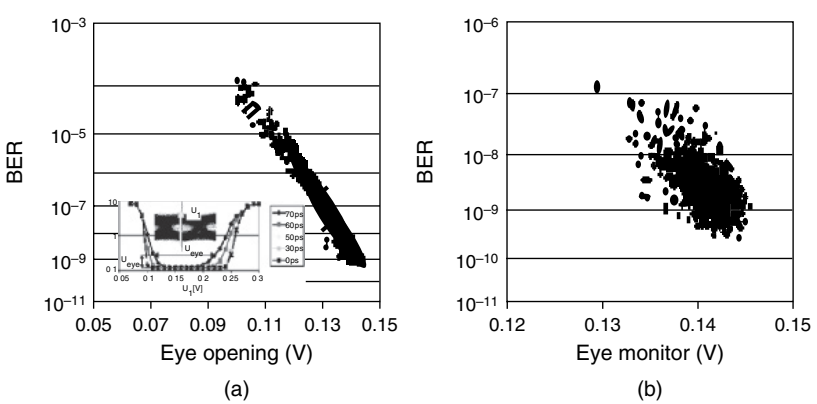

Figure 7.44 (a) BER vs eye opening for all orders PMD statistics (inset shows the typical monitor voltage vs monitor threshold for first order PMD signals with variable DGD and 0.5 splitting ratio). (b) BER after compensation vs eye opening using eye monitoring. (After Ref. [135]. © 2001 IEEE/OSA.)

eye opening and BER after optical compensation is good down to 3×10^{-10} as shown in Figure 7.44(b). The key drawbacks of eye monitoring are the requirement of clock recovery and the difficulties to isolate different impairments.

7.6.3 Asynchronous Histogram Monitoring Techniques

An eye diagram is actually a synchronous amplitude distribution within an entire bit period. When the clock information is absent, the signal can only be asynchronously sampled. The amplitude histogram is obtained by random sampling that spans the entire bit period. With a sufficient number of random samples, an asynchronous histogram can evenly represent the pulse amplitude distribution in a bit period [136]. The asynchronous amplitude histogram technique may be a promising method for low-cost, bit-rate transparent channel performance monitoring due to unnecessary clock recovery.

A comparison of synchronous and asynchronous diagram has been shown in Figure 7.45 [136]. Figure 7.45(a) is the synchronous temporal window (solid line box) at the

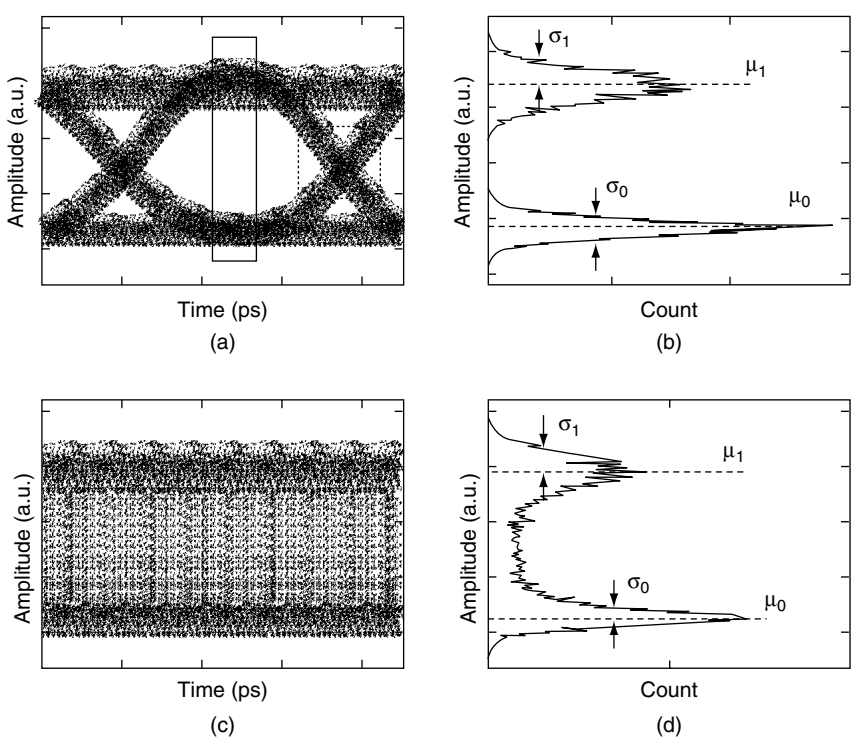

Figure 7.45 (a) Eye diagram and (b) histogram with synchronous sampling. (c) Eye diagram and (d) histogram with asynchronous sampling. (After Ref. [136]. © 2004 IEEE/OSA.)

widest eye opening. Figure 7.45(b) is the corresponding histogram. Based on the histogram, the factor and the BER can be estimated [130]. Figure 7.45(c) and (d) are the asynchronously sampled eye diagram and histogram obtained within the entire bit period. The main difference between the asynchronous and the synchronous histograms lies at the middle counts, the "cross" in the eye diagram, between the mark and space levels. Within the cross-point region, the asynchronous histogram [Figure 7.45(d)] contains counts, while the synchronous histogram [Figure 7.45(b)] contains essentially no counts. The cross-point count is related to the pulse rise time and fall time that may be affected by dispersion-related impairment.

In fact, asynchronous histogram can evaluate the signal quality. It is sensitive to both OSNR and other fiber impairment such as CD and PMD. It has been suggested to monitor the *Q*-factor or OSNR for both OOK and DPSK signals using this method [137 139]. Monitoring of both CD and PMD has also been investigated and demonstrated theoretically and experimentally [140, 141]. However, since this is the electrical domain measurement, the challenge is how to measure the absolute value of *Q*-factor or OSNR, CD, and PMD simultaneously.

Recently, an asynchronous sampling technique is demonstrated that can measure multiple simultaneous impairments [142 145]. The optical waveform is sampled in pairs separated by a known physical delay Δt, as shown in Figure 7.46. The sample

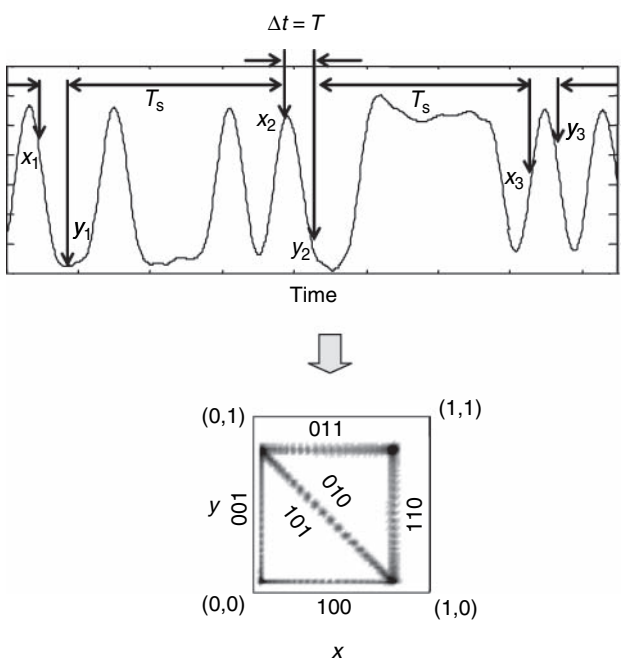

Figure 7.46 Portraits processing of delay tap sample pairs to create phase. The labels on the phase portrait represent the sampled bit sequences. (After Ref. [142]. © 2007 IEEE/OSA.)

time between the pairs, T_s, is not related to the monitored signal bit rate, and can be many orders of magnitude slower. Plotting the pairs produces information-rich patterns called phase portraits, which are of similar complexity to eye diagrams, but do not require clock recovery. A fundamental difference between the two techniques is that the phase portrait contains information about the probability distributions of closely spaced samples, or equivalently, distributions of waveform slopes. This information is absent in eye diagrams, which are constructed from samples separated by large periods. For a one-bit delay, $\Delta t = T$, the technique geometrically separates the various three bit sequences, and in particular separates out the 010 and 101 sequences, which are generally most susceptible to signal distortion.

The effects of OSNR, CD, PMD, and interferometric crosstalk on a 10 Gbit/s NRZ signal have been simulated. The resulting phase portraits and eye diagrams are shown in Figure 7.47. In each case the tap delay for the phase portrait was chosen to be 1-bit

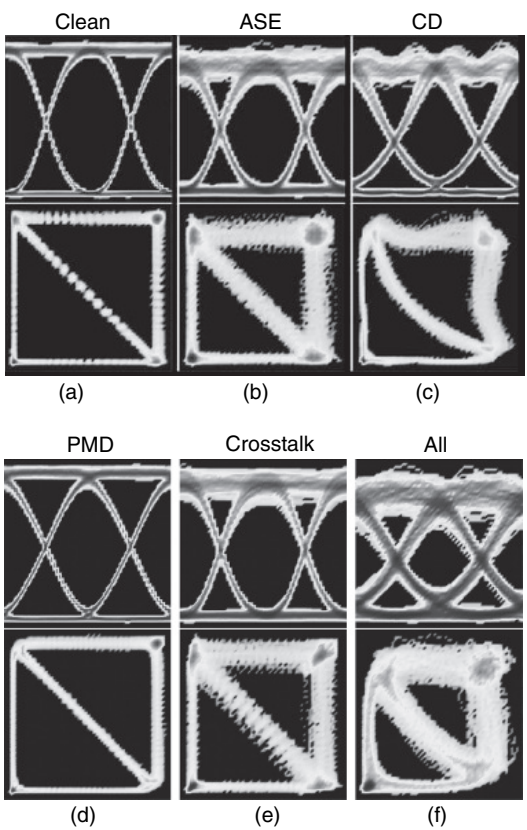

Figure 7.47 Eye diagrams and phase portraits for NRZ (a) OSNR 35 dB and no impairment, (b) OSNR 25 dB, (c) OSNR 35 dB and CD 800 ps/nm, (d) OSNR 35 dB and PMD 40 ps, (e) OSNR 35 dB and crosstalk 25 dB, and (f) OSNR 25 dB, CD 800 ps/nm, PMD 40 ps, and crosstalk 25 dB. (After Ref. [142]. © 2007 IEEE/OSA.)

period. Figure 7.2(a) shows the results for no optical impairment (OSNR 35 dB), with a clean eye and a well-defined geometric shape in the phase portrait. Figure 7.47(b) shows the effects of reducing the OSNR to 25 dB. The predominant effect is to broaden the high-power regions of both the eye and the two-tap plots, but the underlying geometric shapes are not affected. Figure 7.47(c) shows OSNR of 35 dB with 800 ps/nm of CD, corresponding to 50 km of SMF. The eye diagram shows the characteristic narrowing of the peaks. In the phase portrait, the dispersion causes the diagonal to curve in toward the origin. This curvature increases with dispersion, offering a potential dispersion monitoring tool. Figure 7.47(d) shows an OSNR of 35 dB with 30 ps of first-order PMD, with the power split equally between the polarization axes. The eye shows the characteristic "triangularization." And a closer inspection shows significant differences in the distribution of points along the 3-bit transitions. Figure 7.47(e) shows OSNR of 35 dB with a single source of interferometric crosstalk at −25 dB. Both the eye and two-tap plots show similar broadening to the OSNR degradation, but different noise statistics. Finally Figure 7.47(f) shows OSNR of 25 dB with the combined degradations of CD, PMD, and crosstalk. These results show that the phase portraits contained impairment signatures that could be exploited to separate and measure impairments even in cases where they occur simultaneously.

Figure 7.48 shows the simulation results of extracting the signal quality and the underlying cause of signal degradation by analyzing the phase portraits, including OSNR, CD, PMD, filter offset, jitter, or some combinations [145].

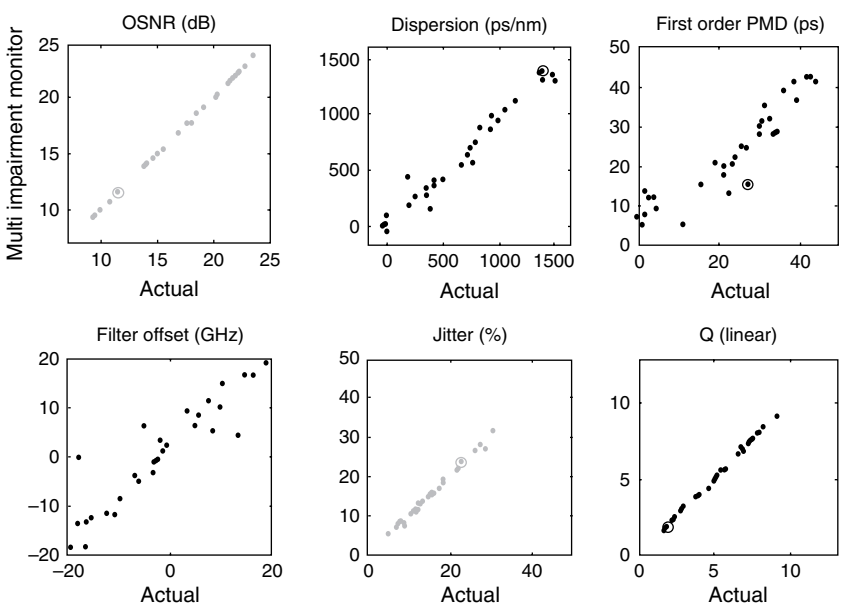

Figure 7.48 Monitor vs actual values of various impairments and signal quality measures, for simultaneous mixtures of OSNR, CD, PMD, filter offset, and jitter, from 10 Gbit/s NRZ simulations. (After Ref. [145]. © 2007 IEEE/OSA.)

Table 7.1
Summary of some advanced OPM techniques.

Techniques	RF tone measurement	Clock tone measurement	Phase measurement (w/VSB filtering)	DOP measurement	Histogram analysis
Monitor	• CD • PMD • OSNR • Channel Power	• CD • PMD • OSNR • Channel Power	• CD	• PMD	• CD • PMD • OSNR
Comments	Fast response time (sub ms); requires to modify transmitter; requires additional consideration to isolate CD and PMD effects	Fast response time (sub ms); no requirement of modification of transmitter; only for single channel operation; requires additional consideration to isolate CD and PMD effects	No modification at the transmitter; unaffected by PMD; can be applied to WDM signals by sweeping the optical filter, requires a high performance phase detector	No requirement of high speed circuit and insensitive to the other degrading effects; requires additional technique to increase the dynamic range	In band and cost effective monitoring; response time may be relatively slow; isolating different impairments are still under investigation

7.7 SUMMARY

In summary, there are many channel-degrading effects in optical networks that affect system performance and that might need to be monitored. However, depending upon the specific network, it might not be necessary to monitor all the above mentioned parameters.

We have covered a variety of topics and techniques on OPM in this chapter. Some advanced OPM techniques are summarized in Table 7.1.

To enable robust and cost-effective automated operation of high-speed reconfigurable optical networks, it is desired to intelligently monitor the state of the network as well as the quality of propagating data signals, isolate specific impairments and locate faults, and automatically diagnose and repair the network. The value of monitoring increases with increasing intelligence and bit rates. And we should keep the right balance between monitoring coverage, sensitivity, and cost.

ACKNOWLEDGMENTS

The authors wish to acknowledge the kind help and insight of the following individuals, listed in alphabetical order: Vahid Reza Arbab, Hunter Boudreaux, Dr. Loukas Paraschis, Dr. Yannick Lizé, Dr. Ting Luo, Xiaoxia Wu, Jing Yang, Jeng-Yuan Yang, Dr. Qian Yu and Lin Zhang.

REFERENCES

[1] F. Forghieri, R. W. Tkach, and A. R. Chraplyvy, "Fiber nonlinearities and their impact on transmission systems" in *Optical Fiber Telecommunications IIIB* (I. P. Kaminow and T. L. Koch, eds), San Diego, CA, USA, Academic Press, pp. 69 114, 1997.

[2] A. E. Willner, "The optical network of the future: Can optical performance monitoring enable automated, intelligent and robust systems?" *Optics and Photonics News*, March 2006.

[3] W. Shieh, R. S. Tucker, W. Chen et al., "Optical performance monitoring in coherent optical OFDM systems," *Opt. Express*, 15, 350 356, 2007.

[4] J. Strand, A. Chiu, and R. Tkach, "Issues for routing in the optical layer," *IEEE Commun. Mag.*, 39, 81 87, February 2001.

[5] K. Guild, "Impairment Aware Routing for OBS and OPS Networks" in Proc. *ICTON 2006*, 3, Nottingham, UK, 2006, pp. 61.

[6] Y. Huang, J. P. Heritage, and B. Mukherjee, "Connection provisioning with transmission impair ment consideration in optical WDM networks with high speed channels," *IEEE/OSA J. Lightw. Technol.*, 23, 982 993, 2005.

[7] T. Carpenter, D. Shallcross, J. Gannett et al., "Maximizing the Transparency Advantage in Optical Networks," in Proc. *OFC*, 2, Atlanta, GA, 2003, pp. 616 617.

[8] N. Andriolli, P. Castoldi, J. Cornelias et al., "Challenges and requirements for introducing impair ment awareness into the management and control planes of ASON/GMPLS WDM networks," *IEEE Commun. Mag.*, 44, 76 85, 2006.

[9] R. Rejeb, I. Pavlosoglou, M. S. Leeson, and R. J. Green, "Management Issues in Transparent Optical Networks," in Proc. 6th *ICTON*, 1, Wroclaw, Poland, July 2004, pp. 248 254.
[10] K. Shaneman and S. Gray, "Optical Network Security: Technical Analysis of Fiber Tapping Mechanisms and Methods for Detection & Prevention," in Proc. *MILCOM*, 2, Monterey, CA, November 2004, pp. 711 716.
[11] M. W. Maeda, "Management and control of transparent optical networks," *IEEE Journal on Sel. Areas in Commun.*, 16, 1018 1023, September 1998.
[12] H. J. Lee, J. H. Bang, J. S. Ko et al., "Dynamic Gain Control of Booster Amplifier (EDFA) using an Optical Supervisory Channel Power Adjustment in WDM Transmission Systems," in Proc. *Joint 4th IEEEICATM*, Seoul, Korea, April 2001, pp. 278 281.
[13] J. Shin, Y. Kwon, and J. Ko, "Optical Supervisory Channel Subsystem for 1.6T WDM Transmis sion System," in Proc. *TheICALT 2004*, 1, Phoenix Park, Korea, 2004, pp. 402 404.
[14] http://www.ciena.com/files/Optical Supervisory Channel Module DS.pdf.
[15] D. C. Kilper, R. Bach, D. J. Blumenthal et al., "Optical performance monitoring," *IEEE/OSA J. Lightwave Technol.*, 22(1), 294 304, 2004.
[16] R. Friskney, K. Warbrick, S. Poliakoff, and R. Heath, "Link Based Photonic Path Performance Prediction and Control," in Proc. *ECOC*, 3, Copenhagen, Denmark, 2002, pp. 1 2.
[17] G. P. Agrawal (1997) "*Fiber Optics Communication Systems,* New York, NY, USA, John Wiley & Sons, 1997.
[18] http://www.optoplex.com/Optical Channel Monitor.htm
[19] http://www.soon link.com.tw/html/pdf/Optical Channel Monitor.pdf
[20] http://www.bayspec.com/pdf/OCPM W.pdf
[21] http://www.axsun.com/html/products omx.htm
[22] http://www.princetonlightwave.com/i products subs ocm.html
[23] K. W. Lim, E. S. Son, K. H. Han, and Y. C. Chung, "Fault localization in WDM passive optical network by reusing downstream light sources," *IEEE Photon. Technol. Lett.*, 17(12), 2691 2693, December 2005.
[24] Y. Li, D. Wang, and J. Li, "FTTH Remote Fiber Monitoring using Optical Wavelength Domain Reflectometry (OWDR) and Wavelength Coded Tag (WCT)," in Proc. *OFC*, paper OThu3, Anaheim, CA, March 2006.
[25] K. Motoshima, L. Leba, D. Chen et al., "Dynamic compensation of transient gain saturation in erbium doped fiber amplifiers by pump feedback control," *IEEE Photon. Technol. Lett.*, 5, 1423 1426, 1993.
[26] A. Srivastava, J. Zyskind, Y. Sun et al., "Fast link control protection of surviving channels in multiwavelength optical networks," *IEEE Photon. Technol. Lett.*, 9, 1667 1669, 1997.
[27] G. Luo, J. Zyskind, Y. Sun et al., "Performace degradation of all optical gain clamped EDFA's due to relaxation oscillations and spectral hole burning in amplified WDM networks," *IEEE Photon. Technol. lett.*, 9, 1346 1348, 1997.
[28] J. Cai, K. Feng, X. Chen, and A. E. Willner, "Experimental demonstration of dynamic high speed equalization of three WDM channels using acousto optic modulators and a wavelength demultiplexer," *IEEE Photon. Technol. Lett.*, 9, 678 680, 1997.
[29] S. Huang, X. Zou, A. E. Willner et al., "Experimental demonstration of active equalization and ASE suppression of three 2.5 Gb/s WDM network channels over 2500 km using AOTF as transmission filters," *IEEE Photon. Technol. Lett.*, 9, 389 391, 1997.
[30] D. Starodubov, V. Grubsky, J. Feinberg et al., "Novel Fiber Amplitude Modulators for Dynamic Channel Power Equalization in WDM Systems," in Proc. *OFC*, paper PD 8, San Jose, CA, February 1998.
[31] J. Ford and J. Walker, "Dynamic spectral power equalization using Micro Opto Mechanics," *IEEE Photon. Technol. Lett.*, 10, 1440 1442, 1998.
[32] C. Doerr, C. Joyner, and L. Stulz, "Integrated WDM dynamic power equalizer with low insertion loss," *IEEE Photon. Technol. Lett.*, 10, 1443 1445, 1998.
[33] C. R. Doerr and K. Okamoto, "Advances in silica planar lightwave circuits," *J. Lightw. Technol.*, 24(12), 4673 4789, 2006.

[34] C. R. Doerr, L. W. Stulz, R. Pafchek et al., "Automatic Wavelength Channel By channel Equal izer," in Proc. *OFC*, 4, Baltimore, Maryland, 2000, pp. 227 229.
[35] C. J. Youn, S. K. Shin, K. J. Park, and Y. C. Chung, "Optical frequency monitoring technique using arrayed waveguide grating and pilot tones," *IEE Electron. Lett.*, 37, 1032 1033, 2001.
[36] L. E. Nelson, S. T. Cundiff, and C. R. Giles, "Optical monitoring using data correlation for WDM systems," *IEEE Photon. Technol. Lett.*, 10, 1030 1032, 1998.
[37] M. Teshima, M. Koga, and K. I. Sato, "Performance of multiwavelength simultaneous monitoring circuit employing arrayed waveguide grating," *IEEE/OSA J. Lightwave Technol.*, 14, 2277 2286, 1996.
[38] D. C. Kilper, S. Chandrasekhar, L. Buhl et al., "Spectral monitoring of OSNR in high speed networks," in Proc. *ECOC*, paper 7.4.4, Copenhagen, Denmark, 2002.
[39] O. Shalitin, G. Shabtay, and Z. Zalevsky, "Future wave in optical network monitoring," *Lightwave Web*, June 2003.
[40] S. K. Shin, K. J. Park, and Y. C. Chung, "A novel optical signal to noise ratio monitoring technique for WDM networks," *OSA Trends in Opt. and Photon. (TOPS)*, 54, 182 184, 2000.
[41] J. H. Lee, D. K. Jung, C. H. Kim, and Y. C. Chung, "OSNR monitoring technique using polarization nulling method," *IEEE Photon. Technol. Lett.*, 13, 88 90, 2001.
[42] J. H. Lee, H. Y. Choi, S. K. Shin, and Y. C. Chung, "A review of the polarization nulling technique for monitoring optical signal to noise ratio in dynamic WDM networks," *IEEE/OSA J. Lightw. Technol.*, 24, 4162 4171, November 2006.
[43] X. Tian, Y. Su, W. Hu et al., "Nonlinearity Tolerant In Band OSNR Monitoring for Synchronous Traffic using Gated Signal RF Spectral Analysis," in Proc. *OFC*, paper OThPl, Anaheim, CA, 2006.
[44] M. Rohde, E. J. Bachus, and F. Raub, "Monitoring of Transmission Impairments in Long Haul Transmission Systems using the Novel Digital Control Modulation Technique," in Proc. *ECOC*, Paper 3.13, Copenhagen, Denmark, 2002.
[45] G. R Hill, P. J. Chidgey, F. Kaufhold et al., "A transport network layer based on optical network elements," *IEEE/OSA J. Lightw. Technol.*, 11, 667 679, 1993.
[46] G. Rossi, T. E. Dimmick, and D. J. Blumenthal, "Optical performance monitoring in reconfigur able WDM optical networks using subcarrier multiplexing," *IEEE/OSA J. Lightw. Technol.*, 18, 1639 1648, 2000.
[47] D. C. Kilper and W. Weingartner, "Monitoring optical network performance degradation due to amplifier noise," *IEEE/OSA J. Lightw. Technol.*, 21, 1171 1178, May 2003.
[48] K. P. Ho and J. M. Kahn, "Methods for crosstalk measurement and reduction in dense WDM systems," *IEEE/OSA J. Lightw. Technol.*, 14, 1127 1135, 1996.
[49] X. Yi, W. Chen, and W. Shieh, "An OSNR monitor for optical packet switched networks," *IEEE Photon. Technol. Lett.,* 18, 1448 1450, 2006.
[50] A. E. Willner and B. Hoanca, "Fixed and tunable management of fiber chromatic dispersion," in *Optical Fiber Telecommunications IVB* (I. Kaminow and T. Li, eds), San Diego, CA, USA, Academic Press, 2002, pp. 642 724.
[51] M. N. Petersen, Z. Pan, S. Lee et al., "Online chromatic dispersion monitoring and compensation using a single inband subcarrier tone," *IEEE Photon. Technol. Lett.*, 14, 570 572, 2002.
[52] G. Ishikawa and H. Ooi, "Polarization mode dispersion sensitivity and monitoring in 40 Gbit/s OTDM and 10 Gbit/s NRZ transmission experiments," in Proc. *OFC*, Washington, DC, 1998, pp. 117 119.
[53] T. Takahashi, T. Imai, and M. Aiki, "Automatic compensation technique for timewise fluctuating polarization mode dispersion in in line amplifier systems," *Electron. Lett.*, 30, 348 349, 1994.
[54] S. M. R. Motaghian Nezam Y. W. Song et al., "First order PMD monitoring for NRZ data using optical clock regeneration techniques," *IEEE/OSA J. Lightw. Technol.*, 22, 1086 1093, April 2004.
[55] X. Liu and Y. H. Kao, "A Simple OSNR Monitoring Technique Independent of PMD and Chromatic Dispersion based on a 1 bit Delay Interferometer," in Proc. *ECOC*, paper Mo4.4.5, Cannes, France, 2006.

[56] Y. K. Lizé, J. Y. Yang, L. C. Christen et al., "Simultaneous and Independent Monitoring of OSNR, Chromatic and Polarization Mode Dispersion for NRZ OOK, DPSK and Duobinary," in Proc. *OFC*, paper OThN2, Anaheim, CA, March 2007.

[57] Y. K. Lizé, L. Christen, J. Y. Yang et al., "Independent and simultaneous monitoring of chromatic and polarization mode dispersion in OOK and DPSK transmission," *IEEE Photon. Technol. Lett.*, 19, 3 5, 2007.

[58] W. Chen, R. S. Tucker, X. Yi et al., "Optical signal to noise ratio monitoring using uncorrelated beat noise," *IEEE Photon. Technol. Lett.*, 17, 2484 2486, 2005.

[59] C. Xie, D. C. Kilper, L. Moller, and R. Ryf, "Orthogonal polarization heterodyne OSNR monitor ing insensitive to polarization mode dispersion and nonlinear polarization scattering," *J. Lightw. Technol.*, 25, 177 183, 2007.

[60] G. W. Lu and L. K. Chen, "Enhancing the monitoring sensitivity of DOP based OSNR monitoring in high OSNR region using off center narrow band optical filtering," *Optics Express*, 15, 823 828, 2007.

[61] T. T. Ng, J. L. Blows, M. Rochette et al., "In band OSNR and chromatic dispersion monitoring using a fibre optical parametric amplifier," *Opt. Express*, 13, 5542 5552, 2005.

[62] T. T. Ng, J. L. Blows, J. T. Mok et al., "Cascaded four wave mixing in fiber optical parametric amplifiers: Application to residual dispersion monitoring," *IEEE/OSA J. Lightw. Technol.*, 23, 818 826, 2005.

[63] T. T. Ng, J. L. Blows, and B. J. Eggleton, "In band OSNR monitoring using fibre optical parametric amplifier," *IEE Electron. Lett.*, 41, 352 353, 2005.

[64] R. Adams, M. Rochette, T. T. Ng, and B. J. Eggleton, "All optical in band OSNR monitoring at 40 Gb/s using a nonlinear optical loop mirror," *IEEE Photon. Technol. Lett.*, 18, 469 471, 2006.

[65 L. D. Garrett, "All About chromatic dispersion in dense WDM optical fiber transmission," Invited Short Course at *OFC*, Anaheim, CA, 2001.

[66] C. D. Poole, "Statistical treatment of polarization dispersion in single mode fiber," *Opt. Lett.*, 13, 687 689, 1988.

[67] C. D. Poole, "Measurement of polarization mode dispersion in single mode fibers with random mode coupling," *Opt. Lett.*, 14, 523 525, 1989.

[68] Y. Namihira and H. Wakabayashi, "Fiber length dependence of polarization mode dispersion measurement in long length optical fibers and installed optical submarine cables," *J. Opt. Com mun.*, 12, 1 8, 1991.

[69] C. D. Poole, R. W. Tkach, A. R. Chraplyvy, and D. A. Fishman, "Fading in lightwave systems due to polarization mode dispersion," *IEEE Photon. Technol. Lett.*, 3, 68 70, 1991.

[70] V. J. Mazurczyk and J. L. Zyskind, "Polarization Hole Burning in Erbium Doped Fiber Amplifiers," in Proc. *Conf. on CLEO/QELS*, paper CPD26, 1993.

[71] H. F. Haunstein and H. M. Kallert, "Influence of PMD on the Performance of Optical Transmission Systems in the Presence of PDL," in Proc. *OFC*, 3, paper WT4, Anaheim, CA, 2001, pp. 17 22.

[72] N. Gisin and B. Huttner, "Combined effects of polarization mode dispersion and polarization dependent loss," *Opt. Commun.*, 142(1 3), 119 125, 1997.

[73] B. Huttner, C. Geiser, and N. Gisin, "Polarization induced distortions in optical fiber networks with polarization mode dispersion and polarization dependent losses," *IEEE J. Sel. Top. Quantum Electron.*, 6, 317 329, 2000.

[74] L. S. Yan, Q. Yu, Y. Xie, and A. E. Willner, "Experimental demonstration of the system performance degradation due to the combined effect of polarization dependent loss with polariza tion mode dispersion," *IEEE Photon. Technol. Lett.*, 14(2), 224 226, 2002.

[75] L. S. Yan, Q. Yu, T. Luo et al., "Deleterious system effects due to low frequency polarization scrambling in the presence of nonnegligible polarization dependent loss," *IEEE Photon. Technol. Lett.*, 15, 464 466, 2003.

[76] A. Chraplyvy, R. Tkach, L. Buhl, and R. Alferness, "Phase modulation to amplitude modulation conversion of CW laser light in optical fibers," *IEE Electron. Lett.*, 22, 409 411, 1986.

[77] N. Liu, W. D. Zhong, Y. J. Wen, and Z. Li, "New transmitter configuration for subcarrier multi plexed DPSK systems and its applications to CD monitoring," *Opt. Express*, 15(3), 839 944, 2007.

[78] M. Murakami, T. Imai, and M. Aoyama, "A remote supervisory system based on subcarrier overmodulation for submarine optical amplifier systems," *IEEE/OSA J. Lightw. Technol.*, 14, 671 677, 1996.

[79] T. E. Dimmick, G. Rossi, and D. J. Blumenthal, "Optical dispersion monitoring technique using double sideband subcarriers," *IEEE Photon. Technol. Lett.*, 12, 900 902, 2000.

[80] A. Liu, G. J. Pendock, and R. S. Tucker, "Chromatic Dispersion Monitoring using Time Multiplexed In Band RF Tones," in Proc. *OFC*, paper OThH6, Anaheim, CA, 2005.

[81] K. T. Tsai and W. I. Way, "Chromatic dispersion monitoring using an optical delay and add filter," *IEEE/OSA J. Lightw. Technol.*, 23(11), 3737 3747, November 2005.

[82] Y. Wang, Z. Pan, A. B. Sahin et al., "In Line Chromatic Dispersion Monitoring using Optically Added Phase Modulated In Band Tones for 10 Gb/s System," in Proc. *OFC*, paper WP3, Atlanta, GA, USA, March 2003.

[83] G. Ishikawa and H. Ooi, "Demonstration of Automatic Dispersion Equalization in 40 Gb/s OTDM Transmission," in Proc. *ECOC*, Madrid, Spain, 1998, pp. 519 520.

[84] Z. Pan, Q. Yu, Y. Xie et al., "Real time group velocity dispersion monitoring and automated compensation without modifications of the transmitter," *Opt. Commun.*, 230(1 3), 145 149, 2004.

[85] K. J. Park, C. J. Youn, J. H. Lee, and Y. C. Chung, "Performance comparisons of chromatic dispersion monitoring techniques using pilot tones," *IEEE Photon. Technol. Lett.*, 15, 873 875, 2003.

[86] F. Devaux, Y. Sorel, and J. F. Kerdiles, "Simple measurement of fiber dispersion and of chirp parameter of intensity modulated light emitter," *IEEE/OSA J. Lightw. Technol.*, 11, 1937 1940, 1993.

[87] N. Liu, W. D. Zhong, Y. J. Wen et al., "PMD and chirp effects suppression in RF tone based chromatic dispersion monitoring," *IEEE Photon. Technol. Lett.*, 18, 673 675, 2006.

[88] Q. Yu, Z. Pan, L. S. Yan, and A. E. Willner, "Chromatic dispersion monitoring technique using sideband optical filtering and clock phase shift detection," *IEEE/OSA J. Lightw. Technol.*, 20(12), 2267 2271, 2002.

[89] S. Li and D.V. Kuksenkov, "A novel dispersion monitoring technique based on four wave mixing in optical fiber," *IEEE Photon. Technol. Lett.*, 16, 942 944, 2004.

[90] M. Westlund, P. A. Andrekson, H. Sunnerud et al., "High performance optical fiber nonlinearity based optical waveform monitoring," *IEEE/OSA J. Lightw. Technol.*, 23(6), 2012 2022, 2005.

[91] S. Wielandy, M. Fishteyn, and B. Zhu, "Optical performance monitoring using nonlinear detection," *IEEE/OSA J. Lightw. Technol.*, 22, 784 793, 2004.

[92] S. Wielandy, M. Fishteyn, T. Her et al., "Dispersion Monitoring and Automatic Compensation based on a Differential Nonlinear Detection Scheme," in Proc. *OFC*1, Atlanta, Georgia, March 2003, pp. 166 168.

[93] P. S. Westbrook, B. J. Eggleton, T. Her et al., "Application of Self Phase Modulation and Optical Filtering to Measurement of Residual Chromatic Dispersion," in Proc. *OFC*, Anaheim, CA, March 2002, pp. 335 336.

[94] Y. Shi, M. Chen, and S. Xie, "A novel low power chromatic dispersion monitoring technique employing SOA spectral shift," *Opt. Commun.*, 230, 297 300, 2004.

[95] T. Luo, C. Yu, Z. Pan et al., "All optical chromatic dispersion monitoring of a 40 Gb/s RZ signal by measuring the XPM generated optical tone power in a highly nonlinear fiber," *IEEE Photon. Technol. Lett.*, 18, 430 432, 2006.

[96] B. Fu and R. Hui, "Fiber chromatic dispersion and polarization mode dispersion monitoring using coherent detection," *IEEE Photon. Technol. Lett.*, 7, 1561 1563, 2005.

[97] A. L. Campillo, "Chromatic dispersion monitoring technique based on phase sensitive detection," *IEEE Photon. Technol. Lett.*, 17, 1241 1243, 2005.

[98] P. J. Maguire, K. Bondarczuk, L. P. Barry et al., "Dispersion Monitoring for High Speed WDM Networks via Two Photon Absorption in a Semiconductor Microcavity," in Proc. *ICTON*, 4, Nottingham, UK, June 2006, pp. 138 141.

[99] S. D. Yang, Z. Jiang, A. M. Weiner et al., "Ultrasensitive chromatic dispersion monitoring for 10 GHz pulse train by quasi phase matched $LiNbO_3$ waveguides," *IEE Electron. Lett.*, 41, 554 556, 2005.

[100] M. Dinu, D. C. Kilper, and H. R. Stuart, "Optical performance monitoring using data stream intensity autocorrelation," *IEEE J. Lightw. Technol.*, 24, 1194 1202, 2006.

[101] M. Bohn, W. Rosenkranz, P. Krummrich et al., "Experimental Verification of Combined Adaptive PMD and GVD Compensation in a 40 Gb/s Transmission using Integrated FIR filters and Spectrum Monitoring," in Proc. *OFC*, paper TuG3, Los Angeles, CA, 2004.

[102] H. Y. Pua, K. Peddanarappagari, B. Zhu et al., "An adaptive first order polarization mode dispersion compensation system aided by polarization scrambling: theory and demonstration," *IEEE/OSA J. Lightw. Technol.*, 18, 832 841, 2000.

[103] A. E. Willner, S. M. R. Motaghian, L. S. Yan et al., "Monitoring and control of polarization related impairments in optical fiber systems," *IEEE/OSA J. Lightw. Technol.*, 22, 106 125, January 2004.

[104] R. Noe, D. Sandel, M. Yoshida Dierolf et al., "Polarization mode dispersion compensation at 10, 20, and 40 Gb/s with various optical equalizers," *IEEE/OSA J. Lightw. Technol.*, 17, 1602 1616, 1999.

[105] T. Luo, C. Yu, Z. Pan et al., "Dispersive effects monitoring for RZ data by adding a frequency shifted carrier along the orthogonal polarization state," *IEEE/OSA J. Lightw. Technol.*, 23, 3295 3301, 2005.

[106] T. Luo, Z. Pan, S.M.R.M. Nezam et al., "PMD monitoring by tracking the chromatic dispersion insensitive RF power of the vestigial sideband," *IEEE Photon. Technol. Letters*, 16, 2177 2179, 2004.

[107] C. Yu, Y. Wang, T. Luo et al., "Chromatic Dispersion Insensitive PMD Monitoring for NRZ Data based on Clock Power Measurement using a Narrowband FBG Notch Filter," in Proc. *ECOC*, paper Tu4.2.3, Rimini, Italy, 2003.

[108] J. Y. Yang, L. Zhang, L. C. Christen et al., "Chromatic Dispersion Insensitive PMD Monitoring of 20 Gb/s DQPSK and 10 Gb/s DPSK using DGD Generated Polarization based Interferometer Filter," in Proc. *ECOC*, paper 3.5.3, Berlin, Germany, 2007.

[109] F. Roy, C. Francia, F. Bruyere, and D. Penninckx, "Simple Dynamic Polarization Mode Dispersion Compensator," in Proc. *Opt. Fiber Commun. Conf.*, 1, 275 278, San Diego, CA, 1999.

[110] S. Lanne, W. Idler, J. P. Thiery, and J. P. Hamaide, "Fully Automatic PMD Compensation at 40 Gbit/s," *IEE Electron. Lett.*, 38, 40 41, 2002.

[111] N. Kikuchi, "Analysis of signal degree of polarization degradation used as control signal for optical polarization mode dispersion compensation," *IEEE/OSA J. Lightw. Technol.*, 19, 480 486, 2001.

[112] H. Rosenfeldt, C. Knothe, R. Ulrich et al., "Automatic PMD Compensation at 40 Gbit/s and 80 Gbit/s using a 3 Dimensional DOP Evaluation for Feedback," in Proc. *OFC*, 4, Anaheim, CA, 2001, pp. PD27 1 PD27 3.

[113] S. M. R. Motaghian Nezam, L. S. Yan, J. E. McGeehan et al., "Wide Dynamic Range DGD Monitoring by Partial Optical Signal Spectrum DOP Measurement," in Proc. *OFC*, Anaheim, CA, 2002, pp. 924 926.

[114] B. W. Hakki, "Polarization mode dispersion compensation by phase diversity detection," *IEEE Photon. Technol. Lett.*, 9, 121 123, 1997.

[115] G. W. Lu, C. Xie, Y. C. Ku et al., "Enhanced PMD monitoring with frequency resolved SOP rotation by self phase modulation," *IEEE Photon. Technol. Lett.*, 16, 2180 2182, 2004.

[116] T. Ito, R. Sato, R. Kasahara et al., "Bit rate and format independent PMD compensation with differential group delay monitoring using SOA/PLC hybrid integrated wavelength converter," *IEE Electron. Lett.*, 39, 84 86, 2003.

[117] I. Roudas, G. A. Piech, M. Mlejnek et al., "Coherent frequency selective polarimeter for polarization mode dispersion monitoring," *IEEE/OSA J. Lightw. Technol.*, 22, 953 967, 2004.

[118] R. Llorente, R. Clavero, and J. Marti, "PMD Monitoring by Spectral SOP Rotation using a Real Time Optical Fourier Transformer," in Proc. *OFC*, paper OME26, Anahaeim, CA, 2005.

[119] M. Boroditsky, K. Cornick, C. Antonelli et al., "Comparison of system penalties from first and multiorder polarization mode dispersion," *IEEE Photon. Technol. Lett.*, 17, 1650 1652, 2005.
[120] P. P. Mitra and K. B. Stark, "Nonlinear limits to the information capacity of optical fiber communications," *Nature*, 411, 1027 1030, 2001.
[121] C. Xu and X. Liu, "Postnonlinearity compensation with data driven phase modulators in phase shift keying transmission," *Opt. Lett.*, 27, 1619 1621, 2002.
[122] E. Yamazaki, F. Inuzuka, K. Yonenaga et al., "Compensation of interchannel crosstalk induced by optical fiber nonlinearity in carrier phase locked WDM system," *IEEE Photon. Technol. Lett.*, 19, 9 12, 2007.
[123] M. N. Petersen and M. L. Nielsen, "Experimental and theoretical demonstration of launch power optimisation using subcarrier fibre nonlinearity monitor," *IEE Electron. Lett.*, 41, 268 269, 2005.
[124] J. P. Gordon and L. F. Mollenauer, "Phase noise in photonic communications systems using linear amplifiers," *Opt. Lett.*, 15, 1351 1353, December 1990.
[125] K. P. Ho and J. M. Kahn, "Electronic compensation technique to mitigate nonlinear phase noise," *IEEE/OSA J. Lightw. Technol.*, 20, 779 783, 2004.
[126] X. Liu, "Nonlinear Effects in Phase Shift Keyed Transmission," in Proc. *OFC*, 2, paper ThM4, Los Angeles, CA, February 2004.
[127] X. Wei and X. Liu, "Analysis of intrachannel four wave mixing in differential phase shift keying transmission with large dispersion," *Opt. Lett.,* 28, 2300 2302, 2003.
[128] S. D. Dods, D. F. Hewitt, P. M. Farrell, and K. Hinton, "A Novel Broadband Asynchronous Histogram Technique for Optical Performance Monitoring," in Proc. *OFC*, paper OThH2, Anaheim, CA, March 2005.
[129] L. Meflah, B. Thomsen, J. E. Mitchell et al., "Advanced optical performance monitoring for dynamically reconfigurable networks," in Proc. 10th *NOC*, London, UK, 2005, pp. 554 561.
[130] N. S. Bergano, F. W. Kerfoot, and C. R. Davidson, "Margin measurements in optical amplifier systems," *IEEE Photon. Technol. Lett.*, 5, 304 306, 1993.
[131] ITU T Recommendation O.201.
[132] R. Wiesmann, O. Bleck, and H. Heppner, "Cost Effective Performance Monitoring in WDM Systems," in Proc. *OFC*, Baltimore, Maryland, 2000, pp. 171 173.
[133] J. D. Downie and D. J. Tebben, "Performance Monitoring of Optical Networks with Synchronous and Asynchronous Sampling," in Proc. *OFC*, paper WDD50, Anaheim, CA, 2001.
[134] W. B. Jones, Jr, *Introduction to Optical Fiber Communication Systems*, New York, Holt, Rinehart, and Winston, 1988.
[135] F. Buchali, S. Lanne, J. P. Thiery et al., "Fast Eye Monitor for 10 Gbit/s and its Application for Optical PMD Compensation," in Proc. *OFC*, paper TuP5, Anaheim, CA, 2001.
[136] H. Chen, A. W. Poon, and X. R. Cao, "Transparent monitoring of rise time using asynchronous amplitude histograms in optical transmission systems," *IEEE/OSA J. Lightw. Technol.*, 22, 1661 1667, 2004.
[137] N. Hanik, A. Gladisch, C. Caspar, and B. Strebel, "Application of amplitude histograms to monitor the performance of optical channels," *IEE Electron. Lett.*, 35(5), 403 404, 1999.
[138] Z. Li and G. Li, "In line performance monitoring for RZ DPSK signals using asynchronous amplitude histogram evaluation," *IEEE Photon. Technol. Lett.*, 18(3), 472 474, 2006.
[139] I. Shake and H. Takara, "Averaged Q factor method using amplitude histogram evaluation for transparent monitoring of optical signal to noise ratio degradation in optical transmission sys tem," *IEEE/OSA J. Lightw. Technol.*, 20(8), 1367 1373, 2002.
[140] Z. Li and G. Li, "Chromatic dispersion and polarization mode dispersion monitoring for RZ DPSK signals based on asynchronous amplitude histogram evaluation," *IEEE/OSA J. Lightw. Technol.*, 24(7), 2859 2866, 2006.
[141] I. Shake and H. Takara, "Chromatic dispersion dependence of asynchronous amplitude histogram evaluation of NRZ signal," *IEEE/OSA J. Lightw. Technol.*, 21(10), 2154 2161, 2003.

[142] Trevor B. Anderson, Sarah D. Dods, Ken Clarke et al., "Multi Impairment Monitoring for Photonic Networks," in Proc. *ECOC*, paper 3.5.1, Berlin, Germany, 2007.
[143] S. D. Dods and T. B. Anderson, "Optical Performance Monitoring Technique using Delay Tap Asynchronous Waveform Sampling," in Proc. *OFC*, Paper OThP5, Anaheim, CA, 2006.
[144] T. B. Anderson and S. D. Dods, "Asynchronous measurement of chromatic dispersion from waveform distortion," *Proc. OFC*, Paper OWN4, Anaheim, CA, 2006.
[145] S. D. Dods, T. B. Anderson, K. Clarke et al., "Simultaneous and Independent Monitoring of OSNR, Chromatic and Polarization Mode Dispersion for NRZ OOK, DPSK and Duobinary," in Proc. *OFC*, Paper OMM5, Anaheim, CA, 2007.

8

ROADMs and their system applications

Mark D. Feuer[*], Daniel C. Kilper[†], and Sheryl L. Woodward[*]

[*]*Optical Systems Research, AT&T Labs, Middletown, NJ, USA*
[†]*Bell Laboratories, Alcatel-Lucent, Holmdel, NJ, USA*

In less than a decade, the state of the art in fiber-optic transport systems has evolved from simple point-to-point chains of optically amplified fiber spans to massive networks with hundreds of optically amplified spans connecting transparent add/drop nodes spread over transcontinental distances. The primary driver for this transformation has been a remarkable improvement in cost, while its primary enabler has been the emergence of the reconfigurable optical add/drop multiplexer (ROADM) as a network element (NE).

This chapter begins with a brief description of how optical networks have progressed since their first deployments, and how ROADMs fit into this on-going evolution. In Section 8.2 the diverse nomenclature of ROADM technologies and architectures is reviewed and organized. Section 8.3 compares a network with ROADMs to three alternative architectures without ROADMs, to illustrate the economic advantages that ROADMs provide. Section 8.4 is a detailed analysis of the routing functionality offered by various types of ROADMs, while Section 8.5 discusses other features often included in ROADMs and requirements typical of many large carriers' networks. Section 8.6 focuses on switch design, including a brief summary of the underlying component technologies. Sections 8.7 and 8.8 discuss the design of ROADM transmission systems and the interplay between the ROADM and transmission performance. We conclude in Section 8.9 with a brief synopsis, and we identify some challenges remaining for ROADM-enabled networks to achieve their full potential.

Optical Fiber Telecommunications V B: Systems and Networks

ISBN: 978 0 12 374172 1

8.1 ROADMs—A KEY COMPONENT IN THE EVOLUTION OF OPTICAL SYSTEMS

Since optical transmission systems were first deployed there has been a constant push to improve system reach and capacity. A high-level overview of the evolution of optical transmission systems is shown in Figure 8.1. The development of wavelength-division multiplexing (WDM) and optical amplifiers, such as the erbium-doped fiber amplifier (EDFA), has led to cost-effective long-haul, high-capacity systems. Optical transmission has been realized over distances greater than the longest

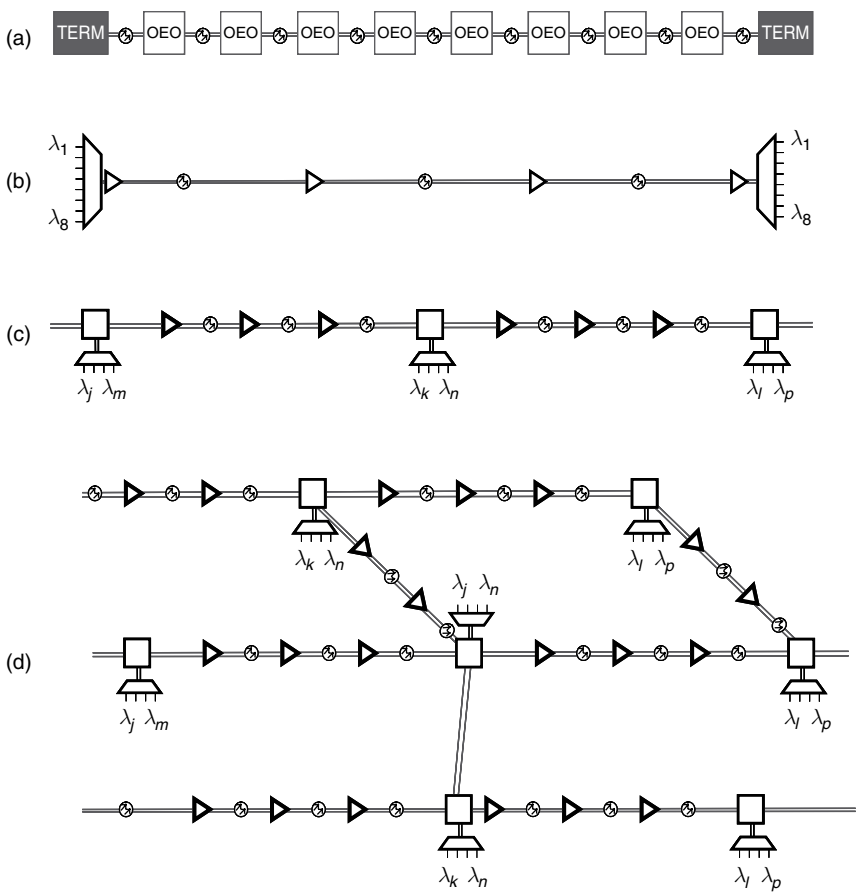

Figure 8.1 The evolution of optical transmission systems: (a) Early systems required full regeneration at each node; (b) WDM and the EDFA provide significant economies, enabling the reach and capacity of the systems to grow; (c) Further improvements in reach and capacity have driven the demand for OADMs, so that the same line system can serve intermediate nodes; (d) Switching in the optical domain will continue the evolution from the simple point to point systems (shown in b) to optical mesh networks (as shown in d) (this figure may be seen in color on the included CD ROM).

circuits in terrestrial networks, with a single-fiber capacity greater than the amount of traffic that currently needs to terminate at any single node [1].

These advances in transmission technology make it desirable for systems to have optical add/drop capability. Exploiting the inherent wavelength granularity of WDM, an optical add/drop multiplexer (OADM) allows some WDM channels (also referred to as wavelengths) to be dropped at a node, while the others traverse the same node without electronic regeneration. Previously, it was necessary to terminate line systems at each node served, and then regenerate the wavelength signals destined for other nodes. The ability to optically add/drop a fraction of a system's wavelengths at a node was first achieved using fixed OADMs. These were constructed from optical filters, and by enabling wavelengths to optically bypass nodes and eliminate unnecessary regeneration, they provided significant cost savings. However, because traffic growth is inherently unpredictable, it is advantageous for the add/drop capability to be reconfigurable. Therefore, although fixed OADMs are usually lower in cost, ROADMs are supplanting them in all but the most cost-sensitive applications.

ROADMs provide many advantages beyond the savings achieved by optically bypassing nodes. In the future, multidegree ROADMs with adequate reconfiguration speeds may enable shared-mesh restoration at the optical layer [2]. Shared-mesh restoration significantly reduces the number of wavelength channels that must be installed as redundant protection circuits. ROADMs also provide operational advantages. Because ROADMs can be reconfigured remotely, they enable new wavelength channels to be installed by simply placing transponders at the end points, without needing to visit multiple intermediate sites. In addition to these cost-saving benefits, ROADMs will enable new services. For example, if transponders are preinstalled, then new circuits can be provided on-demand. The rapid network reconfiguration provided by ROADMs could also become an enabler of dynamic network services, such as switched video for IPTV. For all of these reasons, ROADMs will continue to have a significant effect on the design of optical networks.

8.2 TERMINOLOGY—A ROADM IS A NETWORK ELEMENT

Generally, a ROADM is defined as an NE that permits the active selection of add and drop wavelengths within a WDM signal, while allowing the remaining wavelengths to be passed through transparently to other network nodes. Thus, the simplest ROADM will have two line ports (East and West) that connect to other nodes and one local port (add/drop) that connects to local transceivers. In today's networks, optical links are typically bidirectional, so each line port represents a pair of fibers. When using conventional local transceivers that can process only a single wavelength at a time, the number of fibers in the add/drop port sets the maximum number of wavelengths that can be added or dropped at a given node. As shown in Figure 8.2, at the heart of the ROADM are wavelength add/drop

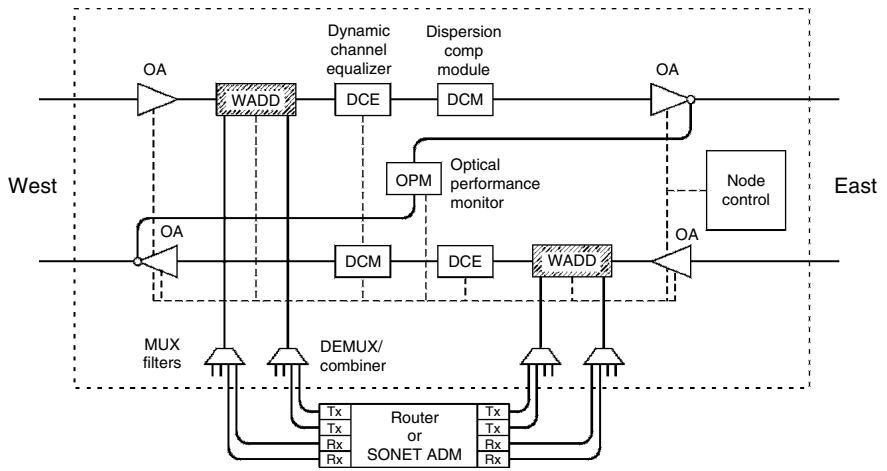

Figure 8.2 A two degree ROADM connects the add/drop port at a node to the optical line. The WADD is a key element of the ROADM, capable of switching individual wavelengths between its input and output ports. Some ROADMs support additional functions, such as dynamic channel equalization.

devices (WADD) that perform the wavelength switching, but many other subsystems, such as amplifiers, performance monitors, and dispersion compensation modules, are needed to complete the NE. Depending on the particular technology chosen, wavelength multiplexing/demultiplexing, channel equalization or other functions may be integrated into the WADD module. Popular WADD types are outlined below, and include modules based on the two-fiber wavelength blocker (WB), the multifiber wavelength-selective switch (WSS), and the integrated DEMUX/switch array/MUX fabricated as a planar lightwave circuit (PLC).

Many of the elements shown in Figure 8.2 are also present in a photonic crossconnect (PXC, also sometimes referred to as a transparent crossconnect or an all-optical crossconnect[1]), defined here as an NE that interconnects WDM signals on multiple line fibers. An example of a PXC connecting three fiber routes is shown in Figure 8.3. Like the ROADM of Figure 8.2, the PXC of Figure 8.3 has three bidirectional ports. However, in the PXC case, each port consists of a single fiber pair, each handles WDM signals, and each maintains the full optical signal quality needed for propagation through a further cascade of fiber spans, PXCs, or ROADMs. (In a ROADM, it may be allowable for signals in the add/drop path to be degraded slightly, since full 3R regeneration immediately follows the drop process.)

In practical networks, locations suitable for a PXC usually need local add/drop capability as well, leading to the concept of a multidegree ROADM that combines both PXC and ROADM functions. In the language of Section 8.5.6, the *fiber degree* of a multidegree ROADM is equal to the number of line fiber pairs it supports.

[1] To avoid confusion, the phrase "optical crossconnect" is not used in this chapter. It has been applied ambiguously in the literature to both electronic and all optical switches.

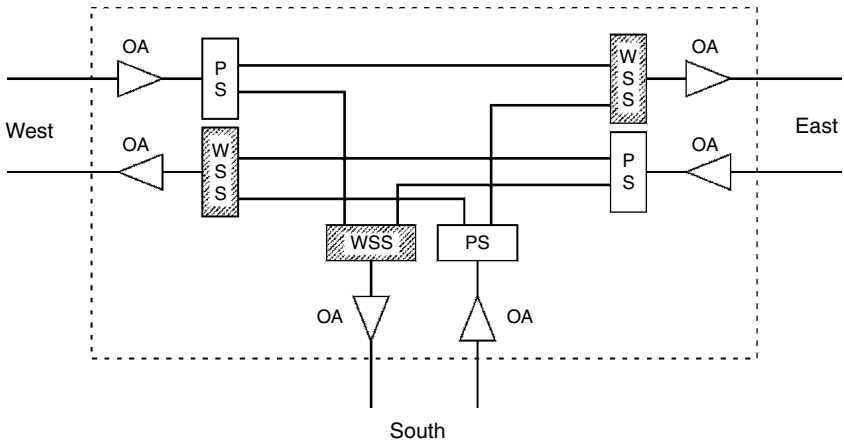

Figure 8.3 Simplified layout of a three degree, broadcast and select type photonic crossconnect (PXC), made up of power splitters (PS), wavelength selective switches (WSS), and optical amplifiers (OA). Ancillary subsystems have been omitted for clarity.

Several other terms describing aspects of add/drop operation are worthy of note. A *full* ROADM is one that provides add/drop (de)multiplexing of any arbitrary combination of wavelengths supported by the system with no maximum, minimum, or grouping constraints. If a ROADM has access to only a subset of the wavelengths, or the choice of the first wavelength introduces constraints on other wavelengths to be dropped, it is called *partial* ROADM. The *drop fraction* of a ROADM is the maximum number of wavelengths that can be simultaneously dropped, divided by the total number of wavelengths in the WDM signal. (Typically, the analogously defined *add fraction* is equal to the *drop fraction*.) If a given add or drop fiber is capable of handling any wavelength, it is said to be *colorless*. If a given add or drop fiber can be set to address any of the line ports (e.g., East or West for a two-degree ROADM), it is said to be *steerable*. An NE is said to be *directionally separable* if there is no single failure that will cause loss of add/drop service to any two of its line ports. The path followed by a particular WDM channel from its source through various ROADMs and PXCs to its termination is denoted a *lightpath*.

8.3 SIMPLE COMPARISON OF FOUR COMPETING NETWORK ARCHITECTURES

The economic advantages of optical bypass have long been recognized [3]. Because it is impossible to predict future traffic requirements, realizing the full advantages of optical bypass demands OADMs that are reconfigurable.

Figure 8.4 illustrates the savings in transponders achieved by deploying ROADMs over various alternative network architectures. For simplicity, we

consider only a linear segment of a larger network, consisting of four nodes denoted as A D [as shown in Figure 8.4(a)]. We assume that a 40-wavelength transmission system is deployed to serve this network, and investigate two alternative end-of-life scenarios. The traffic demands for Case I and Case II (in parentheses) are shown in Figure 8.4(b). In both cases for every west-bound wavelength there is an additional east-bound wavelength provisioned for protection both are included in the wavelength count shown in Figure 8.4(b).

Case I shows an end state in which 20 wavelengths express through this segment of the network. Case II (wavelength counts in parentheses) assumes that node B

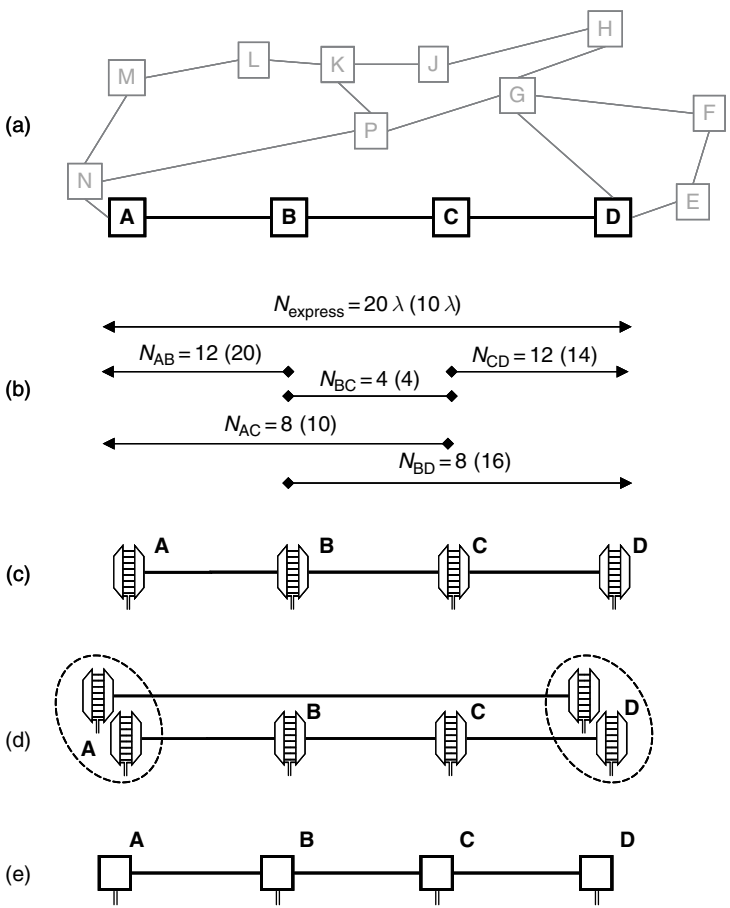

Figure 8.4 (a) Nodes A D are a linear segment of a larger network. By examining how the number of transponders required varies as a function of architecture and traffic, one can develop a qualitative feel for the advantages of ROADMs. Two traffic scenarios (Cases I and II) and four different architectures are considered; (b) the two different traffic scenarios; (c) an architecture with full regeneration at each node; (d) a layered architecture that utilizes an express and local path; (e) two architectures optical bypass can be achieved with either fixed OADMs or ROADMs at each node.

becomes a major traffic destination, with 20 wavelengths terminating there, and only 10 wavelengths express through the segment. A meticulous study would consider many cases, and take into account traffic growth from the beginning of life until the end, considering such factors as the relative costs of equipment, and how traffic churn affects the final state. While our illustrative examples do not represent a rigorous study, these two cases do illustrate the relative strengths of the various architectures. Our results are summarized in Table 8.1 and described in detail below.

One of the four competing architectures, shown in Figure 8.4(c), has full regeneration at each node. This architecture requires transponders at every node, regardless of the circuit's final destination. Figure 8.4(d) shows a network architecture that employs two transmission systems in parallel one for express traffic and one for local traffic. This architecture requires twice the number of fibers be used, and roughly twice the number of amplifiers. Local traffic is regenerated at every node, while express traffic is transmitted over the express system, which only terminates at major nodes. The third architecture, shown in Figure 8.4(e), utilizes fixed OADMs. While fixed OADMs are less expensive than ROADMs, the efficiency of this architecture is dependent upon having a network with predictable and very stable traffic demand. If the network is designed assuming that ½ the traffic will be express, and the rest capable of dropping at each node, then this architecture will require the same number of transponders as the parallel express/local architecture shown in Figure 8.4(d). However, it will not be able to meet the traffic demands of Case II between the node A and the node B and the network would need major work either an additional transmission system would need to be deployed, or the preexisting network would need to be entirely reconfigured, which would interrupt all traffic on the route. Alternatively, the planners might have designed this fixed OADM architecture with many drops, to minimize the possibility that disruptive upgrades would be necessary. If the fixed OADMs were designed to express 10 wavelengths and to drop all others at each node, then both cases could be served by this architecture, but with less than optimal efficiency.

The final architecture schematically looks like Figure 8.4(e); however, it utilizes ROADMs, rather than fixed OADMs. By deploying ROADMs, this segment can meet traffic demands with the minimal number of transponders. Not only does this architecture require fewer transponders than any of the others,

Table 8.1

The number of transponder pairs needed for each of the architectures in Figure 8.4.

# Transponder pairs	Case I (20 express)	Case II (10 express)
Full regeneration	120	120
Parallel systems	80	100
Fixed OADM (20 express)	80	Not served
Fixed OADM (10 express)	100	100
ROADM	64	74

it can also be more easily maintained. When provisioning new wavelengths, only the end terminals for that circuit need to be visited, whereas the other architectures will frequently require that transponders be installed at midpoints.

The number of transponder pairs needed for each architecture is summarized in Table 8.1. This example was intentionally simplified only a short segment of a network was considered, and only end-of-life traffic was modeled, without any of the complications that can be caused by wavelength blocking when traffic grows randomly. However, the trends illustrated in this example are in agreement with far more detailed studies that have taken traffic growth, and even relative equipment costs, into account [4, 5]. The example above only considered degree 2 ROADMs, as did the detailed studies just cited. When comparing higher-degree ROADMs to networks using only degree 2 ROADMs, the savings in transponder count are not as great, as more wavelength blocking is likely to occur forcing the deployment of transponders for wavelength conversion [6]. However, the deployment of high-degree ROADMs offers additional advantages beyond transponder savings, including dynamic provisioning, and the possibility of providing mesh-based shared restoration at the optical layer [2].

8.4 ROUTING PROPERTIES—FULL FLEXIBILITY IS BEST

As a rule, the most desirable ROADMs are the ones with the greatest flexibility: i.e., full ROADMs with 100% add/drop fraction, and colorless, steerable add/drop fibers. However, these are also the most costly solutions, so less ideal options, such as partial ROADMs, have also been extensively investigated. In the analysis below, we will make use of the following parameters:

N = the number of wavelength channels supported by a WDM system,
k = maximum number of channels dropped by a WADD,
J = fiber degree of (i.e., number of line side fiber pairs supported by) a ROADM,
M = the number of input or output fibers provided by a WSS,
R = routing power.

Depending on their internal structure [7, 8] partial ROADMs may be limited to a simple contiguous band of wavelengths, or to a periodic comb of wavelengths, or they may have very complex wavelength constraints. Typically, the wavelength constraints in a partial ROADM are set by the WADDs that perform the wavelength switching. Feuer and Al-Salameh [9] introduced a figure of merit called routing power that provides a framework for comparisons of WADDs. The routing power describes the WADD's ability to establish network connectivity by counting how many distinct connection states [10] it supports. The routing power of a WADD is given by

$$R = \frac{\log(\text{no. of connection states supported by WADD})}{\log(\text{no. of connection states supported by fully flexible WADD})}. \quad (8.1)$$

A fully flexible four-fiber WADD without drop-and-continue function supports 2^N connection states, so we see that

$$R = \frac{\log(\text{no. of connection states supported by WADD})}{N\log(2)}. \quad (8.2)$$

Routing power ranges from zero (for fixed optical add/drop) to unity (for an ideal, fully flexible WADD), and it gives a fair representation of a ROADM's effectiveness in supporting networks with mesh-like traffic demands. Figure 8.5 shows a variety of partial WADD designs with a drop fraction of 0.25, together with the routing power of each. The full crossconnect type [Figure 8.5(a)] has no wavelength constraints except for the maximum drop fraction, so it has the highest routing power. The three banded designs [Figures 8.5(b d)] allow access to only a fraction of the input wavelengths, so they have a low routing power. The tunable filter design of Figure 8.5(e) allows access to any wavelength, but not to two wavelengths in the same band, so it has an intermediate value of R.

The relationship of routing power to network value has been confirmed by simulations of traffic growth in a 32-wavelength, 8-node metro ring constructed from partial ROADMs [11]. In the simulations, ROADMs began with one partial WADD at each ring node. Randomly generated traffic demands (each representing a lightpath with $1+1$ protection) were added to the ring sequentially. When a demand could not be satisfied by the existing ROADMs, an additional WADD module was added to one or both endpoint nodes to increase the drop fraction as

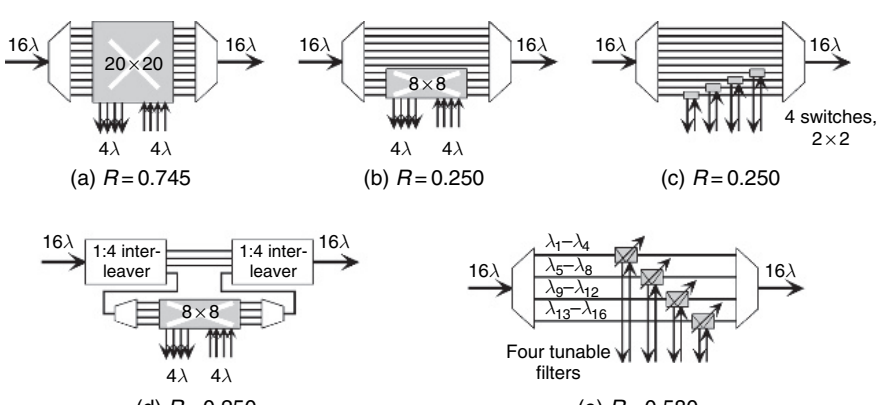

Figure 8.5 Five partial WADD designs with the same add/drop fraction (k/N 25%), but different wavelength constraints.

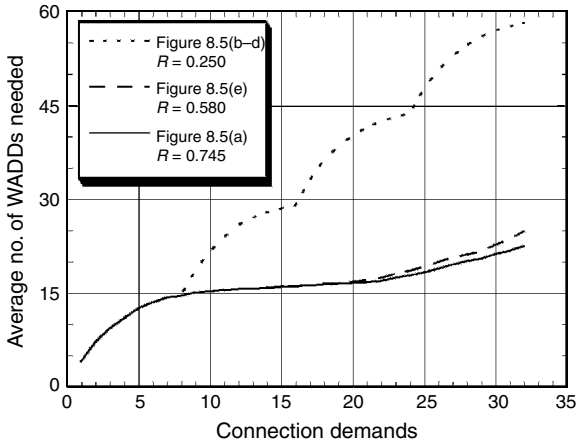

Figure 8.6 Average number of partial WADDs needed to satisfy traffic demands in an 8 node, 32 wavelength ring network with uniform random demands. For designs with a high routing power, fewer WADDs are needed.

needed. Accumulating the results of 1000 randomized trials, one obtains the average number of WADD modules required vs the number of traffic demands, as shown in Figure 8.6. Comparing ROADMs based on Figure 8.5(a), 8.5(b), and 8.5(e), it is clear that the low R of the banded WADD [Figure 8.5(b)] leads to a need for many more module installations, while the crossconnect WADD [Figure 8.5(a)] can satisfy the largest number of traffic demands. R can also be increased by using WADDs with a larger drop fraction, and Figure 8.7 shows the average number of demands satisfied per WADD, at full ring fill, for drop fraction of 0.125, 0.25, and 0.5, for all the three WADD types. Whether R is increased by adding drop fibers to the WADD or by changing the internal switch arrangement, there is a strong, roughly linear correlation between demands satisfied and routing power, confirming the usefulness of R as a figure of merit for WADDs.

It is worth noting that routing power, which effectively assigns equal value to all possible network connection states, is most appropriate for networks with mesh-like (i.e., uniform) traffic demands. In networks with highly structured traffic patterns, such as hubbed rings, WADDs with lower R may be satisfactory. For example, in an access ring with a single hub, only connections with one endpoint at the hub are needed, and a WADD based on a three-fiber tunable filter with variable bandpass width has been proposed [12].

The WADD designs of Figures 8.5(b) and 8.5(c) illustrate the difference between colored and colorless add and drop fibers. In the colored case [Figure 8.5(c)], each add/drop fiber pair is locked to a single wavelength. Even if the transponder attached to it is tunable, service cannot be switched to a new wavelength without manual reconnection to a new fiber pair. This makes pre-need deployment of transponders less practical, and prohibits applications such as bandwidth-on-demand

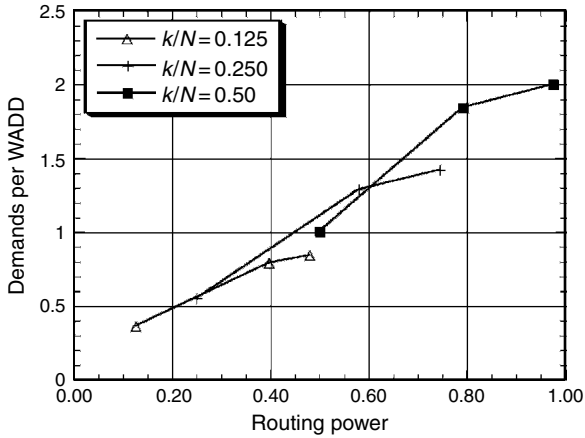

Figure 8.7 Demands satisfied per WADD as a function of the WADD's routing power in the network of Figure 8.6 with fully filled links. *k*/*N* is the drop fraction of the WADD.

and 1:*N* protection against transponder failures. The routing power can be adapted to compare colored and colorless operation by treating each add/drop fiber pair as a separate port and applying the general definition of Eqn (8.1). The result is the fiber routing power R_f, plotted in Figure 8.8 as a function of add/drop fraction. Figure 8.8 shows that the advantage of colorless operation is most dramatic for WADDs that permit full add/drop.

To understand the role of directional steering of transponders, it is necessary to move up from the WADD to the level of the complete ROADM. With a ROADM design like that of Figure 8.2, each transponder is dedicated to a single line fiber

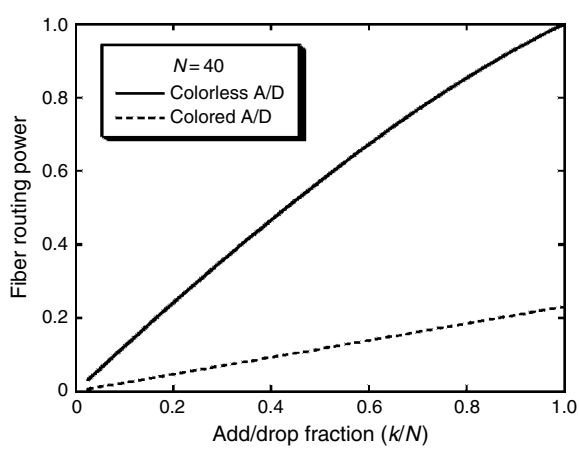

Figure 8.8 Fiber routing power for colored and colorless WADD designs.

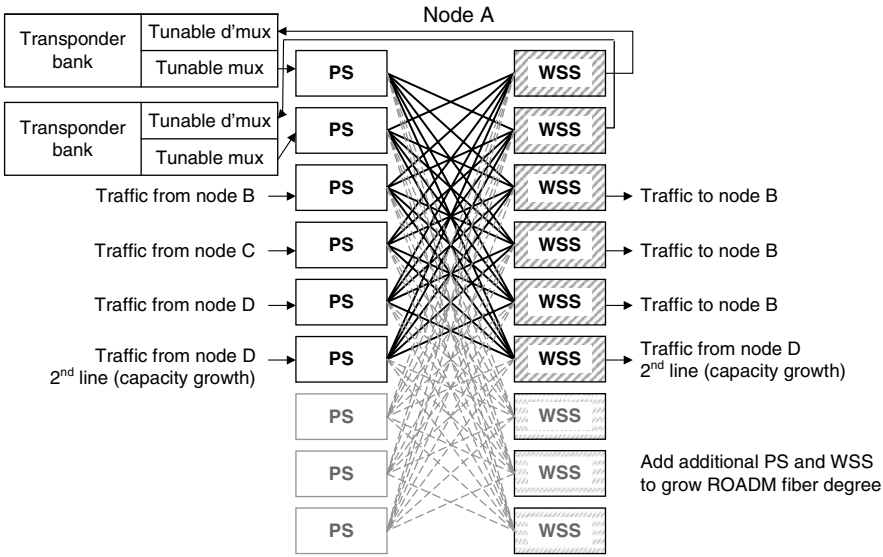

Figure 8.9 This multidegree ROADM supporting colorless, steerable add/drop is assembled from 1×8 power splitters and 8×1 wavelength selective switches (WSSs). This node can grow in service to degree 9 by adding additional power splitters and WSS.

pair, limiting its use for mesh protection or bandwidth-on-demand applications. An alternative approach is to begin with the PXC of Figure 8.3 and add a wavelength MUX/DMUX pair to one fiber pair to transform that fiber pair into an add/drop port. This creates a two-degree ROADM with one steerable add/drop port: transponders attached to such a ROADM can serve either the East or West direction. The design of Figure 8.3 is readily scalable, as shown in Figure 8.9, up to the limit set by the splitter loss or by the number of fibers supported by the WSS. The routing power of the complete ROADM, R_R, is derived from Eqn (8.1) by counting the add/drop connection possibilities associated with different directions, as well as different wavelengths. (We have not counted the line interconnection possibilities of the multidegree ROADM. Because we require that all possible line interconnections be supported, they will cancel out. We have also not included optical multicast connections, though that is a possible extension of the concept.) Figure 8.10 compares the ROADM routing power of an 8-degree, 40-wavelength ROADM with k add/drop fiber pairs, in a steerable, colorless design, a non-steerable, colorless design, and a nonsteerable, colored design. Although the results demonstrate the expected correspondence between routing power and ROADM flexibility, one should keep in mind that network design studies validating the use of routing power for colorless and steerable ROADMs have not yet been carried out.

The discussion so far has excluded any consideration of optical multicast, the process of splitting a WDM channel and sending it to two or more destinations. Broadcast is the traditional method of distributing one-way services such as cable

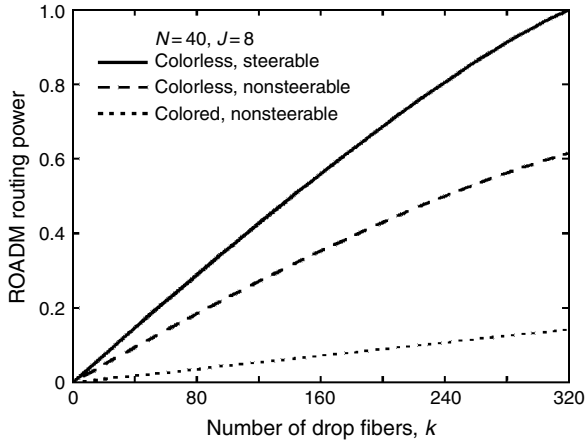

Figure 8.10 Effect of colorless and/or steerable add/drop capability on the fiber routing power of a 40 wavelength ROADM of fiber degree $J = 8$.

television, and some consider it a valuable element of future optical access as well [13, 14]. Multicast is an important tool for optimizing IP networks, and it promises to become more so as IP video and other streaming media continue to expand. Some ROADMs, typically those with power splitters at the drop branch, support optical multicast easily. The multidegree ROADM of Figure 8.9 is one example. Multicast-capable $1 \times M$ WSS have also been demonstrated [15], but these WSS are not yet able to broadcast to all M ports at the same time. For a two-degree OADM, optical multicast is equivalent to a drop-and-continue function, and it has been demonstrated with both fixed OADMs [16] and ROADMs [13]. In small networks where wavelength reuse is considered dispensable, an entire ring can be operated in broadcast and select mode [13]. In larger mesh networks, multicast operation alters the paradigm of bidirectional links that usually pertains to optical transmission, so it may require significant rethinking of network management schemes.

8.5 ADDITIONAL ATTRIBUTES—ROUNDING OUT THE PICTURE

Section 8.4 has described the routing function of the ROADM, but other basic characteristics and attractive features also exist. The most basic are often required because their absence would adversely affect network reliability. Some features are necessary for the ROADM to be cost-effective for a particular application, while others enhance the transmission performance of the optical network. In this section we outline various additional attributes of a ROADM, and discuss what drives carriers to request, or even require, these features.

8.5.1 Hitless Operation

Hitless operation is typically a "must-have" requirement. In most transmission system applications, a ROADM must be capable of switching one wavelength without inducing any errors on the other wavelengths [17]. It has been suggested that forward error correction (FEC) could handle the short burst of errors that might be created in such circumstances; however, this is usually unacceptable for two reasons. First, the performance enhancement provided by FEC is often relied upon by the transmission system itself, and it might not be capable of handling additional errors. Second, FEC is optimized for dealing with uncorrelated errors, rather than bursts of errors as might be caused by switching an adjacent channel in a nonhitless ROADM. Note that it is possible to design a hitless ROADM using a nonhitless WADD by using other elements to block a wavelength before switching.

8.5.2 Directional Separability

Separability is a design principle meant to insure that a single component failure will not affect both the working and protection paths of any circuit. In ring based Synchronous Optical NETwork (SONET) systems, the key precept is East West separability: SONET add/drop multiplexers (ADMs) are constructed so that no single point of failure will disrupt both East-facing and West-facing traffic. This principle is applied even to redundant node controllers and power supply systems. Note that *East-facing* means traffic dropped *from* the East and added *to* the East it is not the same as *Eastbound*. The principle of East West separability can be easily extended to degree 2 ROADMs. In a multidegree ROADM this concept expands to directional separability the requirement that no single point of failure disrupts local add/drop traffic on more than one of its line fiber pairs. This definition assures that subtending SONET or similar equipment will be able to perform client-level protection regardless of which direction is used for the protection path. Achieving directional separability is discussed in more detail in Section 8.6.

8.5.3 Modular Deployment

Carriers wish to deploy systems in the most cost-effective manner possible. Today, it is far more cost-effective to initially deploy the minimal amount of equipment that can smoothly evolve to meet future needs, rather than to deploy a fully loaded system configuration from the very beginning. Currently (and for the foreseeable future), transponders make up the dominant cost of a fully loaded optical communication system. If a full set of transponders were included in the initial deployment, then a substantial cost would be incurred before the network had sufficient traffic to support the expense. Therefore, systems are routinely designed to permit

incremental deployment of transponders on an as-needed basis. Similar considerations also apply to multiplexers, although the economic drivers are not as strong. In general, modular growth will be supported whenever the additional cost and complication of upgrading to higher capacity in the future is small compared to the financial impact of a full equipment deployment at startup.

This pay-as-you-grow approach should be designed into ROADMs, so that the network itself can grow in a cost-effective manner. Traditional networks grow by adding and interconnecting stand-alone line systems, incurring substantial cost and complexity. By using ROADMs that allow for modular deployment of additional ports, network growth can benefit from both the equipment and operational efficiencies of integrating line systems as they are needed into a seamless network (see Section 8.5.4). Because networks are deployed over the course of years, carriers prefer to be able to grow the nodes of the network from terminals or amplifiers, into degree 2 ROADMs, and eventually into multidegree ROADMs [18]. This not only allows the expense to be spread out over years, it also enables the network designers to respond to unforeseen traffic growth patterns.

8.5.4 High Degree for Span Relief

As multidegree ROADMs become more common in backbone and metro networks, equipment builders and network operators must decide on the maximum number of line ports (degree) they will support. NE cost is expected to grow with the degree of the node, and a route-level view of national and continental-scale backbone networks would suggest that a degree higher than four is rare. However, as noted in Ref. [19], there are several reasons why the number of fiber pairs (fiber degree) needed might substantially exceed the number of intersecting routes (route degree).

Continuing growth of traffic (often in directions unpredictable at the time of the original system layout) will eventually require the lighting of additional fiber pairs (overlay) on one or more routes. If these fiber pairs are not connected to the rest of the network via the ROADM, then they will be isolated from the existing optical domain, and many of the advantages provided by transparent optical networking will be lost [20]. Traffic traversing these overlay fibers would need to be dropped, regenerated, and added at the node before it could travel farther in the network. Unless steerable add functionality were available, such overlay traffic would also lose the directional reconfigurability enjoyed by the original traffic. With a ROADM architecture capable of serving a sufficient number of fiber pairs, this isolation of new capacity can be avoided, and the network will be tolerant of uncertain traffic forecasts. Even with a ROADM design capable of modular deployment, as described in Section 8.5.3, the maximum degree of the ROADM is usually determined at the time it is initially deployed. The ability to expand the ROADM to serve a large number of fiber pairs must be designed into the ROADM from the beginning.

Additional line ports may also be needed to provide steerability for local add/drop. As noted in Section 8.4, each steerable transponder bank consumes one fiber pair. Thus, it is not unreasonable to expect the fiber degree to be atleast twice the route degree. Since current WSS-based designs are manageable for a fiber degree of 8 10, many network plans are aiming at multidegree ROADMs in this range. To date, there is no widely accepted strategy for dealing with exceptional cases requiring growth to a higher degree (e.g., a four-route intersection with overlay on three routes and 100% drop fraction with full steerability). This could present a fruitful opportunity for future research.

8.5.5 Network Scaling—How Many Is Enough?

A key parameter in the design of wavelength-routed networks is the number of ROADMs to be cascaded by any given lightpath. Insertion of a ROADM necessarily involves some impairment of the transmitted signal, such as signal-to-noise degradation due to loss, signal distortion due to channel spectrum narrowing, and polarization-dependent loss (see Section 8.7.2). The ROADM design should balance the cost of improved performance against the cost of additional regeneration given the maximum number of cascaded nodes required by the network. The maximum number of cascaded ROADMs may be different for national or continental backbone networks, which traverse long distances, than it is for metro/regional core or feeder networks, which must connect many relatively dense access locations. Expectations for metro systems are also influenced by today's SONET capability of up to 16 cascaded nodes. A maximum cascade of 8 10 ROADM nodes is typically adequate for today's continental backbones, while interconnected metro rings may be asked to support up to 16 or more cascaded ROADM nodes [11]. This places stringent demands on the ROADM implementation, as discussed in Section 8.7.

8.5.6 Channel Conditioning

One beneficial feature of ROADMs is that the WADD is often capable of more than simply transmitting or blocking a wavelength. For example, many WADDs can also act as a channel-specific variable optical attenuators (VOAs). This enables the ROADM to perform channel power equalization. Channel power equalization is particularly useful in networks where not all signals travel the same lightpath, and in long-reach systems that require correction of accumulated gain ripple. This aspect is discussed in detail in Sections 8.7 and 8.8. Channel power equalization is such a useful feature, that many WADDs have been redesigned to incorporate VOAs.

To perform channel power equalization, a ROADM must be able to accurately measure the channel powers, typically with better than 0.5 dB accuracy. A channel monitor provides such additional measurement capability. More advanced types of optical performance monitors [21] (Chapter 7 of this volume) may provide channel monitoring capability plus other measures of signal quality such as the optical signal-to-noise ratio or the polarization mode dispersion. At a minimum, channel monitoring must be provided on the line at some point after the channel power equalization device to provide feedback for that component. Between 1% and 10% of the line power might be tapped for this purpose. Since power equalization is performed infrequently, a single monitor may potentially be shared among power equalization components in a multidegree or multidirection ROADM node as shown in Figure 8.2. In systems with distributed Raman amplification, channel monitoring may also be desirable at the input to the ROADM (output of the transmission span) or output of the dispersion compensating module (DCM) to optimize the Raman pumps for flat channel gain [22].

The technical challenges associated with the channel monitoring function should not be underestimated [21] (Chapter 7 of this volume). An accurate power reading is needed under all operating conditions of the transparent network. This potentially includes monitoring signals with different modulation formats and bit rates, large channel to channel power variations, and signal spectral shaping over different distances and node pass-through. The accumulated optical noise can also impact the accuracy of the signal power measurement [21].

In addition to providing feedback for power equalization, a channel monitoring device can also provide channel path telemetry and identification/discovery capabilities. Channel telemetry is used to trace the path of different WDM channels through the network. Telemetry information can be either explicit or implicit. Explicit telemetry (also called lightpath labeling) involves the use of a channel tag that is carried by the channel along its propagation path and provides an unambiguous indication of channel presence at a ROADM. Most commonly these tags are sinusoidal modulation tones placed on the channel power [23], although more recently an all-digital label coding scheme was introduced [24, 25]. The digital label scheme obviates the need for extra optical modulators and eliminates linear crosstalk between the label and the data information, though it adds a slight overhead ($\sim$2%) to the line data rate. In contrast, implicit telemetry information is transferred between nodes through conventional signaling (e.g., using the optical supervisory channel) and then cross-checked with a total power or channel power measurement. Thus, the node is told by the physical layer management software which channels should be present and the ROADM then confirms their presence by the power reading from the channel monitor. Additional information from a sophisticated channel monitor, such as modulation format or bit rate, can enhance the reliability of this implicit technique, as it provides additional cross-referencing of the correct channel presence.

This telemetry function is a natural adjunct of the wavelength-routing capability built into ROADM networks, needed to verify the accuracy of the routing and to

diagnose and locate routing faults. With explicit telemetry, label reading is a local process implemented within each node, while the implicit type involves correlation of information from many nodes. Implicit path trace can be implemented with technology that is already present in the network, but it may be unable to detect certain hardware or software flaws that cause a ROADM to report its status incorrectly. In addition, amplified spontaneous emission (ASE) noise can be spectrally shaped by the ROADM nodes such that over long distances the accumulated ASE may acquire the spectral signature of a low power channel. Both types of telemetry are susceptible to some of the same challenges that complicate channel monitoring (see above), due to signal impairments and the diversity of spectra possible in transparent systems.

8.5.7 Switching Speed

The switching speed required from the ROADMs will depend strongly on the kinds of network services they are expected to provide. The initial application of photonic (optically transparent) networks is circuit provisioning, a process which has historically taken weeks or months to complete. Even with the expectation that photonic networking will streamline the provisioning process, a ROADM switching time of seconds or even minutes is quite acceptable for present purposes. Dynamic wavelength services, in which a customer turns up additional bandwidth on an on-demand basis, are under active investigation with an eye to unlocking additional revenue streams for network providers. Although this kind of service might set more stringent limits on the ROADM switching time, the primary obstacles to implementation come from software, network management (including the physical layer), and operational issues. In addition, finding the right economic model to support the preinstallation of transponders before they are actually used presents a challenge. Implementation of dynamic wavelength services might drive ROADM switching times down to $\sim$1 s, which should be accessible to most of today's leading component technology families. The next step in ROADM speed might be driven by burst or flow switching since a data burst duration might be as brief as a few seconds, ROADM speeds of $\sim$100 ms would be adequate. Some have suggested that millisecond wavelength services may be desirable [26], which is challenging for some technologies. An alternative driver for improved ROADM speed would be shared wavelength protection/restoration strategies. Since SONET has set a benchmark of 50 ms for the complete decision and switching process, ROADM speeds of $\sim$10 ms or less would be desirable for this application. Although shared protection can offer substantial efficiencies compared to $1+1$ protection, network reconfiguration on these time scales presents many challenges beyond the ROADM switching, including the need for colorless and steerable add/drops, control of transient phenomena in the optical amplifier chains along each affected lightpath, and strategies to manage control message latency and path computation/selection delays in complex mesh networks.

8.6 ROADM/WADD ARCHITECTURE—THINKING INSIDE THE BOX

Many WADD designs suitable for use in the ROADM framework shown in Figure 8.2 can be grouped into two classes: the parallel WADD, in which an assembly of space switches is sandwiched between the DMUX and MUX components [Figure 8.5(a), 8.5(b), or 8.5(c)]; and the serial WADD composed of cascaded tunable filters (Figure 8.11). However, years of active ingenuity have also produced proposals or demonstrations of a wide variety of hybrid designs and unique reconfigurable components. Rather than try to catalog them all here, we will concentrate on three common designs that are commercially available.

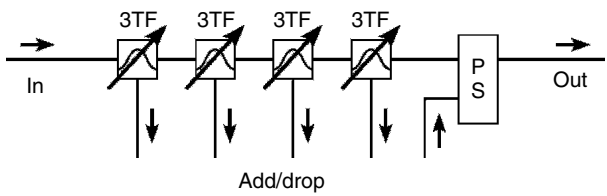

Figure 8.11 Serial WADD assembled from three port tunable filters (3TF) and a wavelength insensitive power splitter/combiner (PS).

8.6.1 Common Designs

In the earliest commercial ROADMs, the classic parallel WADD of Figure 8.5(c) was implemented using arrayed waveguide gratings for DMUX and MUX, bracketing an array of 1×2 or 2×2 switches. Although parallel WADDs assembled from discrete components have been deployed, the discrete approach has been superseded by more highly integrated designs. WADDs based on PLC (see Section 8.6.4 and Chapter 9 of Volume A) technology have been quite successful in systems with moderate wavelength counts, and PLC WADDs have been demonstrated with over 40 wavelengths. These designs have built-in MUX/DMUX of the add/drop channels, which is convenient for ROADMs, but inconvenient for PXC operation such as ring interconnect. Due to insertion loss and passband narrowing, these early ROADMs had limited cascadability, and the discrete-component implementations were bulky. Per-channel equalization has been achieved by incorporating an array of VOAs in series with the switches. Colorless or steerable add/drops would require the addition of an external matrix switch in the local port. Extension of this design to a PXC or multidegree ROADM would involve a large increase in the number and complexity of components, so practical implementation of either integrated or discrete versions may be challenging.

To improve cascadability and cost in systems with 40 or more wavelengths, broadcast-and-select WADDs based on WBs have been extensively deployed in

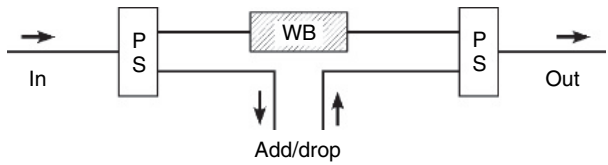

Figure 8.12 In this widely deployed WADD design, the wavelength blocker serves to block individual WDM channels to permit wavelength reuse. WB is a wavelength blocker and PS is a wavelength independent power splitter/combiner.

core networks. The WB is a component with one input fiber and one output fiber, capable of independently blocking or transmitting wavelength channels in any arbitrary pattern. It is assembled with wavelength-independent power couplers to construct a WADD, as shown in Figure 8.12 (see, e.g., Ref. [27]). The typical WB is a free-beam optical device actuated by an array of MEMS or liquid crystal (LC) cells. The add and drop fibers carry WDM signals, so external DMUX/MUX subsystems are needed for local add/drop. Per-channel equalization of express wavelengths is achieved by partial blocking, and colorless add/drop is possible with appropriate choices of DMUX and MUX. Building a PXC or multidegree ROADM with WB-based WADDs is possible, but the number of WBs needed scales as $J(J-1)$, where J is the fiber degree of the ROADM, making this an unattractive approach for ROADMs with $J > 3$.

To enable a smooth upgrade to multidegree ROADMs (see Section 8.5.3), WADDs based on WSSs are gaining in popularity [28]. The WSS is a component with three or more fibers that can be set to establish independent connections for each wavelength, from any input fiber to any output fiber. In a typical WSS, micro electromechanical systems (MEMS), or LC elements are used to steer a free-space beam for each wavelength toward its chosen connection. Although the free-space optics are intrinsically reciprocal, practical considerations such as beam control and back reflection mean that devices are usually personalized at the factory as either $1 \times M$ (multi-output) or $M \times 1$ (multi-input) versions. Either version, or both, may be used in a WADD, as shown in Figure 8.13. Values of M up to 10 and N up to 80 are commercially available, and per-channel equalization is provided. Since each WADD provides multiple drop fibers and multiple add fibers, construction of a multidegree ROADM is straightforward (at least from a hardware perspective) as shown in Figure 8.9. Incremental growth of the fiber degree J up to a maximum of $J = M + 1$ is also possible, using only J or $2J$ WSS modules (the additional degree is possible by eliminating loop back capability, so that signals input on one fiber pair can only be output on other fiber pairs). Steerable add/drop is automatically achieved by the design of Figure 8.9, in which an add/drop fiber pair is interchangeable with a line side pair. However, as fiber pairs are dedicated to steerable add/drop, the maximum fiber degree of the node is decreased proportionately. Thus, to guarantee a steerable 100% add/drop for all directions, one must reduce the maximum value of J to $(M + 1)/2$. Possible responses to this limit include: (a) develop

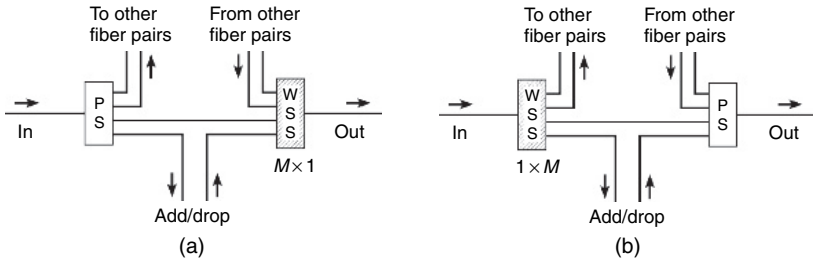

Figure 8.13 Two WADD designs based on wavelength selective switches (WSSs). Only variant (a) is East West separable under all WSS failure modes.

WSS modules with increased M; (b) provide power taps on each line fiber pair to provide some nonsteerable add/drop capability; (c) adopt a more complex multidegree ROADM for high-degree nodes; or (d) design the network so that 100% add/drop is not needed at locations with high fiber degree.

8.6.2 Designs for Colorless Add/Drop

Although colorless add/drop capability is highly desirable, cost-effective means for implementing the flexible MUX/DMUX are still under debate. For the WADD of Figure 8.5(c), which effectively incorporates fixed MUX/DMUX into the WADD itself, the only option is an external matrix switch. A two-degree ROADM based on Figure 8.5(c) would need four switches of dimension $N \times N$ to achieve 100% add/drop that is colorless but nonsteerable. If the add/drop is required to be steerable as well, two matrix switches of dimension $2N \times 2N$ are required. With recent progress that has reduced the cost and optical loss of such matrix switches, this could become a realistic option, at least for systems with $N \leq 40$. As noted above, this WADD is not attractive for multidegree ROADMs.

WADDs based on WBs or WSSs require external MUX/DMUX modules attached to their add/drop fibers. We first consider the drop side under the assumption that 100% add/drop must be supported. One early proposal was to use a $1 \times N$ power splitter followed by tunable filters, as shown in Figure 8.14(a). This approach is attractive for its simplicity and its pay-as-you-grow economics (see Section 8.5.3). If the first stage of deployment includes only a single dropped wavelength, only a single tunable filter need be installed. In practice, however, the large loss associated with the splitting process demands extra amplifiers in the DMUX chain, raising the cost and failure rate of the complete system and degrading the signal-to-noise ratio at the receiver. The performance demanded from the tunable filters is quite high and the cost at increasing drop fractions quickly becomes higher than other alternatives.

Colorless drop for WB-based and WSS-based ROADMs can also be realized by following fixed DMUXs with matrix switches, as shown in Figure 8.14(b). To

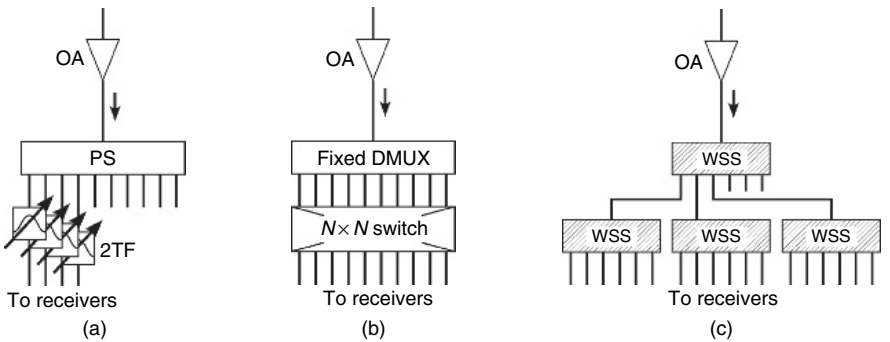

Figure 8.14 Three demultiplexing structures that achieve colorless operation of drop fibers. The labels 2TF, PS, OA, WSS represent two port tunable filters, power splitters, optical amplifiers, and wave length selective switches, respectively.

enable 100% colorless add/drop in a ROADM of fiber degree J, $2J$ matrix switches of dimension $N \times N$ are needed. Steerability may be supported by enlarging the matrix switches to dimension $JN \times JN$ (only two switches are then needed), or by consuming some fiber degrees of the ROADM for local add/drop, as discussed in connection with Figure 8.9.

Figure 8.14(c) illustrates a third approach to colorless drop, using $1 \times M$ WSSs as configurable DMUXs. Since M is usually less than N, a cascaded structure is needed to support 100% drop. For $M^2 \geq N$, a two-layer cascade is adequate. Depending on the split ratio N/M, the higher layer of the cascade could be a power coupler or a WSS. Assuming a two-layer cascade of WSSs, a ROADM serving $J/2$ line fiber pairs with colorless, steerable, 100% drop would employ $(J/2) \times (1 + N/M)$ WSS modules, showing the powerful incentive to develop WSS modules with higher values of M, especially when the wavelength count N is large.

Many variants and combinations of the three approaches outlined in Figure 8.14 have been devised, but no solution has yet achieved commercial dominance. Multiplexing structures for colorless add function are generally analogous to the demultiplexing structures, but there is a fundamental difference. Whereas the color of the light detected is determined in the drop demultiplexers, the wavelength of the light transmitted is determined in the transponder. Therefore, in systems with few WDM channels, it may be practical to implement a power combiner without tunable filters for the add function.

8.6.3 Separability and Failure Modes

As mentioned in Section 8.5.2, management of equipment failures is an essential part of NE design. A requirement that ROADMs have directional separability has far-reaching consequences on how ROADM elements are partitioned onto cards,

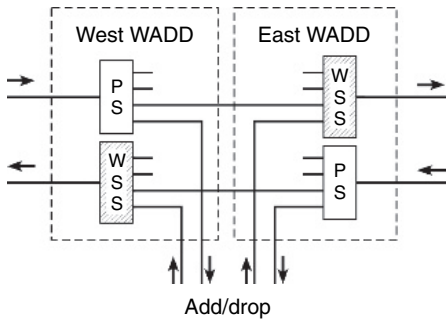

Figure 8.15 A typical scheme of partitioning WADD elements on separate line cards to achieve East West separability.

since all elements on a given card will be disrupted when the card is replaced. For example, if a booster amplifier drives an East-facing fiber, it cannot be packaged on a card with a preamplifier that receives traffic from the West. To assure separability, the WADD subsystems discussed above must be divided among two cards. A typical arrangement is shown in Figure 8.15. Somewhat surprisingly, the two WADD configurations of Figure 8.13 show different separability properties. Configuration (a) can be East West separable (with appropriate partitioning), since no failure of the WSS can disrupt both West-facing drop and East-facing add. Configuration (b), on the other hand, is not fully East West separable, since a WSS that transmits when it should be blocking a wavelength will disrupt the East-facing add (due to optical interference), even as it fails to drop the West-facing channel(s). If this "fail-to-white" condition and the related "fail-to-gray" state (i.e., some light is transmitted in the failed mode) are rare enough to be negligible, this conditional separability may be acceptable. This example highlights the importance of understanding failure modes of these new optical subsystems.

The WADD partitioning of Figure 8.15 can be applied to the multidegree ROADM design of Figure 8.9 to obtain a directionally separable solution. This simple definition of directional separability does present a problem for a shared transponder bank that uses steerable add/drop to serve multiple line fiber pairs. In this case it is wise to consider what drives the separability requirement that working and protection paths are not both vulnerable to the same single point of failure. This can be achieved by taking care when provisioning circuits to insure that the working and protection paths of any circuit are on separate transponder banks. Unfortunately, this solution may complicate the implementation of shared-mesh protection.

8.6.4 Underlying WADD Technologies

Although ROADMs have been built from discrete components, the cost, size, and performance targets of high-volume deployment will demand technologies

capable of a high degree of functional integration. For ROADMs of today and the near future, such integration is provided by PLC (Chapter 9 in Volume A), MEMS (Chapter 19 in Volume A), and LC technologies [28]. The PLCs of greatest interest for ROADMs are made up of index-guided waveguides fabricated on silica or related glassy materials. Passive devices such as fixed waveguide DMUXs and power splitters built from PLCs offer excellent accuracy, reliability, and fiber coupling. Tuning and switching functions are typically integrated as thermo-optic elements driven by microheaters integrated onto the PLC. A wavelength multiplexer with an integrated array of VOAs (often called a VMUX) is an example of a successful PLC product. In very large-scale integration, as needed for a 1×9 WSS, thermo-optically controlled PLCs can have problems with total power dissipation, thermal crosstalk among different elements, and polarization dependence. The basic element of LC technology is a variable optical phase delay. In combination with crossed polarizers, a switch/attenuator is realized. If a diffraction grating or PLC DMUX is used to spatially separate the wavelength channels of a WDM signal, an array of LC switch/attenuator elements can be used to construct a WB, and in fact such WBs have achieved significant commercial success. Although the LC switch is intrinsically a two-mode device, multiple LC phase-delay elements per wavelength can be used to achieve diffractive steering, enabling the LC-based WSS [15]. MEMS was the original technology used to build WSSs, and it is still the technology platform of most WSS vendors. An array of beam-steering mirrors, one per wavelength channel, is used to direct each wavelength to its appropriate input and output fibers. Diffractive steering with MEMS is also possible, but has been less popular to date. As of this writing, it is not clear whether the marketplace will ultimately prefer ROADMs based on LC technology, MEMS technology, or a hybrid of the two.

8.7 ROADM TRANSMISSION SYSTEM DESIGN

The design of ROADM-based fiber-optic transmission systems shares many common elements with traditional point-to-point transmission system design. Balancing the degrading effects of noise and nonlinear phenomena is still a fundamental driver for system performance. However, in ROADM systems the bandwidth management flexibility is another dimension that is traded off against longer reach. For example, the loss associated with internal ROADM elements can be significant and require additional amplification that leads to a corresponding reduction in the noise-limited system reach. The ROADMs can also add new forms of signal impairment such as bandwidth narrowing penalties associated with passes through multiple cascaded ROADMs. Along with new penalties, ROADMs can add complexity to the system design. For example, while point-to-point systems can be designed for a specific desired reach, ROADM systems must accommodate WDM channels with different reach requirements, as well as channels with overlapping lightpaths that start and end at different nodes. In this

section we describe the design elements shared by most ROADM-based transmission systems. In Section 8.9 we explore the additional challenges that arise when mesh networks are considered.

8.7.1 Designing for Reach Diversity

The ability to launch traffic from any ROADM node and drop traffic at any distance within the maximum reach capability creates a paradigm shift in transmission system design. Whereas previously the figure of merit for optical transport was the distance bandwidth product alone, in ROADM systems, the bandwidth management flexibility must be taken into account.

Traditionally, the system dispersion map, which describes the accumulated dispersion as a function of transmission distance, was designed to enable optimized transmission to a specified distance. A dispersion map can include some combination of dispersion precompensation at the channel add location, in-line dispersion compensation and dispersion postcompensation [29]. In some cases, system designers may intentionally introduce or allow large accumulated dispersion during transmission, to avoid nonlinear effects that are enhanced by the propagation of well-formed bit patterns and long dispersion walk-off distances [30]. While this can enable good performance for the design distance, additional signal conditioning may be required to drop a signal at an intermediate distance and the performance will not be optimized for that distance. Several strategies have been proposed to address the problem of add anywhere, drop at any distance dispersion mapping, which we divide into three categories: (1) optimization for shared singly periodic dispersion maps, (2) return to zero and doubly periodic dispersion maps, and (3) per-channel dispersion management.

A singly periodic dispersion map [Figure 8.16(a)] is characterized by a constant residual dispersion per span (RDPS). Although optimized transmission can be achieved by using different RDPS values for different transmission distances, fixed RDPS values that are optimized for all distances up to the maximum reach have also been identified [31]. Different combinations of pre- and postcompensation can be incorporated to facilitate a single RDPS. The RDPS can be chosen such that the positive dispersion walk-off of the RDPS balances the nonlinear shaping due to self-phase modulation along the transmission path. This soliton-like dispersion map design is effective for nonreturn to zero formats as well as return to zero formats that can be configured for dispersion-managed soliton propagation, and has been demonstrated in a variety of ROADM experiments and field trials [22, 32, 33].

In general, doubly periodic dispersion maps [Figure 8.16(b)] provide an extra degree of freedom that can be exploited to achieve improved performance over singly periodic maps, albeit at the cost of greater complexity. A doubly periodic map will use a constant RDPS through some number of nodes followed by compensation to a new value and the pattern repeats, thus accommodating a

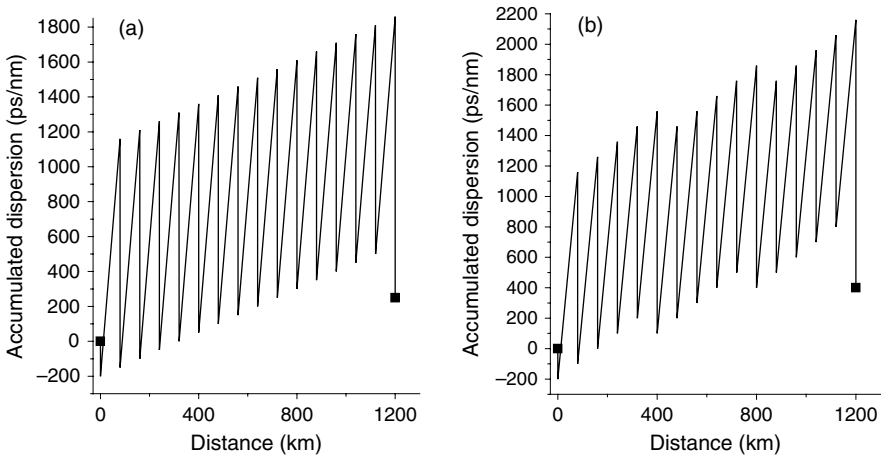

Figure 8.16 Examples of singly and doubly periodic dispersion maps for use in ROADM systems; (a) singly periodic dispersion map with 200 ps/nm precompensation, 50 ps/nm RDPS, and 300 ps/nm postcompensation and (b) doubly periodic map with 200 ps/nm precompensation, 100 ps/nm RDPS, 300 ps/nm postcompensation, and an additional 200 ps/nm after every five spans.

wider range of transmission constraints. However, a common approach is to use a large RDPS at amplifier repeater sites and then bring the accumulated dispersion back down to a target value at each ROADM node. Returning the dispersion to zero at each ROADM is attractive because each channel will have the same nominal dispersion at the add/drop location. Interchannel nonlinear interactions, however, are increased because the bits are re-formed and re-aligned. This effect is particularly problematic for the extreme case of returning the dispersion to zero (or any fixed value) after every span. Several methods have been proposed to reduce such nonlinear crosstalk by de-correlating neighboring channels. For interleaver-based ROADM architectures [as shown in Figure 8.5(d)], this de-correlation may come largely for free due to the inevitable path-length differences among even and odd interleaver branches [34].

Per-channel dispersion compensation can be viewed as an alternative to dispersion maps or used in combination with a dispersion map. Much attention has been focused on compensation at the optical transceivers. Both electronic and optical dispersion compensation have been implemented in commercial optical receiver modules and are considered extensively elsewhere (Chapter 18 in Volume A). A given technology will have a maximum amount of accumulated dispersion that can be compensated. When used without other compensation devices, this maximum range will limit the size of network that can be accommodated for a given transmission format and rate. When used with a dispersion map, per-channel dispersion compensation at the receiver will increase the tolerance to dispersion variations (see Section 8.8.1). Likewise, per-channel dispersion trimming along the transmission path can further mitigate accumulated

dispersion penalties, although at the expense of additional stand-alone single-channel compensation elements. However, integrating dispersion compensation into the WADD devices along with the power leveling capability would allow tuning at each ROADM node (see Section 8.7.2). Per-channel dispersion management also can be facilitated by modifying the optical transmitters. In one such technique distortion is applied to the transmitted waveform such that the waveform will be undistorted at the receiver [35]. This approach requires communication between the source and the destination nodes, and since the predistortion is path specific, the range of distances accommodated for drop and continue ROADM applications will be limited. Another approach is to apply a controlled chirp to the transmitted signal, which has an effect similar to using dispersion compensating fiber for precompensation [36]. As with postcompensation, these methods can be used with a dispersion map to provide greater tolerance to dispersion variations. Another alternative is to modify the modulation format and bit rate to achieve greater dispersion tolerance [37] (Chapter 2 in this volume). Recently, coherent receivers have attracted renewed attention because of their potential to provide electric field re-construction enabling one to correct for dispersion, as well as other sources of signal distortion (Chapters 3 and 4 in this volume).

Other dispersion management techniques, such as the use of nonlinear optical phase conjugators, have been proposed and are discussed elsewhere [38]. The most commonly used dispersion management method for transmission beyond a few hundred kilometers is the singly periodic dispersion map. Return-to-zero dispersion maps at every ROADM or at every span are sometimes used for simplicity, although at the price of reducing the transmission reach and power budget. More complex doubly periodic maps have generated research interest, but they generally do not provide sufficient improvement over singly periodic maps to justify their added complexity. Recently, per-channel dispersion management has been employed in 40 Gb/s transponders for transmission over in-line compensated links [22] and is commercially available at 10 Gb/s both for relaxing dispersion map engineering rules, e.g., Ref. [36] and providing transmission without broadband dispersion compensation [39].

8.7.2 ROADM Cascade Penalties

Signals transmitted through multiple ROADMs will accumulate additional penalties due to the ROADM transmission characteristics. The optical signal-to-noise ratio (OSNR) will be degraded due to optical losses and associated amplifier noise in the ROADM, which can be characterized by an effective noise figure. The effective noise figure is defined for each input port to output port path (including add and drop ports) as the noise figure of an equivalent amplifier used to replace the ROADM for that lightpath, with the same gain and noise performance. A multidegree ROADM core, as shown in Figure 8.9, will have 5 10 dB loss

associated with the WSS and another 6 9 dB from the passive drop split. In addition, power leveling in the WSS requires an average loss of at least ½ of the maximum peak-to-peak channel power ripple, 2 4 dB. This leads to a total loss in the range 13 23 dB, not unlike the loss of a fiber span.

Wavelength multiplexing and demultiplexing for both the wavelength add/drop and switching functions incur optical filtering. The details of the optical passband can impact the ROADM transmission performance. The passband must be sufficiently wide to accommodate the signal bandwidth over the full range of operating conditions, including the effects of spectral broadening due to fiber nonlinearities. Cascaded filtering results in a narrowing of the passband [28]. Figure 8.17 shows the passband narrowing of a WSS placed in a recirculating loop. Broadband ASE noise was incident on the input to the loop and subsequently shaped by each pass through the WSS. In Figure 8.17, the passband ripple growth is proportional to the number of ROADMs traversed because the filter shaping is identical with each pass. For most practical ROADM systems, the passband ripple will grow more slowly because the filter shape will vary for different ROADMs. In general, with transmission through multiple ROADMs the signal bandwidth will tend to broaden due to nonlinearities while the cascaded ROADM bandwidth narrows. The resulting transmission penalty is a complicated function of the interaction between the ROADM filtering and the signal spectral shaping. It will depend on the details of the system design, such as modulation format and dispersion map, as well as the filter characteristics of the ROADMs. System studies have shown both positive and negative impact from cascaded filtering [40 42]. In addition to the amplitude response, the group-delay ripple,

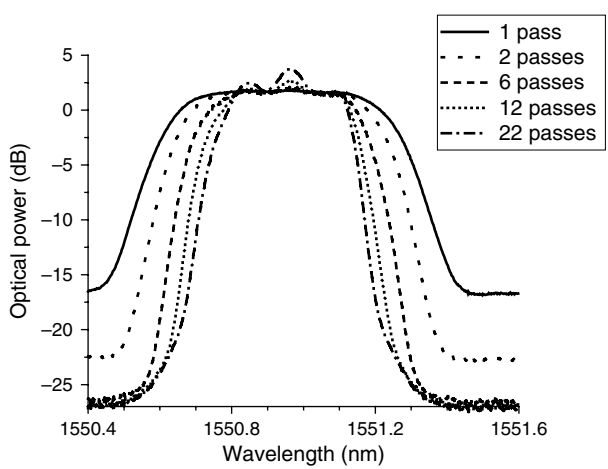

Figure 8.17 Filter narrowing due to multiple passes through a wavelength selective switch (WSS). The noise floor is due to an amplifier after the WSS and the slight broadening below 20 dB is due to the accumulated ASE from many passes.

polarization-dependent loss, and polarization mode dispersion need to be characterized over the full passband.

Channel crosstalk is another parameter that must be carefully controlled in ROADM design. Crosstalk can be separated into in-band and out-of-band, as well as coherent and incoherent. In-band crosstalk is taken relative to the receiver bandwidth and includes any corresponding beat terms that fall within this bandwidth. In-band crosstalk can result in signal signal beating on the one bits, in general inducing the largest penalties [43]. This beating is also polarization and signal quality dependent and will be worse if the interfering signal is a coherent copy of the original signal. In contrast, out-of-band crosstalk contributes a uniform background noise due to the total CW light detected. Primary sources of crosstalk in ROADM systems (Figure 8.18) include in-band interference due to channel blocking leakage, neighboring channel interference due to WDM channel filter leakage, and in-band multipath interference. The worst-case crosstalk transmission penalty will typically grow linearly with the number of occurrences at low crosstalk levels. However, the penalty depends on many factors including the characteristics of the signal and interferers (bit rate, modulation format, extinction ratio, OSNR, etc.) [44 46]. Therefore, one characterizes the worst-case penalty $p_{1\text{pass}}(\varepsilon)$ as a function of the crosstalk power to signal power ratio ε, and then scales ε by the worst-case number of occurrences expected within the network, N, to determine the estimated penalty for transmission margin allocation: $P_{\text{crosstalk}} = 10 \log[p_{1\text{pass}}(N\varepsilon)]$. Usually $P_{\text{crosstalk}}$ is chosen to be a small value and this result is inverted to determine the required crosstalk rejection ratio ε for a given $P_{\text{crosstalk}}$ and N. In some systems, the precise dependence of the penalty with N may need to be determined through careful measurements. With on the order of 10 interferers, less than 1 dB penalty is typically obtained for crosstalk rejection ratios in the range of 10^{-3} 10^{-4}.

In-band multiple interferers due to channel blocking leakage is often the limiting case for ROADM crosstalk, particularly in mesh systems. When a channel is first added to the system, upstream traffic at that wavelength must be blocked. At each subsequent node, traffic at the same wavelength incident from a different input port, also must be blocked to express the channel of interest. Thus, for each ROADM that a signal cascades through there may potentially be traffic on the same wavelength that is blocked and thus a potential source of crosstalk if the

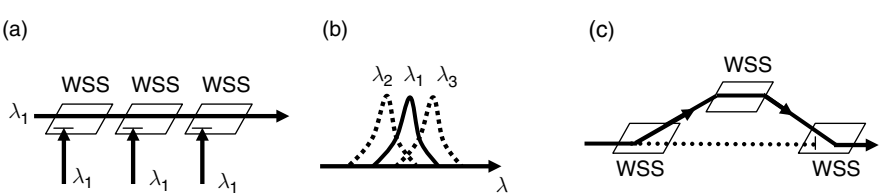

Figure 8.18 Sources of crosstalk in ROADM systems: (a) in band multiple interferers, (b) WDM neighboring channel filter leakage, and (c) in band multiple path interference.

ROADM blocking is not adequate. On the other hand, encroachment from neighboring channels is more of an issue related to the filter function. For the tight channel spacing, steep filter skirts will reduce crosstalk while minimizing the filter narrowing. Multipath interference (MPI) is a general problem in transmission systems. For the mesh systems, one has the additional source shown in Figure 8.18(c) in which different mesh lightpaths can lead to MPI, although this tends to be an infrequent source that is usually avoided due to the strong blocking required for the multiple interferer problem. MPI can also exist within ROADM components. Stray light scatter in the optical switching and MUX/DMUX elements can lead to MPI effects, which will occur with each ROADM pass and can be coherent. The crosstalk rejection of ROADM components is tested across the full channel passband. Often, the rejection is not uniform across the passband and the worst case may not reflect the channel performance because it is not present over the full passband. An appropriate weighting function can be incorporated to help relax the rejection requirements in these cases [47]. The behavior of crosstalk with channel attenuation must also be understood, since WBs and WSSs often provide a channel equalization function (see Section 8.5.5). In particular, some WSS designs can develop undesirable passband sidelobes when attenuated, e.g., due to diffraction effects. If present, these sidelobes must be accounted for in the system design. Ideally, the crosstalk rejection of ROADM components would be tested over all possible device configurations, but the large number of configurations for a WSS may render it impractical to characterize every device shipped in this way.

A promising approach for managing the limitations of the ROADM passband is to use WADDs that support channel passband adaptation. Recently, WSS devices have been introduced that can allow for variable channel spacing and passband width [15]. This capability could be particularly beneficial for supporting networks with mixed bit-rate and/or modulation-format signals. The WSS passband can be adapted to the width required for the different signal bandwidths or possibly even for different transmission distance/ROADM pass-through requirements. Furthermore, adaptation of the dispersion and optical loss across the passband has been demonstrated [48, 49], allowing for functionality such as dispersion compensation and optical signal equalization within the WADD.

8.7.3 ROADM System Margin Calculations and Planning Tools

Transmission margin calculations for ROADM systems will take into account additional penalties due to the ROADM transmission characteristics, and penalties associated with reconfiguration and transparency. Table 8.2 is a sample margin allocation table for a WDM 10.7 Gb/s non-return-to-zero, on-off keyed (NRZ-OOK) ROADM system with a maximum transmission distance of 2000 km and up to 15 ROADM passes. This table relates the received OSNR requirement for a system to the OSNR required in a back-to-back case. Note that the specific values

Table 8.2

Sample margin allocation table for a ROADM transmission system (10.7 Gb/s NRZ-OOK, 2000 km, 15 ROADMs).

Line	Parameter	Value or penalty (dB)
1	Back to back required OSNR for BER 10 ^{3}	10.0
2	Transmitter/Receiver mismatch between vendors	0.5
3	Nonlinear transmission penalty (single channel)	1.0
4	Interchannel crosstalk penalty (WDM)	0.5
5	Polarization mode dispersion penalty	1.0
6	Dispersion slope penalty	0.5
7	Penalty due to channel power ripple and tilt	0.5
8	Polarization dependent loss (including ROADM PDL) penalty	0.5
9	ROADM in band crosstalk penalty	0.2
10	ROADM optical filtering penalty	0.2
11	ROADM network dispersion walk off/error penalty	1.0
12	ROADM power control inaccuracy	0.5
13	Aging and repairs	1.5
14	Total margin allocation	7.9
15	Required EOL minimum received OSNR	17.9

and penalties will depend sensitively on the details of the system design and the numbers used here do not correspond to any particular system, but rather indicate possible values. Penalties on lines 2 8 are common to most transmission systems; whereas the penalties on lines 9 12 are unique to ROADMs. An overview of margin allocation for common transmission penalties can be found in Ref. [50]. Starting from the back-to-back transceiver required OSNR, the transmission penalties and margins are applied to determine the minimum received OSNR for the channel at its drop location. If the predicted end of life (EOL) delivered OSNR of a channel along a particular lightpath falls below the EOL minimum required OSNR on line 15, then the channel will need regeneration at an intermediate site to be provisioned along that connection.

If the penalties vary significantly between different network configurations, then multiple margin tables can be used to cover the different cases. For example, separate margin allocation will typically be provided for 10 and 40 Gb/s transmission cases. Separate margins may also be used for different fiber types or channel spacing. The penalties will correspond to the maximum value for transmission up to a particular distance and number of ROADM passes. Clearly a wide range of different distances and ROADM passes could be specified. However, including a broad range of system configurations in the margin allocation may unnecessarily increase the margins. The use of a planning tool can help to tighten the margins by calculating unique penalties for the different configurations.

Network planning tools have gained increased attention in ROADM systems to automate the complexity associated with the system engineering rules. These tools

are used to optimally select equipment and also provide wavelength assignment and routing to minimize regeneration and cost. This includes incorporating differences in the margin allocation for each channel along its transmission path. These differences can be implemented as unique fixed values as in Table 8.2 or using algorithms to determine the accumulated penalty along the channel path. The planning tool can also be used to calculate the OSNR along the channel path to estimate whether the channel will reach its drop location and identify regenerator locations. Recently, there has been much interest in defining quality of transmission functions to estimate channel performance in planning tools [51]. These algorithms can be derived from detailed off-line simulation results covering the range of channel performance expected in the system and often accumulated over many months. The algorithms should then be validated against simulations and laboratory measurements of specific test cases [52]. Planning tools may include a suite of physical layer channel management and system configuration modules that in some cases intersect with network management software [53]. Planning tools are considered in more detail in Chapter 20 of this volume.

8.7.4 WDM Channel Power Management

Perhaps the most significant impact of ROADMs on transmission system design is related to the WDM channel management aspects. In opaque networks, the channels are terminated at every node and the optical powers at the outputs of a node are generated by new transmitters and therefore decoupled from the optical power at the node inputs. The optical transparency engendered by ROADMs provides a continuous optical connection between the node inputs and outputs to enable selected channels to transparently bypass the node. This can potentially create optical coupling through the entire network. The system design must manage this coupling to prevent effects adverse to the system performance. A combination of architectural choices together with appropriate power control mechanisms can ensure stable system operation.

Steady-State Channel Power Control

Transmission control can be segregated into steady-state and transient modes. Steady-state algorithms maintain the state of the system at or close to the optimum transmission parameters and manage planned transitions between such states, e.g., when new channels are provisioned. The steady-state control in ROADM systems is similar to the transmission control used in traditional point-to-point systems. Channel power levels are maintained near their designed targets and amplifier pump settings adjusted for minimum noise figure. The use of ROADMs, however, also introduces some unique requirements on the steady-state system control.

The power of WDM channels will evolve along the transmission path due to both time- and wavelength-dependent variations in the transmission spectra of the system components and fiber plant. Deviation of the channel power from the target value will lead to a penalty that increases with distance. Furthermore, the receiver will tolerate a range of input powers beyond which signal penalties will accrue. For short transmission distances, the receiver power tolerance will limit the allowable power error. Beyond a certain distance, the transmission impairments will dominate. In point-to-point links, deviations in WDM channel power are often characterized by a total power or average channel power error and channel power ripple and tilt. In ROADM systems there will also be a channel group power error, corresponding to groups of channels that originate from different node inputs and add ports. Changes in the total output power of an amplifier on a ROADM add path, e.g., will result in a power error unique to that group of add channels. Channel power interactions due to amplifier characteristics or fiber nonlinearities (notably stimulated Raman scattering) may cause this error to be transferred to other groups of channels.

Much of the channel power error can be accommodated by tuning the amplifier settings. These steady-state amplifier adjustments in ROADM systems are complicated due to the variability of the channel assignment. In point-to-point systems, wavelength channels can be turned up in a controlled pattern to minimize the impact on amplifier performance and simplify the amplifier control. In ROADM networks, the growth pattern implemented on a particular add port will be constrained by the wavelengths of channels already present from upstream nodes. Since the network must accommodate the unpredictable growth patterns of local traffic, it becomes important to maintain the target power levels and amplifier noise figures in the presence of arbitrary channel configurations. This can be a challenging task as the maximum number of channels supported by the system increases. Arbitrary channel configurations also complicate the detection of a loss of signal condition. Monitor photodiodes must be able to distinguish between the power of a single channel vs the total ASE noise power with no channels present. As the number of channels increases, allowing for a single channel at any location in the spectrum and allowing for the worst-case ASE growth can make discrimination difficult. Blocking unoccupied upstream channels will help to minimize ASE accumulation; however, one must still account for the maximum number of high loss spans between ROADMs.

Optical amplifiers in high-capacity ROADM systems are operated with some level of gain saturation. EDFAs are strongly saturated with gain compression similar to or greater than the range of channel loading [54]. Raman amplifiers will be mildly saturated, such that the gain will change <5 dB for the maximum variation in the number of input channels, even up to >100 channels [55]. Therefore, in each case, the amplifier must be adjusted to maintain a constant channel output power as the number of the input channels is varied. The channel power can be regulated by using either constant gain or constant output power control. In ROADM systems, amplifiers are usually operated with constant gain to allow for potentially large unplanned

variations in channel loading, including those due to power transient events (see the section on Transient Control below). Constant power can be used if the unplanned changes in channel powers are within the system power tolerance or if other techniques are used to minimize the impact of gain saturation, such as using saturating lasers [56] or gain clamping [57]. Even with constant gain control, however, an amplifier will exhibit a constant power response until the action of the control system can adapt to a rapid input power change.

In ROADM systems, the amplifier control is complicated by the wavelength dependence of the channel loading. Here we focus on EDFA control, which is predominantly used in today's optical communication systems. With a single-channel growth pattern, e.g., adding channels from the shortest to the longest wavelength, and a flat input channel power spectrum, the gain and total output power for a single EDFA stage will come close to a one-to-one relationship with the pump power, simplifying the control design. However, for arbitrary channel loading the required pump power becomes a complicated function of the channel spectrum. In the example of Figure 8.19, the control process gain, defined as the pump power to total output power transfer function, is mapped out varying the EDFA input power by changing the number of channels at the input from 32 to 1, either starting from the long-wavelength end or from the short-wavelength end [58]. This single pump input stage amplifier is designed to operate with a 10.4-dB gain to yield a flat output spectrum using the gain-flattening filter. These results illustrate the wavelength dependence of the control gain and the amplifier gain saturation. For a given pump power, the control process gain will vary linearly with input power (on a linear scale) following a slope equal to the signal gain divided by the pump power, if the amplifier is linear. The fact that the amplifier control process gain is not constant indicates that nonlinear control techniques are necessary for optimal performance and the nonlinear parameters must account for differences due to different channel configurations. Such methods for characterizing amplifier behavior take into account the channel loading dependence. Besides the control process gain, another important parameter is the gain saturation measured as a function of channel loading, referred to as the channel gain saturation [59]. This quantity is more relevant to ROADM channel power dynamics than the amplifier gain saturation, which is typically measured as a function of total input power for a single reference channel configuration [60].

For a given mode of amplifier operation, constant gain or constant power, there will be different forms of channel power coupling that will impact the steady-state system control. For ROADM systems such coupling is particularly important with respect to the power control of channel groups associated with different mesh paths. These coupling mechanisms were first studied in constant power operation, typical of point-to-point systems. In the case of ideal, complete saturation, the total output power is a constant and equal to the product of the gain and the sum of the per-channel input powers. Assuming a flat gain spectrum with gain G, the total output power can be written in terms of the total input power P_{in}: $P_{\text{T}} = GP_1 + GP_2 = G[(1 \quad \eta)P_{\text{in}} + \eta P_{\text{in}}]$, where η is the fraction of input power (or channel

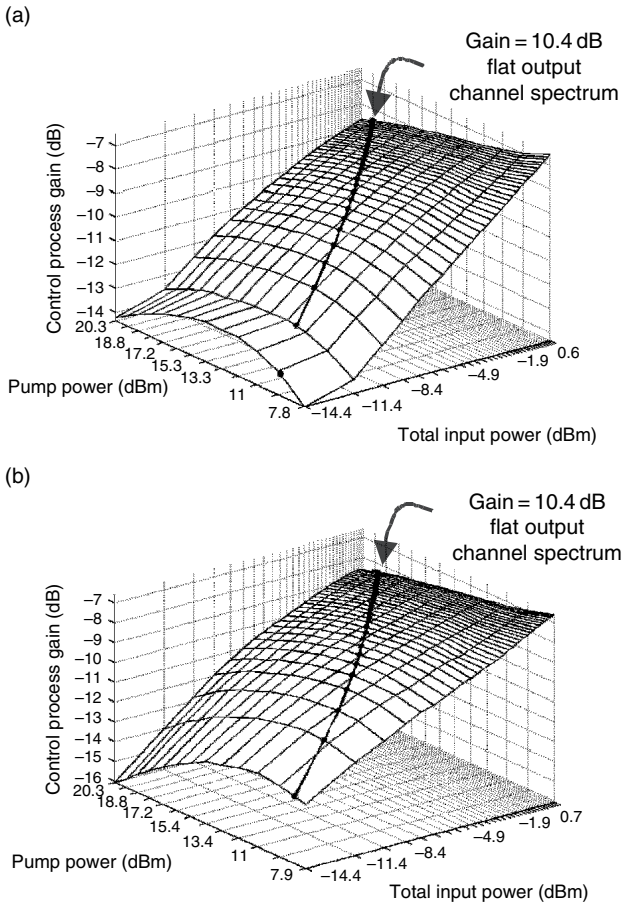

Figure 8.19 Control process gain ($k \quad P_{out}/P_{pump}$) for the input stage of a 32 channel WDM line amplifier (a) dropping channels from long to short wavelength and (b) from short to long wavelength; each input power grid line corresponds to a particular number of channels: 14.4 dBm corresponds to one channel, 11.4 corresponds to two channels, etc (this figure may be seen in color on the included CD ROM).

number if the input channel powers are equal) initially in the second of two groups of channels, represented by total group input powers P_1 and P_2. If the first group of channels is adjusted in power by a factor f, P_T will remain fixed and the total group output power in channel group 2 will become [61]:

$$P_{o2\,(dB)} = 10\log(G'\eta P_{in}) = 10\log(\eta P_T) - 10\log[\eta + (1-\eta)f] \qquad (8.3)$$

due to the change in $G \rightarrow G'$ required to maintain constant P_T. For the case that one channel group is completely dropped, $f = 0$ and $P_{o2\,(dB)}$ is increased by the usual

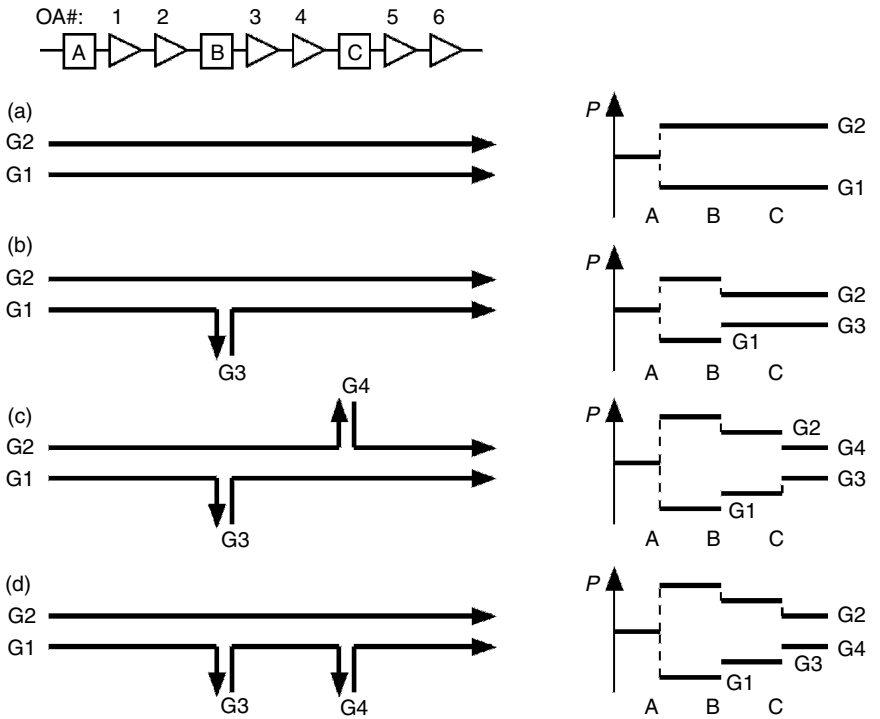

Figure 8.20 Channel power deviations for constant power amplified ROADM systems. As channel group G1 is reduced in power, (a) positive excursion occurs on neighboring channels G2 through a first order interaction; (b) second order interaction creates negative excursion in G3; (c) third order interaction creates positive excursion in group G4; (d) first , second , and third order interactions with groups G2, G3, and G4; the plots on the right hand side illustrate the group power deviations as a function of distance corresponding to the add/drop patterns.

factor of $10\log\eta$. The impact of such channel power coupling in constant power networks is illustrated in Figure 8.20. In the ideal case and neglecting tilt, this effect is modified by the addition or deletion of channel groups, but does not vary with the number of amplifiers. As new groups of channels interact with groups carrying a deviation, higher products of the channel power/number ratio will appear and we refer to these successive interactions as being high order. Examples of first-, second-, and third-order channel power interactions are shown in Figure 8.20. From Figure 8.20 it is evident that the channel group power deviations decrease with higher order coupling. If more than two channel groups are involved, then additional features can be observed. Power coupling will only occur if the total power at the input to an amplifier changes. Thus, for case (b), if group G1 was not dropped at node B, then group G3 would be unaffected. The power deviation on group G1 was compensated by group G2 and the total input

power to amplifier number three would remain unchanged. This effect can lead to situations in which a power error shared by groups of channels can propagate through a network without impacting other channel groups until an affected group reaches its drop location. Furthermore, dropping groups of channels from a set that are influenced by a particular interaction, will result in a larger deviation for the remainder of the channels in the set, because the channel fraction η will decrease. Finally, it is important to note that if all of the channels at the input to an amplifier experience the same power deviation, then the constant power condition of the amplifier will remove the deviation and reset the channels to their correct power levels.

While the simple configurations in Figure 8.20 are useful to understand how groups of channels interact, in practice, very complex channel configurations may exist and numerical simulations are required to evaluate the dynamics. Figure 8.21 shows results from a simulation of a 64 ROADM node linear chain interconnected by single transmission spans (modeled as a simple loss element) and ideal constant power amplifiers [61]. Channel groups with a mean of four WDM channels were added and dropped between different ROADM nodes up to a maximum of 128 WDM channels per link. The channel groups were randomly distributed in wavelength, location, and distance such that the mean number of hops was 9 and the full-width at half-maximum was 2.5. A 3-dB power drop was applied to all of the add channels at a given node and the resulting power deviation ($\Delta P/P$) of the other channels as a function of hops from the event location is plotted after averaging over results from events occurring at every node. The deviation falls off rapidly with distance beyond the mean demand length as expected from interactions of the type illustrated in Figure 8.20. Here the absolute value of the deviation is plotted and the sharp dips correspond to sign changes as seen in Figure 8.20(c) such that the periodicity of the full oscillation is equal to the mean demand length. These features soften as the channel distance distribution broadens. Similar behavior

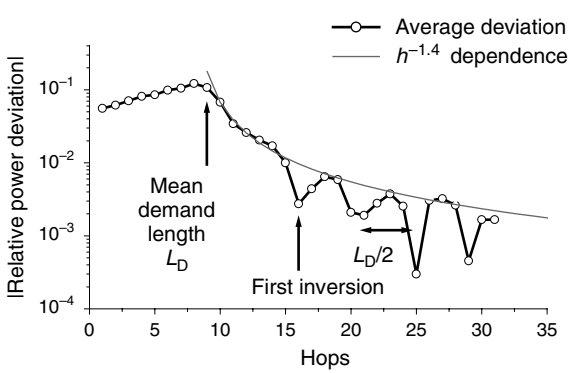

Figure 8.21 Simulated power deviations in a constant power amplified 64 node degree 2 ROADM system as a function of hop distance from the initial event location (this figure may be seen in color on the included CD ROM).

was found in simulations for which the ideal amplifiers were replaced by EDFAs operating in deep saturation typical of transmission systems [61].

Although constant gain control was shown to mitigate the channel power coupling in early constant power experiments, gain ripple and tilt can give rise to coupling in constant gain amplification systems [62]. The impact of gain ripple and tilt can be understood by considering two groups of channels occupying different portions of the amplifier gain spectrum. Groups with total group input powers P_1 and P_2 experience different gains G_1 and G_2, respectively. A constant gain controlled amplifier maintains the total power gain such that $G = (G_1P_1 + G_2P_2)/(P_1 + P_2)$ is constant. For $G_1 \neq G_2$, cross-coupling will occur when P_1 and P_2 are adjusted independently. For $G_1 > G_2$, an increase in P_1 will result in a change in the amplifier's total output power that is greater than the change in the total input power. As a result, the amplifier gain must be reduced to maintain constant total power gain. This gain change impacts both the channel groups and can result in additional gain tilt or ripple. We can write the individual group gains as $G_{1,2} = fG_{A0}g_{1,2}t_{1,2}$, where G_{A0} is the nominal amplifier total power gain, $g_{1,2}$ is the nominal gain ripple and tilt, $t_{1,2}$ is the gain dependent tilt, and f is the change required to maintain constant total power gain G. For an EDFA, the tilt is a function of the gain through the amplifier inversion level, and therefore it will also change, potentially exacerbating or mitigating the effect through the factor $t_{1,2}$. Unlike the channel power deviations in constant power amplifiers, the resulting errors in G_1 and G_2 grow linearly in cascade, modified by amplifier saturation and fiber nonlinearities.

Other mechanisms can also contribute to channel power coupling. Depending on the power and the number of channels (i.e., range of channel wavelengths), short-wavelength channels transfer power to longer wavelength channels through stimulated Raman scattering in the fiber. Also, there can be errors in the amplifier automatic gain control algorithm due to electronic noise and power measurement inaccuracy (usually only a potential problem in systems that require a large power adjustment dynamic range), optical noise (ASE) that contributes to the total power [63], spectral hole burning, and other nonlinearities in the amplifier [64 67]. Figure 8.22 illustrates how gain error in the automatic gain control can potentially evolve over distance and time when compensating for power changes on one channel group (G1) relative to another channel group (G2).

In addition to modifying amplifier settings, the steady-state control algorithm will tune control devices that often have much longer response times than the amplifiers. For example, the channel power attenuation in the WADD device may require one second or longer to adjust a full set of channels. Furthermore, the steady-state control algorithm must propagate from node to node around the network. In part because of the channel power coupling mechanisms mentioned above, the adjustments made at one node can influence adjustments at other nodes. Therefore the settling time for a steady-state control algorithm can be quite long, depending on the size of the system. For this reason, a separate fast control mechanism is often implemented.

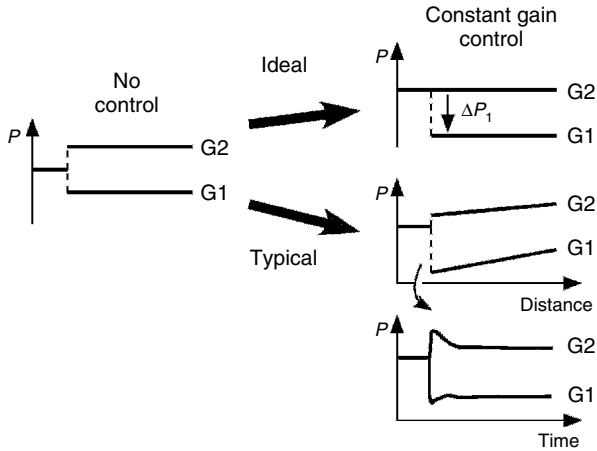

Figure 8.22 Ideal constant gain control of a saturated amplifier provides linear amplification and maintains the output power of the channels in group G2 at their target when channel group G1 falls below its target power by ΔP_1 (dB). In practice, both the channel groups will experience a finite gain error that varies over distance and time.

Transient Control

A fast control algorithm is implemented in ROADM systems to handle rapid and potentially large variations in channel power, e.g., due to fiber cuts. This form of transient control will suppress the channel performance degradation that may occur between the time of the fault and the time required for the steady-state control to adapt. In EDFA systems, transient control is usually implemented through a constant gain amplifier fast control algorithm. The speed required of the amplifier control is determined by the minimum rise time of the channel power excursions during transient events. If a set of channels loading an amplifier is rapidly removed, the remaining or surviving channels will increase in power due to the amplifier saturation as described above [68]. In Figure 8.23(a), the power excursion experienced by a surviving channel due to a 16 8 channel drop is shown for a cascade of 6 amplifiers [69]. Figure 8.23(b) shows maximum derivative of the rising edge of the excursion as a function of the number of amplifiers in the cascade. It is well known that the slope of the rising edge of the EDFA gain transient response will increase linearly in cascade according to [70]:

$$\dot{G}_n(0^+) \sim -\sum_{j=1}^{n} \Delta p_j^{in} g_j(0), \tag{8.4}$$

where G_n is the logarithmic gain of the nth amplifier, Δp_j^{in} is the change in input power for amplifier j, and $g_j(0)$ is the linear amplifier gain immediately prior to the event. Notice, however, in Figure 8.23(a) that the size of the excursion also varies

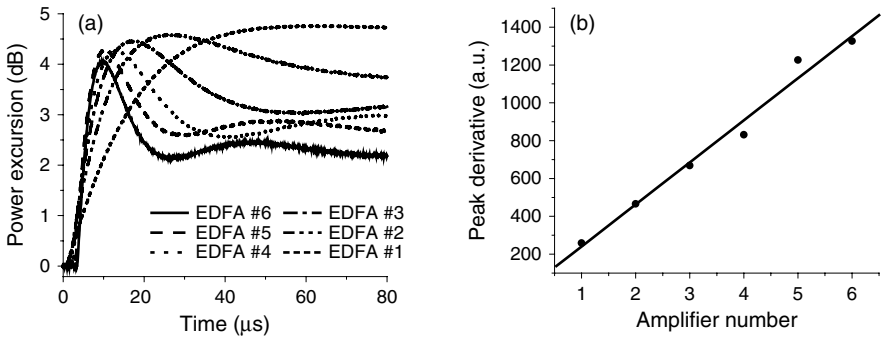

Figure 8.23 (a) Channel power excursion in an uncontrolled EDFA cascade experienced by 1 of 8 surviving channels after a drop from 16 to 8 channels. (b) Peak slope of rising edge grows linearly with number of amplifiers.

in the cascade; this is due to channel power tilt and ripple. The same power coupling and gain errors discussed above for the steady control will also apply for the transient control. For these experiments there was no transmission fiber. If transmission fiber and DCF were included, the response would be further modified by the nonlinear interactions in the fiber.

The transient response in Raman amplifiers has several strong differences from the EDFA response. Figure 8.24 shows the uncontrolled transient response of an all-Raman amplified recirculating loop for surviving channels at the long- and short-wavelength ends of the spectrum [71]. The power excursions have been normalized to the final power after the event and correspond to the input of the indicated span number. Each transmission span consists of co-propagating

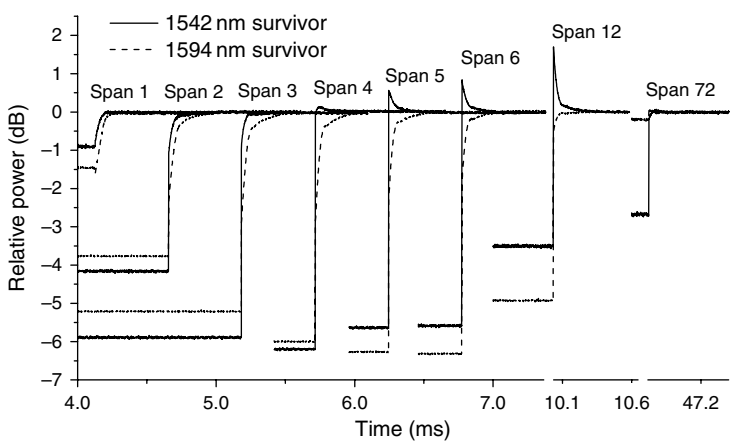

Figure 8.24 Surviving channel power excursions in an uncontrolled all Raman amplified recirculating loop system following a 109 16 channel drop with 50 GHz spaced channels.

and counter-propagating multipump amplifiers in the span and counter-propagating multipump amplifiers in the DCM fiber. The maximum power excursion is not reached until the input to the fourth span. Each of the three line amplifier types is characterized by a different characteristic response time. The DCM and span counter-pumped amplifiers create the double exponential rise evident on the curves from the long-wavelength channel at spans 3 and 4. The co-propagating pump and Raman channel interactions act on nanosecond time scales and result in the sharp edges. In the case of the short-wavelength channels, the co-propagating pump and channel Raman interactions add to create an overshoot, whereas the opposite is true for the long-wavelength channels. Beyond span 6, the growth of ASE noise reduces the power change and creates channel tilt.

Due to the large power excursions shown in Figures 8.23 and 8.24, amplifiers in ROADM systems are typically operated with constant gain control for fast power transient mitigation [72]. Both the Raman and the EDFA amplifiers are commercially available with fast pump power control to maintain constant gain. Feed-forward pump control was shown to be particularly effective in EDFAs to suppress the initial overshoot response [73]. Other EDFA techniques include replacing the lost signal power with power from additional control signals or counter-propagating signals and gain clamping methods [56, 57]. As noted above, spectral hole burning in EDFAs, which results in channel wavelength- and power-dependent gain variations, was shown to lead to significant gain error in long distance transmission [64 66]. EDFA amplifier control does not correct tilt variations due to interchannel Raman interactions in the transmission fiber. Fast tilt control techniques have been investigated to correct for Raman tilt errors [67, 74]. A variety of techniques have also been proposed for transient control in Raman amplifiers [75, 76], including multipump algorithms [77].

The responses in Figures 8.23 and 8.24 correspond to a simple amplifier cascade and not in general to the response of a network with ROADMs, in which channels are added and dropped all along the transmission path. As with the steady-state power errors discussed above, transient effects may be transferred from one channel group to another, persisting to other portions of the network in which the channel loading did not change [69]. In principle, such transient effects could propagate beyond the reach of any single lightpath. For example, the EDFA cascade used to obtain the results in Figure 8.23 was modified such that after the first two amplifiers in the cascade, all of channels that are cut in the transient event are dropped at a ROADM between amplifiers 2 and 3. However, the surviving channels continue and a new set of eight channels is added, maintaining amplifiers 3 6 at constant channel loading during the transient event [as in Figure 8.20(b) for the case that group G1 is cut upstream]. However, the positive power excursion of the surviving channels stimulates a negative power excursion in the channels that add at the ROADM (Figure 8.25). Several features of this response are important for transient control in ROADM systems: (1) the rising edge of the original surviving channels no longer steepen, (2) the magnitude of the power excursion

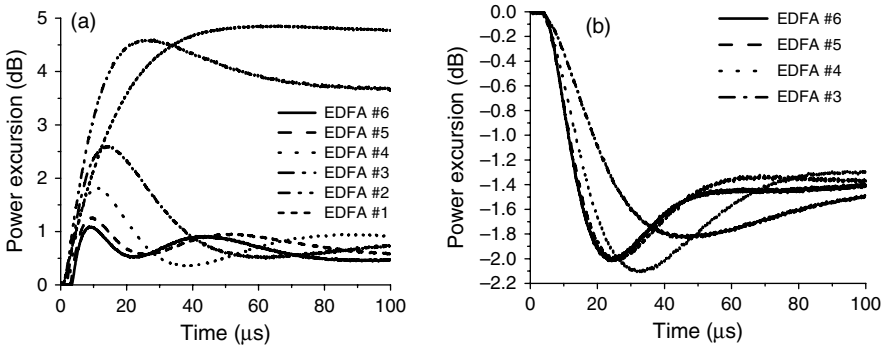

Figure 8.25 (a) Power excursion in an uncontrolled EDFA cascade experienced by 1 of 8 surviving channels following a 16 8 channel drop with channel reconfiguration after the second amplifier (as in Figure 8.20b). (b) Power excursion on 1 of 8 channels added after second amplifier due to second order channel power interaction.

is reduced, being shared with the add channels to maintain constant power, and (3) the falling edge of the add channels steepens; however, it is bounded by the maximum slope of the rising edge of the surviving channels. Feature (3) is also true for the rising edge of the surviving channels relative to the falling edge of the cut channels. The consequence of (1) and (3) is that the control response time need only be as fast as the longest path shared by two independent channel groups in a transient event. No further steepening will occur. From (2) it is seen that the magnitude of the transient event will damp out in ROADM systems with a constant power constraint, both simplifying the power control and mitigating the propagation of power excursions.

8.8 ROADM NETWORKS

The use of ROADMs in mesh configurations requires additional considerations due to the complexity of optically transparent mesh networks. These issues include mesh dispersion map walk-off, wavelength routing, and mesh power control.

8.8.1 Optically Transparent Mesh Transmission Issues

Transmission in optically transparent mesh systems is a new topic of research. Much of the work to date has involved straight-line transmission experiments with mesh NEs such as ROADMs introduced to quantify the additional element penalties [27, 78]. Due to their size, mesh systems are difficult to study both from a computational [79] and a hardware point of view. Conventional recirculating loop experiments are well suited for the study of point-to-point systems. To study mesh-related effects, transmission experiments have been carried out using multiple

interconnected recirculating loops [80, 81]. Another approach has been to use large laboratory experiments or field trials [22, 72, 82]. Recently, the issue of mesh dispersion map walk-off was studied using a dynamically reconfigurable recirculating loop experiment and is discussed below as an example of the types issues currently under investigation [83].

Dispersion map design will usually incorporate some allowance for deviations from the map. As mentioned in Section 8.7.1, these deviations can result from span dispersion measurement uncertainty or error and from systematic errors due to the dispersion slope across the band and granularity of available DCMs. In addition to these errors, in mesh systems a dispersion walk-off can occur due to intersecting line systems at nodes with degree greater than 2. Consider, e.g., a degree 3 ROADM for which the channels at one input have a span compensation error of 3 km because the closest available DCM value corresponds to spans 3 km longer than the span on the input. Suppose that the channels at the other input port experience a -4 km under compensation, again because of the DCM granularity. If the ROADM has only the first input port, then the compensation on the span at the ROADM output would be chosen for a target 3 km shorter than the actual span to correct for the compensation error on the previous span. Notice that this introduces a one time -3 km error on the add channels at the ROADM, even for a degree 2 ROADM. However, the channels on the second input port would experience a -7 km error because of the original error at the input plus the compensation for the other ROADM input port. This error can continue to grow with each ROADM for which the path of interest is not chosen for compensation at the ROADM output. Therefore, this walk-off must be included in the transmission penalties for a mesh design and will depend on the size of the DCM value granularity.

Experimentally verifying the system performance under conditions of DCM granularity can be challenging since many ROADMs would be required for a full system implementation. Recently, a dynamically reconfigurable recirculating loop was used to quantify transmission performance in the presence of compensation granularity error and walk-off [83]. Fast switches were placed at the output of each span so that different spools of fiber could be selected for the end of each span, varying the span length, while maintaining constant DCMs at mid-stage on each of the amplifiers at the span output. The switches were operated synchronous with the recirculating loop loading switches such that 34 different dispersion maps could be realized. Figure 8.26(a) shows the maps and corresponding required OSNR for a BER of 10^{-3}. Figure 8.26(b) shows the corresponding required OSNR as a function of the mean RDPS over 24 and 28 spans, with the mean taken over 28 spans.

8.8.2 Wavelength Routing and Assignment

Wavelength routing and assignment in mesh networks is a challenging optimization problem [84]. A full account of the issues and literature is beyond the scope of

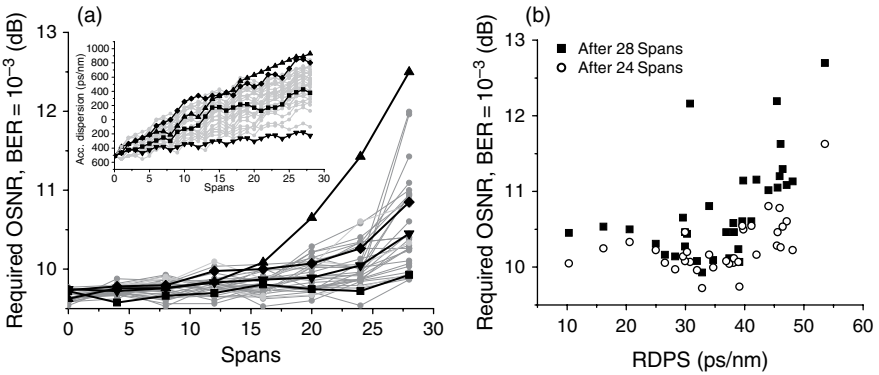

Figure 8.26 (a) Required OSNR for WDM channel at 1551 nm as a function of distance for 34 different dispersion maps (inset) realized using a dynamically reconfigurable recirculating loop. (b) Corresponding required OSNR as a function of RDPS.

this chapter. Because of the computational complexity of the problem, much of the optimization is reserved for predeployment system configuration planning. This need has led to the emergence of network planning tools (Section 8.7.3), which are distinct from network management and control software. Planning tools can be viewed as a collection of software packages that are needed for the development and deployment of ROADM systems. At a minimum, they will configure the channel wavelengths and routing in a network deployment, taking into account the system engineering rules and traffic matrices. More advanced tools will include data layer traffic engineering, equipment selection, physical layer transmission performance simulation, and maintenance/trouble shooting features. An important asset of planning tools is that they can incorporate known system performance data or measurements for a particular deployment and use that information to aid in the network optimization. In particular, whereas point-to-point systems need to provide margins that account for all channels traversing the longest reach, planning tools allow one to incorporate transmission-distance-dependent rules. This provides the potential to use impairment-constrained wavelength routing, which is a challenging optimization problem.

8.8.3 Optically Transparent Mesh Channel Management

Due to power coupling mechanisms in ROADM systems, mesh networks have the potential to form undesirable feedback paths around closed loops. The worst case involves direct optical power coupling at a single wavelength around a closed loop. Such closed loops can cause control mechanisms to run away and lead to optical lasing effects if enough amplification is available. Wavelength routing

rules, ROADM control algorithms, and in many cases the physical switch design should prevent a single wavelength channel from being routed around a closed loop. Due to lightpath diversity requirements for protection, however, channels may be forced to take circuitous routes that could travel much of the distance around a loop. This will not lead to direct power feedback that would create optical closed loops, but care must be taken to avoid forming complete loops in these cases due to single switch failures or during provisioning and reconfiguration. A well-designed physical layer system control algorithm will include safeguards to prevent the possibility of forming closed loops, as well as channel collisions during normal operation. Likewise, ASE noise, both out-of-band and in-band, must be blocked. WSSs or blockers should be kept in the blocked position unless explicitly provisioned to create a planned path.

In addition to direct optical power coupling at a single wavelength, other power coupling mechanisms considered in Section 8.7.4 should be taken into account. Yoo et al. [85] demonstrated that the WDM channel power coupling that results from constant power amplifier operation can result in feedback and instability for ROADM mesh systems. In this case, no channel travels around the complete loop. However, a change in power for one channel can influence the power level of other channels that may travel the remaining distance around the loop to complete the feedback path. This situation is illustrated in Figure 8.27. Channel groups G1 and G2 add at nodes A and D, respectively, and travel partially around the ring formed by nodes B, C, D, E. The groups do not take the shortest routes, which may occur, e.g., when a channel wavelength is already used by another channel in the link that provides the shorter route (this problem is referred to as wavelength blocking). Other groups of channels may also be present in this example, helping to facilitate the power coupling. However, as shown in Section 8.7.4, the amplitude of the power excursion is damped with the

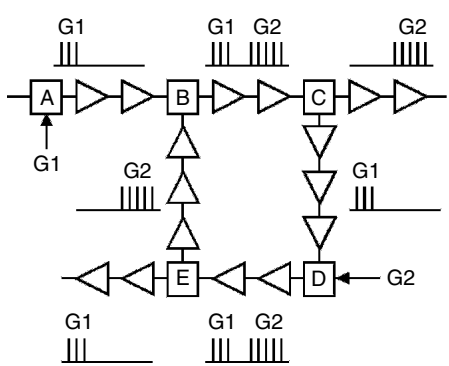

Figure 8.27 Mesh ROADM system with a closed loop. Three channels in group G1 add at node A and follow path A B C D E ; five channels in group G2 add at node D and follow path D E B C . Simultaneous adjustments at ROADMs B and E can couple through channel interactions due to overlapping paths.

number of power coupling events and in proportion to the channel number or power ratio of the two groups of channels involved in the transfer. Therefore, the requirement that the amplitude of the feedback around a closed loop be greater than 1 is generally not met. A channel group with a large number of channels can transfer much of its power deviations to a smaller group, however, but the smaller group will not be effective at coupling the deviations back on the large group to complete a closed loop. Thus channel groups of similar size generally give the largest coupling around a ring. Another important factor is the channel power control algorithms that are used [86]. If the channel power controls operate simultaneously and independently, then this can lead to instability [85]. This does not occur if the power adjustments by the controllers are sequenced. While independent power control at each node is attractive in scaling the network, it leaves open the potential for instability.

For constant gain amplification, which is more common in ROADM systems, channel power coupling will occur through gain ripple and tilt, as well as fiber nonlinearities (see Section 8.7.4). Again, proper sequencing of the channel power control in different nodes is important to ensure stability. Figure 8.28(a) shows the oscillations that can occur for simultaneously adjusting nodes [62]. In this case, three WSS ROADM nodes similar to the architecture in Figure 8.13(a) were assembled in a ring configuration with four transmission spans. Groups of eight channels were placed at either end of the EDFA gain spectrum. The control algorithms were simultaneously stepwise executed and the power tilt between the two channel groups was measured after each iteration of a control cycle. The outputs of two ROADMs are shown to have opposite tilt that oscillates between positive and negative swings with each

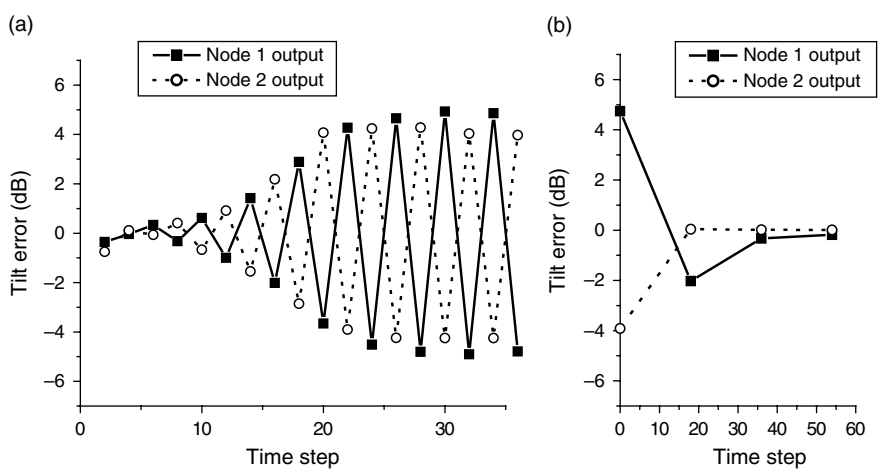

Figure 8.28 (a) Channel tilt oscillations created by simultaneous WSS channel power leveling in a ring configuration with constant gain amplification. (b) Tilt error correction when sequenced WSS channel power leveling is used.

adjustment. These oscillations grew from a small initial tilt error. In Figure 8.28(b), the simultaneous control stepping was stopped and instead each WSS was adjusted through three control iterations before moving sequentially to the next ROADM. The resulting tilt error is shown after all three ROADMs have been adjusted. After just two adjustments around the loop, the tilt error is negligible.

The use of node-sequenced channel power tuning avoids instabilities due to competing channel power adjustments. Sequencing through all nodes in a network, however, does not scale well. The time required to adjust the network can become large. The dynamic domains technique uses the channel paths in the network to define domains between which strong channel power coupling will not exist. These domains are allowed to adjust simultaneously allowing for scalable control [62].

8.9 CONCLUSIONS

In this chapter, we have reviewed the motivations, subsystem technologies, and network architectures underlying ROADMs and ROADM-based optical networks. Simple examples have been used to show the economic value of ROADMs. A variety of ROADM designs has been assessed and compared in terms of wavelength routing capability and other features, including modular growth, directional separability, and maximum fiber degree. An overview of the most successful current implementations has been presented, with an eye toward identifying appropriate network niches for each. The complex interplay between ROADM properties and optical transmission has also been explored, including a detailed discussion of static and dynamic channel power control. Finally, issues specific to optical networks containing ROADMs, such as dispersion map walk-off error and optically transparent mesh channel management, have been addressed.

ROADMs enable an automated and transparent network capable of rapid reconfiguration. To fully realize this vision within the growing global communication fabric, transmission systems must be capable of dealing with continual changes, including power transients and varying transmission conditions. Network management systems must solve complex problems in routing and wavelength blocking, path verification, and more as the photonic layer assumes some of the tasks previously handled by higher layers. Going forward, we can expect network operators to make more and more use of the capabilities of ROADMs, both to meet the growing traffic demand and to offer new services, such as providing entire wavelengths on demand. Advanced ROADM functionality, such as colorless add/drop ports, steerable transponders, and adaptive passbands, will be increasingly sought after, as will new and better solutions for signaling, network management, and mesh transmission. By meeting these challenges, the optical R&D community will help address the world's need for flexible, economical, and scalable networks.

ACKNOWLEDGMENTS

The authors would like to acknowledge the help and support of their colleagues at AT&T, Bell Laboratories, and the Alcatel-Lucent Optical Networks Business division, and to extend special thanks to Martin Birk, S. Chandrasekhar, Randy Giles, Dah-Min Huang, Peter Magill, Patrick Mock, and Chris White.

REFERENCES

[1] A. H. Gnauck and P. J. Winzer, "Optical phase shift keyed transmission," *J. Lightw. Technol.*, 23, 115 130, 2005 and references therein.
[2] J. Strand and A. Chiu, "Realizing the advantages of optical reconfigurability and restoration with integrated optical cross connects," *J. Lightw. Technol.*, 21, 2871 2882, 2003.
[3] J. M. Simmons, E. L. Goldstein, and A. A. M. Saleh, "Quantifying the benefit of wavelength add drop in WDM rings with distance independent and dependent traffic," *J. Lightw. Technol.*, 17, 48 57, 1999.
[4] S. Chaudhuri and E. Goldstein, "On the value of optical layer reconfigurability in IP over WDM lightwave networks," *IEEE Photon. Technol. Lett.*, 12, 1097 1099, 2000.
[5] A. F. Wallace, "Ultra Long Haul DWDM: Network Economics," in *Proc. OFC.*, paper TuT1, 2001.
[6] A. Chiu and C. Yu, "Economic Benefits of Transparent OXC Networks as Compared to Long Systems with OADMs," in *Proc. OFC.*, paper WQ2, 2003.
[7] C. F. Lam, N. J. Frigo, and M. D. Feuer, "A taxonomical consideration of optical add/drop multiplexers," *Photonic Netw. Commun.*, 3, 327 333, 2001.
[8] J. Ford, "Micromechanical Wavelength Add/Drop Switching: From Device to Network Architecture," in "*Proc. OFC*, 2003, pp. 253 255.
[9] M. D. Feuer and D. Al Salameh, "Routing Power: A Metric for Reconfigurable Wavelength Add/ Drops," in "*Proc. OFC*, 2002, pp. 156 158.
[10] C. R. Giles and M. Spector, "The wavelength add/drop multiplexer for lightwave communication networks," *Bell Labs Technical Journal*, 4, 207 229, 1999.
[11] P. Mock and M. D. Feuer, private communication.
[12] T. Strasser, "ROADMs turn economical for edge networks," *Lightwave Mag.*, 24(7), 2007.
[13] C. F. Lam, "Next Generation Metropolitan Area WDM Optical Networks," in *Proc. APOC.*, paper 6354 42, 2006.
[14] E. B. Basch, R. Egorov, S. Gringeri, and S. Elby, "Architectural tradeoffs for reconfigurable dense wavelength division multiplexing systems," *IEEE J. Sel. Top. Quantum Electron.*, 12, 615 626, 2006.
[15] G. Baxter, S. Frisken, D. Abakoumov et al., "Highly Programmable Wavelength Selective Switch Based on Liquid Crystal on Silicon Switching Elements," in *Proc. OFC*, paper OTuF2, 2006.
[16] S. L. Woodward, M. D. Feuer, C. F. Lam et al., "Broadcasting a Single Wavelength Over a WDM Network," in *Proc. OFC.*, paper WBB2, 2001.
[17] C. F. Lam, M. Boroditsky, B. Desai, and N. J. Frigo, "A novel dynamic crosstalk characterization technique for 3 D photonic crossconnects," *IEEE Photon. Technol. Lett.*, 15, 141 143, 2003.
[18] T. Afferton, quoted in P. A. Bonenfant, and M. L. Jones, "OFC 2003 workshop on wavelength selective switching based optical networks," *J. Lightw. Technol.*, 22, 305 309, 2004.
[19] S. L. Woodward, M. D. Feuer, J. Calvitti et al., "A High Degree Photonic Cross Connect for Transparent Networking, Flexible Provisioning & Capacity Growth," in *Proc. ECOC*, paper Th1.2.2, 2006.
[20] Dah Min Huang, private communication.

[21] D. C. Kilper, R. Bach, D. J. Blumenthal et al., "Optical performance monitoring," *J. Lightw. Technol.*, 22, 294 304, 2004.
[22] D. A. Fishman, W. A. Thompson, and L. Vallone, "*LambdaXtreme*® transport system: R&D of a high capacity system for low cost, ultra long haul DWDM transport," *Bell Labs Technical Journal*, 11, 27 53, 2006.
[23] For a general review of the use of pilot tones in WDM systems see, H. C. Ji et al., "Optical performance monitoring based on pilot tones for WDM network applications," *J. Opt. Netwk.*, 3, 510 533, 2004.
[24] M. D. Feuer and V. A. Vaishampayan, "Demonstration of an in Band Auxiliary Channel for Path Trace in Photonic Networks," in *Proc. OFC.*, paper OWB6, 2005.
[25] M. D. Feuer and V. A. Vaishampayan, "Rejection of interlabel crosstalk in a digital lightpath labeling system with low cost all wavelength receivers," *J. Lightw. Technol.*, 24, 1121 1128, 2006.
[26] A. A. M. Saleh and J. M. Simmons, "Evolution toward the next generation core optical network," *J. Lightw. Technol.*, 24, 3303 3321, 2006.
[27] I. Tomkos, M. Vasilyev, J. K. Rhee et al., "80 × 10.7 Gb/s Ultra Long Haul (+4200 km) DWDM Network with Reconfigurable 'Broadcast & Select' OADMs," in *Proc. OFC*, paper FC1, 2002.
[28] D. T. Neilson, C. R. Doerr, D. M. Marom et al., "Wavelength selective switching for optical bandwidth management," *Bell Labs Technical Journal*, 11, 105 128, 2006.
[29] X. Xiao, S. Gao, Y. Tian, and C. Yang, "Analytical optimization of the net residual dispersion in SPM limited dispersion managed systems," *J. Lightw. Technol.*, 24, 2038 2044, 2006; including a discussion of recent map design considerations and references therein.
[30] J. R. Essiambre, G. Raybon, and B. Mikkelsen, "Pseudo linear transmission of high speed TDM signals: 40 and 160 Gb/s," in *Optical Fiber Telecommunications IV B Systems and Impairments* (I. Kaminow and T. Li, eds), New York: Academic, pp. 232 304, 2002.
[31] N. Hanik, A. Ehrhardt, A. Gladisch et al., "Extension of all optical network transparent domains based on normalized transmission sections," *J. Lightw. Technol.*, 22, 1439 1453, 2004.
[32] D. F. Grosz, A. Agarwal, S. Banerjee et al., "All Raman ultralong haul single wideband DWDM transmission systems with OADM capability," *J. Lightw. Technol.*, 22, 423 432, 2004.
[33] A. R. Pratt, P. Harper, S. B. Alleston et al.,"5,745 km DWDM Transcontinental Field Trial Using 10 Gbit/s Dispersion Managed Solitons and Dynamic Gain Equalization," in *Proc. OFC.*, paper PD26, 2003.
[34] C. Xie, "A doubly periodic dispersion map for ultralong haul 10 and 40 Gb/s hybrid DWDM optical mesh networks," *IEEE Photon. Technol. Lett.*, 17, 1091 1093, 2005.
[35] J. McNicol, M. O'Sullivan, K. Roberts et al., "Electrical Domain Compensation of Optical Dispersion" in *Proc. OFC.*, paper OThJ3, 2005.
[36] S. Chandrasekhar, D. C. Kilper, X. Zheng et al., "Evaluation of Chirp Managed Lasers in a Dispersion Managed DWDM Transmission Over 24 spans," in *Proc. OFC.*, paper OthL7, 2007.
[37] P. J. Winzer and R. J. Essiambre, "Advanced modulation formats for high capacity optical transport networks," *J. Lightw. Technol.*, 24, 4711 4728, 2006; see also Chapter 2 in this volume.
[38] R. D. Li, P. Kumar, and W. L. Kath, "Dispersion compensation with phase sensitive optical amplifiers," *J. Lightw. Technol.*, 12, 541 549, 1994.
[39] M. Birk, X. Zhou, M. Boroditsky et al., "WDM Technical Trial with Complete Electronic Dispersion Compensation," in *Proc. ECOC*, paper Th2.5.6, 2006.
[40] H. K. Kim, S. Chandrasekhar, M. Spector, and L. Buhl, "Error free operation of large scale (16 nodes cascaded over total distance of 600 km) optical network based on dense WDM (15 100 GHz spaced l0 Gbit/s/channel) Channels," *Electron. Lett.*, 36, 654 655, 2000.
[41] E. Pincemin et al., "Robustness of 40 Gb/s ASK modulation formats in the practical system infrastructure," *Opt. Express*, 14, 12049 12062, 2006.
[42] J. Wiesenfeld, L. D. Garrett, M. Shtaif et al., "Effects of DGE Channel Bandwidth on Nonlinear ULH Systems," in *Proc. OFC.*, paper OWA2, 2005.
[43] E. L. Goldstein and L. Eskildsen, "Scaling limitations in transparent optical networks due to low level crosstalk," *IEEE Photon. Technol. Lett.*, 7, 93 94, 1995.

[44] F. Liu, C. J. Rasmussen, and R. S. J. Pedersen, "Experimental verification of a new model describing the influence of incomplete signal extinction ratio on the sensitivity degradation due to multiple interferometric crosstalk," *IEEE Photon. Technol. Lett.*, 11, 137 139, 1999.
[45] H. K. Kim and S. Chandrasekhar, "Dependence of in band crosstalk penalty on the signal quality in optical network systems," *IEEE Photon. Technol. Lett.*, 12, 1273 1274, 2000.
[46] P. J. Winzer, M. Pfennigbauer, and R. J. Essiambre, "Coherent crosstalk in ultradense WDM systems," *J. Lightw. Technol.*, 23, 1734 1744, 2005.
[47] T. Zami, B. Lavigne, E. Balmefrezol et al., "Comparative Study of Crosstalk Created in 50 GHz Spaced Wavelength Selective Switch for Various Modulation Formats at 43 Gbit/s," in *Proc. ECOC*, paper We3.P.81, 2006.
[48] R. Ryf, Y. Su, L. Moeller et al., "Wavelength blocking filter with flexible data rates and channel spacing," *J. Lightw. Technol.*, 23, 54 60, 2005.
[49] M. A. F. Roelens, J. Bolger, G. Baxter et al., "Tunable Dispersion Trimming in Dynamic Wavelength Processor at 80 Gbit/s per Channel," in *Proc. OFC.*, paper PDP44, 2007.
[50] ITU T G Series Recommendation Supplement 39, "Optical system design and engineering considerations," *International Telecommunication Union*, 2006.
[51] D. Penninckx and C. Perret, "New physical analysis of 10 Gb/s transparent optical networks," *IEEE Photon. Technol. Lett.*, 15, 778 780, 2003.
[52] S. Herbst, H. Lucken, C. Furst et al., "Routing Criterion for XPM Limited Transmission in Transparent Optical Networks," in *Proc. ECOC*, 2003.
[53] S. A. Taegar, D. A. Fishman, and D. L. Correa, "Engineering and Planning Tool for an Ultra Long Haul Optical Mesh Transport System," in *Proc. NFOEC.*, paper NTuF4, 2006.
[54] E. L. Goldstein, L. Eskildsen, C. Lin, and R. E. Tench, "Multiwavelength propagation in lightwave systems with strongly inverted amplifiers," *IEEE Photon. Technol. Lett.*, 6, 266 269, 1994.
[55] M. Karasek and M. Menif, "Channel addition/removal response in raman fiber amplifiers: modeling and experimentation," *J. Lightw. Technol.*, 20, 1680 1687, 2002.
[56] A. K. Srivastava, J. L. Zyskind, Y. Sun et al., "Fast link control protection of surviving channels in multiwavelength optical networks," *IEEE Photon. Technol. Lett.*, 9, 1667 1669, 1997.
[57] D. H. Richards and J. L. Jackel, "A theoretical investigation of dynamic all optical gain control in multichannel EDFA's and EDFA cascades," *IEEE J. Sel. Top. Quantum Electron.*, 3, 1027 1036, 1997.
[58] D. C. Kilper, M. Waldow, W. Etter, and C. Xie, "Control Process Gain of Erbium Doped Fiber Amplifiers with Wavelength Division Multiplexed Signals," in *Proc. OAA*, 2006.
[59] P. Vorreau, D. C. Kilper, and C. White, "Gain saturation spectrum of backward pumped broad band Raman amplifiers," *IEEE Photon. Technol. Lett.*, 17, 1405 1407, 2005.
[60] N. Takahashi, T. Hirono, H. Akashi et al., "An output power stabilized erbium doped fiber amplifier with automatic gain control," *IEEE J. Sel. Top. Quantum Electron.*, 3, 1019 1026, 1997.
[61] D. C. Kilper and C. A. White, "Fundamental Saturated Amplifier Dynamics in Transparent Networks," in *Proc. ECOC*, paper We4.P.96, 2005.
[62] D. C. Kilper, C. A. White, and S. Chandrasekhar, "Control of Channel Power Instabilities in Transparent Networks Using Scalable Mesh Scheduling," in *Proc. OFC.*, paper PDP11, 2007.
[63] C. Simonneau and V. Leng, "Impact of Spectral Hole Burning and ASE in Constant Gain EDFA with Input Channel Count Variation," in *Proc. ECOC*, paper We3.P.9, 2006.
[64] H. Nakaji and M. Shigematsu, "Wavelength dependence of dynamic gain fluctuation in a high speed automatic gain controlled erbium doped fiber amplifier," *IEEE Photon. Technol. Lett.*, 15, 203, 2003.
[65] C. Fuerst et al. "Impact of Spectral Hole Burning and Raman Effect in Transparent Optical Networks," in *Proc. ECOC*, paper Tu.4.2.5, 2003.
[66] M. Bolshtyanski, "Spectral hole burning in erbium doped fiber amplifiers," *J. Lightw. Technol.*, 21, 1032 1038, 2003.
[67] P. Krummrich and M. Birk, "Experimental investigation of compensation of Raman induced power transients from WDM channel interactions," *IEEE Photon. Technol. Lett.*, 17, 1094 1096, 2005.

[68] Y. Sun, A. K. Srivastava, J. L. Zyskind et al., "Fast power transients in WDM optical networks with cascaded EDFAs," *Electron. Lett.*, 33, 313 314, 1997.
[69] D. C. Kilper, S. Chandrasekhar, and C. A. White, "Transient Gain Dynamics of Cascaded Erbium Doped Fiber Amplifiers with Re Configured Channel Loading," in *Proc. OFC.*, paper OtuK6, 2006.
[70] A. Bononi and L. Rusch, "Doped fiber amplifier dynamics: a system perspective," *J. Lightw. Technol.*, 16, 945 956, 1998.
[71] A. R. Grant and D. C. Kilper, "Signal Transient Propagation in an All Raman Amplified System," in *Proc. OFC.*, paper ThT3, 2004.
[72] N. Madamopoulos, D. C. Friedman, I. Tomkos, and A. Boskovic, "Study of the performance of a transparent and reconfigurable metropolitan area network," *J. Lightw. Technol.*, 20, 937 945, 2002.
[73] C. Tian and S. Kinoshita, "Analysis and control of transient dynamics of EDFA pumped by 1480 and 980 nm lasers," *J. Lightw. Technol.*, 21, 1728, 2003.
[74] K. Motoshima, N. Suzuki, K. Shimizu et al., "A channel number insensitive erbium doped fiber amplifier with automatic gain and power regulation function," *J. Lightw. Technol.*, 19, 1759 1767, 2001.
[75] C. J. Chen and W. S. Wong, "Transient effects in saturated Raman amplifiers," *Electron. Lett.*, 37, 371 372, 2001.
[76] Y. Sugaya, S. Muro, Y. Sato, and E. Ishikawa, "Suppression Method of Transient Power Response of Raman Amplifier Caused by Channel Adddrop," in *Proc. ECOC*, paper 5.2.3, 2002.
[77] X. Zhou, M. Feuer, and M. Birk, "Sub microsecond transient control for a forward pumped Raman amplifier," *IEEE Photon. Technol. Lett.*, 17, 2059 2061, 2005.
[78] G. Raybon, S. Chandrasekhar, A. H. Gnauck et al., "Experimental Investigation of Long Haul Transport at 42.7 Gb/s Through Concatenated Optical Add/Drop Nodes," in *Proc. OFC*, paper ThE4, 2002.
[79] C. Checkuri, P. Claisse, R. J. Essiambre et al., "Design tools for transparent optical networks," *Bell Labs Technical Journal*, 11, 129 143, 2006.
[80] P. Peloso, D. Penninckx, M. Prunaire, and L. Noirie, "Optical transparency of a heterogeneous pan European network," *J. Lightw. Technol.*, 22, 242 248, 2004.
[81] L. M. Gleeson et al., in *Proc. ECOC*, Postdeadline paper Th.4.4.7, 2003.
[82] A. R. Pratt, B. Charbonnier, P. Harper et al., "40×10.7 Gbit/s DWDM Transmission Over a Meshed ULH Network with Dynamically Re configurable Optical Cross Connects," in *Proc. OFC.*, paper PD9, 2003.
[83] D. Kilper, S. Chandrasekhar, E. Burrows et al., "Local Dispersion Map Deviations in Metro Regional Transmission Investigated Using a Dynamically Re configurable Re circulating Loop," in *Proc. OFC*, paper OThL5, 2007.
[84] H. Zang, J. P. Jue, and B. Mukherjee, "A Review of Routing and Wavelength Assignment Approaches for Wavelength Routed Optical WDM Networks," *Opt. Netw. Mag.*, 1, 2000.
[85] S. B. J. Yoo, W. Xin, L. D. Garrett et al., "Observation of prolonged power transients in a reconfigurable multiwavelength network and their suppression by gain clamping of optical amplifiers," *IEEE Photon. Technol. Lett.*, 10, 1659 1661, 1989.
[86] D. Gorinevsky and G. Farber, "System analysis of power transients in advanced WDM networks," *J. Lightw. Technol.*, 22, 2245 2255, 2004.

This page intentionally left blank

9

Optical Ethernet: Protocols, management, and 1–100 G technologies

Cedric F. Lam and Winston I. Way

OpVista, Milpitas, CA, USA

9.1 INTRODUCTION

After years of harsh winter in the telecom industry, which started from the burst of the technology bubble in the beginning of this century, telecom service providers are again hard working with vendors to deploy the next-generation equipment to prepare for the growing bandwidth demands, which are propelled by a slew of new broadband applications such as internet protocol television (IPTV), network gaming, peer-to-peer networking, video/web conferencing, telecommuting, and voice over IP (VOIP).

As the vehicle that interconnects billions of users and devices on the Internet, Ethernet has become the most successful networking technology in history. Even during the years of harsh winter, Ethernet development has never slowed down. The work of 10GBASE-T (IEEE 802.3an, 10-Gigabit Ethernet over twisted pair) was started in November 2002. In the following year (November 2003), IEEE 802.3 launched the project of 10GBASE-LRM (IEEE 802.3aq, 10-Gigabit Ethernet over 300 m of multimode fiber, MMF). The standard for Ethernet in the First Mile (EFM, IEEE 802.3ah) was finished in June 2004. Ethernet continues to evolve rapidly as the human society marches further into the information era.

Originally developed as an unmanaged technology for connecting desktops in local area networks (LANs) [1], nowadays Ethernet has also become a technology for metro and backbone networks. The success of Ethernet is attributed to its simplicity, low cost, standard implementation, and interoperability guarantee [2]. These attributes helped Ethernet and the data networking community it serves to prosper [3], hence producing the economy of scale.

Optical Fiber Telecommunications V B: Systems and Networks

ISBN: 978 0 12 374172 1

The Internet, which was initially devised for data connectivity, is now being transformed into a converged platform to deliver voice, data, and video services (the so-called triple-play) through the universal Ethernet interface. Such convergence is made possible by several factors: (1) new mpeg compression technologies which tremendously reduced the bandwidth and storage required for both standard and high-definition broadcast quality videos to reasonable values, (2) advances in electronic memory, storage, and processing technologies, which allows thousands of movies to be stored and switched in practical size video servers, (3) abundance of bandwidth made available by low-cost wavelength-division multiplexing (WDM) and high-speed Ethernet technologies, (4) improvements in the availability and quality of service (QoS) offered by data networks, which made it possible to support always-on and delay-sensitive services such as voice. As an example, with mpeg2 compression [4], a Gigabit Ethernet link is capable of carrying 240 streams of standard-resolution video signals, each of which requires 3.75 Mb/s bandwidth.

Traditional data services offered on internet protocol (IP) and Ethernet networks are best-effort services. Such no-frills approach helps the Internet and Ethernet to penetrate with low initial cost at the beginning [5]. However, as the network grows and the information society becomes more and more network-dependent, best-effort services will no longer be sufficient. This requires the network infrastructure and its underlying technology to evolve in order to satisfy the growing needs as well as increasing levels of service quality expectations.

To cope with this trend, Ethernet itself has gone through many changes and is now taking many forms very different from its initial design. Yet, such changes have been carefully introduced in a controlled manner to allow the existing broad deployment base to grow smoothly. In this chapter, we review some of the evolutions in Ethernet technology development.

9.2 STANDARDS ACTIVITIES

Ethernet is developed within the IEEE 802 LAN/MAN Standard Committee (LMSC) [6]. The LMSC is responsible for developing standards for equipment used in LANs and metropolitan area networks (MANs). Some of the well-known works in LMSC include Ethernet (802.3), wireless LAN (802.11), token ring (802.6), resilient packet ring (802.17), and bridging (802.1). (Figure 9.1).

The IEEE 802.3 Ethernet standard covers the physical layer (PHY) and the medium access control (MAC) function of the data link layer in the OSI (open system interface) seven-layer reference model. Ethernet frame (packet) forwarding and switching is defined in various 802.1 bridging standards.

In addition, there are many other consortiums and standards organizations working on various Ethernet-related issues. For example, MSA (multisource agreement) consortiums such as Gigabit interface convertor (GBIC), small form factor pluggable (SFP), XENPAK, and XFP [7 10] have been formed by component manufacturers to specify transceiver modules (the so-called PMD or physical

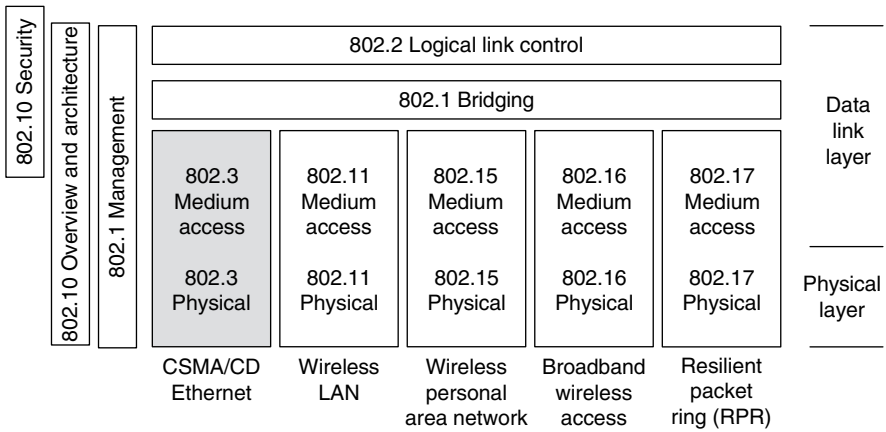

Figure 9.1 The IEEE 802 LMSC organization overview (this figure may be seen in color on the included CD ROM).

medium dependent in Ethernet terminology) with common form factors and common electrical interfaces, which can be used interchangeably with different systems. Metro Ethernet Forum (MEF) [11], another industry consortium, is defining Ethernet service types, operation, administration, and maintenance (OAM) functions, and service level agreements (SLAs).

Within the international telecommunication union (ITU), standards have been published on carrying Ethernet over time-division multiplexing (TDM) circuits. These include the generic framing procedure (GFP) defined in ITU-T G.7041 [12], virtual concatenation (VCAT) defined in ITU-T G.7043 [13], and link capacity adjustment scheme (LCAS) defined in ITU-T G.7042 [14]. ITU-T G.8031 [15] is concerned with Ethernet protection switching. ITU-T Y.1731 [16] deals with OAM functions and mechanisms for Ethernet-based networks.

Optical Internet Forum (OIF) has defined user network interface (UNI) for signaling Ethernet connections in a generalized multiprotocol label switching (GMPLS) enabled optical networks [17].

The overwhelming standard work around Ethernet implies that it is impossible to cover everything in this chapter. Therefore, our goal is to offer a direction to those interested readers to explore in-depth the rest of this rich subject.

9.3 POINT-TO-POINT ETHERNET DEVELOPMENT

9.3.1 Modern Ethernet Layering Architecture

Figure 9.2 shows the layering architecture of modern Ethernet as defined in the IEEE 802.3 standard [18]. In this figure, the MAC layer and the PHY layer are connected with an media-independent interface (MII) for 100 Mb/s Ethernet, GMII

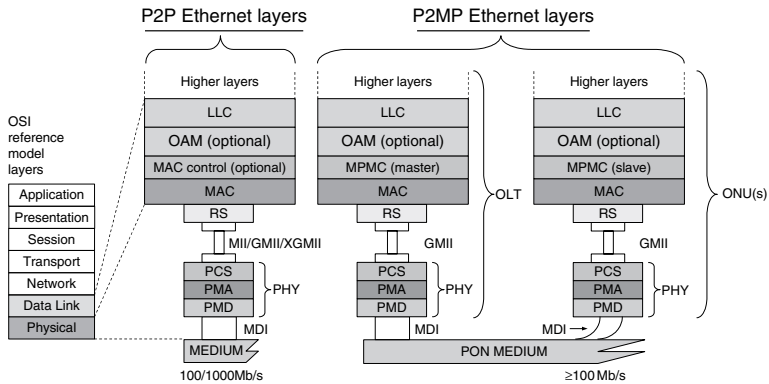

MAC: media access control
MDI: medium dependent interface
MII: media independent interface
XGMII: 10 Gigabit media-independent interface
PHY: physical layer device
RS: reconciliation sublayer
MPMC: multipoint media access control
PCS: physical coding sublayer
GMII: Gigabit media-independent interface
PMA: physical medium attachment
PMD: physical medium dependent

Figure 9.2 Modern Ethernet layering architecture (this figure may be seen in color on the included CD ROM).

(Gigabit media-independent interface) for Gigabit Ethernet and XGMII (10 G MII) for 10 Gb/s Ethernet.

This idea of separating the MAC layer from the physical layer started from the very beginning of the Ethernet history to allow the reuse of the same MAC design with different physical layer technologies and transmission media for Ethernet. Within the PHY layer, the physical coding sublayer (PCS) generates the line coding suitable for the channel characteristics of the transmission medium. The physical medium attachment (PMA) layer performs transmission, reception, collision detection, clock recovery, and skew alignment functions within the physical layer. The physical medium dependent (PMD) layer defines the optoelectronic characteristics of the actual physical transceiver. The term MDI (medium-dependent interface) is simply a fancy way to describe a connector. More detailed discussions of Ethernet layering functions can be found in Ref. [18].

9.3.2 Physical Layer Development

All the modern Ethernet systems are formed with full-duplex links, which do not have the speed and distance limitations imposed by the original CSMA/CD (carrier sense multiple access with collision detection) protocol [19]. Full-duplex Ethernets adopt a star-shaped hub-and-spoke architecture with point-to-point (P2P) connections between the hosts and a hub bridge. The distances between the bridge and hosts are only limited by physical transmission impairments. As mentioned before,

Ethernet embraces different physical layer technologies with a standard interface between the MAC layer and the physical layer. The MAC layer for P2P Ethernet has not changed much for a considerable period of time. Most of the developments in Ethernet happened in the physical layer in the last 10 years.

Gigabit Ethernet Physical Layer

10/100 Mbps Ethernets are mostly deployed on copper medium (coaxial cable or unshielded twisted pair, i.e., UTP). Gigabit Ethernet was first standardized on optical fiber in 1998. Two designs were ratified in IEEE 802.3z to transmit Gigabit Ethernet signals: the 1000BASE-SX uses short-wavelength lasers (850 nm) on MMFs, and the 1000BASE-LX uses long-wavelength laser (1310 nm) on the standard single-mode fiber. At that time, transmitting 1000 Mbps signals on the widely deployed Category 5 UTP was a significant challenge for silicon-chip designers. It requires tremendous signal processing to mitigate the channel impairments in copper wires such as ISI (intersymbol interference) introduced by limited channel bandwidth and signal crosstalks between pairs of copper wires.[1] It was not until a year later that the 1000BASE-T standard (IEEE 802.3ab) was finished.

Although Gigabit Ethernet is now mainly deployed with UTP interfaces, early Gigabit Ethernet was mostly deployed with optical interfaces. Fiber has the advantage of little signal impairments and wide bandwidth. It is suitable for backbone transmission which is the major application for early Gigabit Ethernet. To keep the cost of Gigabit Ethernet low, the IEEE 802.3z committee very conservatively defined the transmission distance limit of 1000BASE-SX as 300m, and that of 1000BASE-LX as 5 km.

Both 1000BASE-SX and 1000BASE-LX share the 8B10B 1000BASE-X PCS line coding [18, Clause 36]. Besides the transmission media, the only difference between 1000BASE-SX and 1000BASE-LX lies in the PMD layer which defines the laser transmitter and photodetector. The interface between the PMA and PMD layer is simply a serial interface. This made it easy to reuse all the designs between 1000BASE-SX and 1000BASE-LX except the PMD transceiver, which cannot interoperate with each other.

Although the IEEE 802.3z standard committee has made the PMD specification extremely conservative, it still represented a significant portion of the Gigabit Ethernet cost.[2] The cost of optical transceivers would explode in Gigabit Ethernet switches and routers containing high port counts. Luckily, the well-thought layered design of Ethernet allows the optical transceiver modules to be separated from the rest of system.

The IEEE 802.3z standard did not specify an exposed interface between the PMA and PMD. Nevertheless, transceiver manufactures formed MSA consortiums [20] that defined optical transceiver modules (i.e., PMDs) with a common electrical

[1] 1000 BASE T uses four pairs of unshielded Category 5 cables simultaneously for signal transmis sion and reception.

[2] The cost of optical transceivers dominated the cost of Gigabit Ethernet. It is also well known that the cost of silicon is always difficult to compete with.

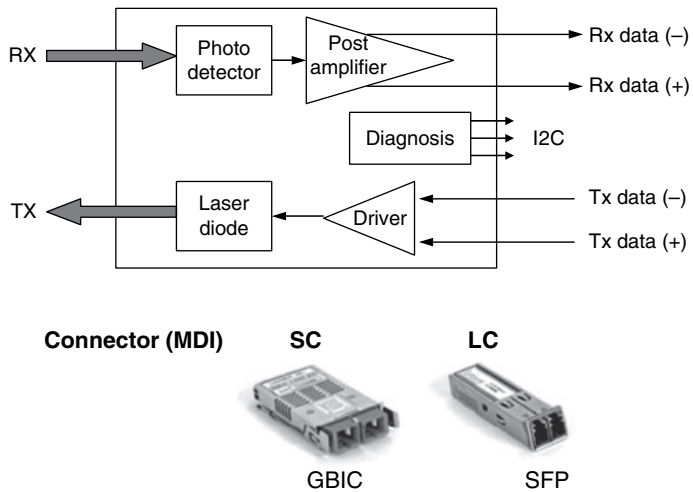

Figure 9.3 GBIC and SFP MSA modules: block diagram (top) and picture (bottom) (this figure may be seen in color on the included CD ROM).

interface and uniform mechanical dimensions. The most commonly seen Gigabit Ethernet MSA PMD modules are GBIC [7] and SFP [8] (Figure 9.3). SFP modules are much smaller in size and became the most popular Gigabit PMD. To improve system density, SFPs use the compact-form LC connector not specified in the IEEE 802.3 standard. Both GBIC and SFP modules are hot swappable so that a router/switch does not need to be populated with expensive optical modules when they are manufactured. Instead, optical transceivers can be inserted when a port needs to be connected. In addition, one does not need to decide ahead of the time which type of optical PMD to be populated at the time of purchasing a piece of Ethernet equipment.

As shown in Figure 9.3, the GBIC and SFP MSA modules contain no data-rate[3] and protocol-specific processing blocks. Therefore, such modules can also be used for other applications such as Fiber Channel and Synchronous Optical NETwork/Synchronous Digital Hierarchy (SONET/SDH). Therefore, the MSA concept not only created a pay-as-you-grow upgrade scenario, but also the economy of scale for optical transceivers which helps to reduce their costs through mass production.

Besides the basic necessary optical electrical (OE) and electrical optical (EO) conversion functions, MSA modules also offer a digital diagnostic I2C (Inter-IC bus) interface, which provides information such as PMD type, laser wavelength, input, and output optical power to the host system. This interface can be used for optical link trouble shooting and performance monitoring.

Another advantage offered by MSA is the ease to incorporate new improved PMD capabilities when they are available. As mentioned before, the IEEE 802.3z committee selected an extremely conservative optical reach of 5 km for the

[3] Clock and data recovery is performed in the PMA layer.

1000BASE-LX PMD. Fueled by the explosion of WDM transmission systems, optical transceiver capabilities have been advancing rapidly. For example, an industry accepted 1000BASE-ZX (not in the IEEE standard) MSA specification exists which enables link transmission distances to be extended to 70 km using APD (avalanche photodiode) receivers. SFP modules with dense wavelength-division multiplexing (DWDM) lasers also exist, which allow users to easily improve fiber utilizations by using parallel wavelengths to multiply the link capacity. All these improvements only involve changes confined to MSA modules.

10 Gigabit Ethernet Physical Layer

10 Gigabit Ethernet Layering Architecture The technology of 10 Gigabit Ethernet was significantly more challenging than that of Gigabit Ethernet. When it was being standardized, 10 Gb/s transmission was still the state-of-the art technology. Many different schemes had been proposed to realize 10 Gigabit Ethernet. As expected, 10 Gigabit Ethernet was also first standardized on the optical fiber medium. At 10 Gb/s data rate, the 8B10B PCS code with 25% overhead (used in 1000BASE-X standard for optical fiber media) would lead to a physical symbol rate of 12.5 Gbaud/s, which is much higher than the conventional OC192/STM64 transmission rate. In order to contain the symbol rate and minimize the cost and technical challenge for 10 Gigabit Ethernet transceivers, 10 Gigabit Ethernet uses a new PCS code (64B66B) with only 3% of the coding overhead. Figure 9.4 shows the summary of 10 Gigabit Ethernet architectures. Two 10GBASE standards using the 64B66B PCS coding [18, Clause 49] were initially produced: the 10GBASE-R LAN standard carrying native Ethernet frames in the physical layer, and the 10GBASE-W WAN standard using SONET/SDH compliant frames in the physical layer.

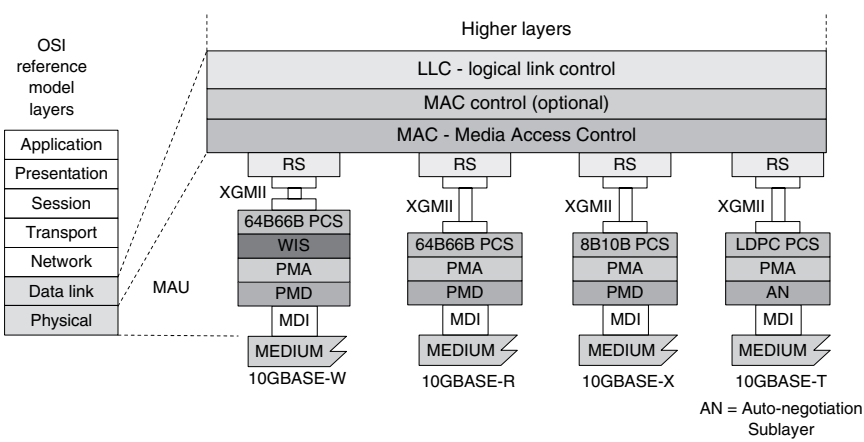

Figure 9.4 10 Gigabit Ethernet layering architecture summary (this figure may be seen in color on the included CD ROM).

The 10GBASE-W PHY contains a WAN interface sublayer (WIS) (Figure 9.4), which encapsulates Ethernet MAC frames within a SONET/SDH compliant frame [18, Clause 50]. The WIS layer also performs rate adaptation function by stretching the gaps between adjacent Ethernet frames so that the output data rate generated by the WAN interface matches the SONET/SDH OC-192 data rate of 9.953Gb/s.[4]

The 10GBASE-W PHY was created because most of the 10 Gb/s transport system existed in SONET/SDH forms at that time. At the time, 10 Gb/s Ethernet was envisioned as an aggregation technology for backbone applications. So it seemed logical to create a WAN standard which was compatible with the existing deployment base of 10 Gb/s transport systems. Nevertheless, the data communication world never liked the WAN standard and most of the 10 Gigabit Ethernet equipment deployed today uses the 10BASE-R standard.

Parallel to 10GBASE-R and 10GBASE-W, a 10GBASE-X standard was created. Similar to 1000BASE-X, the 10GBASE-X standard uses the 8B10B encoding scheme. Instead of transmitting on a single serial interface, the 10GBASE-X PHY transmits signals on a four-lane parallel interface, using four coarsely spaced wavelengths (4×2.5 Gbps) around the 1300 nm spectral region to form the so-called 10GBASE-LX4. It was the first time that the WDM technology was used in Ethernet standard. Even though the LX-4 interface has better dispersion tolerance and was easier to design than 10 Gb/s serial interfaces from a transmission viewpoint, it requires four sets of lasers and photoreceivers, which increase the packaging size, complexity, and cost. Within only a few years, 10 Gb/s serial PHYs have advanced so rapidly that they rendered the LX4 interface obsolete. Three types of 10 Gb/s serial optical PHY standards were initially created: 10GBASE-S, 10GBASE-L, and 10GBASE-E, which are summarized in Table 9.1. The 10GBASE-E interface uses the minimum loss wavelength region of 1550 nm minimum in the silica fiber (the first time in 802.3 standard) to support transmission distances up to 40 km.

The 10GBASE-LRM standard was not finished until 2006, 4 years after the first 10 Gigabit Ethernet Standard IEEE 802.3ae was finished. It enables the use of low-cost Fabry Perot (FP) lasers to transmit up to 220 m on legacy MMF which has

Table 9.1

Summary of 10GBASE optical standards.

PHY standard	Wavelength (nm)	Serial/parallel	Link distance	Medium
10GBASE SR/W	850	Serial	300/33 m	50 μm/62.5 μm MMF
10GBASE LRM	1310	Serial	220 m	50 μm/62.5 μm MMF
10GBASE LX4	1310	WDM (parallel)	300 m	50 μm/62.5 μm MMF
			10 km	Single mode fiber
10GBASE LR/W	1310	Serial	10 km	Single mode fiber
10GBASE ER/W	1550	Serial	40 km	Single mode fiber

[4] 10GBASE Ethernet has a MAC throughout of 10 Gb/s.

been widely deployed in the early 1990s for FDDI and Fast Ethernet applications. To realize 10GBASE-LRM requires advanced electronic dispersion compensation (EDC) techniques in the receiver [21]. Chapter 18 (Volume A) by Yu, Shanbhag, and Choma discusses electronic dispersion compensation (EDC) techniques in detail.

10GBASE-T Interface The 1000BASE-T UTP standard was ratified a year after the standardization of 1000BASE-X. It quickly became the dominating Gigabit Ethernet interface. UTP interfaces have proven to be popular for interconnecting servers, switches, and routers because of the ease in their cable termination and handling. However, it was not until 4 years after the standardization of 10GBASE optical Ethernet that the 10GBASE-T interface standard had been finished [22].

The 10GBASE-T interface uses an low-density parity check (LDPC) PCS. It employees a two-dimensional 16-level pulse amplitude modulation (PAM) encoding scheme on copper wire. The traditional ubiquitous Category 5 cables are no longer capable of supporting 10GBASE-T. 10GBASE-T allows transmission distances of up to 55 m on Category 6 cables. To reach the 100 m distance achieved by 10/100/1000BASE-T interfaces, 10GBASE-T requires a new Augmented Category 6 (or CAT-6A) cable, which has the frequency responses, crosstalk, and alien crosstalk[5] characteristics specified up to 500 MHz [23].

It can be expected that for a considerable period time, optical PHYs will still dominate in 10GBASE Ethernets.

The XAUI Interface 10GBASE PHY and 10GBASE MACs are interconnected with the XGMII. The XGMII interface uses a 32-bit wide data bus with a limited distance support of 7cm.

To facilitate module interconnect, an XGXS (10 Gigabit extender) interface was defined to extend the reaches of XGII. The XGXS interface reduces the 32-bit XGMII data path into a 4-bit 8B10B encoded XAUI (10 Gigabit attachment unit interface) interface as shown in Figure 9.5 [18, Clause 47]. The XAUI interface uses the exactly same coding scheme used in 10GBASE-LX4 standard. It also has a longer reach of 25 cm to facilitate the connection between a PHY device and the MAC layer. Even though the 10GBASE-LX4 PHY using the same coding scheme has never been popular, the XAUI interface has been used in many 10 Gb/s MSA modules.

10Gb/s MSA Modules 10 Gb/s MSA modules are divided into two major categories, MSA transceivers and MSA transponders, which are shown in Figure 9.6. The main difference is that transceivers interface with the host system using a serial interface whereas transponders using a parallel interface. Therefore an electrical MUX/DMUX (multiplexer/demultiplexer) (also called SERDES serializer/deserializer) is included in a transponder.

[5] Alien crosstalk refers to the crosstalk between neighboring UTP cables in a bundle.

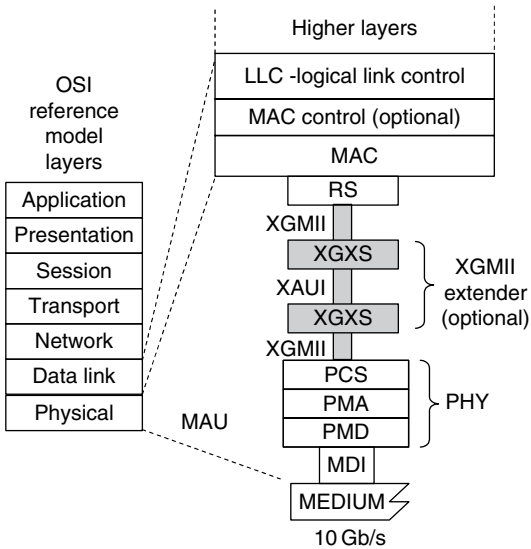

Figure 9.5 The XAUI interface (this figure may be seen in color on the included CD ROM).

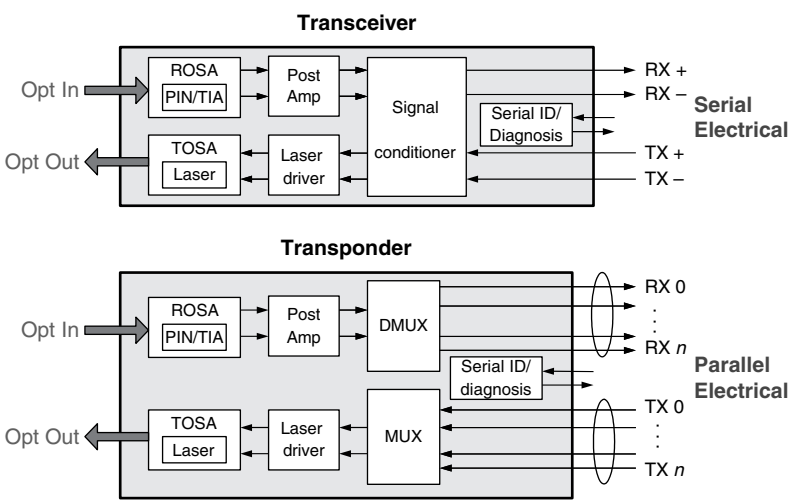

Figure 9.6 MSA transceiver (top) vs transponder (bottom) (this figure may be seen in color on the included CD ROM).

Figure 9.7 shows the diagrams of three types of commonly seen 10 Gb/s MSA modules. The XENPAK and XFP modules are hot swappable modules while the 300-pin module is not. Both XENPAK and 300-pin MSA are transponders while XFP belongs to the transceiver family. Standard 300-pin module implements the

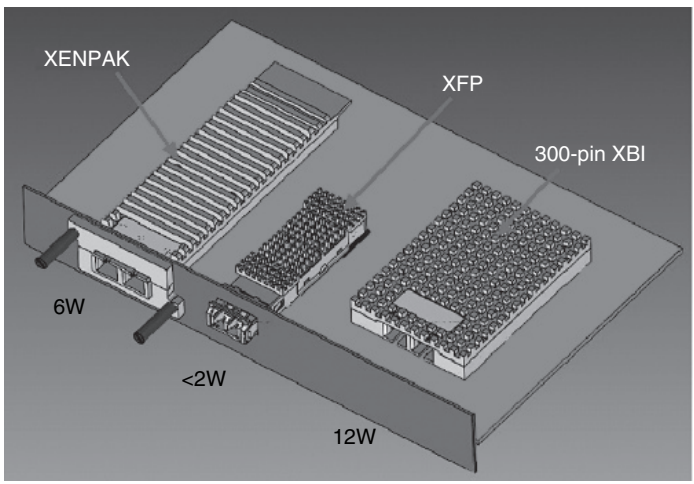

Figure 9.7 Commonly seen 10 Gb/s MSA modules. (this figure may be seen in color on the included CD ROM)

16-bit wide OIF SFI-4 (SERDES framer interface, Release 4) electrical interface for SONET/10G-WAN/10G-LAN signals [76].

Transponders produce lower-speed parallel signals, which are easier to handle on electrical printed circuit boards (PCBs). In contrast, they also require bigger packages and complicated processing circuits. Moreover, transponders are also often format and bit-rate dependent, which limit them to a single application.

Despite the challenge in handling serial 10 Gb/s signals at the electrical interface, MSA transceiver modules are more compact and consume less power. Figure 9.8 compares the block diagrams and applications of 10 Gigabit Ethernet MSA transponders and transceivers. XENPAK and XFP are the most popular 10 Gb/s MSA transponder and transceiver, respectively. Besides maintaining the signal integrity, heat dissipation is a challenge for 10 Gigabit MSA modules, which limits the compactness of their sizes. XPAK and X2 are essentially more compact versions of XENPAK. Significant progresses have been made in the recent years to reduce MSA module power consumptions. A new MSA transceiver standard called SFP + with form factor compatible with SFP is being standardized at the time of writing [24]. It provides even higher density and lower power than XFP transceivers.

Figure 9.8 illustrates that all three 10 Gigabit Ethernet transponders (XENPAK, XPAK, and X2) share the same design with embedded PCS and PMA sublayers and a XAUI interface to the host system. This allows the host system to use any type of the PHY device irrespective of the PCS line coding scheme (i.e., whether 10GBASE-R, 10GBASE-W, or 10GBASE-X PHY is required). For Layer-2/3 switch and router manufactures, this has the advantage of allowing their switching equipment to interface with any PHY devices. Nonetheless, as silicon design advances and the Ethernet community converges to the LAN interface, this

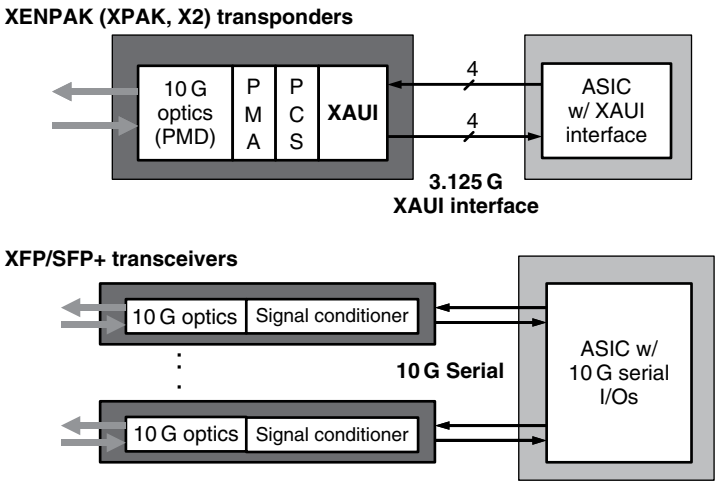

Figure 9.8 10 Gigabit Ethernet transponder (top) vs transceiver (bottom) (this figure may be seen in color on the included CD ROM).

flexibility advantage gives way to the high port-count density and integration benefit offered by transceiver modules. There is a growing industry trend to converge to XFP- and SFP+-based systems. Furthermore, for operational and management efficiencies, the industry prefers only a small handful number of 10GBASE PHY interface types than having many different flavors.

Like their Gigabit counterparts, 10 Gigabit MSA transceivers can be designed to operate at multiple data rates so that they can be used with other 10Gb/s transport systems such as SONET OC-192 and ITU-T OTU-2. Unlike GBIC and SFP transceivers, which normally only have a simple laser driver and postamplifier, to maintain high-speed signal quality and integrity, 10 Gb/s MSA transceivers are normally built with a signal conditioner which performs regeneration to clean up the distortions introduced by the electrical reshape, retime, and reamplify interface between the module and the host system. The signal conditioner can represent (3-R) clock data recovery (CDR) units in transmit and receive paths, or even electronic dispersion compensators. To improve integration and further reduce power consumptions, most of the SFP+ modules will not have built-in CDR to achieve less than 1 W power consumption. A transport equipment manufacturer would usually prefer transceiver-based MSA modules because (1) they can design transponders to work with different format signals and (2) they may not want to deal with the management and configuration complexity associated with the XAUI interface.

Nevertheless, 10 Gb/s transponders still represent the state-of-the-art commercial technology. New 10 Gb/s transmission techniques with higher performance continue to emerge. Transponder manufacturers are taking the advantages of the extra spaces available in 300-pin and XENPAK modules to embed new

transmission capabilities. For example, EDC [21], tunable laser [25], and duobinary [26] modulated transmitters have been incorporated in commercial 300-pin modules. These improved capabilities simplify the job of transport system integrators.

Link Diagnosis in 10 Gb/s Ethernet Traditionally, for cost and simplicity, Ethernet does not include much diagnosis capabilities besides CRC frame integrity check and PHY layer link-up/link-down verification. This was adequate when Ethernet was mainly used in LAN environments. 10-Gigabit Ethernet was intended for MAN applications. To improve network troubleshooting capabilities, for the first time, the IEEE 802.3 standard group introduced loopback and remote link fault diagnosis functions into 10-Gigabit Ethernet designs. These capabilities are shown in Figure 9.9.

The 10-Gigabit Ethernet standard includes optional loopback functions at various PHY sublayers as indicated in Figure 9.9. These loopback functions can be implemented in MSA modules and invoked through the digital diagnosis interfaces so that when a port is not functioning properly, the problem can be isolated and localized with various loopback tests.

Another capability introduced in 10-Gigabit Ethernet is the local fault (LF) and remote fault (RF) signals, which are conceptually similar to the loss of signal (LOS) and remote fault inductor (RDI) maintenance signals on a SONET link. When a link error is detected, if the local receiver receives a corrupted signal, it will generate the LF code words (called LF ordered set, or LFOS) to the reconciliation sublayer (RS) layer [18, Clause 46]. At the same time, the local RS layer inserts RF ordered set (RFOS) to the transmitter which will be received by the link partner. The LF/RF

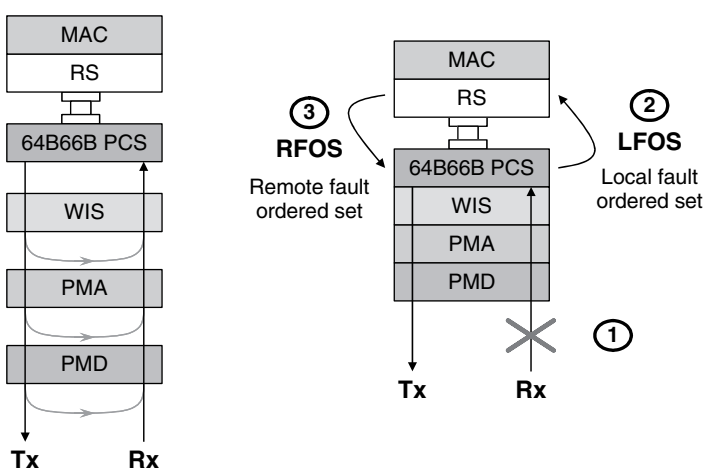

Figure 9.9 Loop back modes (left) and link fault signaling (right) in 10 Gigabit Ethernet (this figure may be seen in color on the included CD ROM).

signals are represented using special 64B66B code words. Thus they are terminated in the physical layer and not passed up to the upper layers.

9.4 LAYER-2 FUNCTIONS IN ETHERNETS

Layer-2 functions include MAC and Ethernet frame switching, which is also called bridging. Unlike traditional circuit switched networks, Ethernet is a packet switched technology. Every Ethernet frame is labeled with a source address (SA) and a destination address (DA) which are used by Ethernet bridges to forward the frame to the proper destination. The IEEE 802.3 standard only covers the MAC portion. Ethernet bridging is covered by the IEEE 802.1 standards. The most important idea for Ethernet bridging is the IEEE 802.1D Spanning Tree Protocol (STP) [27].

9.4.1 Ethernet MAC Frames

To discuss the bridging operation, one needs to first understand the format of Ethernet frames. Figure 9.10 shows the basic Ethernet frame format. This basic format has remained invariant for a considerable period of time, despite the rapid development in Ethernet speed and different physical layer technologies.

Ethernet is a multimedia technology because it operates on different media with various speeds. Ethernet devices are designed with clearly defined interfaces between the MAC layer and the PHY layer. This layered approach allows the physical layer to evolve independent of the MAC layer. Ethernet frames represent the data format at the MAC layer. It is the common MAC layer specification and MAC frame formats that allows Ethernet devices of different speeds and PHY technologies to interoperate with one another. In fact, switches are often built with ports of different speeds and medium types.

Ethernet frames are variable length with a payload area between 46 and 1500 octets. An invariant MAC frame format allows each generation Ethernet to be backward compatible with early generations so that users do not need to upgrade

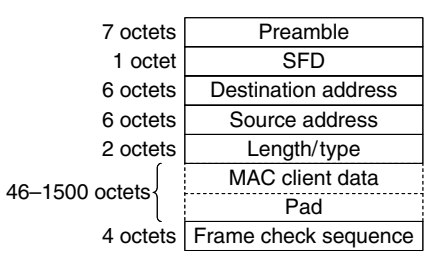

Figure 9.10 Basic Ethernet frame format (SFD: start frame delimiter).

upper layer software and applications when the network speed is increased. This played an important role to ensure the commercial successes of Ethernet. An Ethernet frame starts with a preamble field with alternating 0's and 1's, which is used in early days by burst-mode receivers at a destination node to recover the signal clock. When Ethernet connections became P2P, transmitter and receiver synchronization is always maintained by transmitting idle symbols when there is no data to send. This obviates the need of the preamble field, which nonetheless, is kept for backward compatibility.

The preamble is followed by an start frame delimiter (SFD) to signify the beginning of a frame. Following the SFD is the DA and SA. The first bit of DA determines if the frame is a unicast or broadcast frame. A unicast frame is represented by a 0 value in the first bit of the DA and a multicast packet by a 1 value. The all 1 address is reserved as the universal broadcast address. Normally, a bridge receiving a frame with a broadcast/multicast address will forward the frame to all other ports except the incoming port. A block of multicast addresses has also been reserved by IEEE for protocol implementations. Packets with these reserved addresses are interpreted as protocol data units (PDUs) with special meanings. A station receiving these special multicast packets will normally terminate such packets without forwarding them. In other words, if a bridge receives a multicast frame with its DA in the reserved address block and the switch does not understand the frame, it will simply drop the frame.

Ethernet frames also have a two-octet length/type field to represent the length of the payload field. Since the allowed maximum payload frame is only 1500 bytes, a length/type value above 1536 represents the type of the Ethernet frames. It is often used to represent the upper layer protocol or the type of management information contained in the payload. The frame check sequence (FCS) field uses a four-octet cyclic redundancy check value (CRC) to protect the frame.

Figure 9.10 shows that Ethernet frames contain minimum management information. Such simple frame structure helped to keep the network equipment simple and low-cost. However, as network infrastructures continue to grow and Ethernet service management becomes more and more important, the original frame format with minimal overhead designs is no longer sufficient. Expansions in Ethernet frames have been carefully introduced in the recent years to allow the growths of Ethernets while minimizing the impacts on legacy Ethernet devices [28].

9.4.2 Transparent Bridging

A CSMA/CD collision domain is a multipoint-to-multipoint mesh-connected broadcast domain. Any station in a broadcast domain can directly communicate with any other station in the same domain by broadcasting the frame in the domain. In fact, a station just sends a frame to its destination assuming that the frame will eventually arrive at the destination. As explained before, stations in a broadcast domain share the common medium and its capacity. As the number of hosts in a domain grows and network size increases, the network performance will be degrade.

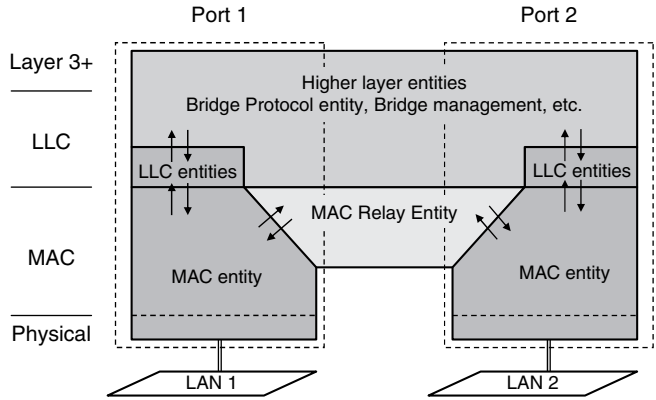

Figure 9.11 Architecture layering of a bridge (this figure may be seen in color on the included CD ROM).

A bridge improves the network performance by limiting the size of a collision domain. The term switch and bridge are used interchangeably in the networking industry. A bridge is a multiport device with a layering architecture shown in Figure 9.11. Each bridge port is connected to a separate LAN (i.e., separate collision domain). A bridge contains a MAC relay entity to forward MAC frames from one port to another.

Normally, besides broadcast/multicast frames, an Ethernet port only accepts unicast frames with DA matching its own MAC address. A bridge port, in contrast, works in a promiscuous mode. It receives frames with any destination addresses and performs one of the three functions:

(1) Broadcast (flooding)
(2) Forwarding
(3) Filtering

Figure 9.12 shows the functional diagram of a bridge, which contains a source address table (SAT), a filter/forward lookup logic and a learning logic associated with port interfaces. When an Ethernet frame arrives at a port interface, the filter/forward lookup logic makes use of the DA and SAT to decide whether the frame needs to be broadcast, forwarded, or filtered.

The SAT is populated automatically through the learning logic or manually through management provision. Each entry of the SAT contains the association of a host address and the bridge port that the addressed host can be reached from. In automatic learning, when a new frame arrives at a bridge port, the learning logic examines its SA. If that address is not yet in the SAT, the learning logic will populate the SA and the port number in the SAT, so that next time, when a frame with the DA matching that address arrives at the bridge, the bridges knows how to forward the frame. Notice that the bridge operation assumes bidirectional links.

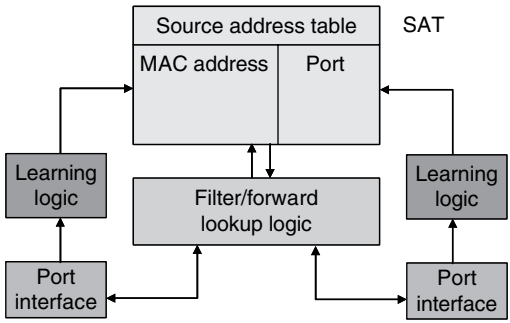

Figure 9.12 Bridge functional diagram (this figure may be seen in color on the included CD ROM).

Automatically learned SAT entries will be aged out (i.e., deleted) if a source address becomes inactive for a certain period of time. This allows the MAC host to be moved from one location to another without the tedious requirement to reconfigure the SAT manually.

Figure 9.13 illustrates the three functions performed by a bridge. In Figure 9.13(a), user Y attached to bridge port 2 sends a frame to user X attached to bridge port 1. Upon receiving the frame at port 2, the bridge looks up X in the SAT and found it associated with port 1. The frame is thus forward to user X through port 1. In Figure 9.13(b), user X is sending a frame to user T. User X's frame is intercepted by the bridge at port 1. The bridge looks up the SAT and find that both user X and user T are both attached to port 1. So it filters the frame at port 1. A third example is shown in Figure 9.13(c). In this case, user Y's frame for user Z

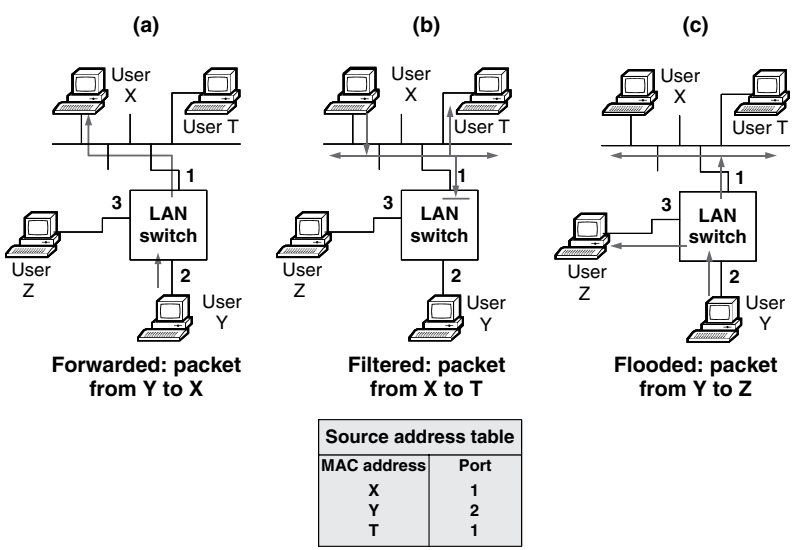

Figure 9.13 Illustration of bridge operation (this figure may be seen in color on the included CD ROM).

arrives at bridge port Z. Since Z is not contained in the SAT, that frame for user Z is flooded by the bridge to all ports except the incoming one. This way, Z will eventually receive its frame. When Z starts to transmit frames to other users (e.g., Z responds to the received frame), Z's SA will be learned by the bridge so that the next frame bounded for Z will not need to be flooded again.

Another situation an incoming frame is flooded is when the received frame is a broadcast or multicast frame. It can be seen that forwarding and filtering help to preserve the bandwidth in other parts of the network where the frame does not need to be flooded. As far as the end users are concerned, the existence of the bridge is transparent as all the LANs (collision domains) interconnected by a bridge form a single broadcast domain. An outgoing user frame will "magically" arrive at its destination host no matter which bridge port it is attached to. There is no address translation or frame encapsulation required when Ethernet frames are forwarded from one section of the network to another section.[6] Thus Ethernet bridging is also called transparent bridging.

9.4.3 Spanning Tree Protocol

It is not difficult to imagine that two or more bridged LANs can be transparently joined to form a larger LAN network by interconnecting bridge ports. When multiple bridges are connected together, there is a possibility to form loops of forwarding paths. Forwarding loops cause a problem called broadcast storm. An example is shown in Figure 9.14. Imagine a broadcast frame arriving at one bridge port. This frame will be broadcast to all other outgoing ports to arrive at another bridge. Each bridge seeing the broadcast frame will broadcast it to all outgoing ports. We end up with a situation that the broadcast frame is circulating and replicating itself exponentially in the network, eventually exhausting all the bandwidth resources.

Another problem of having loops in a system is that a host can be reached through multiple paths. This creates confusions in the bridge learning and forwarding logic. Nonetheless, the availability of multiple paths offers redundancy to allow network resilience in the case of link failures, because traffic can take alternate route to the destination.

The solution to the above problems is to avoid multiple forwarding paths from being formed in a bridged network using the STP. In the STP, all bridge ports regularly send out Bridge Protocol Data Units (BPDUs) to its link partner to exchange the topology information. The BPDUs are well-formed Ethernet frames using one of the aforementioned reserved multicast protocol destination addresses. (BPDUs use the MAC address 01 80-C2 00 00 00h). Each bridge port will only exchange BPDUs with its link partner, which will not be forwarded. Any host receiving a BPDU without being able to understand it will simply discard the

[6] Ethernet MAC address space is large enough to give each host a universally unique six octect address.

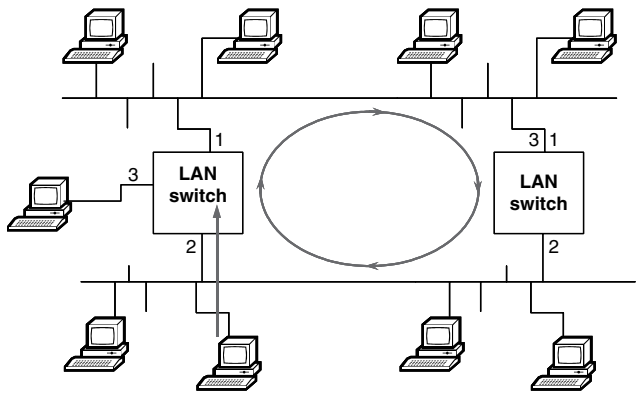

Figure 9.14 Loops formed by multiple bridges. Broadcast traffic sent from a host will keep looping in the network; eventually use up the bandwidth resources (this figure may be seen in color on the included CD ROM).

BPDU. After exchanging enough BPDUs, a root bridge is elected by the bridges participating in the STP. The redundant links are disabled from forwarding traffic (i.e., user data frames) by putting the ports connecting the link ends into the blocked state so that each LAN is connected to the root bridge only through a designated port on a designated bridge. Bridges elect the root bridge, designated bridge and designated ports based on a set of priority criterions such as port speed, bridge and port IDs, and/or manually provisioned cost parameters. For space reasons, the details of the spanning tree algorithm will not be discussed here. Interested readers should refer to IEEE 802.1D [27] for the details.

An example is given here in Figure 9.15. Figure 9.15(a) shows the physical connectivity of a LAN with multiple interconnected bridges. Multiple paths of forwarding loops are possible in this physical topology. After running the spanning tree protocol, the ports marked with crosses [Figure 9.15(b)] are put into blocking mode. The forwarding loops are removed and an active tree topology with Bridge 1 as the root bridge is formed.

One should realize that links blocked from forwarding traffic are still existent in the resultant physical network. Whether a port is in the active forwarding state or blocked state, STP is running continuously with every port constantly exchanging BPDUs with its link partner. The blocked ports only block user data frames from being forward.

When an active forwarding link goes down, the expected BPDU frames will be lost and the ports on its two ends will time out. This will trigger the STP to send advertisement messages to all connected bridges to recalculate the new active topology. Redundant links which were blocked before may then be activated (i.e., changed into forwarding state) to restore the traffic.

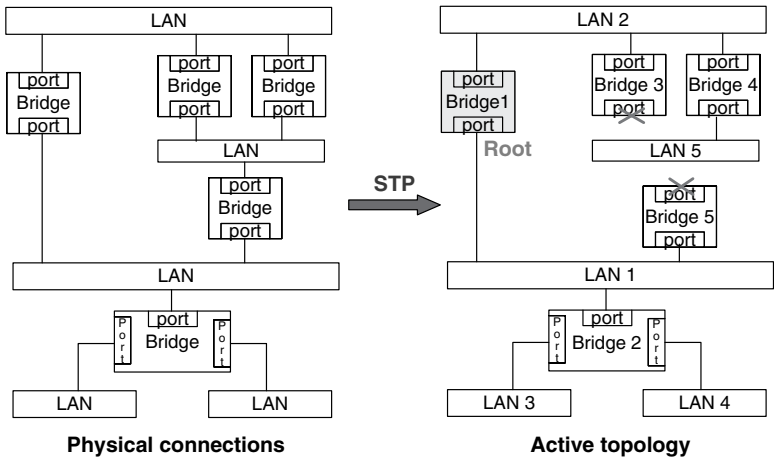

Figure 9.15 (a) Physical connections of a local area network connected with multiple bridges. (b) After running STP, the ports marked with crosses are set into block state so that forwarding loops are removed in the resulting active tree topology with Bridge 1 as the root of the tree (this figure may be seen in color on the included CD ROM).

9.4.4 Limitations of STP

Standard spanning tree protocol usually takes tens of seconds to restore the traffic in the case of a link failure. For burst mode links, when the network is inactive, there is no physical signal activity in the transmission channel. A link down can only be determined by BPDU time out. In the case of P2P full duplex links, when a physical link goes down, it will cause the keep-alive idle symbols to be lost or PCS coding violation, so that bridges do not need to wait for BPDU time out to notice a link failure.

A later variation of the spanning tree protocol called Rapid Spanning Tree Protocol (RSTP) was standardized as IEEE 802.1w [29], which restores traffic in a matter of a few seconds after a link failure.

The STP has the advantage of self-configuration. Once bridge ports are connected, there is no need for operator configuration and provision. However, for a given physical connectivity, the active logical tree topology formed by STP is static and cannot be adapted to the actual traffic pattern. An example is shown in Figure 9.16. In this figure, N1 to N5 represent bridges connected in a physical ring topology. Under normal conditions, the STP will elect bridge N1 as the root bridge and block the link between bridges N3 and N4 to remove the forwarding loop (i.e., the link between N3 and N4 will not forward traffic unless some other links in the ring becomes broken). As a result, any traffic between LAN3 and LAN 4 needs to travel across a long link through bridge N1, even though there is a direct path between bridge N3 and N4. The root bridge N1 can easily become the network performance bottleneck. In contrast, Layer 3 protocols use other mechanisms to

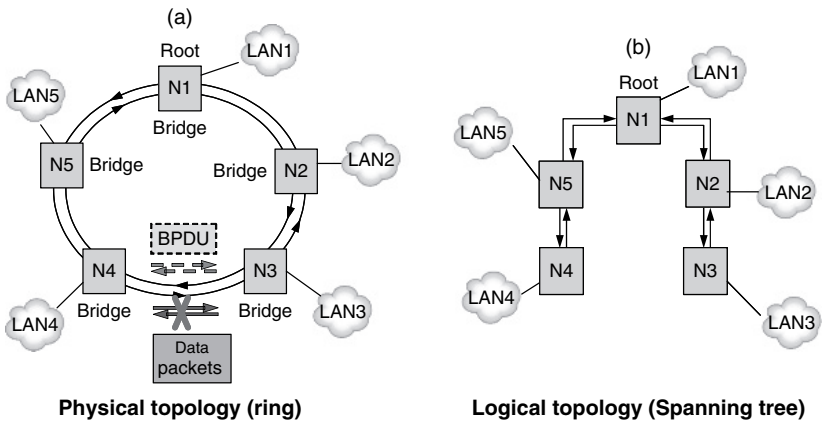

Figure 9.16 Inefficient use of link resources in STP. (a) Physical topology and (b) logical topology after running STP (this figure may be seen in color on the included CD ROM).

avoid infinite data loops and broadcast storms.[7] They can also make use of multiple routing paths for load distribution.

MPLS (Multiprotocol Label Switching) is another method to perform IP/Ethernet traffic switching and engineering. In a packet-switching world, to achieve SONET-like rapid reroute and traffic restoration (on the scale of 50 ms) in response to link failures, MPLS fast reroute can be employed. Packet streams in an MPLS network are routed on circuit-like label switched paths (LSPs), which are formed between the source and destination nodes. A back-up LSP on a diverse route is precalculated when an LSP is formed. Path statuses are monitored by end-nodes exchanging "Hello" messages. An example of MPLS fast reroute protocol is the RSVP-TE (Resource Reservation Protocol Traffic Engineering) protocol [30]. By default, in RSVP-TE, a "Hello" message is exchanged between the nodes at ends of a link every 5 ms. A node receiving the "Hello" message should respond to its link partner with "Hello Ack." A link is declared failure when proper "Hello Ack" is missed in 3.5 "Hello" intervals (i.e., 16.5 ms). When the primary path fails, traffic is quickly rerouted to the backup path.

9.4.5 VLAN and VLAN Stacks

VLAN Basic

As explained before, network hosts connected by bridges form a single broadcast domain. The virtual bridged LAN (VLAN) technology [31] segregates a

[7] A method called time to live (TTL) is widely used in routing protocols to prevent infinite loops and remove orphanage packets.

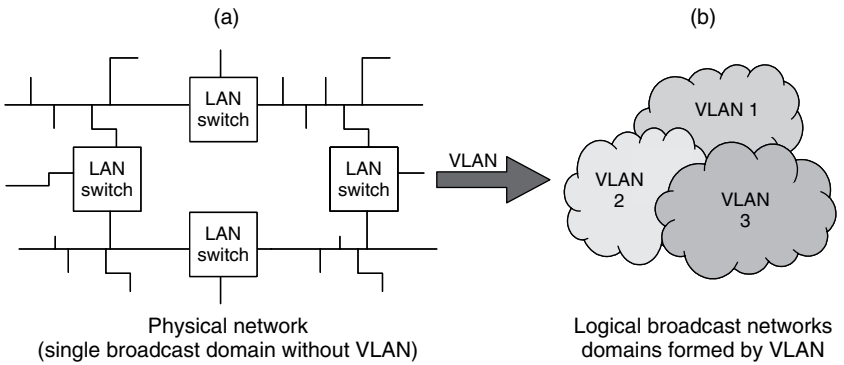

Figure 9.17 VLANs segregate physically connected LAN network (a) into multiple logical broadcast networks (b) (this figure may be seen in color on the included CD ROM).

network physically connected by bridges into multiple logical broadcast domains (Figure 9.17).

VLAN offers the following network advantages:

(1) It limits broadcast traffic to smaller groups and improves network performance.
(2) It provides network privacy and security by separating traffic belonging to different organizations.
(3) It eases network management by allowing operators to assign network ports to different VLAN groups.

VLAN bridges can be implemented so that each logical broadcast domain can have its own separate spanning tree, thus allowing operators to have better control of the resulting logical network topology and traffic distribution [29].

VLAN bridges need to classify and tag data frames so that they can be segregated according to the VLAN they belonged to. This is achieved by adding a four-octect VLAN tag (also called Q-tag) after the SA field of the original Ethernet frame as shown in Figure 9.18. The first two octets correspond to the length/type field of the original Ethernet frame and contain a length/type field value of hexadecimal value $0\times81\text{-}00$. The next two octets represent the tag control information which includes a 3-bit user priority field, a 1-bit canonical format indicator (CFI), and a 12-bit VLAN ID (VID). The 3-bit user priority field can be used to implement eight service quality classes. The CFI field was designed for use with token ring technologies and has no significance any more except for backward compatibility. The 12-bit VID allows 4094 different VLANs to be supported. (The 0 VID is used to represent priority frames and VID $0\times FFF$ is reserved.) Frames belonging to a particular VLAN will only be broadcast/forwarded to hosts on the same VLAN.

Figure 9.19 shows the block diagram and operation of a VLAN bridge. In a VLAN capable environment, there are three types of Ethernet frames: (1) untagged

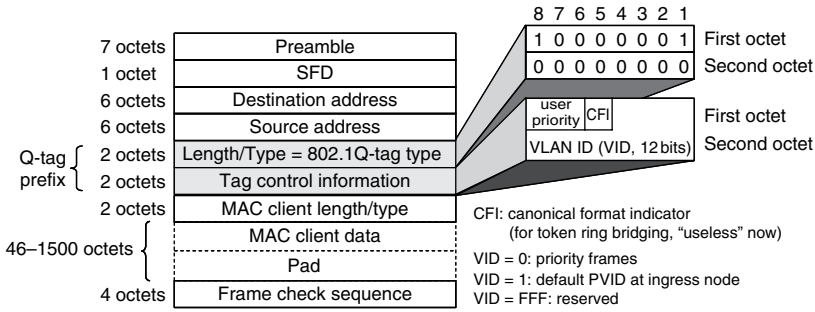

Figure 9.18 VLAN tagged Ethernet frame format (this figure may be seen in color on the included CD ROM).

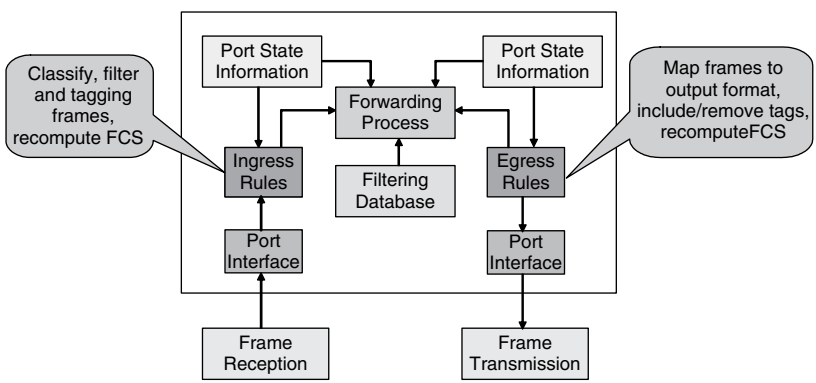

Figure 9.19 Block diagram of a VLAN bridge (this figure may be seen in color on the included CD ROM).

frame, (2) priority-tagged frame (VID = 0), and (3) VLAN-tagged frame. Similar to the transparent bridging philosophy described previously, as far as end users are concerned, the existence of VLAN is transparent.

All end user frames in access networks are normally untagged frames. When a user frame is received by a VLAN bridge port shown in Figure 9.19, it is processed by a set of ingress rules. The ingress rules add a VLAN tag to the user frame based on some provisioned rules. The most common type of VLAN classification is port-based in which each access port is assigned with a provisioned VID. VLANs can also be associated with MAC addresses or upper layer protocol identifiers encapsulated within Ethernet frames. In the latter two cases, the ingress rules also need to perform filtering and classification functions. Another function performed by the ingress rule is recalculation of the FCS after inserting the VLAN tag. At the output of a VLAN bridge port, a set of egress rules are performed to remove the tag and recalculate the FCS. Thus the end users have no idea of the existence of VLANs.

In a port-based VLAN, the operator can easily change a user from one broadcast domain to another broadcast domain by changing the VID of the port that the

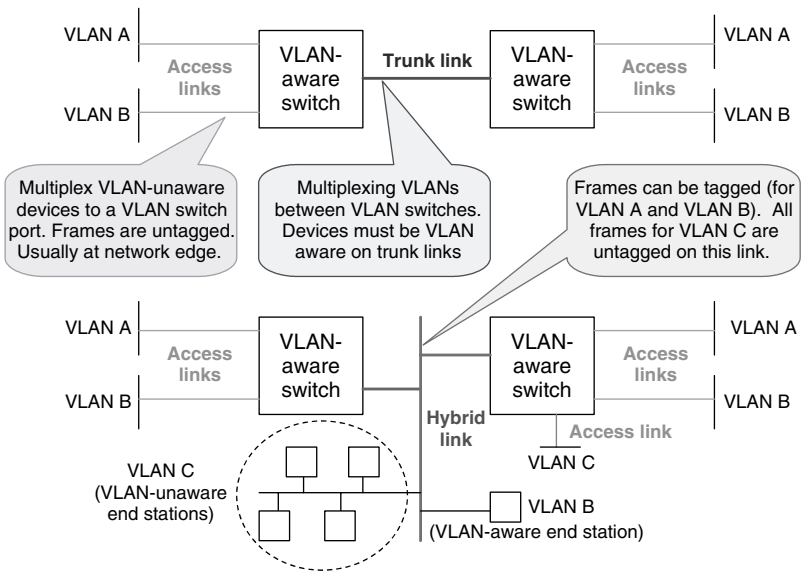

Figure 9.20 Access, trunk and hybrid links in a VLAN enabled network (this figure may be seen in color on the included CD ROM).

user is connected to. An IT manager can also separate users in different departments on different VLANs so that they do not have access to each other's network without going through a gateway.

Figure 9.20 shows three different types of links in a VLAN-enabled network. Frames transported in access links are traditional Ethernet frames with no VLAN tags. These links are usually connected to end users. The trunk links are usually links between VLAN bridges. All the frames on trunk links are VLAN tagged. In other words, trunk links are in effect multiplexing links of different VLANs. A third type of link is the less common hybrid link which can transmit both VLAN-tagged and untagged frames. In this case, all the untagged VLAN frames must belong to one and only one VLAN.

VLAN Stacks

The VLAN idea can be used by service providers to provide virtual layer-2 connectivity services to users over wide area backbone networks. However, two issues must be solved.

(1) The 12-bit VID supports only about 4000 different VLANs. This is very limiting in a carrier environment.
(2) VLAN has already been widely deployed in corporate LANs. Customers subscribing to the services would like to preserve their VIDs and be able to manage their own VID space.

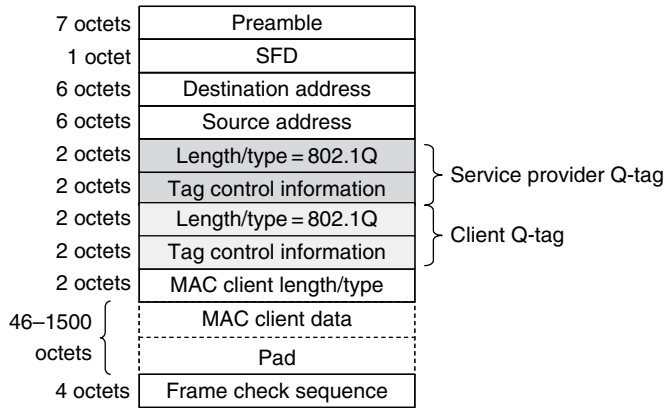

Figure 9.21 Q tag stacking in IEEE 802.1ad provider bridges (this figure may be seen in color on the included CD ROM).

The simple way to resolve the second problem is to stack another VLAN tag, called service VLAN tag (or S-tag), on top of the customer VLAN tag (or C-tag) as shown in Figure 9.21. This technique is also called Q-tag-in-Q-tag, or QiQ, and is standardized as IEEE 802.1ad Provider Bridges [32]. The QiQ technique nested customer VLANs (C-VLANs) inside service VLANs (S-VLANs) to achieve C-VLAN transparency from a customer point of view.

9.5 CARRIER ETHERNET

The cost advantage of Ethernet and the convergence of voice, data, and video services on packet-oriented network infrastructure made Ethernet services the fastest growing services in the telecommunication industry. Instead of requesting traditional TDM-based leased line services, more and more customers are now requesting Ethernet leased lines which not only are cheaper and but also have wider bandwidths.

Traditionally, Ethernet has been managed by corporate IT personnel. Ethernet service definitions and management are new territories to telecom service providers. The new challenges facing a carrier class Ethernet transport system includes scalability, OAM, availability, and security. We will touch some of these subjects in the following sections.

9.5.1 Scalability

To solve the limited 802.1ad VLAN address issue, the IEEE 802.1ah [33] provider backbone bridge (PBB) standard was created. In the IEEE 802.1ah standard, a service provider SA and DA is stacked on top of the customer addresses. This provides a virtually unlimited address space for operators to support as many

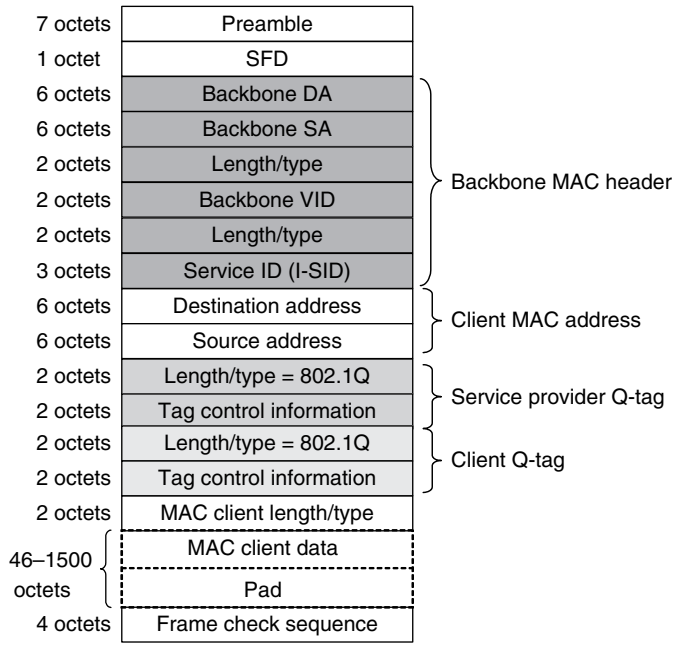

Figure 9.22 Provider backbone bridge (PBB) MAC frames (this figure may be seen in color on the included CD ROM).

customer VLANs as they want. Since the customer MAC addresses are nested within service provider addresses, this method is also nicknamed as MAC-in-MAC or MiM. The Mac-in-Mac stacking is shown in Figure 9.22. Interested readers are referred to [33] find more details from IEEE 802.1ah.

9.5.2 Ethernet Transport

The simplest Ethernet service is the P2P Ethernet signal transport over long distances, traditionally called transparent LAN. Figure 9.23 shows two approaches to Ethernet signal transport over a long distance WDM optical network. The first approach puts native Ethernet frames directly on optical wavelengths. The symbols transmitted on the physical link use Ethernet PCS line coding (i.e., 8B10B for Gigabit Ethernet and 64B66B for 10 Gigabit Ethernet). In this case, the transport signal is identical to the signal presented at the UNI and complete physical layer transparency is achieved.

Another approach to transport Ethernet frames is to make use of the widely deployed legacy transport networks which were built with other technologies such as SONET/SDH [34] or ITU-T G.709 OTN (optical transport network) [35]. Ethernet frames are encapsulated in other transport frames such as the SONET SPE

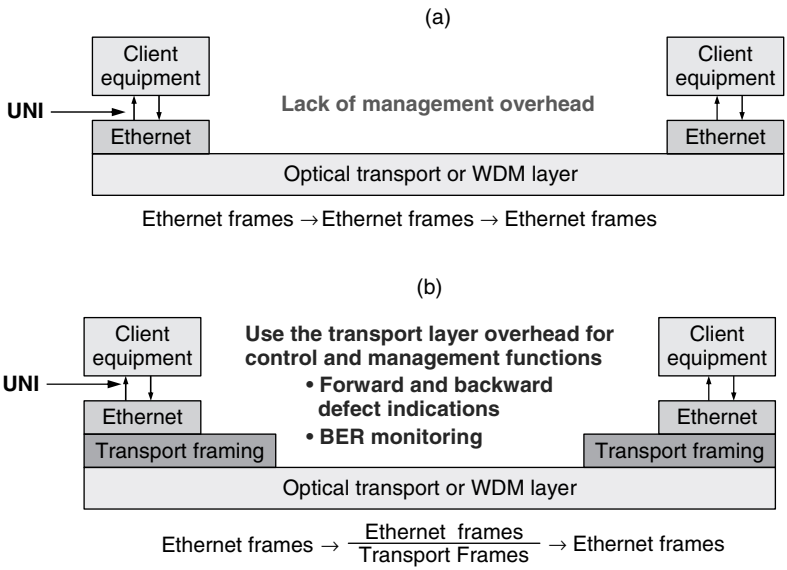

Figure 9.23 (a) Direct native Ethernet transport over WDM optical layer and (b) Ethernet transport over transport framing (this figure may be seen in color on the included CD ROM).

(synchronous payload envelope) before being placed on the optical layer [36, 37]. In this approach, Ethernet is only used as the UNI between the client equipment and the transport network. Legacy transport networks were built with extensive management facilities and mechanisms for fault tolerance and fast recovery, which complements the corresponding inadequacies of Ethernets, at least during the transitional period before the Ethernet community develops its own.

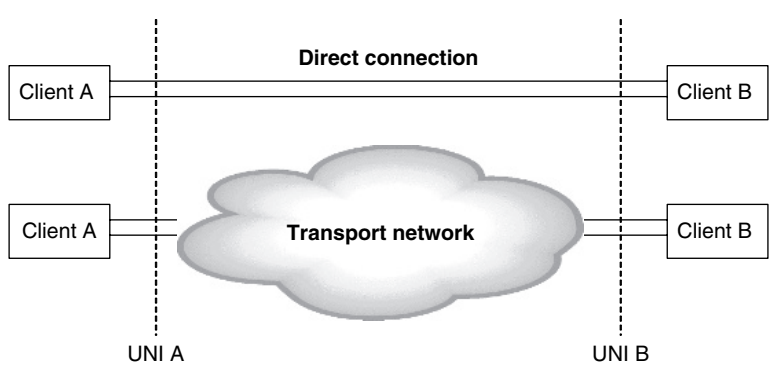

Figure 9.24 Client equipment joined by direct fiber connection (top) and transport network (bottom). From a user's perspective, the transport network should be transparent to client equipment, i.e., ideally it should behaves as a pair of wires joining UNI A and UNI B as in the top diagram (this figure may be seen in color on the included CD ROM).

From a user's perspective, the underlying technology employed for transporting the client Ethernet frames should be transparent. Figure 9.24 shows the comparison of client equipment joined by direct fiber connections between clients' Ethernet interfaces (top) and by a transport network (bottom). Ideally, from a customer's perspective, the transport network between the two dash lines which indicate the UNI demarcation between a service provider and the customer network, should behave as a pair of wires.

In reality, the ideal transparency as described above cannot always be achieved and may not always be the desired behavior either. Despite the difficulty to maintain complete transparency, the transport equipment should provide MAC frame transparency at the minimum, i.e., no filtering and dropping of customer Ethernet frames should occur within the transport network.

Figure 9.25 shows an example of multiplexing dual Gigabit Ethernet (GbE) over a SONET OC-48 link. A SONET OC-48 link has a data rate of 2.488Gb/s. Although the MAC data of GbE runs at 1.0 Gb/s, after the 8B10B PCS encoding, a GbE interface has a symbol rate of 1.25 Gbaud/s. So it is impossible to multiplex two GbE physical layer signals onto an OC-48 payload and maintain both client interfaces at line rate at the same time. As indicated in the figure, the client signals are terminated at the MAC layer to strip off 8B10B encoding before being multiplexed using POS [36, 37]. Physical layer functions implemented using Ethernet PCS control codes such as auto-negotiation [18, Clause 37] are terminated locally. In addition, the clocks at the Ethernet interfaces need to be decoupled from the SONET clock because of the differences in clock rate and accuracy requirements.[8]

In return for the loss of physical layer transparency, one has obtained the SONET manageability in the transport network, as well as better optical layer utilization by multiplexing two Ethernet streams onto one single SONET wavelength. In addition, forward error correction (FEC) such as that available from

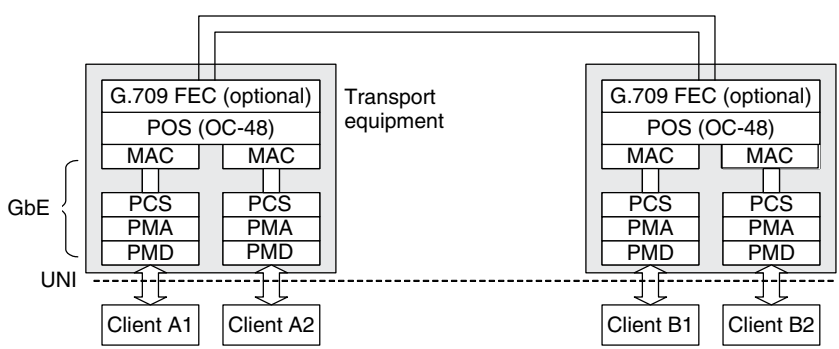

Figure 9.25 Gigabit Ethernet (GbE) multiplexing using packet over SONET (POS) (this figure may be seen in color on the included CD ROM).

[8] Ethernet uses asynchronous transmitters. Each receiver recovers the clock from the received signal. The transmitter clock and receiver clock are completely independent.

G.709 OTN can be added to increase the signal transmission distance without intermediate regeneration.

In a later section, we will see the implications of client/transport interface decoupling in different network protection switching scenarios.

9.5.3 Generic Framing Procedure

GFP is standardized as ITU-T G.7041 [12, 38], which is used to encapsulate packet data (including Ethernet frames) for transport. There are two different types of GFP: frame based GFP (GFP-F) and transparent GFP (GFP-T), which are shown in Figure 9.26 and Figure 9.27.

As shown in Figure 9.26, GFP-F only encapsulates the contents of Ethernet frames. It starts with a payload length indictor and header error control (HEC) fields, which also marks the beginning of GFP frames. Ethernet line coding overhead, the redundant preamble and SFD fields are removed in GFP-F encoding and recreated in GFP-F decoding. Therefore, GFP-F helps to preserve the transport bandwidth.

GFP-T was designed to transparently transport 8B10B code words. In addition to the actual data words, the 8B10B code words also include idle symbols transmitted during IFGs (interframe gaps) between adjacent Ethernet frames, and the physical layer control codes such as the link negotiation words used by Gigabit Ethernet. Not all the 10-bit words are used in 8B10B codes. GFP-T converts fixed-length blocks of 8B10B code words and convert them into 64B65B codes [38].

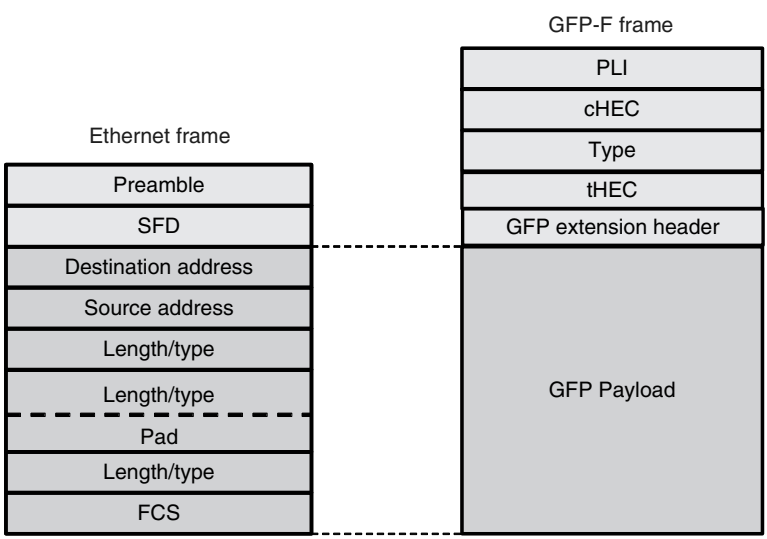

Figure 9.26 Frame based GFP (GFP F). PLI: payload length indicator, cHEC: core header error control, tHEC: type header error control (this figure may be seen in color on the included CD ROM).

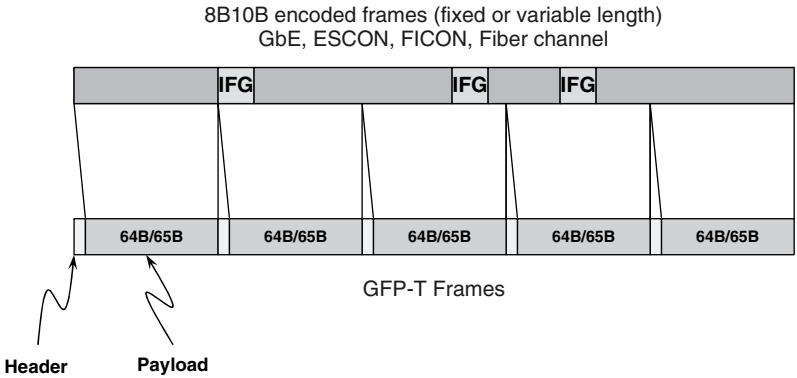

Figure 9.27 Transparent GFP (GFP T). IFG: interframe gap (this figure may be seen in color on the included CD ROM).

All the physical layer control codes in 8B10B codes are included in 64B65B codes and recreated at the other end of the link.

The advantage of GFP-T is that it transparently preserves the end-to-end 8B10B physical layer signaling with a reduced overhead of only 1.5% as opposed to 25%. Moreover, there is no need to wait for the whole frame to be received before encapsulation and thus reduces the transport latency.

GFP frames are usually further encapsulated in SONET or OTN frames. Ethernet speeds increase by multiple of 10 from generation to generation. However, SONET signal rates increase by multiples of 4. The lowest SONET rate, OC3, is 155 Mb/s. This mismatch makes it difficult to efficiently map Ethernet signals on SONET signal hierarchies. To make efficient use of the transport network bandwidth, the ITU-T VCAT standard G.7043 [13] was created to allow GFP frames to be inversely multiplexed to SONET/SDH tributaries with 1.5 Mb/s VC-1.5 granularity. The ITU-T G.7042 [14] LCAS allows dynamic adjustment of the number of inverse multiplexed tributary streams and thus the bandwidths used for carrying Ethernet traffic in a transport network.

9.5.4 Protection Switching

There are many different ways to perform Ethernet protection switching at various network layers. In this section, we briefly describe some approaches and considerations besides the spanning tree protocol described before.

Link Aggregation

Link aggregation [18, Clause 43] is a method to increase data throughput by bundling multiple Ethernet links in parallel to form a link aggregation group

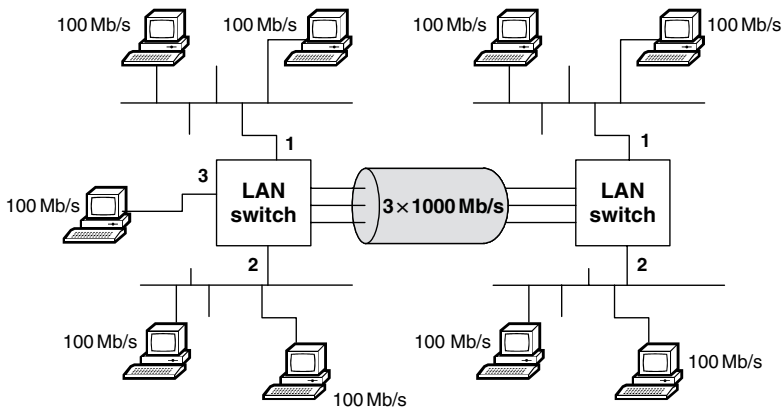

Figure 9.28 Link aggregation increases the throughout by bundling parallel Ethernet links (this figure may be seen in color on the included CD ROM).

(LAG) as shown in Figure 9.28. In this figure, the three 1000 Mb/s links form a single logical link with an effective throughput of 3000 Mb/s.

In normal bridge connections, parallel links will form forwarding loops and the STP will block all but one link for forwarding traffic. In a LAG, all the parallel links represent a single logical link. All the Ethernet interfaces at one end of a LAG represent a single logical MAC interface with one shared MAC address, which can be the MAC address of one of the parallel interfaces.

One of the requirements in Ethernet frame delivery is to maintain the order of frames as there is no sequence number embedded in Ethernet frames for reordering out of sequence frames at the destination node. The parallel links in a LAG create the opportunity for out-of-order frame delivery at the egress point. To avoid this issue, link aggregation makes use of higher layer protocol signatures (such as IP source and destination addresses, and TCP/UDP port numbers) in load balancing so that Ethernet frames belonging to the same application stream (i.e., identified by the same IP SA, IP DA, and/or TCP port number) are always sent through the same component link in an LAG. Thus the frame delivery order is preserved from source to destination on a per application basis. A hash function based on upper layer protocol signatures is usually used to calculate the link in an LAG that will be used for a particular stream of data frames.

Before 100GbE becomes available, LAG is used by many service providers to aggregate multiple lanes of 10 GbE traffic. There are, however, many problems associated with LAG, which motivate the industry to go for a full-fledged 100 GbE [39 42]:

(a) LAG distributes traffic over parallel links via flow-based hash mechanism, which cannot be used to re-order frames from parallel links and cannot guarantee equal distribution of load.
(b) "Special" traffic (multicast, broadcast, control traffic, etc.) usually traverses a single component link, and load balance is lost.

(c) The unpredictable link removal and insertion make LAG operational cumbersome.
(d) Transponder cost for multiple 10 GbE LAG in WAN is very high.

Link aggregation offers resiliency to link failures. If one of the component links in an LAG fails, its traffic will be redistributed to the remaining links, thus providing a graceful degradation. The disadvantage of link aggregation is that it only works as P2P links and with interfaces of the same speed.

Protection in the Presence of the Transport Layer

An advantage of using an optical transport layer for Ethernet backbone is the ability to implement protection switching in the transport layer. Transport equipment generally offers much faster protection switching than data equipment in a network failure, usually within 50 ms. Understanding the interaction between the data layer and the transport layer is important in designing wide area Ethernet backbones that gives the best protection performance.

Figure 9.29 shows a pair of routers/bridges connected back-to-back directly by an Ethernet link. In general, routers or bridges will also continuously verify the link integrity by exchanging keep-alive PDUs (the so-called Hello message). To reduce the bandwidth overhead, such keep-alive PDUs are exchanged with a very low frequency. By default, the "Hello" message interval in a 802.1D bridge is set to 2 sec. When a predetermined number of PDUs are not received after a timeout period, the link is declared lost. As a result, routers/bridges will send topology advertisement messages to the rest of the network to recalculate the routing table or the new spanning tree so that an alternative data path can be found. In addition to PDU timeout, when the link is broken as shown in the figure, both port interfaces connecting to the link detects the physical link down condition immediately. A physical link down can trigger new forwarding path calculation in real time, thus minimizing the network unavailable time.

When a transport layer is present, as mentioned before, the transport layer and the Ethernet layer are physically decoupled. Consequently, a failure in the transport interface may not necessarily cause link down at the Ethernet interface as shown in Figure 9.30. In such a scenario, the client devices have no choice but to rely on the PDU timeout mechanism to detect the link outage (which can cause a delay as long as 20 sec). To overcome this problem, the transport equipment could bring down the client interface intentionally when a transport link fault is detected.

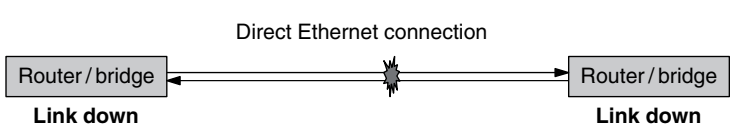

Figure 9.29 A physical link failure will trigger link down at both port interfaces immediately (this figure may be seen in color on the included CD ROM).

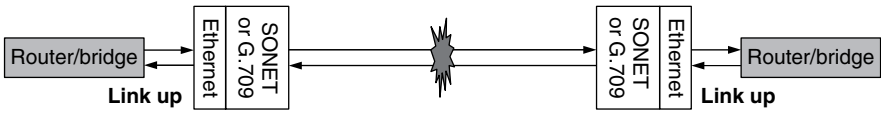

Figure 9.30 A physical link failure on the transport side may not necessarily cause the client interface link down (this figure may be seen in color on the included CD ROM).

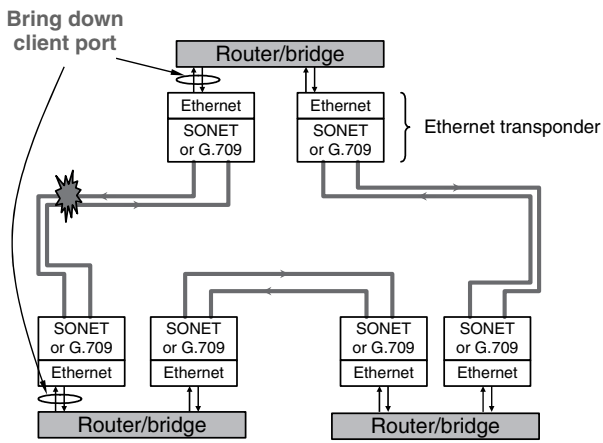

Figure 9.31 A wide area Ethernet ring network using SONET/G.709 for transport. Restoration is performed at Layer 3 or Layer 2 by routers or bridges. To speed up traffic restoration time, when the transport link is lost, the associated client ports are brought down (this figure may be seen in color on the included CD ROM).

Figure 9.31 shows a wide area Ethernet using SONET/G.709 as P2P transport layer only. Protection and restoration is performed by the router/bridges. In this case, a failure at the transport interface brings down the associated client ports to speed up the restoration time.

Figure 9.32 shows a scenario that the transport link is protected. The tail-end switches move the transport link to the protection path within 50 ms when the working path fails. This happens at a timescale much faster than timeout period of Layer 2/Layer 3 PDUs. In this case, if the transport equipment brings down the client interface upon detecting transport link failures, the client equipment will sense the link outage and start to recalculate the spanning tree or routing table right away. For L2 bridges, this will also cause the SAT to be flushed out and relearned, increasing the volume of broadcast traffic in the network temporarily. Therefore, the decoupling between the client and the transport interfaces is actually beneficial because it avoids racing between the data networking layer and transport layer in restoring the traffic when a failure in the transport network occurs.

Thus Ethernet transport equipment (or transponders) should be built so that the ability to bring down the client Ethernet interfaces can be enabled or disabled at appropriate times, depending on the actual network configuration.

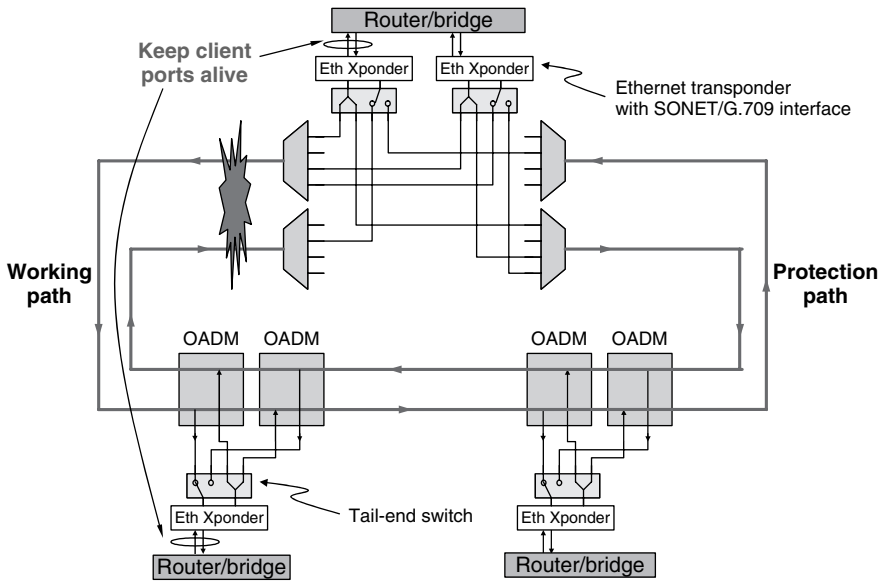

Figure 9.32 Ethernet transport with optical layer protection. A protected transport link should not cause the client link to go down to avoid racing conditions in protection switching (this figure may be seen in color on the included CD ROM).

9.5.5 Ethernet Service Models and Service Level Agreements

It has been a challenge for carriers to offer Ethernet services because of the lack of standards in SLA definitions. The MEF was initially formed by equipment vendors to tackle Ethernet service models, SLA, and OAM issues [11]. The business value of a common set of languages and standards to specify Ethernet services was quickly recognized by carriers [both telecom operators and cable TV multiple service operators (MSOs)] who have later become the dominating participants at MEF.

MEF does not specify the technology used to implement networks. Instead, it defines the bandwidth and PDU behaviors at the UNI between customers and service providers, or the NNI (network network interface) between service providers. MEF specifies Ethernet services as P2P (called E-Line) and multipoint-to-multipoint (called E-LAN) in terms of EVCs (Ethernet virtual circuits) [43]. From a customer's perspective, E-Line behaves as an Ethernet transport link whereas E-LAN behaves as a bridged network. EVC attributes include performance specifications such as bandwidth profile, packet loss rate, packet delay, and delay variations.

On the physical layer, Ethernet port interface speeds are all fixed. The effective data throughput, however, depends on actual frame lengths and IFG widths which can be stretched to limit the data throughput and perform ingress bandwidth shaping. MEF uses committed information rate (CIR), excess information rate (EIR), committed burst rate (CBR), and excess burst rate (EBR) as bandwidth profile attributes to specify SLA [43]. The CIR and EIR represent average bandwidth throughput over defined timing periods

and are measured in bits per second, whereas CBR and EBR are measured in bytes per second. MEF10.1 [43] specifies three levels of bandwidth profile compliances. Green represents service frames within the limits of CIR/CBR and will be guaranteed (i.e., subject to SLA). Yellow represents service frames exceeding CIR/CBR but within EIR/EBR. These are allowed but not subject to SLA. Red represents service frames exceeding EIR/EBR which are not allowed and will result in packet loss.

In addition to Ethernet service attribute model definition, MEF technical documents also cover the aspects of control plane, management plane [44], circuit emulation on Ethernet [45], mobile data back hauling using Ethernet, protection switching etc. Because of space limitation, it is impossible to thoroughly discuss MEF works in great details. Interested readers could download MEF technical specifications at MEF website free of charge [46].

9.6 ETHERNET PASSIVE OPTICAL NETWORKS

9.6.1 Ethernet Passive Optical Network Architecture

PON (passive optical network) is an access network technology with point-to-multipoint (P2MP) connectivity. More details on PON technologies can be found in Chapter 10 by Wagner. The P2MP connectivity makes EPON (Ethernet PON) very different (both from a transmission viewpoint and protocol view point) from the traditional CSMA/CD and P2P full-duplex Ethernets.

A PON is characterized by a passive remote node (RN) to distribute signals from an optical line terminal (OLT) located at a central office to a number of optical network units (ONUs) at customer sites [47]. Ideally, the fiber plant from the OLT to the ONUs is completely passive. A TDM-PON uses a passive power splitter as the RN. The same signal from the OLT is broadcast to different ONUs by the splitter. Signals for different ONUs are multiplexed in the time domain. ONUs recognize their own data through the address labels embedded in the downstream broadcast signal. EPON falls into the category of TDM-PON. A WDM-PON uses a passive WDM coupler as the remote terminal. Signals for different ONUs are carried on different wavelengths and routed by the WDM coupler to the proper ONU in a virtual P2P fashion. Since each ONU only receives its own wavelength, a WDM-PON has better privacy and better scalability. However, WDM devices are significantly more expensive, which made WDM-PONs economically less attractive at this moment.

The EPON protocol layering diagram can be found in Figure 9.2, along side with standard modern Ethernet layering. Figure 9.33 shows the architecture of an EPON infrastructure. Ethernet frames are used to carry the data between the OLT and ONUs in an EPON. The upstream traffic and downstream traffic are separated on 1.31 μm and 1.49 μm wavelengths, i.e., by wavelength division duplex. Usually, an OLT will serve 16 32 ONUs, which are separated by up to 20 km away from the OLT. The optical power budget between the OLT and ONU eventually limit the transmission distance as well as the number of ONUs that can be supported.

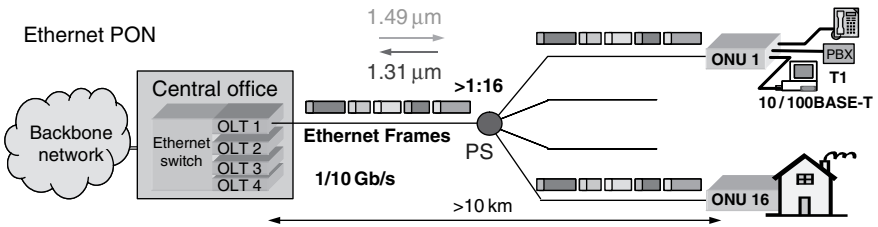

Figure 9.33 Architecture of an EPON infrastructure (this figure may be seen in color on the included CD ROM).

Current EPON standard (802.3ah) specifies 1000 Mb/s data throughput (1.25 Gbaud/s physical symbol rate) on the feeder link between the OLT and ONU. The downstream signal is broadcast to all ONUs in continuous mode. Upstream signals from different ONUs all merge at the power splitting RN. Because a single OLT receiver is shared among all ONUs, when an ONU is not transmitting, it should turn off its transmitter to avoid interfering with other ONUs' upstream signal. Without coordination, upstream frames from different ONUs will collide in time.

9.6.2 Multipoint Control Protocol

In order to avoid collision, all the upstream transmission is scheduled by the OLT centrally. The CSMA/CD mechanism cannot be used in a PON system for the following reasons: (1) the directional power splitter makes carrier sense and collision detection impossible because without using special tricks no ONU can monitor the optical transmission from other ONUs on the same PON; and (2) the data rate and distance covered by a PON system greatly exceeds the limits imposed by the CSMA/CD protocol. The CSMA/CD protocol becomes very inefficient under conditions of high bandwidth and long transmission distance [48].

In EPON, scheduling is performed by the MPMC (multipoint MAC control) layer using the Multipoint Control Protocol (MPCP) [18, Clause 64]. As indicated in Figure 9.2, the MPCP protocol entities in the OLT and ONU form a master-slave relationship with the OLT as the master. In the MPCP protocol, the OLT schedules the starting time and duration for an ONU to transmit upstream data bursts using the Gate MPCPDU (Multipoint Control Protocol Data Unit). ONUs inform the OLT their buffer status using the Report MPCPDU. Based on the reported information, the OLT can dynamically allocate the upstream bandwidth to make the most efficient use of the shared link between the OLT and ONUs.

Since ONUs are located at different distances from the OLT, signals from different ONUs will experience different delays before reaching the OLT. It is therefore important to establish a timing reference between the OLT and an ONU so that after accounting for the fiber delay, when the ONU signal arrives at the OLT, it arrives at precisely the same moment that the OLT intends for the ONU to transmit. The timing reference between the OLT and ONUs is established through the *ranging* process.

Ranging measures the round trip delay between the ONU and OLT, also using the Gate and Report MPCPDUs, which have time stamps embedded. From the time stamps in Gate and Report MPCPDUs, the OLT measures the round trip time (RTT), which is then stored and used to adjust the time that data frames from an ONU should be transmitted. All ONUs are thus aligned to a common logical time reference after ranging so that collision does not occur in a PON system.

From time to time, an EPON OLT will periodically broadcast Discovery Gate messages to discover unregistered ONUs. A new ONU joining the network detects the Discovery Gate and responses with a Register Request to the OLT. After sending the Discovery Gate, an OLT must reserve a time period called discovery window for ONUs that have not been ranged to response. The size of the discovery window depends on the maximum differential delays between the closest ONU and the furthest ONU. Optical signal delay in 1 km of fiber is 5 µs. Therefore, for 20 km of differential distances between ONUs, an RTT difference of 200 µs needs to be reserved in the discovery window. It should be realized that if the upper bound and lower bound of ONU distances are known to the OLT (e.g., through management provision), then instead of reserving a ranging window covering the maximum allowed separation between an ONU and an OLT, the size of ranging window can be reduced to cover only the maximum differential distance among ONUs. If multiple ONUs attempt to join the PON at the same time, collision may occur during discovery. This is resolved by ONUs backing off with a random delay in EPON.

If the register request is properly received by the OLT, the OLT will issue the Register message to the ONU, followed by a Gate message. The Gate message schedules the ONU to transmit an upstream Register Acknowledgment which completes the new ONU registration. Figure 9.34 depicts the auto-discovery

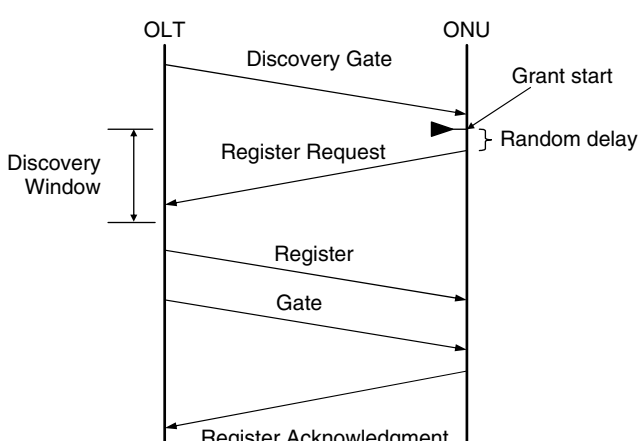

Figure 9.34 Auto discovery process in EPON (reprinted with permission from IEEE Std. IEEE Std. 802.3, 2005, *Carrier Sense Multiple Access with Collision Detection (CSMA/CD) Access Method and Physical Layer Specifications*, Copyright [2005] by IEEE)

process in EPON. During operation, the ONU and OLT may continuously monitor the fluctuation of RTT due to changes such as temperature fluctuation, and perform fine adjustment by updating the RTT register value.

9.6.3 Point-to-Point Emulation in EPON

In an Ethernet environment, L2 connection is achieved using IEEE 802.1-based bridges [27]. As explained earlier, a bridge performs L2 forwarding function by examining the SA and DA of each received frame. If both of them are connected to bridge through the same port, the bridge filters out the packet without forwarding it. This helps to preserve the bandwidth in other parts of the network and improves the network performance.

In an EPON system, the P2P symmetric Ethernet connectivity is replaced by the asymmetric P2MP connectivity. Because of the directional nature of the remote node, ONUs cannot see each other's upstream traffic directly (Figure 9.35). In a subscriber network, this directional property provides an inherent security advantage. Nevertheless, it also requires the OLT to help forwarding inter-ONU transmissions.

Without any treatment, an IEEE 802.1 bridge connected to the OLT would see all the inter-ONU frames with SA and DA belonging to MAC entities connected to the same bridge port, and would thus determine that they were within the same broadcast domain. As a result, the switch would not forward the traffic between different ONUs connected to the same OLT.

To resolve this issue, a point-to-point emulation (P2PE) function has been created in the RS. The P2PE function maps EPON frames from each ONU to a different virtual MAC in the OLT, which is then connected to a higher layer entity such as L2 switch (Figure 9.36).

The P2PE function is achieved by modifying the preamble in front of the MAC frame to include a logical link ID (LLID) [18, Clause 65]. The modified preamble with the LLID is used in the PON section between the OLT and ONUs. The format of the modified EPON preamble is shown in Figure 9.37. It starts with an SLD

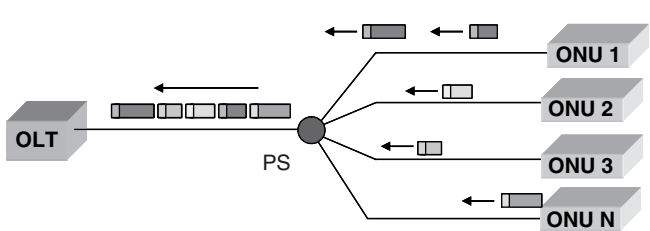

Figure 9.35 Although all the ONU traffic arrives at the same physical port at the OLT, because of the directional power splitting coupler used at the remote node, ONUs cannot see each other's traffic without the forwarding aid of OLT (this figure may be seen in color on the included CD ROM).

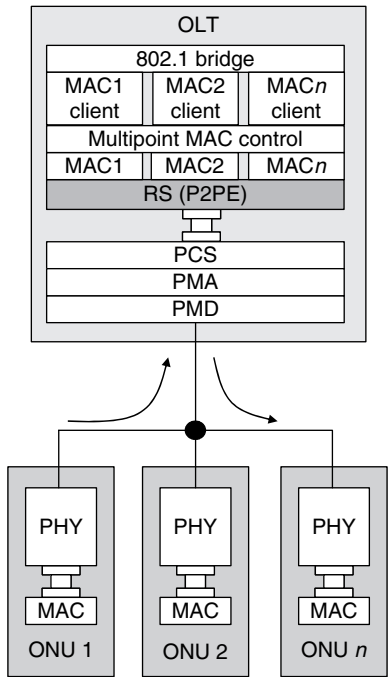

Figure 9.36 Point to point emulation in EPON.

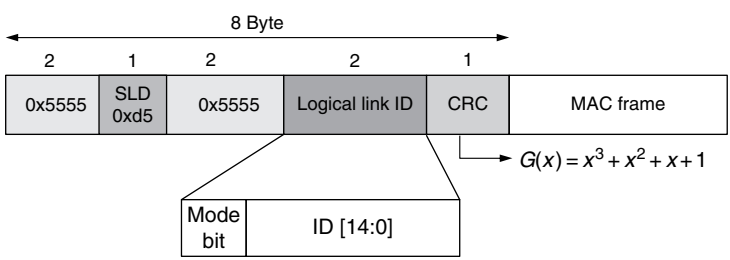

Figure 9.37 Modified preamble with LLID for point to point emulation in EPON (this figure may be seen in color on the included CD ROM).

(start LLID delimiter) field, followed with a two-byte offset and a two-byte LLID. A one-byte CRC field protects the data from the SLD to the LLID inclusive. The first bit of the LLID is a mode bit indicating broadcast or unicast traffic. The rest of the 15 bits are capable of supporting 32 768 different logical ONUs. As mentioned earlier, the actual number of ONUs that can be supported per PON is limited by the power budget. LLIDs are assigned to ONUs at ONU registration time.

The mode bit is set to 0 for P2PE operation. Figure 9.38 shows principle of EPON P2PE. When the mode bit is set to 1, the OLT uses the so-called SCB

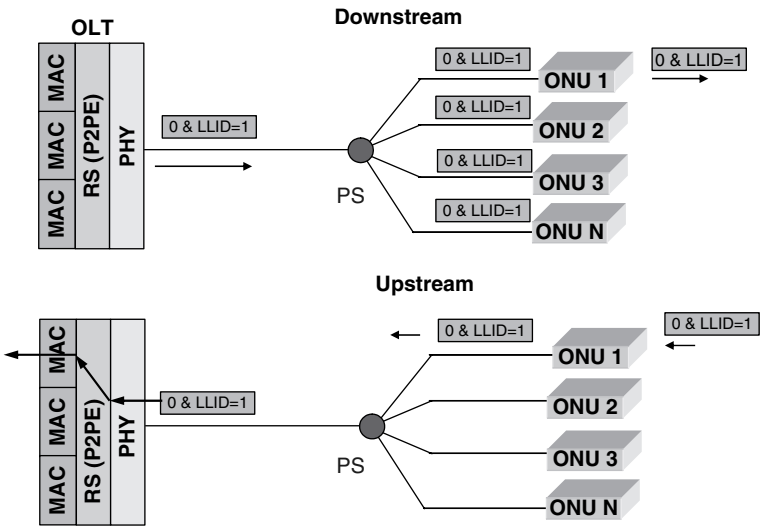

Figure 9.38 EPON point to point emulation operation (this figure may be seen in color on the included CD ROM).

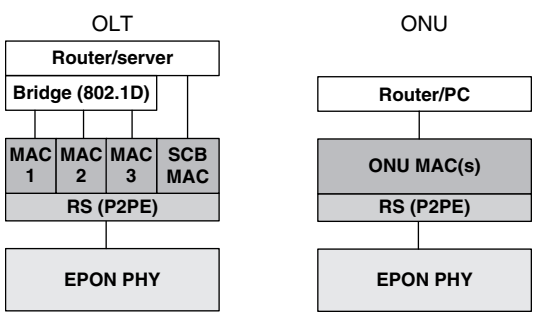

Figure 9.39 Point to point and single copy broadcast (SCB) MACs in an EPON model (this figure may be seen in color on the included CD ROM).

(single-copy broadcast) MAC to broadcast traffic to all ONUs. It takes the advantage of native EPON downstream broadcast operation. To prevent broadcast storm in L2 switches, EPON standard recommends avoiding the connection of the SCB port to 802.1 switches, and use it only to connect to L3 routers[9] or servers for the purpose of disseminating broadcast information. Figure 9.39 illustrates the SCB MAC and emulated P2P MACs in an EPON model.

[9] L2 switches uses STP to ensure no multiple paths exist between two nodes and thus avoid the possibility of forming loops and creating broadcast storms. When both the emulated P2P link and SBC link exist between the OLT and ONU, STP will get confused. Unlike L2 switches, L3 routing protocols can make use of multiple signal paths for load balancing. They can also use the TTL field to avoid loops.

9.6.4 Burst Mode Operation and Loop Timing in EPON

Ethernet protocol is a burst mode protocol. However, modern P2P Ethernet uses dedicated transmitting and receiving paths between a hub and Ethernet workstations. Such a system maintains the clock synchronization between the receiver and transmitter by transmitting idle symbols when there is no data to be sent. Therefore, even though the Ethernet protocol itself is bursty, the physical layer of modern P2P Ethernets is no longer bursty. Although the preamble has been preserved in modern P2P Ethernet, they have no practical significance except for backward compatibility with first-generation Ethernet devices.

Since EPON upstream physical connectivity is bursty, preambles are needed again to help the OLT burst mode receiver to synchronize with the ONU. Moreover, preambles are modified in EPON to carry the LLID used in P2PE [18, Clause 65].

To maintain low cost, traditionally all Ethernet transmitters are running asynchronously on their own local clock domains. There is no global synchronization. A receiver derives the clock signal for gating the received data from its received digital symbols. Mismatches between clock sources are accounted for by adjusting the IFG between Ethernet frames.

In an EPON system, the downstream physical link maintains continuous signal stream and clock synchronization. In the upstream direction, to maintain a common timing reference with the OLT, ONUs use loop timing for the upstream burst mode transmission, i.e., the clock for upstream signal transmission is derived from the downstream received signal.

9.6.5 PCS Layer and Forward Error Correction

EPON defines a symmetric throughput of 1.0 Gbps both in the upstream and downstream directions, and adopted the 8B/10B line PCS coding used in the IEEE 802.3z gigabit Ethernet standard [18, Clause 36]. To take advantage of the low-cost silicon processing capability, EPON has included FEC as an optional choice in the physical layer so that a relaxed optical PMD specification, a higher splitting ratio, or a longer transmission distance can be achieved.

The use of FEC is optional in EPON. The IEEE 802.3ah standard defines RS (255, 239) block codes in the EPON PCS layer [18, Clause 65]. Parity bits are appended at the end of each frame. Since the clock rate does not change when FEC parities are appended, the data throughput is decreased by about 7% when FEC is used. The RS(255, 239) block code does not change the information bits. This allows ONUs which do not support FEC to coexist with ONUs supporting FEC coded frames. An ONU with no FEC support will simply ignore the parity bits albeit running at a higher bit error rate (BER).

9.7 ETHERNET OAM

OAM is an active field of interest and research in Ethernet. One of the charters of the IEEE 802.3ah EFM study group was to specify the Ethernet OAM sublayer functions. The OAM sublayer is situated above the MAC control layer as an optional layer as shown in Fig. 9.2.

The OAM sublayer [18, Clause 57] implements a P2P slow protocol between two interconnected MAC entities using OAMPDUs. Slow protocol PDUs are identified with an Ethernet Type value of 0x88 09 in hexadecimal. To minimize the protocol overhead, slow protocol PDUs are limited to 10 PDUs per second. The formats of OAMPDUs are show next to the OAM layer block diagram in Figure 9.40.

As shown in the figure, the OAM sublayer multiplexes OAMPDUs with data frames from the regular data MAC layer in the transmit path. In the receive path, the OAM sub-layer parses the incoming frames to the OAM client or regular data MAC client. Functions of the OAM layer include:

- OAM capability discovery
- Link monitoring
- Remote loopback
- Remote fault indication

Network management functions such as protection switching, MIB (Management Information Base) read/write, and authentication are not included in the Ethernet OAM layer.

There are two ways for OAM layer to pass protocol information between link partners. A two-octet flag provides quick indication of critical events such as link

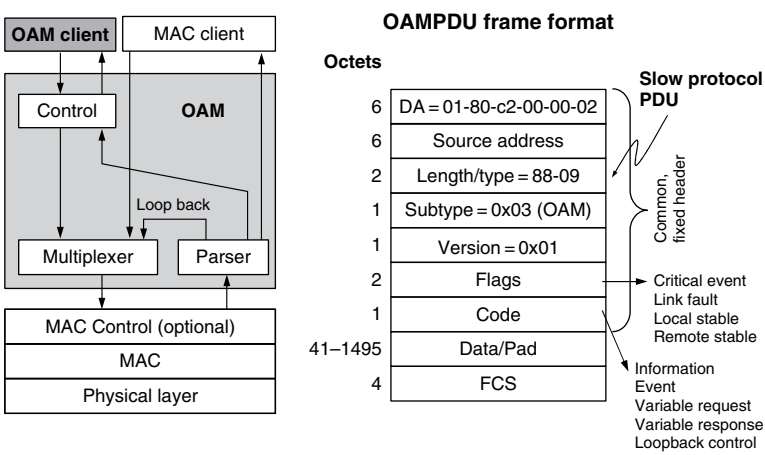

Figure 9.40 OAM sub layer block diagram and OAMPDU frame format (this figure may be seen in color on the included CD ROM).

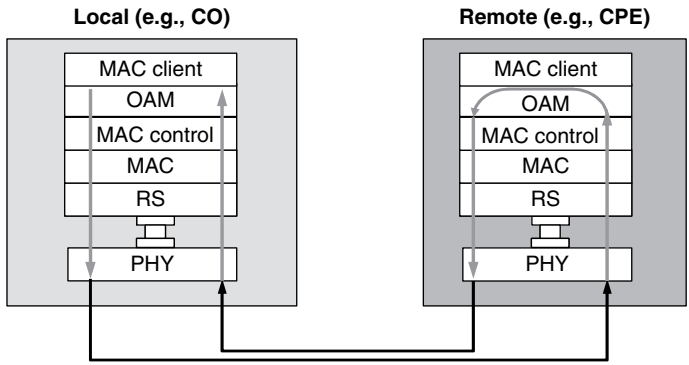

Figure 9.41 OAM loopback function (this figure may be seen in color on the included CD ROM).

fault, local stable, and remote stable using status bits. The OAM sublayer can also send event and information to the link partner using OAM variable request and response messages.

A very important function implemented in OAM is remote loopback, which is shown in Figure 9.41. Figure 9.40 also indicates the loopback path in the OAM sublayer. In the case of a network failure, the remote loopback function allows an operator to quickly test the transmission link and narrow down the fault location.

The MEF and ITU are now busy working on service provider OAM (SOAM) functions for Ethernet services [16, 44], which we cannot cover here because of space limits.

9.8 LATEST ETHERNET DEVELOPMENTS

9.8.1 10 Gb/s Ethernet Passive Optical Networks

As the human society marches further into the information age, demand for bandwidth keeps increasing. Broadband access has become a norm in industrialized nations. Riding on the tremendous success of the 802.3ah EPON, also called GE-PON, in March 2006, IEEE started the study group on the next generation 10 Gigabit Ethernet passive optical network (10GE-PON) standardization, which became the 802.3av task force [49].

10GE-PON offers 10 Gb/s downstream throughput. Two different speeds for the upstream transmission will be available. In the symmetric design, both the downstream and upstream speeds are 10 Gb/s while 1Gb/s upstream is used in the asymmetric design. This will be the first time that Ethernet systems are designed with asymmetric data throughput in the downstream and upstream directions.

One important consideration in 10GE-PON design is the smooth upgrade from the current base of deployed E-PON or GE-PON. To achieve this, 10GE-PON will

adopt a different wavelength (e.g., 1550 nm C-band has been proposed) for the 10 Gb/s downstream traffic [50]. This 15xx nm 10 Gb/s wavelength is blocked by a wavelength filter at legacy GE-PON ONUs which receive the 1490 nm GE-PON downstream signal. In fact, most of the GE-PON ONUs deployed today already have the blocking filter preinstalled. For those systems without blocking filters, a blocking filter will be installed at ONUs which do not need to be upgraded to 10 Gb/s when the OLT is upgraded to support 10 Gb/s downstream speed. Therefore, Gigabit and 10 Gigabit downstream signals are overlaid in the wavelength domain and extracted with appropriate filters at ONUs. To ensure upstream compatibility with legacy GE-PON, either a separate wavelength is used for the 10 Gb/s upstream signal in the WDM overlay approach, or the OLT receiver will switch between GE and 10GE mode in the time domain automatically (TDM overlay approach), depending on the upstream burst [51].

The higher speeds offered by 10GE-PON can be shared among larger user groups to achieve better economy. This means larger remote node splitting ratios and longer transmission distances. It is envisioned that 10GE-PON may need to support splitting ratios of up to 1:64 or 1:128, and transmission distances of up to 60 km between OLT and ONUs. One goal of the 10GE-PON standard is to achieve an enhanced power budget of 29dB (called Class B $++$) between the OLT and an ONU [52]. Instead of specifying the remote node splitting ratio, IEEE standardizes the power budget between the OLT and ONU and lets users decide how to use the available power budget for splitting loss, fiber attenuation, and transmission penalties.

In addition to sustaining higher splitting ratios and longer transmission distances, higher power is also required for the higher transmission speed. Theoretically, given everything else is the same, 9.1 dB more received power is required for a 10GE-PON link compared to a GE-PON link, which is 8.24 times faster after accounting for the difference in 8B10B and 64B66B PCS code rates. To achieve the transmission performance of 10GE-PON, many new optical and electronic technologies will be used. First, FEC and APD will be used to improve the receiver sensitivities [53, 54]. Secondly, compared with GE-PON, the dispersion effect increases by 68 times in 10GE-PON. So EDC is being considered to enhance dispersion tolerance and alleviate the dispersion penalties especially for extended reaches [55]. Thirdly, to achieve the power budget requirement, erbium-doped fiber amplifier (EDFA) and SOAs (semiconductor optical amplifiers) are proposed to overcome the signal loss [56, 57].

PON equipment is extremely cost-sensitive. To achieve the best cost structure, EDFA and SOA will be deployed at the OLT instead of distributed at individual ONUs. In the downstream direction, the 10 Gb/s 15xx nm downstream signal will be from a low-cost distributed feedback (DFB) or electroabsorption modulated laser (EML) laser, whose output power is boosted up by an EDFA or SOA to meet the requirement of ONU receivers, which are preferably low-cost and less-sensitive PIN receivers. Use of APD in the downstream direction has not been ruled out either. In the upstream direction, an SOA $+$ APD configuration is used to receive the bursty

upstream signal at the OLT. SOA has the advantage of wideband, very compact in size, and using mass-manufacturable planar technologies. Nevertheless, EDFAs have dominated in the traditional long-haul DWDM market because of their superior noise figure, low polarization dependence, and gain dynamics which results in low interchannel crosstalk. However, EDFAs only work in the C and L bands. Significant advances in SOA have been made in the last several years [58, 59] that practical devices with satisfactory performances are now available. As a matter of fact, the fast SOA carrier dynamics actually makes it better for the bursty PON signals than EDFAs [77]. 10GE-PON upstream signal amplification is an excellent application which could help nurturing the SOA component industry.

Nonlinear effects, which are traditionally seen only in long-haul transmission systems, will now need to be considered in 10 GE-PON. For example, the downstream output power will eventually be limited by SBS (stimulated brillouin scattering) to about 8 to 10 dBm [60] (see also, Chapter 10 on Fiber-Based Broadband Access Technology and Deployment). Another effect is the stimulated Raman scattering (SRS) effect. The original 1490 nm GE downstream signal copropagates with the 1550 nm 10GE-PON downstream signal and serves a Raman pump to the latter [61]. These two wavelengths are separated such that the 1490 nm wavelength forms a quite efficient Raman pump for the C-band 1550 nm wavelength. The strong 10 Gb/s downstream wavelength will deplete the 1490 nm GE-PON downstream signal, causing penalties to this signal, especially when the transmission fiber length is long.

9.8.2 100 Gb/s Ethernet Development

With the continuing growth in broadband access networks and the introduction of higher bandwidth access technologies such as 10-Gigabit Ethernet PONs, backbone capacities also need to scale proportionally. After a few years of deployment, 10-Gigabit Ethernet has now been commoditized in metro and long-haul backbone systems.

Companies such as Google and Yahoo running high-speed ISP backbones and data centers already need links that operate at 10 Gb/s and higher to support their bandwidth-hungry applications. Telecom and MSO carriers also need Ethernet connections with much higher throughput to maintain their fast growing IPTV services [62]. LAG is used to obtain the required throughput with current technologies. As explained before, LAG load balances the traffic across multiple parallel Ethernet links according to higher-layer protocol identifiers using a hashing algorithm. For video streams, which have higher bandwidth granularity and longer connection time, it is more difficult to load balance the traffic. Moreover, LAG requires complicated configuration and management.

Today, more than a 100 companies have expressed interests in participating in the study of higher-speed Ethernet. Traditionally the speed of a new generation Ethernet is always 10 times that of the previous generation. Accordingly the next-generation Ethernet would be 100Gb/s. However, a 40 Gb/s interim standard

has been proposed because of the current technological and economical challenge in 100 Gb/s transmission. Even though 100Gb/s transmission and processing are still a quite a few years away from commercial use and deployment, optical technologies (such as WDM) exist today and 100Gb/s serial data transmission on field optical fibers have been demonstrated [63 65]. High-speed electronics are also available for MAC processing at 100 Gb/s speed [66 68].

Both serial and parallel PHY implementations for 100 Gb/s Ethernet have been suggested at IEEE 802.3 Higher Speed Study Group (HSSG) meetings. The serial PHY approach transmits 100 Gb/s of data on a single wavelength whereas the parallel approach breaks the data into multiple lanes using parallel fibers or wavelengths. For short haul transmission (i.e., a transmission distance shorter than 40 km), parallel PHYs dominate the proposed solutions. For long-haul transmission, there are both serial and parallel PHYs proposed. It should be noted that today's commercial SONET OC-768 systems running at 40 Gb/s serial transmission already requires re-engineering the fiber plant with carefully controlled dispersion maps, as well as new fibers with very low PMD (polarization mode dispersion). Adaptive PMD compensations are required to ensure system availability. Chromatic and polarization mode dispersion effects increase as the square of the data rate. Therefore, 100 Gb/s serial transmission, even though possible, requires extremely demanding component tolerance and very rigorous system tune-up. Consequently, 100 GbE transmissions in metro and long-haul networks should consider not only the transceiver cost at terminals, but also the transmission system infrastructure cost.

Serial 100 GbE transmission has benefited from bandwidth-efficient modulations such as duobinary and DQPSK (differential quadrature phase-shift keying) [64, 69]. For more details of modulation formats, please refer to Chapter 2 by Winzer and Essiambre on "Advanced Optical Modulation Formats". Moreover, FEC and EDC (electronic dispersion compensation, also refer to Chapter 18 (Volume A) by Shanbhag, Yu, and Choma) are used to increase system tolerances to OSNR (optical signal to noise ratio) degradation and dispersion effects.

Parallel 100GbE transmission can easily bundle 10 wavelengths in a 10Gb/s DWDM system. Commercial 10 Gb/s DWDM systems with 100 and 50 GHz channel spacing are mature and readily available. With the current component and technology cost, this approach will offer the fastest time to market and the lowest system cost. However, this brute force approach has a serious problem of offering low spectral efficiency. Figure 9.42 plots the number of 100 Gb/s Ethernet links that can be supported in the C-band of a single-mode fiber versus the transmission spectral efficiency [70]. Therefore, a parallel PHY based on highly spectral efficient 10 G transmission (e.g., with 10 G channel spacing as low as 12.5 GHz) is highly desirable. This approach has the advantage over alternative parallel PHY approaches (4×25 or 5×20 Gb/s) in the fact that the 100 GbE can be transported in many existing 10 G infrastructure without concerns about dispersion map and fiber PMD issues.

Most likely 100 Gb/s Ethernet will be firstly used in data centers for interconnecting high-capacity servers and data switches. We do not expect 100 Gb/s serial interfaces will be economically competitive for the next several years. Photonic IC (PIC)

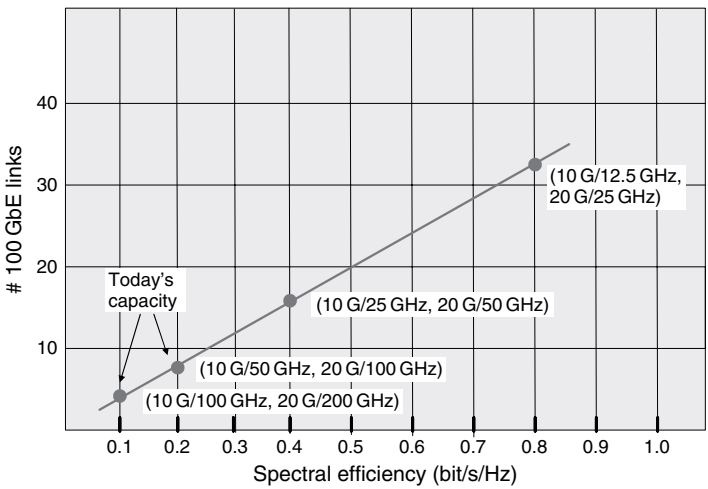

Figure 9.42 Number of 100 Gb/s Ethernet links that can be supported on a single mode fiber in C band (this figure may be seen in color on the included CD ROM).

[78] will be the important technology to realize low-cost and high-density parallel-lane 100 Gb/s Ethernet systems. Both silicon- and InP-based PIC platforms are being considered. The current yield issue to generate InP PICs with channel spacings less than 200 GHz [71] will be a serious road block to their practical use in spectrally efficient 100 GbE systems. Chapter 10 (Volume A) by Welch et al. on "III V Photonic Circuits and their Impact on Optical Network Architectures" explains PICs in more details. Furthermore, electronic transmission mitigation techniques such as FEC and EDC will be used in 100 Gb/s Ethernet systems. For short distance interconnect applications, spectral efficiency will not be very important so that wavelength spacing can be wide to increase optical component tolerances and reduce system costs. For metro and long distance transmissions, spectral efficiency is very important. So ultra-dense WDM transmission can be the solution to (1) maintain the spectral efficiency and (2) alleviate the fiber plant requirements to support 100 Gb/s Ethernet. It would be most ideal if one can transport 100 Gb/s Ethernet with 10 Gb/s transmission engineering rules and yet maintain the high spectral efficiency [70]. Such systems enable smooth upgrade to 100 Gb/s without fork-lifting upgrades.

9.9 HIGH-SPEED ETHERNET APPLICATION EXAMPLE

9.9.1 An IPTV Example

Recently, video services in the form of IPTV have become the most important high-bandwidth application that drives the growth of broadband networks and high-speed Ethernet. Digital TV signals are much easier to transport than their analog ancestors

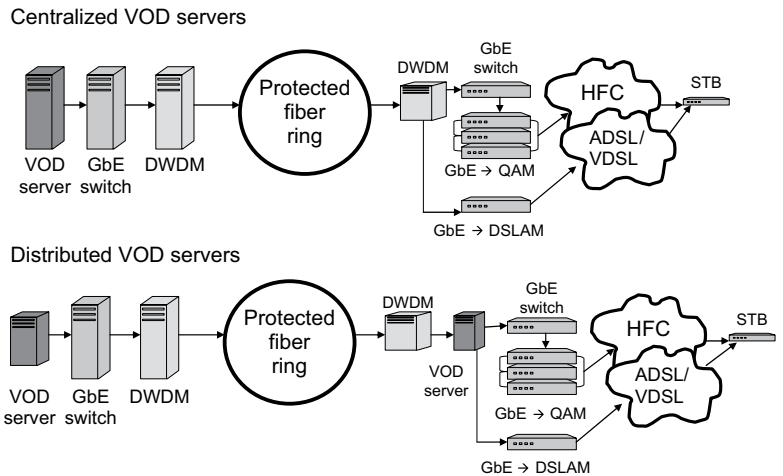

Figure 9.43 VOD delivery network architecture using high speed Ethernet (this figure may be seen in color on the included CD ROM).

because of the much lower system linearity and signal-to-noise ratio requirements. As mentioned at the beginning of this chapter, with the new mpeg compressing technology, a Gigabit Ethernet link is capable of carrying 240 streams of standard resolution video signals, each of which requires 3.75 Mb/s bandwidth.

A state-of-the-art approach to implement a VOD network is shown in Figure 9.43, in which traditional SONET wavelengths are replaced by Ethernet wavelengths. Video servers at the head-end node are connected to the WDM optical layer through a Gigabit or 10 Gigabit Ethernet L2/L3 switch [72]. Video signals are transmitted as MPEG over IP packets which are encapsulated in Ethernet frames. At a hub node, an edge quadrature amplitude modulation (QAM) device converts the video signals in Ethernet frames into QAM formats. This architecture not only replaces all the expensive SONET interfaces with low-cost Ethernet interfaces but also improves the network flexibility. With the help of the L2/L3 switch, video signal streams on IP packets can now be arbitrarily switched to any wavelength, and hence any hub node. In effect, the servers at the head end now form a server farm shared by all the hub nodes. The utilization of the expensive video servers is thus improved. Careful readers will realize that this infrastructure for VOD is also the very same infrastructure needed for offering IP data services. Instead of managing separate networks for data and video streaming, carriers now can offer bundled services on a single network with reduced operation and management costs.

9.9.2 Undirectional Ethernet Broadcast

Broadcast is a cost- and bandwidth-efficient way to supply entertainment audio/video services and disseminate information such as stock market quotes and

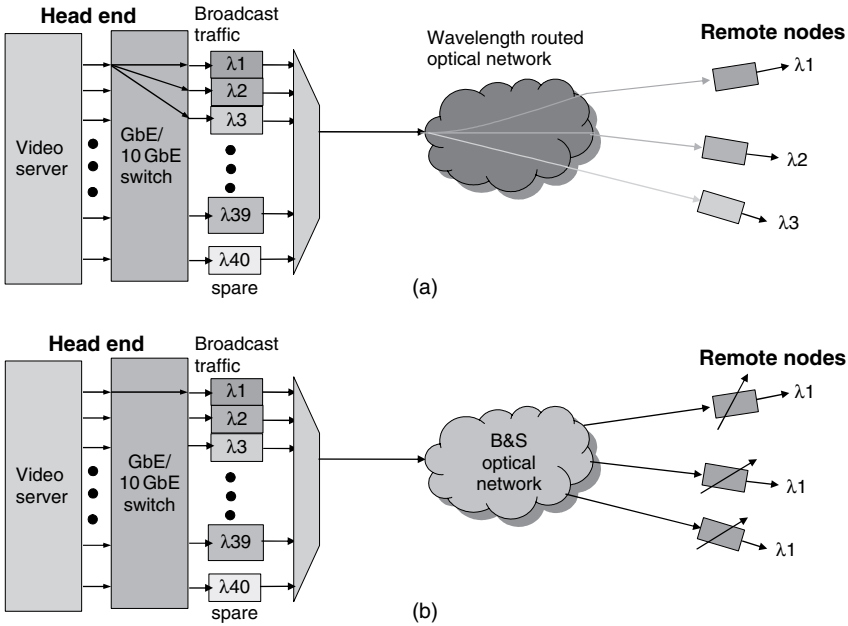

Figure 9.44 Distributing broadcast services in a wavelength routed network (a) and a broadcast and select (B & S) network (b) (this figure may be seen in color on the included CD ROM).

weather forecast to a large number of users. Broadcast can be easily achieved in the optical layer using optical power splitters.

Figure 9.44(a) shows an example of distributing broadcast video in a traditional wavelength-routed metro WDM network, in which different wavelengths are add/dropped at individual remote nodes. Since each remote node drops a different wavelength, the head-end switch needs to replicate the signal three times using three different wavelength transmitters, which is very inefficient in use of the wavelengths, head-end transmitters, switch ports and switch bandwidths. In a broadcast-and-select network [Figure 9.44(b)] [73], only a single switch port and a single head-end transmitter are required, producing significant cost savings.

Traditional Ethernet connections are always bidirectional. Although by nature, IP routing protocols treats a bidirectional Ethernet connection as two independent unidirectional links, bi-directionality has been inherently assumed in many Ethernet and IP protocols such as STP and ARP (Address Resolution Protocol) [74]. Currently, there is no standard of unidirectional Ethernet interfaces for broadcasting on optical networks. To take the advantage of unidirectional Ethernet broadcast, work is needed to resolve the protocol layer issues such as (1) link discovery, (2) link fault monitoring, reporting and trouble shooting, and (3) SAT and ARP table populating, which are generally easier with bidirectional links. The UDLR (unidirectional link routing) protocol [75], which was originally designed

for satellite networks, solves some of these issues by creating a return tunnel on a separate lower bandwidth link. The physical layer realization of a unidirectional Ethernet link is not difficult because full-duplex Ethernet essentially consists of two independent propagating paths. One just needs to disable the auto-negotiation function and remote fault monitoring on a standard bidirectional Ethernet physical layer. From a capital cost perspective, a unidirectional links saves a laser transmitter at the receiving end and a photo-receiver at the transmitting end.

9.10 CONCLUSION

Ethernet has been firmly established as the technology of choice for building the infrastructure of the information society. To cope with the fast evolving requirements for the rapidly growing Internet, Ethernet is also evolving at a breath-taking speed, with new features and capabilities being proposed and introduced almost every day by many companies, standard bodies and research organizations. Technologies to realize 10 GE-PON and 100 Gigabit Ethernet are now hot items on the active agenda list of the IEEE 802.3 standard group. R&D efforts on Ethernet service and OAM models are solving the issues that carriers are facing in offering Ethernet services. In the very near future, carrier class Ethernet equipment will play a key role in tomorrow's triple- or quadruple-play networks to provide converged services.

LIST OF ACRONYMS

3-R	Reshape, retime, and reamplify
10 GE-PON	10 Gigabit Ethernet passive optical network
APD	Avalanche photodiode
ARP	Address Resolution Protocol
BER	Bit error rate
BPDU	Bridge Protocol Data Unit
CBR	Committed burst rate
CDR	Clock data recovery
CFI	Canonical format indicator
CIR	Committed information rate
CRC	Cyclic redundancy check
CSMA/CD	Carrier sense multiple access with collision detection
C-VLAN	Customer VLAN
DA	Destination address
DFB	Distributed feedBack (laser)
DMUX	Demultiplexer
DWDM	Dense wavelength division multiplexing
EBR	Excess burst rate

EDC	Electronic dispersion compensation
EDFA	Erbium-doped fiber amplifier
EFM	Ethernet for the First Mile
EIR	Excess information rate
EML	Electroabsorption modulated laser
EO	Eletrical optical
EPON	Ethernet passive optical network
EVC	Ethernet virtual circuit
FCS	Frame Check Sequence
FDDI	Fiber Distributed Data Interface
FEC	Forward error correction
FP	Fabry Perot
GBIC	Gigabit interface converter
GE-PON	Gigabit Ethernet passive optical network
GFP	Generic framing procedure
GFP-F	Frame-based GFP
GFP-T	Transparent GFP
GMPLS	Generalized multiprotocol label switching
HEC	Header error control
I2C	Inter-IC (bus)
IEEE	Institute of Electrical and Electronics Engineers
IFG	Interframe gap
IP	Internet Protocol
IPTV	Internet Protocol television
ISI	Inter symbol interference
ITU	International Telecommunication Union
LAG	Link aggregation group
LAN	Local area network
LCAS	Link capacity adjustment scheme
LDPC	Low-density parity code
LF	Local fault
LFOS	Local Fault Ordered Set
LLID	Logical link identifier
LMSC	LAN/MAN Standard Committee
LOS	Loss of signal
LSP	Label switched path
MAC	Medium access control
MAN	Metropolitan area networks
MDI	Medium-dependent interface
MEF	Metro Ethernet Forum
MII	Media-independent interface
MiM	MAC-in-MAC
MMF	Multimode fiber
MPCP	Multipoint Control Protocol

MPCPDU	Mutlipoint Control Protocol Data Unit
MPEG	Motion Picture Expert Group
MPLS	Multiprotocol label switching
MPMC	Multipoint MAC control
MSA	Multisource agreement
MSO	Multiple service operator (i.e., CATV operator)
MUX	Multiplexer
NNI	Network network interface
OAM	Operation, administration, and maintenance
OAMPDU	OAM Protcol Data Unit
OE	Optical electrical
OIF	Optical Internet Forum
OLT	Optical Line Terminal
ONU	Optical network unit
OSI	Open system interconnect
OTN	Optical transport network
P2MP	Point-to-multipoint
P2P	Point-to-point
PAM	Pulse amplitude modulation
PBB	Provider backbone bridge
PCB	Printed circuit board
PCS	Physical coding sublayer
PDU	Protocol Data Unit
PHY	PHYsical Layer
PIC	Photonic IC
PMA	Physical medium attachment
PMD	Physical medium dependent
	Polarization mode dispersion
POS	Packet over SONET
QAM	Quadrature amplitude modulation
QiQ	Q-tag-in-Q-tag
QoS	Quality of Service
RDI	Remote fault indicator
RF	Remote fault
RFOS	Remote Fault Ordered Set
RN	Remote node
RS	Reconciliation sublayer
RS	Reed Solomon (code)
RSTP	Rapid Spanning Tree Protocol
RSVP-TE	Resource Reservation Protocol-Traffic Engineering
RTT	Round trip time
SA	Source address
SAT	Source address table
SBS	Stimulated Brillouin scattering

SCB	Single-copy broadcast
SDH	Synchronous digital hierarchy
SERDES	Serializer deserializer
SFD	Start frame delimiter
SFI-4	SERDES framer interface, Release 4
SFP	Small form factor pluggable
SLA	Service level agreement
SLD	Start LLID Delimiter
SOA	Semiconductor optical amplifier
SOAM	Service provider OAM
SONET	Synchronous Optical NETwork
SPE	Synchronous payload envelop
SRS	Stimulated Raman scattering
STP	Spanning Tree Protocol
S-VLAN	Service VLAN
TDM	Time-division multiplexing
TTL	Time to live
UDLR	Unidirectional link routing
UNI	User network interface
UTP	Unshielded twisted pair
VCAT	Virtual conCATenation
VID	VLAN ID
VLAN	Virtual bridged LAN
VOIP	Voice over IP
WDM	Wavelength-division multiplexing
WIS	WAN interface sublayer
XAUI	10 Gigabit Attachment Unit Interface
XGMII	10 Gigabit media-independent interface
XGXS	10 Gigabit extender

REFERENCES

[1] R. M. Metcalfe and D. R. Boggs, "Ethernet: Distributed packet switching for local computer networks," *Communications of the ACM*, 19(7), July 1976.
[2] R. Seifert, *Gigabit Ethernet*, Addison Wesley, 1998, Reading, Massachusetts.
[3] R. H. Caro, "Ethernet wins over industrial automation," *IEEE Spectrum*, 114, January 2000.
[4] ISO/IEC 13818 5:2005. Also see: http://www.mpeg.org/MPEG/index.html
[5] K. G. Coffman and A. M. Odlyzko, "Growth of the Internet," in *Optical Fiber Telecommuncations IV B* (I. Kaminow and T. Li, eds), Academic Press, 2002, pp. 17 59, San Diego, California.
[6] http://grouper.ieee.org/groups/802
[7] *SFF 8053 Specification for GBIC (Gigabit Interface Converter)*, SFF Committee, Rev. 5.5, September 2000, available from: http://www.schelto.com/t11 2/GBIC/sff 8053.pdf
[8] *INF 8074i Specification for SFP (Small Formfactor Pluggable) Transceiver*, Rev 1.0 May 12, 2001, SFF Committee, available from ftp://ftp.seagate.com/sff/INF 8074.PDF

[9] http://www.xenpak.org/
[10] http://www.xfpmsa.org/
[11] http://www.metroethernetforum.org/
[12] ITU T G.7041, *Generic framing procedure (GFP)*, August 2005.
[13] ITU T G.7043, *Virtual Concatenation of Plesiochronous Digital Hierarchy (PDH) signals*, July 2004.
[14] ITU T G.7042, *Link Capacity Adjustment Scheme (LCAS) for Virtual Concatenated Signals*, March 2006.
[15] ITU T G.8031, *Ethernet Protection Switching*, June 2006.
[16] ITU T Y.1731, *OAM Functions and Mechanisms for Ethernet Based Networks*, May 2006.
[17] Optical Internetworking Forum, Document OIF2005.204.17, *User Network Interface (UNI) 2.0 Signaling Specification: Common Part*, June 26 2007.
[18] IEEE Standard 802.3, 2005 Edition, *Carrier Sense Multiple Access with Collision Detection (CSMA/CD) access method and physical layer specifications*.
[19] C. F. Lam, "Beyond Gigabit, Application and Development of High Speed Ethernet Technology" in *Optical Fiber Telecommuncations IV B* (I. Kaminow and T. Li, eds), Academic Press, 2002, pp. 514 563.
[20] Website address of Small Form Factor (SFF) Committee, http://www.sffcommittee.com/ie/#
[21] A. Ghiasi et al., "Experimental Results of EDC Based Receivers for 2400 ps/ nm at 10.7 Gb/s for Emerging Telecom Standards," *OFC/NFOEC* 2006, paper OTuE3, http://www.asipinc.com/pdf/OFC06 EDC10c.pdf
[22] IEEE 802.3an, Physical Layer and Management Parameters for 10 Gb/s Operation, Type 10GBASE T, 2006.
[23] ANSI/TIA TSB 155, "Additional Guidelines For 4 Pair 100 Ω Category 6 Cabling For 10gbase T Applications," October 2004, http://www.ieee802.org/3/an/public/nov04/TR42.7 04 10 142a TSB155 d1.1a.pdf
[24] SFF 8431 Specifications for Enhanced 8.5 and 10 Gigabit Small Form Factor Pluggable Module "SFP+", Revision 2.0, 26 April 2007, ftp://ftp.seagate.com/sff/SFF 8431.PDF
[25] OIF ITLA MSA 01.1, Integrable Tunable Laser Assembly MSA, Novomber 2005, http://www.oiforum.com/public/documents/OIF ITLA MSA 01.1.pdf.
[26] J. Conradi, "Bandwidth Efficient Modulation Formats for Digital Fiber Transmission Systems," in *Optical Fiber Telecommuncations IV B* (I. Kaminow and T. Li, eds), Academic Press, 2002, pp. 862 901.
[27] IEEE Standard 802.1d, *Media Access Control Bridge*, 1993.
[28] IEEE 802.3as, *Frame Format Extensions*, 2006.
[29] IEEE 802.1w, *IEEE Standard for Local and metropolitan area networks Common specifications Part 3: Media Access Control (MAC) Bridges Amendment 2: Rapid Reconfiguration*, 2001.
[30] D. Awduche, "RSVP TE: Extensions to RSVP for LSP Tunnels," *RFC* 3209, December 2001.
[31] IEEE 802.1Q 2005, *IEEE Standard for Local and Metropolitan Area Networks Virtual Bridged Local Area Networks*.
[32] IEEE 802.1ad, *IEEE Standard for Local and Metropolitan Area Networks: Virtual Bridged Local Area Networks Amendment 4: Provider Bridges*, May 2006.
[33] IEEE 802.1ah, *Provider Backbone Bridge*, Draft 3.5, April 2007.
[34] Bell Communications Research GR253 Core, *SONET Transport Systems: Common Generic Criteria*, Issue 2 Revision 2, January 1999.
[35] ITU T G.709, *Interfaces for the Optical Transport Network (OTN)*, March 2003.
[36] IETF RFC 1619, Point to Point Protocol (PPP) over SONET/SDH Specification, May 1994.
[37] IETF RFC 1662, PPP in HDLC like framing, July 1994.
[38] IEEE Communications Magazine, (Feature Issue on *Generic Framing Procedure and Data over SONET/SDH and OTN*) May 2002.
[39] V. Saxena, "*Bandwidth drivers 100G Ethernet*," IEEE HSSG, January 2007, available from http://grouper.ieee.org/groups/802/3/hssg/public/jan07/Saxena 01 0107.pdf.

[40] D. Lee, "*Saturating 100G and 1T pipes*," IEEE HSSG, March 2007, available from http://group er.ieee.org/groups/802/3/hssg/public/mar07/lee 01 0307.pdf.
[41] A. Bechtel, "*A web company's view on Ethernet*," IEEE HSSG, March 2007, available from http:// grouper.ieee.org/groups/802/3/hssg/public/mar07/bechtel 01 0307.pdf.
[42] T. Seely, "*Carrier hurdles to meeting 10GE demand*," IEEE HSSG, March 2007, available from http://grouper.ieee.org/groups/802/3/hssg/public/mar07/seely 01 0307.pdf.
[43] MEF 10.1, *Ethernet Services Attributes Phase 2*, November 2006, available from http:// metroethernetforum.org/PDFs/Standards/MEF10.1.doc
[44] MEF17, *Service OAM Framework and Requirements*, April 2007, available from http:// metroethernetforum.org/MEF17.doc.
[45] MEF3, *Circuit Emulation Service Definitions, Framework and Requirements in Metro Ethernet Networks*, April 2004, available from http://metroethernetforum.org/PDFs/Standards/MEF3.doc.
[46] MEF Technical Specification Website: http://metroethernetforum.org/page loader.php?p id 29
[47] N. J. Frigo, "A survey of fiber optics in local access architectures," in *Optical Fiber Telecommu nications, III A* (I. Kaminow and T. L. Koch, eds), Academic Press, 1997, pp. 461 522.
[48] A. S. Tanenbaum, *Computer Networks*, 3/e, Prentice Hall, 1996.
[49] IEEE802.3av 10GE PON website: http://grouper.ieee.org/groups/802/3/av/index.html
[50] S. Tsuji, "Issues for Wavelength Allocation," IEEE802.3av Task Force Meeting, Knoxville, TN, September 18 19, 2006, http://grouper.ieee.org/groups/802/3/av/public/2006 09/3av 0609 tsuji 1.pdf.
[51] G. Kramer, "10G EPON 1G EPON Coexistence," *IEEE802.3av Task Force Meeting*, Monterey, CA, January 15 17, 2007, http://grouper.ieee.org/groups/802/3/av/public/2007 01/3av 0701 kramer 1.pdf
[52] D S Lee, "Overview of TX/RX technology for high split EPON systems," *IEEE802.3av Task Force Meeting*, November 13 16, 2006, Dallas, TX, http://grouper.ieee.org/groups/802/3/av/pub lic/2006 11/3av 0611 lee 1.pdf.
[53] F. Chang, "10G EPON Optical Budget Considerations," 10 Gb/s PHY for EPON Study Group Meeting, San Diego, CA, July 17 20, 2006, http://grouper.ieee.org/groups/802/3/10GEPON study/public/july06/chang 1 0706.pd
[54] M. Takizawa, "Progress and Issues Concerning the Power Budget Discussions in the Power Budget Ad Hoc," *IEEE802.3av Task Force Meeting*, Orlando, FL, March 12 16, 2007, http:// grouper.ieee.org/groups/802/3/av/public/2007 03/3av 0703 takizawa 1.pdf
[55] F. Chang, "10G EDC for SMF," *IEEE802.3av Task Force Interim Meeting*, Knoxville, TN, September 18 19, 2006, http://grouper.ieee.org/groups/802/3/av/public/2006 09/3av 0609 chang 1.pdf
[56] L. Spiekman and D. Piehler, "Semiconductor Amplifier for Passive Optical Networks," *IEEE802.3av Task Force Meeting*, November 13 16, 2006, Dallas, TX, http://grouper.ieee.org/ groups/802/3/av/public/2006 11/3av 0611 spiekman 1.pdf
[57] P. Doussiere, E. Mao, and W. Jiang, "Technical Feasibility of EDFA based network architecture for 10GEPON," *IEEE802.3av Task Force Meeting*, November 13 16, 2006, Dallas, TX, http:// grouper.ieee.org/groups/802/3/av/public/2006 11/3av 0611 doussiere 1.pdf
[58] L. H. Spiekman, J. M. Wiesenfeld, A. H. Gnauck et al., "8×10 Gb/s DWDM transmission over 240 km of standard fiber using a cascade of semiconductor optical amplifiers," *IEEE Photon. Technol. Lett.*, 12(8), 1082 1084, August 2000.
[59] K. Morito, S. Tanaka, "Record high saturation power ($+22$ dBm) and low noise figure (5.7 dB) polarizationinsensitive SOA module," *IEEE Photon. Technol. Lett.*, 17(6), 1298 1300, 2005.
[60] S. Ten, "SBS Degradation of 10 Gb/s Digital Signal in EPON: Experimental and Model," *IEEE 802.3av Task Force Meeting*, Monterey, CA, 15 16 January 2007, http://grouper.ieee.org/groups/ 802/3/av/public/2007 01/3av 0701 ten 1.pdf
[61] S. Ten and M. Hajduczenia, "Raman Induced Power Penalty in PONs using 0 order Approximation," *IEEE 802.3av Task Force Meeting*, Monterey, CA, January 15 16, 2007, http://grouper.ieee.org/groups/802/3/av/public/2007 01/3av 0701 ten 2.pdf
[62] "Higher Speed Study Group Call for Interests," *IEEE 802.3 HSSG Meeting Presentation*, San Diego, CA, July 18, 2006, http://grouper.ieee.org/groups/802/3/cfi/0706 1/CFI 01 0706.pdf

[63] J. Peter Winzer, Greg Raybon, and Marcus Duelk, "107 Gb/s optical ETDM transmitter for 100 G Ethernet transport," *ECOC 2005*, Post deadline paper Th4.1.1, 2005.
[64] P. J. Winzer et al., "2000 km WDM transmission of 10×107 Gb/s RZ DQPSK," *ECOC 2006* Post deadline paper Th4.1.3, 2006.
[65] E. Lach and K. Schuh, "Recent Advances in Ultrahigh Bit Rate ETDM Transmission Systems," *J. Lightw. Technol.*, 24(12), 4455 4467, December 2006.
[66] Y. Suzuki, Z. Yamazaki, Y. Amamiya et al., "120 Gb/s multiplexing and 110 Gb/s demultiplexing ICs," *IEEE J. Solid St. Cir.*, 39(12), 2397 2402, December 2004.
[67] M. Belhadj, "More on the feasibility of a 100 GE MAC," *IEEE 802.3 HSSG Meeting*, Monterey CA, January 17 19, 2007, http://grouper.ieee.org/groups/802/3/hssg/public/jan07/belhadj 01 0107.pdf
[68] F. Shafai, "Technical Feasibility of 100 G Designs," *IEEE802.3 HSSG Meeting*, Ottawa, ON, CA, April 17 19, 2007. http://grouper.ieee.org/groups/802/3/hssg/public/apr07/shafai 01 0407.pdf
[69] M. Duelk and S. Trowbridge, "Serial PHY for Higher Speed Ethernet," *IEEE802.3 HSSG Meeting*, Knoxville, TN, September 18 21, 2006. http://grouper.ieee.org/groups/802/3/hssg/public/sep06/duelk 01 0906.pdf
[70] W. I. Way, "Spectral Efficient 100 G Parallel PHY in Metro/Regional Networks," *IEEE802.3 HSSG Meeting*, Monterey, CA, January 17 19. http://grouper.ieee.org/groups/802/3/hssg/public/jan07/way 01 0107.pdf
[71] S. Khodja, "*100 GbE Silicon Photonics Platform Considerations*," *IEEE HSSG*, January 2007, available from http://grouper.ieee.org/groups/802/3/hssg/public/jan07/khodja 01 0107.pdf
[72] C. F. Lam, "Metropolitan Area Ethernet Development, Applications and Management," *OECC 2005*, Seoul, Korea, July 4 8, 2005.
[73] C. F. Lam, "Next Generation Metropolitan Area WDM Optical Networks," *APOC 2006*, paper 6354 42, 2006.
[74] IETF RFC 826, David C. Plummer, An Ethernet Address Resolution Protocol, November 1982.
[75] IETF RFC 3077, E. Duros, et al., Link Layer Tunneling Mechanism for Unidirectional Links, March 2001.
[76] OIF SFI4 02.0, *SERDES Framer Interface Level 4 (SFI 4) Phase 2: Implementation Agreement for 10 Gb/s Interface for Physical Layer Device*, http://www.oiforum.com/public/documents/OIFSFI4 02.0.pdf
[77] B. Stefanov, L. Spiekman and D. Piehler, "Semiconductor Optical Amplifiers High Power Operation," *IEEE802.3av Task Force Meeting*, Orlando, FL, March 13 15, 2007, http://grouper.ieee.org/groups/802/3/av/public/2007 03/3av 0703 stefanov 1.pdf
[78] R. Nagarajan, et al., "Large Scale Photonic Integrated Circuits," *IEEE J. Sel. Top. in Quantum Electron.,* 11(1), 5 65, 2005.

10

Fiber-based broadband access technology and deployment

Richard E. Wagner

Corning International, Corning, New York, USA

Abstract

After more than 20 years of research and development, a combination of technolo gical, regulatory, and competitive forces are finally bringing fiber based broadband access to commercial fruition. Three main approaches, hybrid fiber coax, fiber to the cabinet, and fiber to the home, are each vying for a leading position in the industry, and each has significant future potential to grow customers and increase bandwidth and associated service offerings. Further technical advances and cost reductions will be adopted, eventually bringing performance levels and bandwidth to Gb/s rates when user demand warrants while keeping service costs affordable.

10.1 INTRODUCTION

The use of fiber-optic technology in telecommunications systems has grown over the past 25 years, since its introduction as a transmission media for linking metropolitan central offices in 1980. In the decade after that, long-distance networks deployed fiber-based systems extensively, followed by significant construction of metropolitan interoffice network infrastructure. During that time the reliability and availability of transport systems improved dramatically due largely to the low failure rates of the technology. As a result, researchers and developers dreamed of a time when fiber-optic technology could be economically applied in access networks [1] to replace the copper-based systems extending from central offices to residences and businesses (see Figure 10.1 for a diagram [2] of such scenarios). A perfect example of this visionary dream was articulated by Paul Shumate and Richard Snelling in an *IEEE Communications Magazine* article published in 1989 [3], where they predicted that a fiber-to-the-home (FTTH) solution could be at economic parity with copper-based solutions by 1995 if a carrier were to deploy 1 3 million lines (see Figure 10.2 for a replication of their prediction chart). They went on to explain that it could be possible

Optical Fiber Telecommunications V B: Systems and Networks

ISBN: 978 0 12 374172 1

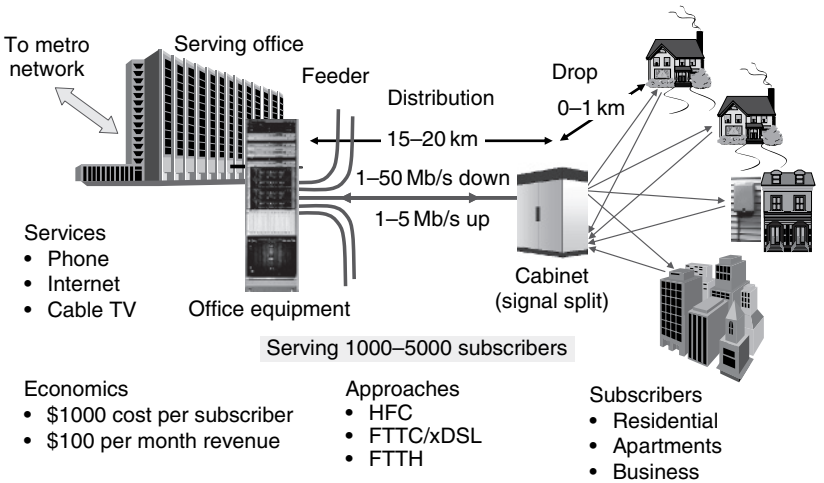

Figure 10.1 FTTx access network reference models (this figure may be seen in color on the included CD ROM).

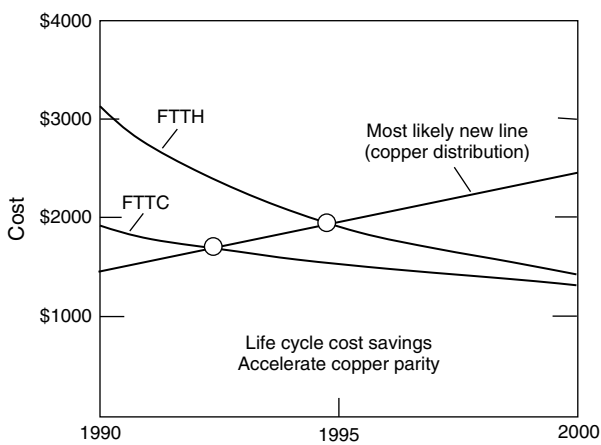

Figure 10.2 FTTH vs copper introduction cross over date (C. 1991 Shumate).

to convert the entire US network to FTTH over a 25-year period, producing a broadband network for the Information Age. They further noted that there were many details to be worked out, including standardization, network interfaces, powering at the customer end, video capability, and network evolution. This work was pioneering and prophetic, as we now know today.

But what those authors, and others with them, did not foresee was the dramatic effect of the telecommunications consent decree on competition in the United States, the dampening effect of the federal communications commission (FCC) policy allowing competing carriers to lease infrastructure at cost or below, the

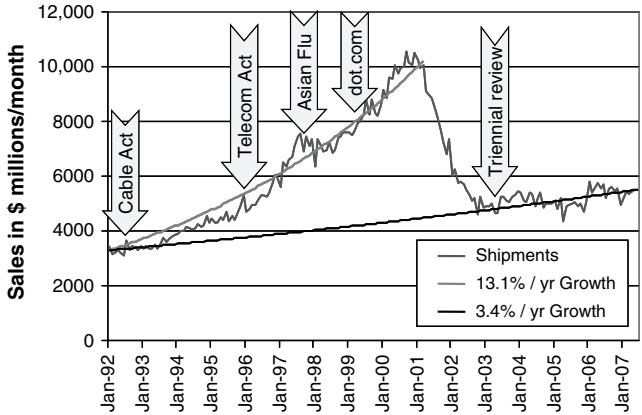

Figure 10.3 Telecom bubble telecom equipment shipped in the united states vs time (this figure may be seen in color on the included CD ROM).

delaying effect of the telecom "bubble" bursting [4] (Figure 10.3), and the bandwidth growth driver of the Internet when used for business and entertainment.

Now, in Asia, North America, Europe, and globally, we are seeing significant capital spending on fiber-based broadband access infrastructure [5, 6]. Some of the earliest spending was in Japan, where government funding and initiatives helped to push carriers toward fiber-based access network technologies. Soon after, in the United States, spending was driven by three events: the FCC has made an historic policy decision in 2003 to free fiber-based solutions from competitive regulations, cable TV (CATV) operators have increased telecommunications industry competition by offering high data rate Internet service and telephone service over the Internet, and users have grown accustomed to using the Internet for sharing large digital files containing e-mail messages, photos, music, video, and news clips.

In response to these drivers, the three major local exchange carriers in the United States (Verizon, BellSouth, and SBC) issued a common request for information to broadband access system suppliers, trusting that the resulting volume manufacturing incentives would bring the cost of deploying such systems in line with associated service revenues. Now it appears that this risky move was justified, because in North America we have seen about 8 million fiber-based broadband access lines deployed to homes since then, with more than 1.5 million customers taking the services being offered. Globally there are, by the end of 2007, about 11 million fiber-based access customers. The overall result of this is lowered costs for the technology and its installation, significant technological advancements in the equipment and installation methods, and improved service offerings to customers at affordable rates.

In alignment with this trend, European carriers are now committing funds to fiber-based access networks as well, and in a few years China will ramp up spending for this purpose.

This chapter will focus on the fiber-based approaches to broadband access worldwide, including some of the drivers for deployment, the architectural options, the capital and operational costs, the technological advances, and the future potential of these systems. Three variants of fiber-based broadband access, collectively called FTTx (fiber to the x) in this chapter, have emerged as particularly important. They are hybrid-fiber-coax (HFC) systems, fiber-to-the-cabinet (FTTC) systems, and FTTH systems.

10.2 USER DEMOGRAPHICS

One of the most dramatic and unexpected drivers for fiber-based broadband access has been the explosive growth of the internet and its associated applications. As early as April 1993, when the Mosaic browser became available, the public began to use the internet for transfer of text messages, photos, and data files. Building on that initial application, the number of Internet users has grown to 211 million in the United States alone, and represents about 70% of the population now, while globally there are about 1.2 billion internet user representing about 18% of the world population [7, 8] (Figure 10.4). Not only has the number of users grown, but individual usage has expanded exponentially, until today we routinely exchange music, photos, videos, and software files as large as 10's of megabytes each.

A close look at the bandwidth available to access the Internet shows that it was gated by the technology being offered [9 11] (Figure 10.5), with new ones adopted in cycles of roughly 5 6 years each [2] (Figure 10.6). For example, the earliest users bought phone modems, initially at 9.6 kb/s, then increasing in performance to 14.4 kb/s, 28 kb/s, and finally 56 kb/s [10]. Typically, a group of early users (indicated as Initial Users in Figure 10.6, representing the top 25% of users) adopt the new technology first; the mainstream follows, and finally everybody else (Slow Adopters in Figure 10.6,

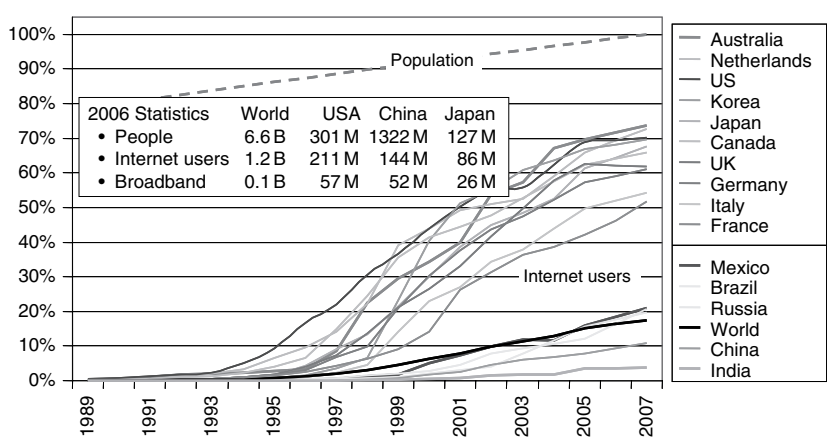

Figure 10.4 Internet usage worldwide (this figure may be seen in color on the included CD ROM).

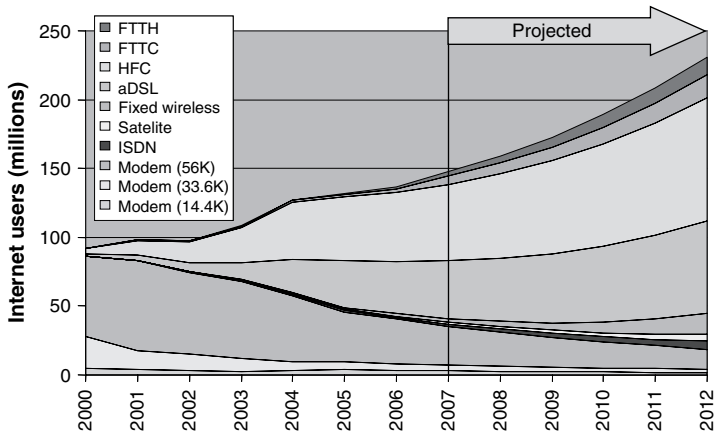

Figure 10.5 US residential access technology adoption over time (this figure may be seen in color on the included CD ROM).

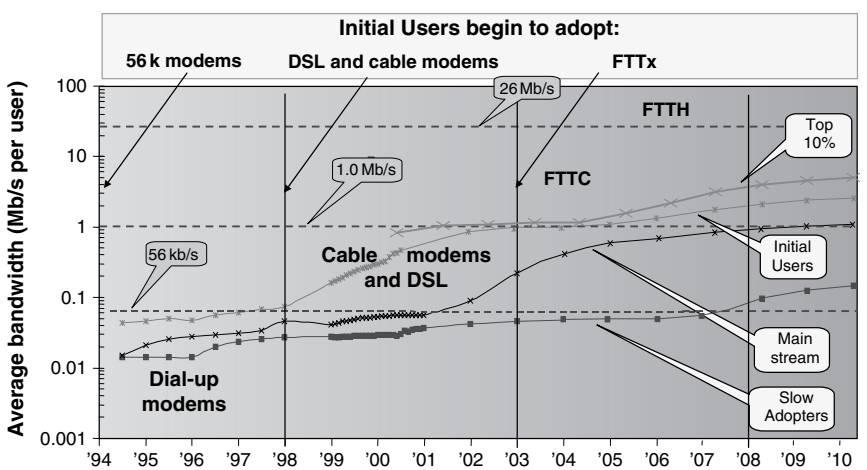

Figure 10.6 US user downstream connection speed trend and projection over time (this figure may be seen in color on the included CD ROM).

representing the bottom 25% of users) takes advantage of the technology. While the entire adoption cycle takes 8 10 years from introduction to 50% adoption, newer technology is introduced before even half of the users have the old in place. By the time the Slow Adopters begin to use one approach, another newer approach is being offered and adopted by a new set of Initial Users. The cycle of technology adoption by Initial Users, Mainstream Users, and Slow Adopters has experienced two full cycles now, and is into its third cycle: phone modems, then cable modems and asymmetric digital subscriber line (aDSL) modems, and now fiber-based access.

In Figure 10.6, phone modems were introduced in 1993 and by 2001 the overall average user bandwidth exceeded 56 kb/s. Cable modems, introduced in late 1997, were adopted similarly with average user bandwidth exceeding the 1 Mb/s cable modem bandwidth by 2006. Now that FTTH has been introduced, with primary service offerings ranging from 5 to 30 Mb/s, initial users are beginning to subscribe to this technology, especially at 10 15 Mb/s, which will take several years to reach the 25% penetration level and a few more years to achieve the mainstream. We can expect that by 2010 a significant number (perhaps a few million) of those users will be looking for something more, very likely 100 Mb/s service or higher. It is interesting to note that each of these technology cycles has resulted in bandwidth offerings about an order of magnitude larger than the previous, even though the price of the service offerings has only doubled for each cycle.

If we extend this trend into the future, we can expect at least two more cycles of technology adoption by users (Figure 10.7). One of these would offer 100 Mb/s service, projected by this data to have a few million subscribers by 2010, and another higher service offering of 1 Gb/s Ethernet projected to be penetrating the customer base by 2016. The earlier cycle that utilized cable modems and DSL technologies was characterized by asymmetric traffic, in which the downstream signals from the service provider to the user employed a much higher data rate than the upstream signals for both technological and service reasons because subscribers were more likely to view content than to generate content. The recent and future cycles, though, need to support nearly symmetric traffic because subscribers desire to share high-resolution images, large files, and video recorder clips with other users which requires upstream data rates that are similar to downstream rates.

Beyond service offerings of 1 Gb/s with symmetric traffic, it is difficult now to envision what might be the next advance, because completely unimagined applications, spurred by the increased bandwidth offerings, are very likely to arise in the interim. But it is interesting to note that the raw bandwidth of high-definition TV (HDTV) signals for large-screen displays is nearly 10 Gb/s, leading to the expectation that even higher access speeds could be of interest in the very long term.

Against this backdrop of continued bandwidth enhancements stands the much less variable location of the users. For example, residential users in metropolitan

Technology	Per user	Start	50%	
Phone modems	<100 kb/s	1993	2001	History
Cable modems	1 Mb/s	1998	2006	
FTTx approaches	10 Mb/s	2004	2012	
Next generation fiber technology	100 Mb/s	2010	2018	Forecast
Big broadband technology	1 Gb/s	2016	2024	

Figure 10.7 Projection of user demand for bandwidth, showing a Gb/s target eventually (this figure may be seen in color on the included CD ROM).

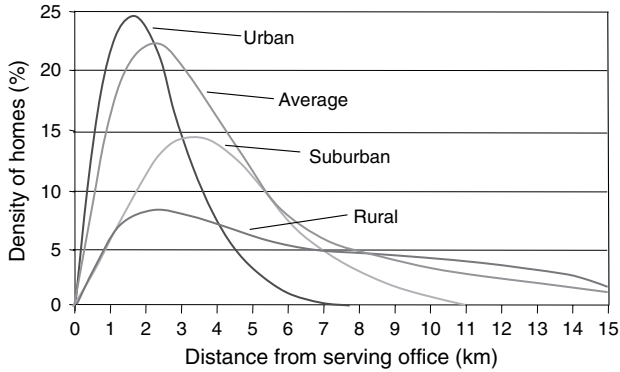

Figure 10.8 Distribution of homes from a serving office in the United States (this figure may be seen in color on the included CD ROM).

areas in the United States are typically located within 5 km of the central offices that serve them, and in suburban and rural areas this range extends at the greatest to about 10 and 20 km, respectively [12, 13] (Figure 10.8). In Asia and Europe, where the population density is higher, the users are typically closer to the central offices that serve them than they are in the United States. This density of users is not changing much over decades because it is determined by the cultural and socio-economic norms of suitable living arrangements. So the technologies that carriers deploy need to be capable of serving customers within this rather fixed range, while being able to be upgraded to provide ever higher user bandwidth. In practice, carriers have tended to provide options that offer cost or performance advantages in shorter-reach, higher density metropolitan locations compared to suburban and rural areas. But until recently they have paid little attention to the looming issue of extending the user bandwidth to Gb/s rates.

Ultimately, the introduction of FTTx technologies and their subsequent adoption by mainstream users will have an effect on the traffic load offered to the metropolitan networks that serve the users [14]. This means that the metropolitan interoffice network demands will be advanced by a couple of years compared to a scenario where such technology is not introduced (see Figure 10.9). Such an effect is just now beginning to be felt by service providers as a result of their introduction of FTTx technologies.

10.3 REGULATORY POLICY

Still, with all of these drivers, applications and technology advances available to carriers, they were reluctant to invest in new broadband access infrastructure until recently. In the United States, the 1996 Telecom Act [15] and the regulatory policy of the FCC stipulated that new infrastructure was regulated and had to be offered to competitors at a price set by strict policy rules. This discouraged new network

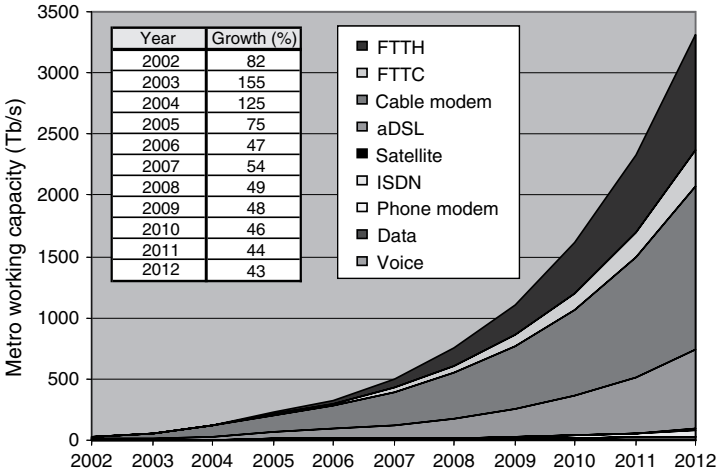

Figure 10.9 US Metro Internet traffic growth over time and in the future, with FTTx factored in (this figure may be seen in color on the included CD ROM).

builds, because investors feared that their expenditures would be exploited by competitors at costs lower than their own investments would support. Fortunately, this roadblock was removed to a great extent in February 2003, when the FCC adopted new rules for local phone carriers relating to broadband access networks, and issued a notice of proposed rule-making intended to give relief to major carriers of this burden by allowing new FTTx infrastructure to be built without being required to be offered to competitors at regulated prices . This was followed in August 2003 by the actual decree that formalized the FCC policy decision [16]. During this period, SBC, BellSouth, and Verizon issued a common Request For Proposals for FTTx broadband systems, offering encouragement to system houses to design and supply standard FTTx systems. While the initial FCC decision applied to FTTH architectures, follow-up clarifications and decisions related to the 2003 FCC ruling gave adequate relief to some FTTC architectures as well. Somewhat earlier, the Japanese and Korean governments instituted initiatives to help drive their carriers to deploy FTTx technologies, and recently European carriers are finding ways to overcome regulatory issues in the countries they serve. At the same time, municipal governments, independent contractors, and housing builders began to offer FTTx systems as part of their economic development packages. With regulatory relief in the United States, the number of fiber-based access homes passed in North America grew to 8 million in 4 years. In the same time the number of homes connected grew to nearly 1.5 million [17, 18], representing a penetration of about 19% of the homes passed (Figure 10.10). This growth is expected to continue to nearly 40 million homes passed by 2012, with a 44% penetration of homes connected.

Worldwide the number of homes connected has grown in this same period to about 11 million [19 24] and this is expected to grow to 110 million by 2012

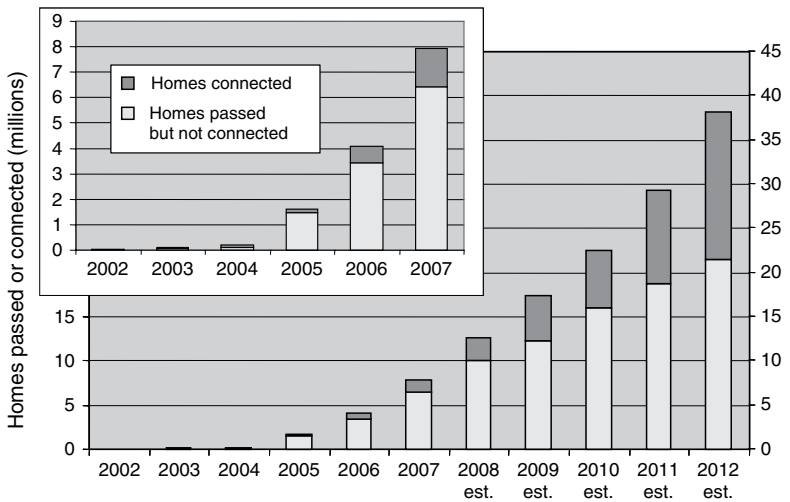

Figure 10.10 FTTx deployments in North America (this figure may be seen in color on the included CD ROM).

(Figure 10.11). Initially Japan, with its national push, was the leading country to deploy FTTx technology, followed by the United States as a result of the regulatory policy changes that took place there, and then by Europe and finally in a few years by China.

Looking toward the future, there are several global policy issues in active debate today that may impact continued broadband deployment. These include video franchise reform to streamline competitive entry, municipal broadband

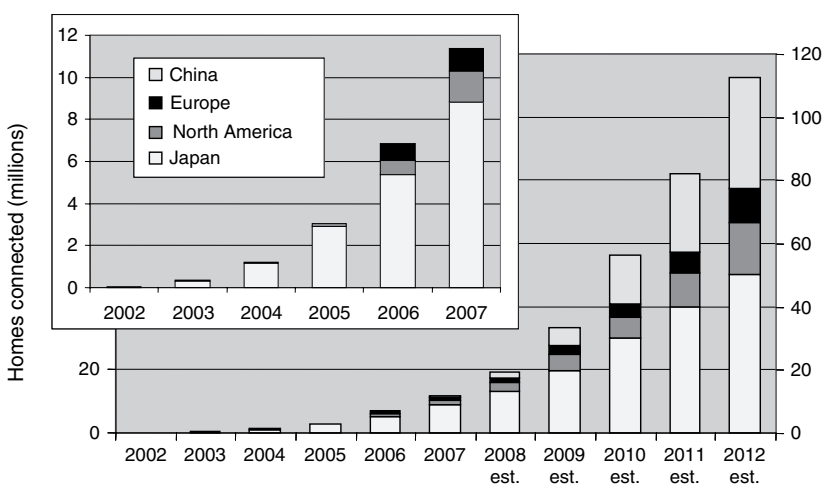

Figure 10.11 FTTx deployments globally (this figure may be seen in color on the included CD ROM).

deployment allowing local governments to deploy and operate broadband networks, and a universal service fund ensuring fair deployment to all communities regardless of socioeconomic status. It is too early to tell, but the outcome of these policy decisions could encourage further spending by carriers if it is favorable to them.

10.4 NETWORK ARCHITECTURES

In the past 15 years, global service providers have gradually pushed fiber technologies farther out from the serving offices and closer to the users. This trend started with the deployment of Subscriber Loop Carrier systems, which simply replaced multiple aging copper lines with fiber transport for the first few km from the serving office. Later, beginning in the early 1990s, CATV operators began to enhance their broadcast TV infrastructure by deploying HFC systems [25], which brought fiber out to within a kilometer or so of the users. Beginning in 1998, BellSouth began to use fiber-to-the-curb systems whenever they needed to refurbish aging copper plant or had new housing start installations, bringing fiber out to within 150 m of the users. These systems are a variant of FTTC systems, with the cabinet placed close to the home at the curb. FTTC is also a hybrid approach, as it uses digital subscriber line (DSL) technology over the existing copper twisted pair infrastructure in the drop portion of the network [26]. In 2002, Japan began deploying FTTH systems, using a point-to-point architecture. Shortly after that, in 2004, Verizon began deploying FTTH systems using a passive optical network (PON) architecture in the USA, pushing fiber all the way to the user. Verizon generalized the approach, calling their system fiber-to-the-premises (FTTP) to allow for the possibility of serving multiple dwelling unit structures (duplex homes and apartments) as well as businesses with the same fiber-based approach. AT&T is now deploying fiber to the node (FTTN) in the United States, a variant of FTTC that brings fiber to within 1.0 km of the user. For the hybrid approaches, longer distances from the termination of the fiber plant to the user have an adverse effect on the bandwidth that can be delivered to the user over copper twisted pairs or coaxial cable.

The network architectures of each of these three variants of fiber-based broadband access are very similar (Figure 10.12). They each have office terminal equipment, large fiber count feeder plant, medium fiber count distribution plant, a drop cable, and customer premises equipment. The three variants differ in a very important respect: the transmission media used for the drop portion of the network. In HFC the drop is coaxial cable, in FTTC the drop is twisted wire pairs, and in FTTH the drop is fiber. They also differ in another important respect: HFC and FTTC require active devices and powering in the outside plant, while FTTH has a totally passive outside plant that requires no power. These variants contribute to differences in the possible user service offerings, as well as differences in the cost structure for deployment and operations.

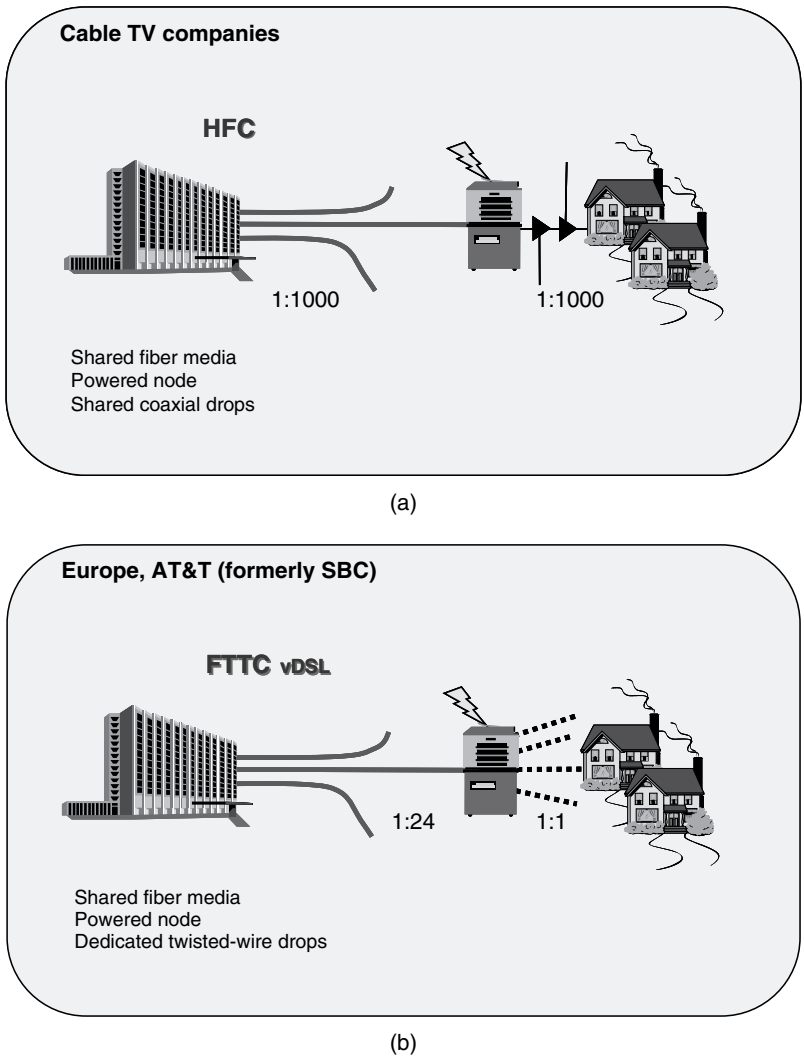

Figure 10.12 Broadband access network architectures for (a) HFC, (b) FTTC/xDSL, (c) FTTH PON, and (d) FTTH Pt Pt (this figure may be seen in color on the included CD ROM).

There are three basic services that each of these architectures is expected to deliver: telephone service, entertainment video service, and high-speed Internet data service. These represent the so-called triple play in FTTx architectures. Since entertainment video has historically been offered using NTSC (National Television System Committee) analog video standards, these systems typically

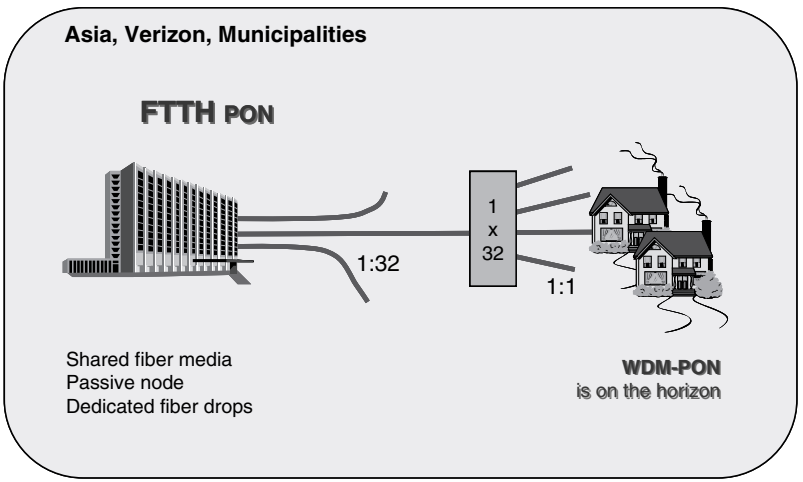

(c)

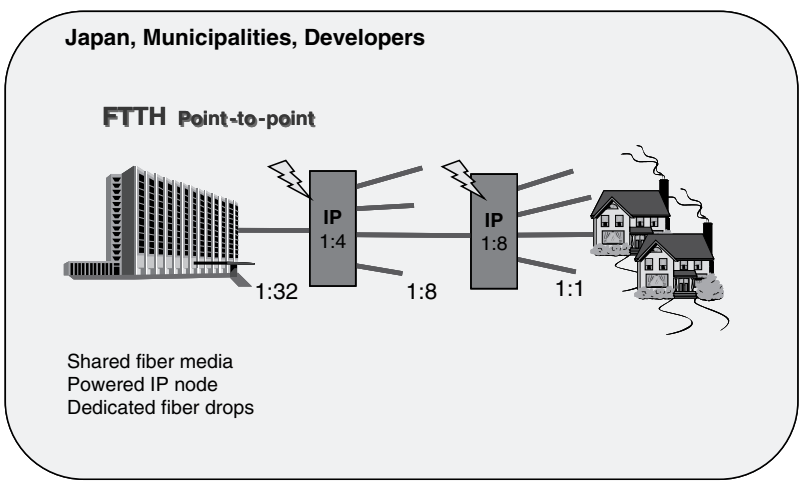

(d)

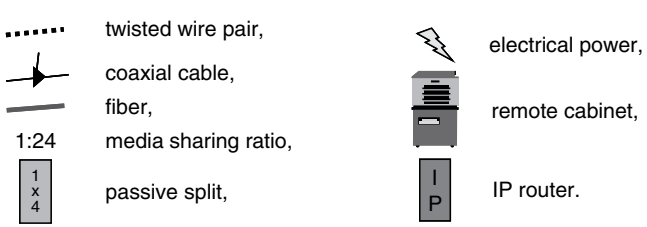

Figure 10.12 (*Continued*)

strive to support both conventional analog video channels as well as digital data channels. In HFC systems, both analog and digital channels are multiplexed onto the same optical carrier; in FTTH systems, the analog and digital signals are multiplexed onto different optical carriers (different wavelengths); and in FTTC systems only digital data channels are supported. Digital TV (DTV) services are normally delivered on the analog channels, while video-on-demand (VoD) is handled by the high-speed data channel. Since FTTC has no analog support, it can not simultaneously carry all of the entertainment channels, but is limited to offering VoD services and a limited number of DTV channels.

FTTC differs from HFC and FTTH in that it must seek to deliver entertainment video services in a digital format. In the long run, this distinction about how entertainment video is supported (either analog or digital) may disappear, since there is a significant trend to shift to digital formats, such as DTV and HDTV. Such a transition to digital television is mandated in the United States by the FCC for over-the-air broadcast TV signals to be completed by February 17, 2009 [27], but for video signals carried in a closed medium (fiber, coaxial cable, twisted pair) there is no equivalent mandated timetable. Other countries have similar timetables for conversion of TV signals to HDTV formats. Still, users are becoming increasingly aware of the advantages of digital video, as they become accustomed to digital video monitors, Video iPODs™, Digital Video Recorders, and other similar visual display appliances. Consequently, it is very likely that by the end of this decade the most common format for video signals will be digital formats that can store and retrieve video content from digital storage devices.

10.4.1 HFC Network Architecture and its Potential

The multiple service operators (MSOs) have deployed HFC networks to more than 40 million customers to date. These architectures include fiber-based transport from a service office to a powered node, which typically supports 500 1000 homes. The modulation format on the transport is subcarrier multiplexed (SCM) analog TV channels on a 1550 nm optical carrier. Since the TV signals are analog in nature, the transmitter must be exceptionally linear to avoid second- and third-order intermodulation impairments among the multiplexed TV channels, and the optical receiver power must be high to avoid noise impairments. This means that high-power erbium-doped fiber amplifier (EDFAs) are used at the serving office, to boost the analog signals to high power and to enable splitting the analog signals to serve many nodes. Every node receives the same set of analog TV channels. In addition, each individual node receives its own channel that is dedicated to Internet service for that node. This means that the unique Internet data must be multiplexed onto the Internet channel for its particular node. Since all users of the node get the same signal, they are all sharing the Internet channel, so none of them can benefit from the full Internet channel bandwidth. At the node, all of the

channels are amplified and split to feed to each subscriber associated with that node. Each subscriber receives the same analog signal as every other subscriber fed by that node, and their cable modem must filter out the TV channels they want to watch and select the Internet packets destined for their account. Cable modems sold today separate the Internet channel from the TV channels and deliver 42 Mb/s of Internet data downstream shared by all users, in compliance with a Data Over Cable Interface Specification (DOCSIS) 2.0 standard. In the upstream direction, Internet data from each subscriber is multiplexed onto a single upstream channel, which in DOCSIS 2.0 is 30 Mb/s shared by all users of the node. The upstream channel is limited by the coaxial amplifiers in the distribution plant, and this is the main limitation of HFC systems for high-speed Internet service.

Over time, there has been a progression of standards for HFC networks, with the DOCSIS cable modem standard being the controlling factor for user bandwidth. The trend has been to increase available downstream user bandwidth, then to increase upstream user bandwidth, then to use more channels for Internet access, and eventually to remove coaxial amplifiers from the distribution plant to allow more channels in the upstream direction. This progression of standardization is intended to increase user bandwidth for Internet service, and that trend is illustrated in Figure 10.13. Note that to achieve such increases, it is necessary to limit the number of customers that a node supports, and correspondingly to move the nodes closer to the user. Eventually, when the drop distances are short enough to remove all amplifiers, and when the node supports 25 users, an HFC network architecture should be able to deliver Gb/s data rate services to fulfill the demands of future users.

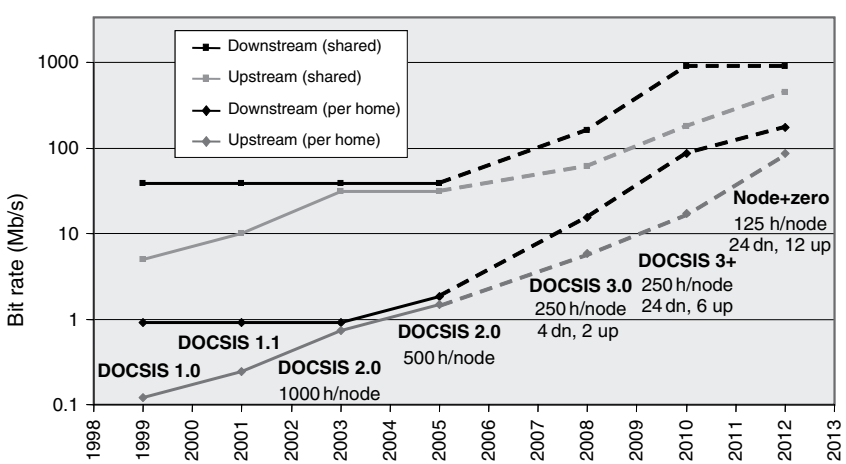

Figure 10.13 Standards progress over time for HFC (CableLabs) (this figure may be seen in color on the included CD ROM).

10.4.2 FTTC Network Architecture and its Potential

BellSouth has deployed FTTC to more than 1.3 million customers by 2006, AT&T has a plan to deploy FTTN widely to their customers, and BT in the United Kingdom offers this architecture to its customers. These architectures, originally standardized by ANSI (American National Standards Institute) and FSAN (Full Service Access Network Group) with the local exchange carriers input and later standardized by International Telecommunications Union (ITU), use GbE transport from a serving office to a remote cabinet. The optical signal formats and system are simple single-channel digital systems at 1310 nm, with either time-division multiplexed (TDM) or packet multiplexing of individual subscriber's information at the office and corresponding electronic demultiplexing at the remote cabinet in the downstream direction. Normally a single fiber supports the downstream multiplexed signals of 24 subscribers, and at the remote cabinet these are separated and remodulated using DSL formats that can be applied to the individual twisted wire pair drops. A similar arrangement is used in the upstream direction, using a second fiber with electronic multiplexers at the remote cabinet and corresponding demultiplexers at the office.

Over time, the standards and commercial DSL products have evolved to support ever higher user bandwidths. These standards prescribe a discrete multitone (DMT) modulation format, which uses a large number of 4 kHz-spaced orthogonal subcarriers in the band, each modulated at a low rate, which allows the system to cope with severe impairments that may be introduced by the twisted-pair copper medium [28]. Early DSL systems used 1.1 MHz of spectrum on the copper wires to achieve a bit rate of 364 kb/s, but this spectrum use has been increased to 2.2 MHz for aDSL2, then to 12 MHz for very high-speed Digital Subscriber Line (vDSL) and most recently to 30 MHz for vDSL2 technology.

In each case, the noise within the usable spectrum is the limiting transmission impairment, and as the bandwidth increases the total noise increases correspondingly. The noise limitation translates to a distance limit the distance for which the signal-to-noise ratio produces satisfactory error rates decreases as the usable bandwidth increases. So DSL using 1.1 MHz of spectrum can support drop distances of 2.5 km, while the latest vDSL2 standard using 30 MHz of spectrum supports drop distances of only 300 m. Consequently, the FTTN system of AT&T, with drop distance of 1.0 km can probably support a user bandwidth of about 25 Mb/s, while the FTTC system of BellSouth (now known as AT&T Southeast), with a drop distance of 300 m can probably support a vDSL2 user bandwidth of about 100 Mb/s.

A summary of the standards evolution is depicted in Figure 10.14. In the future, if DSL standards should move to an even higher utilization of copper spectrum of 50 MHz, and if service providers are willing to dedicate two twisted pairs per user and maintain drop distances less than 150 m, it is conceivable that DSL technology can support 1 Gb/s data rate services to individual users.

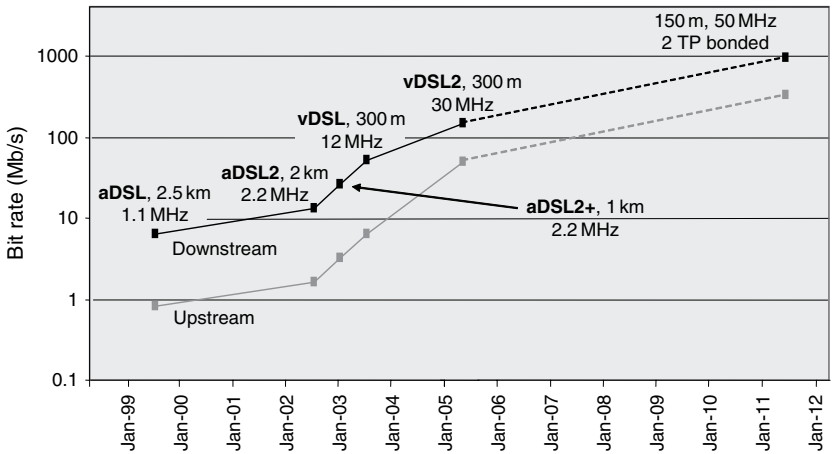

Figure 10.14 Standards progress over time for xDSL (ITU T) (this figure may be seen in color on the included CD ROM).

10.4.3 FTTH Network Architecture and its Potential

Verizon began deploying FTTH (they use the term FTTP to include homes, multidwelling units, and businesses) in May 2004 and by July 2007 had passed more than 7 million homes and had an estimated 1.5 million subscribers. Carriers in Asia and Europe, as well as many municipalities globally deploy this architecture as well. The FTTH systems use a PON architecture, transporting common signals from a serving office to multiple users with a 1:32 optical power split at a passive cabinet [29], and then a fiber drop to a network interface unit on the outside of the house. The analog and digital signals are carried on different wavelengths, with the downstream analog signals at 1550 nm and the downstream digital signals at 1490 nm. Remember, though, that analog channels can carry DTV signals via quadrature amplitude modulation. Upstream signals are carried in the same fiber as the downstream signals at a wavelength of 1310 nm, and are coupled to the fiber through coupling filters at each end of the network. The upstream data signals are multiplexed together using time-division multiple access (TDMA) methods, and each user is assigned one or more unique timeslots. A key problem in PON networks is that each user's upstream signal will arrive at a variable time determined by the distance the user is from the serving office and the transit time of the signal in fiber, potentially causing signal contention at the point where the upstream TDMA signals are to be multiplexed. This is handled by an autoranging synchronization signal that prompts each user when to transmit so that their signal arrives at the multiplex point in the correct timeslot.

Initially, the PON standards addressed FTTH systems with a downstream data rate of 622 Mb/s and an upstream data rate of 155 Mb/s using the asynchronous

transfer mode (ATM) format (A-PON), but later this was enhanced to include the analog channel for broadband access (B-PON). Eventually the ATM approach was extended to 2.5 Gb/s downstream and 622 Mb/s upstream (G-PON), and another approach using GbEthernet without an analog overlay was standardized as well (GE-PON). With the ATM format, the user has a well-defined and guaranteed bandwidth and quality of service, while with the Ethernet format the user shares the full bandwidth on a best-effort basis. The ATM-based PON systems are favored by US carriers, since the ATM format is compliant with their legacy transport systems, while the Ethernet format requires other capital-intensive changes to how they build their legacy networks. The user bandwidth characteristics of these various options for FTTH systems are summarized in Figure 10.15, and it is clear that user bandwidths of 100 Mb/s are quite reasonable today, and these can very likely move to Gb/s data rates [30] by making use of the statistical multiplexing inherent in Ethernet protocols.

While each of the FTTx architectures can be extended to provide significantly more bandwidth per user, even up to Gb/s rates per user, inside the home there is still the issue of how to distribute those signals to multiple rooms. The FTTH and FTTC systems provide the user an interface at the side of the home and the HFC systems provide a cable modem interface inside the home, but from a user perspective the signals must reach each PC, Internet appliance, display, and entertainment system in the household for the bandwidth to be useful. In Japan and in China, the FTTH system are installed with the user interface inside the home, allowing this interface to have substantially less environmental stress from temperature and the elements, and offering the possibility of tailoring the interface to the specific needs of the user. In-home networking has been identified as a key

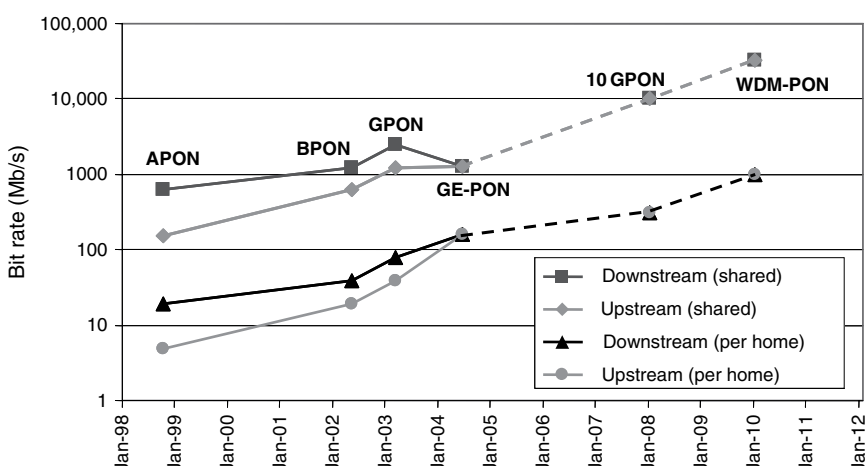

Figure 10.15 Standards progress over time for PON (ITU T) (this figure may be seen in color on the included CD ROM).

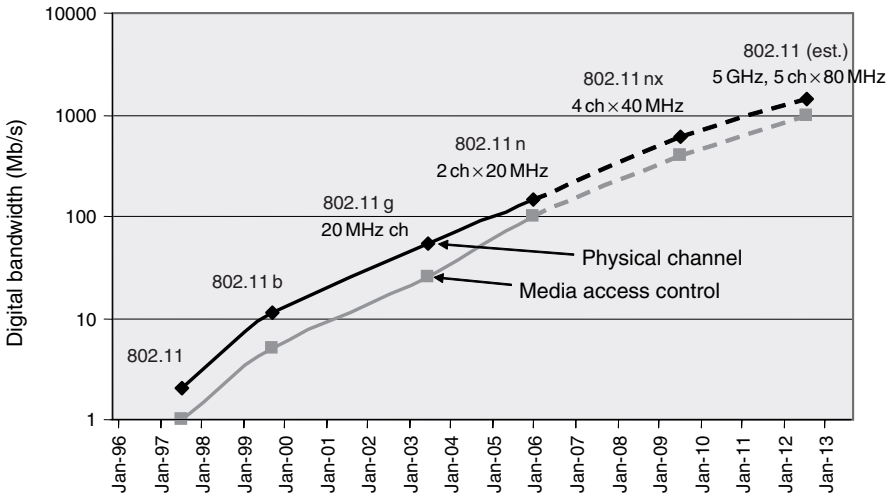

Figure 10.16 Standards progress over time for Wi Fi (IEEE) (this figure may be seen in color on the included CD ROM).

problem in the recent introduction of FTTP in the United States and Japan, and has been a lingering issue for HFC installations with multiple PCs. While this is not strictly the carriers issue to address, they will increasingly be in the position to suggest solutions to the homeowner in order to gain the maximum adoption of their service offerings. Fortunately, each of these system interfaces can be equipped with wireless (Wi-Fi, wireless-fidelity) base stations which today are capable of distributing several Mb/s of data anywhere inside a typical home. But as FTTx bandwidth increases over time, the demands of in-home networking capability will grow correspondingly to bandwidths of Gb/s. While the standards activity for Wi-Fi is on track to keep pace with the introduction of FTTx technologies (Figure 10.16), another option is to deploy specially designed fiber [31] in structured cabling arrangements for in-home networks.

10.5 CAPITAL INVESTMENT

While any one of these FTTx approaches can satisfy the current demands and affordability of the current market, they each require substantial capital investment to deploy widely. By way of example, imagine that the estimated 110 million homes is served by fiber-based access in 2012 as shown in Figure 10.11, that this represents a penetration of homes passed of 30%, and that each home passed could be provided for as little as $1000 per household. This would require about $370 billion in cumulative capital expenditures over a 5-year period. This represents a combined annual capital spending for fiber-based access related systems of about

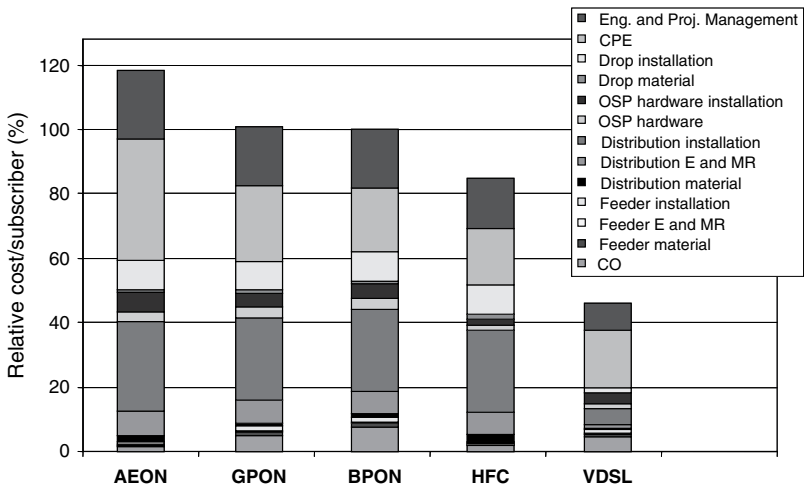

Figure 10.17 Comparison of relative capital costs per subscriber of HFC, FTTC/xDSL, and FTTH options, with B PON arbitrarily chosen as a reference (this figure may be seen in color on the included CD ROM).

$75 billion by all carriers globally. But 110 million homes is only about 5% of those available in the developing countries, so it will require a 20-year or more infrastructure commitment to bring fiber to all homes worldwide. A comparison of the FTTx approaches indicates that $1000 per home is a target that is eventually achievable, with the more expensive approaches providing more capability in the long run.

A comparative assessment of the capital costs for FTTx systems is illustrated in Figure 10.17, where it is assumed that 100% of homes passed are taking service, that there is a mix of 70% aerial and 30% buried plant, that the density of users is typical of a combination of urban and suburban customers, and that all of the equipment, installation, project, and subscriber costs are included in the comparison and averaged over all customers. At the lower end, FTTC/vDSL requires the smallest capital expenditures because it capitalizes on the existing telephone copper wire drop plant, but it also provides the most restrictive service options because it does not support analog TV programming. In the mid-range, HFC capital expenditures are higher than for FTTC/vDSL, and the extra expenditure buys the capability for analog TV programming, although HFC systems offer shared and therefore somewhat limited bandwidth for high-speed Internet services. At the upper end of capital expenditures are the FTTH systems, which provide for analog TV services as well as the highest potential digital Internet bandwidth. Because the MSO and ILECs (Incumbent Local Exchange Carriers) already have coaxial cable and twisted-pair drop cables in place, those two options represent lower spending and medium-term risk positions for satisfying future bandwidth demand growth. On the other hand, FTTH requires new infrastructure all the way to the home, making it the most capital intensive but also offering a better longer-term risk for satisfying future growing bandwidth demands.

10.6 OPERATIONAL SAVINGS

Given that FTTx deployments consume so much capital, a carrier is bound to ask: "Why would it benefit my company to take the risk to offer such services?" Of course, the answer is twofold: there are new service-related revenues to reap, and there are also operational cost savings associated with fiber-based systems. Taking a lesson from long-haul and metro transport systems, carriers have learned that fiber systems have fewer failures, higher availability, are more reliable [32], and have more capacity than copper-based systems. So FTTx solutions have a strong historical track-record on which to rely for both good reliability and high bandwidth at long distances. In addition, passive plant is especially attractive, because the number of active devices can be made much smaller in the outside plant where the parts are less accessible, and because passive devices in the outside plant are highly reliable [33]. For this reason alone, fiber-based systems are more attractive than copper-based systems that require periodic amplification and signal shaping. Further, new operational savings can be built into new infrastructure that take into account the ability to use sophisticated computer algorithms to enable faster and more efficient service provisioning, churn, administration, and easier fault location. All of these network operations and "back office" functions add up to significant annual operational savings compared to the way things are done today.

As an example, a comparison between FTTH annual operations expenditures relative to today's copper-based wireline technology [34, 35] is illustrated in Figure 10.18. While details of the customer contact and billing, central office, outside plant and network operations costs have been analyzed for both FTTH and today's technology [34], only the overall operations costs have been estimated for HFC and FTTC solutions [35]. This information indicates that more than $150 per year per subscriber can be saved in operational expenditures for FTTH compared to the labor-intensive wireline operations activities associated with customer

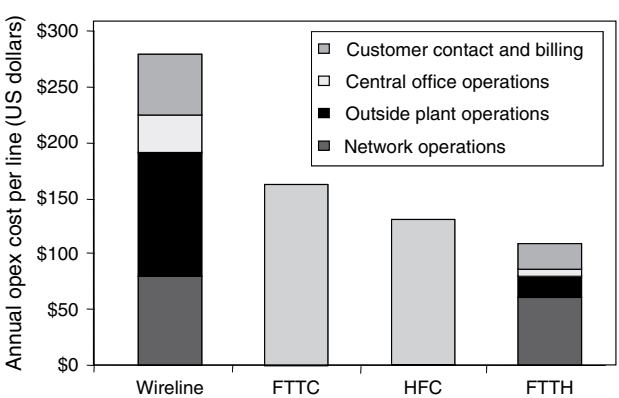

Figure 10.18 Comparison of operations costs per subscriber for FTT (this figure may be seen in color on the included CD ROM).

service requests, as well as provisioning, terminating, and re-provisioning service. Over a 7-year period, this nearly pays for the installation expenses, without even taking service revenue into account. A similar, but less dramatic, scenario is the case for HFC and FTTC solutions as well, but their reliance on active plant prevents them from reaping the benefits of a fully passive outside plant.

10.7 TECHNOLOGICAL ADVANCEMENTS

Over the last decade, system suppliers have worked at reducing the cost of equipment, the first installed costs of active and passive cable plant and the operations costs of FTTx systems. Both HFC and FTTC solutions have been deployed for most of the decade, and are relatively simple optically, consisting of point-to-point fiber transmission followed by more complex electronic splitting in a cabinet near the customers. Consequently, a major cost reduction driver has been electronics advances of IC integration. For HFC, this has resulted from the DOCSIS 1.0 and 2.0 standards, which allows IC designers to build special-purpose ICs to a common standard and increase the IC volumes dramatically. In a similar vein, the xDSL standardization process has allowed aDSL and vDSL to be implemented in standard IC designs, so that the most recent vDSL2 IC designs are capable of supporting all previous standards by firmware control. As a result of the standardization and volume manufacture of chip sets for HFC and FTTC, the OEM chip costs have been reduced, leading to lower first installed costs for carriers. In both cases, these IC advances also reduce the serving office, outside plant, and customer equipment size, power consumption, and number of active parts in the system. These changes tend to reduce the installation costs as well as the ongoing operations costs of these systems. We can expect similar IC advances in FTTH systems as well when the annual deployment rates are large enough to justify custom IC development costs for FTTH systems thus bringing down the cost of FTTH equipment in like manner.

10.7.1 Optical Transmitter and Receiver Technology Advances

For all three FTTx options, the photonics parts costs have been driven down by volume manufacturing. A prime example of this is the triplexer that is used in FTTH systems to receive downstream digital and analog signals and transmit upstream digital signals. Only a few years ago triplexers were manufactured using packaged photodiodes, packaged lasers, thin-film filter components, and bulk coupling and splitting optics resulting in labor-intensive packaging costs and a triplexer price of $350 per unit. Now, with volume demands for triplexers at a few million per year, the manufacturing approaches have turned to integrated

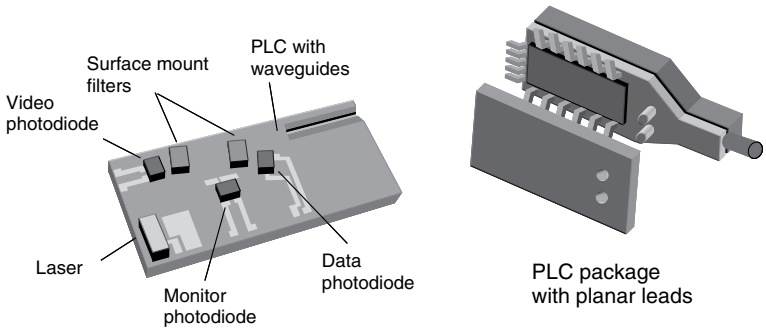

Figure 10.19 Sketch of triplexer solution enabling volume manufacturing (this figure may be seen in color on the included CD ROM).

solutions, where automated pick-and-place can be applied. For example, planar lightwave circuits [36 39] are used to form the coupling waveguides and wavelength filters, photodiode, and laser chips are flip-chip mounted directly on the PLC substrate, and fiber alignment is done by direct coupling via precision grooves in the PLC substrate [40] (Figure 10.19). These approaches bring the advantage that they can reliably achieve fiber alignment tolerances and good fiber coupling efficiency with a controlled waveguide transition design to the PLC waveguide, by using the precision and yield associated with IC fabrication processes [41]. The result of all these technology improvements is a triplexer that can be offered at a price of $50 or lower to system suppliers. Since the triplexer is a dedicated part (one per subscriber), its cost reduction has a dollar-for-dollar impact on the cost of the overall system. The cost reduction of this single component alone has made a significant impact on lowering the per subscriber cost of FTTH systems.

10.7.2 Cable Management Technology Advances

Installation of optical fiber cable, cabinets and other passive plant components in the feeder, distribution, and drop portions of the outside plant can account for more than half of the cost of installation of an FTTx system. This cost component has received a lot of attention to simplify installation techniques, to speed deployment, and to improve labor efficiency and effectiveness. One way to accomplish this is to integrate much of the time-consuming cable management parts together in the factory [42], where volume manufacturing methods and sophisticated assembly equipment can be easily supported. This means that the distribution cable, branch entry points, and cable terminations must be uniquely designed for a specific location and assembled under controlled conditions in the factory. Since each location has a different set of physical measurements along its route from distribution cable to branch entry point to splitter cabinet, this requires careful network planning and advance engineering effort by the carrier. In any installation, whether

using field installed terminations or terminations installed at the factory, it is necessary to engineer and plan the network for a specific location. But when you integrate the cable assembly in the factory, the engineering measurements must be more accurate because there is no chance to make a final cable length adjustment in the field by cutting the cable shorter.

For cable assemblies that are integrated in the factory, the carrier's craft personnel are sent into the field prior to ordering the outside plant products, where they use precise laser rangefinders, measuring wheels, and pull-tapes to determine the distances of each cable, branch point, and termination on the specific route. These measurements are provided to a few inches tolerance for the cable manufacturer via an online configuration manager, which generates a bill of materials automatically. Then each cable management assembly is custom-manufactured to those demanding specifications and delivered to the installation site ready to roll off the reel and fasten in place without any field-related cutting of cables or splicing of cable branch entry points, splice points, or closures [43, 44]. Figure 10.20 shows photos of

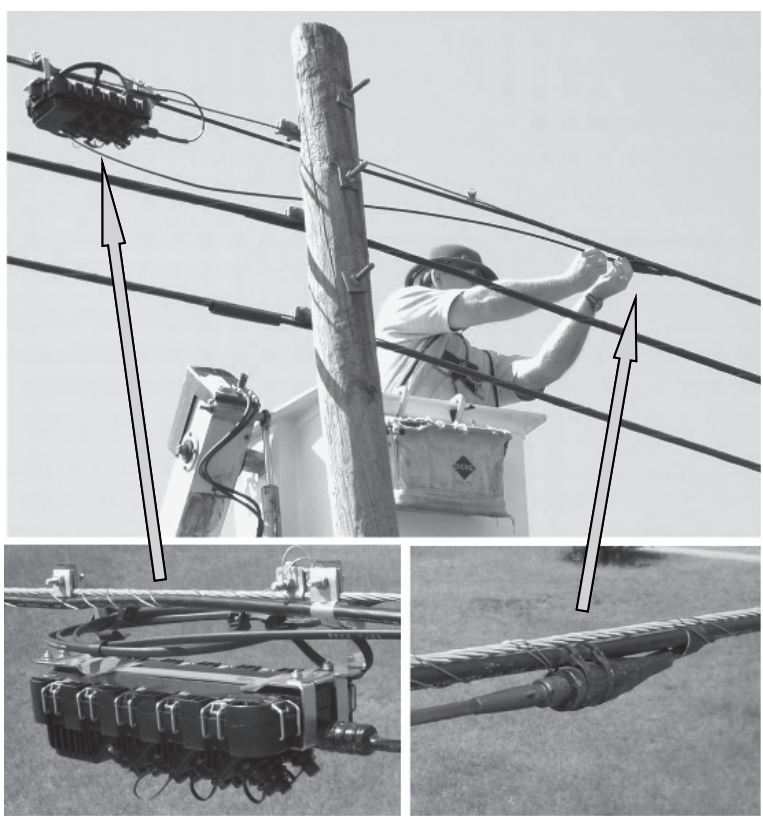

Figure 10.20 Factory installed aerial cable branch point and fiber drop terminal closure (photos) (this figure may be seen in color on the included CD ROM).

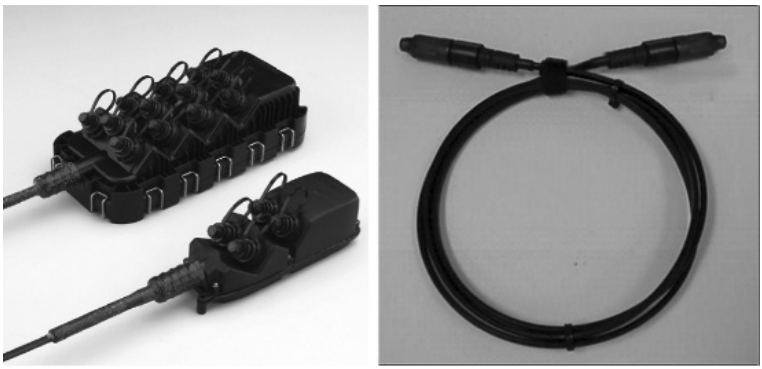

Figure 10.21 Fiber drop terminals and drop cable with robust connectors installed at the factory (photos) (this figure may be seen in color on the included CD ROM).

aerial cable terminal closure and branch points being installed, and Figure 10.21 shows photos of drop cable terminations and drop cable with robust connectors manufactured for this method. With this technique, installation times can be cut from nearly 2 days to less than 3 hours, and the entire process takes fewer truck rolls, fewer tools, and requires much less time working overhead in a bucket. To further ease installation, and to assure a minimum of future maintenance events, the splitter cabinets, enclosures, branch points, terminals, and drop cables are all fitted with connectors at the factory, making them waterproof and environmentally robust while minimizing splicing in the field.

10.7.3 Outside Plant Cabinet Technology Advances

In a similar fashion, the cabinets that house the splitters are factory assembled and internally preconnected according to an engineering design, so that they can be set in place and attached to their dedicated cables without further craft involvement interior to the cabinet. The initial designs of the cabinets were rather massive, requiring several laborers and a crane to unload and place them. Subsequent technology advances allowed the cabinets to be miniaturized so that they can be lifted by hand and set in place by an individual [45]. An enabling step toward this objective was to improve the bend tolerance of the fiber [19, 46, 47] used in the 1:32 splitters, from 75 mm bending radius to 30 mm bending radius. This was combined with a reduction in the fiber jumper diameter from 2.9 to 2.0 mm, to allow the 1:32 splitters [33] to be reduced in size from 191 mm $\times$ 131 mm to 125 mm $\times$ 63 mm on the long dimensions, because the excess fiber coiled inside the splitter package could be correspondingly reduced in diameter. Overall this resulted in a 78% reduction in the spatial volume taken up by the splitters (Figure 10.22). At the same time, the layout of the cabinet was improved to make it

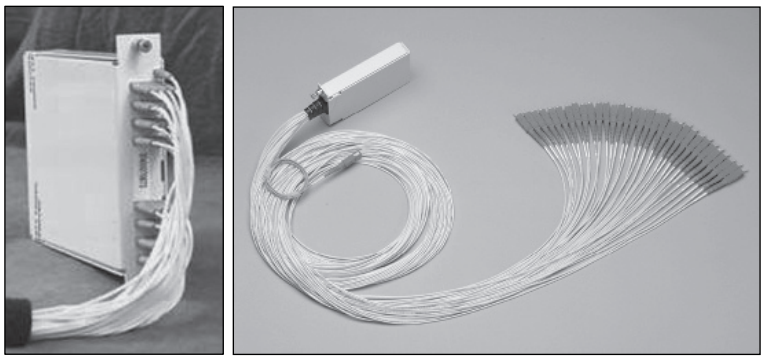

Figure 10.22 Splitter size reduction associated with bend tolerant fiber (a) before and (b) after size reduction (photos) (this figure may be seen in color on the included CD ROM).

more craft friendly. The splitter size reduction together with the improved cabinet layout then enabled the splitter cabinets to be redesigned to allow a smaller footprint, resulting in a smaller cabinet with less metal, making it much lighter. An example of the cabinet size reduction that resulted from improved fiber bend tolerance is shown in Figure 10.23, where it is clear that the cabinet volume was reduced by more than a factor of four. Such size reductions have diverse impact on costs; ranging from reduced space to store inventory prior to installation, reduced shipping fees, reduced need for heavy equipment to install the cabinets, and reduced labor during cabinet installation. In addition, the smaller cabinets are

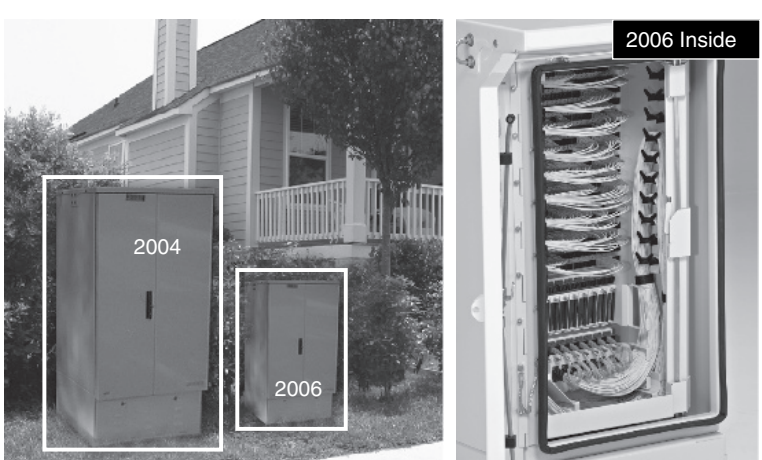

Figure 10.23 Cabinet size reduction associated with bend tolerant fiber, smaller cable diameter, and smaller splitters (photos) (this figure may be seen in color on the included CD ROM).

less intrusive to the environment, can be more easily placed in a wider variety of locations than the bigger cabinets and experience less vandalism.

10.7.4 Fiber Performance Technology Advances

There is another important technology development that is beginning to play a role in reducing the overall FTTx system cost. This is the discovery that the stimulated Brillouin scattering (SBS) threshold in fiber can be increased, allowing higher launch power for analog signals without introducing more system impairments [48, 49]. To begin with, in both HFC and FTTH systems, the analog signal loss budget is the limiting factor in determining the reach from the serving office out to the active optoelectronics (see Figure 10.24). The loss budget is set at the subscriber end by the receiver noise limitations at a level of -5 dBm to -10 dBm, depending on the system under consideration. Then to get a high enough loss budget for reasonable reach, the launch power has to be very high in excess of $+15$ dBm. With standard single-mode fiber (meeting G.652 standards), increasing the launch power above about $+17$ dBm for the analog signals introduces significant impairments due to the reflected SBS power, which emphasizes all of the key analog impairments [50]. The received noise is increased [carrier-to-noise ratio (CNR) is reduced] as a result of laser phase-to-intensity conversion by the SBS, and intermodulation distortions [CSO and composite triple beat (CTB)] are introduced in the modulated carrier because the optical carrier wave is above the

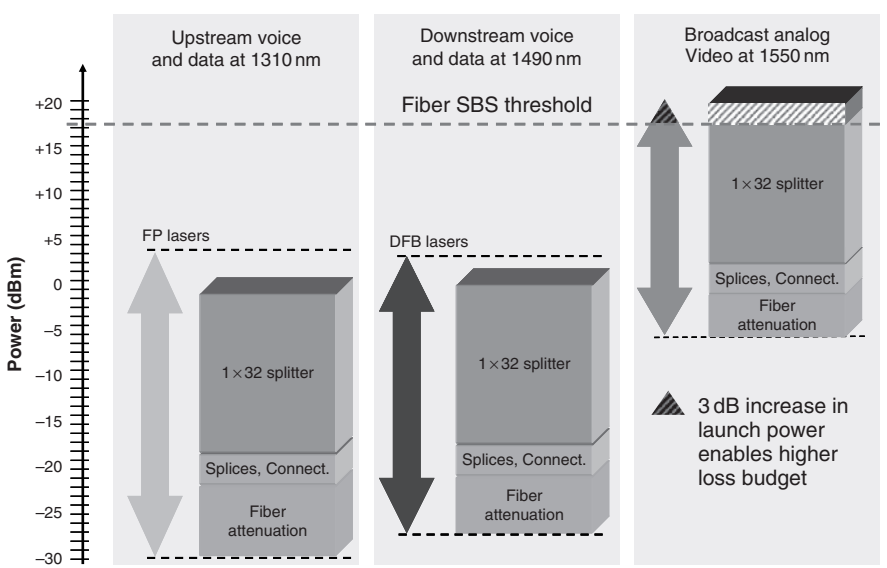

Figure 10.24 System loss budget for analog and digital transmission (this figure may be seen in color on the included CD ROM).

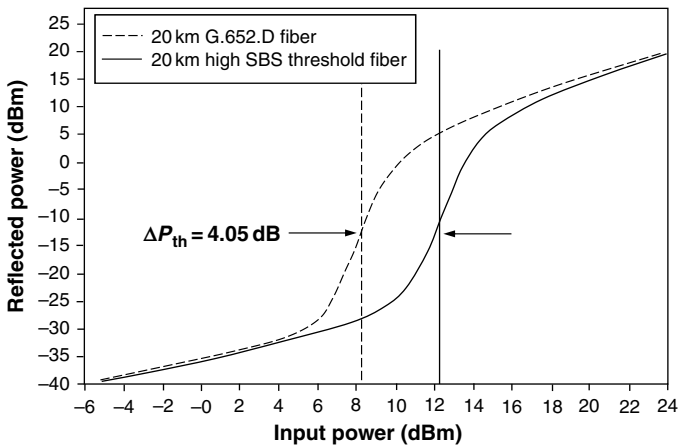

Figure 10.25 Comparison of fiber meeting G.652 standards and high SBS threshold fiber performance.

SBS threshold and attenuated relative to the modulated sidebands which are below the SBS threshold. Fortunately, this SBS threshold can be controlled to some extent by the design of the fiber profile, which can be optimized to reduce the interaction between the acoustic wave and the optical field in the waveguide and ameliorate the cause of SBS [51, 52] (see Figure 10.25). A suitable fiber design can produce Brillouin gain spectra that are only about 35 40% as strong as the Brillouin gain spectra in standard single-mode fiber [50, 53] (see Figure 10.26).

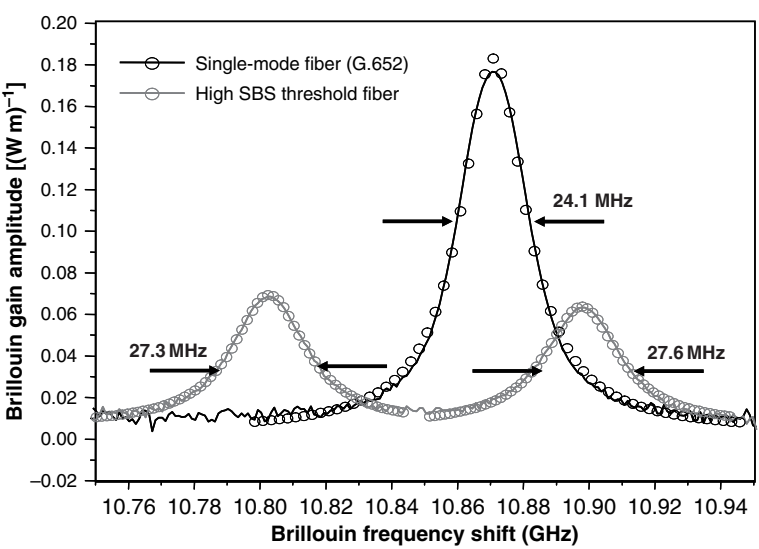

Figure 10.26 Fiber theory for improving SBS threshold (this figure may be seen in color on the included CD ROM).

The result is a fiber that can accommodate about 4 dB higher launch power, while still retaining the same analog impairments seen in standard single-mode fiber. Since the fiber design itself avoids excess SBS impairments, cheaper video transmitters can be used because they don't have to compensate for that impairment.

The impact of the high-threshold SBS fiber is to provide relief to the system in several potential ways. In HFC systems, it is possible to launch higher power and place the node farther from the serving office. In FTTH systems, the higher launch power enables twice the splitting with a corresponding increase in cost sharing of key system components [54], or alternatively an increased reach of 10 km or so which enables more subscribers to be accessible to the serving office. Since this fiber performance has to be designed into the system, the impact of this improvement in fiber attributes is only now beginning to be felt in the industry. But laboratory measurements confirm that the system improvements suggested by the Brillouin gain spectrum reductions can in fact be realized (Figure 10.27). Since the improved fiber is completely compatible with standard single-mode fiber, achieving similar or better attenuation, fiber coupling, and splicing attributes, these system cost savings can be passed on to a large extent to system suppliers, to the carriers and ultimately to the subscribers as lower access fees.

Taken together, all of these technological advancements have made a steady impact on the costs of FTTx systems. For example, a progression over time of the system costs for FTTH approaches is shown in Figure 10.28, where the system cost has declined about 15% per year during the 1990s and about 20% per year between 2000 and 2004 [35], to a point where the cost is about $1300 per subscriber in 2006. With continued deployment, increasing volumes, improved system range

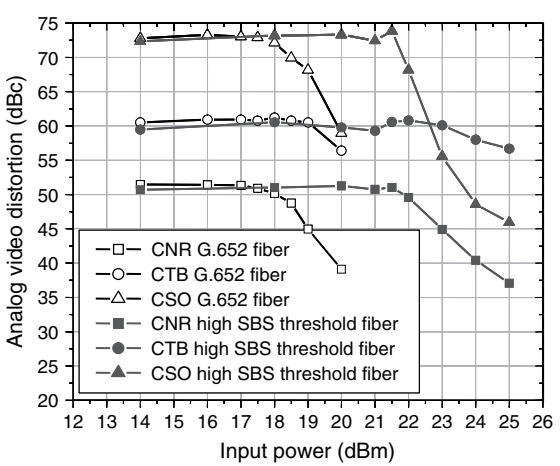

Figure 10.27 Analog impairments with fiber meeting G.652 standards and high SBS threshold fiber (this figure may be seen in color on the included CD ROM).

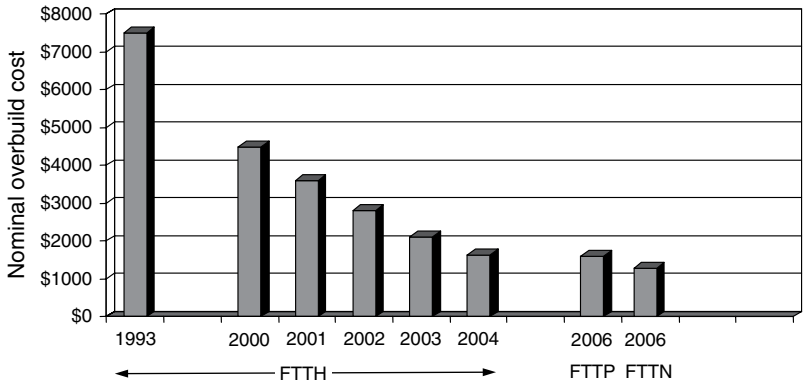

Figure 10.28 Cost decline of FTTx solutions with time (this figure may be seen in color on the included CD ROM).

and split ratio [13, 55], and competitive pricing the cost per subscriber will likely continue moving downward toward the $1000 target.

10.8 FUTURE BANDWIDTH ADVANCEMENTS

While technology advancements are helping to bring infrastructure and operations costs down, they also introduce the potential for increased user bandwidth performance. This is fortuitous, as the cycle of user technology adoption points toward a 10-fold increase in user bandwidth by 2010 to 100 Mb/s per user [56] for a few million users, and 5 years later to 1 Gb/s per user [57] with a similar user base. These changes in the industry and in user needs are going to drive the technologies that carriers deploy. In fact, the trends in standard products for HFC, FTTC, and FTTH all show the potential for achieving upgrades to 1 Gb/s per user by the time such needs develop, but this requires pushing fiber closer to the home than is currently the case for FTTC and HFC networks. So those service providers will have to consider carefully their evolution and capital spending plans to assure they can continue to meet the competitive needs of users in the long term.

Of course, it is difficult to envision exactly how 1 Gb/s per user could be useful a decade from now. But we have seen technology transform our social and entertainment behavior in the past. Phonograph records gave way to CDs, which have much higher fidelity for music, and letters gave way to e-mail, which is faster and can go to multiple recipients. Film gave way to digital images, which enable instant proofing and sharing with friends and family. Black and white TV gave way to color TV, and now analog TV is being replaced by digital TV, which can enable interactive viewing and game playing. Movie theaters are giving way to DVD players with wide screens, surround sound, and home theater arrangements. Each of these technical advances has ushered in new ways to view and share

information and entertainment content, leading to unexpected demands for higher bandwidth in our daily lives. As the trend continues, there will inevitably be more sharing of digital images, digital music files, digital movie files, digital home movie clips, digital news feeds, with the consumer electronics industry fueling the trend by offering a whole host of innovative communications and entertainment appliances catering to our growing wants and needs. Ultimately, the increased capability and fidelity of sharing and displaying images and movies will lead to the adoption of 1 Gb/s data rates being delivered to our homes and distributed throughout the household, most likely with capabilities for symmetric traffic flows in both directions.

With some imagination, and imperfect knowledge that the historical trends presented here project into the future, it is possible to envision the following scenario playing out over the next two decades.

- *Applications*: all industrial and entertainment content is digital, and able to be delivered to (and from) homes and businesses at Gb/s rates, where it is stored for on-demand use at the subscriber's convenience, and viewed on large-screen digital displays.
- *Technology*: fiber-based systems are used exclusively for broadband access, with many homes and business connected directly to fiber and the remainder connected from cabinets within 150 m of their building.
- *Deployment*: carriers offer integrated multimedia service packages that include entertainment (music and movies), high-speed Internet, cellular communications, as well as voice services. They also offer in-home networking using wireless and structured cabling options, so subscribers can effectively utilize their bandwidth.
- *Economics*: the capital expenditures for broadband access have been largely recovered and the business cases are positive because of reduced operations costs, allowing carriers to compete on price and bandwidth, and to expand infrastructure to support heavy use of Gb/s access rates.

By the time that 1 Gb/s per user is needed and affordable, much of the broadband access infrastructure will already have been installed and in service in the world. Because of this, upgrade strategies are of key importance for how to evolve from today's architectures to those that support Gb/s per user capacity 10 15 years from now. Even beyond this time frame, WDM-PON (wavelength-division multiplexed-PON) and 10G-PON (10 Gb/s-PON) approaches could enable even higher capacity, and complicate the evolution strategy and planning further [58]. While FTTH systems can accommodate such change by replacing or upgrading the transmission equipment at the ends of the access network, the FTTC and HFC systems may require labor-intensive changes in the drop plant as well. These are complex techno-economic issues and worthy of study and experimental investigation right now, although the issues will linger so that there is time to work through the possibilities to arrive at sound solutions before it is too late.

10.9 SUMMARY

After more than 20 years of research and development, a combination of technological, regulatory, and competitive forces are finally bringing fiber-based broadband access to commercial fruition. Three main approaches, HFC, FTTC/vDSL, and FTTH, are each vying for a leading position in the industry, and each has significant future potential to grow customers and increase bandwidth and associated service offerings. No matter which approach wins, or even if all three remain important, construction of the infrastructure needed to serve the entire global network will take one or two decades to complete, because the capital requirements are enormous. During this time it is almost certain that further technical advances and cost reductions will be adopted, bringing performance levels and bandwidth ever higher and keeping service costs affordable. Ultimately, the potential for Gb/s access speeds is on the horizon, and is a target that can be reached economically, when user demand warrants it, through evolution of the infrastructure that is being deployed today.

ACKNOWLEDGMENTS

The author would like to acknowledge the very broad base of work at Corning Incorporated, from which significant content of this paper is drawn. Contributors to that base of work include colleagues from Corning Science and Technology, Corning Optical Fiber, and Corning Cable Systems organizations. In particular, the author would like to thank John Igel, Robert Whitman, Mark Vaughn, Boh Ruffin, and Scott Bickham for specific contributions to this work. In addition, the author would like to thank Paul Shumate and Tingye Li for sharing their perspective on the historical trends for fiber to the home.

LIST OF ACRONYMS

ANSI	American National Standards Institute, standardizing T1E1 for DSL formats
ATM	Asynchronos Transfer Mode, a signal format for combining digital signals
CATV	Cable TV, a means to provide TV via coaxial cable to homes
CNR	Carrier-to-Noise-Ratio, which is the RF carrier strength relative to the noise
CSO	Composite Second Order, an analog impairment due to non-linear effects
CTB	Composite Triple Beat, an analog impairment due to non-linear effects

DMT	Discrete Multi-Tone modulation format, the line code used by aDSL and vDSL systems
DOCSIS	Data Over Cable Interface Specification, a standard to describe cable modems
aDSL, aDSL2	Asymmetric Digital Subscriber Line, a standard for providing digital signals over copper wires used with FTTC systems
vDSL, vDSL2	Very high speed Digital Subscriber Line, a standard for providing digital signals over copper wires used with FTTC systems
DTV	Digital TV, provides digital television with resolution comparable to analog TV
EDFA	Erbium Doped Fiber Amplifier, provides gain in the 1550 nm band
FCC	Federal Communications Commission, a US regulatory body for communications
FSAN	Full Service Access Network Group, broadband access network standards forum
FTTC	Fiber to the cabinet, which brings fiber to a powered cabinet near the subscribers
FTTH	Fiber to the Home, which brings fiber all the way to the side of the home
FTTN	Fiber to the Node, AT&Ts name for FTTC with the cabinet being at a node up to 1.0 km from the subscribers
FTTP	Fiber to the Premises, Verizon's name for expanded FTTH systems to include fiber to business and multiple dwelling units
FTTx	Fiber to the X, describes fiber-based access systems, such as HFC, FTTC, FTTH
G.652	Standard single mode fiber, meeting the ITU-T standard named G.652
GbE	1.0 Gb/s Ethernet, a standard for Ethernet connections
HDTV	High Definition TV, provides high resolution digital television
HFC	Hybrid Fiber Coax, which brings fiber to a powered cabinet near the subscribers
ILEC	Incumbent Local Exchange Carriers, offer local telephone services
ITU	International Telecommunications Union, a standards body for communications
MSO	Multiple Service Operators, companies offering cable TV, internet and phone service
NTSC	National Television System Committee, analog television standard body
10G-PON	10 Gb/s PON, a system with downstream data rates of 10 Gb/s
PON	Passive Optical Network, a method of providing passive splitter and handling upstream congestion by auto-ranging used with FTTH systems

A-PON	ATM-PON, a passive system using the ATM signal format
B-PON	Broadband-PON, a passive system using ATM signals and an analog overlay
G-PON	Gb/s PON, a system with Gb/s data rates and ATM signal formats
GE-PON	Gigabit Ethernet-PON, a system using GbE for downstream signals
WDM-PON	Wavelength Division Multiplexed-PON, a system using multiple wavelengths, one for each subscriber
SBS	Stimulated Brillouin Scattering, due to an interaction of acoustic and optical waves
SCM	Sub-Carrier Multiplexed, a means to combine multiple analog signals by interleaving RF carriers, each of which are modulated with analog signals
TDM	Time Division Multiplexed, combines signals by interleaving digital streams
TDMA	Time Division Multiple Access, combines the signals from many users into one
Wi-Fi	Wireless-Fidelity, system for broadcasting internet signals inside homes

REFERENCES

[1] R. E. Wagner, J. I. Igel, R. Whitman et al., "Fiber based broadband access deployment in the United States," *J. Lightw. Technol.*, 24(12), 4526, December 2006.

[2] R. E. Wagner, "Broadband Access Network Options," OIDA Workshop on Broadband Access for the Home and Small Business, Palo Alto, April 22 23, 2003.

[3] P. W. Shumate and R. K. Snelling, "Evolution of fiber in the residential loop plant," *IEEE Commun. Mag.*, 29(3), 68 74, March 1991.

[4] US Census Bureau, "Manufacturing, Mining and Construction Statistics" Manufacturers' Ship ments Historic Timeseries, http://www.census.gov/indicator/www/m3/hist/naicshist.htm, August 29, 2005.

[5] R. L. Whitman, "Global FTTH Risks and Rewards," FTTH Council Conference, Las Vegas, October 3 6, 2005.

[6] J. B. Bourgeouis, "FTTx in the US: Can we see the Light?" FTTH Council paper, http:// www.ftthcouncil.org/documents/763530.pdf, November 2005.

[7] "Internet Users (ITU estimates)," United Nations Statistics Division, Millennium Indicators Database, http://millenniumindicators.un.org/unsd/mdg/Handlers/ExportHandler.ashx?Type Excel& Series 608, March 10, 2005.

[8] "World Internet Usage and Population Statistics," Miniwatts Marketing Group, http://www. internetworldstats.com/stats.htm, June 30, 2007.

[9] Nielsons NetRatings, "NetView Usage Metrics," http://www.nielsen netratings.com/news.jsp? section dat to&country us, published monthly.

[10] C. Kehoe, J. Pitkow, K. Sutton et al., GVU Tenth World Wide Web User Survey, Georgia Institute of Technology, www.cc.gatech.edu/gvu/user surveys, May 14, 1999.

[11] M. J. Flanigan, "*TIA's 2006 Telecommunications Market Review and Forecast*," Telecommunica tions Industry Association, Arlington, VA, February 2006.

[12] M. D. Vaughn, "FTTH Cost Modeling: Impact of Split Location and Value of Added Splits, Extended Reach and Equipment Consolidation," 2003 FTTH Council Conference, Session B06, New Orleans, October 7 9, 2003.
[13] M. D. Vaughn, Member, IEEE, David Kozischek, David Meis, Aleksandra Boskovic, and Richard E. Wagner, "Value of reach and split ratio increase in FTTH Access networks," *J. Lightw. Technol.*, 22, 2617 2622, November 2004.
[14] M. D. Vaughn, M. C. Meow, and R. E. Wagner, "A bottom up traffic demand model for LH and metro optical networks," *OFC 2003 Technical Digest*, Paper MF111, Atlanta, March 23 28, 2003.
[15] Telecommunications Act of 1996, Pub. L. No. 104 104, 110 Stat. 56.
[16] M. H. Dortch, Secretary FCC, "Review of the Section 251 Unbundling Obligations of Incumbent Local Exchange Carriers" FCC 03 36, *Report and Order and Order on Remand and Further Notice of Proposed Rulemaking* in CC Docket No. 01 338, adopted February 20, released August 21, 2003.
[17] M. Render, "FTTH/FTTP Update" 2005 FTTH Council Conference, Render, Vanderslice and Associates Research, www.ftthcouncil.org/documents/732751.pdf, Las Vegas, October 3 6, 2005.
[18] M. Render, "Fiber to the Home: Advanced Broadband 2007 Volume One," Render, Vanderslice and Associates Research, http://www.rvallc.com/ftth reports.aspx, June 2007.
[19] J. George and S. Mettler, "FTTP market and drivers in the USA," ITU T Study Group 6, TD 227A1 (GEN/6), Geneva, May 14 18, 2007.
[20] G. Finnie, "Heavy Reading European FTTH Market report," FTTH Council Europe Annual Conference, Barcelona, February 7 8, 2007.
[21] D. van der Woude, "An overview of Fiber to the Home and Fiber backbone projects," FTTH Council Europe Annual Conference, Barcelona, February 7 8, 2007.
[22] R. Montagne, "FTTH deployment dynamics: Overview and French case," IDATE Consulting and Research, FTTH Council Europe Annual Conference, Barcelona, February 7 8, 2007.
[23] X. Zhuang, S. Huiping, Xuemengchi, and W. Hong, "FTTH in China," Ministry of Information Industry of China, ITU T Study Group 6, TD 227A1 Rev.1 (GEN/6), Geneva, May 14 18, 2007.
[24] M. Coppet, J. F. Hillier, J. C. Hodulik et al., "Global Communications," UBS Investment Research Q series, July 10, 2007.
[25] W. Ciciora, J. Farmer, D. Large, and M. Adams, "Chapter 18 Architectural Elements and Examples," *Modern Cable Television Technology*, Second Edition, Morgan Kufmann Publishers in an Imprint of Elsevier, San Francisco, pp. 733 766, 2004.
[26] M. D. Nava and C. Del Toso, "A Short Overview of theVDSL System Requirements," *IEEE Commun. Mag.*, December 82 90, 2002.
[27] W. F. Caton, Acting Secretary FCC, "Advanced Television Systems and Their Impact Upon the Existing Television Broadcast Service," FCC 97 115, 6th Report And Order on MM Docket No. 87 268, adopted April 3, 1997.
[28] P. Eriksson and B. Odenhammar, "VDSL2: Next important broadband technology," http://www.ericsson.com/ericsson/corpinfo/publications/review/2006 01/06.shtml, Ericcson Review, Issue No. 1 2006.
[29] D. Meis et al., "Centralized vs Distributed Splitting in Passive Optical Networks," NFOEC'05, Paper NWI4, Anaheim, March 6 11, 2005.
[30] D. Faulkner, "Recent Developments in PON Systems Standards in ITU T," SPIE Optics East 2005, Paper 6012 27, Tutorial IV, Boston, October 23 26, 2005.
[31] K. Nakajima, K. Hogari, J. Zhou et al., "Hole assisted fiber design for small bending and splice losses," *IEEE Photon. Technol. Lett.*, 15, 1737 1739, 2003.
[32] See, for example, transport availability standards requirements listed in Bellcore GR 418 CORE (downtime minutes per year), ETSI standard EN 300 416 (outages per year), and ITU T standard G.828 (errored seconds per year).
[33] C. Saravanos, "Reliability Performance of Optical Components in the Outside Plant Environment," 2004 FTTH Council Conference, www.ftthcouncil.org/documents/212550.pdf, Orlando, October 4 6, 2004.

[34] J. Halpern, G. Garceau, and S. Thomas, "Fiber to the Premises: Revolutionizing the Bell's Tele com Networks," Bernstein Research & Telcordia Research Study, http://www.telcordia.com/products/fttp/bernstein telcordia.pdf, May 20, 2004.

[35] P. Garvey, "Making Cents of it All Costs/Key Drivers for Profitable FTTH," FTTH Council Conference, Las Vegas, October 3 6, 2005.

[36] M. Pearson, S. Bidnyk, A. Balakrishnan, and M. Gao, "PLC Platform for Low Cost Optical Access Components," *Technical Digest IEEE LEOS 2005*, Paper WX1, Sidney, October 23 27, 2005.

[37] Y. Nakanishi, H. Hirota, K. Watanabe et al., "PLC based WDM Transceiver with Modular Structure using Chip Scale Packaged OE Devices," *Technical Digest IEEE LEOS 2005*, Paper WX2, Sidney, October 23 27, 2005.

[38] W. Chen, K. B. Little, W. Chen et al. "Compact, Low cost Chip Scale Triplexer WDM Filters," *OFC 2006 Technical Digest*, Paper PDP12, Anaheim, March 5 10, 2006.

[39] H. Sasaki, M. Uekawa, Y. Maeno et al., "A low cost micro BOSA using Si microlens integrated on Si optical bench for PON application," *OFC 2006 Technical Digest*, Paper OWL6, Anaheim, March 5 10, 2006.

[40] D. W. Vernooy, J. S. Paslaski, H. A. Blauvelt et al., "Alignment Insensitive Coupling for PLC Based Surface Mount Photonics," *IEEE PTL*, 16(1), 269 271, 2004.

[41] Wenhua Lin, and T. Smith, "Silicon Opto Electronic Integrated Circuits: Bringing the Excellence of Silicon into Optical Communications The Key to Large Scale Integration" http://www.kotura.com/SOEIC Technology.pdf, February 2004.

[42] M. Turner, "Moving backwards in the OSP: Improving the FTTH distribution segment helps advanced services move forward," OutsidePlant Magazine, Article EVO 634, January 2006.

[43] D. Meis, "Get big savings in time and money," Broadband Properties Magazine, p. 20, August 2005.

[44] V. O'Byrne, D. Kokkinos, D. Meis et al., "UPC vs APC Connector Performance in Passive Optical Networks," NFOEC'05, Paper NTuF3, Anaheim, March 6 11, 2005.

[45] A. Woodfin, "Access makes the Parts Grow Stronger," FTTH Council Conference, Las Vegas, October 3 6, 2005.

[46] K. Himeno, S. Matsuo, N. Guan, and A. Wada, "Low Bending Loss Single Mode Fibers for Fiber to the Home," *JLT*, 23(11), November 3494 3499, 2005.

[47] G.S. Glaesemann, M.J. Winningham, and S.R. Bickham, "Single Mode Fiber for High Power Applications with Small Bend Radii," in Proc. *SPIE Photonics Europe*, paper 6193 23, Strasbourg, April 3 7, 2006.

[48] A. Woodfin, A. B. Ruffin, and J. Painter, "Advances in optical fiber technology for analog transport: technical advantages and recent deployment experience," National Cable and Telecommunications Association, NCTA Technical Papers, 44th Edition, pp. 93 100, Chicago, June 8 11, 2003.

[49] A. Woodfin, J. Painter, and A. Boh Ruffin, "Stimulated Brillouin Scattering Suppression with Alternate Fiber Types Analysis and Deployment Experience," NFOEC'03, *Technical Digest*, 4, (1265), Orlando, September 7 11, 2003.

[50] A. B. Ruffin, F. Annunziata, S. Bickham et al., "Passive Stimulated Brillouin Scattering Suppression for Broadband Passive Optical Networks," *Technical Digest LEOS'04*, Paper ThE2, Puerto Rico, November 7 11, 2004.

[51] A. Kobyakov, S. Kumar, D. Q. Chowdhury et al., "Design concept for optical fibers with enhanced SBS threshold," *Opt. Express*, 13, 5338 5346, July 2005.

[52] M. J. Li, X. Chen, J. Wang et al., "Fiber Designs for Reducing Stimulated Brillouin Scattering," *OFC 2006 Technical Digest*, Paper OTuA4, Anaheim, March 5 10, 2006.

[53] A. B. Ruffin, Ming Jun Li, Xin Chen et al., "Brillouin gain analysis for fibers with different refractive indices," *Opt. Lett.*, 30(23), 3123 3125, December 1, 2005.

[54] M. D. Vaughn, A. B. Ruffin, A. Kobyakov et al., "Techno economic study of the value of high stimulated Brillouin scattering threshold single mode fiber utilization in fiber to the home access networks," *JON*, 5(1), January 4, 2006.

[55] J. Lepley, M. Thakur, I. Tsalamanis et al., "VDSL transmission over a fiber extended access network," *J. Opt. Netw.*, 4, 517 523, 2005.
[56] R. Hunt, "Reforming Telecom Policy for the Big Broadband Era," New America Foundation article, http://www.newamerica.net/index.cfm?pg publications&SecID 30&Al lOf 2003, December 19, 2003.
[57] IEEE USA Committee on Communications and Information Policy, "FTTH Policy: The Case for Ubiquitous Gigabit Open Access Nets," *Broadband Properties Magazine*, p. 12, August 2005.
[58] R. Heron, "FTTx Architecture Transition Strategies," *NFOEC'2007*, Paper NThF, Anaheim, March 25 29, 2007.

11

Global landscape in broadband: Politics, economics, and applications

Richard Mack

KMI Research, CRU Group, Mount Pleasant, London, UK

11.1 INTRODUCTION: USE OF FIBER IN ACCESS NETWORKS—DRIVEN BY BROADBAND SERVICES

The first installations of fiber-optic systems for commercial communications occurred in the late 1970s. "Commercial" means that the network operator was selling communication services and carrying traffic for residential, government, or business customers. In the 30 years since then, the public network operators or "carriers" have installed more than 600 million km of cabled fiber in telecom networks throughout the world.

The average number of fibers per cable has been increasing since the early years, but in most carrier networks it falls between 30 and 50. Thus, the installed base of optical fiber is arrayed over 15 20 million km of network cable routes. About a million of these route-km use submarine cable for tying together continents, islands, and coastal cities.[1] The vast majority of routes, however, use terrestrial cable for linking cities, central offices (COs), feeder locations, businesses, and recently, some homes.

Altogether, the world's telecom networks provide service to 1.25 billion telecom customers, of which 75% are residences.[2] Barely 1% of these customers have an "all-fiber" connection to the carrier network. Specifically, there are about 10 million fiber-to-the-premises (FTTP) customers worldwide.[3] There is another slightly larger group of residential and business customers that have fiber to the apartment building, the office building, or the office park. The number or

Optical Fiber Telecommunications V B: Systems and Networks

ISBN: 978 0 12 374172 1

customers served by FTTP or fiber-to-the-building (FTTB) is about 30 million, or about 2.5% of the world's wireline customers.

The low penetration of fiber-optic customer connections into all wireline connections reflects the comparatively recent status of this network application. Until about 2000, there were few cases in which the telecom network operators could justify the cost of installing and equipping fiber for access network applications. This is changing rapidly. Of the 10 million FTTP lines now in service, 7 million were turned up in 2005 and 2006.

Another indication that this is a new phenomenon: the number of customers passed by fiber in the access network is two to three times higher than the number subscribing fewer than 30% of the households that could be equipped with FTTP have signed up. For one reason, some have been passed so recently that the operator has not had a chance to sell them the service. Another reason is that they already have broadband service, such as digital subscriber line (DSL) service or cable-modem service, from another service provider and need to be "marketed" to switch.

As of year-end 2006, only two carriers had more than a million FTTP customers: NTT East and NTT West. This will change in early 2007, as Verizon continues marketing and signing up customers. Much of the early FTTP activity was with small "pioneering" network operators. Only a handful of the world's large incumbent telecom operators have made significant investments in FTTP. Altogether, these factors emphasize that 2007 is an early year for FTTP or access network applications. Table 11.1 shows some demographic and telecom indicators to highlight the early status of FTTP.

Even though FTTP systems currently serve only 1% of wireline access subscribers, they represent 9% of the fiber installed in telecom networks worldwide. Similarly, FTTP systems represent 11% of all transceivers shipped to date. The potential for more widespread FTTP deployment therefore offers high-unit-quantity market potential to companies manufacturing fiber, cable, transmission systems, and related products.

The table also shows data on other fiber-based broadband access network architectures FTTB, FTTC, and FTTN. These architectures extend fiber from the CO to a point closer to the customer's premises, but use copper cable for the actual drop. This approach provides greater bandwidth than an all-copper access network but shares the optical cable, transmission, and installation costs among multiple customers. The table shows that FTTB, FTTC, and FTTN are a smaller percentage of the world's fiber plant but a higher percentage of its broadband subscribers.

The experience in early 2007 shows a continuation of the recent growth in FTTH network construction and new subscriptions. Verizon in the United States, for example, is passing three million homes per year with its FTTP construction and reporting that subscription rates are accelerating. Other operators in such markets as the United States, China, France, Korea, the Netherlands, Singapore, and Taiwan have announced large FTTx projects during the first half of 2007.[4] As these new projects get underway, the number of homes passed by FTTx systems worldwide will increase by several million per year in 2008 and 2009.

Table 11.1

Demographic, telecom, broadband, and fiber-optic indicators worldwide totals as of year-end 2006[5,6,7] (all data in millions, except percentages).

Population	6589
Households	2196
Households with Internet	512
Wireline access lines	1295
Residential wireline access lines	950
Broadband access lines	292
FTTP subscribers	10
FTTP subscribers/total access lines	**0.8%**
FTTP subscribers/broadband access lines	**3.4%**
FTTB, C, N subscribers	64
FTTx subscribers	74
FTTx subscribers/wireline access lines	**5.7%**
FTTx subscribers/broadband access lines	**25.3%**
Installed base F km, all applications	790
Installed base F km, telecom only	620
F km in FTTP, cumulative	56
FTTP F km/WW telecom installed base	**9.0%**
F km in FTTB,C,N, cumulative	39
FTTB,C,N/WW telecom installed base	**4.9%**
FTTx F km/WW Inst. base.	15.3%
TRX shipped, all applications, cumulative	133
TRX shipped, FTTH (fiber to the home), cumulative	14
TRX in FTTx/Total TRX shipped	**10.5%**

Sources:

1. Telecom and broadband data: ITU, Internet World Stats, Neilsen/Net Ratings, DSL Forum, Company Reports.
2. Fiber optic data: KMI Reseach, CRU Group, and LightCounting (transceiver data).

There is no question that the fiber optics industry has entered a major new phase characterized by high-quantity FTTP deployment. The questions discussed in this chapter include:

(1) Why is this deployment happening now (or why did it not happen sooner)?
(2) Could this FTTP-deployment phase extend to all telecom networks, all operators, all customer premises?
(3) How long could it take to deploy FTTP in all markets, or to upgrade all telecom networks, and what technologies will be used?

For the first question, the discussion will show that FTTP technology was too costly to deploy relative to revenues from the services that could be carried in the 1980s and 1990s. Now, costs have dropped, but the main development is that new

revenue-generating services, such as high-speed Internet and digital television, have improved the business case for FTTP.

The next questions, however, are more complex. To put it simply, the business case for FTTP has not improved so that it is uniformly attractive for every operator in every market. Factors such as regulatory policies, competitor's capabilities, and the services offered vary significantly among countries, and in many cases among the states, regions, or cities within a country. Further, the regulatory, competitive, and service-related factors are changing and may remain in a state of flux for years in some markets. As a result, the next few years will continue to have operators in different markets arriving at different conclusions about FTTP's attractiveness.

In several respects, the fiber optics technology is *not* the problem. FTTH systems use well-established technologies. Some, such as 1310-nm Fabry Perot diode lasers, standard single-mode (ITU G.652) fiber, 2.5-mm ferrule connectors, have decades of manufacturing experience. Carriers can design FTTH systems with products having the following key characteristics:

(1) compliance with strong international standards (IEEE or ITU);[8]
(2) compatibility with standards-based network management and operations systems;
(3) robust features for outside-plant engineering;
(4) demonstrated reliability based on field experience in Japan, United States, and other early FTTH markets.

In addition, the equipment suppliers have addressed earlier problems and continue to develop improvements in such areas as powering or battery backup, installation costs, equipment size or "real-estate" requirements, in-home network interfaces, and other parts of the entire system.

The costs associated with FTTP deployments will continue decreasing due to higher production volumes, increased integration in electronics and optoelectronics, improved manufacturing processes, and new technologies for construction, testing, and operational functions. So the uncertainties about future FTTP deployments are mainly due to the regulatory policies, competition for customers, and service revenues.

The menu of services offered has been a huge factor. In the 1990s, FTTP did not prove-in for business cases based only on voice or other narrowband services such as dial-up modem or FAX. Since then, the advent of new web services and the associated requirement for faster Internet access has given service providers an entirely new revenue opportunity.

For example, the number of US households with DSL or cable-modem service increased from zero to about 50 million in 10 years. Depending on bit rate and competition, the monthly fees range from less than $20 to more than $40 per household. The result is a residential broadband Internet market worth tens of billions of dollars per year to community antenna television (CATV) and telecom operators a market that did not exist 10 years ago.

In the next few years, Internet-speed requirements will continue to scale up, plus there will be new revenue opportunities associated with IPTV and other new entertainment services. The potential to attract customers by offering a "triple-play" package combining voice telephony, high-speed Internet, and video entertainment into one monthly bill will be a major factor in FTTP system revenue calculations.

With the apparent trends in bandwidth requirements and new video services, it is likely that most of the world's telecom networks *someday* will use fiber to link every household, business, or fixed-site end-user facility. It is not unusual to hear technology pundits and telecom analysts describe fiber-to-the-home (or premises) as the "end-game" in access networks.[9] In analyzing when this end-game might materialize, it is useful to think of FTTP in terms of different deployment scenarios, each with its own set of business-case factors, as shown in Table 11.2.

The greenfield scenario is usually in developments or new communities above a specific size, typically hundreds or thousands of homes, such that all new infrastructure is being built new roads, water and sewer pipes, and utility systems. Fiber-optic cable can be installed with other utilities, before the streets are paved, so there is no additional construction cost to pay back.

Many developers and telecom operators have concluded that fiber is preferred over copper in this environment. Zoomy Communications, which builds and operates FTTH networks for real-estate development projects, projected that the United States would have 1.6 2.0 million new homes built in 2006, that 50% of those would be in "master-planned communities;" and that at least 45% of those were considering FTTH.[10] The expression "master-planned communities" usually refers to lower-density, suburban or exurban housing, often for high-income households. FTTH has been used in these communities for several years.

Table 11.2

Business case scenarios for FTTP deployment.

Scenario	Operator	Key factor/characteristic	Number of lines
Greenfield	Incumbent, developer, other	New community or housing development	<2% of total homes, usually in developed economies
"Re hab"	Incumbent	Replace old network or one with many failures/ trouble tickets	<2 or 3% of existing lines/yr
Upgrade	Incumbent	Increase capacity, add services, may include re hab in large areas	Could be large area, entire region, or country
Overlay	Not the incumbent; e.g., CLEC, utility, municipality, other	Often in single communities; Sometimes "open access" network with multiple service providers	Select communities, or regions, usually where incumbent has not upgraded

Since 2005 there also have been increasing reports of FTTP or FTTB for new housing in higher-density communities, often serving lower incomes. For example, Tierra Urbana, a developer in Mexico, has begun working with a CATV operator called Interfibra to install FTTC and FTTP for up to 4000 new working-class homes in Monterrey.[11]

Examples of re-hab, in which FTTH systems are installed specifically to rebuild older copper networks, are infrequent but have been reported. By 2006 such installations were largely indistinguishable from broader upgrade applications, in which the operator wants to increase capacity and support new higher-bandwidth services. In fact, more then 95% of all FTTP deployments are either upgrade or overlay projects: "upgrade" if it is a telecom operator already serving the area, such as the incumbent local exchange carrier, or "overlay" if it is a new operator building a network that will compete with the incumbent.

With NTT East, NTT West, and Verizon passing and serving millions of homes, there are more subscribers in the "upgrade" segment, but there are more projects in the "overlay" segment, typically serving a smaller number of homes per project.

The United States, for example, had about 1.3 million FTTP subscribers in March, 2007, but 0.9 million were Verizon households.[12] The remainder are attributed to about 350 operators, including independent (non-Bell) telephone companies, municipalities, utilities, and other operators.[13] The average number of subscribers for the non-Bell systems was between 1000 and 2000.

In Austria, Denmark, the Netherlands, Norway, and Sweden, there are dozens of community-based FTTH projects, operated by municipalities, utilities, housing corporations, or innovative partnerships and consortia that may include various local governments, utilities, corporations, and other investors. With the exception of larger municipal systems in Amsterdam and Austria, most of these community projects have 2000 to 20,000 subscribers.

Considering the costs and revenue opportunities, it is unlikely that more than one operator will build FTTP systems to serve the same community. This is one reason FTTP is sometimes called the "end-game," or why FTTP operators are said to have "first-mover advantage." Most communities probably will be served by either an incumbent (upgrade) or a competitor (overlay) but not both. The competitive situation is therefore a critical factor in the FTTP business-case analysis.

11.2 CURRENT STATUS OF FIBER OPTICS IN TELECOM AND ACCESS NETWORKS

As noted in Table 11.1, the amount of cabled fiber installed in FTTx systems is 15% of all fiber installed to date in telecom networks. It is 12% of all fiber installed for all applications. But these percentages are changing as FTTx installations progress at faster rates than other applications.

In the United States, for example, more than 50% of the fiber installed in 2006 was in FTTx applications. This high percentage reflects the large-scale projects underway at Verizon, which has ramped up its FiOS initiative to a level where it is passing three million homes per year with FTTP technology, and AT&T's Project Lightspeed, which is using FTTN plus very high-bit-rate digital subscriber line (VDSL2) to pass more than three million homes per year. The US FTTx deployments also include hundreds of smaller projects being implemented by municipalities, utilities, and real-estate developers.

In Europe, Asia, and other regions, the amount of fiber in FTTx systems ranged from 1% to 21% of the total fiber kilometers installed in all applications during 2006. These lower percentages, when combined with the 54% for North America, resulted in a weighted average of 28% for the amount fiber installed in FTTx systems relative to the amount in all applications for the entire world in 2006. As FTTx becomes more widespread in Europe, Asia, and other markets, the percentage of annual fiber demand in FTTx installations will increase so that the worldwide percentage will average more than 40% by 2010.

Figure 11.1 shows the amount of fiber installed each year in major applications, including FTTP and other FTTx (FTTB, FTTC, FTTN). Figure 11.2 shows the cumulative amount of fiber installed, or the "installed base" in the same application segments. The "Other S-M" segment includes single-mode fiber installed for utility, railway, highway, campus, and other private networks. The "Other Local Tel." segment includes fiber installed in metropolitan rings, central-office trunks, and feeder systems fiber that has not been installed specifically as part of FTTx systems. Applications might include large-business customer connections or other local telecom links.

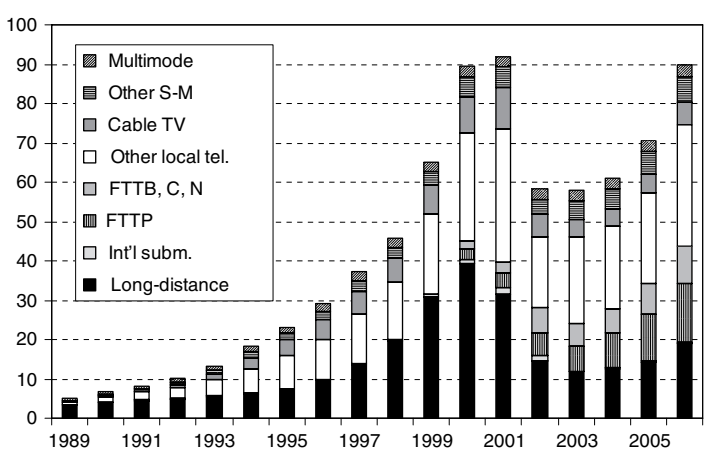

Figure 11.1 Annual fiber installations by application segment, 1989 2006 (this figure may be seen in color on the included CD ROM).

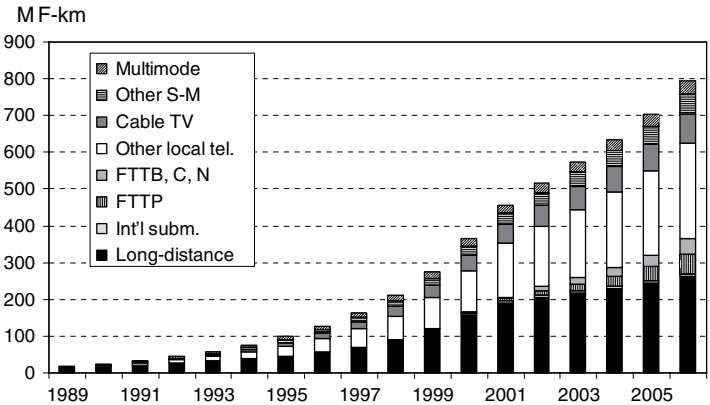

Figure 11.2 Cumulative fiber installations by application segment, 1989 2006 (this figure may be seen in color on the included CD ROM).

The dotted FTTP segment and the stripped "FTTB,C,N" together make up the FTTx fiber quantities. In Figure 11.1, FTTx amounts to 28% of 2006 annual installations, and in Figure 11.2, it is 12% of all fiber installed as of year-end 2006.[14]

Fiber-km is a convenient measure of optical network construction trends, and it can be useful for comparing markets, regions, carriers, or groups of countries, such as developed vs developing economies. But it is *not* a useful measure of network capacity or network utilization. One big reason is that most fiber is installed with the intention of sitting unused initially and possibly for years.

This intention refers to the practice of specifying cables with higher fiber counts than needed initially. Many telecom cables therefore contain a combination of "lit" and "dark" fibers, a distinction which refers to whether the fiber is connected to transmission equipment or sitting unequipped for future use.

Telecom network operators are well aware that the labor and construction costs are almost always much higher than the cost of the cable itself when building "outside-plant" cable routes. The cabled fiber has typical lifetime specifications of 30 years. These two factors have led telecom engineers to specify cables with many times the fiber needed so as to avoid future construction. The additional fiber is often "incremental" to the construction as low as a few percentage points of the route-construction costs.[15]

The other main reason why fiber-km is not an indicator of network capacity is the vast range of transmission products that can be used to "light up" a fiber pair. A single pair (used for transmission in both directions) can be connected to lower-speed single-wavelength-channel equipment so that it is carrying megabits per second of capacity, or it can be connected to wavelength-division-multiplexing systems capable of dozens of channels, each at 10 Gbps, resulting in aggregated capacity levels such as 640 Gbps per fiber pair.

This means that data comparing fiber-km in long-distance, FTTP, and other applications do not indicate any specific trends in overall network capacity or

investment. The main conclusion is that FTTx is becoming an increasingly important part of the entire fiber optics market, and that telecom operators as a group are shifting a greater percentage of their network investments into the access network.

The equipment for lighting up fiber not only has a wide range of bandwidth capabilities, but there also are diverse approaches to achieving fault tolerance, route redundancy, network management, and other operational features. As a result, there is no readily tabulated product to serve as a unit for measuring and comparing equipment markets. In theory, a figure-of-merit for analyzing equipment markets might be expressed in some bandwidth-times-distance units (e.g., Mbps-kilometers), but there is no convenient way to collect or analyze such data on the installed base or current purchases.

In general, the cable market, as can be measured in fiber-km, is a good indicator of network construction. The equipment market, if there were a convenient unit of measure, would be an indicator of network capacity requirements sent over fiber. With this understanding, one broad conclusion from Figures 11.1 and 11.2 is that single-mode fiber-optic technology generally started out in long-distance applications and has been progressing into shorter-distance applications over the past 20 years.

This history of fiber optics applications where, when, what applications has been heavily influenced by two main factors. One is the bandwidth-times-distance figure of merit noted above, and the second is cost. There are many elements in a system's cost, some of which are summarized in Table 11.3.

Material and construction costs will be part of every system. Costs associated with legal work, permitting, rights-of-way, government fees, and financing may be present with some projects and not others. For most telecom applications, materials are typically about half of total costs. In FTTx applications, construction can be the largest single-cost element, and in some cases can be more than half of total system costs.

The table shows only the costs associated with building the system, sometimes known as installed first costs. These costs typically appear in financial statements as capital expenditures or additions to plant, property, and equipment. Labor associated with network construction is considered a capital cost.

In addition to these costs, there are lifetime costs or operational costs, which are reported under operating expenses in financial statements. For a fiber-optic network, these costs can include monitoring and maintenance, database management, software upgrades, provisioning expenses, and other operational functions. The distinction between system costs and operating costs can be important in the business case

Table 11.3

Summary of fiber-optic system costs.

Materials	Cable, transmission equipment, Interconnect and Splice hardware, support hardware
Labor/services	Planning, permitting and other legal, engineering, construction, testing and certification
Other	Rights of ways, work permits, government fees, finance costs

for FTTx construction. A fiber-based access system may have higher construction and material costs than some competing technologies, but it may offer advantages in operating expenses, due to reliability, density, size, power, and other characteristics.

The bandwidth-times-distance performance and the cost factors together represent one side of the business-case equation, with the other side represented by revenues from network services or other financial benefits. Experience shows that fiber-optic systems were first used for long-distance applications and over the three decades of commercial deployments have been penetrating shorter-distance applications.

This has resulted from two phenomena. First, fiber-optic system costs have been decreasing with quantity, design and process improvements, manufacturing experience, and competition among vendors. At the same time, system bit rates have scaled up, so that the costs per bit transmitted have decreased substantially. Table 11.4 shows the progress in transmission capacity with separate columns for single-channel bit rates and number of wavelength channels, based on the year that commercial systems were introduced.

The second phenomenon in the feasibility of shorter-distance fiber systems has been the increase in revenues for local communications. This has been due mainly to the shift from voice to data services. To explain more fully, the costs for long-distance applications are offset by revenues from a larger number of customers, whose traffic is multiplexed together to share a long-distance communications "pipe." As network applications get shorter, or closer to the individual customer, there will be fewer customers sharing a pipe. An FTTH or FTTP system, for example, has no sharing and therefore must be supported by revenues from only that home or premises. With revenues based mainly on voice telephone, fiber systems would not prove in, but with revenues based on voice, data, and video, or some combination of services, fiber can be more readily justified.

Table 11.4

Advances in TDM rates and WDM channel counts by year.

	TDM rate[16]	No. wavelengths
1980	45 Mbps	
1983	90 Mbps	
1984	140 Mbps	
1985	560 Mbps	
1986	810 Mbps	
1987	1.7 Gbps	
1990	2.5 Gbps	
1995		4
1996	10 Gbps	8
1997		16
1998		32
1999		80
2000		160
2004[17]	40 Gbps	

The business cases for fiber-optic systems have many complexities associated with various trade-offs between performance and cost factors and also against the revenue opportunities. In a simple example, large-core multimode fiber costs more than single-mode fiber but it allows use of lower-cost sources, detectors, and connectors. The large-core, lower-cost interfaces allow multimode fiber to be competitive with copper for distances in campus or building networks. In another example, higher-cost NZDS fiber can be justified in long-distance DWDM systems because the high aggregate bandwidth can support a huge number of revenue-generating circuits as well as efficient and cost-effective wavelength routing or switching technologies.

The result of these cost, performance, and revenue factors has been a 30-year history with fiber-optic systems progressing from long-distance to loop applications as shown in Table 11.5. What's not shown in the table is the parallel development of Internet technology and a new realm of telecommunication-network applications carrying data for PC users.[18]

Also not shown in the table are other major technologies that have evolved or phased into telecom networks. One example is the "digitization" of switching, which began in the mid-1970s and was a major initiative for telecom companies through the 1980s and into the 1990s when digitization was nearly complete. In addition to such technological evolution, there have been on-going changes in the regulatory and competitive factors affecting telecom operators, as well as the services offered.

These parallel phenomena in some cases contributed to the demand for fiber-optic technology, and in other cases fiber optics enabled or contributed to the evolution of

Table 11.5

History of fiber-optic systems in commercial telecom network applications.

1978	Early trunk and niche applications, limited by LED source and MM fiber performance
1981	Long distance installations begin on AT&T's Northeast Corridor
Early 1980s	First undersea cables installed (Denmark and other islands)
1983	Central office trunk and long distance applications are underway in United States, Europe, and Japan
1984	US has multiple competitors installing long distance fiber, S M technology phased in
1986	CO trunks being configured in metropolitan rings, SONET/STM systems available
Mid 1980s	Fiber versions of SLC 96 feeder system available, limited early acceptance
1988	First transoceanic undersea cable (TAT 8) in Atlantic
Late 1980s	Fiber optic feeder systems becoming more widespread
Late 1980s	FTTH and FTTC trials getting underway
Early 1990s	Fiber used routinely for telecom long distance, CO trunk, and some feeder applications
1992	AM DFB lasers meet criteria for CATV distribution, HFC deployments begin
Mid 1990s	Long distance, metro rings, CO trunks, and feeder installations increase in volume
2000	FTTH deployment is underway in Japan, FTTC in the United States
2002	Community based FTTH underway in US and Europe
2003	Verizon, BellSouth, and SBC issue joint RFP for high quantity FTTP equipment

new markets and carrier businesses. This mix of technology "push" and "pull" currently is evident in the early phases of FTTx deployments. Many operators are designing access networks with more fiber to meet customer requests for higher-bandwidth service. At the same time, some operators that already have begun installing fiber in access applications are taking advantage of the higher capacity to introduce new services or new "features" for their subscribers.

NTT East and West, for example, have been offering voice and data services as part of their "B-FLETS" FTTH services for several years but in early 2007 have announced plans to add Internet Protocol television (IPTV) to the service menu beginning in 2008.[19] Verizon has used its FTTP technology to introduce new services and features such as Internet data showing weather and traffic in part of a home's TV screen, ways to "play" Internet-based photographs and music on the TV, and new features for game players.

In early 2007, it is clear that services are evolving at the same time that other business case factors are changing. Although this represents uncertainty for carriers or network operators, the evolution of technology and other factors will drive more FTTP deployments, not fewer, because the demand-side requirement is for more bandwidth, and the supply-side improvements are lowering the installation and operational cost of fiber-optic systems, in terms of per-home cost and even more so in terms of cost-per-bit-transmitted.

This "upside" potential for near-term growth in FTTP deployments was noted earlier in terms of the small percentage of homes already served or passed. Also noted was the number of operators with FTTP systems approximately 500, including incumbent local exchange carries (ILECs), competitive local exchange carriers (CLECs), municipalities, utility companies, real-estate corporations, and various consortia of local community and telecom groups. Most of these operators are providing smaller regional or community-based systems. Large nationwide ILECs have delayed committing to FTTP, for various reasons including financial and regulatory obligations, but this is likely to change in the next 5 years.

Another way to emphasize the "upside" potential for fiber-optic system suppliers is to note that four operators, Verizon, AT&T, NTT East, and NTT West, represented 18% of the cabled fiber installed worldwide in 2006, and that these four represented 70% of the fiber installed for FTTx. As other large incumbents begin large-scale FTTx projects, the demand for cable and other fiber-optic products will have strong growth over many years.

11.3 TELECOM INDUSTRY HISTORY, STRUCTURE, AND BUSINESS CASE-FACTORS

The first telephones were operating in the late 1870s, which means that telecom networks have been evolving for about 125 years, longer if telegraphy is included. This history is rich with important, even stunning, technological and market

developments. Three *major* disruptions have occurred worldwide in the last 20 30 years during the period when fiber-optics technology has moved into widespread deployment:

(1) "Re-regulation" or "liberalization" in which major telecom markets shift from monopoly to at least partial competition, and many markets shift from government-owned to "for-profit" telecom operators.
(2) Evolution of data traffic, especially Internet data, as a critical application of telecom networks.
(3) Development of cellular-mobile telephone technology and rapid business and consumer market acceptance of "cell phones."

A very recent development in telecom markets is emerging as likely to be a fourth major disruption in the fiber-optics era: evolution of digital TV or video technology, especially "IPTV," and use of telecom networks for such video distribution.

The causes and effects of these four disruptions are complex and will be summarized here only to emphasize their role in fiber optics applications and their contribution to the growing need for fiber's bandwidth. Part of this complexity results from a world telecom market that is actually the sum of about 200 distinct markets (countries) each with its own rules, operators, and economic situation.

The world's telecom markets can be grouped into levels of development that track with the countries' economic health. Various telecom indicators, such as telephone-line penetration, telephone usage, and telecom capital expenditures are consistent with a country's GDP per capita, total infrastructure spending, and other economic indicators.

The most advanced telecom markets include United States, Canada, most of Western Europe, Japan, Korea, Taiwan, Singapore, Australia, New Zealand, and several other countries. The developing telecom markets include countries in Africa, Latin America, much of the Asia Pacific region, and most of Eastern Europe/Central Asia.[20] Table 11.6 shows the differences in select telecom indicators among regions.

The table indicates the range of telecom usage in different regions. Some markets of Western Europe, for example, have more than 100 cellular subscribers per 100 population, meaning that most of the population has a cell phone and many individuals have two one for business and one for personal use. On the other hand, there are tens of thousands of villages in China, Indonesia, India, and other developing markets that have no phone service whatsoever. In fact, large diverse markets such as China and India might be viewed as having both advanced and developing markets within the country. That is, they have very sparsely populated regions with low telecom density as well as major metropolitan and business centers with highly developed telecom networks.

Table 11.6

Sample Telecom indicators by region, as of year-end 2005.

Year end 2005 data in millions or number per 100 population	Western Europe	Eastern Europe	Asia Pacific	North America	Latin America, Africa	World total
Population (M)	513	402	3643	435	1525	6518
Households (M)	223	136	1316	145	324	2143
Wireline main lines in use (M)	211	101	571	197	140	1219
Main lines per 100 population	41	25	16	45	9	19
Mobile subscribers (M)	371	249	837	270	402	2129
Mobile subs. per 100 population	72	62	23	62	26	33
Internet users (M)	286	68	329	245	100	1028
Internet users per 100 population	56	17	9	56	7	16
Cable TV basic subscribers (M)	87	25	210	79	19	420
Broadband subscribers (M)	58	5	94	55	8	219
2005 Percent of world total in each region						
Population	8	6	56	7	23	100
Households	10	6	61	7	15	100
Wireline main lines in use	17	8	47	16	11	100
Mobile subscribers	17	12	39	13	19	100
Internet users	28	7	32	24	10	100
Cable TV basic subscribers	21	6	50	19	5	100
Broadband subscribers	26	2	43	25	4	100

Sources: ITU, CIA Factbook, KMI Research.

The advanced telecom markets were the first to shift away from monopoly status and presently have the most competitors. Developing telecom markets generally have lower revenues per subscriber, fewer subscribers per population, and often fewer subscribers per square kilometer. As a result, the developing markets attract less telecom investment and have fewer competing carriers.

Why do markets have competing carriers at all? Why was there a shift away from monopoly telecom operations? For most of the telephone industry's history, the operators enjoyed monopoly status. In the United States for example, there have been thousands of phone companies, but with rare exception these phone companies have served distinct communities or geographic market areas as monopoly operators.[21]

The pressure to introduce competition has come from several sources:

- companies pursuing opportunities to sell services in competition with the "incumbent" or former monopoly operators;
- consumer groups and business customers seeking other choices;
- regulatory authority and government agencies that believe competition between operators will result in better service, lower prices, and overall performance improvements.

These pressures have resulted in new legislation or policies to establish competition in telecom markets throughout the world. The effect is a change in regulations, a process commonly referred to as "de-regulation," even though "re-regulation" may be a better term. With the United States being a notable exception, the telecom network in most countries was formerly owned or operated by the national government, often under an entity known as a Post, Telegraph, and Telephone (PTT) authority.

The regulatory changes therefore have included policies to "privatize" the PTT, or to transfer telecom operations from the government to nongovernment owners and investors, as well as policies to license and oversee new competitors in telecom markets. These processes were underway during the 1980s in some advanced telecom markets such the United States, United Kingdom, and Japan and had gotten underway in most parts of the world during the 1990s.

In the United States, a major milestone was the break-up of AT&T on January 1, 1984, when 22 Bell operating companies were spun out and re-organized under seven regional holding companies. This development can be seen as the culmination of several suits initiated by various competitors and the Department of Justice dating back to the 1940s.[22] During these years, there were four main activities under the AT&T corporate umbrella: (1) long-distance telecom; (2) local exchange carrier operations; (3) manufacturing (Western Electric); (4) R&D (Bell Laboratories). The 1984 break-up was effected to end law suits brought by other manufacturers seeking opportunities for their equipment in Bell company networks and by other long-distance providers seeking access to customers on the Bell local networks.

The agreement specifying the 1984 breakup had terms defining what services the new long-distance and local telecom entities could provide. Other local telecom competitors, however, sought interconnection with local Bell customers, and the local Bells themselves sought to enter other markets, such as video and long-distance. These pressures were addressed by the US Congress in the 1996 Telecommunications Act.

While these changes were happening in the US, government authorities elsewhere also found themselves having to design carefully balanced policies that gave new competitors a fair chance without unduly restricting the former monopoly or incumbent operators. Such policy-making efforts have had to address complex problems of how many and what entities to license, whether foreign ownership is permitted, what are fair interconnection fees and wholesale circuit prices, who pays for maintenance of access locations, etc.

The upshot of this re-regulation is that the world's telecom markets shifted from monopoly to competitive status during the period from 1984 to 2006, approximately the same period when fiber-optic technology was "proving in" for long-distance and local telecom. Table 11.7 shows data from the International Telecommunications Union (ITU) on the status of competition in 190 member countries as of 2004.[23]

The table shows that most markets have full or partial competition in local telecom and domestic long-distance services. Data and mobile markets appear more competitive, partially because these are newer markets, having emerged during the years of pro-competitive re-regulation. Policies to manage competition

Table 11.7

Status of competition in worldwide telecom markets.

	Local service	Domestic L D	Data	DSL	Mobile	Internet service
Full competition	77	73	114	82	86	120
Partial competition	34	31	21	17	56	21
Monopoly	66	63	27	20	20	7
Duopoly	2	1	2	0	1	0
Not available/not reported	11	22	26	71	27	42
Total	190	190	190	190	190	190

Source: ITU Information and Communications Technology database.

in these new industries have been implemented more efficiently without needing negotiations or rule-making procedures to address problems associated with the incumbents and legacy networks.

The 66 or 63 markets listed as having local or long-distance monopolies are mainly in developing telecom markets of Africa and parts of Asia. Some of these markets have been introducing measures to "privatize" government-run telecom and to "liberalize" telecom policies in the early years of the twenty-first century. But progress with telecom reform in these markets sometimes moves more slowly than in other regions because the operating costs and revenues are less attractive to investors.[24]

In Western Europe, a region with unusually high teledensity, network investment, and usage factors, the pro-competitive telecom-market policies have come from both domestic governments and the European Commission (EC). The EC has written policies to promote the advance of information and communications technology for the European Union (EU) member countries as well as to promote the concept of a regional (EU) telecom market rather than a collection of domestic telecom markets.

What has the world's transition to competitive markets meant for fiber optics and for fiber in broadband applications? There are three main effects:

(1) There are more carriers building networks, so more fiber and equipment is purchased and installed. Of course, there are limits to how many carriers can build networks to serve the same market a lesson learned (in some cases quite painfully) after a period of over-investment in the late 1990s and the subsequent collapse of fiber optics and telecom markets in 2001. Such limits are critical in broadband access networks, where the cost of fiber-based equipment is shared by fewer potential customers, or just one subscriber in the case of FTTP.
(2) The carriers are competing to win customers on the basis of reliability, service quality, network flexibility, and price either the price of a bundle of services or the price of individual services on a "menu" of services.

(3) The nongovernmental or for-profit status and the competitive situation mean that carriers must minimize costs as well as maximize revenues. Fixed and variable cost factors installed first costs and operating costs are critical, and telecom operators are pursuing new cost-cutting technologies aggressively.

The increased sensitivity to capital and operating costs is driving product and process innovation, such as increasing levels of microelectronic and optoelectronic integration, plus improvements in test, cable, splice, and interconnect hardware that reduce construction time and costs.

One important concept in telecom policy reform that has affected the use of fiber optics is "local loop unbundling." This refers to a mechanism for letting competitors use parts of the incumbents' local access networks. The requirement involves not only guidelines for physical interconnection or co-location, but also ways to break out various cost elements previously bundled into a single local-service charge. This means the regulators and carriers must agree on fees for switching, CO connections, local-loop outside plant "pairs," or partial use of the network and cable plant. When implemented, unbundling means that a competitor can obtain loops or circuits on a wholesale basis and re-sell them, along with its own "branded" services.

The EC's policies, for example, cover several types of unbundling full unbundling, shared unbundling, and "bitstream" service. The EC also requires that the incumbent not only furnish its loop facilities, but that it provide competitors with published pricing, suitable justification of the prices, spaces for interconnection, and suitable notification and information about its services and facilities.[25]

Some prominent incumbents have seen the EC's unbundling policies as a disincentive to investment in FTTP networks. The issue is whether the incumbent will achieve suitable payback on its investment if it must share the network and potentially dilute its own revenue stream.

In the United States, a key decision by the FCC in 2003 was seen as favorable to incumbents, especially the local Bell companies, because it exempted them from the requirement to unbundle and share fiber-based broadband access facilities.[26] The FCC's decision was intended to stimulate investment in broadband access networks by interpreting unbundling requirements as applicable only to narrowband or voice facilities.

In addition to unbundling, new regulatory policies must address other factors that can affect FTTP deployment. Examples include rules for sharing or leasing rights-of-way and the fees for such sharing; concepts of network ownership and service provision that may separate the transport and content businesses; contributions to universal service funds, number portability, level-of-service guarantees, and many other issues.

Much of the world's pro-competitive regulatory change was occurring at the same time as the Internet revolution the transition of the Internet from initially a

US defense network, to a worldwide science and education network, to a widely used commercial and consumer communications tool, to a ubiquitous "cloud" for delivering a rapidly changing array of information, entertainment, household, business, and personal services.

It is impossible to overstate the implications of Internet applications and Internet traffic on telecom networks. In the past 10 20 years, network operators have invested heavily to replace, upgrade, or overlay switching, backbone (inter-switch), and access (switch-to-customer) facilities to support their customers' Internet usage. The quantity of connections, the bandwidth required per connection, and the bandwidth required of different network segments have been increasing with double-digit growth rates (or faster) for the years between 1994 and 2007, compared with growth rates of 4 8% for voice-telephony connections.

Bandwidth requirements will be discussed in a subsequent section of this chapter. For the purposes of this section on the telecom industry's history, the objective is to stress that broadband access and Internet services have come to represent a new market for the network operators a market that has emerged during the era of re-regulation and increasing competition among operators. Table 11.8 shows the current decade's growth trend in terms of subscribers or lines.

To further emphasize the importance of the Internet-services market and higher-bandwidth access, it is important to note that revenues for wireline local service voice telephony have been decreasing in advanced telecom markets, mainly due to the rise of cellular-mobile telephony. This means that the telecom companies are eager to develop new sources of revenue, and broadband service is a critical element in their business plans. Figure 11.3 shows the trend in local telecom service revenues for the US incumbent local exchange carriers.[27]

The major US local exchange carriers have been able to offset the decline in local-telephone service revenues since 2000 by adding revenues from DSL and long-distance services. The former AT&T companies were excluded from the long-distance market after the 1984 divestiture, but the 1996 Telecommunications Act included terms and conditions for offering long-distance service. The opportunity to continue increasing revenues from DSL or fiber-based broadband services is critical to the major local exchange carriers in every market.

Table 11.8

Compound annual growth rates in wireline, CATV, and broadband subscribers.

	2000	2006 est.	2000 2006 CAGR (%)
Wireline main lines	979	1302	5
Households with internet	168	512	20
Broadband internet subscribers	21	292	56
CATV subscribers	323	450	6

Sources: ITU, KMI Research.

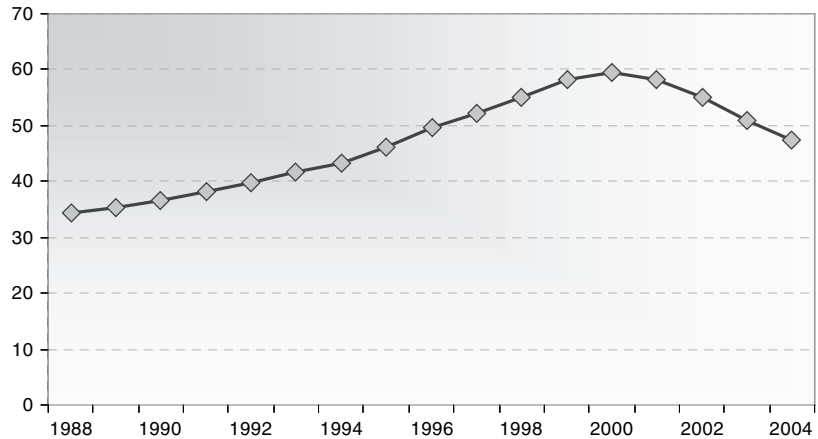

Figure 11.3 US wireline revenues for local service and local calls completed, 1988 2004 in $ billion. (*Source*: FCC Statistics of Communications Common Carriers 2004/2005.) (this figure may be seen in color on the included CD ROM)

The downward trend in local-exchange carrier revenues parallels the erosion in the number of wireline access lines operated by these carriers. The number of lines has been dropping 3 7% per year since 2000 in the United States, and a similar trend is underway in other advanced telecom markets. There are several reasons for this decrease:

(1) Households and small businesses are eliminating their second line, which may have been taken for facsimile machines, dial-up Internet, or other household members (e.g., teenage children). More recently, these customers are substituting, DSL, VOIP (voice over IP), or other services.
(2) A small percentage of telephone customers are switching entirely to VOIP, CATV-provided telephony, or other non-local-exchange carrier services for voice telephony.
(3) The main reason is that more of the population is opting to use cellular services in lieu of wireline access lines. In the United States, for example, the percent of population living in households with no wireline telephone service increased from 3% in 2003 to 10% in 2006.[28] This phenomenon includes young adults who have had cell phones while in school and see no reason to open a wireline account when they establish a household, as well as households that decide to discontinue their wireline service and use only their cell phones, a decision called "cutting the cord."

The proliferation of cellular telephones throughout the world has been one of the most dramatic developments in telecommunications. In about 15 years, the number of cellular telephone subscribers went from near zero to more than two billion, almost double the number of wireline accounts (Figure 11.4).

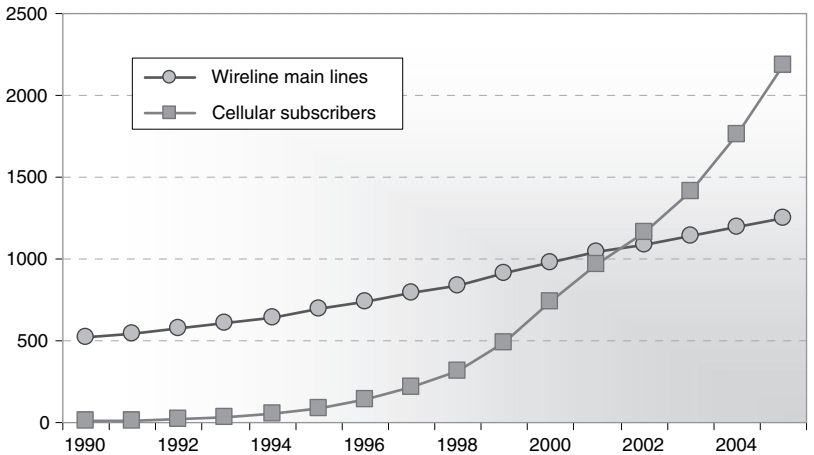

Figure 11.4 Wireline and cellular telephone subscribers worldwide, 1990 2004, in millions of subscribers. (*Source*: ITU Telecom Statistics Database.) (this figure may be seen in color on the included CD ROM)

In advanced telecom markets, cellular technology has been used in addition to wireline service for mobility or constant connectivity. In many lower-income markets, wireless technology has been used to provide service to villages and rural populations where there never had been any wireline infrastructure. Prepaid services and low-fee options have contributed to usage in low-income areas. As seen in Table 11.6, the penetration of cellular telephony into the population is higher than wireline teledensity in every region, and it is two to three times higher in Africa, Latin America, and Eastern Europe.

The growth of wireless in developing telecom markets is expected to continue through the present decade. For example, the number of cellular subscribers in China increased from 91 million in 2000 to 393 million in 2005, and it has been projected to pass 500 million in 2007.[29] The number in India increased from 4 million in 2000 to 90 million in 2005, and it has been projected to pass 150 million in early 2007.[30] These markets are adding cellular subscribers at rates of 3 5 million per month. In advanced telecom markets, the number of new subscribers is not increasing in this fashion, but the operators are adding new services and continuing to increase revenues per user.

What is the effect of cellular technology on fiber optics and on broadband access? The cellular market has a limited but positive demand on fiber-optic systems in two respects. First, it puts more traffic on the trunks and intercity backbones, since more customers are accessing the network and using more minutes of long-distance capacity. Second, there has been limited use of fiber for backhaul or local infrastructure, to link cell sites to switching stations, although copper-based T-1 lines are used more commonly.

The indirect effects of wireless systems may prove more important in the fiber-optics market. As noted above, the use of wireline facilities for voice telephony is

decreasing and will continue to decrease. The local exchange carriers therefore are focusing on Internet access and broadband services to increase revenues.

A recent telecom industry development — mainly since 2002 — has been the upgrade of cellular networks to provide data (Internet) services. This has been referred to as "3G" or third-generation cellular technology. As of early 2007, operators in some markets also had introduced video services for their cellular-mobile subscribers. Such mobile data and video services can address the need for "ubiquity" or constant access, but limitations in the display (screen size), interface (keyboard), and capacity will prevent cellular-based data services from displacing "wireline" broadband access.

Another development that has begun to enter mainstream telecommunications since 2000 is video on the Internet, including IPTV. The following statements indicate the disruptive potential of video:

(1) "YouTube (a web-based video-sharing website launched in February, 2005) today consumes as much bandwidth as the entire Internet consumed in the year 2000."[31]
(2) "Each year the original content on the world's radio, cable and broadcast television channels adds up to about 75 petabytes of data — or, 10 to the 15th power. If current estimates are correct, the 2-year-old YouTube streams that much data in about 3 months. But a shift to high-definition video clips by YouTube users would flood the Internet with enough data to more than double the traffic of the entire cybersphere. And YouTube is just one company with one application that is itself only in its infancy. Given the growth of video cameras around the world, we could soon produce 5 exabytes of amateur video annually. Upgrades to high-definition will in time increase that number by another order of magnitude to some 50 exabytes or more, or 10 times the Internet's current yearly traffic."[32,33]
(3) "BitTorrent [a web-based Internet television provider] said traffic generated by millions of its users now accounts for as much as 40% of all worldwide Internet traffic."[34]

These statements suggest that video on the Internet will have a huge effect on bandwidth requirements, in turn driving more fiber into broadband access networks. The second statement about YouTube notes the potential role of high-definition television (HDTV). But there also is on-going development of other advanced video display technology, such as 3-D TV. Various 3-D technologies have been used for more than 10 years in commercial applications (engineering workstations, movie theaters, etc.). Systems for home entertainment are under development with the potential for market introduction before 2010. Although early reports suggest that one consumer product may operate within the limits of asynchronous digital subscriber line (ADSL) bandwidths,[35] there also is potential for much higher-bandwidth requirements.

Video developments have several complex facets: who generates content; who owns and transmits the content; which content is broadcast vs switched; where

content is cached, etc. For example, the YouTube phenomenon is indicative of the upsurge in the amount of "user-generated" content, which increases the demand for upstream bandwidth (from the customer's premises towards the CO or network facility) and possibly for symmetric service offerings.

This raises the question, what exactly is "broadband?" In the United States, the FCC has defined broadband as more than 200 kbps.[36] The OECD has defined it as more than 256 kbps downstream and 128 kbps upstream. The ITU has defined it as faster than primary rate ISDN, which is 1.5 Mbps in many markets. OfTel in the United Kingdom has defined it as more than 128 kbps. Some analysts have proposed a definition that scales up through "generations" starting at 256 or 384 kpbs for the first generation, rising to 2 Mbps for the second, and possibly a third generation will be more than 5 Mbps or 10 Mbps. Other government groups have concurred with the OECD at 256 kbps.[37]

Although the widely used figures of 200 or 256 kbps may seem low by some standards, they represent a threshold separating dial-up modem from DSL and faster technologies. As speeds increase above hundreds of kbps into the Mbps regime, the operators must make a greater investment, and the transmission plant is more likely to include fiber.

11.4 HISTORY OF FIBER OPTICS IN ACCESS NETWORKS

FTTH and FTTC are not recent phenomena. The first discussions and technology trials date back to the 1970s. The 1980s and 1990s saw a bewildering mix of expensive trials, technology developments, unfulfilled requests for proposals from carriers, changing service requirements, improvements in competitive media, and of course the regulatory changes. The upshot appears to be a 15-year history with numerous false starts, failed initiatives, and other reversals. Table 11.9 shows events that highlight early efforts with FTTH and some of the various market, regulatory, and technical developments in the 1970s, 1980s, and 1990s.

When FTTH was first discussed in the 1970s, fiber optics was mainly used for trunk routes, but the bandwidth-times-distance performance led telecom visionaries to propose "wired cities" with voice, video, and what were then called "futuristic" (probably meaning "not fully understood") services deployed directly to homes.

In 1976, the Japanese Ministry of International Trade and Industry announced plans for the Hi-OVIS (highly interactive optical visual information system) project in a new community called Higashi-Ikoma, which is near Osaka in the Nara Prefecture. The first FTTH links were activated in 1978, and the project ran through 1986, ultimately involving 156 homes. The fiber system supported a range of voice, video, and data applications, including experimental educational, "social," and entertainment services.

Other early trials were getting underway at about the same time. In 1978, France Telecom announced a 1500-home FTTH project in Biarritz. The first

Table 11.9

Sample of FTTH developments in three decades.

1978	Japan's MITI announces Hi Ovis project, 156 homes served with FTTH
1981	Elie, Manitoba FTTH project begun, serving 158 rural homes
1986	GTE announces first US FTTH trial for Cerritos, Calif.
1987	British Telecom Research Labs technical paper describes TPON architecture with 128 way split
1988	Raynet announces tap based bus architecture for FTTH or FTTC, joint effort with BellSouth Enterprises for operations software, and trials with NYNEX
1991	NTT reveals "Optical Fiber Loop 21" goal of "all fiber" network by 2015; developments to include 4000 fiber cable, 100 fiber connectors, etc.
1991	Deutsche Bundespost Telekom issues RFP for initial "OPAL" trials to begin in 1992 with plans to deploy for 1.2 million homes from 1993 to 1995
1992	US FCC video dialtone ruling allows local telephone companies to transport (but not originate) video traffic without obtaining cable television franchise
1993	US carriers have announced more than 50 FTTH/FTTC field trials, largest with 1000 homes
1994	GTE and four regional Bells announced major deployments (serving millions of homes) for video dialtone using HFC or FTTC with coax overlay
1995	European PTTs and other operators have announced more than 40 FTTH and FTTC trials
1995	BT, other major carriers, and equipment vendors form FSAN (the Full Service Access Network Coalition) committee to develop standards
1995	BellSouth begins deploying FTTC for new construction projects
1995	First of 5 years (1995 2000) in which US CATV operators install more fiber than regional Bell companies
1996	US Telecommunications Act signed, video dialtone opportunity changed, LECs except BellSouth drop FITL deployment plans
1996	LANcity (now Arris) ships its 20,000th cable modem to CATV operators and says it expects to ship it's millionth within 18 months
1997	CATV operators start offering voice services in addition to data and video on their networks
1998	BellSouth, GTE, USWest, and Ameritech announce major DSL initiatives, covering millions of customers
1999	Massive buildup of long distance, regional, and metro networks causes fiber and component shortages; FTTH receives little attention.
2001	Japan's USEN launches first commercial FTTH service in March, NTT follows shortly thereafter
2003	NTT says FTTH "B FLETS" service is available in every major Japanese city
2003	FCC's Triennial Review exempts incumbent FTTx projects from unbundling requirement they don't have to share broadband facilities

homes were turned up in 1983, and all 1500 were operational by 1986. In North America, the first FTTH project got underway in 1981 and served 158 rural customers in Elie, Manitoba with voice and television signals.

After the mid-1980s, however, the number of trials increased significantly as the large US local exchange carriers began both lab and field evaluations. GTE (now part of Verizon) was the first to announce a US FTTH field trial in December 1986. This trial would provide telephone, CATV, and experimental services over fiber to 700 homes in Cerritos, Calif. GTE would operate the trial in conjunction with a local CATV operator, Apollo Cablevision. Services began in 1989.

By the end of the 1980s, US operators had announced 21 trials, ranging in size from 12 to 700 homes. The participating carriers included GTE, Contel, Alltel, and six of the seven regional Bell companies.

The early field trials focused on system cost, reliability, operational costs, and performance factors. The experience clearly showed carriers and vendors that fiber-based system costs would need to fall dramatically if there were to be any chance of practical deployments. Anecdotal reports indicate that the costs of early FTTH trials in the United States ran as high as $10,000 per home. Other issues included power supply, footprint/rack size, and systems for provisioning and other operational functions.

In addressing the cost problem, the early developers introduced two important concepts for sharing the transmit-receive electronics to lower costs per subscriber. The first was to locate the remote "electronics" or optical network unit (ONU) in a pedestal, pole-mounted cabinet, hand-hole, or building basement so that it could be shared among multiple subscribers. The second was to split the optical power from a single CO laser source into multiple output fibers. British Telecom Research Labs first demonstrated this concept and termed it "telephony over passive optical network" or "TPON," and the term "PON" has become widely used for such splitter-based architectures.[38]

The PON concept was made feasible by the development of reliable, repeatable single-mode coupler and splitter products, first introduced in the early 1980s. The first introduction of Raynet's fiber-in-the loop (FITL) system used a multimode fiber bus with passive taps based on patented variable tap/coupler hardware. The large local exchange carriers showed little interest in multimode fiber or the tapped-bus architecture, and Raynet quickly shifted its development to PON architectures based on single-mode fiber.

During the early 1990s, fiber-optic equipment vendors and carriers expressed the general view that FITL would progress from field trials to "first office applications" and then to widespread deployment, often seen as taking a period of 3 5 years. This progression would be facilitated by "learning-curve" phenomena in which the cost of the optical cable, transceivers, and associated products all decreased as "experience" or production quantities increased. The FITL costs were projected to "cross over" and fall below the costs of twisted-pair copper systems.

This crossover was complicated or delayed for several reasons. First, the carriers needed revenues from services other than voice telephony to justify higher-quantity procurements. Second, the regulations affecting telephone company transmission of information and entertainment services were in a state of flux in the 1990s. Also, twisted-pair (TWP) copper was not the only competitive medium. Coaxial networks were enhanced with new hybrid-fiber coaxial (HFC) architectures and cable-modem technology, so that CATV operators became a major competitive threat for potential FITL service revenues. And development of DSL technology, especially ADSL, allowed the embedded TWP network to support new revenue opportunities with significantly lower costs than fiber.

This history shows the importance of two main factors in triggering carrier spending on fiber in access networks. The first is the menu of services and fees that

can be marketed. As Internet applications became richer with images, video, and audio content, the demand for higher-speed service became more attractive. The second factor is competitive what other carriers are offering services to these customers and what technology do they use?

In hindsight, the 1990s might be characterized as years in which the fiber proponents were looking for a "killer application." or seeking ways to justify initial volume deployments of FITL. The present decade (2000 2010) might be characterized as years when the fiber proponents have identified high-speed Internet access (covering a diverse family of applications including video) as a the main revenue source and are seeking ways to tailor the fiber network or "right-size" it to maximize cost-effectiveness.

11.5 APPLICATIONS AND BANDWIDTH REQUIREMENTS

This "tailoring" of fiber in the loop involves how far to take the fiber, how much to share the optoelectronics, and what transmission speed to use, which also affects optoelectronic costs. Recalling that the fundamental performance factor in fiber-optic systems is bandwidth-times-distance, the question of how far to take the fiber into the loop raises the question what bandwidth requirement must be supported?

The answer is not a simple matter. Different carriers have arrived at different conclusions, reflecting different strategies for modulating video channels, different approaches to the amount of switching vs broadcasting, and different approaches to providing content vs transporting it for other providers.

A major issue is whether video services are part of the digital stream or whether the operator will use a second downstream wavelength channel for video using AM transmission techniques. The AM transmission techniques have been used for about 15 years in CATV networks and are well understood a "mature" technology. Verizon, for example, has incorporated a 1550-nm channel for AM video services in its wide-scale FTTP project, starting with its first installations in 2004.

AT&T, on the other hand, has chosen all-digital video transmission, using IPTV technology. The critics of AT&T's approach have questioned whether the VDSL bandwidth will be able to provide enough capacity for customers wanting multiple video channels at once, specifically if more than one HDTV channel is to be streamed at the same time.

The matter of bandwidth requirement is further complicated by uncertainty about future requirements it is clearly a moving target. The Internet experience to date has shown a steady progression in the most widely used Internet access speeds, starting with 14-kpbs, then 28-kbps and 56-kbps dial-up modems in the 1990s. In the current decade ADSL and cable-modem technology have moved consumers into hundreds of kbps or single-digit Mbps. And now FTTx operators are signing up subscribers at 10s of Mbps. The result is a 1000-fold increase from 14 kbps to 15 Mbps in about 15 years.

For typical loop lengths in North America, 15 Mbps with xDSL technology will require a DSLAM (digital subscriber line access multiplexer) somewhere in the outside plant between the COP and the subscriber.[39] The DSL Forum has publicized the following guidelines for xDSL bit rates and distances:[40]

- ADSL typically supports 8 Mbps within 5000 feet;
- ADSL2+ extends this to 20 Mbps, within 5000 feet;
- VDSL2 will achieve higher up to 50 Mbps for distances within 1000 feet, possibly to 100 Mbps, if distances are 500 feet or less (e.g., FTTC).

Data on US Bell company local operations prior to the divestiture in 1984 show average loop lengths greater than 15,000 feet (4.6 km), and data from rural operators in the 1990s show average loop lengths greater than 20,000 feet (6.1 km). This means that data rates of 8 Mbps and higher can not be served from the CO for most customers. Loop lengths in Japan, Korea, Western Europe, and other markets tend to be somewhat shorter, typically ranging from 2.0 to 3.5 km.

A shift from ADSL speeds to faster Internet services beyond 5 Mbps download speeds already is underway in the United States and Canada. Thus, many telecom operators are upgrading to FTTN or FTTC even without immediate plans to transport IPTV or streaming video services. The triggers for such Internet speeds will include audio and video downloads, gaming, and video conferencing. In some cases, home-office requirements for accessing corporate servers and downloading large data files also may trigger demand for higher speeds.

HDTV is becoming an increasingly important factor in bandwidth requirements. The digital transmission speeds needed to support HDTV depend on the compression technology. With MPEG-2 compression, an HDTV signal will require 15 20 Mbps per second. Several industry participants have cited 16 18 Mpbs. As of early 2007, MPEG-4 compression products were not widely available, but operators expected that HDTV could be streamed over digital channels of 4 8 Mbps, with levels of 5 or 6 Mbps generally cited.

The bandwidth required per video channel with MPEG-2 and MPEG-4 is stated as a range because different video streams can be compressed to smaller file sizes. For example, basketball games or other sports events are said to require the largest file size, or can not be compressed as much, because there is constant motion, shifting of angles, and widely varied backgrounds. Programs such as movies, on the other hand, may have less motion, fewer shifts in camera angle, and more constant backgrounds for longer intervals or scenes. Table 11.10 summarizes the compression rates for standard-definition and high-definition digital video channels.

The data on HDTV penetration into TV households suggests potential demand for more than one HDTV signal. In 2006, consumer data indicated that a non-negligible percentage of HDTV households already had acquired a second HDTV set, and this percentage was expected to continue increasing. There is also the possibility of subscribers seeking to watch one HDTV program while receiving

Table 11.10

Bit rates per video channel with compression.

(Rates in Mbps)	Range	Typicial
SDTV/channel w MPEG 2	2 5	3
SDTV/channel w MPEG 4	1.5 2	1.5
HDTV/channel w MPEG 2	15 20	16
HDTV/channel w MPEG 4	5 10	8

and recording another. For these reasons, many companies providing video service acknowledge the need to support more than one simultaneous HDTV transmission.

Table 11.11 shows the bandwidth requirement per household if the entertainment TV channels are part of the downstream digital payload, with two scenarios for compression and Internet use. Upstream transmission has a lower bit rate in most service providers' offerings. "Power users" require higher-speed Internet for video editing, video downloads, high-end gaming, etc. The 10 Mbps proposed for "power user" requirements in this table was probably conservative as of 2006. The high-end offerings in some markets already had extended to 30 or 50 Mbps. Operators in Japan and Korea already had introduced 100-Mbps services.

The table shows that the bandwidth requirement for all-digital triple-play (voice + Internet + video) might range from 16 to 48 Mbps per household. A typical household in 2007 or 2008 might require 27 Mbps for a mix of digital video channels for multiple television sets and video recorders, games, and Internet. A "power user" might be require more than 35 or 40 Mbps.

Although it is difficult to envision a 1000-fold increase in Internet bandwidths per customer, as happened from the mid-1990s 2006, it would be foolhardy to say that 30 Mbps is the maximum household bandwidth requirement for the next 10 years. The history of Internet applications shows they can evolve quite rapidly, and they always have used more bandwidth.

Table 11.11

Bandwidth required per household (Mbps).

Video services with MPEG 2 compression			
Internet (average)	5	Internet (Power user)	10
Telephony	0.1	Telephony	0.1
2 SDTV channels	6	2 SDTV channels	6
1 HDTV channel	16	2 HDTV channels	32
Total (Mbps)	27.1	Total (Mbps)	48.1
Video services with MPEG 4 compression			
Internet (average)	5	Internet (Power user)	10
Telephony	0.1	Telephony	0.1
2 SDTV channels	3	2 SDTV channels	3
1 HDTV channel	8	2 HDTV channels	16
Total (Mbps)	16.1	Total (Mbps)	29.1

11.6 FACTORS AFFECTING DEPLOYMENTS

The different scenarios for near-term video-service opportunities can shift the bandwidth requirement per household by tens of megabits per second. There are other variables that will affect the decision as to how far to take the fiber, or to what extent the fiber and optoelectronic facilities are to be shared among multiple subscribers.

The regulatory factors mentioned previously, especially the rules concerning unbundling are critical. Even when there are no concerns that an operator must share its broadband facilities with competitors, there can still be concerns about competitors using other technologies, such as CATV operators with HFC networks. In this case, the competitors might capture some of the available market, and reduce the FTTx operator's "take rate." This means that there will be fewer subscribers served by the operator, and a lower percentage of the homes passed will be generating revenues to offset capital and operational expenses.

The competitive situation, the regulatory framework in place, and the bandwidth requirement may be the most critical factors in network-design decisions, but there are many other factors, as shown in Table 11.12.

Several items listed in this table are worth noting as having a significant effect in specific markets. For example, NTT's outside-plant infrastructure incorporates underground feeder routes and aerial distribution, except in the densest downtown areas. NTT designed its FTTH architecture to take advantage of this infrastructure, adopting a PON concept with two stages of splitters one located in the CO and one located at the distribution area interface. NTT had upgraded almost all of its feeder routes to fiber several years before it began turning up millions of FTTH subscribers.

With this resource already in place, when NTT receives an order for its high-speed "B-FLETS" service, it will install a fiber-optic distribution cable, if it has not already done so in that distribution area, and it will install the fiber-optic drop and optical network terminal (ONT). This approach, of having preinstalled fiber-optic feeder infrastructure, that already "passes" the homes, allows NTT to turn up new subscribers in a relatively short period of time days or weeks, depending on the distribution facilities in place. It also allows NTT to wait until a customer orders the service before incurring the costs associated with the drop and ONT.

The demographic, distance, and density factors also have affected network architectures in other Asian markets. In dense urban areas of China, Taiwan, Korea, and Singapore, there has been widespread use of fiber-to-the-building (FTTB) architectures, with the subscriber connection using ADSL or Ethernet technology on copper cable. This architecture is less common in the United States, where fewer than 20% of customers live in multifamily dwelling units (MDUs).

The factors concerning video markets may be the most volatile, or subject to change in a relatively small number of years. As of year-end 2006, the worldwide market had about 450 million CATV subscribers, but fewer than 10 million IPTV subscribers. During 2007, however, trade publications cited analysts' projections that IPTV subscribers might increase to 48 million in 2010 or 60 million in 2011.[41] This emphasizes the relatively early stages of TV programming on the Internet.

Table 11.12
Factors in Deciding what FTTx architecture is optimal.

A. Network characteristics
Distance (loop length)
Infrastructure What is available, usable, or obsolete?
Copper loop pairs
Feeder electronics
Feeder fiber
Cabinets, huts, handholes
Rights of way availability and fees
B. Demographics
Population density and distribution
Extent of single family vs MDU housing
PC penetration, Internet usage
Personal Income/Disposable Income
Work at home market
C. Competitive situation and "take rate" factors
Cable TV Industry
Number and strength of CATV operators
Offer high speed Internet, telephony, triple play?
DSL and wireless competitors
Number and services offered
VOIP, wireless users "cutting the cord"
Rates for unbundled facilities
End user fees for servicer or packages
D. Regulatory
Unbundling several types, fees
Government support
Competitive policies
Funding, tax credits, loan subsidies
Video franchise regulations
Access to rights of way
E. Service requirements or service opportunity
Internet bit rates market demand and competitor's offerings
IPTV potential revenue stream
Bundling e.g., triple play, or other "package plans"
F. Financial
Sources of funding
Commitment of government officials, corporate executives
Revenue opportunity

Finally, there is an element of choice or vision in the decision making, in addition to more rigorously quantified cost and payback factors. This is particularly evident in the different choices of AT&T and Verizon in the US market during the years of 2003 2007. Both companies operate with the same regulatory factors. They have similar competitive situations largely up against CATV

operators with cable-modem service. They have similar density and demographic situations. Verizon has a little more aerial plant, which allows for less costly FTTP construction, but otherwise, the two companies encounter mostly the same network, policy, and market factors.

Yet Verizon has committed to FTTP, with plans to spend about $20 billion from 2003 to 2010, and AT&T has committed to FTTN, with plans to spend about $7 billion. In this case, the element noted as "executive commitment" is important. It is a matter of how the top officers have weighed the risks associated with FTTP and FTTN investments risks of not achieving timely payback criteria vs the risks of investing in a lower-capacity facility that may require costly upgrades, possibly even before it is fully depreciated.[42]

As noted previously, the "unbundling" requirements have had a significant effect in the US and Western Europe. Carriers in Australia and other markets also are struggling to justify FTTx investments if they must share the facilities with competitors. In the case of Western Europe, a court case that is likely to get underway in 2007 will receive close scrutiny. The European Commission has said it will launch a suit in the European Court of Justice to overturn a domestic policy in Germany that exempts DT from unbundling its FTTN network. This policy was implemented by the German parliament in early 2007 in defiance of EU telecom rules.

11.7 FTTx MARKET SCENARIOS

Figure 11.5 shows the results of these deployment factors in the world's broadband access market. That is, the figure shows the networks implemented in terms of the number of subscribers served by the different broadband-access technologies. The "Other" category includes broadband over power line (BPL), ISDN, (symmetric) DSL, and some satellite-based technologies used mainly in remote areas with limited wireline infrastructure. The fixed wireless segment includes LMDS and MMDS technologies, a small amount of municipal Wi-Fi usage, but not Wi-Fi hotspots. In the future, fixed wireless may include WiMAX standards, but this technology was not in commercial use as of 2006.

The outlook for beyond 2006 is for FTTB and FTTP to displace CO-ADSL in increasing numbers, as carriers in advanced telecom markets upgrade their networks to support video and other services that require faster transmission speeds. Depending on the decisions of major incumbent carriers in Western Europe, the 5-year forecast from 2007 to 2012 could see the number of FTTB-plus-FTTP subscribers rising to a level between 50 and 100 million.

This figure could include 30 million subscribers in Japan (this is the target for NTT East and West combined), plus 10 20 million in the United States, another 10 20 million in Western Europe, and large quantities in China, Korea, Singapore, Taiwan, and other rapidly growing or advanced telecom markets.[43]

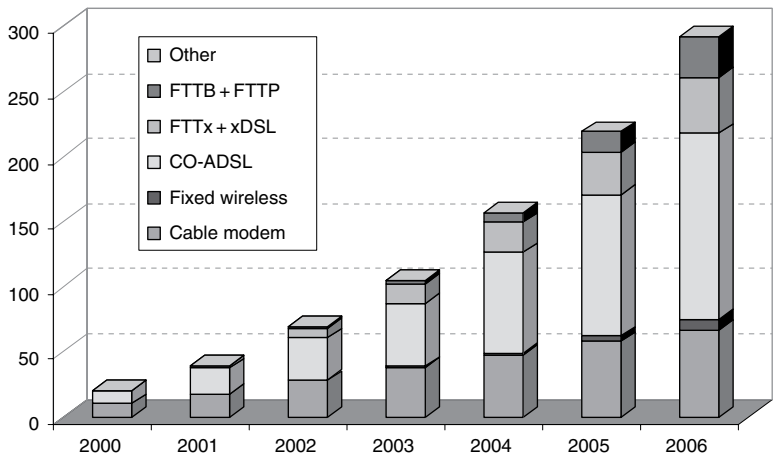

Figure 11.5 Broadband access subscribers by main technology, 2000 2006, million subscribers cumulative (this figure may be seen in color on the included CD ROM).

The experience of the small municipal and utility FTTH projects in the United States and northern Europe has demonstrated high subscription rates and also reasonable payback criteria consistent or better than business-plan expectations. These utility or community-based markets are not necessarily representative of all FTTH deployment. This is because many municipalities initiated FTTx investment plans specifically because incumbents' telecom operators did not provide adequate broadband service. That is, these markets had "pent-up" demand for broadband service and no real competition.

In these cases the absence of broadband service may have been a trigger for new deployments or at least a positive decision criterion. In other cases, the presence of competitors has provided stimulus for some operators to invest in FTTH as a way to differentiate themselves from the competitors.

The presence of competition has stimulated carriers in markets, such as France, Korea, and Japan, to announce aggressive FTTH targets. As these deployments get underway, the world will be watching Verizon, which said in its September 2006 quarterly financial briefing that it expected its FTTP deployments to be "EBITDA positive by year three" and "operating income positive by year four."[44] Verizon started FTTP deployments in the Dallas area and other communities during 2004, so the year-three and year-four milestones will be falling between 2005 and 2010.

In quarterly results announced after the September 2006 briefing, Verizion has said that that the subscriber sign-up rate has been meeting or exceeding its expectations for both the video and the data services. Verizon will represent a good indicator of a phone company's ability to increase revenues in video and data services by deploying new FTTP technology in markets with strong CATV

competitors. As of early 2007, there is little evidence, if any, that FTTP operators are encountering any major sources of operational or financial failure.

11.8 CONCLUSIONS

Commercial fiber optics technology has developed over 30 years with consistent improvements in terms of bandwidth-times-distance performance. At the same time, prices for cable, transmission systems, and related apparatus have decreased with product and process improvements. As a result, fiber optics have been deployed cost-effectively for increasingly shorter distances in telecom networks, as well as for applications with a smaller bandwidth-times-distance product, such as FTTH.

As the twenty-first century got underway, fiber-optic systems for access networks were in early deployment. Standards, low-cost construction techniques, powering technologies, operating system software, and other objectives needed for practical fiber-in-the-loop deployments all had been addressed and were in stages of improvement or subsequent generations.

With this progress on network technologies and cost problems well underway, the biggest remaining variable for FTTx system "success" has been the revenue stream, or the business-case profit line. And the evolution of Internet applications, somewhat in parallel with developments in fiber-optic technologies, appears promising as the basis of new revenue-generating services for telecom network operators installing FTTx systems.

The matter of purchasing fiber-optic products, building a network, and selling broadband services is complicated by a large number of regulatory, competitive, political, and "infrastructure" factors. Policies concerning unbundled local loops, for example, have proven to be critical factors in several major markets. In the United States, for example, Verizon and AT&T initiated wide-scale FTTx projects after an FCC ruling exempted the RBOCs (Regional Bell Operating Companies) from having to "unbundled" and share new fiber networks. FTTx installations by some European incumbents, on the other hand, have been delayed by unbundling policies that require them to share new fiber facilities on a wholesale basis to competitive carriers.

Such factors complicate the carriers' decisions as to when to start FTTx projects or how far to take the fiber whether all the way to the home or to some shared node. Plus, regulatory factors and customer applications, such as video services, are in a state of flux they can change rapidly (in months, not years). There are only 10 15 years of World Wide Web and consumer Internet history to evaluate, but one clear and overwhelming history lesson is that Internet applications can emerge or change in a very short period of time. Heavy-traffic applications such as Napster and YouTube achieved wide-spread usage in 12 24 months.

In some greenfield housing projects, the business case may be the most straightforward there is no infrastructure already in place, construction costs are competitive, and there may be interest in integrating broadband services into the overall community plan.

But greenfield communities are a small percentage of customers about 2% in North America, for example. This means that companies evaluating the use of FTTP or other fiber-based broadband access systems, must look at ways to phase in the new systems, operate a hybrid network until all homes are passed, meet unbundling and other regulatory requirements, market their services possibly against established competitors, and continue to modify their network to meet new service requirements or opportunities.

The fundamental proposition for network equipment manufacturers and operators, in short, is to use the power of semiconductors, software, and fiber optics to upgrade telecom networks and provide services to customers that have adopted or are adopting increasingly powerful PCs, Internet applications, video display systems, and other advanced technologies. It is a safe bet that the customer premise equipment and the end-use applications will continue evolving. The ongoing development and business plans of PC, software, entertainment, security, medical, education, and consumer electronic companies are likely to assure a steady stream of innovations. And it is an even safer bet that these innovations will need more network bandwidth in the future, not less.

LIST OF ACRONYMS

ADSL	Asynchronous digital subscriber line
CAGR	Compound annual growth rate
CATV	Community antenna television. More commonly called cable television.
CLEC	Competitive local exchange carrier. A carrier competing with the ILEC for local telephone subscribers in the ILEC's home serving area.
CO	Central office
CO-ADSL	ADSL service provided entirely over copper telephone lines. The DSLAM is located in the central office
CPE	Customer premises equipment
DSL	Digital subscriber line
DSLAM	Digital subscriber line access multiplexer
FCC	Federal Communications Commission US telecom regulatory agency
FITL	Fiber-in-the-loop

FSAN	The Full Service Access Network coalition
FTTB	Fiber to the building, or sometimes, fiber-to-the-basement. Generally NOT understood as fiber-to-the-business
FTTC	Fiber-to-the-curb
FTTH	Fiber-to-the-home
FTTN	Fiber-to-the-node. A fiber-based system in which the optical network unit is located in a node that may serve 50 500 homes. The distinction between FTTN and FTTC is the number of homes served by the optical unit. For FTTC, the number typically range from 4 to 32; whereas FTTN is usually a "larger" node, or one that serves more homes as many as 500 or 600
FTTP	Fiber-to-the-premises. This is similar to FTTH, but more inclusive the subscriber premises may be retail or other small businesses as well as residential customers
FTTx	Refers to FTTB, FTTC, FTTN, and FTTP collectively meaning any type of fiber-in-the-loop architecture for broadband services
HDTV	High-definition television
HFC	Hybrid-fiber coax, a network architecture carrying AM signals on fiber from the head-end to a node for optical to electronic conversion, then using coaxial cable from the node to the customer premises. Two-way HFC transmission was developed in the 1990s
ILEC	Incumbent local exchange carrier. In the United States, one of the RBOCs or any of the hundreds of other incumbent local phone companies. In other countries, the ILEC is often the former PTT or government-run telecom monopoly.
IP	Internet Protocol
ITU	International Telecommunications Union
LEC	Local exchange carrier. In some contexts, the incumbent local exchange carrier. With the advent of competition and the coining of the term "CLEC," LEC can now refer to either an ILEC or a CLEC
LLU	Local loop unbundling
MDU	Multiple dwelling unit or multifamily dwelling unit
ONT	Optical network terminal. The device, providing an on/off ramp to the fiber, much like an ONU in a FTTC system, The ONT is situated at the home or customer's premises in an FTTP system.
ONU	Optical network unit. The device that converts and splits signals from fiber to copper and/or coaxial cable at the residents' end of a FTTC system.
PON	Passive optical network. An FITL architecture that uses optical splitters to share an optical transmitter among two or more fibers.

	The FSAN committee has specified split ratios up to 64:1 in the standards adopted by the ITU ITU G.983 (BPON) and G.984 (GPON).
POTS	"Plain Old Telephone Service." The term refers to standard voice-grade telephone service and is used to distinguish standard voice-grade service from video or high-speed data service.
RBOC	Regional Bell Operating Company, also called a "Baby Bell." Refers to Qwest, AT&T (formerly SBC, Ameritech, Pacific Telesis, and BellSouth) and Verizon
TWP	Twisted pair, refers to copper-wire telecom cable technology
VDSL	Very high-bit-rate digital subscriber line
VOIP	Voice over IP
Wi-Fi	802.11 short-range broadband wireless access
WiMAX	802.16 wide range broadband wireless access
WW	Worldwide (abbreviation used with some market data to clarify geographic segment).
xDSL	A generic way of referring to several types of DSL technologies as a group, including ADSL, VDSL, ADSL2, and VDSL2, in which the lower-case "x" denotes a variable.

NOTES

1. KMI estimates that domestic and international submarine cable routes installed to date total about 990,000, but several early systems were made obsolete by newer generations of transmission technology and taken out of service. Obsolete means that the maintenance fees on older cables using lower-bit-rate transmission were higher than the cost to purchase a similar amount of transmission capacity on newer systems having higher bit rates and DWDM technology.
2. International Telecommunications Union (ITU), Telecom Indicators Database.
3. As of December 31, 2006, there were 7 million FTTP customers in Japan, 1.2 million in the United States, 1 million in Europe, and 0.5 1 million in other major markets of Asia and other regions. In the first quarter of 2007, the world's operators have been signing up about 350 000 new FTTP subscribers per month, and this rate is increasing.
4. It is impossible to list every project, telecom operator, or country. The number of projects, communities, regions, or countries has been increasing exponentially since 2005. In previous years, a telecom operator might pursue a process of field trial, then "first-office" application, then wide-scale deployment. The interval from launching the field trial to deployment might have been 2 years or more. By 2007, many operators have compressed or eliminated this

multiphase process, reflecting high levels of confidence and well-documented field experience with the products and technologies among vendors and carriers worldwide.

5. The "FTTx" notation: fiber-to-the-premises (FTTP), fiber-to-the-building (FTTB), fiber-to-the-curb (FTTC), and fiber-to-the-node (FTTN) collectively are labeled FTTx. In this context, the fiber-to-the-node networks are those using a remote DSLAM unit or digitally multiplexed telecom system, and not the RF-based hybrid-fiber-coax systems commonly operated by CATV companies. A "TRX" is a transmit-receive module or a pair of separate transmitter and receiver modules.
6. The table shows a distinction between the installed base of cabled fiber (F-km) in all applications, vs the quantity in telecom applications. The nontelecom applications would include CATV networks, utility, railway, highway, campus, intrabuilding, and sensor networks. This distinction is included to show the role of FTTP and FTTx in the market for products used in telecom networks.
7. International Telecommunication Union (ITU), World Telecommunication/ICT Indicators Database, http://www.itu.int/net/home/index.aspx
8. ITU-T G.983, ITU-T G-984, IEEE 802.3ah.
9. Tauber, Hartwig (IMC University of Applied Sciences Krems, Austria and 2005 2006 President, FTTH Council-Europe); "Why a Competitive Europe needs FTTH?," ECOC 2006 Plenary Session.
10. Kruse, Diane (CEO Zoomy Corporation); "Separating Network Ownership from Service Providers," 2006 US FTTH Council Exposition, http://www.ftthcouncil.org.
11. Zager, Masha, "Triple-Play Services Delivered to Workers' Housing in Mexico," Broadband Properties, June 2006.
12. Render, Michael, "FTTH/FTTP Update, April 2007," (Teleconference), FTTH Council. See also Verizon's Financial Reports for First Quarter, 2007.
13. The US has about, 1200 independent telephone companies, 3300 power "providers" (from American Public Power Assoc., which cites DOE's Energy Info. Admin.), 19,000 municipal governments, 3000 county governments, and 17,000 town or township governments (from National League of Cities). Even though the United States has two phone companies (AT&T and Verizon) representing two-thirds of the country's lines, there are thousands of "non-Bell" communities, and the independent carriers, power utilities, local governments, or other operators serving these communities increasingly are evaluating FTTx to provide new broadband services.
14. One observation from this data is that cumulative worldwide installations will pass the one-billion-kilometer level sometime in late 2008 or early 2009. The second billion will be getting underway with a different mix of applications and fiber types. Also, some of the early long-distance

systems will be operating with fiber that is 30 years old, affording opportunities to collect new data on field reliability and long-term operating characteristics.

15. For example, cable construction can cost as low as $10,000 per km for some aerial installations, or more than $250,000 per km for underground installations in metropolitan areas, where it may be necessary to block traffic, open up streets, and repave them afterwards. A *typical* project might have right-of-way, engineering, permitting, and construction costs totalling $45,000 per km, and the price of a typical 60-fiber loose-tube cable might be $2000 per km, or less than 5% of all other cable-route costs.
16. Note that the bit rate shown represents the fastest product on the market that year. SONET systems with 155 and 622 Mbps rates were sold in the 1980s, but their introductions are not shown because faster asynchronous systems were on the market. The goal of the table is to highlight the progression of transmission capacity over time. Also note that the bit rate and channel columns represent separate product introductions, so it should not be inferred, for example, that any vendor introduced an 8-wavelength WDM system with each channel capable of 10 Gbps in 1996. Rather, there were 10-Gbps systems available, and 8-channel systems in 1996. Shortly thereafter, however, the system vendors became become able to support 10-Gbps rates in DWDM systems, and more recent products have supported 40-Gbps rates in DWDM configurations.
17. The first year that 40-Gbps transmission systems were available is difficult to establish, because this technology received considerable "advance marketing" during the 2 3 years of laboratory demonstrations and field trials leading up to working applications. Transmission components and subsystems were publicized as early as 2001, and early proof-of-concept demonstrations occupied the next 2 3 years. By 2004, start-up system companies such as Mintera and StrataLight were marketing systems, and customer applications were underway in 2005. In 2006 and 2007, other major telecom equipment vendors have announced customers for 40-Gbps systems.
18. Important early developments in the widespread adoption of Internet applications occurred in the early 1990s; e.g., the 1991 proposal for World Wide Web software by Tim Berners-Lee, the 1993 introduction of Mosaic web-browser software, the Netscape browser in 1994, and Microsoft's Internet Explorer in 1995. Easy-to-use browser and e-mail software contributed to a dramatic, even unprecedented, rise in residential and business use. The Internet Systems Consortium reports data on host PCs, based on surveys of named domains, showing growth from 2.2 million (M) hosts in 1994, 9.4 M in 1996, 29.6 M in 1998, 72.4 M in 2000, and 147.3 M in 2002, and 233.3 M in 2004. This is a CAGR of 59% over 10 years in the number of hosts. Note that the amount of use (hours) and the application richness (kbps) also increased during this time.

19. Shinohara, Hiromichi (NTT Access Network Service Systems Labs), "Overview of Japanese FTTH Market and Lessons Learned from FTTH Deployment in NTT," FTTH-Council Europe Annual Conference, Barcelona, Spain, February 8, 2007.
20. It is possible to define various criteria or combinations of demographic, economic, and telecom indicators for grouping markets into levels of advanced or developing. "Teledensity" or the number of wireline main lines per 100 population offers a convenient single-indicator criterion. KMI has used 40 lines per 100 as a threshold to separate advanced and developing markets.
21. On January 1, 1984, when AT&T was broken up, there were about 1400 independent telephone companies operating in the United States, in addition to the 22 Bell operating companies. By virtue of acquisitions and mergers, the number of independent operators had dropped to about 1200 by 2006. At times in the US industry's history, this number was greater than 2000. Sources: the FCC, the Organization for the Promotion and Advancement of Small Telecommunication Companies (OPASTCO) and the United States Telecom Association (USTA).
22. For example, 1949 Dept. of Justice antitrust suit against AT&T and Western Electric; 1966 suit by Carter Electronics resolved by FCC "Carterphone" ruling; 1974 Dept. of Justice antitrust suit; 1974 MCI suit against AT&T.
23. The ITU had 191 member countries in 2006. In other statistical reports, the ITU provides data on telecom indicators for more than 200 countries.
24. There also are reports from the ITU, the World Bank, and other international development agencies that political instability, government corruption, lack of roads and other utility infrastructure, and related financial problems have delayed programs to introduce telecom competition in some developing markets.
25. EC Regulation No. 2887/2000 of the European Parliament and of the Council of December 18, 2000, "Unbundled Access to the Local Loop," Official Journal L 336, 30/12/2000 pp. 0004 0008. Plus subsequent directives. For summary, see *Regulatory Framework for Electronic Communications in the European Union: Situation in September 2003*, Luxembourg: Office for Official Publications of the European Communities, 2004; ISBN 92-894-4304-9.
26. February 20, 2003, *The FCC Adopts New Rules for Network Unbundling Obligations of Incumbent Local Phone Carriers*, FCC Wireline Competition Bureau Doc. 231344, From the FCC summary release: "The Commission provides substantial unbundling relief for loops utilizing fiber facilities: (1) the Commission requires no unbundling of fiber-to-the-home loops; (2) the Commission elects not to unbundle bandwidth for the provision of broadband services for loops where incumbent LECs deploy fiber further into the neighborhood but short of the customer's home (hybrid loops), although requesting carriers that provide broadband services today over

high capacity facilities will continue to get that same access even after this relief is granted; and (3) the Commission will no longer require that line-sharing be available as an unbundled element. The Commission also provides clarification on its UNE pricing rules that will send appropriate economic signals to carriers."

27. These revenues are for 56 incumbent local exchange carriers that report data to the FCC. The revenues do not include any special access, L-D access fees (origination or termination), unbundled-network-element (wholesale) line revenue, or DSL service revenue. As of 2005, the 56 reporting ILECs represented 96 million or about 86% of US residential access lines and 143 total access lines or about 82% of the US total. The access lines not included in this data are owned by smaller independent (non-"Bell") and competitive local exchange carriers.
28. "Wireless Substitution: Preliminary Data from the January June 2006 National Health Interview Survey," by Stephen J. Blumberg, Ph.D., and Julian V. Luke, Division of Health Interview Statistics, National Center for Health Statistics, CDS, (http://www.cdc.gov/nchs/products/pubs/pubd/hestats/wireless2006/wireless2006.htm)
29. ITU Telecom Statistics Database; projection by KMI Research.
30. ITU Telecom Statistics Database; Cellular Operators Association of India, Cellular Statistics Web Page (http://www.coai.in/archives statistics 2006 q4.htm); Association of Unified Telecom Service Providers of India, Subscriber Data Web Page (http://www.auspi.in/show-subscribber.asp).
31. Dell, Michael. "Consumer Electronics Show Las Vegas," (http://www.cesweb.org/docs/Dell 2007transcript.doc), January 2007; referenced in *The Broadband Factbook*, The Internet Innovation Alliance, p. 35 (http://www.internetinnovation.org/iia/downloads/IIA Fact Book.pdf).
32. Swanson, Bret, "The coming exaflood," *Wall Street Journal*, January 2007; referenced in Ibid. p. 41.
33. This statement is generally corroborated by comments of major-carrier executives, including AT&T's G. Keith Cambron who said AT&T's global network carried 5.1 petabytes/day in 2006 (OFC 2006 plenary address), and Verizon's Mark Wegleitner, who said Verizon traffic was 700 petabytes/month in 2007 (OFC 2007 plenary address).
34. "BitTorrent Secures $20 Million in Venture Capital," (http://www.bittorrent.com/about/press/bittorrent-secures-20-million-in-venture-capital), December 2006; referenced in Ibid., p. 42.
35. Philips 3D Display used for Deutsche Telekom to demonstrate interactive 3D-TV at CeBIT, March 15, 2007, Philips Press Release (http://www.business-sites.philips.com/3dsolutions/news/article-15369.html).
36. FCC Consumer and Government Affairs, Consumer Facts website, (http://www.fcc.gov/cgb/consumerfacts/highspeedinternet.html).

37. Organization for Economic Cooperation and Development; Directorate for Science, Technology, and Industry; Committee for Information, Computer, and Communications Policy; Working Party on Telecommunication and Information Services Policy, "Universal Service Obligations and Broadband," January, 2003.
38. "Passive Optical Local Networks for Telephony Applications and Beyond," *Electronics Letters*, 32(24), November 19, 1987.
39. There are several types of loop equipment that can incorporate this DSLAM. The variants use different protocols for the CO-to-remote-DSLAM link, as well as different capabilities for routing, grooming, and multiplexing functions.
40. DSL Forum Website (http://www.dslforum.org) see pages for VDSL Tutorial, ADSL Tutorial, and Technical Reports.
41. Buckley, Sean, "Telcos enter the video village," *Telecommunications Magazine*, May 29, 2007, and "Parks Associates Predicts 60 Million IPTV Subscribers by 2012," http://www.parksassociates.com.
42. In other markets, the ownership structure can vary, for example, with less or zero shares publicly traded. Ownership, government policies, and even cultural factors can affect long-term strategies and decisions about payback and risk. The NTT group in Japan has invested more in FTTH than any other company. High-count feeder cables, intended to support FTTH were being installed by 2000, and since then NTT has progressed from "media-converter" to EPON, turning up millions of subscribers. The financial reports indicate a long-term vision of FTTH, not plans for short-term (1 3 year) payback. This is consistent with policy-makers' statements in Japan.
43. The FTTP or FTTB subscribers that sign up after 2006 will include many that are upgrading to faster service from CO-ADSL. The number of subscribers converting from dial-up modems and the number of first-time broadband subscribers will be smaller percentages. This trend already has affected the growth of CO-ADSL lines the number of new CO-ADSL lines added each year. In 2 3 years, in 2009 or 2010, the FTTx upgrades may start to erode the installed base (the cumulative number after churn) of CO-ADSL.
44. Verizon Communications, Inc., FiOS Briefing Session, September 27, 2006.x

12

Metro networks: Services and technologies

Loukas Paraschis[*], Ori Gerstel[*], and Michael Y. Frankel[†]

[*]*Cisco Systems, San Jose, CA, USA*
[†]*CTO Office, Ciena, Linthicum, MD, USA*

Abstract

This chapter summarizes the innovation in network architectures and optical transport that has enabled metropolitan networks to meet the diverse service needs of enterprise and residential applications, and cost effectively scale to hundreds of Gb/s of capacity, and hundreds of kilometers of reach. A converged metro network, where IP/Ethernet services and traditional time division multiplexed (TDM) traffic operate over a common intelligent wavelength division multiplexed (WDM) transport layer, has become the most appropriate architecture for significantly reduced network operational cost. At the same time, advanced technology, and system level intelligence have improved the deployment and manageability of WDM transport. The most important application drivers, system advancements, and associated technology innovations in metropolitan optical networks are being reviewed.

12.1 INTRODUCTION AND DEFINITIONS

This chapter discusses the evolution of optical metropolitan networks. We start from the evolution of services over the past several years and next few years, and drill down into increasing details about the implementation of the solution. To understand why the network is evolving the way it is and how it will continue to

Optical Fiber Telecommunications V B: Systems and Networks

ISBN: 978 0 12 374172 1

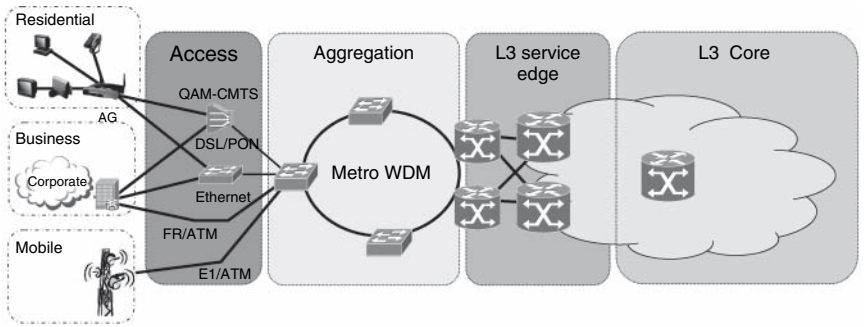

L0–L1	SONET, CWDM	CWDM, DWDM, OTN	N/A	DWDM, OTN
L2–L3	Ethernet	Ethernet, IP, MPLS	IP, MPLS	IP, MPLS

Figure 12.1 Context for metro networking within the entire network and technologies typically deployed (this figure may be seen in color on the included CD ROM).

evolve, one has to first understand how services are evolving from simple point-to-point transport services to sophisticated packet services for video and other applications. This is covered in Section 12.2. The services, in turn, drive the architecture of the entire network, and this is covered in the Section 12.3. Once the architecture is defined, we are ready to delve into the implications of the architecture on the physical layer as described in the Section 12.4, while Section 12.5 discusses network automation tools required for successful design, deployment, and operation. We summarize the chapter in Section 12.6 and provide an outlook into the future of the network in Section 12.7.

Figure 12.1 depicts several network layers based on their packet functionality: access to customers, aggregation of traffic from various access points into larger central offices, the edge of the packet layer, and the core of the network. The table below the figure represents the most common technologies per layer, from a transport perspective (L0 L1 typically) and a packet perspective (L2 L3). A different segmentation is mostly based on geographical reach: access, metro, regional, and long-haul networks. While aggregation networks often correspond to metro/regional networks and core networks are often long-haul, this is not always the case: regional service providers (SPs) often run a metro core network, and access networks in sparsely populated areas often cover regional distances. In the rest of the section, we focus on the geographic segmentation as we find it more meaningful for dense wavelength-division multiplexing (DWDM) technology.

Access networks are typically classified by reaches below 50 km. Access networks are commonly deployed in a ring-based architecture to provide protection against fiber cuts, and are historically SONET/SDH (Synchronous Optical NETwork/Synchronous digital hierarchy), and more recently coarse

wavelength-division multiplexed (CWDM) systems. A 10-nm spacing of channel wavelengths in a CWDM system drives down the cost of pluggable transceivers by eliminating component cooling requirements, and simplifies optical filter design and manufacture. These systems also tend not to have optical amplification. Optical channel data rates in the access network today are predominantly at or below 2.48 Gb/s, with 4 and 10 Gb/s gaining some recent deployments.

Metro systems may be classified by reaches typically below ~300 km, with currently typical node traffic capacities of one to several 10's Gb/s. Given the reach, number of nodes and optical add/drop granularity, Metro networks are typically equipped with optical amplifiers and support DWDM with wavelength channel spacing of 0.8 nm (100 GHz). The lasers now require cooling, but can still be operated without active wavelength locking. The majority of channels in deployment operate at 2.48 Gb/s, but 10-Gb/s data rates are gaining in market share, and higher data rates are starting to see some spot deployments.

Regional systems are classified by reaches on the order of 600 km and below, and long haul is anything above 600 km. Traffic capacities are on the order of multiple 100's of Gb/s. These networks are always equipped with optical amplifiers. Data rates of 10 Gb/s are prevalent for these systems, with channel spacing as low as 0.2 nm (25 GHz), though 0.4 nm (50 GHz) is much more widely deployed. Active wavelength locking is mandatory for such tight channel spacing, with data rates of 40 Gb/s seeing deployments, and 100 Gb/s being pursued within standards bodies and industry development groups.

12.2 METRO NETWORK APPLICATIONS AND SERVICES

SPs have traditionally relied on different networks to address different consumer and enterprise market needs. POTS, TDM/PSTN, and to some extend ISDN, have typically served the voice-dominated consumer applications, while Frame Relay, asynchronous transfer mode (ATM) and TDM leased-line networks have served the more data-intensive enterprise applications. At the same time, video has been mostly distributed on separate, extensively analog, networks. Internet access, while representing a significant departure from the 64-kB/s voice access lines, has been relatively lightly used mainly carrying content limited by human participation such as e-mail and web access. In recent years, the paradigm has undergone a dramatic shift toward streaming and peer-to-peer applications, driving significant growth in the utilization of access lines as well as the core, as it is less dependent on the presence of a human being at the computer to drive the utilization of the network.

Whether the cause is, the spread of cell phones or voice over IP (VoIP), SPs have seen a steady decline in revenues from traditional telephony and a steep increase in voice-originated and other packet traffic. As a result, SPs are trying to find new revenue streams from residential customers via a strategy commonly referred to as

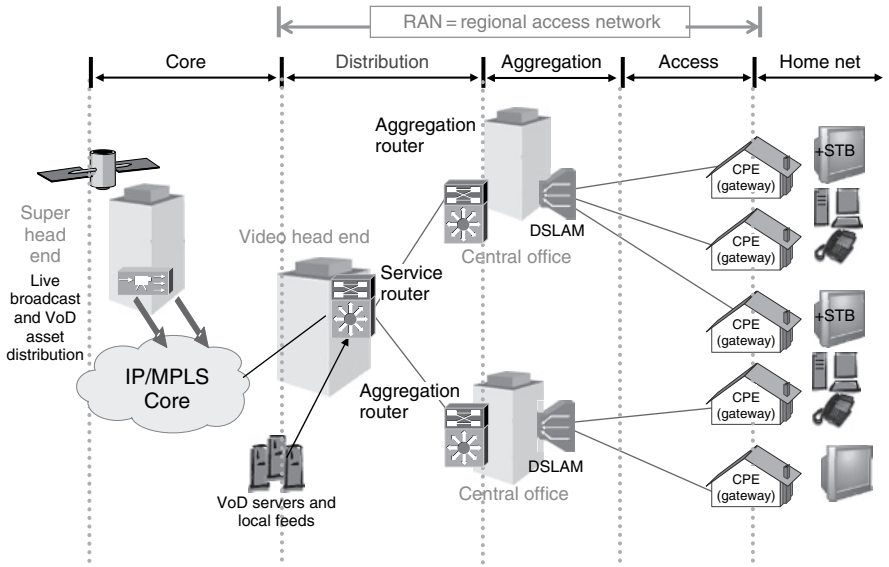

Figure 12.2 Video over broadband architecture overview (this figure may be seen in color on the included CD ROM).

"triple (or even quadruple) play": providing voice, video, and Internet over a common packet infrastructure. This infrastructure requires significant investment in upgrading residential access, as well as back-end systems to create functions and generate content that will increase customer loyalty. The primary example for such applications is video including high-definition broadcast and on-demand content. In an ideal SP world, customers will receive all their video needs from a network that is engineered around video delivery. Such a network is shown in Figure 12.2.

However in many geographic locations, particularly in the USA, SPs are facing tough competition from cable providers, who are much more experienced in delivering video content and are also building their own triple play networks over a coax cable infrastructure that is less bandwidth-constrained than the twisted-pairs SPs own. This, in turn, drives SPs to revamp the actual access medium to fiber (to the home, curb, or neighborhood). Perhaps the most serious competition, for both SPs and cable providers, comes from companies who are providing more innovation over the Internet. These "over-the-top" providers use the high-speed Internet access that is part of triple play to deliver video, music, photo sharing, peer-to-peer, virtual communities, multiparty gaming, and many other services without facing the access infrastructure costs. This competition for the hearts and pockets of consumers is driven by application-level innovation delivered over the Internet Protocol (IP), and therefore the transport network should be optimized for either IP or for Ethernet, which is its closely related lower-layer packet transport mechanism.

Enterprise services are experiencing an equally phenomenal growth. The wide-scale adoption of e-commerce, data warehousing, business continuance, server consolidation, application hosting, and supply chain management applications, has fueled significant bandwidth growth in the enterprise network connectivity and storage needs. The business critical nature of most of these applications also calls for uninterrupted and unconstrained connectivity of employees and customers. To best support this, most enterprises have upgraded their networks, replacing ATM, Frame Relay, and TDM private lines, with a ubiquitous Ethernet (GE and 10 GE) transport. In addition, regulatory requirements in the financial and insurance industries increased significantly the bandwidth needed to support disaster recovery. The large financial firms became the early adopters of enterprise WDM metro networks, driven by the need to support very high-bandwidth storage applications for disaster recovery such as asynchronous and synchronous data replication over metro/regional distances. An overview of storage-related services can be found in Figure 12.3.

To increase the value of the service and the resulting revenue per bit, carriers are looking for ways to provide higher level connectivity beyond simple point-to-point connections between a pair of Ethernet ports. This includes multiplexed services in which multiple services may be delivered over the same port distinguished by a "virtual LAN" (VLAN) tag, and handled differently inside the network. It also includes point-to-multipoint and even multipoint-to-multipoint services, in which the network appears to the user switches and routers as a distributed Ethernet switch. These services are realized via various Layer 2 and even Layer 3 mechanisms. A summary of the various Metro Ethernet services can be found in Figure 12.4.

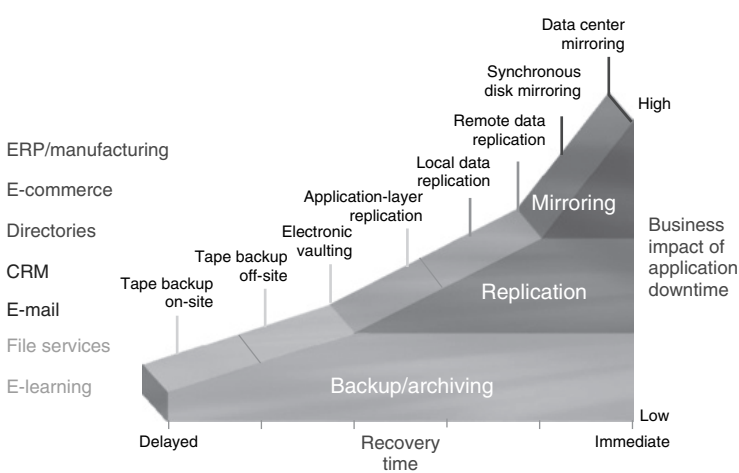

Figure 12.3 Mapping business continuance solutions (this figure may be seen in color on the included CD ROM).

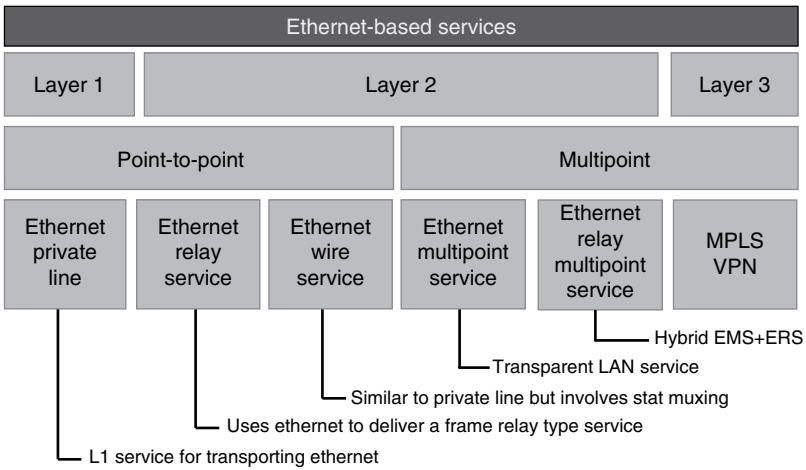

Figure 12.4 Overview of Ethernet based services (this figure may be seen in color on the included CD ROM).

12.3 EVOLUTION OF METRO NETWORK ARCHITECTURES

12.3.1 Network Architecture Drivers

In an environment of an ever increasing richness of services, at progressively higher bit rates, but with a price point that must grow slower (or even decline) than their required bandwidth, service providers must build very efficient networks with the lowest possible Capital expenditure (CAPEX), as well as low operational costs (OPEX).

CAPEX can be optimized by the following means:

- Allowing for as much bandwidth oversubscription as possible, while still respecting the quality of service (QoS) customers are expecting. This cannot be achieved by connections with fixed preallocated bandwidth such as SONET private lines, and drives toward the adoption of packet technologies in the access and aggregation layers,
- Convergence of multiple per-service layers into a unified network. This allows for a better utilization of the network and for better economies of scale, as bandwidth can freely move from one application to another,
- Service flexibility. As new services are introduced, the existing infrastructure must be able to support them, even when the service deviates from the original design of the network.

- Hardware modularity. Hardware must be designed and deployed in a manner that can accept new technologies as they become available, without requiring complete new overbuilds.

OPEX can be optimized by the following means:

- Convergence of layers also helps reduce OPEX as operators do not have to be trained on diverse network elements and distinctive network management capabilities, but rather on one technology. This also allows for more efficient use of the resources as the same operators can work across the entire network instead of working in a "silo" dedicated to one service.
- Increasing the level of automation. Yesterday's transport systems required manual intervention for any change in connection bandwidth and endpoints. Moving to a network that adapts automatically to changes in traffic pattern and bandwidth allow reduction in manual work and cost.

Another related consideration is a barrier to entry and speed of deployment of a new service. Clearly new services will be introduced at an ever increasing rate, sometimes without a clear understanding of their commercial viability. Therefore, it is critical that they can be introduced with minor changes to the existing gear, without requiring a large capital and operational investment that goes with a new infrastructure. This can only be achieved with a converged network that is flexible enough.

So how does a carrier meet these requirements? By converging on a small number of very flexible and cost effective network technologies. Specifically, the following technologies have a good track record of meeting these needs:

- DWDM transport: since photonic systems are less sensitive to protocol, format, and even bit rate, they are able to meet diverse needs over the same fiber infrastructure with tremendous scaling properties,
- Optical transport network (OTN) standard describes a digital wrapper technology for providing a unified way to transport both synchronous (i.e., SONET, SDH) and asynchronous (i.e., Ethernet) protocols, and provide a unified way to manage a diverse services infrastructure [1, 2].
- Ethernet: this technology has morphed over a large number of years to support Enterprise services as well as effective transport for TCP/IP, predominantly in metro aggregation networks,
- TCP/IP: has proven resilient to the mind-boggling changes that the Internet has gone through, and is the basis for much of the application level innovation.

Metropolitan area networks (MANs) have been the most appropriate initial convergence points for multiservice architectures. The significant growth of applications with extensive metropolitan networking requirements has placed increased

emphasis on the scalability of multiservice MANs [3]. MAN architecture has thus evolved; Internetworking multiple "access" traffic-collector fiber rings in "logical" star or mesh, through a larger "regional" network [4, 5]. A converged metro network architecture of Ethernet/IP and high-speed OTN services operating over a common intelligent WDM layer, reduces CAPEX, and even more importantly OPEX, by enabling easier deployment and manageability of services.

12.3.2 Metro Optical Transport Convergence

WDM has been acknowledged early as the most promising technology for scalable metro networks [5, 6]. Its initial deployment, however, remained rather limited, addressing mostly fiber exhaust applications. Metro optical transport is particularly sensitive to the initial cost of the deployed systems, and the CAPEX cost of WDM technologies had been prohibitively high. Attempts to control CAPEX through the use of systems with coarse WDM channel spacing (i.e., 10 or 20 nm) has met with only limited success, as system costs are still set by the transponders, and total unregenerated optical reach and total system capacity is limited. Attempts to increase system capacity by introducing denser channel spacing (i.e., DWDM with 100 GHz spacing) while still avoiding expensive optical amplifiers, resulted in systems with a severe limitation on the number of accessible nodes and total reach.

However, metro networks have critical requirements for service flexibility, and operational simplicity. Moreover, metro WDM cost has to account not only for a fully deployed network, but also for its ability to scale with the amount of deployed bandwidth; as most metro networks do not employ all (or most) WDM channels at the initial deployment phase, but rather "light" unused channels only when actually needed to serve (often unpredictable) network growth. As a result, network operators delayed WDM deployment in their metro networks until these problems were solved with mature technologies from a stable supply base.

At the same time, the evolution of the SONET/SDH transport standards, enabled a successful generation of systems that supported efficient bandwidth provisioning, addressing most of the initial MAN needs, leveraging the advancements in electronics, and 2.5-Gb/s (STM-16) and 10-Gb/s transport (STM-64) [7]. These "next-generation" SONET/SDH systems further allowed improved packet-based transport over the existing time-division multiplexed (TDM) infrastructure, based on data encapsulation and transport protocols (GFP, VCAT, LCAS). Packet-aware service provisioning enabled Ethernet "virtual" private network (VPN) over a common service provider MAN. The initial rate-limited best-effort Ethernet service architectures, evolved to offer QoS guarantees for Ethernet, as well as IP services (like VOIP), and packet-aware ring architecture, like the resilient packet ring (RPR) IEEE 802.17 standard, provided bandwidth spatial reuse. Such Layer-2, and eventually Layer-3, intelligent multiservice provisioning has enabled significant statistical multiplexing gains, enhancing network scalability. The table

illustrates an example of a network with VC-4 granularity that serves a VPN with 4 gigabit Ethernet (GE) sites, six additional point-to-point GE connections, and a storage area network with 2 GE and two fiber channel (FC) services. A "purely" optical solution would require at least six STM-64 rings that, even after leveraging VCAT, would be at least 75% full. An advanced multilayer implementation that employs packet level aggregation and QoS in conjunction with VCAT (ML + VCAT) could be based on just four STM-64 rings, each with less than 40% of capacity utilization, saving more than 50% in network capacity. This new generation of multiservice platforms allowed, for the first time, different services to be deployed over a common network infrastructure, instead of separate networks, improving network operations.

	Required VC4:	
VCAT Only		ML + VCAT
91	Ring 1	30
84	Ring 2	30
49	Ring 3	26
21	Ring 4	8
245	Total VC4	94
(6) 75% full	STM64 Rings	(4) 40% full

As traffic needs grew beyond 10 Gb/s per fiber, however, WDM transport became the best alternative for network scalability. To this end, multi-service systems evolved to "incorporate" WDM interfaces that connect them directly onto metro fibers, thus eliminating client optoelectronic (OEO) conversions and costs. The integration of WDM interfaces in the service platforms also changed the traditional "service demarcation point" in the network architecture. This seemingly straightforward convergence of the transport and service layers has introduced additional requirements for improved manageability in the WDM transport. The introduction of many different "wavelength services" amplified the value for "open" WDM architectures that provide robust and flexible transport. In this sense, a converged, flexible WDM metro transport architecture that supports all the different services with the lowest possible OPEX, leveraging elaborate planning and operational tools, and enabling standards-based interoperability, has become increasingly important.

A related but somewhat opposite trend is the integration of increased service layer functionality into the DWDM layer: as packet processors and other service handling mechanisms have become more compact and less expensive, transponders in the DWDM system are no longer restricted to converting client signals to WDM, but have taken on the task of multiplexing services into a wavelength, switching these services to their destination potentially adding new services along the path, and the related management and control functions. Thus, ADM,

MSPP and Ethernet switch platforms "on a blade" have been introduced, replacing small ADMs and small Ethernet switches that would be managed separately from the DWDM layer by devices that are fully integrated into the DWDM layer. These devices typically have only a few WDM interfaces and are limited in size, and they can be logically interconnected in rings over the WDM layer. An example of such a device and its usage in the network can be found in Figure 12.5.

Figure 12.5(a)shows a conceptual drawing of a DWDM shelf with 3 ADM on a blade cards, each terminating a number of client interfaces and a single WDM wavelength each. These concepts hold for Ethernet-based cards as well.

Figure 12.5(b)shows a typical use of these cards on a physical ring topology. Each rectangle represents an ADM on a blade card and the color codes represent rings of ADMs on a blade. In some cases, these cards are concatenated in the same site to terminate a higher amount of traffic.

Figure 12.5(c) shows how these cards can be deployed over a physical mesh topology.

Another example is fiber channel (FC) "port extenders" which adapt FC over long distances by "spoofing" acknowledgements from the remote device toward the local device, thereby allowing the local device to increase its throughput without waiting a round trip delay for the remote device to acknowledge the

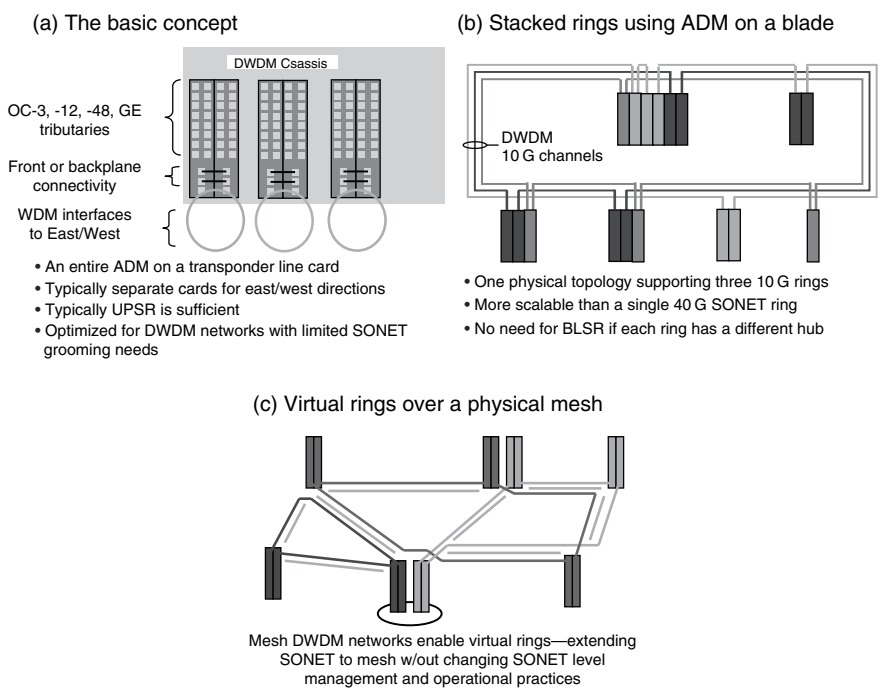

Figure 12.5 The ADM on a blade concept (this figure may be seen in color on the included CD ROM).

messages. Another value such devices provide is that they give the SP visibility into application level issues and therefore enhance the SPs ability to troubleshoot the system.

Eventually, a new generation of metro-optimized WDM transport (often referred to as multiservice transport platforms or MSTPs) has contributed significantly to the recent progress in MAN WDM deployments. This WDM transport enables elaborate optical add drop multiplexing (OADM) architectures that transparently interconnect the different MAN nodes. Moreover, such MSTP WDM systems have scaled cost-effectively to hundreds of Gb/s, and to hundreds of kilometers, and have significantly enhanced ease of deployment and operation, by automated control and integrated management of the optical transport layer [8].

12.3.3 Network Survivability

Due to the critical nature and volume of information carried over the network, carriers must ensure that network failures do not result in a loss of customer data. There are a number of schemes that may be implemented, with a general characteristic of providing redundancy in physical transmission route and equipment. At a high level there are two approaches to survivability: (1) protection in the optical layer and (2) protection in the client layer. While optical layer protection provides lower cost, it does not protect against all failures and cannot differentiate between traffic that requires protection and traffic that does not. Therefore, typically, intelligent clients such as routers are in charge of protecting their own traffic over unprotected wavelengths, while less intelligent clients rely on optical layer protection. In the rest of this section, we first focus on optical layer protection and then move to client layer protection.

A common optical layer protection scheme arranges nodes into a physical ring topology, such that a connection between any pair of nodes can take one of two possible physical routes. Should one physical routes experience a breakdown in fiber or equipment, an automatic protection switch (APS) is executed.

Figure 12.6 shows a four-node ring arrangement that is used to clarify various protection schemes encountered in metro networks, i.e., ULSR, UPSR, BLSR, BPSR. First letter indicates data flow direction around the ring, such that Unidirectional (U) implies that Node 1 communicates to Node 2 in a clockwise (CW) direction, and Node 2 also communicates to Node 1 in the same CW direction passing via Nodes 3 and 4. In this case, the counter-clockwise (CCW) direction serves a protection function. Bidirectional (B) implies that Node 1 communicates to Node 2 in a CW direction, while Node 2 communicates to Node 1 in a CCW direction. In this case, the other ring portion serves a protection function. Second letter refers to the whether protection is done at a Line (L) or Path (P) level. SR refers to the basic switched-ring network architecture.

While the terminology varies, the above schemes are generally applicable to both SONET/SDH, DWDM, and optical transport network (OTN) protection (see

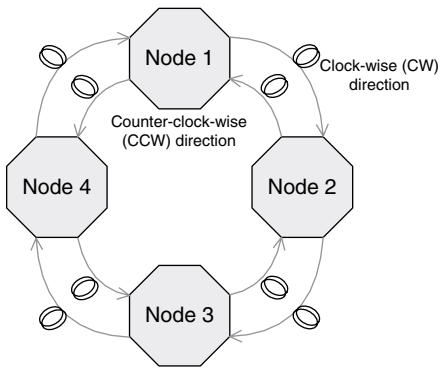

Figure 12.6 Two fiber (2F) optical ring architecture (this figure may be seen in color on the included CD ROM).

G.872). The scheme deployed vary based on ease of implementation and changes in demand patterns: in SONET/SDH networks, the most common protection is UPSR followed by BLSR for some core networks. In the DWDM layer, simple $1+1$ protection is typically implemented, which is equivalent to BPSR in the above notation.

It should be noted that the outlined protection approach inherently doubles the overall network bandwidth requirements relative to actual demand load. Unidirectional case allocates one fiber fully to work data, and one to protection data; bidirectional case allocates each fiber's bandwidth to work/protect in a 50%/50% split.

Figure 12.6 provides a very high-level view of the metro network ring architecture. Actual protection switching within a node can also be done in many different ways. For example, Figure 12.7 shows a few that see common implementation, in a general order of increasing cost. Figure 12.7(b) shows an implementation that protects against fiber cuts only, but minimizes hardware requirements. Figure 12.7(c) shows an implementation that both protects against fiber cuts and provides transport hardware redundancy, but requires only a single connection to the client equipment. Finally, Figure 12.7(d) shows that protection may be implemented at the electronic router/switch level, while increasing the required size of the electronic fabrics. All of these approaches fall into a general category of $1+1$ protection schemes, i.e., each work demand has a dedicated corresponding protection demand through a geographically disjoint route, and all approaches are capable of providing protection within a 50-ms SONET/SDH requirement.

All of the above approaches require an effective doubling of the network capacity, while providing protection only against a single route failure. The demands placed on the networks continue to grow in geographic extent, number of interconnected nodes, and in an overall network demand load [9]. As the size grows, a single ring implementation may not be practical from reliability and bandwidth capacity perspectives. The network may still be partitioned into a set of

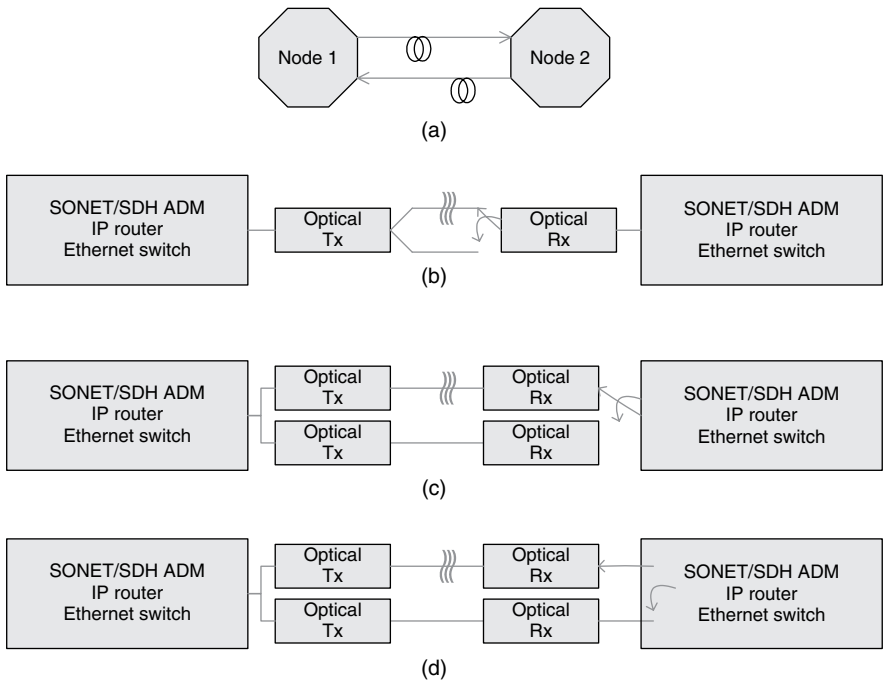

Figure 12.7 Protection switch options within a Node: (a) Generic node 2F connection, (b) Line side optical switch, (c) client side optical switch, (d) Line Terminating equipment switch (this figure may be seen in color on the included CD ROM).

ring connections, with ring-to-ring interconnections. A single ring-to-ring connection will look like a single point of failure in a network, and rings may need to be joined at multiple points: physically the network starts to look like a mesh arrangement of nodes, as shown in Figure 12.8.

The rich physical connectivity of a mesh network is obvious as a node-to-node demand connection may take many diverse routes through the network. This diverse connectivity offers an opportunity to significantly improve network's utilization efficiency. Recall that a fully protected ring-based network required dedicated doubling of its capacity relative to the actual bandwidth. A shared protection scheme allocates protection only after a failure has occurred. Thus, assuming that a network suffers only a small number of simultaneous failures, and that a rich physical network connectivity affords several route choices for the protection capacity, each optical route needs to carry only an incremental amount of excess protection bandwidth [10, 11] reduced by a factor of $1/(d\text{-}1)$, where d is the average number of diverse routes connected to nodes. In addition to reduced cost, another benefit of this approach is an ability to gracefully handle multiple network failures. The actual capacity is consumed only after a failure is detected. However, the trade-off is a substantially more complicated restoration algorithm

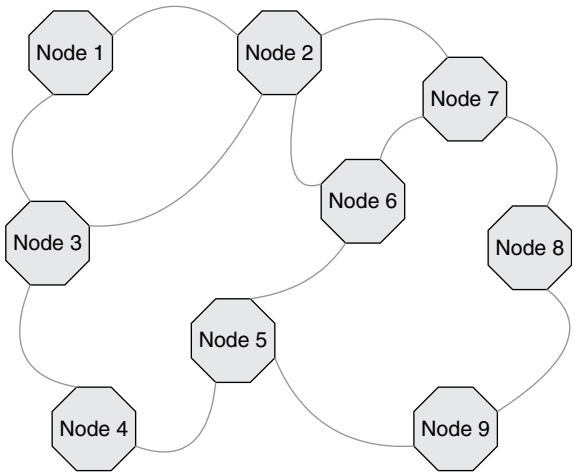

Figure 12.8 Network with a large number of interconnected nodes takes on a "mesh" appearance (this figure may be seen in color on the included CD ROM).

that now requires both network resources and time to compute and configure a protection route [12]. Further, re-routing is done via electronic layer, not optical one, given today's status of optical technology.

As the service layer moves to packet-based devices, new protection mechanisms are being considered. Examples include MPLS fast reroute (FRR), RPR, as well as Ethernet convergence. Out of these mechanisms, RPR is the closest to SONET protection, in that it is mainly confined to rings and loops around the ring in the event of a failure. However, since RPR uses statistical multiplexing, it is able to drop traffic that has low priority depending on the actual amount of high priority traffic currently in the network, whereas the optical layer was limited to protecting the total working bandwidth irrespective of the actual usage of the bandwidth. This added flexibility allows SPs to offer a large number of services, while with SONET the only service that was available was a fully protected service (99.999%). It is worth noting that some SPs tried to also offer a preemptible service using protection bandwidth in SONET, but since this bandwidth was frequently preempted, the service was only useful for niche applications.

MPLS offers a more flexible mechanism that is not restricted to rings, based on a working path and a predefined protection path. Again, thanks to statistical multiplexing, the bandwidth along the protection path does not have to be reserved to a particular working connection, but rather is used by the traffic that requires protection based on priorities. While the packet level mechanism is simple, this scheme does require planning to ensure protection bandwidth is not oversubscribed to a point that the service level agreement cannot be guaranteed.

Finally, Ethernet also offers a convergence mechanism that ensures packet can be forwarded along a new spanning tree should the original spanning tree fail. However, this mechanism is typically slow and does not scale to larger networks.

Given these protection mechanisms, what is the role of the WDM layer in protecting traffic? Quite a bit of research has been performed on how WDM protection can coexist with service layer protection and how the layers coordinate and benefit from the respective protection mechanisms [13, 14]. However in reality, most SPs prefer to keep protection to one layer for simplicity. Naturally, when protection does exist in the service layer, it is more beneficial to use it, as it covers failure modes that are unrecoverable in the optical layer (such as an interface failing on the service box). As discussed, often times service level protection is more efficient driving to an overall lower cost of protection even as service layer equipment is more expensive than WDM equipment [15]. This leaves narrow room for protection at the WDM layer: typically for point-to-point applications that do not have their own protection mechanism, such as SAN applications.

12.4 WDM NETWORK PHYSICAL BUILDING BLOCKS

12.4.1 Client Service Interfaces

Metro networks generally see traffic that has already gone through several levels of aggregation multiplexing, and equipment interconnections are done at 1-Gb/s data rate and above. By definition, these are meant to connect equipment from a wide variety of manufacturers, and several international standards (as well as industry-wide Multi-Sources Agreements) have been developed [16, 17] that cover optical, mechanical, electrical, thermal, etc. aspects. Given the required high data rate and the physical connectivity length, metro equipment client interconnections are almost exclusively optical.

Early systems had interface hardware built from discrete components. A highly beneficial aspect of developing and adhering to standards is an ability of multiple vendors to provide competitive interchangeable solutions. Over the last several years, the optoelectronics industry has seen a tremendous amount of client interface development, and a near complete transition from custom-made interfaces to multi-sourced, hot-pluggable modules. The interfaces have evolved [18] from GBICs offered at 1-Gb/s data rate [19] to SFP for multirate application up to 2.5-Gb/s data rate [20] to XFP at 10 Gb/s [21]. The economics of manufacturing are such that it is frequently simpler to produce a more sophisticated component and use it across multiple applications. Further, providing a single electrical socket on the equipment allows the interfaces to be reconfigured simply by plugging in a different client module, with same interfaces being able to support SONET/SDH, Ethernet, FC, etc. applications. Figure 12.9 shows a comparison of relative physical form factors for a variety of pluggable interfaces targeting 10-Gb/s data rate, and the rapid relative size reduction over the course of a few years.

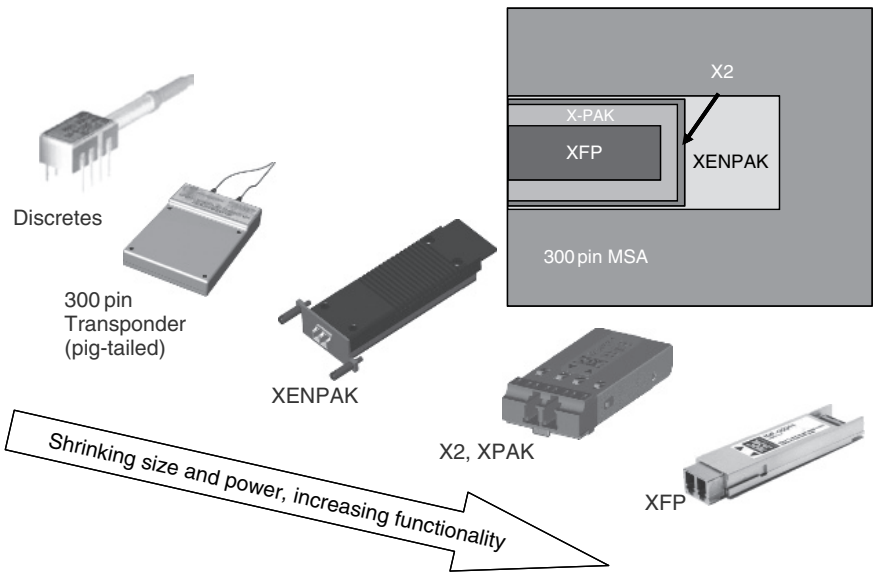

Figure 12.9 Evolution of client size interface form factors (this figure may be seen in color on the included CD ROM).

12.4.2 WDM Network-Side Optical Interfaces

The requirements on the WDM (network-side) of the optical system are more stringent than on the client interfaces. While client interfaces need connectivity over a relatively short distances, with 90% falling within 10-km distance, network side interfaces need to cover distances of hundreds of km and many demands are multiplexed on the same fiber using WDM.

The optical wavelength of client side interfaces has a wide tolerance range and uncooled lasers are most often used. The WDM side, due to multichannel requirement, has lagged the client side interface in size development. Initial network side pluggable modules were developed in GBIC form-factor for 2.5-Gb/s application, and used uncooled lasers for CWDM with relaxed 10 nm wave separation. More recently, 2.5-Gb/s interfaces with DWDM (100-GHz) channel spacing were implemented in SFP form factor, too. As networks evolved to support higher bandwidth services, 10 Gb/s network side interfaces were implemented in 300-pin MSA form factors [22]. Subsequently, MSA modules evolved to support 50-GHz channel spacing with full tunability across all C-band wavelengths. Tunable laser technologies have being increasingly employed in Metro WDM systems to reduce inventory cost, and improve operations [16]. The choice of the appropriate transmitter technology is particularly important, as its cost usually dominates the total cost of a fully deployed transport system [23]. At the same time, much smaller XFP

packages supporting 10-Gb/s WDM interface at 100-GHz channel spacing were developed using lasers without wavelength locking. Such next-generation pluggable transmitters are very important, not only for their enhanced performance or lower cost, but also for more easily integrating into the different service platforms further simplifying the network architecture and thus reducing the overall network cost. At such high data rates, however, optical performance, predominantly dispersion-tolerant (chirp-minimized) modulation, becomes also important. Current development efforts are pursing fully C-band tunable 50-GHz WDM interfaces in XFP form factor. Higher data rate 40-Gb/s interfaces currently require a larger package, but are following the same general trajectory of rapidly decreasing size and increasing capability.

In addition to the extremely rapid advances in the optical technology developments, electronics technology is also providing increased performance, and reduced size and power consumption. Of particular interest are the field programmable gate array (FPGA) technology and the FEC technology. Metro networks are generally called on to support a rich variety of services, such as SONET/SDH, Ethernet, and FC. The protocols and framing formats, overhead, and performance monitoring parameters are very different, while intrinsic data rates may be quite close. Since client interfaces are pluggable, it is highly desirable to provide a software-configurable, flexible electrical processing interface such that a single hardware circuit pack can be field-reconfigured to support different services. FPGA elegantly fulfills such a role, providing high gate count, and low-power and high-speed capability with 65-nm CMOS geometries available in 2007, and 45-nm CMOS geometries expected to be available in 2009 2010 time frame. At the same time, FEC and increasingly enhanced FEC enable much more flexible transmission performance.

12.4.3 Modulation Formats for Metro Networks

Non-return-to-zero on-off keying (NRZ-OOK) is arguably the simplest modulation format to implement for WDM network signal transmission. NRZ-OOK is the format with the widest deployed base of commercial systems, given that excellent propagation characteristics can be achieved with quality implementations having good control over rise/fall times, limited waveform distortions, and high optical extinction ratio. The longer (300 km) demand reach requirements imply that both fiber dispersion and loss become quite important. The intrinsic dispersion tolerance is determined by the modulation format and data rate. For example, NRZ-OOK at 2.5 Gb/s has an intrinsic dispersion tolerance of $\sim$17,000 ps/nm, corresponding to $\sim$1000 km of NDSF fiber. The fact that this is well above reach "sufficiency" for Metro networks permits an engineering trade for a lower-cost, lower-quality implementation. Relaxing transmitter chirp control can lower costs substantially, while still allowing for a dispersion tolerance in 1600-ps/nm to 2400-ps/nm range (i.e., 140 km of NDSF fiber).

Intrinsic optical transceiver characteristics are set by launch power, dispersion tolerance, receiver sensitivity and ASE tolerance. A network must satisfy this multi-dimensional demand simultaneously and preferably with a single modular implementation. Metro networks geographic characteristics and traffic demands cover a broad range from a few tens of kilometers up to 200 km. Such wide range of networks implies that there is no generic target characteristics: networks may be limited by any combination of the above mechanisms, depending on demand reach length, number of nodes, fiber characteristics, etc. Even within the same network some demands may be power-limited, while others may be limited by dispersion, while others may be limited by ASE noise. A desire to minimized network hardware costs, while still supporting the demands, poses a challenging optimization problem.

Unamplified links have two dominant limiting characteristics, and performance is typically expressed in terms of receiver power penalty as a function of dispersion. Noise determined by receiver electronics is independent of input signal power, and affects both "0" and "1" signal levels equally. System performance must be kept above a threshold line defined by a minimum receiver power required to achieve desired bit error rate (BER) performance at a set dispersion. Optically amplified system noise is primarily determined by the beating between signal and ASE components, and impacts primarily "1" level for OOK modulation formats [24, 25]. Its functional form is different from a direct power penalty, and systems need to consider three characteristics: received power, dispersion and OSNR. Amplified systems performance can be expressed in terms of two-dimensional power and dispersion surface, and shown as a target OSNR required to achieve a certain BER, with an example shown in Figure 12.10.

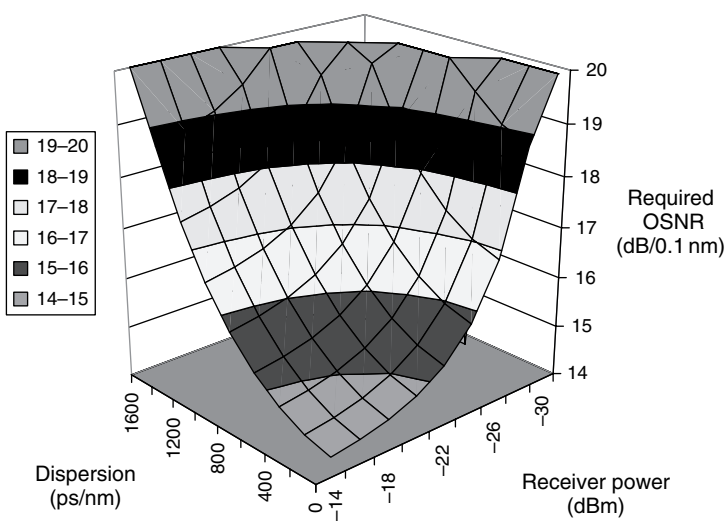

Figure 12.10 Target OSNR required to achieve a BER $\sim 10^{-7}$ for a typical 10 Gb/s NRZ OOK implementation, which assumes a receiver sensitivity of -28 dBm at 10^{-9} BER, and an OSNR sensitivity of 10 dB/0.1 nm at 10^{-3} BER (this figure may be seen in color on the included CD ROM).

Optically amplified, ASE-limited systems exhibit an inverse relationship between required target OSNR and unregenerated optical reach. Thus, a 1-dB increase in required OSNR produces a corresponding reduction in unregenerated reach, and can easily cross the network performance threshold.

12.4.4 Handling Group Velocity Dispersion

As service demands pushed network transport rates to 10 Gb/s, the requirement to cover an identical network geographic extent remained unchanged. Current 10-Gb/s transmission is still most frequently done with NRZ-OOK format, which intrinsic dispersion tolerance is 16 times smaller than equivalent 2.5 Gb/s (i.e., ~1200 ps/nm for unchirped versions). 10-Gb/s data rate crosses the threshold of dispersion tolerance for many Metro networks, and some form of dispersion compensation is required. In-line dispersion compensating fiber (DCF) is the most commonly deployed technology. DCF is very reliable and completely passive, has a spectrally transparent pass band compatible with any format and channel spacing, and can be made to compensate dispersion across the full spectral range for most deployed transmission fiber types. The disadvantages are added insertion loss that is most conveniently "hidden" in the optical amplifier midstage, nonlinear effects requiring controlled optical input power, both of which degrade overall link noise figure. Existing networks cannot be easily retro-fitted with DCFs without significant common equipment disruption.

New ways of handling dispersion based on transponder-based technologies are advantageous for seamless network upgrades. Particularly, transmitter-side modulation formats [26] or receiver-side electronic distortion compensation (EDC) are attractive, if they can be made economically viable. Detailed characteristics and implementations for a variety of modulation formats are described in Chapter 2, and electronic distortion compensation is also described in Chapter 18 of Volume A [27, 28]. However, it is instructive to note some options that have been specifically applied to metro networks: prechirped NRZ-OOK modulation, duobinary modulation, and receiver-side EDC. With both prechirped and duobinary modulation formats optimal dispersion is shifted to higher values, but performance may be degraded for other parameters, such as ASE tolerance or overall dispersion window. Receiver side equalization, whether electronic or optical, is a technology that introduces additional cost, power consumption, and board space. A decision to use transceiver-based dispersion compensation is not simple or universal, though EDC is finding good adoption especially on the client interfaces.

Modulation formats may mitigate some of the dispersion problems. However, the desire to upgrade existing field-deployed networks to support higher channel data rates transport is impeded by several considerations: (1) higher rate signals require OSNR increase of 3 dB for each rate doubling (assuming constant format and FEC), (2) receiver optical power sensitivity increasing by 3 dB for each data

rate doubling, (3) dispersion tolerance decreasing by 6 dB for each data rate doubling, (5) in-line optical filtering, and (4) system software upgrades.

12.4.5 Optical Amplifiers

Optical signal loss in metro networks accumulates from three components: transmission fiber, optical components embedded in the frequent add/drop nodes, and passive fiber segment connections. Metro networks are generally deployed in very active environments, and while not very long, they are subject to frequent mechanical disturbances and breaks. Metro network fiber accumulates passive loss due to frequent repairs and splicing.

There are three main optical amplifier choices available for overcoming the loss: erbium-doped fiber amplifier (EDFA), semiconductor optical amplifier (SOA), and Raman amplifier. Of these, EDFA provides a cost-effective solution to overcome loss in the network with good performance. SOA amplifiers have the advantage of wide amplification bandwidth, but have more limited output power, susceptibility to interchannel crosstalk issues, and high noise figure. Distributed Raman amplifiers' primary benefit is in reducing effective amplifier spacing which lowers the overall link noise figure. Metro nodes are already closely spaced and "distributed" benefit is small. Distributed Raman also relies on transmission fiber quality, and passive losses and reflections have a substantially deleterious effect [29], making use of Raman amplifiers in metro quite rare.

Amplifier response to optical transients is as critical a characteristic as gain, noise figure, output power, and spectral flatness. Rich traffic connectivity patterns require a high level of immunity to possible optical breaks. Figure 12.11 shows an

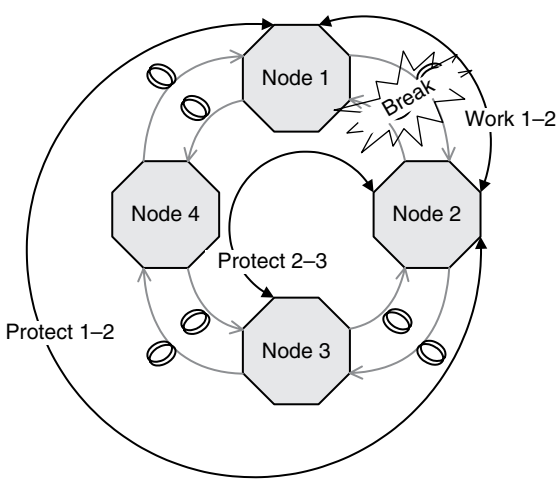

Figure 12.11 Optical interaction between optical work and protect routes (this figure may be seen in color on the included CD ROM).

example whereby a break between Node 1 and Node 2 causes a loss of optical Work 1 2 and Protect 2 3 channels. Protect 2 3 channels are optically coupled to Protect 1 2 channels, and any disruption on Protect 1 2 channels will cause a corresponding loss of connectivity between Node 1 and Node 2.

Table 12.1 below shows a table of typical effects that can lead to EDFA transients and associated time constants. The same physical properties that make EDFA excellent for multichannel transmission with negligible crosstalk also make it hard to suppress optical transients. Techniques based on optical reservoir channels suffer from having to add extra optical hardware, and the fact that EDFA dynamics are spectrally dependent, i.e., loosing channels at short wavelengths does not have the same effect as adding a reservoir channel at long wavelengths. The same is true with gain clamping via lasing [30]. The most cost-effective strategy, and one that has seen actual field deployment, is using optical tap power monitors on the amplifier input and output ports, with electronic feedback to the pump lasers. The electronic feedback loop can be made quite fast, but pump laser electrical bandwidth and intrinsic EDFA gain medium dynamics limit possible control speed. A simple addition of a controlled attenuator is insufficient to guarantee flat spectral output under different channel load.

Figure 12.12 shows an example measurement of an electronically stabilized EDFA amplifier transient response to an optical step function, with step function fall time as the parameter. Several temporal regions can be identified. First, there is an optical power increase due to a redistribution of optical power into surviving channels, with a rise time corresponding to the optical channel power loss fall time. Second, the pump power is rapidly reduced by the electronic feedback control, and the channel power recovers with a time constant set by the control loop dynamics. Third, depending on the parameters of the control loop and their interplay with optical dynamics, there may be some amount of transient undershoot and possibly ringing. Finally, a steady state is reached that is likely to have some finite error in the channel power due to electronic errors, due to finite broadband ASE power, etc.

The transient are shown for a single amplifier, while real systems employ many cascaded amplifiers in a route. Each subsequent amplifier will see not only the

Table 12.1

Table of possible optical transient time constants, in order of increasing speed.

3 mm jacketed fiber slow bending	500 ms
3 mm jacketed fiber caught in shelf cover	100 ms
3 mm jacketed fiber fast bending	7 ms
3 mm jacketed fiber wire stripper cut	5 ms
Connector E2000 fast unplug	2 ms
Bare fiber wire stripper cut	200 µs
Bare fiber knife chop cut	100 µs
Bare fiber (break at splice using tensile force)	2 µs

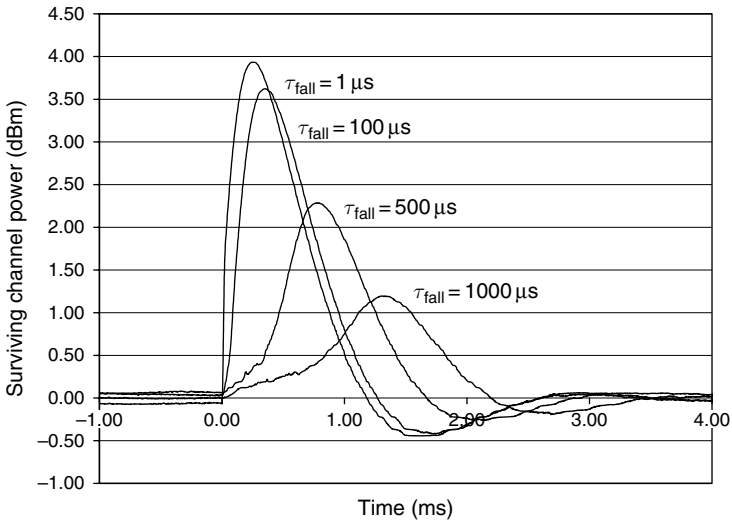

Figure 12.12 Example amplifier optical transient response, with optical channel loss fall time as a parameter.

original step-like loss of the optical signal, but will also experience the accumulated effects of all of the preceding amplifiers. Thus, control loop parameters have to be developed and verified on amplifier cascades, in addition to individual modules [31].

It is fundamentally not possible to completely prevent and eliminate optical transients, and these impact optical channel performance in several ways. Increasing optical power may lead to nonlinear fiber effects and corresponding distortions in the received signal. Low power leads to a decrease in optical SNR. Further, power may exceed the dynamic range of the receivers, and may interact with the dynamic response of the receiver electrical amplification and decision threshold mechanisms. These combined effects may lead to burst errors in the optical channel. Protection switching mechanisms need to be designed with corresponding hold-off times to prevent such events from triggering unnecessary switching.

12.4.6 Optical Add/Drop Nodes

WDM multiplexing and connectivity provides some of the functionality previously supported at the SONET layer, such as multiplexing and circuit provisioning. As discussed previously and shown in Figure 12.11, networks nodes may be arranged on an optical fiber ring. However, demand connections may be such that an optical channel bypasses a node and stays in the optical domain. OADMs accomplish this function. Most of the metro networks were deployed with OADMs implemented with fixed optical spectral filters. The filters are positioned within the optical path

along the ring to both drop and add signals of pre-determined wavelengths. This provides a very cost-effective access to the optical spectrum, minimizes signal insertion loss, and allows for possible wavelength reuse in different segments of the optical ring or mesh network. In a sense, predeployed optical filters associate a specific destination wavelength range address with each node. Optical filters themselves may be based on a wide variety of technologies, and are beyond the scope of this chapter.

Fixed filter based nodes are cost-effective, have low optical loss, and simple to design and deploy. However, they pose an operational challenge due to the intrinsic lack of reconfigurability. Each node must have a predesigned amount of capacity (i.e., wavelength address space) associated with it and cannot be changed without significant traffic interruptions. For example, some portions of the network may experience more than expected capacity growth and may require additional spectral allocations, which would be impossible to achieve without inserting additional filters into the common signal path, thereby interrupting traffic. Others portion of the network may lag expected growth, and will thus strand the bandwidth by removing unused spectrum from being accessible to express paths. Network deployment with fixed filters require significant foresight into the expected capacity growth, and several studies have addressed the question of what happens when actual demands deviate from the expectations [32], with as much as half of the overall network capacity possibly being inaccessible. One of the frequently proposed techniques to overcome such wavelength blocking limits is the use of strategically placed wavelength converters in the network [33, 34], but is quite expensive in terms of additional hardware that must be either predeployed or require as-needed service field trips.

An alternative to deploying wavelength converters is to provide dynamic reconfigurability that is generally associated with electrical switching directly at the optical layer. Developments in optical technology have allowed a new level of functionality to be brought to the OADMs, and fall under a general term of reconfigurable OADM (ROADM). It should be pointed out that while ROADMs substantially reduce wavelength blocking probability [35, 36], they cannot completely eliminate it, especially if all wavelengths remain static after assignment. Some amount of wavelength conversion or dynamic wavelength retuning may be required (see Chapter 8).

A variety of optical ROADM node architectures can be considered, depending on the particular goals of the network designer [37, 38]. These architectures can be subdivided into three broad categories. The first category can be described as a space-switch-based architecture surrounded by MUX/DEMUX elements. An example for a Degree 2 node is shown in Figure 12.13(a). With the current state of the art, the implementation is done with integrated MUX/DEMUX, add/drop switch, and direction-switch elements. The channelized aspect of the architecture introduces optical filtering effects into the express path, thereby limiting bit rate and channel spacing transparency. Increasing the connectivity degree of the node requires a change in the configuration by adding either a new level of integration

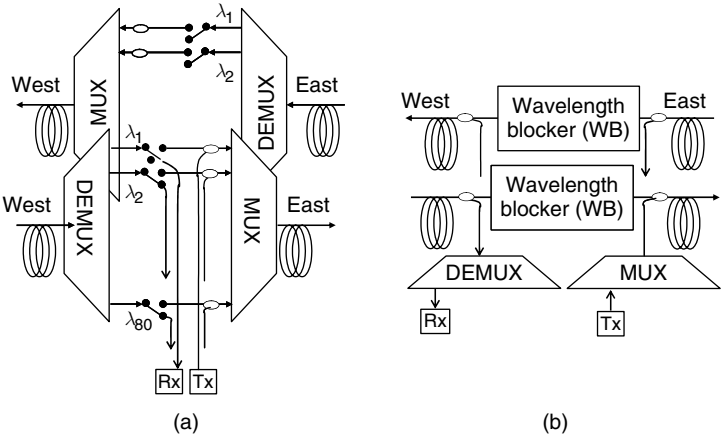

Figure 12.13 (a) Degree 2 space based OADM; (b) Degree 2 broadcast and select OADM.

of additional MUX/DEMUX and switch elements, or externally interconnecting smaller building blocks of Figure 12.13(a) with additional external switching.

The second category can be described as broadcast and select architecture, and is shown in Figure 12.13(b). The architecture relies on an integrated wavelength blocker (WB), which can provide arbitrarily selectable pass and stop bands with continuous spectrum and single-channel resolution. The express path continuous-spectrum attribute reduces channel filtering effects, improves cascadability, and permits a high level of bit rate and channel spacing transparency. One disadvantage of the broadcast and select architecture is its requirement of a separate MUX/DEMUX structure to handle local add/drop traffic, which adds cost and complexity. A second disadvantage is that scaling to a higher Degree N node interconnect requires $N \times (N\ 1)$ WB blocks, with a Degree 4 node requiring 12 WB blocks.

More recently, a third ROADM architecture has been introduced that attempts to combine a high level of integration and express transparency associated with a broadcast and select architecture, with an integrated MUX/DEMUX functionality [39]. The architecture, shown in Figure 12.14, is based on an integrated multi-wavelength, multiport switch (MWS) and is particularly attractive for metro-type applications that are susceptible to frequent traffic and node churn, but have moderate bandwidth requirements. MWS elements have several output ports (in the 4 9 range) and can selectably direct any combination of wavelengths to any output ports. A receiver can be connected directly to the MWS if only a small number of add/drop wavelengths is required, or a second level of DEMUX can be implemented to increase the add/drop capacity. The second level itself can be based on a low-cost fixed architecture, or a more complex wavelength-tunable one.

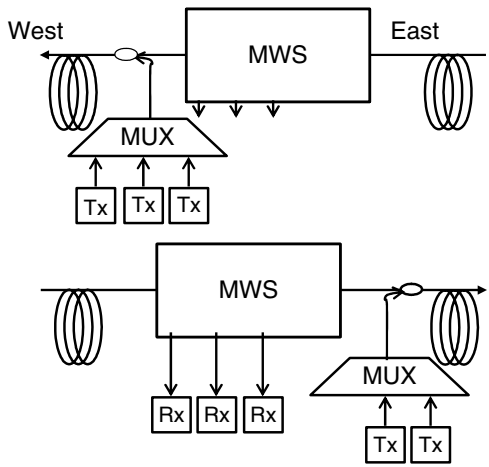

Figure 12.14 Reconfigurable OADM Architecture.

Table 12.2
Comparison of three optical ROADM architectures.

Parameter	Space switched	MWS + MWS DEMUX	MWS + fixed DEMUX
Cost	Independent of # A/D channel	Same up to 8 ch, 5 × at 40 ch	Same up to 8 ch, 2 × at 40 ch
Optical channel monitor	Built in	Usually external	Usually external
Channel power equalization	Yes	Yes	Yes
Multidegree	Highly integration dependent. Difficult in service growth	Up to Degree 8 (in service)	Up to Degree 8 (in service)
0.5 dB passband	~40 GHz	~50 GHz	~50 GHz
Express loss	<12 dB	<13 dB	<13 dB
Flexibility	Add/drop ports have fixed wavelengths	Drop ports are fully tunable. Adds are wavelength independent	Drop ports are commonly fixed wavelengths. Adds are wavelength independent

Table 12.2 shows a comparison table of possible space switch and MWS-based architectures, and associate trade-offs.

Recently, the optoelectronics industry has evolved a new direction toward higher levels of functional integration, which has the potential to reduce the cost

of OE and EO conversion (Chapters 6 and 10 of Volume A). Possible availability of such low-cost optical interface components has prompted a re-evaluation of the existing trade-offs between optical and electrical switching, and proposals for a "Digital ROADM" have been presented (see Chapter 10 of Volume A). A Digital ROADM is more accurately termed a reconfigurable electrical add/drop multiplexer. It is an electrical switching fabric very similar in functionality to the legacy SONET/SDH add/drop Multiplexers or to an Ethernet switch, but updated to operate on signals compliant to the recently developed OTN framing standard. Highly integrated photonics indeed hold a promise of reduced costs; unfortunately, optical interfaces comprise only a small fraction of the overall node cost. The impact of electronically processing every digital bit stream holds both advantages of being able to completely regenerate wavelength signals, monitor bit stream quality, and improve their grooming efficiency, as well as detrimental aspects of substantially increased electronic power consumption and mechanical footprint. Table 12.3 captures the more salient comparison points, and argues that metro networks still preferentially benefit from optical OADM rather than electrical one.

In summary, ROADM has introduced network design flexibility, and automated and scalable link engineering, both critical to the success of metro WDM architectures. Wavelength-level add/drop and pass-through, with automated reconfigurability (ROADM) at each service node, is also only operationally robust solution for WDM deployments that support the uncertain (often unpredictable) future traffic patterns in MANs that scale to hundred of Gb/s. ROADM network flexibility also provides the ability to set up a wavelength connection without visiting any intermediate sites, thus minimizing the risk of erroneous service disruptions during network upgrades. In the context of the present analysis, it is also useful to identify and distinguish between two main functional characteristics of ROADMs at the network level: (1) ROADM solutions allow for switching of each individual wavelength between the WDM ingress and egress, potentially among more that one fiber facility. (2) More elaborate solutions could also allow extraction or insertion of any client interfaces to any wavelength of any fiber. This latter solution has been often proposed, in combination with predeployed tunable transmitters and/or receivers, to realize advanced network automation. Such a network, with the addition of a GMPLS control plane, enables dynamic bandwidth provisioning, and fast shared optical layer mesh protection. Current network deployments, however, are primarily interested in the ROADM functionality and the most cost-effective-related technologies (rather than in the most advanced solution that would meet any conceivable future need, irrespective of price). In this sense, the technologies captured in the above table, are currently the main focus of network deployments, as they have sufficient functionality to meet most customer needs, and are the most mature and thus cost-effective technologies [40].

Table12.3

Comparisons of reconfigurable electrical and optical add/drop nodes.

Parameter	Electrical ADM	Optical ADM
Optical mux/demux	First level external optical Second level integrated within Rx	First level MWS switch Second level fixed filter or MWS
Channel monitor	Full electrical PM	Analog optical wavelength power
Channel regeneration	Yes, but not critical for metro	Only power equalization, OK for metro
Multidegree	Requires highly sophisticated switching fabric with full nonblocking interconnect capability	MWS provide direct degree interconnects, but wavelength blocking may exist
Optical line amps	Requires Rx side and Tx side OLA to deal with MUX/DEMUX loss.	Requires Rx side and Tx side OLA to deal with MUX/DEMUX loss
Per channel power consumption	~50 100 W per 10 Gbps data stream (estimated average from published Ethernet and OTN switch fabrics)	~2.5 W per 10 Gbps wavelength (<100 W for OLA + MWS)
Granularity	Provides subwavelength switching capability	Wavelength level switching capability
Subrate channel flexibility	Subrate channels electrically multiplexed to wavelength	Subrate channels electrically multiplexed to wavelength.
Super rate channels	Must be inverse multiplexed across several wavelengths. For example, 40 Gbps services occupy 4 × 10 Gbps λ's, and may cross integrate part boundary	May be inverse multiplexed. Or may used new modulation format technology for direct transport over existing line system
Total system capacity	Fixed on Day 1 install	Can grow as new XCVR technology is introduced to populate unfilled spectrum, i.e., improved FEC, modulation format, equalization
Relative cost of a high capacity ADM node	Assuming OEO interfaces are low cost, high capacity electrical FEC, framing and switching fabric expected to dominate costs	OEO interfaces maybe relatively higher, but optical switch fabric is much lower cost than comparable electronic one

12.5 NETWORK AUTOMATION

Network design tools are mandatory for proper design, deployment, and operation of an optical WDM network, especially when large degree of reconfigurability is deployed. Network planning process focuses an optimized network design for efficient capacity utilization and optimum network performance for a given service load. Such design and planning tools must combine a set of functions that span multiple layers of the network operation, from a definition of user demands, to service

aggregation and demand routing, and finally to the physical transport layer. Higher (logical) network layers need not worry about the physics of light when calculating paths across a network, with a possible exception of physical latency associated with the connection. However, the physical layer must include important optical propagation effects when deciding demand routing and capacity load attributes.

A typical network design process, graphically illustrated in Figure 12.15, includes several steps. First, a set of "Input" parameters is formed by a combination of logical user service demands and by an abstracted layer describing known physical connectivity and limitations. The inputs may also include a description of existing network configuration, which may be automatically uploaded from field-deployed hardware, or may be a completely new installation. Second, service demands are aggregated into optical wavelengths, considering actual electronic hardware limitations, user-defined constraints, and required network performance. Third, aggregated wavelength demands and a refined definition of the physical layer (i.e., definitions of specific fiber types, lengths, optical losses) are provided as an input to drive physical network design process. The result of this multi-step process is a complete description of the network hardware, with a detailed description of the Bill of Material, deployment process documents and drawings, as well an estimate of the network performance characteristics.

The actual software implementation may partition the overall process into relatively independent modules, with each step performed sequentially. An alternative is to provide coupling between each step to allow a higher level of network optimization and refinement. The software itself may be an off-line design/planning tool driven by a user interested in targeting substantial network configuration

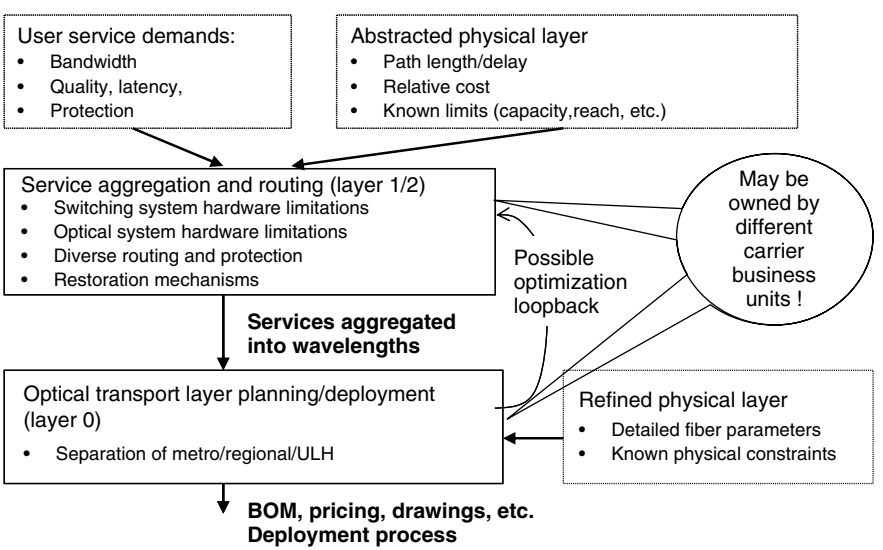

Figure 12.15 Network planning and design process.

changes or upgrades. A similar process and software may also be used for handling new service demand requests that may arrive to the automatically switched optical networks, with the process triggered when a single new service demand arrives to the network and must be satisfied within the shortest amount of time and within constraints of null or minimal hardware change.

The geography of the metro networks is frequently characterized by a wide variability in traffic-generating node separation, which may range from sub-km range for nearly co-located customers to 100 km, and possibly longer. Premise space and power availability, traffic add/drop capacity requirements are also quite variable. Networks with such diversity benefit from a highly modular system transmission design, whereby components such as add/drop filters, optical amplifiers, dispersion compensation modules, and other signal conditioning elements are independent of each other and are deployed on as needed basis. Especially considering the case of closely spaced nodes, the decision to deploy optical amplifiers and dispersion compensation modules cannot be made based on a purely "local, nearest node" basis. The presence of optically transparent degree 3 and higher nodes complicate the configuration process even further by optically coupling multiple network segments and even coupling directions. For example, a purely linear bidirectional system has independent optical propagation for the individual directions. However, a T-branch network geometry couples East-to-West and West-to-East directions, since both share a common Southbound path. The configuration and optimization of such networks cannot be made based on simplified engineering rules in networks that are mostly focused on the cost of the solution. Fortunately, the field of optimization algorithms is very advanced [41] and can be leveraged directly to solving the network problem. The algorithms may be additionally fine-tuned to target specific carrier requirements, such as preferentially focusing on lowest initial cost, highest network flexibility, best capacity scalability, or some other parameters defined by the carrier.

The operational aspects of reconfigurable optical networks require that same algorithms used for network design and planning be applied in-service. Whenever a network receives a new demand request, it must rapidly assess its current operational state and equipment availability, determine if the requested demand can be satisfied either directly or with some dynamic reconfiguration, and consider both logical connectivity and physical layer impairments with the newly proposed wavelength assignment and routing. This is a nontrivial problem requiring a large number of complex computations in near real time, and is currently seeing increasing research interest [42].

12.6 SUMMARY

In this chapter, we discussed innovations in network architectures and optical transport that enable metropolitan networks to cost-effectively scale to hundreds Gb/s of capacity, and to hundreds of kilometers of reach, meeting the diverse

service needs of enterprise and residential applications. A converged metro network, where Ethernet/IP services, along with the traditional TDM traffic, operate over an intelligent WDM transport layer is increasingly becoming the most attractive architecture addressing the primary need of network operators for significantly improved capital and operational network cost. At the same time, the optical layer of this converged network has to introduce intelligence, and leverage advanced technology in order to significantly improve the deployment and manageability of WDM transport. We reviewed the most important operational advancements, and the technologies that cost-effectively enhance the network flexibility, and advance the proliferation of WDM transport in multiservice metro networks.

This chapter has identified the two main trends in the transport layer of the Metro optical networks. First, there is a preference to use standards-based approaches at all layers of the network. Second, high network flexibility as demanded by the extremely rapid evolving market dynamics. Standards-based approaches allow carriers and equipment manufacturers to leverage a wide base of industry-wide efforts. Flexibility, when provided at low incremental costs, allows carriers to be "wrong" at initial network deployment, but still rapidly adapt to the ever changing and evolving markets. Software definable, flexible client interfaces allow a single network to support a rich variety of existing services, as well as to allow real-time changes as older protocols are removed and new ones are added to the same hardware. At the same time, new unanticipated services and protocol developments can be readily added without affecting installed hardware base. A different approach to the same end is a protocol-agnostic open WDM layer that allows alien wavelengths that carry traffic directly from service-optimized and integrated WDM interfaces on client platforms to operate over a common WDM infrastructure. Manufacturing advances and high volumes have made wide-band wavelength tunability a reality for the Metro space, where a single part number could be produced in extremely high quantities to cover all applications. In addition, wavelength tunability offers the promise of reconfigurability with little or no capital outlay for separate optical switch components. Fixed wavelength filters may serve as an effective "optical address" to which a tunable transmitter may be tuned to establish a particular traffic pattern. Tunable optical filters would have a similar application. Reconfigurable optical add/drop multiplexers bring a level of flexibility and optical transparency to optical switching and routing. Again, unanticipated network growth patterns, new services, and evolving channel data rates can be easily added. As new Transceiver technology is developed, overall network capacity may even be increased substantially beyond initial design parameters without requiring new overbuilds. Finally, evolving sophistication of the network planning and design tools lets carriers minimize their CAPEX costs, while at the same time retaining highly desirable flexible OPEX characteristics.

12.7 FUTURE OUTLOOK

From a transport perspective, DWDM is the main growth technology for metro networks as required bitrates on a fiber in particular in the presence of video services outpace the ability of single-wavelength transmission technologies to deliver the bandwidth cost-effectively. Moreover, photonic switching technologies allow for the electrical layer to scale more moderately, as much of the traffic can bypass electronics in most sites.

At the same time, Ethernet has become much more mature and robust, and is incorporating various mechanisms that will allow it to scale more gracefully including fault detection mechanisms, hierarchical addressing schemes (such as 802.1ah and 802.1ad), as well as carrier class switch implementations. In fact, Ethernet, in its various incarnations, is gaining popularity as a replacement of SONET/SDH for sub-wavelength transport.

Finally, the IP layer has clearly become the convergence layer of most services both for the residential and enterprise markets. IP in particular MPLS Pseudowires, has also been used increasingly as a mechanism to converge legacy technologies such as FR and ATM over IP and as a back-haul mechanism to aggregate them into the router. Different approaches exist in terms of role of Ethernet vs IP in the metro. Some carriers see the value of Layer 3 intelligence as close to the customer as possible. This allows for efficient multicast, deep packet inspection and security mechanisms that guarantee that a malicious user will have a minimal impact on the network. Other carriers are trying to centralize Layer 3 functions as much as possible, claiming that this reduces cost and allows for more efficient management. Whatever the right mix of Ethernet and IP may be, it is clear that the network will benefit from tighter integration of the packet layer and the optical layer.

Efficient packet transport based on WDM modules in routers and switches have recently enabled the first such "converged" deployment in the emerging IP-video MAN and WAN architectures [43]. The advents in optical switching and transmission technologies discussed in Section 12.3, further allow a flexible optical infrastructure that efficiently transmits and manages the "optical" bandwidth, enabling advanced network architectures to leverage the IP-WDM convergence, and to realize the associated CAPEX and OPEX savings. These architectures would ideally be based on open "WDM" solutions (like the ones described above), so that the same WDM infrastructure can also continue to support traditional TDM traffic, as well as wavelength services or other emerging applications that may not converge over the IP network, e.g., high-speed (4 or 10 Gb/s) fiber channel. Such open WDM architectures further need to offer performance guarantees for the different types of wavelength services, including "alien" wavelengths, support mesh network configurations, and also benefit from coordinated management, and network control.

ACKNOWLEDGMENTS

The authors would like to acknowledge many colleagues at Cisco and Ciena.

REFERENCES

[1] ITU G.709 standard
[2] A. McCormick, "Service enabled networks aid convergence," *Lightwave*, May 2007
[3] Special Issue on "Metro & access networks," *J. Lightw. Technol*., 22(11), November 2004.
[4] L. Paraschis, "Advancements in metro optical network architectures," *SPIE*, 5626(45), 2004.
[5] N. Ghani et al., "Metropolitan optical networks," in *Optical Fiber Telecommunications IV B: Systems and Impairments*, (I. P. Kaminow and T. Li, eds), Academic Press, 2002, pp. 329 403, Chapter 14.
[6] A. Saleh et al., "Architectural principles of . . . ," *J. Lightw. Technol.*, 17(10), 2431 2448, December 1999.
[7] D. Cavendish, "Evolution of optical transport technologies . . . ," *IEEE Comm.*, 38(6), 2002
[8] M. Macchi, et al., "Design and Demonstration of a Reconfigurable Metro Regional WDM 32 × 10 Gb/s System Scaling beyond 500 km of G.652 Fiber," in *Optical Fiber Communication Technical Digest Series, Conference Edition, 2004*, Paper OTuP2, *Optical Society of America.*
[9] M. J. O'Mahony, et al., "Future optical networks," *J. Lightw. Technol*., 24(12), 4684 4696, December 2006.
[10] S. Ramamurthy, et al., "Survivable WDM mesh networks," *J. Lihgtw. Technol*., 21(4), 870 883, April 2003.
[11] N. Mallick, "Protection Capacity Savings due to an End To End Shared Backup Path Restoration in Optical Mesh Networks," in Proc. *OFC 2006*, paper NThB2, March 2006.
[12] M. Bhardwaj et al., "Simulation and modeling of the restoration performance of path based restoration schemes in planar mesh networks," *J. Opt. Netw.*, 5(12), 967 984, December 2006.
[13] P. Demeester et al., "Resilience in multilayer networks," *IEEE Communications Magazine*, 37(8), 70 76, August 1999.
[14] J. Manchester, P. Bonenfant, and C. Newton, "The evolution of network survivability," *IEEE Communications Magazine*, 37(8), 44 51, August 1999.
[15] R. Batchellor and O. Gerstel, "Protection in Core Packet Networks: Layer 1 or Layer 3?" in proceedings *ECOC Conference*, September 2006, Paper Tu3.6.4.
[16] L. Paraschis, O. Gerstel, and R. Ramaswami, "Tunable Lasers Applications in Metropolitan Networks," in *Optical Fiber Communication Technical Digest Series, Conference Edition, 2004.* Paper MF 105. *Optical Society of America.*
[17] ITU T Rec. G.957, "Optical interfaces for equipment and systems relating to the Synchronous Digital Hierarchy," 1995.
[18] http://www.schelto.com/
[19] ftp://ftp.seagate.com/sff/INF 8053.PDF
[20] ftp://ftp.seagate.com/sff/INF 8074.PDF
[21] http://www.xfpmsa.org/cgi bin/home.cgi
[22] 300 pin Multi Source Agreement web site: http://300pinmsa.org/
[23] L. Paraschis, "Innovations for Cost effective 10 Gb/S Optical Transport in Metro Networks," Invited Presentation in *LEOS 2004: The 17th Annual Meeting of the IEEE Lasers and Electro Optics Society*. *November 2004*, Paper WU1.
[24] S. Norimatsu et al., "Accurate Q factor estimation of optically amplified systems in the presense of waveform distortion," *J. Lightw. Technol*., 20(1), 19 27, January 2002.
[25] J. D. Downie, "Relationship of Q penalty to eye closure penalty for NRZ and RZ signals with signal dependent noise," *J. Lightw. Technol*., 23(6), 2031 2038, June 2005.

[26] A. Tzanakaki, "Performance study of modulation formats for 10 Gb/s WDM metropolitan area networks," *IEEE Photon. Technol. Lett*., 16(7), 1769 1771, July 2004.
[27] Q. Yu and A. Shanbhag, "Electronic data processing for error and dispersion compensation," *J. Lightwave Techn.*, 24(12), 4514 4525, December 2006.
[28] T. Nielsen and S. Chandresekhar, *J. Lightw. Technol.*, 23(1), 131, January 2005.
[29] S. K. Kim et al., "Distributed fiber Raman amplifiers with localized loss," *J. Lightw. Technol*, 21(5), 1286 1293, May 2003.
[30] M. Karasek and J. A. Valles, "Analysis of channel addition/removal response in all optical gain controlled cascade of Erbium doped fiber amplifiers," *J. Lightw. Technol*., 16(10), 1795 1803, October 1998.
[31] S. Pachnicke, et al., "Electronic EDFA Gain Control for the Suppression of Transient Gain Dynamics in Long Haul Transmission Systems," *OFC*, March 2007, paper JWA15.
[32] A. Sridharan, "Blocking in all optical networks," *IEEE/ACM Trans. On Netw.*, 12(2), 384 397, April 2004.
[33] C. C. Sue, "Wavelength routing with spare reconfiguration for all optical WDM networks," *J. Lightwave Technol*., 23(6), 1991 2000, June 2005.
[34] O. Gerstel, et al., "Worst case analysis of dynamic wavelength allocation in optical networks," *IEEE/ACM Trans. On Netw*., 7(6), 833 845, December 1999.
[35] J. Wagener, et al., "Characterization of the economic impact of stranded bandwidth in fixed OADM relative to ROADM networks," *OFC*, March 2006, paper OThM6
[36] H. Zhu, "Online connection provisioning in metro optical WDM networks using reconfigurable OADMs," *J. Lightw. Technol.,* 23(10), 2893 2901, October 2005.
[37] S. Okamoto, A. Watanabe, and K. Sato, "Optical path cross connect node architectures for photonic transport networks," *J. Lightw. Technol.*, 14(6), 1410 1422, June 1996.
[38] E. Iannone and R. Sabella, "Optical path technologies: a comparison among different cross connect architectures," *J. Lightw. Technol*., 14(10), 2184 2196, October 1996.
[39] M. Fuller, "RFP activity boosts ROADM development," *Lightwave*, April 2004. http://lw.pennnet.com/Articles/Article Display.cfm?Section ARTCL8ARTICLE ID 203231&VERSION NUM 1
[40] C. Ferrari, et al., "Flexible and Reconfigurable Metro Regional WDM Scaling beyond 32x10Gb/s and 1000km of G.652 Fiber," in *LEOS 2005: The 18th Annual Meeting of the IEEE Lasers and Electro Optics Society*, November 2005, TuG5.
[41] Optimization Software Guide by Jorge J. Moré and Stephen J. Wright (SIAM Publications, 1993).
[42] G. Markidis, "Impairment constraint based routing in ultralong haul optical networks with 2R regeneration," *Photon. Techn. Lett*., 19(6), 420 422, March 2007.
[43] O. Gerstel, M. Tatipamula, K. Ahuja et al., "Optimizing core networks for IP Transport," *IEC Annual Review of Communications*, 59, 2006.

This page intentionally left blank

13

Commercial optical networks, overlay networks, and services

Robert Doverspike[*] and Peter Magill[†]

[*]*Transport Network Evolution Research AT&T Labs Research, Middletown, NJ, USA*
[†]*Optical Systems Research, AT&T Labs, Middletown, NJ, USA*

13.1 THE TERRESTRIAL NETWORK MODEL

We will describe the architecture of today's service and transport networks for large terrestrial commercial carriers. It is important that those who study optical networks have a comprehensive understanding of what generates the demand for optical networks and the type of network architectures they comprise. A prerequisite of such an understanding is knowledge of the classes of commercial services and how the networks to provide them are constructed, maintained, and engineered.

Figure 13.1 shows a pictorial view of a useful network model for understanding today's commercial telecommunications network. This model breaks the "network" visually according to *horizontal* and *vertical* characterizations. The horizontal axis represents areas of the network divided into territorial and structural segments. The US network can be roughly categorized into three segments: *access*, *metro* [also sometimes called Metropolitan Area Network (MAN)], and *core* (also called *long distance*). Each of these segments consists of a complex interlacing of network layers (the ***vertical*** axis). We also note that European, Asian, North American, and other continental networks will look similar, but will have critical differences that vary with the deployment of different technologies, geographical characteristics, and politico-economic telecommunications organizational structures.

To define this more precisely, a *network layer* (or *overlay network*) consists of *nodes*, *edges* (or links), and *connections*. The nodes represent a particular set of switches or cross-connect equipment that exchange data (in either digital or analog form) among one another via the edges that connect them. Edges can be modeled as *directed* (unidirectional) or *undirected* (bidirectional) communication paths.

Optical Fiber Telecommunications V B: Systems and Networks

ISBN: 978 0 12 374172 1

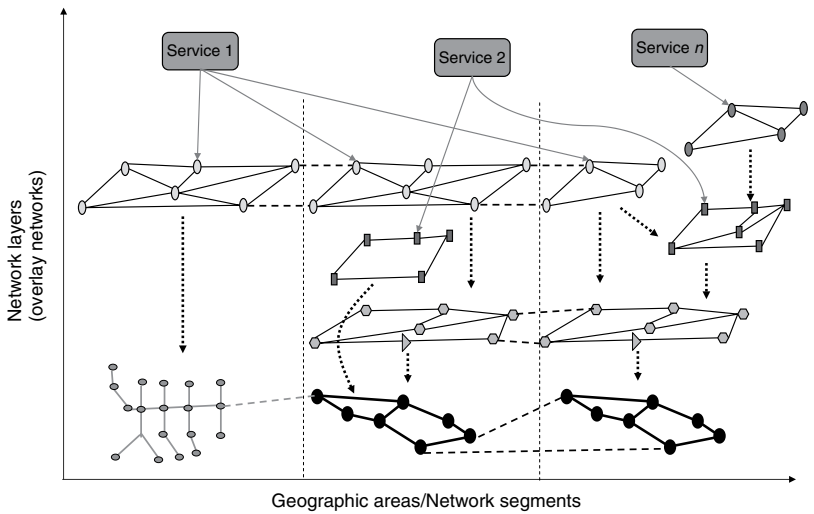

Figure 13.1 Graphical network model (this figure may be seen in color on the included CD ROM).

The combination of nodes and edges transports *connections* from/to sources and destinations. Connections can be *point-to-point* (unidirectional or bidirectional), *point-to-multipoint*, or (more rarely) *multi-point-to-multipoint*. Connections serve two purposes. First, telecommunications services (depicted as large rounded rectangles in Figure 13.1) are transported by connections at various network layers in particular segments. The traffic for a given layer is carried by the connections at that layer. Second, edges of a given network layer are transported by the connections of one or more lower-layer networks. In this way, each layer is providing a "service" for the layer immediately above it to provide connectivity. Additionally, for each layer this connectivity "service" may or may not be guaranteed against failures (fiber cuts, equipment outages, etc.). Some layers provide *restoration* to maintain connectivity, while others do not. This will be explained more thoroughly in Section 13.2.3. Note that in this chapter we use the term "restoration" to include other commonly used terms, such as *protection*, *resiliency*, and *robustness*. An important observation (especially for the student of packet and optical networks) regarding the nodes and edges in these network models is that they should all be considered as *logical*, even for the bottommost layers.

For example, the bottom layer of principal interest to this chapter usually represents some form of fiber transport media. However, an edge or link between two fiber nodes most likely represents multiple physical entities and/or layers. It in fact, can consist of multiple cable segments and splicing technologies, which are inside of ducts or subducts, which are often inside substructures (e.g., concrete conduit or plastic pipe). Thus, such an edge (or link) indeed represents a simplification (usually for routing or planning and engineering purposes) of multiple detailed layers and may consist of hundreds of individual physical components.

Another example is given by the Open Systems Interconnection (OSI) model developed by the ISO standards organization [1] and the colloquial classification of packet layering (e.g., "Layer 1, 2, 3," etc.) which has subsequently emerged in the industry. This relegates everything below Layer 2 [e.g., frame relay, multi-protocol label switching (MPLS), etc.] to the label of *Layer 1* or *physical layer* (PHY). This could include SONET, SDH, or other protocols/signals, which in fact can be one or more layers above the fiber layer and, as such, quite logical in nature. Finally, network technologies like Ethernet encompass multiple layers. Even though it started as a Layer 2 protocol, Ethernet has been standardized with multiple specific Layer 1 (or PHY) transmission technologies (e.g., 10BaseT, 100BaseFX, GigE, etc.). And the various Ethernet PHY definitions are used solely to transport Ethernet frames (Layer 2), and nothing else. The standardization of this tight integration of Layers 1 and 2 is a large factor in the very low cost of Ethernet equipment.

13.1.1 Network Segments

We provide a more specific (but still pictorially suggestive) picture of the three horizontal lower-layer network segments (access, metro, and core) in Figure 13.2. Note that for simplification, these three segments are laid out in partitioned, planar graphs. However, note that the reality is not as clean as depicted, with the segments often geographically intersecting one another.

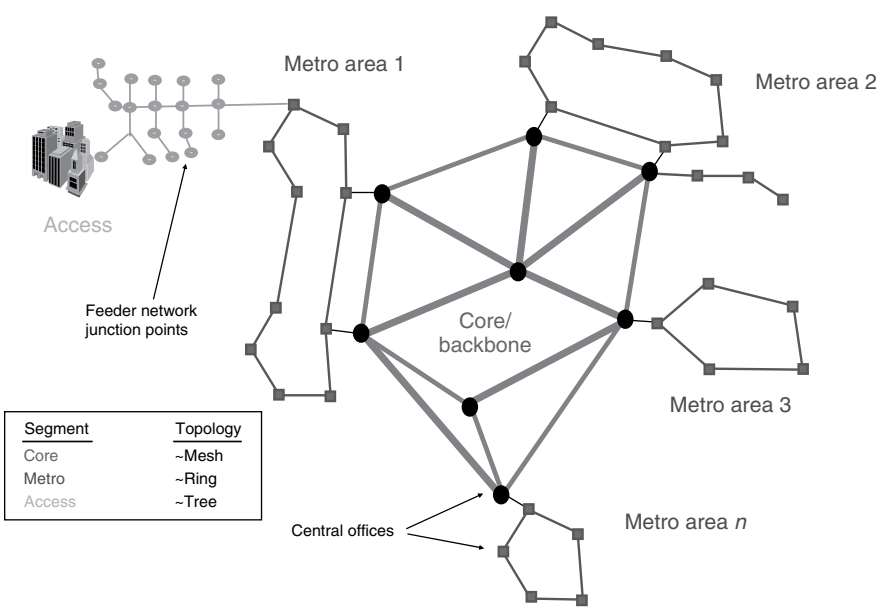

Figure 13.2 Example of geographical (horizontal) network segments (this figure may be seen in color on the included CD ROM).

The lowest layer of the *access* network consists of copper, coaxial, or fiber media and generally has a tree-like graphical structure, especially in residential neighborhoods. The access segment is the "last-mile" to the customer, who is usually categorized as either *residential* (sometimes called *consumer*) or *business* (sometimes called *enterprise*). Note that wireless is also a predominant access-segment lower-layer technology, but we will not explore wireless technology architectures here.

A *metro* network uses time division multiplexing (TDM), packet, and optical multiplexing technologies [like dense wavelength division multiplexing (DWDM)] at the lowest layers. The metro network segment is generally defined as the nodes [central offices (COs)] and edges (connecting COs) within a metropolitan area. The *core* network generally consists of the nodes (each sometimes called a point of presence or *POP*) that are connected by intercity edges. Although various forms of metro packet transport and a *convergence* of TDM and packet technologies have emerged, the SONET/SDH ring continues to be the dominant transport-layer technology for metro networks since the early 1990s (the specific layering will be described in later sections). This is why the metro network segment is depicted as rings in Figure 13.2, although we note most metro networks can indeed support mesh-like topologies. A general description is that the metro network collects traffic from end customers and determines which traffic to route intrametro or intermetro; the intermetro traffic is then handed to the core network segment at the appropriate network layer.

The *core* or intercity network uses similar technologies as the metro, but has different traffic clustering and distance criteria and constraints. The core network tends to have a "mesh" structure at the lowest layer. This is generally justified because it is more economical to connect the many different cities by physically diverse routes, given the large amount of traffic that is aggregated to be carried on the core network. However, note that core networks differ significantly by country or continent. For example, because of smaller distance limitations, European core networks often have different technologies and network graphs than in the United States.

13.1.2 Access-Layer Networks and Technologies

Some of the residential access network layers for a large commercial local *Telco* carrier for the United States are illustrated in Figure 13.3 (a telecommunications carrier with a historical lineage to telephone companies will be referred to as a *Telco*). Note that for access networks there are many different architectural options, both existing and planned. A few of the principal Telco architectures are shown in Figure 13.3. The bottom layer is actually depicted as a composite of three separate layers, *copper loop*, *fiber loop*, and *fiber feeder*. Depending on region, these three layers can be disjoint or can be geographically coincident, as in Figure 13.3. As shown, the loop pairs can either route to a remote terminal (RT) or all the way to the serving CO. Feeder fiber connects the RTs to the CO.

Four architectural examples are illustrated in Figure 13.3, with a given combination of service offerings at the top layer. The reason for so many different

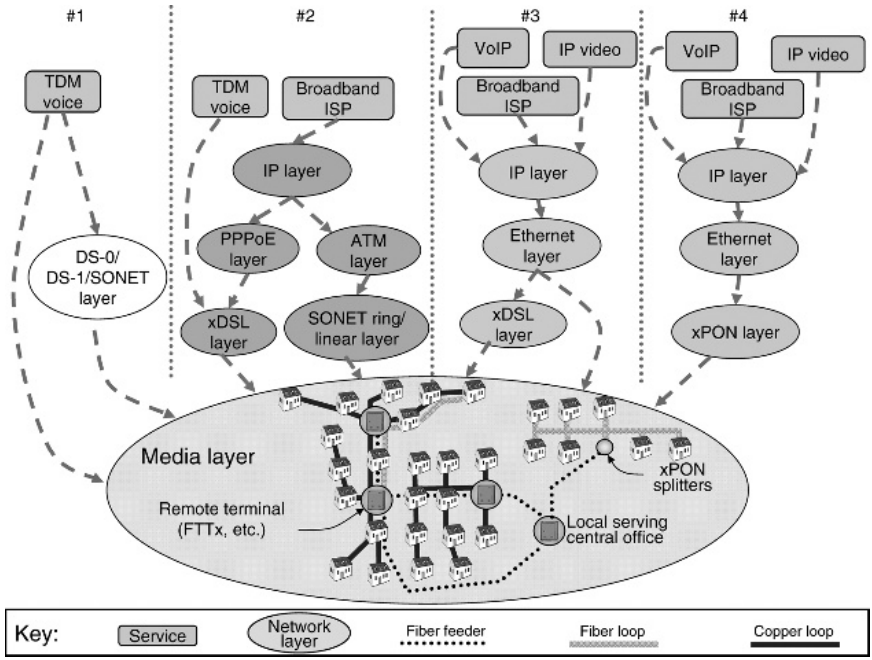

Figure 13.3 Some Telco access segment network layers (residential) (this figure may be seen in color on the included CD ROM).

architectures is mostly due to the historical evolution of technology and services. This brings up an important aspect of real carrier networks: It is generally easier and more acceptable to introduce new architectures and technologies to a commercial network as a new overlay network or geographical segment than it is to remove an older architecture and technology base. This phenomenon is mostly dictated by economics and the reluctance/difficulty for customers to transition their services. As a result, there tends to be a "stacking up" of technologies and architectures, plus a sequence of product vintages and releases, over many years. Note that, as unattractive as it appears, there are some regions where all four of these architectures are geographically co-existent.

Architecture 1 is traditional TDM voice, the grandfather service for all Telcos. The analog voice signal is carried over copper pairs until it reaches an RT where it is digitized and then carried in the TDM channels of SONET systems (older DS-3/DS-1/copper feeder technology also still exists). The SONET systems can be restorable (e.g., UPSR ring) or unrestorable (linear chain).

Architecture 2 shows the evolution to digital subscriber line (DSL) technology, where TDM voice plus broadband ISP service are offered. There are several variations, but the traditional DSL broadband ISP service is shown, architected with point-to-point protocol over Ethernet (PPPoE) technology between the customer modem and the DSL access multiplexer (DSLAM) in the RT or CO.

Analog voice is multiplexed with the packet stream by the DSL technology over the copper wire pairs. Asynchronous transfer mode (ATM) switches are installed in the RT and route individual customer packets over ATM virtual circuits to the ISP edge switch (i.e., typically an *Internet Protocol (IP) router*, which is not shown). The ATM links are routed over SONET rings/chains at a lower layer, whose links in turn route over the feeder fiber layer. In our layered model, the ATM links are implemented as connections in the SONET layer [in units of synchronous transport signal (STS)-*n*, where an STS-1 signal is 51.84 Mb/s and an STS-*n* signal has a data rate of $n \times 51.84$ Mb/s]. There is consideration for using coarse wavelength division multiplexing (CWDM) or other WDM technology to carry the SONET OC-*n* [where the fundamental optical carrier (OC-1) carries an STS-1] links, but this is rare in access networks today.

Architecture 3 shows the more recent IP-over-xDSL technology, which has been installed mostly to carry video. Here, voice service is digitized [Voice over Internet Protocol (VoIP)] and all three services are co-transported over the IP layer. These services and applications per customer are carried via higher-layer protocols [such as Real-Time Protocol (RTP) or video-framing protocols] and separated/differentiated by various *virtual circuit* or *tunneling* methods [such as MPLS Layer 2 pseudo-wire [2] or Ethernet Virtual Local Area Networks (VLANs)]. The IP layer is carried over the Ethernet layer. Ethernet links are routed over xDSL (principally VDSL) to the RT (containing an *IP-DSLAM*) and then routed directly over fiber feeder to the router in the CO. WDM technology can also be used to multiplex the use of access fiber in the feeder network (not shown). Note that there exist hybrid variations where TDM voice service is carried over xDSL up to the RT and then from that point routed to the CO. This is analogous to how TDM voice is handled in architecture 2.

Finally, architecture 4 shows the use of xPON (e.g., BPON, GPON, or EPON) over the fiber loop layer that routes all the way to the customer premises. The upper layers are similar to architecture 3. Note that there are hybrids of architectures 4 and 3 where the xPON stops short of the customer premises (e.g., fiber-to-the-pedestal, -curb, -node, etc.) and xDSL is employed for the last few hundred feet.

The access network layers for business customers include basically the same layers as residential, but there are key differences. The media layers of business access networks have a higher penetration of fiber loop than residential networks, although over the period from 2005 to 2015 large carriers plan to install much more fiber to the residence. However, most business locations, especially the smaller ones, are still connected by copper pairs. For data services, carriers use DS-1 over copper or various xDSL technologies to route to the RT or CO. TDM voice is still a very prevalent service. Most business locations with fiber access (often called *fiber-on-net*) use a SONET ring layer. Ethernet access is growing in penetration and popularity, and there are a variety of Ethernet-over-SONET, Ethernet-over-fiber, and Ethernet-over-copper architectures being deployed.

For access to business customers, the last portion of the network (between the carrier equipment and the customer premise) varies in complexity much more than

for residential access. On the one hand, much of small-business access, especially away from the downtown areas, looks very similar to the residential access in Figure 13.3. In contrast, the configuration becomes more complex in central business districts. For the fiber-on-net locations, there is a mixture of technologies and architectures. One of the key factors in determining the restoration capabilities for the access network is the type or layout of the customers' buildings. In multitenant buildings (where the bulk of demand for bandwidth for Telco business services originates), this is influenced by whether a Telco has *common space* in that building. Common space is a rented area inside the building where the Telco can install its equipment. Today, that consists mostly of fiber or DSX cross-connect patch panels, DS-1/DS-3/STS-1 multiplexing equipment, and SONET ADMs to support voice trunks and private-line services. Ethernet switches are becoming more common, as well.

We illustrate an example multitenant building layout in Figure 13.4. The common space is often in the basement or in a maintenance closet. Fiber, coax, and copper cables are wired to the common space and travel up cable *risers* of the building, which usually are along plumbing or electrical conduits or in elevator shafts. Figure 13.4 shows some DS-1/DS-3 multiplexers and SONET ADMs (OC-12 and OC-48). The customers have equipment (called an M13) on their premises that multiplexes DS-1s into a DS-3 or which terminates an OC-3 or an OC-12, which is then cabled to the basement. Smaller customers simply use

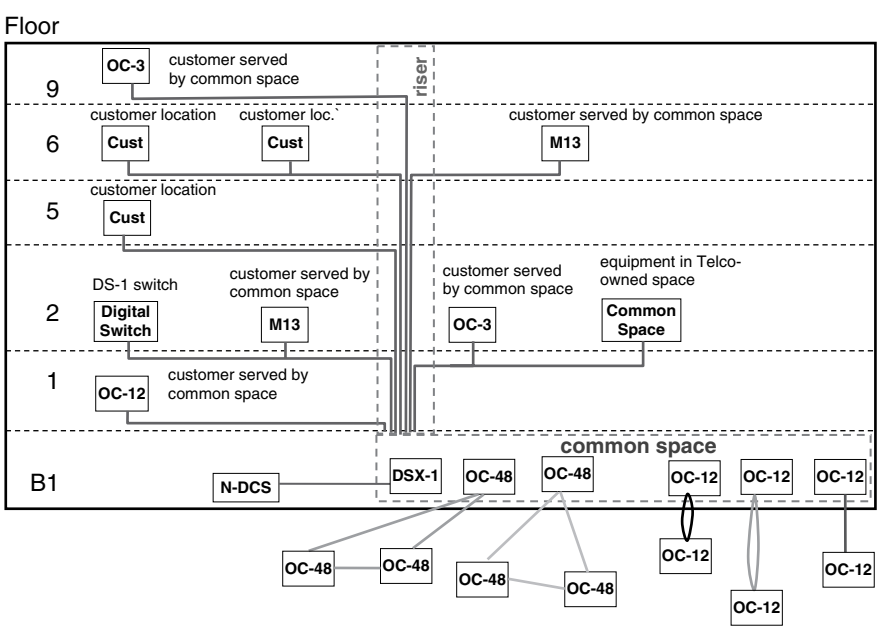

Figure 13.4 Example of building with common space (this figure may be seen in color on the included CD ROM).

copper lines connected directly to the common space. Ethernet customers run their Fast Ethernet lines (copper or fiber) or GigE (fiber) directly to the common space. The common space often resembles a mini CO, where DS-0s and DS-1s are packed into STS-1s (called *grooming*) to ride on SONET rings to their next location, which might be either another customer location (for multinode rings) or a CO. At the CO (in the metro network segment see Section 13.1.3 below), the lower-rate connections (DS-1s) are usually groomed to pack into STS-1 links. (Grooming is better illustrated by the example of Figure 13.7, covered later in the discussion of the metro segment.) Thus, even within the building there can be a complex network. Indeed, intrabuilding networks can be very convoluted because of such factors as constraints on physical access to common space (which usually involves landlord-tenant small-business contracts), the intersecting interests of various carriers, mergers and acquisitions of carriers, building riser restrictions, and, perhaps most of all, different vintages of equipment for both customer and carrier.

Except for voice, the principal business services are different from residential services, although small-business customers may use residential DSL or coaxial-based broadband ISP (cable modem) services. Virtual Private Ethernet (VPE), Virtual Private Network (VPN) (an IP-based service), Virtual Private LAN Service (VPLS), TDM Private Line, and Business ISP are the most typical examples of business data services. Business VoIP (often called *B-VoIP*, in contrast to residential/consumer VoIP, often called *C-VoIP*) is a growing service. This is because most businesses tend to need more bandwidth for data services and thus have more opportunities to use their data networks for their voice services as well. B-VoIP services tend to mostly use the *Session Initiation Protocol (SIP)* [3] to signal to the VoIP network to set up and control their calls and call features. The traditional, bulky Private Branch Exchange (PBX) is slowly being replaced by the more agile and flexible SIP- or IP-PBX. The *IP multimedia subsystem (IMS)* architecture, which is based on SIP, is a higher-layer server and protocol architecture that many carriers are pursuing to provide wired and wireless VoIP and data services [4].

Some of the other significant access-segment architectures not shown are coax and hybrids of coax and fiber feeder and non-IP-based video over fiber.

13.1.3 Metro-Layer Networks and Technologies

The network layers for a typical US metro network are depicted in Figure 13.5. Of the three major network segments, the metro network is particularly complicated because all the access architectures discussed previously (many of which were not shown) have to be transported over the metro segment. Since the access segment is the "last mile," it does not evolve as a unit and some parts have interfaces and technologies that are decades-old vintage. Thus, as newer transport technologies are introduced into the metro segment, it must still provide aggregation and transport for the older access-segment overlays and technologies. Once these services are mapped onto the metro segment, further aggregation can occur before

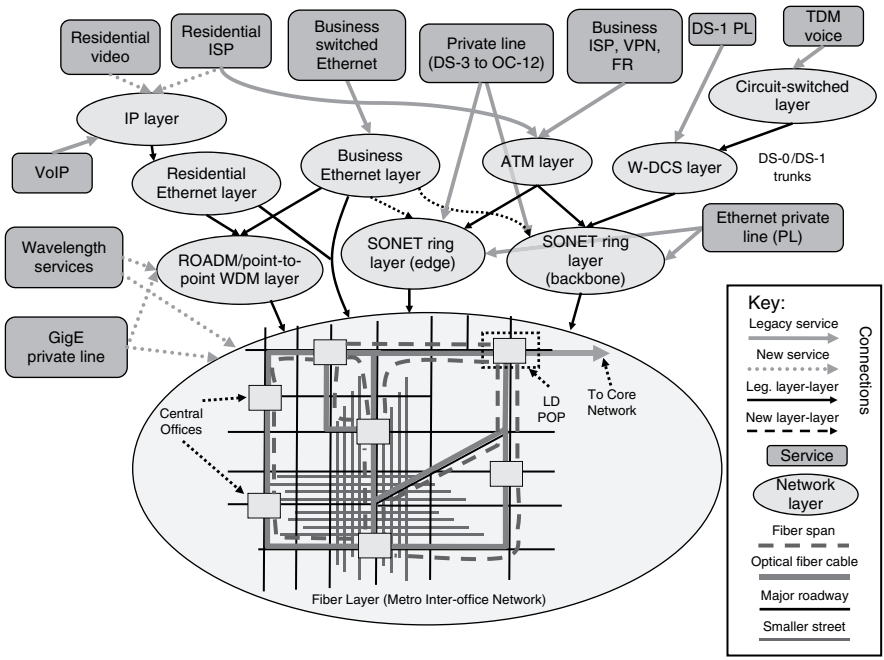

Figure 13.5 Example of Metro Segment Network Layers (this figure may be seen in color on the included CD ROM).

handing off to the core, which tends to simplify core-segment architectures. Furthermore, the large majority of service connections are intra-metro (i.e., both ends are in the same metropolitan area) and, in fact, some services are only offered or targeted as intra-metro service.

The bottom layer of Figure 13.5 is the fiber network. Virtually all Telco COs today are connected via fiber. There are usually one or more COs in each metro area that are each a point-of-presence (POP) where services are handed off to a long-distance entity (which can be another carrier, the same carrier, or a separate business unit of the same carrier). The idea of a POP arose in the years leading up to the breakup of the Bell System in 1984 and became entrenched via its Consent Decree and Federal Communications Commision (FCC) guidelines for its enforcement. That FCC document laid out the boundaries of each Telco metro network more rigorously than the original 161 LATAs (Local Access and Transport Area). This metro-to-core POP handoff can be complex, a mixture of virtual and physical in nature which varies by network layer and service. We illustrate this with the handoff for IP services later.

As we observe in Figure 13.5, most fiber cables run along streets and other public conduits, such as transportation lines (e.g., subways) or sewer/water lines, and bridges. The cables in cities are usually inside hard conduit and ducts or subducts and, in fact, may run in parallel in the same conduit with older copper cables that provide access-segment connectivity. Fiber cables in the city outskirts are often aerial

(on telephone poles or power lines), especially in the Northeastern United States. Furthermore, there is usually no clean geographical boundary between core and metro. For example, core-segment fiber cables often run in parallel with metro-segment cables over the same conduit structures. The factors determining how cables among the various segments are routed are very complex and depend on business factors such as negotiated rights-of-way, or Indefeasible Right of Use agreements (IRUs), capitalized long-term leases, and carrier corporate lineage (mergers, spin-offs, acquisitions, mutual agreements). However, although much industry "buzz" has ensued about the various long-distance overlay networks and services and legislation to govern US Telecommunications policy, the answer to the question of "who owns the cables and rights-of-way for our metro and access segments" is the key economic and business factor that has molded the structure of both our major and minor US carriers. This also ultimately has an impact on the structure of the equipment suppliers who supply those carriers.

As can be seen in Figure 13.5, since most fiber cables run along highways, the fiber network has a noticeable "grid" pattern, and as such, there are typically two and usually no more than four physical cable routes out of a CO. Often, multiple fiber routes exist that share part of their route on the same conduit section. Sometimes, fibers share the same cable and then split into different directions at cross streets or at the entrance to customer buildings. Where fiber cables enter a CO, they are usually wired from the cable vault entrance to some form of fiber patch-panel (often called an *LGX* or Lightguide Cross Connect) which is a physical device with manual or automated (remotely controlled) cross-connects. Some carriers have begun to deploy automated cross-connects based on mechanical fiber switches or MEMS devices at large COs. *Fiber spans* are defined between the patch panels. This is illustrated by the large dashed edges in the fiber layer of Figure 13.5. Mathematically speaking, these edges form another overlay network (nodes = patch panels and links = fiber spans) over the network layer of fiber cables (nodes = buildings and links = cable runs, depicted by large solid lines).

One can now understand why the introduction (Section 13.1) stressed the idea of "logical networks." The "fiber layer" in Figure 13.5 is, in fact, itself composed of multiple layers. If a network provisioner/planner wants to route a higher-layer network link or customer service over fiber, then he/she routes along the network graph corresponding to these fiber spans. The major benefit is that most of the physical splicing of the cable is done when the cable is installed, especially for major carriers. Normally, whenever a connection (higher layer link or service) has to be provisioned over fiber, the only physical installation (splicing and/or installation of fiber patch cords) occurs on the ends of the connection to connect the ports of the equipment interface cards into the patch panel [e.g., the interface card of a router, Ethernet switch, reconfigurable optical add/drop multiplexer (ROADM), Optical Transponder, etc.]. The connection through the intermediate nodes of the metro network can then be set up via remote cross-connect commands to the patch panels. An exception would be for needed intermediate equipment, such as O-E-O optical regenerators at intermediate nodes which, due to their high cost, are

not usually pre-installed and pre-connected into the patch panel. Even if the patch panel is manually cross-connected, no splicing is usually required end-to-end. The difficulty, as one can observe in Figure 13.5, is that the fiber spans (edges) can sometimes run together on portions of the route, called a *shared-risk-link group (SRLG)* originally defined in Ref. [5]. Thus, the planner must be knowledgeable about the actual fiber paths of these fiber spans to ensure that restoration objectives are met for whatever higher-layer network link (or service) is being provisioned. SRLGs are addressed again later in the discussion about network restoration.

Figure 13.5 illustrates only a simplified picture of the common metro layers. The dotted lines signify newer service or network layer connections vs. more traditional (legacy) transport architectures. Four network layers are shown that route over the fiber layer: edge SONET ring, backbone SONET ring, ROADM/point-to-point WDM, and IP. Furthermore, two services are shown that often route directly onto the fiber layer, Gigabit Ethernet Private Line and *wavelength services*. These services are also shown routing directly over the ROADM layer. This is because, in contrast to the core network, WDM is not yet pervasive in the metro segment. Thus, even in metros that have ROADM layers, many customers' connections may have to route directly on fiber for part of their route where the ROADM network has not been installed. Note that in reality, although not pictured at that level of detail, most carriers prefer some sort of network equipment between the customer premises equipment (CPE) and the fiber, a form of "demarcation point" so that they can monitor performance and isolate performance issues.

It is useful to clarify the term "Wavelength Services." For technical readers of an optical technology book, this may be confusing, because the term is, in fact, more marketing-oriented than technically accurate. Wavelength services today usually refer to private-line services corresponding to 2.5, 10, or 40 Gb/s SONET or SDH signals, their emerging ITU (ODU-1,2,3) containers, or 1-, 10-, or 100-Gigabit Ethernet signals. These signals are, in fact, electrical but are often transported over WDM equipment; therefore, they have colloquially been mislabeled as "Wavelength Services."

The metro WDM layer is a mixture of point-to-point and newer ROADM technologies; hence our label "ROADM/Pt-Pt WDM Layer." See Chapter 8 for a full description of the technologies in the ROADM layer. The ROADM overlays tend to be installed in ring-like (two-connected) topologies and, therefore, tend to have a more "network" appearance (for graphs-theorists, the ROADM network is comprised of just one connected subgraph). In contrast, point-to-point WDM was (and is) mostly installed to relieve fiber exhaust and therefore has a more scattered topology (consisting of many disconnected subgraphs). A determining factor for the architecture of the metro segment is minimizing network cost; consequently most carriers must cost-justify every individual installation of WDM technology. Where spare fiber is abundant, this is harder to justify economically. There is also a common industry misconception that installation of ROADM network layers can be justified in terms of reduced operations or provisioning costs. Given the discussion of patch panels above and the observation that the number of daily

connection requests for the ROADM layer (from higher layer links or services) is very small, it is clear the cost savings is insignificant in comparison with the capital cost of the WDM equipment.

We continue the explanation of the configuration of Figure 13.5 by providing some historical perspective. Let us examine the right-most stack of network layers in Figure 13.5. In the 1950s and 1960s, the Bell System (including Western Electric, its equipment supplier division at the time) developed digital encoding (called *pulse code modulation*) of analog voice and its resulting metro multiplexing and transmission technology, the DS-1 (1.54 Mb/s), subsequently, in the 1970s and 1980s the DS-1, with its ability to carry 24 DS-0 (64 Kb/s) voice-bearing trunks, became the mainstay transmission unit in metro network carriers. A natural evolution of the digital DS-0-based switch, the node of the circuit-switched layer in Figure 13.5, the manual DSX-0 and DSX-1 cross-connect frame, and finally the *narrowband digital cross-connect system (N-DCS)* and *wideband digital cross-connect system (W-DCS)* followed. An N-DCS cross-connects DS-0 channels from among its DS-1s interfaces and a W-DCS cross-connects DS-1 or SONET VT-1.5 channels from among its higher rate interfaces. Telcos later expanded their W-DCS layer beyond its original purpose (namely, to transport links of the circuit-switched layer) to establish DS-1 private-line services. This included the wholesaling of DS-1s to other carriers, the price of which was governed by tariffs.

Then packet switches began to offer the ability to encapsulate their data (payloads) inside clear-signal (nonchannelized) DS-1s, which could be readily provisioned by the W-DCS. With the advent of fiber optics and high-speed fiber optic terminals (multiplexers), the impact of single network component failures also grew. Bellcore decided to standardize the collection of fiber optic transmission rates with its SONET standard, as well as take the opportunity to standardize the collection of transmission systems with various restoration (protection) schemes that had emerged; consequently, SONET self-healing ring standards were established. Given the ability of SONET rings and chains to transport DS-3s links between W-DCSs or between DS-1/DS-3 multiplexers at smaller COs, the DS-3 private-line market emerged. The initial customers of the DS-3 private-line service were predominantly other carriers. The STS-*n*c market naturally emerged as the demand for higher rates grew and as the W-DCS was upgraded to have SONET optical interfaces. Thus, even though a revolution was occurring from voice to packet services, a major upheaval of metro network architectures (the rightmost network layer stack) was avoided by the combination of (1) a sustained, multiyear sequence of small advancements in interface rates, (2) gradual reduction of the per-unit costs, (3) marketing/wholesaling of associated private-line services, and (4) encapsulation of packets within TDM signals.

Looking at the emergence of packet networks in more detail, given the provisioning, planning, operations, and service marketing methodologies that evolved around the rightmost stack of Figure 13.5, packet networks had to find a place to fit in a mature stack of overlay networks. In particular, some of the earliest large packet network overlays arose from long-distance frame-relay service. The frame-relay

protocol was a simple layer-2 protocol to encapsulate IP packets and, in particular, through its concept of the permanent virtual circuit (PVC) enabled the setting up of connections in a more flexible and economic packet environment than private line. This provided (and still provides) customers with multiple (say, n) sites in different cities a more economical alternative to the "n-squared" problem; that is, they would require $n(n-1)/2$ point-to-point private-line connections to fully interconnect their sites, whereas with frame relay they only require n interfaces into the long-distance carrier's frame-relay network. The frame-relay customer can then set up a fully-connected mesh of virtual PVCs between his sites. The cost (and associated pricing) is such that customers with high values of n benefit the most. However, as ATM technology emerged, its concept of a *virtual channel* overlapped with that of frame-relay PVC. Thus, today almost all frame-relay services are carried over ATM networks. Frame-relay PVC/DLCIs are mapped to ATM VCs using the concept of a virtual channel identifier (VCI). The DS-1 private-line service continues to be the primary metro service to transport frame-relay signals from customer locations to the ATM network. In fact, as soon as the DS-1 encounters the first ATM switch, all the frame-relay encapsulation is discarded and replaced within the ATM adaptation layer (AAL). The frame-relay encapsulation is recreated at the far end so that it can interface to the customer port at that end. In fact, many customer interfaces on their switches completely bypass the frame-relay stage and originate as ATM cells.

The links of the ATM switches have to be transported at a lower layer, so ATM encapsulation within STS-nc signals was developed and thus could readily use the SONET infrastructure that evolved for private-line services. Furthermore, since ATM standards were not developed with a comprehensive restoration methodology (a major reason why some think SONET succeeded to a far great level than ATM), SONET rings also provided a ready restoration mechanism against lower-layer failures, which helped ATM networks to meet the higher level of QoS often expected for the services it transports. We note ATM vendors did provide various restoration methods, but they were never universally adopted by carriers. These relationships among layers for restoration are discussed below in the sections on restoration.

Given that metro ATM networks were deployed primarily for transport of local frame relay service and some early IP transport, they were the first standardized packet networks the Telcos deployed. Therefore, they naturally evolved to transport the emerging consumer DSL-based ISP services. All this discussion is captured in Figure 13.5, which shows residential (and smaller business) ISP services plus frame relay and business IP services transported over the metro ATM network layer.

Given this history, we observe that the "king" of metro transport for the past 15 years has been the SONET/SDH ring (which, for simplicity, we will confine ourselves to SONET for the remainder of this chapter). We have broken this into two layers to better illustrate the common architecture of the SONET ring layer. In most Telcos, the edge SONET ring layer mostly consists of *unidirectional path-switched rings (UPSRs)* or two-node, $1+1$ or 1:1 protected systems (see Section 13.2.3 below) and the backbone SONET ring layer consisting of *bidirectional*

line-switched rings (BLSRs). The links of these rings are routed over the fiber layer, although some links are routed onto point-to-point WDM systems on some fiber spans that have reached fiber exhaust, as discussed above. The reason for the UPSR/BLSR demarcation is mostly due to network evolution and economics. Generally, the UPSR is more economical for a traffic matrix whose nonzero demands have only one endpoint, while the BLSR is better suited to a more distributed traffic matrix. In reality, since the SONET ring has built-in restoration characteristics, its use established a QoS expectation for most private-line services or overlay networks whose links use the SONET layer. As a result, when Telcos provisioned private-line services, they had to install a ring close to the customer location. For buildings that are on-net, this results in the installation of a (usually) smaller ADM in the building, as illustrated in Figure 13.4. The UPSR predated the emergence of the BLSR by many years. Most initial SONET metro networks were covered with multinode UPSRs. However, as demand grew and higher rate SONET interfaces were offered, the architecture with edge and backbone SONET rings evolved. The typical SONET edge ring deployment migrated toward two-node rings: one at the customer premise and the other at the CO. Smaller customers received lower-rate rings. Furthermore, the end of the two-node ring at the CO is often a port on a card of a larger ADM. The result has evolved into a massive collection of SONET-layer edge rings. Private-line connections (usually called *circuits* in Telco terminology) with ends on two different edge rings route over the backbone rings or share a node at the CO. Alternately, many private-line connections are access links to packet networks or the metro segment of a long-distance private-line circuit, so only have one end on an edge ring of a given metro network. However, note that backbone SONET rings are mostly deployed to transport the links of the other higher layer networks, such as ATM, DCS, or IP layers.

Technically speaking, the SONET layer is not as "pure" a routing layer as in packet networks or a WDM network with multidegree ROADMs. This is because most SONET rings consist of individual Add/Drop Multiplexers (ADMs) that are connected by OC-n (typically $n = 12$, 48, or 192) signals. Because network demand has become enormous compared to the (now) relatively small size of a ring, each metro network consists of hundreds (even thousands) of rings and, consequently, there are enormous numbers of ADMs in large COs. Graphically, each CO consists of many (sometimes hundreds) of individual ring nodes. We illustrate this with a picture of the rings for a large metro network in Figure 13.6. A geographically-correct diagram is virtually impossible to show for large numbers of rings, therefore Figure 13.6 represents a *connectivity graph*, where the nodes and edges of the rings are optimally placed to avoid edge crossings and hence be more visually useful. The heavily shaded areas are in fact a large collection of edges from enormous numbers of rings. As the reader can see, there is no "typical" topological pattern or architecture. This is even more pointed when we note that this figure depicts a medium-sized *competitive local exchange carrier (CLEC)* of a large city. The picture for an incumbent carrier (essentially a Telco) would be an order of magnitude more complex.

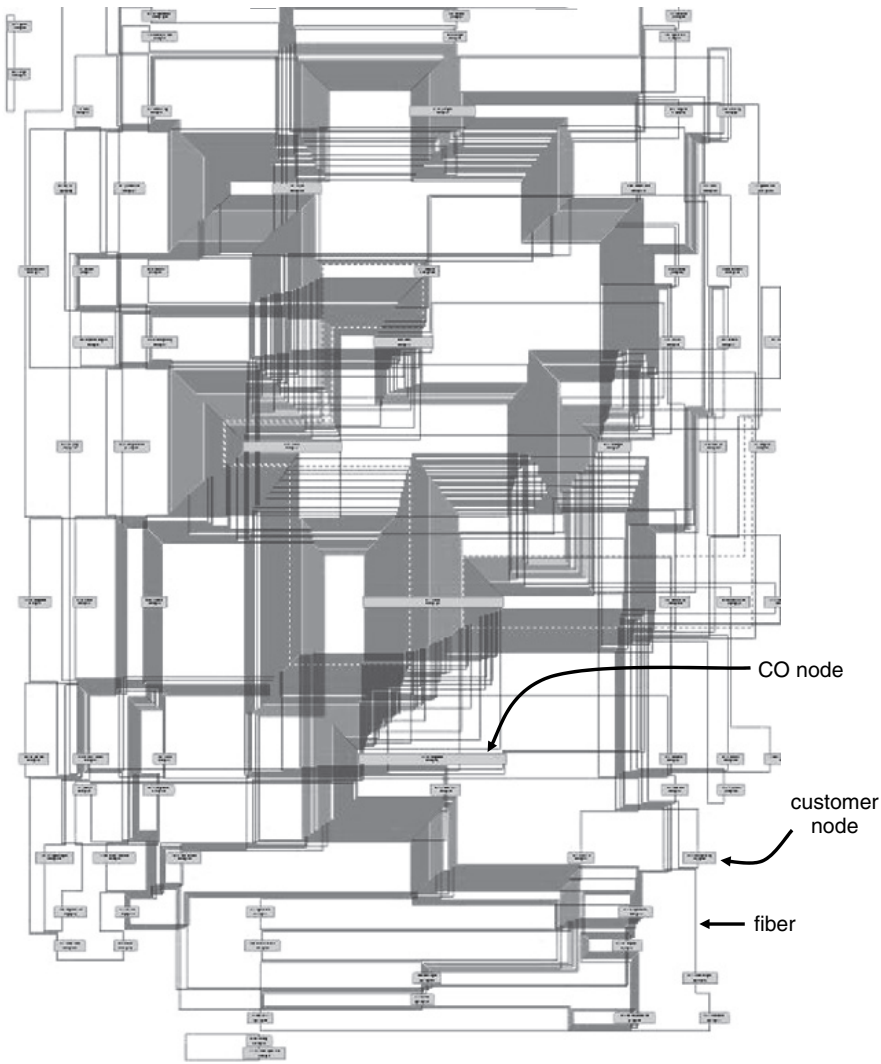

Figure 13.6 Connectivity graph of rings in large metro (this figure may be seen in color on the included CD ROM).

Connections are generally routed across rings by a method called *ring hopping*. The usual approach is to provision tie links among the ADMs. For example, two different OC-192 ring nodes may have installed channelized OC-48 links between them on their *drop-side* or *tributary-side* ports. SONET STS-*n*c connections that have to route between the two rings can be assigned to the spare channels on the tie-links and cross-connected by the cross-connect fabrics of the two ADMs by remote command. The *broadband digital cross-connect system (B-DCS)* is a DCS

that cross-connects at DS-3/STS-1 or higher rates and was developed to mitigate the need for many pair-wise tie links needed for ring-hopping among many ADMs in a given office. In fact, the value of a single B-DCS with multiple interface cards with ports that act as single SONET ring nodes (called *subtending* rings) was studied and recommended many years ago [6]. Basically, this reduced multiple ADMs in a CO to just one equipment platform. However, the B-DCS was not widely adopted in the metro network segment; consequently, although it exists, we do not depict it in Figure 13.5. The reason for its limited deployment was mostly because of overlap issues with regard to the W-DCS, which was widely deployed prior to the advent of the B-DCS, and further coupled with the economics of multiplexing/demultiplexing TDM connections (grooming). However, in contrast, we note that in AT&T's core network segment, an early B-DCS layer (with electrical DS-3 interfaces) was widely deployed in the early 1990s and adapted with a DCS restoration method called FASTAR to provide network restoration [7]; however, this has been superseded by a more modern, restorable TDM cross-connect layer with optical interfaces and distributed intelligence, although the original FASTAR network is still operational. This is described in the next section, as well as later sections on restoration.

In addition to links of higher-layer networks, Ethernet private-line services are routed over the SONET ring layers. Ethernet private line services provide interfaces on ADMs that receive GigE or Fast Ethernet signals and then encapsulate the Ethernet frames into standard SONET payloads in units of STS-1 capacity and then are transported similar to any SONET private line service. *Next-Gen* SONET features, such as Virtual Concatenation (VCAT) (described in other chapters), provide more flexible connection sizing than the historical SONET concatenated STS-1/3c/12c offerings. Even though the interface can be GigE, the interface card usually polices the rate down to the private line rate ($n \times$ STS-1). Full rate GigE private lines are also sometimes provided over SONET rings (e.g., inside STS-24c or VCAT STS-22vc signals), but generally Telcos are choosing to deploy them directly over the fiber layer or ROADM layer (or mixtures of the two) because of the large amount of capacity they use up on SONET rings.

Next the hand-off from the metro to core segments will be illustrated in more detail. Originally, the concept of a "POP" was a simpler concept that was narrowly defined around the Public-Switched Telephone Network (PSTN), mostly for transporting voice service [8]. The POP was a location where the Inter-LATA carrier put a circuit switch that had trunks to a metro (Intra-LATA) carrier *tandem* switch. The term Point of Interface (POI) was further defined, wherein the transport network boundary was established between the two carriers. However, as private line services and packet networks evolved, this has become a far more complex concept that varies by service and the network layers. An example is shown in Figure 13.7. This diagrams the connection of a business customer for a long-distance ISP service. Each gray vertical box represents a different piece of equipment (as labeled above it). The logical and physical links between these elements are shown by line segments along their corresponding layer or

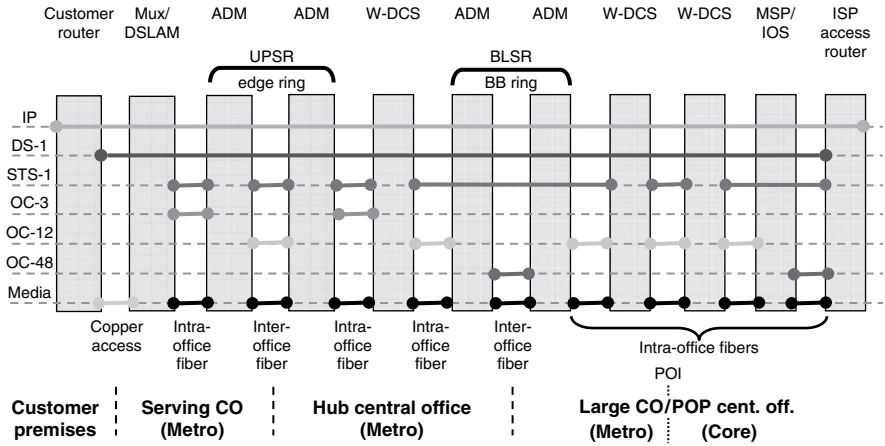

Figure 13.7 ISP POP example TDM backhaul to access router (this figure may be seen in color on the included CD ROM).

connection rate. The lowest horizontal line indicates the actual media used for that link in this example. The customer router has a DS-1 interface. From the point of view of the customer, he/she has a direct DS-1 to a port on the access router (AR) of the Inter-LATA carrier. From the point of view of the metro carrier, this is simply a DS-1 TDM private-line connection between the customer and a port/channel on the metro W-DCS: the metro carrier has no idea what is contained in the DS-1. This sort of encapsulation of packets in a TDM private-line connection to a packet-network interface is often called TDM *backhaul*.

The AR resides in the POP location, along with a lot of other equipment associated with the lower-layer networks that support this connection. As one can see, although the IP protocol stack views the DS-1 as a "physical" connection/layer, it is quite logical in nature. The dotted lines indicate the interface level of the connections between the network equipment, mostly determined by the multiplexing and demultiplexing that the DS-1 experiences as it traverses the metro network and mixes with other connections with different endpoints. Out of the customer premise, the DS-1 is carried over copper (the prevalent media to most customer locations) to a DSLAM or DS-1 multiplexer. The DS-1 multiplexer multiplexes DS-1s into STS-1s (or DS-3s for older equipment) and hands off via an OC-3 containing other STS-1s as well, to a SONET ADM. The signal is then routed on a leg of a UPSR OC-12 ring containing yet more traffic to a larger office with a W-DCS, which is the hub location associated with the serving CO of the customer location. The DS-1 is de-multiplexed into an STS-1 channel of an OC-3 link to the W-DCS. The links between W-DCSs (that form a mesh network) are channelized STS-1s, generally transported by OC-48/192 backbone rings. Figure 13.7 shows the DS-1 riding one link of the W-DCS network, which ends at the POP CO, which is usually co-located in the same building as a large metro CO.

For simplicity, this example assumes that this circuit routes on one leg (a single hop) of each ring.

Once the circuit enters the POP, it hands off from the metro W-DCS to the core W-DCS across the POI. This figure illustrates the interface as an OC-12, although the DS-3 interface is still a common handoff rate. One end can be owned by the metro carrier and the other by the core carrier. Note that as carriers have split up and subsequently merged since 1984, these two carriers might indeed be members of the same corporation. The FCC still has rules concerning separation of services, and some separation is likely to exist for some years following the writing of this chapter. After the DS-1 enters the core W-DCS, it is groomed with all the other DS-1s destined for the AR. The STS-1s destined for the AR are routed usually through a SONET cross-connect, which is a more intelligent and distributed version of a modern B-DCS with optical interfaces [which AT&T termed an *intelligent optical switch (IOS)*]. The purpose of routing through a platform like an IOS is that if there is a need to redirect the STS-1 toward another AR, this can be done easily by rerouting the STS-1 in the IOS network. This flexibility and grooming capability is the key motivation for routing through such cross-connect devices. Note that we depict the IOS along with an multi-service platform (MSP). An MSP multiplexes the lower rate signals to OC-48 or higher to hand off to the IOS. Its use is governed by the economics of pricing for interface cards on high capacity equipment.

The business access segment of the metro network is evolving to Ethernet for both interfaces and transport protocol. This is mainly since businesses prefer Ethernet interfaces into the metro *Wide Area Network (WAN)* because of the consistency with their LAN, simplicity, and low cost. Most Telcos have introduced Ethernet transport services. Initially, the Ethernet layer networks to carry these services have hub-and-spoke topologies that consist of a low number of switches or routers (sometimes just one) in the backbone portion and low cost Ethernet switches at the customer premise.

Figure 13.8 shows the service example of Figure 13.7 using the Business Ethernet layer. This is still basically the same ISP service, but here the customer has an Ethernet interface that is transported as a switched Ethernet service over the Ethernet layer. Currently, few of the links between Ethernet switches are carried over ROADM, but we illustrate a likely scenario for the coming years. It is unlikely that economics will support the use of ROADMs in the COs of the metro network that are currently occupied by the edge SONET ring layer, so we show the link from the *network premise equipment* (NPE), which is generally a low-cost Ethernet switch owned and controlled by the carrier but on or near the customer's premises, to the backbone Ethernet switch. The links between backbone Ethernet switches are shown routed over ROADMs since these are more likely to be in large COs. One major difference with Figure 13.7 is that, in contrast to SONET rings, the ROADM rings generally have no restoration capabilities; restoration has to be handled by the Ethernet layer. The handoff to the core router is typically GigE (or 10 GigE) over fiber. Note that this fiber might route through a fiber patch panel for flexibility. The customer's access link from his/her CPE to the AR is separated and identified by a

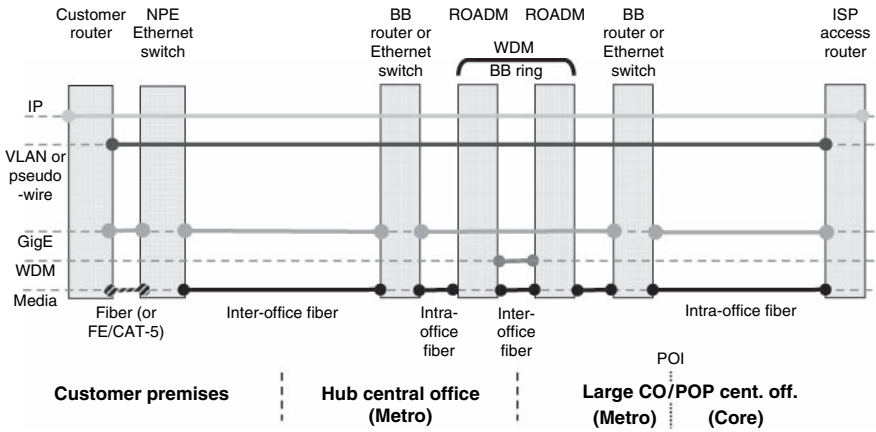

Figure 13.8 ISP POP Example Ethernet transport to access router (this figure may be seen in color on the included CD ROM).

VLAN ID or pseudo-wire ID, if layered with a PWE3-capable protocol, such as MPLS. Comparing Figures 13.7 and 13.8, one can readily see the improved simplicity of carrying packet services over packet networks.

Finally, we briefly mention the IP layer that has emerged to carry IPTV. In this discussion, we have segmented the Ethernet layer into two layers because this is how the Ethernet transport is being implemented in the near-term. Because of the order-of-magnitude size difference between the two Ethernet transport networks (residential/entertainment video vs. business Ethernet services), the residential Ethernet layer is being customized for the video application and most of the ROADM network layers have been economically justified to support the large numbers of GigE or 10 GigE links needed. Furthermore, the business Ethernet services have to support VPLS, spanning tree protocols and other virtual LAN services, which are not generally relevant for residential packet services. At some point, it is possible that the two Ethernet networks will merge, but that evolution is not clear.

13.1.4 Core-Layer Networks and Technologies

The typical network layers of the core network segment for a large US commercial carrier are depicted in Figure 13.9. Note that, as with the metro and access examples, this figure represents a significant simplification and does not describe all the network elements and technologies or all the services and will vary somewhat carrier by carrier; however, it does capture the most predominant layers and principal inter-layer relationships. As with the metro network segment, let us explore first the legacy stack of network layers on the right. Network layers that are essentially capped (not growing or growing very slowly) are hashed. As with the metro segment, this stack was engineered and developed over many decades to provide legacy voice services.

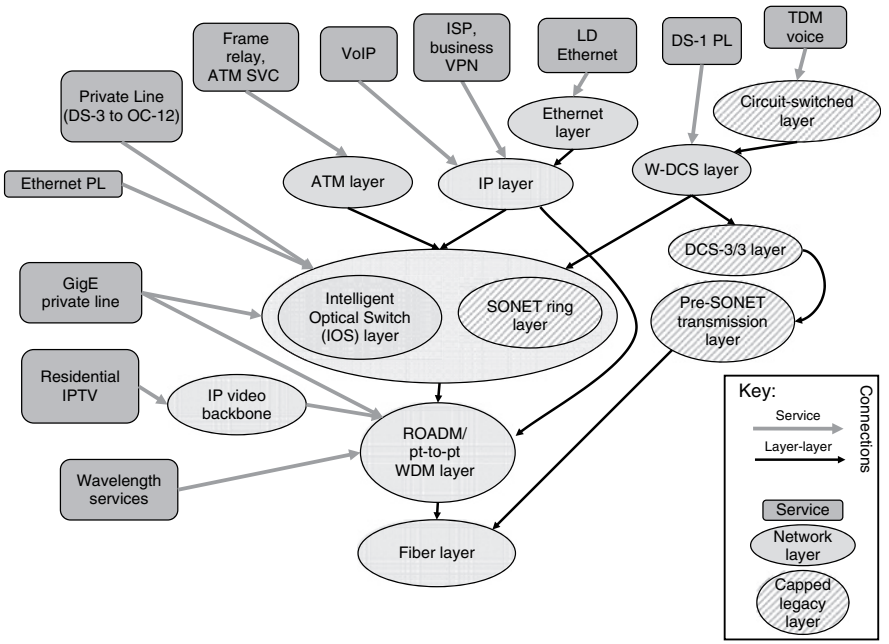

Figure 13.9 Example of core segment network layers (this figure may be seen in color on the included CD ROM).

In the case of the core network segment, the original circuit-switched network was used for the wholesaling of telecommunications services (initially telephone calls). In fact, the wholesaling capability (among various other factors) led to the eventual breakup of the Bell System monopoly in the early 1980s as the AT&T Long Lines business unit was forced to wholesale call minutes to emerging, competitive long-distance companies, from which the US intra-LATA/inter-LATA competitive framework for long-distance carriers eventually emerged. Similar to the metro network segment, the DS-0 trunks (channels of DS-1s) that connect the nodes of the circuit-switched layer route over the W-DCS layer. Continuing down the "legacy" network stack, the DS-3 links of the W-DCS are transported over DCS-3/3s, a DCS that cross-connects DS-3s that interface it (note that the term B-DCS was coined by Bellcore to include both the pre-SONET DCS-3/3 and SONET DCS with its optical interfaces and ability to cross-connect at STS-1 or higher rates). The DS-3 links between the DCS-3/3s are routed over pre-SONET transmission systems. Originally, the DCS-3/3 was developed as a natural evolution of the manual DSX-3 cross-connect frame functionally analogous to the fiber "patch-panel" of today but with coax cables. That is, it was viewed as a remote-controlled DSX frame for cross-connecting the basic unit of transport at the time, the DS-3. The ability of the DCS-3/3 to rapidly (relatively to that era) and automatically reroute DS-3 connections motivated development of the first large-scale transport mesh restoration methods [7].

With the advent of SONET, growth of private line and IP services, the legacy transport stack became inadequate. During a transitional period, SONET rings were introduced into the core network. However, examining Figure 13.6, the impracticality of using SONET rings in a large core segment is obvious. Furthermore, early restoration studies showed SONET rings to be economically inferior to mesh restoration with DCS-type equipment, such as the Intelligent Optical Switch (IOS) [9]. Upon deployment of the IOS, the SONET ring layer was relegated to reaching smaller COs (i.e., edge of the core segment) and is essentially capped in most core network. The other main factor in this evolution is restoration, detailed in Section 13.2.3. The relationship of the other services, discussed for the most part in the metro segment, can be seen in Figure 13.9. Note that the separate IP video backbone layer can be functionally carried over the IP layer. However, full-featured entertainment video has very specialized performance and multicast properties and, hence, is usually carried over a dedicated layer. Perhaps as advanced QoS features of the core IP network are introduced, they will eventually enable the convergence of all IP services, including consumer entertainment video.

Comparing Figure 13.9 with Figure 13.5, the differences between the core network segment and the metro network segment are evident. While the SONET ring layers dominate in the metro, the SONET ring layer is minimal in the core. In the core, the fastest growing layer is the IP layer and almost all upper network layers route over a ubiquitous WDM layer. We thus focus on the IP/OL (read "IP over Optical Layer") architecture as the evolving "network of the future" and examine its migration in more detail in Figure 13.10. One can see that the IP layer is segmented into ARs and backbone routers (BRs). The reasons for this segmentation involve aggregation and restoration and, as such, are covered in the next section.

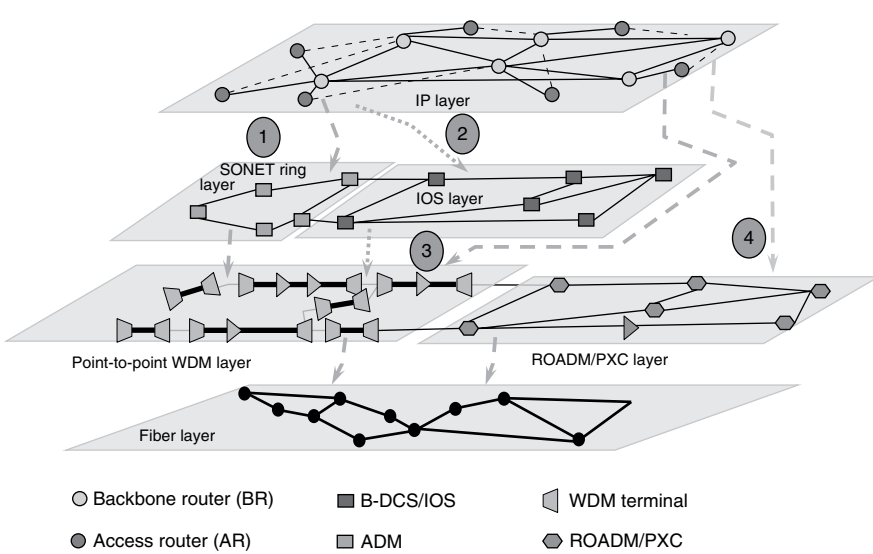

Figure 13.10 Example of core network layers (this figure may be seen in color on the included CD ROM).

The core IP layer originally had its links (e.g., OC-12) route over the SONET ring layer and then the IOS layer (or combinations thereof). As the size of the IP links increased, they routed directly over the WDM layers, skipping all intermediate SONET cross-connect layers. A chief reason for this is that the IP layer is capable of restoration itself using the Internet Engineering Task Force (IETF)-standardized suite of Interior Gateway Protocols (IGPs) [e.g., open shortest path first (OSPF) or intermediate-system-to-intermediate-system (IS-IS) reconvergence]. The economics and other tradeoffs of restoration at the IP layer vs. lower layers are discussed in the next section.

The WDM layer is itself a study in network evolution. Originally, just as in the metro network, point-to-point WDM systems were deployed to relieve cables facing fiber exhaust and their shelf organization was specialized to interface links of SONET rings. However, as WDM became ubiquitous (which involved an evolution and then "de-evolution" of various fiber types and characteristics, as described in other chapters), the economics of core-segment transport became dominated by the short length of these point-to-point WDM systems (around 100 miles on average) and subsequent large use and high price of O-E-O regenerators. This led to the deployment of ultra-long-haul systems that connect ROADMs and photonic cross-connects (PXCs) which route photonic signals i.e., wavelengths. While the subject of ROADMs and PXCs is covered thoroughly in Chapter 8, we will give a brief overview for this discussion.

The simplest ROADMs allow for connections to be added to and dropped from wavelengths. A ROADM is connected to other nodes via links in two directions (often called East and West) and hence is termed a degree-2 node. More sophisticated ROADMs will need to be capable of multidegree routing, or to route wavelengths among more than two interfacing fiber pairs or directions. Multidegree capability is needed when the length of the WDM transmission systems (i.e., the distance between O-E-O regenerators) exceeds the distance between major network nodes. A multidegree node is connected by links to other nodes in more than two geographic directions. These are termed degree-3, degree-4, or higher. Thus, instead of adding/dropping traffic from the various directions in the electronic domain, a multidegree ROADM can add/drop in the photonic domain.

The evolutionary stages of the core network are marked with ovals, numbered 1 4 in Figure 13.10. The first stage had the IP traffic carried over SONET rings. In stage 2, that traffic was carried over the IOS network. In stage 3, IP signals were routed directly over the WDM layer, while in stage 4 that traffic is carried on a ROADM- and PXC-based network. As of this writing, this evolution is still in progress and currently all of the arrows of Figure 13.10 still exist, but the fourth stage is the target architecture and generates the most capacity growth. Today, the links of the IP layer between BRs are 10- and 40-Gb/s POS (Packet-over-SONET). However, 10-Gb/s Ethernet is emerging as well as 100-Gb/s Ethernet. We note that in contrast to enterprise networks, where Ethernet interfaces are significantly less expensive than their SONET counterparts, this relative difference narrows on very-high-speed router interfaces, whose costs are dominated by other factors related to packet switching and routing.

13.2 RELATIONSHIP OF SERVICES TO THE LAYERS

13.2.1 Service Requirements and How They Affect Technologies of the Layers

Network services are provided by network overlays at each layer. Each layer then places requirements on lower layers all the way down to the optical layer. Service requirements differ by the type of service and layer where they are provided. Service requirements can be divided into two basic classes: (1) expectations for provisioning new services or features of existing services, including bandwidth constraints/options, and (2) Quality-of-Service (QoS) parameters, such as Bit Error Rate (BER), packet loss, latency/delay, jitter. As one would expect, all of these requirements can differ by network segment, layer, and type of service. We give some high-level examples in Table 13.1. Note that these are for illustration purposes only and do not represent actual service requirements of any particular commercial carrier.

To achieve the stringent QoS requirements (such as network availability), a commercial carrier must provide various restoration methods in the network segments and layers. These will be described in a Section 13.2.3.

13.2.2 QoS, SLAs, and Network Availability

QoS is a complex function that varies layer by layer. For the TDM and optical layers, it is mostly a function of maximum BER tolerance and delay. Other chapters define and explain BER for optical layer networks in more detail. We will discuss QoS as it relates to the other layers of the network. However, note that all QoS examples we provide in this section are tutorial in nature. In particular, they do not constitute recommendations and are not meant to imply any commercial service guarantees. By modeling BER as a 0/1 function [i.e., either a network link exceeds a maximum and generates a *threshold crossing alert (TCA)* which generates a critical alarm or it does not] and then including whether a link is up or down [e.g., it generates *loss of signal (LOS)* or other critical alarm], one can formulate a *network availability* model for a particular network layer. This subject is complex, involving probability and networking, the details of which are outside the scope of this chapter, but the following will attempt a simple description.

Consider the WDM layer and index all of the n components of it plus its lower fiber layer for a particular specific network (e.g., optical amplifiers, WDM terminals, ROADMs, optical transponders, fiber spans) and then define a 0/1 variable, c_k, for each component k for $k = 1, \ldots, n$. $c_k = 0$ signifies that component k is *unavailable* or *down* and a $c_k = 1$ signifies that the component is *available* or *up*. A given *failure state, s*, of the network can be represented by the n-tuple $s = (c_1, c_2, \ldots, c_n)$. The failure state space is the set of all possible states. For a reasonable size network, n could be hundreds or thousands and thus

Table 13.1
Examples of service requirements for today's services.

Segment	Service	Example provisioning requirements	Example QoS
Access (Residential)	TDM Voice	New line in 7 days	Levels of static, buzz, outage. Repair in 3 days
	Broadband Residential ISP	New service in 3 14 days Various rates (down, up) (512 Kb/s, 125 Kb/s), (1.5 Mb/s, 512 Kb/s), etc.	Refunds for outages ≥6 to 24 hours
	IP Video	Still under development	Must keep jitter and loss very low. Various forms of retransmit, FEC and buffering used to mitigate
Metro	Private Line	New service anywhere from 1 week to 6 months. Rates from DS 0 to OC 192/10 GigE	Jitter/delay meet Bellcore TR 253 Availability range from 0.9995 to 0.9999
	Business ISP	New service in weeks. If uses private line backhaul for access, subject to above Bandwidth limited by access size or other policing SLA	For 95% of the time, no more than 1% packet loss. Latency <10 20 ms
	Voice	Residential: same as access; Wholesale business: varies by contract	≤0.005 blocking
Core	Private Line ≤622 Mb/s	Similar to metro; ends includes metro segment	Jitter/delay meet Bellcore TR 253 Latency varies by distance. Availability similar to metro except core availability is without the metro ends
	Private Line ≥622 Mb/s & Wavelength Services	Generally longer than private line if routed directly over WDM layer	SONET Private Line meets Bellcore TR 253. 1/10/100 GigE not well specified Availability not well specified since usually no restoration provided
	Business VPN	1 day. If uses private line backhaul, access is subject to Private Line requirements	Packet availability QoS similar to metro Latency depends on distance and lower layer routing, sometimes ranging from 5 to 50 ms

the state space, although finite, is intractable in size (2^n). The rate at which components go down is governed by a stochastic process, often a Poisson, which is totally specified by a single parameter for each of them, the mean time between

failure (MTBF). The rate at which components come up is governed by a stochastic process, usually following an exponential distribution specified by the mean time to repair (MTTR). Similar to a massive Markov process, various failure states transition to other states by components going down and coming up (being repaired) with the given rates. Thus, the probability that the network is in a given failure state can be computed. However, the intractable size of the state space must be computationally addressed. The most significant observation is that the nonfailure state (fully operation state) of the network, (1, 1, . . . , 1), typically has a high probability (e.g., 0.8 or more). Failure states are usually rare. For example, if network availability reaches $1 - 10^{-5} = 0.99999$ (the popular "5 nines"), then it is generally considered very reliable. Thus, network states with probability less than a certain tolerance, ε, such as 10^{-5}, need not be explicitly evaluated. Let us index the states, s_i, in order of decreasing probability. Although the size of the state space is exponential, the maximum value k such that $\sum_{i=1}^{k} \Pr\{s_i\} \leq 1 - \varepsilon$ does NOT grow exponentially in the variable n. If we lump the states s_i for $i > k$ into an *unevaluated* set, then we only have to evaluate its complement (the *evaluated* set), which may be of tractable size. We know that we can bound the answer.

To make use of this, we define *performance functions* (PFs) for the QoS parameters of the services carried over the network under study, most of which involve some form of loss. Of course, not every service/customer/user of a network is affected by every failure state. For a network, this is generally defined in terms of the connections that use it. As an example, consider multichannel entertainment digital video (like IPTV) over a WDM backbone network from a central source (e.g., primary Head End) to destination nodes (e.g., secondary Head Ends). Define an availability PF, $a(d, s_i)$, to be 0 if failure state s_i causes destination d to be disconnected from the central source, and 1 otherwise. The expected availability of the video service to node d can be found by computing $\sum_{i=1}^{n} a(d, s_i) \cdot \Pr\{s_i\}$. To make this computation tractable, apply the technique above to only compute the QoS availability over the evaluated set. For example, suppose the availability PF over the evaluated set is found to be 0.999 (3 nines). Then we can bound the expected network availability, $E(a, d)$, is bounded by $0.999 \leq E(a, d) \leq 0.999 + \varepsilon$. The lower bound corresponds to disconnection [unavailable, $a(d, s_i) = 0$] over every state in the unevaluated set while the upper bound corresponds to service-without-loss [service available, $a(d, s_i) = 1$] over every state in the unevaluated set.

However, the catch is that *a priori* one does not know how to order the failure states. Generally, most analysts or network operators/engineers, even academicians, make simplifying assumptions about the evaluated set. For example, in most cases they assume it only consists of single-fiber failures and ignore all other failure states. But, often this only gets us to 0.99 or 0.999 probability of the state space. There are mathematical techniques and algorithms, such as statistical dominance rules, to build analytical performance tools to allow setting of a tight tolerance, ε, such as 10^{-5}. See Ref. [10].

Another issue with QoS parameters is how to define them over multiple connections. Drawing on our previous simple example of video service over WDM layer, we could define the *worst-case* network availability as $E_{\mathrm{WC}}(a) = \min_{d} E(a,\ d)$. Or, we can define the average network availability $E_{\mathrm{AVG}}(a) = \frac{1}{m}\sum_{d} E(a,\ d)$, where m is the number of connections (destinations). However, it should be noted that the average availability is a risky QoS measure to use as a design criterion because networks can be quite uneven in their design and traffic matrices. More sophisticated QoS measures can be defined on the distribution, such as finding the number x, such that the availability is more than x for 95% of the nodes.

Let us now turn our attention "up" the stack to the IP layer. There are many more potential and complex loss QoS PFs. For example, packet loss is the most common QoS for the IP layer. This is now a good place to introduce the notion of a *Service Level Agreement (SLA).* An SLA is a set of guarantees that a carrier provides to a customer for the network service. Typical SLAs for the IP layer contain a packet loss PF based on the probability distribution. An example SLA could be that a customer should expect no more than 5% packet loss 95% of the time. Evaluating packet loss on the model we described above is more difficult than the much simpler network availability for the optical and circuit-switched layers. Because of the complex protocols that run over the IP layer, the somewhat unpredictable behavior of (IP) routers, the buffering and queuing disciplines in the routers, the routing aspect of traffic, and the bursty nature of packet traffic, this is truly challenging. That complexity will not be described in detail here, but refer the reader to Ref. [10] for more detail. Alternatively, for a private-line circuit (connection) over the DCS or SONET layers, an example SLA might be a simple availability QoS PF of network availability $\geq$0.99995. Again these are illustrative examples and do not represent actual SLAs of any particular carrier.

Let us now focus on a three-layer network: IP/WDM/fiber (read "IP over WDM over fiber") from the core segment of the overall network. Following the layered network model of Section 13.1, the IP links form connections transported by the WDM layer. One can then calculate the availability of those connections due to failures in the WDM layer just as done previously for the video example. By including the IP-layer components to the failure state space (e.g., router common cards, router fabric, router line cards, and optical transponders to connect the router links to the WDM terminals), one can then calculate the availability of the IP network. However, if the nonfailure state has a probability of about .8 or even .9 (as is often the case), the astute reader may ask, "How do we get the network closer to an objective in the range four to five nines (.9999 .99999)?" The greatest control that network administrators have to improve *network availability is restoration*. But recall that it has been found to be more cost-effective to limit restoration to certain layers. In this example, assuming that the core WDM layer offers no restoration (the usual situation in today's Telco core network), then restoration must be provided at the IP layer. Now, in addition to the downtime

from an IP-layer link (originating from a failure or planned take-down event, such as maintenance, in any one of the layers) and then subsequent return to the "up" state after repair, automatic restoration must be included, which does not return the IP link to the up state, but reroutes traffic around the down link. However, if indeed we were examining a multilayer network stack (such as the ATM/IOS layers in Figure 13.9) was being examined where restoration was provided at the lower layer, then the upper layer link would in fact experience a short down period while its connection was rerouted at the lower-layer network. These are factors that basically make the computation of the QoS PF, such as $a(d, s_i)$, more complex and dependent on the specific network layers, their interrelationships, and restoration methods at each layer. We examine specific restoration methods in the next section.

13.2.3 Network Restoration

The authors estimate that network operators and engineers spend at least 75% of their time attending to the maintenance of network performance. This involves avoiding, detecting, measuring, or planning for potential network component failures or traffic congestion, as well as maintenance and upgrade of network components to meet their network QoS and SLAs. After the QoS/SLA discussion of the previous section, the reader can now understand why network restoration is the main architectural tool that network operators have for achieving their QoS objectives.

In today's network segments, restoration against network failure can and does occur across several network layers. If one does not understand these layers and their relationship, then fully understanding restoration in large commercial networks is difficult. With the foregoing explanation of the network layers, there are some fundamental properties of network failure analysis that we will list here:

(1) Failures can originate at any layer. As a general rule, failures that originate in a given layer cannot be restored at a lower layer. For example, if an ATM switch fails, all the PVCs that route through that switch will be lost. The links which terminate on that switch cannot be restored at a lower layer since the switch itself has failed. The PVCs must be rerouted around the lost switch at the ATM layer.
(2) Since links at any layer are essentially logical, multiple links may route over the same connection or node at a lower layer. Thus, a network or node failure at a lower layer usually results in multiple link failures at higher layers. This phenomenon means operators must identify the shared-risk-link groups (SRLGs), mentioned earlier, which simply means it is important to identify the lower-layer links that each connection routes over. This is a critical fact often glossed over in some academic circles, where only single-link failures are examined in overlay networks.
(3) Given property 1, to meet even the weakest network availability or QoS objectives, all upper-layer networks must provide restoration in some form,

no matter how rudimentary. The crudest form of restoration is typically accomplished by reprovisioning connections through their connection setup control mechanisms in response to network failure.

(4) It is important to understand how the behavior of a link, X, at a given layer depends on lower-layer restoration. If X is provided as a restorable connection by the lower layer and a failure originates at the lower layer that causes X to go into an unavailable state (go down), then it is down for the (usually very short) period until the connection is restored at the lower layer by rerouting its connection to a nonfailed path, assuming that sufficient restoration capacity is provided to reroute the connection. In contrast, if the lower layer provides no restoration or if link X is provisioned as a nonrestorable connection, then link X stays down until the lower layer failure is repaired. If the failure originates at the same layer as X, then link X stays down until repaired.

Restoration Methods by Network Segment

The restoration methods for each network layer of the network segments discussed in previous sections are summarized below. As usual, there is no claim that this listing is complete or fully represents the architectures or performance of any carrier. The restoration methods for the access-, metro-, and core-segment example networks are summarized in Tables 13.2, 13.3, and 13.4 respectively.

We give brief and simplified descriptions of the most important restoration methods.

UPSR SONET Ring (Figure 13.11a) In this architecture, the ring is configured over two unidirectional transport rings, one transmitting in a counterclockwise direction over the nodes of the ring (sometimes called the *outer ring*) and the other transmitting in the clockwise direction (sometimes called the *inner ring*). An

Table 13.2

Example of access-segment restoration methods.

Network layer	Restoration method(s) against network failures that originate at that layer or lower layers	Example Restoration time scale
Copper/fiber	No automatic rerouting	hours days
xPON, xDSL, PPPoE, ATM	No automatic rerouting	hours days
Ethernet	No automatic rerouting	hours days
IP	No automatic rerouting	hours days
SONET chain (residential)	Hot standbys for card failure. No automatic rerouting	10 ms (hot standby); hours days (otherwise)
SONET ring (business)	UPSR or 1 + 1	10 20 ms

Table 13.3
Example of metro-segment restoration methods.

Network layer	Restoration method(s) against network failures that originate at that layer or lower layers	Example Restoration time scale
Fiber	No automatic rerouting	Hours
ROADM/Pt Pt WDM layer	No automatic rerouting	Hours
ROADM layer with path switched restoration	1 + 1 restoration	10 20ms
SONET ring (backbone)	BLSR	50 ms
SONET ring (edge)	UPSR or 1 + 1	10 20ms
ATM	(1) No automatic rerouting or (2) P NNI reprovisioning of PVCs or (3) centralized mesh restoration	(1) Hours (2) Seconds (3) Seconds
W DCS	No automatic rerouting	Hours
Ethernet or Layer 2 (e.g., MPLS)	(1) No automatic rerouting (2) Spanning tree reconfiguration (3) Rapid spanning tree (RST) (4) Link fast reroute (FRR)	(1) Hours (2) Seconds (3) Subsecond (4) 50 ms
IP	IGP reconfiguration [reroutes new flows and generates new multicast trees (where used)]	10 60 s
Circuit switched	Automatic alternate rerouting of new calls (existing calls dropped)	Seconds

STS-n connection enters and leaves the ring (denoted as nodes A and Z, respectively) via add/drop ports of the ADM at the two end nodes of the connection. For a ring in a nonfailed state, A transmits to Z and Z transmits to A in the same counterclockwise direction (on the outer ring). The connection transmits over n consecutive channels (or time slots), starting at a channel numbered $1 + kn$ (where k is an integer ≥ 0). It sends a signal from A to Z on one ring and a duplicate signal from A to Z in the other direction on the other ring. A port selector switch at the receiver chooses the normal service signal from one direction (usually counterclockwise). If this signal fails (i.e., the ADM receives an alarm), then the port selector switches to the alternate signal. It reverts to the original signal after receipt of a clear signal or under other control messages. Some versions of OC-3 or OC-12 rings are channelized to VT 1.5 channels.

BLSR SONET Ring (two-fiber) (Figure 13.11b) In this architecture, the first half of the channels (time slots) in each direction are used for transmission when the ring is in the nonfailed state. The second half of the channels is reserved for restoration. When a failure occurs, a *loop back* is done at the add/drop

Table 13.4
Example of core-segment restoration methods.

Network layer	Restoration method(s) against network failures that originate at that layer or lower layers	Example Restoration time scale
Fiber	No automatic rerouting	Hours
ROADM/Pt Pt WDM layer	No automatic rerouting	Hours
ROADM layer with path switched restoration	1 + 1 restoration (electrical)	10 20 ms
SONET ring	BLSR	50 100 ms
IOS (DCS) layer	Distributed path based mesh restoration	Subsecond to seconds
ATM	P NNI reprovisioning of PVCs	Seconds
DCS 3/3 layer	FASTAR (DCS mesh restoration under centralized control)	Minutes
W DCS	No automatic rerouting	Hours
Ethernet or Layer 2 (e.g., MPLS)	TBD	
IP and IP video	(1) IGP reconfiguration [generates new multicast trees (where used)]	(1) 10 60s
	(2) Layer 2 fast reroute (FRR)	(2) 50 ms
Circuit switched	Automatic alternate rerouting of new calls (existing calls dropped)	Seconds

port of the nodes surrounding the failed ring segment and the failed segment is patched with (rerouted over) the restoration channels over the links in the opposite direction of the failed segment around the ring. In the case of node failures and multiple failures, complicated procedures using *squelch tables* and other mechanisms are standardized to prevent mis-cross-connection for connections whose ends are in the failed segment. Connections must be assigned to the same channels on each link of the ring over which they route. A BLSR has the advantage over a USPR that the same channels (time slots) on different links can be assigned to different connections whose routes do not overlap over links of the ring and thus save some capacity.

BLSR SONET Ring (four-fiber) Four-fiber BLSR is not a commonly deployed technology and therefore we do not describe it here.

IP-Layer IGP Reconvergence This is the most common method of restoration in large commercial IP-layer networks today. It usually uses either OSPF or IS-IS signaling messages for general topology updates and then to recompute paths for routing IP flows or for MPLS forwarding. The IGP reconvergence mechanism is used whenever the IP topology changes by flooding messages (i.e., sending them to all neighboring nodes, and then recursively over the entire network) called *link state advertisements (LSAs)* in response to the change. Generally, the LSA is a *link-up, link-down*, or *weight change* message. If an IP-layer link changes status

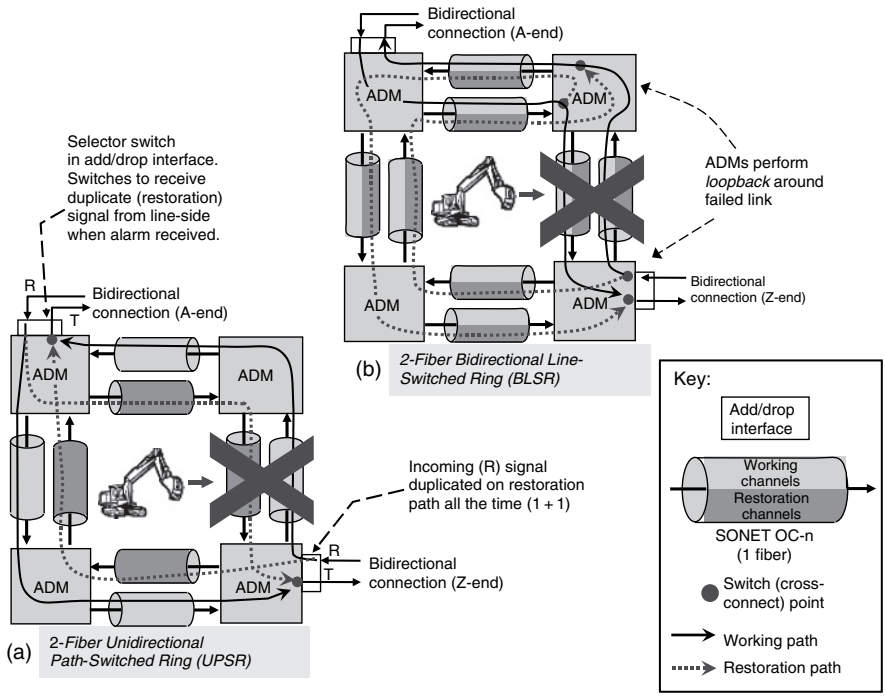

Figure 13.11 SONET self healing rings. (a) UPSR, (b) BLSR (this figure may be seen in color on the included CD ROM).

either by being detected to go down due to a network failure or by being intentionally taken out of service for a maintenance event (or, more commonly, its link weight is changed to a very large value), then that constitutes a topology change. Therefore, the IGP reconvergence mechanism becomes, effectively, a restoration method whereby each router recomputes the shortest paths to each destination router port in the network and then adjusts its routing table accordingly. In practice, this generally takes anywhere from 10 to 60 s; however, experiments and analysis have demonstrated that this can be reduced to less than 5 s, if various required timers are carefully adjusted. However, in practice, these are not easy to control.

IP-Layer MPLS Fast Reroute (FRR) This is a standardized restoration procedure in which primary and backup (restoration) *Label-Switched Paths (LSPs)* are established for next-hop or next-next-hop MPLS FRR. When a failure is detected at the routers surrounding the failure (usually via linecard interfaces), the MPLS forwarding label for the backup LSP is "pushed" on the MPLS shim-header at the first router and "popped" at the second router. These labels are precalculated and stored in the forwarding tables, so restoration is very fast. 100 ms or less

restoration has been demonstrated. While enabling rapid restoration, because these paths are segmental "patches" to the primary paths, the alternate route is often long and capacity inefficient. Furthermore, flows continue routing over the backup paths until the alarms clear, which may span hours or days. To address this inefficiency, there are more sophisticated versions in which the FRR provides rapid restoration and then IGP reconvergence occurs and the IP-layer routing is recalculated to use more efficient end-to-end paths.

IOS-Layer Shared Mesh Restoration This method is a distributed restoration technique. Links of the IOS network are assigned routing weights. When a connection is provisioned, its source node computes and stores both the normal route (usually along a minimum-weight path) and a diverse restoration route through IOSs. The nodes communicate the state of the IOS network connectivity via topology update messages transmitted over the SONET overhead on the links between the IOSs. When a failure occurs, the switches flood failure messages to all nodes indicating the topology change. The source node for each affected connection then instigates the restoration process for its failed connections by sending connection request messages along the links of the (precalculated) restoration path. Restoration is differentiated among priority and nonpriority connections. The failed priority connections use the diverse paths and get first claim at the spare channels. After a time-out that allows all priority connections to be rerouted (restored) and the topology update messages to stabilize, the alternate paths of the failed nonpriority connections are dynamically computed and rerouted along those paths. It is called *shared* restoration because a given spare channel can be used by different connections for nonsimultaneous failures. Shared mesh restoration is generally more capacity-efficient than SONET rings in mesh networks (i.e., networks with average connectivity greater than two).

1:1 or 1 + 1 Tail-End Switch (Electronic) The fastest forms of optical-layer restoration are one-by-one (1:1) and one-plus-one (1 + 1) restoration, which switch at the ends of the connections. With 1 + 1, the signal is sent in duplicate across both the service path and the restoration path; the receiver then chooses the surviving signal upon detection of failure. In 1:1, the transmitted signal is switched to the restoration path upon detection of failure of the service path. Technically speaking, this is actually not "optical" restoration, but rather restoration by the electrical circuits at the ends of a lightpath, usually SONET-based and similar in behavior to a UPSR with only one channel. These techniques can trigger in as little as 20 ms (mostly due to hold-down timers to accommodate fault aging). However, this method requires a dedicated backup connection, which results in more than 100% restoration-overbuild of transport resources because of the longer diverse paths.

Circuit-Switched-Layer Dynamic Routing Restoration in this layer consists of routing new calls on alternate paths that avoid failed nodes or links. Existing

calls at the time of failure are lost. Dynamic routing finds the least utilized paths among many intermediate switches. Hierarchical routing can also provide restoration, but generally in highly connected networks dynamic routing provides significantly more paths than methods based on hierarchical routing and provides the same degree of restoration with more efficient use of capacity.

Ethernet-Layer Spanning Tree Protocol The spanning tree protocol generates paths in Ethernet networks via distributed signaling among switches. The principal development for spanning tree protocols was to avoid loops in Ethernet networks. However, it also generates a minimum-hop path and serves as a restoration method after topology updates settle. Rapid spanning tree is a version that accelerates the tree update process and provides a form of fast restoration.

Note that restoration architectures are not widely deployed in Telco networks in the residential loop and feeder networks (up to the first CO). This is mainly due to their tree-like topology (as illustrated in Figure 13.3), which would make alternate routing prohibitively expensive. However, the situation is more complex in business locations. As mentioned earlier, in the United States, the vast majority of business locations are still connected to the network by copper. For those locations it is somewhat similar to residential. However, for the fiber connected locations, as illustrated with the multitenant building example of Figure 13.4, one of the key factors in determining the restoration capabilities for the access network is the layout of the customer building. Generally, the portion of network up to the common space is not diversely routed since riser diversity is not easy to organize in this way. However, larger customers (e.g., other carriers) often will demand such diversity and be able to obtain it because of their large business presence in the building. Note that almost all SONET ADMs are installed as rings in common space. We note that today most access rings are in fact two-node SONET rings.

The most striking observation about Tables 13.2 13.4 is the variation of restoration capability of the layers directly above fiber. In the metro segment, the layer right above the fiber layer is (and has been) the SONET ring layer, which provides restoration. In contrast, in the core network, the next upper layer above fiber is WDM layer, which *does not* provide restoration. Although it is still early, so far, as ROADM technologies penetrate the metro segment, we are seeing this same trend. What are the reasons for this phenomenon? Are there future services or architectures that are driving this trend? The next sections shed more light on the reasons for this architectural trend.

Failures Across Multiple Network Layers

To describe some various restoration approaches and layer inter-relationships, restoration in the core network segment will be discussed first. Please re-examine the core-segment network layers shown in Figure 13.9. Automatic restoration is provided by the IP layer, SONET ring layer, IOS layer, and IP video backbone

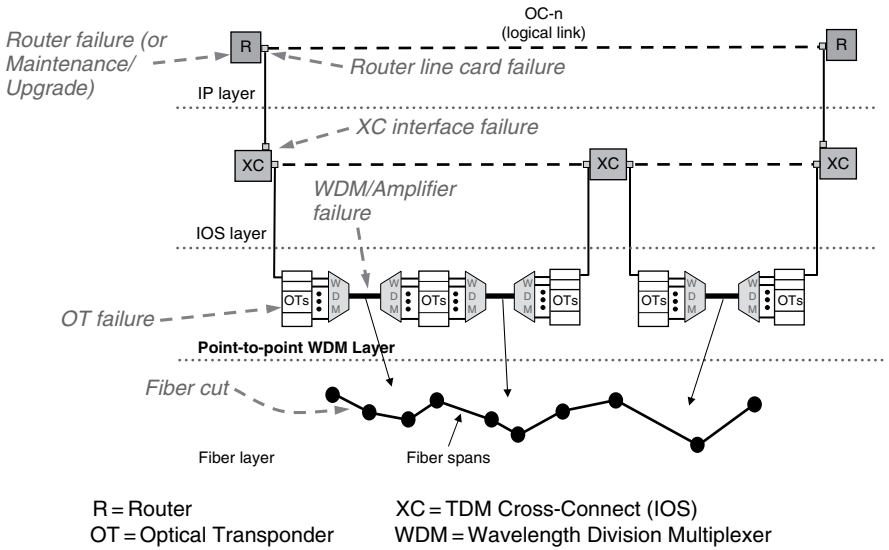

Figure 13.12 Example of Potential network failures at multiple layers (this figure may be seen in color on the included CD ROM).

layer. As Table 13.4 suggests, at present, no automatic restoration is provided in the WDM layers (other than a very limited number of high-speed SONET private lines with 1:1 protection). Examining the typical architecture for the increasingly important IP layer, one can see that IGP reconvergence is used for restoration. Almost all lower-layer failures in the core IP-layer network of Figure 13.9 result in failure of multiple IP-layer links. In fact, some SRLG failures can cause over 10 links to go down in large ISPs. FRR over MPLS (or other tunneling protocols) also is used by some carriers and by the IP video backbone.

The concept of how failures occur at different layers and how the layers are affected is illustrated in Figure 13.12 for the core network segment. This figure depicts, by simple example, the four layers of Figure 13.9 from the IP layer down, with emphasis on potential network failure. It shows an IP-layer link that routes over the IOS layer, like a link between an AR and BR located in different cities. The links of the IOS layer in turn route over the Pt-Pt WDM layer. The links (DWDM systems) of the WDM layer route over the fiber layer. Figure 13.12 only shows a few of the many component failures that can originate in the layers. For example, an amplifier failure at the WDM layers usually results in the failure of multiple IOS links and, as a consequence, multiple IP links. In this example, the IOS network would reroute its failed SONET STS-*n* connections on different paths. Assuming the rerouting is successful, the IP STS-*n* link would go down for a short time and then, after its alarm clears when the rerouting is complete, would be turned back up by the router controller. Alternatively, if some component of the router becomes unavailable (e.g., card failure, fabric failure, system or maintenance, upgrade, etc.), then the

IP layer reroutes the affected flows on different paths via IGP reconvergence. Note that the ability to restore connections at lower layers will not aid the affected IP flows that route through the failed router components. Also, the other overlay networks (frame relay, ATM, and circuit-switched voice) have not been depicted which could also be affected by the lower-layer failures.

It should be clear that to achieve QoS objectives, some form of restoration must be used. Many people in the optical community tend to assume that network operators will provide optical layer restoration as a straight-forward matter of achieving a QoS objective. But, at which layers should QoS objectives be set and how should they be defined? For example as shown, lower-layer failures can cause most of the network unavailability, but lower layers support multiple upper layers each with different QoS objectives. As the reader may have guessed already, the network layering, different service requirements, and choice of restoration architectures make this an inexact science. The situation is exacerbated when commercial carriers must further constrain these decisions by economics. For example, while it is generally true that (per unit of bandwidth) links at lower layers cost less than links at higher layers, it does not always follow that restoration should be fully provided at lower layer(s).

To explain this observation, in Figure 13.10 it can be seen that while some links between ARs and BRs route over the IOS or SONET ring layers, at present all links between core BRs skip the IOS layer and route directly onto the point-to-point WDM or ROADM layers. There is no restoration provided for the router links at these WDM layers. While efficient WDM restoration methods are not widely provided by vendors, in fact the reason for this architectural direction is mostly economic rather than vendor capability. Some of the leading factors for this interesting situation can be briefly summarized:

(1) Many failures (as illustrated by the router component failures in Figure 13.12) originate within the IP layer. Extra link capacity must be provided at that layer for such failures. This extra capacity can then also be used for failures that originate at lower layers. This obviates some of the advantages of lower-layer restoration.
(2) The IP layer can differentiate services by *Class of Service (CoS)* and assign different QoS to them. For example, one such QoS distinction is to restore premium services at a better level of restoration than best-effort services. In contrast, the WDM layer cannot make such fine-grain distinctions; it either restores or does not restore the entire connection supporting an IP-layer link, which contains a mixture of different CoS flows (including non-IP).
(3) Under normal conditions, there is spare capacity available in the IP layer to handle bursty demand. This is because, restoration requirements aside, to handle normal service demand, most IP links are engineered to run below 80% utilization during peak intervals and well below that during off-peak intervals.

Point 1 above is the most crucial driver. To further explain its effect, if we inspect Figure 13.10 in more detail, we see that each AR is *dual-homed* (either via intra-office fiber or via transport over the OL) to two BRs. There are a variety of architectural options to accomplish this. (1) There is just one BR per backbone CO. In this case, for each AR co-located with a BR, it uses intra-office fiber to link to the BR. The link to the mated BR must be transported over the other network transport layers (IOS, SONET ring, WDM, etc.). A remote AR (an AR not co-located with any BR) would use network transport to connect to each of two BRs. (2) Alternatively, there are dual-BRs in each backbone CO. Here, a co-located AR would use intra-office fiber to connect to each BR. A remote AR may either be linked to a mated pair of BRs in one office or link to BRs in different cities.

The reasons for having both ARs and BRs are manifold but, in particular, ARs aggregate lower rate interfaces from various customers. This function requires significant equipment footprint and processor resources (e.g., for customer-facing BGP and VPN processing). Major COs consist of many ARs to accommodate the low-rate customer interfaces. Without the aggregation function of the backbone router, each such office would be a myriad of inter-access-router tie links and inter-office links, which have historically proven to be unmanageable and expensive. To the contrary, backbone routers are primarily designed to be IP transport switches with only the highest speed interfaces. This segregation allows the BRs to be designed for multiterabit per second capacity. When a BR is down (e.g., due to failure of components, upgrade or maintenance), the AR shifts its demand to the alternate BR. This is an essential capability to achieve QoS. For example, key locations serve as peering points to other ISPs, the loss of which causes a significant outage. Thus, sufficient IP-link capacity is installed to reroute the traffic from an AR to its alternate-homed BR if any single-BR fails. However, because of point 2 above, the amount of extra capacity for restoration can be mitigated by allowing utilization levels during a failure event to rise above nonfailure levels. Also note that we have found that the biggest negative impact of the failure of a major BR is the loss of traffic originating at that router, rather than from "through" traffic. When all these three factors were examined the detailed network design optimization studies [11, 12] recommended providing restoration at the IP layer only.

13.3 NETWORK AND SERVICE EVOLUTION

13.3.1 Which Services will Grow and Which will Shrink? Demand and Capacity

Estimating the relative bandwidth impact of services on the network is not as easy as it would seem and, besides the complexity of layering, it also requires some knowledge of network design. First, we must divide service/network sizing into two pieces: *demand* (or *traffic*) and *capacity*.

For example, consider the frame relay service, which is transported over the core ATM overlay network. Define the traffic matrix $d(i,j,t)$ to be the average amount of demand (traffic) from source node i to destination j over time interval t, assuming for simplicity that all flows are point-to-point (in contrast to point-to-multipoint). A typical time interval for measurement purposes is 5 min. Note that packet traffic is typically bursty, so the maximum flow during that interval is even higher. Thus the demand over an interval is the time-averaged demand over that interval. Then the "instantaneous" total network demand at time t is $D(t) = \sum_{i,j} d(i,j,t)$. Of course, for most packet or voice services, $D(t)$ tends to be periodic by time-of-day, week, month, etc. However, in reality it never repeats exactly. We then define the total demand for that layer as $D = \max_t D(t)$ over the period of interest (say, several months). The capacity to carry this traffic is computed by a *network planning process*. In most commercial carriers, this process is akin to a network optimization problem where the objective is to minimize network cost subject to service requirement constraints, such as having enough capacity to provision new service requests and achieving a certain network QoS objective. Suppose for illustration that $D = 30$ Gb/s, the traffic matrix has an average hop count per connection of three hops, and that no link can exceed 80% utilization. Then, the network capacity must be at least 112.5 Gb/s. Of course, in reality this number would likely be higher because links can only be installed in discrete sizes, such as 2.5 or 10 Gb/s. In core networks, because network cost is more influenced by distance, network planners often prefer to express network capacity in units of capacity-distance. This is obtained by converting the capacity of each link in the overlay network to units of an "equivalent bandwidth" and then summing. "OC-48-miles," "DS-3-miles," and "10 Gb/s-km" are examples of such units. But, the major reason it is done this way is the network layering. That is, planners can easily cost out the equipment at the overlay network required to install a link, but it is hard to compute the cost of transporting that link as a connection over lower layers. Continuing the example, suppose these ATM links route over the IOS layer and that the IOS layer provides restoration. Thus, the "demand" for the IOS layer from the ATM layer is 112.5 Gb/s. However, private-line services and other overlays also use the IOS layer. Suppose the IOS layer is composed of 10-Gb/s links. Then the links from the ATM layer plus various private-line services route over the IOS network and share this link capacity. Furthermore, the (normally idle) restoration capacity is shared among these overlays and services. Once the IOS layer is sized, in an analogous, but quite different network optimization process, then one has a capacity estimate for this layer. This capacity then becomes demand for the WDM layer. Then repeat the same process to get demand for the fiber layer.

Now with an idea of how demand and capacity relate to layers, return to the question of how to express the relative size and growth impact of services. Generally, it is best to express it in multiple ways since it is often like comparing apples and oranges. For example, we can express an estimate of the size of the

demand at the highest layer where the service is provided. This is the 30-Gb/s frame relay example above. Then, we can express its impact to the lower layers of the network. In the case of the core network, this is either the WDM layer or fiber layers (or both). Thus, one metric we sometimes use in carrier networks is the amount of equivalent 10 Gb/s of capacity required by the WDM layer for each service. However, it is clear from the above capacity sharing and restoration aspects, that this is not an easy metric to generate. One approach is to generate network designs down the layers all the way to the WDM layer for a given service with only that service generating all the demand. Interestingly, note that it would be erroneous to add those WDM capacity units over all services and then presume the result is the capacity of the combined network. This is because of the sharing of capacity, discrete units of capacity, and restoration at each layer. But, it does give a useful metric to determine relative size. Of course, such numbers are not easy to generate. Most network planners do not even know them because they usually tend to plan layer by layer.

For optical engineers and researchers, the most significant impact of services on the WDM or optical layers is in the metro segment. This is because the core WDM layer is largely built-out. More efficient long-haul WDM technology will be pursued, but there are not major capacity issues to be tackled. In contrast, many metro networks have virtually no WDM and it has been hard to identify economic drivers for its widespread deployment until recently. In metro networks where ROADM layers are deployed, they are deployed in backbone COs, roughly corresponding with the nodes of the metro backbone SONET rings. Therefore, in terms of impact to the telecommunications optical systems industry, the greatest potential impact will be in the metro segment.

To better understand this, in Table 13.5 provides some very rough capacity impacts on a large Telco metro network based on our study of these networks. Note that these are not official size estimates for any given carrier and are only provided to give a very rough perspective. The second column gives the relative

Table 13.5

Rough estimate of impact of services on WDM/fiber layers in a large metro network.

Service	Present estimate of size in terms of WDM layer impact (%)	Relative growth rate
W DCS (Voice + DS 1 Private Line)	5 10	Small
Business ISP, VPN, FR	0 5	Small
Private Line (DS 3 OC 12)	5 10	Medium
Switched Ethernet	0 5	Medium
Residential ISP	0 5	Medium
Residential Video	50 75	Large
Ethernet PL (<GigE)	0 5	Small
Wavelength Services & GigE PL	20 30	Large
Dynamic Bandwidth Services	Negligible	Unknown

impact to the WDM and fiber layer caused by that service in today's network, as a fraction of the total capacity of that metro. This is complex and hard to estimate because with only a partial WDM footprint, many links of higher layer networks route over a combination of direct fiber and links of WDM systems. But, it can be clearly seen that in metros where IP networks are installed to carry residential video, this service dominates. High-rate private line and GigE private line are also large contributors. The demand for these services comes mostly from external overlay networks. Many of these customers are themselves carriers.

The last row lists *dynamic bandwidth services*. These dynamic *constant bit rate (CBR)* services are drivers for fast provisioning. They fall into two categories: subwavelength rate and wavelength rate (the dividing line is now 10 Gb/s and likely to move mostly to 40 Gb/s by 2012). We envisage that the main demand for the wavelength-rate dynamic CBR services will come from government, limited e-Science/grid computing, and large, multisite private networks. For example, AT&T offers a "bandwidth-on-demand" type service called Optical Mesh Service (OMS). This service currently provides rapid (subminute) setup of TDM connections between customer access locations via the IOS layer. Its principal customers are large enterprise customers or other carriers with large multisite networks.

An important point is that we assume traditional subwavelength TDM private-line services will continue to be used. This is an important point because many articles in the late 1990s seemed to dismiss these services. However, it is now many years later and today the capacity of the core network (core segment, IOS layer) needed to provide these sub-OC-48 services today is still large and growing. We assume sub-wavelength private line services will continue to have significant demand over the near future. Our rationale is as follows. Following historical growth patterns, the highest optical transport rates of today (i.e., wavelength services) evolve to subwavelength rates of tomorrow. Today most private lines are in fact links of customer IP networks. Many of these "customers" are indeed other carriers or government entities. The business need for such customer overlay networks is not expected to change, just the highest rates. Today the highest (wavelength) rate is 2.5 or 10 Gb/s. This will increase to 40 Gb/s or even 100 Gb/s in the next 5 years. Clearly, only a small fraction of customers will require private-line links at 40 100Gb/s. To provide these subwavelength private-line services, the most likely migration path is that they will be transported over one of the rapidly growing packet-based networks via pseudo-wire circuit emulation [13] with guaranteed minimum latency and QoS. Also, as the packet networks grow to huge size, PVC-type services will be more readily accepted and so these will grow to replace much of the TDM private line.

13.3.2 Network Evolution

Figure 13.13 depicts a potential evolution of the core segment. The first observation is that it is significantly simpler than today's network. Of course, this is

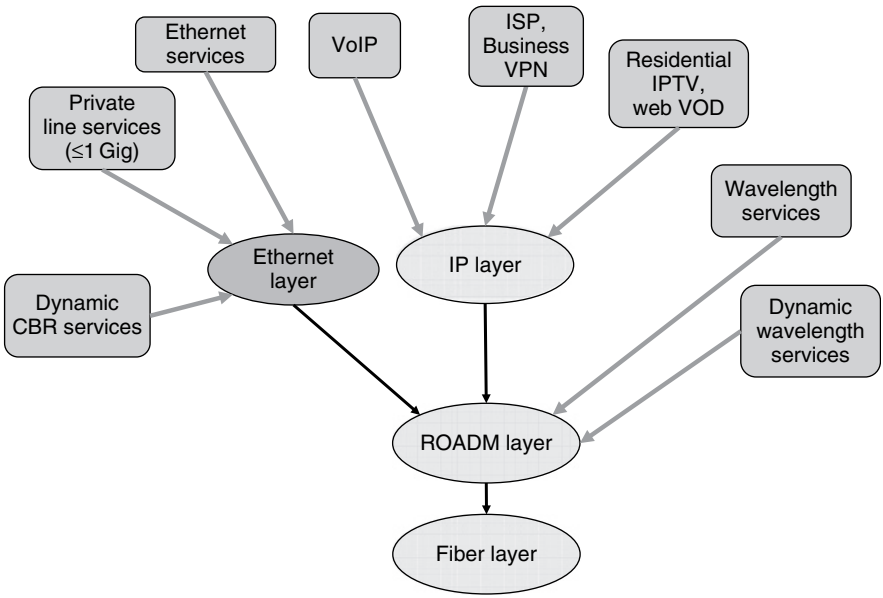

Figure 13.13 Potential future core segment network layers (this figure may be seen in color on the included CD ROM).

idealistic in the sense that commercial networks have shown a difficulty to retire older technologies and architectures. This picture still retains TDM private-line services. These are likely to exist in some form for a long time because they accommodate the links of other overlay networks. We note that perhaps many customers of TDM private-line services migrate to more circuit-oriented virtual flows, such as Ethernet virtual private line or PVCs in some form (not necessarily frame relay or ATM). It is assumed that an evolved Ethernet layer can accommodate both types of flows: PVCs of some type and TDM circuits via circuit emulation. Both the IP layer and the Ethernet layer mostly transport IP packets at their higher layers, but the Ethernet layer is more focused on connecting LANs and transporting PVC-type connections.

To achieve this evolution, some enhancements over today's core packet networks will be needed. The challenges will be to demonstrate when pseudo-wire setup can be optimized for speed and that the latency of circuit emulation (due to its playout buffers) will meet grid-computing requirements. However, note that carrier-grade circuit emulation technologies exist, are generally available (GA) today, and have been shown to be able to meet the private-line service requirements [13, 14]. Uncertainty in the timing of this migration lies more in the metro segment (which evolves more slowly) and the economics of transitioning from legacy network architectures. Furthermore, ITU G.8261 has been established to enable timing (clock) distribution adequate for carrier-grade circuit emulation in Ethernet networks.

Dynamic wavelength-rate CBR services will require an optical control plane that supports fast provisioning and WDM transmission systems and cross-connects that can appropriately meet transient, power, and other optical requirements or, if not possible, cleverly preprovisioned O-E-O methods.

Voice is expected to migrate to VoIP. We note that this migration has been forecast more aggressively in the past, yet has defied predictions. However, despite the economic analysis or preference of carriers and predilection of many customers against change, equipment to feed the circuit-switched layer is being capped by many equipment suppliers and so its lifetime is very limited.

13.3.3 "Killer Apps"

What sorts of future applications will require massive link bandwidth and/or advanced network provisioning and management capabilities? There are many ways to interpret how future applications will affect the various networks discussed, but given the focus of this book, this discussion will be specific to the impact on the optical layers. Just as with the first sections of this chapter, we need to examine this segment by segment and layer by layer.

For the metro and access segments, referring back to Table 13.5 (based on present growth rates), the services that are projected to have the biggest impact on the metro fiber layer are residential IP and video services. The impact on the fiber layer of these two services can probably be lumped together. This is because IP-based transport of residential video services is estimated to become predominant ($\geq$50% of capacity) by 2015 and residential ISP services are carried over the same IP layer. Note that we can lump residential wireline voice services (VoIP) in as well, but its bandwidth usage is so insignificant that it essentially has no impact on the fiber layer. The impact on the DWDM and fiber layers of the metro segment for these services will be gated by the access segment, and therefore it is important to discuss the main technologies available for video transport over the access segment and how they might evolve.

Access Segment

Access-segment technologies fall roughly into five transport architectures: (1) IP layer over copper (xDSL), (2) IP layer over fiber, (3) satellite, (4) RF carrier over fiber, and (5) RF carrier over coaxial cable. A key difference is that architectures 1 and 2 are switched, while 3 5 are broadcast. That is, architectures 1 and 2 transport only the services/flows required to each customer at a given time, while 3 5 transport to each customer the union of services/flows over all customers in a given access subnetwork (or serving area) at a given time. This is a critical point because, under architectures 3, 4, and 5, an increase in the amount of available video entertainment channels plus growth of ISP service requires a commensurate increase in the access transport bandwidth. However, the real-time bandwidth actually required by each household has grown relatively slowly, most recently rising due to the advent of high-definition TV (HDTV) and increased demand for

ISP bandwidth (in the 3 20 Mb/s range). In contrast, the access bandwidth required for architectures 1 and 2 is governed by the maximum cumulative bandwidth required by each household at any instance of time. Thus, for architectures 1 and 2, the breadth of entertainment channels is not limited by access-segment bandwidth and therefore can grow without bound.

Providing video and ISP services under architectures 1 and 2 (which are relatively new compared with architectures 3 5) has required substantial investment in the access and metro segments because the required lower layers of the infrastructure were not pre-existing. The accompanying investment in the core segment has been relatively very small; but we will return to discuss the core segment later. However, while the industry is experiencing an enormous economic "bump" from the access- and metro-segment deployments to realize architectures 1 and 2, based on the argument above and our assumption of predominant IP transport in 5 years, this growth will likely flatten out once the bulk of the network and its layers is deployed in most metropolitan areas. Then, network growth will be gated by growth in the maximum bandwidth per household. At present, based on an ISP service (1 20 Mb/s), four simultaneous video receivers, and anticipated standard definition (SD) (1 3 Mb/s peak) and HDTV (6 8 Mb/s peak) compressed data rates, the anticipated per-household peak demand over the next 5 years has been estimated anywhere from a low of 20 Mb/s to a high of 50 Mb/s. Given these estimates and assuming architecture 1 or 2, the variety of entertainment channels, video-on-demand (VoD), and other applications, which can be more easily accommodated by a switched IP infrastructure, can grow at a frenetic pace [e.g., person-to-person video, home-monitoring, YouTube-type video, intense gaming (high-speed, high-resolution, multiplayer), etc.], yet continue to be accommodated by the anticipated maximum access bandwidth. Therefore, for the residential access segment we would need to see new killer apps which require ~10 Mb/s or more to cause the next "bump" in commercialization or spending.

Alternatively, for business access, there is a completely different situation. Business customers who require large bandwidth usually aggregate many employees or serve many customers, either directly or indirectly through other businesses. While a maximum of 20 50 Mb/s may be adequate for most residential locations, many businesses today require multiple gigabits per second. The distinction, however, is that there are relatively few of these large enterprises when compared with the much larger number of residential customers (by more than three orders of magnitude). Also, almost all business locations with significant bandwidth requirements already have fiber to their locations. We do not anticipate any business killer apps driving access and metro bandwidth requirements much differently than the estimates in Table 13.5, although we will discuss a special class of academic/government customer when we discuss the impact on the core segment later.

Metro Segment

To examine the impact of residential IP (video + ISP service) on the metro segment in more detail, look at how entertainment video might evolve. Today, most entertainment

TV shows are still broadcast on a schedule, typically 300 500 simultaneous SD channel feeds plus 10 100 HD channels, assembled from a variety of entertainment content providers. Some satellite carriers are trying to get a jump on terrestrial carriers by offering hundreds of all-HD channels. To deliver this type of service to residential customers over the metro network, IP *multicast* [using *protocol independent multicast* (PIM)] can be used. Under this methodology, a *video hub office* (VHO) or *headend* for a metro area transmits the IP streams for each channel to downstream routers or switches. Each router or switch in the IP layer takes the channel stream received and duplicates it to each of its downstream links, according to a multicast routing tree that is set up via the PIM signaling protocol for each channel (note that to lower costs, many implementations of IPTV install Ethernet switches closer to the customer. These switches make use of a protocol called Internet Group Management Protocol (IGMP) for multicast, rather than PIM, which is mostly confined to routers). The last router before the customer (usually located in an RT or mini-headend) only transmits the channels that the customer requires in real-time. This tends to equalize the cost of infrastructure when compared to alternate architectures (like 3 5 above) which broadcast all channels to each customer. In contrast, if IP *unicast* is used instead (in which case virtual point-to-point connections are made between the VHO and each customer), then the metro transport cost is much higher. Today, both multicast and unicast are required. Unicast is mostly used for ISP service and VoD, where customers choose their entertainment from a stored catalog of programs.

Continuing with the evolution of residential video entertainment, in 2007 it is estimated that of the 200 500 TV channels, only 10 20 actually require real-time streaming (e.g., sports events, news, and live events). The principal question, then, is how prevalent or even predominant will the VoD model become? Taking this to the next step, how will VoD, as offered by video entertainment providers today, differ from that of video delivered via the Internet? These two forms of entertainment are converging. The main differences today are quality and licensing: TV offers consistently high-quality video and more heavily licensed movies and TV shows, whereas the Internet is a wild repository of anything from content similar to TV itself, to homemade, low-quality webcam movie shorts with no licensing or copyright impact. But, from the standpoint of network layers and technologies, there is little difference! These two services (ISP and IPTV) are only separated by virtual streams inside the IP transport pipe. If the latter model is realized in full (i.e., almost all forms of video entertainment are VoD), this will increase the bandwidth requirements substantially on the metro transport layers because, without many simultaneous channels, multicasting provides little advantage. Thus, the metro transport networks will continue to grow beyond their initial deployments, even though the maximum residential bandwidth remains constant. But, as with the access segment itself, the capacity (e.g., cumulative capacity in units of 10 Gb/s-km) of the metro-segment residential-IP layer will reach a maximum on the order of nd^2 [also denoted $O(nd^2)$], where n is the number of residential customers and d is a parameter that estimates the geographical extent of the access network served (e.g., "network diameter"). Alternatively, if this IP

layer of the metro segment is dominated by multicast transmission, then the capacity scales only as $O(d^2)$. We anticipate that the VoD model will predominate after 5 years. We do not base this prediction on the desires of the carriers, who need to receive return on their rather substantial investment, but rather by the enormous competitive pressure asserted by the Internet, coupled with the lifestyle shift currently underway. These changes include the use of "time-shifting" devices (such as Tivo®) and increasing numbers of teens and younger adults taking entertainment from the Internet. This shift also significantly changes what type and where advertising can be placed, with substantial impact on the overall economics. However, we note that in the past many traditional entertainment distribution models were turned upside down by Internet-based sharing models (such as sharing of music via free music distribution sites), only to be reigned in by the US tort system and copyright and licensing laws. Therefore, we predict this evolution will not be a smooth transition but will move ahead in spurts.

As for the ISP service itself and the previously mentioned estimate of 20 50 Mb/s per household maximum, what sorts of applications will even get close to this limit or, ultimately, push bandwidth beyond this? Since high-quality video channels will be available via VoD for the traditional SD/HD streaming (or VoD) video entertainment portion of the IP pipe, applications that are more distributed and not mass produced will be needed to drive this portion. A very likely candidate is monitoring or surveillance. With heightened concern for safety, two-income households, inexpensive and robotic web-cams, and just plain curiosity, there will be a large increase in local video monitoring. For example, parents might want to monitor their children at home, daycare, or school, or to monitor their pets or check on the security of their home or other locations. More people are also using video conferencing while working at home. Is this enough to stress the 20 Mb/s maximum access bandwidth? The answer is "no," unless the video quality becomes more like SD and there are multiple, simultaneous feeds required. However, another interesting driver for increased access bandwidth and a less stringent metro network has been identified [15]. Because of the current video streaming model described above, the IP layer of the metro network has to deliver incredibly reliable performance. Jitter and small failures or packet loss are not well tolerated. Furthermore, video features, such as "pause," "fast-forward," or "rewind," are somewhat limited under VoD. For example, to maintain the proper encoding and sequencing of differential video frames, a show/movie is usually prerecorded in a separate compressed date file for each "fast-forward" or "rewind" speed offered. When the customer selects a particular direction and speed, the specific prerecorded file is accessed and provided by a separate stream. Some of this can be provided by a digital video recorder (DVR), but it still requires some degree of streaming limitation. However, if we hypothesize an access link with huge bandwidth, then for non-real-time content there is no need for streaming. The customer (or the system) can simply download (or pre-fetch) all or most of the video file and then have a full set of features, similar to a DVD. But, most importantly to the transport network, it alleviates most of the high-availability and low-latency

characteristics of the metro IP layer and furthermore alleviates much of the need for IETF-motivated *diffserve* performance models for high-priority streaming data. Is this enough of a driver to force up the required bandwidth of the access link? We are not prepared to predict this, but it is an interesting viewpoint.

Core Segment

Although some requirements on DWDM and optical technology might be unique to the core segment, its size will be bounded by a function of the access limitations identified above. A key historical factor in the core segment is the $O(n)$ vs $O(n^2)$ effect described in Section 13.1.3. This continues to be a key factor which will be illustrated with an example. Today, residential ISP customers download a VoD service from an IPTV carrier or something similar from the ISP from a few, centralized sources. This, to date, has also applied to Internet gaming, wherein there are large numbers of end users, but who interact mostly via centralized servers. This implies that the impact on the core segment is $O(n)$ because of the small, fixed number of sources compared to the total number of end customers, n. However, there are point-to-point applications (or in Internet lingo *peer-to-peer*) such as residential monitoring and peer-to-peer video, multimedia, and music applications. If the video bandwidth requirement of such a point-to-point session increases to become closer to that of a VoD movie or TV show, then the peer-to-peer applications will dominate the centralized services. Most importantly to the core network segment, its traffic matrix (the matrix $\{d_{ij}\}$ whose entries are demand from AR i and AR j) will have density (number of entries with significant demand) more like $O(n^2)$, rather than $O(n)$. This will increase the required network capacity. However, note that the impact on the household maximum bandwidth in the access segment is unchanged. Rather, it is the networking effect that mostly impacts the core segment layers.

Our observation is supported by the current and historical distribution of types of Internet services. Peer-to-peer applications have constituted a large portion of long-distance ISP traffic and we now estimate they comprise over 25% of flow bandwidth in long-distance ISP networks. However, we note that quoting a reliable distribution of services will be increasingly difficult because many peer-to-peer applications on the Internet are disguised within protocols or encrypted and, as such, are hard to measure.

Distributed sensor networks are another interesting application. These could include extremely low-energy radio signaling between inventory and inventory control systems via RFID. While this application has the potential to be truly massive in n, it is not yet clear if the individual bandwidth requirements are substantial (e.g., on the order of video). It is also unclear whether these connections will aggregate to mostly business locations or mostly residential and whether this will have a $O(n)$ vs $O(n^2)$ effect on the core network.

One particular type of business service that has been highly touted to have a large impact on the core network is grid computing and e-science applications. These include the distributed processing of massive data files from particle accelerators in different countries and advanced distributed genome processing. They

have also spurred some interest in educational and government circles for bandwidth-on-demand services or interactions among control planes to dynamically adjust topologies across network layers. In these applications, the bandwidth connections are truly massive and, for various distributed computer-to-computer interface requirements, need to bypass typical data layer protocols as found in commercial IP layer networks. These applications are of great scientific interest and have spurred a whole academic field of integrated IP/DWDM network management and switching technologies (such as optical burst switching). And while they will generate focused, dynamic, and high-bandwidth connections, these applications have not been shown to generate much impact on total core network capacity due to the paucity of locations. Current large business customers also have interest in bandwidth-on-demand. These large business customers generally have large private networks and bandwidth-on-demand provides them flexibility for their own IP-layer topologies because of the rapidity of ordering point-to-point long-distance connections for their IP-layer links. We feel that the bandwidth-on-demand model would fit both of these applications well [16].

13.4 SUMMARY

The US telecom network has been divided into access, metro, and core segments and their various stages of evolution were illustrated. While the core segment has an almost ubiquitous penetration of fiber and WDM technologies, the opposite is true for access and metro segments in most areas. Thus, while much of the optics literature and industry focuses on advanced optical technologies for the long-distance network, most of the investment and opportunity for growth resides in the metro/access portion. As study shifts through the core, metro, and access segments, it will be seen that networks evolve more slowly and more nonuniformly. Beyond network segmentation, since the optical layer is essentially the workhorse for higher network layers, an understanding of network layering is crucial to understanding the requirements and evolution of the optical layer. A prime example of this correlation is network restoration. One cannot study or propose practical restoration methodologies for the optical layer unless the functionality and formulation of the restoration problem is understood at all network layers. This chapter has attempted to provide the reader a basic understanding of commercial optical network architectures and brought out some of their more practical commercial aspects.

LIST OF ACRONYMS

1 + 1	One-plus-one (signal duplicated across both service path and restoration path; receiver chooses surviving signal upon detection of failure)

1:1	One-by-one (signal switched to restoration path upon detection of failure)
AAL	ATM adaptation layer
ADM	Add/drop multiplexer
AR	Access Router
ATM	Asynchronous transfer mode
B-DCS	Broadband digital cross-connect system (cross-connects at DS-3 or higher rate)
BER	Bit error rate
BGP	Border Gateway Protocol (IP Protocol)
BLSR	Bidirectional line-switched ring
BPON	Broadband Passive Optical Network (each PON downstream carries 622 Mb/s on one wavelength and (optionally) analog video on another; upstream 155 Mb/s; up to 32 endpoints)
BR	Backbone Router
CLEC	Competitive local exchange carrier
CO	Central office
CoS	Class of Service
CPE	Customer premises equipment
CWDM	Coarse wavelength-division multiplexing
DCS	Digital cross-connect system
DLCI	Data link connection identifier
DS-0	Digital signal level 0 [a plesiosynchronous (pre-SONET) signal carrying one voice-frequency channel at 64 kb/s]
DS-1	Digital signal level 1 (a signal carrying 24 DS-0 signals at 1.544 Mb/s)
DS-3	Digital signal level 3 (a signal carrying 28 DS-1 signals at 44.736 Mb/s)
DSL	Digital subscriber line
DSLAM	Digital subscriber line access multiplexer
DSX	Digital cross-connect
DVR	Digital Video Recorder
DWDM	Dense wavelength-division multiplexing
E1	European plesiosynchronous (pre-SDH) rate of 2.0 Mb/s
EPON	Ethernet Passive Optical Network (each PON downstream carries 1 Gb/s; upstream 1 Gb/s; up to 32 endpoints)
FCC	Federal Communications Commission (an agency of the US Government)
FE	Fast Ethernet (100 Mb/s)
FRR	Fast Reroute
GigE	Gigabit Ethernet (nominally 1000 Mb/s)
GPON	Gigabit-per-second-capable Passive Optical Network (each PON downstream carries 2.4 Gb/s on one wavelength and

	(optionally) analog video on another; upstream 1.2 Gb/s; up to 32 endpoints)
HD	High definition (short for HDTV)
HDTV	High definition (television with resolution exceeding 720×1280)
IETF	Internet Engineering Task Force
IGMP	Internet Group Management Protocol
IGP	Interior Gateway Protocol
IOS	Intelligent optical switch
IP	Internet Protocol
IPTV	Internet Protocol television (i.e., entertainment-quality video delivered over IP)
IS-IS	Intermediate-system-to-intermediate-system
ISO	International Organization for Standardization (not an acronym)
ISP	Internet Service Provider
ITU	International Telecommunication Union
LATA	Local access and transport area
LGX	Lightguide cross-connect (fiber patch panel)
LOS	Loss of service
LSA	Link state advertisement
LSP	Label-switched path
MAN	Metropolitan Area Network
MPLS	Multi-Protocol Label Switching
MSP	Multi-Service Platform
MTBF	Mean time between failure
MTTR	Mean time to repair
N-DCS	Narrowband digital cross-connect system (cross-connects at DS0 rate)
NPE	Network premise equipment
OC-*n*	Optical carrier level *n* (designation of optical transport of a SONET STS-*n*)
O-E-O	Optical-to-electrical-to-optical (3R regeneration)
OL	Optical layer
OSPF	Open shortest path first
PBX	Private branch exchange
PIM	Protocol independent multicast
PL	Private Line
P-NNI	Private network-to-network interface
POP	Point of presence
PON	Passive Optical Network (access network with only passive components (glass) in the distribution plant; no electric power needed except at CO and endpoints)
POS	Packet over SONET/SDH
PPP	Point-to-Point Protocol
PPPoE	Point-to-Point Protocol over Ethernet

PVC	Permanent virtual circuit
PWE3	Pseudo-wire emulation edge-to-edge
PXC	Photonic cross-connect
QoS	Quality of service
RF	Radio frequency
RFID	Radio frequency identification (a technology for very low power, low bandwidth communication using small tags)
ROADM	Reconfigurable optical add/drop multiplexer
RST	Rapid spanning tree
RT	Remote terminal
RTP	Real Time Protocol
SD	Standard definition (television with resolution of about 640×480)
SDH	Synchronous digital hierarchy (a synchronous optical networking standard used outside North America, documented by the ITU in G.707 and G.708)
SLA	Service level agreement
SLRG	Shared-link-risk group
SONET	Synchronous Optical Network (a synchronous optical networking standard used in North America, documented in GR-253-CORE from Telcordia)
STS-*n*	Synchronous transport signal level *n* (an electrical signal level of the SONET hierarchy with a data rate of $n \times 51.84$ Mb/s)
SVC	Switched virtual circuit
TCA	Threshold crossing alert
TDM	Time division multiplexing
ULH	Ultra-long haul
UPSR	Unidirectional path-switched ring
VCAT	Virtual concatenation
VCI	Virtual circuit identifier
VoD	Video on demand
VLAN	Virtual Local Area Network
VoIP	Voice over Internet Protocol
VPLS	Virtual Private LAN Service (i.e., Transparent LAN Service)
VPN	Virtual Private Network (IP Protocol)
VT1.5	Virtual Tributary group (encapsulation of asynchronous DS-1 inside SONET STS-1) payload; other VT groups (VT2, VT3, VT6) are similarly defined
WAN	Wide Area Network
W-DCS	Wideband digital cross-connect system (cross-connects at DS-1 or SONET VT*n* rate)
WDM	Wavelength-division multiplexing
xDSL	various digital subscriber line technologies, where x $\in$ {null, A, H, or V}
xPON	various Passive Optical Network technologies, where x $\in$ {B, E, or G}

REFERENCES

[1] H. Zimmermann, "OSI reference model The ISO model of architecture for open systems interconnection," *IEEE Transactions on Communications*, 28(4), 425 432, April 1980.

[2] IETF, Pseudo Wire Emulation Edge to Edge (PWE3) Working Group, http://www.ietf.org/html.charters/pwe3 charter.html.

[3] J. Rosenberg and H. Schulzrinne, "Signaling for Internet Telephony," in Proc. *ICNP* 1998. Sixth International Conference on Network Protocols, IEEE, pp. 298 307.

[4] http://www.telecomspace.com/latesttrends ims.html

[5] S. Chaudhuri, G. Hjálmtýsson, and J. Yates, "Control of lightpaths in an optical network," *Optical Internetworking Forum Submission*, OIF2000.04, January 2000 and *IETF Internet Draft*, February 2000.

[6] R. D. Doverspike, J. Morgan, and W. Leland, "Network design sensitivity studies for use of digital cross connect systems in survivable network architectures," *IEEE J. Sel. Areas in Commun. (JSAC)*, Issue on Integrity of Public Telecommunication Networks, 12(1), 69 78, 1994.

[7] C. W. Chao, H. Eslambolchi, P. Dollard et al., "FASTAR A Robust System for Fast DS 3 Restoration," in Proc. *GLOBECOM'91*, Phoenix, Arizona, December, 1991, pp. 1396 1400.

[8] T. Sheldon, "Encyclopedia of Networking & Telecommunications," McGraw Hill, 2001.

[9] R. Doverspike, S. Phillips, and J. Westbrook, "Future transport network architectures," *IEEE Commun. Mag.*, 37(8), 96 101, August 1999.

[10] K. Oikonomou, R. Sinha, and R. Doverspike, "Multi layer network performance and reliability analysis," Operations Research, to appear.

[11] G. Li, D. Wang, R. Doverspike et al., "Economic Analysis of IP/Optical Network Architectures," in Proc. *OFC 2004*, Los Angeles, CA, March 2004.

[12] G. Li, D. Wang, J. Yates et al., "IP over optical cross connect architectures," *IEEE Commun. Mag.*, 45(2), 34 39, February 2007.

[13] T. Afferton, R. Doverspike, C. Kalmanek, and K. K. Ramakrishnan, "Packet aware transport for metro networks," *IEEE Commun. Mag.*, 120 127, March 2004.

[14] J. Wei, K.K. Ramakrishnan, R. Doverspike et al, "Convergence through Packet Aware Transport," *The Journal of Optical Networking,* Special Issue on Convergence, 5(4), 221 245, April 2006.

[15] A. Odlyzko, "Resource/traffic Management Architectures for NGI." http://www.dtc.umn.edu/~odlyzko/talks/itc2007.pdf

[16] S. Beckett and M. Lazer, "Optical Mesh Service, Service Strategy Capitalizing on Industry Trends," http://www.oiforum.com/public/documents/061016 AT&T.pdf

14

Technologies for global telecommunications using undersea cables

Sébastien Bigo

Alcatel-Lucent Bell Labs, Centre de Villarceaux, Route de Villejust, Nozay, France

14.1 INTRODUCTION

The advent of optical technology in commercial undersea transmission systems dates back to 1987, with the layout of TAT8 and TPC3 fiber cables across the Atlantic Ocean and the Pacific Ocean, respectively [1]. These optical systems carried data at no more than 280 Mbit/s, over light at the wavelength of 1.3 μm. Their successors, namely TAT9 and TPC4, reached the rate of 560 Mbit/s while being operated at 1.55 μm, where fiber loss is lower. However, all these pioneer systems had to be periodically regenerated with electrical repeaters. The replacement of these repeaters by all-optical repeaters, based on erbium-doped fiber amplifiers (EDFAs) marked the beginning of a new era [2]. TAT 12/13 and TPC5, deployed in 1995, were the first cables to rely on such repeaters. In these cables, beside EDFA technology, the fiber manufacturers had come with a new fiber type, of lower-dispersion, making possible the increase of the bit rate to 5 Gbit/s. But, it was the wavelength division multiplexing (WDM) technique which gave a real boost to the system capacity. It consists in modulating a set of lasers in parallel, each carrying independent information at a different wavelength (still in the order of 1.5 1.6 μm), to combine them into a single fiber, and periodically amplify them altogether into the EDFA-based repeaters. At the receiver end, an optical demultiplexing device separates the different wavelengths and sends each of them to a dedicated photodiode. The capacity of such a WDM system is equal the number of modulated wavelengths, referred to next as channels, times the bit rate per wavelength. Because communications are bidirectional, optical fibers and EDFAs always come by pairs, one for each direction, and the

Optical Fiber Telecommunications V B: Systems and Networks

ISBN: 978 0 12 374172 1

Figure 14.1 Picture of the submarine optic network across the Atlantic Ocean, at the beginning of 2007. Reproduced with permission from Alcatel Lucent © Alcatel Lucent, 2007.

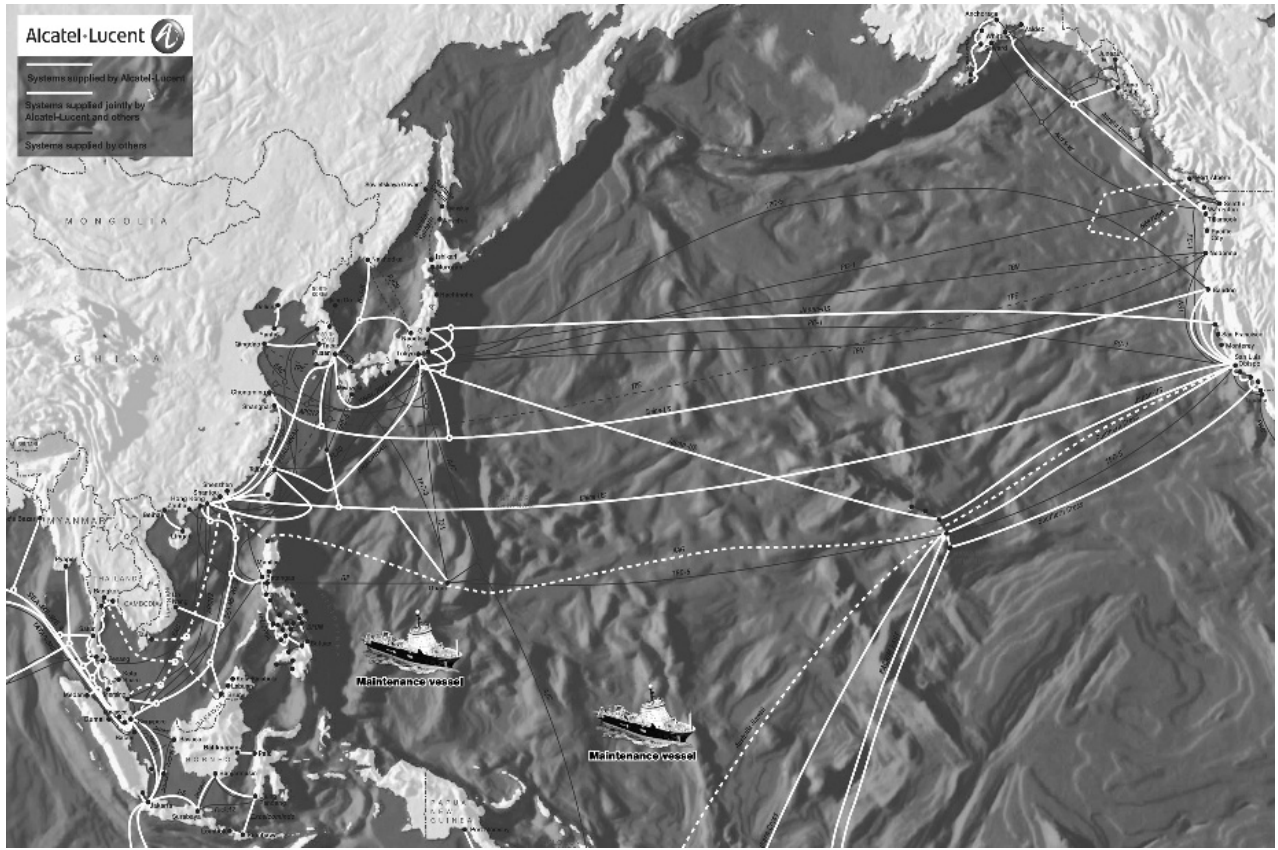

Figure 14.2 Picture of the submarine optic network across the Pacific Ocean, at the beginning of 2007. Reproduced with permission from Alcatel Lucent © Alcatel Lucent, 2007.

terminals are designed such that the incoming (i.e., received) light from one fiber and the outgoing (i.e., transmitted) light into the other fiber are generally processed into a single opto-electronic board per wavelength, called a transponder.

The first generation of WDM undersea systems, namely GEMINI and Sea-Me-We-3 [1], were modulated at a channel bit rate of 2.5 Gbit/s, and the channel number grew from 4 to 8 and, later, to 16. Eventually, the bit rate increased to 10 Gbit/s, which is still the highest commercial rate in 2007. However, the capacity per fiber also grew with the number of WDM channels, from a few units to a typical one hundred today, as made possible by the widening of the EDFA amplification window and the narrowing of the channel-to-channel spectral spacing, down to 50 or 33 GHz in the most advanced undersea cables. It should be emphasized that the system capacity is often further increased by operating several optical fiber pairs in parallel in the same cable. An typical undersea cable contains two to four fiber pairs. After the global downturn of the optical transmission market as a result of overinvestment, capacity growth was removed from the headlines of the operators' requests, but it can be expected that the market recovery started in 2006 will boost capacity needs up again in the years to come. In the meantime, research efforts have been kept high, for supplying the most adequate solutions when demand is ready. The geographical layouts of the undersea fiber optic communication networks across the Atlantic and the Pacific Oceans is displayed in Figure 14.1 and in Figure 14.2, respectively, as they stand at the beginning of the year 2007.

The goal of this chapter is to list the technologies which are used in today's submarine links and to discuss the technologies which could be implemented in future undersea networks. In particular, today's channels are modulated at 10 Gbit/s rate, but the deployment of systems based on the next-generation standard bit rate, namely 40 Gbit/s, has already begun in terrestrial networks. As of mid-2007, the total number of installed transponders at 40 Gbit/s there does not exceed a few tens but is rising jointly with capacity demand. Undersea networks will likely have to catch up in a few years. However, the migration to 40 Gbit/s in these networks can be quite challenging. Over the longest transoceanic distances, it will likely require a thorough re-design of the system, involving higher-performance repeaters and new fiber cables. Over more moderate distances, whenever possible, operators will likely ask that it be conducted over already-laid cables, by upgrading only the terminals with 40 Gbit/s transponders. However, substituting older 10 Gbit/s or older 2.5 Gbit/s terminals by 10 Gbit/s terminals equipped with the latest technological advances has already proved very effective for extracting more capacity out of existing cables [3], sometimes eight times the initially planned load. The 40 Gbit/s technologies will prevail for upgrades once they are competitive enough.

This chapter addresses the challenges associated with both green-field deployments and system upgrades. Original fiber arrangements, alternative modulation formats, alternative detection schemes, new amplifiers, and advanced forward-error correction (FEC) are all potential enablers for making submarine links compatible with 40 Gbit/s channel rate.

14.2 TECHNICAL CHALLENGES IN HIGH-SPEED, LONG-DISTANCE OPTICAL COMMUNICATIONS

14.2.1 An Overview of Transmission Impairments in WDM Systems

This section briefly explains the problems which have to be solved when performing high-speed, long-distance optical transmission. One essential limitation which has been encountered since the early days of optical communications is optical fiber loss. Thanks to the progress of fiber manufacturing, the attenuation of fibers has dropped to slightly below 0.2 dB/km, in the wavelength range where the attenuation is at its minimum, i.e., at $\sim$1.55 µm. Even low as it is, loss must be compensated for by optical amplifiers, such that an optical signal traveling into the fiber can be recovered after the typical long distances under consideration here. Optical amplifiers based on erbium-doped fiber were developed at the end of the 1980s [2] and are now widely deployed within terrestrial and undersea systems. Located in the repeaters, they provide a high gain and a low noise figure, so that several hundreds of erbium-doped fiber amplifiers (EDFAs) can be cascaded in long-distance undersea systems.

Once periodical amplification is implemented in repeaters, fiber chromatic dispersion arises as a major impairment. Chromatic dispersion designates the wavelength (or frequency) dependence of the fiber index of refraction. As a result, each of the spectral components of a given channel do not travel at the same speed and are received delayed with respect to each other at the receiver. Owing to this effect, the neighboring bits of a bit stream experience bit-to-bit overlap, the so-called intersymbol interference, making the distinction between "1" and "0"s possibly erroneous at the output of the receiver photodiode. With a conventional 10 Gbit/s channel, the maximum transmission distance over standard single-mode fiber (SSMF, of chromatic dispersion of 17 18 ps/nm/km) does not exceed 100 km. As an example, the impact of 1000 ps/nm cumulated chromatic dispersion on a sequence of data at 10 Gbit/s is drawn in Figure 14.3. Chromatic dispersion of 1000 ps/nm corresponds to what would be obtained after 60 km of SSMF. Note that the sign does not matter here, i.e., whether the higher frequency spectral components travel faster than the lower frequency components, or vice versa, brings similar intersymbol interference. Due to fiber chromatic dispersion, the "1"s broaden and "0" and "1"s are increasingly difficult to discriminate.

This effect sets a limit on the system length and must be overcome to bridge transoceanic distances. Two main remedies have been used against it. The first one, which was implemented in the first transoceanic cables, is to operate over a fiber with a specific index profile, yielding a dispersion around 0 ps/nm/km. The second one, which is now exclusively used, is to compensate for the chromatic dispersion by concatenating the transmission fiber with another fiber exhibiting a dispersion of opposite sign.

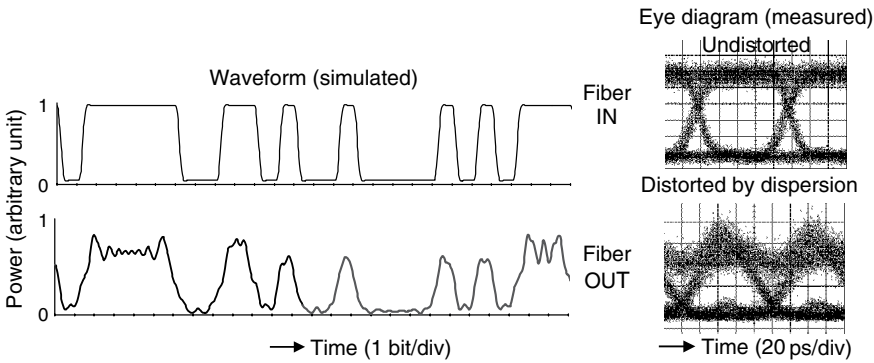

Figure 14.3 Impact of 1000 ps/nm chromatic dispersion on pulse integrity, at 10 Gbit/s channel rate.

When the issues of fiber loss and chromatic dispersion are handled as explained, new issues arise. Unlike the previous ones, these issues cannot be fully compensated for. One of them is the noise generated by the optical amplifiers, which builds up along the transmission path, and reduces the optical signal-to-noise ratio (OSNR). When the OSNR becomes too low, the electrical gate which discriminates between "1"s and "0"s is often mistaken, and the number of errors worsens beyond acceptable limits. The most straightforward solution for improving the OSNR is to increase the signal power at the input of the optical amplifiers. This can be done either by decreasing the distance between two repeaters (which implies more repeaters and generally a higher system cost) or by increasing the signal power P at the output of the amplifiers. However, both approaches only reduce the number of errors up to a certain extent, because other physical effects come into play. These effects, called nonlinear effects [4], result in waveform distortions which become stronger as the channel power grows. Because light travels across very long distances, e.g. several thousands of kilometers, and into a very small fiber core (characterized by its effective area $A_{\text{eff}} \sim 30\,\mu\text{m}^2$ to $100\,\mu\text{m}^2$), any signal with moderate power level P can be affected. One of these effects is the Kerr effect, which consists of an instantaneous modification of the fiber refractive index n proportionally to P, according to $n = n_0 + n_2 P/A_{\text{eff}}$, where n_2 is the nonlinear index coefficient at 2.7 10 $^{20}\,\text{m}^2/\text{W}$.

Kerr effect manifests itself in several phenomena, some of them noticeable when a single channel propagates and others arising only when several WDM channels propagate altogether. The primary single-channel phenomenon that comes to mind is self-phase modulation (SPM), whereby the phase of each channel is altered according to its own power profile. The fact that photodiodes are phase-insensitive could suggest that SPM is harmless, but a complex phase-to-intensity process occurs during propagation as a result of the chromatic dispersion. Therefore, SPM often translates into pulse distortions, which depend on chromatic dispersion. WDM nonlinear effects stemming from Kerr effect are often categorized into cross-phase modulation (XPM), whereby the phase of each channel is

modified proportionally to the power of the neighboring channels, and four wave mixing (FWM), whereby three channels interact to transfer fractions of their energies to a fourth one. Beside Kerr effect, interchannel Stimulated Raman Scattering is another nonlinear effect which can play an important role in optical transmission, especially when the number of WDM channels is large. It consists of a power transfer from higher frequency channels to lower frequency channels [5]. The latter effect will be not discussed further here, except when implicated in Raman amplification (see Section 14.4.2), an amplification technology alternative to EDFAs [2].

Because of nonlinear effects, the setting and control of the amplifier output power is a key issue for optical system designers. The power should stay above a lower bound, otherwise the signal is drown into noise, and below an upper bound, otherwise nonlinear effects cause irretrievable distortions. Therefore, the best system performance, which is generally estimated with the bit-error ratio (BER), i.e., the number of errors over to the number of transmitted bits, is the result of a complex trade-off. We shall see in the following sections that this trade-off depends on the specifications of the fibers and the optical amplifiers. Furthermore, in undersea links, it is generally different from what would be prescribed in terrestrial links. Inset 1 recalls the major differences between the two types of systems.

Inset 14.1 Main differences between undersea and terrestrial systems

Undersea vs terrestrial optical systems: What makes them different?

Whether under water or in the ground, optical transmission systems have been categorized according to the distances to cover, which are often larger when crossing the oceans (from 6000 km to 12,000 km) than when linking major cities over the continents (from 50 km to a few 1000 kilometers). This gap has narrowed in the past 5 years, as terrestrial networks have been growing closer in size to submarine networks. However, the two networks types differ in several fundamental features, other than the mere transmission distance.

In terrestrial networks, electrical power can generally be supplied to each repeater from a nearby power source, whereas, under water, electrical power has to be conveyed by the cable itself. In submarine cables, optical fiber pairs are surrounded by a robust cable structure containing steel wires for strength and a layer of copper, fed with a voltage up to 10 kV. In contrast, in terrestrial cables, fiber pairs are just protected by a polyethylene armor. Even though the issue of power consumption is a major concern in both undersea and terrestrial networks, it truly sets an upper limit to the number of optical amplifiers per submerged repeater and, therefore, to the number of fiber pairs within undersea cables. It also restricts the type of active components which can be used under water. Moreover, in case of failure or damage, the repairs of submarine cables

can take several weeks, especially in deep sea and in the regions of the world where the maintenance ships are relatively scarce resources. Hence, reliability has always been a paramount concern of undersea network operators, even though this concern has been distracted by the attempt to minimize cash burn and maximize profits after the downturn of the millennium. Responses to this concern are dedicated protection and restoration mechanisms (involving route diversity, whenever possible), as in terrestrial networks, but also specific high-reliability amplifier designs. Optical protection mechanisms are most often applied to all channels in submarine systems, whereas they are not systematic in terrestrial systems. More advanced route engineering techniques are also applied in undersea networks, to optimize the physical protection of the cable by choice of armoring and burial in order to minimize the impact of physical aggressions. The design life of submarine systems is typically 25 years, as compared with ~15 years in terrestrial systems.

Nonetheless, the underwater environment liberates some key constraints of the ground environment. In particular, at the early stages of design, terrestrial systems must be made adaptable to complex existing networks topologies, as dictated by geography and legacy. In contrast, submarine systems are mainly designed on a prototyped, customized basis, which opens more possibilities for achieving ultralong distances. Submarine repeaters are protected by a hermetic housing, are just laid on the sea floor when in deep sea, and are possibly buried elsewhere with a plough. In comparison, terrestrial repeaters are mounted in racks and installed in dedicated premises. The premises are selected by the operators, preoccupied by the cost of real estate and maintenance. Thus, when linking large cities with terrestrial cables, systems designers have almost no control on the position of the repeaters, and must adapt the system engineering rules and the amplifier designs to account for possibly highly variable span lengths. Conversely, when bridging continents by undersea links, they can select the exact location of repeaters almost freely. For simplicity, as well as for a better control of propagation impairments, they always make sure that the submerged repeaters are periodically spaced. They can therefore tailor exactly the optical amplifiers to the repeater span length and to obtain excellent noise characteristics. Besides, in undersea links, they generally choose smaller repeater span length, e.g., 35 55 km in older systems, than the typical distance between the premises of terrestrial networks owners, e.g., 100 km. In order to save on costs, they can increase, and have increased this length in recently deployed submarine systems, to a typical 70 80 km over transoceanic distances, and to possibly longer but at the expense of a reduction of the maximum system reach. They would therefore reserve the longest repeater span length (e.g., 100 120 km) to regional systems, of relatively moderate haul.

In addition, the average fiber loss within submarine cables is generally smaller (e.g., ~0.21 dB/km) than the fiber loss within terrestrial cables (e.g., ~0.25 dB/km). Explanations of this discrepancy are that the fibers are

similar but not exactly of the same type and that terrestrial cables suffer from a higher number of fiber cuts during system operation, but more importantly, the installation of a terrestrial cable involves splicing numerous cable sections together, of limited length (e.g., 2 5 km), as imposed by the constraints on weight and volume of road transportation. In comparison, a submarine cable is obtained by concatenating much larger sections of optical fiber, essentially spliced at the cable factory. Not only the number of splices is smaller but the average loss per splice is also smaller. Once manufactured, the submarine cable is loaded into the cable ship by spools of up to several thousands of kilometers. Besides the beneficial impact on cable loss, the above handling process specific to undersea systems, explains why undersea system providers have accepted to combine several fiber types within the same cable, whereas terrestrial network owners have clearly expressed their reluctance to move into this direction. Some of these fiber combinations have proved fruitful for containing propagation impairments and meeting the difficult challenges of ultralong-haul undersea links.

Terrestrial and undersea systems also use terminals which can be quite dissimilar. It partly has to do with the fact that the relative share of terminals in the total system cost is generally smaller in submarine systems than in terrestrial systems. System designers are often tempted to insert relatively expensive technologies in terminals, for enhancing the system performance or reach. Not surprisingly, the leverage created by these technologies to drive the overall system cost down is often greater in undersea applications than in terrestrial applications. For example, the terminals attached to submarine links often rely on dispersion-compensating schemes and modulation formats (all detailed further) unseen in terrestrial systems. Similarly, the channel frequencies of some undersea systems are allocated along grids, e.g., every 33 GHz, which do not comply with the grids of the International Telecommunication Union (ITU). This naturally requires the development of nonstandard components, and adds to the cost of the terminals, but opens opportunities for a better usage of the optical amplifier bandwidth.

Finally, in the past few years, terrestrial operators have been requesting that their network be more transparent. In other words, whenever a flow of data is to be sent from point A to point C via a node in point B, they prefer that the flow of optical data only travels through point B, free of any opto-electronic conversion stages, whenever possible. They have also asked that the network configuration (e.g., which wavelength should be stopped in point B, and which wavelength should just go through) be remotely reconfigurable. This trend has added a lot of complexity to terrestrial networks. The operators of undersea networks are also increasingly asking for cost-effective ways of achieving wavelength pass-through in so-called branch stations (i.e., passive versions of node B in the above example, buried under water), but submarine links are still essentially nonreconfigurable, point-to-point links.

Another physical phenomenon in the fiber, which can severely degrade the system quality, is polarization mode dispersion (PMD) [6]. Because fibers have circular profiles, models tend to overlook the fact that the electric field is better represented by a vector. This approximation is generally true, but should imperfections alter the fiber composition or local geometry during manufacturing, the two polarization components of the electric field may travel at different speeds causing pulse broadening or even pulse splitting at the end an optical link, as illustrated in the example in Figure 14.4. The acronym PMD designates both the physical phenomenon and the parameter which quantifies its magnitude [6]. A good way to explain the phenomenon is to think of the transmission fiber as a concatenation of very small, birefringent fiber sections, randomly oriented with respect to each other. In each of them, the optical index (hence, the speed of the light) is not strictly identical whether light is aligned along any of two principal axes. Thus, when not aligned along one of them, a pulse splits into two sub-pulses (the so-called modes), which get time-delayed by a quantity called differential group delay (DGD). When the DGD is large enough, one of the two sub-pulses can overlap the neighboring (sub-)pulses and make the error-free discrimination between "1"s and "0"s impossible. Contrary to chromatic dispersion, PMD is not a deterministic phenomenon. The principal axes of the small fiber sections rotate randomly with respect to each other when the environmental conditions (stress, temperature) change. Hence, not only the overall fiber principles states but also the DGD vary with time. The PMD value of a fiber is defined as the average value of the DGD over time. Because of its statistical nature, PMD in transmission fibers does not accumulate proportionally with distance as in birefringent fibers, but with the square root of distance. It is generally expressed in ps/$\sqrt{}$km. Besides, it is important to note that the statistics of the DGD are not upper bounded, i.e., that very large DGDs, and therefore strong pulse splitting, are always possible in long-haul systems, even if their likelihood is very small, whatever the PMD value. This means that

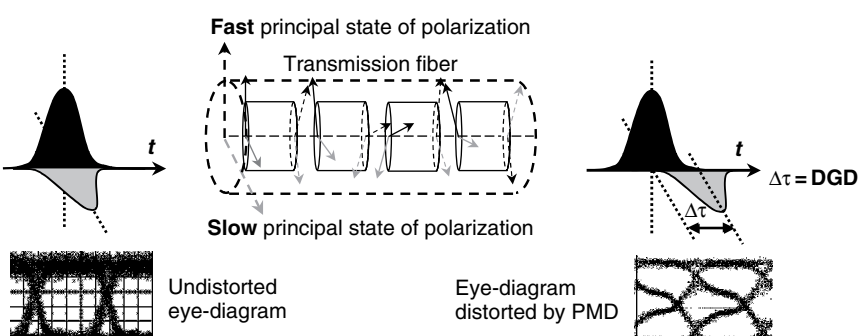

Figure 14.4 Impact of PMD on pulse integrity. Here, a signal at 10 Gbit/s is launched at ~45° of the principal states of polarization of a fiber with 80 ps differential group delay (DGD).

it is not possible to guarantee the performance of a transmission system 100% of the time. Because the PMD distortions vary with time, so does the bit-error ratio performance, which therefore can be attributed a probability density function. It is also customary to define an outage probability when this performance passes an acceptable boundary, i.e., when DGD turns too large, which should not exceed a typical 10^{-5}, i.e., 5 min per year. This amounts to requiring that the cumulated PMD should not exceed 10 15% of bit-duration, e.g., 10 15 ps at 10 Gbit/s [6]. In installed undersea cables, the PMD is generally lower than this value. Hence, the effect of PMD does not limit the performance of current $N \times 10$ Gbit/s submarine systems.

All the above impairments must be contained to guarantee a BER below 10^{-13} throughout the system life. An important building block for meeting this requirement is forward error correcting codes (FEC) codes. This coding technology allows to detect and correct errors at the receiver end, provided the BER before correction is lower than a certain threshold (called FEC threshold). FEC requires that all electrical bit-streams be precoded prior to converted into optical streams (each at a given wavelength) and sent into the transmission fiber. Precoding consists in adding adequate redundant information to the signal, referred to as the overhead. A precoded bit sequence is therefore longer than the original, by a certain amount, generally expressed in percent. Various types of FECs have been used in submarine systems. Some, with a relatively small overhead of 7%, correct BERs as low as 4×10^{-3}; others with a higher overhead of 23% have proved to be able to correct BERs as low as 10^{-2}, very near the theoretical limit. The transition from 2.5 to 10 Gbit/s channel rate in optical systems was largely facilitated by the FEC developments.

14.2.2 From 10 to 40 Gbit/s, Impact of the Transmission Impairments

By increasing the bit rate from 10 to 40 Gbit/s, several physical constraints are strengthened. One of them is chromatic dispersion. Since the bit duration is four times shorter, while the spectrum width is 4 times larger, the maximum distance of a dispersion-uncompensated, dispersion-limited system would be reduced 16-fold. Dispersion-compensating devices are used in order to remove this limitation. These devices are very effective but generally leave some residual dispersion mismatch, which must fall within acceptable boundaries. The maximum acceptable mismatch is naturally reduced by the same factor of 16, when moving from 10 to 40 Gbit/s channel rate. Hence, while at 10 Gbit/s, dispersion compensation can be performed by fixed compensators, tunable compensators will have to be used at 40 Gbit/s in most configurations. In this case, chromatic dispersion as such does not appear as a major limitation for the deployment of 40 Gbit/s system.

Nevertheless, moving from 10 to 40 Gbit/s channel rate increases the system sensitivity to other impairments. The maximum cumulated PMD decreases by a factor of 4, at ~3 ps at 40 Gbit/s. Today's fibers are not compliant with this 3 ps PMD requirement after transoceanic distances, but it can be expected that the fiber PMD will decrease in the coming years, thanks to the progress in fiber manufacturing. Furthermore, devices have been proposed for PDM mitigation. They can extend the tolerable PMD beyond 6 ps. Their principles will be discussed later in this chapter. In spite of their relative complexity, such devices would alleviate the effects of PMD and make transoceanic transmissions at 40 Gbit/s possible.

Another major concern when moving to 40 Gbit/s channel rate is amplifier noise. To recover the full formation at 40 Gbit/s, the receiver electrical bandwidth must be four times larger than at 10 Gbit/s, which means that the receiver catches 6dB more EDFA noise than at 10 Gbit/s for the same signal power. Hence, unless alternative approaches are used, the optical signal-to-noise ratio required to operate at 40 Gbit/s should also be 6 dB higher than at 10 Gbit/s. This suggests increasing the power per channel by the same amount. Unfortunately, the tolerance to nonlinear effects is also reduced at 40 Gbit/s, by an amount which is dependent on the system characteristics [7].

Besides, the most penalizing nonlinear phenomena also differ at 40 Gbit/s from those at 10 Gbit/s. They still stem from the Kerr effect. However, whereas at 10 Gbit/s interchannel (between channels) nonlinear interactions dominate, it is primarily the propagation of each individual channel, free of its neighbors, that should be the primary matter of concern at 40 Gbit/s rate, and also at higher rates. In other words, 40 Gbit/s systems are mainly impaired by self-phase modulation (SPM). To obtain better insight on SPM, the phenomenon itself has been categorized into three basic symptoms, referred to as the intrachannel effects. For the sake of clarity (but without loss of generality), we depict next the optical data stream carried by each channel as a series of optical pulses, i.e., assuming a return-to-zero format. However, the considerations detailed next apply to any modulation format. Each pulse (symbol) of the data stream can have its phase affected by the Self Phase Modulation effect independently from the neighboring pulses, a phenomenon simply referred to as iSPM (for intrapulse SPM). When undergoing chromatic dispersion, the pulses broaden and overlap the neighboring pulses, as represented in Figure 14.5. Over a given fiber configuration, the overlap phenomenon is typically 16 times stronger at 40 Gbit/s than at 10 Gbit/s, both because the bit duration is reduced fourfold and because the spectral width of each channel is increased fourfold. This gives rise to interpulse nonlinear interactions, which naturally vary depending on the transmitted binary sequences. These interactions can be separated into two families, named after their similarities with WDM nonlinear effects. The first one is intrachannel XPM (iXPM), which designates the phase modulation of one symbol proportionally to the power profile of the neighboring symbols.

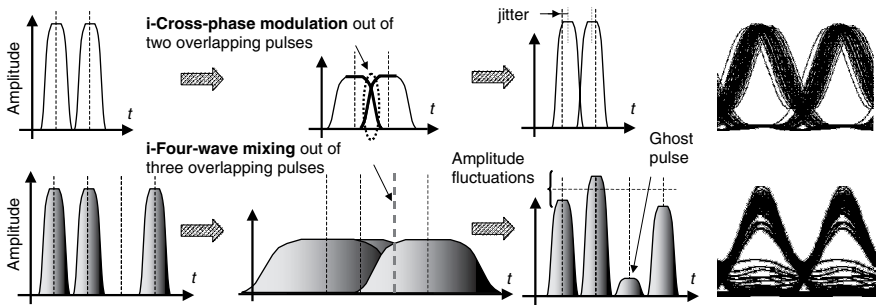

Figure 14.5 Intrachannel cross phase modulation (i XPM) and intrachannel four wave mixing (i FWM) across one repeater span (this figure may be seen in color on the included CD ROM).

The second one is intrachannel FWM (iFWM). iFWM designates a power exchange between different symbols which occurs when three regularly-spaced frequencies from three different symbols interact to generate energy at a fourth frequency, every time all three frequencies coexist within the same small time slot [8].

In Figure 14.5 (bottom), the spectral content of each pulse has been schematized. It spreads over a finite bandwidth before being fed into a fiber span. Through chromatic dispersion (here positive), the leading edge of each pulse experiences a shift toward higher frequencies (blue), whereas the trailing edge experiences a shift toward lower frequencies (red). After broadening, in the temporal overlap zone, the spectral content of each pulse varies from one pulse to the next, which serves as a seed for a four-wave mixing process. At the end of the repeater span, dispersion compensators shrink the pulses back to their original width, but cannot undo the interpulse energy exchanges caused by four-wave mixing. Hence, residual power fluctuations on top of the "1" pulses can be seen, while ghost pulses in the time slots of some "0"s can appear.

When WDM systems are operated at 40 Gbit/s instead of 10 Gbit/s channel rate, the reduced tolerance to noise, to chromatic dispersion, and to PMD, and the strengthening of intrachannel nonlinear effects all explain why the pioneer laboratory demonstrations at 40 Gbit/s reached much shorter distances than the installed 10 Gbit/s transmission systems, typically less than 3000 km [9, 10], as listed in Table 14.1. However, within a few years, distances longer than 6000 km [12, 13], even more than 10,000 km [20, 27], were reported. Over transoceanic distances, the transmitted capacities amounted to several terabit/s [22, 23, 24]. We shall see in the next parts what made the evolution possible and shall discuss the enabling technologies [35]. These technologies need to be appreciated not only in the prospect of designing green-field links, but also in the prospect of upgrading some existing $N \times 10$ Gbit/s systems to 40 Gbit/s without loss of performance.

Table 14.1

WDM laboratory demonstrations at 40 Gbit/s with submarine configurations over long-haul distances (>2000 km) reported in the main conferences and journals.

Date	Capacity (Gbit/s)	Number of Channels	Channel spacing (GHz)	Density (bit/s/Hz)	Modulation format[1]	Distance (km)	Repeater span (km)	Fiber type and arrangement	Amplifier type	PRBS[2] 2^*N*–1	Q^2 factor[3] (dB)	Author et al.	Company	Reference
Sep–00	640	16	100	0.40	C-RZ	2000	40	+ D/–D	EDFA	15	15.3	I. Morita	KDD	[9]
May–01	1280	32	100	0.40	RZ	2400	40	+ D/–D, medium dispersion	Raman	11	11.8	L. du Mouza	Alcatel	[10]
Oct–01	1280	32	140	0.29	RZ	4500	50	+ D/–D	EDFA	15	11.0	J.-X. Cai	Tyco	[11]
Mar–02	3000	75	66	0.61	CS-RZ	4500	51	+ D/–D	EDFA	23	10.0	J.-X. Cai	Tyco	[12]
Mar–02	1520	38	130	0.31	RZ	6200	51	+ D/–D	EFDA	23	10.0	J.-X. Cai	Tyco	[12]
Mar–02	1280	32	100	0.40	CS-RZ	6050	52	+ D/–D/ + D/– D/ + D/–D/ + D/–D	Raman	23	11.7	H. Sugahara	NEC	[13]
Jul–02	2200	55	50	0.80	CS-RZ	2500	43	+ D/–D/ + D	EDFA/ Raman	15	9.6	N. Yoshikane	KDD	[14]
Jul–02	1280	32	100	0.40	CS-RZ	9000	50	+ D/–D/ + D/– D/ + D/–D/ + D/–D	EDFA/ Raman	23	10.6	H. Sugahara	NEC	[15]
Jul–02	2480	62	100	0.40	CS-RZ	2200	40	+ D/–D	Raman	23	10.8	T. Matsuda	NTT	[16]
Sep–02	1000	25	100	0.40	RZ	2055	49	NZDSF	EDFA	15	12.8	G. Mohs	Tyco	[17]
Sep–02	1280	32	100	0.40	CS-RZ	6050	40	+ D/–D/ + D/– D/ + D/–D/ + D	Raman	23	12.1	A. Tanaka	NEC	[18]
Mar–03	1600	40	70	0.57	RZ-DPSK	8700	43.2	+ D/–D/ + D	Raman	23	10.0	T. Tsuritani	KDD	[19]
Mar–03	1600	40	100	0.40	RZ-DPSK	10,000	100	+ D/–D	Raman	31	9.6	C. Ramussen	Mintera	[20]
Sep–03	4000	100	62.5	0.64	RZ-DPSK	6240	65	+ D/–D/ + D	Raman	23	10.2	G. Charlet	Alcatel	[21]
Sep–03	2560	64	50	0.80	RZ-DPSK	8200	43	+ D/–D/ + D	EDFA	31	9.5	I. Morita	KDD	[22]
Nov–03	2560	64	100	0.40	CS-RZ	6000	50	+ D/–D/ + D/–D	Raman	23	11.3	M. Morisaki	NEC	[23]

Feb–04	1680	42	100	0.40	RZ-DPSK	4820	61	NZDSF	EDFA	23	11.8	L. Becouarn	Alcatel	[23]
Feb–04	5960	149	50	0.80	DSPK	6120	65	+ D/–D/ + D	Raman	23	8.9	G. Charlet	Alcatel	[24]
Sep–04	1240	31	100	0.40	DPSK	6120	65	+ D/–D/ + D	Raman	23	12.3	G. Charlet	Alcatel	[25]
Sep–04	2000	50	100	0.40	CSRZ-DPSK	6000	45	+ D/–D, medium dispersion	EDFA	23	9.7	Y. Inada	NEC	[26]
Sep–04	1600	40	100	0.40	APolRZ-DPSK	11,220	65	+ D/–D/ + D	Raman	23	9.9	G. Charlet	Alcatel	[27]
Mar–05	720	18	133	0.30	RZ-DPSK	6250	50	NZDSF	EDFA	23	13.5	J.-X. Cai	Tyco	[28]
Sep–05	6040	151	50	0.80	RZ-DQPSK	4080	65	+ D/–D/ + D	Raman	15	10.0	G. Charlet	Alcatel	[29]
Jan–06	1000	25	100	0.40	CSRZ-DPSK	6250	50	NZDSF-	EDFA	23	12.1	J.-X. Cai	Tyco	[30]
Mar–06	1120	28	133	0.30	CRZ-DQPSK	6550	45	+ D/–D	EDFA	15	12.1	J.-X. Cai	Tyco	[31]
Sep–06	3200	80	50	0.80	QPSK	3060	65	+ D/–D/ + D	Raman	15	9.5	G. Charlet	Alcatel	[32]
Mar–07	1600	40	50	0.80	PDM-QPSK	4080	65	+ D/–D/ + D	Raman	11	10.5	G. Charlet	Alcatel-Lucent	[33]
Mar–07	960	24	133	0.30	RZ-DPSK	4450	150	+ D/–D	EDFA/ Raman	23	12.4	J.-X. Cai	Tyco	[34]

[1] Formats description to be found later in this chapter. PDM stands for polarization division multiplexing.

[2] Value N of the pseudo-random bit sequence length 2^N–1.

[3] All Q factors are given before forward error correction (FEC).

14.3 FIBER INFRASTRUCTURE

14.3.1 In the First-Generation, Single-Channel Optical Systems

The first generation of commercial optically amplified undersea systems relied on dispersion-shifted fiber (DSF). DSF has a very low chromatic dispersion at the wavelength where the signal is transmitted ($\sim$0 ps/nm.km around 1550 nm), so that dispersion accumulation at the end of the link is contained. Soon after its introduction in laboratory experiments, it was observed that DSF was not adapted to wavelength-division multiplexed (WDM) transmissions. As a result of nonlinear effects, especially four-wave mixing, detrimental channel-to-channel interactions prohibit transmission over undersea distances over this fiber.

14.3.2 In the Early WDM Systems

This is the main reason why a new fiber, with a small, but nonzero dispersion was developed, the so-called nonzero DSF, (NZDSF). When designed for undersea applications, this fiber has a negative dispersion ($D \sim 3$ ps/nm/km at 1550 nm) [36]. After propagation over several repeater spans of NZDSF, chromatic dispersion needs to be compensated for. Standard single mode fiber (SSMF), with a positive chromatic dispersion (around 18 ps/nm/km), is used for that purpose.

However, compensation cannot be identically performed for all the WDM channels because dispersion is dependent on wavelength. If this dependence is linear (a fairly good approximation), this effect is fully characterized by the so-called dispersion slope $D' = \partial D/\partial\lambda$. Both the NZDSF and the SSMF have a positive dispersion slope, which means that both fibers contribute to widen the excursion of dispersion as a function of wavelength, i.e., across the multiplex. Figure 14.6 illustrates the extent of the phenomenon over a typical block consisting of six NZDSF spans and one SSMF fiber span. Even if no specific technique was applied against the dispersion slope in the early WDM system demonstrations, it rapidly arose as one of the most detrimental limitations in ultralong-distance systems.

14.3.3 In WDM Systems at 10 Gbit/s

In today's 10 Gbit/s submarine systems, the whole multiplex occupies a typical total bandwidth ranging from 13 nm to 27 nm. In most designs, the dispersion accumulated in five to ten consecutive fiber spans of NZDSF is compensated for by the dispersion accumulated into one span of SSMF, as in the example in Figure 14.6. The overall transmission line can be regarded as concatenation of so-called blocks, which are elementary structures as in Figure 14.6, and which are

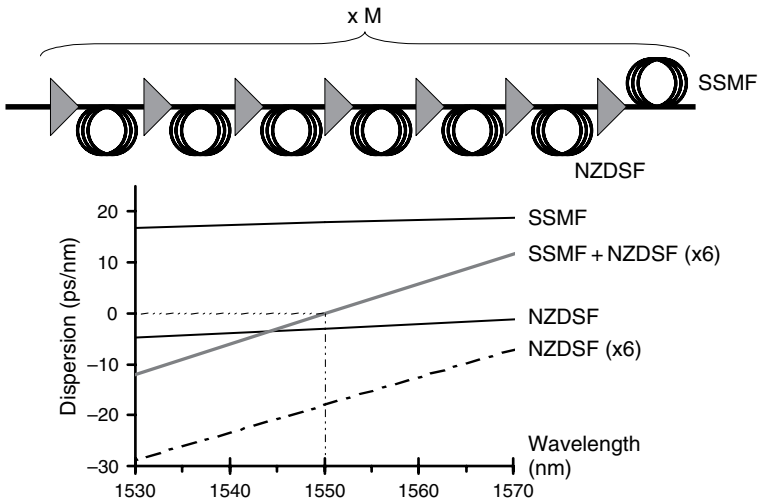

Figure 14.6 Wavelength dependence of chromatic dispersion in a typical NZDSF based undersea systems (this figure may be seen in color on the included CD ROM).

periodically replicated along the cable as represented in Figure 14.7. Dispersion compensation is nearly perfect at the center wavelength of the amplification spectral window, but a residual positive (resp. negative) dispersion builds up at longer (resp. smaller) wavelengths.

After a transpacific distance ($\sim$9000 km or more), the chromatic dispersion excursion across the multiplex approaches 20,000 ps/nm, which causes severe degradations to the leftmost and to the rightmost channels at 10 Gbit/s. A straightforward approach against these distortions has been to further adjust chromatic dispersion in the transmitter (precompensation), and in the receiver (postcompensation) on a per-channel or per-group-of-channels basis, as schematized in Figure 14.8. At the longer wavelengths, sections of fiber with negative dispersion are added in the transmitter and the receiver. Conversely, sections of fiber with positive dispersions are added at the shorter wavelengths.

As a remedy against the large excursion of dispersion across the multiplex, a novel fiber combination was proposed. It consists, in each repeater span, in alternating two types of fibers. The first type ($+$D) has a positive dispersion ($\sim +20$ ps/nm/km), a large effective area (100 μm^2 or more), a low attenuation, and a positive dispersion slope. The second type ($-$D) has a negative dispersion (around -40 ps/nm/km) and a negative dispersion slope, but a higher loss ($\sim$0.23 dB/km or more) and an effective area of just $\sim$30 μm^2 or less. Because of the small effective area, the second type induces comparatively more distortions due to nonlinear effects, unless located where optical power is comparatively smaller. Hence, it is preferably inserted at the end of each repeater span. A typical dispersion map with the $+$D/$-$D fiber combination is depicted in Figure 14.9.

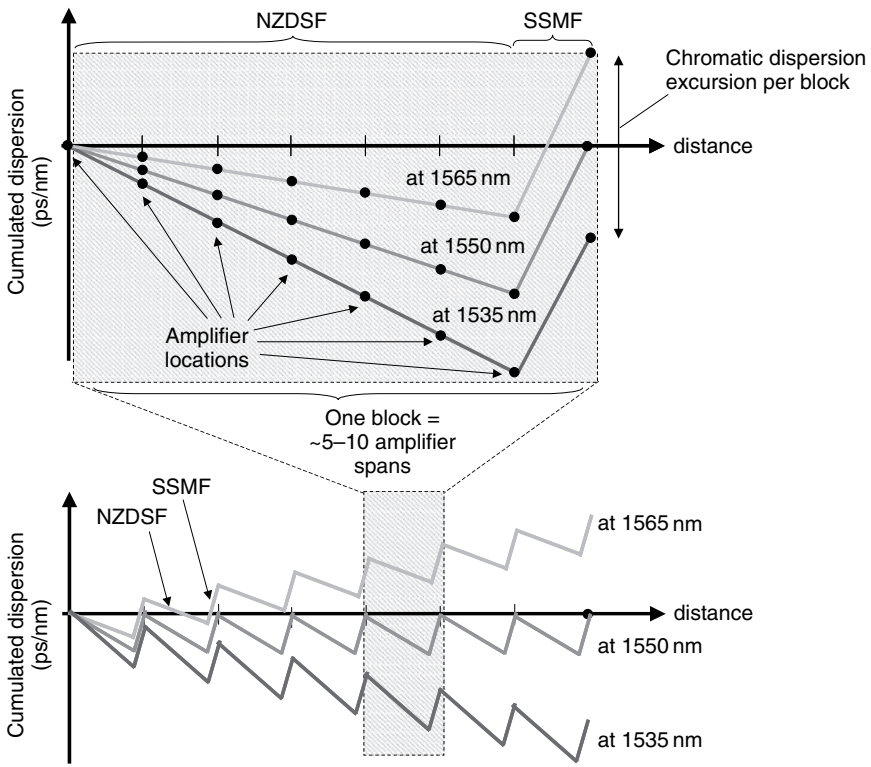

Figure 14.7 Schematic of the evolution of the cumulated dispersion along the line vs wavelength for an NZDSF based system. (After Ref. [35], © IEEE, 2006) (this figure may be seen in color on the included CD ROM).

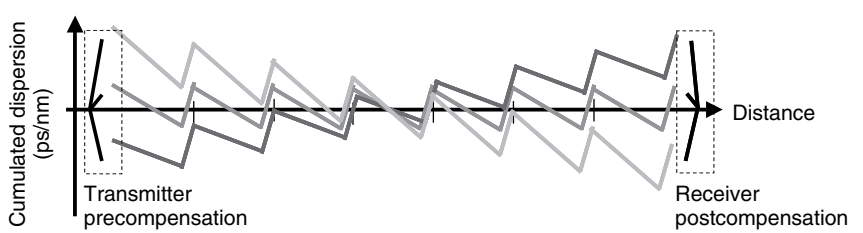

Figure 14.8 Schematic of the evolution of the cumulated dispersion along the whole transmission system vs wavelength for an NZDSF based system. (After Ref. [35], © IEEE, 2006) (This figure may be seen in color on the included CD ROM.)

As above, the line is divided in so-called blocks. They consist of 5 10 repeater spans. Chromatic dispersion is preferably not compensated at the end of each repeater span, such that the impact of WDM nonlinear impairments (XPM and FWM) is better contained [2]. Conversely, the chromatic dispersion is nearly compensated at the end of the blocks.

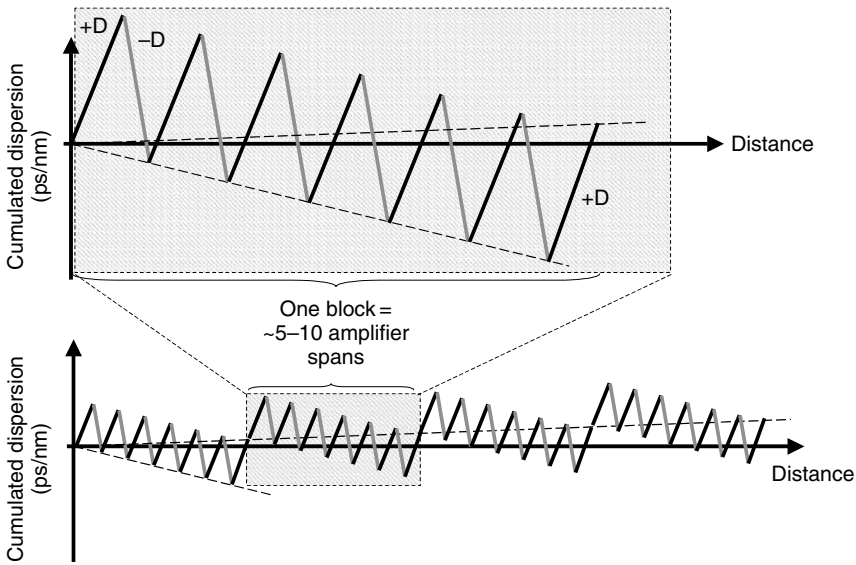

Figure 14.9 Schematic of the evolution of the cumulated dispersion along the line for a +D/ D fiber based system. (After Ref. [35]. © IEEE, 2006.)

The key advantage of the +D/ D fiber combination originates from the fact that +D and D index profiles have been designed such that the dispersion slopes of both fiber types can ideally match. As a result, the excursion of chromatic dispersion across the multiplex (as a function of wavelength) is very small at the end of the link, which favorably reflects onto the performance after transmission with respect to NZDSF systems. The extra cost associated with such fibers have limited the deployment of systems based on +D/ D fibers up to now [37], but such fibers could be mandatory for wideband (>25 nm), long-distance (>9000 km) systems.

14.3.4 Fiber for 40 Gbit/s WDM Systems

At 40 Gbit/s channel rate, the pioneer laboratory experiments also used a slope-compensated alternation of fibers with positive (+D) and negative (D) dispersions [9]. However, at this higher rate, the nature of the most detrimental nonlinear effects changes. In particular, the impact of intrachannel effects increase with pulse-to-pulse overlap in the fiber and therefore increase with chromatic dispersion.

In Ref. [38], several millions of simulation runs have been performed, each emulating a system configuration, in order to assess the impact of intrachannel effects as a function of the bit rate B and the dispersion parameter β_2. β_2 is related

to the chromatic dispersion D in ps/nm.km through $D = 2\pi c\beta_2/\lambda^2$, where c is the speed of light, and λ the signal wavelength. One remarkable conclusion is that intrachannel effects cause identical performance degradation in a system having a bit rate B and a dispersion parameter β_2, and in another system having a bit rate $2B$ and a dispersion parameter $\beta_2/4$. It was found that $\beta_2 B^2 L_{\text{eff}}$ is a good parameter for assessing the impact of intrachannel effects, where $L_{\text{eff}} = (1 \quad \exp(\ \alpha L))/\alpha$ stands for the effective length, L being the span length and α the attenuation coefficient. When $|\beta_2| B^2 L_{\text{eff}} \ll 1$, pulse-to-pulse overlap is very limited and the distortions caused by intrachannel effects remain low. This condition is met in all 10 Gbit/s systems. Conversely, when $|\beta_2| B^2 L_{\text{eff}} >> 1$, each pulse overlaps so many of its neighbor pulses, that all bit-to-bit information exchanges are scrambled and the impairments caused by intrachannel effects remain also relatively low. The most detrimental distortions are found when $|\beta_2| B^2 L_{\text{eff}} \approx 2$, e.g., precisely when propagation takes place over $+$D/ D fiber at 40 Gbit/s.

A way to contain intrachannel effects would therefore be to select a fiber with lower absolute value of chromatic dispersion. This would suggest that a cable based on NZDSF fiber would be preferable against intrachannel effects than a cable based on a $+$D/ D fiber combination. However, the fact that the dispersion slope of the NZDSF fiber cannot be easily compensated inline has a more detrimental impact on the system performance than the reduction of the absolute value of the chromatic dispersion. Another approach would be to use a $+$D/ D fiber combination with smaller dispersion parameters $|\beta_2|$ at 40 Gbit/s than at 10 Gbit/s. In this case, the residual dispersion slope arises again as a possibly strong limitation. Indeed, the excursion of dispersion across the multiplex cannot be contained over as large a wavelength range as with fibers with larger dispersion parameters $|\beta_2|$. For example, an early laboratory demonstration at 40 Gbit/s was based on a combination of fibers with $+8$ ps/nm/km average dispersion and -16 ps/nm/km average dispersion, respectively [10], but the transmission distance was limited to 2400 km. Even if other medium-dispersion fibers were used later in other test beds [39, 26], most of the demonstrations at 40 Gbit/s resorted to the same $+$D/ D fiber as that used for 10 Gbit/s applications, i.e., with larger dispersion ($\sim$20 ps/nm/km and ~ -40 ps/nm.km for the $+$D and the D fibers respectively, e.g., in Ref. [12]).

More complex fibers arrangements have also been proposed, especially in order to enhance the compatibility with the other generations of optical amplifiers, like Raman amplifiers. Configurations with three fibers ($+$D/ D/ $+$D) [14, 19, 21, 22, 24, 27] per repeater span and even with eight fibers per span [13, 15, 18] have been implemented and successfully tested in the laboratories. Besides, some essential characteristics of the fiber were improved. By increasing the fiber effective area, the impact of nonlinear effects are reduced [15], whereas the reduction of fiber attenuation brings a larger optical signal-to-noise at the end of the line. This gives some new margins to system designers, who may use them to propose systems reaching longer distances, or systems having a smaller number of repeaters. A $+$D fiber of impressive characteristics was reported, with 200 μm^2 effective area and

<0.16 dB/km loss [40]. However promising, this fiber is not yet used in systems, nor is it produced in large enough volumes. Conversely, the characteristics of the D fiber have been enhanced, and further benefits are expected out of the recent progress on dispersion compensating fiber (DCF) technology in terrestrial networks. This may result in an increase of effective area of the D fiber and to a reduction of its loss. Any such improvement of the transmission fiber characteristics is expected to facilitate the deployment of systems operated at 40 Gbit/s channel rate.

Before moving to systems based on new + D/ D fibers, some operators would rather upgrade their existing 10 Gbit/s NZDSF-based undersea cables to 40 Gbit/s. One important step to meet this goal was achieved, when 40 Gbit/s data were transmitted over a 4800 km-long, NZDSF-based, straight-line WDM test bed [41]. The compatibility with the already widely-deployed 10 Gbit/s systems was thereby shown for the first time. Nevertheless, for longer distances over the NZDSF, a limitation unseen at 10 Gbit/s arises. To cope with the NZDSF/SSMF positive chromatic dispersion slope, spools of positive- or negative-dispersion fiber are inserted in the terminals for the individual tuning of the cumulated dispersion of each channel, as pre and postcompensation in Figure 14.8. These spools are effective for canceling the dispersion of each channel *in average* but have no effect on the residual wavelength dependence of dispersion within the channel bandwidth, the so-called intrachannel dispersion slope [30]. This effect is harmless at 10 Gbit/s channel rate but can severely distort waveforms at 40 Gbit/s. For example, in Becouarn's experiment [41], the dispersion cumulated over the whole NZDSF/SSMF line varies by as much as 300 ps/nm from one channel to the next, i.e., over just 100 GHz. This corresponds to a residual dispersion slope of 375 ps/nm^2. If the transmission length had been increased to 7600 km, the residual dispersion slope would have amounted to 600 ps/nm^2. In this configuration, the inset of Figure 14.10 depicts the eye diagram at 40 Gbit/s impaired by this sole

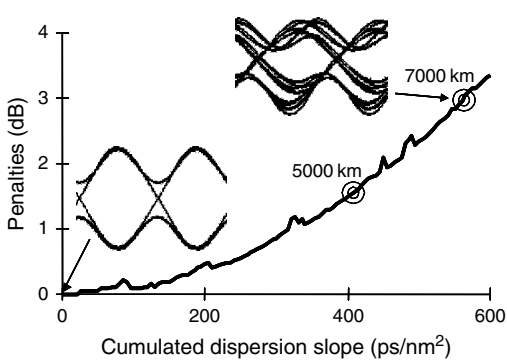

Figure 14.10 Computed penalty as a function of the dispersion slope. Insets: Eye diagrams at 0 km and after 7600 km in a NZDSF based system at 40 Gbit/s. (After Ref. [42]. Reprinted with permission from *Electronics Letters,* 2006.)

detrimental effect, as compared with the undistorted eye-diagram, obtained at 0 km, in the so-called back-to-back configuration.

Distortions of the signal quality can be quantified through the OSNR penalty, expressed in dB and with respect to the back-to-back configuration. When distorted, "1"s are more often mistaken for "0"s and vice versa, unless the relative amount of noise onto the receiver photodiode can be decreased. When a phenomenon generates 1 dB OSNR penalty, it means that it would take a 1 dB higher OSNR onto the receiver than in the back-to-back configuration, in order to recover the phenomenon-free performance. To be fully meaningful, the penalty should be evaluated while the number of errors is close to the maximum guaranteed to the operator throughout the system life. Here, it is evaluated while assuming that a commercial forward error correction board should bring the bit error-rate (BER) to less than 10^{-13}, i.e., to no more than one bit mistaken every 10^5 bits ($\mathrm{BER} = 10^{-5}$) without correction. Figure 14.10 represents the computed penalty at 10^{-5} BER as a function of the dispersion slope [42]. After 7600 km, a >3 dB penalty can be expected, which is unacceptable for system designers. To cope with this effect, an intrachannel dispersion slope compensator should be used. With such a device, a transmission over 6250 km NSDSF, has been reported with similar performance at 40 Gbit/s as at 10 Gbit/s [30].

Another fiber characteristics that worry system designers at 40 Gbit/s is the PMD. At 40 Gbit/s, the tolerable PMD is reduced by a factor of 4 compared to 10 Gbit/s transmission. The stringent impact of PMD at 40 Gbit/s suggests selecting fibers with a lower PMD than at 10 Gbit/s, but limited progress have been reported in this field in the past few years, and a further reduction by a factor of 2 of the PMD seems already challenging. Alternatively, PMD-corrective techniques at the receiver side sound attractive. Such techniques cannot fully compensate for PMD; they only mitigate it to some significant extent. As a rule of thumb, they typically allow a doubling of the maximum tolerable PMD. They can be divided into two major categories, whether they are electrical or optical.

On the one hand, electrical solutions rely on linear or nonlinear equalization, both correcting each bit of the data sequence according to its neighbors in order to reduce intersymbol interference [43]. Linear equalization consists in adding or subtracting weighted parts of the symbols adjacent to the bit under analysis, whereas nonlinear equalization relies on the dynamic adjustment of the threshold of the receiver. On the other hand, optical solutions for PMD mitigation basically involve the adaptation of the signal polarization at the receiver side. A practical approach consists in implementing a polarization controller and a birefringent element before the receiver photodiode, as schematized in Figure 14.11. Using the polarization controller, the principal states of polarization of the birefringent element are rotated so as to become orthogonal to that of the fiber at every moment, while its DGD should be equal (or reasonably close) to the DGD of the transmission fiber. For optimum performance, two (or more) such pairs of polarization controllers and birefringent elements can be cascaded.

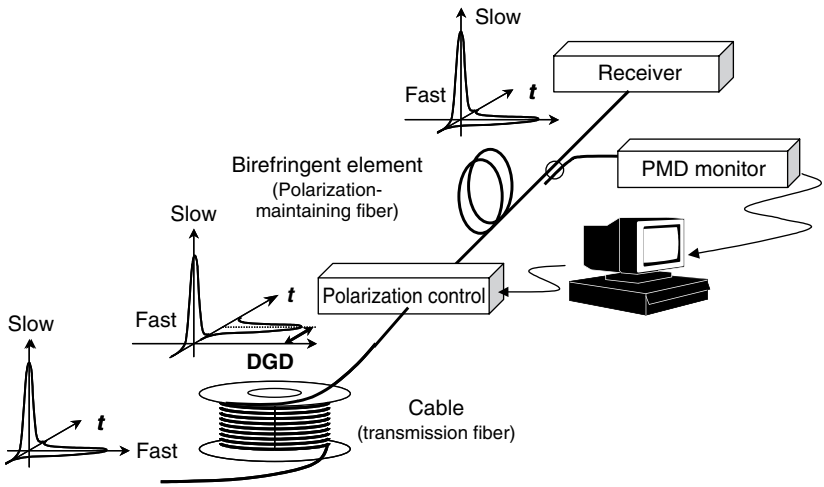

Figure 14.11 Principle of an optical PMD mitigator. (After Ref. [2]. © Wiley, 2002.)

Nevertheless, such PMD mitigators are complex devices and operate only on a per-channel basis. For this reason, system suppliers have been reluctant to their introduction at 10 Gbit/s, but the debate at 40 Gbit/s is different. Alternative approaches against PMD have attracted attention recently. One of them has the advantage of operating on all channels at once. It consists in inserting fast polarization scramblers periodically along the line and to use the possibilities offered by forward error correction (FEC) [44]. The scramblers somehow replicate the natural process which makes the differential group delay (DGD) of the fiber vary randomly, but at a much faster speed. More specifically, their characteristic scrambling time is made smaller than the duration of the so-called FEC frame, i.e., the elementary cell of bits over which error correction is performed (a few hundreds of bits). The possibility for the fiber (DGD) to reach very large values is as likely as without scramblers (generally rare), but whenever such an events occurs, it should last a much smaller time than the FEC frame duration, and therefore fall within the corrective capabilities of the FEC. Hence, the likelihood of true system outages can be significantly reduced.

Another strategy against PMD impairments would be to depart from conventional modulation formats (see further down) and select one which is particularly robust to PMD. In this respect, the most promising formats are multilevel formats, which inherently use longer symbol durations. One of them is quadrature phase shift keying (QPSK), which is twice as tolerant to PMD as the conventional formats used for 40 Gbit/s, but at the expense of some heavy drawbacks, also discussed later.

In summary, the intrachannel dispersion slope compensators and the PMD mitigation techniques are helpful responses to the limitations of fiber technology. Since the downturn of the millennium, the fiber industry has reported limited

progress for undersea applications, but this situation could change quickly when the operators are willing to increase the channel rate to 40 Gbit/s over the submarine routes.

14.4 AMPLIFIER SCHEME AND POWER MANAGEMENT

14.4.1 Erbium-Doped Fiber Amplifiers (EDFAs)

Erbium-doped fiber amplifiers (EDFAs) have been the one of the key constituents of optical undersea systems. The progress in terms of noise figure, bandwidth, gain uniformity vs wavelength, and output power has largely set the pace of the undersea system performance for more than 10 years. Nevertheless, EDFA technology seems to have now reached its pinnacle and little improvement is expected in the next few years.

Figure 14.12 depicts the typical gain shape of a raw erbium-doped fiber. This shape can slightly vary, depending on the concentrations and the types of co-dopants injected in the glass material during manufacturing, but it primarily depends on the inversion parameter. This parameter refers to the ratio of the number of erbium ions in the excited state over the number of erbium ions in the ground state. Assuming carefully-adjusted inversion parameters, the wavelengths windows where the gain excursion vs wavelength is the smallest fall either in the (1528 1568 nm) range or in the (1565 1605 nm) range. The first range is called the C-band and is used in the vast majority of optical transmission systems, and in particular, in all deployed undersea systems. The second range is referred to as the L-band. In order to compensate for the gain excursion, gain-flattening filters (GFFs) with a loss profile matching the inverse of the erbium fiber gain are incorporated within or after the amplifiers. The insertion of GFFs tends to alter the noise properties of the repeater and it is important that their loss be contained. Hence, the largest bandwidth which can be obtained with affordable noise generation is generally accepted to be around 40 nm. The widest bandwidth reported

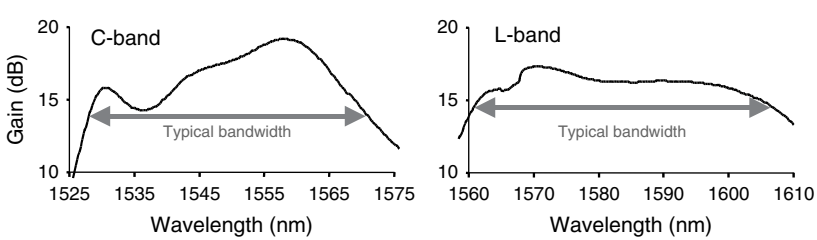

Figure 14.12 Typical gain curves provided by an erbium doped fiber, with a high (left) or a low (right) inversion parameter (this figure may be seen in color on the included CD ROM).

in an EDFA-based submarine experiment is 43 nm [45], with complex and lossy gain-flattening filters. In some laboratory experiments, two EDFAs are operated in parallel, one providing gain in the C-band, the other in the L-band. The bandwidth is then advantageously doubled, but the approach has not yet proved to be cost-effective for implementation in commercial systems.

Owing to the difficulty of repairs, reliability issues are key concerns for submarine cable designers. EDFAs largely attract their attention because most of the electrical power conveyed by the cable copper is used to feed the EDFAs. It is essential that the risk of EDFA breakdown be minimized. In particular, the consequences of possible laser diode failures are contained thanks to a redundancy scheme. It exploits the fact that the repeater must regenerate the signals traveling in both directions of a fiber pair. Figure 14.13 represents the internal structure of a repeater for submarine applications, as well as that of a repeater for terrestrial applications, where repairs are easier. In the undersea repeater, the light from two pump diodes (or sometimes, two pairs of pump diodes) at the wavelength of 980 nm is combined into a 3 dB coupler and equally split, in order to be shared by the two counter-directional amplifiers. In each of these amplifiers, the light at 980 nm is injected into the erbium-doped fiber along with the signal via a fused fiber multiplexer. Then, a gain-flattening filter compensates for the wavelength dependence of erbium-doped fiber response and reduces the overall EDFA gain excursion. Each amplifier is sandwiched into a pair of optical isolators against detrimental back-reflections. With such a redundant structure, if one pump-diode breaks, then the surviving diode can take over and feed the two bidirectional amplifiers.

In contrast, in a terrestrial repeater, the two bidirectional EDFAs are fully independent from each other. In case of pump failure, they block light and must be replaced. Their internal structures are very similar to that of undersea EDFAs, except that they are often designed as a concatenation of two EDFA stages. Thus, they can accommodate terrestrial-specific, lossy components within the so-called interstage.

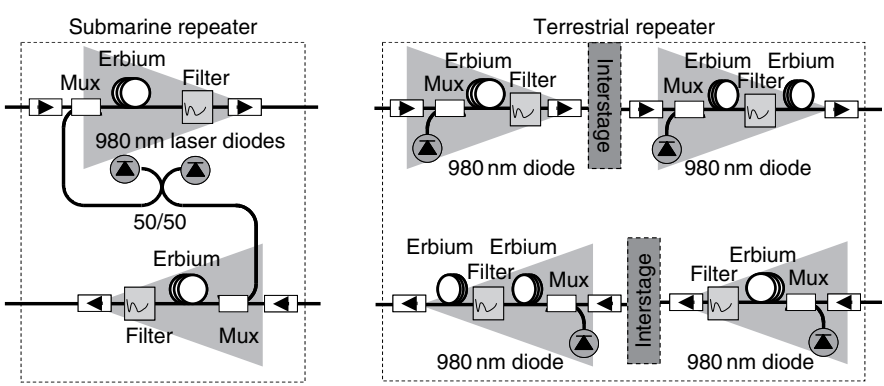

Figure 14.13 Internal structure of an EDFA based submarine repeater, as compared with a terrestrial repeater (this figure may be seen in color on the included CD ROM).

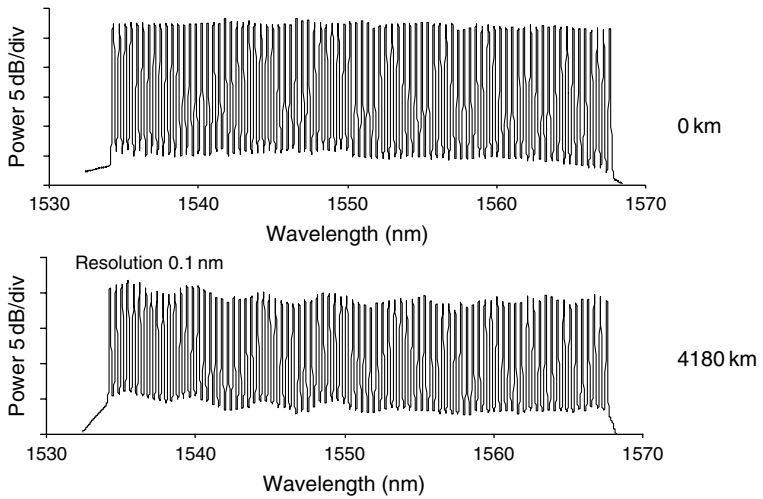

Figure 14.14 Spectrum in back to back (0 km) and at the output of a 4820 km long, straight line, EDFA based test bed. (After Ref. [41]. © IEEE, 2004.)

After a given number of concatenated amplifiers, additional gain flattening filters are sometimes inserted along the line for fine tuning, in order to keep the power excursion within a few dBs over a wide band and after long transmission lengths. Figure 14.14 gives an example of a spectrum recorded after a cascade of 200 repeaters in a straight-line test bed [41]. In this test bed, Fiber-Bragg gratings are used into all 61-km spaced amplifiers. Other Fiber-Bragg gratings are inserted every 15 amplifiers along the line, in order to provide a second-order gain correction. It can be seen that the power excursion does not exceed 4 dB after 4180 km across the entire multiplex.

In a long-term view, it can be expected that system designers will require larger amplifier bandwidths than current EDFAs. This suggests looking for alternative amplification technologies. Raman amplification has come up as one promising candidate. However, it should be recalled that the initial motivation for bringing Raman amplification in the front scene was the quest for additional system margins, to be ultimately converted into longer distances, longer repeater span lengths, or as enabling technology for the upgrade to 40 Gbit/s channel rate.

14.4.2 Raman Amplifiers

Raman amplifiers rely on a phenomenon called Stimulated Raman Scattering (SRS) [4]. This phenomenon designates the nonlinear process whereby some lower energy photons are created at the expense of higher-energy ones via interactions with optical phonons in the silica medium. This nonlinear effect can be used to generate gain in the transmission itself, by sending a high-power pump

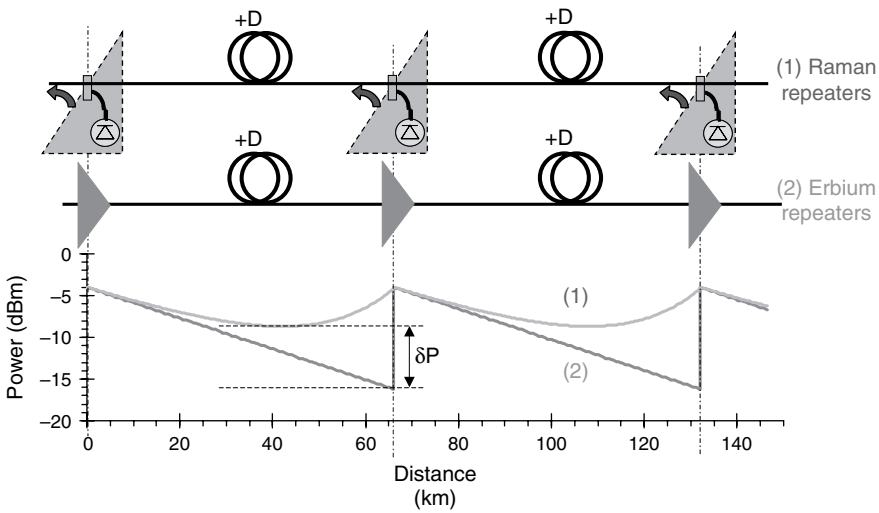

Figure 14.15 Schematic of the power profile along the transmission line for Raman amplifiers and EDFAs (this figure may be seen in color on the included CD ROM).

along with the signal, but generally backwards. The Raman process takes place throughout the transmission fiber and thus can be viewed as distributed. It contrasts with the amplification process within the EDFAs, which takes place over very short sections of doped fiber and thus should be considered as lumped. Because of its distributed nature, the Raman process generates gain with a smaller amount of noise than a lumped process. A better insight into this can be obtained by simulating the relative change in signal power along a 65 km-long repeater span, as depicted in Figure 14.15. In the presence of 12 dB Raman gain, the power decay resulting from fiber loss is stopped at about 20 km before the next repeater. At this point, the power level is $\delta P \sim 6$ dB higher than at the input of a regular EDFA. This minimum power level in the span mainly sets the amount of noise generated by the overall amplification process. Therefore, deploying Raman amplifiers effectively reduces the span loss by several dB, or else effectively increases the optical signal to noise ratio (OSNR) by the same amount.

However, it is not possible to fully benefit from the higher OSNR because the power level averaged along the span is larger than with a lumped amplification process, which enhances the detrimental impairments caused by nonlinear phenomena other than Stimulated Raman Scattering. Hence, the power at the output of Raman amplifiers should be reduced with respect to the recommended power at the output of EDFAs, which, in return, limits the OSNR improvement brought by Raman amplifiers. This suggests the noise/nonlinearity trade-offs in systems based on Raman amplifiers and based on EDFAs differ, but remain in favor of Raman. However, though the performance benefits of Raman amplification can very

noticeable in systems with long repeater spans, they are almost negligible when the span loss is around 10 dB, which is a common case in long submarine cables.

Stimulated Raman Scattering provides gain only over a limited wavelength region, but this region can be easily tuned by changing the pump wavelength. The left part of Figure 14.16 depicts typical, normalized Raman gain curves. Note that the gain in dB scales proportionally with the injected pump power in mW. The Raman gain peaks about 100 nm away from the pump wavelength. Gain uniformity over a wide band can therefore be obtained by inserting several pumps at different wavelengths simultaneously into the transmission fiber. The right part of Figure 14.16 shows the gain response computed after one 65 km-long span of fiber (here, a $+$D/ D/$+$D fiber combination) with three Raman pumps of optimized power at wavelengths 1435, 1455, and 1490 nm. Not more than 3 dB excursion is predicted over a range as large as 1530 1603 nm. Naturally, gain flattening filters must be used, as with EDFAs, in order to reduce the power excursion and enable transmissions over ultralong distances.

Raman amplifiers can also be used in parallel with EDFAs to widen the amplifier bandwidth. In Ref. [46], an EDFA provides gain in the C-band, while a Raman pump located at 1490 nm generates gain at longer wavelengths, up to 1607 nm. With the use of repeaters based on the association of both, 256 channels at 10 Gbit/s were transmitted successfully over 11,000 km.

Because Raman amplification is a distributed process which takes place into the transmission fiber, the characteristics of this fiber must be accurately taken into account when assessing the benefits of Raman amplification. Here, we consider fiber schemes involving two types of fiber with positive ($+$D) and negative (D) dispersion characteristics. The typical loss and effective area for $+$D fiber are 0.185 dB/km and 110 μm^2, respectively, compared with 0.23 dB/km and 30 μm^2, respectively, for the D fiber. The total lengths of $+$D and D fiber are dictated by the need to compensate for the overall dispersion. This still leaves various

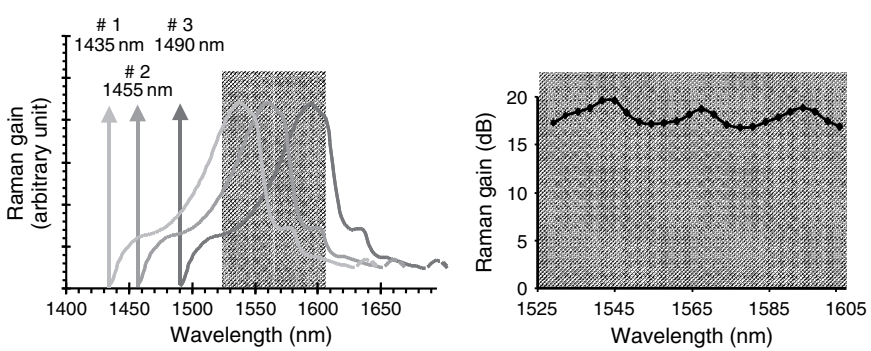

Figure 14.16 Typical normalized Raman gain shapes generated by a three pump schemes (left). Gain response computed after one $+$D/ D/$+$D fiber span, when the three pump power levels are optimized (right) (this figure may be seen in color on the included CD ROM).

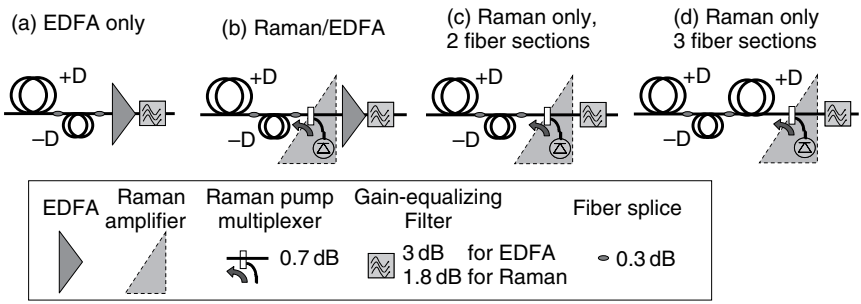

Figure 14.17 Description of the investigated fiber schemes as a function of the repeater type (EDFA, Raman, or hybrid EDFA/Raman). Each schematic depicts all the components of a single repeater span. (After Ref. [47]. © Alcatel, 2005) (this figure may be seen in color on the included CD ROM).

possibilities for concatenating the $+D/-D$ fibers, which we study next as a function of the amplifier configuration [47].

We compare by using numerical simulations four fiber/amplifier configurations, as schematized in Figure 14.17. Configuration (a) is the most standard configuration involving EDFA repeaters. Configuration (b) is the replica of configuration (a) but combines a Raman preamplifier and an EDFA in the repeaters, whereas configuration (c) uses only Raman repeaters. Finally, configuration (d) differs from configuration (c) by the fact the transmission fiber consists of three fiber sections $+D/-D/+D$ instead of two.

We compare the relative performance of all four configurations by evaluating the maximum reachable distance Dmax vs the repeater span length. Dmax is obtained when the lower optical power limit given by the tolerance to noise coincides with the higher optical power limit given by the accumulation of nonlinear impairments [48]. For an accurate evaluation, we have taken into account a realistic insertion loss for all the critical components of the repeaters. In particular, a gain equalizing filter is needed at every amplifier to contain the power excursion vs wavelength along the link. In our simulations, we assume a maximum insertion loss of the gain-equalizing filter, which is 1.2 dB higher with EDFA-based repeaters than with those based on all-Raman. This accounts for the fact that EDFA gain is generally less uniform than Raman amplifier gain. We have also taken into account the relatively high 0.3 dB per splice loss of the D-fiber. Figure 14.18 is a plot of Dmax, normalized to the maximum distance that can be achieved with the optimum 40 km span length in the EDFA configuration (a). Note that the Raman-specific limitations due to double Rayleigh backscattering [49] have been overlooked here.

In most cases, configurations using some form of Raman amplification perform better than those based solely on EDFAs, but the advantage does not translate into more than a 20% increase in the maximum reach Dmax. Besides, with a conventional two-section $+D/-D$ fiber configuration, a hybrid EDFA/Raman configuration (b) slightly outperforms the all-Raman configuration (c), especially when the repeater

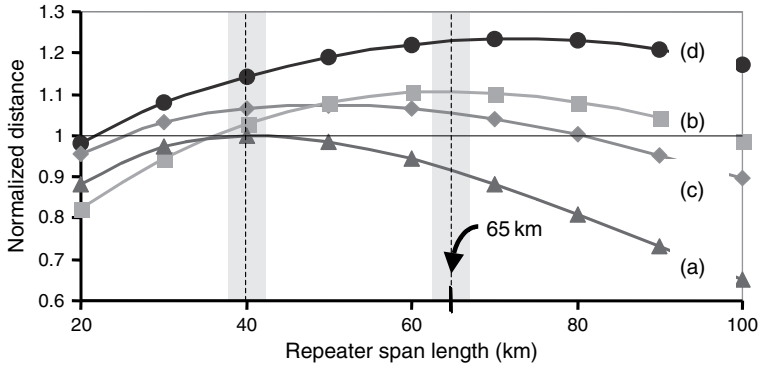

Figure 14.18 Impact of the fiber/amplifier scheme and the span length on the system performance. (After Ref. [47]. © Alcatel, 2005) (this figure may be seen in color on the included CD ROM).

span length exceeds 40 km. Configuration (b) appears particularly interesting for systems with long repeater spans [34, 50]. At 100 km span length, the maximum distance is identical to that which would be achievable with EDFAs spaced by only 40 km. However, the amplification bandwidth is limited by that of the EDFA.

Configuration (d), like (c) [51], does not suffer from this limitation. It involves only Raman but with three $+D/\ D/+D$ sections of fiber and appear as the most performing. Whereas a three-section scheme would be of limited interest with EDFAs, it enhances the benefits of Raman amplification by making sure that the maximum optical power level is found at the beginning and at the end of each repeater span, in the fiber type ($+D$), which has the larger effective area, and therefore is the less sensitive to nonlinear impairments. Note that the greatest benefits are obtained with an optimal repeater span length of $\sim$60 80 km, significantly larger than the conventional optimal span length with configuration (a) based on EDFAs ($\sim$40 km). However, a major drawback of all-Raman amplification is the higher required pump power, and thus the higher electrical power that should be supplied to the submarine cable.

In summary, Raman technology may bring some benefits to system reach, but whether these benefits are worth the development of the associated disruptive repeater design is still a matter of debate. Nonetheless, Raman amplification can be regarded as an enabling technology for 40 Gbit/s systems when the system bandwidth exceeds 70 nm. The optical bandwidth can be increased by more than a factor of 2 as compared with conventional EDFA system. Furthermore, the wider the bandwidth, the better the Raman efficiency is. For example, a Raman amplifier with two pumps at wavelengths 1430 and 1460 nm provides flat gain over a 41 nm bandwidth with $\sim$680 mW of injected pump power (i.e., the pump power per unit of bandwidth is 16.6 mW/nm), whereas a system with three pumps at 1435, 1455, and 1490 nm provides gain over 73.5 nm with only $\sim$850 mW of pump power (i.e., the pump power per unit of bandwidth is just 11.6 mW/nm).

Besides the assessment of Raman benefits in terms of performance and power consumption, several important issues must be addressed before Raman amplifiers are implemented in actual systems. One of these issues is the control of their gain response throughout the life of the system. Because of cable repairs and fiber aging, the beginning-of-life settings for minimal gain excursion may have to be adjusted. In EDFA systems, any increase of loss is converted into a gain tilt of the following repeater, e.g., over a 30 nm multiplex, the leftmost channels experience higher gain than the rightmost channels, by more than 0.5 dB every additional 1 dB loss on the signal path. One cause for time-dependent loss is fiber aging. It results in a typical 0.003 dB/km extra attenuation over 25 years, which amounts to an overall distributed 21 dB loss in a 7000 km-long system. Another cause for time-dependent loss is cable repairs. Such repairs are needed when a failure occurs. The cable is cut at the bottom of the ocean at depth d_0 and brought up to the surface where it is spliced to a new section of cable of typical length $2d_0$, before being laid back onto the sea floor. A typical loss of 2.5 dB is provisioned every 1000 km for such operations, which yields an overall 17.5 dB loss for a 7000 km-long cable. These two estimations clearly illustrate that fiber aging or cable repairs would cause dramatic gain excursions, if periodical active tilters had not been implemented in submerged equipments to counterbalance them.

A submarine system using a wideband Raman amplifier would behave quite differently [52]. Firstly, the occupied optical bandwidth could be much wider, which would naturally complicate gain flatness management. Secondly, the response of a Raman amplifier to fiber aging or cable repairs can quite different from that of an EDFA. The overall Raman gain curve is the combination of various gain curves produced by several pumps' wavelengths (e.g., three to five in order so as to obtain wideband amplification). The Raman effect provides gain to the signal through an energy transfer from the pumps to the signal. But in a multipump configuration, the energy transfer also takes place between the pumps. The lower-wavelength pumps give up a fraction of their power to the longer-wavelength pumps. The wider the amplification bandwidth, the more the pumps need to be spaced apart, and the larger the pump-to-pump interactions are. When fiber attenuation increases uniformly along the line (as a result of aging for example), the Raman gain decreases and pump-to-pump interactions become weaker, which causes a gain tilt. Figure 14.19 shows a computation of this tilt, assuming a multiplex spanning over 1529 1603 nm.

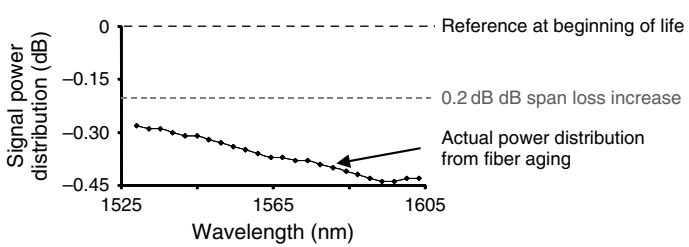

Figure 14.19 Computed impact of distributed fiber aging on the power distribution of a multiplex, after one 65 km long repeater span (this figure may be seen in color on the included CD ROM).

This multiplex is injected with 10 dBm total power at the input of a $+D/-D/+D$ fiber span with 65 km length. The 0 dB reference level corresponds to the power distribution that would be recorded at the repeater span end, at the beginning of life. When the cable is affected by 0.003 dB/km extra attenuation due to distributed fiber aging, the overall repeater span loss increases by 0.2 dB (dotted line), but the Raman gain is also reduced. The resulting power distribution vs wavelength is tilted, as shown by the full line of Figure 14.19.

The impact of fiber repairs can be very different. Since Raman effects take place within the transmission fiber, it should be expected that the location of the fiber cut and the type of fiber used for repairing are important parameters for assessing the spectral distortions of the gain. We compute these distortions in a configuration similar to that of Figure 14.19. We consider that the repair consists in splicing a 10 km-long NZDSF fiber to the existing cable, inserted at six possible locations of a span schematized in the inset of Figure 14.20. A 3 dB repair loss is assumed, including 0.5 dB loss per splice. The power distribution at the end of the span is represented in Figure 14.20, and compared with a reference EDFA-based configuration where 3 dB loss would yield a spectrally uniform 3 dB reduction of power. Most remarkably, in cases 1 and 2, the added fiber section causes negligible Raman gain variation. In contrast, in cases 4 and 5, Raman gain decreases dramatically.

It appears that a 3 dB span loss increase can lead to less than 3 dB (cases 1, 2, and 3) or more than 3 dB (cases 4, 5, and 6) loss at the end of the repaired span. When the repair is done in the first half of the repeater span, the Raman gain increases compared with the reference configuration, as explained by a reduction of the Raman amplifier saturation. At the same time, the multiplex experiences relatively more gain at the longer wavelengths, as a result of stronger pump-to-pump Raman interactions. Conversely, when the repair is performed in the second half of the repeater span, the channels power is affected in average by more than 3 dB (cases 4, 5, and 6). This should not be surprising as the NZDSF fiber used for repair has a significantly larger effective area ($\sim 65\,\mu m^2$) than the $-D$ fiber ($\sim 30\,\mu m^2$). Thus, a Raman pump traveling into an NZDSF fiber generates less

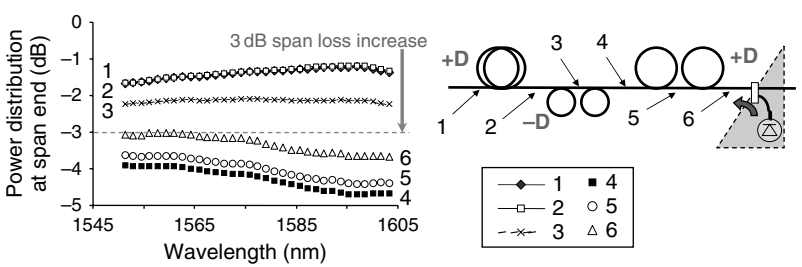

Figure 14.20 Computed impact of a (lumped) fiber repair on the power distribution of a multiplex, as a function of the repair location, after one 65 km long repeater span. (After Ref. [52]. Reprinted with permission from IEE) (this figure may be seen in color on the included CD ROM).

gain than in an NZDSF. Figure 14.20 also shows that, in these cases, the multiplex power distribution is tilted, but in the opposite direction, due to weaker pump-to-pump Raman interactions.

Whether the power variations originate from fiber aging or repairs, they have to be contained. In this respect, Raman amplification provides more flexibility than erbium-doped fiber amplification, because the gain shape can be modified during the system life by adjusting the pump power of each wavelength of the Raman amplifier. This could be viewed as an advantage but multiparameter adjustments add to the complexity of the system. The most straightforward way to control these adjustments would be to rely on optical spectrum monitoring units distributed along the link.

In summary, despite the above advantages in terms gain uniformity management, the limited increment of distance allowed by Raman amplification does not seem to outweigh the cost of development of this alternative amplification technology for undersea applications, at least for the next coming years. It has in store greater opportunities for optical bandwidth extension, when the market trends are ready for it. It is therefore likely that the first generation of submarine systems at 40 Gbit/s will not resort to Raman amplifiers, but to erbium-doped fiber amplifiers.

14.5 MODULATION FORMATS

Since the early laboratory experiments at 40 Gbit/s, one topic has grown into the system designers' minds as one key enabler for the introduction of 40 Gbit/s channel rate, namely the topic of modulation formats. The modulation format designates the approach used to apply the incoming digital information to each of the optical carriers. A large number of such approaches have been proposed in the past 5 years. Notwithstanding complexity and cost considerations in the implementation, the pros and cons of formats should not be limited to the sole issue of compatibility with ultrahigh capacities. Some of them can be immediately recommended for their superior robustness to fiber nonlinearity, others because they exhibit greater tolerance to amplifier noise accumulation. Others have higher resistance to the chromatic dispersion, or to the polarization mode dispersion (PMD). Not surprisingly, these advantages cannot all be obtained from a single format.

Most studies now concur to suggest that the choice of the format has a stronger influence on the system performance at 40 Gbit/s than at 10 Gbit/s. In particular, the interest for phase shift keying (PSK) was renewed in 2002 [53], when used for the first time at 40 Gbit/s in conjunction with a balanced receiver. With such a receiver, the sensitivity to optical noise (namely optical signal-to-noise ratio sensitivity), is improved by nearly 3 dB, compared with more conventional formats like return-to-zero (RZ). Besides, PSK formats turned out to be particularly resistant to nonlinear effects.

14.5.1 In 5 Gbit/s Single-Channel Systems and in N × 2.5 Gbit/s WDM Systems

The most straightforward way to modulate a laser diode at B Gbit/s (e.g., 2.5, 10, or 40 Gbit/s) is to switch its output light intensity ON or OFF, whether the symbol to be transmitted is a mark ("1") or a space ("0"), at a rate equal to the information frequency B GHz (e.g., 2.5, 10, or 40 GHz). This operation, called on-off keying (OOK), is generally achieved by applying the ON/OFF electrical signal to a Mach-Zehnder (MZ) electro-optic modulator fed with the laser light. The modulator acts like a switch, i.e., with a small insertion loss when a "1" is coded and a higher attenuation when a "0" is coded. The power ratio between "1"s and "0"s is usually higher than 10 dB. This produces so-called non-return-to-zero (NRZ) optical data. Figure 14.21 depicts the computed waveform of an eight-bit binary sequence with corresponding intensity, phase, and eye diagram, modulated with NRZ format, as well as with all the formats proposed for submarine applications and discussed next. The associated optical spectra are also drawn, as well as schematics of the conventional ways of producing the formats.

The first generation of submarine WDM systems at 5 or 2.5 Gbit/s all relied on the NRZ format, possibly enhanced by some polarization modulation in order to improve the tolerance to nonlinearities.

14.5.2 In N × 10 Gbit/s WDM Systems

When the bit rate increases from 2.5 to 10 Gbit/s, new physical constraints came up, which suggests departing from NRZ modulation. When the bit rate is increased by a factor of 4 (6 dB), the optical signal-to-noise ratio should ideally scale up by the same amount for the bit error rate to remain unchanged. This requires increasing the channel power by the same amount, but is often obtained at the expense of a stronger impact of nonlinear effects.

The return-to-zero (RZ) format was then viewed as a promising alternative to NRZ. With RZ format, any "1" symbol is represented by a pulse, which can be of variable duration (e.g., $1/(2B)$ at half maximum in Figure 14.21). For best performance, pulses are usually carved into the NRZ waveform, thanks to a second MZ electro-optic modulator in cascade with the NRZ modulator. Alternatively, the RZ waveform can be generated electrically out of the electrical binary sequence and fed to a single Mach-Zehnder (MZ) modulator, directly producing RZ optical data. At 10 Gbit/s, RZ has been praised for its higher tolerance to fiber nonlinear effects. An intuitive explanation for this feature is the fact that with isolated pulses, unlike in NRZ sequences, each "1" symbol (1) is virtually independent from its neighbors and (2) experiences the same nonlinearity. In NRZ, sequences of "1" emulate continuous light-signal packets, which are unstable under nonlinear propagation at the edges. If the RZ pulse power is carefully chosen, distortions due to nonlinear

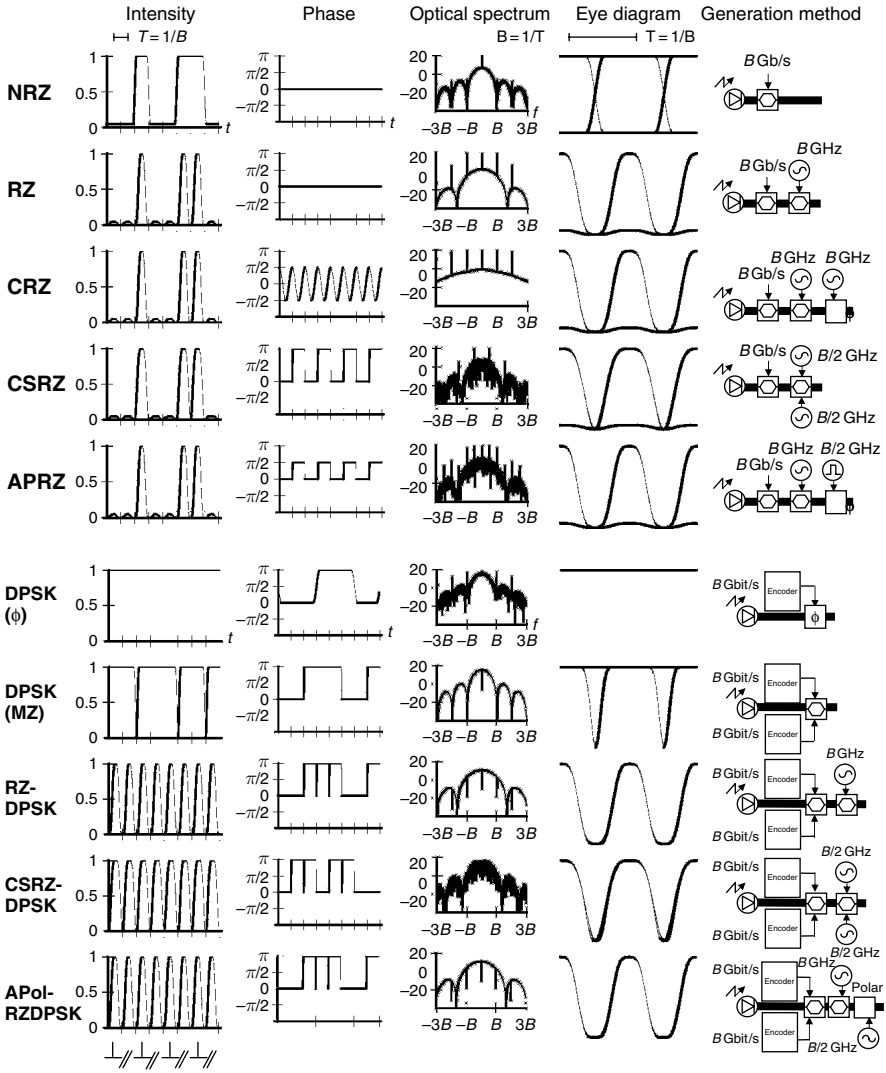

Figure 14.21 Computed waveform of an eight bit sequence with intensity, phase, eye diagram, and optical spectrum for each format. In addition, a schematic of the most conventional generation method is provided. All the amplitude Mach Zehnder (MZ) electro optic modulators are chirp free. Single arm MZ or dual arm MZ indicate that $V\pi$ or $2V\pi$ total driving voltage is needed, respectively, regardless the actual MZ design (push pull configuration or not). NRZ stands for non return to zero, RZ for return to zero, CRZ for chirped return to zero, CSRZ for carrier suppressed return to zero, APRZ for alternate phase return to zero, DPSK for differential phase shift keying, and APol for alternate polarization. (After Ref. [2]. © Wiley 2002.)

effects can be even almost canceled by the effect of chromatic dispersion. In such a regime, the RZ pulses are referred to as "solitons" [54]. Despite the attention they received, solitons never came out of the research laboratories, because they were found quite sensitive to the transmission line parameters (power, dispersion, etc.) and most of their benefits vanish when WDM channels are densely packed, like today's.

The Return-to-Zero (RZ) format has been widely used and deployed for submarine cables, but several enhanced RZ formats have been proposed as alternatives to conventional RZ. Chirped RZ (CRZ) has been one of the most successful. It consists in passing RZ data into a phase modulator driven by a clock at the information frequency B [55]. This scheme produces wider channel spectra than RZ spectra, which limits the maximum number of channels, and thus the system total capacity. However, it has been largely implemented for 10 Gbit/s undersea applications, because it significantly enhances the robustness to nonlinearities. Typically, the larger the phase modulation depth, the larger the spectral width, and the better the enhancement. CRZ is especially efficient against intrachannel nonlinear effects (i.e., those affecting the waveform of each isolated pulse). For the longest transmission distances, RZ modulation formats are used jointly with bit-synchronous phase modulation. This phase modulation induces a further significant channel spectrum broadening and a larger tolerance to nonlinearities.

A major evolution compared with previous 2.5 Gbit/s systems was the introduction of forward error correction (FEC). FEC relaxes the constraints on the bit-error ratio, making possible a significant reduction of the signal power and, hence, nonlinear impairments, while maintaining the bit-error ratio after correction. FEC triggered the possibility to pack channels closer, paving the way for larger system capacities in the same amplifier bandwidth. The interest toward modulation formats with larger spectral width such as CRZ went down and NRZ format was revitalized. In particular, some of the most recently installed 10 Gbit/s WDM undersea systems rely on the simple, cost-effective NRZ format. Other systems rely on NRZ, but only over a fraction of the multiplex. The reason is that over NZDSF fiber, the impact of optical nonlinearities can be very different from channel to channel. The lower wavelength channels are generally more distorted, and in this region, a larger channel spacing is sometimes mandatory to meet the distance and performance requirements, so that RZ or CRZ formats can be used instead of NRZ format.

As the channel spacing went down over the years, nonlinearities affecting the propagation of each individual channel, free of its neighbors, became secondary to nonlinearities resulting from interactions between WDM channels. For very highly-dense 10 Gbit/s WDM systems (e.g., with 25 GHz channel spacing or even less), differential Phase Shift Keying (DPSK) and Return-to-Zero-DPSK (RZ-DPSK) [56, 57] formats were shown to be promising alternatives to NRZ and RZ formats. Since then, they have also proved successful for achieving the longest system distances, or for enabling challenging system capacity upgrades. Next, we shall describe these PSK formats in more detail. We shall show that their potential is even greater at 40 Gbit/s and briefly return to their pros and cons at 10 Gbit/s.

14.5.3 In N × 40 Gbit/s WDM Systems

One major reason for revisiting the issue of modulation formats when moving from 10 Gbit/s channel rate to 40 Gbit/s channel rate is that the nature of nonlinear impairments changes. At 10 Gbit/s, intrachannel nonlinear effects are often negligible. In contrast, at 40 Gbit/s, the broadening ratio of pulses normalized to the bit duration is 16 times stronger than at 10 Gbit/s, and intrachannel effects generally dominate. This acknowledgment gave rise a series of new modulation formats particularly interesting for 40 Gbit/s transmission, while rekindling interest toward older ones [71]. All of them include some form of phase modulation, for breaking the phase-matching conditions essential to the generation of intrachannel four-wave mixing.

The carrier-suppressed RZ (CSRZ) format was initially used in terrestrial links at 40 Gbit/s channel rate [58]. In this format, a π-phase shift is applied to every other bit, as a consequence of RZ pulse carving from a Mach-Zehnder electro-optic modulator driven at half the information frequency (see line 4 of Figure 14.21). However, though widely used in the pioneer 40 Gbit/s laboratory experiments [12, 13, 14, 15, 16, 23], CSRZ is not very efficient against intrachannel nonlinear effects. By applying alternate phase shifts of $\pi/2$ instead of π to consecutive bit slots, to yield the so-called $\pi/2$-alternate-phase RZ ($\pi/2$ APRZ) format [59], the reduction of intrachannel impairments is greater [60]. This ensures that constructive interferences between overlapping pulses are turned into destructive interferences, and reduces the generation of ghost pulses. Figure 14.22 illustrates the computed benefits of the $\pi/2$ modulation over the intensity and phase of a particularly penalized subsequence of seven-bits, after propagation over 1500 km of SSMF fiber. Despite the promises, the potential of the APRZ modulation format in a WDM long-haul, submarine environment remains to be confirmed.

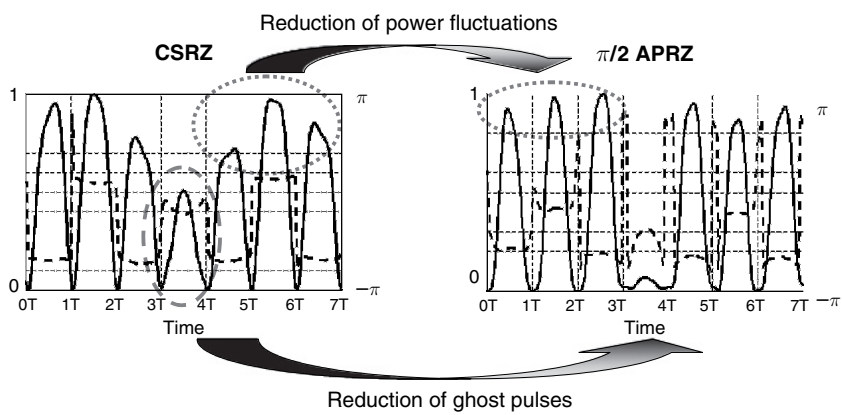

Figure 14.22 Impact of $\pi/2$ periodic phase modulation after 1500 km of SMF fiber onto the phase (dotted line) and intensity (full line) of a seven bit long sequence within the data pattern. (After Ref. [35]. © IEEE, 2006) (this figure may be seen in color on the included CD ROM).

Differential Phase-Shift Keying (DPSK) is another modulation format which has attracted considerable attention for 40 Gbit/s applications. It incorporates numerous π phase jumps, which act similarly as above against intrachannel nonlinear effects, but we shall come back to this feature that later on. In contrast to all the above formats, the information is carried by the phase itself. DPSK optical data are generated by passing laser light into a electro-optic phase modulator, or preferably, into a Mach-Zehnder electro-optic amplitude modulator (see Figure 14.21, lines 6 7), biased such that the intensity levels of the "1" and "0" symbols are identical. Since photodiodes are essentially intensity sensitive, some phase-to-intensity conversion is required in front of the receiver to recover the information. For that purpose, differential detection looks particularly convenient. It consists in comparing the phase of a given bit with that of the following one, before sending the result onto a photodiode, as shown in Figure 14.23. The comparison is performed in a passive fiber Mach-Zehnder interferometer with an arm longer than the other by the length of one bit. Note that differential detection scrambles the data, which can therefore only be recovered if passed into a precoder at the transmitter side. A functional schematic of such a precoder is also depicted in Figure 14.23.

Besides, the passive Mach-Zehnder interferometer has the advantage of having two output arms, one supplying the actual data, the other supplying the complementary of the data. By departing from conventional receivers and attaching the two arms to two distinct photodiodes operating in parallel (their photocurrents being subtracted in the end), it is possible to increase the robustness to low OSNRs of the detected signal by $\sim$3 dB. This result has created another important motivation for rekindling the DPSK format for 40 Gbit/s applications. A receiver with two such photodiodes is called a balanced receiver (Figure 14.23).

A simple way to evaluate the robustness to noise is to draw the constellation diagram for each format (see Figure 14.24), i.e., the electrical field at the expected locations of "0" and "1" symbols in the complex plane, assuming a normalized

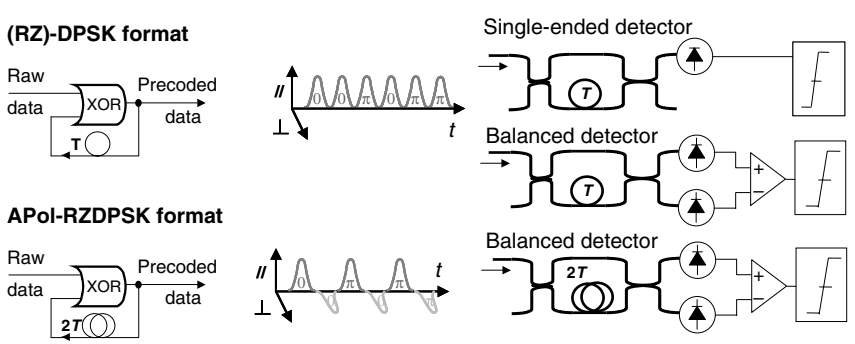

Figure 14.23 Schematics of differential precoders and differential detection schemes for (RZ)DPSK and APol RZDPSK modulation formats (this figure may be seen in color on the included CD ROM).

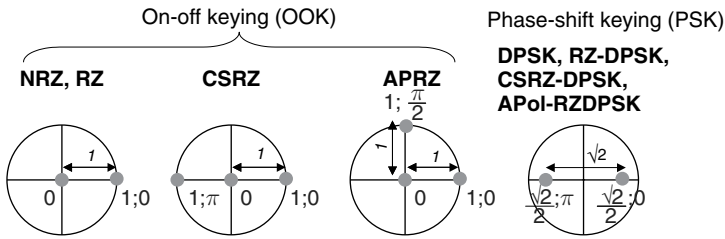

Figure 14.24 Constellation diagrams of formats listed in Figure 14.21 (this figure may be seen in color on the included CD ROM).

signal intensity. For OOK modulation formats (NRZ, RZ, CRZ, CSRZ, or APRZ), a "0" symbol has nearly zero intensity and therefore falls in the center of the diagram, whereas a "1" symbol has an amplitude normalized to 1, and therefore falls on the unit circle. "1" symbols can be located anywhere on this circle, depending on the reference phase from which their phase is evaluated. The reference phase does not matter in our explanation, and we choose to represent them with a zero phase, i.e., along the real axis. Conversely, for the DPSK format (and all the phase-shift-keyed formats of Figure 14.21, discussed later), both "0" and "1" symbols have the same amplitude ($\sqrt{2}/2$) but a phase difference of π. Again, the reference phase is not meaningful here, and we may locate them about along the real axis, about the circle center. For each symbol of the bit stream, any noisy perturbation adds to the electrical field and shifts its coordinate in the complex plane, off the expected values represented by the dots in Figure 14.24. Since the amplitude distance between "0" and "1" symbols is $\sqrt{2}$ larger for the DPSK format than for the on-off keyed (OOK) formats, it takes a larger amount of noise power (by approximately $\sim(\sqrt{2})^2$) for the PSK formats to have a "1" mistaken for a "0', or a "0" mistaken for a "1." These considerations hold only if DPSK data are detected with a receiver which can distinguish between the phase of symbols with no overall power loss, as in the balanced configuration of Figure 14.23. This highlights why the tolerance to noise of DPSK can be approximately 3 dB better than that of the on-off keyed (OOK) formats. The actual figure depends on the true characteristics of the terminal equipment, mostly the bandwidth of the electro-optic modulator and its phase ripples, and on the exact splitting ratio of the balanced Mach-Zehnder passive demodulator [64].

Most experiments reported to date based on DPSK format used a DPSK electro-optic modulator in combination with an RZ pulse carver, yielding return to zero DPSK. Pulse carving can be performed with a electro-optic Mach-Zehnder modulator driven by a clock signal either at (1) frequency B or at (2) frequency $B/2$, i.e., while leaving phase information unchanged or while alternating the phase of every second bit slot by π, yielding the RZ-DPSK and CSRZ-DPSK formats, respectively. It can be easily figured out that the phase alternation of CSRZ has no other effect on DPSK but to turn the signal into its complementary. Hence, any difference in system performance between the two above pulse carving schemes

originate from differences in carving shapes and thus spectral shapes. At 40 Gbit/s, DPSK formats have surpassed all the other formats in terms of performance at 40 Gbit/s [20, 24], not only because of their stronger resistance to noise, but also to their improved tolerance to nonlinear effects.

The multiple phase jumps between bits in any DSPK waveform break the phase-matching conditions for intrachannel four-wave mixing to efficiently occur and thereby provide a superior resistance to distortions at high power [62, 63]. Additionally, the peak power of each pulse is twice as small as that of OOK pulses for the same average power, which also helps provide a higher robustness to nonlinear effects. Further insight on this robustness is given next using computer simulations. RZ and RZ-DPSK formats are compared after propagation over 15 100 km-long spans of SSMF fiber. The channel power P in each repeater span is gradually increased and the performance is evaluated at the receiver end. The Q factor, or its logarithm $Q^2_{\mathrm{dB}} = 20\log_{10}(Q)$, is provided next as a substitute to the bit-error rate (BER). This quality factor is derived from the BER using the following formula:

$$\mathrm{BER} = \frac{1}{\sqrt{2\pi}}\int_{Q}^{+\infty}\exp\left(-\frac{x^2}{2}\right)\mathrm{d}x = \frac{1}{2}\,erfc\left(\frac{Q}{\sqrt{2}}\right) \tag{14.1}$$

Note that other definitions for the Q factor are used by some authors. Here, the calculation of Eqn (14.1) is performed (as often in the literature), regardless of any consideration whether the conditions are met for the other definitions to match. At relatively low power levels of P, when the channel power increases, the optical signal-to-noise ratio (OSNR) at the end of the link increases proportionally. Hence, the factor Q improves with the channel power P. At relatively high power levels in the fiber, the impact of nonlinear effects becomes noticeable and the Q^2 factor drops when P increases. This trend applies to all modulation formats, but Figure 14.25 shows clearly that the RZ-DPSK format outperforms the RZ format for two reasons. The first one is the improved OSNR sensitivity. The second one is the higher tolerance to nonlinear effects and especially to intrachannel four-wave

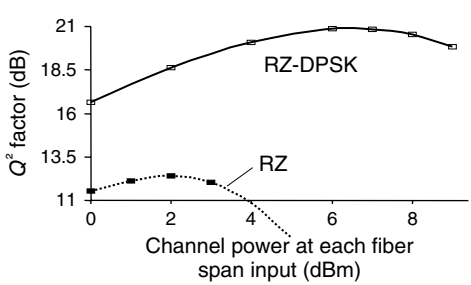

Figure 14.25 Numerical comparison of the performance of RZ and RZ DPSK formats at 40Gbit/s. (After Ref. [35]. © IEEE, 2006.)

mixing, which drastically limits the maximum input power for RZ format. Hence, with DPSK format, it is possible to send higher signal power into the fiber, and hence bridge longer distances, while fulfilling the customer requirements in terms of bit-error ratio (or Q factor).

At 10 Gbit/s, the use of PSK formats does not bring about as many benefits as at 40 Gbit/s channel rate. The first reason is that intrachannel nonlinear effects at 10 Gbit/s are not as penalizing as at 40 Gbit/s. Additionally, at 10 Gbit/s, another detrimental nonlinear effect comes into play when PSK formats are implemented, namely nonlinear phase noise [64, 65]. This effect is another manifestation of the Kerr nonlinear effect. It stems from interactions between the signal and the amplifier noise during propagation along the transmission line. Its impact is most often negligible at 40 Gbit/s, but it can be extremely penalizing at 10 Gbit/s channel rate, particularly with PSK formats [66]. In some undersea cable configurations at 10 Gbit/s, the impact of nonlinear phase noise is so high that the implementation of (RZ-)DPSK is not worth the extra cost compared with the RZ format. However, in other cable configurations, the conditions are met for a successful and cost-effective implementation of RZ-DPSK format. These configurations generally correspond to the longest transoceanic distances, e.g., transpacific distances (>9000 km), where $+$D/ D fiber is preferred [56, 57]. The use of DPSK can there allow a reduction of the number of repeaters and hence system cost savings, despite higher terminal costs. Another application of RZ-DPSK format at 10 Gbit/s is to upgrade the capacity of existing NZDSF-based systems [67]. In such systems, the accumulated chromatic dispersion can be very large (see bottom Figure 14.7), especially, at the leftmost and rightmost wavelengths of the multiplex. In these wavelength windows, the pulse-to-pulse overlap within each channel is large enough for intrachannel four-wave mixing to appreciably distort the waveforms. At the same time, in such highly-dispersive regime, the interactions between signal and amplifier noise are less effective. These two last considerations highlight why the use of the RZ-DPSK format can prove fruitful there at 10 Gbit/s. In contrast, at the center of the multiplex, these considerations do not apply, and the RZ format can outperform the RZ-DPSK format. A careful mix of RZ and RZDPSK formats depending on wavelength can therefore be recommended [68].

At 40 Gbit/s, DPSK formats have undoubtedly surpassed all the other formats for submarine applications. Research studies reported in the recent past in this field have focused either in meeting the ultralong-haul distance requirements or in demonstrating that systems based on 40 Gbit/s channel rate could carry greater capacities than those based on 10 Gbit/s channel rate.

Bridging distances as long at 40 Gbit/s channel rate as at 10 Gbit/s channel rate has been a challenge. The introduction of PSK formats and the progress in FEC technology have been major steps. Another step has been to further improve the modulation/demodulation scheme. Besides the phase and the intensity, exploited by advanced on-off-keying and phase-shift keying, another physical characteristic of light may be used to improve the transmission performance, namely polarization. It is well known that the linear and nonlinear interactions between two

waveforms, whether at the same wavelength or at different ones, depend on their respective polarization. A rule of thumb to remember is that they are maximum when the polarization states of the waveforms are aligned. Considering that the most penalizing nonlinear phenomena at 40 Gbit/s involve the interactions between adjacent bits, it can be easily predicted that a periodical alternation of the polarization state by 90° every other bit should bring some advantage. This scheme can be applied either to RZ or to RZ-DPSK, generating thus alternate-polarization (APol) RZ [69] and APol RZ-DPSK, as represented in Figure 14.23, bottom. However, differential detection with APol-RZ-DPSK cannot be performed with the same passive Mach-Zehnder interferometer as that used in a DPSK receivers, because the state of interference of two electrical fields cannot vary as a function of their phase if they are orthogonally polarized. An interferometer with an arm longer than the other by the length of two bits instead of one bit should be used, so that the bits which are compared in the interferometer are aligned along the same polarization axis instead of being orthogonally polarized. Naturally, the differential precoder feeding the APol-RZDPSK transmitter have to be updated accordingly (Figure 14.23, bottom) [70].

In Figure 14.26, the improvement brought by the polarization modulator on the tolerance to nonlinear effects has been measured after a transmission distance of 9180 km. The optical power at each repeater span input of one typical channel, selected into a full 100 GHz multiplex, is varied by steps of 1 dB. The bit-error ratio is measured, converted into Q factor according to Eqn (1), and reported in Figure 14.26. No difference is noticeable at low power levels (when nonlinear effects are weak), whether the polarization modulator is ON or OFF, but, at higher power levels, the APol RZ-DPSK format clearly outperforms RZ-DPSK format. When the polarization modulator is turned ON, it appears that the power yielding the best bit-error ratio (or Q^2 factor) is improved by nearly 3.5 dB, at around 7 dBm, and that the optimum Q^2 factor is increased by more than 2 dB [27].

Next, the impact of the electrical phase of the polarization-modulator-driving clock is reported after transmission over 9180 km, in the conditions of Figure 14.26, at 7 dBm power per channel. The Q^2 factor is again computed out of bit-error ratio

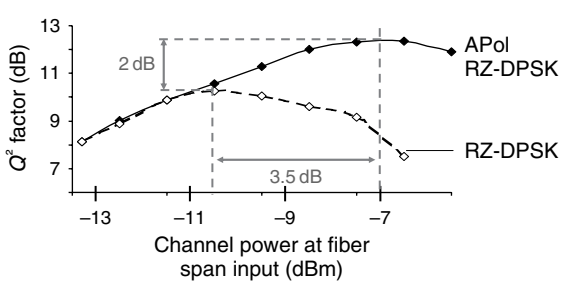

Figure 14.26 Improvement tolerance to nonlinearities, thanks to bit to bit polarization alternation with RZ DPSK format, as measured after 9180 km, over the setup of experiment. (After Ref. [27]) (This figure may be seen in color on the included CD ROM.)

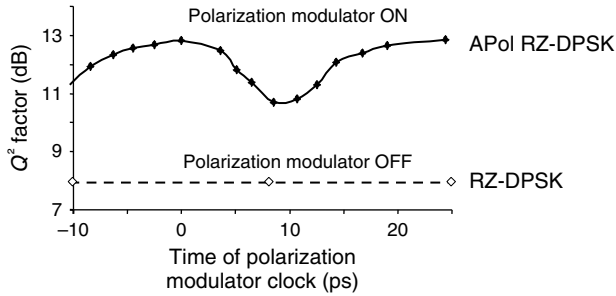

Figure 14.27 Measured impact of the phase detuning of the polarization modulator driving clock after 9180 km, at 7 dBm power per channel [27].

measurements and shown in Figure 14.27. It is found to evolve within ∼2 dB when the electrical clock which drives the polarization modulator is detuned off its optimal adjustment. The dotted line at ∼8 dB corresponds to the measured performance when the polarization modulator is switched off. Interestingly, the system Q factor is always better than without polarization modulation, whatever the phase of the clock.

The APol RZ-DPSK modulation/demodulation scheme appears therefore as an excellent candidate for ultralong-haul undersea transmissions. However, its tolerance to PMD is slightly lower than that of the RZ-DPSK format. The OSNR penalty vs the differential group delay (DGD) has been measured in a back-to-back configuration (no fiber propagation). For that purpose, a low-frequency polarization scrambler (∼1 KHz) and a variable DGD have been inserted between the transmitter and the receiver. The penalty measured at a bit-error ratio of 10^{-5} is plotted in Figure 14.28 for the RZ-DPSK and the APol RZ-DPSK formats vs the DGD. Assuming a maximum penalty of 1 dB, the APol RZ-DPSK format accommodates a maximum DGD no smaller than 7 ps, as compared with 9 ps with RZ-DPSK. This suggests that polarization modulation leads to a reduction of the PMD tolerance. The PMD specifications

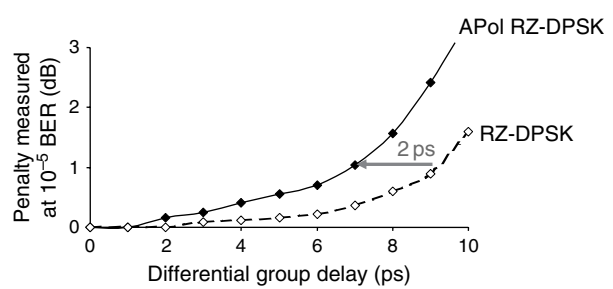

Figure 14.28 Measured tolerance of the APol RZ DPSK and RZ DPSK formats to polarization mode dispersion. (After Ref. [27]) (This figure may be seen in color on the included CD ROM.)

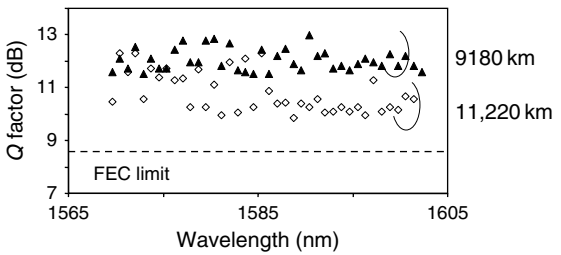

Figure 14.29 Recorded Q^2 factors of 40 × 40 Gbit/s transmission after 9180 and 11,220 km. (After [27].)

of the system constituents need to be tightened accordingly, and/or polarization mitigation devices should be used (see paragraph 14.3.4).

APol RZ-DPSK modulation format has been used to transmit a total 1.6 Tbit/s capacity (40 wavelengths at 40 Gbit/s) over a transpacific distance in a 510 km-long recirculating loop, based on all-Raman repeaters and +D/ D/ + D fiber spans [27]. The Q factors of all the channels are plotted in Figure 14.29. It is generally accepted that approximately 3 dB Q^2 factor margin is needed to cope for the degradation of the system performance during the 25-year lifetime. If we assume a third-generation forward error correcting (FEC) code, which would bring better than 10^{-13} bit-error ratio after correction when the Q^2 factor is higher than 8.5 dB limit (i.e., 4 10^{-3} bit-error ratio), then all 40 channels are found exhibit Q factors at 9180 km which meet the minimum 3 dB margin requirement for industrial implementation. This clearly suggests that ultralong-haul 40 Gbit/s submarine transmission could be deployed in a relatively near future when demand exists. Figure 14.29 also provides the Q factors at a distance of 11220 km. The performance of the worst channel (9.9 dB) is still 1.4 dB above the FEC limit.

Besides research efforts devoted to fully bridging submarine distances at 40 Gbit/s, other efforts have been striving to show that WDM systems based on 40 Gbit/s channel rate could carry more capacity than WDM systems based on 10 Gbit/s. To deliver higher capacities is naturally expected to be one major driver for moving from 10 Gbit/s technologies to 40 Gbit/s technologies in undersea optical systems. This requires a better usage of the available optical bandwidth of the repeaters, which can be evaluated thanks to the so-called information spectral density (ISD). The ISD is equal to the ratio channel bit rate over the channel-to-channel spectral spacing. An ISD of 0.8 bit/s/Hz corresponds to a channel spacing of 50 GHz at 40 Gbit/s or of 12.5 GHz only at 10 Gbit/s. This latter figure should be compared with the standard channel spacing of 33 or 50 GHz in current submarine systems at 10 Gbit/s. Naturally, the larger the ISD, the higher the interactions between channels, whether these interactions stem from multiplexing/demultiplexing or from nonlinear propagation in fiber.

The largest ISD reported in submarine transmission experiments are 0.8 bit/s/Hz at 40 Gbit/s ([22, 24]), while only 0.65 bit/s/Hz has been reported at 10 Gbit/s [57]. All these results have been obtained after propagation over

combinations of +D and D fibers, which should be preferred to NZDSF fiber. Propagation over NZDSF fiber is more impaired by interchannel nonlinear effects, which preclude larger ISDs over this fiber. At 0.4 bit/s/Hz ISD, however, channels at 40 Gbit/s with RZ-DPSK format could be transmitted over NZDSF fiber with similar BERs as with channels at 10 Gbit/s with RZ format [30].

When targeting large ISDs, the modulation format should be carefully chosen in order to minimize the channel spectral occupancy, so that linear (and nonlinear) channel-to-channel crosstalk is more easily contained. For instance, in the aforementioned large-ISD experiment at 10 Gbit/s [57], DPSK was reportedly selected instead of RZ-DPSK, because of its smaller spectral width. However, its width is already relatively broad with respect to the channel spectral spacing. As a consequence, a specific technique against linear and nonlinear channel interactions has to be used, namely channel-to-channel cross-polarization. It consists in interleaving odd and even channels while rotating the polarization axis of every other channel by 90°. This technique has been widely used in the laboratories, but has not yet been implemented in commercial systems. Channel cross-polarization is also needed in 40 Gbit/s experiments, performed with 50 GHz channel spacing [14, 22, 24]. Further reduction of crosstalk is obtained through narrow optical filters at the transmitter side. Such filters are used with a view to reducing the bandwidth of all individual channels before their recombination into the wavelength multiplex. As such, filters become part of the modulation scheme. At the ISD of 0.8 bit/s/Hz, with such filtering and cross-polarization, it was shown that the small advantage in terms of noise sensitivity of the RZ-DPSK format when compared with the DPSK format, vanishes in a back-to-back configuration (i.e., without fiber propagation). After propagation over 6120 km, the Q factor performance across the multiplex is found to be very similar (Figure 14.30), whether RZ-DPSK or DPSK is used. This suggests that an RZ pulse carving stage does not bring noticeable benefits with 40 Gb/s channels packed as close as 50 GHz. Saving this stage simplifies the transponder design, and therefore reduces the system cost.

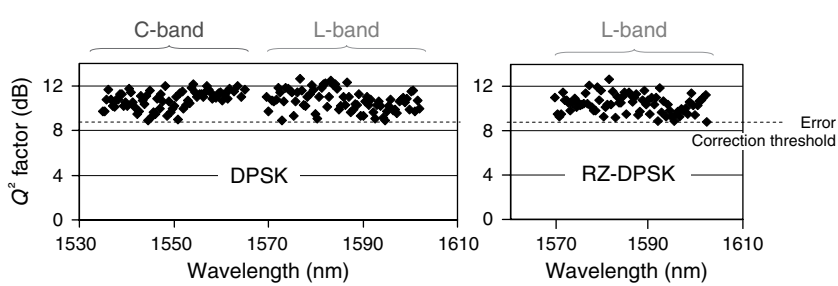

Figure 14.30 Recorded Q^2 factors of 149×40 Gbit/s (6 Tbit/s) transmission after 6120 km based on DPSK format (C band and L band) and RZDPSK format (only L band measured, but C band still present). (After Ref. [24]. © IEEE, 2005) (This figure may be seen in color on the included CD ROM.)

The experimental results in Figure 14.30 correspond to the largest capacity reported after a transoceanic distance at the time of publication. It has been obtained with 149 channels at 40 Gbit/s rate, totalizing 6 Tbit/s capacity [24]. This represents more than 50% capacity improvement when compared with the largest reported capacity at 10 Gbit/s, even if the transmission distance is smaller in the 40 Gbit/s-based experiment.

More recently, the same capacity was transmitted with a modulation format different from than (RZ)DPSK, namely Return to Zero Quadrature Phase Shift Keying (RZ-DQPSK). This format still relies on PSK, but over four possibly phase states instead of two for (RZ)DPSK. Despite its natural compatibility with very high capacities (e.g., 6 Tbit/s [30] or more), and its excellent resilience to linear impairments, the RZ-DQSPK format has proved not as resistant to nonlinear effects as (RZ)DPSK, and is therefore more difficult to use over transoceanic distances [29, 31]. However, this conclusion may have to be updated when the ongoing research on coherent detection [33] becomes mature enough. It could allow a more efficient processing of data modulated with the RZ-DQPSK format and push further some of its limitations.

14.6 CONCLUSION

After the period of over-investment and the economic downturn that followed the beginning of the millennium, the market of undersea cables seems to have now returned to a healthier growth rate. During the recovery period, the reduction of costs came up as first priority, which did not leave much room for technical innovations in new cables. At the same time, the demand for very high capacity slowed down drastically. As cables are gradually filling up, this demand should return on track in the years to come. While the maturation of 10 Gbit/s technologies has opened remarkable opportunities to extract more capacity out of already laid cables, the research efforts on 40 Gbit/s technologies detailed in this chapter should serve as ground for the development of next-generation systems.

ACKNOWLEDGMENTS

The author especially acknowledges the help of Gabriel Charlet for providing material to this work and for fruitful discussions.

REFERENCES

[1] J. Chesnoy, "*Undersea Fiber Communication Systems*," New York, Academic Press, 2002.
[2] E. Desurvire, B. Desthieux, D. Bayart, and S. Bigo, "Erbium Doped Fiber Amplifiers : Device and System Developments," New York, J. Wiley & Sons, 2002.

[3] M. André and M. Brochier, "Overview of Submarine Systems Upgrades," in Proc. *SubOptic'07*, Baltimore, May 2007, pp. 14 17.
[4] G. P. Agrawal, *"Nonlinear Fiber Optics,"* 3rd edition, New York, Academic Press, 2001.
[5] S. Bigo, S. Gauchard, A. Bertaina, and J. P. Hamaide, "Experimental investigation of Stimulated Raman scattering limitation on WDM transmission over various types of fiber infrastructures," *IEEE Photon. Technol. Lett.*, 11(6), 671 673, 1999.
[6] S. Bigo, "Optimizing Terrestrial Systems for 40 Gbit/s Channel Rate," tutorial paper, in Proc. *ECOC'05*, paper Tu1.1, Glasgow, September 25 29, 2005.
[7] H. Kogelnik, R. M. Jopson, and L. E. Nelson, "Polarization mode dispersion," *Optical Fiber Communications IVB*, New York, Academic Press, pp. 725 861, 2002.
[8] P. J. Winzer and R. J. Essiambre, "Advanced Modulation Formats," in Proc.of the *IEEE*, 94(5), May 2006, pp. 952 985.
[9] I. Morita, K. Tanaka, N. Edagawa, and M. Suzuki, "40 Gbit/s × 16 WDM Transmission over 2000 km using Dispersion Managed Low Nonlinear Fiber Span," in Proc. *ECOC'00*, paper 10.1.5, 4(25), Munich, Germany, September 3 7, 2000.
[10] L. du Mouza, G. Le Meur, H. Mardoyan et al., "1.28 Tbit/s (32 × 40 Gbit/s) WDM Transmission over 2400 km of TeraLight™/Reverse TeraLight Fibres using Distributed All Raman Amplification," in Proc. *SubOptic'01*, paper PD 2, Kyoto, Japan and, from the same authors, "1.28 Tbit/s (32 × 40 Gbit/s) WDM transmission over 2400 km of TeraLight™/Reverse TeraLight fibres using distributed all Raman amplification," *Electron. Lett*., 37(21), 2001, pp. 1300 1302.
[11] J. X. Cai, M. Nissov, A. N. Pilipetskii et al., "1.28 Tbit/s (32 × 40 Gbit/s) Transmission over 4500 km," in *Proc. ECOC'01*, paper PD.M.1.2, Amsterdam, Netherlands, October 1 4, 2001.
[12] J. X. Cai, M. Nissov, C. R. Davidson et al., "Transmission of Thirty Eight 40 Gbit/s Channels (>1.5 Tb/s) Over Transoceanic Distance," in Proc. *OFC'02*, paper FC4 1, Anaheim, California, March 17 22, 2002.
[13] H. Sugahara, K. Fukuchi, A. Tanaka et al., "6050 km Transmission of 32 × 42.7 Gbit/s DWDM Signals using Raman Amplified Quadruple Hybrid Span Configuration," in *Proc. OFC'02*, FC6 1, Anaheim, California, March 17 22, 2002.
[14] N. Yoshikane, I. Morita, A. Agata, T. Tsuritani, and N. Edagawa, "50 GHz Spaced 55 × 42.7 Gb/s Transmission over 2500 km using SPM Based All Optical Reshaper," in Proc. Topical Meeting on *OAA'02*, paper PDP6, Vancouver, Canada, July 14 17, 2002.
[15] H. Sugahara, M. Morisaki, T. Ito, K. Fukuchi, and T. Ono, "9000 km transmission of 32 × 42.7 Gb/t dense WDM signals using 195 mm2 Aeff Fiber and Inverse Double Hybrid Span Config uration," In Proc. Topical Meeting on *OAA'02*, paper PDP3, Vancouver, Canada, July 14 17, 2002.
[16] T. Matsuda, T. Kotanigawa, A. Naka, and T. Imai, "62 × 42.7 Gbit/s (2.5 Tbit/s) WDM signal transmission over 2200 km with broadband distributed Raman amplification," *Electron Lett.*, 38(15), 818 819 2002.
[17] G. Mohs, J. X. Cai, K. E. Colovchenko et al., "40 Gb/s WDM Long Haul Transmission on Non Slope Matched Fiber," in Proc. *ECOC'02*, paper 10.1.3, Copenhagen, Denmark, September 8 12, 2002.
[18] A. Tanaka, Y. Inada, H. Sugahara et al., "Study on Span Configurations for Long Distance 40 Gb/s Based WDM Transmissions with All Raman Amplification," in Proc. *ECOC'02*, paper 10.1.4, Copenhagen, Denmark, September 8 12, 2002
[19] T. Tsuritani, K. Ishida, A. Agata et al., "70 GHz spaced 40 × 42.7 Gbit/s transmission over 8700 km using CS RZ DPSK signal, all Raman repeaters and symmetrically dispersion manged fiber span," and from same authors, "70G Hz spaced 40 × 42.7 Gbit/s transpacific transmission over 9400 km using prefiltred CSRZ DPSK signals, all Raman repeaters, and symmetrically disper sion managed fiber spans," *J. Lightw. Technol*., 22(1), 215 223, 2004.
[20] C. Rasmussen, T. Fjelde, J. Bennike et al., "DWDM 40 G Transmission over Trans Pacific Distance (10 000 km) using CSRZ DPSK, Enhanced FEC and All Raman Amplified 100 km Ultrawave™ Fiber Spans," in Proc. *OFC'03*, paper PD18, Atlanta, March 23 28, 2003.

[21] G. Charlet, J. Lazaro, E. Corbel et al., "One Hundred WDM Channel Transatlantic Transmission Experiment at 43 Gbit/s using Raman Repeaters with Large 65 km Spacing," in Proc. *ECOC'03*, paper Th.4.3.3, Rimini, September 21 25, 2003.

[22] I. Morita and N. Edagawa, "50 GHz Spaced 64 × 42.7 Gbit/s Transmission over 8200 km using Pre Filtered CS RZ DPSK Signal and EDFA Repeaters," in Proc. *ECOC'03*, paper Th4.3.1., Rimini, Italy, September 21 25, 2003.

[23] M. Morisaki, H. Sugahara, T. Ito, and T. Ono, "2.56 Tbit/s (64 × 42.7 Gb/s) WDM transmission over 6000 km using all Raman amplified inverse double hybrid spans," *Photon. Technol. Lett*., 15(11), 1615 1617 2003.

[24] G. Charlet, E. Corbel, J. Lazaro et al., "WDM transmission at 6 Tbit/s capacity over transatlantic distance, using 42.7 Gbit/s differential phase shift Keying without pulse carver," *J. Lightw. Technol*., 23(1), 104 107, 2005.

[25] G. Charlet, E. Corbel, J. Lazaro et al., "Performance Comparison of DPSK and RZ DPSK Formats in N × 43Gb/s Submarine Transmission with 100 GHz Channel Spacing," in Proc. *ECOC'04*, paper Th3.5.3., Stockholm, September 5 9, 2004.

[26] Y. Inada, T. Ito, K. Mino et al., "Error Free Transmission over 6000 km of 50 × 42.8 Gb/s, FEC Coded CS RZ WDM Signal in EDFA and Medial Dispersion MDF Systems," in Proc. *ECOC'04*, paper Th.3.5.4., Stockholm, September 5 9, 2004.

[27] G. Charlet, R. Dischler, A. Klekamp et al., "WDM Bit to Bit Alternate Polarisation RZ DPSK Transmission at 40 × 42.7 Gbit/s over Transpacific Distance with Large Q Factor Margin," in Proc. *ECOC'04*, paper Th4.4.5., Stockholm, September 5 9, 2004.

[28] J. X. Cai, C. R. Davidson, M. Nissov et al., "Transmission of 40 Gb/s WDM Signals over 6250 km of Conventional NZ DSF with >4 dB FEC Margin," in Proc. *OFC'05*, paper PDP 26, Anaheim, California, March 6 11, 2005.

[29] G. Charlet, P. Tran, H. Mardoyan et al., "151 × 43 Gb/s Transmission over 4080 km Based on Return to Zero Differential Quadrature Phase Shift Keying," in Proc. *ECOC'05*, paper Th4.1.3, Glasgow, September 25 29, 2005.

[30] J. X. Cai, C. R. Davidson, M. Nissov et al., "Transmission of 40 Gbit/s WDM Signals over Transoceanic Distance using Conventional NZ DSF with Receiver Dispersion Slope Compensation," *J. of Lightw. Technol.*, 24(1), 191 200, January 2006.

[31] J. X. Cai, M. Nissov, C. R. Davidson et al., "Improved Margin in Long Haul 40 Gb/s Systems using Bit Synchronously Modulated RZ DQPSK," in Proc. *OFC'06*, paper PDP 33, Anaheim, CA, 2006.

[32] G. Charlet, N. Maaref, J. Renaudier et al., "Transmission of 40 Gbit/s QPSK with Coherent Detection over Ultra Long Distance Improved by Nonlinearity Mitigation," in Proc. *ECOC'06*, paper Th.4.3.4, Cannes, 2006.

[33] G. Charlet, J. Renaudier, M. Salsi et al., "Efficient Mitigation of Fiber Impairments in an Ultra Long Haul Transmission of 40 Gbit/s Polarization Multiplexed Data, by Digital Processing in a Coherent Receiver," in Proc. *OFC'07*, paper PDP 17, Anaheim, CA, 2007.

[34] J. X. Cai, D. G. Foursa, A. J. Lucero et al., "Long Haul 40 Gb/s RZ DPSK Transmision over 4450 km with 150 km Repeater Spacing using Raman Assisted EDFAs," in Proc. *OFC'07*, paper OWM3, Anaheim, CA, 2007.

[35] G. Charlet and S. Bigo, "Upgrading WDM Submarine Systems to 40 Gbit/s Channel Bit Rate," in Proc. *IEEE*, 94(5), 935 951, May 2006.

[36] N. S. Bergano, C. R. Davidson, B. M. Nyman et al., "40 Gbit/s WDM Transmission of Eight 5 Gbit/s Data Channels over Transoceanic Distance using the Conventional NRZ Modulation Format," in Proc. *OFC'95*, paper PD19, San Diego, California, February 26 March 3, 2005.

[37] B. Bakhshi, M. Manna, G. Mohs et al., "First dispersion flattened transpacific undersea system: From design to Terabit/s field trial," *J. of Lightw. Technol*., 22(1), January 2004, pp. 233 241.

[38] A. Cauvin, Y. Frignac, and S. Bigo, "Nonlinear impairments at various bit rates in single channel dispersion managed systems," *Electron. Lett.*, 39(23), 1670 1671, 2003.

[39] K. Mukaza, K. Imamura, and T. Yagi, "Dispersion Management Line Consisted of Medial Dispersion Fiber (MDF)," in Proc. *ECOC'04*, paper We 3.3.3, Stockholm, Sweden, September 5 9, 2004.

[40] M. Tsukitani, M. Matsui, K. Nagayama, and E. Sasaoka, "Ultra Low Non Linearity Pure Silica Core Fiber with an Effective Area of 211 μm^2 and Transmission Loss of 0.159 db/km," in Proc. *ECOC'02*, paper 3.2.2, Copenhagen, Denmark, September 8 12, 2002.

[41] L. Becouarn, G. Vareille, S. Dupont et al., "42 $\times$ 42.7 Gbit/s RZ DPSK Transmission over a 4820 km Long NZDSF Deployed Line using C Band Only EDFAs," in Proc. *OFC'04*, PDP37, Los Angeles, California, March 22 27, 2004.

[42] M. Lefrançois, G. Charlet, and S. Bigo, "Impact of very large cumulated dispersion on perfor mance of 40Gbit/s submarine systems over non zero dispersion shifted fibres," *Electron. Lett.*, 42(3) 2006.

[43] M. Z. Win and J. H. Winters, "Equalization techniques for mitigating transmission impairments," *Optical Fiber Communications IVB*, New York, Academic Press, 2002, pp. 965 997.

[44] X. Liu, C. Xie, and A. J. van Wijngaarden, "Multichannel PMD mitigation and outage reduction through FEC with sub burst error correction period PMD scrambling," *IEEE Photon. Technol. Lett*., 16(9), 2183 2185, September 2004.

[45] J. X. Cai, M. Nissov, A. N. Pilipetskii et al., "2.4Tb/s (120 $\times$ 20 Gbit/s) Transmission over Transoceanic Distance using Optimum FEC Overhead and 48% Spectral Efficiency," in Proc. *OFC'01*, paper PD20, Anaheim, California, March 17 22, 2001.

[46] D. G. Foursa, C. R. Davidson, M. Nissov et al., "2.56 Tb/s (256 $\times$ 10Gbit/s) Transmission over 11 000 km using Hybrid Raman/EDFAs with 80 nm of Continuous Bandwidth," in Proc. *OFC'02*, FC3 1, Anaheim, California, March 17 22, 2002.

[47] S. Bigo and G. Charlet, "Technical challenges of 40 Gbit/s in WDM submarine transmission," *Alcatel Telecommunications Review*, 3rd quarter 2005, 211 215 2005.

[48] J. C. Antona, S. Bigo, and J. P. Faure, "Nonlinear Cumulated Phase as a Criterion to Assess Performance of Terrestrial WDM Systems," in Proc. *OFC'02*, paper WX5, Anaheim,California, March 17 22, 2002.

[49] C. R. S. Fludger and R. J. Mears, "Electrical measurement of multipath interference in distributed Raman amplifiers," *J. of Lightw. Technol*., 19(4), 536 545, April 2001.

[50] T. Inoue, K. Ishida, T. Tokura et al., "150 km Repeater Span Transmission Experiment over 9000 km," in Proc. *ECOC'04*, paper Th 4.1.4, Stockholm, Sweden, September 5 9, 2004.

[51] N. Shimojoh, T. Naito, T. Tanaka, H. Nakamoto, T. Ueki, A. Sugiyama, K. Torii and M. Suyama, "2.4 Tbit/s WDM Transmission over 7400 km using all Raman Amplifier Repeartesr with 74 nm Contin uous Single Band," in Proc. *ECOC'01*, paper PD.M.1.4, Amsterdam, Netherlands, October 1 4, 2001.

[52] G. Charlet, P. Tran, and S. Bigo, "System Impact of Fibre Repairs on a N $\times$ 40 Gbit/s All Raman Amplified Submarine Transmission," in Proc. *ECOC'05*, paper Mo3.2.3, Glasgow, September 25 29, 2005.

[53] A. H. Gnauck, G. Raybon, S. Chandrasekhar et al., "2.5 Tb/s (64 $\times$ 42.7 Gbit/s) Transmission over 40 $\times$ 100 km NZDSF using RZ DPSK Format and All Raman Amplified Spans," in Proc. *OFC'02*, FC2 1, Anaheim, California, March 17 22, 2002.

[54] L. F. Mollenauer, P. V. Mamyshev, and M. J. Neubelt, "Demonstration of Soliton WDM Transmission at up to 8 $\times$ 10 Gbit/s Error Free over Transoceanic Distance," in Proc. *OFC'96*, paper PD22, San Jose, California, February 29, 1996.

[55] E. A. Golovchenko, A. N. Pilipetskii, and Neal S. Bergano, "Transmission Properties of Chirped Return tomzero Pulses and Nonlinear Intersymbol Interference in 10 Gb/s WDM Transmission," in Proc. *OFC'00*, paper FC3, 4, Baltimore, March 7 10, 2000, pp. 38 40.

[56] J. X. Cai, D. G. Foursa, C. R. Davidson et al., "A DWDM Demonstration of 3.72 Tb/s over 11 000 km using 373 RZ DPSK Channels at 10 Gbit/s," in Proc. *OFC'03*, paper PD22, Atlanta, March 27, 2003.

[57] L. Becouarn, G. Vareille, P. Pecci, and J. F. Marcerou, "3 Tbit/s Transmission (301 DPSK Channels at 10.709 Gbit/s) over 10270 km with a Record Efficiency of 0.65(bit/s)/Hz," in Proc. *ECOC'03*, paper Th.4.3.2, Rimini, Italy, September 21 25, 2003.

[58] Y. Miyamoto, K. Yonenaga, S. Kuwahara et al., "1.2 Tbit/s (30×42.7 Gbit/s ETDM Optical Channel) WDM Transmission over 376 km with 125 km Spacing using Forward Error Correction and Suppressed Carrier RZ Format," in Proc. *OFC'00*, PD 26, Baltimore, MD, March 3 10, 2000.

[59] P. Johannisson, D. Anderson, M. Marklund et al., "Suppression on nonlinear effects by phase alternation in strongly dispersion managed optical transmission," *Opt. Lett.*, 27, 1177 1179, 2002.

[60] D. M. Gill, X. Liu, X. Wei et al., "$\pi/2$ Alternate Phase On Off Keyed 40 Gbit/s transmission on Standard Single Mode Fiber," *Photon. Techol. Lett.*, 15(12), 1776 1778, December 2003.

[61] A. H. Gnauck and P. J. Winzer, "Optical phase shift keyed transmission," *J. Lightw. Technol.*, 23(1), 115 130, January 2005.

[62] A. H. Gnauck, X. Liu, X. Wei et al., "Comparison of modulation format for 42.7 Gbit/s single channel transmission through 1980km of SSMF," *Photon. Technol. Lett.*, 16(3), 909 911, March 2004.

[63] A. V. Kanaev, G. G. Luther, V. Kovanis et al., "Ghost pulse generation suppression in phase modulated 40 Gbit/s RZ transmission," *J. Lightw. Technol.*, 21(6), 1486 1489, June 2003.

[64] J. P. Gordon and L. F. Mollenauer, "Phase noise in photonic communications systems using linear amplifier," *Opt. Lett.*, 15(23), 1351 1353, December 1990.

[65] H. Kim and A. H. Gnauck, "Experimental investigation of the performance limitation of DPSK systems due to non linear phase noise," *IEEE Photon. Technol. Lett.,* 15(2), 320 322, February 2003.

[66] T. Mizuochi, K. Ishida, T. Kobayashi et al., "A comparative srtudy of DPSK and OOK WDM transmission over transoceanic distances and their performance degradations due to nonlinear phase noise" *J. Lightw. Technol.*, 22(9), 1933 1943, September 2003.

[67] J. X. Cai, D. G. Foursa, L. Liu et al., "RZ DPSK Field Trial over 13100 km of installed non slope matched submarine fibers," *J. Lightw. Technol.*, 23(1), 95 103, 2005.

[68] S. Dupont, P. Marmier, L. du Mouza et al., "70×10 Gbps (Mixed RZ OOK and RZ DPSK) Upgrade of a 7224 km Conventional 32×10 Gbps Designed System," in Proc. *ECOC'07*, Berlin, Germany, 2007.

[69] G. Le Meur, P. Brindel, S. Cussat Blanc et al., "Experimental Validation of the Bit to Bit Alternate Polarization Technique for $N \times 43$ Gb/s Submarine Transmission," in Proc. *ECOC'04*, paper We4.P.105, Stockholm, September 5 9, 2004.

[70] I. Kang, C. Xie, C. Dorrer, and A. Gnauck, "Implementations of alternate polarisation differential phase shift keying transmission," *Electron. Lett.*, 40(5), 2004.

[71] S. Bigo, G. Charlet, and E. Corbel, "What has Hybrid Phase/Intensity Encoding Brought to 40 Gb/s Ultralong Haul Systems?," in Proc. *ECOC'04*, paper Th2.5.1., Stockholm, September 5 9, 2004.

15

Future optical networks

Michael O'Mahony

Department of Electronic System Engineering, University of Essex, Colchester, UK

(Portions reprinted, with permission, from *Journal of Lightwave Technology*, Vol. 24, No. 12, December 2006, © 2006 IEEE)

15.1 INTRODUCTION

All developed regions of the world are experiencing huge growth in the volume of digital data being generated. Figure 15.1 shows the historical growth, where for example between 2000 and 2006 the volume of data grew by a factor >50, from 3 to 160 BGB, an unimaginable growth a decade or so ago. In this context, it is also predicted that by 2010, 70% of this data will be generated by consumers. Although all of this data will not flow across networks, increasing amounts will, and hence current networks must evolve to support this staggering growth and provide appropriate services to the end users for manipulating and processing their data.

This growing data wave and its consequent demands on communication networks for capacity and services arise from many different user communities spread across the globe, a phenomenon which has accelerated in the twenty-first century. Figure 15.2 illustrates the global networking situation, wherein different user groups have their own networking domains, but increasingly wish to interconnect and share networking resources. These networks may, e.g., be domestic/national telecommunication networks, national research and educational networks (NRENs) (e.g., interconnecting national research and educational institutes), major research test beds (e.g., funded by governments), or enterprise/business networks. Currently, major processing and storage resources (such as supercomputers) distributed on a global basis are shared by high-end (scientific) users (grid computing) and will likely, in time, become accessible to domestic users and other groups; however, moving from specialized networks designed for thousands of scientific users to one designed for sharing globally distributed resources to millions of users requires significant research and development. Requirements from some of these users groups are as follows:

Optical Fiber Telecommunications V B: Systems and Networks

ISBN: 978 0 12 374172 1

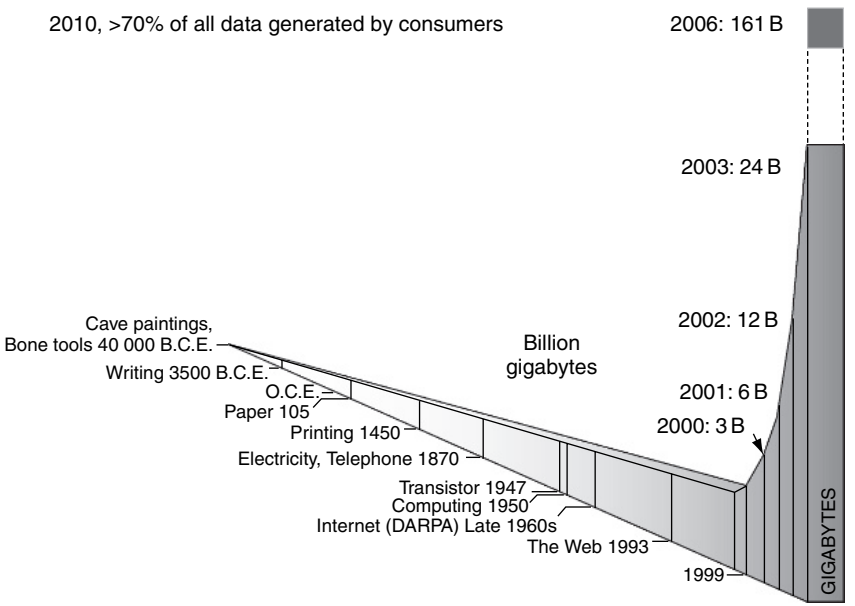

Figure 15.1 Growth of data (derived from idea by da Silva, Director Network & Communication Technologies, CEC.) (This figure may be seen in color on the included CD ROM).

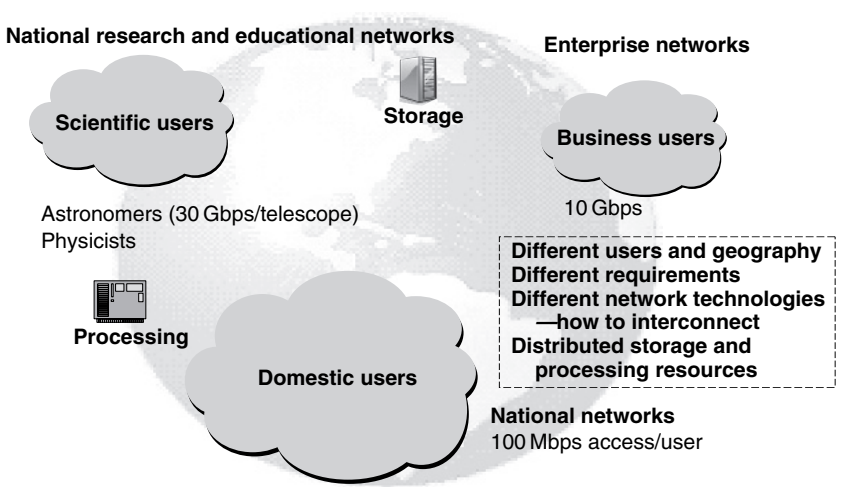

Figure 15.2 User communities and networks (this figure may be seen in color on the included CD ROM).

15.1.1 Domestic Users

Based on national telecommunication networks, domestic users will increasingly look to store and manipulate video images, play interactive games, and download increasingly large files. Much of this capability is enhanced through the greater penetration of broadband access, which in its ultimate form will be provided via optical fiber interconnections offering bandwidth of 100 Mbps, as currently in countries such as Japan [1]. As summarized in Table 15.1, access at 100 Mbps is seen as a target that would support most services being considered, including "Triple Play" services, which include voice data and video; mobile users will also require high-bandwidth access, estimated as 30 Mbps in this model. These figures would be greatly increased, if super high definition TV would also become a broadcast service, requiring Gbps access speeds.

It is likely that, in the future, such users will make use of network resources such as storage (already BT Vault, in the UK, is a service for storage) and processing power. As mentioned above, networking technologies such as the grid computing [2], where global computing resources can be accessed for any location, will become available to domestic users (consumer grids), enabling new services, e.g., video processing, to be done online. In the era of mobility, it is likely also that personal storage will follow the user across the globe, so that wherever he/she is, all personal data can be instantly accessed. Major challenges here include security, as well as adaptable network architectures.

15.1.2 Large Business/Enterprise Users

They require access to high symmetric bandwidths (e.g., up to 10 Gbps) for virtual private network (VPNs), disaster recovery, storage, etc. Such services will be supplied through Fiber to the Premises (FTTP) technologies.

Table 15.1

Residential service requirements.

Application	Downstream requirement	Upstream requirement
HDTV (3 per home at 20 Mbit/s each) Standard TV 4.5 Mbit/s	60 Mbit/s	<1 Mbit/s
Online gaming	2 20 Mbit/s	2 20 Mbit/s
VoIP Telephone (3 per home at 100 kbit/s)	0.3 Mbit/s	0.3 Mbit/s
Data/Email, etc.	10 Mbit/s	10 Mbit/s
DVD download for rental Assume download must take <10 mins, i.e., ~ the time to get one from a rental store	14 Mbit/s	<1 Mbit/s
Total	**~100 Mbit/s**	**~30 Mbit/s**

Scientific Users (High-End Users)

These users are currently served by (NRENs) or large dedicated test beds. Application examples include:

High-Energy Particle Physics: The next generation of experiments at the Large Hadron Collider (LHC) in European Laboratory for Particle Physics (CERN) will produce data sets measured in tens of petabytes per year that can only be processed and analyzed by globally distributed computing resources. Experiments require deterministic transport of 10 100 terabyte data sets, and a 100 terabyte data set requires a throughput of 10 Gbps for delivery within 24 hours. Thus optical network services will be crucial to this discipline where dedicated and guaranteed bandwidth is required for periods of days.

Very-Long-Baseline Interferometry (VLBI): VLBI is used by radio astronomers to obtain detailed images of cosmic radio sources, where the combination of signals from two or more widely separated radio telescopes can effectively create an instrument with a resolving power proportional to their spatial separation. e-VLBI [3] will use high-speed networks to transfer telescope data to a correlator, and the availability of optical network services at multi-Gbps (10 40 Gbps) throughput will greatly increase capability.

e-Health: Remote mammography poses challenges for the deployment of supporting IT systems due to both the size and the quantity of images, with networks required to transport 1.2 GB of data every 30 s. The availability of optical network services offering real-time guarantees is important in this field.

15.2 REGIONAL ACTIVITIES

With these new demands for data services, the traditional voice-centric telecommunications network is in the process of transforming to a data-centric network. The vision is to have a communications environment comprising wired and wireless networks where any individual can access information and network resources in an effortless manner. To achieve this, the ultimate network will have as its building blocks a fixed optical network platform, accessed though wireless (Wi-Fi, WiMax, UMTS) and wired infrastructures, such as FTTP. Such an all-pervasive networked society, however, puts increased demands on network reliability and security.

The importance of future national network infrastructures is mirrored in the ongoing discussions on how a new Internet might be realized. It has been commented [4] that the Internet is expanding from an "Information Service" to a "Critical Infrastructure" for all aspects of society and so new network architectures must evolve to overcome many of the problems inherent in the current Internet. NRENs as well as experimental network test beds are currently being used (in part) to understand how a new Internet might be constructed. The inference is that at all levels communication networks are no longer just desirable but critical for a nation's development and security.

Regional views on expected growth in capacity demands, traffic profiles of new services, and the need to move to data-centric networking are reflected in the scope of the major research programs and their associated projects funded by regional governments.

In *Europe*, currently there are no overarching roadmaps for future networks, but a number of very large "Integrated Projects" funded through the European Commission (EC) identify their own vision of the future. The NOBEL project [5], e.g., studies the evolution of core and metropolitan optical transport networks, supporting end-to-end quality of service (QoS), with intelligent data-centric solutions based on automatic switched optical network (ASON) [6] and generalized multiprotocol label switching (GMPLS) [6], together with optical burst and packet switching; these topics are discussed later in this chapter.

Optical packet switching (OPS) has had long-term support within the EU and national programs, with projects such as DAVID [7] and OPSNET/OPORON [8, 9] developing the technology and its application over a period of about 15 years; however, it is still seen as a very future technology. By contrast, optical burst switching (OBS) and GMPLS approaches are viewed as realistic possibilities for more near-term deployment, and research in these areas is also echoed in national funding in many countries.

Recently, BT (UK) has committed itself to moving to a converged national network solution (BT 21CN Network), with an Internet protocol/multiprotocol label switching (IP/MPLS) core [10]. This change is also under way in other countries (Netherlands, Australia) and is significant in that the architecture opens the path to a full optical transport network at some point in the future, with the possible replacement of optical-electronic-optical (OEO) switches and regenerators with optical-optical-optical (OOO) technologies.

Europe is characterized by a large number of NRENs which exist in most member countries. These networks are nationally funded and commonly used for research into scientific applications (of the type discussed above). The EC funds an overlay network GEANT [11], which provides interconnections between these national networks and provides international connections, e.g., to the USA. These networks look to lambda networking based on scheduled or dynamic provision of lightpaths.

The Pacific Rim countries of Japan and Korea are well known for their ambitious plans in relation to broadband deployment and enhanced network infrastructures.

Japan has well-defined R&D programs; some are initiated by the Japanese Government with a view to evolving a legacy telecommunications network to an IP over wavelength division multiplexing (WDM) network. Such programs move in tandem with operator plans, e.g., NTT plan to migrate 30 million customers to FTTP and IP telephony by 2010. The most recent program focused on developing an all-optical transport network with terabit capability [12]; this research comprised the study and development of photonic nodes such as fast optical cross-connect (OXC) based on MEMS together with control plane (such as GMPLS), OBS, and high-bit-rate, ultralong transmission based on dense wavelength division multiplexing (DWDM) (up to 1000 channels) and optical time division

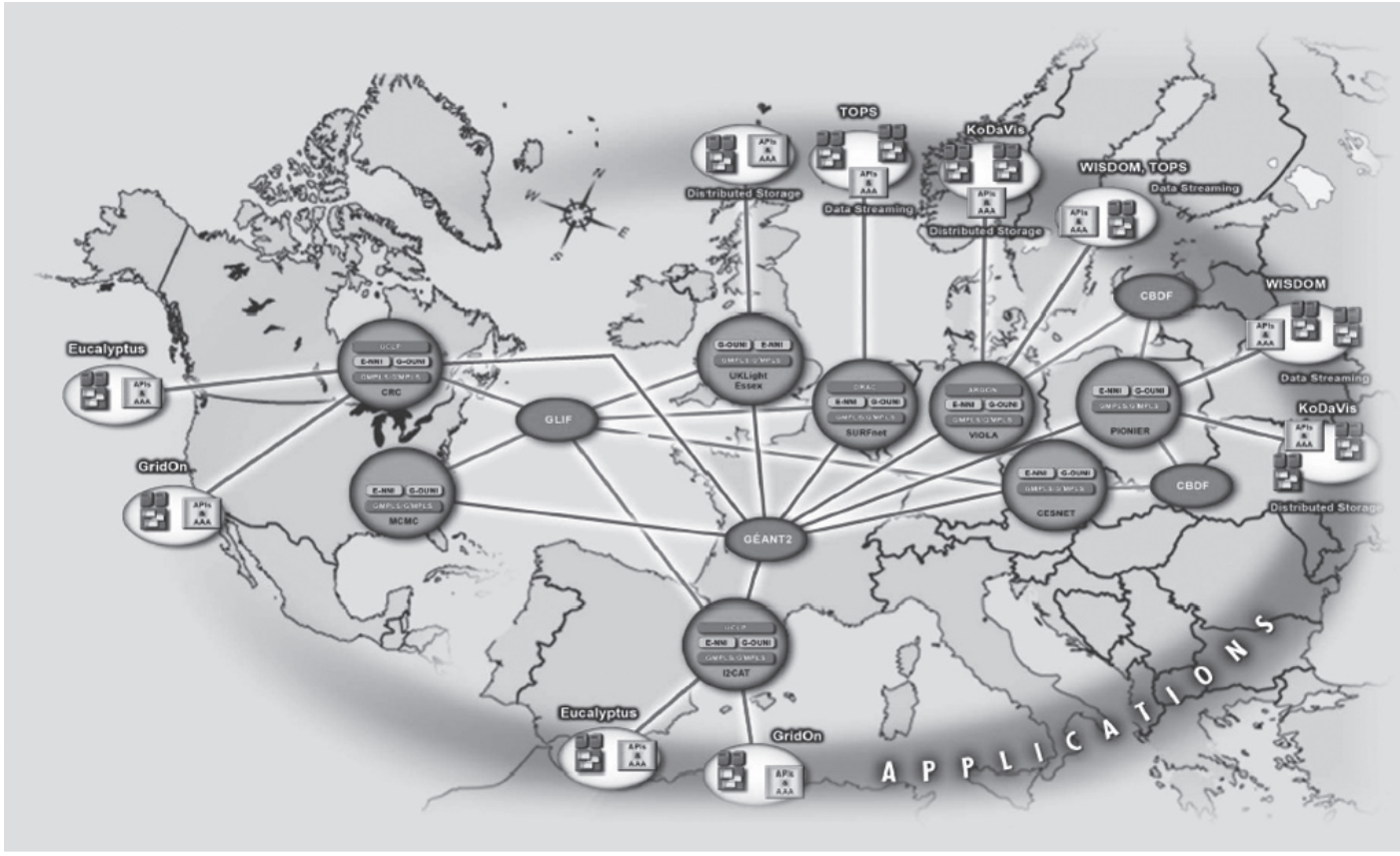

Figure 15.3 Global test bed (*Source*: IST PHOSPHOROUS Project D. Simeonidou.) (This figure may be seen in color on the included CD ROM).

multiplexing (OTDM). For photonic routing, targets are related to the feasibility of 10-Tbps routers and network architectures appropriate to a Tb-class wavelength-routed optical network. The current program seeks to understand how this optical platform can support new bandwidth, demanding applications such as grid computing, and real-time applications like video, digital cinema, and network storage. Key targets include 160 Gbps multilevel transmission systems, using DQPSK/QAM, etc. aiming at bandwidth utilization of more than 2 bits/Hz by 2010.

In the *USA* funding for research (nonindustrial) is through the National Science Foundation and for large projects often through DARPA. Current major photonic activities include studies on optical code division multiple access (OCDMA) and terabit router technology, the latter represented by projects IRIS [13] and LASOR [14], whose goal is to realize 100-Tbps routers. Both projects take the route of OPS, which offers attractions in terms of footprint and power requirements.

The strong interest in optical networking in the USA is reflected in the existence of a number of national test beds, which enable the interconnection of scientific users and support research into future networks. For example, National LambdaRail (NLR) [15] is a high-speed national computer network which is also used as a network test bed for experimentation with next-generation large-scale networks. Links in the network use DWDM at 10 Gbps/channel. NLR's services are already in use by many network research projects, e.g., the NSF OptIPuter project and Internet 2's Hybrid Optical Packet Infrastructure (HOPI) project, which looks at a future infrastructure comprising an IP core network together with an optically switched wavelength set, for dynamic provisioning of high-capacity paths. Currently being proposed is a new national facility GENI [16], which includes a global experimental facility designed to explore new network architectures with the broad scope of understanding new paradigms for Internet-type networks.

The global nature of communications means that there is much interaction and common research between world regions. Organizations like Global Lambda Integrated Facility (GLIF) [17] provide a structure to enable global test beds to be interconnected to undertake research activities of common interest. Thus there exists a global test bed interconnection, as illustrated in Figure 15.3.

15.3 A BRIEF HISTORY OF OPTICAL NETWORKING

The invention of the laser by Schawlow and Townes in 1958 followed by the work of Kao and Hockham on optical fibers (in 1965) and the subsequent demonstration of optical fiber as a practical communication medium by Maurer, Keck, Schultz, and Zimar in 1970 brought into being a technology platform capable of supporting national and global communication requirements for the twenty-first century and beyond. In the late 1970s, fiber began to replace coaxial cable as the transmission medium in the trunk systems of telecommunication networks bringing many advantages both technical and economic. The creation of the Internet (with TCP/IP) in 1983 and subsequently the World Wide Web in 1993 sparked the growth of data

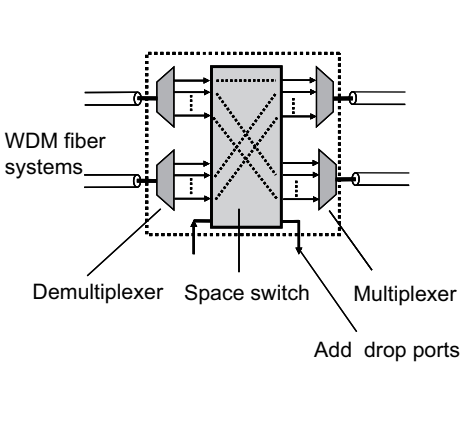

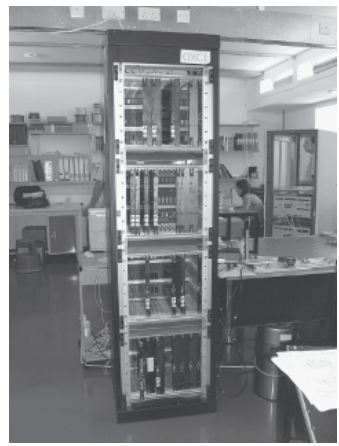

Figure 15.4 Optical cross connect (this figure may be seen in color on the included CD ROM).

traffic on the network, and in 2002, or thereabouts, the amount of network data traffic exceeded that of voice traffic. In the decade from 1985 to 1995, four significant events heralded the possibility of optical networking where both transmission and switching might be based on optics. These were (1) the realization of optical amplifiers allowing (2) the economic deployment of WDM, (3) the demonstration of an OXC enabling the rapid reconfiguration of lightpaths based on wavelength channels, and (4) the convergence of service and transport transmission rate.

The early view of optical networking considered an "Optical Layer" to form an extension to the existing SDH/SONET network layers. Figure 15.4 shows an OXC (and its realization), which comprises input demultiplexers, a space switch, and output multiplexers. Each incoming fiber supports a number of wavelengths; these are demultiplexed and then either switched (by the space switch) to an output multiplexer and hence outgoing fiber or dropped off locally. Hence the OXC is defined as a general wavelength switch which can be realized in (a) an all-optical (transparent) manner (OOO optical input, optical switch fabric, optical output) or in an opaque manner (OEO optical input, electrical switch fabric, optical output) through choice of technologies.

Figure 15.5 shows the original concept of an optical layer, which was envisaged as an extension to the existing SDH/SONET network layers. In the UK, e.g., it was typical that about 60% of the traffic entering a main node was transit traffic; thus, an OXC might be deployed within the optical layer to enable long-haul transit traffic to bypass the main switch nodes and hence reduce the size and cost of the digital cross-connects. Demonstrations of such reconfigurable networks were carried out in Europe and the USA in 1994 [18, 19].

The convergence of service and transport wavelength bit rates around the year 2000 (Figure 15.6), at a bit rate of 10 Gbps, opened the possibility of direct interfacing between, e.g., an IP network and an optical transport network

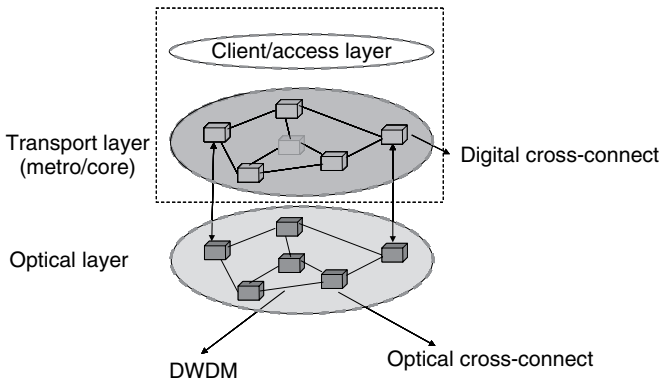

Figure 15.5 The optical layer (this figure may be seen in color on the included CD ROM).

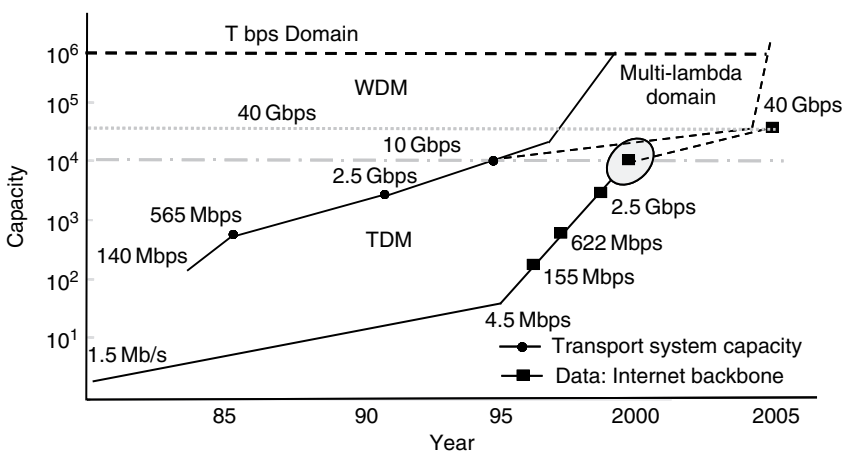

Figure 15.6 Service and line rates.

employing WDM and OXCs, where the granularity of the network directly matched the router interface rate. This was an important step in the evolution of optical networks as a router output stream could flow directly on a wavelength channel. The diagram also shows that convergence at 40 Gbps occurred in 2005, with the availability of 40-Gbps routers and engineered 40-Gbps DWDM transmission systems [20]. Each wavelength, of course, may support many traffic streams.

Figure 15.7 is the schematic of a possible future telecommunications network showing core, metro, and access layers. The core cloud represents an optical network comprising a number of nodes interconnected by amplified fiber links employing DWDM. The nodes comprise an OXC in conjunction with a network service element (SE). The OXC supports the bypass function and allows specific wavelength channels to be dropped to the SE, which e.g., could be an

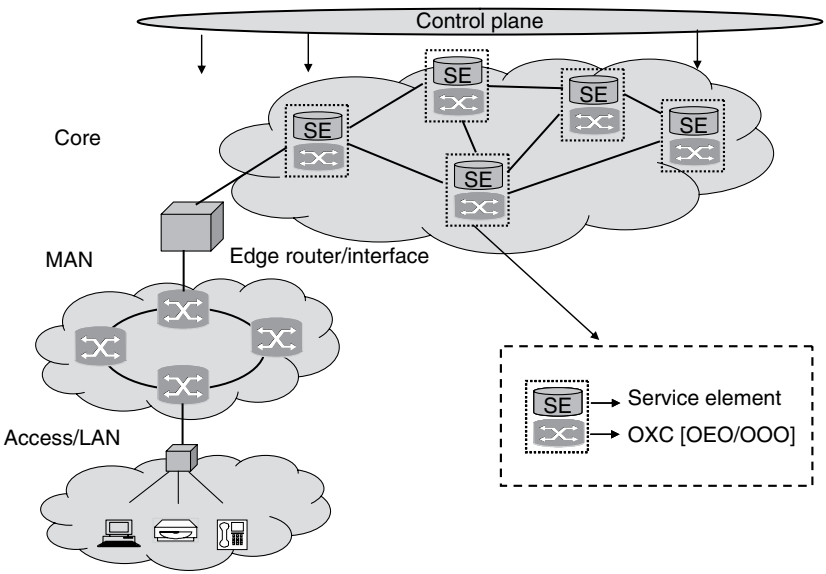

Figure 15.7 A national telecoms network (this figure may be seen in color on the included CD ROM).

IP/MPLS router, an SDH/SONET digital cross-connect, or an optical burst, packet, or Ethernet switch, as discussed later. At the network edge, traffic is mapped onto the network services via an edge interface/router, which can perform either User Network Interface (UNI) or Network Network Interface (NNI) functionality as defined by the Optical Internetworking Forum (OIF) [6] depending on what is connected to the core. A control plane is required to establish paths across the data plane as requested at the network edge, mapping, e.g., an IP/MPLS stream from the MAN onto a specific wavelength; this path establishment can be done in a centralized or distributed manner. The deployment of optical technology brings many potential benefits, as outlined in Figure 15.8.

Some of these are:

Transmission: Optical systems enable low-cost high-capacity systems based on high-speed channels combined with DWDM technology.

Switching: A major benefit from optical switching (discussed below) is the reduced power and size in comparison with electronics for the same throughput. This is a very important factor as exchange buildings are often limited in size, especially within urban environments.

Interoperability: As discussed above, there are many different user communities distributed globally who wish to interconnect (e.g., for grid computing) for purposes of experiments or sharing resources. Interoperabilty is a key issue as each network domain may use different technologies at data and control plane level. It is likely that networks based on optical technologies will offer much

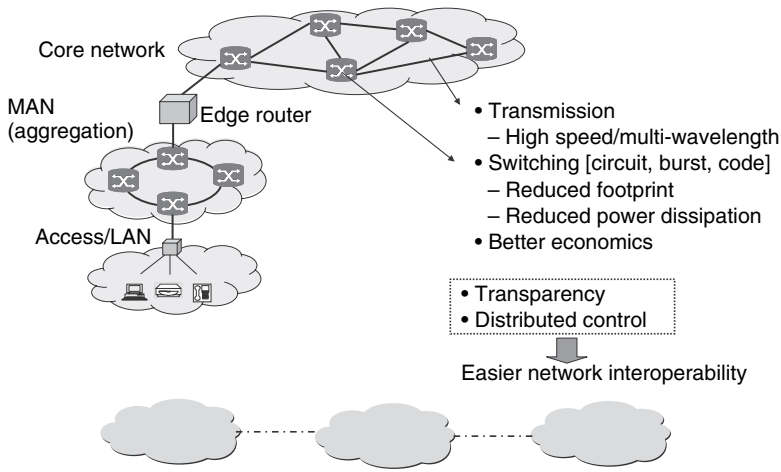

Figure 15.8 Optics and the network (this figure may be seen in color on the included CD ROM).

greater ease of interoperability, through e.g., the exploitation of transparency (signals remaining in the optical domain across the network), allowing wavelengths at the network edge to be dynamically aligned to another domain, or support distributed control though the use of fast optical switches.

This chapter addresses some of the key optical functionalities of future optical networks, rather than the detail of all the technology issues which are inevitable part of any evolution. It is recognized that a number of functions, e.g., dispersion compensation, are currently migrating to the electronic domain, but these topics are not considered here. As discussed earlier, optical networking includes the concept of OXCs (wavelength switches) using either an OEO switching or an OOO approach. The OEO approach requires that all the wavelength paths terminating at the switch go through OE conversion prior to the switch and EO conversion following the switch; this is costly but enables a well-established electronic switch technology to be used; it also supports finer granularity switching. The OOO approach has the great attraction that no OE/EO conversions are needed, but the transparent systems it offers (with signals staying in the optical domain across the network) mean that careful design of the use of wavelengths is needed and make it likely that wavelength conversion (ideally all-optical) would be needed.

15.4 A DIVERSITY OF ARCHITECTURES AND TECHNOLOGIES

As Figure 15.7 shows, national networks comprise a number of interconnected subnetworks, access (user to local exchange), metro (interconnection of local exchanges to the core), and core network which transports data over long

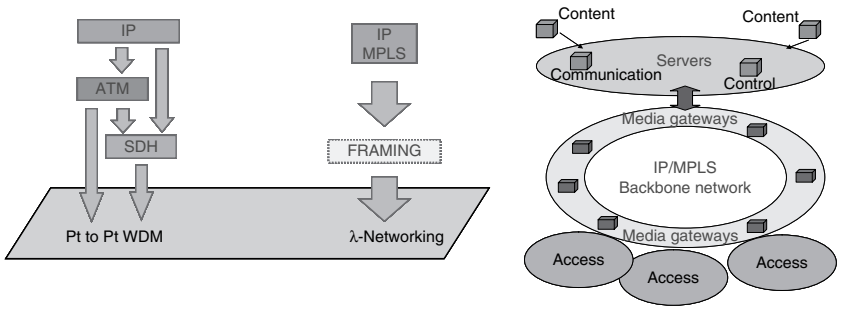

Figure 15.9 The changing network (this figure may be seen in color on the included CD ROM).

distances. Each of these subnetworks has its own architectural designs which respond to issues specific to its position in the overall network; for example, the access connects to every individual and hence cost is a major issue; the core networked carries data from many users and so its costs are shared. In this discussion, we focus on the often-called transport network, which spans metro and core carrying aggregated traffic across the network. As the total traffic across the network increases and the demand for new fast services increases, design of the transport network and its control and management are increasingly important.

Much research has focused on moving from the traditional circuit-based switching to a more dynamic and data-centric network enabling rapid lightpath reconfiguration and providing subwavelength granularity, as needed by the new applications discussed earlier. In its present form, the network has a complex layering to allow the simultaneous support of data and voice services as shown in Figure 15.9.

The left-hand side of Figure 15.9 shows how data (IP) may be encapsulated into ATM cells (or SDH/SONET frames) for transmission across the point-to-point connections in the WDM network; currently, the network is changing to a more data-oriented version of SDH/SONET [next generation (NG) SDH/SONET]. Much effort has been made to minimize this complex layering, which is expensive to maintain. The right side of the diagram shows an example (discussed again below) where the core of the network is based on IP data streams with MPLS at the network nodes a purely data network.

Figure 15.10 outlines a possible evolution route for the network structures and technologies that may appear in the future optical (transport) network; as illustrated, it is a version of many such diagrams presented over the years. Working from the bottom left-hand corner of the diagram:

Progress toward optical networking has been much slower than envisaged in the late 1990s, and currently the first real steps toward networking are seen in the deployment of reconfigurable optical add drop multiplexers (ROADMs), in particular those based on a multiport wavelength-selective switch (WSS) [21]; these devices have the functionality of OXCs (Figure 15.3) with an optical switch

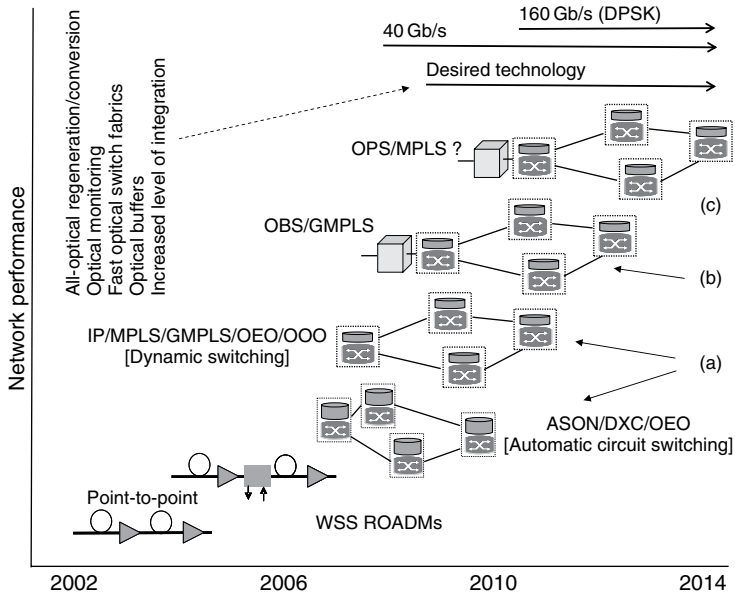

Figure 15.10 Network evolution (this figure may be seen in color on the included CD ROM).

core; a selected wavelength on an incoming port can be dropped or transmitted under control and so represents the first introduction of optical wavelength switching.

15.4.1 Network Switching

Figure 15.10 illustrates possible further stages in the network switching evolution. In the figure, (a) represents the move to a more data-centric and dynamic switching model using an ASON [6] architecture which would allow automated lighpath provisioning and supports NG-SDH/SONET with digital cross-connect (DXC) or OXC (OEO) switching in the data plane. Figure 15.10(a) also shows that a move to an IP/MPLS (i.e., IP routers) or GMPLS (with OEO or OOO wavelength switches) architectures is foreseen, which provides an enhanced dynamic capability. GMPLS allows all transport modes, circuits, burst, and packets to be supported and can be deployed in either a centralized or a distributed mode. This represents one of the options to build a "converged network," where the backbone is a multitechnology IP/GMPLS/OEO/OOO network supporting all services (voice, data, video), which may overtake the ASON architecture. It is also the case that in recent times Carrier Ethernet [22] (based on native Ethernet or MPLS) looks increasingly attractive across all layers of the network, and indeed within the UK some (small) network providers already operate national converged networks with Ethernet switching

elements. The move toward 100 GbE standards illustrates the importance of this technology and hints of future major roles in the next-generation networks. Figure 15.10(b) represents a move to a user-centric design, based on OBS with GMPLS (OBS/GMPLS); this technology provides subwavelength granularity and is also of interest to future optical grid networks [23]. Finally, Figure 15.10(c) represents the move to an OPS network where MPLS provides a common (across electrical/optical domains) control plane. OPS offers the finest granularity and is still seen as the ultimate switching technique, but its success will depend on many technology advances; these options are discussed in more detail in the following sections.

A recent development relating to network architectures is the move toward programmable networks. Figure 15.11 illustrates the concept. In this case, the core and edge nodes of the network are directly associated with electronic processors, allowing node functions to be dynamically altered.

The Metro/aggregation network (Figure 15.8) delivers data from the access to the edge device for processing, and will likely use DWDM supporting, e.g., Carrier Ethernet, but it is the access network that provides the key to the future, in particular the move toward FTTP.

Access-PONs: FTTP supports the Passive Optical Network (PON) concept, which has been studied for over 20 years, but now increasingly deployed. PONs offer multiservice (voice, data, video, and telemetry) and multiprotocol (IP, TDM, ATM) support and thus are a very flexibly infrastructure. A number of possibilities have been studied, which exploit the basic PON concept, but with a view to reduce costs. Two examples follow:

Long-reach PONs: Some operators [24] see the possibility of merging metro and access in a long-reach (amplified) PON. Optical amplification is included to boost the power budget and increase bandwidth, range, and number of splits. The long reach is used to bypass the metro network and terminate at a core edge node; this enables the removal of the local

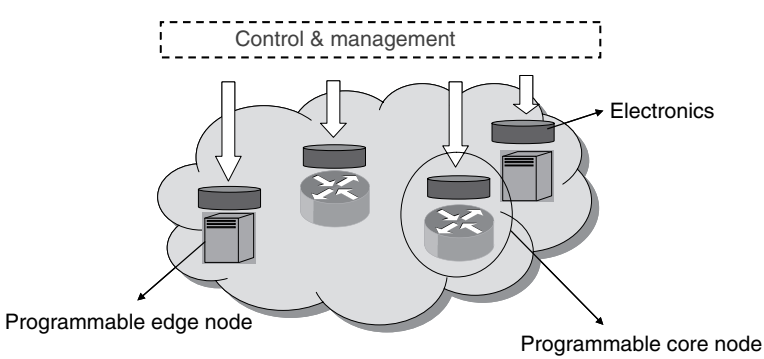

Figure 15.11 Progammable Networks (*Source*: FON Workshop OFC 2006: P Morton, GENI; Simeonidou IST PHOSPHOROUS.) (This figure may be seen in color on the included CD ROM).

exchange or remote concentrator site. In the UK this would require 100 of these core edge nodes with long-reach spans of 100 km and bit rates of at least 10 Gbps.

CWDMA/OCDMA PONs: Coarse WDM (CWDM) allows low-cost WDM to be deployed (as device cooling is not required); CWDM uses channel spacing of 20 nm, so only eight or so channels can normally be deployed. OCDMA (see below) has been demonstrated [25, 26] as a robust complementary technology that could also be deployed in conjunction with CWDM to increase the number of users. As with WDM, OCDMA offers the possibility of translation from one channel to another (code translation), opening many interesting possibilities.

Transmission speed

Current networks employ amplified DWDM systems with individual channel bit rates up to 10 Gbps to connect main switching centres, and currently 40-Gbps systems are being deployed. There are many reasons for believing that bit rates will increase beyond 10 Gbps and perhaps even to 160 Gbps (Figure 15.6). For example, (a) in the past it has always been advantageous to move to high bit rates from a cost viewpoint; (b) although optical amplifiers are reasonably bit rate agnostic, most of the more advanced functions currently considered for future networks such as all-optical regeneration, wavelength conversion, dispersion compensators, etc. can only operate on a single wavelength; (c) when future OOO switches are deployed then increasing the bit rate can help in reducing the port count required of the switch fabrics [26], as large OOO switch fabrics are difficult to realize, e.g., in the case of an optical packet switch where it is difficult to scale fabrics; for wavelength switching, waveband approaches [24] can be used to mitigate these technology issues, and (d) studies show that as the overall traffic on a network increases then the optimum line rate also increases thus as network traffic increases by factors of 10 or 100 over the next decade, high bit rates may be of increasing interest. Increasing bit rate, however, leads to a more demanding requirement for system design to minimize the effects of dispersion (chromatic and polarization) and nonlinear effects; thus there is the increasing interest in modulation techniques such as differential phase-shift keying (DPSK), which is more robust to transmission impairments than intensity modulation; PSK systems are already being deployed and 160-G systems are being investigated in field trials.

15.5 KEY TECHNOLOGIES AND SUBSYSTEMS

15.5.1 Switching Technologies

Figure 15.12 is the schematic of the switching options currently under consideration for future networks, namely optical circuit, burst, and packet switching, together with optical code switching and possible hybrid solutions involving

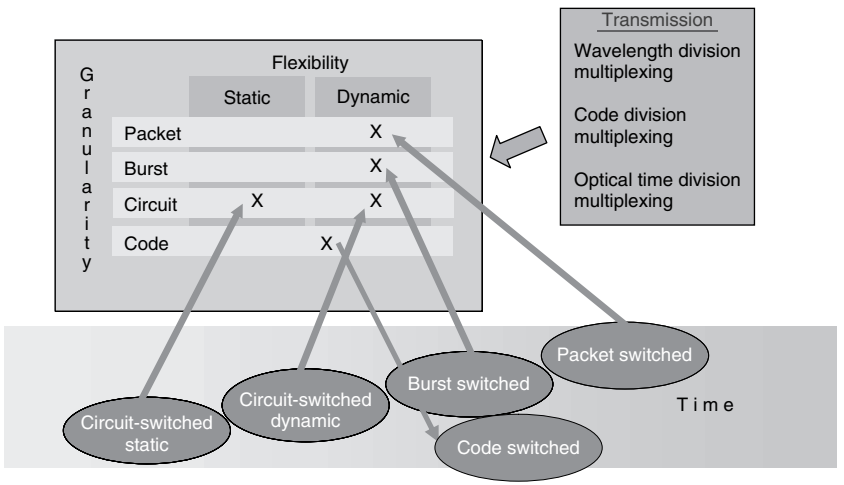

Figure 15.12 Network switching options (*Source*: IST OPTIMIST Project.) (this figure may be seen in color on the included CD ROM).

burst and circuit switching. The diagram illustrates the key features of these differing options, particularly in respect to granularity and flexibility. Granularity concerns, in these cases, the ability to have many users operate across one wavelength channel, thus as described below, burst-, packet-, and code-based systems demonstrate this feature; in contrast, circuit switching simple sets up a wavelength path for a specific information stream. Flexibility implies the ability to dynamically respond to network demands, setting up and tearing down new paths, etc. All the technologies discussed can be deployed in a dynamic manner by the incorporation of optical switches and a suitable control plane to enable rapid configuration. As we move to more dynamic and granular solutions of course, the technology becomes more complex and deployment moves out in time. These switching options are now discussed in greater detail.

Dynamic Optical Circuit Switching

Circuit switching technology, where end-to-end circuits are established upon request, is currently moving toward the deployment of fast and automatically reconfigurable nodes with switching granularity at the wavelength level and is represented by the ASON architecture standard. To enable dynamic networking, the provisioning of lightpaths is automated; this is illustrated in Figure 15.13. The diagram shows an advanced control plane (associated with the data plane), which provides the necessary signaling capabilities for configuring paths through the network. The user can request, through the UNI, a new lightpath, and the controllers in the network nodes exchange, through the NNIs, the necessary information for the lightpath setup (allocation of wavelengths, etc.) activating the node

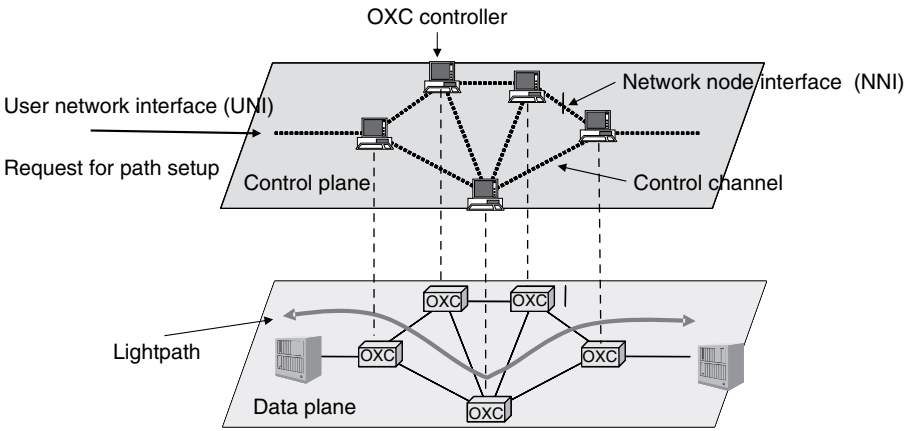

Figure 15.13 Dynamic circuit switching (this figure may be seen in color on the included CD ROM).

switches. The node switches themselves can be DXCs or OEO OXCs as illustrated in Figure 15.13.

As currently viewed, the ASON network, which is based on NG-SDH/SONET, has advantages in terms of QoS, management, and security. However, due to the domination of IP-centric traffic, future solutions are focusing on bursty networking models able to handle dynamic segments instead of continuous data, or combinations of burst and circuit switching.

Optical Burst Switching

In recent years, much research has focused on OBS. It is a technology which is suited to bursty traffic (and can be viewed as application-centric) but can be realized in a less complex way than OPS (see below). Indeed some commercial equipment is now available [27].

OBS [28] is based on the separation of data and control plane and is seen as a cut-through technology, i.e., data transfers directly though the network without being stored at intermediate nodes. It has become of great interest as it enables many data streams to share a wavelength channel, i.e., it offers subwavelength granularity. This sharing of a wavelength channel will become increasingly important as channel bit rates increase to 40 Gbps and beyond. Figure 15.14 illustrates the operation of OBS. Prior to data burst transmission, a burst control packet (BCP) is created and sent toward the destination by an OBS ingress node (the edge router). The BCP is typically sent out-of-band over a separate signaling wavelength and processed at intermediate OBS routers. It informs each node of the impending data burst and sets up an optical path for its corresponding data burst. Data bursts remain in the optical plane end-to-end and are typically not buffered as they transit the network core. The bursts' content, protocol, bit rate, modulation

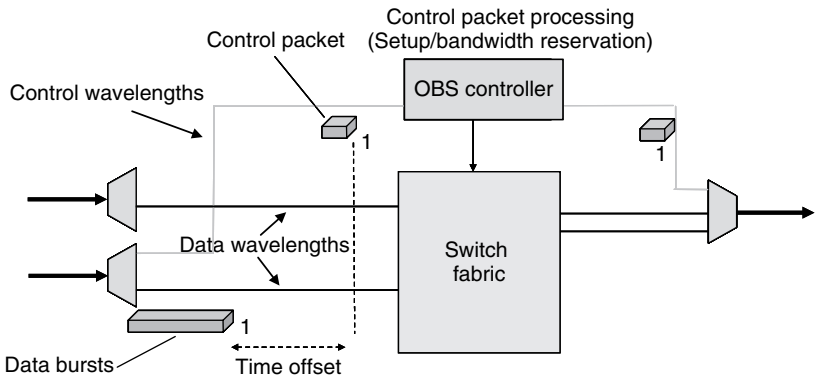

Figure 15.14 Optical burst switching concept (this figure may be seen in color on the included CD ROM).

format, and encoding are completely transparent to the intermediate routers. The main advantages of the OBS in comparison with the other optical networking schemes are that unlike the optical wavelength switched networks, the optical bandwidth is reserved only for the duration of the burst, and that unlike the OPS network it can be bufferless; but it also needs a switch reconfiguration speed in the order of microseconds; switch speed is important as it has an impact on the size of burst that can be handled. Figure 15.15 shows a schematic of an OBS network scenario. At the edge of the network, Figure 15.15, data are aggregated into classified bursts, giving some, e.g., short burst lengths for QoS. A GMPLS control plane supports the data plane and switch reconfiguration; the node switches ideally have reconfiguration speeds in the microsecond regime.

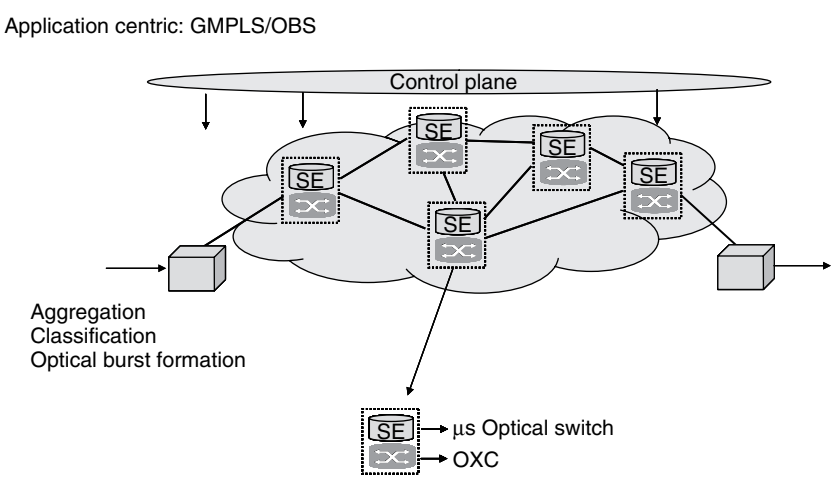

Figure 15.15 Optical burst switching network (this figure may be seen in color on the included CD ROM).

Due to these implementation issues (easier processing, bufferless/reduced buffer operation, and relatively slow switching requirements), OBS is seen as a practical solution and is considered as the next evolution step in future optical networking. The feasibility of OBS technology can be identified by a number of reported results from field trials and test beds. The most complete demonstrator was set up in Japan under the "OBS network" project and accommodated six nodes with MEMS-based switches, achieving switching times of 1 ms for bursts with a minimum size of 100 ms [29].

OBS is currently being considered for deployment in Metro/WAN networks. Currently, the only way to build such networks with more than 10 GBPS of bandwidth requires the use of DWDM technology to enable point-to-point circuits to be established for every required path across the network; clearly, this can be both expensive, inefficient, and difficult to manage. OBS, with its multiplexing capabilities, offers a new approach by enabling communications with multiple destinations across a network. This means no circuits need be preprovisioned, and high-speed transponders need not be dedicated for every single communication path. This frees up capital, simplifies network design, and enables the creation of packet metro aggregation networks where bandwidth shifts in real-time to where it is needed in the network. On the negative side, the use OBS may have a detrimental effect on network utilization, a topic still under study. The lack of buffering at the OBS nodes and the challenges in efficient scheduling of variable size bursts, which lead to poor utilization, make this a serious aspect of network design.

OBS has been also identified as a compatible solution for the physical layer infrastructure in grid computing applications, with possible realization on NRENs [30].

Optical Packet Switching

Figure 15.12 shows that OPS is seen as the highest granularity of the proposed schemes; it is also the most difficult and complex to realize; hence, for many years it has appeared on the edges of any network evolution roadmap (such as in Figure 15.10). OPS is a store and forward technology so optical packets are buffered at network nodes; hence, buffering is a key issue and challenge in OPS networks.

Figure 15.16 illustrates the operation of an optical packet switch. The top of the diagram shows the form of an optical packet, which comprises a number of IP packets aggregated to form a payload with a serial header, header, and payload separated by a time duration sufficient for the optical switch to reconfigure; this time is typically in the order of nanoseconds. At the switch node, the header is decoded, by means of detection followed by electronic processing, and used to set the switch fabric. The switch operates on a store and forward mode, so if contention exists where more than one input seeks the same output, buffering is necessary. This is problematic for optics as, to date, it is only possible to delay a packet (rather than store) usually by means of a length of fiber; in a discussion below, a means of buffering using advanced technology is outlined. At the switch output, a

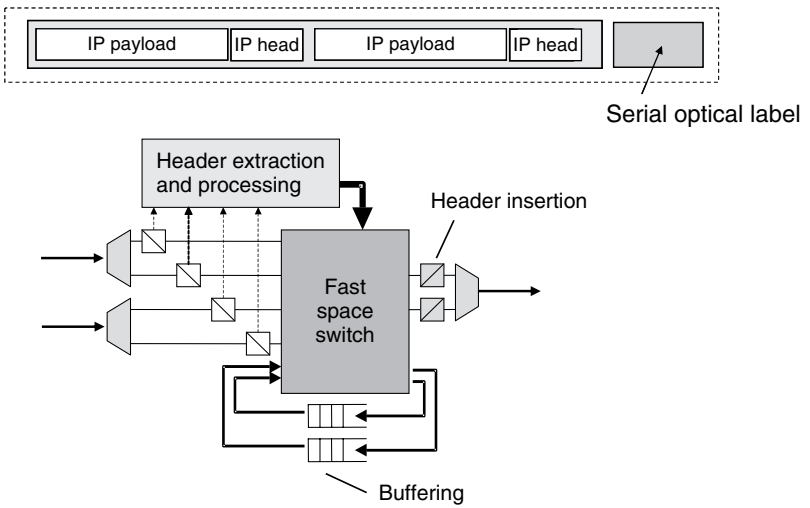

Figure 15.16 Optical packet switching (this figure may be seen in color on the included CD ROM).

new optical header is inserted (and the old deleted) before the packet exits to the network. OPS requires the use of more demanding subsystems (than OBS) with intrinsic intelligence to realize adequate packet processing and routing on the fly. The main challenges in OPS are the implementation of the optical header processing mechanism, the development of an intelligent switch controller, the realization of ultrafast switching in nanoseconds timescale, and the exploitation of buffering mechanisms to reduce packet blocking.

A common realization of a switch node is illustrated in Figure 15.17, which shows a possible switch fabric but does not include other necessary subsystems such as buffering or routing table implementations; buffering is commonly realized using fiber delay lines or their equivalent [31]. Each incoming fiber (a total of m fibers) supports a number of wavelengths (n), which are demultiplexed at the switch input. The stream of optical packets (on each wavelength) is first sampled by a splitter, to allow the optical header to be decoded, converted to an electrical signal for electronic processing, then used as a control signal to the tunable wavelength converter (TWC). The TWC in conjunction with the arrayed waveguide (AWG) forms the equivalent of a space switch functionality as follows. The path through the AWG is determined by the wavelength at its input port. The header decoder and processing sets the electrical signal to the TWC to change the wavelength of the optical packet payload to that required to ensure it exits the AWG at the port specified by the packet header. The combination of tunable laser and AWG enables switch times in the order of nanoseconds to be achieved, and this enables relatively short packets to be formed in an efficient manner.

In contrast to OBS, complete OPS demonstrators are mainly restricted to the development of fully functional but small switching elements that simply show the

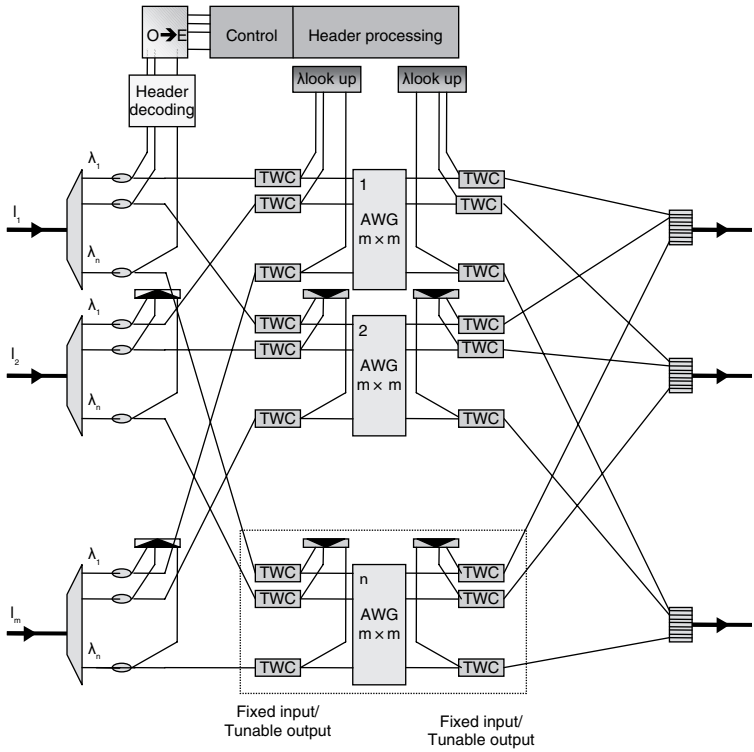

Figure 15.17 Optical packet switch node (this figure may be seen in color on the included CD ROM).

feasibility of fast packet switching on the physical layer with some extensions to the link layer. In the OPSNET project [32], dynamic switching of asynchronous optical packets at 40 Gbps has been demonstrated in a fully controllable setup able to identify and process the header and route the payload accordingly. In Ref. [32], contention resolution on the wavelength level is also considered on a 10 Gbps packet switching node. A more feasible approach toward the implementation of OPS considers the use of synchronously (slotted) transmitted packets with fixed lengths, but in this case the hardware overhead is on the implementation of the packet synchronizer at the input. However, slotted solutions are attractive for other applications like computer interconnects. More recent approaches take the view of a multiwavelength packet [33], where the payload comprises a number of wavelengths, e.g., 16 wavelengths each supporting 10 Gbps enable a 160-Gbps OPS transmission link to be demonstrated. This approach takes OPS a long way forward in terms of practical realization.

Despite their feasibility limitations, OPS demonstrators assisted the development of numerous ultrafast switching and processing techniques regarding

wavelength conversion, header encoding/decoding and processing, label swapping, fast clock extraction, regeneration, and optical contention resolution. Additionally, various switch architectural designs and control protocols have been proposed, which in combination with the significant technological advances over the last years, indicate the possible deployment of OPS in future. However, its future relies on advances in photonic integration that will enable cost-effective subsystems to be constructed, including the all important buffer.

Optical Code Division Multiple Access

OCDMA has been studied as an alternative networking solution able to increase passively the number of users per wavelength. The advantages of OCDMA have been evident for some time through its successful use in wireless networks. For optical networking, its potential for enhanced security, decentralized control, and flexibility in bandwidth granularity provides interesting possibilities to solve these well-known issues in the development of future networks. Additionally, the feasibility of OCDMA has been assisted by newly developed components able to provide simple ways of coding and decoding signals in a passive manner, a particularly attractive and cost-effective feature. Figure 15.18 shows a coder/decoder based on a fiber Bragg grating (FBG). Sections of the grating are arranged so that an input pulse (at the Bragg wavelength) is reflected with an appropriate phase so that the output from the input pulse is represented by a series of reflections of differing phases. Thus the input pulse is coded into a chip sequence which is dependent on the grating design. Gratings have been designed to give up to 511 chips.

The operation of OCDMA relies on each user having a unique code, but sharing the same bandwidth. User signals are multiplexed at the transmitter on to a common wavelength: at the receiver each incoming signal is matched against locally stored

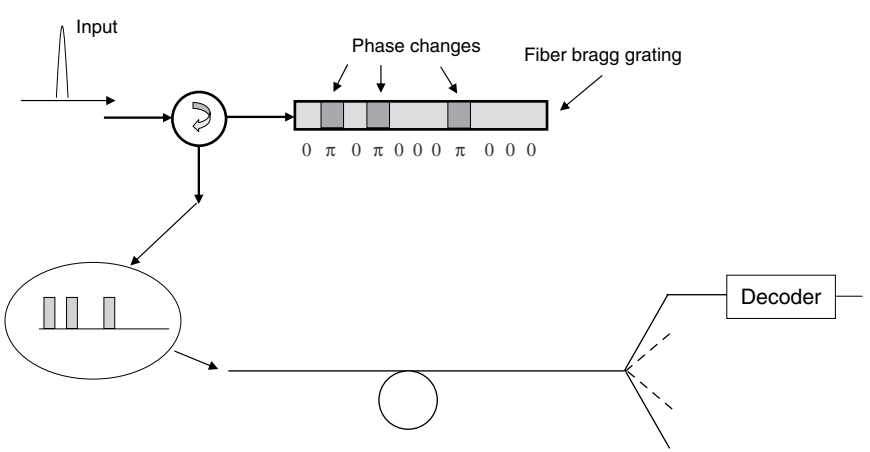

Figure 15.18 OCDMA (this figure may be seen in color on the included CD ROM).

copies of the codes through the process of autocorrelation. The major problem in OCDMA is the interference between user signals, called multiple access interference (MAI). The discrimination achieved between user signals is determined primarily by the set of codes chosen. Essentially good discrimination means long codes, but recall from above that long codes mean a high channel chip rate and hence high channel bandwidths are required, e.g., if each user were to require 1 GBPS and the code length was 50 chips, then the channel bandwidth would be required to be 50 GBPS; codes must be chosen so that the cross-correlation function between codes is low when compared with the peak autocorrelation value. The combination of OCDMA with CWDM technology in access environments is an interesting example of how the technology can help boost the number of users sharing a PON, as recently demonstrated in Ref. [34]. The paper reported the field trial of a 3-WDM $\times$ 10 OCDMA $\times$ 10.71 Gbps system over a 111-km field trial. Key aspects of the approach were (a) the use of a multiport encoder/decoder in the central office which can give multiple optical codes in multiple wavelength bands; this device gives good correlation properties to suppress MAI and beat noise; (b) the use of an super-structural fibre Bragg grating (SSFBG) (or tunable transversal filter) at the optical network unit (ONU). The use of the DPSK-OCDMA with balanced detection is seen as a key enabler over conventional on/off keying OCDMA with superior noise performance.

In recent times other interesting possibilities for OCDMA have been reported [35]. For example, the FBGs illustrated in Figure 15.18 have been modified to incorporate the inclusion of tungsten wires at intervals along the grating; by passing current though these wires, the local refractive index can be modified and a reconfigurable coder/decoder can be achieved. Thus a user assigned a particular code on a particular wavelength can alter his code (switching) as required. Finally, the use of optical codes under a different concept has shown the feasibility to implement an OPS node [36]. Here optical codes are used as labels in order to distinguish the different headers of the transmitted packets. After header matching, the autocorrelation peak triggers an electronic controller that shows the output port where the packet should be routed.

In summary, research on OCDMA in recent years has demonstrated that it provides an interesting extension to the usual dimensions of space, time, and wavelength deployed in optical networks. However, it faces challenges if used in areas of the network involving long distances and high bit rates, and so at present most consider the access network the most likely area for deployment. As the access network is very cost sensitive, however, severe demands are placed on the technology to allow it to be competitive with legacy solutions.

15.6 KEY SUBSYSTEMS AND TECHNOLOGIES

The roadmap of Figure 15.10, and the above discussion, broadly outlines a much argued route forward to the future; with switching or transmission aspects relevant to a future global optical network. Generally, the picture is that transmission

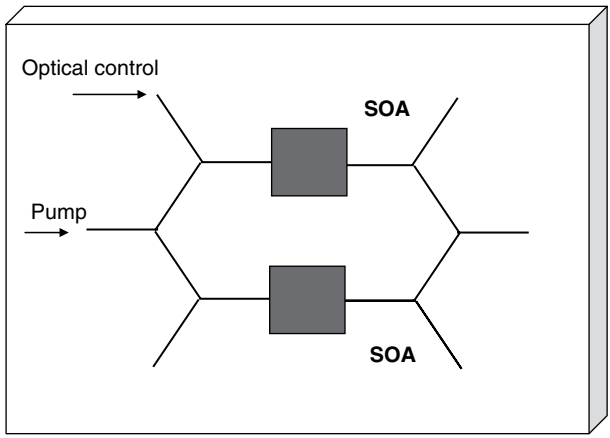

Figure 15.19 Mach Zehnder Interferometer (MZI) (this figure may be seen in color on the included CD ROM).

speeds are still predicted to increase as before (e.g., to 160 Gbps probably using DPSK), within the context of a more dynamic and granular network, supported by appropriate control plane (e.g., GMPLS with extensions). Many of the key functional subsystems needed for this future flexible network have already been described, with experimental demonstrations (e.g., all-optical regeneration at 40 Gbps has been widely reported [37], as has wavelength conversion, fast tunable lasers, tunable dispersion compensators, MEMs-based switch fabrics, etc.), others are still gleams in the eye of the network designer with, as yet, no sure route for realization, e.g., optical memory and multiwavelength optical regeneration.

However, what has become well recognized is that the future of realizing the full potential of optical networks, at affordable cost, lies in the ability to perform good levels of photonic integration. This has not been an easy route to date, but some interesting examples of future approaches are starting to appear. Generally, the integration of photonic components is not straightforward as the substrate technology for various components differs (e.g., lasers are grown on InP whereas filters benefit from silicon technology). Existing photonic integration approaches are based on hybrid integration, where individual components are laid down and interconnected on a suitable substrate (e.g., silicon) (hybrid integration offers full functionality, lower cost, and shorter development times), or on monolithic integration, where a limited set of functions, realizable on a common material, are combined. Photonic integration also faces a challenge from approaches such as Infinera [38], where large number of OEO interfaces are integrated on an IP chip, allowing similar functionality in many cases at comparable costs.

Advances in the integration of Mach Zehnder Interferometers (MZI) illustrate the benefits of integration. Figure 15.19 shows the structure of such a device, where a pump signal is split between the two interferometer arms and the phase difference between the arms is controlled by an optical signal operating on a

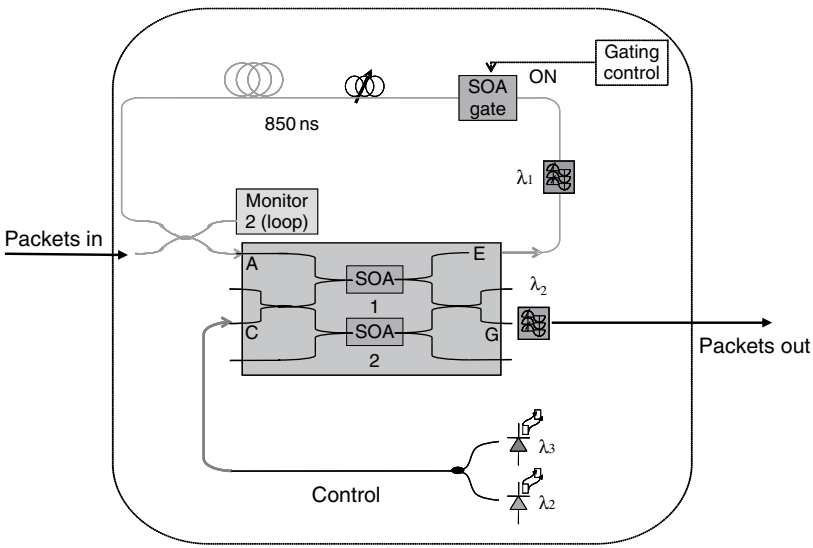

Figure 15.20 MZI buffer (this figure may be seen in color on the included CD ROM).

nonlinear element, typically a semiconductor optical amplifier (SOA). Integrated MZIs can be used for a variety of functions needed in future systems and cannot be realized by assembling discrete components because of the need for stability in the physical dimensions of the device. Commercial devices are available for operation at 40 Gbps and can be used to realize a variety of functions such as 2R regeneration and wavelength conversion [39]. Research currently shows how, through the use of push-pull configurations where phase changes are applied in both arms, the performance can be significantly enhanced, with up to 160 Gbps operation reported [40]. This configuration has been used in a number of different signal-processing applications such as regeneration, add drop multiplexing, and time slot interchange switching [41]. Currently, devices are becoming available where multiple MZIs are integrated on to one substrate enabling futuristic functional subsystems to be achieved such as bursty receivers [42]. Figure 15.20 shows the use of such a device to realize an optical buffer, suitable for an OPS system. The data bursts enter the MZI at port A. A control signal comprising a continuous train of return-to-zero (RZ) pulses at the same bit rate as the data is injected at input C; the wavelength of this pulse train can be altered between one of two wavelengths. The data exit the MZI at port E and circulates around the buffer loop, which as shown is set to give a round trip delay of 850 ns a packet length in this example. Data continue to circulate around the loop until the control wavelength is switched to the other state, in which case the data exit through port G through a bandpass filter. The SOA gate in the upper loop is used (by switching off) to clear the loop for the next input of original data.

Recently, novel approaches based on silicon photonic integration (Silicon Photonics) have been reported by Intel [43] (see also Chapter 11 on "Silicon Photonics" by Cary Gunn and Thomas L. Koch). Silicon is a well-understood material and the basis of low-cost electronics. It is transparent at infrared wavelengths so can be used to guide light, but cannot emit light. Intel are pioneering a process whereby a laser chip mounted in a silicon external cavity forms a tunable laser, which together with silicon modulators (realized by MZI configurations) and photodetectors (with Ge doping) shows promise as a future low-cost integration strategy; current performance is at the 1 Gbps, but 10 40 Gbps is predicted.

There are a number of key functions necessary, at a link and network level, to enable efficient operation of the future optical network. Examples are:

Optical switching: To fully advance to transparent networking, OOO switches are required, at microsecond (for OBS), millisecond (for OXCs), and nanosecond (for OPS) reconfiguration times. 3-D MEMS switches (ms reconfiguration) are now available with port counts to 160×160 [44], and the recent interest in the deployment of ROADMs means that the functionality of OOO switches is now available. Fast (ns) switch fabrics (of high dimension) are realized through the combination of tunable lasers/wavelength converters together with arrayed waveguides; it is hard to see this situation changing. Nevertheless, low-dimension ns switch modules are available [45], an example based on total internal reflection in a compound semiconductor PLC [46], which forms the core of a commercially deployed OPS system (see also Chapter 17 by R. Tucker for discussion on key issues for optical switching).

Optical monitoring (see also Chapter 7 on "Optical Performance Monitoring" by Alan Willner): As the network performance increases, it is crucial to understand the state of the physical layer so that appropriate routing and remedial actions can be taken. For example, within a network, a variety of bit rates from 10 to 160 Gbps may exist, with some routes more appropriate to one bit rate than another from the point of view of optical signal-to-noise ratio (OSNR), residual dispersion channel power, etc. Information should be available through optical monitoring to inform routing decisions at network nodes; this trend now appears in the area of cross-layer routing and is important one for research.

All-optical wavelength conversion and regeneration: All-optical wavelength conversion and regeneration is desirable (including from a power and footprint viewpoint as well as cost) for networks operating at speeds >40 Gbps (see also Chapter 20 in Volume A "Nonlinear Optical Circuits for Signal Processing" by Ben Eggleton and Stojan Radic). To achieve conversion, the physical properties of a nonlinear element are used to perform a logic function between the input signal and a pump. The main nonlinear elements used are an SOA, electro-absorption modulator (EAM), fiber, photonic crystal, and periodically poled $LiNbO_3$ (PPLN) waveguides. SOA-based devices, especially quantum dot, and EAMs have the added advantages of compactness and low-energy requirements to trigger

nonlinearities. Fibers have an instantaneous response to pulses but have limited nonlinearity, even in specially designed photonic crystal fibers; hence long lengths are required. PPLN requires intermediate lengths, and very fast conversion (40 160 Gbps) has been demonstrated.

Considerable research has been done in the area of single-wavelength subsystems, and e.g., advanced all-optical regenerative schemes at bit rates beyond 100 Gbps have been recently proposed in Ref. [47], as well as well-reported demonstrations at 40 Gbps [48]. Multiwavelength all-optical regeneration, if feasible, will dramatically decrease the cost of DWDM transmission links. A number of techniques are currently being considered, e.g., (a) through the mechanism of self-phase modulation, which in principle enables operation at speeds $>$160 Gbps, and (b) based on the inhomogeneously-broadened gain of self-assembled quantum dots in Quantum Dot SOAs [49].

Optical memory: All-optical buffering through fiber delay lines is an approach that requires complex control, and packets are delayed rather than stored. Recently, in the framework of LASOR [14], integrated delay lines have been developed as it has been shown [50] that a small number of low-depth buffers are sufficient for an OPS network. Recent research has focused on the possibility of controlling the velocity of light pulses propagating through a material, and measurements in SOA quantum wells showed controllable delay up to 1 ns; this results in a direct measurement of group velocity of $<$200 m/s giving a slow down factor up to 1.5×10^6 [51]. However, there is an indication that such phenomenon exhibit a specific delay-bandwidth product which means for high bit rates the achievable delay is low.

15.7 CONCLUSION

The drive toward an optical network, by which we mean a network comprising optical transmission and switching has taken about 20 years from original concept to the start of deployment of limited optical switching. The huge growth in demand for capacity from domestic users, due to the penetration of broadband service, together with the increasing needs of scientific high-end users, has made the economic deployment of advanced optical technology economic in a growing number of application areas. It is also the case that the maturity and ready availability of optical technologies have made it possible for communities to construct their own networks independent of operators, a situation that has greatly changed in the past decade.

New network architectures do not suddenly appear and real networks must evolve carefully, and this chapter discussed the current roadmap for the choice of switching technologies future networks might employ, representing research studies in current and recent years. The main changes represent the recognition that the world has changed to a data rather than voice-centric model; it was shown that between 2000 and 2006 the volume of data generated grew by a factor of 50. Thus initial network changes are to move the current SDH/SONET transmission and

switching technologies to one more amenable to data (NG-SDH) and these changes are now implemented. In conjunction with these near term changes, there is a strong move toward carrier-grade Ethernet, in particular 100 G Ethernet on a single channel, and it is likely that this trend will come to dominate. Other immediate changes required are to move toward a more dynamic network where circuits can be established and torn down in minutes rather than hours or days, and such architectures are represented in the standardized ASON architecture, where requests from users activate a control plane which initiates automatic node switching. These two changes represent desired changes in the current circuit-switched network, but the accelerating changes in demand (capacity, quality) require more significant changes. Discussed were:

(1) the move to all IP-based network where the core network comprises an IP router together with an OXC. This is an approach currently being adopted by BT UK.
(2) the move to an application-centric network based on OBS or OPS. Here appropriate network interfaces can assemble bursts representing required QoS at the network edge. The core of the network required optical switch fabrics, ideally in the microsecond switching regime.

From a transmission viewpoint current networks operate mainly at 10 GBPS, but 40-GBPS technology is now available for deployment. As the overall network load increases, studies show that the optimum line rate also increases, so line rates of $>$100 GBPS must not be discounted.

Finally, it was noted that there have been in recent times significant advances in subsystems and components and in device integration seen as the key to future optical networking. This integration enables the realization of many of the key functionalities for optical networking to be realized in a manner appropriate to real deployment; examples are all-optical wavelength conversion and optical regeneration.

REFERENCES

[1] H. Shinohara, "Overview of Japanese FTTH Market and NTT Strategy for Entering Full FTTH Era," in Proc. *ECOC 2006*, paper Th1.1.1, Cannes, September 2006.
[2] R. Smith, Grid Computing: A Brief Technology Analysis, CTO Network Library, 2005.
[3] http://www.jb.man.ac.uk/news/evlbi/
[4] Bill St Arnaud, "Future Internet Issues," *OECD ICCP Workshop*, March 2006, Paris, France.
[5] C. Cavazzoni, D. Colle, A. Di Giglio et al., "Evolution of Optical Transport Networks in Europe: The NOBEL Project Vision," in Proc. *Broadband Europe Conf.*, paper T04A.01, Bordeaux, December 2005 (www.bbeurope.org).
[6] N. Larkin, "ASON & GMPLS; the battle for the optical control plane"; http://www.dataconnection.com/network/download/whitepapers/asongmpls.pdf.
[7] Stavdas, S. Sygletos, M. O. Mahony et al., "IST DAVID: Concept presentation and physical layer modelling of the metropolitan area network," *J. Lightw. Technol.*, 21(2), 372 384, February 2003.

[8] Dimitrios Klonidis, Christina (T.) Politi, Reza Nejabati, Mike J. O. Mahony, and Dimitra Simeonidou; OPSnet: "Design and demonstration of an asynchronous high speed optical packet switch," *IEEE J. Lightw. Technol.*, 23(10), 2914 2925, October 2005.
[9] R. Nejabati, D. Klonidis, G. Zervas et al., "Demonstration of a Complete and Fully Functional End to End Asynchronous Optical Packet Switched Network," in Proc. *OFC 2006*, paper OWP5, Anaheim, USA, March 2006.
[10] J. Ryan, "An Outlook for Optical Executatives," in Proc. *OSA Executative Program*, Anaheim, USA, March 2006.www.osa.org/partner/network/program/Ryan%20John.ppt
[11] B. Fabianek, "Optical Networking Testbeds in Europe," in Proc. *OFC 2006*, paper OWU1, Anaheim, USA, March 2006.
[12] Kenichi Kitayama, Tetsuya Miki, Toshio Morioka et al., "Photonic network r&d activities in Japan current activities and future prospects," *J. Lightw. Technol.*, 23(10), 3404 3418, October 2005.
[13] D. T. Neilson, D. Stiliadis, and P. Bernasconi, "Ultra High Capacity Optical Ip Routers for the Networks of Tomorrow: Iris Project," in Proc. *ECOC 2005*, paper We 1.1.4, Glasgow, UK, September 2005.
[14] D. J. Blumenthal, "LASOR (Label Switched Optical Router): Architecture and Under lying Integration Technologies," in Proc. *ECOC 2005*, paper No XX, Glasgow, UK, September 2005.
[15] http://www.nlr.net/ess/index.html.
[16] P. Freeman, "GENI: Global Environment for Networking Innovations," in Proc. *The Future of the Internet*, OECD, Paris, France, March 2006 (http://www.oecd.org/dataoecd/43/63/36274169.pdf.)
[17] http://www.glif.is/
[18] J. Zhou, R. Cadeddu, E. Casaccia et al., "Crosstalk in multiwavelength optical cross connect networks," *J. Lightw. Technol.*, 14, 1423 1435, June 1996.
[19] R. E. Wagner et al., "Monet: Multiwavelength optical networking," *J. Lightw. Technol.*, 14, 1349 1355, June 1996.
[20] T. Freeman, "DWDM platform set for 40 G deployment," *Fibre Systems*, 3(1), 23, January/ February 2006.
[21] L. Zong, P. Ji, T. Wang et al., "Study on Wavelength Cross Connect Realised with Wavelength Selective Switches," in Proc. *OFC 2006*, paper NThC3, Anaheim, USA, March 2006.
[22] E. Hernandez Valencia and H. Menendez, "Exploiting Carrier Ethernet to Deliver Profitable New Services, in Proc. *OFC 2006*, paper NTUD1, Anaheim, USA, March 2006.
[23] D. Simeonidou, R. Nejabati, B. St. Arnaud et al., "Optical Network Infrastructure for Grid," http:// www.ggf.org/gf/docs/?final
[24] K. Kitayama, X. Wang, and N. Wada, "A Solution Path to Gigabit Symmetric FTTH: OCDMA over WDM PON," in Proc. *Broadband Europe Conf.*, paper T01A.02, Bordeaux, December 2005. (www.bbeurope.org)
[25] R. C. Mendez, P. Toliver, S. Galli et al., "Network applications of cascaded code translation for wdm comaptible spectrally phase encoded optical cdma," *J. Lightw. Technol.*, 23(10), 3129 3231, October 2006.
[26] Esther Le Rouzic and Stephanie Gosselin "160 Gb/s Optical networking: A prospective techno economic analysis," *IEE J. Lightw. Technol.*, 23(10), 3024 3033, October 2005.
[27] http://www.matissenetworkks.com.
[28] C. Qiao and M. Yoo, "Optical burst switching A new paradigm for an optical internet," *J. High Speed Netw.*, Special Issue on Optical Networks, 8(1), 69 84, 1999.
[29] A. Sahara, R. Kasahara, E. Yamazaki et al., "The Demonstration of Congestion Controlled Optical Burst Switching Network Utilizing Two Way Signaling Field Trial in Jgn Ii Testbed," in Proc. *OFC 2005*, paper OFA7, Anaheim, CA, USA, March 2005.
[30] Dimitra Simeonidou, Reza Nejabati, Georgios Zervas et al., "Dynamic optical network architec tures and technologies for existing and emerging grid services," *J. Lightw. Technol. Member*, 23(10), 3347 3357, October 2005.
[31] J. Gripp, D. Stiliadis, J. E. Simsarian et al., "IRIS optical packet router, [Invited]," *J. Opt. Netw.*, 5, 589 597, 2006.

[32] Dimitrios Klonidis, Christina (T.) Politi, Reza Nejabati, Mike J. O. Mahony et al., "OPSnet: Design and demonstration of an asynchronous high speed optical packet switch," *IEEE J. Lightw. Technol.*, 23(10), 2914 2925, October 2005.

[33] H. Furukawa, N. Wada, H. Harai et al., "Field Trial of IP over 160 Gbit/s Colored Optical Packet Switching Network with transient Response Suppressed EDFAand 320 Gbit/s toughput Optical Packet Switch Demonstrator," in Proc. *OFC 2007*, PDL, Anaheim, USA, March 2007.

[34] K. Kitayama, X. Wang, and N. Wada, "A Solution Path to Gigabit Symmetric FTTH: OCDMA over WDM PON," in Proc. *Broadband Europe Conf.*, paper T01A.02, Bordeaux, December 2005. (www.bbeurope.org)

[35] C. Tian, Z. Zhang, M. Ibsen et al., "Demonstration of a 16 channel code reconfigurable OCDMA/ DWDM system," in Proc. *OFC 2007*, paper OMO2, Anaheim, USA, March 2007.

[36] X. Wang and N. Wada, "Demonstration of OCDMA Traffic over Optical Packet Switching Networks with PLC and SSFBG En/decoders for Time Domain OC Processing," in Proc. *ECOC 2005*, paper PDL We1.4.5, Glasgow, UK, September 2005.

[37] K. Stubkjaer, "Semiconductor optical amplifier based all optical gates for high speed optical processing, *IEEE J. Sel. Top. Quantum Electron.*, 6(6), 1428, November 2000.

[38] R. Nagarajan, C. Joyner, and R. Schneider, "Large scale photonic integrated circuits," *IEEE J. Sel. Top. Quantum Electron.*, 11(1), January/February 2005.

[39] G. Maxwell, R. McDougall, R. Harmon et al., "WDM enabled, 40 GB/s Hybrid Integrated All optical Regenerator," in Proc. *ECOC 2005*, paper PDL 4.2.2, Glasgow, UK, September 2005.

[40] S. Nakamura, Y. Ueno, and K. Tajima, "168 Gbit/s all optical wavelength conversion with a symmetric Mach Zehnder type switch," *IEEE Photon. Technol. Lett.*, 13, 1091, 2001.

[41] S. Pau, Y. Jianjun, K. Kojima et al., "160 Gb/s all optical MEMS time slot switch for OTDM and WDM applications," *IEEE Photon. Technol. Lett.*, 14(10), 1460 1462, October 2002.

[42] Dimitrios Petrantonakis, George T. Kanellos, Panagiotis Zakynthinos et al., "A 40 Gb/s 3R Burst Mode Receiver with 4 Integrated MZI Switches," in Proc. *OFC 2006*, paper PDP 25, Anaheim, USA, March 2006.

[43] P. Koonath, T. Indukuri, and B. Jalali, "Monolithic 3 D silicon photonics," *J. Lightw. Technol.*, 24(4), 1796 1804, April 2006.

[44] http://www.glimmerglass.com

[45] R. Varrazza, I. B. Djordjevic, and Y. Siyuan, "Active vertical coupler based optical crosspoint switch matrix for optical packet switching applications," *J. Lightw. Technol.*, 22(9), 2034 2042, 2004.

[46] http://www.yokogawa.com

[47] Yong Liu, Eduward Tangdiongga, Zhonggui Li et al., Eindhoven Univ. of Technology, The Netherlands, Aston Univ., UK. "Error Free 320 Gb/s SOA Based Wavelength Conversion Using Optical Filtering," in Proc. *OFC 2006*, paper PDP 28, Anaheim, USA, March 2006.

[48] O. Lecrec et al., "Optical regeneration at 40 Gb/s and beyond," *J. Lightw. Technol.*, 21(11), 2779 2790, 2003.

[49] T. Akiyama et al., "Application of Spectral Hole Burning in the Inhomogeneously Broadened Gain of Self Assembled Quantum Dots to a Multi Channel Nonlinear Optical Device," *Photon. Technol. Lett.*, 12(10), 1301 1303, 2000.

[50] N. Beheshti, Y. Ganjali, R. Rajaduray et al., "Buffer Sizing in All Optical Packet Switches," in Proc. *OFC 2006*, paper OThF8, Anaheim, USA, March 2006.

[51] C. Chang Hasnain, "Controlling Light Speed in Semiconductors," in Proc. *ECOC 2005*, paper Mo3.1.3, Glasgow, UK, September 2005.

16

Optical burst and packet switching

S. J. Ben Yoo

Department of Electrical and Computer Engineering,
University of California, Davis, CA, USA

Abstract

This chapter discusses optical burst and packet switching technologies in detail and examines their roles in the future Internet. We will first discuss the role of optical circuit, burst, and packet switching systems in photonic networks and will cover the benefit and trade off issues in optical circuit, burst, and packet switching networks. Following an introductory section, we will review the networking architecture/pro tocols, systems, and technologies pertaining to optical burst switching and will repeat careful investigations into optical packet switching. Finally, we will look into the optical label switching (OLS) technology, which provides a unified platform for interoperating optical circuit, burst, and packet switching techniques. Test bed demonstrations employing OLS edge routers show high performance networking in support of multimedia and data communications applications over the Internet with the packets and bursts switched directly at the optical layer.

16.1 INTRODUCTION

The initial phase of optical networking, often referred to as the first-generation optical networking, started its deployment in 1997 and focused its attention on point-to-point link capacity increases. This deployment successfully provided scalable solutions to the rapidly growing network capacity demands driven by exponential increases in data and multimedia services. By contrast, network applications and services have connectivity and capacity requirements that vary in the long term (monthly, yearly) or short term (daily, hourly) such that network reconfigurations become necessary. In the first-generation optical networking, reconfigurations must take place using electronic switches or routers because optical networking supports only point-to-point connectivity. However, the true

Optical Fiber Telecommunications V B: Systems and Networks

ISBN: 978 0 12 374172 1

benefit of optical networking may rise from its capability to reconfigure the vast bandwidth directly in the optical layer, possibly without involving electronics in the data plane. The second-generation optical networking achieves reconfigurations of optical wavelength circuit paths (lightpaths) by properly configuring the optics (e.g., filters, beam splitters, switches, etc.) which reside in optical network elements. The second-generation optical networking supports format and protocol transparency and simplifies the hardware requirements in the data plane. Generalized multiprotocol label switching (GMPLS), Automatic Switched Optical Network (ASON), and emerging optical Ethernet technologies support the second-generation optical networking by defining the optical control plane, separately from the data plane, in order to set up and release lightpaths. As the deployment of the second-generation optical networking elements reconfigurable optical add drop multiplexers (ROADMs), optical cross-connects (OXCs), etc. is in progress today, we anticipate introduction of the third-generation optical networking in a foreseeable future. The third-generation optical network is capable of switching data *packets* or *bursts* directly in the optical layer. Today's voice, data, and multimedia services are rapidly converging toward Internet Protocol (IP)-based packetized services, and the data traffic is already dominant in today's networks. The third-generation optical networking will seek integration of data networking and optical networking by supporting packet switching of datagrams on a wavelength division multiplexing (WDM) optical networking platform. The optical packet switching (OPS) technology is particularly attractive from the viewpoint of a true IP-over-WDM architecture, where the IP packets are switched or forwarded over the all-optical WDM network without excessive electronic processing in the data plane. The optical network is currently evolving from traditional point-to-point static WDM networking to dynamically reconfigurable optical networking. Its continuing evolution is likely to lead to optical networking capable of dynamic switching of optical bursts and packets. The third-generation optical networking is expected to offer flexible and cost-effective network operation by exploiting statistical multiplexing and high network capacity utilization, similarly to what electronic packet switching networks have offered. Figure 16.1 shows the network evolution trend from the first-generation optical networking to the second- and the third-generation optical networking employing reconfigurable optical network elements (ROADMs and OXCs) and optical routers. Optical burst switching (OBS) is implemented either as a fast reconfiguring optical circuit switching (OCS) with tell-and-go (TAG) signaling or as an OPS with large aggregated packets. Figure 16.2 illustrates the trend of evolutions in optical networking protocol stacks, and Figure 16.3 shows typical node architectures for (a) all-optical OCS, (b) O/E/O OCS, (c) all-optical OPS, and (d) all-optical OBS.

The benefit of OPS and OBS compared with OCS rises from the higher network utilization at a subwavelength granularity and from the supporting of more diverse services with bursty traffic patterns. The benefit of using "all-optical" routers/switches in OPS and OBS can rise from the reduction in power and size

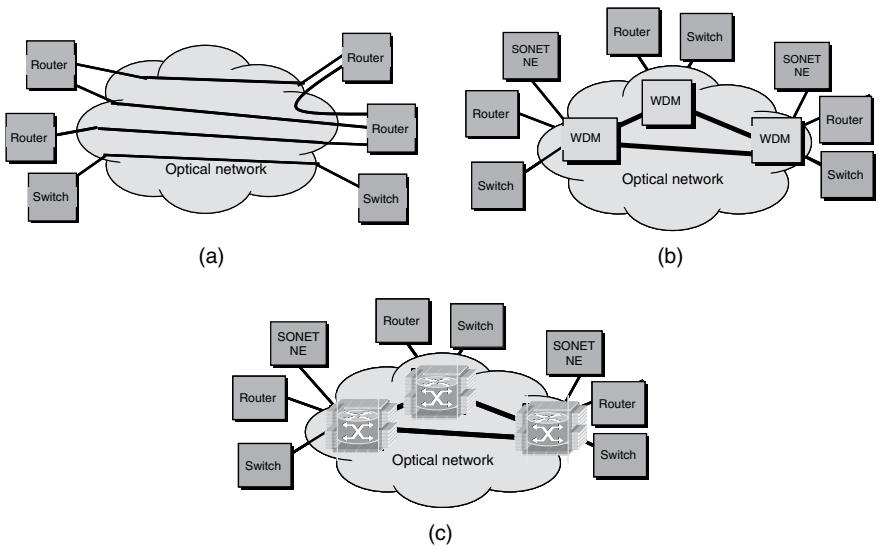

Figure 16.1 Evolution of optical Internetworking from (a) first generation optical networking involving point to point static optical networking, (b) second generation optical networking involving wavelength routed OCS, and (c) third generation optical networking involving OPS and OBS routers interfacing with other network elements (NE) (this figure may be seen in color on the included CD ROM).

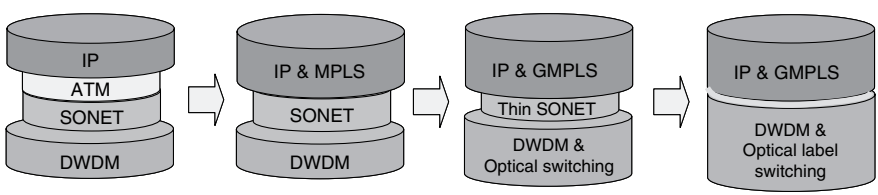

Figure 16.2 The evolution trend of protocol stacks from today's IP/ATM/SONET/WDM paradigm to a new paradigm IP over WDM with optical label switching (OLS). The future protocol exploits added capabilities in OLS and WDM to greatly simplify today's protocol stacks requiring heavy electronic data processing (this figure may be seen in color on the included CD ROM).

requirements. However, such comparisons must carefully consider underlying physical layer constraints and technical challenges, as well as higher layer functions. For example, conventional electronic routers adopt "store-and-forward" mechanisms with packet buffering, deaggregation, synchronization, contention resolution/arbitration, and reassembly, whereas all-optical routers can exploit the newly available dimension in the wavelength domain to resolve contention. Optical label switching (OLS) is a new networking technology designed in 1997 [1] fortuitously in the same year as IETF's introduction of multiprotocol label switching (MPLS). OLS supports optical packet, burst, and circuit switching by using optical labels and the wavelength-time-space domain all-optical contention

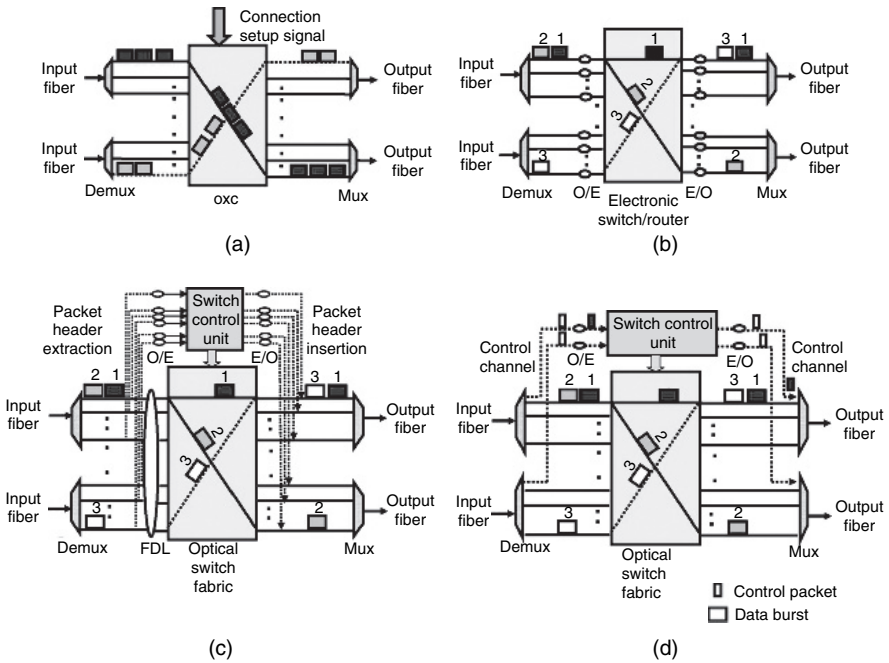

Figure 16.3 Optical node architectures employing (a) all optical optical circuit switching (OCS) involving out of band signaling for setting up and tearing down lightpaths, (b) O/E/O switching involving an electronic switch fabric with optoelectronic interfaces, (c) all optical optical packet switching (OPS) involving built in optical buffers and a fast optical switch, and (d) all optical optical burst switching (OBS) involving tell and go signaling without built in optical buffers. OCS can provide guaranteed quality of service (QoS) but the connection time can be slow and it does not provide subwavelength granularity. While OBS and OPS can provide higher network utilization with subwavelength granularity and rapid reconfiguration, it is difficult to achieve guaranteed QoS (this figure may be seen in color on the included CD ROM).

resolution [2, 3]. MPLS has no consideration for "wavelengths" and was enhanced to MPLambdaS in 1999 to adopt multiwavelength optical networking, and then it was further generalized into GMPLS to map integrated time, space, and wavelength domain multiplexing of packet and circuit services. While today's GMPLS standard does not include the possibility of packet switching and burst switching directly in the optical layer, its future extensions may include such features to adopt OLS capabilities.

This chapter discusses technology and system aspects of OPS and OBS in the context of the future Internet. Section 16.2 covers OBS technologies. Section 16.3 reviews OPS technologies in detail, including optical header, optical switching, and systems technologies. Section 16.4 briefly introduces OLS and shows experimental results in systems and networking test beds. Section 16.5 summarizes this chapter and lists the key issues of OBS and OPS for the future Internet.

16.2 OPTICAL BURST SWITCHING TECHNOLOGIES

Second-generation optical networking is based on reconfigurable OCS where lightpath provisioning processes require assurances in meeting service layer agreements based on reserving available resources including protection paths/links. The overlay data communication network (DCN) uses a data communication channel (DCC) to support communications for provisioning the lightpaths. While OCS can support quality-of-service (QoS) assurances associated with the lightpaths, provisioning of lightpaths can take relatively a long time (many seconds or minutes), and it is not uncommon that the service providers take several months in manually provisioning lightpaths. OBS networks [4, 5] initially emerged as very fast reconfigurable OCS networks with a special signaling method (e.g., just-in-time (JIT) [6], or just-enough-time (JET) [7]) instead of a typical circuit provisioning process. The emergence of OBS was driven by the desire to quickly transport a large amount of data across a high-capacity optical network without having to provision long-lasting circuits and also by the preference of achieving this agile networking on optical cross-connects without having to deploy new optical routers. Since the second-generation optical networking is currently in the early stage of deployment, OBS experimental demonstrations have been limited to research network test beds, and most of the publications have concentrated on theoretical analyses of OBS signaling protocols and studies of OBS network performance.

The fundamental concept of OBS [4, 5] emerges from burst assembly, signaling with the burst header cell (BHC), and burst disassembly [8]. The BHC contains the usual header information plus the burst length. Typically, OBS uses electronic processing in the control plane to read the BHC and to control the switching fabric. In the data plane, the data bursts can be switched all-optically, if an all-optical switching fabric and interfaces are involved. The data bursts can possibly contain multiple packets with various data rates and formats limited only by the optical characteristics of the optical switching fabric and interfaces. As Figure 16.4 indicates, the edge routers in the OBS network provide important burst assembly and disassembly operations at the ingress and egress, respectively [5]. When an end system has a burst of data to send, an idle channel on the access link is selected, and the data burst is sent on that idle channel. As the following subsection will discuss in detail, there are a number of different OBS protocols including two-way signaling (e.g., wavelength-routed OBS [9]) and one-way signaling (e.g., TAG-OBS, JET-OBS) methods. In the JET-OBS protocol, a BHC is sent on the control channel shortly before the burst transmission begins, specifying the destination of the burst and the channel on which the burst is being transmitted. A burst switch, on receiving the BHC, selects an outgoing link leading toward the desired destination with an idle channel available, and then establishes a path between the specified channel on the access link and the channel selected to carry the burst. It also forwards the BHC on the control channel of the selected link, after modifying the cell to specify the channel on which the burst is being forwarded. This process is repeated at every switch along

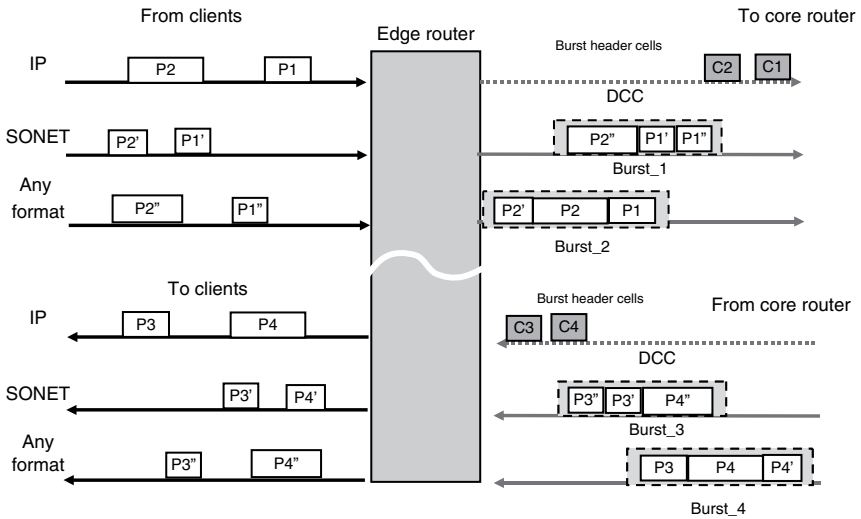

Figure 16.4 Optical burst switching (OBS) edge router's burst assembly at ingress, and burst disassembly at egress based on forward equivalent class (including class of service). In this figure, out of band burst header cells will indicate the information pertaining to each burst and will be communicated over the data communication channel (DCC). In band burst label allows attaching the label to each burst on the same wavelength channel [3] (this figure may be seen in color on the included CD ROM).

the path to the destination. The BHC also includes a length field specifying the amount of data in the burst. This is used to release the path at the end of the burst. If there is no channel available to accommodate the burst when it arrives, the burst will undergo contention resolution and arbitration procedures discussed later in this section.

16.2.1 Various OBS Protocols and Architectures

Numerous publications have covered various OBS control protocols. Two-way reservation protocols such as reservation/scheduling with just-in-time (RIT) and tell-and-wait (TAW) protocols, which require acknowledgment from the receiving node before sending the burst. Wavelength-routing OBS (WR-OBS) [9] utilizes TAW and routing-and-wavelength-assignment (RWA) method. One-way reservation protocols such as TAG protocols require no acknowledgment from the receiving node in order to reduce latency. Terabit burst switching [4] uses TAG protocols to achieve both datagram mode and virtual circuit mode of routing. TAG-based OBS utilizes either JET signaling [5,7] or signaling with built-in offset in the node (similarly to the OPS with built-in delays at the nodes to require no offset time between the BHC and the burst). The following discusses these protocols in more detail.

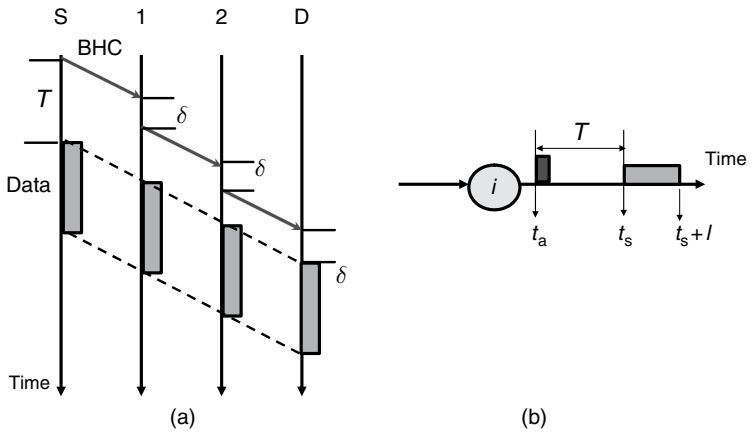

Figure 16.5 OBS using the JET signaling with offset time [10]. (a) The burst header cell (BHC) propagates from source (S) to Destination (D) via intermediate nodes "1" and "2" with processing delay δ at each node. (b) The intermediate node i reserves the bandwidth for the burst starting from the burst arrival time (t_s) instead of the arrival time of the BHC (t_a); in this case, the offset time $T(i)$ at node i is t_s t_a. Here, the reservation of the bandwidth is from t_s to $t_s + l$ for the burst with length l (this figure may be seen in color on the included CD ROM).

Figure 16.5 illustrates the basic concept of JET [10]. As shown, a source node having a burst to transmit first sends a BHC on a signaling channel toward the destination node. The BHC is processed at each subsequent node in order to establish an all-optical data path for the following burst. Based on the information carried in the BHC, each node chooses an appropriate wavelength on the outgoing link, reserves the bandwidth on it, and configures the optical switch. Meanwhile, the burst waits at the source in the electronic domain. After an offset time, T, whose value is to be determined next, the burst is sent in optical signals on the chosen wavelength. To ensure that all intermediate OBS nodes have enough time to complete the processing of the BHC before the burst arrives, JET sets the offset time T to be $\delta \times H$, where δ is the BHC processing delay per node, and H is the number of hops along the path (e.g., $H = 3$ in Figure 16.5(a)). In practice, the network is likely to include reconfigurable network elements with nonuniform BHC processing delays (e.g., optical cross-connects and optical add drop multiplexers having different processing delays) so that the offset time needs to be integrated over the expected lightpath ($T = \Sigma_i^H \delta_i$, where δ_i is the BHC processing delay at node i). The JET signaling lets each BHC carry the offset time information and makes the delayed reservation for the corresponding burst, that is, the reservation starts at the expected arrival time of the burst. As Figure 16.5(b) shows, at the intermediate node i, the bandwidth is reserved for the burst starting from the burst arrival time (t_s) instead of the arrival time of the BHC (t_a); in this case, the offset time $T(i)$ at node i is t_s t_a. In addition, the BHC also contains the burst length information to enable the bandwidth reservation only for the burst duration with

automatic release. For example, in Figure 16.5(b), the bandwidth is reserved from t_s to $t_s + l$ for the burst with length l. All these features are useful in achieving effective bandwidth utilization in OBS networks [10].

It is worth mentioning that the JET signaling requires a careful precomputation of the offset time T; if the offset time T cannot compensate the total latency experienced by the BHC, the burst will be lost. At higher load, there is higher probability of contention and higher burst loss rates. A number of publications [10 12] have discussed improving or varying QoS [more accurately, priority-based class of service (CoS)] by adjusting the offset time T to provide statistically higher probability of burst delivery. There is no guaranteed QoS; however, a greater offset time provides a higher probability [10] of successful forwarding, and thus provides a higher level of CoS. While the burst blocking probability rises with higher offered load, higher class burst services experience relatively lower blocking probability compared with lower class burst services. Another point to note is that the end-to-end delay in JET OBS networks includes the burst assembly time, the time it takes to estimate the offset time T, the transit time across the network, and the offset time T itself. Since the BHC contains information pertaining to the length of the burst, the BHC will be sent out after the burst assembly is complete and the offset time T is computed. Then the BHC ingresses into the network, while the burst waits for the offset time T before it ingresses into the network. The burst assembly using timer-based, or combined timer and burst-length-based [13, 14] algorithms to be discussed in the following section can limit the amount of delay associated with burst assembly.

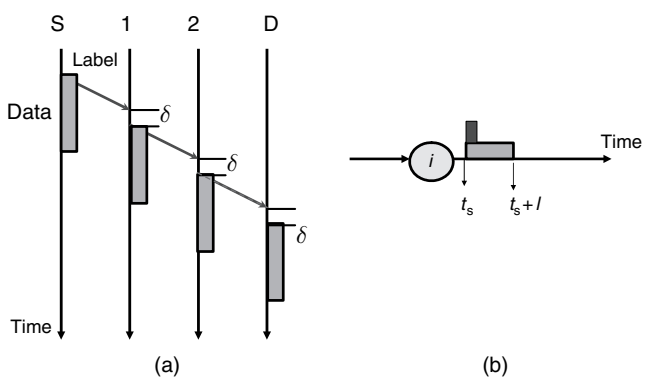

Figure 16.6 Timing diagram of optical packet switching (OPS) or OPS like optical burst switching (OBS) networking, where each node contains a built in optical buffer that matches the total time it takes to process the BHC and to switch the data burst. (a) The optical label propagates together with the datagram from source (S) to destination (D) via intermediate nodes "1" and "2" with processing delay δ at each node. (b) The intermediate node i reserves the bandwidth for the burst starting from the datagram arrival time (t_s) which coincides with the optical label arrival time (t_a), and the reservation of the bandwidth is from t_s to $t_s + l$ for the datagram with length l (this figure may be seen in color on the included CD ROM).

The second type of TAG-OBS protocol mentioned earlier is to follow the scheme used for OPS where each node is equipped with a built-in optical buffer that matches the total time it takes to process the BHC and to switch the burst [15]. Figure 16.6 illustrates the timing. Since the latency is controlled and managed at each intermediate node, there is no need to precompute the estimated sum of latency across the expected transit nodes over the expected path. In most cases, the BHC and the data burst are positioned in time with little offset ($T \sim 0$) and intermediate OBS routers maintain this proximity of the low offset. The built-in optical fiber delay line (FDL) buffer in the OBS node matches the time it takes to read the BHC, look up the forwarding table, resolve contention, arbitrate packets, and switch the optical switch [3]. The FDL can be as short as 10 m for 50 ns latency, or as unrealistically long as 10 km for 50 μs latency. Hence, employing a fast optical switch and a fast electronic control is essential for this OPS-like OBS [16]. In contrast, this method avoids the need for precomputations of the offset time T and circumvents the scalability limit seen in the first type of OBS networks [17]. Section 16.4 will discuss OPS-like OBS using optical labels to support interoperability between OPS, OBS, and OCS.

The scalability limit of two-way signaling based OBS networks has been covered in Ref. [17], where a practical limit of 20 35 and 50 116 nodes have been estimated based on the time it takes for RWA to complete using Adaptive Unconstrained Routing Exhaustive and Shortest Path First Fit methods, respectively. The scalability of JET-based OBS networks is expected to be limited by the rise in the blocking probability affecting the network throughput at high network load levels.

16.2.2 OBS Core and Edge Routers

Most of the proposed OBS architectures and protocols are based on the assumption that the core of the optical network does not need any substantial hardware upgrades when transitioning from the reconfigurable OCS networks. In practice, most of the existing core networking elements have relatively slow (>5 ms) response time even if the software and firmware upgrades take place to allow fast switching based on TAG signaling. The optical-label-based OPS-like OBS discussed in Section 16.4 will exploit a fast (~1 ns) switching fabric with agile firmware which interfaces with the network control and management software system. Hence, the OBS core and edge routers have focused on the "fast-core" and "smart-edge" architecture [18, 19] where the core routers support very high-capacity, low-latency, and all-optical transparent switching and the edge routers support computation of BHC or labels, burst or datagram assembly and disassembly, and electronic packet inspection.

In all OBS schemes, the burst assembly algorithm and the traffic statistics play key roles in the performance of the OBS network [18]. As mentioned above, burst assembly and disassembly processes take place at OBS edge routers at the ingress and egress of the OBS network. Bursts with identical forward equivalent class

(FEC) will be assembled and processed in one burst assembly unit [18]. The burst scheduler handles creating bursts and their corresponding BHCs, adjusting the offset time for each burst, scheduling bursts on each output link, and forwarding the bursts and their BHCs to the OBS control network [20]. The burst assembly algorithms can be classified as timer-based, burst-length-based, and combined timer and burst-length-based [13, 14]. The assembled traffic characteristics differ from the original traffic statistics [21], and the OBS network performance also varies in its throughput, latency, burst loss probability, etc., due to this burst assembly process.

In the Internet based on electronic packet-switching, it is commonly believed that the long-range dependency is an important factor affecting the performance including data losses and delay. In the OBS- and OPS-based Internet, when equipped with very little optical buffering at each node, the short-range dependency is more important than the long-range dependency [19]. A number of studies [13, 20] indicated that the burst assembly gives no influence on the long-range dependency of the assembled burst traffic. Further simulation studies [18, 19] indicated significant benefit of burst assembly in the network performance by reducing the short-term correlation of the traffic processes.

16.2.3 OBS Contention Resolution and Network Performance

Burst contention occurs in OBS nodes when two or more bursts attempt to go to the same output port of the same wavelength channel at the same time. The contention resolution can utilize alternative forwarding in wavelength, time, and/or space domains [2, 22, 23].

- Wavelength domain: Contending bursts can take alternative wavelengths for forwarding. This is the most effective contention resolution not incurring additional latency while maintaining the shortest path or minimum hop distance.
- Time domain: Contending bursts can be delayed in a time buffer (e.g., FDL) to be forwarded later. Since FDLs are strict FIFO queues with fixed delays, they are less effective than electronic RAMs. Multiple FDL array with various buffer lengths in a switching fabric is desirable.
- Space domain: Contending bursts can be forwarded to another output port than the preferred one so that another OBS router will forward the bursts. This method uses part of the network as a buffer and can cause the bursts to arrive out of sequence.

If contention resolution in the three domains is unsuccessful due to unavailability of alternative wavelength, port, or time-delay combinations, there exists one

additional means of contention resolution by buffering in the electronic RAMs in the OBS edge router [3, 24]. Otherwise data losses due to dropping or preempting the burst are inevitable. While unified contention resolution [23] combining the three optical domains with electronic RAMs in the edge router [3, 24] is most effective, most of the OBS research focuses on simpler schemes without wavelength conversion using space domain deflection [25] alone, or burst scheduling [26] alone. Other studies [27, 28] investigated hybrid schemes involving optical buffering (i.e., FDLs) and partial wavelength conversion.

16.2.4 Optical Switching Technologies for OBS

As mentioned earlier, the main attraction of OBS compared with OCS is that it can more effectively accommodate bursty traffic at a subwavelength granularity, without requiring very fast switching speeds like OPS does. While OPS seeks to achieve nanosecond switching speeds, JET-OBS can function with microsecond or even millisecond switching speeds. By contrast, slower OBS switching speeds can cause inefficiency and unpredictability in the OBS network performance especially at high network load levels.

OBS can exploit hybrid optical and electrical switching technologies, but its main benefit rises from using an all-optical switching fabric. Optical switching broadly defines switching in the space, time, and wavelength domains. When switching in all three domains is available, most effective contention resolution and diverse switching functions are achievable. In most cases, however, optical switching fabrics are capable of space switching only, or capable of space switching with limited wavelength conversion. Time switching is considered most difficult, and it typically utilizes a combination of space switching and FDL to realize the necessary discrete time delays. In selecting optical switch fabrics for OCS, OBS, and OPS applications, there are countless attributes that need to be considered. Table 16.1 summarizes this consideration. These attributes fall into three general categories: signal quality, configuration, and performance. *Signal quality* includes the signal-to-noise ratio, jitter, chirp, amplitude distortion, crosstalk, and extinction ratio, and it largely determines the bit error rate and the cascadability of the switch fabric. *Configuration* is related to the implementation of the switch fabric and includes scalability, blocking characteristics (e.g., wide-sense, rearrangeably, strick-sense nonblocking), control requirements, dynamic ranges, polarization dependence, degrees of multicast (if any) [29], latching/non-latching, promptness (store-and-forward vs cut-through), upgradeability (hitless vs non-hitless), and wall-plug power requirements. Size, cost, and cost-effectiveness can be also included in this category. Lastly, the *performance* includes optical bandwidth, insertion loss, switching speed, bit-rate limit, bit-pattern dependence, uniformity, and optical transparency. Selected parameters are described below. Papadimitriou [30] provides a tutorial summary of various optical switching fabrics.

Table 16.1
Optical switching technologies for OCS, OBS, and OPS.

	Optomechanical switches	Optical MEMS	Thermooptical PLC	PLZT switch	Wavelength routing switch (e.g., AWG and Tunable λ)	SOA broadcast and select	SOA crosspoint	Semiconductor optical phase array	Optical RAM
Switching time	~4 ms	3D: ~10 ms 2D: ~3 ms	~3 ms	~300 ns	~1 ns	~1 ns	~1 ns	~30 ns	~1 ns
Scalability	16×16	1000×1000 for 3D 32×32 for 2D	4×4	4×4	65336×65336	32×32	4×4	64×64	64×64
Applications	OCS, OBS	OCS, OBS	OCS, OBS	OCS, OBS	OCS, OBS, OPS	OCS, OBS, OPS	OCS, OBS, OPS	OCS, OBS, OPS	OCS, OBS, OPS
Level of transparency	Strict	Strict	Strict	Strict	λ conversion dependent	Strict	Strict	Strict	Opaque
Crosstalk	$<$ 55 dB	$<$ 45 dB	$<$ 35 dB	$<$ 25 dB	$<$ 35 dB	$<$ 45 dB	$<$ 45 dB	$<$ 25 dB	$<$ 35 dB
PDL	<0.1 dB	<0.5 dB	<0.5 dB	<1 dB	λ conversion dependent	Strict	<3 dB	<3 dB	<3 dB
Switching	Space	Space	Space	Space	λ & Space	Space	Space	Space	Space
Reference	[31]	[32]	[33, 34]	[35]	[36 38]	[39]	[40, 41]	[42]	[43 47]

Signal Quality Issues

- Crosstalk: the ratio of the power at a specific output from the desired input to the power from other inputs.
- Jitter: the accumulated additional jitter in the switching fabric due to switching elements (SOA) or any time-dependent element.
- Chirp: the ratio of added frequency modulation vs amplitude modulation as a result of switching.
- Q-factor and optical signal-to-noise ratio (OSNR): the signal quality at input and at output. Caution must be taken to carefully evaluate optical regeneration, if any, in the switching fabric since OSNR may appear to improve but Q-factor can stay low.

Configuration Issues

- Scalability: It is the maximum size of the optical switch in terms of total port counts.
- Latching/nonlatching: whether the switching fabric can latch its switching state or it cannot latch its state without additional control when power fails.
- Blocking/nonblocking: The switch fabric is blocking (nonblocking) if it cannot (can) establish connection states for all possible desired connections. Rearrangeably nonblocking means that it maybe necessary to rearrange currently active connections to support a request for a new connection between a pair of idle input and output ports. Wide-sense nonblocking networks are those that can realize any connection pattern without rearranging active connections *provided that* correct rules are used for routing each new connection through the switch fabric. Strict-sense nonblocking networks require no rearrangement and no complex routing algorithm so that new connection requests are allowed to use any free path in the switch.
- Promptness: Store-and-forward switching stores the entire frame in the memory and waits until the entire frame has arrived prior to forwarding it. Once the frame is in the memory, the switch can check the destination address, the source address, the cyclic redundancy check, etc. Cut-through switching will begin forwarding the frame as soon as the destination address is identified.
- Degree of switching capability in space, wavelength, and time domains: The switching fabric can switch in the space, wavelength, and/or time domains, and if the switching has any limitations in the range of the switching in these domains.
- All-optical vs optoelectronic switching: The switching fabric can contain interfaces and switching elements that are all-optical, electrical, or hybrid.
- Cost, size, reliability, and power consumption: The deployment and maintenance costs, physical size, reliability, and power consumption of the switching node are important factors to be considered. Integration of components reduces unreliable component-to-component interfaces and simplifies packaging for reduced cost, size, and power consumption.

Performance Issues:

- Insertion loss: the power ratio between the output signal and the input signal.
- Polarization-dependent loss: the variance in insertion losses between two principal states of polarization.
- Polarization mode dispersion: the variance in time delays between two principal states of polarization.
- Switching speed: the time it takes for the switch to change its state.
- Uniformity: the variance of the above parameters measured from port to port, or from wavelength to wavelength.
- Level of transparency [48]: the level of signal transparency maintained after the switching. There are three levels of transparency: strict, amplitude, or digital transparency. Strict transparency fully maintains amplitude and phase information of the signal after switching. Amplitude transparency fully maintains the amplitude information but loses phase information of the signal after switching. Digital transparency maintains digital amplitude information but loses analog amplitude or phase information of the signal after switching. Opaqueness refers to not retaining any level of transparency.

Section 16.3 will discuss the optical switching technologies for OPS. Here, we provide a short summary of space switching technologies and show possible combinations with wavelength conversion or time delay units (e.g., FDL). Most of the optical space switching technologies do not restrict transparency; however, when combined with wavelength conversion technologies, the optical switching fabric will exhibit different levels of transparency (strict, amplitude, or digital transparency, vs opaqueness) [48] depending on the wavelength conversion technologies used [49].

Figure 16.7 illustrates optical switching fabric architectures. Figure 16.7(a) is a wavelength selective space switching with a $K \times K$ space switch on each of W wavelength layers having no wavelength capabilities. Figure 16.7(b) allows shared wavelength conversion or shared time switching/delays in addition to the wavelength selective space switching in Figure 16.7(a). Figure 16.7(c) offers nonblocking wavelength interchanging switching with full space and wavelength switching capability; however, it requires a relatively large space switch fabric of size $KW \times KW$. Figure 16.7(d) allows shared time switching/delays in addition to the space and wavelength switching in Figure 16.7(c). Since the FDL is the only practical time buffer technology available today, the architecture in Figure 16.7(d) allows only FIFO-based time delay unless multiple FDLs are combined with another reconfigurable switching fabric. Section 16.3 will discuss time switching in further detail.

There has been active research in OBS networking and system test bed studies around the world. Alcatel implemented a KEOPS optical burst/packet router prototype [39] using one 64×64 highly integrated semiconductor optical amplifier (SOA) switch matrix and 16 burst aggregation/de-aggregation boards with ATM

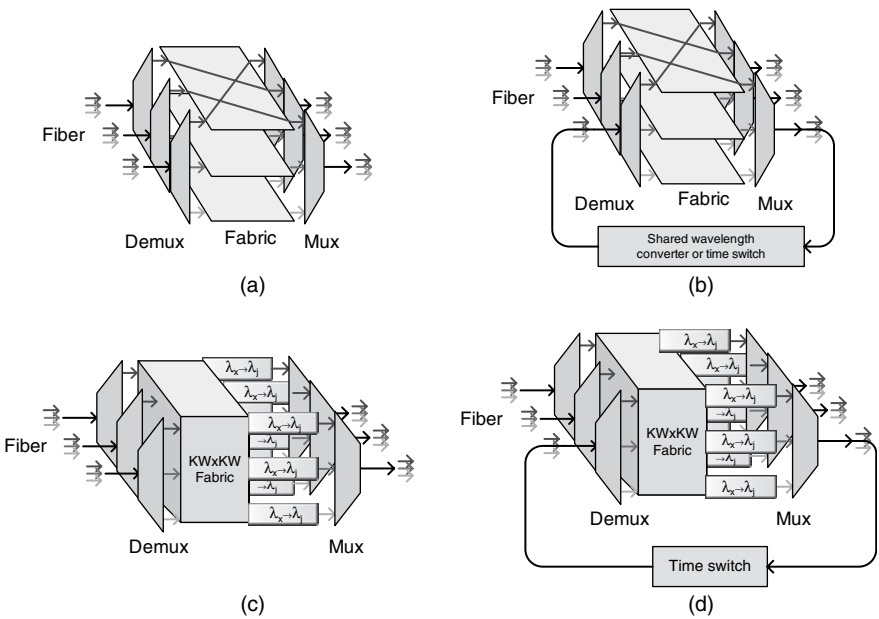

Figure 16.7 Optical switching fabric architectures with (a) wavelength selective space switching only, (b) wavelength selective space switching with shared wavelength conversion or time switching, (c) space and wavelength switching, and (d) space wavelength switching with shared time switching (delay) (this figure may be seen in color on the included CD ROM).

interfaces. MCNC [32] focused on a one-way JIT signaling protocol; it set up an OBS test bed using three sites comprising JIT controller and micro-electromechanical system (MEMS) OXC of ATDnet. NTT and Fujitsu demonstrated [50] optical burst switching with GMPLS-based two-way signaling protocol by utilizing planar lightwave circuit (PLC) and MEMS switches. Hikari router [33, 34] is designed as a GMPLS-based optical and electrical multilayer router, which includes both an OXC and an IP router to support dynamic cooperations of optical and IP layers. A recent study on PLZT (lanthanum-doped lead zirconium titanate) switch [35] with shared wavelength conversion allowed variable-length 3.5 μs optical burst switching. The following section includes detailed discussions on optical switching fabrics for OPS systems.

16.3 OPTICAL PACKET SWITCHING TECHNOLOGIES

OPS technologies offer a new capability to process packets directly at the optical layer for the future Internet. OPS systems can be categorized in a number of ways: synchronous vs asynchronous packet switching, fixed-length vs variable-length packet switching, and store-and-forward vs cut-through packet switching. Optical

packet multiplexing schemes also differ and can exploit time division multiplexing (TDM), WDM, and optical code division multiplexing (CDM). A great deal of recent research in optical networks has focused on a method in which multiple streams of packets are multiplexed in the wavelength domain. In comparison, TDM- and optical CDM-based OPS work has been much less active, primarily due to difficulties in developing demultiplexing devices for optical TDM or for optical CDM. This section will first review conventional electronic packet switching, then discuss OPS based on WDM schemes in detail, and finally cover OPS based on TDM schemes briefly.

16.3.1 OPS Protocols and Architectures

Conventional Electronic Packet Switching Router Architecture Overview

Today's electronic packet switching routers are all based on store-and-forward, fixed-length, and synchronous packet switching. Figure 16.8 shows the schematic of an electronic router. Here, each line card on the electronic router is equipped with relatively large electronic random access memories (RAMs) so that the line card can receive asynchronously arriving variable-length packets, buffer them, segment them into fixed size cells, schedule the cells, and forward them synchronously through the switching fabric. The output port line card with RAMs will reassemble the received fixed-length cells into variable-length packets. Each line card is configured in duplex. The electronic RAM provides significant flexibility in electronic packet switching. First, contention resolution and arbitration exploit well-known time domain processes in the RAM. Secondly, the switching speed of the switching fabric need not be faster than the bit rate, and there is no need to include a "guard time" used in OPS. Thirdly, the electronic router can conduct advanced electronic processing and queuing on the packets while the packets are in the buffer memory.

In contrast, this store-and-forward approach imposes the following shortcomings. First, the line card needs to store and process every bit in the packet. As a

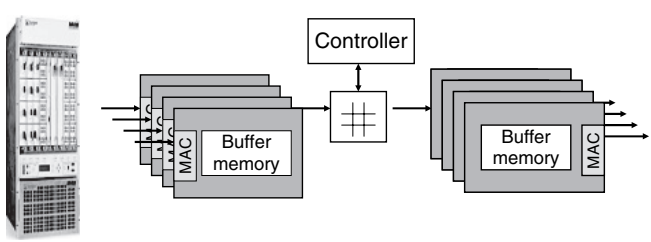

Figure 16.8 A schematic of an electronic router (this figure may be seen in color on the included CD ROM).

consequence, the line card must run at the specified line-rate, and it becomes sophisticated and power consuming, especially at high data rates. Secondly, the advances in router technologies will depend strongly on the advances in dynamic RAM (DRAM) technologies whose access speed has been rising only at 7% per year [51]. Thirdly, the finite capacity in electronic switching [52 54] forces the electronic routers to be clustered with each other to achieve higher capacity. This clustering consumes a number of line card ports for simple interconnection between the routers within the cluster.

OPS Router Architecture

The lack of a viable optical RAM technology is a significant handicap in realizing an all-optical router, especially if the store-and-forward router architecture were to be directly adopted in the optical router. In contrast, an all-optical router can exploit the newly available wavelength domain in switching and contention resolution. Optical routers exploiting the wavelength domain can potentially support high line-rate multiwavelength data signals with typically much lower power consumption and less signal interference than its electronic counterpart.

OPS routers utilize the "optical header" attached to the associated "optical data payload" for forwarding at each optical router. Since the optical header needs to contain only relatively a small number of bits (typically ~40 bits) for source (~10 bits), destination (~10 bits), optical time-to-live (TTL) (~4 bits), QoS (~3 bits), etc., the bit rate for the optical header can be much lower than that for the optical data payload. As in OBS, a typical OPS system utilizes an electronic control plane and an all-optical data plane so that electronics will look up the content of the header, make switching decisions, and reconfigure the all-optical switching fabric to forward the optical data payload. Normally during this process, optical header replacement takes place. The optical header replacement and optical label swapping processes are identical at the physical layer (although logically different).

Figure 16.9(a) illustrates the system architecture of synchronous and fixed-length OPS systems and (b) shows that of asynchronous and variable-length OPS systems. In the former, the input interface must synchronize the packets, whereas in the latter, no synchronization is necessary. The input interface in both cases extracts the headers; the input control detects the headers and sends the header content information to the switch controller where forwarding table lookup, contention resolution, arbitration, and forwarding decision take place. The switch controller then sends the new switching state command to the switching fabric and also sends new header information to the output control so that theswitching fabric will switch and the output interface can replace the header (and possibly data signal regeneration as well). While the asynchronous, variable-length packet switching systems need no packet synchronization processing, the

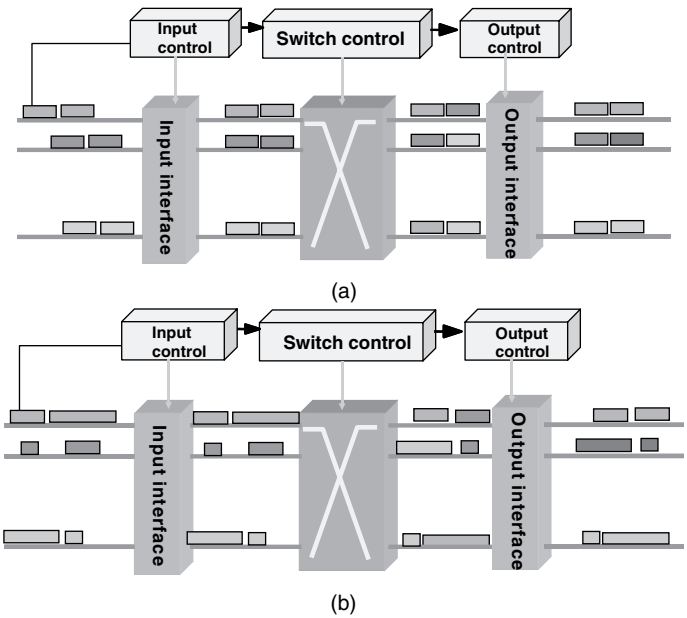

Figure 16.9 Optical router architecture with (a) synchronous and fixed length packet forwarding, and (b) asynchronous and variable length packet forwarding (this figure may be seen in color on the included CD ROM).

contention probability is higher in the asynchronous systems than in the synchronous counterparts, so that more effective contention resolution schemes become necessary.

16.3.2 OPS Router Systems

Optical Header (Label) Processing Technologies

Unlike OBS, which employs a separate channel (DCC) for electronic BHC processing and replacement, OPS should exploit optical headers that can be easily attached and detached from the optical data payload, preferably by using a simple all-optical technology. For this reason, the format of optical headers is a very important design consideration in determining the optical router architecture. The header replacement capability helps provide flexibility in the OPS network, although it is not absolutely necessary in certain deterministic system or network architectures [55]. Table 16.2 shows the summary of header (or label) placement technology.

The header can be placed in series or in parallel to the data payload using a number of technologies. In choosing the technology, the optical header scheme should (a) impose a minimum overhead to the data networking capacity, (b) support simple header replacement techniques, (c) maintain high signal fidelity across fiber

Table 16.2
Optical header (label) encoding technique comparisons.

	Separation domain	Method	Spectral efficiency	All optical label swapping complexity	Payload label crosstalk	Interoperability OCS/OBS/OPS	References
Serial	Time	Bit serial	Good <0.8	Complicated; strict timing required between label and payload	Low ~ 20 dB	Difficult (requires time domain processing)	[39, 56 58]
Parallel		Double sideband subcarrier	Fair <0.5	Complicated	Low ~ 17 dB	Possible	[5, 59, 62]
		Single sideband subcarrier	Good <0.7	Complicated	Low ~ 17 dB	Possible	[4, 63, 64]
	Frequency	Carrier suppression and separation	Good <0.7	Complicated	Low ~ 17 dB	Possible	[65]
		Out of band label (wavelength multiplexing header technique)	Poor <0.2	Simple	very low ~ 35 dB	Possible	[66, 67]
	Code	Optical code	Fair <0.4	Medium	Medium ~ 10 dB	Possible	[68, 69 71]
	Modulation format	ASK (OOK) payload DPSK/FSK label	Very good <0.8	Complicated	High ~ 6 dB	Possible	[72 75]
		DPSK/FSK payload ASK (OOK) label	Very good <0.8	Complicated	High ~ 6 dB	Possible	[76 78]
		PolSK label ASK (OOK) payload	Very good <0.8	Complicated	High ~ 6 dB	Possible	[79]

transmission and cascaded nodes, and (d) impose low crosstalk between the header and the payload. The serial header techniques place the header bit-serial to the payload in the time domain and require a relatively strict control of the timing. The parallel header techniques place the header on a separate wavelength, frequency, modulation format, or code. The parallel header architecture facilitates the header replacement process because a separate channel allows parallel processing of the header. It also provides better support for asynchronous variable-length packet switching, offers possible interoperability between OPS with OCS and OBS, and relaxes the stringent timing control requirement seen in serial header techniques.

Time Domain Header Technique Early OPS technologies including TDM OPS technologies utilized a time domain header technique. They primarily pursued synchronous and fixed-length packet switching mainly because the TDM label already required relatively strict timing control. Figure 16.10 shows an example of a time domain header format used in the KEOPS OPS system demonstration [39].

In this example, a fixed time slot of 1.646 μs includes the 180 ns optical header (optical routing tag), the >26 ns guard time, the 1.35 μs data payload, and another >64.3 ns guard time to separate packets. KEOPS utilized the header line rate of 622 Mb/s and the flexible payload line rate up to 10 Gb/s [80]. Both headers and payloads are led by synchronization bits to facilitate the burst mode clock recovery. Upon reading the packet headers, the optical synchronizer synchronized all packets entering the OPS system. The time domain header replacement requires time switching to remove the old header and to attach a new header to the payload. Since the header format includes a small number of header bits (typically less than 100 bits), the overhead is relatively low especially if a large data payload format (>15k bytes) is adopted. Like in other OPS technologies, typical line rates for the header are much lower than those for the data payload, and thus relatively simple electronics can read the header, look up the forwarding table, and provide the new header content.

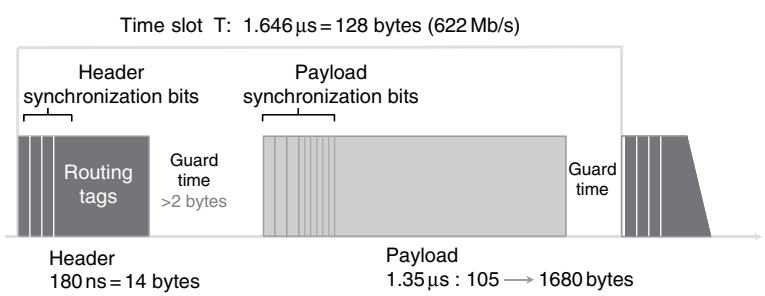

Figure 16.10 KEOPS optical packet format (courtesy of [39]) (this figure may be seen in color on the included CD ROM).

Subcarrier Multiplexing Header Technique One of the most popular optical header techniques is based on subcarrier multiplexing of the header with the data payload on the baseband. Initially, double-sideband SCM optical header techniques were widely utilized [83 85]; however, the double-sideband SCM signal multiplexing studied in the mid-1980s [86, 87] for video transmission revealed signal reception problems due to RF fading at particular distances in the network. The RF fading is a result of coherent interference between the carrier and the two sidebands, which constructively or destructively interfere depending on their relative phases determined by the initial phase conditions and the total dispersion (the product of the dispersion coefficient and the fiber transmission length). To defeat the RF fading effect, a number of new techniques including carrier suppression method in optical header extraction and replacement [88] as well as single-side optical labeling technique with carrier suppression [63, 65] have been investigated. Figure 16.11 shows subcarrier multiplexed optical header techniques involving (a) double-sideband label with baseband data payload involving a compact integrated electro-absorption modulator laser [81, 89], and (b) carrier-suppressed subcarrier multiplexing with label and data signals occupying each sideband [65]. Both techniques utilized relatively simple optical filtering techniques such as fiber Bragg gratings (FBGs) or arrayed waveguide gratings (AWGs) for separating subcarrier components, and showed successful penalty-free operations. Cascaded optical router

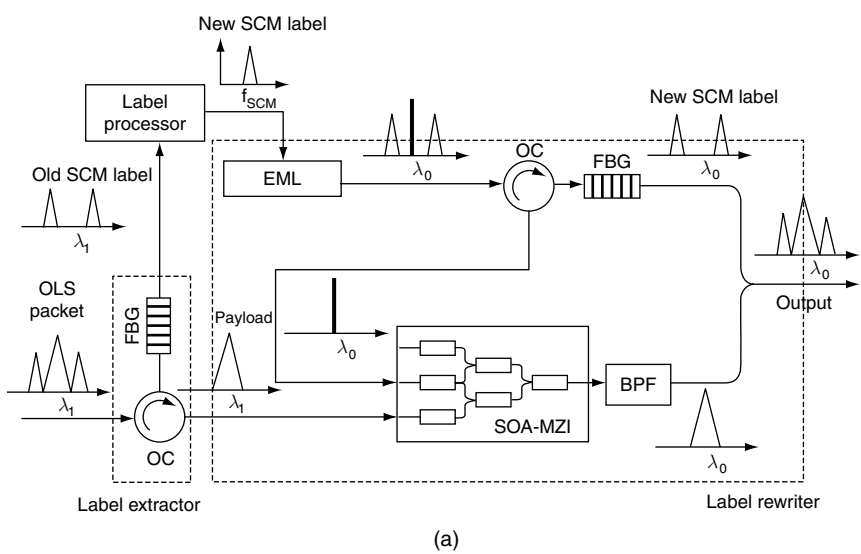

Figure 16.11 Subcarrier multiplex optical header technique involving (a) double sideband label with baseband data payload with a compact integrated electro absorption modulator laser (courtesy of [81]), and (b) carrier suppressed subcarrier multiplexing with label and data signals occupying each sideband (courtesy of [65, 82]).

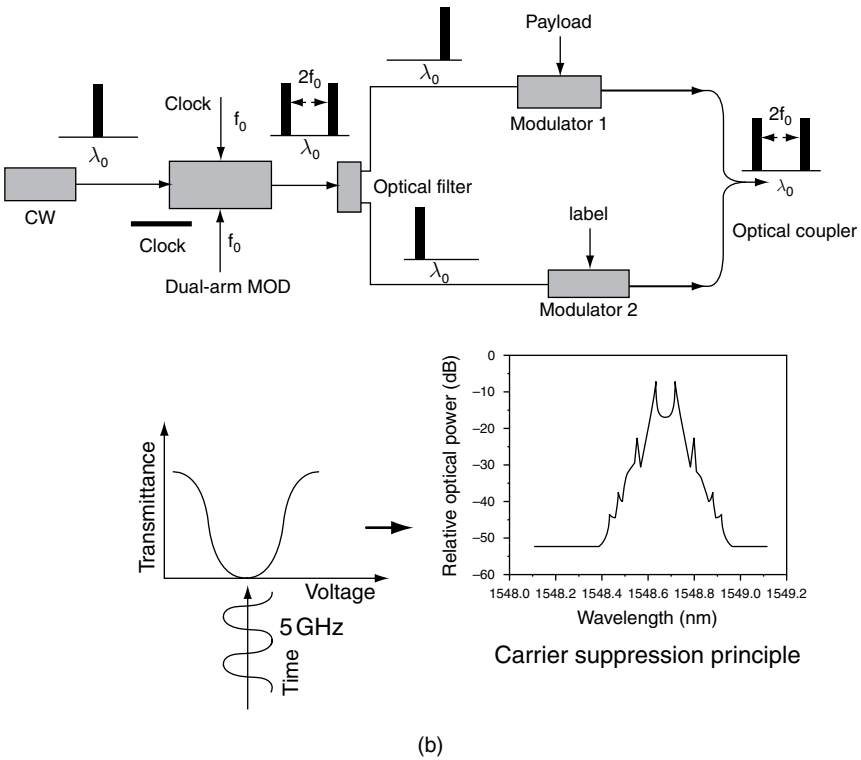

Figure 16.11 Continued.

operation [90], polarization and dispersion independent fiber transmission [61], and the first field trial across 477 km have been demonstrated [91] using the double-sideband optical header technique.

Wavelength Multiplexing Header Technique The wavelength-multiplexed header methods support extremely simple all-optical header extraction and replacement processes. The optical header takes a separate wavelength [66] or multiple wavelength channels [92] to carry information pertaining to the data packets, similarly to the DCC (typically at 1510 nm or at 1310 nm) used for the network control and management system in WDM networks. The accuracy of the relative timing between the header and the data is affected by the relative accumulated dispersion between the data communications channel (header) and the data channel (data payload). A 100 km internode distance causes a timing drift of 0.4 μs between the header at 1310 nm and the payload at 1550 nm due to dispersion of a standard single-mode fiber (dispersion coefficient at 17 ps/nm/km). This may be acceptable for OBS but is too large for OPS. In addition, this method requires an additional wavelength(s) for the headers to carry relatively low bandwidth

information, and the headers may contend with each other to indicate control information of multiple payloads when they are present at the same time.

Orthogonal Modulation Header Technique One of the most innovative optical header technologies maps, the header and the data information modulated in orthogonal modulation formats (e.g., in amplitude and phase domains) [73, 75, 76, 93 98]. It is also possible to place two levels of labels [93] in phase and wavelength domains, while keeping the data in the amplitude domain. Demonstrated techniques involve on-off keying intensity-modulated (OOK-IM) data payloads with frequency-shifted keying (FSK) headers [94] as well as 2.5 Gb/s OOK-IM headers with 40 Gb/s RZ-DPSK data payloads [76]. Reference [73] demonstrated a header (label) replacement technique involving SOAs, electro-absorption modulators (EAM), and highly-nonlinear-fiber (HNLF) for 10 Gb/s IM data payloads and two-level optical header (labels) at 2.5 Gb/s DPSK and the wavelength domain. In both cases (ASK labels and FSK/PSK labels), there are trade-offs between crosstalk vs extinction ratios in the two orthogonal domains. Isolating crosstalk in real optical systems become often difficult since the two domains are coupled with each other due to, for example, unintended frequency chirping during amplitude modulations and vice versa. Reference [74] uses integrated EAM distributed feedback (DFB) lasers for FSK label modulation, where offsetting amplitude modulations applied to the EAM cancels the unintentional amplitude modulation induced during the FSK label modulation. Additional orthogonal modulation schemes include polarization modulations [79, 99, 100], wavelength shifted keying for pulse position modulation [101], and embedded DPSK label in ASK data payload [102].

Figure 16.12 shows the experimental setup involving 156 Mb/s FSK header and 10 Gb/s IM data payload. The optical 156 Mb/s FSK-modulated signal is obtained by directly modulating the electrical current of an integrated EAM-DFB laser. The optical FSK-modulated signal, with a tone spacing of 20 GHz, is then fed into an optical Mach Zehnder intensity modulator operating at 10 Gb/s, resulting in a combined FSK and intensity modulation format. The extinction ratio of the intensity modulation is adjusted to 6 dB to allow both the FSK and the intensity modulation detection. In the core router, the new FSK header signal is generated by modulating the phase current of the grating-assisted codirectional coupler with sampled rear reflector (GCSR) laser. Figure 16.12 inset (a) shows the optical spectrum at the output of the SOA-MZI wavelength converter which achieves wavelength conversion with label swapping, with clear label and payload eye diagrams in Figure 16.12 inset (b).

Optical Code based Optical Header Technique Optical code division multiple access (O-CDMA) networking uses optical codes instead of optical wavelength or time slot channels for networking. The optical code is typically a combination of wavelength and time domain attributes. The same encoding and decoding method for O-CDMA networking can be used for optical header encoding and decoding in OPS networks, where a set of optical codes can represent optical

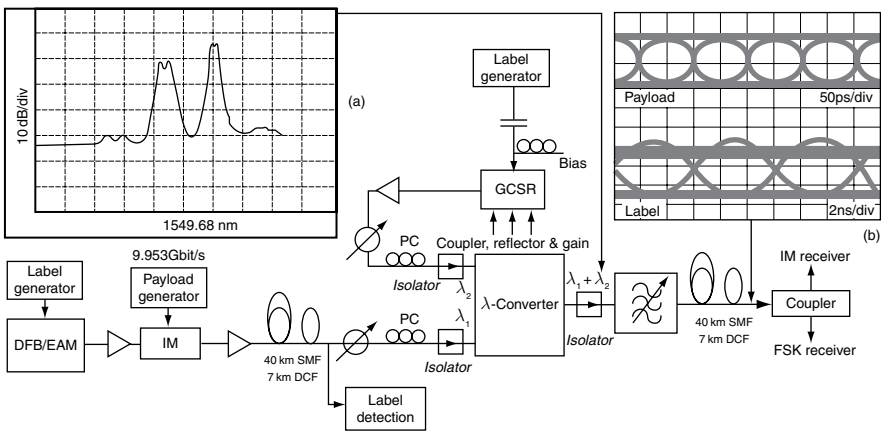

Figure 16.12 Experimental setup for frequency shifted keying/intensity modulated (FSK/IM) label generation, and label swapping in a single semiconductor optical amplifier/Mach Zehnder interferometer (SOA MZI) wavelength converter. (a) Optical spectrum at the output of the SOA MZI with 4 nm span. (b) Eye diagrams of the 10 Gb/s IM payload (top). (Courtesy of [75]).

header contents and the decoders with matching optical codes can identify optical headers that match the look-up table content [68, 103, 67, 69 71]. Since this all-optical correlation technique consumes far less time in identifying a match than electronic forwarding table look-up, the O-CDMA header can help reduce the latency in the OPS router at the expense of requiring multiple O-CDMA decoder optical circuits in parallel. Initial O-CDMA header encoding/decoding utilized FBGs in parallel [68], and later utilized very compact AWGs with multiple ports for multiple header recognitions in parallel [71]. References [104, 69] utilized 160 Gb/s OTDM data payload on eight wavelengths with O-CDMA headers to demonstrate 1.28 Tb/sec variable length OPS. Figure 16.13 [103] shows the spectrum and time domain traces of the header where the matched header shows sharp and strong correlations for the matched header using the O-CDMA technique. The unmatched optical header will have an unnoticeably low peak optical intensity value, although the total integrated pulse energy levels are identical in both matched and unmatched cases.

All-Optical Header and Packet Processing

In addition to header replacement and packet forwarding, a number of innovative research activities are leading to novel all-optical header processing. Reference [105] demonstrated reconfigurable optical header recognition via time-to-wavelength mapping in SOA and tunable correlation decoding in two FBG arrays, Ref. [106] realized an optical TTL decrementing module incorporating two difference-frequency generators, and Ref. [107 109] experimented on all-optical performance monitoring and selective packet dropping by monitoring the error of

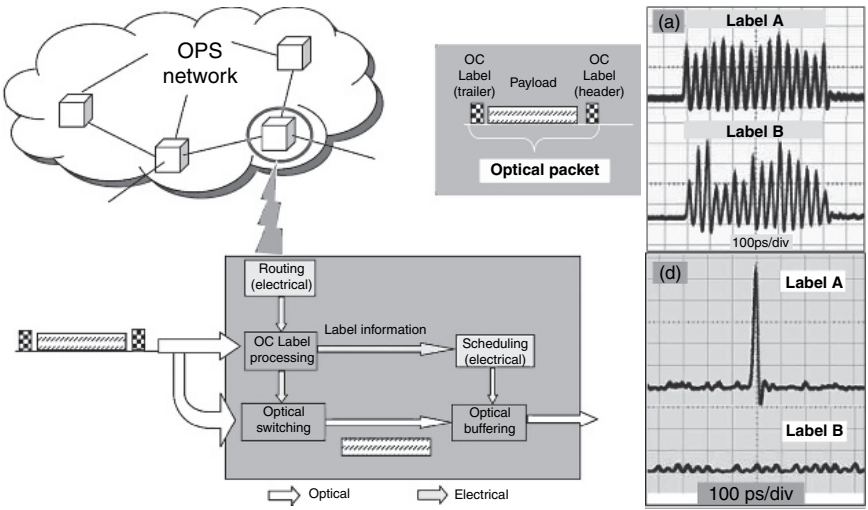

Figure 16.13 Optical code label based optical packet switching (OPS) networks, and waveforms of (a) encoded label A and label B, (d) correlations of label A and label B with SSFBG decoder. (Courtesy of [103]).

the optical header field to infer the error of the data payload. Moreover, recently developed all-optical flip-flop [110] and optical logic gate [111] technologies are likely to find new applications in all-optical header processing in OPS systems.

Optical Packet Synchronizer/Time Switch/Optical Buffers

In synchronous OPS systems, it is necessary to synchronize the packets before they are switched in the switching fabric. Even for asynchronous and variable-length OPS systems, studies in Refs [112, 113] showed the benefit of synchronization. Since there is no viable optical RAM technology available today, typical optical synchronizers involve a number of modules providing fixed amount of time delays placed in parallel or in series with each other. Each module is typically a combination of an optical FDL and an optical switch so that switching to this module will provide a predetermined amount of time delay. If there are N levels of granularity in the time delay in a switching fabric containing K number of ports and W number of wavelengths, the OPS system requires a total of $N \times K \times W$ synchronizing modules with FDLs and optical switches. For typical (large) N values, the synchronization stage can be even more complex than the optical switching fabric itself. Shared buffer and loop back buffer architectures can greatly reduce this complexity.

The CORD project [114] employed optical delay lines with 2×2 switches to achieve contention resolution in the time domain. Figure 16.14 shows a design from Ref. [115] employing SOA gates (SOAGs) and optical FDLs in parallel ($N = 8$). However, this stage is preceded by a tunable wavelength converter ($m = 8$) and is followed by another stage of FDLs with a DEMUX and a MUX

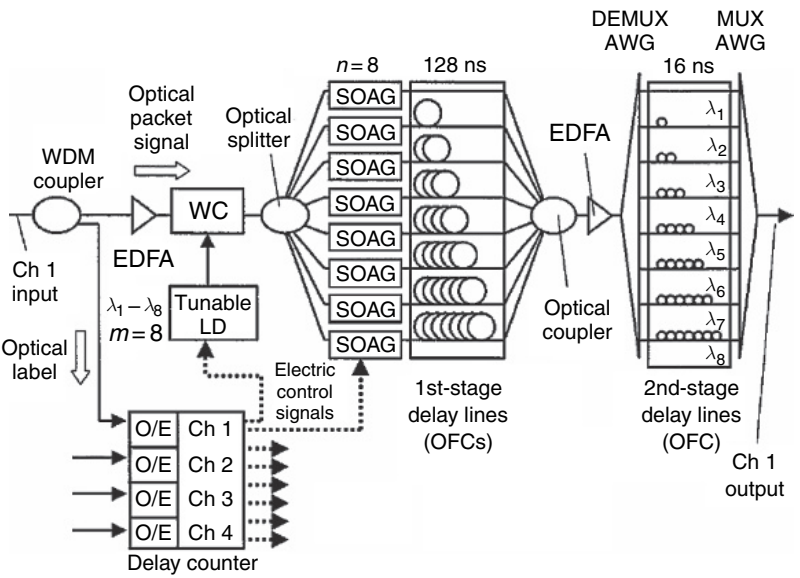

Figure 16.14 Optical packet synchronizer: T_d, delay of input packets with respect to reference time; WC, wavelength converter; SOAG, semiconductor optical amplifier gate; OFC, optical fiber circuit. (Courtesy of [115]).

to achieve synchronization with a time resolution of 16 ns with 64 optical path choices ($N \times m$), each with a different length.

The KEOPS project also utilized a combination of parallel optical modules in multiple serial stages [80]. Figure 16.15 shows the schematic. As in the previous case, SOAGs compensate for the splitting losses. The synchronizer is composed of

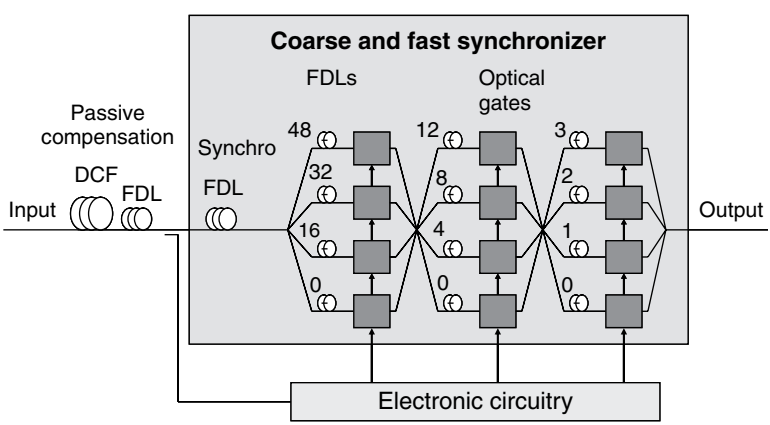

Figure 16.15 Structure of the all optical synchronizer. (Courtesy of [80]).

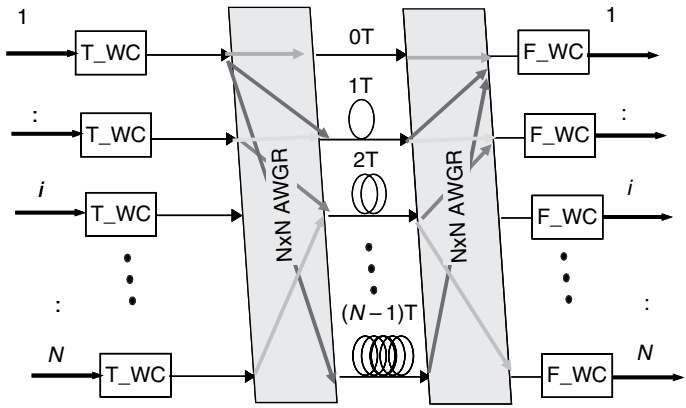

Figure 16.16 Wavelength routing $N \times N$ optical synchronizer. (Courtesy of [116, 117]) (this figure may be seen in color on the included CD ROM).

a number of stages including passive couplers and optically gated calibrated FDLs. The delays are taken to be some multiple of the synchronizer resolution. The maximum delay should be higher than the maximum expected fluctuations, and will impact the number of stages to be added. The KEOPS design achieves a resolution of about 3.2 ns by implementing three stages of four delay lines.

Reference [116] made a theoretical proposal for a wavelength-routed shared optical buffer stage including traveling delay lines with delay-line loops. The design was for time-slotted, fixed-length packet switching. Reference [117] has experimentally demonstrated the applicability of the wavelength-routed optical buffer architecture as a time-slot interchanger to be used in a synchronous OPS networks, as well as a synchronizer for both variable and fixed-length OPS networks. Figure 16.16 shows the architecture used for an experimental demonstration.

Synchronizer architectures must carefully consider packet contention rising from the head of the packet colliding with the tail part of the same packet itself, or other contention cases where multiple packets collide into each other at the output port. The architecture of the synchronizer can limit its applicability to fixed-length packet switching because of the contention. Wavelength conversion in the synchronizer can resolve such contending cases. Loopback FDLs, which allow packets to recirculate back to the input of the synchronization stage, can enhance the limited optical buffering and synchronization capabilities. Synchronization stages precede switching stage(s) to achieve OPS with lower packet contention probabilities. Figure 16.17 shows an OPS switching fabric with a wavelength-routing packet synchronizer of Figure 16.16 combined with a wavelength-routing switching fabric of Ref. [36] described in Figure 16.21 in the next section. Reference [112] provides detailed performance analyses and simulations of this two-stage architecture for asynchronous variable-length OPS. More than one order of magnitude packet loss rate reduction and throughput increase can be achieved in the switching fabric by including the optical synchronizer [112].

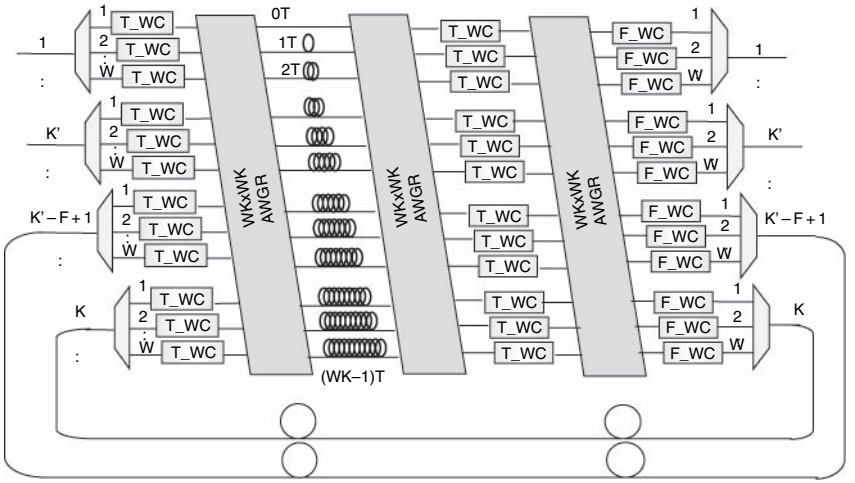

Figure 16.17 A schematic of a two stage optical switch architecture. (Courtesy of [112]) (this figure may be seen in color on the included CD ROM).

There ultimate packet synchronization and optical buffering could perhaps be achieved by utilizing the slow-light effect. It is known that light can be slowed down in dispersive materials near resonances [118]. Dramatic reduction of the light group velocity has been demonstrated recently in various atomic [119 121] and solid state systems [122 129]. Many of these technologies utilize the material resonance with the optical wave, and must operate within a narrow frequency range determined by the material resonance and at a low temperature in order to achieve sharp material resonance. Brillouin, Raman, and four-wave mixing (FWM) effects in fiber can offer room temperature operation at a tunable operating wavelength determined by the pump wavelength. Hole-burning in SOAs and vertical cavity surface emitting lasers (VCSELs) can also provide slow-light effect near the pump wavelength in a more compact geometry. References [127, 128, 130] experimentally demonstrate slow-light effects in a low-loss submicron silicon photonic crystal waveguide with controlled variable time delay in a very compact, room temperature operation without requiring an external pump wave. A future photonic crystal structure utilizing electro-optical material (e.g., GaAs, InP, $LiNbO_3$), switching of slow-light effects in less than a nanosecond time scale, is possible if a traveling wave configuration is adopted [131]. References [132 134] discuss fundamental limits and figure-of-merit of the slow-light buffers, and Chapter 13 examines practical aspects of the currently available slow-light buffers in the context of a conventional store-and-forward router architecture, in which each packet needs to be buffered, segmented, and forwarded at the input buffer before reassembled at the output buffer. Such an architecture requires relatively large buffers, whereas even the best slow-light optical buffer experimentally demonstrated so far cannot store more than several bits; hence as

Chapter 13 concludes, the current slow-light buffering technologies are not practical in conventional store-and-forward optical router architectures.

In contrast, a number of recent works [1, 2, 23, 135 139, 140] indicated the utility of wavelength conversion in OPS systems, and [2, 3, 23, 140, 141] utilized pipelined wavelength, time, and space domain contention resolution to avoid buffering each packet, resulting in an OPS router with essentially no buffers. An OPS system utilizing wavelength, time, and space domain contention resolution [113] showed that only a small amount of variable optical buffer (∼200 bytes) can provide a significant boost in the OPS network performance (∼100 times lower packet loss rate) [112, 131, 142]. The architecture in [112, 113, 131, 142 144] utilizes slow-light variable optical buffers to avoid head-of-line blocking and achieves significant network performance improvement in variable-length asynchronous OPS routers with wavelength-time-space contention resolution.

Another argument on reduced optical buffering can be found from statistical multiplexing of Transmission Control Protocol (TCP) flows. Ninety-five percent of the traffic today is on TCP, and TCP's congestion control algorithm determines the size of the buffer. The rule of thumb is that each link needs a buffer of size equivalent to the product of the average round-trip time and the data rate of the link. For OPS systems in core networks, both the round-trip time and the data rate can be extremely high, and the required buffer size can be extremely large. Recent studies [145 149] at Stanford University and at University College of London have indicated that core routers with a large number N of TCP flows will require square root of N times smaller buffers as dictated by the rule of thumb. Since N can be typically on the order of 10,000, the required buffer can be 100 times smaller. This corresponds to the 320 MByte memory requirement reducing to 3.2 MByte for a typical 10 Gb/s linecard. However, the counterpoint [150] argued unpredictability, high packet loss rates, and lower throughput would prevail in such a router during large TCP transfers. More importantly, the above analyses and simulations are conducted based on a single-channel packet switching system, using a store-and-forward router architecture, without wavelength domain contention resolution capability. Active research is in progress to investigate the impact of bufferless and reduced buffer OPS systems, possibly with pipelined (cut-through with no store-and-forward) router architecture [113, 131].

Optical Switching Technology for OPS

Section 16.2 briefly covered optical switching technologies for OBS. This section will discuss the switching fabric technologies for OPS systems. Since optical packets are considered to be much shorter in duration than optical bursts, OPS systems require rapid switching, typically on a nanosecond time scale. This is especially important because the OPS system does not have a viable optical RAM technology today. In an electronic router, the store-and-forward process allows a switching fabric to switch more slowly than the bit time without losing a bit in a packet. In an optical router without optical buffering, slow switching can cause loss of bits in a packet during the

switching transition, unless there is enough time gap between the packets to accommodate the switching transition. This gap, called "guard time," must be longer than the switching time of the slowest packet switch in the path, and must provide room for any additional uncertainty in timing. Hence, efficient OPS networking requires fast switching and accurate timing in all OPS systems in the network.

In addition, OPS systems should be scalable to support many wavelengths and ports. For instance, the number of switching elements (control points) increases as N^2 in an $N \times N$ crosspoint switch, where N is a product of the number of ports K and the number of wavelengths W. Even a larger number of control points are necessary for a dilated switch fabric. Hence, even with a switching fabric containing nanosecond switching devices, the OPS system may switch significantly slower due to control signal interfaces. Likewise, the complexity in packet contention resolution and arbitration quickly rises as the number of ports and wavelengths increases. OPS can significantly benefit from a switching fabric whose switching elements and control points scale linearly rather than hyperlinearly (e.g., $\sim N^2$, or $\sim N^*\log N$), and whose switching architecture readily adopts hierarchical contention resolution and arbitration. Reference [113] discusses a novel hierarchical contention resolution and arbitration in wavelength-time-space domains applied to asynchronous and variable-length packet switching.

Space Switching The KEOPS project [80] investigated a wavelength-routing switch utilizing tunable wavelength converters and a broadcast-and-select switching fabric consisting of SOA gates. Figure 16.18 shows the switching fabric, composed of the following three main blocks [80].

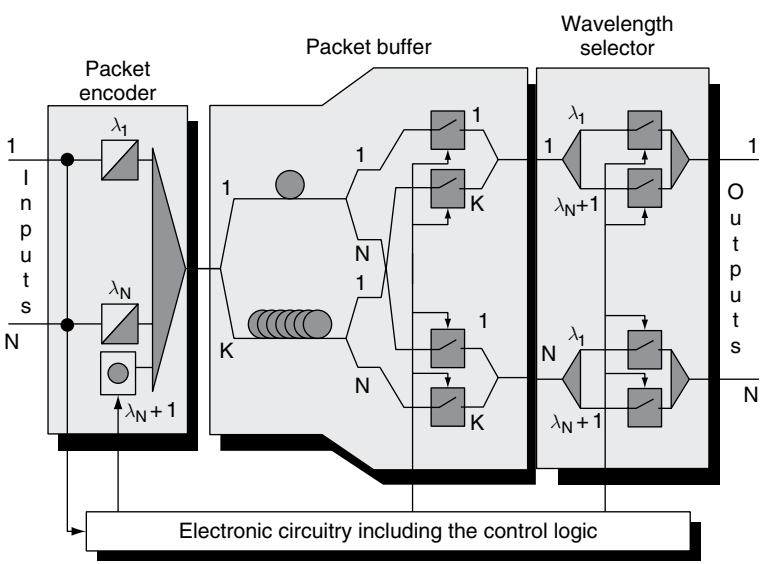

Figure 16.18 Structure of the broadcast and select switch. (Courtesy of [80]).

- A wavelength encoding block, which consists of a set of all-optical wavelength converters (AOWCs) based on cross-gain-modulation in SOAs, one per input and each being assigned a fixed output wavelength;
- A buffering and time switching block which includes FDLs and a space switch built up with SOA gates;
- A wavelength selection block based on a set of wavelength selectors (WS).

In this switching fabric, each incoming packet is assigned to one wavelength for identifying its input port, and then is fed into the packet buffer shared between all wavelengths according to the output queuing principle. All packets are broadcast to experience all possible delays achievable. For each output port and time slot, optical gates within the buffer and within the wavelength demultiplexer select the input port (represented by the wavelength) and the proper delay (FDL). While the switching fabric loses a large fraction of optical power in this broadcast-and-select scenario, the SOA gates compensate for the power loss. The sub-blocks rely mostly on the SOA technology, which is capable of high-speed optical processing including optical gating, wavelength selection, and regenerative wavelength conversion. SOAs achieve subnanosecond optical gating and adopt gain-clamped structures to avoid the cross-saturation effects when multiwavelengths are used. Wavelength conversion may be achieved using the cross-gain-modulation effect in SOAs. SOA-MZIs exploit their nonlinear transfer functions to provide amplitude reshaping properties at high bit rates (up to $\sim$40 Gb/s). In addition to the switching matrix, the KEOPS system included the input interface, defined as a "coarse-and-fast" synchronizer that aligns the incoming packets in real time according to a delineation process of the payload, and an output interface that regenerates the data streams. Fast power equalizers reduce packet-by-packet power nonuniformity. An optical "3R" structure regenerates the payload in both amplitude and time domains. Reference [80] discusses 40 cascaded hop OPS using a broadcast-and-select switch fabric with optical 3R regeneration.

Optical crosspoint switches (OXSs) are analogous to electronic crosspoint switches (EXSs) in providing $N \times N$ space switching using N^2 switching elements at the crosspoints. Reference [40] utilized SOA gates whereas Refs [41, 151] employed active vertical couplers (AVCs) (SOA with vertical coupling) at the crosspoints. Figure 16.19 shows the latter at a crosspoint, where two AVCs are formed between the passive waveguide and an upper layer of the active waveguide (dark shade). A total internal reflection (TIR) mirror vertically penetrates the active waveguide layer with an angle of 45° with respect to the two couplers directions. This deflects the optical signal from the input AVC to the output AVC. The crosspoint switches exhibit switching-state-dependent losses; however, the SOA allows compensation of the optical losses to possibly achieve uniform losses. In practice, this is difficult since the power level needs to be equalized at the output for many different switching paths, and the number of control points increases as N^2.

Figure 16.20 shows the experimentally measured gated BER performance of switching units along the diagonal of the matrix (paths D1, C2, B3, and A4) with

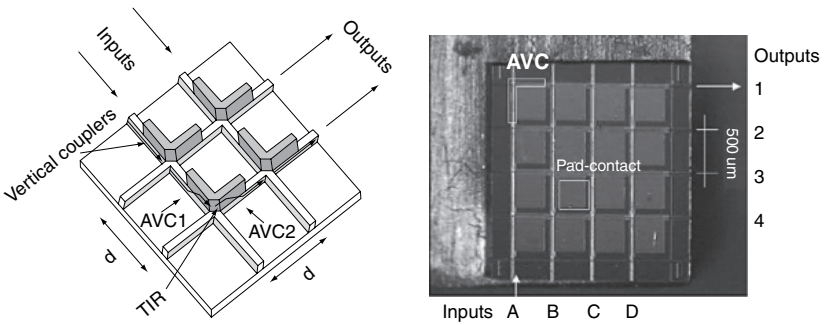

Figure 16.19 Optical crosspoint switch based on SOA based active vertical couplers. (Courtesy of Ref. [41]).

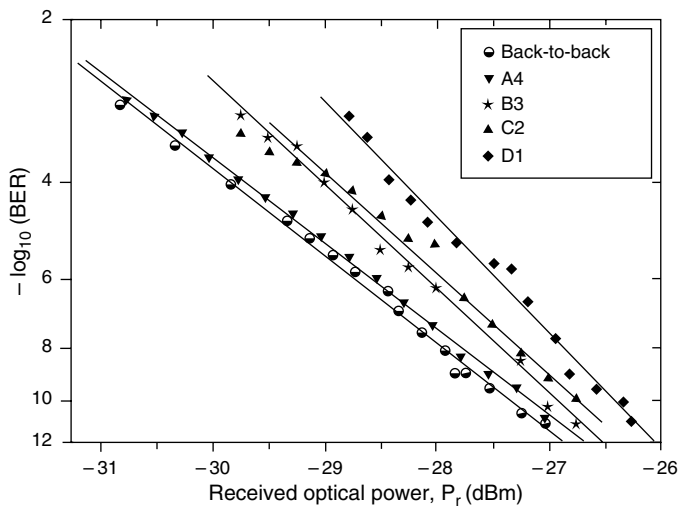

Figure 16.20 Gated mode BER performances of switching units on the diagonal [41].

error-free performance [41]. BER with power penalties of less than 1 dB are observed for all diagonal switch cells, with larger penalties for longer paths as expected due to the existence of residual path-dependent losses.

Wavelength-Routing Switching Fabric A wavelength-routing switching fabric involving tunable wavelength converters and wavelength routers provides an effective and scalable method of realizing a switching fabric with wavelength and space switching. Figure 16.21 shows the wavelength-routing optical switching architecture utilizing tunable wavelength converters (T WCs), fixed wavelength converters (F WCs), AWG routers (AWGRs), and recirculating FDLs [36]. It includes $KW \times KW$ AWGR with F shared recirculating FDLs.

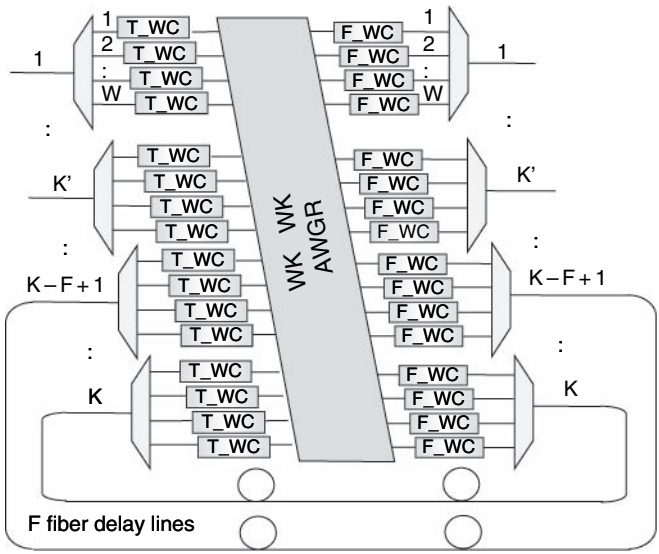

Figure 16.21 The wavelength routing optical switching architecture utilizing tunable wavelength converters (T WCs), fixed wavelength converters (F WCs), arrayed waveguide grating routers (AWGRs), and recirculating fiber delay lines [36] (this figure may be seen in color on the included CD ROM).

Similar architectures have also been discussed in WASPNet architectures [152], NTT's local area network architectures [153], loopback cross-connect architectures [154], IRIS [155], LASOR projects [156], and OPSnet demonstrations [37, 38]. In Ref. [36], the T WC consisted of a tunable superstructure grating distributed Bragg reflector (SSG-DBR) laser and a SOA-MZI wavelength converter. The F WC architecture was identical to T WC architecture except for using a fixed wavelength DFB laser. The SOA-MZIs provide 2R optical regeneration capability, which helped obtain 11 hop cascaded operation in Ref. [90]. In Refs [157] and [80], SOA-MZIs with all-optical clock recovery for 3R regeneration were utilized for 101 hop and 40 hop cascaded operations, respectively. In Refs [37, 38], FWM wavelength conversion in SOAs were used in the T WC in order to support DPSK/ASK optical header/data formats. For tunable lasers in the T WC, SSG-DBR lasers as well as sampled grating-DBR (SG-DBR) lasers [158] have been utilized to tune over a broad (>60 nm) spectral range in a relatively short amount of time ($\sim$nanosecond) limited by the carrier dynamics in the DBR region. Figure 16.22 illustrates the (a) SG-DBR laser, (b) SSG-DBR laser, and (c) tunable output wavelength spectrum from a SSG-DBR laser. In Ref. [36], the AWGR with cyclic and uniform loss properties [159] were used to provide uniform optical power at the F WC where all-optical regeneration and conversion to a fixed wavelength take place. This uniformity is extremely important in achieving optical regeneration for all possible $N \times N$ switching states.

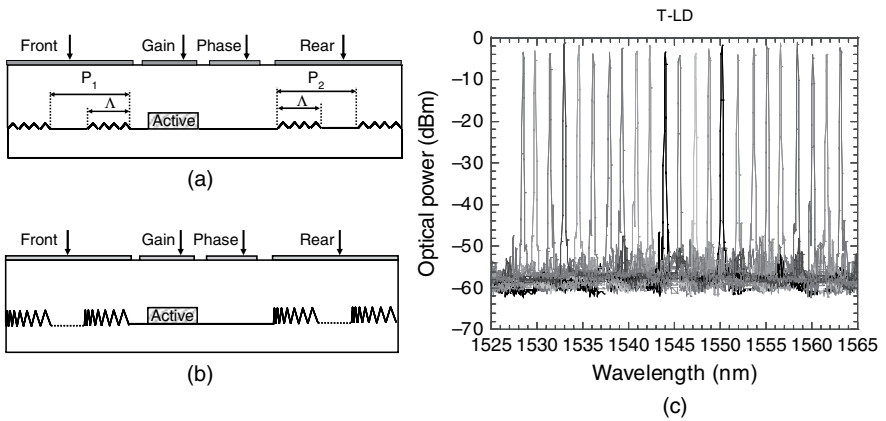

Figure 16.22 Monolithic tunable lasers capable of switching at nanosecond time scales based on (a) sampled grating DBR (SG DBR) lasers, (b) superstructure grating distributed Bragg reflector (SSG DBR) lasers, and (c) tunable output wavelength spectrum from a SSG DBR laser (this figure may be seen in color on the included CD ROM).

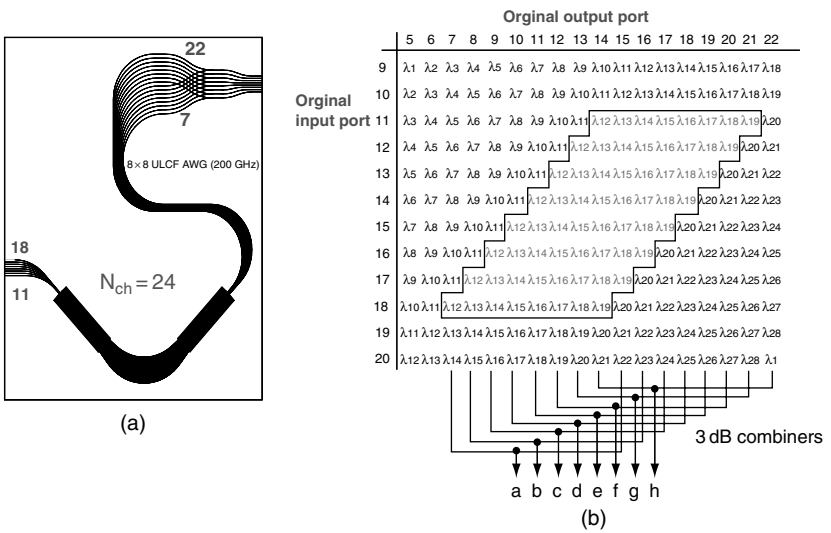

Figure 16.23 $N \times N$ uniform loss cyclic frequency arrayed waveguide grating router (a) layout and (b) the routing table (N 8 case). (Courtesy of Ref. [159]) (this figure may be seen in color on the included CD ROM).

Figure 16.23 shows the $N \times N$ uniform loss cyclic frequency AWGR (ULCF-AWGR) (a) layout and (b) the routing table for $N = 8$ case [159]. Figure 16.24 shows the measured transmission spectra of $N \times N$ ULCF-AWGR ($N = 32$ case), indicating less than ±0.5 dB nonuniformity in transmission from any N input port.

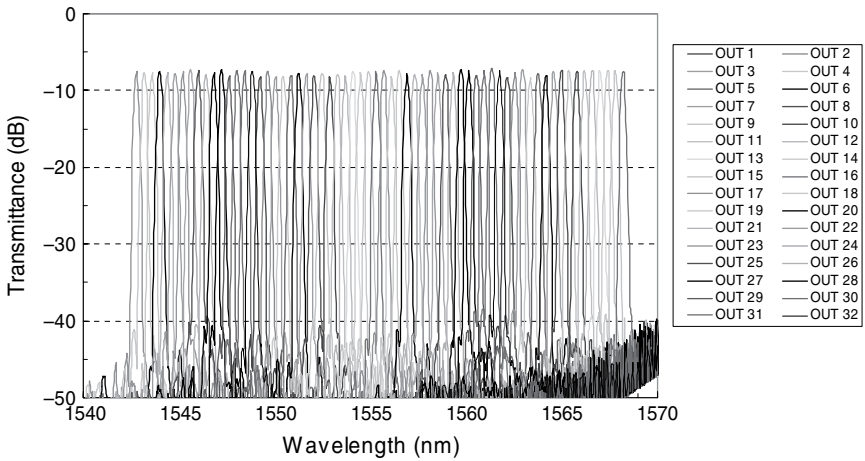

Figure 16.24 Measured transmission spectra of $N \times N$ uniform loss cyclic frequency arrayed waveguide grating router (N 32 case) (this figure may be seen in color on the included CD ROM).

The switching fabric configuration in Figure 16.21 with W wavelength channels, K fiber ports, and F loopback fibers is capable of achieving switching and contention resolution in wavelength, time, and space domains, by only tuning the wavelengths in the T WCs. Unlike other switching fabric architectures which require $O(N^2)$ or $O(N \log N)$, it requires only N number of elements to control to achieve $N \times N$ switching. Scalability beyond $N \times N$ using a $N \times N$ AWGR can be achieved if each input port on AWGR can accommodate N number of T WCs so long as each of them gives a distinct output wavelength. Therefore, a $N \times N$ AWGR can support a switching fabric of $N^2 \times N^2$ connectvity. For a 256×256 AWGR with 25 GHz channel spacing, this would correspond to 65536×65536 connectivity. Even greater scalability is possible by stacking multiple AWGRs and providing limited wavelength conversion in the architecture, to provide 42 petabit/sec switching capacity in a single OPS switching fabric with 32 layers of 256×256 AWGRs.

Reference [37] utilized a similar switching fabric architecture with FWM-based wavelength converters in T WC stages at the front and rear of the AWGR to achieve excellent 40 Gb/s packet switching results. Figure 16.25 shows the experimental result using phase-modulated (PM) header bits and IM data payload [37]. Filtering of the strong pump and nonconjugate signals after FWM is a challenge, but the demonstrated system applies very effective filtering schemes.

16.3.3 TDM Optical Packet Switching Technologies

As mentioned at the beginning of this section, the concept of OCS, OBS, and OPS networking can exploit TDM, WDM, and OCDM techniques. A great deal of

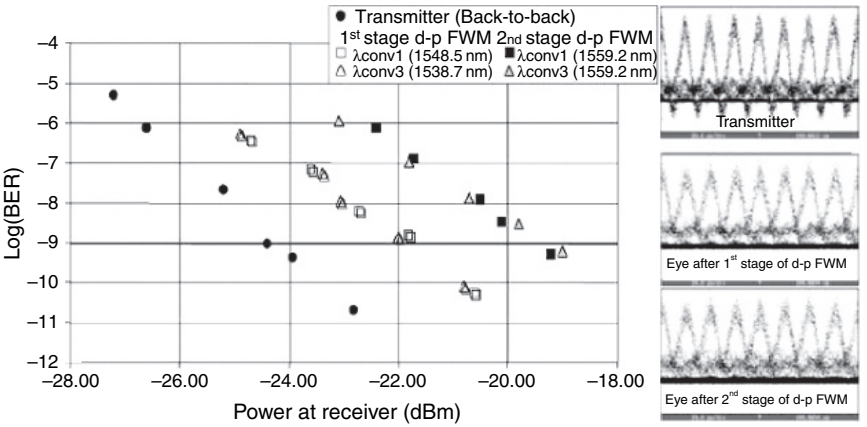

Figure 16.25 Packet BER measurements and eye diagrams from optical packet switching (OPS) experiments utilizing four wave mixing (FWM) based wavelength converters, tunable lasers, and AWGRs. (Courtesy of Ref. [37]).

recent research in optical networks has been focused in the area of WDM OPS. In comparison, TDM- and CDM-based OPS research is much less active, primarily due to difficulties in developing ultrafast demultiplexing and processing devices for optical TDM or optical CDM technologies. Princeton researchers have demonstrated [160] 100 Gb/s TDM OPS technologies based on the terahertz optical asymmetric demultiplexer (TOAD) [160]. The TOAD is a nonlinear interferometer based on a nonlinear loop mirror containing a SOA placed asymmetrically inside the fiber loop. Effectively, the clock pulse can open a "switching window" in time for which the incoming data stream will be transmitted. TDM header processing requires time domain switches that can rapidly switch the header and the payload. Bintjas et al. [57] utilized an ultrafast nonlinear interferometer (UNI) [161, 162] gate and a Fabry Pérot filter to extract a packet clock and a second UNI gate to separate the header and the payload both at 10.3 Gb/s.

16.3.4 Hybrid (Optical-Electrical) Packet Switching Using CMOS Random Access Memory/Switch

A very interesting OPS approach [43 47] is to use electronic CMOS technologies and high-speed "serial-to-parallel" converter (SPC) and "parallel-to-serial" converter (PSC) technologies to combine the dexterity of electronics with the high capacity of optics. This approach was used in three functional blocks of the OPS system [30], namely (1) the opto-electronic hybrid RAM, (2) the opto-electronic switching fabric, and (3) the opto-electronic header (label) swapping. Each functional block combines an optical SPC, a CMOS circuit, an optical PSC, an optical clock generator (OCG), and an electrical clock generator (ECG) [43 47].

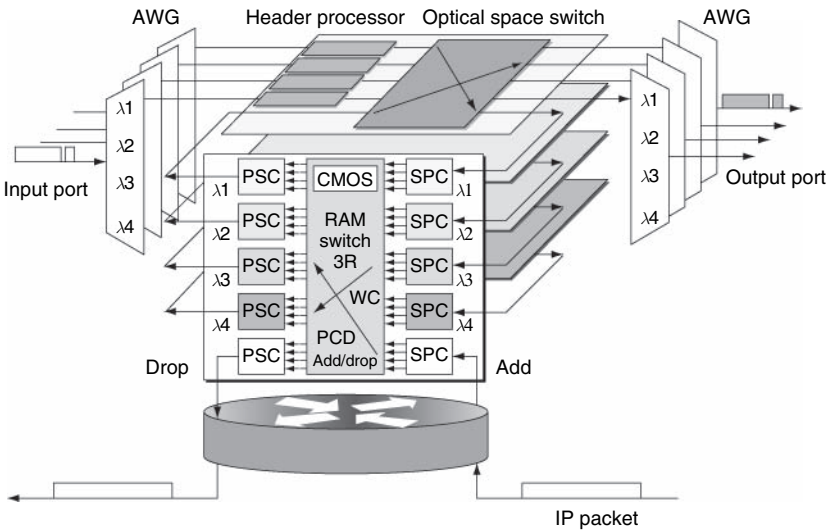

Figure 16.26 Optical packet switching fabric architecture involving CMOS RAM switching in a shared loopback configuration. (Courtesy of Ref. [43]) (this figure may be seen in color on the included CD ROM).

Figure 16.26 shows the OPS switching fabric containing a standard wavelength-selective space switch architecture and a shared opto-electronic CMOS RAM with SPC and PSC for time-buffering-based contention resolution. CMOS RAM also conducts wavelength conversion and 3R signal regeneration. The required CMOS RAM size for this operation is relatively large, especially at high line rates; however, the flexibility offered by the CMOS is very attractive. The key to this technology is an all-optical SPC and PSC. Figure 16.27 shows (a) the schematic and

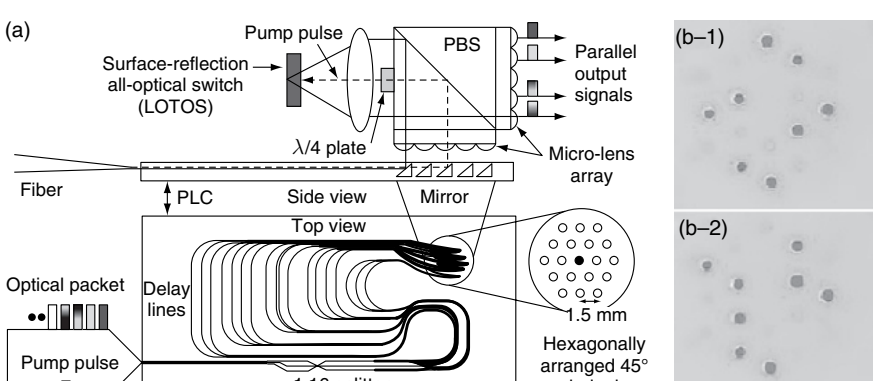

Figure 16.27 (a) All optical, serial to parallel converter. (b) Camera images of parallel output optical signals for input packets (1) 1001011011010010 and (2) 1000111001110001. (Courtesy of Ref. [43]) (this figure may be seen in color on the included CD ROM).

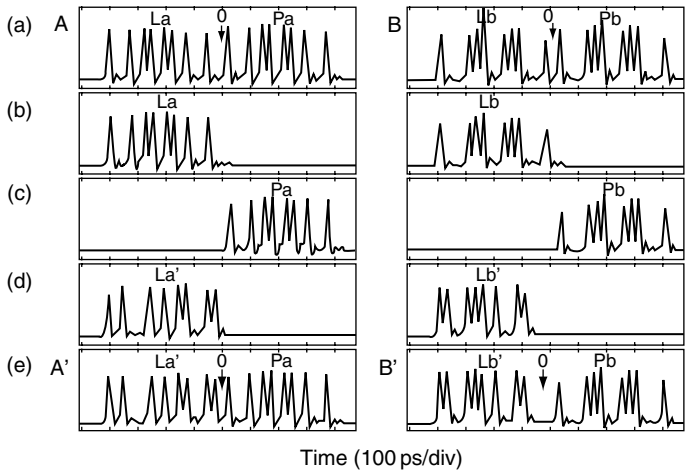

Figure 16.28 (a) Input packets. (b) Separated old labels. (c) Separated payloads. (d) Generated new labels. (e) Output packets with new labels. (0 is a 1 bit guard band.) (Courtesy of Ref. [41]).

(b) the camera images of SPCs in operation. Here, a very advanced low-temperature grown surface-reflection all-optical switch exploiting spin-polarization interactions in quantum wells has been utilized for high-speed switching. Using similar architectures, optical header swapping and opto-electronic buffer modules including CMOS have been implemented and demonstrated [43]. Both modules contain electrical or optical clock generators (ECG, OCG) to provide synchronization clock signals for asynchronously arriving headers (labels) or payloads. Figure 16.28 shows experimentally obtained results [43]. Figure 16.28(a) shows an input packet stream consisting of two alternating 40 Gbit/s, 33-bit packets at a packet rate of 42 MHz; (b) and (c) show the input label and payload separated by a 600-ps-long electrical pulse generated from the ECG. Figure 16.28(d, e) shows new labels match the forwarding table instructions, confirming successful operation of the SPC, PSC, and label processor [43].

16.4 OLS TECHNOLOGIES

OLS emerged as a vehicle for the next-generation Internet and is currently investigated widely around the world [56, 60, 67, 70, 75, 78, 88, 93, 95, 163 165]. The term "optical-label switching" was first introduced when the DARPA proposal and the patent [1] initially used "optical-tag switching" to describe the new IP-over-WDM Next Generation Internet (NGI) technology, and then DARPA recommended it to be renamed as "optical-label switching." While OLS was designed independently of MPLS and MPLambdaS, its interoperability with MPLS and MPLambdaS implies flexibility in network planning, operations, and

upgrades. This interoperability is facilitated by GMPLS with a newly proposed extension, which introduces OLS specifically to facilitate interoperability between OCS, OBS, and OPS, and to address packet and burst switching capabilities directly at the optical layer. The OLS technology has made notable progress since its birth leading to demonstrations of the OLS router all-optical label swapping and the first field trial of the OLS technology [166]. OLS is used in many different contexts including store-and-forward based OPS using optical labels or JET signaling-based optical burst switching. This section will focus on the OLS system integration based on the pipelined cut-through method architecture [16] in support of interoperability with OBS, OPS, OCS, as well as GMPLS in the future [55].

16.4.1 Unified OCS, OBS, and OPS Platform

The OLS router discussed in this section (1) discards the store-and-forward architecture, (2) adopts parallel optical labeling (utilizing optical SCM), and (3) employs the optical switching fabric based on wavelength routing illustrated in Figure 16.21. These three elements greatly facilitate interoperability between OCS, OBS, and OPS on a single OLS platform, in which the OLS routers can support multiple services on multiple wavelengths and flows at the same time. To support this further, the OLS network adopts four classes of optical label formats that are 40 bits long. Reference [55] discusses the details of the OLS protocol. Class A is a destination-oriented optical label format similar to an IP header containing destination, source, QoS, CoS, ToS, optical-TTL, and experimental bits. Class B is identical to Class A but includes traffic engineering features encoded in the experimental bits. Class C is for label-based forwarding similar to MPLS labels. Class D is for circuit switching label. The Class A, B, and D labels not necessarily require label swapping at each node [55]. Another important aspect of the OLS router is to use a unified and pipelined contention resolution scheme in the wavelength, time, and space domains to facilitate the interoperability of multi-service OPS, OBS, and OCS networking.

Wavelength–Time–Space Domain Contention Resolution, Multicast, and Scalable Networking

OLS core router systems integration included the full control plane with interoperability, so that asynchronous, variable-length packet contention resolution and packet forwarding are possible in wavelength, time, and space domains. Figure 16.29 shows the error-free performance for contention resolution in the three domains [167]. In order to test the scalability of the OLS network, the OLS network test bed was configured to test cascaded stages of the OLS router with all-optical burst-mode 3R regeneration. Figure 16.30 shows the simplified perspective of the OLS router experiment involving looping experiments extending to 101 cascaded router hops [168]. At each hop, the optical data payload undergoes

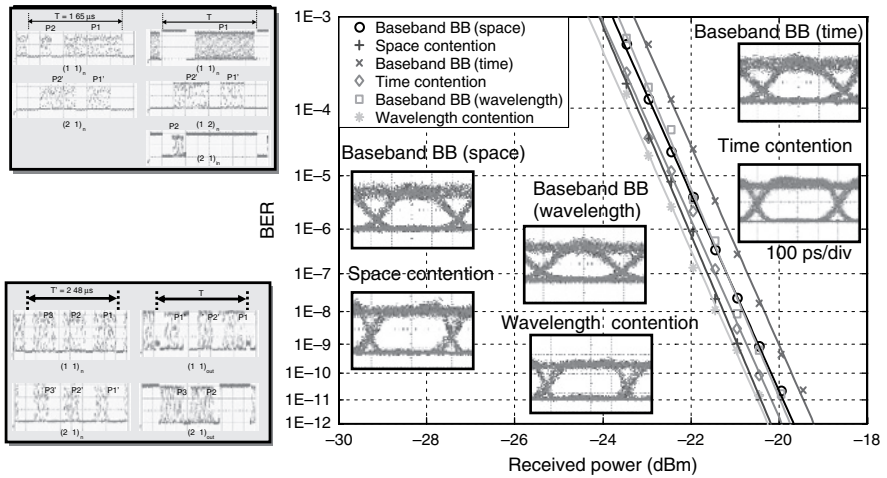

Figure 16.29 Variable length packet switching BER with packet by packet contention resolution in wavelength, time, and space domains. (Courtesy of Ref. [167]) (this figure may be seen in color on the included CD ROM).

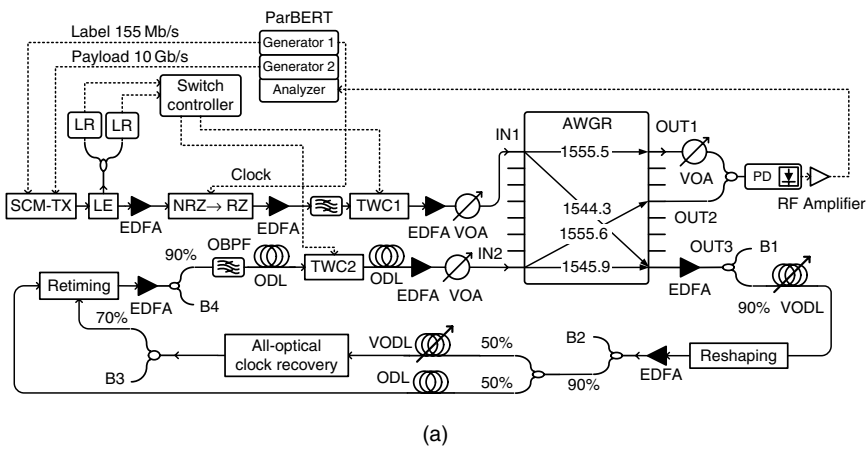

Figure 16.30 (a) Experimental setup for cascaded optical label switching (OLS) routing experiments. (b) Details of the functional blocks in (a). (c), (d) Output packets recorded on digital communication analyzer after cascaded number of hops up to 101. (e) Measured bit error rates up to 101 hops. Here, AWGR: arrayed waveguide grating router; CIR: circulator; DFB: distributed feedback laser; EDFA: erbium doped fiber amplifier; FBG: fiber Bragg grating; FFP: Fabry Perot filter; FWC: fixed wavelength converter; LE: label extractor; LO: local oscillator; LR: label receiver; MZI: Mach Zehnder interferometer; MZM: Mach Zehnder modulator; NRZ: non return to zero; OBPF: optical band pass filter; ODL: optical delay line; ParBERT: parallel bit error rate tester; PC: polarization controller; PD: photo detector; RZ: return to zero; SCM: subcarrier multiplexing; SOA: semiconductor optical amplifier; TLD: tunable laser diode; TWC: tunable wavelength converter; TX: transmitter; VOA: variable optical attenuator; VODL: variable optical delay line. (Courtesy of Ref. [168]) (this figure may be seen in color on the included CD ROM).

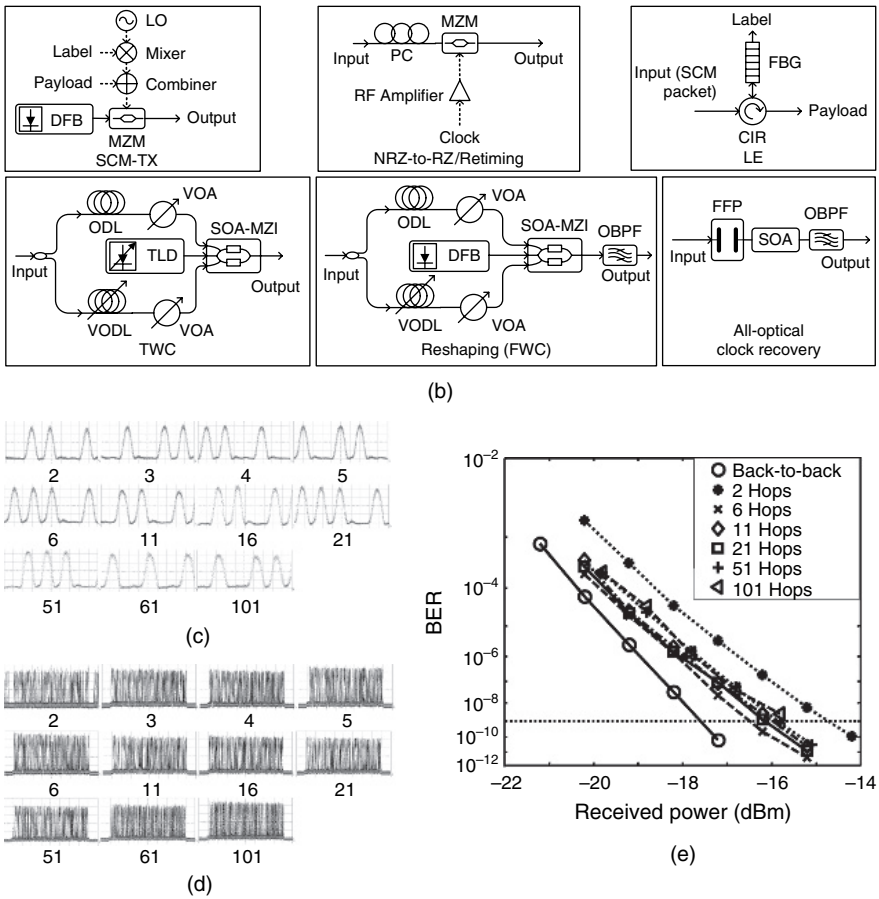

Figure 16.30 Continued.

3R optical regeneration using all-optical burst-mode clock recovery using a fiber Fabry Perot filter (FFP) and a SOA. The FFP extracts the optical clock component from the optical data payload, and the SOA reduces the pattern dependence in the clock [168]. This method provides rapid burst-mode clock recovery in ∼1 ns, and reduces the minimum packet guard time to ∼2 ns [169]. Error-free 101 hop cascaded OLS router operation has been demonstrated using the burst-mode 3R regeneration [168].

In addition to the OLS core router systems integration including the full control plane with interoperability, OLS edge router integration is important for interfacing with clients and for conducting packet and burst aggregation/deaggregation. The OLS edge routers function from layer-1 up to layer-4: the layer-3 and layer-4 processing performs policy-based IP packet forwarding while layer-1 and layer-2

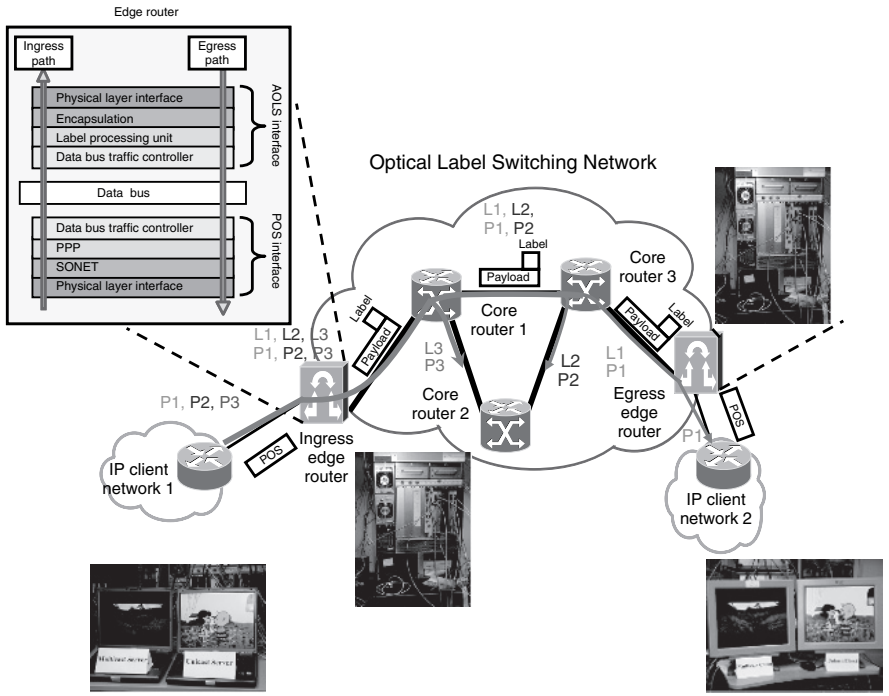

Figure 16.31 Optical label switching (OLS) network test bed with cascaded stages of OLS core routers and ingress and egress OLS edge routers interfacing with IP clients running multicast and unitcast FTP and video stream experiments (this figure may be seen in color on the included CD ROM).

adapt the interfaces to the OLS network. Figure 16.31 illustrates the UC Davis OLS network test bed including OLS core and edge routers. On this test bed a number of experiments have been conducted addressing layer 3 and 4 issues. They included IP-client to IP-client packet transport over cascaded OLS core router [170] and combined multicast and unicast video streaming over OLS router networks [171]. The video streaming traffic starts from the multicast and unicast servers and ends at the Ethernet client networks. The edge router aggregates the traffic from the servers based on the destination address and CoS, attaches an optical label, and forwards it to the OLS core network. The OLS core routers in the OLS network process the labels and make the forwarding decisions. For multicast packets, the OLS core routers utilize wavelength converters with multiple tunable lasers so that multiple copies of the same input packet can be forwarded to desired multiple outputs. The unicast traffic is processed similarly with the multicast traffic, except that each OLS core router forwards it to exactly one downstream link, until it reaches the destination. The OLS edge router features mapping of the CoS attributes to the optical label and intelligently adapts the maximum transport unit (MTU) to dynamically aggregate the packets from the client networks based on the traffic load and the characteristics of the OLS

network. The egress OLS edge routers deaggregate the packets. The unicast and multicast video as well as the background FTP traffic all performed with no noticeable additional errors.

Edge router research and development have made excellent progress around the world [147, 172, 173], allowing interfacing with higher layer applications.

Optical Routers and Integration efforts

As mentioned in Section 16.3.1., today's electronic routers consume relatively large space and power. The state-of-the-art CISCO CRS-1 router with 640 Gb/s capacity (16 slots of 40 Gb/s line cards in one shelf) occupies $213 \times 60 \times 91\,\text{cm}^3$ space, consumes 15.5 kW power, and weighs 751 kg [174]. The multishelf configuration of the CRS-1 router can scale up to 46 Tb/s capacity [1152 slots of 40 Gb/s line cards in 80 shelves (72 line card shelves and 8 fabric shelves)], consumes 0.86 MW power [175]. All-optical label switching routers have the following opportunities for reducing the size and power consumption. The comparison must consider the entire network perspective including both core and edge routers. For instance, the OLS core/edge routers support OLS-based packet forwarding, whereas the CISCO CRS-1 router supports the true IP routing function with deep packet inspection capability.

- Use optical labels running at manageable bit rates (e.g., 155 Mb/s $\sim$1 Gb/s) while keeping high-speed data (e.g., 40 Gb/s) in the all-optical domain so that the optical label switching router will only involve simple electronics in the control plane and transparent optics in the data plane (no high-speed electronics necessary).
- Discard the store-and-forward router architecture and adopt the pipelined router architecture to avoid bit-by-bit buffering and processing of data (no optical RAMs, serial-to-parallel/parallel-to-serial signal processors necessary).
- Migrate from hop-by-hop deep packet inspections and security functions running at high data rates to optical-label-based security, performance monitoring, and network control and management.
- Exploit further integration and optical interconnects without repeated O/E and E/O conversion steps or on-chip/off-chip coupling stages.
- Adopt a fast-core, smart-edge label switching paradigm with OLS core routers and OLS edge routers so that data stays in the all-optical domain in the core while intelligent queuing and packet inspection can take place at the edge.

Just from the first three steps above, all-optical label switching routers achieve dramatic reduction in power consumption and size. 1.28 Tb/s capacity optical label switching routers with 32×32 AWGR, 40 Gb/s wavelength converters (two sets of 32), diode lasers (32 tunable and 32 fixed DFB lasers) [176], and

control electronics are expected to consume approximately 128 Watts and occupy $32 \times 60 \times 32\,\text{cm}^3$ space, as opposed to 34 kW, $213 \times 120 \times 91\,\text{cm}^3$ for an electronic counterpart. Monolithic integration [176] of the optical switch fabric, in principle, allows even greater reduction of power consumption down to 14 Watts and physical size to $5 \times 5 \times 10\ \text{cm}^3$. Recent research activities around the world [155, 156, 177 180] have involved integration of many functional optical components on a chip. Integration of multiple optical components is expected to reduce size, power consumption, and manufacturing cost, and to improve reliability.

16.5 SUMMARY

OPS and OBS technologies seek powerful combinations of the vast optical bandwidth and the agile subwavelength granularity by switching and routing packets and bursts directly in the optical layer. OBS offers best-effort burst transport and switching with one-way signaling so that high network utilization for bursty traffic can be achieved. OBS can be realized even with nodes employing relatively simple optical switching fabrics with ms$\sim$$\mu$s switching speeds. OPS requires fast switching speeds (in the nanosecond range) to be effective. Recent advances in optical header (label) processing and optical switching led to asynchronous and variable-length OPS with contention resolution in wavelength, time, and space domains at nanosecond switching speeds. Unlike electronic packet switching routers, optical routers can exploit the wavelength domain to greatly reduce the buffer requirement and to discard store-and-buffer architecture involving packet processing in the data plane. OLS facilitates seamless interoperability between OPS, OBS, and OCS. OLS test bed demonstrations around the world have successfully achieved support of multi-service applications, 101 cascaded network element operations, and field trial spanning 477 km packet transport. In addition to the reduced complexity and power requirements in OLS routers resulting from significantly reduced high-speed electronic processing in the data plane, further advances in integrated optoelectronic technologies may eventually allow chip-scale integration of OLS routers for the agile, robust, and high-performance Internet in the future.

ACKNOWLEDGMENT

The author thanks many researchers around the world who contributed to this chapter. The author acknowledges the support by DARPA NGI Initiative F30602 98-C-0216 and F30602 00 2 0543, and by the National Science Foundation under grant number ANI-998665, NRT-0335301, NETS-0435529. The author is indebted to many UC Davis researchers, especially Z. Pan, F. Xue, H. Yang, and Z. Zhu.

REFERENCES

[1] S. J. B. Yoo and G. K. Chang, "High Throughput, Low Latency Next Generation Internet Using Optical Tag Switching," in US Patent 6,111,673, August 29, 1997.

[2] S. Yao, S. J. Ben Yoo, B. Mukherjee, and S. Dixit, "All optical packet switching for metropolitan area networks: Opportunities and challenges," *IEEE Commun. Mag.*, 39, 142 148, 2001.

[3] F. Xue, Z. Pan, Y. Bansal et al., "End to end contention resolution schemes for an optical packet switching network with enhanced edge routers," *J. Lightw. Technol.*, 21, 2595 2604, 2003.

[4] J. S. Turner, "Terabit burst switching," *J. High Speed Netw.*, 8, 3 16, 1999.

[5] C. M. Qiao and M. S. Yoo, "Optical burst switching (OBS) a new paradigm for an optical Internet," *J. High Speed Netw.*, 8, 69 84, 1999.

[6] J. Y. Wei and R. I. McFarland, "Just in time signaling for WDM optical burst switching networks," *J. Lightw. Technol.*, 18, 2019 2037, 2000.

[7] M. Yoo and C. Qiao, "Just Enough Time (JET): A High Speed Protocol for Bursty Traffic in Optical Networks," presented at *1997 Digest of the IEEE/LEOS Summer Topical Meetings: Vertical Cavity Lasers/Technologies for a Global Information Infrastructure/WDM Components Technology/ Advanced Semiconductor Lasers and Applications/Gallium Nitride Materials, Processing, and Devices* (Cat. No.97TH8276), IEEE, New York, NY, USA, 1997, pp. 26 27.

[8] J. S. Turner, "WDM burst switching for petabit data networks," presented at *OFC*, Technical Digest Postconference Edition, Trends in Optics and Photonics Vol. 37 (IEEE Cat. No. 00CH37079), Opt. Soc. America, Part Vol. 2, pp. 47 49, Vol. 2, Washington, DC, USA, 2000.

[9] M. Duser and P. Bayvel, "Performance of a dynamically wavelength routed optical burst switched network," *IEEE Photon. Technol. Lett.*, 14, 239 241, 2002.

[10] M. Yoo, C. M. Qiao, and S. Dixit, "Optical burst switching for service differentiation in the next generation optical internet," *IEEE Commun. Mag.*, 39, 98 104, 2001.

[11] M. Yoo, C. Qiao, and S. Dixit, "QoS performance of optical burst switching in IP over WDM networks," *IEEE J. Sel. Areas Commun.*, 18, 2062 2071, 2000.

[12] A. K. Turuk and R. Kumar, "Delay on demand: A signaling protocol to reduce blocking prob ability in optical burst switching networks," *Photon. Netw. Commun.*, 10, 253 266, 2005.

[13] X. Yu, J. K. Li, X. J. Cao et al., "Traffic statistics and performance evaluation in optical burst switched networks," *J. Lightw. Technol.*, 22, 2722 2738, 2004.

[14] A. Ge, F. Callegati, and L. S. Tamil, "On optical burst switching and self similar traffic," *IEEE Commun. Lett.*, 4, 98 100, 2000.

[15] S. J. B. Yoo, H. J. Lee, S. Vaidianathan et al., "Optical Label Switching and Routing by Rapidly Tunable Wavelength Conversion and Uniform Loss Cyclic Frequency Array Waveguide Grating," presented at *OFC 2001*, Optical Fiber Communication Conference and Exhibit, Technical Digest Postconference Edition (IEEE Cat. 01CH37171), Opt. Soc. America, Part Vol. 3, pp. WDD49 1 3, Vol. 3, Washington, DC, USA, 2001.

[16] S. J. B. Yoo, L. Hyuek Jae, P. Zhong et al., "Rapidly switching all optical packet routing system with optical label swapping incorporating tunable wavelength conversion and a uniform loss cyclic frequency AWGR," *IEEE Photon. Technol. Lett.*, 14, 1211 1213, 2002.

[17] A. Zapata and P. Bayvel, "Dynamic Wavelength Routed Optical Burst Switched Networks: Scal ability Analysis and Comparison with Static Wavelength Routed Optical Networks," presented at *OFC* (Trends in Optics and Photonics Series Vol.86) Postconference Digest (IEEE Cat. No.03CH37403), Opt. Soc. America, Part Vol. 1, pp. 212 213, Vol. 1, Washington, DC, USA, 2003.

[18] F. Xue, Z. Pan, Y. Bansal et al., "End to end contention resolution schemes for an optical packet switching network with enhanced edge routers," *J. Lightw. Technol.*, 21, 2595 2604, 2003.

[19] F. Xue and S. J. B. Yoo, "Self Similar Traffic Shaping at the Edge Router in Optical Packet Switched Networks," presented at *ICC 2002*, Conference Proceedings (Cat. No.02CH37333), IEEE, Part Vol. 4, pp. 2449 2453, Vol. 4, Piscataway, NJ, USA, 2002.

[20] Y. J. Xiong, M. Vandenhoute, and H. C. Cankaya, "Control architecture in optical burst switched WDM networks," *IEEE J. Sel. Areas Commun.*, 18, 1838 1851, 2000.

[21] F. Xue, Z. Pan, H. Yang et al., "Design and Experimental Demonstration of a Variable Length Optical Packet Routing System With Unified Contention Resolution," *J. Lightw. Technol.*, 22, 2570 2581, 2004.

[22] S. Yao, B. Mukherjee, S. J. B. Yoo, and S. Dixit, "All Optical Packet Switched Networks: A Study of Contention Resolution Schemes in An Irregular Mesh Network with Variable Sized Packets," presented at *SPIE Int. Soc. Opt. Eng*. Proceedings of the SPIE The International Society for Optical Engineering, vol. 4233, USA, 2000, pp. 235 246.

[23] S. Yao, B. Mukherjee, S. J. B. Yoo, and S. Dixit, "A unified study of contention resolution schemes in optical packet switched networks," *J. Lightw. Technol.*, 21, 672 683, 2003.

[24] S. Yao, F. Xue, B. Mukherjee et al., "Electrical ingress buffering and traffic aggregation for optical packet switching and their effect on TCP level performance in optical mesh networks," *IEEE Commun. Mag.*, 40, 66 72, 2002.

[25] S. Lee, K. Sriram, H. Kim, and J. Song, "Performance improvement of deflection routing in Optical Burst Switching networks," in Proc. *ICCS 2003*, Pt Iii, Proceedings, Vol. 2659, Lecture Notes In Computer Science, Berlin, Springer Verlag Berlin, 2003, pp. 445 452.

[26] J. K. Li and C. M. Qiao, "Schedule burst proactively for optical burst switched networks," *Comp. Netw. The International Journal Of Computer And Telecommunications Networking*, 44, 617 629, 2004.

[27] N. L. Bin Wang, "Dynamic Contention Resolution in Optical Burst Switched Networks with Partial Wavelength Conversion and Fiber Delay Lines," in *GLOBECOM '04. IEEE*, 3, 2004, pp.1862 1866.

[28] C. M. Gauger, "Optimized combination of converter pools and FDL buffers for contention resolution in optical burst switching," *Photon. Netw. Commun.*, 8, 139 148, 2004.

[29] Z. Pan, H. J. Yang, J. Q. Yang et al., "Advanced optical label routing system supporting multicast, optical TTL, and multimedia applications," *J. Lightw. Technol.*, 23, 3270 3281, 2005.

[30] G. I. Papadimitriou, C. Papazoglou, and A. S. Pomportsis, "Optical switching: Switch fabrics, techniques, and architectures," *J. Lightw. Technol.*, 21, 384 405, 2003.

[31] M. K. Panda, T. Venkatesh, V. Sridhar, and Y. N. Singh, "Architecture for a Class of Scalable Optical Cross Connects," in Proc. *BROADNETS 2004*, IEEE Comput. Soc. 2004, Los Alamitos, CA, USA, 2004, pp. 233 242.

[32] I. Baldine, A. Bragg, G. Evans et al., "JumpStart deployments in ultra high performance optical networking testbeds," *IEEE Commun. Mag.*, S18 S25, 2005.

[33] Y. Yamabayashi, M. Koga, and S. Okamoto, "Autonomously controlled multiprotocol wavelength switching network for Internet backbones," *IEICE Trans. Commun.*, E83B, 2210 2215, 2000.

[34] K. Sato, N. Yamanaka, Y. Takigawa et al., "GMPLS based photonic multilayer router (Hikari router) architecture: An overview of traffic engineering and signaling technology," *IEEE Com mun. Mag.*, 40, 96 101, 2002.

[35] A. A. Amin, K. Shimizu, M. Takenaka et al., "Label Based Path Switching and Error Free Forwarding in a Prototype Optical Burst Switching Node Using a Fast 4×4 Optical Switch and Shared Wavelength Conversion," in Proc. *OFC'06*. Anaheim, CA, 2006.

[36] S. J. B. Yoo, H. J. Lee, Z. Pan et al., "Rapidly switching all optical packet routing system with optical label swapping incorporating tunable wavelength conversion and a uniform loss cyclic frequency AWGR," *IEEE Photon. Technol. Lett.*, 14, 1211 1213, 2002.

[37] D. Klonidis, C. T. Politi, R. Nejabati et al., "OPSnet: Design and demonstration of an asynchro nous high speed optical packet switch," *J. Lightw. Technol.*, 23, 2914 2925, 2005.

[38] D. Klonidis, C. Politi, M. O'Mahony, and D. Simeonidou, "Fast and widely tunable optical packet switching scheme based on tunable laser and dual pump four wave mixing," *IEEE Photon. Technol. Lett.*, 16, 1412 1414, 2004.

[39] C. Guillemot, M. Renaud, P. Gambini et al., "Transparent optical packet switching: The European ACTS KEOPS project approach," *J. Lightw. Technol.*, 16, 2117 2134, 1998.

[40] G. A. Fish, L. A. Coldren, and S. P. DenBaars, "Suppressed modal interference switches with integrated curved amplifiers for scaleable photonic crossconnects," *IEEE Photon. Technol. Lett.*, 10, 230 232, 1998.

[41] R. Varrazza, I. B. Djordjevic, and S. Yu, "Active vertical coupler based optical crosspoint switch matrix for optical packet switching applications," *J. Lightw. Technol.*, 22, 2034 2042, 2004.
[42] E. Shekel, D. Majer, G. Matmon et al., "Broadband Testing of a 64&Times;64 Nanosecond Optical Switch," presented at *LEOS 2002*, 2002 IEEE/LEOS Annual Meeting Conference Pro ceedings, 15th Annual Meeting of the IEEE Lasers and Electro Optics Society (Cat. No.02CH37369), IEEE, Part Vol. 2, pp. 371 372, Vol. 2, Piscataway, NJ, USA, 2002.
[43] R. Takahashi, T. Nakahara, K. Takahata et al., "Ultrafast optoelectronic packet processing for asynchronous, optical packet switched networks," *J. Opt. Netw.*, 3, 914 930, 2004.
[44] T. Nakahara, H. Takenouchi, R. Takahashi et al., "32 Bit Label Swapping of 40 Gbit/S Burst Optical Packets with Intensity Tracking of Input Label," presented at 30th*ECOC*, Stockholm, Sweden, 2004.
[45] R. Takahashi, T. Nakahara, K. Takahata et al., "Photonic random access memory for 40 Gb/s 16 b burst optical packets," *IEEE Photon. Technol. Lett.*, 16, 1185 1187, 2004.
[46] R. Takahashi, T. Nakahara, H. Takenouchi, and H. Suzuki, "40 Gbit/s label recognition and 1×4 self routing using self serial to parallel conversion," *IEEE Photon. Technol. Lett.*, 16, 692 694, 2004.
[47] R. Takahashi and H. Suzuki, "1 Tb/s 16 b all optical serial to parallel conversion using a surface reflection optical switch," *IEEE Photon. Technol. Lett.*, 15, 287 289, 2003.
[48] A. A. M. Saleh, "Transparent optical networks for the next generation information infrastructure," presented at *OFC '95*, Summaries of Papers Presented at the Conference on Optical Fiber Communication, Vol. 8. 1995 Technical Digest Series, Postconference Edition, Opt. Soc. Amer ica, p. 241, Washington, DC, USA, 1995.
[49] S. J. B. Yoo, "Wavelength conversion technologies for WDM network applications," *J. Lightw. Technol.*, 14, 955 966, 1996.
[50] A. Sahara, Y. Tsukishima, K. Shimano et al., "Demonstration of connection oriented optical burst switching network utilising PLC and MEMS switches," *Electron. Lett.*, 40, 1597 1599, 2004.
[51] S. Iyer, R. Zhang, and N. McKeown, "Routers with a single stage of buffering," *Comp. Commun. Rev.*, 32, 251 264, 2002.
[52] J. Kleban and A. Wieczorek, "CRRD OG: a packet dispatching algorithm with open grants for three stage buffered clos network switches," presented at *2006 Workshop on High Performance Switching and Routing* (IEEE Cat. No. 06EX1229C) IEEE, p. 6, Piscataway, NJ, USA, 2006.
[53] J. Cheyns, C. Develder, E. Van Breusegem et al., "Clos lives on in optical packet switching," *IEEE Commun. Mag.*, 42, 114 21, 2004.
[54] F. K. Liotopoulos, "Issues on gigabit switching using 3 stage Clos networks," *Informatica*, 23, 335 346, 1999.
[55] S. J. B. Yoo, "Optical label switching, MPLS, MPLambdaS, and GMPLS," *Opt. Netw. Mag.*, 4, 17 31, 2003.
[56] D. J. Blumenthal, B. E. Olsson, G. Rossi et al., "All optical label swapping networks and technologies," *J. Lightw. Technol.*, 18, 2058 75, 2000.
[57] C. Bintjas, N. Pleros, K. Yiannopoulos et al., "All optical packet address and payload separation," *IEEE Photon. Technol. Lett.*, 14, 1728 1730, 2002.
[58] W. I. Way, Y. M. Lin, and G. K. Chang, "A Novel Optical Label Swapping Technique Using Erasable Optical Single Sideband Subcarrier Label," presented at *OFC*, Technical Digest Post conference Edition, Trends in Optics and Photonics Vol.37 (IEEE Cat. No. 00CH37079), Opt. Soc. America, Part Vol. 2, 2000, pp. 59 61 Vol. 2, Washington, DC, USA, 2000.
[59] D. J. Blumenthal, A. Carena, L. Rau et al., "All optical label swapping with wavelength conver sion for WDM IP networks with subcarrier multiplexed addressing," *IEEE Photon. Technol. Lett.*, 11, 1497 1499, 1999.
[60] B. Meagher, G. K. Chang, G. Ellinas et al., "Design and implementation of ultra low latency optical label switching for packet switched WDM networks," *J. Lightw. Technol.*, 18, 1978 1987, 2000.

[61] H. J. Lee, V. Hernandez, V. K. Tsui, and S. J. B. Yoo, "Simple, polarisation independent, and dispersion insensitive SCM signal extraction technique for optical switching systems applications," *Electron. Lett.*, 37, 1240 1241, 2001.

[62] M. Y. Jeon, Z. Pan, J. Cao et al., "Demonstration of all optical packet switching routers with optical label swapping and 2R regeneration for scalable optical label switching network applications," *J. Lightw. Technol.*, 21, 2723 2733, 2003.

[63] Y. M. Lin, W. I. Way, and G. K. Chang, "A novel optical label swapping technique using erasable optical single sideband subcarrier label," *IEEE Photon. Technol. Lett.*, 12, 1088 1090, 2000.

[64] H. Chen, M. Chen, S. Xie, and B. Zhou, "Single sideband payload and label scheme for 40 Gb/s all optical label switching," presented at 30th *ECOC 2004*, Royal Inst. of Technol, Part Vol. 4, 2004, pp. 948 949, Vol. 4, Kista, Sweden, 2004.

[65] J. J. Yu, G. K. Chang, and Q. M. Yang, "Optical label swapping in a packet switched optical network using optical carrier suppression, separation, and wavelength conversion," *IEEE Photon. Technol. Lett.*, 16, 2156 2158, 2004.

[66] A. Okada, "All Optical Packet Routing in Awg Based Wavelength Routing Networks Using an Out of Band Optical Label," presented at *OFC*, Postconference Technical Digest (IEEE Cat. No.02CH37339), Opt. Soc. America, Part Vol. 1, pp. 213 215, Vol. 1, Washington, DC, USA, 2002.

[67] N. Wada, H. Harai, and W. Chujo, "Multi Hop, 40 Gbit/S Variable Length Photonic Packet Routing Based on Multi Wavelength Label Switching, Waveband Routing and Label Swapping," presented at *OFC*, Postconference Technical Digest (IEEE Cat. No.02CH37339), Opt. Soc. America, Part Vol. 1, pp. 216 217, Vol. 1. Washington, DC, USA, 2002.

[68] K. Kitayama and N. Wada, "Photon. IP routing," *IEEE Photon. Technol. Lett.*, 11, 1689 1691, 1999.

[69] N. Wada, W. Chujo, and K. Kitayama, "1.28 Tbit/s (160 Gbit/s*8 Wavelengths) Throughput Variable Length Packet Switching Using Optical Code Based Label Switch," presented at Pro ceedings Post Deadline Papers, 27th *ECOC* (Cat. No.01TH8551) IEEE, Part Vol. 6, pp. 62 63, Vol. 6, Piscataway, NJ, USA, 2001.

[70] H. Furukawa, N. Wada, and T. Miyazaki, "Specification and Operation of 160 Gbit/S/ Port Interface Optical Packet Switch Prototype with Narrow Band Optical Code Label Processor and High Extinction Ratio Optical Buffer," in Proc. *OFC'06*, Anaheim, CA, 2006.

[71] N. Wada, G. Cincotti, S. Yoshima et al., "Characterization of a full encoder/decoder in the AWG configuration for code based photonic routers Part II: Expertiments and applications," *J. Lightw. Technol.*, 24, 113 121, 2006.

[72] E. N. Lallas, N. Skarmoutsos, and D. Syvridis, "An optical FSK based label coding technique for the realization of the all optical label swapping," *IEEE Photon. Technol. Lett.*, 14, 1472 1474, 2002.

[73] N. Chi, L. Xu, L. Christiansen et al., "Optical Label Swapping and Packet Transmission Based on Ask/Dpsk Orthogonal Modulation Format in Ip Over Wdm Networks," presented at *OFC* (Trends in Optics and Photonics Series Vol. 86) Technical Digest (IEEE Cat. No.03CH37403), Opt. Soc. America, Part vol. 2, pp. 792 794, vol. 2, Washington, DC, USA, 2003.

[74] J. F. Zhang, N. Chi, P. V. Holm Nielsen et al., "An optical FSK transmitter based on an integrated DFB laser EA modulator and its application in optical labeling," *IEEE Photon. Technol. Lett.*, 15, 984 986, 2003.

[75] J. J. V. Olmos, J. Zhang, P. V. Holm Nielsen et al., "Simultaneous optical label erasure and insertion in a single wavelength conversion stage of combined FSK/IM modulated signals," *IEEE Photon. Technol. Lett.*, 16, 2144 2146, 2004.

[76] N. Chi, C. Mikkelsen, L. Xu et al., "Transmission and label encoding/erasure of orthogonally labelled signal using 40 Gbit/s RZ DPSK payload and 2.5 Gbit/s IM label," *Electron. Lett.*, 39, 1335 1337, 2003.

[77] N. Deng, Y. Yang, C. K. Chan et al., "Intensity modulated labeling and all optical label swapping on angle modulated optical packets," *IEEE Photon. Technol. Lett.*, 16, 1218 1220, 2004.

[78] X. Liu, X. Wei, Y. K. Su et al., "Transmission of an ASK labeled RZ DPSK signal and label erasure using a saturated SOA," *IEEE Photon. Technol. Lett.*, 16, 1594 1596, 2004.
[79] C. W. Chow, C. S. Wong, and H. K. Tsang, "Optical packet labeling based on simultaneous polarization shift keying and amplitude shift keying," *Opt. Lett.*, 29, 1861 1863, 2004.
[80] D. Chiaroni, B. Lavigne, A. Jourdan et al., "Physical and logical validation of a network based on all optical packet switching systems," *J. Lightw. Technol.*, 16, 2255 2264, 1998.
[81] Z. Q. Zhu, Z. Pan, and S. J. B. Yoo, "A compact all optical subcarrier label swapping system using an integrated EML for 10 Gb/s optical label switching networks," *IEEE Photon. Technol. Lett.*, 17, 426 428, 2005.
[82] J. J. Yu and G. K. Chang, "A novel technique for optical label and payload generation and multiplexing using optical carrier suppression and separation," *IEEE Photon. Technol. Lett.*, 16, 320 322, 2004.
[83] M. Cerisola, T. K. Fong, R. T. Hofmeister et al., "Subcarrier multiplexing of packet headers in a WDM optical network and a novel ultrafast header clock recovery technique," presented at *OFC '95*, Summaries of Papers Presented at the Conference on Optical Fiber Communication, Vol. 8, 1995 Technical Digest Series. Postconference Edition, Opt. Soc. America, pp. 273 274, Washing ton, DC, USA, 1995.
[84] C. L. Lu, D. J. M. Sabido, P. Poggiolini et al., "Cord A Wdma optical network Subcarrier based signaling and control scheme," *IEEE Photon. Technol. Lett.*, 7, 555 557, 1995.
[85] E. Park and A. E. Willner, "Self routing of wavelength packets using an all optical wavelength shifter and QPSK subcarrier routing control headers," *IEEE Photon. Technol. Lett.*, 8, 938 940, 1996.
[86] R. Olshansky, "Microwave subcarrier multiplexing: new approach to wideband lightwave sys tems," *IEEE Circuits and Devices Mag.*, 4, 8 14, 1988.
[87] R. Olshansky and V. A. Lanzisera, "60 channel FM video subcarrier multiplexed optical commu nication system," *Electron. Lett.*, 23, 1196 1198, 1987.
[88] H. J. Lee, S. J. B. Yoo, V. K. Tsui, and S. K. H. Fong, "A simple all optical label detection and swapping technique incorporating a fiber Bragg grating filter," *IEEE Photon. Technol. Lett.*, 13, 635 637, 2001.
[89] Z. Q. Zhu, V. J. Hernandez, M. Y. Jeon et al., "RF photonics signal processing in subcarrier multiplexed optical label switching communication systems," *J. Lightw. Technol.*, 21, 3155 3166, 2003.
[90] J. Cao, M. Y. Jeon, Z. Pan et al., "11 Hop Operation of Optical Label Switching System with All Optical Label Swapping," presented at *ECOC*, 2003.
[91] V. J. Hernandez, Z. Pan, J. Cao et al., "First Field Trial of Optical Label Based Switching And Packet Drop on A 477 Km Nton/Sprint Link," presented at *OFC*, Postconference Technical Digest (IEEE Cat. No.02CH37339), Opt. Soc. America, Part Vol. 1, 2002, pp. 168 169, Vol. 1, Washington, DC, USA, 2002.
[92] H. Tsushima, M. Shabeer, P. Barnsley, and D. Pitcher, "Demonstration of an optical packet add drop with wavelength coded header," *IEEE Photon. Technol. Lett.*, 7, 212 214, 1995.
[93] T. Koonen, G. Morthier, J. Jennen et al., "Optical Packet Routing in Ip Over Wdm Networks Deploying Two Level Optical Labeling," in Proc. 27th *ECOC* (Cat. No.01TH8551), IEEE, Part Vol. 4, pp. 608 609, Vol. 4. Piscataway, NJ, USA, 2001.
[94] N. Chi, B. Kozicki, J. Zhang et al., "Transmission Properties of an All Optical Labelled Signal Using Orthogonal Im/Fsk Modulation Format," in Proc. *ECOC'03*, Rimini, Italy, 2003.
[95] I. T. Monroy, J. J. V. Olmos, A. M. J. Koonen et al., "Optical label switching by using differential phase shift keying and in band subcarrier multiplexing modulation format," *Opt. Eng.*, 43, 1476 1477, 2004.
[96] J. J. V. Olmos, I. T. Monroy, F. M. Huijskens, and A. M. J. Koonen, "In band time to live signaling system for combined DPSK/SCM scheme in OLS," *IEEE Photon. Technol. Lett.*, 16, 2386 2388, 2004.

[97] J. J. V. Olmos, I. T. Monroy, Y. Liu et al., "Asynchronous, self controlled, all optical label and payload separator using nonlinear polarization rotation in a semiconductor optical amplifier," *Opt. Express*, 12, 4214 4219, 2004.
[98] I. T. Monroy, E. J. M. Verdurmen, S. Sulur et al., "Performance of a SOA MZI wavelength converter for label swapping using combined FSK/IM modulation format," *Opt. Fib. Technol.*, 10, 31 49, 2004.
[99] C. W. Chow and H. K. Tsang, "Orthogonal label switching using polarization shift keying payload and amplitude shift keying label," *IEEE Photon. Technol. Lett.*, 17, 2475 2477, 2005.
[100] L. Xu, N. Chi, L. K. Oxenlowe et al., "A new orthogonal labeling scheme based on a 40 Gb/s DPSK payload and a 2.5 Gb/s PolSK label," *IEEE Photon. Technol. Lett.*, 17, 2772 2774, 2005.
[101] L. Xu, T. Wang, O. Matsuda et al., "Wavelength shift keying (WSK) encoded pulses for optical labeling applications," *IEEE Photon. Technol. Lett.*, 17, 2775 2777, 2005.
[102] W. Hung, C. K. Chan, L. K. Chen, and F. Tong, "A Novel Phase Encoding Scheme for Optical Packet Label Processing," in Proc. *ECOC'03*, Rimini, Italy, 2003.
[103] W. Xu and W. Naoya, "Experimental demonstration of OCDMA traffic over optical packet switching network with hybrid PLC and SSFBG en/decoders," *J. Lightw. Technol.*, 24, 3012 3020, 2006.
[104] N. Wada, H. Harai, and F. Kubota, "Optical packet switching network based on ultra fast optical code label processing," *IEICE Transactions On Electron.*, E87C, 1090 1096, 2004.
[105] M. C. Cardakli, S. Lee, A. E. Willner et al., "Reconfigurable optical packet header recognition and routing using time to wavelength mapping and tunable fiber Bragg gratings for correlation decoding," *IEEE Photon. Technol. Lett.*, 12, 552 554, 2000.
[106] J. E. McGeehan, S. Kumar, D. Gurkan et al., "All optical decrementing of a packet's time to live (TTL) field and subsequent dropping of a zero TTL packet," *J. Lightw. Technol.*, 21, 2746 2752, 2003.
[107] J. Yang, M. Y. Jeon, J. Cao et al., "Performance monitoring by sub carrier multiplexing in optical label switching networks," presented at *CLEO*, Baltimore, Maryland USA, 2003.
[108] J. Yang, M. Y. Jeon, J. Cao et al., "Performance monitoring in transparent optical networks using self monitoring optical labels," *Electron. Lett.*, 40, 1370 1372, 2004.
[109] J. Q. Yang, Z. Zhu, H. Yang, Z. Pan, and S. J. B. Yoo, "All Optical Time to Live Using Error Checking Labels in Optical Label Switching Networks," presented at 30th *ECOC*, Stockholm, Sweden, 2004.
[110] H. J. S. Dorren, M. T. Hill, Y. Liu et al., "Optical packet switching and buffering by using all optical signal processing methods," *J. Lightw. Technol.*, 21, 2 12, 2003.
[111] J. P. Wang, B. S. Robinson, S. A. Hamilton, and E. P. Ippen, "40 Gbit/s All Optical Header Processing for Packet Routing," in Proc. *OFC'06,* Anaheim, CA, 2006.
[112] H. Yang, H. Junqiang, P. Zhong et al., "An asynchronous, variable length two stage packet switch fabric architecture with look ahead and load balance scheduling schemes for optical label switching networks," presented at *GLOBECOM '04*, IEEE Global Telecommunications Conference (IEEE Cat. No. 04CH37615), IEEE, Part Vol. 3, 2004, pp. 1828 1834, Vol. 3, Piscataway, NJ, USA, 2004.
[113] H. Yang, V. Akella, C. N. Chuah, and S. J. B. Yoo, "Scheduling Optical Packets in Wavelength, Time, and Space Domains for All Optical Packet Switching Routers," presented at 2005 IEEE ICC (IEEE Cat. No. 05CH37648), IEEE. Part Vol. 3, 2005, pp. 1836 1842, Vol. 3. Piscataway, NJ, USA, 2005.
[114] R. T. Hofmeister, L. G. Kazovsky, C. L. Lu et al., "CORD: Optical packet switched network testbed," *Fib. and Integrated Opt.*, 16, 199 219, 1997.
[115] T. Sakamoto, A. Okada, M. Hirayama et al., "Optical packet synchronizer using wavelength and space switching," *IEEE Photon. Technol. Lett.*, 14, 1360 1362, 2002.
[116] W. D. Zhong and R. S. Tucker, "A new wavelength routed photonic packet buffer combining traveling delay lines with delay line loops," *J. Lightw. Technol.*, 19, 1085 1092, 2001.

[117] Z. Pan, J. Cao, Y. Bansal et al., "All Optical Programmable Time Slot Interchanger Using Optical Label Switching with Tunable Wavelength Conversion and N by N Arrayed Waveguide Grating Routers," presented at *OFC*. Postconference Technical Digest (IEEE Cat. No. 02CH37339), Opt. Soc. America, Part Vol. 1, pp. 267 268, Vol. 1. Washington, DC, USA, Anaheim, CA, 2002.
[118] L. Brillouin, "Wave propagation and group velocity," New York, Academic Press, 1960.
[119] L. V. Hau, S. E. Harris, Z. Dutton, and C. H. Behroozi, "Light speed reduction to 17 metres per second in an ultracold atomic gas," *Nature*, 397, 594 598, 1999.
[120] C. Liu, Z. Dutton, C. H. Behroozi, and L. V. Hau, "Observation of coherent optical information storage in an atomic medium using halted light pulses," *Nature*, 409, 490 493, 2001.
[121] M. Bajcsy, A. S. Zibrov, and M. D. Lukin, "Stationary pulses of light in an atomic medium," *Nature*, 426, 638 641, 2003.
[122] M. D. Lukin and A. Imamoglu, "Controlling photons using electromagnetically induced trans parency," *Nature*, 413, 273 276, 2001.
[123] P. C. Ku, C. J. Chang Hasnain, and S. L. Chuang, "Variable semiconductor all optical buffer," *Electron. Lett.*, 38, 1581 1583, 2002.
[124] J. Mork, R. Kjaer, M. van der Poel, and K. Yvind, "Slow light in a semiconductor waveguide at gigahertz frequencies," *Opt. Express*, 13(20), 3, October 2005.
[125] J. E. Heebner, R. W. Boyd, and Q. H. Park, "Slow light, induced dispersion, enhanced non linearity, and optical solitons in a resonator array waveguide," *Phys. Rev. E (Statistical, Non linear, and Soft Matter Physics)*, 65, 0366191 0366194, 2002.
[126] Y. Okawachi, J. E. Sharping, A. L. Gaeta et al., "All optical tunable slow light delays via stimulated scattering," *Opt. & Photon. News*, 16, 42, 2005.
[127] Y. A. Vlasov, M. O'Boyle, H. F. Hamann, and S. J. McNab, "Active control of slow light on a chip with photonic crystal waveguides," *Nature*, 438, 65 69, November 2005.
[128] Y. A. Vlasov and S. J. McNab, "Coupling into the slow light mode in slab type photonic crystal waveguides," *Opt. Lett.*, 31, 50 52, January 2006.
[129] R. W. Boyd, N. N. Lepeshkin, and P. Zerom, "Slow light in a collection of collisionally broadened two level atoms," *Laser Phys.*, 15, 1389 1392, 2005.
[130] H. Altug and J. Vuckovic, "Experimental demonstration of the slow group velocity of light in two dimensional coupled photonic crystal microcavity arrays," *Appl. Phys. Lett.*, 86, 111 102, 2004.
[131] H. J. Yang and S. J. B. Yoo, "All optical variable buffering strategies and switch fabric, architectures for future all optical data routers," *J. Lightw. Technol.*, 23, 3321 3330, 2005.
[132] R. W. Boyd, D. L. Gauthier, A. L. Gaeta, and A. E. Willner, "Limits on the Time Delay Induced by Slow Light Propagation," presented at 2005 *QELS* (IEEE Cat. No. 05CH37696) IEEE, Part Vol. 1, 2005, pp. 214 216, Vol. 1, Piscataway, NJ, USA.
[133] R. S. Tucker, P. C. Ku, and C. J. Chang Hasnain, "Fundamental limitations of slow light optical buffers," in Proc. *IEEE/OSA OFC 2005*, paper JWA32, Anaheim, California, 2005.
[134] R. S. Tucker, P. C. Ku, and C. J. Chang Hasnain, "Delay bandwidth product and storage density in slow light optical buffers," *Electron. Lett.*, 41, 208 209, February 2005.
[135] S. L. Danielsen, C. Joergensen, B. Mikkelsen, and K. E. Stubkjaer, "Optical packet switched network layer without optical buffers," *IEEE Photon. Technol. Lett.*, 10, 896 898, 1998.
[136] S. L. Danielsen, P. B. Hansen, and K. E. Stubkjaer, "Wavelength conversion in optical packet switching," *J. Lightw. Technol.*, 16, 2095 2108, 1998.
[137] V. Eramo and M. Listanti, "Wavelength converter sharing in a WDM optical packet switch: dimensioning and performance issues," *Comp. Netw. The International J. Comp. And Telecom mun. Netw.*, 32, 633 651, 2000.
[138] V. Eramo and M. Listanti, "Packet loss in a bufferless optical WDM switch employing shared tunable wavelength converters," *J. Lightw. Technol.*, 18, 1818 1833, 2000.
[139] V. Eramo, M. Listanti, and M. Di Donato, "Performance evaluation of a bufferless optical packet switch with limited range wavelength converters," *IEEE Photon. Technol. Lett.*, 16, 644 646, 2004.

[140] S. Yao, B. Mukherjee, and S. Dixit, "Advances in photonic packet switching: an overview," *IEEE Commun. Mag.*, 38, 84 94, 2000.
[141] F. Xue and S. J. Ben Yoo, "High capacity multiservice optical label switching for the next generation Internet," *IEEE Commun. Mag.*, S16 S22, 2004.
[142] H. Yang and S. J. B. Yoo, "A New Optical Switching Fabric Architecture Incorporating Rapidly Switching All Optical Variable Delay Buffers," presented at *OFC* (IEEE Cat. No.04CH37532), Opt. Soc. America, Part Vol. 2, 2004, p. 3, Vol. 2. Washington, DC, USA,.
[143] H. J. Yang and S. J. Ben Yoo, "Combined input and output all optical variable buffered, switch architecture for future optical routers," *IEEE Photon. Technol. Lett.*, 17, 1292 1294, 2005.
[144] H. Yang and S. J. B. Yoo, "New Optical Switching Fabric Architecture Incorporating Load Balanced Parallel Rapidly Switching All Optical Variable Delay Buffer Arrays," presented at 2005 *OFC*, Technical Digest (IEEE Cat. No. 05CH37672), IEEE, Part Vol. 1, 2005, p. 3, Vol. 1, Piscataway, NJ, USA.
[145] D. Wischik, "Fairness, QoS, and buffer sizing," *Comp. Commun. Rev.*, 36, 93 95, 2006.
[146] G. Raina, D. Towsley, and D. Wischik, "Part II: Control theory for buffer sizing," *Comp. Commun. Rev.*, 35, 79 82, 2005.
[147] R. Rajaduray, S. Ovadia, and D. J. Blumenthal, "Analysis of an edge router for span constrained optical burst switched (OBS) networks," *J. Lightw. Technol.*, 22, 2693 2705, 2004.
[148] M. Enachescu, Y. Ganjali, A. Goel et al., "Part III: Routers with very small buffers," *Comp. Commun. Rev.*, 35, 83 89, 2005.
[149] G. Appenzeller, I. Keslassy, and N. McKeown, "Sizing router buffers," *Comp. Commun. Rev*. 34, 281 292, 2004.
[150] A. Dhamdhere and C. Dovrolis, "Open issues in router buffer sizing," *Comp. Commun. Rev.*, 36, 87 92, 2006.
[151] K. A. Williams, G. F. Roberts, T. Lin et al., "Integrated optical 2×2 switch for wavelength multiplexed interconnects," *IEEE J. Sel. Top. Quantum Electron.*, 11, 78 85, 2005.
[152] D. K. Hunter, M. H. M. Nizam, M. C. Chia et al., "WASPNET: A wavelength switched packet network," *IEEE Commun. Mag.*, 37, 120 129, 1999.
[153] A. Okada, H. Tanobe, and M. Matsuoka, "Reconfigurable information sharing network system based on a cyclic frequency AWG and wavelength tunable lasers," *IEICE Transactions On Commun.*, E88B, 2449 2455, 2005.
[154] C. C. Wang and R. S. Tucker, "Tunable optical wavelength converters with reconfigurable functionality," *IEEE J. Sel. Top. Quantum Electron.*, 3, 1181 1189, 1997.
[155] M. Zirngibl, "IRIS: Optical Switching Technologies for Scalable Data Networks," in Proc. *OFC'06,* Anaheim, CA, 2006.
[156] M. L. Masanovic, V. Lal, J. A. Summers et al., "Widely tunable monolithically integrated all optical wavelength converters in InP," *J. Lightw. Technol.*, 23, 1350 1362, 2005.
[157] Z. Pan, Z. Zhu, M. Funabashi et al., "Error Free 31 Hop Cascaded Operation of an Optical Packet Switching Router with All Optical 3r Regeneration," in Proc. *OFC'06,* Anaheim, CA, 2006.
[158] V. Jayaraman, D. A. Cohen, and L. A. Coldren, "Demonstration of broad band tunability in a semiconductor laser using sampled gratings," *Appl. Phys. Lett.*, 60, 2321 2323, 1992.
[159] K. Kato, A. Okada, Y. Sakai et al., "32×32 full mesh (1024 path) wavelength routing WDM network based on uniformloss cyclic frequency arrayed waveguide grating," *Electron. Lett.*, 36, 1294 1296, 2000.
[160] P. Toliver, I. Glesk, R. J. Runser et al., "Routing of 100 Gb/s words in a packet switched optical networking demonstration (POND) node," *J. Lightw. Technol.*, 16, 2169 2180, 1998.
[161] N. S. Patel, K. L. Hall, and K. A. Rauschenbach, "40 Gbit/s cascadable all optical logic with an ultrafast nonlinear interferometer," *Opt. Lett.*, 21, 1466 1468, 1996.
[162] V. W. S. Chan, K. L. Hall, E. Modiano, and K. A. Rauschenbach, "Architectures and technol ogies for high speed optical data networks," *J. Lightw. Technol.*, 16, 2146 2168, 1998.
[163] Z. Pan, H. Yang, Z. Zhu, and S. J. B. Yoo, "Experimental Demonstration of a Multicast Capable Optical Label Switching Router," presented at *OFC*, Anaheim, CA, 2005.

[164] W. Hung, K. Chan, L. K. Chen et al., "A Routing Loop Control Scheme in Optical Layer for Optical Packet Networks," presented at *OFC*, Postconference Technical Digest (IEEE Cat. No.02CH37339), Opt. Soc. America, Part Vol. 1, 2002, pp. 770 771, Vol. 1, Washington, DC, USA.

[165] J. W. Kim, T. I. Chae, and Y. H. Won, "Simple and Robust All Optical Label Detection Using 2nd Harmonic Scm Technique," presented at 6th *ICACT* (IEEE Cat. No.04EX801), IEEE, Part Vol. 1, 2004, pp. 183 185, Vol. 1, Piscataway, NJ, USA.

[166] V. J. Hernandez, Z. Pan, J. Cao et al., "First Field Trial of Optical Label Based Switching And Packet Drop on a 477 Km Nton/Sprint Link," presented at *OFC* Postconference Technical Digest (IEEE Cat. No.02CH37339), Opt. Soc. America, Part Vol. 1, 2002, pp. 168 169, Vol. 1, Washington, DC, USA.

[167] Z. Pan, H. Yang, Z. Zhu et al., "Demonstration of variable length packet contention resolution and packet forwarding in an optical label switching router," *IEEE Photon. Technol. Lett.*, 16, 1772 1774, 2004.

[168] Z. Pan, Z. Zhu, M. Funabashi et al., "101 hop cascaded operation of an optical label switching router with all optical clock recovery and 3R regeneration," *IEEE Photon. Technol. Lett.*, 18, 1654 1656, 2006.

[169] M. Funabashi, P. Zhong, Z. Zuqing, and S. J. B. Yoo, "Nanosecond guard time packet by packet burst mode optical 3R regeneration in an optical label switching router," *IEEE Photon. Technol. Lett.*, 18, 1091 1093, 2006.

[170] J. Taylor, Y. Bansal, M. Y. Jeon et al., "Demonstration of Ip Client To Ip Client Packet Transport Over an Optical Label Switching Network with Edge Routers," presented at 29th *ECOC*, Rimini, Italy, 2003.

[171] J. Hu, Z. Pan, Z. Zhu et al., "First Experimental Demonstration of Combined Multicast and Unicast Video Streaming Over an Optical Label Switching Network," presented at *OFC* in the Technical Digest of IEEE/OSA, paper OTuJ2, Anaheim, CA, 2006.

[172] R. Nejabati, D. Klonidis, G. Zervas et al., "Demonstration of a Complete and Fully Functional End To End Asynchronous Optical Packet Switched Network," in Proc. *OFC'06*, Anaheim, CA, 2006.

[173] Y. M. Sun, T. Hashiguchi, V. Q. Minh et al., "Design and implementation of an optical burst switched network testbed," *IEEE Commun. Mag.*, S48 S55, 2005.

[174] *CISCO*, "CISCO CRS 1 Carrier Routing System," CISCO, 2006.

[175] *CISCO*, "CISCO CRS 1 MultiShelf System Data Sheet," 2006.

[176] S. J. B. Yoo, "Integrated Optical Router," in Proc. *US Patent,* USA UC, Davis, 2004.

[177] D. Chiaroni, "Packet switching matrix: A key element for the backbone and the metro," *IEEE J. Sel. Areas Commun.*, 21, 1018 1025, 2003.

[178] L. Dittmann, C. Develder, D. Chiaroni et al., "The European IST project DAVID: A viable approach toward optical packet switching," *IEEE J. Sel. Areas Commun.*, 21, 1026 1040, 2003.

[179] Z. Hu, B. R. Koch, J. E. Bowers, and D. J. Blumenthal, "Integrated Photonic/RF 40 Gb/s Burst mode Optical Clock Recovery for Asynchronous Optical Packet Switching," in Proc. *OFC'06*, Anaheim, CA, 2006.

[180] M. Takenaka, M. Raburn, K. Takeda, and Y. Nakano, "All Optical Packet Switching by MMI BLD Optical Flip Flop," in Proc. *OFC'06*, Anaheim, CA, 2006.

This page intentionally left blank

17

Optical and electronic technologies for packet switching

Rodney S. Tucker

Department of Electrical and Electronic Engineering, University of Melbourne, Australia

17.1 INTRODUCTION

Packet switches are arguably the most important items of equipment in any Internet Protocol (IP) network. Packet switches provide an efficient mechanism for routing IP packets through the network, from source to destination. Each packet switch inspects the incoming IP packets, determines the appropriate next hop for the packets, provides buffering for the packets while they wait for an available output port, and schedules the orderly departure of outgoing packets taking into account packet priority and service quality metrics. This scheduling of outgoing packets enables the all-important statistical time multiplexing of data on each outgoing wavelength channel and ensures that many users who are communicating at relatively low data rates can share a wavelength channel that operates at a high bit rate, such as 10 or 40 Gb/s. Without the statistical multiplexing function provided by packet switches, it would not be possible to provide end-to-end connectivity for the millions of users on the Internet. Without collision avoidance, the throughput of the network would be significantly reduced.

The packet switches or routers in today's IP network are sophisticated electronic systems. They rely heavily on advanced electronic buffering, fast switching, and powerful processing technologies. Incoming packets arrive at the router via optical fiber links. Packets on the fiber links are optical signals and are converted to electronic signals by optical-to-electronic (O/E) converters located at the inputs to the router. Apart from the optical interconnects between separate equipment racks, the vast majority of the components and circuits in today's routers are electronic. The outgoing packets from the router pass through E/O converters before being launched onto the next optical fiber transmission link in the network.

Optical Fiber Telecommunications V B: Systems and Networks

ISBN: 978 0 12 374172 1

Optical packet switching[1] is a potential alternative to electronic packet switching. A key difference between electronic packet switching and optical packet switching is that optical packet switching eliminates the need for O/E and E/O converters at the input and output ports of electronic packet switches. Optical packet switches (OPSs) use optical components for the buffering, switching and other processing such as signal regeneration and wavelength conversion. Because an OPS does not require O/E and E/O converters in the data path, the payload data in each packet remains in optical form as it passes through the switch. In other words, an OPS is optically transparent.

For a number of years, researchers (including the present author) have argued that optical packet switching will become an essential part of the future IP networks as the size and capacity of networks expand. This notion is based on the belief that optical packet switching (i.e., packet switching without O/E and E/O conversions in the signal path) provides a number of key advantages. These claimed advantages include (i) higher bandwidths due to the inherent broadband nature of optics compared with electronics, (ii) data format independence, and (iii) compatibility with the vision of all-optical networking, in which data pass transparently through the network from source to destination in optical form without undergoing any O/E or E/O conversions.

A major obstacle to the development of practical OPS hardware has been the lack of a suitable optical memory technology that can store high-bit-rate optical packets. Another obstacle has been the need for reconfigurable cross-connects that can be switched in around 1 ns or less and that can accommodate the large number of ports (hundreds to thousands) required in practical packet switching network applications. Also limiting the application of optical packet switching has been the relatively immature state of optical component integration technologies compared with electronic integration technologies. As a result, OPS demonstrations using today's components have tended to become cumbersome, even for small networks with limited total capacity.

This chapter examines the potential role of both optical and electronic technologies in future high-capacity packet switches. The chapter begins with an introduction to the functionality of routers and the key functional building blocks of high-capacity routers. A brief overview is provided of state-of-the-art routers, and the critically important consideration of power consumption in router design is highlighted. The chapter then focuses on the following key physical layer building-blocks in packet switches: (i) buffers, (ii) interface components including interconnects, wavelength converters, and regenerators, and (iii) switch fabrics or cross-connects. In each case, we consider alternative technologies and compare electronic and optical realizations of the building-blocks. Advantages and

[1] In this chapter, the term "optical packet switching" refers to a packet switch in which the payload data in the packets remains in optical form as it passes through the switch. The term includes optical packet switches in which electronics is used for processing and control functions that do not involve the payload data.

disadvantages of different technologies are presented. These comparisons focus on energy dissipation and the potential for integration and miniaturization.

Finally, to bring the various threads of the chapter together, the projected power consumption is estimated for high-capacity packet switches using a variety of optical and electronic technologies. Two key conclusions of this chapter are (a) there is no solution in sight to the optical buffer problem, and (b) optoelectronic switch fabrics using optoelectronic wavelength converters and arrayed-waveguide grating multiplexers (AWGs) appear to potentially offer the lowest-power solutions. Therefore, electronic buffers, and optoelectronic wavelength converters and regenerators are likely to remain as integral components in future high-capacity routers. Future packet switches will likely be optoelectronic packet switches rather than OPSs.

17.2 PACKET SWITCH ARCHITECTURES AND PERFORMANCE

17.2.1 Architectures

Figure 17.1 is a simplified picture of the basic architecture of electronic packet switches and OPSs. Figure 17.1(a) represents an electronic packet switch, and the switch in Figure 17.1(b) is an OPS. The key functional bocks in electronic packet switches and OPSs are the same. However, in the OPS [Figure 17.1(b)], the incoming optical packets remain in the optical domain as they pass through the switch. (Note that the functional blocks in Figure 17.1 are shaded differently to indicate whether they are electronic or optical.) The input/output ports on the electronic packet switch are usually located on line cards as indicated in Figure 17.1(a). The header and payload of the incoming optical packets are converted to electronic form in O/E converters located at the input ports on the line cards, and outgoing packets are converted back to optical form in E/O converters at the output ports on the line cards. Interfaces on the line cards provide synchronization of the incoming packets, and the forwarding engine controls the movement of packets through the buffers and the switch fabric.

In the OPS in Figure 17.1(b), incoming optical packets pass through an optical input interface to optical buffers and an optical switch fabric. O/E converter converts the packet header to the electronic domain for processing. Some researchers have proposed all-optical signal processing for header processing and packet forwarding in OPSs. However in IP networks, these processes are computationally intensive and not suited to the very limited processing power of all-optical computing. Therefore, in this chapter we consider a more practical scenario, in which header processing, route processing, and forwarding are carried out in the electrical domain. In the electronic packet switch, both the header and the payload of the incoming optical packets are converted to electronic form in O/E converters

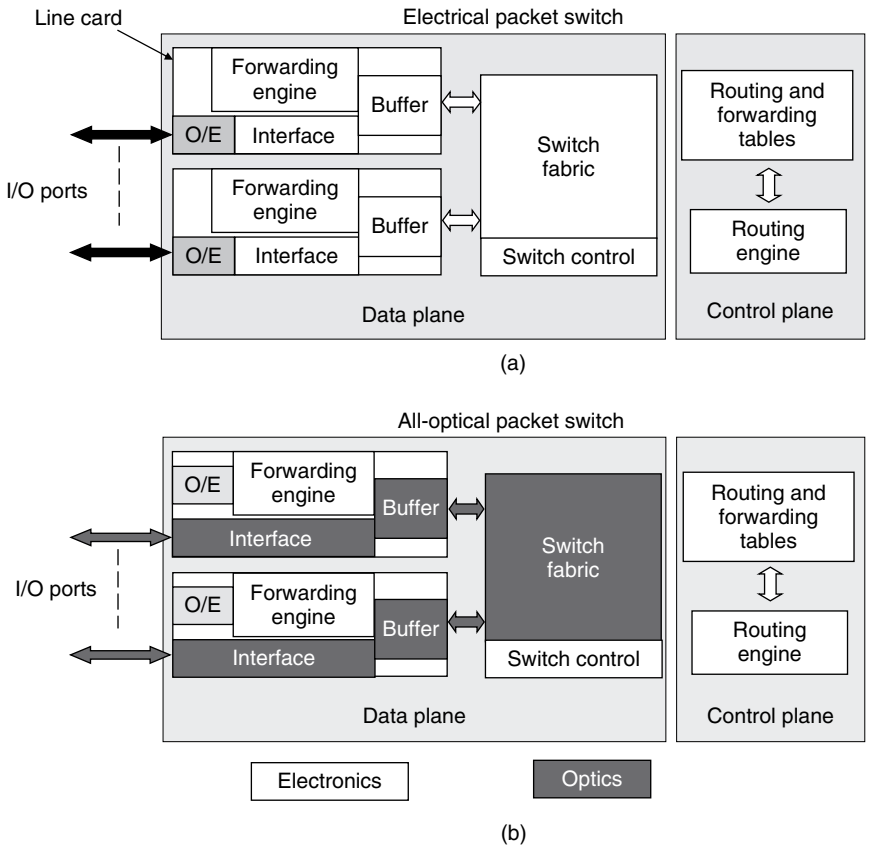

Figure 17.1 Packet switch architectures. (a) Electrical packet switch. (b) Optical packet switch.

for buffering and switching, and are converted back to optical form in E/O converters at the output ports. Thus, the O/E converters in Figure 17.1(b) are not located in the signal path as they are in Figure 17.1(a). Optical interconnects are sometimes used in state-of-the-art electronic packet switches to provide interconnects between racks, but this is clearly not the same as optical packet switching. For simplicity, the optical interconnects are not shown in Figure 17.1.

Figure 17.1 highlights the distinction between the data plane and the control plane. The data plane contains the key functional blocks that manipulate the IP packets as they pass through the router. The control plane contains the routing and forwarding tables, and the routing engine, which controls IP packet routing. The control plane is a computationally intensive block and, like the forwarding engine, it is not suited to implementation in optical form. The control plane is therefore shown as electronic in both Figure 17.1(a) and Figure 17.1(b). Electronic packet switches and OPSs both employ an electronic switch fabric controller which,

together with the forwarding engine on the line cards, is part of the data plane. Details of the control plane, the routing and forwarding engines, and the switch control circuitry are beyond the scope of this chapter.

In electronic packet switches, the incoming packets are generally spit into cells for buffering and switching and are then reassembled into packets before retransmission on the network. Figure 17.2 shows a simplified picture of part of the data plane in an electronic packet switch. In Figure 17.2, incoming packets are converted to electrical form in the O/E converters on the line cards and then are split into cells (usually 64 bytes long) in the forwarding engine. (Figure 17.1 shows only one O/E converter per line card, but in general, there can be more than this, as shown in Figure 17.2.) In electronic packet switches, the individual cells from one input packet are often distributed among a number of parallel switch fabrics (shown in Figure 17.2). This splitting of packets into cells provides a number of advantages. In particular, provided there are sufficient parallel switch fabrics in the packet switch, it is possible to operate the individual switch fabrics at a lower data rate than the incoming packets. Splitting of packets into cells is generally not desirable in optical packet switching because it would defeat one of the key motivations of optical packet switching, which is to maintain transparency and to avoid any processing of the payload data. Some electronic routers include some internal buffering located between stages of the switch [1]. This helps to reduce blocking in the switch fabric.

Figure 17.3 shows how the I/O ports on a packet switch are connected to the incoming and outgoing fibers via wavelength division multiplexing (WDM) demultiplexers and multiplexers, respectively. There are F incoming fibers in Figure 17.3 and F outgoing fibers. Each fiber carries K wavelengths. Figure 17.3(a,b) shows the key components of the data plane of an electronic packet switch and an OPS, respectively.

Buffering in a packet switch can be placed at the input ports or at the output ports, or shared between the inputs and outputs. In Figure 17.3, the buffers are located at the

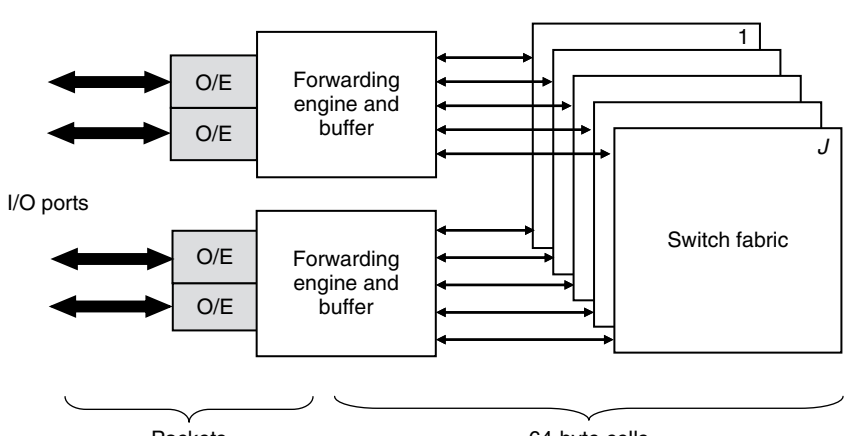

Figure 17.2 Data plane in an electronic packet switch.

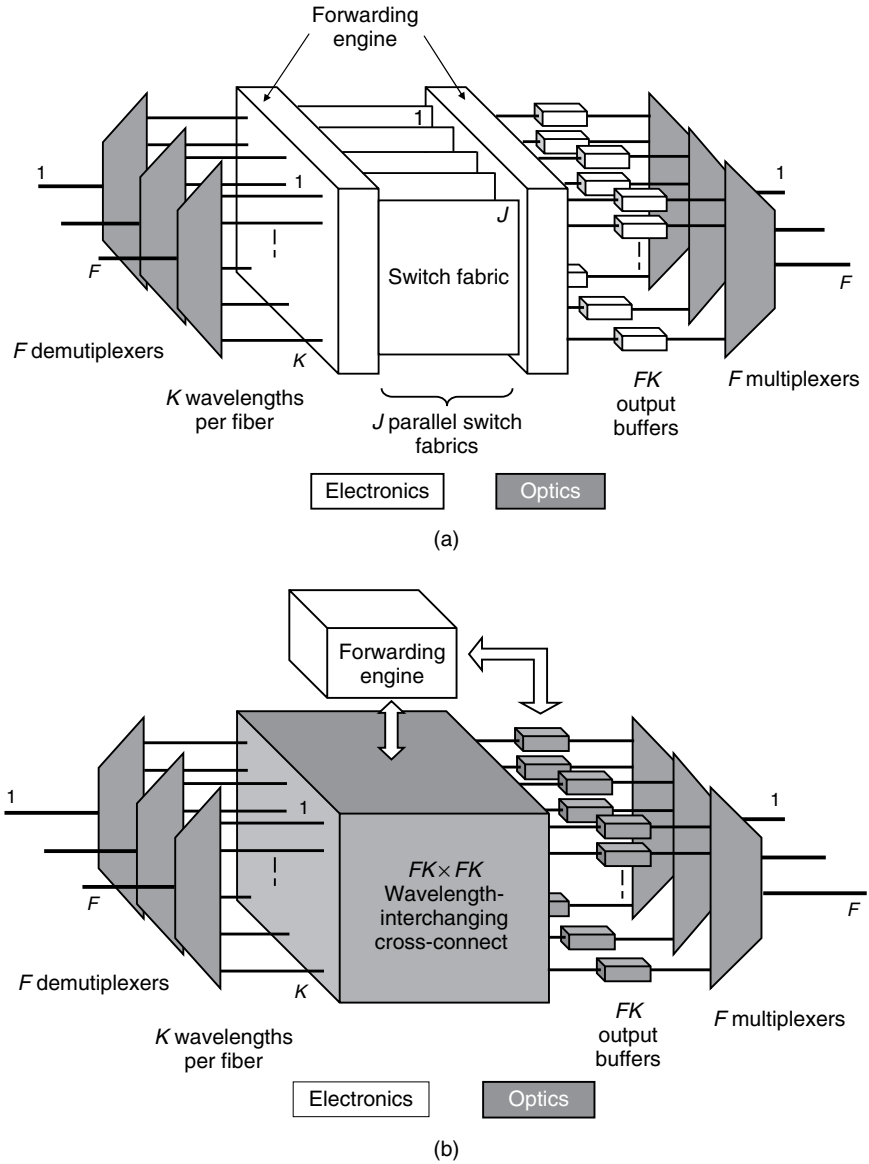

Figure 17.3 Data plane and demultiplexers/multiplexers. (a) Electrical packet switch. (b) Optical packet switch.

output ports, for simplicity. The number of output buffers is FK. A total of FK O/E converters [not shown in Figure 17.3(a)] are required at each of the FK input ports, and FK E/O converters (also not shown) are required at each input to the output multiplexers. The wavelengths of these E/O converters are configured so that each one of

them matches the wavelength of its multiplexer port. In the electronic packet switch in Figure 17.3(a), the forwarding engines are linked directly to the J parallel switching fabrics shown in Figure 17.2. In the OPS in Figure 17.3. (b), the forwarding engine is an electronic processor that sits outside the switch fabric. The switch fabric is an $FK \times FK$ wavelength-interchanging cross-connect. If the packet switch is to be optical, this fabric must also be optical.

The $FK \times FK$ wavelength-interchanging cross-connect in Figure 17.3(b) performs the same function as the signal path of the routing engines in Figure 17.3(a), together with the J parallel electronic switch fabrics in Figure 17.3(a). One advantage of the electronic switch fabric in Figure 17.3(a) over the optical switch fabric in Figure 17.3(b) is that it does not require tuneable wavelength converters (TWCs). This is because an electronic switch fabric uses electronic switching to direct each data stream to the appropriate output port, where the E/O converter only requires a fixed wavelength.

Optical packet switching has been studied by researchers in many laboratories for around 20 years [2 8]. More recently, research in the related field of optical burst switching has also gained momentum [8, 9]. In optical burst switching, the optical buffering problem is eliminated by removing the buffers. By aggregating a number of IP packets into a longer burst, the need for a cross-connect with a fast switching time on the order of 1 ns is relaxed. However, some studies indicate that the throughput limitations in OBS networks may increase network costs [10]. In addition, it is not clear whether OBS is compatible with conventional Transmission Control Protocol/Internet Protocol (TCP/IP) networking. Chapter 16 of this volume contains an overview of optical packet switching and optical burst switching, and the reader is referred to Chapter 16 for a more detailed description of the architecture of optical burst switches.

17.2.2 Energy and Power in Electronic Routers

Figure 17.4 shows how the performance (measured in terms of throughput in bits of data per second) of routers has grown over the period 1993 2004 [11]. The vertical axis is normalized to the capacity achieved in 1993. This particular graph refers to a succession of router models from Cisco, but similar growth has been achieved by other manufacturers [12]. Since 1993, the capacity of routers has increased by a factor of about 2 2.5 every 18 months [12, 13]. Large routers generally come equipped with 10 or 40 Gb/s line cards and are scaleable in capacity, depending on the number of installed line cards and the number of racks. Figure 17.5 shows three equipment racks of one of the largest commercially available routers the Cisco CRS-1. Line cards are visible on the front of the outer two racks. The O/E converters, input/output fibers, and interconnects between racks are out of view at the rear of the racks. The CRS-1 can be scaled, by increasing the number of racks, up to a capacity of 40 Tb/s. A full-configured 40 Tb/s CRS-1 router consumes approximately 1 MW of power, and occupies approximately 100 racks.

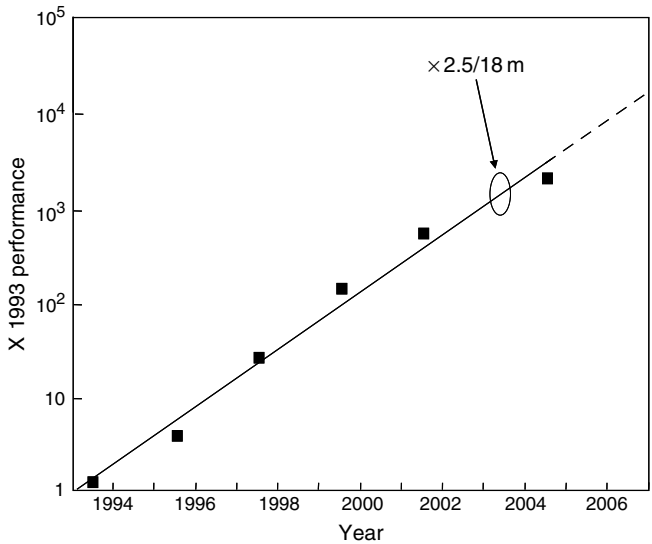

Figure 17.4 Packet switch performance against time since 1993.

Figure 17.5 CRS 1Router. Courtesy of Cisco Systems, Inc. Unauthorized use not permitted (this figure may be seen in color on the included CD ROM).

An issue that is causing concern in the telecommunications industry is the growing energy consumption and heat dissipation in telecommunications equipment. Figure 17.6 [14] shows the calculated energy consumption of an IP network, obtained using a network model based on power consumption figures published in equipment vendors' data sheets. The model network used in these calculations uses a gigabit Ethernet passive optical network (EPON) for access. The data in Figure 17.6 are normalized to a customer base of 1 million users, and the energy consumption is plotted against the average access rate per user. Figure 17.6 shows that the power consumption of the WDM fiber links (mainly due to power consumption in optical line amplifiers), the power consumption of the metro and access networks, the power consumption of the core network, and the total power consumption of the network.

It is clear from Figure 17.6 that the power consumption is dominated by the access, metro, and core network equipment. The WDM fiber links consume only about 2% of the total power. Apart from the passive optical network (PON) equipment in the local exchanges and on the outside wall of the home, most of the power in the network is consumed by IP routers, both in the metro network and in the core network. If we consider an average access rate of 30 Mb/s, and compare the power consumed by the network with the total electric power consumption of 1 million people in an Organization for Economic Co-operation and Development (OECD) country, the power consumed by the network is about 1% of the total electricity supply. While 1% may seem to be small, this percentage is rising rapidly. In addition, it needs to be recognized that the power consumed by the network is dominated by the power consumed by routers, and the routers are concentrated in a relatively small number of buildings. The engineering challenges in supplying power to these buildings and removing the dissipated heat are becoming quite challenging.

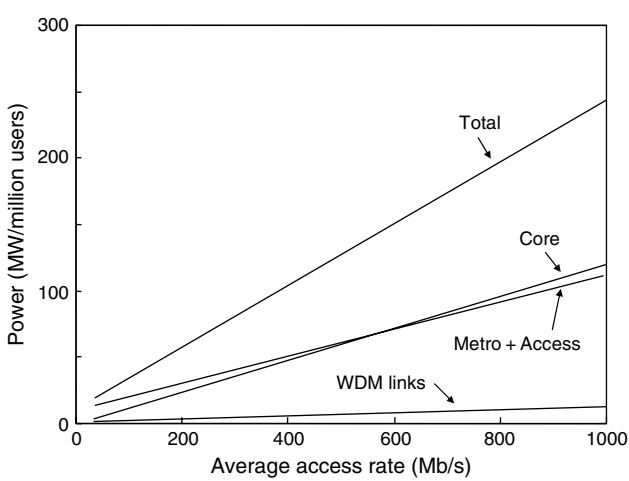

Figure 17.6 Energy consumption of an IP network per million users vs access rate.

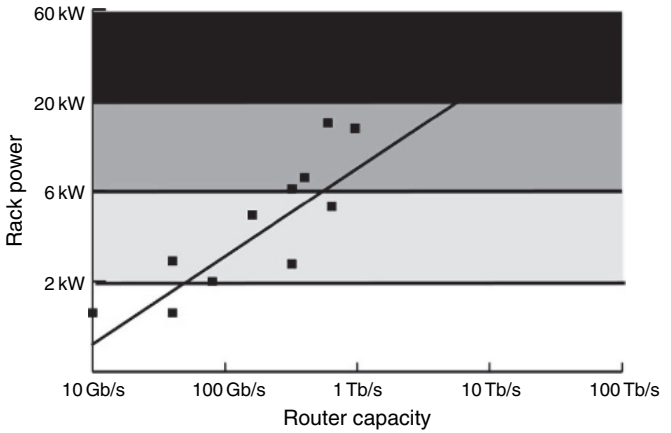

Figure 17.7 Energy consumption of routers against time since 1993 [12]. © 2006 IEEE.

Figure 7 [12] shows the energy consumption per rack in routers as a function of time from 1993 to 2004. Comparing Figs 17.4 and 17.7, it can be seen that that the energy increases by a factor of about 1.5 for every factor of 2 increase in capacity [12]. This is a rapid growth rate, but is less rapid than the growth rate of the capacity. This means that the energy dissipated per bit of data that passes through a router is decreasing by 20% per year [12]. While this small improvement in efficiency is useful, it is not sufficient to circumvent the serious power dissipation challenges facing router designers.

Figure 17.8 [11] provides a breakdown of the power consumption of a typical large single-rack router. The power consumed by the buffers is 5% of the total

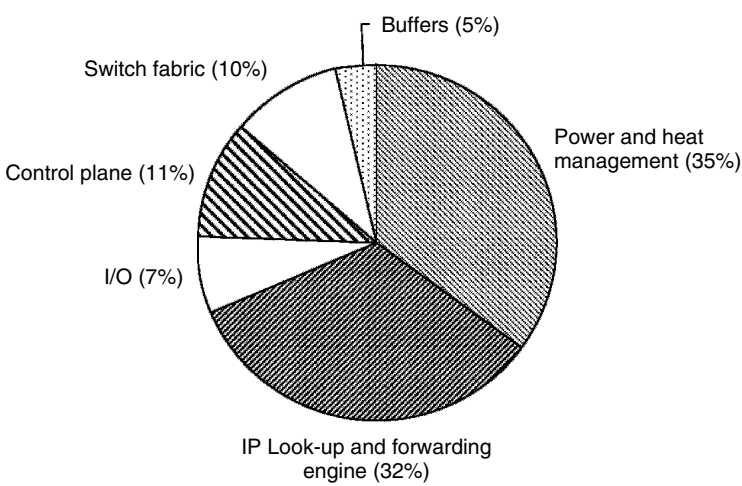

Figure 17.8 Breakdown of power consumption in a large single rack router.

power consumption, and the power consumed by the switch fabric is 10% of the total power. An additional 11% is consumed in the control plane. The I/O between boards and racks consumes 7%. The largest contributions to energy consumption are the routing processor and forwarding engine, which together consume 32% of the total power, and inefficiencies in the power supplies and air blowers to remove heat, which together use 35% of the total power. A common misconception sometimes stated in the optical packet switching literature is that the buffers and switch fabric in electronic packet switches consume most of the power in a router. However, Figure 17.8 shows that the power consumed by the buffers and the switch fabric is only a small part of the total.

The amount of data that can be transmitted over an optical fiber communications link has been increasing steadily for many years, and obeys an "optical Moore's law" [15]. While the capacity and transmission distance is increasing, in today's network, the capacity of the optical fibers is vastly underutilized. It is interesting to note that from an energy consumption point of view, the fiber transmission medium is a very minor contributor to the total power consumption in a network (see Figure 17.6). However, as shown in Figure 17.6, the energy consumption of the routers is much larger. A consequence of this will be a major shift in thinking about the ultimate capacity of the network. It is possible that energy constraints rather than fiber transmission bandwidth limitations or cost constraints will ultimately limit the capacity of the network.

One of the key objectives of this chapter is to compare optical and electronic packet switching technologies, with a focus on device and system energy consumption. A key parameter for these comparisons is the energy required to pass each bit of data through the packet switch. The energy per bit, and to a lesser extent, the size of each device, will be the most fundamentally important parameter for comparing technologies in future packet switches. Whichever technology dominates in the future (optics or electronics), it will have to consume significantly less energy than the electronic devices in current-day packet switches, and it will need to be able to be integrated into very small packages.

17.2.3 Electronic and Photonic Bottlenecks

It is often argued in the literature that optical packet switching will circumvent the so-called "electronic bottleneck" associated with electronic packet switching. The electronic bottleneck is a term used to signify the limited bandwidth or bit rate of electronic components and electronic systems such as packet switches or routers. The looming electronic bottleneck has been a major motivation for research in optical packet switching. It has also motivated developments in optical time division multiplexing (OTDM) [16,17] which could possibly be used as a replacement for electronic time division multiplexing (ETDM) in very high bit rate systems. However, while the electronic bottleneck has been seen as an issue in the past, the speed of electronics has continued to improve rapidly. ETDM now

supports commercial 40 Gb/s transmission systems, and it is expected that 100 Gb/s electronic systems will become available in the next few years [18]. ETDM at 160 Gb/s is likely to follow several years later. In addition, electronic technologies for data processing for error correction and dispersion compensation [19] are advancing into the 40 Gb/s regime and beyond, and integrated WDM optoelectronic circuits [20] are replacing conventional hybrid circuits.

As the speed of electronic switching and signal processing increases, the threat posed by the electronic bottleneck recedes. Arguably, the electronic bottleneck is no longer a major issue. Instead, a bottleneck in energy consumption is now looming as a major problem. To fully understand the relative advantages of optical and electronic technologies, it is necessary to carefully evaluate the energy consumption of competing optical and electronic components. In this chapter it is shown that the energy consumption in some optical circuits is larger than in corresponding electronic circuits. This gives rise to the notion of a photonic bottleneck [21], which could place severe limitations on system capacity on OPSs and other high-speed optical circuits.

The comparisons in this chapter are based on aggressive but plausible projections of current optical technology, and projections of CMOS electronics based on the ITRS Semiconductor Roadmap [22]. The analysis presented here uses a bit rate of 40 Gb/s, but the results can be scaled to higher bit rates such as 100 Gb/s. By way of introduction to our comparison of optical and electronic technologies, Figure 17.9 shows the switching energy of CMOS gates over the time frame 1995 2025 [22]. This curve highlights the improvements that have been achieved in CMOS technology in recent years, and the further improvements that can be expected in the near future. Also shown in Figure 17.9, for reference, is the power level of a bit stream at 40 Gb/s corresponding to the given switching energy. The numbers beside the CMOS curve refer to the feature size of each CMOS generation, in nm.

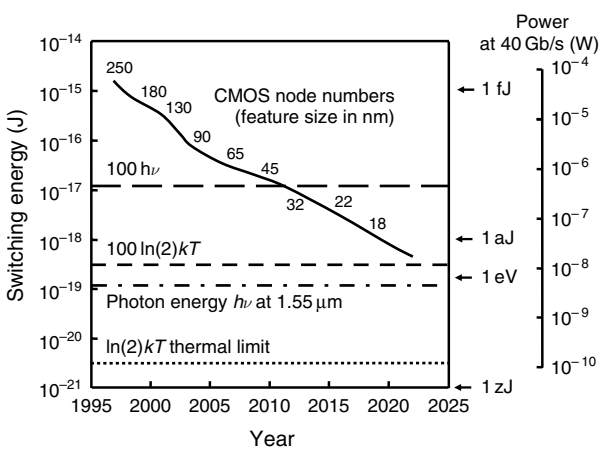

Figure 17.9 Switching energy of CMOS gates against time.

The ultimate thermal switching energy limit $\ln(2)kT$ of an electronic gate and the ultimate quantum switching energy $h\nu$ of an optical gate (i.e., the photon energy at a wavelength of 1.55 μm) are included in Figure 17.9 for comparison with CMOS gate switching energies. The actual switching energy for reliable operation will always be larger than these lower theoretical limits, and we have therefore also included the more practical lower limits of $100\ln(2)kT$ and $100\,h\nu$, respectively. It is interesting to note that around the in the year 2011, the switching energy of a CMOS gate will be equal to this $100\,h\nu$ lower limit on switching energy for an optical gate.

The energy dissipation in electronic circuits is influenced not only by the gate switching energy but also by the energy dissipated conveying data from device to device in capacitive interconnecting wires. Therefore, the total energy dissipation per logic operation is always larger than the gate switching energy. Nevertheless, it is important to recognize that CMOS and other electronic technologies are very advanced, and continue to improve. To be competitive with CMOS in terms of power dissipation, optical devices will need to achieve extremely low switching energies.

17.3 BUFFERS

17.3.1 TCP/IP and Buffering

TCP manages the flow of IP packets between each source destination pair in a network. Data sources generally have a large buffer, and data flow from this buffer is managed in collaboration with the associated receiver at the destination. Routers in the transmission path from the source to the destination also include buffers to smooth out data flows and to maximize throughput across and congested links. The required size of the router buffer is ultimately linked to the behavior of TCP sessions over links that use the buffer. Modern electronic routers are often equipped with buffers having capacities that are equivalent to delays as large as 250 ms per port. Thus, a router with 40 Gb/s line cards could have as much as 10 Gb of buffering, or about 1 GB per port. It is arguable that the buffer capacities as large as this are excessive, but it has become conventional for router manufacturers to offer this much buffer capacity.

The congestion control mechanism in TCP operates independently on each of the data flows in the network. Figure 17.10 illustrates how TCP controls the size of the so-called window as a series of packets in a single flow is sent from a source (on the left) to a destination (on the right). In Figure 17.10, the position of the data packets and acknowledgment packets (labeled Ack) are plotted against time in a form of zig-zag diagram. The packets propagate from the source, on the left, to the destination, on the right, and acknowledgments of successful packet reception are propagated back from the destination to the source. The round-trip time for a packet transmission and the return acknowledgments is RTT. In this example, the

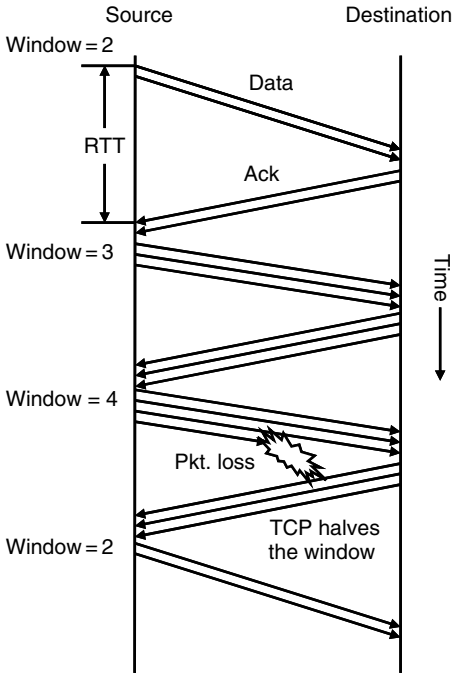

Figure 17.10 Evolution of packets under control of TCP.

window size starts with a value of 2, and accordingly, two IP packets are sent from the source toward the destination. The destination confirms that two packets have been successfully received. When the source receives this information, the window size is incremented to a value of 3 and three packets are sent. This process is repeated, with increasing numbers of packets being sent in each RTT until a packet is lost somewhere in the system when a buffer in an intermediate router overflows. In Figure 17.10, a packet is lost when the window size is 4, and at this point, the TCP forces the number of packets per round trip to be halved (i.e., the window size becomes 2).

Figure 17.11 shows a simple picture that can be used to explain how fluctuations in the window size are related to the RTT associated with an end-to-end connection between users. The example in Figure 17.11 has a single source and a single destination with a router containing buffers located between them, and with a bottleneck in the link between the router and the destination. The bandwidth B of the bottleneck link following the router is less than the bandwidth B' of the link from the source to the router. The bit rate on the bottleneck link is constant and equal to B. In this example, the transmission system uses paced TCP which, unlike the scheme shown in Figure 17.10, forces the source to distribute the outgoing packets evenly over the RTT. Because the packet transmissions are paced, the data rate on the link from the source follows a smooth sawtooth waveform as shown on

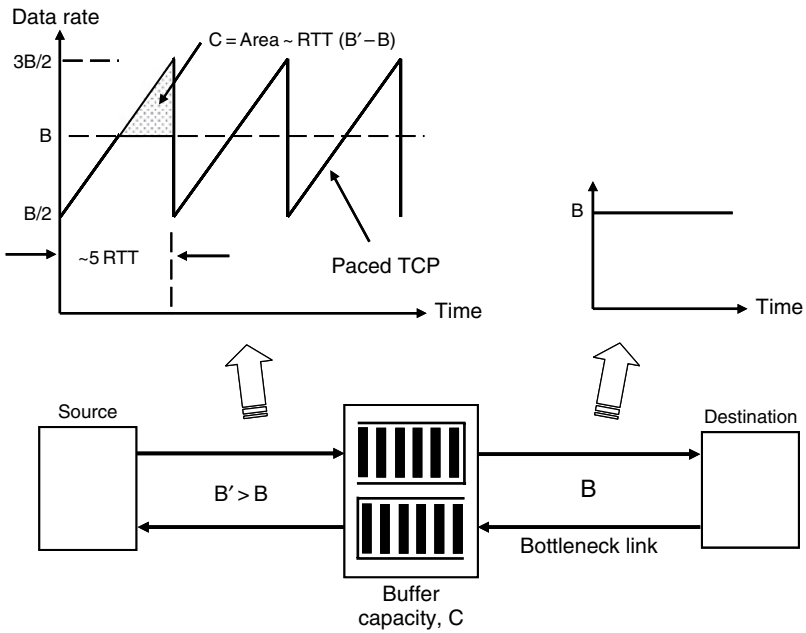

Figure 17.11 Relationship of fluctuations in window size to round trip time.

the upper left of Figure 17.11. It has an average value of B and fluctuates between $3B/2$ and $B/2$. The period of the sawtooth is roughly 5RTT, and the capacity of the buffer is equal to the area of the shaded triangle. This area is approximately $\text{RTT} \times B$. In other words, the required buffer delay for each port is roughly equal to the round-trip time, which could be as large as 250 ms for intercontinental transmission, especially if data traverse a number of routers with buffer delays.

The amplitude of the fluctuations in window size is smaller in real networks than in the simple picture given in Figure 17.11. However, in a typical network, many TCP sessions share the bottleneck link and share the buffer. With many packets from simultaneous TCP sessions sharing the buffer, the fluctuations in total data rate tend to become smoothed out. As a result, the excursions in the data rate from their average value are much less than in Figure 17.11, and it may be possible to significantly reduce the size of buffers on routers in the network. Based on a more detailed analysis, it has been suggested recently [23] that the capacity of the buffer on each port could be reduced from $\text{RTT} \times B$ to $\text{RTT} \times B/\sqrt{n}$, where n is the number of TCP sessions (i.e., the number of users sharing the same wavelength).

If each user has an access rate of 10 Mb/s and the line rate at each port is $B = 40$ Gb/s, the maximum number of users per wavelength is $n = 4000$. On this basis, the buffer capacity per port could be reduced by a factor of $1/\sqrt{4000}$, from 10 to 160 Mb, or about 16×10^3 IP packets with an average packet length of 10 kb. If the access rate for each user increases to 1 Gb/s, the required buffer capacity

increases to 1.6 Gb or 160×10^3 IP packets. More recently, it has been suggested that the buffer capacity could be reduced to around $\log(W)$, where W is the maximum window size [24], which suggests [25] that the buffer capacity could be as small as 10 20 packets, or around 200 Kb. The suggestion that buffers could be as small as this has rekindled interest in optical packet switching. However, it remains an open question as to whether buffers as small as this will be viable in practice.

17.3.2 Buffer Parameters

In our comparison of optical and electronic technologies for buffers, we focus on two key parameters: power dissipation and footprint (i.e., size). As pointed out in Section 17.2.2, the energy consumption of the buffers in a router is only a small fraction of the total energy consumption in the router. In addition, the board area occupied by buffer dynamic random-access memory (DRAM) memory chips is only a small fraction of the total board area. In comparison, we will show that the power dissipation and footprint of optical buffers are generally larger than for electronic buffers. To provide a consistent frame of reference, we will consider the write/store/read energy per bit in each buffer and the size of a stored bit. The total size of a buffer is the size of a stored bit multiplied by the capacity of the buffer, and the dissipated power of a buffer is the write/read/store energy per bit multiplied by the bit rate of the data passing through the buffer.

17.3.3 Delay Line Buffers

It has been widely recognized since the early days of optical packet switching that a key limitation on the viability of optical packet switching is the lack of a viable optical buffer technology. There have been many practical demonstrations of small-scale OPSs using a variety of buffer arrangements based on optical delay lines. Overviews of buffering for optical packet switching are given in Refs [26] and [27]. Figure 17.12 [28] summarizes some of the key delay line buffer structures that have been reported in the literature. Figure 17.12(a) is a simple variable delay line. In this figure, the broad arrows represent a control signal that is used to adjust the delay time. This control of the delay time is essential because any buffering or storage of data requires that the process of reading the data from the buffer is controllable. Figure 17.12(b) shows a variable (or fixed) optical delay line, combined with a crosspoint, in a feedback (recirculating loop) configuration. Unlike Figure 17.12(a), the delay time in Figure 17.12(b) does not need to be controllable because data can be read out by controlling the state of the crosspoint. Figure 17.12(c) is a feed-forward arrangement with crosspoints and delay lines.

Buffers can be constructed by combining the building-blocks in Figure 17.12 either in cascade, as shown in Figure 17.13(a), or in parallel as shown in Figure 17.13(b) [28]. If the cascaded stages in Figure 17.12(a) are simple variable delay

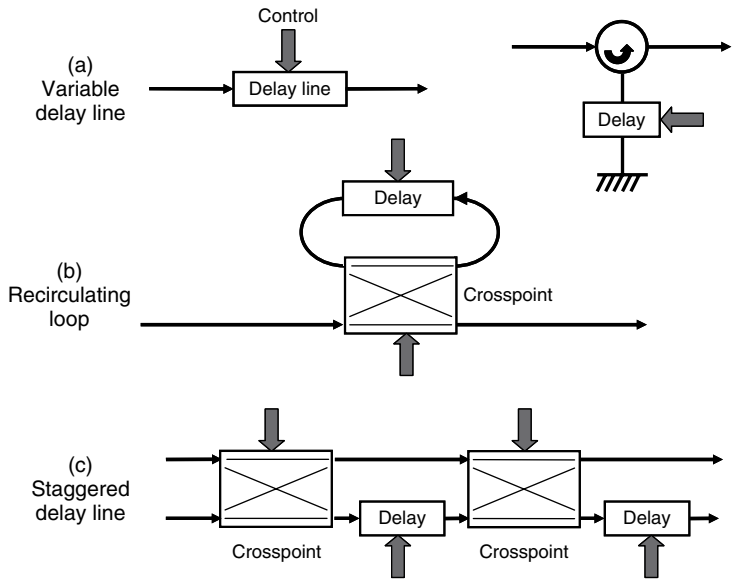

Figure 17.12 Some key delay line buffer structures [28]. (a) Variable delay line. (b) Recirculating loop. (c) Staggered delay line. © 2006 IEEE.

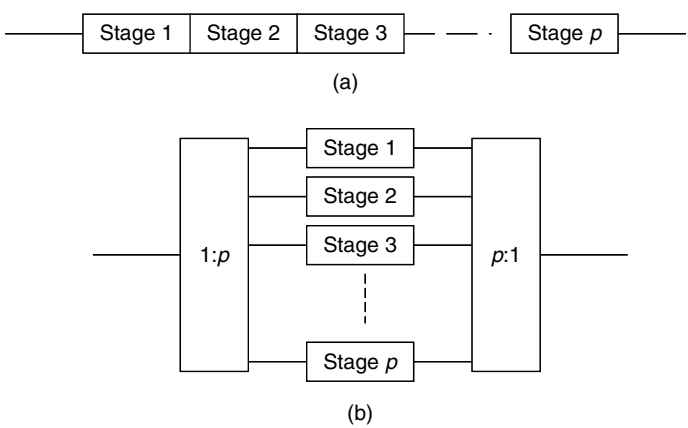

Figure 17.13 (a) Cascaded buffers. (b) Parallel buffers. [28] © 2006 IEEE.

lines of the type shown in Figure 17.12(a), the cascade is a first-in-first-out (FIFO) buffer, in which the order of packets emerging from the buffer is the same as the order of packets entering it. The recirculating loop buffer in Figure 17.12(b) can operate as a FIFO buffer, but if more than one packet is stored in the delay, the order of the packets can be changed. There is a common misconception that less waveguide delay is required in recirculating buffers than other buffer memories.

However, the reality is that while a packet is circulating in the loop, no other packets can enter it. Therefore, if it is necessary to buffer a stream of closely spaced incoming packets, multiple recirculating loops are required. This can be achieved using the cascade configuration of Figure 17.13(a) or the parallel configuration in Figure 17.13(b).

Many of the optical buffers in OPS system experiments in the literature are based on delay lines using optical fiber as the waveguide. A wide variety of buffers based on fiber delays have been reported. A possible alternative to fiber delay lines are low-loss integrated silica delay lines [29]. While these waveguides are more compact than fiber delay lines, their data storage capacity is limited by waveguide losses.

A recent surge of research activity in slow-light technologies [30 34] suggests that slow light may prove useful for buffer applications. Because of the lower group velocity, the physical size of the individual bits of data is smaller and the required length of the waveguide for a given storage capacity is reduced. This in illustrated in Figure 17.14, which shows the group velocity, bit rate, bit period and, the physical bit length as a function of position x in a waveguide that undergoes a sudden transition from a regular waveguide to a slow-light waveguide with a reduced group velocity [35]. The length of an individual bit of data is equal to the bit period times the group velocity. Consequently, the physical length of the bits is reduced from L_{in} on the input line to the smaller length L_{bit} on the slow-light waveguide.

The group velocity ν_{g} in a slow-light waveguide can be written in terms of the free-space velocity c, the effective refractive index n of the waveguide, and the optical frequency ω:

$$\nu_{\text{g}} = \frac{c}{n + \omega \dfrac{dn}{d\omega}} \tag{17.1}$$

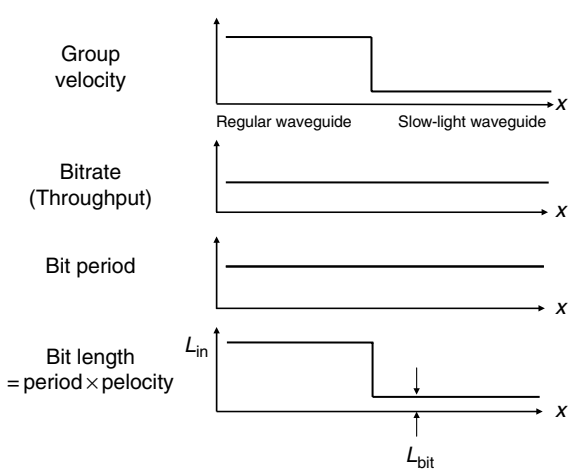

Figure 17.14 Group velocity, bit rate, bit period, and bit length in slow light waveguide [28]. © 2006 IEEE.

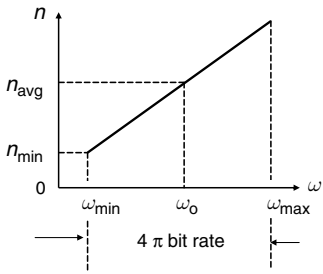

Figure 17.15 Effective refractive index vs optical frequency in an ideal slow light waveguide.

It is easy to see from Eqn. (17.1) that the group velocity can be much smaller than c if the $\omega(dn/d\omega)$ term is large. For distortionless slow-light propagation, the term $\omega(dn/d\omega)$ needs to be large and independent of the optical frequency across the signal pass-band. Figure 17.15 shows this effective refractive index against the optical frequency [35]. The ideal refractive index profile is approximately a straight line against frequency and has a minimum value $n_{\min}$ at optical frequency $\omega_{\min}$ and a maximum value at optical frequency $\omega_{\max}$. The average effective refractive index across the signal band is n_{avg}, and the centre frequency ω_0 of the signal is aligned with the center of the region of linear slope. To minimize the length L_{bit} of the stored bits, the optical radian frequency bandwidth of the data signal (shown as 4π *bitrate* in Figure 17.15) should fully occupy the device bandwidth from $\omega_{\min}$ to $\omega_{\max}$ [35]. The fundamental lower limit on the bit size L_{bit} is one optical wavelength, and is obtained when $n_{\min} = 0$ [35]. In other words, no matter which slow-light technology is employed, one can never compress a bit of data to a dimension less than a wavelength. In practice, it would be difficult to achieve such a small value for L_{bit}.

Slow-light technologies that can approximate the ideal characteristic in Figure 17.15 include electromagnetically induced transparency (EIT) [32], coupled-resonator waveguides (CRWs) [36], and photonic crystal (PC) waveguides [33]. While slow-light delay lines show some promise, it is important to recognize that the capacity of slow-light delay line buffers is limited by a number of factors. At a very fundamental level, delay-bandwidth product or delay-throughput product is limited by bandwidth of the slow-light medium. The delay-throughput product can never exceed this limitation [35, 37]. In addition, as pointed out in the previous paragraph, the length of waveguide occupied by a single bit of data cannot be less than a wavelength. At a more practical level, the capacity of slow-light delay lines is limited by dispersion in the waveguide [37, 38] and by losses in the waveguide [28, 39].

To reduce the effect of loss and dispersion in a delay line buffer, it may be necessary to provide loss and dispersion compensation. Figure 17.16 shows a schematic diagram of a delay line buffer, including dispersion compensation and gain to overcome losses. The delay line in Figure 17.16 comprises n cascaded stages,

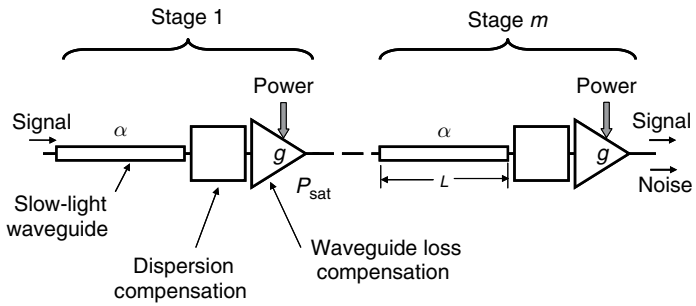

Figure 17.16 Buffer delay line structure showing dispersion compensation and gain blocks for loss compensation.

with each stage including a length of slow-light waveguide of length L and with a loss coefficient α, a lossless dispersion compensator, and a gain block of gain g that compensates the waveguide loss α. Using this model of a loss-compensated delay line, it is possible to determine the limitations on performance of a delay line buffer. These limitations are governed by the properties of the delay line, by the amplified spontaneous emission (ASE) noise generated in the loss-compensating amplifiers, and by the saturation of these amplifiers as the ASE noise accumulates [28].

Figure 17.17 shows the buffer length (i.e., the length of a stored bit L_{bit} times the capacity of the buffer in bits) as a function of the bit rate for various slow light delay lines, with buffer capacities N_{bit} of 100 and 10,000 [28]. In Figure 17.17 it is assumed that there are no dispersion compensators in the delay line model of

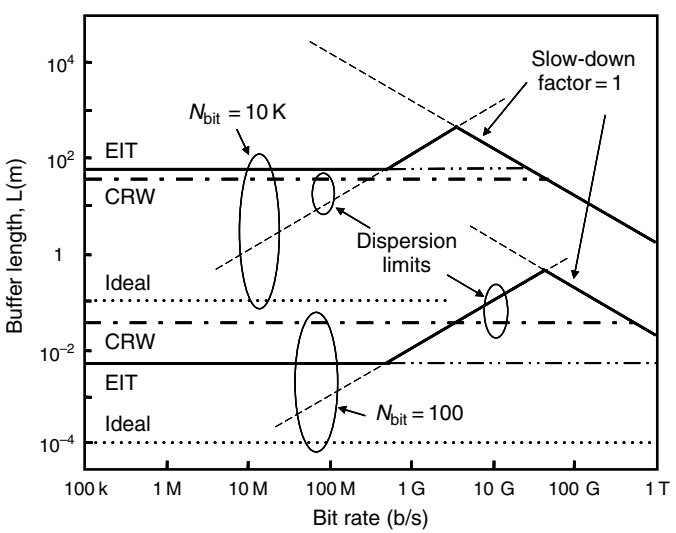

Figure 17.17 Buffer length vs bit rate for 100 bit and 10 kb delay line buffers [28]. © 2006 IEEE.

Figure 17.16. It is also assumed that at all bit rates, the bandwidth of the slow light medium is adjusted to match the full optical bandwidth of the data (see Figure 17.15). The three slow-light delay line technologies represented in Figure 17.17 are EIT and CRW delay lines (solid and broken lines) and an ideal slow-light delay line that is dispersionless and that has a minimum bit length of one wavelength. At low bit rates, all of the buffer lengths are independent of bit rate. This is because the slope of the effective refractive index in Figure 17.15 increases as the bit rate decreases. Above about 500 Mb/s, the buffer length increases in EIT devices due to dispersion. The solid lines with negative slopes in Figure 17.17 represent a slow-down factor of 1. On this line, the light is not slowed.

The influence of losses on the maximum achievable capacity of a delay line buffer at a bit rate of 40 Gb/s is illustrated in Figure 17.18 [28]. The left-hand vertical axis in Figure 17.18 is the maximum capacity of lossy delay lines in which optical amplification is used to overcome the losses (see Figure 17.16). The saturation power on the horizontal axis of Figure 17.18 is the saturation power of the loss-compensating amplifiers in Figure 17.16. The maximum achievable capacity for a delay line using semiconductor optical amplifiers (SOAs) with a saturation power of 10 mW and with an attenuation of 0.01 dB/cm is about 40 Kb. For an attenuation of 0.1 dB/cm, the maximum capacity is about 1 Kb. These capacities are not large enough for buffering in optical packet switching. Therefore, the attenuation coefficient of a slow-light waveguide (and, in fact, any waveguide delay line) needs to be significantly smaller than 0.05 dB/cm if the delay line is to be used as a buffer in an OPS.

Also shown in Figure 17.18 is the energy per bit, which is plotted against the right-hand axis. This energy has been calculated by determining the total pump power into the amplifiers and dividing this by the bit rate [28]. The energy curve in Figure 17.18 applies to all delay lines. For the examples considered in the previous

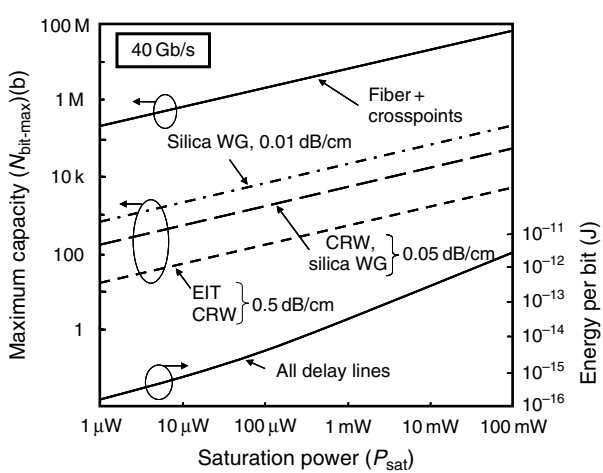

Figure 17.18 Buffer capacity vs saturation power of loss compensating amplifiers [28]. © 2006 IEEE.

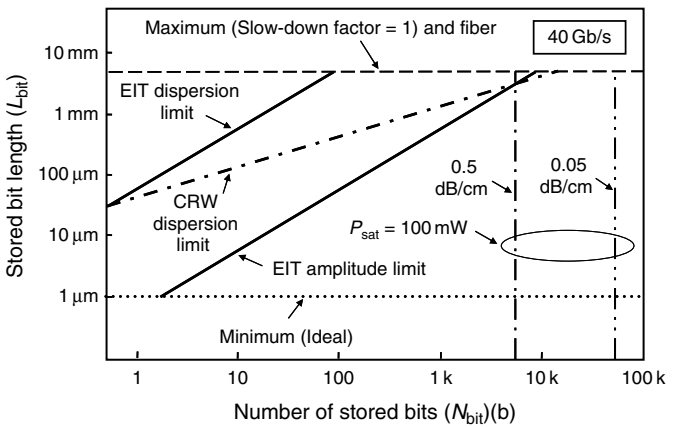

Figure 17.19 Length of a stored bit vs the number of stored bits [28]. © 2006 IEEE.

paragraph, the write/store/read energy per bit is 0.5 pW. Figure 17.19 shows the length L_{bit} of a stored bit against the capacity N_{bit} for a bit rate of 40 Gb/s. This figure includes limitations caused by dispersion (when no dispersion compensation is included) and the limitations caused by losses, in this case for a saturation power of 100 mW. The maximum size of a stored bit (broken line) is the length of a 40 Gb/s bit in a regular waveguide (approximately 5 mm). The minimum L_{bit} that can be achieved with any slow-light delay line is one optical wavelength (approximately 1 µm) and is indicated in Figure 17.17 with a dotted line. The allowed region of operation of a slow-light delay line lies above the "ideal" minimum length, below the least of the EIT or CRW dispersion limits and the EIT amplitude limit, below the "slow-down factor = 1" line, and to the left of the attenuation limits.

There are two distinct classes of slow-light delay lines Class A and Class B (Class B is also referred to as "adiabatically tuneable") [35]. In Class A delay lines, the group velocity of the light is slowed across an interface between two waveguides with different group velocities as shown in Figure 17.14. In Class B delay lines, the velocity of the light is reduced adiabatically and uniformly across a data packet. A common misconception in the literature is that Class B delay lines circumvent the delay-throughput product limitation encountered in Class A delay lines. However, this is not the case. The reason is that in Class B delay lines it is necessary to load an entire packet or segment of a packet into the delay line before the velocity is adiabatically reduced [35, 40]. Thus, a single Class B delay line cannot continuously accept input data, and as a result, its effective bandwidth or throughput is limited [35].

As pointed out earlier, the minimum length of a stored bit of data in any slow-light delay line is approximately one wavelength λ. This is much smaller than could be achieved with fiber delay lines. Figure 17.20 shows a folded waveguide layout with an interwaveguide spacing of 5λ [28]. In an ideal slow-light delay line, where each bit is compressed down to a size of λ, the storage density is $1/5\lambda^2$ or

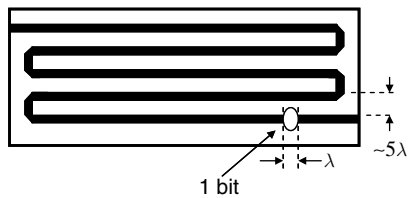

Figure 17.20 Folded layout of planar waveguide delay line [28]. © 2006 IEEE.

approximately 200 Gb/m^2. In a more realistic scenario, where a bit is compressed down to a size of 100 λ, the storage density is 2 Gb/m^2. Note that these calculations of storage density do not include any crosspoints or other control or switching devices in the buffer.

17.3.4 Resonator Buffers

A possible alternative to delay line buffers is an array of high-Q optical resonators that trap the energy of individual data pulses [41]. Optical resonators with Q values in the range $10^5 - 10^6$ have been reported in PC [41] and in microring resonators [42], and even higher Q's have been reported in a crystalline whispering gallery resonator [43]. These high-Q resonators can trap energy for a nanosecond or more [41].

Figure 17.21 shows a possible structure for an optical ring resonator RAM that can store a number of multiple-bit words or packets. This memory is a true RAM because words can be retrieved in random order. A packet to be written in the

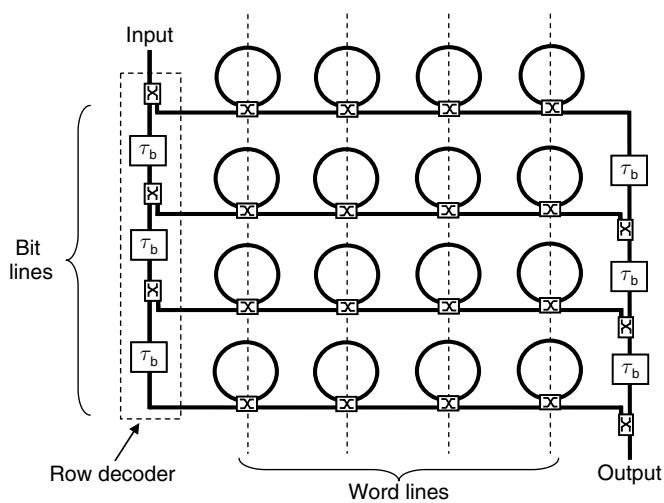

Figure 17.21 Optical ring resonator random access memory. © 2008 IEEE.

RAM enters from the top left into a serial-to-parallel demultiplexer (i.e., a row decoder) comprising a cascade of delay lines of length equal to a bit period τ_b, with a crosspoint between each delay line. To store the packet, once all the bits in a data word have entered the cascaded τ_b delay lines, the crosspoints in the serial-to-parallel demultiplexer, are simultaneously switched and the parallel bits enter the horizontal waveguides in Figure 17.21 (i.e., the bit lines).

Similarly, when data are read out from the RAM, bits from the ring resonators are converted from parallel-to-serial in a parallel to serial converter comprising another cascade of delay lines of length equal to one bit period, with a crosspoint between each delay line. The word lines in Figure 17.21 control the variable couplers in the cells. If the variable couplers are electro-optical directional couplers, these word lines are electrical wires.

Like delay line buffers, ring resonator RAM buffers suffer from optical losses. With a resonator Q of 10^6, the retention time of a stored pulse is approximately 5 ns. By way of comparison, the retention time needed to store 10 IP packets at 40 Gb/s is around 2.5 μs, or about three orders of magnitude larger than this. Clearly resonator buffers will not be suitable for packet switching without incorporating some gain to overcoming the losses. But just as with delay line buffers, optical amplification in resonator buffers will come at a cost of noise and gain saturation. The storage density in ring resonator RAM is limited by the size of the resonators and the crosspoint switches. If the diameter of the ring resonator is 100 μm and the resonators are spaced by 50 μm, the storage density is on the order of 40 Mb/m^2.

17.3.5 Electronic Buffers

Projections to the year 2018, based on the 2005 *International Technology Roadmap for Semiconductors* [22], indicate embedded DRAM (eDRAM) with an intrinsic storage capacitance of around 1 fF, a read/write energy of 1.6×10^{-16} J/bit for each cell, a retention time of 64 ms, and a read/write cycle time of 200 ps. The projected cell area is approximately 0.0064 μm^2. Figure 17.22 shows a simplified layout and cell circuit model for an eDRAM chip, showing an effective cell pitch of 80 nm. Using this cell pitch, and with an array area efficiency of 60% [22], one can observe that the projected storage density of eDRAM is approximately 100 Tb/m^2. This means that the storage density of eDRAM is almost five orders of magnitude larger than in an EIT or CRS delay line with a capacity of 100 b, where the bit length is around 100 μm and the storage density is around 2 Gb/m^2. It is clear that on the basis of chip area, optical delay lines are not competitive with electronic buffers.

The read/write energy of an eDRAM is orders of magnitude larger than the intrinsic read/write energy of a single cell. This is because significant energy is consumed by a range of on-chip devices including word and bit lines, decoders, sense amplifiers, and buffers. For our comparisons with optical buffers, we assume that the total power consumption of 20-nm feature-size CMOS eDRAM together with 40 Gb/s I/O interfaces (which dominate the power consumption) will be

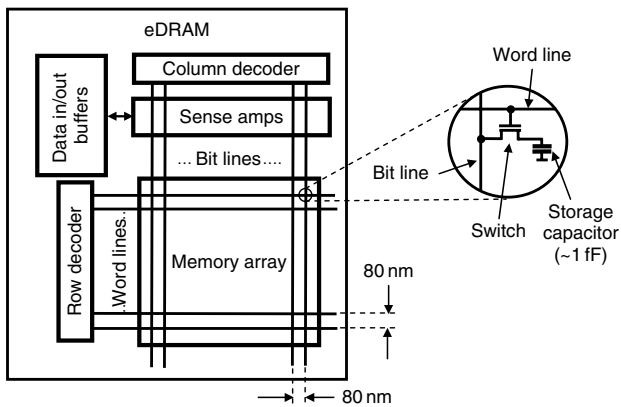

ITRS 2018: eDRAM	
Read/write energy*	1.6×10^{-16} J
Array storage density*	150 Tbit/m^2
Retention time	64 ms
Read/Write time	200 ps

*Excludes decoders and buffers

Figure 17.22 CMOS random access memory.

around 40 mW, or 1 mW/Gb/s. For the purposes of the comparisons presented here, it is assumed that the on-chip peripheral circuits occupy the same chip area as the memory cells. Thus overall storage density (not including the I/O interfaces) is estimated to be 50 Tb/m^2.

17.3.6 Comparison of Buffer Technologies

Table 17.1 compares the energy per bit and power dissipation of optically amplified delay line buffers and CMOS eDRAM for buffers with capacities of 5 IP packets (50 kb) and 100 IP packets (1 Mb), at a bit rate of 40 Gb/s. The delay line buffers are subdivided into slow-light delay lines, with attenuation coefficients of 0.05 dB/cm and 0.5 dB/cm, and fiber delay lines, with an attenuation of 0.2 dB/km [28]. Note that the energy and power figures for slow-light delay lines also apply to single-chip non-slow-light delay lines such as silicon planar waveguides [29]. Except where noted, the parameters used in Table 17.1 are the same as used for Figure 17.16. Table 17.1 uses output signal-to-noise ratios (SNRs) of 30 so that multiple optical devices can be cascaded. Each of the entries in Table 17.1 applies to a single buffer of the specified capacity. A router with n ports will require n of these buffers. In all slow-light delay lines and the fiber delay lines in Table 17.1,

Table 17.1
Energy per bit and power dissipation of optically-amplified delay line buffers and CMOS eDRAM.

			Capacity			
			5 IP packets (50 kb)		100 IP packets (1 Mb)	
	α	SNR (dB)	E_{bit}	Power	E_{bit}	Power
Slow light	0.05 dB/cm	30	1.2 pJ	50 mW		
	0.5 dB/cm	30				
Fiber	0.2 dB/km	30	1.3×10^{-2} fJ	5 μW	6.9 fJ	260 nW
CMOS			0.2 pJ	8 mW	0.2 pJ	8 mW

single-wavelength operation is assumed. As pointed out earlier, some efficiency in device area could be achieved through WDM. However, the energy per bit and total power dissipation cannot be improved by employing WDM.

The lowest power consumption in Table 17.1 is achieved with fiber delay lines. However, because of their physical bulk, fiber delay lines are generally not considered to be practical. The next lowest power consumption is in CMOS buffers, and the largest consumption is in slow-light delay lines and other planar waveguide delay lines, which consume the same amount of power as slow-light delay lines with the same waveguide losses and the same buffer capacity. The blank entries in Table 17.1 indicate where slow-light buffers cannot be realized in practice because the power dissipation is impractically large and/or because bandwidth limitations are not met.

17.4 INTERCONNECTS, WAVELENGTH CONVERTERS, AND REGENERATORS

Interconnects are a key component in any large-scale optical or electronic packet switch [12]. Today's large multirack routers use optical interconnects between racks and a range of optical and electronic interconnects between boards. As the number of boards and racks increase in future generations of routers, so will the power consumption of the interconnects. In any OPS, all interconnects need to be optical. Otherwise optical transparency through the system will be lost. Interconnects in OPSs will simply be lengths of fiber between optical circuits or boards. In large switching fabrics using wavelength converters in conjunction with wavelength-selective devices such as AWGs, interconnects may include or be interfaced to wavelength converters and possibly signal regenerators. Therefore, it is useful to consider interconnects, wavelength converters, and regenerators together.

In this section, we present some simple models of interconnects, 2R regenerators, and wavelength converters. We focus on optical interconnects for electronic packet

switches and wavelength-converting interconnects for OPSs. In interconnects for electronic packet switches, an electrical signal is converted to the optical domain via an E/O converter for transmission and then returned to the electronic domain via an O/E converter. In contrast, wavelength-converting optical interconnects include optical to electronic to optical (O/E/O) devices, in which the incoming optical signal is converted to the electronic domain and then converted back to the optical domain at the output, and optical (O/O) devices, in which the signal remains in the optical domain at all times. It is beyond the scope of this chapter to give a detailed review of wavelength converters and regenerators. Detailed overviews of optical wavelength converters and regenerators are presented elsewhere [44].

A key figure of merit that is used in the literature to characterize interconnects (electronic and optical) is the energy consumption per bit of data transferred. This energy is often expressed in terms of power consumption per Gb/s of data, with units of mW/Gb/s. It is interesting to note that while the interconnect research community pays great attention to the energy consumption per bit, researchers working on optical wavelength converters and optical regenerators (including the present author) have, to date, largely ignored this very important figure of merit. As these devices move from the research laboratory into possible practical applications, there will be much greater need to pay close attention to their energy consumption. In this section, we will present a simple energy model of interconnects, wavelength converters, and 2R regenerators, and use this model to optoelectronic and optical devices.

17.4.1 Interconnects

Recent examples of low-power, low-cost E/O/E optical interconnects include a high-capacity 250 Gb/s 48-channel interconnect for back plane applications, with a power dissipation of 1.5 W, or 6 mW/Gb/s [45], and a 4-channel 10 Gb/s transceiver using 80-nm CMOS and VCSELs with a power consumption of 2.5 mW/Gb/s [46]. Near-term projections of and power dissipation in optical interconnects [47] suggest that power dissipations below 2 mW/Gb/s are achievable, and it is reasonable to expect that even lower dissipation will be obtained with future generations of CMOS and other electronic technologies. In this chapter, estimates of interconnect performance are based on the optimized designs presented in Ref. [47] and are projected to 22-nm CMOS technology. Using this approach, one can find the energy per bit to be 0.4 mW/Gb/s in an optimized E/O/E interconnect with a path loss of 6 dB. The model is shown in detail in Figure 17.23, which shows power levels for an interconnect operating at 40 Gb/s.

The O/E/O interconnect model in Figure 17.23 uses a CW laser and an external modulator. In principle, the modulator could be eliminated and the laser could instead be directly modulated. However, it is difficult to achieve efficient direct modulation in the 40 GHz region when the laser is operated at low power levels. Nevertheless, if 40 GHz direct modulation could be achieved, the total energy of

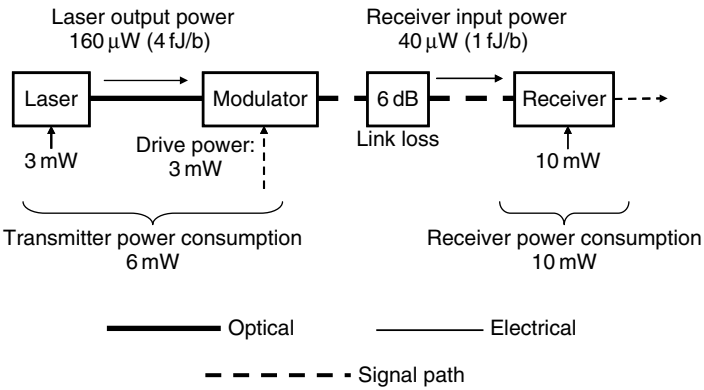

Figure 17.23 Power consumption model of optical interconnect.

an interconnect using directly modulated lasers would be a little smaller than the total energy in Figure 17.23. The receiver sensitivity in Figure 17.23 is 40 μW, or 1 fJ/b at 40 Gb/s, the laser output power is 160 μW, the total power consumed by the transmitter is 6 mW (150 fJ/b), and the total power consumed by the receiver is 10 mW (250 fJ/b). The total energy consumption per bit is 0.4 pJ.

17.4.2 2R Regenerators and Wavelength Converters

An O/E/O 2R regenerator and an O/E/O wavelength converter are both similar to the interconnect in Figure 17.23, but the receiver is at the input and the modulator is at the output. Figure 17.24 shows the model used here for an O/E/O 2R

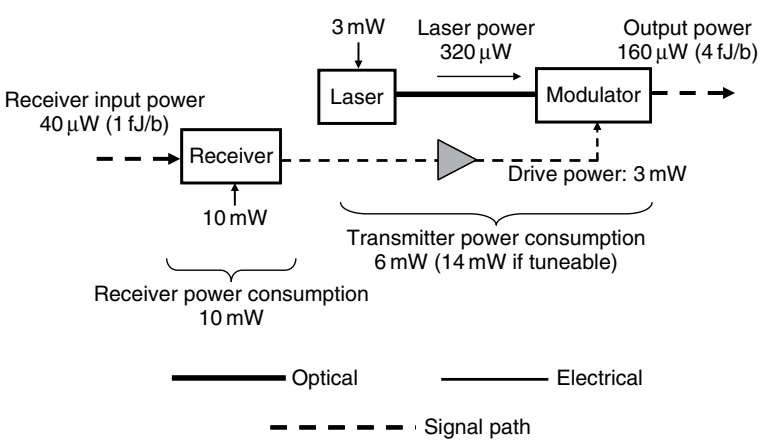

Figure 17.24 Power consumption model of O/E/O wavelength converter.

regenerator and wavelength converter. The figure summarizes the drive power levels and the optical signal levels. If the 2R regenerator or wavelength converter has a fixed output wavelength, the total power consumption is the same as for the E/O/E interconnect in Figure 17.23. If the regenerator or wavelength converter is tuneable, additional drive current (power) is required to drive the tuning region of the tuneable laser chip. In our model, this additional power is 3 mW.

Two candidate technologies for optical regenerators and wavelength converters are SOAs [48] and highly nonlinear optical fibers [49]. Highly nonlinear fiber devices currently operate at optical power levels of at least 1 W [50], which is two orders of magnitude larger than practical power levels. Failing an unexpected large improvement in the nonlinearity of these fibers, they do not appear likely to provide a viable platform for wavelength conversion or regeneration. A reduction in the attenuation of highly nonlinear fibers would enable operation at lower power levels, but this would require device lengths of 100 m or more, which would not be practical for use in packet switches that require thousands of devices in one piece of equipment.

SOAs are able to operate at relatively low optical power levels, but they require a large electrical drive power typically on the order of 200 mW or more (~100 mA of drive current or more). There has been some improvement in the efficiency of SOAs, but the power consumption of SOAs and laser diodes is not falling as rapidly with time as the power consumption of CMOS gates. Figure 17.25 shows the model used here for an SOA-based wavelength converter. A very low electrical drive power of 50 mW (~25 mA) is assumed and a drive power to the laser is 2 mW. These are aggressively small power levels, but not impossible targets for device drive powers in the 2020 timeframe.

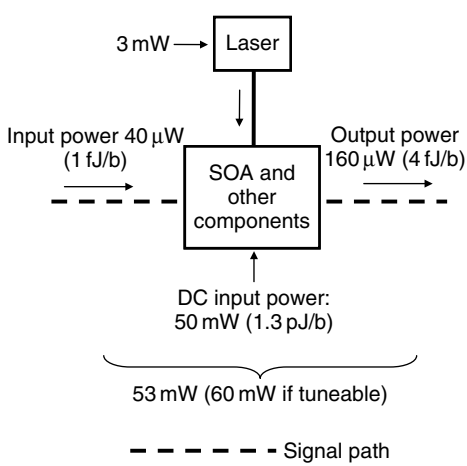

Figure 17.25 Power consumption model of semiconductor optical amplifier (SOA) O/O wavelength converter.

17.5 SWITCH FABRICS

This section explores a range of switch fabrics and presents a model of energy consumption in different switch fabric technologies.

17.5.1 Optical Switch Fabrics

Overviews of optical cross-connect switch fabrics are provided in Refs [51 53]. Chapter 16 of this volume includes a discussion of optical switch fabric technologies for optical packet switching. A key requirement of switch fabrics for packet switches is that the switching time is small compared with the packet length. The length of an IP packet at 40 Gb/s can be between as small as 13 ns and as large as 300 ns. Therefore, in order to avoid inefficiencies in utilization of the transmission channel, the switching of the fabric time needs to be around 1 ns or less. Another key requirement of any optical (or electronic) switch fabric for optical packet switching is that the power dissipation is manageably small. In this section, we develop an energy dissipation model of an optical switch fabric and use this model to identify power dissipation "hot spots" in the switch fabric.

Figure 17.26 shows a general picture of the internal components of a wavelength-interchanging optical cross-connect switch fabric for packet switching. Also shown in Figure 17.26 is one of the input demultiplexers, one of the output multiplexers, and three of the output buffers. The shaded rectangle in Figure 17.26 represents the $FK \times FK$ wavelength-interchanging switch fabric in Figure 17.3(b). The number of incoming and outgoing fibers is F. Each fiber carries K wavelengths as shown. The number of bits in each packet at each wavelength is N and the input power of each packet is P_{in}. The cross-connect sends packets on each

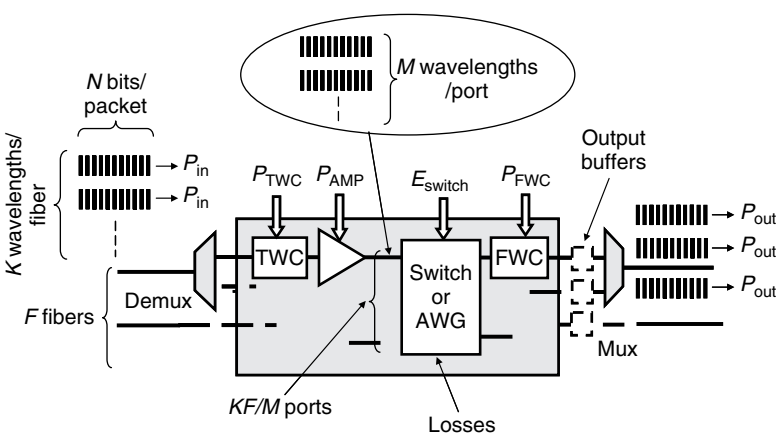

Figure 17.26 Power and energy model of wavelength interchanging optical switch fabric.

input port to an appropriate output port where the packets are buffered and re-multiplexed back onto a set of outgoing fibers at a power level of P_{out}.

The key functional blocks in the switch fabric are TWCs and fixed wavelength converters (FWCs), switches or AWGs, and amplifiers to overcome losses. For simplicity, Figure 17.26 shows only one stage of TWCs. However, as shown in Section AWG-based Switch Fabrics, multiple stages will generally be required. The output wavelength converter stages connect, via buffers, to multiplexer ports with defined wavelengths. For this reason, these wavelength converters are fixed. As shown in Figure 17.26, losses in the switch fabric typically arise in the AWGs and/or the switches. In addition, some wavelength converter technologies introduce losses that need to be compensated. Other potential causes of loss are interconnects between components of the switch fabric.

It is sometimes argued that an advantage of optical packet switching is that it permits so-called deflection routing in the wavelength domain and in the space (i.e., fiber) domain to reduce the required capacity of the buffers. In other words, packets that experience a contention at the output port can be diverted either to a different wavelength on the desired fiber or onto another fiber, provided this alternate fiber ultimately leads to the desired destination. In principle, deflection routing can also be used in electronic packet switching. However, this requires some form of alternate route processing and is likely to result in out-of-order packet delivery. Out-of-order packet deliver can be handled by TCP but is a problem for the User Datagram Protocol (UDP).

Another potential advantage of optical switching is that it is possible, in principle, to route a group of wavelengths or a waveband through the switch fabric. This is illustrated in Figure 17.26, where M packets are simultaneously switched at one port of a switch or AWG internal to the switch fabric. By routing a waveband of M wavelengths on each port of the internal switch, the number of ports on the internal switch is reduced from KF to KF/M, as shown in Figure 17.26. The benefit of this arrangement is that by reducing the number of internal switch ports, the switch structure is simplified and power consumption may potentially be reduced. A disadvantage is that the number of ports on the packet switch is reduced, and this could reduce the number of other packet switches in the network that it could connect to. In some switch fabrics, such as the TWC/AWG architecture described later in Section AWG-based Switch Fabrics, routing of wavebands is difficult to achieve in practice.

It is sometimes argued that OPSs will consume less power than electronic packet switches because in electronic packet switches, the data are routed on a bit-by-bit basis, while in OPSs, the data are routed on a packet-by-packet basis. A simple model of power dissipation in the switch fabric in Figure 17.26 is now developed to explore this proposition. This leads to a better understanding of the energy consumption of an OPS fabric and the potential of waveband routing.

The power required per wavelength in the TWCs, amplifiers, and FWCs in Figure 17.26 is P_{TWC}, P_{AMP}, and P_{FWC}, respectively. The energy to change the state of one optical path from the input to the output of the switch is E_{switch}.

Assuming that the gain of the amplifiers is equal to the losses in the switch fabric and that the quantum efficiency of the amplifiers is 100%, then the power consumed by the amplifiers is equal to the optical power dissipated in losses. The power dissipated in the losses depends on the distribution of the gain blocks in the switch fabric and on the total losses. If a gain block is used after every 6 dB of loss, the number of amplifiers is $L_{\text{total}}/6$, where L_{total} is the total loss in dB. If $P_{\text{out}} = P_{\text{in}}$, and if the amplifiers have 100% quantum efficiency, the power consumed by each amplifier is approximately $P_{\text{out}} - P_{\text{out}}/4 = 0.75P_{\text{in}}$. Therefore, the total power consumption in all the amplifiers is approximately $P_{\text{AMP}} = 0.75K\ F\ P_{\text{in}}(L_{\text{total}}/6)$, where, as before, K is the number of input wavelengths on each input fiber and F is the number of input fibers.

Because the internal switch in Figure 17.26 has to change state only once per packet, the energy required to switch one complete packet through the switch in Figure 17.26 is the energy E_{switch} to change the state of one path in the switch fabric. The energy per bit is E_{switch} divided by the number M of wavelengths simultaneously switched by the internal switch and divided by the number N of bits per packet. Therefore, the total energy consumption per bit of data E_{bit} in the switch fabric is

$$E_{\text{bit}} = \frac{P_{\text{in}}(L_{\text{total}}/6) + P_{\text{TWC}} + P_{\text{FWC}}}{B_{\text{rate}}} + \frac{E_{\text{switch}}}{MN} \tag{17.2}$$

and the total power dissipation in the switch fabric is $P_{\text{total}} = K\ F\ B_{\text{rate}} E_{\text{bit}}$ or

$$P_{\text{Total}} = KF\left[P_{\text{in}}(L_{\text{total}}/6) + P_{\text{TWC}} + P_{\text{FWC}} + \frac{B_{\text{rate}} E_{\text{switch}}}{MN}\right]. \tag{17.3}$$

Equation (17.3) shows how the contribution of the switch energy is decreased by the factor MN. Using the O/E/O wavelength converter model in Figure 17.24, and with three stages of TWCs, one can find that the power consumption of the TWC's is $P_{\text{TWC}} = 3 \times 24 \times 10^{-3} \times K$ and the power consumption of one stage of FWCs is $P_{\text{FWC}} = 16 \times 10^{-3} \times K$. Similarly, using the O/O wavelength converter model in Figure 17.23, one can find that $P_{\text{TWC}} = 3 \times 60 \times 10^{-3} \times K$ and $P_{\text{FWC}} = 53 \times 10^{-3} \times K$. If $P_{\text{in}}(L_{\text{total}}/6) < 1$ mW, and $B_{\text{rate}} = 40$ Gb/s, (17.2) becomes

$$E_{\text{bit}} = E_{\text{WC}} + \frac{E_{\text{switch}}}{MN}, \tag{17.4}$$

where $E_{\text{WC}} = E_{\text{TWC}} + E_{\text{FWC}} = 2.1 \times 10^{-12}$ J for O/E/O wavelength converters, and $E_{\text{WC}} = 2.8 \times 10^{-12}$ J for O/O wavelength converters.

From (17.4) it is clear that the energy per bit E_{bit} is dominated by the wavelength converter energy consumption E_{WC} if E_{switch} is of the same order of magnitude as E_{WC} and the product MN is large. The magnitude of E_{switch} can vary widely, depending on the switch technology. For example, in Lithium Niobate crosspoint switches, the electrical port is usually terminated with a 50 Ω

load. If the switching voltage is 3 V, the power dissipation is 180 mW, and the switching energy per bit is this power multiplied by the bit length (25 ps at 40 Gb/s) In this case, $E_{\text{switch}} = 4.5 \times 10^{-12}$ J. In switches using SOA gate arrays (see Section SOA-based Switch Fabrics below), the electrical power consumed by a single crosspoint can be as large as 500 mW, which corresponds to $E_{\text{switch}} = 12.5 \times 10^{-12}$ J. For AWG-based switch fabrics (see Section AWG-based Switch Fabrics below), there is no electrical switch and the second term in (17.4) is zero.

The following three subsections consider two possible realizations of optical switch fabrics and an electronic switch fabric.

AWG-Based Switch Fabrics

Figure 17.27 shows the structure of an optical switch fabric using three-stage Clos architecture. The switch fabric in Figure 17.27 has 25,600 ports, and at 40 Gb/s, this switch fabric would have a total throughput of 1 Pb/s. The cross-connect has four stages of wavelength conversion. The first three stages use TWCs, and the last stage uses FWCs. Arrays of AWGs are located between the wavelength converters. The interconnections between the wavelength converters and AWGs are optical, and fiber would be the preferred interconnection medium. Nevertheless, there would be many challenges in building and maintaining such a large switch fabric because of the very large number of interconnecting fibers and the very wide

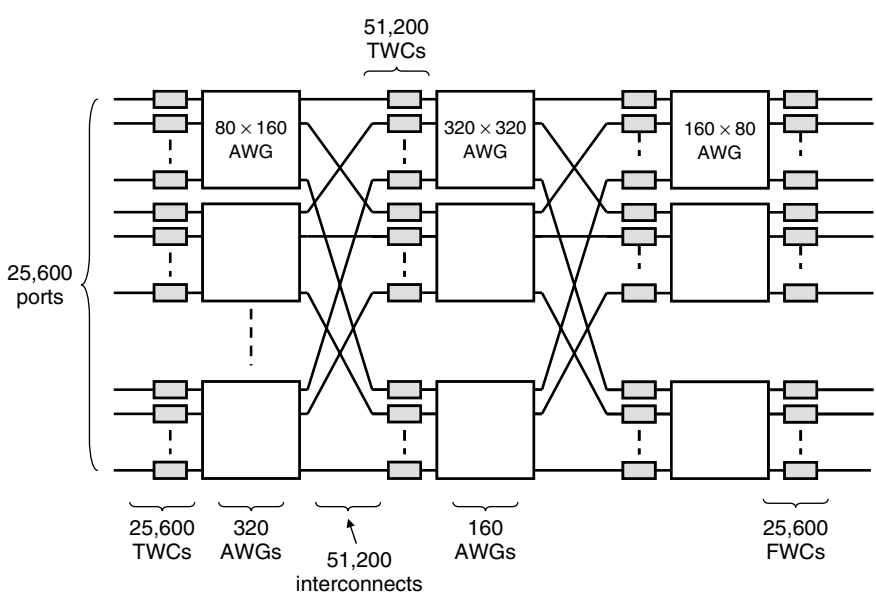

Figure 17.27 Petabit per second optical switch fabric using arrayed waveguide grating multiplexers (AWGs) and wavelength converters.

tuning range required by the tuneable lasers. However, Figure 17.27 shows that at least in principle it is possible to scale optical switches to very large capacities.

SOA-Based Switch Fabrics

There have been many reports in the literature of switch fabrics using SOA gate arrays [7, 54 59]. SOA gate arrays are potentially attractive for optical packet switching because they offer wide optical bandwidth and they can be switched on and off on a time scale of around 1 ns. Figure 17.28 shows an example of a 4×4 Benes switch using an array of SOA gates [56]. Each of the SOA gates is driven by a control circuit that switches the gate on and off. As indicated in Figure 17.28, the 4×4 switch is made up of a number of 1×2 and 2×2 switches, each of which uses a number of 3 dB couplers and SOA gates.

There are three key issues that limit the ability of SOA gate arrays to scale to large size and to operate at low power dissipation [56]. The first of these limitations is crosstalk. In order for a large array of SOA gates to have low crosstalk, the on-off ratio of each SOA gate needs to be very large typically on the order of 50 dB. To achieve an on-off ratio of this order, each individual SOA either needs to be long or needs to be cascaded with an optical attenuator. The problem with these approaches is that they both require the SOA to be operated at a high on-level drive current in order to overcome the high losses that are needed to produce the high on-off ratio. Typically, high on-off ratio SOA gates consume around 0.5 W when biased in the "on" state.

The second limitation on SOA gate arrays is caused by the build up of spontaneous noise as the size of the fabric and the number of cascaded amplifiers increased. In addition to reducing the SNR, this build up of spontaneous noise leads to the third limitation, namely a build up in the total noise and signal power through the fabric. This build up of signal power means that SOAs toward the output stages of the switch fabric need to operate at hight power levels. This leads

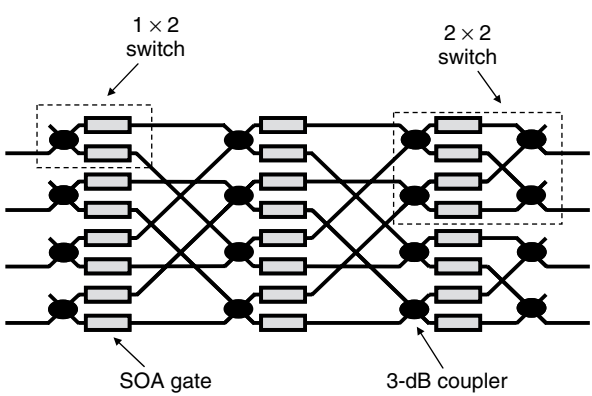

Figure 17.28 4×4 Benes switch using an array of semiconductor optical amplifier (SOA) gates.

to an increase in the required drive power to the SOAs and a consequent increase in the overall power consumption. Further, the accumulation of noise as the optical signal passes through a large switch negates one of the prime original reasons for seeking optical transparency, because a large part of the network noise budget is consumed in the switches.

Electronic Switch Fabrics

A typical high-capacity commercial single-chip electronic cross-connect currently provides throughputs of around 50 Gbit/s at a line rate of 4 Gb/s, with a power consumption of 16 W [60]. This power consumption corresponds to 30 pJ of energy per bit. Szymanski et al. [61] have estimated that with readily available 180-nm CMOS technology, single-chip throughputs on the order of 5 Tbit/s will be achievable, with power consumption on the order of 26 W per chip (5 pJ/b). Extrapolating these results to 22-nm CMOS technology, and assuming that single-chip throughputs of 10 Tbit/s will be achievable, this leads to an estimate of a switching energy of 1 pJ/b. As pointed out earlier, some electronic routers include some buffering between stages of the switch. For simplicity, this buffering is not considered in the present analysis.

It is instructive to estimate the power dissipation of an electronic switch fabric, and to compare this with the power consumption of an optical switch fabric. Figure 17.29 shows a switch fabric using the same three-stage Clos architecture as in the optical switch fabric in Figure 17.25. The three stages of switch blocks in

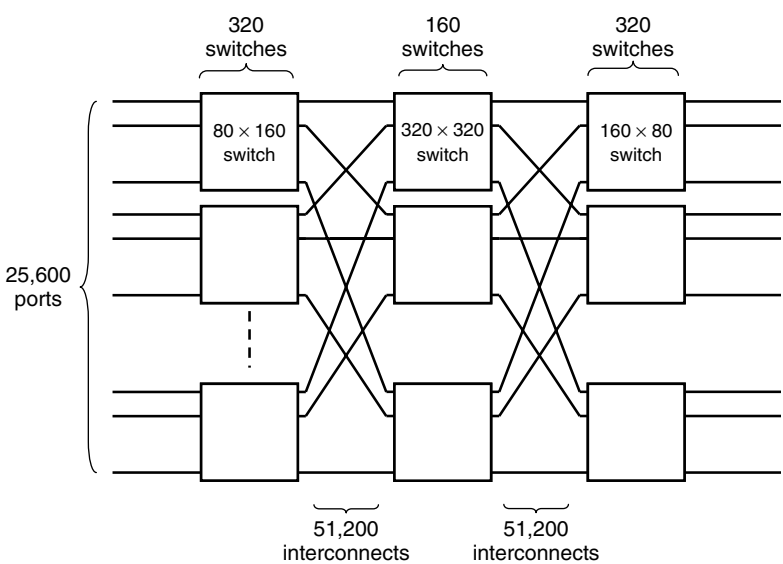

Figure 17.29 One switch plane of a petabit per second electronic switch fabric.

Figure 17.27 comprise a total of 800 switch blocks. Each of these switch blocks is strictly nonblocking and contains a number of interconnected chips. Optical or high-speed electronic interconnects are provided between the switch blocks. The calculations presented here are based on the optical interconnect model in Figure 17.23. It is worth noting that in the optical switch fabric in Figure 17.27 and the electronic switch fabric in Figure 17.29, only those interconnects between stages that are carrying data need to be active. This control strategy can save a considerable amount of power.

As pointed out in Section 17.2.1, the switch fabric in electronic routers usually comprises a number J of parallel switch fabrics (see Figure 17.2). Each of these J parallel fabrics has the structure shown in Figure 17.27. The effective bit rate of the cells as they pass through each of the J parallel switch fabrics is $40/J$ Gb/s in a packet switch with a line rate of 40 Gb/s. To estimate the power consumption of the switch blocks, the energy per bit in each switch block is taken to be 1 pJ/b and is assumed to be independent of the bit rate in the J parallel fabrics (i.e., independent of J). The power consumption of the interconnects in Figure 17.29 (see Figure 17.23) is also assumed to be independent of bit rate in the J parallel fabrics.

As shown in Figure 17.3(a), the forwarding engine in electronic routers plays an active role in switching the cells to the J parallel switching planes. In OPSs [Figure 17.3(b)], the forwarding engine does not provide this function. To provide a fair comparison between optical and electronic switch fabrics, it is necessary to include the energy consumed by the forwarding engine in switching the cells to and from the electronic switch fabric. In the data presented in the next paragraph, we have assumed that an additional 1 pJ of switching energy per bit is consumed by the forwarding engine.

17.5.2 Comparison of Switch Fabric Technologies

Table 17.2 summarizes the total power consumption and the energy per bit, for a 1 Pb/s switch fabric operating at 40 Gb/s. Data are presented for AWG-based switch fabrics, for an SOA gate array, and for a CMOS switch fabric. The AWG-based switch fabrics are subdivided into fabrics using optical (O/O)

Table 17.2

Total power consumption and the energy per bit for a 1 Pb/s switch fabric operating at 40 Gb/s.

		Total power (kW)	Energy per bit (pJ)
AWG based cross connect	O/O WC's	5.8	5.8
	O/E/O WC's	2.2	2.2
SOA gate array		70	70
CMOS		5.2	5.2

wavelength converters, and fabrics using optoelectronic (O/E/O) wavelength converters. The power consumption for each of the devices is as shown in Figs 17.23 17.25. The power consumption of each of the SOA gates in the Benes fabric is taken (optimistically) as 100 mW. The data in Table 17.2 were obtained by counting the number of active devices and interconnects in the structures shown in Figs 17.27 and 17.29 for the AWG and CMOS switch fabrics, and in a large Benes array scaled up from the structure shown in Figure 17.28 [56]. Note that only half of the 51,200 TWCs between the first and second and the second and third stages of AWGs in Figure 17.27 are active at any one time. Similarly, only half of the 51,200 interconnects between the first and second and the second and third stages of CMOS switches in Figure 17.29 are active at any one time.

The calculated power dissipation in Table 17.2 for the optical switch fabric is about the same as the power dissipation in the CMOS switch fabric (5.8 kW vs 5.2 kW). This does not support the common assumption that optical switching using AWGs and TWCs consumes less power than electronic switches. The power dissipation in the optoelectronic switch fabric (2.2 kW) is about half of the power consumption in the optical switch fabric and the CMOS switch fabric. This is because the energy consumption of the O/E/O wavelength converters used in the modeling is lower than the power consumption of the O/O wavelength converters. The AWG-based switch fabric with O/E/O wavelength converters has the lowest power consumption and the lowest energy per bit (2.2 kW and 2.2 pJ/b).

The power dissipation of the SOA gate array scaled up to a large Benes array is 70 kW. This is more than an order of magnitude larger than any of the other switch fabrics considered here. Note that it would be very difficult to construct a large Benes array of SOA gates due to the very large number of interconnects required. A more practical solution might be to use smaller Benes arrays of SOAs and to interconnect these smaller arrays using a Clos structure similar to the switch fabric in Figure 17.29. The power dissipation for this arrangement would be 105 kW. Considering this larger power consumption and the degraded SNR at the output of SOA gate arrays, SOA gate arrays do not appear to be competitive with electronic and AWG-based switch fabrics technologies for large-scale switch fabrics. For this reason, SOA gate arrays are not considered in the remaining analysis in this chapter.

17.6 POWER CONSUMPTION IN HIGH-CAPACITY ROUTERS

This chapter has focused so far on the energy consumption of various components of OPSs and electronic packet switches. A full and complete comparison of energy consumption in optical and electronic routers requires models of a complete optical router and a complete electronic router. As a step in this direction, we have compared routers comprising the four possible combinations of optical and

electronic buffers and switch fabrics [28]. This analysis includes the buffers, switch fabrics, and some of the I/O between boards. However, it does not include IP-lookup and forwarding, the control plane, some of the I/O between boards, or the power supply inefficiency and power consumed in heat management. While the power dissipation attributed to these functions is larger than the power dissipation in the buffers and switch fabrics (see Figure 17.7), the power dissipation in IP-lookup and forwarding and the control plane will scale with the capacity of the router and the power consumed by the power supply inefficiency and heat management will scale with the power consumed in the remainder of the router. Therefore, a comparison of power dissipation based only on the buffers and switch fabrics can be used to give an indication of some key differences between optical and electronic packet switching.

Figure 17.30 [28] shows the four possible combinations of electronic and optical switch fabrics and buffers for routers with buffers located at the output ports. To provide a common framework for comparison, it is assumed that the routers operate with full-reach optical fiber links at the input and output ports. Therefore, the optical power level at each input port is at the sensitivity-limited level determined by high-performance optical receivers, and the optical power level at each output is set at the level of a standard optical transmitter [28]. In addition, amplifiers and other components are required as shown in Figure 17.30.

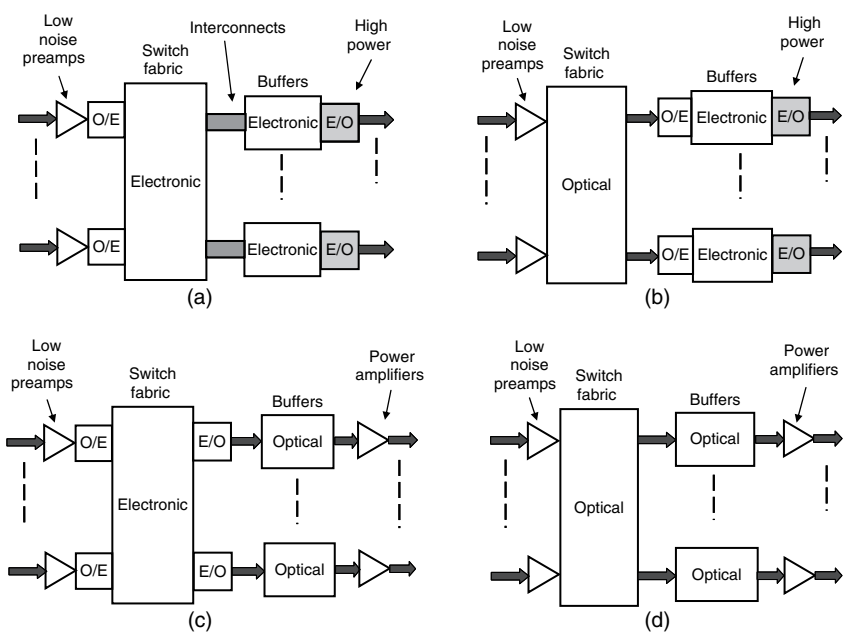

Figure 17.30 Four possible arrangements of optical and electronic buffering and switching [28]. © 2006 IEEE.

Table 17.3 summarizes the calculated power consumptions for a 1 Pb/s router with output buffering as shown in Figure 17.30. The entry labeled "extra power" in the table corresponds to the additional power consumed by the additional amplifiers and other components in Figure 17.30. The power figures for the optical switch fabrics are subdivided into optoelectronic switch fabrics (incorporating O/E/O WCs) and optical switch fabrics (incorporating O/O WC's). The total power consumption for each of the six combinations of buffer and switch fabric are highlighted with shading. The size of each output buffer is set at 5 IP packets (i.e., 50 kb). This is close to the maximum size achievable in a delay line buffer (slow light or conventional delay line) with an attenuation of 0.05 dB/cm. If significantly larger buffers are needed, the only solution would be to use fiber or electronic buffers. Fiber-based delay lines would be technically feasible, but very bulky. In comparison, the size of electronic buffers in the 1 Tb/s router could easily be increased by many orders of magnitude beyond 50 kb, and this would have minimal impact on the total power dissipation. Taking these considerations into account, electronic buffering appears to offer significant advantage over optical buffering.

Table 17.3 summarizes that the smallest power dissipation of the six different combinations of switch fabric and buffer is 4.9 kW. This is achieved using AWG-based optoelectronic switch fabrics (incorporating O/E/O WCs) and electronic buffers. Therefore, the lowest power dissipation is achieved in routers that combine optoelectronic switch fabrics and electronic buffers. The power consumption of a router with an optical buffer and an optoelectronic switch fabric (6.1 kW) is slightly larger, but the optical buffer will be bulkier than an electronic buffer. Furthermore, there would be little point in combining an optical buffer with an optoelectronic switch fabric because the router would not be optically transparent. The power consumption of a true OPS (i.e., with an optical buffer and an optical switch fabric) is 9.7 kW, which is around twice the 4.9 kW power consumption of a router using an optoelectronic switch fabric and electronic buffers.

The conclusions in the previous paragraph provide some guidance as to the relative power consumption of competing technologies. However, the difference

Table 17.3

Power consumptions of 1 Pb/s router with output buffering.

		Buffer							
		Optical				Electronic			
		Buffer (kW)	Cross connect (kW)	Extra power (kW)	Total (kW)	Buffer (kW)	Cross connect (kW)	Extra power (kW)	Total (kW)
Switch fabric	Optical	1.3	5.8	2.6	9.7	0.2	5.8	2.5	8.5
	Optoelectronic	1.3	2.2	2.6	6.1	0.2	2.2	2.5	4.9
	Electronic	1.3	5.2	2.2	8.7	0.2	5.2	2.1	7.5

between the maximum and minimum powers in Table 17.3 is only a factor of 2. Considering the approximations made in the analysis, some caution is needed. Perhaps the most important conclusion that can be drawn from these results is that optical packet switching with optical buffering and optical switch fabrics does not appear to provide any dramatic power savings when compared with electronic packet switching. If there is no significant difference in power dissipation, other factors such as cost, physical realizability, and footprint will decide. Given the huge challenges in optical buffering compared with electronic buffering, and the lack of a clear power consumption advantage in optical packet switching, it would appear that electronics will remain the technology of choice in future high-capacity packet switches.

17.7 CONCLUSIONS

This chapter has examined some of the major factors influencing the choice of technologies in packet switches or routers for high-capacity telecommunications networks. The most important consideration in the design of future high-capacity routers will be energy consumption and the associated heat dissipation problems. The energy bottleneck has become a major problem in the design of high-capacity electronic routers, and designers are looking for alternative design approaches for the future. At a superficial level, optical packet switching appears to offer a way forward. Optical switching is a potentially low-power technology, and the concept of optical packet switching is consistent with the dream of an all-optical network.

It has long been recognized that the lack of a practical optical buffer technology is a major impediment to the development of optical packet switching. Recent theoretical results indicate that optical buffers might not need to have large capacity. However, this chapter has shown that even low-capacity optical buffers are difficult to build, are bulky, and consume a significant amount of energy. On the basis of power consumption alone, slow-light technologies and other optical buffering techniques such as those based on high-Q micro-resonators are unlikely to be able to compete with electronic buffer technologies.

There is some potential for reduction of the power consumption in router switch fabrics that use optical technologies such as AWGs and rapidly tuneable wavelength converters. Continuing progress in low-power optical receiver and transmitter technologies suggests that optoelectronic wavelength converters rather than optical wavelength converters will be the technology of choice for these switch fabrics. A key conclusion of this chapter is that future generations of high-capacity router will use more optical components and more optoelectronic components than today, particularly in interconnects. However, optically transparent OPSs are unlikely to become competitive with optoelectronic packet switches.

The search for low-energy approaches to packet switching will continue. In the near term, some advances will be possible through the reduced energy requirements of smaller-scale generations of CMOS. But these advances will not continue

for ever, and in the present climate, the required capacity of routers is growing faster than Moore's law. A large proportion of the energy dissipation in high-capacity routers occurs in the routing engines. Therefore, considerable energy dissipation could be saved if it was possible to simplify the routing algorithms. This is a topic of equal relevance to optical packet switching and to electronic packet switching, but it is beyond the scope of this chapter.

REFERENCES

[1] G. Sapountzis and M. Katevenis "Benes Switching Fabrics with O(N) Complexity Internal Back pressure," in Proc. *IEEE Workshop on HPSR*, Torino, Italy, 2003.

[2] P. A. Perrier and P. R. Prucnal, "Self clocked optical control of a self routed photonic switch," *J. Lightw. Technol.*, 7, 983 989, 1989.

[3] J. Spring and R. S. Tucker, "Photonic 2 × 2 packet switch with input buffers," *Electron. Lett.*, 29, 284, 1993.

[4] D. Blumenthal, P. Prucnal, and J. Sauer, "Photonic Packet Switches: Architectures and Experi mental Implementations," in Proc. *IEEE*, 82, 1650 1667, November 1994.

[5] D. K. Hunter, W. D. Cornwell, T. H. Gilfedder et al., "SLOB: A switch with large optical buffers for packet switching," *J. Lightw. Technol.*, 16, 1725 1736, October 1998.

[6] R. S. Tucker and W. Zhong, "Photonic packet switching: an overview," *IEICE Transactions*, E82 B, 254 264, 1999.

[7] D. Chiaroni, P. Bonno, O. Rofidal et al., "First Demonstration of An Asynchronous Optical Packet Switching Matrix Prototype for Multi Terabit Class Routers/Switches," in Proc. 27th *ECOC*, 2001, pp. 60 61.

[8] S. J. Yoo, "Optical packet and burst switching technologies for the future photonic internet," *J. Lightw. Technol.*, 24, 4468 4492, December 2006.

[9] C. Qiao and M. Yoo, "Optical burst switching OBS a new paragigm for an optical internet," *J. High Speed Netw.*, 8, 69 84, 1999.

[10] R. Parthiban, R. S. Tucker, C. Leckie et al., "Does Optical Burst Switching Have a Role in the Core Network?," in Proc. *OFC/NFOEC 2005*, 2005, p. 3.

[11] G. Epps, *Private Communication*, 2007.

[12] D. T. Neilson, "Photonics for switching and routing," *IEEE J. Sel. Top. Quantum Electron.*, 12, 669 677, July/August 2006.

[13] G. Epps, D. Tsiang,and T. Boures, "System power challenges," http://www.cisco.com/web/about/ac50/ac207/proceedings/*POWER GEPPS rev3.ppt*.

[14] J. Baliga, K. Hinton, and R. S. Tucker, "Energy Consumption of the Internet," in Proc. *COIN ACOFT*, Melbourne Australia, 2007.

[15] E. B. Desurvire, "Capacity demand and technology challenges for lightwave systems in the next two decades," *J. Lightw. Technol.*, 24, 4697 4710, December 2006.

[16] R. S. Tucker, G. Eisenstein, and S. K. Korotky, "Optical time division multiplexing for very high bit rate transmission," *J. Lightw. Technol.*, 6, 1737 1749, November 1988.

[17] H. G. Weber, R. Ludwig, S. Ferber et al., "Ultrahigh speed OTDM transmission technology," *J. Lightw. Technol.*, 24, 4616 4627, 2006.

[18] E. Lach and K. Schuh, "Recent advances in ultrahigh bit rate ETDM transmission systems," *J. Lightw. Technol.*, 24, 4455 4467, 2006.

[19] Q. Yu and A. Shanbhag, "Electronic data processing for error and dispersion compensation," *J. Lightw. Technol.*, 24, 4514 4525, 2006.

[20] D. F. Welch, F. A. Kish, R. Nagarajan et al., "The realization of large scale photonic integrated circuits and the associated impact on fiber optic communication systems," *J. Lightw. Technol.*, 24, 4674 4683, 2006.

[21] K. Hinton, P. Farrell, and R. S. Tucker, "The Photonic Bottleneck," in Proc. *OFC*, Anaheim, CA, 2007.
[22] "International Technology Roadmap for Semiconductors, 2005 Edition (2005). [Online]. Avail able: http://public.itrs.net/," 2005.
[23] G. Appenzeller, I. Keslassy, and N. McKeown, "Sizing Router Buffers," in Proc. *SIGCOMM'04*, Portland, Oregon, 2004, p. 2.
[24] M. Enachescu, Y. Ganjali, A. Goel, and N. McKeowan, "Part III: Routers with very small buffers," *ACM/SIGCOMM Comp. Commun. Rev.*, 35, 83 89, July 2005.
[25] N. Beheshti, Y. Ganjali, R. Rajaduray et al., "Buffer Sizing in All Optical Packet Switches," in Proc. *OFC/NFOEC 2006*, Anaheim, CA, 2006, p. 3.
[26] D. K. Hunter, M. C. Chia, and I. Andonovic, "Buffering in optical packet switches," *J. Lightw. Technol.*, 16, 2081 2094, 1998.
[27] H. Yang and S. J. B. Yoo, "All optical variable buffering strategies and switch fabric architectures for future all optical data routers," *J. Lightw. Technol.*, 23, 3321 3330, October 2005.
[28] R. S. Tucker, "The role of optics and electronics in high capacity routers," *J. Lightw. Technol.*, 24, 4655 4673, December 2006.
[29] H. Park, E. F. Burmeister, S. Bjorlin, and J. E. Bowers, "40 Gb/s Optical Buffer Design and Simulation," in Proc. *NUSOD '04*, 2004, pp. 19 20.
[30] L. V. Hau, S. E. Harris, Z. Dutton, and C. H. Behroozi, "Light speed reduction to 17 meters per second in an ultracold atomic gas," *Nature*, 397, 594 598, February 18, 1999.
[31] P. C. Ku, F. Sedgwich, C. Chang Hasnain et al., "Slow light in semiconductor quantum wells," *Opt. Lett.*, 29, 2291 2293, 2004.
[32] R. W. Boyd, M. S. Bigelow, N. Lepeshkin et al., "Fundamentals and Applications of Slow Light in Room Temperature Solids," in Proc. *IEEE LEOS 2004*, Annual Meeting, 2004, pp. 835 836.
[33] Y. A. Vlasov, M. O'Boyle, H. F. Hamann, and S. McNab," Active control of slow light on a chip with photonic crystal waveguides," *Nature*, 438, 3, November 2005.
[34] C. J. Chang Hasnain and S. L. Chuang, "Slow and fast light in semiconductor quantum well and quantum dot devices," *J. Lightw. Technol.*, 24, 4642 4654, 2006.
[35] R. S. Tucker, P. C. Ku, and C. J. Chang Hasnain, "Slow light optical buffers: capabilities and fundamental limitations," *J. Lightw. Technol.*, 23, 4046 4066, December 2005.
[36] A. Melloni, F. Morichetti, and Martnelli, "Linear and nonlinear pulse propagation in coupled resonator slow wave optical structures," *Opt. Quantum Electron.*, 35, 365 378, 2003.
[37] J. B. Khurgin, "Optical buffers based on slow light in electromagnetically induced transparent media and coupled resonator structures: comparative analysis," *J. Opt. Soc. Am. B.*, 22, 1062 1074, May 2005.
[38] R. S. Tucker, "Petabit Per Second Routers: Optical vs Electronic Implementations," in Proc. *OFC'2006*, Anaheim, CA, 2006, p. 2.
[39] J. Khurgin, "Power dissipation in slow light devices comparative analysis," *Opt. Lett.*, 32, 163 165, December 2006.
[40] J. Khurgin, "Adiabatically tunable optical delay lines and their performance limitations," *Opt. Lett.*, 30, 2778 2780, October 2005.
[41] T. Asano and S. Noda, "Ultra High q Photonic Nanocavities and Trapping of Ultra Short Optical Pulses," in Proc. *Topical Meeting on Slow and Fast Light*, Washington DC, 2006, pp. MB41 2.
[42] J. Guo, M. J. Shaw, G. A. Vawter et al., "High Q Integrated on Chip Micro Ring Resonator," in Proc. *IEEE LEOS* Annual Meeting, 2004, pp. 745 746.
[43] A. A. Savchenkov, A. B. Matsko, V. S. Ilchenko, and L. Maleki, "Ultrahigh Q Crystalline Optical Wispering Gallery Mode Resonators," in Proc. *LEOS* Summer Topical Meeting on Biophotonics/ Optical Interconnects and VLSI Photonics, 2004, pp. 29 30.
[44] O. Leclerc, B. Lavigne, D. Chiaroni, and E. Desurvire, "All optical regeneration: principles and WDM implementation," in *Optical Fiber Telecommunications IVA*, (I. Kaminow and T. Li, eds), San Diego, Academic Press, 2002, pp. 732 783.
[45] M. E. Ali, G. Panotopoulos, E. de Groot et al., "Demonstration of a High Density Parallel WDM Optical Interconnect," in Proc. *IEEE LEOS* 2004, Annual Meeting, 2004, pp. 459 460.

[46] C. Kromer, G. Sialm, C. Berger et al., "A 100 mW 4×10 Gb/s transceiver in 80 nm CMOS for high density optical interconnects," *IEEE Journal of Solid St. Cir.*, 40, 2667 2679, December 2005.

[47] H. Cho, P. Kapur, and K. C. Saraswat, "Power comparison between high speed electrical and optical interconnects for interchip communication," *J. Lightw. Technol.*, 22, 2021 2033, Septem ber 2004.

[48] M. L. Masanovic, V. Lal, J. A. Summers et al., "Widely tunable monolithically integrated all optical wavelength converters in InP," *J. Lightw. Technol.*, 23, 1350 1362, 2005.

[49] L. Ju Han, T. Nagashima, T. Hasegawa et al., "Output performance investigation of self phase modulation based 2R regenerator using bismuth oxide nonlinear fiber," *IEEE Photon. Technol. Lett.*, 18, 1296 1298, 2006.

[50] T. Okuno, T. Nakanishi, M. Hirano, M. Onishi, "Practical Considerations for the Application of Highly Nonlinear Fibers," in Proc. *OFC 2007*, Anaheim, CA, 2007.

[51] G. I. Papadimitriou, C. Papazoglou, and A. S. Pomportsis, "Optical switching: switch fabrics, techniques, and architectures," *J. Lightw. Technology*, 21, 384 405, 2003.

[52] J. Gripp, M. Duelk, J. E. Simsarian et al., "Optical switch fabrics for ultra high capacity IP routers," *J. Lightw. Technol.*, 21, 2839 2850, 2003.

[53] M. Zirngibl, "Applications for optical switch fabrics," in *Optical Fiber Telecommunications IVA*, (I. Kaminow and T. Li, eds), San Diego, Academic Press, 2002, pp. 374 404.

[54] J. D. Evankow, Jr. and R. A. Thompson, "Photonic switching modules designed with laser diode amplifiers," *IEEE J. Sel. Areas Commun.*, 6, 1087, 1988.

[55] R. Fortenberry, A. J. Lowery, W. L. Ha, and R. S. Tucker, "Photonic packet switch using semiconductor optical amplifier gates," *Electron. Lett.*, 27, 1305, 1991.

[56] R. F. Kalman, L. G. Kazovsky, and J. W. Goodman, "Space division switches based on semi conductor optical amplifiers," *IEEE Photon. Technol. Lett.*, 4, 1048, 1992.

[57] J. Gibong and J. W. Goodman, "Gain optimization in switches based on semiconductor optical amplifiers," *J. Lightw. Technol.*, 13, 598 605, 1995.

[58] N. Sahri, D. Prieto, S. Silvestre et al., "A Highly Integrated 32 Soa Gates Optoelectronic Module Suitable for Ip Multi Terabit Optical Packet Routers," in Proc. *OFC 2001*, 2001, pp. PD32 1 PD32 3.

[59] D. Chiaroni, "Packet switching matrix: a key element for the backbone and the metro," *IEEE J. Sel. Areas in Commun.*, 21, 1018, 2003.

[60] Vitesse, "4.25 Gbps 144×144 Crosspoint Switch Datasheet, http://www.vitesse.com/products/ product.php?number VSC3140," 2005.

[61] T. H. Szymanski, H. Wu, and A. Gourgy, "Power complexity of multiplexer based optoelectronic crossbar switches," *IEEE VLSI* Systems, 13, 604 617, May 2005.

This page intentionally left blank

18

Microwave-over-fiber systems

Alwyn J. Seeds

Department of Electronic and Electrical Engineering, University College London, London, England

18.1 INTRODUCTION

Optical fiber is now established as the medium of choice for high-capacity long-haul digital transmission systems and is moving rapidly into the access area. Its use in high-speed local area networks is also widespread. A less well-known applications area is its use for the transmission of microwave signals for cable television, cellular radio, wireless local area networks (WLAN), and microwave antenna remoting. The object of this chapter is to review the technologies involved, consider the basic performance parameters, and present recent work on such systems.

The chapter is organized as follows. Section 18.2 will introduce and present models for both intensity modulation direct detection (IMDD) and coherent transmission systems and compare their performance capabilities. Section 18.3 will review opto-electronic components for use in optical microwave transmission systems, including sources, optical amplifiers, and detectors. Section 18.4 will review recent research results on microwave-over-fiber systems. Finally, Section 18.5 will discuss future prospects for optical transmission of microwave signals.

18.2 OPTICAL FIBER TRANSMISSION OF MICROWAVE SIGNALS

Figure 18.1 shows an optical transmission link with its equivalent in conventional microwave technology. The use of optical transmission requires the input signal to be converted into optical form at the input to the fiber and to be returned to the electrical domain at the output. The extra components required to effect this have to be weighed against the advantages of the fiber transmission medium.

Optical Fiber Telecommunications V B: Systems and Networks

ISBN: 978 0 12 374172 1

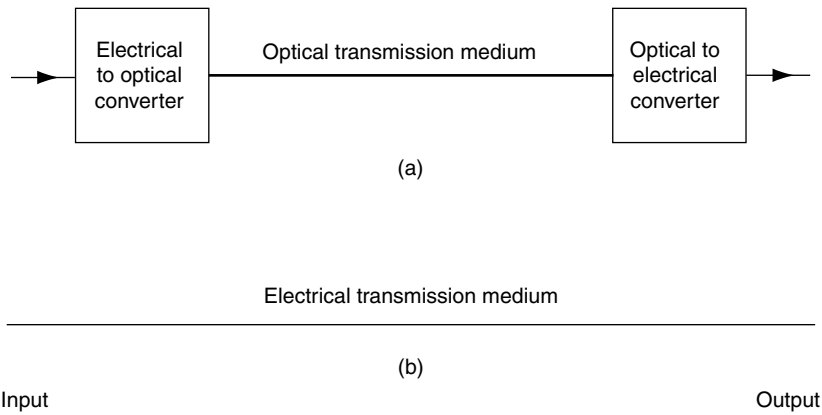

Figure 18.1 Optical and electrical transmission links for microwave signals.

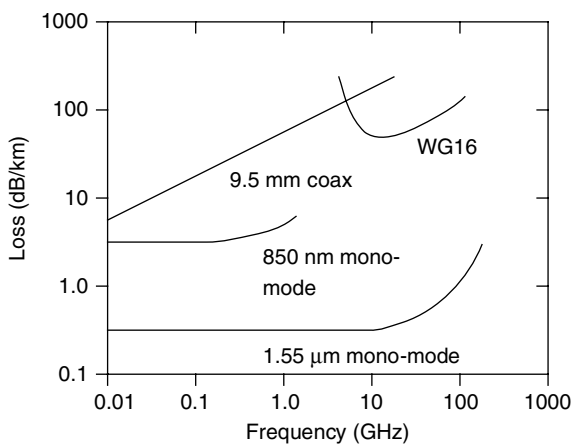

Figure 18.2 Losses of various transmission media as a function of signal frequency.

The most obvious advantage of fiber transmission is reduced losses relative to metallic media. Figure 18.2 compares the loss of silica fiber, at wavelengths of 850 nm and 1550 nm, with that of representative metallic media. Clearly, fiber has substantially lower losses at microwave signal frequencies; indeed for transmission distances above a few kilometres at frequencies in excess of 10 GHz, it is unrivalled. The rise in effective loss at the higher microwave frequencies is due to dispersion power penalties. For a 1 dB penalty, the fiber bandwidth can be approximated by Ref. [1]

$$B = \frac{1}{4\Delta\lambda DL} \tag{18.1}$$

where $\Delta\lambda$ is the source linewidth, D is the fiber dispersion, and L the fiber length. Thus, for silica fiber having $D = 90$ ps/(km.nm) at a wavelength of 850 nm and <4 ps/(km.nm) at 1550 nm (dispersion-flattened fiber), the 1 dB/km penalty bandwidths for wide linewidth (1 nm) optical sources are 2.8 and 70 GHz, respectively. For microwave transmission purposes, the preferred wavelengths are either 1550 nm, using dispersion-shifted or dispersion-flattened fiber, or 1300 nm, using standard fiber and accepting the $\sim$0.2 dB/km loss penalty.

Two basic approaches to optical signal modulation and recovery are possible. In the simplest IMDD [Figure 18.3(a)], the optical source intensity is either directly modulated by the input microwave signal or passed through an external intensity modulator. The resulting intensity-modulated signal passes through the optical fiber to the photodiode where the modulation is returned to the electrical domain.

In the coherent system [Figure 18.3(b)], the optical source is modulated in intensity, frequency, or phase by the input microwave signal, either directly or by passage

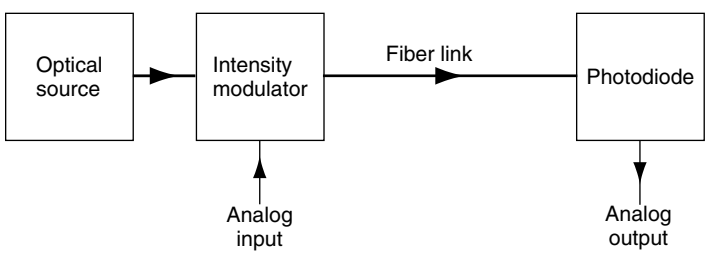

(a) IMDD transmission system

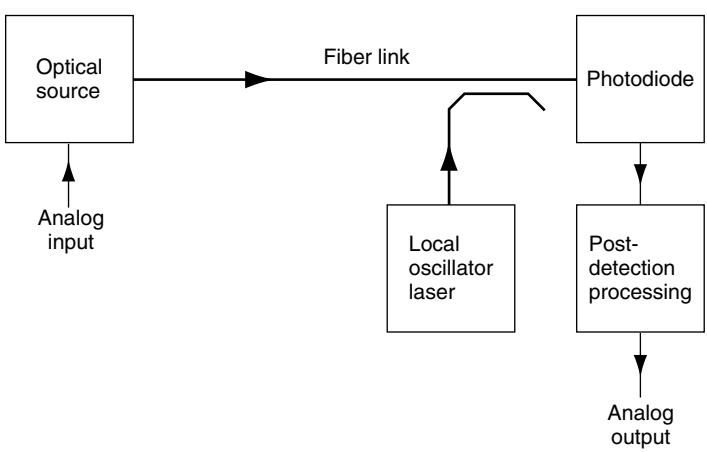

(b) Coherent transmission system

Figure 18.3 Optical transmission link architectures: (a) Intensity modulation direct detection; (b) Coherent.

through an external modulator. The modulated signal passes through the optical fiber to the receiver, where it is combined with the output from a local oscillator (LO) laser. The combined signal illuminates the photodiode to produce an electrical signal centered on the difference frequency between the unmodulated optical source and the LO laser. This signal is further processed to recover the analog output signal.

18.2.1 Transmission System Model—Direct Detection

Consider first the IMDD system [Figure 18.3(a)]. Let the microwave signal to be transmitted be represented by $m\{t\}$. The optical power at the output of the intensity modulator is

$$P_0 = P_u(1 + k\, m\{t\}), \tag{18.2}$$

where P_u is the mean optical power and k is the modulation sensitivity ($k\, m\{t\} > \quad 1$). The mean squared signal current at the detector output is

$$I_s^2 = (RG_l P_u k)^2\, \overline{m^2\{t\}}, \tag{18.3}$$

where R is the photodiode responsivity and G_l the fiber path gain ($G_l < 1$ unless optical amplifiers are used).

Noise at the detector output arises from several sources. These include

(i) Thermal noise current generated in the photodiode load, with mean square value

$$I_{nt}^2 = \frac{4kT\,B}{R_L}, \tag{18.4}$$

where k is Boltzmann's constant, T the absolute temperature, B the bandwidth, and R_L the load resistance value.

(ii) Shot noise generated in the photodiode

$$I_{ns}^2 = 2e\left(\bar{i}_d + i_{dk}\right)B, \tag{18.5}$$

where e is the electronic charge, i_d is the mean optically generated current in the photodiode, and i_{dk} is the photodiode dark current.

(iii) Optical source relative intensity noise

$$I_{nRIN}^2 = \overline{i_d}^2 \mathrm{RIN}\, B, \tag{18.6}$$

where RIN is the source relative intensity noise value.

(iv) Noise generated by any optical amplifiers used, I_{na}^2.

Assuming these noise sources to be uncorrelated, the signal-to-noise ratio (SNR) at the detector output can be written

$$\mathrm{SNR} = \frac{(RG_{\mathrm{l}}P_{\mathrm{u}}k)^2\,\overline{m^2\{t\}}}{\left(\frac{4kT}{R_{\mathrm{L}}} + 2e(RG_{\mathrm{l}}P_{\mathrm{u}} + i_{\mathrm{dk}}) + (RG_{\mathrm{l}}P_{\mathrm{u}})^2\mathrm{RIN}\right)B + I_{\mathrm{na}}^2}. \tag{18.7}$$

It can be seen that the thermal noise contribution is independent of unmodulated optical power, P_{u}, as is the optical amplifier noise contribution if nonlinear effects can be neglected. Thus the SNR can be improved by increasing the unmodulated optical power until the source relative intensity noise limit is reached, giving

$$\mathrm{SNR} = \frac{k^2\,\overline{m^2\{t\}}}{\mathrm{RIN}B} \tag{18.8}$$

For optical powers below the RIN limit, shot-noise-limited reception can be achieved if the thermal and optical amplifier contributions are sufficiently small, giving

$$\mathrm{SNR} = \frac{RG_{\mathrm{l}}P_{\mathrm{u}}k^2\,\overline{m^2\{t\}}}{2eB}, \tag{18.9}$$

where the photodiode dark current has been assumed negligible relative to the photocurrent. For low received optical powers, thermal and optical amplifier contributions are dominant.

18.2.2 Transmission System Model—Coherent Detection

Consider now the coherent system [Figure 18.3(b)], and assume that polarization control techniques are used so that the signal and LO electric fields incident on the photodiode have the same polarization. The signal electric field is defined by

$$E_{\mathrm{s}} = E_{\mathrm{sp}}\cos(\omega_{\mathrm{s}}\,t + \phi_{\mathrm{s}}), \tag{18.10}$$

where ω_{s} is the signal frequency and ϕ_{s} the signal phase, and the LO field by

$$E_{\mathrm{LO}} = E_{\mathrm{LOp}}\cos(\omega_{\mathrm{LO}}\,t + \phi_{\mathrm{LO}}) \tag{18.11}$$

with ω_{LO} the LO frequency and ϕ_{LO} the LO phase. Defining the intermediate frequency (IF), ω_{I}, by $\omega_{\mathrm{I}} = \omega_{\mathrm{LO}} \quad \omega_{\mathrm{s}}$ the analytic signal incident on the photodiode is

$$V_{\mathrm{in}} = \left(E_{\mathrm{sp}}\exp j\phi_{\mathrm{s}} + E_{\mathrm{LOp}}\exp j(\omega_{\mathrm{I}} + \phi_{\mathrm{LO}})\right)\exp j\omega_{\mathrm{s}}t \tag{18.12}$$

For $\omega_I << \omega_s$ the output current from the photodiode is proportional to $V_{in} V_{in}^*$ so that

$$i \propto E_{sp}^2 + E_{LOp}^2 + 2\,E_{sp}\,E_{LOp}\cos(\omega_I t + \phi_{LO} - \phi_s) \tag{18.13}$$

It is convenient to rewrite Eqn (18.13) in terms of optical power since that is a directly measurable quantity. Using

$$E_{sp}^2 = \frac{2Z_o\,P_o\,G_l}{A} \tag{18.14}$$

and

$$E_{LOp}^2 = \frac{2Z_o\,P_{LO}}{A}, \tag{18.15}$$

where Z_o is the impedance of the medium where the power is measured, P_o is the source output power, and A is the photodiode area,

$$i = R\left(P_o G_l + P_{LO} + 2\sqrt{P_o G_l P_{LO}}\cos(\omega_I t + \phi_{LO} - \phi_s)\right) \tag{18.16}$$

The first two terms represent direct detection of the signal and LO, respectively. The third term is of more interest. First, its magnitude is proportional to the square root of the LO power. Thus, the detected signal can be made larger simply by increasing the LO power. Second, the detected signal is proportional to the square root of the source output power. Thus, linear modulation of the source electric field will yield linear modulation of the detected photocurrent at the IF. Alternatively, linear modulation of the source intensity will yield linear modulation of the output of a square law detector fed with the photodetected IF signal. Third, the term is at the IF, ω_I, so that modulation of the source frequency, ω_s, leads directly to modulation of the IF, which can be recovered using a suitable discriminator. Fourth, the term contains the signal phase, ϕ_s, and the LO phase, ϕ_{LO}, so that phase modulation of the source leads directly to phase modulation of the IF output. Thus, coherent systems can use amplitude, intensity, frequency, or phase modulation while direct detection systems are limited to either amplitude or intensity modulation. When $\omega_I = 0$, the coherent system is said to be homodyne, but when $\omega_I \neq 0$, the coherent system is said to be heterodyne.

The sources of noise in a coherent system are similar to those in a direct detection system (Section 18.2.1), giving an IF carrier-to-noise ratio (CNR) after photodetection of

$$\mathrm{CNR} = \frac{2\;P_o\;G_l\;P_{LO}\;R^2}{\left(\frac{4kT}{R_L} + 2e(RP_{LO} + i_{dk}) + (RP_{LO})^2\mathrm{RIN}\right)B + I_{na}^2}, \tag{18.17}$$

where it is assumed that $P_{LO} >> P_o G_l$ and RIN is the relative intensity noise of the local oscillator laser. It is normal practice in coherent receivers to use a balanced detection scheme to cancel LO laser RIN [2] so that by increasing the LO power, shot-noise-limited reception is obtained, giving

$$\mathrm{CNR} = \frac{P_o G_l R}{e B} \tag{18.18}$$

18.2.3 Comparison Between Coherent and Direct Detection Systems

Coherent transmission systems offer three main advantages over systems using direct detection:

(i) Shot-noise-limited reception can be achieved even at low received signal powers, simply by increasing the LO power.
(ii) Intensity, frequency, or phase modulation modes can be used whereas direct detection systems are limited to intensity modulation (the use of angle modulation with interferometric detection at the receiver results in an intensity-modulated signal at the photodiode that has then to be detected conventionally and therefore does not yield SNR improvements).
(iii) The excellent frequency selectivity that can be achieved using electrical post-photodetector filters is translated into the optical domain by the coherent detection technique enabling the realization of dense wavelength division multiplex schemes for multichannel transmission or channel selection schemes.

Reviewing these advantages in turn, the first is of reduced importance for systems operating at a wavelength of 1550 nm now that effective optical amplifiers are available. However, there is interest in systems operating at 1300 nm wavelength in order to take advantage of the silica fiber dispersion minimum and the low noise and high output power of semiconductor-laser-pumped Nd-YAG lasers. There is also interest in systems operating at 850 nm wavelength for compatibility with GaAs microwave monolithic integrated circuit (MMIC) technology. Efficient optical fiber amplifiers are not available for either of these wavelengths.

The alternative strategy for shot-noise-limited IMDD systems of increasing the source power P_u is limited by the onset of stimulated Brillouin scattering (SBS) and other nonlinear effects in optical fiber [3]. The SBS threshold for 1 dB forward transmission loss is given by [4]

$$P_c = \frac{42 A_e}{g_B L_e}, \qquad L_e = \frac{1 - e^{-\alpha L}}{\alpha}, \tag{18.19}$$

where A_e is the core area of the fiber, g_B is the Brillouin gain coefficient, L_e is the effective interaction length, L is the fiber length, and α is the fiber loss. For a 30 km-long 1550 nm wavelength system using silica fiber of 9 μm core diameter and 0.2 dB/km loss, with $g_B = 4 \times 10^{-9}$ cm/W and continuous wave (CW) excitation, $P_c = 4.1$ mW. Thus, from Eqn (18.9), the shot-noise-limited SNR, for a narrow bandwidth link with photodiode responsivity 0.9 A/W and $k^2\overline{m^2\{t\}} = 1$, would be limited by SBS to 155 dB.Hz. Thus, coherent transmission remains of interest for other than short distance systems, where high SNR is required.

The second advantage enables SBS to be reduced by broadening the optical signal bandwidth beyond the SBS linewidth (~20 MHz at 1550 nm wavelength) using frequency or phase modulation. Use of frequency or phase modulation also enables a trade-off to be made between optical signal bandwidth and received SNR [5].

The importance of the third advantage depends upon whether the ability to switch between many sources carried on the same fiber is required. An example of such a requirement would be a distributed receive antenna remoting application.

There are three main disadvantages of coherent transmission systems relative to those using direct detection:

(i) The frequencies of the LO laser and signal must be controlled to differ by the required IF, whereas in the direct detection system, it is only necessary that the source laser frequency be suitable for the photodiode used.
(ii) The linewidths of source and LO lasers must be suitable for the modulation mode used, whereas in direct detection systems, the required source linewidth is mainly determined by the optical fiber dispersion penalty.
(iii) The polarization state of the LO and signal must be matched at the photodiode.

The requirement for source frequency control is an exacting one. An operating wavelength of 1550 nm corresponds to a frequency of 194 THz, so that to maintain an heterodyne signal within 10% of band center in an IF bandwidth of 2 GHz, control to within 1 part in 10^6 is required. For semiconductor lasers with typical temperature-tuning sensitivities of 30 GHz/K and current-tuning sensitivities of 3 GHz/mA, this requires temperature control to within 7 mK and current control to within 7 μA.

Advanced semiconductor lasers can offer linewidths in the kHz region coupled with wavelength-tuning ranges in excess of 10 nm [6] although the commercial availability of such lasers is currently limited. Homodyne systems require the LO frequency to be phase-locked to that of the received signal in an optical phase-lock loop (OPLL). Realizing such loops with other than narrow linewidth lasers presents formidable challenges [7].

Polarization matching can be achieved by active polarization control of the LO signal for maximum detected signal output [8] or using polarization diversity reception [9].

Whilst the disadvantages of coherent transmission systems can all be overcome, the penalty is a significant increase in system complexity relative to direct detection systems.

18.3 COMPONENTS FOR OPTICAL TRANSMISSION OF MICROWAVE SIGNALS

In this section, the performance of the key components used in microwave-over-fiber systems will be reviewed.

18.3.1 Optical Sources

The key performance parameters for sources used in intensity-modulated microwave-over fiber-systems are

(i) Output wavelength
(ii) Output power
(iii) Intensity noise
(iv) Modulation response for directly modulated sources

and additionally for coherent systems

(v) Linewidth
(vi) Tunability

The main optical sources are fiber lasers, crystal and waveguide lasers, and semiconductor lasers. Only semiconductor lasers offer direct modulation capability; thus external modulator technology must also be considered. The capabilities and limitations of the various laser and modulator technologies are discussed below.

Fiber lasers

The use of optically pumped fiber doped with an appropriate lasing ion has made a key contribution to optical communication through the optical fiber amplifier. With appropriate feedback, fiber optical sources can also be realized.

The required doped fiber length depends on cavity losses, pump power, and lasing ion doping concentration. The latter is limited by clustering, so that practical erbium-doped fiber lasers for operation at 1530 nm wavelength typically require doped fiber lengths of 1 5 m, giving laser mode separations of 100 20 MHz. Obtaining stable single-mode operation is therefore difficult. Unidirectional ring configurations, which eliminate spatial hole burning, can offer narrow (kHz)

linewidths [10], but active stabilization of the fiber length and polarization state is required to eliminate mode hopping. The performance of the 1550 nm wavelength erbium laser is presently being advanced [11] in both silica and phosphate glass hosts because of the natural overlap with the mature erbium-doped fiber amplifier technology.

Crystal and waveguide lasers

Diode-pumped crystal lasers are attractive sources of high-power (>100 mW), narrow linewidth (<1 kHz), low RIN ($<$ 170 dBc/Hz) optical signals [12]. They offer superior amplitude and phase noise characteristics to those available from semiconductor designs due to the slow gain dynamics of the active rare earth ions. The most successful designs are based on the 1320 nm wavelength transition in Nd:YAG [13] and the 1530 1550 nm wavelength range transitions in Er:Glass. They are finding application as sources in wide dynamic range direct detection analog optical transmission systems for cable TV and related applications. For general application, they suffer from limited tunability (<60 GHz) and high optical complexity.

Improved optical confinement and potential for integration with other optical and electro-optic components make rare-earth-doped waveguide lasers of interest. The two main fabrication technologies are silica on silicon and titanium in-diffused lithium niobate. To realize lasers with reasonably small chip area, it is necessary to achieve doping densities much higher than for fiber lasers. This is especially challenging for erbium-doped guides. Kitagawa et al. [14] have achieved an output power of 1 2 mW from a 45 mm-long erbium-doped silica on silicon laser pumped at 980 nm wavelength. In-diffusion has been used to realize an erbium-doped laser in lithium niobate. A waveguide of length 10.5 mm gave a theshold of 8 mW for pumping at 1477 nm wavelength [15]. Nonsemiconductor waveguide lasers require an optical pump source, which is generally desired to be a diode laser. Thus a fully integrated source technology is not possible.

Semiconductor lasers

Semiconductor lasers are used as sources in most current optical communication systems. They offer the advantages of direct electrical pumping and modulation capability. At frequencies below the photon electron resonance, the modulation response is uniform and given by

$$P_{\mathrm{om}} = \eta_1 i_{\mathrm{m}}, \tag{18.20}$$

where P_{om} is the modulated component of the laser output power, i_{m} the modulating current, and η_1 the modulation sensitivity, defined by

$$\eta_{\mathrm{l}} = \frac{\mathrm{d}P_{\mathrm{u}}}{\mathrm{d}i_{\mathrm{L}}}, \tag{18.21}$$

with i_{L} the laser bias current. Thus maximizing η_{l} minimizes transmission system loss in IMDD systems. The simplicity of direct modulation of semiconductor lasers has proved attractive for many applications, and following early work on modulation characteristics [16], rapid progress has been made in reducing electrical parasitics of laser structures and optimizing laser parameters for high-speed operation. The introduction of multiple-quantum-well (MQW) active regions [17] led to considerable reductions in threshold current and an increase in differential gain by up to a factor of 2 relative to bulk devices. An important limitation is gain compression, which has so far limited reliable 1550 nm room temperature operation lasers to bandwidths of about 30 GHz [18 20] despite much research effort.

Semiconductor lasers for coherent analog optical transmission systems generally require tunability for source/LO laser wavelength matching and channel selection, uniform FM frequency response for optical FM and phase-locked applications, and narrow linewidth for high SNR in angle-modulated systems.

Renewed interest in wavelength division multiplexed (WDM) systems, both for increased channel capacity and for their use in all-optical routeing, has placed emphasis on the need for widely tuneable laser sources. A number of approaches are possible. Multi-section distributed feedback (DFB) lasers have been realized with tuning ranges of 10 nm, while maintaining linewidths less than 20 MHz [21]. Wider tuning ranges have been achieved in vertically coupled structures [22], culminating in the 55 nm tuning range reported by Kim et al. [23], although the linewidth obtained was not reported.

A novel approach, yielding discontinuous tuning over a wide range with simple control, is the Y junction laser [24], where vernier effects have been used to increase the tuning range to 38 nm.

For use as an optical FM source and current-controlled oscillator (CCO) operation in phase-locked applications, a major difficulty has been the interaction between thermal and carrier density effects, leading to an highly nonuniform FM response. The most common approach to achieving uniform FM response has been to use a multisection DFB laser with the section currents adjusted for best uniformity of response. Using this approach, Ogita et al. [25] have achieved a 3 dB bandwidth of 15 GHz, although neither the peak frequency deviation nor the residual intensity modulation is stated. An alternative approach, capable of an intrinsically flat FM response, is to use the refractive index change resulting from the quantum-confined Stark effect (QCSE) in a reverse biased MQW section. The technique was first demonstrated in external cavity laser systems [26] achieving a response uniformity of ± 1.6 dB over the frequency range 20 kHz to 1.3 GHz, limited by tuning element capacitance. More recently, monolithically integrated sources using the same technique have been realized in both the GaAs/AlGaAs [27] and InGaAsP [28] systems. Figure 18.4 shows the measured FM frequency

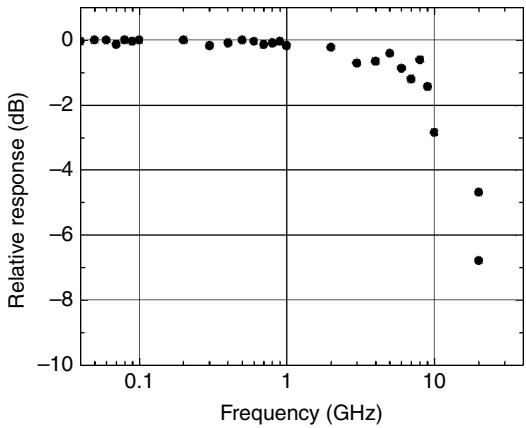

Figure 18.4 Measured FM frequency response of MQW tuned semiconductor laser (after Ref. [28]).

response for a three-section QCSE-tuned laser [28]. Again, the upper frequency limit is set by the tuning element capacitance.

Careful design of semiconductor laser structures to minimize spatial hole burning effects has led to the realization of MQW DFB lasers having linewidths below 100 kHz [6], a value sufficiently small to permit high SNRs in angle-modulated systems.

Semiconductor lasers can also be used with external modulators. The advantage that external modulation offers the link designer is the ability to design the laser separately from the modulation bandwidth or link linearity, which are determined by the modulator design. Since improvements in link loss, noise figure, and compression dynamic range rely on high detector photocurrents to obtain shot-noise-limited operation, research has focused on the design of high-power low-noise lasers. Examples of high-power semiconductor lasers include DFB [30] as well as low-gain designs [31] where power outputs have exceeded 150 mW and are nearing 1 W.

Reviewing the state of semiconductor laser research, it is clear that sources suitable for high-performance IMDD and coherent microwave transmission systems are realizable and such lasers have the attraction of low-cost manufacture.

External modulators

Where the source technology is not capable of direct modulation at microwave rates or it is desired to avoid transmission system gain limitation due to limited source modulation sensitivity, an external modulator can be considered. For a Mach Zehnder interferometric modulator [32] operated well within its bandwidth, the modulation response is uniform and given by

$$P_{\mathrm{om}} = \frac{\pi G_{\mathrm{M}} R_{\mathrm{in}} P_{\mathrm{I}}}{V_{\pi}} i_{\mathrm{m}}, \tag{18.22}$$

where G_{M} (normally <1) is the optical power gain of the modulator when biased for maximum transmission, R_{in} the input resistance of the modulator, P_{I} the incident unmodulated laser power, and V_{π} the input voltage required to produce a phase shift of π between the arms of the interferometer and hence extinguish the optical output.

Since P_{om} is proportional to P_{I}, the gain of the transmission system can be increased by increasing P_{I}, the limit being set by available laser power, the onset of optical damage in the modulator, nonlinear limitations in the optical fiber as discussed in Section 18.2.3 or saturation of the detector. Use of this feature enabled the first demonstration of an optical link exhibiting gain without the use of electrical amplification [32]. Interferometric external modulators have been realized in both lithium niobate [33, 34] and III V semiconductor technologies [35, 36] with bandwidths well in excess of 30 GHz. Polymer modulators have also achieved impressive high-frequency capability [37] and represent an attractive technology if problems of stability, high temperature, and high-power operation can be overcome. Minimizing V_{π} and maximizing G_{M} without compromising the operating bandwidth are key challenges to modulator designers.

Electro-absorption modulators operate by converting the incident light into photocurrent in their absorbing state. Waveguide modulators using the Franz Keldysh effect in bulk semiconductor materials or the QCSE in quantum well materials have been studied extensively. Bulk modulators at 1530 nm wavelength have achieved 3 dB electrical bandwidths of 50 GHz with 3.5 V drive for 20 dB extinction and fiber-to-fiber insertion loss of about 8 dB [38]. To obtain sufficiently low capacitance for such high-speed operation, the active section of the waveguide must be kept very short, 50 μm in this example, limiting the modulation sensitivity. Traveling wave approaches can be used to improve this parameter [39, 40] and a 1300 nm wavelength traveling wave modulator with 3 dB electrical bandwidth exceeding 5 40 GHz, small signal modulation sensitivity 0.65 V^{-1}, and fiber-to-fiber insertion loss of 11.3 dB has recently been demonstrated [40]. An attractive feature of electro-absorption modulators is that they can be integrated with semiconductor lasers to form compact optical sources capable of ultrafast modulation [41]. Recent advances in high-power semiconductor modulators have also been made with devices capable of handling over 100 mW of optical power [42], where careful quantum well and waveguide design was employed to prevent carrier bleaching at high power.

Coupling losses between optical fiber and semiconductor waveguide modulators can be reduced by moving to nonwaveguide reflective modulator designs in which the light is incident perpendicular to the junction plane, as in the asymmetric Fabry Perot modulator (AFPM). In common with other electro-absorption modulators, these devices can also be used as detectors to create a duplex system, as described in Section 18.4 [43].

18.3.2 Optical Amplifiers

The development of optical amplifiers has made it possible to realize systems in which the optical transmission parameter, G_l is greater than unity. They can also be used to compensate for splitting losses in multipoint distribution systems.

The most important optical amplifier technologies for microwave signal transmission applications are the traveling wave semiconductor laser amplifier (SLA) [44] and the doped fiber amplifier (DFA) [45]. Figure 18.5 shows the modeled distortion performance of a typical SLA as a function of the intensity modulation frequency of the incident light [44]. When the modulation frequency is greater than the reciprocal of the carrier lifetime, typically 2 ns, the distortion is seen to be small. This restricts the minimum intensity modulation frequency to several GHz, making them unsuitable for a number of wireless system applications, such as cellular radio signal distribution.

Figure 18.6 shows the structure and typical performance of an erbium-doped fiber amplifier. The DFA is pumped using a semiconductor laser and has the advantage that it can be spliced directly into a fiber system, avoiding significant coupling losses. Since the fluorescence lifetime of erbium is long (>10 ms), low distortion performance can be maintained for modulation frequencies down to the kHz region.

The noise contribution from optical amplifiers can be included through the I_{na}^2 term in Eqns (18.7) and (18.17). Desurvire [46] gives a full analysis of the noise contributions for transmission systems using a variety of amplifier configurations. As an example, consider an IMDD system with low fiber loss using

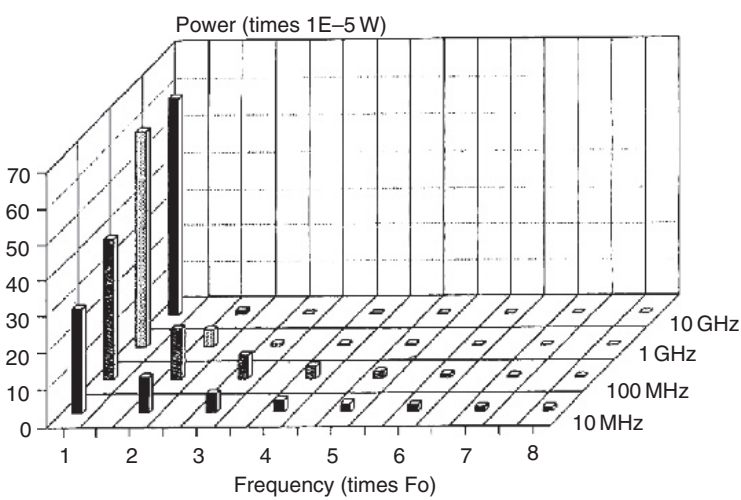

Figure 18.5 Modeled harmonic distortion performance of semiconductor laser amplifier for intensity modulated inputs as a function of signal frequency.

Centre wavelength: 1.53 μm	3 dB Bandwidth: 35 nm
Optical gain: 20 dB	Noise figure: 5 dB
Pump wavelength: 1.48 μm	Sat. O/P power: 25 mW

Figure 18.6 Structure and typical performance of the erbium doped fiber amplifier (EDFA).

an optical preamplifier immediately before the photodetector. I_{na}^2 will comprise three terms:

(i) Additional shot noise due to the amplified spontaneous emission power:

$$I_{\mathrm{sn}}^2 = \frac{4eRn_{\mathrm{sp}}hc(G_{\mathrm{l}} - 1)}{\lambda} B_{\mathrm{o}}\, B, \tag{18.23}$$

where n_{sp} is the amplifier spontaneous emission factor, h Planck's constant, c the velocity of light in vacuo, B_{o} the bandwidth of the optical amplifier output filter, G_{l} the amplifier gain, and λ the operating wavelength.

(ii) Spontaneous-spontaneous beat noise:

$$I_{\mathrm{sp.sp}}^2 = 4\left(\frac{Rn_{\mathrm{sp}}hc(G_{\mathrm{l}} - 1)}{\lambda}\right)^2 B_{\mathrm{o}}B, \tag{18.24}$$

where it is assumed that $B_{\mathrm{o}} >> B$.

(iii) Signal-spontaneous beat noise:

$$I_{\mathrm{s.sp}}^2 = \frac{4R^2P_{\mathrm{u}}n_{\mathrm{sp}}hcG_{\mathrm{l}}(G_{\mathrm{l}} - 1)}{\lambda} B \tag{18.25}$$

The first two terms can be minimized by reducing B_{o} to the minimum compatible with the modulated signal bandwidth and source wavelength drift tolerance, so that in practical systems the third term is the only significant one. For full population inversion, $n_{\mathrm{sp}} = 1$, and an optical source of low RIN, increasing the amplifier gain ($G_{\mathrm{l}} >> 1$) gives an amplifier-noise-limited SNR of

$$\mathrm{SNR} = \frac{P_{\mathrm{u}} k^2 \overline{m^2\{t\}} \lambda}{4hc\,B} \tag{18.26}$$

Substituting for the responsivity in Eqn (18.9), according to Section 18.3.3, the shot-noise-limited SNR for a nonpreamplified system with the same assumptions is

$$\mathrm{SNR} = \eta \frac{P_{\mathrm{u}} k^2 \overline{m^2\{t\}} \lambda}{2hc\,B}, \tag{18.27}$$

where η is the photodetector quantum efficiency. Thus, for an ideal photodetector, the preamplifier degrades the SNR by 3 dB. In practical systems, the preamplifier is attractive because it enables the SNR of Eqn (18.26) to be achieved even for weak received optical signals where thermal noise in detector and receiver normally predominates.

The choice between SLAs and DFAs for microwave transmission application will depend on the systems context. SLAs can be integrated into opto-electronic integrated circuits (OEICs) whereas DFAs interface naturally with fiber systems. SLAs offer greater power-added efficiency, whereas DFAs offer lower added noise and much lower minimum modulation frequency, which is important since there are extensive wireless communication allocations in the range 150 MHz to 2.5 GHz. Thus it seems likely that SLAs will see growing application in integrated systems for higher frequency services, such as WiMax.

18.3.3 Photodetectors

For microwave signal transmission, depletion layer photodetectors are preferred for their speed and good quantum efficiency. For such devices, 3 dB bandwidths in excess of 100 GHz were demonstrated some years ago [47]. For operation well within the 3 dB bandwidth, a simple current generator model for the photodiode can be used, giving

$$i_{\mathrm{s}} = RG_{\mathrm{l}} P_{\mathrm{u}}\, km\{\mathrm{t}\}, \tag{18.28}$$

where the responsivity, R, is given by

$$R = \eta \frac{\mathrm{e}\lambda}{hc} \tag{18.29}$$

The upper limit to depletion photodiode frequency response is set by transit time effects [48] and by the depletion capacitance of the diode unless traveling wave techniques are implemented [49]. Optimization involves conflicting requirements

since reducing the depletion width to increase the transit-time-limited frequency increases the depletion capacitance and can lead to incomplete absorption of light in geometries where light is incident normal to the junction plane. Loss of quantum efficiency can be compensated for in thin depletion layer devices by adding doped absorbing layers [50] adjacent to the depletion region, but with a general increase in some of their nonlinear characteristics. For high-speed operation, waveguide photodiodes with light incident parallel to the junction plane have been extensively studied [49] with multimode designs offering 110 GHz bandwidth with 50% quantum efficiency [51].

In high dynamic range microwave photonic systems, detector power handling and nonlinear effects are of great importance. The effect of the generated carriers on the electric field within the detector is an important limiting factor, which has been studied theoretically [52] and experimentally [53]. Traveling wave configurations have been suggested to reduce the space charge density and obtain increased power handling capability [54], but surface-illuminated designs, such as the partially depleted-absorber photodiode (PDA-PD), have yielded the highest current handling performance to date [55]. These high current handling designs make use of thin depletion regions combined with doped absorbers for increased efficiency. Other devices utilizing doped rather than fully depleted absorbers include the uni-traveling-carrier photodiode (UTC-PD) [56]. Thin depletion regions are key to obtaining high photocurrent for two reasons. First, since most photodiodes fail because of high thermal dissipation, the thin depletion region can attain higher electric fields for the same applied voltages, thus lowering Joule heating. Second, the space-charge effect is reduced because the space-charge-field is proportional to the number and separation of carriers within the depletion region, which are both reduced because of the short transit time. While doped absorber photodiode designs can offer operation at frequencies into the THz band [56, 57], excessive minority electron transit time can lead to additional small nonlinearities including current-dependent bandwidth [55], nonlinear responsivity [58], and harmonic distortion [59]. PDA-PDs have achieved record performance in terms of output RF power at ultrahigh frequencies, with over $+24$ dBm directly from the PD being reported at 2 GHz [60] with good power conversion efficiency. At higher frequencies, the use of the UTC-PD approach in an optimized waveguide detector has given record output powers of $+12$ dBm at 110 GHz [29], -8 dBm at 450 GHz, and -17 dBm at over 900 GHz [57].

The main design challenges for photodiodes in microwave transmission systems are to achieve wide bandwidth, high linearity, and high quantum efficiency, without compromising the optical power handling requirements for shot-noise-limited systems.

Amongst other photodetector technologies, perhaps the most exciting for microwave applications, due to its internal current gain, is the heterostructure photo-transistor (HPT). Wake et al. [61] have reported a waveguide HPT with unity gain bandwidth exceeding 30 GHz.

18.4 MICROWAVE-OVER-FIBER SYSTEMS

18.4.1 Wireless-Over-Fiber Systems

The principal attraction of wireless-over-fiber technology is that it centralizes most of the transceiver functionality by transmitting the wireless signals in their modulated format over fiber, and reduces the fielded access points to antennas with associated amplifiers and frequency converters. Standards-independent and multiservice operation is facilitated.

At frequencies used for existing cellular systems (900 MHz and 1.8 GHz for Groupe speciale mobile (GSM), 2 2.3 GHz for Universal mobile telecommunication system (UMTS)), semiconductor lasers, directly modulated with the data-modulated radio frequency (RF) signals, are favored on cost grounds, with single-mode-fiber (SMF) and wide bandwidth photodiodes to complete the system. Figure 18.7 shows a typical system layout. Wireless base stations are located in a central communications room and their outputs/inputs fed through RF multiplexers to lasers/photodiodes contained within the optical transceiver hub. The modulated optical signals are linked to/from the remote antenna units (AUs) in the building using single-mode optical fiber. A major cost saving is becoming available in such links with the development of high linearity, uncooled laser diodes [62].

Strong growth in the use of IEEE 802.11 a/b/g WLAN has led to the development of systems for the simultaneous transmission of multiple WLAN channels

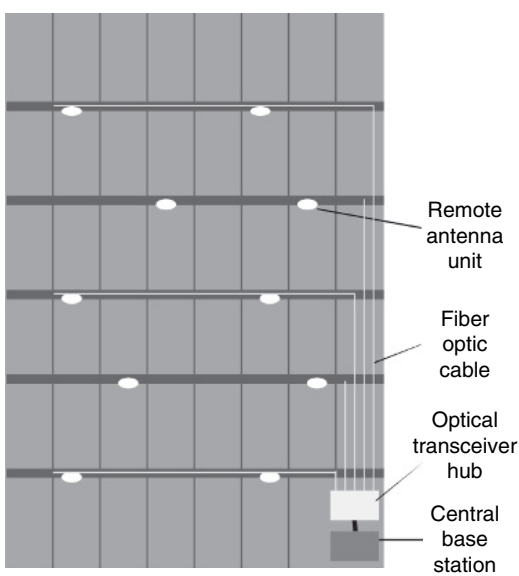

Figure 18.7 In building wireless over fiber system (this figure may be seen in color on the included CD ROM).

over a single wireless over fiber link [63], showing the wide dynamic range capabilities available with modern directly modulated lasers.

For in-building applications, there has been considerable interest in the passive picocell concept [64], in which the base station uses a combined detector/optical modulator, which is directly coupled to the antenna, so that no electrical amplification or other processing is required. Typically, a waveguide electro-absorption modulator is used as the detector/modulator. However, this leads to system penalties due to the polarization dependence of the modulator and the high optical insertion loss. A more recent approach uses a normal incidence AFPM to give polarization independence and a low optical insertion loss by direct coupling to single mode optical fiber [43]. Passive picocell technology requires non-eye-safe high optical power (>10 mW), high (mW) output power capability from the detector, and high modulation sensitivity to provide whole-room coverage for high data rate services, such as WLAN. Its application area is therefore likely to be limited to low data rate services, such as emergency voice coverage.

Multimode fiber, although forming by far the majority of the in-building installed fiber base, has seen restricted use for wireless-over-fiber applications, since its small bandwidth $\times$ distance product (typically <500 MHz.km) requires signal transmission at IF with up/down conversion at each AU [65]. Above the multimode fiber cut-off frequency, the transmission response is fairly uniform, but at a lower level, and it has been shown to be possible to use this frequency range for wireless-over-fiber transmission without down/up conversion [66].

To cater for growth in broadband wireless access applications, spectrum has been made available in the 28, 40, and 60 GHz bands. Here, single-sideband techniques are preferred to overcome dispersion limits on propagation in standard SMF. At the higher frequencies, where direct modulation or external modulators are not available, a wide variety of techniques have been investigated [6 7, 67 74] to provide broadband wireless-over-fiber access, while minimizing the fiber dispersion penalties resulting from the high carrier frequency. These include dispersion compensation [69], frequency multiplying modulators with sideband filtering for modulation [70], optical single-sideband modulators [71], synchronization of a mode-locked laser to a subharmonic optical clock [72], optical injection locking of two slave lasers to spectral lines from a directly modulated master laser [73], and phase locking of two lasers in an OPLL [75]. Of these methods, dispersion compensation requires adjustment if the fiber span length is changed; modulator approaches suffer substantial optical loss whereas the power output at the required modulation frequency from mode-locked lasers is usually small so that optical amplifiers are required, increasing system cost. Injection locking approaches offer high launch power, reducing the need for optical amplifiers, but require milliKelvin temperature control of the slave lasers for reliable operation, while OPLLs require special low propagation delay optics and electronics for use with semiconductor lasers. Use of the optical injection phase lock loop (OIPLL) technique overcomes these limitations [76, 77]. Figure 18.8 shows a 36 GHz binary phase shift keyed (BPSK) wireless link which makes use of the wide loop bandwidth of the OIPLL to allow direct data modulation of the reference source, thus removing the need for an optical modulator [74].

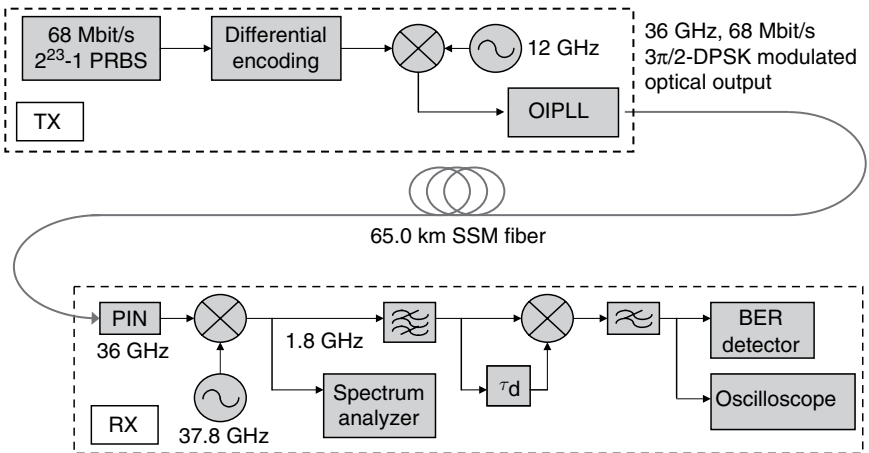

Figure 18.8 36 GHz BPSK wireless over fiber system. (after. Ref. [74]) (this figure may be seen in color on the included CD ROM).

18.4.2 Antenna Remoting and Cable Television Applications

Microwave antenna remoting for satellite earth stations and similar applications has used microwave-over-fiber technology for a number of years [78]. The cable television industry has long used broadband fiber technology for distribution of both analog and digital signals [79]. Each modulated channel is mixed with a subcarrier in the electrical domain to form a composite signal, which is used to modulate the optical source. Linearity requirements in such systems are stringent [80]; however, the value of the traffic to be carried and the number of end-customers is sufficient to support the use of externally modulated and linearized sources. As discussed in Section 18.2, the use of high-power externally modulated optical sources enables links having significant transmission gain without the use of electrical amplifiers leading to low link noise figures and enhanced spurious-free dynamic ranges (SFDRs) [32, 81, 82].

In analog links employing external Mach Zehnder modulators (MZM), the sinusoidal transfer function usually dictates the linearity of the link unless fiber [83] or photodetector [84] nonlinearities dominate. Biasing the modulator at quadrature yields the highest slope and the highest link gain or lowest loss. In addition to being the point of highest slope, operation at quadrature yields an odd transfer function thus minimizing the second-order distortion output. Third-order distortion from the sinusoidal transfer function is a weak function of bias [85] and limits most practical links as it yields two-tone third-order distortions within typical signal bandwidths. Intermodulation distortion is usually quantified with the SFDR, defined as the largest input SNR signal possible without observation of measurable distortion products above the noise floor. For quadrature-biased

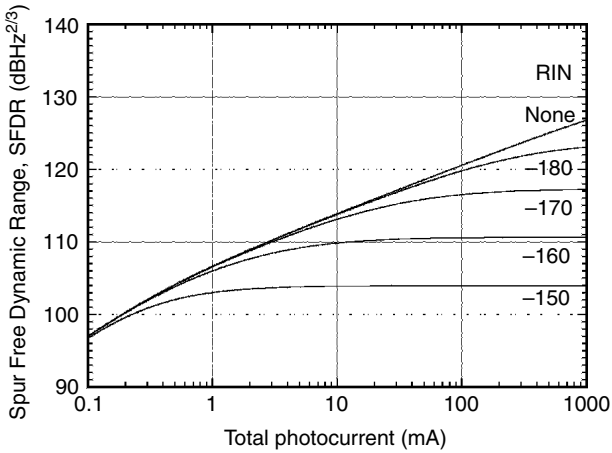

Figure 18.9 Spurious free dynamic range performance as a function of photocurrent (after Ref. [86]).

MZMs, the SFDR is only a function of photocurrent [86] and laser RIN as shown in Figure 18.9 unless the modulator sensitivity becomes so high that input thermal noise appears at the output of the link. SFDR values of greater than 120 dB-Hz$^{2/3}$[84] have been achieved for a 100 mA balanced detection link over multi-octave bandwidths. Higher multi-octave dynamic range links are likely to use techniques to linearize the MZM transfer function [87, 88 89], feedback or feed forward compensation [90], or coherent frequency or phase (angle) modulation links.

As discussed in Section 18.2 coherent analog transmission systems offer the choice of intensity, amplitude, frequency, or phase modulation. Fong et al. [91] report amplitude-modulated links which are insensitive to source linewidth, while Kalman and Kazovsky [92] describe a highly linear phase-modulated link. Cai and Seeds [93] report a frequency-modulated link, which enables high SNR to be obtained in long unamplified links.

18.5 CONCLUSION—FUTURE PROSPECTS

In this chapter, systems for the optical transmission of microwave signals have been analyzed and technologies for their implementation reviewed. IMDD systems offer the advantage of simplicity. However, large received optical power is necessary in order to overcome receiver thermal noise. In systems of length more than a few kilometres, the maximum source power is limited by the onset of nonlinear effects, especially SBS, in the optical fiber. In short systems, the limit is set by source and detector power handling limits. Optical preampliers enable near shot-noise-limited detection to be achieved even for low received powers. In particular, the availability of high-quality optical fiber amplifiers for the 1550 nm

optical fiber transmission window makes it possible to realize high-quality IMDD transmission systems at that wavelength. There is much scope for further work to improve component performance, particularly source output power, RIN, and modulation sensitivity; modulator insertion loss, power handling, and V_π; and photodetector power handling.

The capability of coherent systems to select between many channels present on the same optical fiber makes them attractive in applications such as multiple antenna remoting. They also enable wide dynamic range transmission systems to be realized at wavelengths where high-quality optical amplifiers are not available, and, using angle modulation, to obtain SNRs beyond those obtainable with IMDD systems for long links where fiber nonlinearity limits the fiber launch power. These are, however, niche applications.

Of the applications for this technology, wireless-over-fiber systems and cable television transmission have both found widespread commercial adoption. Microwave antenna remoting is also now well established. For the future, millimeter-wave personal communications using fiber-fed base stations is an area of intense interest.

ACKNOWLEDGMENTS

The author thanks the members of his research group and his colleagues worldwide for their many contributions to the work described here. The International Union for Radio Science (URSI) is thanked for permission to include the microwave-over-fiber link analysis first presented by the author in the Review of Radio Science 1993 1996. Particular thanks are due to Keith Williams (US Naval Research Laboratory), who provided key references and commentary on link technology. Aspects of the work described here were supported by the UK Engineering and Physical Sciences Research Council, the United States Air Force Office of Scientific Research, and the 5th and 6th European Union Framework Research Projects, NEFERTITI, GANDALPH, ISIS, e-PhotonONE, and IPHOBAC.

REFERENCES

[1] P. S. Henry, R. A. Linke, and A. H. Gnauck, "Introduction to lightwave systems," in *Optical Fiber Telecommunications II* (S. E. Miller and I. P. Kaminow, eds.), Orlando, Academic Press, 1988.

[2] G. L. Abbas, V. W. S. Chan, and T. K. Lee, "Local oscillator excess noise suppression for heterodyne and homodyne detection," *Opt. Lett.*, 8, 419 421, 1983.

[3] A. R. Chraplavy, "Nonlinear effects in optical fibers," in *Topics in Lightwave Transmission Systems* (T. Li, ed.), San Diego, Academic Press, 1991, pp. 267 295.

[4] R. G. Smith, "Optical power handling capacity of low loss optical fibers as determined by stimulated Raman and Brillouin scattering," *Appl. Opt.*, 11, 2489 2495, 1972.

[5] B. Cai and A. J. Seeds, "Optical frequency modulation link for microwave signal transmission," *IEEE MTT S Digest*, San Diego, 163 166, 1994.

[6] M. Okai and T. Tsuchiya, "Tunable DFB lasers with ultra narrow spectral linewidth," *Electron. Lett.*, 29, 349 351, 1993.
[7] R. T. Ramos and A. J. Seeds, "Delay, linewidth and bandwidth limitations in optical phase locked loop design," *Electron. Lett.*, 26, 389 391, 1990.
[8] N. G. Walker and G. R. Walker, "Polarisation control for coherent communications," *J. Lightw. Technol.*, LT 8, 438 458, 1990.
[9] B. Glance, "Polarisation independent optical receiver," *J. Lightw. Technol.*, LT 5, 274 276, 1987.
[10] P. R. Morkel, G. J. Cowle, and D. N. Payne, "Travelling wave erbium fiber ring laser with 60 kHz linewidth," *Electron. Lett.*, 26, 632 634.
[11] C. Spiegelberg, J. Geng, Y. Hu et al., "Low noise narrow linewidth fiber laser at 1550 nm," *J. Lightw. Technol*., LT 22(1), 57 62, 2004.
[12] K. J. Williams, A. Dandridge, A. D. Kersey et al., "Interferometric measurement of low frequency phase noise characteristics of diode laser pumped Nd:YAG ring laser," *Electron. Lett.*, 25, 774 776, 1989.
[13] T. J. Kane and R. L. Byer, "Monolithic unidirectional single mode Nd:YAG Ring Laser," *Opt. Lett*., 10, 65 67, 1985.
[14] T. Kitagawa, K. Hattori, M. Shimizu et al., "Guided wave laser based on erbium doped silica planar lightwave circuit," *Electron. Lett.*, 27, 334 335, 1991.
[15] R. Brinkmann, W. Sohler and M. Suche, "Continuous wave erbium diffused $LiNb0_3$ waveguide laser," *Electron. Lett.*, 27, 415 416, 1991.
[16] T. Ikegami and Y. Suematsu, "Resonance Like Characteristics of the Direct Modulation of a Junction Laser," in Proc. *IEEE 1967*, 55(1), 1967, pp. 122 123.
[17] J. P. van der Ziel, R. Dingle, R. C. Miller et al., "Laser oscillation from quantum states in very thin GaAs $Al_{0.2}Ga_{0.8}$ As multilayer structures," *Appl. Phys. Lett.,* 26(8), 463 465, 1975.
[18] R. S. Tucker and I. P. Kaminow, "High frequency characteristics of directly modulated InGaAsP ridge waveguide and buried heterostructure lasers," *J. Lightw. Technol.*, LT 2, 385 393, 1984.
[19] O. Kjebon, R. Schatz, S. Lourdudoss et al., "30 GHz direct modulation bandwidth in detuned loaded InGaAsP DBR lasers at 1.55 mm wavelength," *Electron. Lett*., 33, 488 489, 1997.
[20] Y. Matsui, H. Murai, S. Arahira et al., "30 GHz bandwidth 1.55 μm strain compensated InGaAlAs InGaAsP MQW laser," *IEEE Photon. Technol. Lett*., 9, 25 27, 1997.
[21] T. L. Koch and U. Koren, "Semiconductor lasers for coherent optical fiber communications," *J. Lightw. Technol.*, LT 8, 274 293, 1990.
[22] S. Illek, W. Thulke, and M. C. Amann, "Codirectionally coupled twin guided laser diode for broadband electronic wavelength tuning," *Electron. Lett.*, 27, 2207 2209, 1991.
[23] I. Kim, R. C. Alferness, L. L. Buhl et al., "Broadly tunable InGaAsP/InP vertical coupler filtered laser with low tuning current," *Electron. Lett.*, 29, 664 666, 1993.
[24] W. Idler, M. Schilling, D. Baums et al., "Y Laser with 38 nm tuning range," *Electron. Lett.*, 27, 2268 2270, 1991.
[25] S. Ogita, Y. Kotaki, M. Matsuda et al., "FM response of narrow linewidth, multielectrode, $\lambda/4$ shift DFB laser," *IEEE Photon. Technol. Lett.*, 2, 165 166, 1990.
[26] B. Cai, A. J. Seeds, and J. S. Roberts, "MQW tuned semiconductor lasers with uniform frequency response," *IEEE Photon. Technol. Lett.*, 6, 496 498, 1994.
[27] X. Huang, A. J. Seeds, J. S. Roberts, and A. P. Knights, "Monolithically integrated quantum confined Stark effect tuned laser with uniform frequency modulation response," *IEEE Photon. Technol. Lett*., 10, 1697 1699, 1998.
[28] M. I. Pantouvaki, C. C. Renaud, P. Cannard et al., "Fast tuneable InGaAsP DBR laser using quantum confined Stark effect induced refractive index change," IEEE *J. Sel. Top. Quantum Electron.*, JSTQE 13(5), 1112 1121.
[29] C. Renaud, D. Moodie, M. Robertson, and A. J. Seeds "High Output Power at 110 GHz with a Waveguide Uni Travelling Carrier Photodiode," in Proc. *IEEE LEOS Annual Meeting 2007*, Orange, October, 2007, 782 783.
[30] Y. Inaba, H. Nakayama, M. Kito et al., "High power 1.55 μm Mass Transport Grating DFB lasers for externally modulated systems," *IEEE J. Sel. Top. Quantum. Electron*., JSTQE 7(2), 152, 2001.

[31] J. J. Plant, P. W. Juodawlkis, R. B. Huang et al., "1.5 μm InGaAsP InP Slab Coupled Optical Waveguide Lasers," *IEEE Photon. Technol. Lett*., 17(4), 735 737, 2005.
[32] C. H. Cox, G. E. Betts, and L. M. Johnson, "An analytic and experimental comparison of direct and external modulation in analogue fiber optic links," *IEEE Trans.*, MTT 38, 501 509, 1990.
[33] D. W. Dolfi and T. R. Ranganath, "50 GHz velocity matched, broad wavelength $LiNbO_3$ modulator with multimode active section," *Electron. Lett.*, 28, 1197 1198, 1992.
[34] K. Noguchi, O. Mitomi, and H. Miyazawa, "Millimeter wave Ti:LiNbO3 optical modulators," *J. Lightw. Technol*., 16, 615 619, 1998.
[35] R. G. Walker and I. Bennion, "GaAs/AlGaAs Travelling Wave Modulators for Millimetre Wave Frequencies," in Proc. *ECOC 1991*, Paris, 1991, pp. 437 440.
[36] R. G. Walker, "Electro optic Modulation at mm Wave Frequencies in GaAs/AlGaAs Guided Wave Devices," in Proc. *8th IEEE LEOS Annual Meeting*, San Francisco, 1995, pp. 118 119.
[37] D. Chen, H. Fetterman, A. Chen et al., "Demonstration of 110 GHz electro optic polymer modulators," *Appl. Phys. Lett*., 70, 3335 3337, 1997.
[38] T. Ido, S. Tanaka, M. Suzuki et al., "Ultra high speed multiple quantum well electro absorption optical modulators with integrated waveguides," *J. Lightw. Technol*., LT 14, 2026 2034, 1996.
[39] S. Z. Zhang, Y. J. Chiu, P. Abraham, and J. E. Bowers, "25 GHz Polarisation insensitive electroabsorption modulators with travelling wave electrodes," *IEEE Photon. Technol. Lett*., 12, 1471 1473, 2000.
[40] G. L. Li, S. A. Pappert, C. K. Sun et al., "Wide Bandwidth Travelling Wave InGaAsP/InP Electro Absorption Modulator for Millimetre Wave Applications," in Proc. *IEEE MTT S Symposium Dig*., paper Tu1C 2, Phoenix, AZ vol. 1, 2001, pp. 61 64.
[41] H. Kawanishi, Y. Yamauchi, N. Mineo et al., "EAM integrated DFB laser modules with more than 40 GHz bandwidth," *IEEE Photon. Technol. Lett*., 13, 954 956, 2001.
[42] Y. Zhuang, W. S. C. Chang, and P. K. L. Yu, "Peripheral coupled waveguide mqw electroabsorp tion modulator for near transparency and high spurious free dynamic range rf fiber optic link," *IEEE Photon. Technol. Lett*., 16(9), 2033 2035, 2004.
[43] C. Liu, et al., "Bi Directional Transmission of Broadband 5.2 GHz Wireless Signals Over Fiber Using a Multiple Quantum Well Asymmetric Fabry Perot Modulator/Photodetector," in Proc. *IEEE/OSA OFC'2003,* Atlanta., March 2003, pp. 738 740.
[44] C. Zaglanikis and A. J. Seeds, "Computer Model for Semiconductor Laser Amplifiers with Rf Intensity Modulated Inputs", in Proc. *IEE 1992, Pt. J. Optoelectronics,* paper 139, pp. 254 262, 1992.
[45] R. I. Laming and D. N. Payne, "Progress in the Optimisation of Erbium Doped Fiber Amplifiers (EDFAs)," in Proc. *OFC 1990*, San Diego, 1990, p. 178.
[46] E. Desurvire, *Erbium Doped Fiber Amplifiers*, New York, Wiley, pp. 65 203, 1994.
[47] D. G. Parker, P. G. Say, and A. M. Hansom, "110 GHz high efficiency photo diodes fabricated from indium tin oxide/GaAs," *Electron. Lett.*, 23, 527 528, 1987.
[48] W. Gartner, "Depletion layer photoeffects in semiconductors," *Phys. Rev*., 116, 84 87, 1959.
[49] J. E. Bowers and C. A. Burrus, "High speed zero bias waveguide photodetectors," *Electron. Lett.*, 22, 905 906, 1986.
[50] G. A. Davis, R. E. Weiss, R. A. LaRue et al., "A 920 1650 nm High Current Photodector," *IEEE Photon. Technol. Lett.*, 8(10), 1373 1375, 1996.
[51] K. Kato, A. Kozen, Y. Muramoto et al., "110 GHz 50% efficiency mushroom mesa waveguide p i n photodiode for a 1.55 μm wavelength," *IEEE Photon. Technol. Lett*., 6, 719 721, 1994.
[52] M. Dentan and B. D. de Cremoux, "Numerical simulation of a p i n photodiode under high illlumination," *J. Lightw. Technol*., LT 8, 1137 1144, 1990. 'M. Denton' or 'M. Dentan'.
[53] P. L. Liu, K. J. Williams, M. Y. Frankel, and R. D. Esman, "Saturation characteristics of fast photodetectors," *IEEE Trans*., MTT 47, 1297 1303, 1999.
[54] L. Y. Lin, M. C. Wu, T. Itoh et al., "High power, high speed photodetectors design, analysis and experimental demonstration," *IEEE Trans*., MTT 45, 1320 1331, 1997.

[55] X. Li, N. Li, S. Demiguel et al., "A Comparison of front and backside illuminated high saturation power partially depleted absorber photodetectors," *IEEE J. Quantum Electron*., 40, 1321 1325, 2004.

[56] H. Ito, T. Furata, S. Kodama, and T. Ishibashi, "InP/InGaAs Uni travelling carrier photodiode with 310 GHz bandwidth," *Electron. Lett*., 36, 1809 1810, 2000.

[57] A. J. Seeds, C. Renaud, M. Pantouvaki et al., "Photonic Synthesis of THz Signals," in Proc. *EMC 2006*, Manchester, September 2006, pp. 1107 1110.

[58] K. J. Williams and R. D. Esman, "Photodiode DC and Microwave Nonlinerity at high current due to carrier recombination nonlinearities," *IEEE Photon. Technol. Lett*., 10, 1015 1017, 1998.

[59] K. J. Williams, R. D. Esman, and M. Dagenais, "Nonlinearities in p i n microwave photo detectors," *J. Lightw. Technol*., LT 14, 84 96, 1996.

[60] K. J. Williams, D. A. Tulchinsky, and J. C. Campbell, "High Power Photodetectors," IEEE Int. Tropical Meeting on Microwave Photonics, Victoria, Canada, October 2007, pp. 9 13.

[61] D. Wake, D. J. Newson, M. J. Harlow, and I. D. Henning, "Optically biased edge coupled InP/InGaAs heterostructure photo transistor," *Electron. Lett*., 29, 2217 2218, 1993.

[62] J. D. Ingham et al, "Wide Frequency Range Operation of a High Linearity Uncooled DFB Laser for Next Generation Radio Over Fiber," in Proc. *IEEE/OSA OFC 2003*, Atlanta, March, 2003, pp. 754 756.

[63] T. Niiho, M. Nakaso, K. Masuda et al., "Multi Channel Wireless LAN Distributed Antenna System Based on Radio Over Fiber Techniques," in Proc. *IEEE LEOS Annual Meeting*, *Puerto Rico*, October, 2004, pp. 57 58.

[64] D. Wake, D. Johansson, and D. G. Moodie, "Passive picocell a new concept in wireless network infrastructure," *Electron. Lett*., 33, 404 406, 1997.

[65] LGC Wireless, 2006, http://www.lgcwireless.com/products/lgcell.html

[66] P. Hartmann, M. Webster, A. Wonfor et al., "Low Cost Multimode Fiber Based Wireless LAN Distribution System Using Uncooled Directly Modulated Dfb Laser Diodes," in Proc. *ECOC 2003, Rimini*, September, 2003, We4.P.124.

[67] H. Ogawa, D. Polifko, and S. Bamba, "Millimetre wave fiber optic systems for personal radio communication," *IEEE Trans*., MTT 40, 2285 2292, 1992.

[68] H. Schmuck and R. Heidemann, "High Capacity Hybrid Fiber Radio Field Experiments at 60 GHz," in Proc. *IEEE/IEICE ITM MWP 1996*, Kyoto, 1996, pp. 65 68.

[69] K. Kitayama, "Fading Free Transport of 60 GHz Optical DSB Signal in Non Dispersion Shifted Fiber Using Chirped Fiber Grating," in proc. *IEEE ITMMWP 1998*, Princeton, 1998, pp. 223 226.

[70] J. J. O'Reilly, P. M. Lane, and M. H. Capstick, "Optical generation and delivery of modulated mm waves for mobile communications," in *Analogue Optical Fiber Communications* (B. Wilson, Z. Ghassemlooy, and I. Darwazeh, eds), London, England, Institution of Electrical Engineers, 1995, pp. 229 256.

[71] G. H. Smith and D. Novak, "Broadband millimetre wave (38 GHz) fiber wireless transmission system using electrical and optical SSB modulation to overcome dispersion effects," *IEEE Photon. Technol. Lett*., 10, 141 143, 1998.

[72] K. I. Kitayama, T. Kuri, H. Yokoyama, and M. Okuno, "60 GHz Millimetre Wave Generation and Transport over OFDM Fiber Optic Networks," in Proc. *IEEE/IEICE ITMMWP 1996*, Kyoto, 1996, pp. 49 52.

[73] R. P. Braun, G. Grosskopf, D. Rohde, and F. Schmidt, "Fiber Optic Millimetre Wave Generation and Bandwidth Efficient Data Transmission for Broadband Mobile 18 20 and 60 GHz Band Communications," in proc. *IEEE ITMMWP'1997,* Essen., 1997, pp. 235 238.

[74] L. A. Johansson, D, Wake, and A. J. Seeds, "Millimetre Wave Over Fiber Transmission using a BPSK Reference Modulated Optical Injection Phase Lock Loop," in Proc. *IEEE/OSA OFC 2001*, paper WV3 1 WV3 3, Anaheim, March, 2001, p. 3.

[75] L. N. Langley, M. D. Elkin, C. Edge et al., "Packaged semiconductor laser optical phase locked loop (opll) for photonic generation, processing and transmission of microwave signals," *IEEE Trans*., MTT 47, 1257 1264, 1999.

[76] A. C. Bordonalli, C. Walton, and A. J. Seeds, "High performance phase locking of wide linewidth semiconductor lasers by combined use of optical injection locking and optical phase lock loop," *J. Lightw. Technol*., 17, 328 342, 1999.

[77] L. A. Johansson and A. J. Seeds, "Millimeter wave modulated optical signal generation with high spectral purity and wide locking bandwidth using a fiber integrated optical phase lock loop," *IEEE Photon. Technol. Lett*., 12, 690 693, 2000.

[78] J. E. Bowers, A. C. Chipa'loski, S. Boodaghians, and J. W. Carlin, "Long distance fiber optic transmission of C band microwave signals to and from a satellite antenna," *J. Lightw. Technol.,* LT 5, 1733 1741, 1987.

[79] T. E. Darcie and G. E. Bodeep, "Lightwave subcarrier catv transmission systems," *IEEE Trans*., MTT 38, 524 533, 1990.

[80] P. A. Davies and N. J. Gomes, "Subcarrier multiplexing in optical communication networks," in *Analogue Optical Fiber Communications* (B. Wilson, Z. Ghassemlooy, and I. Darwazeh, eds), London, England, Institution of Electrical Engineers, 1995, pp. 1 32.

[81] V. J. Urick, M. S. Rogge, F. Bucholtz, and K. J. Williams, "Wideband (0.045 6.25 GHz) 40 km analog fiber optic link with ultra High (>40 dB) all photonic gain," *Electron. Lett*., 42(9), 552 553, 2006.

[82] E. I. Ackerman and C. H. Cox III, "Microwave photonic links with gain and low noise figure," in Proc. *IEEE LEOS Annual Meeting*, Lake Buena Vista, Florida, October, 2007, pp. 38 39.

[83] E. E. Funk, A. L. Campillo, and D. L. Tulchinsky, "Nonlinear Distortion and Crosstalk in Microwave Fiber Radio Links," in Proc. *IEEE* MTT S Int. Microwave Symp. Digest (Cat. No. O2CH37278), 3 June, 2002, pt. 3, Seattle, WA, pp. 1691 93.

[84] K. J. Williams, L. T. Nichols, and R. D. Esman, "Photodetector nonlinearity limitations on a high dynamic range 3 GHz fiber optic link," *J. Lightw. Technol*., LT 16(2), 192 199, 1998.

[85] L. T. Nichols, K. J. Williams, and R. D. Esman, "Optimizing the ultrawide band photonic link," *IEEE Trans.*, MTT 45(8), 1384 1389, 1997.

[86] B. H. Kolner and D. W. Dolfi, "Intermodulation distortion and compression in an integrated electrooptic modulator," *Appl. Opt*., 26(17), 3676 3680, 1987.

[87] P. L. Liu, B. J. Li, and Y. S. Trisno, "In Search of a linear electrooptic amplitude modulator," *IEEE Photon. Technol. Lett*., 3(2), 144 146, 1991.

[88] W. K. Burns, "Linearized optical modulator with fifth order correction," *IEEE J. Lightw. Technol*., LT 13, 1724 1727, 1995.

[89] W. B. Bridges and J. H. Schaffner, "Distortion in linearized electrooptic modulators," *IEEE Trans. on Microwave Theory and Tech*., MTT 43, 2184 2197, 1995.

[90] T. Ismail, J. E. Mitchell, and A. J. Seeds, "Linearity Enhancement of a Directly Modulated Uncooled DFB Laser in a Multi channel Wireless over Fiber Systems," in Proc. *IEEE MTT S Symposium*, Long Beach, paper Tu1A 2, June, 2005, pp. 7 10.

[91] T. Fong, T. Ong, D. J. M. Sabido IX, and L. G. Kazovsky, "Linewidth insensitive coherent AM analog optical links using semiconductor lasers," *IEEE Photon. Technol. Lett.*, 4, 469 471, 1993.

[92] R. F. Kalman and L. G. Kazovsky, "Demonstration of an analog heterodyne interferometric phase modulated link," *IEEE Photon. Technol. Lett.*, 6, 1271 1273, 1994.

[93] B. Cai and A. J. Seeds, "Optical frequency modulation links: Theory and experiments," *IEEE Trans*., MTT 45, 505 511, 1997.

19

Optical interconnection networks in advanced computing systems

Keren Bergman

Department of Electrical Engineering, Columbia University, New York, NY, USA

19.1 COMPUTING SYSTEMS TRENDS AND THE PHOTONICS OPPORTUNITY

Over the past four decades, the progress of computing systems was largely dominated by the underlying acceleration in microprocessor performance and extraordinary advances in semiconductor technology. Improved fabrication methods and increasing die sizes were manifested in Moore's law, predicting in 1965 that the number of transistors integrated on a single die will be roughly doubled every 2 years [1]. Along with additional advances in circuit design techniques and processor microarchitectures, these improvements led to rapidly increasing clock speeds and to the extremely high performance presented by CMOS-based microprocessors [2].

The past trend of continuous acceleration in single microprocessor performance is currently undergoing a major paradigm shift as critical technologies have simultaneously converged on fundamental performance limits. Essentially, the scaling in transistor speeds and integration densities can no longer drive the expected congruent multiples in computation performance. Local processing frequencies have clearly reached a point of diminishing returns: further increases in speed lead to tighter bounds on the logic on-chip coherently accessed in a single clock cycle, and the associated power dissipation is exacerbated in an exponential fashion. Evidence of this is unmistakable in practically every commercial manufacturer of high-performance microprocessors with the introductions of chip multiprocessors (CMPs). CMPs and multicore architectures aim to optimize performance per Watt by operating multiple parallel processors at lower clock frequencies [3 9]. Thus, these new CMP architectures are leading a major design shift from "computation-bound" to "communication-bound": the chip becomes a distributed parallel system

Optical Fiber Telecommunications V B: Systems and Networks

ISBN: 978 0 12 374172 1

in which global on-chip communication plays a dominant role in design and ultimate performance.

At the system level, the underlying transformation in microprocessors toward CMPs with increasing numbers of cores will have profound impact on the interconnect infrastructure in modern advanced computing. Top supercomputers today are already composed of tens and hundreds of thousands ($10^4 \sim 10^5$) of individual processing elements. For example, one of the fastest supercomputers in the world, the Blue Gene/L at Lawrence Livermore, contains 131 072 individual PowerPC compute nodes [10]. The interconnection network that enables these over 100 k compute elements to communicate with each other and essentially work as one coherent unit on critical computations is a $64 \times 32 \times 32$ three-dimensional torus that supports the passing of over 100 terabits per second across its bisection. The interconnection networks of these large-scale supercomputers typically consume a significant portion of the system footprint and power dissipation budget. With the eminent use of multicore architectures and CMPs in the processing elements of next-generation computing systems, it is clear that multimillion-node systems are on the near-term horizon. For these systems, the communications infrastructure and interconnection networks will play an increasingly important role in the computing performance. This represents a stark shift from the historical performance drivers of processor speeds and memory densities to the communications-bound systems in which efficient information exchange among compute and memory elements is paramount.

In this context, optical interconnection networks (OINs) offer a potentially disruptive technology solution that can provide ultrahigh throughput, minimal access latencies, and low-power dissipation that remains independent of capacity. By realizing the enormous bandwidth capacities and stringent latency requirements of interconnecting the growing number of compute elements in a scalable fashion, OINs can become key to relieving what is perhaps the most daunting challenge to performance of future computing systems.

In order to best address this application, novel optical transmission and photonic switching paradigms must be developed. Although conventional fiberoptic components and engineering principles can be leveraged in the design of OINs, high-bandwidth low-latency systems often require different approaches not found in long-haul network designs. Similarly, the principles used for designing electronic interconnection networks are no longer applicable since the optical domain offers unique advantages and challenges which differ markedly from high-speed electronics.

In this chapter, we first review the theoretical behavior of interconnection networks and acquire the nomenclature and methods unique to interconnection network design and characterization. This includes formal definitions of network effective bandwidth, latency, and other performance metrics, as well as classifications of switching elements, network control mechanisms, and routing protocols. The common trade-offs between performance metrics for a variety of network topologies and network management schemes are also considered. With this

foundation, the details of interconnection network functionality and architectural principles can further be developed.

The technological toolbox used for OINs borrows heavily from that for long-haul networks, but some elements are used in unconventional ways, and it is important to understand the differences. Most significant among these is the maximization of channel bandwidth through multiple-wavelength transmission schemes. The structure of network subsystems and componentry is discussed in some detail, while keeping in mind the requirements of OINs in advanced computing systems applications. Technology-specific design considerations such as power consumption, system cost, robustness, and flexibility are examined as well.

We then consider whole OIN systems, emphasizing a few which have been successfully implemented as well as a few prototypes. The successful and unsuccessful features offer further insight into the optimal utilization of optical technologies for the aforementioned design requirements. The future direction of OIN technologies and the system design implications of likely advances conclude the chapter.

19.2 INTERCONNECTION NETWORKS PERFORMANCE CONSIDERATIONS

The goal of the interconnection network is to serve as the communications infrastructure for transferring data among the growing massive numbers of processing and memory elements. The performance of advanced computing systems clearly relies upon the efficiency and capabilities of the interconnect. Interconnection networks, unfortunately, have traditionally failed to match the fast progress pace exhibited by microprocessors [2]. Unlike microprocessors, the performance of interconnection networks is not dominated by the transistor gate size, it is rather dependent on the dynamics of signal propagation through electronic transmission lines (e.g., coaxial cables or backplane differential traces). Losses caused by skin effect limit the bandwidth of transmission lines to a few gigahertz and the transmission distance at high data rates to a few meters for cables and less than 1 m for backplanes [11]. Careful impedance matching, required to avoid reflections, prohibits the employment of shared busses and dictates the use of point-to-point links, contributing to long network diameters and high latencies in large-scale systems [11, 12].

In the past, microprocessors were not fast enough to approach these fundamental communication limits and their off-chip bandwidth requirements were modest. The performance of advanced computing systems was largely dominated by processor speeds and not by the network. With recently improved performance of microprocessors, dramatically accelerated by CMPs, bandwidth and latency requirements have increased at a rate much faster than the network's ability to provide them. The performance bottleneck has clearly shifted from the processors to the interconnection infrastructure.

The communication bottleneck is critical. In most large-scale systems, the memory is distributed among a large number of nodes, spread over substantial

space [2]. As a result, a significant fraction of memory accesses travel through the interconnection network which must provide high-bandwidth, low-latency communication to memory to achieve efficient utilization of the processing capabilities. This is especially true for classes of applications where instruction-level parallelism (ILP) is low and branches are often hard to predict [2]. In these applications, aggressive latency-hiding techniques are inefficient and an underperforming memory connection can quickly translate to pipeline stalls and to discarded speculative work [2, 13]. Software techniques, therefore, cannot mask the dire need for high-bandwidth, low-latency communications access to memory. Achieving maximum utilization of compute resources particularly as the number of nodes scales profusely with the emergence of CMPs falls increasingly on the efficiency of the information exchange among those resources. Thus, the interconnection network communications plays an increasingly central and dominant role in the ultimate system performance.

A high-bandwidth, low-latency, and, perhaps most importantly, low-power communication infrastructure is clearly required for next-generation performance computing systems. Parallel advanced computing environments, particularly CMP-based architectures, require interconnect solutions that provide the necessary bandwidth and latency while maintaining manageable power consumption figures. Current shared-bus topologies in multicore processors are envisioned to be replaced by scalable interconnection network topologies. Interconnection network performance may be defined along three metrics: latency, bandwidth, and power dissipation.

19.2.1 Latency

The latency of a message through a network has three contributing components:

(1) Time-of-flight (t_p), governed by the speed of light and the physical distance between the nodes, and assumed to be fixed.
(2) Store-and-forward latency, or serialization latency (t_b), in each individual router in the path affected by the packet size (b) and the transmission rate (R) as $t_b = b/R$.
(3) Routing latency (t_r) in each router, which is the sum of a forwarding latency (t_f), a queuing latency (t_q), and the serialization latency, t_b.

The total latency across an interconnection network can therefore be expressed as:

$$D = t_p + t_b + (h-1) \times t_r = t_p + h \times \frac{b}{R} + (h-1) \times (t_f + t_q),$$

where h is the number of hops traversed by the message path in the network including the source and the destination [14]. As systems scale to large port counts,

their diameter, defined as the length of the minimal path connecting the most distant pair of nodes [12], grows. The resulting hop count experienced by packets (h) is larger, contributing to a high latency which, as described above, may be detrimental to the overall system performance.

From the simple latency equation above, one can envision three methods by which the message latency can be reduced:

- Reducing the network diameter by using high radix routers[1] (see, e.g., [15]).
- Increasing the transmission rate (R).
- Lowering the queuing latency (t_q) in the routers.

Reducing memory access latency by a combination of these methods is key to improving the performance of future computing systems [13]. The challenges presented by the increase in the latency in absolute terms are even graver when one considers the fact that the processor clock speeds are constantly increasing. The increase in latency in terms of clock cycles is, obviously, much faster. In contemporary processors, the access time to a remote memory module across an interconnection network in large-scale distributed systems is as large as thousands of clock cycles [2, 10].

19.2.2 Bandwidth

As microprocessors' compute power continues to grow with the recently accelerating adoption of multicore and multithreaded designs in CMPs, off-chip bandwidth requirements must follow. Perhaps the most pronounced evidence of this accelerated trend is in the recent unveiling of Intel's 80-core multiprocessor that delivers TeraFlops "supercomputer-on-chip" performance [3]. When multiple processing cores are integrated on a chip, and a fast memory link is required for each core, the aggregate bandwidth of the chip can become very large. Table 19.1 provides information about the off-chip bandwidth requirements of current commercial high-performance microprocessors. Supplying the bandwidth demands of these processors is crucial to enable continued scaling of computing systems performance by effectively removing the critical communications bottleneck.[1]

The bandwidth that can be routed by an interconnection network or its effective throughput is a key performance metric that is dependent upon several factors. These include the network topology, transmission rates, flow control, routing algorithms, and traffic patterns or applications. Extensive numerical simulations are used to model the network behavior under specific applications loads and

[1] High radix routers or switching nodes have a large number of input/output ports.

Table 19.1
Off-chip bandwidth requirements of commercial microprocessors.

Processor	Vendor	Release year	Off chip bandwidth (GB/s)
Cell Broadband Engine [6]	IBM, Sony, Toshiba	2006	50.6
Montecito [9]	Intel	2005	10.7
Niagara [8]	Sun	2003	>20
Opteron [5]	AMD	2003	24.5

predict its throughput performance. Broadly, the network effective bandwidth depends upon three major components [2]:

- Injection bandwidth $N \times BW_{\text{LinkInjection}}$
- Bisection bandwidth $BW_{\text{Bisection}}$
- Reception bandwidth $N \times BW_{\text{Link Reception}}$

where N is the number of ports or nodes interconnected by the network. The injection bandwidth refers to the aggregate bandwidth that can enter the network and is equal to the number of available input ports multiplied by the bandwidth capacity of each injection port. Similarly, the reception bandwidth refers to the aggregate bandwidth that can exit from the network and is equal to the number of available output ports multiplied by the bandwidth capacity of each ejection port. The network bisection is a plane that cuts the network nearly in half, such that the number of channels and the bandwidth crossing the plane are nearly equal. The bisection bandwidth is the total bandwidth crossing the bisection plane. The three components reflect the network raw capabilities and are scaled according to the traffic characteristics. The effective bandwidth is given as:

$$BW_{\text{EFF}} = \min\left(N \times BW_{\text{LinkInjection}},\ \rho \times \frac{BW_{\text{Bisection}}}{\gamma},\ \sigma \times n \times BW_{\text{Link Reception}}\right),$$

where ρ is an efficiency factor reflecting the collective contributions of routing, arbitration, and switching on the network utilization, γ expresses the fraction of the total traffic which is routed through the network bisection, and σ is the average reception factor, which captures the effects of traffic contention. The scaling factors depend on the application and are typically obtained using simulations. An interconnection network should be designed such that its effective bandwidth supplies the demands of all the processors in the system. An underperforming network can lead to processor-stalls and thus have a direct impact on the application's execution time. The effective bandwidth required from an interconnection network is expected to grow from tens of Tb/s in today's top supercomputers to well over tens of Pb/s in future systems.

19.2.3 Power

Supplying the immense bandwidth demands of advanced computing systems typically accomplished via parallelism or bit-slicing techniques is consuming a rapidly increasing fraction of the power budget [12]. The power expended on transmission, buffering, and switching of electronic signals grows quadratically (and in some cases, even cubically) with the data rate [16 18]. Additionally, as systems become spatially larger, more power is required to overcome the losses in long transmission lines (cables and backplanes). These losses are overcome by power hungry methods such as high-amplitude signaling, periodic regeneration, and sophisticated signal-processing techniques including pre-emphasis or equalization [19]. For next-generation performance computing, power dissipation is clearly emerging as perhaps the greatest challenge to future scaling. Machine performance measures have recently shifted from raw Flops/s toward emphasizing energy efficiency with performance/Watt metrics. In many datacenters, server farms, and high-performance computing systems installations, power consumption and cooling issues become significant operational factors, taxing the limits of available power densities and increasing operational costs [20]. Additional concerns such as cabling density, bending radii, and cooling airflow also present ever increasing challenges to interconnection networks designers.

19.3 OPTICAL INTERCONNECTION NETWORKS DESIGN CONSIDERATION

Optical interconnections offer a potentially disruptive technology solution by directly addressing the bandwidth and power limitations of electronic interconnects [21]. Parallel optical links for board-level interchip communication or interboard communication through a backplane have been recently demonstrated to offer impressively high data throughput with relatively low power consumption [22]. But as off-chip bandwidth demands of CMPs continue to accelerate, the power dissipation associated with multiple parallel electro/optical signal conversion grows rapidly.

Optical transmission technologies have the potential to mitigate or even eliminate most of the daunting computing systems interconnect challenges. The bandwidth of optical fibers can be utilized through wavelength division multiplexing (WDM) to carry very high data rates, exceeding 10 Tb/s [23]. The low loss in optical fibers alleviates the need for regeneration and sophisticated signal-processing techniques. Bending radii and spatial volumes challenges are also addressed when optical fibers are used [11]. These reasons lead to an increasing trend toward using multimode fibers with relatively low cost and easy-to-use connectors, as point-to-point links in local area networks, HPC systems, and enterprise server installations [11].

Point-to-point optical links, however, provide only partial relief to the growing power consumption and bandwidth scaling difficulties. In order to comprehensively address the power, bandwidth, and latency challenges, optical switching must be employed in a manner that fully exploits bit-rate transparency across the network. Bit-rate transparency refers to the property of optical switches whereby the power consumption and switching rate are essentially independent of the bit rate [24]. An optical switching gate, e.g., is turned on and off at the message or packet rate, and the power expended to control it is independent of the amount of data routed through its transparent bandwidth window. An electronic switch, conversely, switches on and off with every bit transition while dissipating dynamic power. The transmission rate in optical communication systems can, therefore, be increased and additional wavelengths can be multiplexed without an increase in the power expended on switching. OINs of various structures and topologies have therefore been suggested by many researchers as solutions for advanced computing systems interconnection networks [25 30].

Optical networks should capitalize on the advantages of photonic technology while acknowledging its current shortcomings. Two architectural challenges stem from inherent limitations of the optical medium: the lack of efficient buffering technologies and the limited processing capabilities of optics. Electronic interconnection networks rely heavily on memory elements such as registers and random access memories (RAM) to perform essential contention resolution functions and to store data while control information is processed. Header and address processing are also easily performed in the electronic domain. An OIN, conversely, has no such luxuries. Contentions must be resolved without (or with minimal) buffering and processing must be simple and executed as quickly as possible since data cannot be arbitrarily delayed. Optical switching devices also present challenges that are negligible or nonexistent in CMOS-based digital electronics, such as noise, optical nonlinearities, and signal degradation. All these limitations and factors must be carefully considered and addressed.

19.3.1 Capitalizing on WDM Transmission

The single most important advantage of optical signal encoding is the enormous bandwidth it can support, both because of the high modulation bandwidth available to a signal channel (i.e., carrier frequency or carrier wavelength) and because of the number of wavelength channels that can be transmitted simultaneously. With a total of 6 THz of bandwidth available for optical transmission using readily available components over the C-band, efficient coding techniques can certainly support transmission capacities of more than 1 Tb/s [23]. In summary, OIN designs should capitalize on the gargantuan bandwidth available to fiberoptic technologies while minimizing the burden of computation and buffering on the photonic network components. Indeed, it is even beneficial to distinguish between the path and devices through which the high-bandwidth payload travels, and the

path and components that carry the routing information and execute the routing decision. That is, an ideal OIN design leaves the transmission capacity to the optical domain and relies on better suited technologies for routing and decision mechanisms.

19.3.2 Multistage Topologies

Additionally, in order to address general networking concerns such as scalability and modularity, multiple-stage distributed topologies are often employed in interconnection networks, independent of the transmission medium [12, 31] (Figure 19.1). For a large number of network input and output terminals, it is important that the number of switching nodes required to implement a complete topology scales efficiently. Further, it can be beneficial for a given implementation to comprise nearly identical switching nodes that only need to be configured with their position within the interconnection network, as is common for various multiple-stage topologies. For a large number of input and output terminals, it is also important for the control and routing mechanism to scale efficiently. Whereas centralized arbitration algorithms can become computationally burdensome for large numbers of network terminals at fast packet injection rates, a distributed control scheme that delegates routing to each individual switching node can simplify the routing mechanism [1, 32].

In order to further simplify routing and architectural organization, packet or message switching is a method by which multiple input terminals can freely communicate with multiple output terminals. Designated transmission lines between every input and every output is clearly wasteful of resources. Moreover, because the optical switching nodes would likely subtend only 100s of bit periods of latency, the model of circuit switching may not provide the necessary granularity. A packet switching network based on distributed switching nodes in a multiple-stage topological configuration may therefore define the target architectural design space.

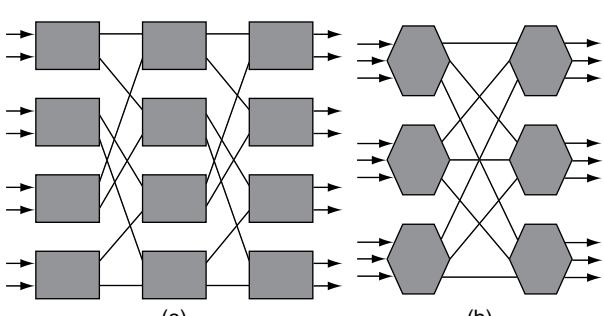

Figure 19.1 Schematics of banyan butterfly topologies for (a) 2×2 nodes and (b) 3×3 switching nodes.

19.4 PACKET SWITCHING NODE AND MESSAGE STRUCTURE

The building block of any scalable photonic switching network is the switching node, the crosspoint where optical pathways intersect and allow optical packets to traverse the network from one of multiple input terminals to one of multiple outputs. OIN topological specifications, along with the aforementioned delegation of capacity and functionality, yield design considerations for the switching node and message format.

The motivation for implementing an optical packet switching fabric from simple switching node building blocks is twofold: (1) optical components are still expensive and not easily integratable, and (2) architectures composed of simple switches with a distributed control scheme scale straightforwardly to large port counts. Thus, the switching node design presented here represents the simplest possible switching junction: it is a primitive single-packet 2×2 switching structure (also called "1×2" in some contexts) which can easily be expanded to full 2×2 nonblocking functionality for common multiple-stage (i.e., banyan) topologies. In addition to its structure being simple, its flow control logic is also as minimal as possible to achieve low routing latencies. The switching node relies on only two header bits to make a decision: one framing bit (*frame*) and one bit from the packet's destination address. When an interconnection network structure is based on a banyan or binary routing tree multiple-stage structure, it is sufficient to route packets in such a way that only one bit of the address is considered at a particular stage of the architecture [12]. In addition to this basic functionality, a switching node used with distributed control may be required to generate a deflection signal for another adjacent switching node. It must take an incoming deflection signal into account when processing a routing decision.

From the perspective of the optical packet, the node needs to be transparent; i.e., the signal going in must resemble the signal coming out as closely as possible (in terms of optical power, signal-to-noise ratio, etc.), thus maximizing the scalability and modularity of the OIN. In order to accommodate this requirement with photonic technologies, the most practical solution is to allow for the packet to traverse a straightforward optical data pathway while diverting a small amount of optical power for the requisite header detection. In this way, the optical signals which are routed to subsequent switching nodes are left relatively undisturbed. The optical data pathway contains a two-way fiberoptic splitter with switch gates [typically implemented with semiconductor optical amplifiers (SOAs)] on each side; the state of the switching node is set by enabling one of these gates (or by leaving both disabled).

From the perspective of the routing control, the routing decision is based on electronic signals detected from the diverted optical stream in addition to an external electronic deflection signal from an adjacent node; the decision is executed by enabling one of the two gates, as noted above. Simultaneously, an

outgoing deflection signal is generated for another adjacent switching node. The latencies of the optical pathway and of the routing decision processing must be matched so that the gates are enabled just as the optical packet is incident on them, in order to avoid truncation of the packet payload.

19.4.1 Wavelength-Striped Message Format

The prevalent use of SOAs as the gate elements in the switching node design is owing to SOAs' switching speed and gain. The gain is necessary for the preservation of transparent routing: the couplers and splitters in the first part of the node introduce loss which must be overcome before the optical packet exits the switching node. Very few devices can both provide gain and switch on the time scales required for packet switched OINs. SOAs meet these two needs in addition to providing a third beneficial feature: they can amplify signals over a very wide range of wavelengths.

Therefore, the packets used in this kind of SOA-based OPS network can contain multiple wavelengths which are transmitted in parallel. These wavelengths are modulated with data which are physically independent but logically contiguous. Encoding can be entirely bit-parallel, segmented, or any other format since the physical layer is transparent to all possible data encoding schemes. The entire wavelength-parallel packet structure is routed through the network as one unit, simultaneously in time and space. It should be noted that chromatic dispersion is irrelevant for the target distance scales.

In addition to the payload being composed of a multiple-wavelength data structure (also referred to as wavelength striping), the routing headers are also encoded in a wavelength-parallel manner. Each address bit, along with the packet frame, is encoded on one wavelength each, such that the wavelength is either 0 or 1 (i.e., high power or low power) for the entire duration of the packet (Figure 19.2). This primitive bit-parallel header encoding scheme allows for extraordinarily simple detection at the switching nodes, minimizing latency and maximizing robustness.

It is important to note the timing structure of the packet: a dead-time spacing is inserted between consecutive packets, and guard times for the packet payload are placed at the beginning and end of each packet. The dead time allows time for the SOAs to open and close completely between packets, in an effort to minimize routing transients. The guard time serves a similar purpose but also accommodates for small path-delay timing mismatches within the individual switching nodes. It is especially important that payload information not be corrupted during its propagation through the switching fabric whereas the single-bit header signals are far less critical.

Ultimately, because the SOA switching elements are capable of providing gain to all of the wavelengths used in the optical packet, this multiple-wavelength scheme easily allows for packet transmission that truly exploits the ultrahigh bandwidths of optical communications.

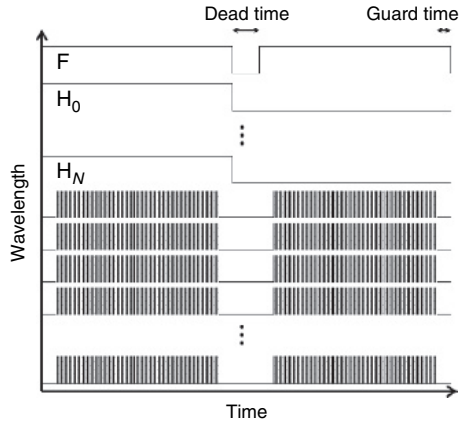

Figure 19.2 Diagram of the packet structure with multiple headers and multiple packets transmitted in a wavelength parallel fashion. The dead time (time between packets) and guard time (margin between packet frame and payload) are shown.

19.4.2 Optical Packet Switching Node for Multistage Interconnection Networks

The packet routing information is contained in the header field along designated wavelengths. In order to simplify detection, each of the header bits is encoded on a distinct wavelength stripe. Thus, an *n*-bit header requires an additional *n* wavelengths more than those designated for the packet payload. However, having only one bit of information to decode on each wavelength for the entire duration of the packet dramatically simplifies header detection. One function which is simpler with photonic devices than with electronic devices is channel demultiplexing, and isolating one of these header wavelengths only requires an optical filter. For a two-way switching node, two header bits are sufficient to establish all possible switching states. The control plane of the switching nodes is therefore driven by two simple optical filters and two low-speed optical receivers. After the optically encoded header bits have been decoded into electrical signals, all switching node routing logic can utilize electronic logic devices with relative simplicity. Then the routing decision is executed by enabling one of the two SOA switching elements [33, 34]. The routing for each node is entirely contained within that node, resulting in a distributed switching architecture.

Moreover, the packets traverse the node structure in a manner which is almost perfectly transparent: optical power is preserved and very little signal distortion is introduced. Specifically for optical multistage interconnection networks (MINs), great care must be taken to ensure that the signal exiting the switching node is almost identical to the one that entered. The losses introduced by the Y-junction and other passive optical components are exactly matched by the gain introduced by the SOA.

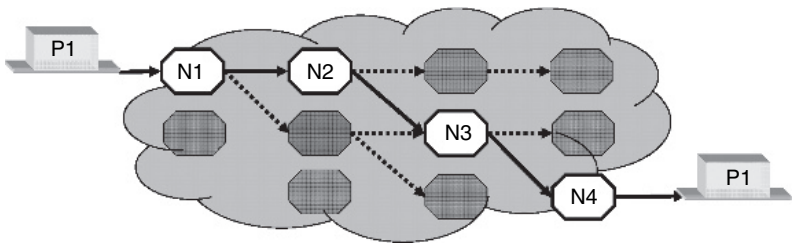

Figure 19.3 Illustration of a packet (PI) propagating transparently through a cascade of switching nodes (N1 N4) of a multistage interconnection network (MIN) (this figure may be seen in color on the included CD ROM).

The SOA is also operated in a regime where very few nonlinearities occur in order to best preserve signal integrity [35, 36]. This structure allows for many switching nodes to be cascaded in a modular way that is almost independent of the path through the network and the number of nodes traversed. The packets fly through the system without significant degradation, traveling from one node to the next (Figure 19.3).

In order to best serve this switching node design, the network must follow a bufferless topology. Clearly, the simple switching node design that has been developed above lacks buffering and store-and-forward capabilities. The optical packets traverse the Y-junction at exactly the speed of light in fiber, and there is no means of halting the packet flow or even slowing it down. These restrictions are easily serviced by the architectural implementation of deflection routing or, similarly, hot-potato routing [12, 37, 38].

Optical MINs, along with the switching node design and optical packet format presented, are intended to leverage the unique benefits of fiberoptic and photonic technologies while avoiding their shortcomings. Buffering and packet storage are not required; this is avoided by deflection routing. Logical computations executed in optical media are not required; instead digital electronic devices compute the switching node routing decision. Moreover, the packet payload is encoded optically as a high-bandwidth multiple-wavelength structure that transparently propagates the network as a unit, staying in the optical domain throughout the entire network. Only the low-bandwidth headers are converted to the electronic domain, allowing packets to fly through the network uninhibited, with time-of-flight latencies approaching speed-of-light limitations. The benefits of fiberoptics are complemented, not hindered, by electronics in a cooperative arrangement that maximizes the throughput of the interconnection network and minimizes transmission latencies.

19.5 OPTICAL INTERCONNECTION NETWORK DESIGN AND PERFORMANCE ANALYSIS

Employing the building blocks, tools, and performance metrics covered thus far, one can consider the complete design and performance analysis of an OIN.

The design is based on SPINet (Scalable Photonic Integrated Network), an architecture designed to be implemented using photonic integration technology [34, 39, 40]. Based on an indirect MIN topology, SPINet exploits WDM to simplify the network design and to provide very high bandwidths. SPINet does not employ buffering and resolves contention by dropping contending messages. A physical layer acknowledgment protocol provides immediate feedback notifying the terminals whether their messages are accepted and facilitates retransmissions when necessary, in a manner resembling traditional multiple-access media. In this section, the SPINet design is considered in detail and performance is investigated under various scenarios.

19.5.1 Architecture Overview

The SPINet network is a transparent optical MIN, comprised of 2×2 bufferless photonic switching nodes. The class of topologies most appropriate for the implementation of SPINet network are banyan networks (also known as *butterfly* [12] networks or *baseline* [31] networks). A k-ary n-stage banyan connects N_T source terminals to N_T destination terminals, where $N_T = k^n$. The network comprises of n stages and each stage comprises of $k^n/2$ nonblocking crossbar switches of radix k (i.e., $k \times k$ switching nodes). The switch radix, k, is typically selected to be a power of 2, facilitating simplicity in addressing and implementation.

The topology chosen for the implementation of the SPINet architecture is binary banyan topology (i.e., $k = 2$) to enable simple implementation using 2×2 switching nodes based on optical switching gates. There are several binary banyan network topologies that differ in the interconnection patterns between the stages (i.e., the rule determining the interconnection between switches' output ports in stage i to switches' input ports in stage $i + 1$) [31, 41]. The Omega topology, first presented by Lawrie [42], is chosen because it offers an identical interconnection pattern across all stages thus simplifying implementation especially in a photonic integration environment.

An $N_T \times N_T$ Omega network, therefore, is comprised of $N_S = \log_2 N_T$ identical stages. Each stage consists of a perfect shuffle interconnection followed by $N_T/2$ switching elements, as shown in Figure 19.4(a). In the Omega network, each switching node has four allowed states (straight, interchange, upper broadcast, and lower broadcast). In the SPINet implementation, the switching nodes are modified such that the broadcast states are removed and four new states are introduced (upper straight, upper interchange, lower straight, lower interchange), in which only data from one input port are passed to an output port while the data from the other port are dropped [see Figure 19.4(b)].

The SPINet was designed to facilitate photonic integration, and in its envisioned implementation, the entire network is integrated on a photonic integrated circuit (PIC) within a single chip. The terminals are physically located on the computing nodes and are connected to the PIC by optical fibers. In the performance evaluation,

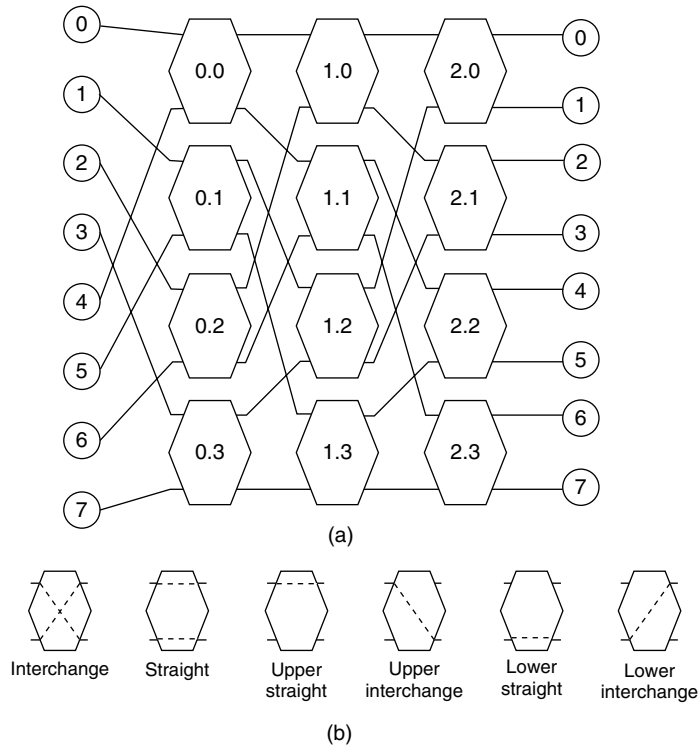

Figure 19.4 (a) 8×8 Omega network; (b) switching node states.

the terminals are assumed to be synchronized, the network is slotted and synchronous, and messages have a fixed duration. The minimal slot duration is determined by the round-trip propagation time of the optical signal from the terminals to the PIC. A slot time of 100 ns can, therefore, accommodate a 20-m-long propagation path and thus a distance of 10 m between the terminals and the PIC.

19.5.2 Flow Control

At the beginning of each slot, any terminal may start transmitting a message, without a prior request or grant. The messages propagate in the fibers to the input modules on the PIC and are forwarded to the switching nodes of the first stage. At every routing stage when the leading edges of the messages are received from one or both input ports, a routing decision is made and the messages continue to propagate to their requested output ports. In the case of output-port contention in a switching node, one of the contending messages is dropped. The choice of which message to drop can be random, alternating, or priority-based. Since the

propagation delay through every stage is identical, all the leading edges of the transmitted messages reach all the nodes of each stage at the same time.

The switching states of the nodes, as determined by leading edges, remain constant throughout the duration of the message so the entire message follows the path acquired by the leading edge. Since the propagation delay through the PIC is very short (a few nanoseconds) compared with the duration of the messages (tens or hundreds of nanoseconds), the messages stretch across the PIC, effectively creating transparent lightpaths between the inputs and outputs. When the messages reach the output modules, they are forwarded on the output fibers to the appropriate terminals while at the same time an acknowledgment optical pulse is generated and sent on the previously acquired lightpath in the opposite direction. Since the switching elements in the node preserve their states and support bidirectional transmission, the acknowledgment pulse is received in the source terminal and the successful reception of the message is confirmed.

When the slot time is over, all terminals cease transmission simultaneously, the switching nodes reset their switching states, and the system is ready for a new slot. The slot duration is chosen such that the acknowledgment pulses are received at the source terminals before the slot ends. Hence, before the beginning of the following slot, every terminal knows whether its message was accepted and it can, therefore, choose to immediately retransmit the message when necessary.

Utilizing the ultralow-latency propagation through the PIC, the SPINet architecture eliminates the need for central scheduling employing the distributed computing power of the switching nodes to produce an input output match at every slot. This process of implicit arbitration enables scalability to large port counts without burdening a central arbiter with computing complex maximal matches.

Because blocking topologies are used, to reduce hardware complexity, the network's utilization is lower than that of a traditional maximum matched nonblocking network [43]. Techniques can be used, however, that exploit the properties of integrated photonics, namely the small area of the switching nodes and their low latency, to increase utilization. This can be achieved by adding a small number of stages to the network and thus increase the number of available paths between each source destination pair.

19.5.3 Wavelength Speedup

The message header is encoded on dedicated wavelengths (Section 19.4) such that it can be instantly decoded in the switching nodes and the routing decision executed immediately upon receiving the leading edges of the messages. The message payload is segmented and the individual wavelength stripes are simultaneously encoded at a higher data rate (e.g., 10 Gb/s per wavelength) [30, 44]. The complete multiwavelength message is routed together as a single unit.

For high-end systems, wavelength striping can offer unparalleled transmission bandwidth which is practically not achievable using alternative electronic transmission or even serial single-wavelength optical transmission techniques. For low-cost systems, alternatively, the wavelength-striped packet structure is compatible with the trend toward parallel optical transmission adopted in low-cost local area optical networks [11, 22, 45].

The achievable low-cost bandwidth and the network's inherent wide switching band and bit-rate transparency suggest a bandwidth-time trading: for a given required peak bandwidth, a $\times S$ speed-up is used in the wavelength domain, while the packet rate (the load offered to the network) is reduced by a $1/S$ factor. For example, for a port designed to provide a peak bandwidth of 40 Gb/s, eight wavelengths are modulated at 10 Gb/s each, and a new packet is generated once every two slots on average. This $\times 2$ speed-up lowers the load offered to the network thus leading to reduced queuing latency. The peak bandwidth can therefore be described as:

$$B_{\text{Peak}} = \frac{R \times N_{\text{Payload}} \times \eta}{S},$$

where R is the serial data rate (e.g., 10 Gb/s), N_{Payload} is the number of payload wavelengths used, and η is the slot efficiency parameter. The slot efficiency η is defined as:

$$\eta = \frac{T_{\text{Slot}} - T_{\text{G}}}{T_{\text{Slot}}},$$

where T_{Slot} is the slot duration and T_{G} is the guard time. The guard time is allocated before payload transmission, necessary to accommodate the optical gates' switching time, for clock recovery in the payload receivers, and for synchronization inaccuracies.

19.5.4 Performance Analysis and Metrics

The performances of banyan networks have been studied extensively using analytical models as well as simulations [31, 41]. Nonetheless, the performance evaluation of the SPINet architecture and OINs more generally present a different problem space. Banyan networks are often analyzed as packet switching networks in which each packet progresses one stage per time slot. Additionally, because most of the work was done in the context of VLSI switches, the switches typically offer some buffering space while they try to maximize the link utilization and conserve bandwidth.

In OINs, the large bandwidth available in the photonic links and switches suggests that the optimization variable should not necessarily be the link

utilization as is often employed in electronic interconnect design. Link utilization can, instead, be traded off to overcome the absence of efficient buffers. The ultralow latency of optical signals, enabling path adjustments within the same time slot, is a new technical possibility unique to photonic network and thus requiring a different analysis. These differences among others clearly require a new study of the network performance and the parameters that affect it.

Analysis of the network performance under different workload scenarios and traffic conditions requires numerical simulations. It is beneficial if the simulation program is highly modular such that switching nodes, traffic generation modules, and traffic analyzers can be interconnected according to various topologies. The key performance metrics include:

(1) Throughput, the number of packets successfully routed by the network in each slot, on average. The throughput is divided by the number of input ports, and thus normalized to receive values between 0 and 1.
(2) Acceptance rate, defined as the throughput divided by the offered load, is the probability that a packet injected in a given slot will be successfully routed to its destination and are not blocked.
(3) Queuing latency, the average number of slots a message spends in the input queue before successfully injected. The queuing latency can be divided to the time spent in the queue until reaching the head-of-line (HOL) spot, and the time spent on injection attempts from the HOL spot.

19.5.5 Topology Modifications

The SPINet architecture based on the Omega topology is internally blocking an unavoidable property of banyan topologies. In evaluating topological modifications that mitigate internal blocking, it is important to study their effect on performance.

There are several types of nonblocking multistage topologies:

- *Strictly nonblocking topologies* (e.g., crossbar), requiring N^2 crosspoints to implement an $N \times N$ port network. These topologies are clearly not scalable and become prohibitively expensive in the implementation of integrated large port count switches and networks.
- *Batcher banyan networks* are based on a property of the banyan topology: sorted traffic does not face internal blocking. When the banyan network is preceded with a Batcher sorting network, any traffic pattern can be routed without internal blocking. An N-port (radix-N) Batcher network, however, comprises of $\frac{1}{2}\log_2 N(\log_2 N + 1)$ stages, and the sorting nodes must be capable of inspecting the entire routing header. For these reasons, using this topology presents significant challenges on the optical technology.
- *Rearrangeably nonblocking* topologies such as Clos, or Beněs networks. In order to exploit the rearrangeability property, however, the network must use

some kind of central management module that selects paths and rearranges them when necessary. Since one of the key concepts in OINs is self-routing, to facilitate the low latency of the switching nodes, rearrangeably nonblocking networks are clearly not advantageous.

There are other solutions, however, that maintain the binary structure and the self-routing paradigm, and are thus more appropriate for use with the SPINet architecture. In OINs, it is generally straightforward to increase the network connectivity by adding waveguide or fiber paths. Increasing the path diversity in the network can significantly mitigate the internal blocking and dramatically improve performance. In a network with a higher degree of path diversity, more paths exist between each source destination pair. Different messages can, therefore, travel through different paths without blocking each other while the simplicity of the network and the switching nodes is preserved [12].

Deflecting Nodes

To enable these methods, a new type of switching node is introduced: the deflecting node. The deflecting nodes are completely identical to the routing nodes except for the manner in which they deal with contending messages. Whereas in the routing node one of the contending messages is dropped, in the deflecting node it is deflected to the undesired port. In order to convert a routing node to a deflecting node, only a minor change has to take place in truth table controlling the electronic logic. Messages are never lost in deflecting nodes, but it is noted that in order to avoid routing errors, restrictions are placed on the location of deflecting nodes in the network.

Enhanced Omega Topology

In the Enhanced Omega (EOM) topology (Figure 19.5), a stage of deflecting nodes (ovals in Figure 19.5), termed scattering stage, is placed before each routing stage (hexagons in Figure 19.5), except for the last one. Each pair of deflecting nodes in the scattering stage is connected to a pair of routing nodes which are buddies. According to the banyan buddy property, any node in a banyan network has a buddy node which is connected to the same nodes in the following stage [31]. The deflecting nodes examine the same address bit as the subsequent routing nodes, identify messages that would contend, and attempt to scatter them to different routing nodes. The buddy property guarantees that no routing errors are caused by the scattering operation. Scattering stages cannot be inserted before the last routing stage because each of these routing nodes is connected to two output modules and has no buddy. Therefore, in order to construct an EOM network, $N_S - 1$ stages are added to the original N_S stage Omega network.

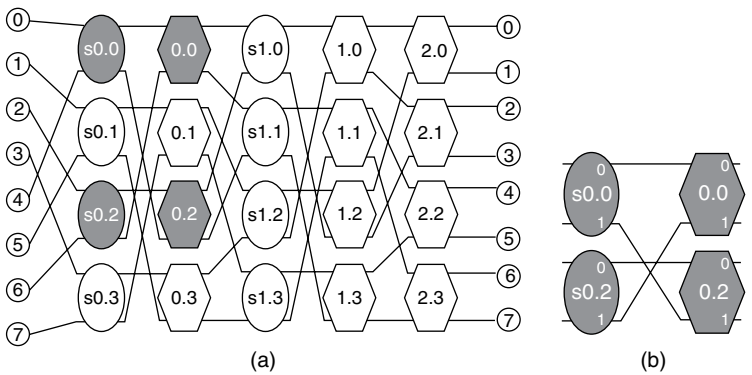

Figure 19.5 (a) 8×8 Enhanced Omega network; (b) Deflecting nodes connected to buddy routing nodes.

Inset (b) in Figure 19.5 shows the four-node structure comprising of two scattering nodes followed by two buddy routing nodes. The structure has four input port and four output ports. It is easy to see that in cases where two packets are received with the same requested output port, the contention will be avoided regardless of the input ports through which the packets arrive. Contentions are also avoided also for three-packet and four-packet combinations.

Distribution Network and Path Adjustments

An additional technique to increase utilization makes use of the ultralow-propagation latency of the optical signals to make path adjustments before the payload transmission begins. To support this mechanism, a distribution network of deflecting nodes, with an Omega topology, is inserted before the routing network [46]. A distribution address, encoded on dedicated wavelengths, is attached by the input modules to incoming messages when they are injected into the network. The messages are routed through the distribution network and then to their destination by the routing network.

The advantages of the distribution network are twofold: First, by encoding a random distribution address, the load on the routing network can be balanced regardless of the real traffic pattern [12]. Second, the physical layer acknowledgment protocol can be exploited to make path adjustments by changing the distribution address if the message is dropped in the first attempt. These path adjustments can be made in several iterations within the same time slot, during the guard time that precedes the payload transmission. Each iteration takes as long as the *ack* reception latency, the sum of the round-trip time across the switching fabric and the response time of the output modules in generating the acknowledgment pulses ($T_{\text{Sw\_Fab}} + T_{\text{Ack}}$). The guard time has to be

appropriately increased affecting the slot efficiency parameter (η). The improved utilization gained from multiple iterations has to be weight against the number of iterations.

19.5.6 Performance Evaluation

To evaluate the performance gain offered by the EOM topology over the standard banyan implementation, the Omega is used as reference in the numerical simulations. Results from these simulations are provided here for the throughput, scalability, and path adjustment iterations (latency) while more extensive performance evaluation can be found in Ref. [47].

In Figure 19.6, the performance of the Omega and EOM topologies is compared under uniform Bernoulli traffic for varying loads. The improvement offered by the EOM topology by mitigating the internal contentions is evident. For example, a queuing latency of 1.0 slot is attained by an Omega network under a load of 0.42 and, conversely, an EOM network under a load of 0.62. To evaluate scalability, Omega and EOM topologies are also compared for varying switch radices (Figure 19.7). Since the plain Omega topology saturates at an offered load of $p \approx 0.65$, this simulation is performed under a load of $p = 0.50$. The steep decline in performance as networks scale in size is attributed to the increased probability or blocking as the number of stages rises, and is especially evident in Omega networks. The EOM network shows a remarkable improvement in mitigating the blocking and, therefore, significantly contributes to an improved scalability.

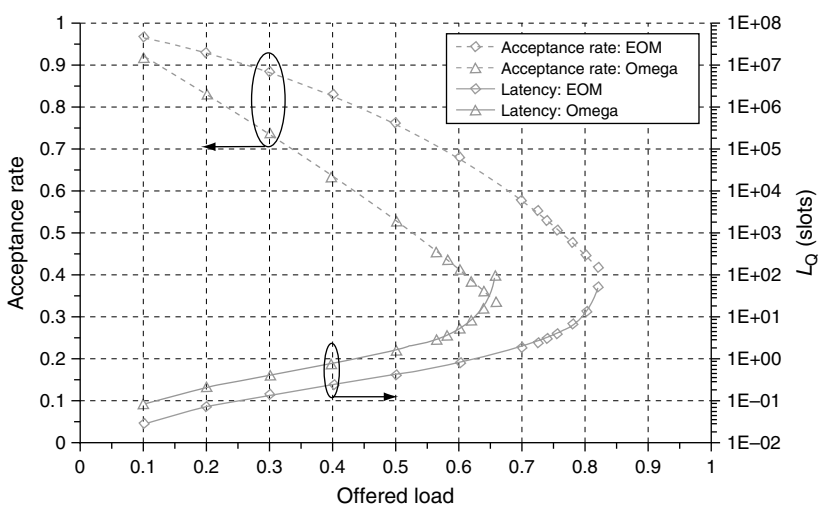

Figure 19.6 Performance of Omega and Enhanced Omega networks under varying offered loads (this figure may be seen in color on the included CD ROM).

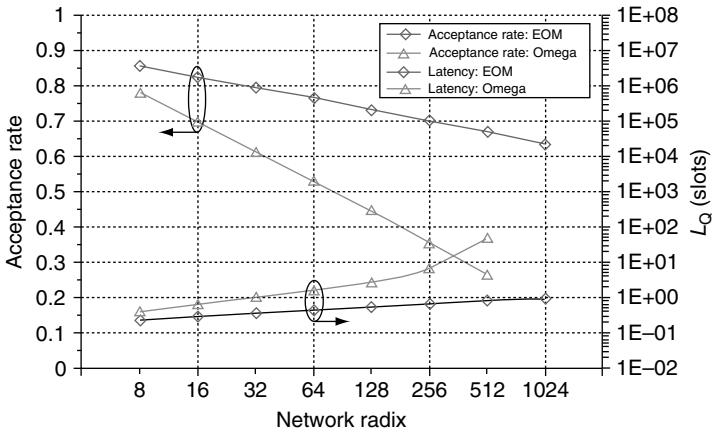

Figure 19.7 Performance of Omega and Enhanced Omega networks for varying port counts (this figure may be seen in color on the included CD ROM).

As described earlier, path adjustment iterations contribute to utilization but reduce the slot efficiency parameter (η) because they require a longer guard time in each slot. It is, therefore, important to study their contribution. The performance of a 64×64 EOM network, with a four-stage distribution network (15 stages in total), is simulated under uniform Bernoulli traffic with a varying number of path adjustment iterations (nPA) and the results are given in Figure 19.8. The performance gain is noticeable but seems to have a diminishing return which becomes very small for $n\text{PA} > 2$.

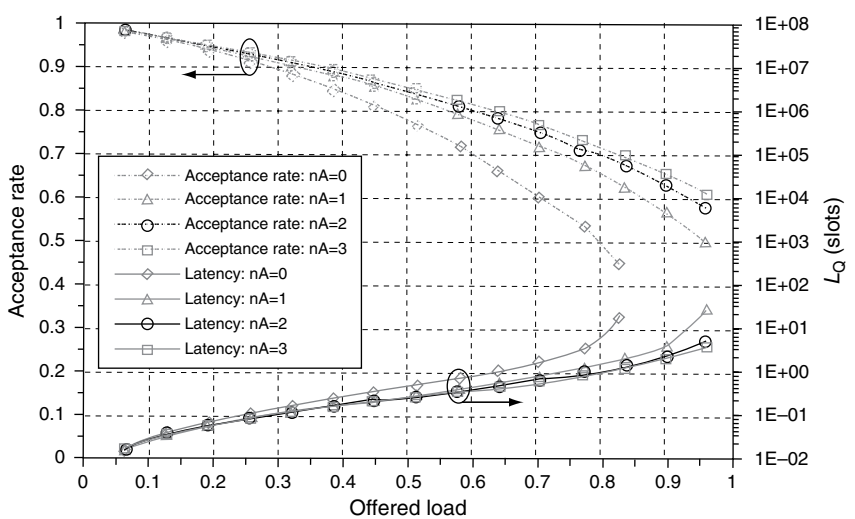

Figure 19.8 The effect of the number of path adjustment iterations (nPA) on the performance of a 64×64 EOM network (N_S 15) (this figure may be seen in color on the included CD ROM).

19.6 OIN DESIGN DRIVER IMPLEMENTATION CONSIDERATIONS

In this section, the implementation of an integrated 64×64 OIN design based on the SPINet architecture is considered. The design driver is an EOM network with $N_T = 64$ I/O terminals and a four-stage distribution network that will require $N_S = (2 \times \log_2 N_T - 1) + 4 = 15$ stages, of $N_T/2 = 32$ switching nodes each, or a total of $N = 480$ switching nodes. The envisioned integrated SOA-based 2×2 switching element as in Ref. [48], has an area of 1 mm^2, and consumes an average power of 15 mW. The area and power consumed by the additional components required in the node construction, namely the CMOS electronics and passive optical devices, are negligible compared with the size of the switching element. A reasonable estimate for the total area of a switching node is 1 mm × 2 mm, including the interstage waveguides. A reasonable estimate for the average total power of the 64-port PIC would be 10 W.

The input modules and output modules contain laser sources and some electronic circuitry for the generation of distribution addresses and acknowledgment pulses. The added area and power dissipation of these modules are not large compared with the network size, because only 64 input and output modules are required. Similar degree of integration on a single-InP PIC has been recently introduced in commercial modules for telecom applications [49, 50]. It can be reasonably projected that a whole network can fit on a 4 cm × 4 cm PIC implemented on a hybrid integration platform of InP and silicon.

The latency of a routing node is governed by latency of the passive optics, photodetectors, the electronic logic gates, and the switching time of the SOAs. The combined latency, for an integrated device, can be approximated at less than 300 ps taking into account the simplicity of the logic circuit and current trends in device performance. The total message latency is, therefore, lower than 4.5 ns for the 15-stage network, and the round-trip latency can thus be estimated at 9 ns. Table 19.2 summarizes the specifications of an envisioned 64×64 integrated SPINet network implementation.

Table 19.2

Specifications of envisioned 64×64 integrated SPINet implementation.

Item	Value
Switch radix (N_T)	64
Topology	Enhanced Omega (EOM) with a 4 stage distribution network
Number of stages (N_S)	15
Number of 2×2 switching nodes (N)	480
Number of switching gates (SOAs)	1920
Average power consumption (estimated)	10 W
Total area (estimated)	4 cm × 4 cm
Round trip latency (estimated)	9 ns

According to the results from Figure 19.8, when operated at an offered load of $p = 0.8$ with two path adjustment iterations ($n\text{PA} = 2$), the network attains an acceptance rate of 0.7 and a mean queuing latency $L_Q = 1.0$ slots. When 100 ns slots are used ($T_S = 100$ ns), with a guard time (T_G) of 6 ns for synchronization and clock recovery, and assuming the *ack* round-trip latency ($T_{Sw\_Fab} + T_{Ack}$) is 9 ns, the slot efficiency parameter can be computed:

$$\eta = \frac{T_{Slot} - T_G - n_{Pa}(T_{Sw\_Fab} + T_{Ack})}{T_{Slot}} = 0.76$$

Using wavelength-parallel messages (8 wavelength × 10 Gb/s, as experimentally demonstrated in [39]) one can calculate the average bandwidth per port and the bisection bandwidth:

$$B_{Peak} = \frac{R \times N_{Payload} \times \eta}{S} = 30.4\,\text{Gb/s}$$

$$B_{Average} = B_{Peak} \times p = 24.3\,\text{Tb/s}$$

The aggregate injection bandwidth is therefore,

$$B_{Agg\ \ Injection} = N_T \times B_{Average} = 1.55\,\text{Tb/s}$$

In order to scale to larger systems, a designer can choose either to construct a PIC with a larger port count, if the required integration level is available, or use multistage topologies. The latency effects of each one of these options can be simulated and straightforwardly computed. For the discussed single-stage 64-port system, where t_b is the slot time (100 ns), and maximum fiber length (l_f) is 16 m, the mean message latency (D) is found to be:

$$t_p = \frac{l_f}{c_f} + \frac{T_{Sw\_Fab}}{2} = 84.5\,\text{ns}$$

$$t_r = t_q + t_b = L_Q \times T_{Slot} + t_b = 200\,\text{ns}$$

$$D = t_p + t_b + t_r = 384.5\,\text{ns}$$

where t_r is the routing latency, including the queuing latency incurred by retransmissions, and c_f is the speed of light in silica (2×10^8 m/s). Table 19.3 summarizes the implementation design results.

Table 19.3

Performance results for a 64-terminal optical interconnection network based on an integrated 64×64 SPINet architecture.

Item	Value
Tributary transmission rate (R)	10 Gb/s
Number of wavelengths (N_{Payload})	8
Speed up (S)	2
Peak data rate (B_{Peak})	30.4 Gb/s
Average data rate at load r 0.8 (B_{Average})	24.3 Gb/s
Queueing latency at load r 0.8 (L_{Q})	1.0 slots
Total average latency at load r 0.8 (D)	384.5 ns

19.7 OIN ARCHITECTURES AND SYSTEM DEMONSTRATIONS

Significant research efforts have focused on the use of optical communications in the context of interconnection networks [25, 26, 28, 29, 30, 44, 51]. In this section, we review a subset of these architectures that are specifically aimed at advanced computing systems. The particular points of interest by which an architecture is evaluated are bandwidth, latency, scalability, and system integration. Additionally, since contention resolution is one of the key challenges in the design of OIN, the contention resolution mechanism in each architecture is described. The Data Vortex architecture and system demonstration are covered in greater detail.

19.7.1 RAPID, OSMOSIS, and Gemini

The Reconfigurable All-Photonic Interconnect for parallel and Distributed systems (RAPID) architecture, proposed by Kodi and Louri [26, 69], suggests the use of a hierarchical structure of passive optical networks, with fixed wavelength receivers, tunable transmitters, and dynamic time slot pre-allocation (Figure 19.9). RAPID exploits both WDM and space division multiplexing (SDM) as well as the employment of multiple-domains where wavelengths may be reused to achieve high bandwidths. The network architecture also offers high connectivity which reduced the network diameter and results in lower queueing and routing delays for packet transmission. Scaling is linear with added terminal nodes. Some key advantages of this architecture are its implementation simplicity and lack of requirement for active optical switching elements. As messages hop between different networks (or clusters) however, O/E/O conversions, queuing, and reallocation of time slots must be performed, which contribute adversely to latency and complexity. The use of passive networks based on power splitting also limits the scalability to large node count systems. Recent modifications to the architecture and the addition of electronic flow control have been shown to result in improved performance.

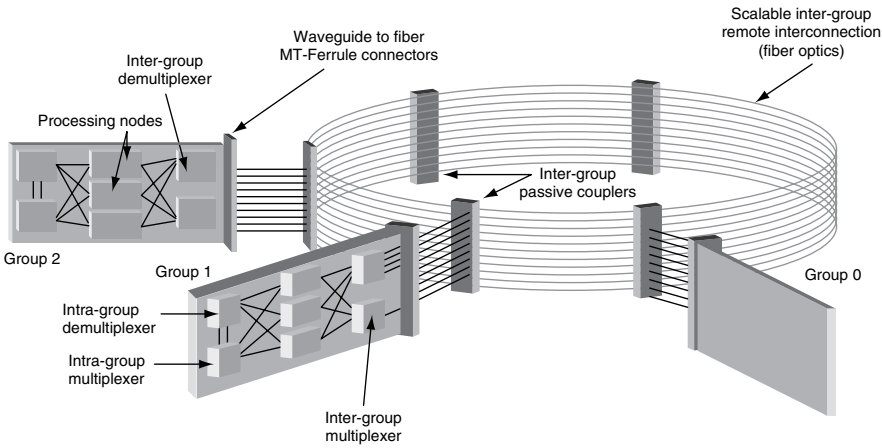

Figure 19.9 RAPID interconnection network conceptual diagram [26] (this figure may be seen in color on the included CD ROM).

Contentions in the RAPID network are avoided at the time of slot allocation, using an appropriate assignment algorithm. This approach presents a reasonably good and reliable performance in small networks, but may have scalability problems when many terminals are connected in the same network.

In the Optical Shared Memory Supercomputer Interconnect System (OSMOSIS) project, pursued by IBM and Corning [29], an SOA-based 64×64 broadcast-and-select crossbar switching fabric has been constructed and a high-speed scheduling algorithm has been developed to maximize its utilization (Figure 19.10). SOAs are used as the switching gates in the switching fabric, and serial 40 Gb/s peak bandwidth per port is demonstrated. Internal paths are wavelength multiplexed in the switching fabric to reduce the number of SOAs and the total cost. Scaling the OSMOSIS beyond the 64-port system is suggested using a fat tree topology, performing O/E/O conversion and queuing between stages.

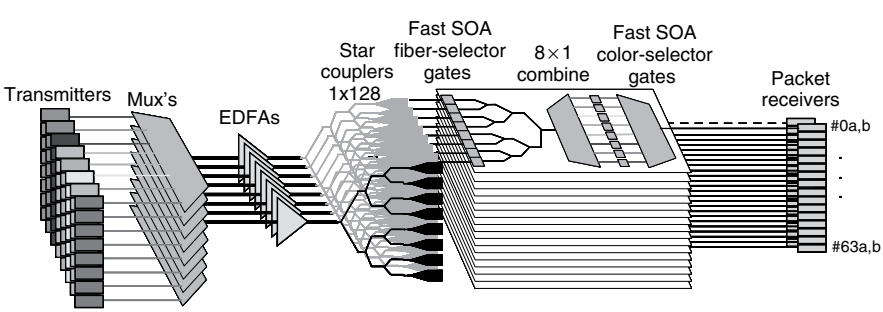

Figure 19.10 OSMOSIS broadcast and select network architecture overview [29] (this figure may be seen in color on the included CD ROM).

The OSMOSIS demonstration is perhaps the closest to actual computing system implementation and possible commercialization, having shown a running prototype. The OSMOSIS architecture employs a fast scheduler which requires additional communication lines with the interconnection switching fabric. This design was shown to work for the 64-port fully implemented system although may present some scalability challenges to large systems with over 1000s terminals. The wavelength domain is used for switching among ports (and planes), and scaling the bandwidth per node is achieved by increasing the serial (40 Gb/s) data rate.

As in the RAPID architecture, contentions in OSMOSIS are avoided by centrally scheduling the traffic on the switching before transmission. This approach enables the establishment of nonblocking optical paths and the reliable transmission of the high-bandwidth optical signals, but communications with the central controller can incur significant latency penalties and limit the ultimate scalability.

The Gemini OIN [25] architecture is designed with dual optical/electronic technology planes (Figure 19.11). It includes an end-to-end optical data path for large message traffic in conjunction with an electrical path used to control the

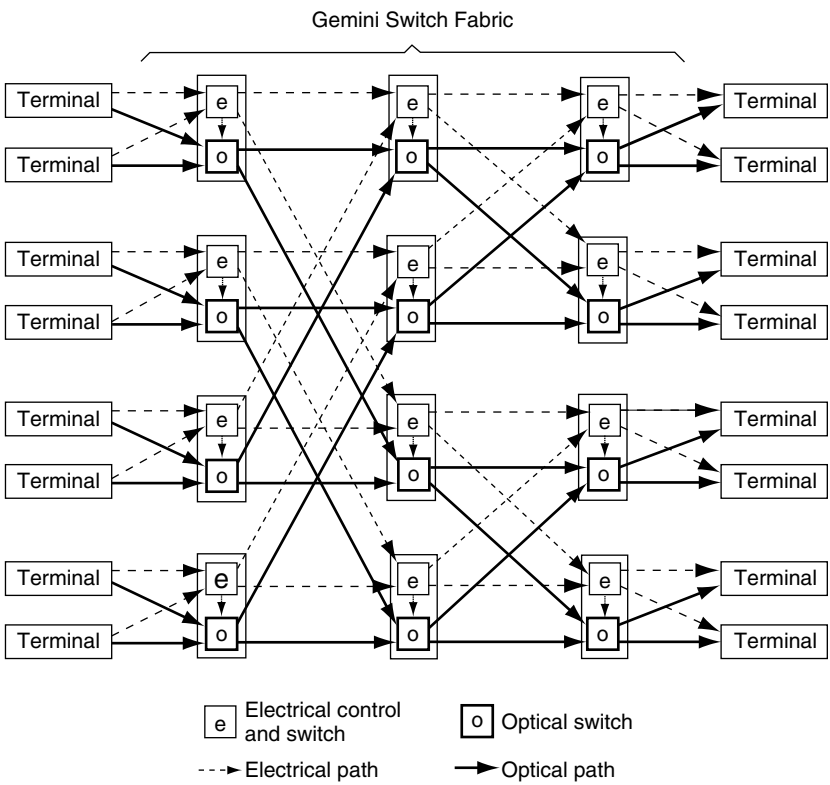

Figure 19.11 An 8×8 Gemini interconnection network [25].

setup of the optical path as well as for transmission of smaller data volume message traffic. Switching of the optical messages is accomplished with $LiNbO_3$ electro-optic 2×2 switch elements. The Gemini network interface, which requires a complex data organization engine, is used to collect messages from memory for delivery to the network and for distributing messages from the network into memory.

In the innovative approach used in Gemini, routing is accomplished by the dual electronic control network which sends setup, acknowledgment, blocking, and tear down signaling to establish the optical paths. Buffering of the electronic messages is used to address contention. The use of distributed control in Gemini is advantageous for scalability; however, substantial data organization operations are required at the network interfaces which can consume significant computation resources for setting up the dual networks communications and may adversely impact the parallel applications programmability.

The Data Vortex, developed and studied in Columbia University [30], is an optical packet switching MIN, scalable to a very large port count, and comprised of simple, SOA-based, bufferless switching nodes. Contentions are resolved by delaying contending packets to in the same stage via deflection to alternative intrastage paths. The wavelength-striped packets and the optically encoded addresses are maintained in the optical domain from source to destination. The Data Vortex scheme has been proven feasible on a 12×12 network fully implemented in a laboratory setup, and error-free transmission of 160-Gb/s peak bandwidth has been confirmed [30].

The limitations of the Data Vortex architecture arise from the unpredictable path a packet may take in the network, resulting from the complex topology and the use of deflection routing [52]. The different number of switch element hops taken by each packet has a performance penalty of unpredictable latency and packet reordering. The varying length paths also places constraints on the physical design of the optical and optoelectronic elements such as the SOAs and receivers.

19.7.2 The Data Vortex OIN

The Data Vortex topology, as first described in [53, 54], integrates internalized buffering with banyan routing to result in a bufferless network, specifically for implementation with fiberoptic components. The structure can be visualized as a set of concentric cylinders or routing stages which are cyclic subgroups that allow for deflections without loss of routing progress. Moreover, the hierarchical multiple-stage structure is easily scaled to larger network sizes while uniformly maintaining fundamental architectural concepts [30, 32, 55].

The Data Vortex architecture is a fully-implemented directed deflection routing topology composed of simple 2×2 switching nodes. The nodes are arranged in hierarchal levels or cylinders, each affixing an additional bit in the packet's destination address, in a manner similar to banyan network addressing. It is

designed to facilitate optical implementation by maintaining simple routing and eliminating the need for internal physical buffering. The Data Vortex is an input-blocking architecture that exhibits no internal blocking and no output blocking. Contention within the network is resolved by simple deflection routing techniques. Deflection routing removes the need for buffers by allowing packet contention to be resolved without blocking within the network and without blocking at the output. Therefore, the need for O/E and E/O data signal conversion is eliminated.

The Data Vortex architecture incorporates both deflection routing and banyan-style hierarchal addressing while utilizing bufferless switching nodes. This is accomplished by extending the paths in a conventional butterfly network to allow for routes which are always available for packet deflection. The topology of Data Vortex networks are thus best visualized in three dimensions (Figure 19.12). Because the packet paths are arranged angularly in this three-dimensional arrangement with traffic generally flowing inward, the aggregate flow of traffic resembles a physical spiral or vortex.

The Data Vortex topology is composed entirely of 2×2 switching nodes that are wholly distributed and require no centralized arbitration. The topology is divided into C hierarchies or *cylinders* which are analogous to the stages in a conventional banyan network (e.g., butterfly). The architecture also incorporates deflection routing, which is implemented at every node; deflection signal paths are placed only between different cylinders. Each cylinder (or stage) contains A nodes around its circumference and $H = 2^{C-1}$ nodes down its length. The topology contains a total of $N = A \times H \times C = A \times H \ (\log_2 H + 1)$ switching elements, with $N_t = A \times H$ possible input terminal nodes and the same number of possible

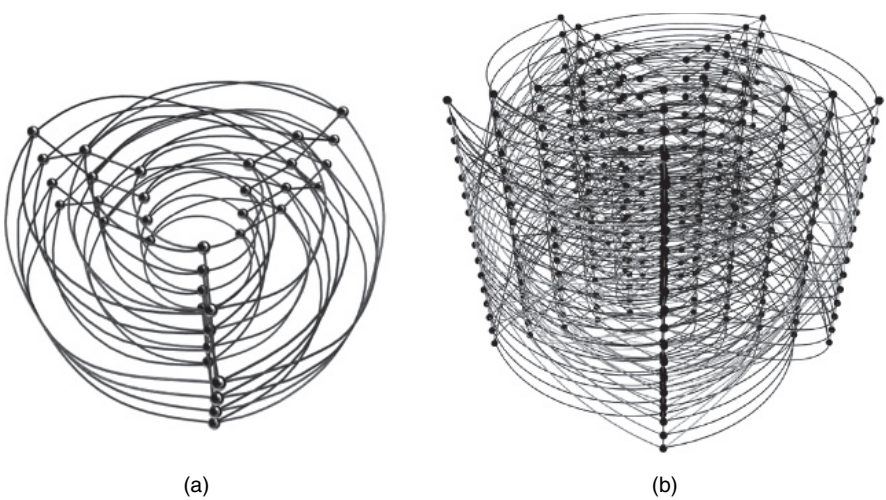

Figure 19.12 (a) Illustration of an example Data Vortex topology with 3 angles (A), a total height of 4 (H), and 3 cylinders (C). (b) A second example of a Data Vortex topology with A 5, H 16, and C 5.

output terminal nodes. The position of each node is given by the triplet (a, c, h), $0 \le a \le A-1$, $0 \le c \le C-1$, $0 \le h \le H-1$.

Paths within a cylinder exist only between nodes of adjacent angle values and never between nodes with the same position around the circumference of the cylinder, i.e., only from (a, c, h) to $(\mathrm{mod}_A\, a+1, c, G_c(h))$. These edges are often termed *deflection paths* because, while they are also used for address resolution, they are the only links available for deflections. Additional edges are present between cylinders called *ingression paths*, which connect nodes of the same height and of adjacent angle values, i.e., from (a, c, h) to $(\mathrm{mod}_A\, a+1, c+1, h)$. Thus, all paths between nodes progress one angle dimension forward and either continue around the same cylinder while moving to a different height or ingress to the next hierarchal cylinder at the same height. Deflection signals connect only nodes on adjacent cylinders with the same angular dimension, i.e., from $(a, c+1, h)$ to a node at position $(a, c, G_{c+1}(h))$. The conventional nomenclature illustrates packets routing to progressively higher numbered cylinders as moving inward toward the network outputs (Figure 19.13).

The paths within a cylinder differ depending upon the level c of the cylinder. The crossing or sorting pattern (i.e., the connections between height values defined by $G_c(h)$) of the outermost cylinder ($c = 0$) must guarantee that all paths cross from the upper half of the cylinder to the lower half of the cylinder so that the graph of the topology remains fully connected, and so that the banyan-like bitwise addressing scheme functions properly. The cylindrical crossings ensure that destinations can be addressed in a binary tree-like configuration, similar to binary banyan networks.

Addressing within the Data Vortex architecture is entirely distributed and bitwise, similar to banyan architectures: as a packet progresses inward, each

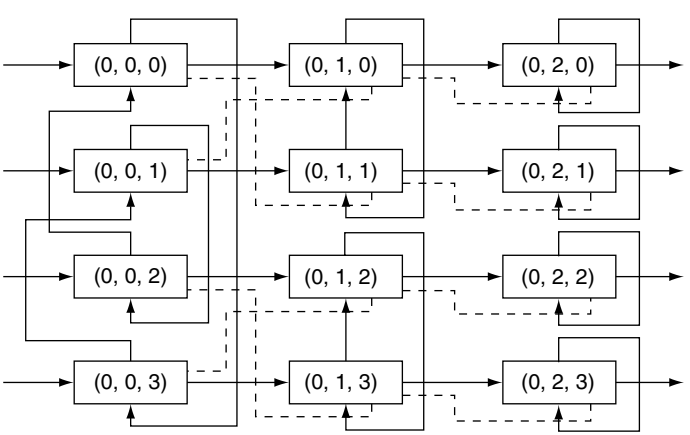

Figure 19.13 Schematic of an A 1, C 3, H 4 Data Vortex network. Directed optical paths are shown as solid arrows, and electronic deflection signals as dashed lines. The 12 nodes are labeled with coordinates (a, c, h).

successive bit of the binary address is matched to the destination. Each cylinder tests only one bit (except for the innermost one), and half of the height values permit ingression for "1" values, and half for "0" values, arranged in a banyan-like binary tree configuration. Within a cylinder c, nodes at all angles at a particular height (i.e., (•, c, h)) match the same $c+1$st significant bit value while paths guarantee preservation of the c most significant address bits. Thus, with each ingression to a successive cylinder, progressively more precision is guaranteed in the destination address. Finally, on the last cylinder $c = C - 1$, each node in the angular dimension is assigned a least significant value in the destination address so that the packets circulate within cylinder $c = C - 1$ until a match is found for the last angular address.

Each switching element is bufferless and is designed to check exactly one bit of the destination address, in addition to a general *presence* bit (or packet *frame*). When the selected address bit matches the value assigned to the node because of its position with the cylinder, the packet is allowed to ingress into the next cylinder, unless a deflection signal is received. When the selected address bit does not match, or when a deflection signal is received, the packet is routed within the same cylinder, and the node sends a deflection signal indicating that the next node will soon be busy with that packet. Therefore, every switching element always has an available deflection path and has an ingression path used for routing matches.

While it may seem wasteful to have twice as many optical paths as necessary, having a guaranteed deflection path allows for an extraordinarily simple routing logic which can be executed extremely quickly [33]. The distributed bitwise addressing scheme also helps ensure that routing decisions do not dominate network latency. No buffers are used, so the network latency can be reduced to the optical time-of-flight.

The nodes within the Data Vortex architecture are made to be as simple as possible and are designed to route only one packet per time slot (Figure 19.14).

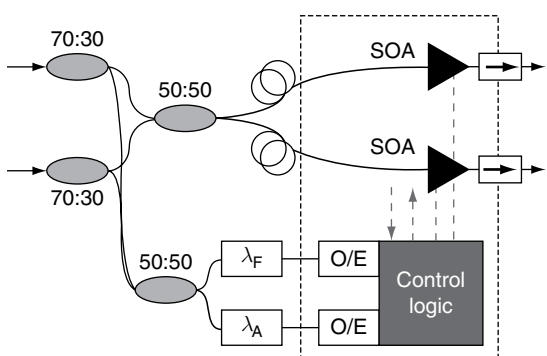

Figure 19.14 Schematic of the Data Vortex switching node (ovals for optical couplers, λ filters, O/E photodetectors, and boxed arrows for isolators, dashed arrows for deflection signal I/O).

This constraint requires a deflection mechanism within the Data Vortex which is somewhat different from conventional techniques. The Data Vortex deflection implementation prevents two packets from ever entering the same switching element by controlling one of the two possible source nodes. Thus, deflections occur only when a packet in cylinder $c+1$ is deflected or remains in cylinder $c+1$ due to its destination address. A packet which would otherwise ingress into that node on cylinder $c+1$ from its node on cylinder c is thus required to remain in cylinder c, since the deflection signal indicates that the desired node will be busy. This deflection structure results in a "backpressure" from the inner cylinders ($c = C-1,\ C-2,\ \ldots$) to the outer cylinders ($c = 0,\ 1,\ \ldots$). A deflected packet must traverse two additional node hops before the address again matches.

The deflection signaling structure continues to the nodes on the output and input terminals such that output nodes can receive *busy* signals from the output queuing subsystem, and the input nodes can transmit similar *busy* signals to the input interface. Thus, packets which attempt input at the first cylinder $c = 0$ may receive a signal which indicates that the desired input node is busy; the packet must therefore be queued to reattempt injection.

In considering the scalability of the Data Vortex, the critical issue becomes the physical layer and the degradation of the optical payload. However, it was shown in Ref. [56] that there exists a trade-off between the maximum number of wavelengths available for a packet and the number of node hops through which it can propagate error-free. That is, a packet with fewer payload wavelengths can in general traverse more nodes before significant errors accumulate. The optical signal-to-noise ratio (OSNR) of a packet shrinks due to the accumulation of SOA amplified spontaneous emission (ASE) noise through a long cascade of switching nodes. In general, however, utilizing the current technology, nearly 1 Tb/s of bandwidth can be utilized for networks that require $\sim$20 node hops [56], which corresponds to scaling the Data Vortex to a 4096×4096 interconnection network.

As an example of a large-scale system, we consider the design of a 4096-port Data Vortex network. In order to provide $H = 4096$, the number of cylinders must be $C = 13$. In order to achieve high acceptance rate, five or more angles should be used, implying a total switching node count of $N = 266240$. This number may seem large, but consider that each packet propagates through only $\sim$20 nodes on average. The extra nodes provide alternate routing and deflection paths, which enable the Data Vortex topology to achieve such high acceptance rates (Figure 19.15). In designing a complete optical packet switching interconnection solution, it is important not to forget the cost of the packet generation modules and the packet receivers. In order to maximize the effectiveness of these, the appropriate Data Vortex topology can be constructed to provide high acceptance rates with single-angle injection. Although the total number of switching nodes can be very great, the modular and systematic arrangement of the Data Vortex architecture makes design tractable and ultimately feasible for large port counts and ultrahigh-bandwidth, low-latency switching.

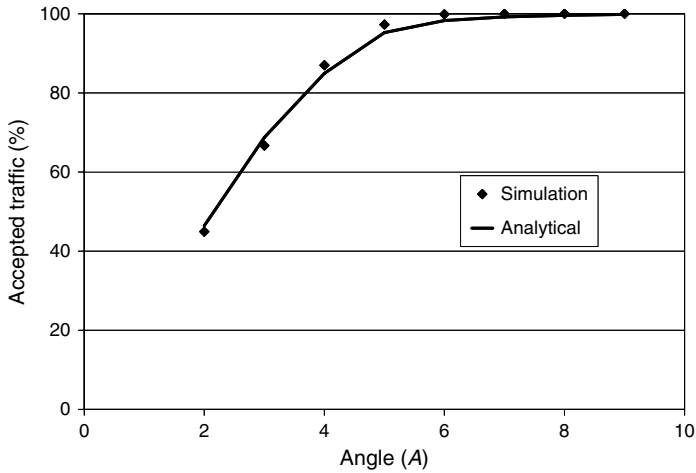

Figure 19.15 Accepted traffic vs angle size for maximum random workload. The network simulated has H 4096 ports and maximum load. For angle sizes greater than 6, the network accepts more than 99.99% of all traffic offered, even under maximum offered load.

19.8 FUTURE DIRECTIONS: OPTICAL INTERCONNECTION NETWORKS-ON-CHIP

Looking forward to the future opportunities for OINs, the emerging field of networks-on-chip (NoC) for multicore processors may significantly benefit from the insertion of photonic interconnect technologies. The last few years have seen remarkable advances in the integration of photonic elements in silicon with critical components such as modulators, waveguides, and optical receivers (based on SiGe) now available as library cells in standard CMOS processes [20, 57 61]. Concurrently with these advances in integrated silicon photonics, as discussed in Section 19.1, microprocessors are undergoing a major paradigm shift with the emergence of multicore architectures and CMPs. The quest for both high performance and low power has set a clear trend for CMPs as each technology generation will likely feature chips that host a larger number of smaller processing cores.

The distributed nature of the multicore architecture, accompanied by the increasing clock-speeds, die-areas, and complexity of chips, have led to an increasing consensus that NoCs are to be used as the communication infrastructure for these systems. The alternative, an increasingly large number of point-to-point links, has become too complex to design and to implement. An increasing number of researchers have adopted this concept of a shared, packet-switched medium for on-chip communications, and a large body of works has been dedicated to developing architectures, algorithms, circuit techniques, and performance studies of NoCs [62 66]. While NoCs dissipate less power than a set of point-to-point

links to provide the same communication performance, they do not completely alleviate the power dissipation problem. Power dissipation has been identified as a key limitation to improving the performance in intrachip communications as a growing fraction of the total power dissipated in VLSI chip is expended on communications rather than computation.

Photonic channels can support large amounts of data traffic across longer distances in a bandwidth-oriented design of a network connecting processing cores and memories. The communications can occur at very high throughputs with extraordinary energy efficiencies compared with equivalent electronic technologies. In a field that was dominated for decades by a race for performance, performance-per-unit-power is now becoming the accepted figure of merit. As such, photonic interconnection network solutions, which can provide scalable ultrahigh throughputs with low-power dissipation for on- and off-chip communications, can potentially offer unparalleled advantages in terms of GFLOPS-per-Watt performance [67, 68].

REFERENCES

[1] G. E. Moore, "Cramming more components onto integrated circuits," *Electron.*, 38(8), 114 117, April 1965.

[2] J. L. Hennessy and D. A. Patterson, *Computer Architecture: A Quantitative Approach*, San Francisco, CA: Morgan Kaufmann, 4th edition, 2007.

[3] S. Vangal, J. Howard, G. Ruhl et al., "An 80 Tile 1.28TFLOPS Network on Chip in 65 nm CMOS," in Proc. *ISSCC*, Dig. Tech. paper 5.2, February 2007.

[4] R. Kalla, B. Sinharoy, and J. M. Tendler, "IBM Power5 chip: A dualcore multithreaded processor," *IEEE Micro*, 24(2), 40 47, March 2004.

[5] C. N. Keltcher, K. J. McGrath, A. Ahmed, and P. Conway, "The AMD Opteron processor for multiprocessor servers," *IEEE Micro*, 23(2), 66 76, March/April 2003.

[6] J. A. Kahle, M. N. Day, H. P. Hofsteee et al., "Introduction to the cell multiprocessor," *IBM J. Res. Develop.*, 49(4 5), 589 604, September 2005.

[7] M. Kistler, M. Perrone, and F. Petrini, "Cell multiprocessor communication network: Built for speed," *IEEE Micro*, 26(3), 10 23, May/June 2006.

[8] P. Kongetira, K. Aingaran, and K. Olukotun, "Niagara: A 32way multithreaded SPARC processor," *IEEE Micro*, 25(2), 21 29, March/April 2005.

[9] C. McNairy and R. Bhatia, "Montecito: A dual core, dual thread Itanium processor," *IEEE Micro*, 25(2), 10 20, March/April 2005.

[10] A. Gara, M. A. Blumrich, D. Chen et al., "Overview of the blue gene/l system architecture," *IBM J. Res. Develop.*, 49(2 3), 195 212, May 2005.

[11] A. F. Benner, M. Ignatowski, J. A. Kash et al., "Exploitation of optical interconnects in future server architectures," *IBM J. Res. Develop.*, 49(4/5), 755 775, July 2005.

[12] W. J. Dally and B. Towles. *Principles and Practices of Interconnection Networks*, San Francisco, CA: Morgan Kaufmann, 2004.

[13] D. Dai and D. K. Panda, "How can we design better networks for DSM systems?" *Lecture Notes in Computer Science*, 1417, 171 184, January 1998.

[14] J. P. G. Sterbenz and J. D. Touch, *High Speed Networking: A Systematic Approach to High Bandwidth Low Latency Communication*, New York, NY: Wiley and Sons, 2001.

[15] J. Kim, W. J. Dally, B. Towles, and A. K. Gupta, "Microarchitecture of a high radix router," in 32nd *ISCA '05*, June 2005, pp. 420 431.

[16] T. Mudge, "Power: A first class architectural design constraint," *IEEE Computer*, 34(4), 52 58, 2001.
[17] R. Ho, K. W. Mai, and M. A. Horowitz, "The Future of Wires," in Proc. *IEEE*, 89(4), 490 504, April 2001.
[18] M. A. Horowitz, E. Alon, D. Patil et al., "Scaling, power, and the future of CMOS," in *IEEE Intl. Electron Devices Meeting*, December 2005.
[19] J. Liu and X. Lin, "Equalization in high speed communication systems," *IEEE Circuits Syst. Mag.*, 4(2), 4 17, 2004.
[20] L. A. Barroso, J. Dean, and U. Holzle, "Web search for a planet: The Google cluster architecture," *IEEE Micro*, 23(2), 22 28, March/April 2003.
[21] D. Miller, "Rationale and Challenges for Optical Interconnects to Electronic Chips," in Proc. *IEEE*, 88(6), 728 749, June 2000.
[22] C. L. Schow, F. E. Doany, O. Liboiron Ladouceur et al., "160 Gb/s, 16 Channel Full Duplex, Single Chip CMOS Optical Transceiver," in Proc. *OFC*, OThG4, March 25 29, 2007.
[23] G. P. Agrawal, *Fiberoptic Communication Systems*, New York, NY: Wiley and Sons, 2002.
[24] R. Ramaswami and K. N. Sivarajan, *Optical Networks: A Practical Perspective*, San Francisco, CA: Morgan Kaufmann, 2nd edition, 2002.
[25] R. D. Chamberlain, M. A. Franklin, and C. S. Baw, "Gemini: An optical interconnection network for parallel processing," *IEEE Trans. Parallel Distrib. Syst.*, 13(10), 1038 1055, October 2002.
[26] A. K. Kodi and A. Louri, "Design of a high speed optical interconnect for scalable shared memory multiprocessors," *IEEE Micro*, 25(1), 41 49, January/February 2005.
[27] T. Lin, K. A. Williams, R. V. Penty et al., "Performance and scalability of a single stage SOA switch for 10×10 Gb/s wavelength striped packet routing," *IEEE Photon. Technol. Lett.*, 18(5), 691 693, March 1, 2006.
[28] A. Louri and A. K. Kodi, "SYMNET: An optical interconnection network for scalable high performance symmetric multiprocessors," *Appl. Opt.*, 42(17), 3407 3417, June 10, 2003.
[29] R. Luijten, C. Minkenberg, B. R. Hemenway et al., "Viable Optoelectronic HPC Interconnect Fabrics," in *ACM/IEEE SC '05*, November 2005, p. 18.
[30] A. Shacham, B. A. Small, O. Liboiron Ladouceur, and K. Bergman, "A fully implemented 12×12 data vortex optical packet switching interconnection network," *J. Lightw. Technol.*, 23(10), 3066 3075, October 2005.
[31] A. Pattavina, *Switching Theory Architecture and Performance in Broadband ATM Networks*, New York, NY: Wiley and Sons, 1998.
[32] Q. Yang and K. Bergman, "Traffic control and WDM routing in the data vortex packet switch," *IEEE Photon. Technol. Lett.*, 14(2), 236 238, February 2002.
[33] B. A. Small, A. Shacham, and K. Bergman, "Ultra low latency optical packet switching node," *IEEE Photon. Technol. Lett.*, 17(7), 1564 1566, July 2005.
[34] A. Shacham, B. G. Lee, and K. Bergman, "A wideband, non blocking, 2×2 switching node for a SPINet network," *IEEE Photon. Technol. Lett.*, 17(12), 2742 2744, December 2005.
[35] B. A. Small, T. Kato, and K. Bergman, "Measurements of very low bit error rates for an optical packet switching node," *IEEE Photon. Technol. Lett.*, 17(11), 2379 2381, November 2005.
[36] O. Liboiron Ladouceur, B. A. Small, and K. Bergman, "Physical layer scalability of WDM optical packet interconnection networks," *J. Lightw. Technol.*, 24(1), January 2006.
[37] N. F. Maxemchuk, "Regular and mesh topologies in local and metropolitan area networks," *AT&T Tech. J.,* 64(7), 1659 1686, September 1985.
[38] P. Baran, "On distributed communications networks," *IEEE Trans. Commun.,* 12(1), 1 9, March 1964.
[39] A. Shacham, B. G. Lee, and K. Bergman, "A Scalable, Self Routed, Terabit Capacity, Photonic Interconnection Network," in *Hot Interconnects: IEEE 13th Annual Symposium on High Performance Interconnects*, August 2005, pp. 147 150.
[40] A. Shacham and K. Bergman, "Utilizing Path Diversity in Optical Packet Switched Interconnection Networks," in Proc. *OFC 2006*, OTuN5, Anaheim, CA, March 2006.

[41] C. L. Wu and T. Y. Feng, *Interconnection Networks for Parallel and Distributed Processing*, Los Alamitos, CA: IEEE Computer Society Press, 1984.
[42] D. H. Lawrie, "Access and alignment of data in an array processor," *IEEE Trans. Comput.*, 24, 1145 1155, December 1975.
[43] N. McKeown, A. Mekkittikul, V. Anantharam, and J. Walrand, "Achieving 100% throughput in an input queued switch," *IEEE Trans. Commun.*, 47(8), 1260 1267, August 1999.
[44] T. Lin, K. A. Williams, R. V. Penty et al., "Performance and scalability of a single stage SOA switch for 10×10 Gb/s wavelength striped packet routing," *IEEE Photon. Technol. Lett.*, 18(5), 691 693, March 1, 2006.
[45] L. A. B. Windover et al., "Parallel optical interconnects >100 Gb/s," *J. Lightw. Technol.*, 22(9), 2055 2073, September 2004.
[46] F. Tobagi, "Fast packet switch architectures for broadband integrated services digital networks," in Proc. *IEEE.*, 78(1), 133 167, January 1990.
[47] A. Shacham and K. Bergman, "Building ultra low latency interconnection networks using photo nic integration," *IEEE Micro*, May/June 2007.
[48] K. A. Williams, G. F. Roberts, T. Lin et al., "Integrated optical 2×2 switch for wavelength multiplexed interconnects," *IEEE J. Sel. Top. Quantum Electron.*, 11(1), 78 85, January/February 2005.
[49] R. Nagarajan et al., "Large scale photonic integrated circuits," *IEEE J. Sel. Top. Quantum Electron.*, 11(1), 50 65, January/February 2005.
[50] R. Nagarajan et al., "Large scale photonic integrated circuits for long haul transmission and switching," *J. Optical Netw.*, 6(2), 102 111, February 2007.
[51] I. Keslassy, S.T. Chuang, K. Yu et al., "Scaling internet routers using optics," *ACM SIGCOMM*, August 2003.
[52] A. Shacham and K. Bergman, "Optimizing the performance of a data vortex interconnection network," *J. Optical Netw.*, 6(4), 369 374, April 2007.
[53] C. Reed, "Multiple level minimum logic network," US Patent 5 996 020, November 30, 1999.
[54] Q. Yang, K. Bergman, G. D. Hughes, and F. G. Johnson, "WDM packet routing for high capacity data networks," *J. Lightw. Technol.*, 19(10), 1420 1426, October 2001.
[55] B. A. Small, O. Liboiron Ladouceur, A. Shacham et al., "Demonstration of a Complete 12 port Terabit Capacity Optical Packet Switching Fabric," in Proc. *OFC*, paper OWK1, Anaheim, March 2005.
[56] O. Liboiron Ladouceur, B. A. Small, and K. Bergman, "Physical layer scalability of WDM optical packet interconnection networks," *J. Lightw. Technol.*, 24(1), January 2006.
[57] C. Gunn, "CMOS photonics for highspeed interconnects," *IEEE Micro*, 26(2), 58 66, March/ April 2006.
[58] F. Xia, L. Sekaric, and Y. A. Vlasov, "Ultracompact optical buffers on a silicon chip," *Nat. Photon.*, 1, 65 71, January 2007.
[59] Q. Xu, S. Manipatruni, B. Schmidt, J. Shakya, and M. Lipson, 12.5 Gbit/s carrier injection based silicon microring silicon modulators," *Opt. Express*, 15(2), 430 436, 22 January 2007.
[60] Q. Xu, B. Schmidt, S. Pradhan, and M. Lipson, "Micrometer scale silicon electro optic mod ulator," *Nature*, 435, 325 327, May 19, 2005.
[61] B. G. Lee, B. A. Small, Q. Xu et al., "Characterization of a 4×4 Gb/s Parallel electronic bus to WDM Optical link silicon photonic translator," *IEEE Photon. Technol. Lett.,* 19(7), 456 458, April 1, 2007.
[62] L. Benini and G. D. Micheli, "Networks on chip: A new SoC paradigm," *IEEE Computer*, 49(2/3), 70 71, January 2002.
[63] W. J. Dally and B. Towles, "Route packets, not wires: On chip interconnection networks," in Proc. *Design Automation Conf.*, June 2001, pp. 684 689.
[64] S. Heo and K. Asanović, "Replacing global wires with an on chip network: A power analysis," in *ISLPED 2005*, August 2005, pp. 369 374.

[65] R. Kumar, V. Zyuban, and D. M. Tullsen, "Interconnections in multicore architectures: Under standing mechanism, overheads, scaling," in 32nd annual *ISCA '05*, June 2005.
[66] T. M. Pinkston and J. Shin, "Trends toward on chip networked microsystems," *Intl. J. High Perform. C. and Netw.*, 3(1), 3 18, 2001.
[67] A. Shacham, K. Bergman, and L. P. Carloni, "The Case for Low Power Photonic Networks on Chip," in Proc. *DAC 2007*, paper 8.5, June 2007.
[68] Shacham, K. Bergman, and L. P. Carloni, "On the Design of a Photonic Network on Chip," in Proc. *NOCS 2007*, paper 2.1, May 2007.
[69] C. Kochar, A Kodi, and A. Louri, "nD RAPID: A multidimensional scalable fault tolerant optoelectronic interconnection for high performance computing systems," *J. Optical Netw.*, 6(4), 465 481, May 2007.

This page intentionally left blank

20

Simulation tools for devices, systems, and networks

Robert Scarmozzino

RSoft Design Group, Ossining, NY, USA

20.1 INTRODUCTION

The ability of optical fiber-based telecommunications to satisfy the enormous demand for network capacity that exists in today's society is a testament to the efforts of researchers and engineers in the field and the resulting advancements in technology over the last 30+ years. These advancements come from thorough understanding of the physics and other disciplines underlying the technology, and the ability to recognize sources for limitation, develop ideas for solution, and predict, test, and demonstrate those ideas. The field of numerical modeling, the subject of this chapter, has already been an important facilitator in the above process, and its influence is expected to increase further as photonics, the technology as the core of optical fiber telecom (OFT), matures to the level of integration and market penetration as the electronics industry.

The scope of numerical modeling in OFT is very broad, and can be categorized in many ways. For the purposes here, we will divide the discussion into three groups:

- Device/component-level modeling
- System-level modeling
- Network-level modeling

The device/component layer considers individual elements at the core of the OFT hierarchy. These are further divided into passive components (e.g., the fiber itself, splitters, couplers, wavelength-division multiplexing (WDM) components) and active components (e.g., lasers, detectors, modulators). The principle objective at this layer of modeling is to understand the detailed physical behavior of the

Optical Fiber Telecommunications V B: Systems and Networks

ISBN: 978 0 12 374172 1

component with respect to is ability to generate, modify, transmit, and detect light. Modeling generally considers the full 3D spatial behavior of the electromagnetic field and/or the electron device characteristics, as well as the temporal aspects, either directly in the time domain or indirectly in the frequency domain.

The system layer considers how collections of components function together to form a system for transmission of information (digital or analog). The primary objective is to determine the quality of transmission [e.g., BER (bit error rate) or SNR (signal-to-noise ratio)] of a given system configuration. The larger scale of systems simulation (in space, length of time, and number of components) necessitates some form of abstraction or simplification compared to device level modeling. For example, in modeling of the fiber, the space dimension is reduced from three dimensions (3D) to one dimension (1D) by assuming a constant modal profile. Nevertheless, systems modeling includes detailed physics, such as nonlinear phenomenon in fiber propagation, that enables accurate prediction of system characteristics.

The configurations considered in systems modeling are in many cases single point-to-point links (e.g., source transmit receive configuration), but can be small networks as well. However, as the number of network nodes becomes large, full systems simulation becomes prohibitive, and additional abstraction is necessary. Furthermore, at the network layer additional questions arise, such as capacity planning and network protocols that are outside the scope of the type of modeling described above for components and systems. It becomes useful at this point to distinguish between modeling the physical aspects of light transmission, and the other questions mentioned above. The former, we refer to as physical layer modeling. While it is possible to model large networks at the physical layer, for the purposes of this chapter, we will use the term network modeling to refer to these higher-level questions. In capacity planning, for example, the fundamental question is: given a set of network demands between locations, find the set and distribution of equipment that optimizes some metric (e.g., cost).

In this chapter, we will describe several methods for device, systems, and network modeling, and give examples of each. This survey is by no means exhaustive. Finally, it should be noted that many of the methods described here, in the references therein, and elsewhere in the literature have been embodied in commercially available simulation tools.

20.2 DEVICE SIMULATION

In this section we explore device-level modeling. As noted earlier, this can loosely be divided into two broad classes, passive and active. In passive modeling, the fundamental problem is to analyze the propagation of light in a device, such as a waveguide, of a given geometry and materials. The optical properties of the materials are considered given, and fixed throughout the computation. The propagation of light is thus determined entirely via Maxwell's equations. In contrast, in active device modeling, the optical properties of the material are not fixed, but

depend on other physical variables that need to be solved for. For example, in a semiconductor electro-optic modulator, the optical index of refraction depends on the quasistatic electric field, which in turn depends on the carrier distribution in the semiconductor. Thus additional equations (e.g., Poisson's equation, carrier transport equations) need to be solved. Select examples of both passive and active modeling are discussed in the following.

20.2.1 Passive Device Modeling Methods—Solving Maxwell's Equations

As noted above, the modeling of passive devices essentially involves the numerical solution of Maxwell's equations, for which there are many approaches. The time evolution behavior of these equations can be handled directly in the time domain, or alternatively considered in the frequency domain through Fourier transformation. The spatial behavior can be represented through gridded methods, which represent the field at a discrete set of points or regions in space, or through semianalytic methods, in which a portion of the field behavior is represented by analytic solutions, and the rest by an expansion in numerical or analytic basis functions. Approaches can be "rigorous," meaning that theoretically they can include all aspects of the physical behavior in their solution, or approximate in nature, meaning that they simplify Maxwell's equations in ways that are appropriate only for certain physical phenomenon. All numerical methods are approximate by virtue of the truncation of continuous differential equations to a discrete problem (e.g., a finite number of discrete grid points in gridded methods, or a finite number of basis functions in semianalytic methods). Well-formulated methods should converge to the correct solution as the number of grid points or basis functions is increased. Methods differ in how well they converge, and how their computational cost (i.e. computer time and memory) scales as the computational size of the problem increases.

The next section will review selected methods and give a number of application examples for each. The review is not intended to be comprehensive, but give a representative cross section of those methods that are in common use. Some of the methods presented are for general propagation problems, while others consider special subproblems, such as finding waveguide modes or modeling periodic structures.

The Beam Propagation Method

This section reviews the beam propagation method (BPM) [1 3]. The simplest version of this technique uses finite difference methods to solve the well-known parabolic or paraxial approximation of the Helmholtz equation. The fundamental physical limitation of the above approach limits the solution to forward traveling waves and implies a paraxiality condition on the primary direction of propagation.

These limitations can be reduced using more advanced methods reviewed in Ref. [3]. Even with these restrictions, the BPM can be used to model a wide variety of problems in photonics, and is the only viable method in many cases due to practical computational limits.

Scalar, Paraxial BPM The simplest form of BPM considers a scalar field (i.e., neglects polarization effects) and assumes paraxiality (i.e. propagation is restricted to a narrow range of angles). In this case, the wave equation can be written in the form of the well-known Helmholtz equation for monochromatic waves:

$$\frac{\partial^2 \phi}{\partial x^2} + \frac{\partial^2 \phi}{\partial y^2} + \frac{\partial^2 \phi}{\partial z^2} + k(x, y, z)^2 \phi = 0. \tag{20.1}$$

Here the scalar electric field has been written as $E(x, y, z, t) = \phi(x, y, z)\, \mathrm{e}^{-\mathrm{i}\omega x}$ and the notation $k(x, y, z) = k_0\, n(x, y, z)$ has been introduced for the spatially dependent wavenumber, with $k_0 = 2\pi/\lambda$ being the wavenumber in free space. The geometry of the problem is defined entirely by the refractive index distribution $n(x, y, z)$.

Aside from the scalar assumption, the above equation is exact. Considering that in typical guided-wave problems the most rapid variation in the field ϕ is the phase variation due to propagation along the guiding axis, and assuming that axis is predominantly along the z direction, it is beneficial to factor this rapid variation out of the problem by introducing a so-called slowly varying field u via the ansatz

$$\phi(x, y, z) = u(x, y, z)\, \mathrm{e}^{i\bar{k}z}. \tag{20.2}$$

Here k is a constant number to be chosen to represent the average phase variation of the field ϕ, and is referred to as the reference wavenumber. The reference wavenumber is frequently expressed in terms of a reference refractive index, n, via $k = k_0 n$. Introducing the above expression into the Helmholtz equation, and making the parabolic approximation by neglecting the second derivative u_{zz}, yields the following equation for the slowly varying field:

$$\frac{\partial u}{\partial z} = \frac{i}{2\bar{k}} \left(\frac{\partial^2 u}{\partial x^2} + \frac{\partial^2 u}{\partial y^2} + \left(k^2 - \bar{k}^2 \right) u \right). \tag{20.3}$$

This is the basic BPM equation in 3D; simplification to two dimensions (2D) is obtained by omitting any dependence on y. Given an input field, $u(x, y, z = 0)$, the above equation determines the evolution of the field in the space $z > 0$.

Numerical Solution Equation (20.3) is a parabolic partial differential equation that can be "integrated" forward in z by a number of standard numerical techniques. The most common is the finite difference method. For simplicity, the

approach is illustrated for a scalar field in 2D (xz). Let u_i^n denote the field at transverse grid point i and longitudinal plane n, and assume the grid points and planes are equally spaced by Δx and Δz apart, respectively. Using a Crank Nicholson scheme, Eqn (20.3) is represented at the midplane between the known plane n and the unknown plane $n+1$ as follows:

$$\frac{u_i^{n+1}-u_i^n}{\Delta z}=\frac{i}{2\bar{k}}\left(\frac{\delta^2}{\Delta x^2}+\left(k\left(x_i,z_{n+1/2}\right)^2-\bar{k}^2\right)\right)\frac{u_i^{n+1}+u_i^n}{2}. \tag{20.4}$$

Here δ^2 represents the standard second-order difference operator, $\delta^2 u_i=(u_{i+1}+u_{i-1}\quad 2u_i)$, and $z_{n+1/2}\equiv z_n+\Delta z/2$. The above equation represents a matrix equation for the unknown field u_i^{n+1} in terms of known quantities, and can be solved with standard techniques to propagate the field at each step.

Applications Since the BPM can efficiently accommodate large problem domains even if the geometry or material changes at every step, it has become the preferred method for simulating many of the components found in photonic integrated circuits (PICs). These include couplers, power dividers, multi-mode interference devices (MMIs), Mach Zehnder modulators, and arrayed waveguide routers (AWGRs). Furthermore, several of these devices can be simulated together in order to study the coupling efficiency between them.

Figures 20.1 and 20.2 depict a Mach Zehnder modulator comprised of channel waveguides and three electrodes. The operational state of the device is switched when the voltage applied to the center electrode is changed. Since the direction of the applied field is different in each branch the refractive index perturbations (due to electro-optic effect) are in opposite directions. An optical path-length

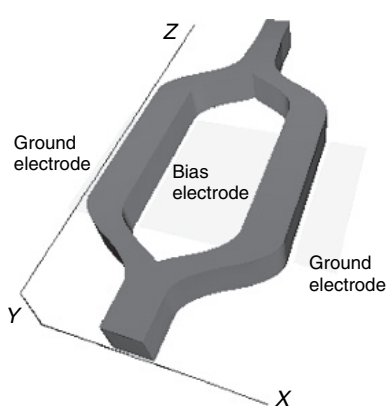

Figure 20.1 Schematic of a channel waveguide Mach Zehnder Modulator controlled by applied voltage (this figure may be seen in color on the included CD ROM).

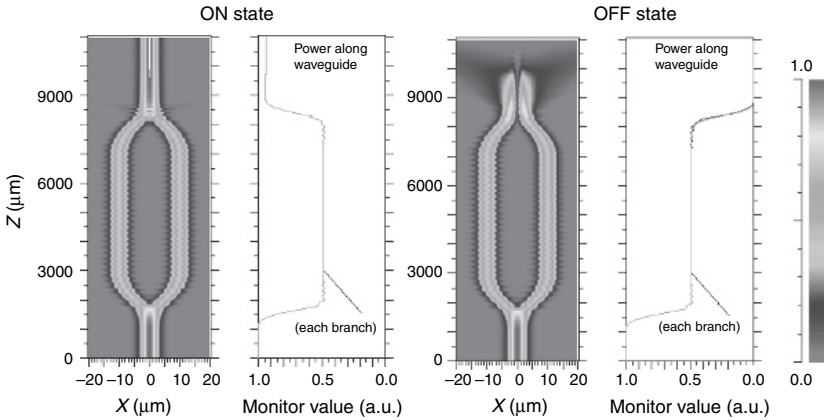

Figure 20.2 Simulation results for a Mach Zehnder Modulator showing both the ON (left) and the OFF (right) states. In the ON state, nearly all power incident on the device will be transmitted to the output waveguide, while nearly all incident power is radiated away in the OFF state (this figure may be seen in color on the included CD ROM).

differential results that causes the propagating field to constructively (ON state) or destructively (OFF state) interfere with itself at the output of the device.

Figure 20.3 shows a 1 16 AWGR with flattened spectral response. The device is comprised of input and output star couplers connected by an array of 80 waveguides. There are 16 output waveguides, each corresponding to a single wavelength channel, and a single input waveguide that has a nonlinear taper.

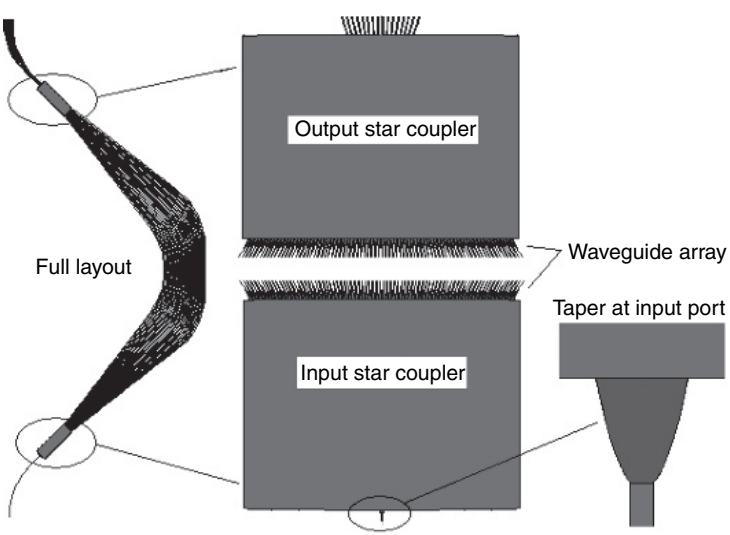

Figure 20.3 Scale view of an AWGR layout along with expanded views of the star couplers and tapered input port (this figure may be seen in color on the included CD ROM).

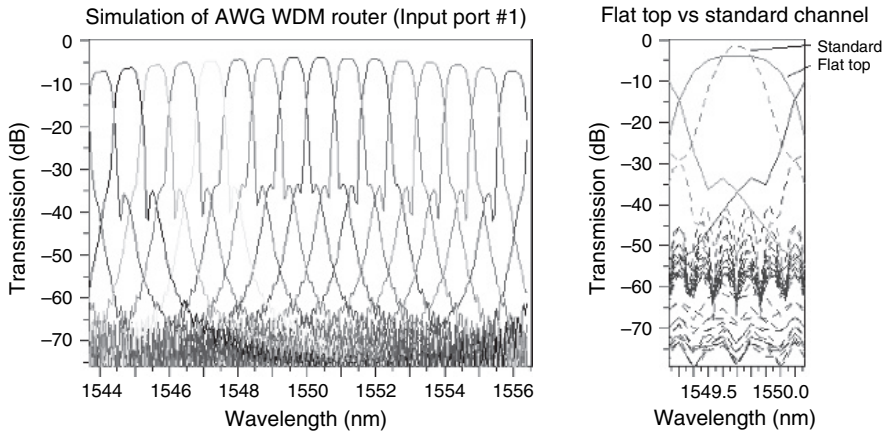

Figure 20.4 Spectral response of the 16 channel AWGR (left) with tapered input port, and comparison (left) of a single channel with (flat top) and without (standard) the taper (this figure may be seen in color on the included CD ROM).

This taper gives rise to the flattened spectral response of each channel, which can be seen in Figure 20.4, along with a magnified view of a single channel with both flattened and un-flattened responses. Precise simulation of this taper is critical for accurate prediction of this device's spectral performance, which is important due to the trade-off between flatness and crosstalk.

The Finite-Difference Time-Domain (FDTD) Method

This section describes the well-known finite-difference time-domain (FDTD) technique [4, 5]. The FDTD method is a rigorous solution to Maxwell's equations and does not have any approximations or theoretical restrictions. This method is widely employed as a propagation solution technique in integrated optics, especially in situations where solutions obtained via other methods such as the BPM cannot cope with the structure geometry or other aspects of the problem.

Background The FDTD method is essentially a direct solution of Maxwell's curl equations. Consider a region of space that contains no flowing currents or isolated charges. Maxwell's curl equations in can be written in Cartesian coordinates as six coupled equations for the components of **E** and **H**. Two examples are

$$\begin{aligned} \frac{\partial H_x}{\partial t} &= -\frac{1}{\mu}\left(\frac{\partial E_y}{\partial z} - \frac{\partial E_z}{\partial y}\right), \\ \frac{\partial E_y}{\partial t} &= -\frac{1}{\varepsilon}\left(\frac{\partial H_x}{\partial z} - \frac{\partial H_z}{\partial x}\right). \end{aligned} \tag{20.5}$$

The other four equations are analogous.

Maxwell's equations describe a situation in which the temporal change in the **E** field is dependent upon the spatial variation of the **H** field, and vice versa. The FDTD method solves Maxwell's equations by first discretizing the equations via central differences in time and space and then numerically solving these equations in software.

The most common method to solve these equations is based on Yee's mesh [4] and computes the **E** and **H** field components at points on a grid with grid points spaced Δx, Δy, and Δz apart. The **E** and the **H** field components are then interlaced in all three spatial dimensions as shown in Figure 20.5. Furthermore, time is broken up into discrete steps of Δt. The **E** field components are then computed at times $t = n\Delta t$ and the **H** fields at times $t = (n + 1/2)\ \Delta t$, where n is an integer representing the compute step. This method results in six equations that can be used to compute the field at a given time and mesh point, denoted by integers i, j, k, from neighboring field components at prior times. For example, two of the six are

$$\begin{aligned} H^{n+1/2}_{x(i,j,k)} &= H^{n\ \ 1/2}_{x(i,j,k)} + \frac{\Delta t}{\mu \Delta z}\left(E^{n}_{y(i,j,k)} - E^{n}_{y(i,j,k\ \ 1)}\right) - \frac{\Delta t}{\mu \Delta y}\left(E^{n}_{z(i,j,k)} - E^{n}_{z(i,j\ \ 1,k)}\right), \\ E^{n+1}_{x(i,j,k)} &= E^{n}_{x(i,j,k)} + \frac{\Delta t}{\varepsilon \Delta y}\left(H^{n+1/2}_{z(i,j+1,k)} - H^{n+1/2}_{z(i,j,k)}\right) - \frac{\Delta t}{\varepsilon \Delta z}\left(H^{n+1/2}_{y(i,j,k+1)} - H^{n+1/2}_{y(i,j,k)}\right). \end{aligned} \tag{20.6}$$

These equations are iteratively solved in a leapfrog manner, alternating between computing the **E** and **H** fields at subsequent $\Delta t/2$ intervals.

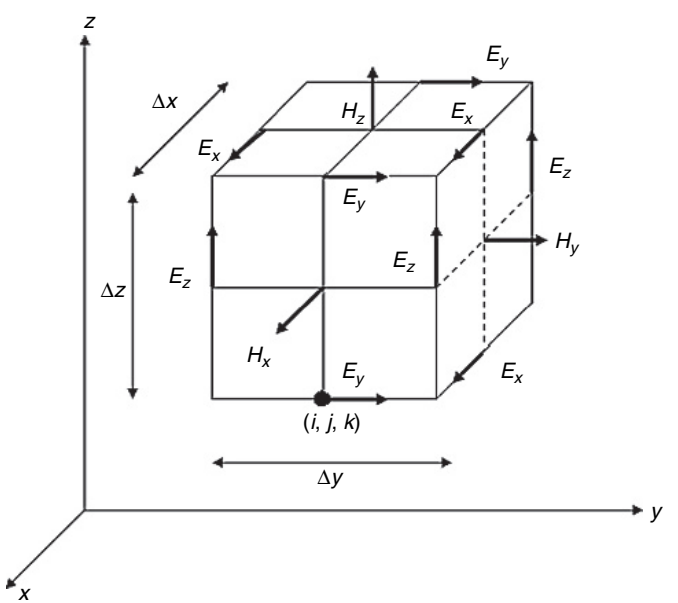

Figure 20.5 The Yee cell showing the placement of field components in FDTD [4].

While the above brief overview considers only the simplest physical situation, the FDTD method is very general and can be used to model anisotropic materials, dispersion, gain, and nonlinearities, for example. Further details of the method can be found in many well-known texts (e.g., Ref. [5]).

Applications The first FDTD example demonstrates guiding the flow of light through a two-dimensional (2D) photonic crystal (PC) by the introduction of 1D line defects. The PC structure consists of a rectangular array of silicon rods ($n = 3.4$), with a period $a = 0.6\,\mu\text{m}$, surrounded by air. Since we are simulating a 2D structure the rods are considered to extend to infinity outside the plane of the page.

The bandgap of the above structure for the TE polarization lies between 0.4 and 0.5 $\omega a/2\pi c$. When light at $\lambda = 1.33\,\mu\text{m}$ (corresponding to $\omega a/2\pi c = 0.45$) is introduced into the defect, it is guided by the line defect and does not escape into the PC, since the frequency of the guided mode falls within the photonic band gap. Figure 20.6(a) demonstrates that linear defects in PBG materials can act as efficient waveguides, transmitting light around extremely sharp corners (radius of curvature $\sim\lambda$) with relatively small losses. Figure 20.6(b) shows light being guided along a "T" defect in the 2D PC. In addition to the above simple examples, more complex devices like resonant add drop filters and other integrated optical components can be easily studied using the FDTD technique. Potentially, these applications can lead to the design of new compact integrated optoelectronic or all-optical circuits [6, 7].

The second FDTD example is a GaN-based light-emitting diode (LED) with a structured PC pattern at the traditional semiconductor air interface. The PC pattern on top has a periodic variation characterized by a period, duty cycle, depth, indices, and variation profile. FDTD can be used to study the performance of the LED device and to verify the final design. The structure shown schematically in Figure 20.7(a) is comprised of 0.5 μm of GaN ($n = 2.67$) grown on top of a sapphire substrate. The PC pattern on top has a period of 0.5 μm and an etch depth of 0.1 μm.

To simulate a realistic multiple quantum well launch the FDTD excitation consists of a large array of dipole sources with random orientations and phases, distributed

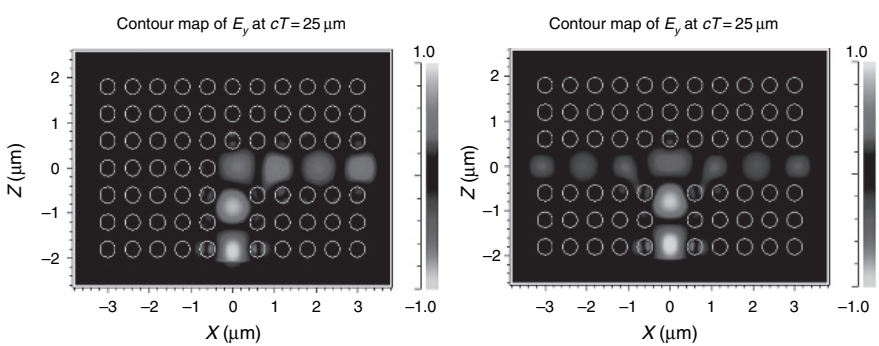

Figure 20.6 Field being guided along (a) sharp 90° bend and (b) "T" structure, generated by introducing line defects in a 2D photonic crystal (this figure may be seen in color on the included CD ROM).

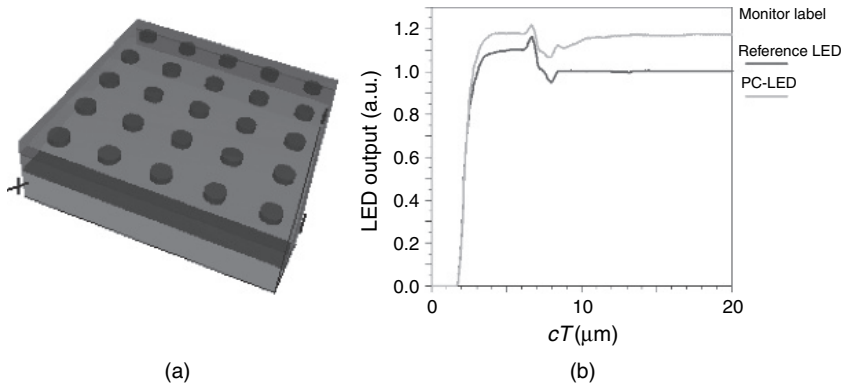

Figure 20.7 (a) Schematic of LED structure with an air hole array. (b) Time evolution of the output power of the LED (right). Patterning a PC structure at the material air interface on top enhances the light extraction efficiency. Data are normalized such that the saturated value for the reference LED, i.e., without the PC structure on top, is 1 (this figure may be seen in color on the included CD ROM).

evenly over an active layer plane. Two simulations are run: one with a structured PC pattern on top and another with an unstructured semiconductor air interface (reference LED). The results presented in Figure 20.7(b) show that the structured PC pattern clearly allows more light to pass through the semiconductor air interface. In addition, several simulations can be performed to maximize the light extraction efficiency to find optimal values for the parameters that describe the periodic variation of the PC.

The Finite Element Method

A prominent method for solving boundary value problems is the finite element method (FEM). While prominent in a wide variety of fields, such as thermodynamics and fluid mechanics, there are versions of the method that can be used to solve the vector wave equation of electromagnetics.

Background Consider the source-free time-harmonic form of the wave equation in a lossy anisotropic media is given by [8]

$$\nabla \times \left(\frac{1}{\mu_r} \times \left(\nabla \times \vec{E} \right) \right) - k_0^2 \varepsilon_r \vec{E} = 0, \quad \hat{n} \times \vec{E} = 0 \tag{20.7}$$

where μ and ϵ are complex diagonal tensors, and the field is assumed to vanish at the edge of the domain. The FEM does not solve the boundary value problem of Eqn (20.7) directly, but rather a related equation that can be arrived at in several ways. The first is the Ritz method, whereby a variational expression, or functional, is constructed from the operator of the differential equation. If the operator is self-adjoint and positive definite, the solution can be found by minimizing this functional. The second approach is the Galerkin method, a weighted residual method in

which the residual of the differential equation is minimized to determine the solution. Both methods use an expansion basis that exists over the entire domain, to represent the solution. Since such a basis may be difficult to find for an arbitrary problem, the FEM subdivides the domain into a collection of cells, or elements, for which a simple basis can be defined. This basis vanishes outside the element, so that the final solution is just a summation over the solutions of all the elements in the domain.

For the electromagnetics problem defined by Eqn (20.7), the hybrid node/edge vector FEM with perfectly matched layer (PML) boundary conditions is most commonly used. PML allows for leaky propagating and dielectric cavity modes to be determined. The functional for Eqn (20.7), in 2D, over domain A, as generated by the Ritz method, is given by [8]

$$F(\vec{E}) = \frac{1}{2}\iint_A \left[\left(\nabla \times \vec{E}\right) \cdot \frac{1}{\mu} \cdot \left(\nabla \times \vec{E}\right) - k_0^2 \vec{E} \cdot \varepsilon \cdot \vec{E}\right] \mathrm{d}A \tag{20.8}$$

For propagating [9 13] and leaky modes [14], a separable field ansatz, $E(x, y, z) = E(x, y)\exp(\ \mathrm{j}\beta z)$, where β is the modal propagation constant along z, is substituted in, and the following field transform is made:

$$\begin{aligned} \vec{E}'_{\mathrm{T}} &= \beta \vec{E}_{\mathrm{T}}, \\ E'_z &= -\mathrm{j}E_z. \end{aligned} \tag{20.9}$$

and the interpolant basis is applied. The transverse components are expanded in a vector (edge element) basis,

$$\vec{E}'_{\mathrm{T}}(x, y)\mathrm{e}^{\ \mathrm{j}\beta z} = \sum_{i=1}^{n} \vec{N}_i E'_{\mathrm{T}i} = \sum_{i=1}^{n} \{U\hat{x} + V\hat{y}\}_i E'_{\mathrm{T}i}, \tag{20.10}$$

where the $E'_{\mathrm{T}i}$ are the values of the (transformed) field along each edge (or portion of each edge, depending on the order). The longitudinal component (perpendicular to the plane of the element) is represented by a scalar (node element) basis,

$$E'_z(x, y)\mathrm{e}^{\ \mathrm{j}\beta z} = \sum_{i=1}^{n} N_i E'_{zi}, \tag{20.11}$$

where the E'_{zi} are the values of the (transformed) field at each node, and n is the dimension of the basis, which depends on the geometry of the element and the order of the interpolation. Lastly, the functional is minimized,

$$\frac{\partial F}{\partial E_i} = 0, \tag{20.12}$$

yielding a matrix eigenvalue equation with β^2 as the eigenvalue. Scattering and cavity modes [15 17] can also be determined from nearly the same functional. The

initial form of the interpolant basis functions, *N*, for the edge-based vector FEM is most commonly attributed to Nedelec [18].

Applications The FEM, described in the previous section, has several advantages over other methods. Since it is fully vectorial, so all the field components can be generated simultaneously. The elements can be a variety of shapes and sizes [13], amenable to both structured and unstructured meshes. Other efficiencies of FEM include the rapid convergence of the eigenvalues in higher order FEM, even on coarse grids. Furthermore, boundary conditions may be applied to exploit the symmetry of a problem. For example a common formulation treats azimuthal symmetry [16, 17] (i.e., body of revolution BOR) which is ideal for cylindrical vertical cavity surface-emitting lasers (VCSELs) and microdisk resonators. Thus, the FEM can be efficiently applied to complex geometries and in various coordinate systems. Lossy and high index contrast materials can also be accommodated. Multiple modes can be calculated simultaneously with the FEM, and depending on the type of eigenvalue solver, modes near a certain eigenvalue can be selected. A wide variety of applications benefit from the use of FEM, including photonic crystal fibers (PCFs) (even those not governed by total internal reflection), VCSELs, polarization converters, and slotted waveguides, to name a few.

Example 1: Fundamental Propagating Mode of a PCF Fiber. The first FEM example is an air-core PCF. PCFs are typically formed from the extrusion of a stack of glass rods or tubes, which gives the fiber a finite periodic lattice-like cross section. Numerous variations are possible, allowing the designer to control the number of modes, modal and coupling losses, polarization, and dispersion of the fiber. One such structure is shown schematically (length along *Z* not to scale) in Figure 20.8. It is comprised of several rings of hexagonally stacked air holes of

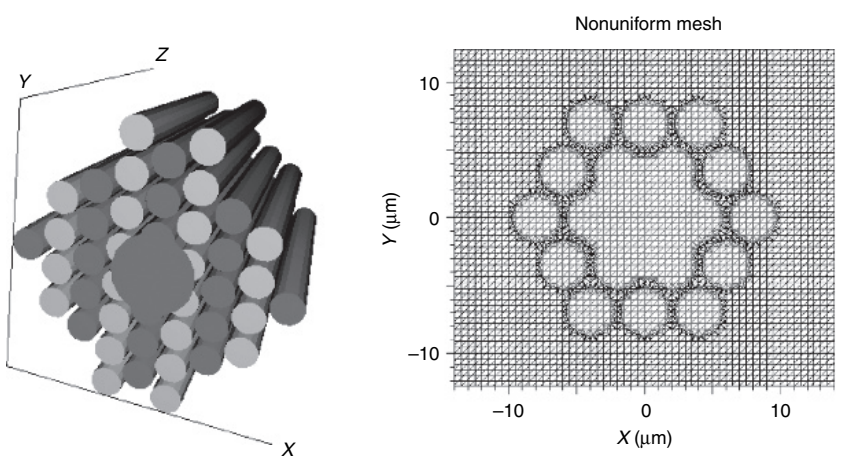

Figure 20.8 Schematic of the PCR (left) and corresponding nonuniform mesh (right) (this figure may be seen in color on the included CD ROM).

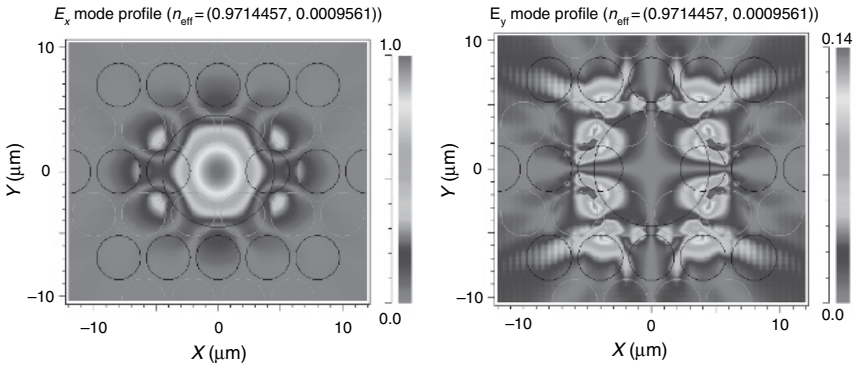

Figure 20.9 E_x component (left) and E_y component (right) of the fundamental PCF mode (this figure may be seen in color on the included CD ROM).

diameter ∼3.514 μm with center-to-center separation of 4 μm within a silica medium ($nr \sim 1.45$). The larger air hole in the center (red) intersects with the smaller holes forming a noncylindrical central core of air, the actual shape of which can be seen clearly, also in Figure 20.8.

Figure 20.9 shows the E_x and E_y components of the fundamental mode superimposed on the outline of the structure. Calculated at a free space wavelength of ∼2.79 μm, the mode is clearly well confined to the core, though some of the evanescent tail extends into the first ring. Note that the E_y component has only ∼14% the peak amplitude of the E_x component (the E_z component, not shown, has ∼25%).

Example 2: Fundamental Propagating Mode of a Polarization Converter. The second FEM example is a polarization converter, a necessary component in PICs that have polarization sensitivity, such as filters, interferometers, and switches. In this example, an asymmetric slanted ridge waveguide is used to rotate the polarization of a linearly polarized launch field. This results from the beating between the two strongly hybridized fundamental modes that are excited by the launch field with almost equal intensity. FEM is well suited to the design of waveguides that support such modes and that have the desired beat length. The structure shown schematically in Figure 20.10 is comprised of 1.3 μm of GaAs ($nr = 3.37$) grown on 6 μm of $Al_{0.1}Ga_{0.9}As$ ($nr = 3.324$). The ridge width is 2.45 μm and the etch depth is 1.2 μm with a sidewall elevation angle of 53° [19]. The nonuniform mesh used in the simulation is also shown in Figure 20.10.

Figure 20.11 shows the E_x and E_y components of the first fundamental hybridized mode, superimposed on the outline of the waveguide structure. Calculated at a free space wavelength of 1.55 μm, the mode clearly shows nearly equal amplitude in both the components (E_y ∼86% of E_x). The other mode would have a slightly dominant E_y component. The resulting half beat length for this device is ∼724 μm, making it relatively compact, a desirable quality for minimizing chip real estate.

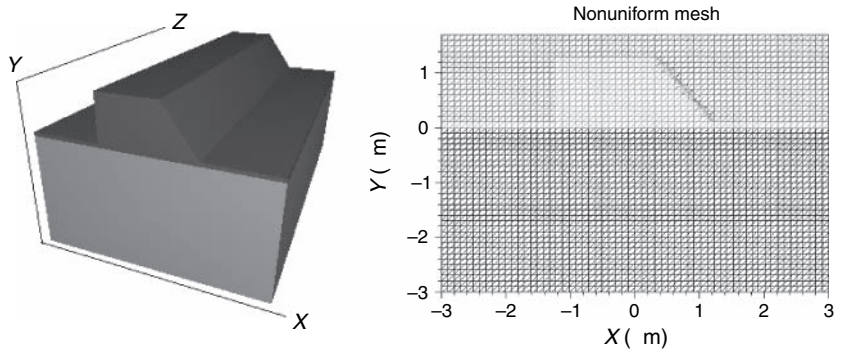

Figure 20.10. Schematic representation of the polarization rotator (left) and corresponding nonuniform mesh (right) (this figure may be seen in color on the included CD ROM).

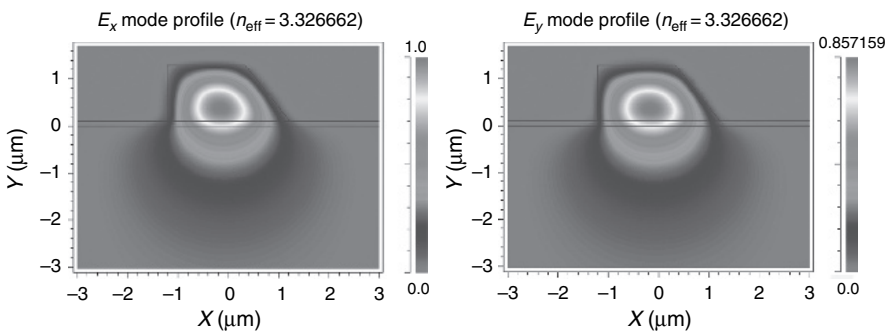

Figure 20.11 E_x component (left) and E_y component (right) of one of the fundamental hybridized modes (this figure may be seen in color on the included CD ROM).

The Plane Wave Expansion Method for Photonic Band Structure Calculation

The introduction of the concept of photonic band gap materials by Yablonovitch [20] and John [21] in the late 1990s created the need for rigorous calculation of the electromagnetic properties of periodic media. Transmission and propagation problems in these systems is largely modeled using FDTD and other finite-difference methods, but the basic physics of perfectly periodic photonic systems has largely been revealed through the plane wave expansion (PWE) method.

Background and Theory Consider harmonic-time solutions to Maxwell's equations propagating in an arbitrary system at frequency $\omega = 2\pi c/\lambda$. From Maxwell's

equations, it is easy to derive the vector Helmholtz equation for the magnetic field $\mathbf{H}(\mathbf{x})$[1]

$$\nabla \times \left(\frac{1}{e(\mathbf{x})} \nabla \times \right) \mathbf{H}(\mathbf{x}) = \frac{w^2}{c^2} \mathbf{H}(\mathbf{x}). \tag{20.13}$$

Now suppose that the dielectric constant function $e(\mathbf{x})$ varies periodically in one, two or three dimensions, a system known as a *PC* (though 1D structures probably do not warrant the term PC [22]). For example, for 3D periodicity we have $e(\mathbf{x}) = e(\mathbf{x} + l\mathbf{a} + m\mathbf{b} + n\mathbf{c})$ for some *lattice vectors* **a**, **b**, and **c**. By the Bloch Floquet theorem [23], we immediately know that the solutions must be expressible in the form

$$\mathbf{H}_{n,\mathbf{k}}(\mathbf{x}) = \mathrm{e}^{\mathrm{i}\mathbf{k}\cdot\mathbf{x}} \mathbf{u}_{n,\mathbf{k}}(\mathbf{x}), \tag{20.14}$$

where the $\mathbf{u}_{n,\mathbf{k}}(\mathbf{x})$ are functions that have the same periodicity as the medium, the Bloch vector **k** lies in the *first Brillouin zone* [23], and the index n labels the solutions by their *photonic band*. We can then express the Bloch functions as a Fourier series over the *reciprocal lattice* $\mathbf{G}_j$ of the structure (i.e., a PWE) so that

$$\mathbf{H}_{n,\mathbf{k}}(\mathbf{x}) = \sum_{j=\ \infty,\, s=0,1}^{j=\infty} c_{j,s} \hat{\mathbf{h}}_{j,s} \mathrm{e}^{\mathrm{i}\left(\mathbf{k}+\mathbf{G}_j\right)\cdot\mathbf{x}} \tag{20.15}$$

with $\hat{\mathbf{h}}_{j,s}$ a set of polarization vectors. To solve the problem, we insert Eqn (20.15) in Eqn (20.13) and then find the expansion coefficients $c_{j,s}$ and eigenvalues w_n for a given Bloch vector **k**.

Numerical Solution To obtain a numerical solution, we truncate the expansion Eqn (20.15) at a number of plane waves N large enough to resolve the modes and structure accurately, and yet small enough to solve in an acceptable amount of time. A direct substitution of Eqn (20.15) into Eqn (20.13) then yields a matrix eigenvalue problem of finite size. Solving this equation, Ho et al. [24] were the first to show that certain 3D PCs could exhibit a complete *photonic band gap* a range of frequencies for which no electromagnetic states exist. Figure 20.12 shows the *photonic band structure* and first Brillouin zone for a lattice of spheres in a diamond configuration. The range of forbidden frequencies is clearly visible. In fact, plots such as that in Figure 20.12(a) do not show the complete band structure which is defined throughout the first Brillouin zone (so each band would be a surface in a four-dimensional space). Instead, it is convenient and universal to display the bands along certain high-symmetry directions of the Brillouin zone. The extrema of bands and hence the boundaries of the gaps always occur along such directions.

[1] In the photonic crystal literature, this equation is frequently (and somewhat regrettably), referred to as the "master equation."

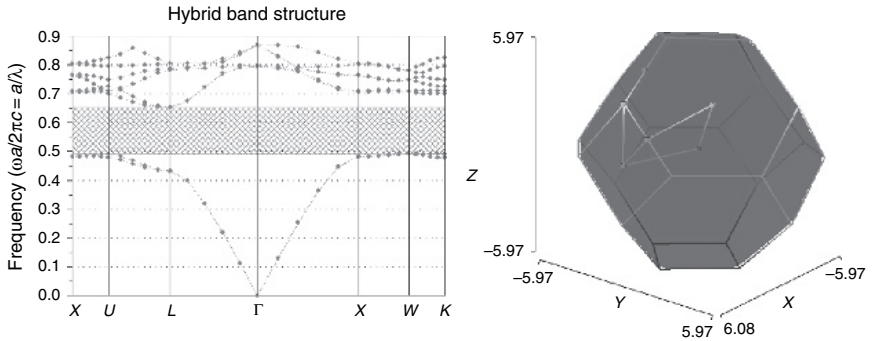

Figure 20.12 (a) 3D band structure for a diamond lattice of spherical air holes of radius 0.325*a* in a background of refractive index 3.606 (*a* is the lattice period). (b) First Brillouin zone for the diamond lattice (this figure may be seen in color on the included CD ROM).

Figure 20.13 illustrates the relationship between the complete band structure and the conventional display for a 2D square lattice of rods.

The formulation of Eqn (20.13) as a matrix eigenproblem has two significant difficulties it is numerically intensive and demanding in memory, and there is an ambiguity in how to perform the inversion of the dielectric tensor in a truncated basis. These difficulties were resolved in a landmark paper by Meade et al. [25]. Following the ideas from the condensed matter literature, they consider Eqn (20.13) as a sequence of linear operators applied to the magnetic field **H(x)**. The curl operations are performed in Fourier space and the multiplication by the reciprocal of the dielectric tensor is performed in real space. Conversion between the two domains is accomplished using fast Fourier transforms (FFTs) for which

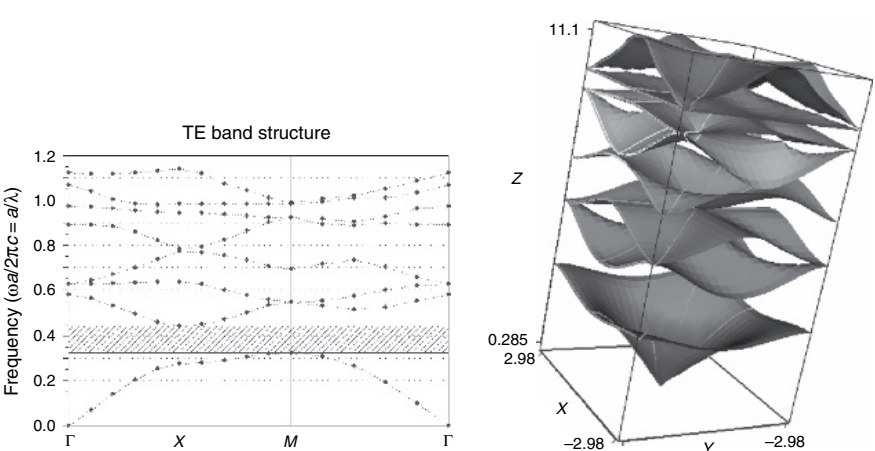

Figure 20.13 (a) Conventional band structure for a 2D lattice of cylindrical rods of index 2.983 and radius 0.2*a*. (b) Complete band structure for the same system (this figure may be seen in color on the included CD ROM).

very fast implementations are available. In this way, all operations are diagonal and the memory required is of the order of the number of expansion coefficients, rather than the square of this number. The linear operator in Eqn (20.13) turns out to be Hermitian, and so the actual eigensolutions can be obtained in a Rayleigh Ritz fashion by minimizing the functional $\langle \mathbf{H}(\mathbf{x})|\hat{\Theta}|\mathbf{H}(\mathbf{x})\rangle / \langle \mathbf{H}(\mathbf{x})|\mathbf{H}(\mathbf{x})\rangle$. Typically, this is done using a standard algorithm such as conjugate gradients or more sophisticated variants [26]. The vast majority of plane wave calculations in the last 15 years have being performed with this approach. Extensions to include anisotropy and improve the moderate convergence properties associated with PWE of discrete jumps in refractive index have also been developed [26].

Advantages, Restrictions, and Extensions The PWE method has a number of advantages. It is fast, relatively easy to implement and robust in the sense that it automatically finds all the bands from the lowest up, and is untroubled by degenerate bands. Modal field profiles are available without extra cost and derived quantities such as group velocities [27] and densities of states can be found [28]. It is also easy to incorporate certain symmetry properties to improve performance and separate modes of different type.

However, due to its mathematical structure, the PWE method suffers from a number of restrictions. Firstly, the requirement of a Hermitian dielectric tensor means that lossy materials including metals can not be handled. Similarly, the standard approach of finding each band successively at fixed $\mathbf{k}$ means that material dispersion is also not easily incorporated. While these problems have been solved in a number of special cases, the solutions tend to involve specific dispersion relations or restrictions to particular polarization or 2D problems. When dispersion or loss must be accounted for, a better approach is to adopt a formalism in which the frequency w is the free parameter and the eigenvalue is $\mathbf{k}$. Pearce et al. [29] have presented a detailed example of such a method but to date it seems to have been largely applied to PCFs only.

Nonperiodic Problems Although we have presented the PWE method in terms of periodic structures, in fact many of its applications involve systems that are not strictly periodic. Two well-known examples are modeling the properties of the resonances of defects in finite PCs and the guided modes of PCFs. In such cases, the *supercell approximation* is invoked. To recover a periodic system, one considers an infinite array of the finite structures. If the repeated unit is sufficiently large, then the coupling between neighboring defects is negligible and the eigenvalues of the supercell system approach those of the isolated system. By imposing this artificial periodicity, we do change some of the physics. For example, the resonances of a defect in a finite crystal are strictly leaky modes with loss rates that can only be found with a calculation involving open boundaries. In contrast, the frequency eigenvalues of a supercell calculation are always real. Often this approximation is unimportant though. For example, the modes of air-core PCFs are strictly leaky. In practice, however, the loss due to the finite crystal is small

compared to other loss channels due to structural imperfections, and the PWE has found important application in these fibers [30].

Applications In terms of the sheer numbers of calculations performed, the PWE method certainly finds the most use as a tool for calculating the band structures of perfect PCs and modes of defect states. However, it has been applied to a host of other interesting systems such as dispersive modes of defect waveguides in 2D PC slabs [31] or the symmetry properties of modes of unusual waveguides [32]. Here we briefly discuss a particularly diverting application the superprism [33].

Superprism dispersion An interesting aspect of PC physics that is less well-known than the photonic band gap effects is the behavior of light propagation *within* bands. Even though propagation is permitted at such frequencies, it involves highly unusual dispersive behaviour such as autocollimation and beam-steering which is highly dependent on input angle and wavelength. Understanding this behavior requires accurate knowledge of the dispersion. The behavior of light at the interface to a PC is particularly interesting. The diagram in Figure 20.14(a) shows how to determine the direction of a refracted beam. The argument is based on conservation of the component of the wavevector parallel to the crystal surface which is oriented vertically. The curves represent the *iso-frequency contours* outside and inside the crystal which are the allowed wave solutions and are found by PWE. Wavevector conservation shows that the allowed outgoing wavevectors are the red arrows. But the direction of energy propagation is given by the normal to the iso-frequency contour shown by the green arrows. It is apparent that a small change in the direction of the incoming (blue) wavevector can produce dramatic changes in the direction of the outgoing (green) vector. The performance of a superprism is a remarkably sensitive phenomenon given the relative simplicity of the device. Figure 20.14(b) shows the *resolution parameter* of a superprism constructed from a square PC [34, 35]. The light areas are regions of very high resolution, and the dark regions of low resolution. Such detail requires calculation of the band structure at tens of thousands of points throughout the first Brillouin zone and depends upon the high speed of the PWE method.

Rigorous Coupled Wave Analysis for Periodic Structures

In many cases, it is desired to model propagation through a periodic structure. In this case, the periodicity can be exploited in a manner similar to the PWE method of the previous section. In the literature, several algorithms exist which are based on rigorous coupled wave analysis (RCWA) [36 38] and enhanced with modal transmission line (MTL) theory [39, 40], and are fully vectorial rigorous solutions of Maxwell's equations.

Background The RCWA [36 38] represents the electromagnetic fields as a sum over coupled waves. A periodic permittivity function is represented using Fourier harmonics. Each coupled wave is related to a Fourier harmonic, allowing the full

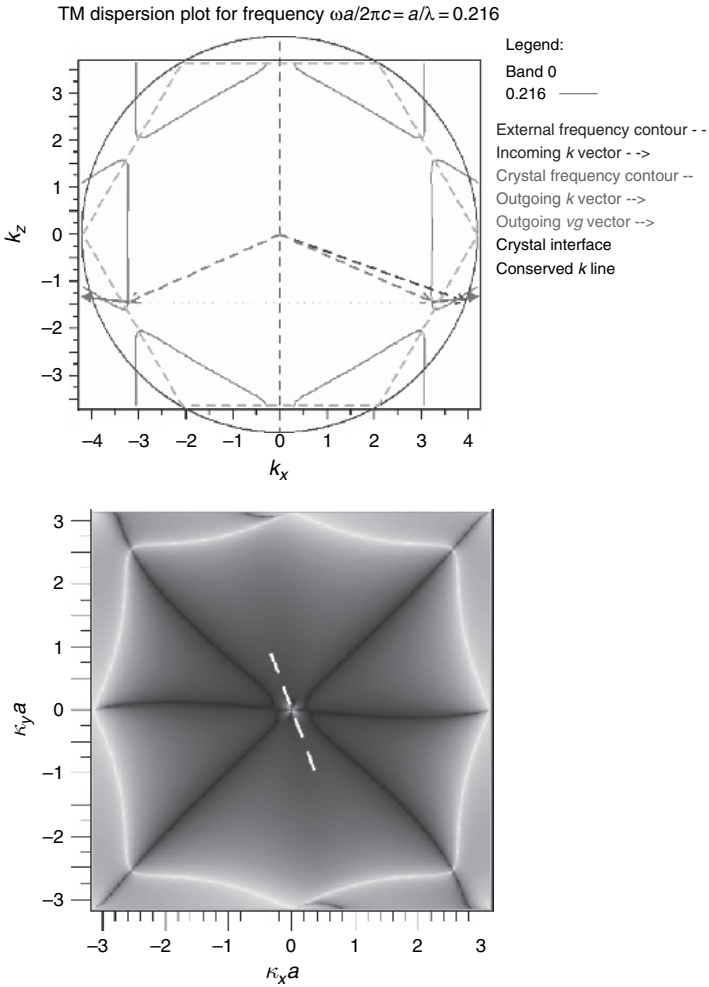

Figure 20.14 (a) Wavevector construction for superprism refraction at the surface of a 2D hexagonal photonic crystal. A wave in free space (blue arrow) is refracted into a wave in the crystal lying on the red iso frequency contour. The refraction direction is determined by conservation of the tangential component of momentum. (b) Map of the resolving power of a superprism (this figure may be seen in color on the included CD ROM).

vectorial Maxwell's equations to be solved in the Fourier domain. The MTL [39, 40] approach is equivalent to RCWA, except that MTL uses summations over individual modes to represent the electromagnetic fields. This method has the advantage of describing the fields in terms of an equivalent transmission-line network, which yields physical insight for various applications using different mechanisms. Another benefit of the MTL method is that it eliminates possible stability problems, which may be encountered in other numerical schemes, such as the transfer matrix method.

The geometry is assumed to consist of homogenous incident and outgoing regions, with an arbitrary, but periodic structure sandwiched between them. For typical scattering problems, we want to calculate the reflected and transmitted light waves from the incident field. The structure is sliced along the primary direction, z, into "layers." Within each layer the structure is assumed independent of z, and periodic in the transverse directions x and y. According to Bloch's Theorem, the transverse field components in a periodic layer can be expressed as

$$E_x = e^{i\left(k_{x,0}x+k_{y,0}y\right)} \sum_p \sum_q e^{i\left(\frac{2\pi}{\Lambda_x}px+\frac{2\pi}{\Lambda_y}qy\right)} \sum_m a_{x,m,p,q}\left(f_m e^{i\kappa_m z} + g_m e^{\ i\kappa_m z}\right),$$

$$E_y = e^{i\left(k_{x,0}x+k_{y,0}y\right)} \sum_p \sum_q e^{i\left(\frac{2\pi}{\Lambda_x}px+\frac{2\pi}{\Lambda_y}qy\right)} \sum_m a_{y,m,p,q}\left(f_m e^{i\kappa_m z} + g_m e^{\ i\kappa_m z}\right),$$

$$H_x = e^{i\left(k_{x,0}x+k_{y,0}y\right)} \sum_p \sum_q e^{i\left(\frac{2\pi}{\Lambda_x}px+\frac{2\pi}{\Lambda_y}qy\right)} \sum_m b_{x,m,p,q}\left(f_m e^{i\kappa_m z} - g_m e^{\ i\kappa_m z}\right),$$

$$H_y = e^{i\left(k_{x,0}x+k_{y,0}y\right)} \sum_p \sum_q e^{i\left(\frac{2\pi}{\Lambda_x}px+\frac{2\pi}{\Lambda_y}qy\right)} \sum_m b_{y,m,p,q}\left(f_m e^{i\kappa_m z} - g_m e^{\ i\kappa_m z}\right).$$

Substituting the above into Maxwell's equations results in an eigenvalue problem for the modes:

$$\mathbf{A}\mathbf{x} = \lambda\mathbf{x},$$

where $\lambda = \kappa_m^2$ is the eigenvalue to be calculated, and the a and b coefficients in the field representations are derived from the corresponding eigenvectors.

A solution for the entire structure can be obtained using well-known transmission-line methods to solve the required boundary-value problem. The scattering characteristics can then be obtained in the following systematic fashion. The modal voltage and current amplitude for jth layer are

$$v_m^{(j)} = f_m^{(j)} e^{i\kappa_m z} + g_m^{(j)} e^{\ i\kappa_m z},$$
$$i_m^{(j)} = f_m^{(j)} e^{i\kappa_m z} - g_m^{(j)} e^{\ i\kappa_m z}.$$

The superscript j indicates that the various quantities are for a specific (jth) layer. Imposing the required boundary condition (at z_j^{j+1}) between the jth and $(j+1)$th layers result in

$$\sum_m \begin{pmatrix} a_{x,m,p,q} \\ a_{y,m,p,q} \end{pmatrix}^{(j)} v_m^{(j)}(z_j^{j+1}) = \sum_m \begin{pmatrix} a_{x,m,p,q} \\ a_{y,m,p,q} \end{pmatrix}^{(j+1)} v_m^{(j+1)}(z_j^{j+1}),$$

$$\sum_m \begin{pmatrix} b_{x,m,p,q} \\ b_{y,m,p,q} \end{pmatrix}^{(j)} i_m^{(j)}(z_j^{j+1}) = \sum_m \begin{pmatrix} b_{x,m,p,q} \\ b_{y,m,p,q} \end{pmatrix}^{(j+1)} i_m^{(j+1)}(z_j^{j+1}).$$

This approach not only facilitates physical insights into the problem but also provides important numerical advantages [39, 40].

Applications RCWA can be used to determine the reflection and transmission, from a periodic structure, of a plane wave, as a function of wavelength and incident angle. Numerous applications can benefit from this technique including out-coupling from surface gratings, diffractive optical element design, and metrology.

Figure 20.15 shows several reflected orders of a blazed surface grating at a particular wavelength. Each order is peaked at a different angle. The simulation can also be stepped through wavelength at a particular angle, to produce the optical spectrum. Figure 20.16 shows the field pattern of the 1 reflected order which is peaked at an angle of 20°. The periodicity is along x in this example.

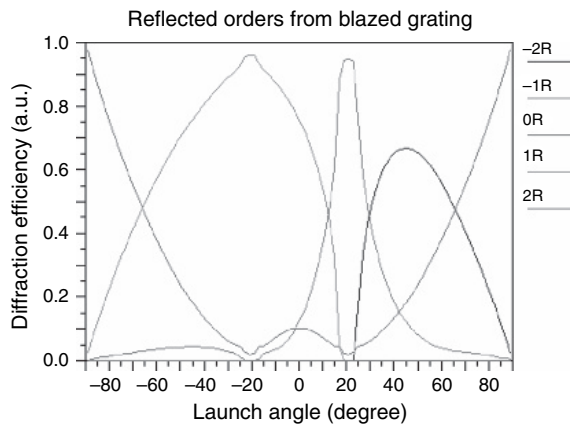

Figure 20.15 Diffraction efficiency of five reflected orders of a blazed surface grating (this figure may be seen in color on the included CD ROM).

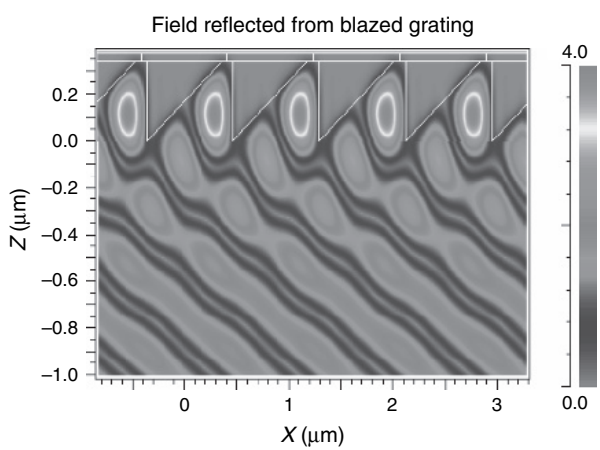

Figure 20.16 Field of the 1 reflected order (20° from normal) of a blazed grating (shown outlined in white and inverted, at top of figure) (this figure may be seen in color on the included CD ROM).

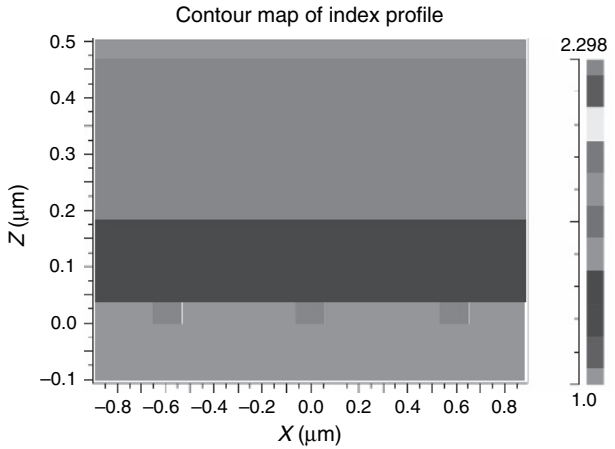

Figure 20.17 Surface filter with a very sharp resonance that is both a function of incident angle and wavelength (this figure may be seen in color on the included CD ROM).

Figure 20.17 depicts several periods of a resonant grating filter (RGF). These exploit a resonance condition that arises when incident light gets trapped in the waveguide via evanescent coupling. When this light is out-coupling again, it interferes destructively with the incoming light, producing very sharp resonances for narrow ranges of incident angle and wavelength. Hence only a few layers are needed for narrow band reflection. The angular dependence also provides a mechanism for tunability. The response of this filter is shown in Figure 20.18 as a contour plot of angle and wavelength. The first inset shows a cut along wavelength taken at 40° and the other inset shows a cut along angle taken at 1.55 μm.

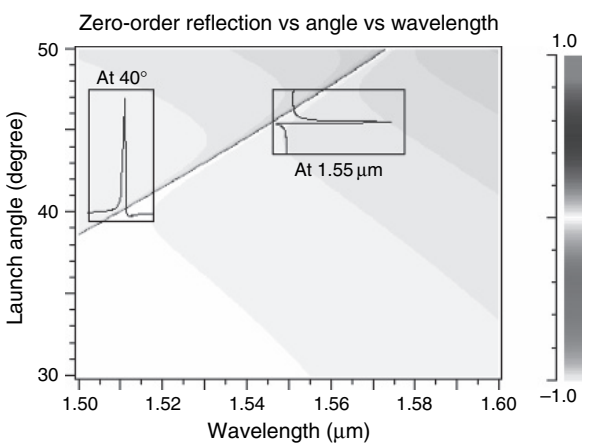

Figure 20.18 Filter response showing the linear variation of the peak with angle and wavelength along with insets showing a single angle (40°) and a single wavelength (1.55 μm) (this figure may be seen in color on the included CD ROM).

20.2.2 Active Optical Device Modeling

Active optical device modeling requires the simultaneous calculation of the optical field and the gain medium. For semiconductor-based active optical devices such as lasers, amplifiers, and modulators, the gain medium is pumped by carrier injection, requiring the solution of the electronic transport equations, and in some cases, the thermal transport equation as well. Various approaches are present in the literature, but generally fall into two broad categories; those that solve the coupled rate equations in time only and those that solve the transport equations on a spatial mesh. Additionally, there is a traveling wave approach which falls somewhere in between, accounting for time and one spatial dimension.

Background

The standard rate-equation approach typically includes the following three equations: the carrier density Eqn (20.16), the photon density Eqn (20.17), and the phase of the cavity mode Eqn (20.18) [41 46].

$$\frac{\mathrm{d}N}{\mathrm{d}t} = \frac{\eta_i I}{qV} - R^{\mathrm{spon}}(N) - R^{\mathrm{nr}}(N) - G(N,S)S, \tag{20.16}$$

$$\frac{\mathrm{d}S}{\mathrm{d}t} = -\frac{S}{\tau} + \Gamma\beta^{\mathrm{spon}}R^{\mathrm{spon}}(N) + \Gamma G(N,S)S, \tag{20.17}$$

$$\frac{\mathrm{d}\phi}{\mathrm{d}t} = \frac{\alpha}{2}\left(\Gamma G(N,S) - \frac{1}{\tau} + \frac{\varepsilon S}{\tau}\right). \tag{20.18}$$

Here, I is the injection current, N is the carrier density, S is the photon density, ϕ is the optical phase, η is the current injection efficiency, q is the electron charge, V is the cavity volume, τ is the photon lifetime, Γ is the confinement factor, β is the spontaneous emission coupling coefficient, α is the linewidth enhancement factor, and ϵ is a gain saturation parameter. Also, R represents the spontaneous and nonradiative recombination and G is the optical gain, both of which depend on carrier density and temperature. R and G have various analytic forms depending on which physical processes are being modeled. Standard methods for solving sets of coupled first-order differential equations, such as the fourth-order Runge Kutta method, are typically employed to resolve the above system.

The second approach, which is attempts to include the spatial variations of the carriers and fields, resolves the physical equations at the nodes of a spatial mesh, and is hence much more computationally intensive [49 51].

$$\nabla \cdot \varepsilon_{\mathrm{stat}} \nabla\varphi + q\left(N_{\mathrm{D}}^{+} - N_{\mathrm{A}} + p - n\right) = 0, \tag{20.19}$$

$$\frac{\partial n}{\partial t} + \nabla \cdot j_n + U = 0, \tag{20.20}$$

$$\frac{\partial p}{\partial t} + \nabla \cdot j_p + U = 0, \tag{20.21}$$

$$\nabla^2 E_m + \varepsilon_{\text{opt}} k_0^2 E_m = 0, \tag{20.22}$$

$$\frac{\partial S_{m,\omega}}{\partial t} = \left(G_{m,\omega} - \frac{1}{\tau_{n,\omega}} \right) S_{m,\omega} + R_{m,\omega}^{\text{spon}}. \tag{20.23}$$

The carrier dynamics are governed by the Poisson equation (20.19) and the continuity equations for electrons (20.20) and holes (20.21). Here, ϕ is the electrostatic potential, n and p are the electron and hole densities, respectively, and N_{D} and N_{A} are the ionized donor and acceptor concentrations, respectively. U represents the total generation and recombination, both radiative and nonradiative (such as Auger and Shockley Read Hall (SRH) recombination), while j is the current density. The optical equations are split into two parts; the first being a spatial part (20.22) from which the modal eigenvalues and field patterns, E, are determined. The second is the photon rate equation (20.23), which connects the photon population to the carrier densities via the modal gain, G, and spontaneous recombination R^{spon}. In most modern devices, there is the additional complication of quantum wells, which are used engineer the gain spectrum. These necessitate the solution of a multiband Schroedinger equation to determine the carrier distributions in energy and space, as well as their transition rates. The most common numerical approach for this is the KP method [52 57], which is a perturbation technique, typically employing a basis of four or eight bands. This system of equations must be solved self-consistently; usually by iterating between a fully coupled Newton Raphson solution of the transport (20.19 20.21) and photon rate equation (20.23), and independent solutions of the modes (20.22) and gain (KP method). Such an approach is inherently unstable and a variety of techniques are required to insure a convergent simulation.

Applications A broad range of devices may be simulated by the methods described in the previous section; Fabry Perot (FP) edge-emitting lasers, VCSELs, distributed feedback lasers (DFBs), semiconductor optical amplifiers (SOAs), LEDs, electroabsorptive (EA) modulators, and photodetectors (PDs) to name a few. The particular approach used depends on the information desired. For example, if the system performance (discussed in subsequent sections of this chapter) of the device is required, the rate-equation approach is better suited. However, if a particular geometry or material composition must be optimized to improve the design, then a spatial simulation is necessary. While empirical models for spatial hole burning, self-heating, and mode competition, can be found in the rate equation approach, a spatial simulation can give a clear picture of these effects and how they impact device performance. Additionally, numerous parameters can be calculated directly from the simulation results, such as modal confinement factors, nearfield and farfield patterns, energy bands, carrier densities, current fluxes, and

lattice temperature profiles. The following examples are spatial simulations of an FP laser and a VCSEL, and will be used to demonstrate the type of information that can be obtained from the spatial mesh approach, and its importance to device design.

Example 1: Fabry Perot Edge-Emitting Laser Diode. An FP laser is typically formed with a single or multiple quantum well active region surrounded by a separate confinement layer for optical confinement in the vertical (Y) direction. An etched ridge structure is used for optical confinement in the lateral direction (X). Finally, the device is cleaved front and back (Z), creating semiconductor air interfaces ($\sim$30% reflectivity) which form an FP cavity (shown schematically in Figure 20.19).

Figure 20.19 also shows the nonuniform simulation mesh that digitizes the structure. Note that the symmetry of the problem has been exploited for computational efficiency, and only the right half of the structure is simulated. Nonuniform meshing is critical to resolve all the layers of the device, which can vary in thickness by orders of magnitude, especially if quantum wells are present.

The simulation begins with a cold cavity mode calculation and the calculation of the material gain, both shown in Figure 20.20. In the case of FP lasers, the (longitudinal) mode density is so high that the lasing wavelength is assumed to track the gain peak (about 980 nm for this example). In other types of lasers, such as VCSELs and DFBs the cavity has better mode selectivity, and must be carefully designed so that the fundamental resonance collocates closely with the peak of the gain.

Next, the transport can be simulated, giving rise to the $L\ I\ V$ curve shown in Figure 20.21. From this information, the lasing threshold ($\sim$10 mA) and slope efficiency of the device can be determined. If temperature is included in the simulation, the $L\ I$ curve can begin to roll-off due to self-heating effects in the active region that cause the gain to saturate. The dynamic performance of the

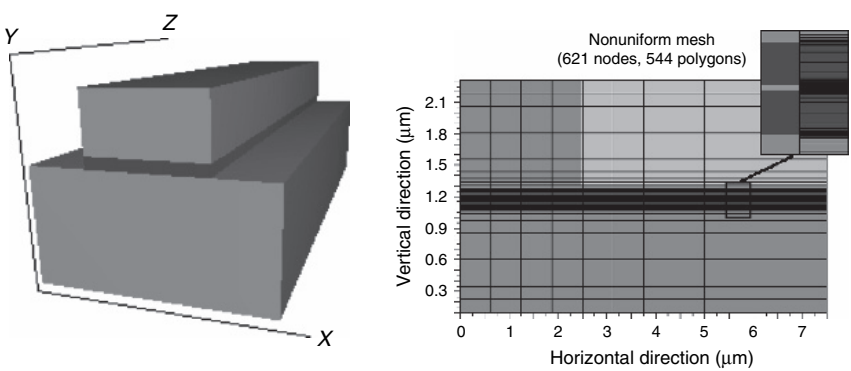

Figure 20.19 Schematic of a ridge (FP) laser (shown left), and nonuniform simulation mesh (shown right) superimposed on the device structure (only right half is simulated). The active region, with single quantum well, is shown in the inset (with and without the mesh) (this figure may be seen in color on the included CD ROM).

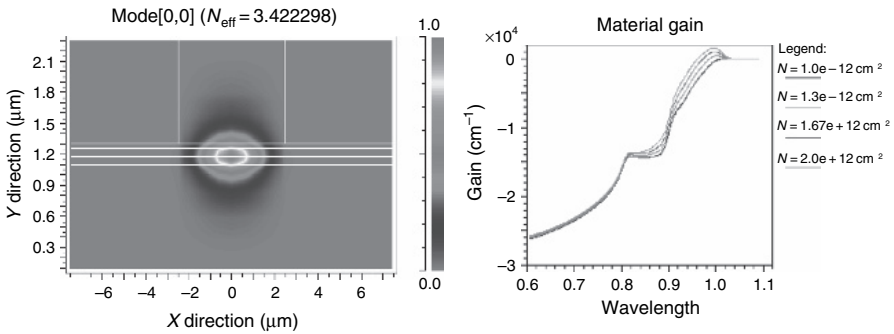

Figure 20.20 Fundamental mode (left) along with an outline of the structure (white), and material gain spectra (right) at several carrier densities, as generated by the KP method, for a single InGaAs/AlGaAs quantum well (this figure may be seen in color on the included CD ROM).

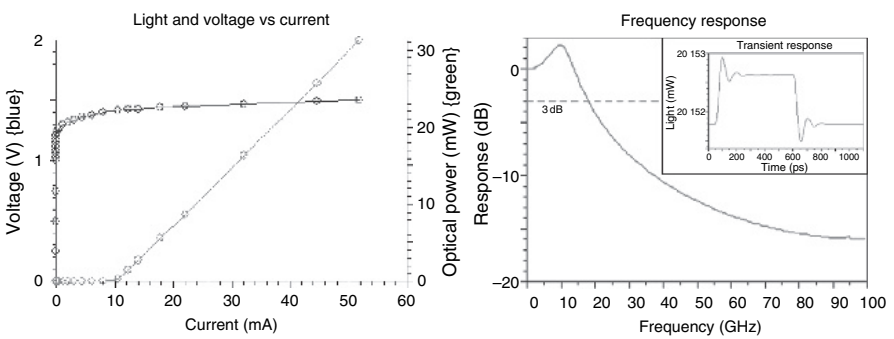

Figure 20.21 *L I V* curve for this device (left), and frequency response (right) at a bias of about 20 mA. The transient response of the light output to a small injected square pulse (right) is shown in the inset (this figure may be seen in color on the included CD ROM).

device can also be obtained from this type of simulation. For example, a small signal response can be obtained by injecting a small current pulse into the bias contact of the device and observing the resulting perturbation in the optical output power. Figure 20.21 also depicts both the time- and frequency-domain responses, revealing a 3dB cutoff frequency in the 15 20 GHz range, for this device.

Example 2: Vertical Cavity Surface-Emitting Laser. A VCSEL has several advantages over FP lasers. It emits from the surface of the chip, taking up less real estate, and has a mode that couples better to fibers. Also, the cavity mode selectivity ensures better stability of the lasing wavelength. However, a commensurate disadvantage is the increased thermal sensitivity, caused by temperature detuning between the lasing wavelength and the gain peak. Hence, many factors must be considered in the proper design of a VCSEL, making the use of simulation critical. In the following example, a cylindrical oxide aperture VCSEL is discussed. Shown schematically in Figure 20.22, this device has several GaAs/$Al_{0.2}Ga_{0.8}As$

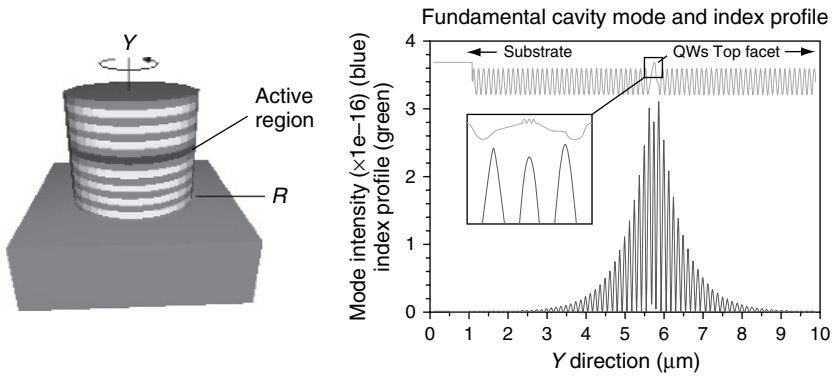

Figure 20.22 Schematic of a cylindrical VCSEL (left), and simulated mode and index profiles (right) (this figure may be seen in color on the included CD ROM).

quantum wells centered in a lambda cavity that is terminated by top (32 periods) and bottom (36 periods) DBR mirrors. Also, near the center of the cavity is a thin oxide layer with small diameter aperture that is responsible for confining modes and carriers toward the center of the cylinder, where their overlap will be optimal.

The vertical profile of the mode is also shown in Figure 20.22, along with the index profile. The inset shows an expanded view of the quantum wells and their overlap with the central intensity peak. Device operation is strongly dependent not only on how the mode overlaps with the quantum wells, but also on how it intersects with the oxide aperture. Figure 20.23 shows the transmission spectrum of the cavity superimposed with the material gain, at several temperatures and a constant sheet carrier density of 2×10^{12} cm^{-2}. Clearly, the gain peak undergoes a red shift with increasing temperature, that changes its relative position with respect to the lasing resonance, which remains fixed. This detuning results in a roll-over of

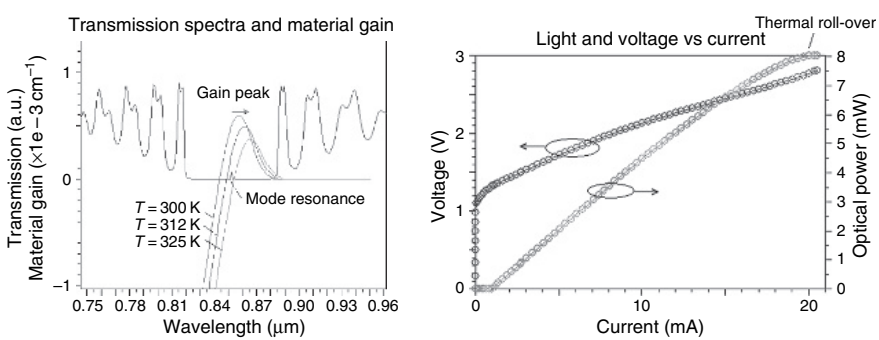

Figure 20.23 Transmission spectrum of the cavity shown superimposed with the material gain at several temperatures (left), and the *L I V* curve depicting the effects of thermal roll over (right) (this figure may be seen in color on the included CD ROM).

the $L\ I$ curve, also shown in Figure 20.23, and can actually cause the device to turn off at higher bias currents.

A caveat with active device simulation on a spatial mesh is that it requires accurate knowledge of many material parameters, and in the end, may still deviate from experimental results due to the un-simulated portions of the problem (i.e., those not within the simulation domain). For example, parasitic effects due to the laser die or package, or even due to the measurement apparatus itself, may cause discrepancies between simulation and experiment. The power of these simulations comes from their ability to show the performance trends of the device, as its material or geometric parameters are varied.

20.3 OPTICAL COMMUNICATION SYSTEM SIMULATION

In this section we explore system-level modeling. In optical communication system modeling, the information is represented by optical, electrical, and binary signals and is propagated from a transmitter to a receiver through various network components. Each component is modeled with equations representing the underlying physics to capture the way it processes its input signal to produce an output signal. Network components include optical fiber, DFB and VCSEL lasers, EDFA and SOA amplifiers, electrical and optical filters, photodetectors, electrical amplifiers, and many others.

The optical fiber is the medium in which the signal propagates for distances of up to thousands of kilometers. The fiber type divides optical communication systems into two main categories, single-mode and multimode. In single-mode systems the small fiber core diameter enables the propagation of only two degenerate modes, the X and Y polarizations. These systems ensure the highest bandwidth and reach. In multi-mode systems a larger fiber core enables the propagation of multiple modes, each characterized by its own loss, propagation constant, and spatial profile. These systems have lower bandwidth, but also advantage in terms of cost.

In this section, we describe some of the available methods for single- and multi-mode system simulation, with particular emphasis on optical fiber modeling. We also present some of the methods available for estimating system performance in terms of bit error rate (BER) and the related Q parameter. The following discussion is by no means exhaustive, and the interested reader can find further material in the references section.

20.3.1 Single-Mode Systems

As outlined above, single-mode systems incorporate a wide range of network components. Simulation requires modeling of each of these elements, thereby allowing a designer to assess the impact of transmitters, transmission media, and receivers on an optical link's overall performance. For example, a designer may

wish to compare the advantages and disadvantages of direct versus external modulation in the transmitter, or the impact of different optical amplification schemes on system performance. Arguably the fiber itself plays the largest role in determining a single-mode link's performance. Linear effects such as loss, dispersion, and polarization mode dispersion (PMD) can lead to pulse spreading which ultimately undermines the optical signal-to-noise ratio (OSNR) at the receiver. Nonlinear behaviors such as four-wave mixing (FWM), self-phase modulation (SPM), cross phase modulation (XPM), stimulated Brillouin scattering (SBS), stimulated Raman scattering (SRS), modulation instability, and parametric gain can further degrade a signal's transmission due to crosstalk and additional distortion effects. In this section, we discuss the system-level modeling of single-mode fiber, and present an example of single-mode system simulation.

The propagation of an optical pulse in a single-mode fiber is governed by the nonlinear Schrödinger equation, which can be written as

$$\frac{\partial A}{\partial z} + \beta_1 \frac{\partial A}{\partial t} + \frac{i}{2}\beta_2 \frac{\partial^2 A}{\partial t^2} + \frac{\alpha}{2}A = i\gamma |A|^2 A. \tag{20.24}$$

In Eqn (20.24), A is the complex field envelope, z is the distance, β_1 is inversely proportional to the group velocity ν_g, β_2 accounts for the group velocity dispersion (GVD), α accounts for the effects of fiber loss, and γ is the nonlinear coefficient. Equation (20.24) can be modified to include the effects of third-order dispersion, amplification, amplified spontaneous emission noise, and PMD to represent a more comprehensive model of single-mode optical fiber transmission [58 63].

Only the HE_{11} mode propagation is relevant in single-mode optical fiber systems. However, due to the circular symmetry of the fiber, there are two orthogonal HE_{11} solutions. Ideally, the two HE_{11} modes should be degenerate, but fiber birefringence can break the degeneracy. Therefore, it is important to account for the fact that the fiber propagation is bimodal, and that both linear and nonlinear phenomena shuffle optical power between the two modes in complicated ways. This mode mixing of the propagating light can impact certain effects that need a high degree of coherence to develop. Linear and nonlinear birefringence, PMD, FWM, and sideband instability (SI) are a few of the phenomena that require a bimodal or vector signal representation to be properly investigated. To include bimodal effects, the mode amplitude in the spectral domain can be written as

$$\underline{A} = \underline{A}(\Omega, z) = \begin{bmatrix} A_x(\Omega, z) \\ A_y(\Omega, z) \end{bmatrix}, \tag{20.25}$$

where $A_x(\Omega, z)$ and $A_y(\Omega, z)$ are the components of the mode amplitude vector that are defined with respect to a linear $(\hat{x}, \hat{y})$ polarization basis. The frequency Ω refers to the complex envelope representation [58], i.e., $\Omega = \omega \quad \omega_0$, where ω_0 is the nominal optical transmission frequency.

The Split-Step Method

The propagation equation (Eqn (20.24)) is a second-order nonlinear partial differential equation that does not generally have an analytical solution. In almost all cases, numerical approaches have to be employed. The split-step Fourier method is the most commonly used numerical scheme that is employed for solving Eqn (20.24). This method is considerably faster than most finite difference methods due to the use of FFT algorithms [64]. It is also a very convenient method due to its simplicity and flexibility in dealing with higher order dispersion, Raman effects, and filtering [58].

All commercial optical system simulation tools use the split-step method to perform the integration of the fiber propagation equation. The form of such an equation is as follows:

$$\frac{\partial A(t,z)}{\partial z} = \{L + N\}A(t,z), \tag{20.26}$$

where $A(t,z)$ is the optical field, L is the linear operator responsible for dispersion and other linear effects, and N is the nonlinear operator that accounts for the Kerr effect and other nonlinear effects like SRS or pulse self-steepening.

The split-step integration algorithm works by separately applying L and N to $A(t,z)$ over small spans of fiber Δz. The distribution of the step sizes along the fiber is an important factor in determining the efficiency of the split-step method. A number of step-size selection criteria, mostly based on physical intuition, have been used to optimize the split-step method. A computational cost for a given global accuracy serves as the figure of merit for each criterion. Some of the more commonly used methods are discussed in Ref. [65]. The split-step method is based on an approximate solution that assumes that over a small distance Δz, the dispersive and nonlinear effects can be considered to act independently. For this two-step approach, the solution of Eqn (20.26) can be expressed as

$$A(z + \Delta z) = \exp(\Delta z L)\exp(\Delta z N)A(z,t). \tag{20.27}$$

A more commonly used solution, referred to as symmetric split-step, includes the effect of nonlinearity in the middle of the segment rather than at the segment boundary. For the symmetric split-step, the solution to Eqn (20.26) is expressed as

$$A(z + \Delta z) \approx \exp\left(\frac{\Delta z}{2}L\right)\exp\left\{\Delta z N\left[A\left(z + \frac{\Delta z}{2}, t\right)\right]\right\}\exp\left(\frac{\Delta z}{2}L\right). \tag{20.28}$$

Since the linear and nonlinear operators do not commute in general, both solutions (20.27) and (20.28) are only approximations to the exact solution. Using the Baker Hausdorff formula [66], it can be shown that the symmetric

split-step method improves the leading-order error term from second-order to third-order in the step size Δz when compared to solution (20.27).

The frequency-domain split-step (FDSS) and the time-domain split-step (TDSS) methods are the two popular approaches that are used to numerically solve Eqn (20.28). These two methods differ in the way L is calculated. The nonlinear operator N is always calculated in the time domain by both methods. The techniques are briefly discussed in the next two subsections.

Frequency-Domain Split-Step

FDSS calculates L in the frequency domain [58], by multiplying the FFT of $A[n]$, the signal in sampled time, with the FFT of $h[n]$, the impulse response in sampled time. The resulting array is converted back to the time domain with an inverse FFT, as expressed in the following formula:

$$\text{FDSS} \Rightarrow A'_L[n] = A[n] \otimes h[n] = \text{FFT}^{-1}(\text{FFT}(A[n]) \times \text{FFT}(h[n])). \qquad (20.29)$$

It is well known from signal processing and simulation theory that FDSS as calculated above does not implement a linear convolution product, but a circular convolution, as indicated by the $\otimes$ symbol. The circular convolution can create a signal fold-over error effect, or aliasing, in the resulting array $A'_L[n]$, which may contain less samples than needed to compute the actual convolution product $A_L[n]$. The use of the FFT algorithm implies periodic boundary conditions. In cases where the pulse energy spreads rapidly, it may be difficult to avoid hitting the window boundary. This fundamental issue with the FDSS method can lead to numerical instabilities as the energy reaching one edge of the window automatically reenters the window from the other edge. Initially, it may appear that this approach introduces unphysical correlations due to the wrapping of signals and noise. In fact, these correlations may have only a very minor effect and can always be essentially eliminated by using longer bit patterns. Moreover, periodic boundary conditions are important for WDM simulations using FDSS since initially coincident pulses in different channels quickly separate due to walk-off. If the pulses did not re-enter the time window, interchannel interactions would be grossly underestimated leading to overoptimistic predictions for cross talk, gain tilt, and XPM effects. However, the wrapping of the signals and noise is intrinsic to the method, thus it is difficult to avoid when the effect is undesirable and extreme care must be exercised to ensure that the FDSS method is used properly.

Time-Domain Split-Step

Being a linear operator, L is fully characterized by its impulse response $h(t)$ and the mathematically correct way to compute its effect on $A(t,z)$ is via a convolution

product in time. TDSS calculates L in the time domain by calculating the convolution product in sampled time [67], which can be written as

$$\text{TDSS} \Rightarrow A_L[n] = A[n] * h[n] = \sum_{k=-\infty}^{\infty} A[k]h[n-k]. \tag{20.30}$$

The effective implementation of TDSS is more difficult than FDSS to achieve. In the TDSS method, the linear operator L can be either implemented by means of infinite impulse response (IIR) filters [67] or finite impulse response (FIR) filters. The FIR implementation can be achieved by automatically truncating the theoretically infinite $h(t)$ impulse response of L and calculating the FIR filter with a sophisticated technique that ensures full control on the overall end-to-end error. One of the best implementations of the FIR filter algorithm in terms of complexity is the famous overlap-and-add algorithm [68] that takes advantage of FFTs while correcting the aliasing problems that affect FDSS. To filter M signal samples of $A[n]$, the computational effort of L at each Δz (i.e., for each filter) is on the order of $M[\log_2(K)+2]$, where K is the number of samples of the impulse response $h(t)$ of the FIR filter which implements L. The drawback of this FIR filter implementation is the need to segment, block-process, and then streamline the data. For comparison, the computational complexity of FDSS for each L is on the order of $M[\log_2(M)+1]$, which can be considerably larger.

The intrinsic signal and noise wrapping that could possibly lead to numerical errors in the FDSS method do not occur in the TDSS method. TDSS imposes no constraints whatsoever on the shape and spectra of the optical signals. Furthermore, TDSS requires no tricky workarounds since it guarantees the absence of intrinsic errors. TDSS computes a true convolution in the time domain and therefore channels are free to shift in time. It should be noted that distant channels in a WDM system shift with respect to each other to an extent that they only partially overlap. Thus to preserve accuracy, the nonoverlapping bits are cut off at the end and only the bits that have always beaten with all channels are preserved in an efficient TDSS method.

40 Gbit/s NRZ, Duobinary, DPSK, and CSRZ-DPSK Single-Mode System Simulation Example

The split-step methods described above can be used to simulate the propagation in optical fiber of single- and dual-polarization signals described in terms of amplitude and phase information sampled over the simulation time span. The analog nature of the signal representation makes the methods suitable for study of the performance of different modulation formats at a given bitrate.

In the following we show the simulation results of four different modulation formats in ultrahigh spectrally efficient WDM systems. Besides standard nonreturn-to-zero (NRZ) intensity modulation, we analyze duobinary, DPSK, and

CSRZ-DPSK formats, and optimize the system dispersion map for each of them. These examples were used to obtain results presented in [69]. The transmitter and receiver layout of the four analyzed modulation formats is shown in Figure 20.24.

The different architectures, based on seven-channel WDM transmission, were simulated using a commercial optical communication system design tool. Each transmitter uses the ad hoc setup obtained after optimization of each modulation format under analysis. The channel spacing is set to 50 GHz and the bit rate to 42.65 Gbit/s (40 Gbit/s + typical FEC overhead). The transmission line is a

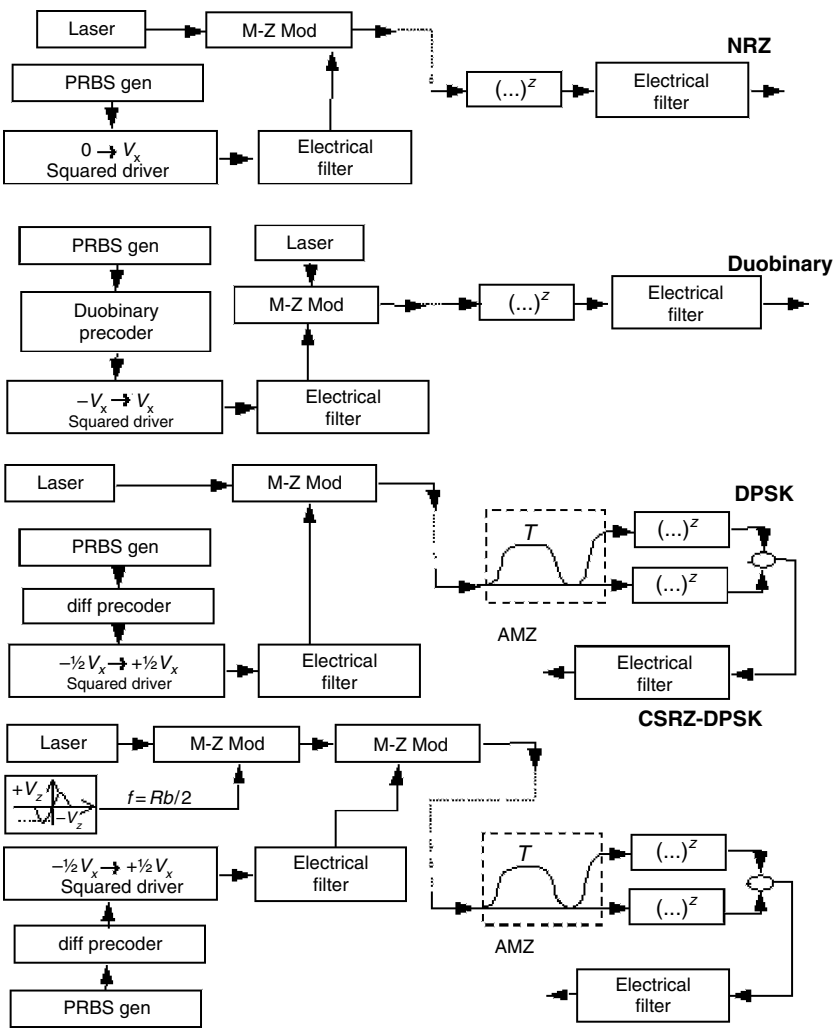

Figure 20.24 From top to bottom: NRZ, duobinary, DPSK, and CSRZ DPSK transmitter and receiver layout [69].

five-span periodically amplified fiber link based on nonzero dispersion-shifted fiber (NZDSF) with dispersion parameter $D = 4.46$ ps/nm/km, dispersion slope $S = 0.09$ ps/nm^2/km, and loss $\alpha_{\text{dB}} = 0.22$ dB/km. All values are referred to the wavelength of the WDM comb's center channel. The length of each span is 100 km, and a variable attenuator is used after the fiber spans to set the overall span loss to a fixed value α_{tot}. Dispersion management is obtained via a Dispersion compensation unit (DCU) inserted between two amplification stages after the attenuator. The noise figure F of both the erbium-doped fiber amplifiers (EDFAs) is equal to 6.5 dB ($n_{sp} = 2.23$). A further DCU is placed before the receiver to adjust the overall link dispersion. Like the transmitter structure, the receiver is configured as defined in the back-to-back optimization phase. For each modulation format, the OSNR at the input of the receiver is set to give a target BER of 10^{-6} in the back-to-back WDM condition. This target OSNR (a different value for each modulation format) can be achieved by choosing the proper transmitted power, depending on the overall span loss α_{tot}.

The resilience of each modulation format to variation of the dispersion was tested by varying the amount of dispersion $D_{\text{in-line}}$ and D_{RX} (measured in ps/nm) introduced by the in-line DCU and the receiver DCU, respectively. The Q surface at the receiver vs in-line and predetection dispersion is shown in Figure 20.25. The size of the Q interval is 5.5, 1.5, 1.2, and 1 dB, respectively, for NRZ, duobinary,

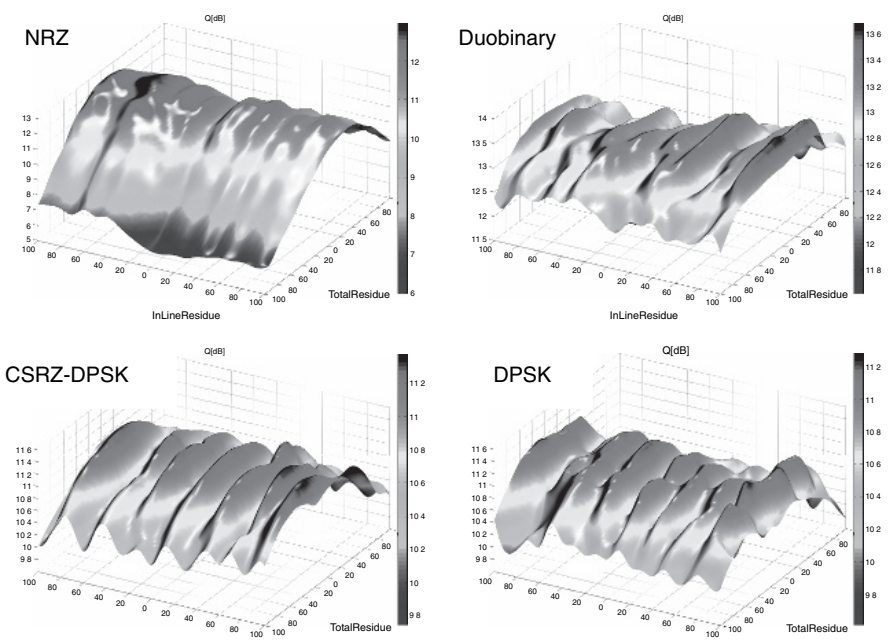

Figure 20.25 Clockwise from top left: Q surface at the receiver vs. in line and predetection dispersion for NRZ, duobinary, DPSK, and CSRZ DPSK modulation formats (this figure may be seen in color on the included CD ROM).

DPSK, and CSRZ-DPSK modulation formats. The simulation results show that advanced modulation formats have greater dispersion resilience than the standard NRZ intensity modulation scheme.

20.3.2 Multi-mode Systems

Recent advances and standards efforts [70] in Ethernet-based multigigabit optical data links have revived interest in design optimization of optical communication systems that use multi-mode fibers and multi-mode light sources. Some of the typical multi-mode design objectives, among others, include optimization of system bandwidth, compliance with standards requirements, evaluation of chromatic and modal dispersion, and calculation of differential mode delay (DMD) and encircled flux (EF), all of which can be studied via suitable multi-mode system simulation tools.

Unlike single-mode systems, multi-mode designs require analyses of both temporal and spatial effects [71 73]. For example, it is relatively easy to analyze coupling between a single-mode fiber and a single-mode laser. In contrast, analysis of coupling between a multi-mode fiber and a multi-mode laser requires knowledge of the spatial distributions of both the laser's optical field profiles and the fiber's transverse mode profiles. Misalignment between the fiber and laser also affects the analysis. Furthermore, as shown in Figure 20.26, an optical pulse launched into a multi-mode fiber simultaneously excites multiple fiber modes, each having a different group velocity [74 77]. This causes each mode to arrive at the end of the fiber at different times, thereby creating a spreading of the pulse, also known as modal dispersion.

Below we elaborate on these issues with particular emphasis on the multi-mode fiber, and then present an example of a multi-mode link simulation.

Representation of an Optical Signal

For single-mode simulations, it is sufficient to consider only the time-varying amplitude of a particular mode. Multi-mode systems, however, with their complicated mode couplings between components, demand that each mode's transverse

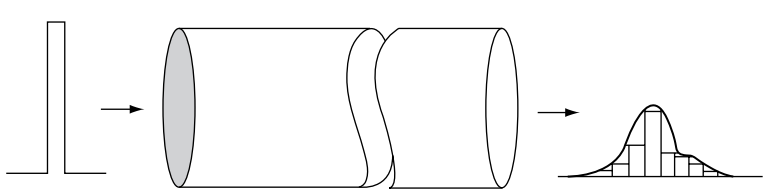

Figure 20.26 Modal dispersion in a multi mode fiber.

shape be explicitly accounted for within the optical field representation. Hence, we include transverse mode profiles for both polarizations as part of the optical signal.

The complete representation of an optical field for a single mode, *including unique shapes for the X and Y polarizations*, is

$$E(t) = \gamma\{\hat{x} \cdot [A_x(t)\psi_x(x,y)\mathrm{e}^{\ \mathrm{j}2\pi f_o t} + \mathrm{c.c.}] + \hat{y} \cdot [A_y(t)\psi_y(x,y)\mathrm{e}^{\ \mathrm{j}2\pi f_o t} + \mathrm{c.c.}]\}, \quad (20.31)$$

where γ is a scaling factor, f_o is the optical carrier frequency, t is time, x is the X coordinate, y is the Y coordinate, and c.c. denotes complex conjugate. The field amplitudes for the X and Y polarizations are $A_x(t)$ and $A_y(t)$, respectively, while the normalized transverse mode profiles for the X and Y polarizations are $\psi_x(x, y)$ and $\psi_y(x, y)$, respectively. The profiles are normalized to ensure that the full optical power is carried inside the amplitude functions. In most cases, the mode profiles for the X and Y polarizations will be identical, but for generality, they can be specified separately. These mode shapes include donut and spot modes, Laguerre Gaussian (LG) and Hermite Gaussian modes, and linearly polarized (LP) fiber modes. These profiles will generally vary depending on the component from which they are generated. For example, VCSELs can often be characterized by LG modes.

Typically, the multi-mode output of a given component can be treated at a single wavelength with mutually orthogonal transverse modes.

Propagation of Light in a Multi-mode Fiber

As seen earlier in Figure 20.26, the modal dispersion causes different fiber modes to arrive at the fiber output with different delays. Typically, a multi-mode fiber would support hundreds of transverse modes at a particular wavelength, thereby making the analysis of modal delays a very involved one. There are various approaches for these calculations.

One approach is to use the BPM to determine the transverse optical modes of a multi-mode fiber and their respective propagation constants [78 82]. A second approach is to assume a parabolic refractive index profile for which analytical expressions exist for fiber modes and delays [83, 84]. Of course, this assumption would not permit studies on the effects of index perturbations. A third approach determines the modes of a fiber by solving the radial Helmholtz equation subject to a radially varying index profile $n(r)$. The individual propagation constants are determined by using Maxwell's equations to match boundary conditions, and then solving the resulting characteristic equation. The advantage of this approach is that the index profile can be an arbitrary function.

When performing system-level analysis of modal delays, a common approximation is the so-called degenerate mode group (DMG) formulation. This technique is based on the observation that modal delay values tend to fall into clusters; the DMG formulation takes advantage of this fact by analyzing the clusters rather than the individual delays themselves. The well-known Wentzel-Kramers-Brillouin

(WKB) approximation [72, 73] of electromagnetic theory is based on the scalar Helmholtz equation

$$\frac{d^2\psi}{dr^2} + \frac{1}{r}\frac{d\psi}{dr} + \left[k^2 n^2(r) - \beta^2 - \frac{l^2}{r^2}\right]\psi = 0 \tag{20.32}$$

with assumed solutions of the form

$$\psi(r) = \psi_0 \exp[ikS(r)], \tag{20.33}$$

where r is the radial distance from the center of the fiber core, k is the wave number, $n(r)$ is the multi-mode fiber's radially varying index profile, β is the modal propagation constant, and l is the given azimuthal index for which solutions $\psi_{lm}(r)$ for each radial index m are found.

Furthermore, $S(r)$ can be expanded in powers of $1/k$:

$$S(r) = S_0(r) + \frac{1}{k}S_1(r) + \cdots \tag{20.34}$$

The fundamental WKB assumption is that if the index varies only slightly over the distance of a wavelength, terms of higher order in Eqn (20.34) can be neglected [73], leading to reasonable approximations for $\psi(r)$.

In Refs [72] and [73], it is shown that under the WKB approximation, the modal delays for the parabolic index fiber can be approximated by

$$\tau_{\mathrm{WKB}} = \frac{Ln_1}{2c}\left(\frac{n_1}{N_{\mathrm{eff}}} + \frac{N_{\mathrm{eff}}}{n_1}\right), \tag{20.35}$$

where L is the fiber length, n_1 is the peak index at the fiber center, c is the speed of light, and N_{eff} is the effective index.

An Example of the System-Level Impact of Modal Delays

Consider the layout for a typical multi-mode system simulated using a commercial tool [85] as shown in Figure 20.27.

From left to right, the components are a PRBS pattern generator, a laser driver, a VCSEL, a coupler, a multi-mode fiber, a photoreceiver, and an eye diagram analyzer. The VCSEL is modulated by a 10-Gb/s NRZ data stream and produces an 820-nm Gaussian beam with a 5-μm waist. The coupler is set to provide an offset of 25 μm between the VCSEL and the multi-mode fiber axis. After the simulation is over, the multi-mode fiber model produces a plot of the relative power coupled into each mode as a function of the modal delay as shown in Figure 20.28, where the received eye diagram is also shown. Reducing the lateral offset to

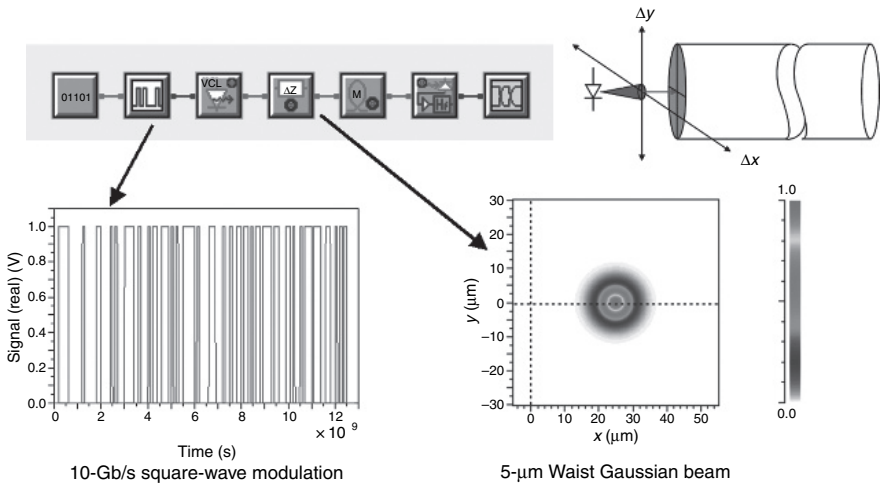

Figure 20.27 A simple multi mode link (this figure may be seen in color on the included CD ROM).

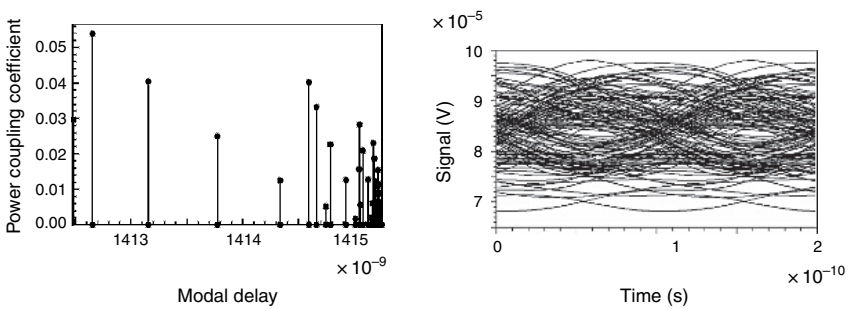

Figure 20.28 Modal delay plot (left) and received eye (right) for a 25 μm laser fiber offset.

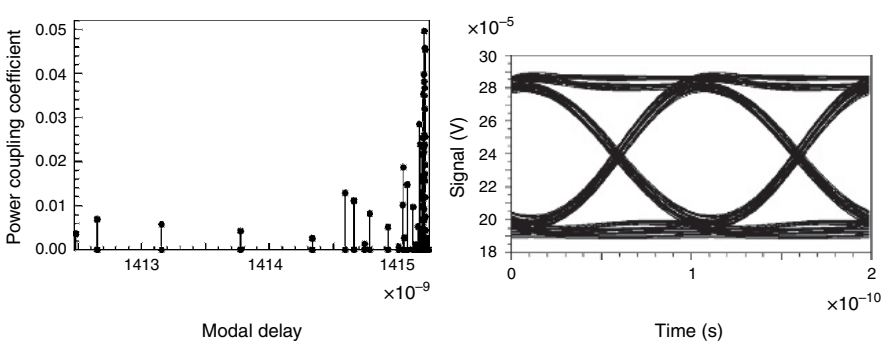

Figure 20.29 Modal delay plot (left) and received eye (right) for a 5 μm laser fiber offset.

5 μm results in more tightly clustered delay values, and hence a better received eye diagram, as shown in Figure 20.29.

20.3.3 Performance Estimation

Introduction

The simulation of an optical communication system requires not only implementation of detailed models for the link subsystems and components, but also handling of stochastic physical processes and accurate techniques for the evaluation of the system performance.

The stochastic physical processes taking place in an optical communication system are the following:

- noise [ASE (amplified spontaneous emission) thermal, shot, phase noise, etc.]
- statistics of systems parameters (length, dispersion value, PMD, etc.)
- statistics of digital sources (random digital sequences)

Focusing our attention on binary digital systems, the most commonly used performance parameters are

- BER
- Q-factor, defined as

$$Q = \frac{m_1 - m_0}{\sigma_1 + \sigma_0},$$

where m_1, σ_1 (m_0, σ_0) are the mean and the standard deviation of the received signal at the sampling instant when a logical "1" ("0") is transmitted.

In a laboratory or field experiment, BER can be easily and accurately measured using commercial BER testers, which are based on direct error counting by comparison of the input and output digital streams. Otherwise, BER evaluation is usually a very difficult task in a software simulation environment for the following reasons:

- the reference BER for an optical communication system is very low (10^{-9} and lower),
- the signal at the output of the link is usually effected by intersymbol interference,
- the number of simulated bits is limited with respect to the available CPU time.

The most commonly used techniques in communications system simulations are direct error counting, Monte Carlo methods, and semianalytical techniques. A detailed analysis of these techniques may be found in Ref. [86]. Direct error

counting is seldom used in the simulation of optical systems. In fact, a BER close to 10^{-9} requires [86, Figure 2] the simulation of at least 10^{10} bits to achieve a reasonable accuracy, and would thus need a prohibitively large CPU time even for extremely simple link setups.

Monte Carlo Method

In the Monte Carlo approach, all the stochastic processes are simulated by extracting a random variable from a random number generator. All noise sources are simulated by extracting a noise sample, adding it to each signal sample and propagating them together. The system parameters are simulated by extracting random numbers once at the beginning of the simulation. The digital signal sources are simulated through pseudo-random sequence generators.

The system performance is then estimated calculating a few moments typically mean and variance of the received signal.

In the Monte Carlo approach the noise is propagated in the same way as the signal, reflecting physical reality. In case nonlinearities are relevant, the method is accurate since signal and noise can mix together nonlinearly. Moreover for very complex transmission systems, Monte Carlo is often the only available general purpose approach because the noise statistics at the receiver can only be handled with a Gaussian approximation.

Simulated Number of Bits and Confidence Interval The estimate of the system performance over a finite and typically small time frame using the Monte Carlo method is affected by statistical fluctuations of the results.

A very common parameter for the estimation of system performance by simulation is the well-known Q-factor, defined as

$$Q = \frac{m_1 - m_0}{\sigma_1 + \sigma_0}, \tag{20.36}$$

The BER is then often evaluated as

$$\mathrm{BER} = \frac{1}{2}\mathrm{erfc}\left(\frac{Q}{\sqrt{2}}\right) \tag{20.37}$$

This last relation is exact only when:

- noise at the receiver is Gaussian,
- ISI is negligible.

There is usually a widespread perception among the users of simulation tools of the scope and consequences of these two assumptions. On the contrary, it is much

less understood that there is an intrinsic uncertainty in the evaluation of the Q-factor whenever it is measured over a finite number of bits.

To investigate this point, let us suppose that the above assumptions are exactly met, i.e., that the signal is not significantly affected by intersymbol interference and that the noise is Gaussian. Let us start by focusing on the estimate m^* of the mean of a Gaussian-distributed variable of mean m and standard deviation σ . The estimate is evaluated over N samples of the variable as

$$m^* = \frac{1}{N}\sum_{i=1}^{N} s_i, \tag{20.38}$$

where s_i are the N samples of the variable. From standard estimation theory [87], it can be demonstrated that the estimate m^* has an uncertainty whose standard deviation is given by

$$\mathrm{dev}[m^*] = \frac{\sigma}{\sqrt{N}}. \tag{20.39}$$

Similarly, the estimate of the variance σ^{2*} has an uncertainty whose standard deviation is given by [87]:

$$\mathrm{dev}[\sigma^{2*}] = \sqrt{\frac{2}{N}}\sigma^2. \tag{20.40}$$

Starting from these results, and assuming that we are simulating N_{tot} bits and that we have an equal number of "1" and "0" symbols, it can be shown that the uncertainty in the estimation of the Q-factor has a standard deviation which is approximately given by

$$\mathrm{dev}[Q^*] \cong \frac{Q}{\sqrt{2N_{\mathrm{tot}}}}. \tag{20.41}$$

As commonly accepted, we will now assume as a "confidence interval" of the estimate a range given by two standard deviations, which, for Gaussian variables, accounts for a 95% probability. We can interpret the confidence interval as follows: the estimate Q^* has a 95% probability to be in the range:

$$[Q - 2\,\mathrm{dev}[Q^*], Q + 2\,\mathrm{dev}[Q^*]]. \tag{20.42}$$

In Figures 20.30 and 20.31, we report this range for a nominal $Q = 6$ (15.56 dB) and $Q = 8.2$ (18.2 dB), corresponding to the two commonly used reference BERs of 10^{-9} and 10^{-16}, respectively.

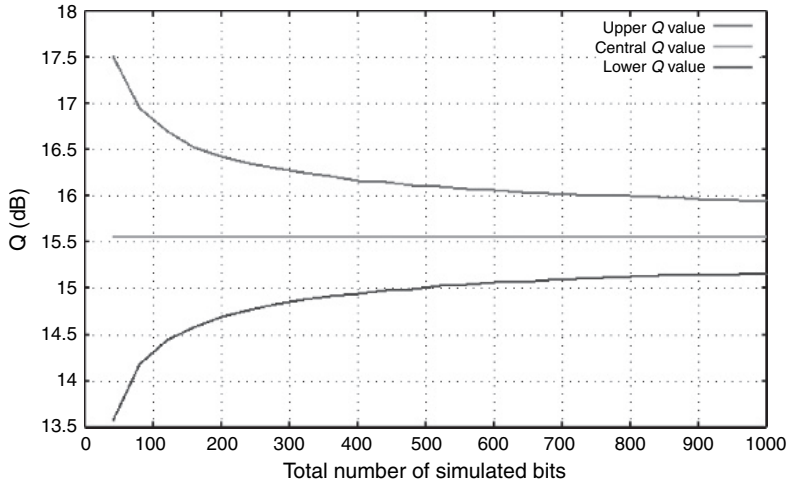

Figure 20.30 Q factor estimate range (95% confidence interval) for a nominal Q 6 (15.56 dB), corresponding to BER 10^{-9} (this figure may be seen in color on the included CD ROM).

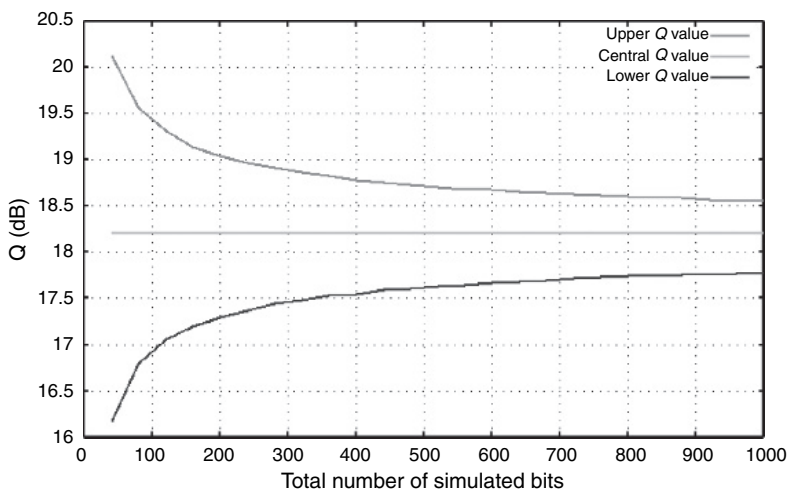

Figure 20.31 Q factor estimate range (95% confidence interval) for a nominal Q 8.2 (18.2 dB), corresponding to BER 10^{-16} (this figure may be seen in color on the included CD ROM).

It is interesting to note that, in both cases, approximately 500 bits are required to have Q-factor confidence intervals of ± 1 dB. Moreover, it should be noted that, even though this is often done in a simulation environment, the estimation over less than 100 bits leads to an exceedingly high confidence interval, greater than ± 2 dB.

In order to asses the "error" in the evaluation of the Q-factor over a finite number of bits, we consider the two extremes of the 95% confidence interval given by

$$\begin{cases} Q^*_{\min} = Q - 2\,\mathrm{dev}[Q^*], \\ Q^*_{\max} = Q + 2\,\mathrm{dev}[Q^*]. \end{cases} \tag{20.43}$$

The estimate range can be expressed as

$$\mathrm{range} = Q^*_{\max} - Q^*_{\min} \tag{20.44}$$

and is given by

$$\mathrm{range} = 20\log_{10}\left(\frac{1+\sqrt{\dfrac{2}{N_{\mathrm{tot}}}}}{1-\sqrt{\dfrac{2}{N_{\mathrm{tot}}}}}\right). \tag{20.45}$$

This is a very useful formula, which shows that the Q-factor range is independent from the Q-factor nominal value and is only dependent on the total number of bits N_{tot}. The following table reports this range in dB vs the number of simulated bits.

Number of simulated bits N_{tot}	Q factor uncertainty range (dB)
32	4.43
64	3.10
128	2.18
256	1.53
512	1.09
1024	0.77

An even more useful insight into this description of the estimation accuracy can be obtained by Figures 20.32 and 20.33, where the BER range (evaluated from the Q-factor in the Gaussian approximation) is plotted vs the number of simulated bits for the two nominal BERs equal to 10^{-9} and 10^{-16}.

As it can be shown by direct comparison, the confidence interval at a BER around 10^{-9} is given by roughly ± 1 order of magnitude for $N_{\mathrm{tot}} = 512$. We believe that this is an acceptable range for most applications and we thus advise the user to simulate at least 512 bits when even the accurate indication of the BER value is in the 10^{-9} range.

The situation is worst at lower bit rates, as it can be seen from the graphs at $\mathrm{BER} = 10^{-16}$. In fact for a given N_{tot}, the range in terms of BER increases while decreasing the reference BER. This is due to the fact that the BER vs Q-function is

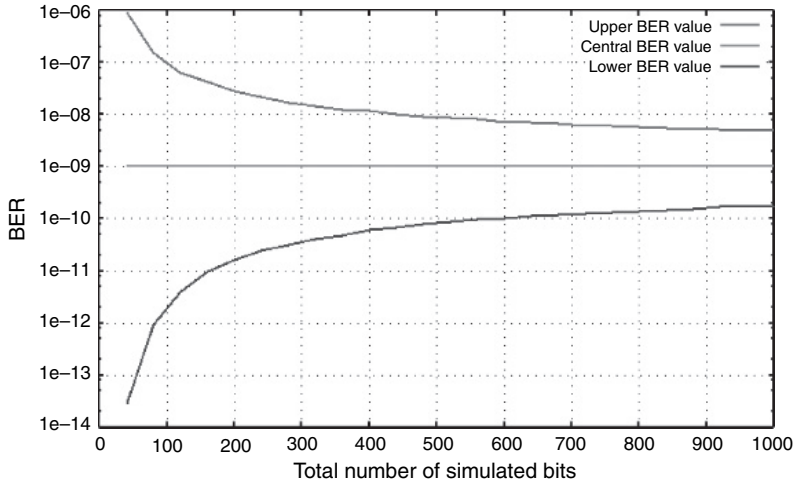

Figure 20.32 BER estimate range (95% confidence interval) for a nominal BER 10^{-9} (this figure may be seen in color on the included CD ROM).

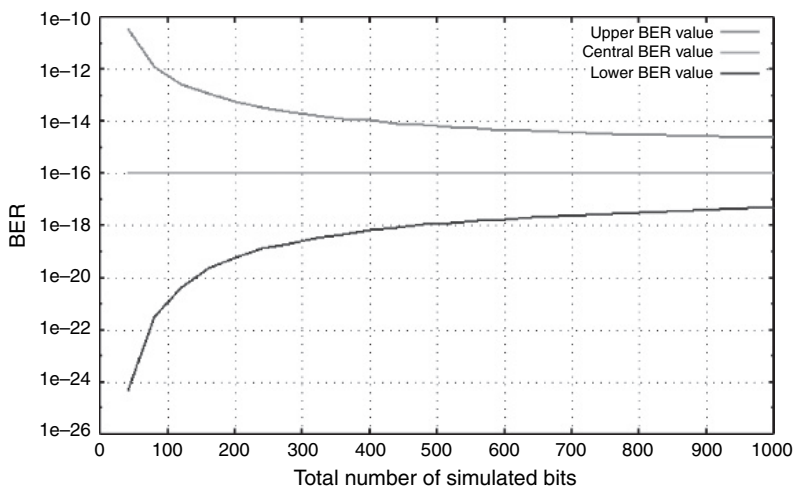

Figure 20.33 BER estimate range (95% confidence interval) for a nominal BER 10^{-16} (this figure may be seen in color on the included CD ROM).

steeper for smaller BER. Thus for a fixed range in term of Q-factor correspond to a BER range that increases for the decreasing reference BER, as shown in Figure 20.34. For example when simulating 512 bits at BER $= 10^{-16}$, the range is more than ± 2 orders of magnitude.

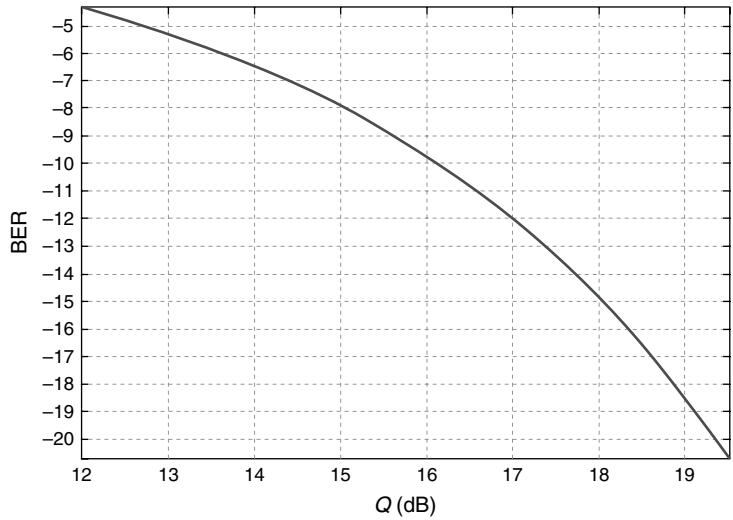

Figure 20.34 BER vs Q factor (this figure may be seen in color on the included CD ROM).

Semianalytical Techniques

In the semianalytical techniques, the stochastic processes related to the noise are taken into account analytically. The signal is simulated without noise, the noise is propagated analytically, and explicit analytic formulas are used to evaluate the BER.

Several versions of semianalytical techniques are available. The common requirement to all these techniques is the exact knowledge of the noise distribution at the receiver. Whenever this is true, the semianalytical techniques are very powerful and provide extremely accurate results even when a few bits are simulated (see Ref. [86, Section VI]). Moreover, since the noise statistics do not have to be recovered from the signal, the semianalytical techniques seamlessly handle systems with strong ISI.

Karhunen–Loève Technique The exact probability density functions (PDFs) of the received signal after pre- and postdetection optical and electrical filtering can be efficiently evaluated by using the method described in Ref. [86], based on the Karhunen Loève decomposition of signal and noise in the frequency domain.

It can be shown (see Refs [88, 89]) that the received signal after optical and electrical filtering can be written in the form:

$$v(t) = \sum_i |b_i(t) + \nu_i(t)|^2 \tau_i, \tag{20.46}$$

where $b_i(t)$ and $\nu_i(t)$ are the coefficients of the series expansion of the Fourier transform $S(f)$ and $N_{\mathrm{ASE}}(f)$ of the noiseless received signal $s(t)$ and of the ASE noise random process $n_{\mathrm{ASE}}(t)$, respectively:

$$\begin{aligned} b_n(t) &= \int S(f)\exp[\mathrm{j}2\pi ft]\,\phi_n^*(f)\mathrm{d}f, \\ v_n(t) &= \int N_{\mathrm{ASE}}(f)\exp[\mathrm{j}2\pi ft]\,\phi_n^*(f)\mathrm{d}f. \end{aligned} \tag{20.47}$$

$\{\phi_m(t)\}$ is a set of orthornormal functions satisfying the following eigenvalue integral equation:

$$\int \phi_m(f_2)K(f_1,f_2)\mathrm{d}f_2 = \tau_m\phi_m(f_1). \tag{20.48}$$

For a direct detection receiver:

$$K_{\mathrm{DD}}(f_1,f_2) = RGH_{\mathrm{o}}(f_1)H_{\mathrm{L}}(f_1 - f_2)H_{\mathrm{o}}^*(-f_2), \tag{20.49}$$

where R and G are the photodiode responsivity and avalanche gain, respectively, and H_{O} and H_{L} are the optical and electrical filter transfer functions, respectively. Similar expressions can be obtained for differential receivers.

Using numerical integration algorithms (see Ref. [90, Chapter 4]), the solution of Eqn (20.48) can be reduced to the eigenvalue and eigenvector problem for a Hermitian matrix:

$$\int \phi_m(f_2)K(f_1,f_2)\mathrm{d}f_2 \approx \int_{f_{\mathrm{MAX}}}^{f_{\mathrm{MAX}}} \phi_m(f_2)K(f_1,f_2)\mathrm{d}f_2 \approx \sum_{i\ \ 0}^{2k} \phi_m(x_i)K(f_1,x_i), \tag{20.50}$$

where $x_i = f_{\mathrm{MAX}}\left(\frac{(i\ \ k)}{k}\right)$. The integration interval $[\ f_{\mathrm{MAX}}, f_{\mathrm{MAX}}]$ must be chosen in a way that the integrand evaluated for $f > f_{\mathrm{MAX}}$ is sufficiently small and does not affect the result. Equation (20.48) can thus be rewritten as

$$\sum_{i=0}^{2k} \phi_m(x_i)K(x_n,x_i) = \tau_m\phi_m(x_n), \quad n,m = 0,\ldots,2k, \tag{20.51}$$

i.e., in matrix form:

$$\mathbf{K}\cdot\boldsymbol{\varphi} = \boldsymbol{\tau}\cdot\boldsymbol{\varphi}. \tag{20.52}$$

with $K_{i,j} = K(x_i,x_j)$, $\varphi_{\mathrm{ij}} = \varphi_{\mathrm{j}}(\mathrm{x_i})$, $\tau_{ij} = \tau_i\delta_{i,j}$. Since K is Hermitian, the problem Eqn (20.53) is straightforward to solve using the Jacobi routines in Ref. [90, Chapter 11].

Since $n_{\mathrm{ASE}}(t)$ is a white random process, it can be shown that the noise expansion coefficients $n_i(t)$ are statistically independent Gaussian random variables with zero mean and variance $N_0\tau_i$. Thus Eqn (20.46) represents a weighted sum of nonzero mean-squared Gaussian random variables, whose moment generating function (MGF) is equal to [91]:

$$h(t,z) = \prod_{i=0}^{n_{\mathrm{val}}-1} \frac{\exp\left[-\dfrac{z|b_i|^2\tau_i}{1+z\tau_i N_0}\right]}{(1+z\tau_i N_0)^M} \tag{20.53}$$

with $M = 1$ and 2 for single- and dual-polarization representations, respectively.

If additive electrical noise sources, which are statistically independent from the optical ASE noise, are also present (like shot or thermal noise), the overall MGF of the decision variable can be evaluated by multiplying Eqn (20.53) by the MGF of a Gaussian random process with zero mean and variance $\sigma^2(t) = (\sigma_{\mathrm{sh}}(t))^2 + (\sigma_{\mathrm{th}})^2$, i.e.,

$$h_{\mathrm{el}}(t,z) = \exp\left[-\frac{1}{2}\sigma^2(t)\,z^2\right]. \tag{20.54}$$

Using the steepest descent approximation method [92], the probability of error can be evaluated as

$$\begin{aligned} P^0_{e,k}(s_{\mathrm{th}},t) &= \int_{s_{\mathrm{th}}}^{\infty} PDF_k(s,t)\,\mathrm{d}s \approx \frac{\exp[\theta(t,z_0)]}{\sqrt{2\pi\theta''(t,z_0)}}, \\ P^i_{e,k}(s_{\mathrm{th}},t) &= \int_{\infty}^{s_{th}} PDF_k(s,t)\,\mathrm{d}s \approx \frac{\exp[\theta(t,z_1)]}{\sqrt{2\pi\theta''(t,z_1)}} \end{aligned} \tag{20.55}$$

with $\theta(t,z)$ defined as

$$\theta(t,z) = \ln\left[\frac{\exp[-zs_{\mathrm{th}}]\,h(t,-z)\exp\left[-\frac{1}{2}\sigma^2(t)z^2\right]}{|z|}\right]. \tag{20.56}$$

θ'' is the second derivative of θ with respect to z, and z_0 and z_1 are, respectively, the positive and negative roots of the equation:

$$\vartheta'(t,z) = \frac{\partial\theta(t,z)}{\partial z} = 0. \tag{20.57}$$

Equation (20.57) can be efficiently solved using the bisection method described in Ref. [90, Chapter 9].

Finally the overall BER at a given decision threshold s_{th} and sampling instant t_{s} is evaluated as

$$\text{BER}(s_{\text{th}}, t_{\text{s}}) = \frac{1}{N}\sum_{k=1}^{N} P_{e,k}^{0,1}(s_{\text{th}}, t_{\text{s}} + kT). \tag{20.58}$$

20.4 NETWORK MODELING

20.4.1 Introduction

In this section, we discuss optical network modeling, which allows for the study of high-level optical network behaviors under various conditions. The networks under study are generally comprised of a WDM-based optical layer along with a service operator network and traditional transport network technologies like Synchronized Optical NETwork (SONET) and synchronized digital hierarchy (SDH). A variety of optical network architectures are available in the optical layer, and generally incorporate optical terminal multiplexers (OTM), Optical Add and Drop Multiplexers (OADM) and Optical Cross Connects (OXCs). Furthermore, the transparent nature of the optical network supports a wide range of physical and logical topologies, as well as different routing and protection mechanisms. Examples of some network modeling applications include network dimensioning, protection and restoration mechanisms, and protocol behaviors and throughputs. Below we discuss a small subset of the topics related to optical network modeling. For further information, the interested reader is referred to the references section.

20.4.2 Network Dimensioning

Network dimensioning finds out the resources required to implement an optical network. The allocation of resources includes fiber, wavelengths, and WDM equipment required to build the physical topology to satisfy the given set of traffic demands. In the network planning process, traffic demands are the forecasted traffic demands. Network planning can be done either with static traffic or dynamic traffic. With static traffic planning, the traffic is known in advance, the planning can be done for a single period or multiple periods. With dynamic traffic planning, the traffic is uncertain. The traffic forecasts are given in terms of statistical data. For example, it can be given as the level of traffic churn or number of hubs in the network or number of nodes in the optical ring. In this case the designed network should be flexible enough to accommodate the traffic dynamism and minimize the network cost [101 103].

Network design/planning software helps to achieve the design goals quickly and to do a systematic planning process [99, 100]. During the network planning process, the planner needs to collect an initial data set, which will be used to plan the network later. This initial data set includes

- Fiber connectivity between the locations: in the ideal case, physical connections between all locations are need. However, creating full mesh connectivity with independent fiber routes between locations is very expensive. So it is required to consider physical connectivity limitations to determine the possible permitted links during the network planning process.
- Traffic demands (logical level demands): traffic demand specifies the number of wavelength channels required between two nodes. These wavelength channels are routed through the fiber links in the network in such a way that it minimizes the network cost.

Each traffic demand has parameters such as

(a) Start and end nodes.
(b) Bandwidth.
(c) Quantity.
(d) Protection/restoration requirements.
(e) Routing diversity requirements.

- Network elements: there are three types of technologies available today. WDM terminal multiplexers and demultiplexers (OTM), OADM and OXC. In each of these elements, there are constraints due to available technology at the time of planning. For example, there is a limited number of optical add and drop channels in an OADM, or number of EDFAs that can cascade along an optical path. Also in the planning process one should consider technologies that will mature in the near future. Input parameters required for the network elements include
  (a) Number of wavelengths available per fiber.
  (b) OADM capacity number of add drop channels.
  (c) OXC capacity number of optical cross connections it supports.
  (d) Power budget (span loss) for the EDFA.
  (e) Number of cascaded EDFAs possible before regeneration.
- Routing and survivability schemes: the routing of the optical path should take into consideration the client layer requirements. For example, the client layer may require several channels between two nodes with a guarantee of carrying all channels of the given demand together along with the same path. This is called grouped routing of set of optical channels. Another very important aspect of optical network planning is the planning of optical protection and restoration. Parameters used in the routing and survivability schemes are
  (1) Routing metric shortest path, minimum hops, minimum cost, maximum availability.

(2) Diversity requirements node diverse, line diverse and nondiverse.
(3) Client layer protection requirements $1+1$ protection, 1:1 protection, optical ring protection schemes like optical channel layer protection, Optical multiplexer layer protection, optical multiplexer section shared protection (OMS-SPRing).
(4) Restoration requirements end-to-end path restoration, link restoration, and adjacent node restoration.

Let us consider the design of WDM rings with known traffic demands. There are three types of popular WDM rings:

- WDM rings with dedicated protection: this is also called path-protected ring. These can be unidirectional (UPSR) or bidirectional (BPSR). Every optical channel is protected from fiber cuts by another dedicated protection channel, which runs on the opposite side of the ring.
- WDM rings with shared protection: these rings are always bidirectional, although in some cases it is advantageous to route some optical demands unidirectionally. In case of a fiber break on one section of the ring, enough spare transmission capacity is provisioned on the rest of the ring to restore the optical demands interrupted on the broken section. An example of this type of ring is the OMS-SPRing.
- WDM rings with no protection: protection may be carried out in client layers in this case, using capacity on the same ring or elsewhere in the network, but the WDM ring does not need to reserve any wavelengths for protection purposes.

Consider the capacity planning for the WDM ring with dedicated protection, the working and protection channels can share the same wavelength since it travels in the opposite direction of the ring. So each optical demand can be assigned one wavelength. Consider a ring with N nodes and full mesh connectivity with one wavelength demand between each node. This means there are $N(N\ \ 1)/2$ demands present in this case and we need $N(N\ \ 1)/2$ wavelengths to satisfy the entire demands.

20.4.3 Discrete Event Simulations for Optical Networks

Apart from the network planning/design, network modeling also deals with the study of optical network protocols, protection mechanisms and quality of service. In this section, we will see discrete event simulations and a few optical network applications using discrete event simulation models.

A popular methodology to generate discrete event systems is Petri Nets [111 117]. Petri Nets are an efficient, visual approach to model the dynamic behavior of queues and protocols. The basic Petri Nets formalism consists of a

very small set of symbols [117 119]. This makes the approach easy to learn. Concepts like parallelism and synchronization are expressed with a few icons. Petri Nets are defined in terms of three symbols. *Place* (represented by a circle) to model states, conditions, events, and queues. *Transition* (represented by a rectangle) to model state transitions and activities. *Arc* (represented by oriented lines) to define cause effect relationships by connecting places and transitions. Arcs going from places to a transition define the transition's input places; whereas arcs going from a transition to places define the transition's output places. A place is often an input to a transition and an output from other transitions at the same time. Current state (true conditions or occurring events) is represented by drawing a dot within the suitable place. Such a dot is called a token. Petri Nets evolve by moving tokens from an initial state defined by a set of initial tokens until no more tokens can be moved according to the following simple rule: "When all the input places of a transition contain at least one token the transition can fire. The effect of a transition firing is to remove tokens from some places and to create tokens in some other places. When a transition fires, it fetches one token from each of its input places and releases a new token in each of its output places."

Example: Protection Scheme in Packet Transmission

We would like to evaluate the protection switching mechanism of a WDM ring. For example consider a WDM ring with four nodes. In normal working conditions, the traffic will flow in the main (normal) ring, in case of a fiber cut, the traffic will flow in the protection ring. There is a supervisory link, which is used to transmit messages between the nodes. The objective is to study the series of events and messages required to invoke a protection mechanism in a WDM ring and predict the robustness of the protection protocol.

To simulate such a scenario, we need four objects, the node, the working link, the protection link and the supervisory link. Top-level view of the ring is given in Figure 20.35. Both normal and protection rings are unidirectional, while the supervisor link transmits in both directions. The packets are generated from each node and circulated in the ring. Each packet carries a value to model the carrier signal status: TRUE means that there is a carrier signal and the link is working properly. FALSE means absence of the carrier signal. If a FALSE value is detected, then the receiver node sends a special message to the adjacent nodes informing of the detection of a failure and starts switching the transmission to the protection link.

The Node Object The node object is made of two states: NORMAL and PROTECTION. The node is initially in the normal state. The node has a TX section, RX section, Fault management section and a restoration management section as shown in Figure 20.36. Each section behavior is described below.

The TX section generates packets at a particular rate, which is user defined. For example, it generates one packet every 0.01 time units. When the state is

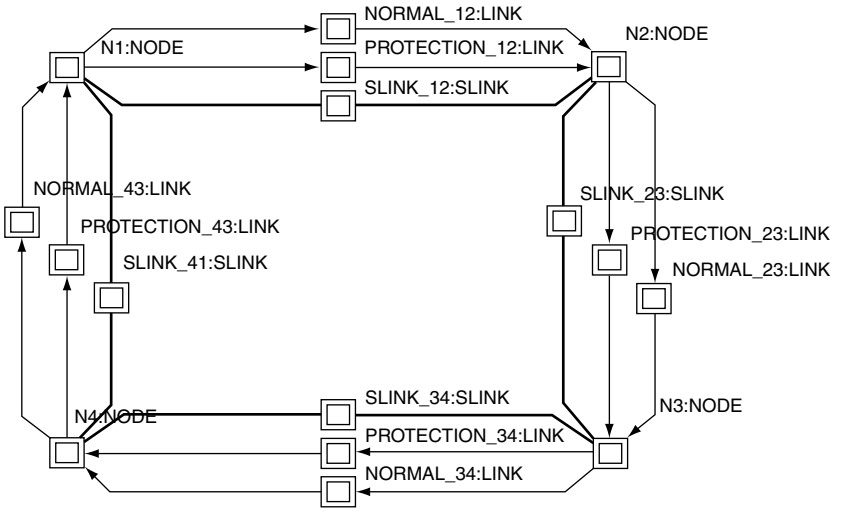

Figure 20.35 The top level view.

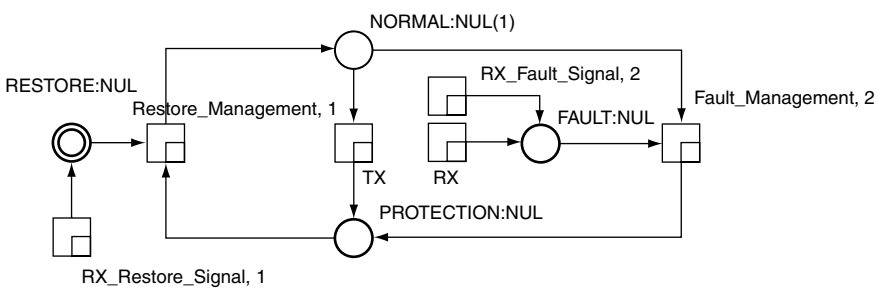

Figure 20.36 Main view of node object.

NORMAL, the packet is transmitted on the normal ring, and when the state is PROTECTION it will go on the protection ring. The details of the TX section are given in Figure 20.37.

When the RX section as shown in Figure 20.38 receives a packet with a FALSE value, meaning that the carrier signal is lost, it detects the fault on the link and immediately activates a procedure at higher priority (2) managed by the Fault Management section. Any packet received on the working link when the node is not in normal state is then discarded, and these are the packets that the node lost.

When a FAULT is detected by the Fault Management section as shown in Figure 20.39, it switches the mode from NORMAL to PROTECTION. A GO PROTECTED signal is sent to the adjacent nodes, predecessor and follower,

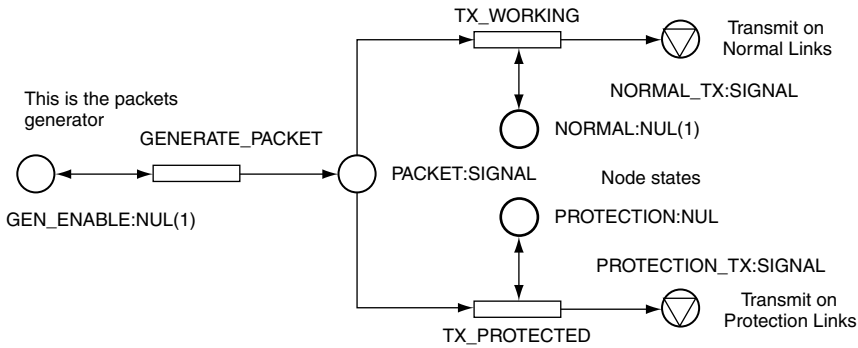

Figure 20.37 The TX section.

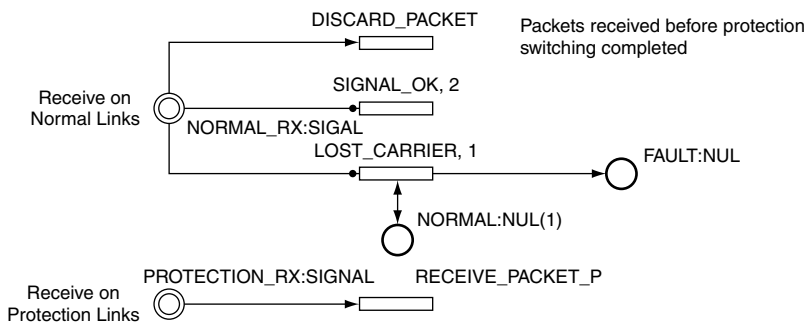

Figure 20.38 The RX section.

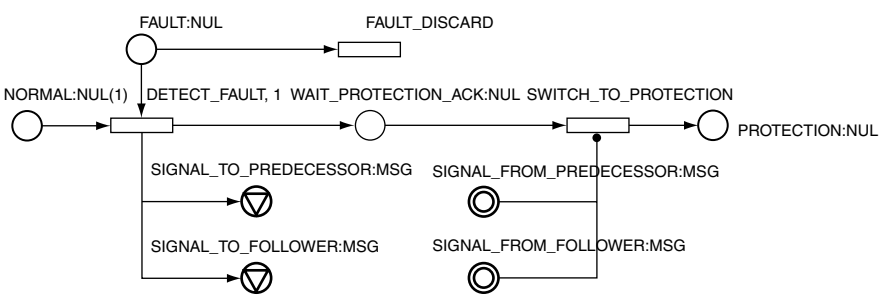

Figure 20.39 The fault management section.

through the supervisor LINK and then the Fault Management subnet waits to get an ACK signal from both adjacent nodes.

When the ACK signals are received, the node switches to PROTECTION State, which disables transmission on the normal link and switches transmission of

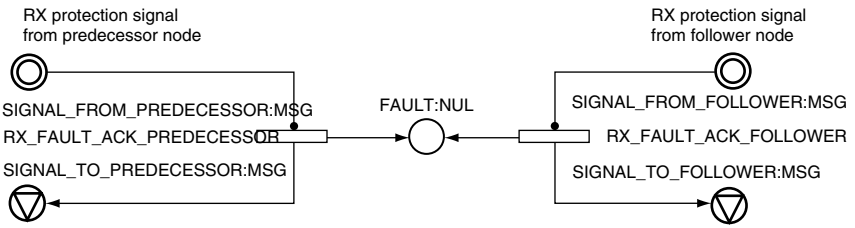

Figure 20.40 RX Fault signal.

packets on the protection link, as described in the packet generation TX subnet of Figure 20.37.

While in the protection mode, a state simply receives packets, without examining the carrier presence, as it is assumed, in this simple example, that the protection link is always working.

When the RX Fault Signal section (Figure 20.40) receives the GO PROTECTION signal from an adjacent node, the ACK signal is sent back to that node and an internal fault generated, which is managed as described in the fault management section Figure 20.39.

Restoration To restore normal mode of operations, the node must receive a signal in place RESTORE, which activates the Restore Management section. This section works the same way the Fault Management section does, but this time it switches the nodes from PROTECTION mode to NORMAL. The restore action will be taken inside the Restore Management section (Figure 20.41).

If in protection mode, the restore command make the node exit the protection state, inform the adjacent nodes of the changes, and when both predecessor and follower nodes send back an ACK message, the node switches eventually in the normal state, so that packets will be sent through the normal link again, as described in the TX section.

When the Restore Management section receives the restore command, it sends an ACK message as reply; an internal restore is generated to be managed as

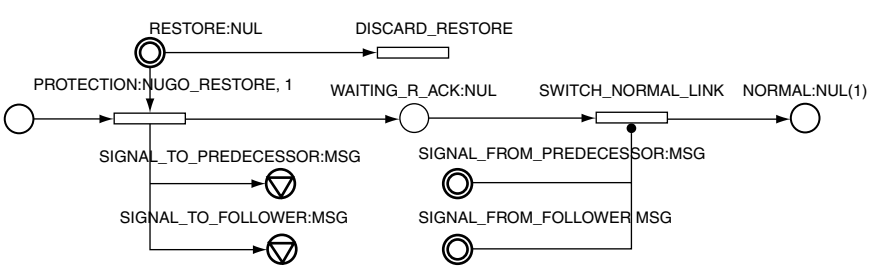

Figure 20.41 Restore Management section.

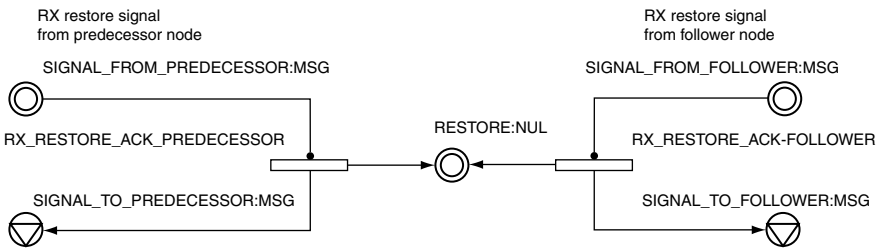

Figure 20.42 RX Restore Signal section.

described in the previous view, and to communicate to all the adjacent nodes to switch to the normal link (Figure 20.42).

The Link Object Each single link is unidirectional; the link object propagates packets with a propagation delay, for example 0.005 time unit. The link object is having two states: WORKING and BROKEN, where WORKING is the initial state.

The user can make any link working or broken by a toggle switch (Figure 20.43).

The Supervisor Link Object The fourth object is the supervisor link, which propagates supervisor signals among nodes. All messages simply pass through the supervisor link with a propagation delay, for example at 0.005 time units (Figure 20.44).

Simulation The WDM ring shown in Figure 20.35 is simulated under various parameter values. Figure 20.45 shows one of the simulation results obtained. In this graph, time is marked in the X-axis and discrete events (fault detection and switch to protection) are marked in the Y-axis. At time $t = 1.0$ a link fault is simulated

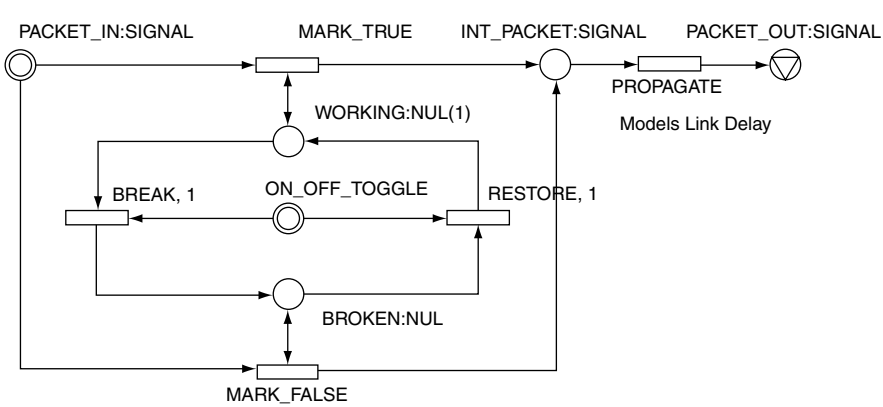

Figure 20.43 The link object.

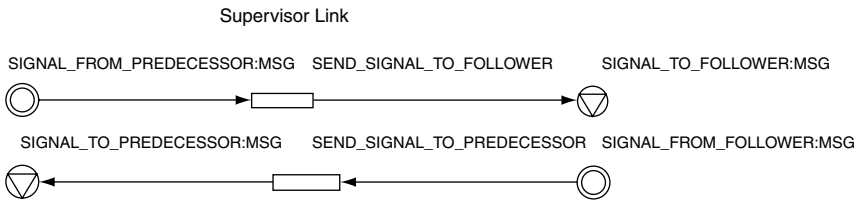

Figure 20.44 The supervisory link.

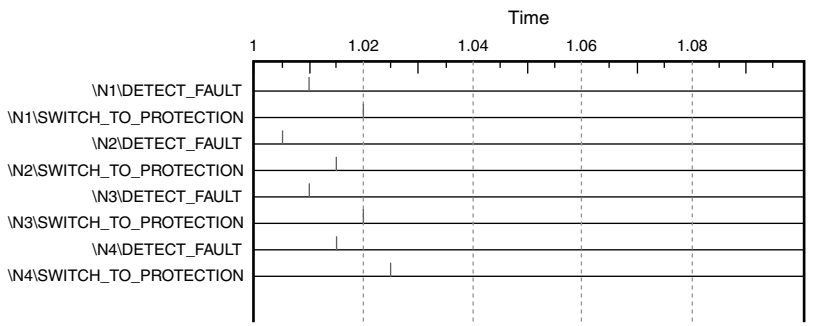

Figure 20.45 Simulation results (this figure may be seen in color on the included CD ROM).

by the user. Since the link propagation delay time in this simulation run is 0.005 time units, N2 (Node 2) detects the fault at time 1.005. Both N1 and N3 are then informed of the fault event, at time 1.01 (\N1\DETECT FAULT and \N3\DETECT FAULT), after the propagation delay time of the supervisor link. At time 1.015 N2 receives both ACKs from N1 and N3 and switches to protection mode (\N2\SWITCH TO PROTECTION). At the same time N4 is informed of the fault (\N4\DETECT FAULT). At time 1.02 N1 and N3 receive their ACK and switch to protection mode (\N1\SWITCH TO PROTECTION and \N3\SWITCH TO PROTECTION). At time 1.025 N4 receives ACK from N1 and N3 and finally switches to protection mode (\N4\SWITCH TO PROTECTION). At this point, all nodes are transmitting and receiving packets into the protection link.

From this graph it is easy to understand the system behavior, and to predict the performance of the protection and restoration protocols and their robustness.

ACKNOWLEDGMENTS

The author would like to acknowledge the contributions and assistance of several colleagues at RSoft: Evan Heller, Michael J. Steel, Mayank Bahl, and Mingming Jiang (device/component portion); Enrico Ghillino, Jigesh Patel, Dwight Richards, and Pablo Mena (system portion); Anil Ramapanicker (network portion).

REFERENCES

[1] M. D. Feit and J. A. Fleck, "Light propagation in graded index optical fibers,", *Appl. Opt*., 17, 3990, 1978.

[2] See references in D. Yevick, "A guide to electric field propagation techniques for guided wave optics," *J. Opt. Quantum Electron.,* 26, S185, 1994.

[3] R. Scarmozzino, A. Gopinath, R. Pregla, and S. Helfert, "Numerical techniques for modeling guided wave photonic devices," *J. Sel. Top. Quantum Electron.*, 6, 150, 2000.

[4] K. S. Yee, "Numerical solution of initial boundary value problems involving Maxwell's equations in isotropic media," *IEEE Trans. Antennas Propagat*., AP 14, 302, 1966.

[5] Tavlove, "Computational electrodynamics: The finite difference time domain method," Artech House, Norwood, MA, 1995.

[6] M. Bahl, N. C. Panoiu, R. M. Osgood, Jr, "Nonlinear optical effects due to 1D Kerr defects in a 2D photonic crystal," *Phys. Rev. E*, 056604, 2003.

[7] N. Panoiu, M. Bahl, and R. Osgood, Jr, *Opt. Express.*, 12 18, 1605.

[8] J. Jin, *The Finite Element Method In Electromagnetics*, 2nd edition, New York, John Wiley & Sons, 2002.

[9] K. Saitoh and M. Koshiba, "Full vectorial imaginary distance beam propagation method based on a finite element scheme: application to photonic crystal fibers," *IEEE J. Quantum Electron*., 38(7), 927, 2002.

[10] M. Koshiba, S. Maruyama, and K. Hirayama, "A vector finite element method with the high order mixed interpolation type triangular elements for optical waveguiding problems," *IEEE J. Lightw. Technol.*, 12(3), 495, 1994.

[11] D. Schulz, C. Glingener, M. Bludszuweit, and E. Voges, "Mixed finite element beam propagation method," *IEEE J. Lightw. Technol.*, 16(7), 1336, 1998.

[12] Y. Tsuji, M. Koshiba, and T. Shiraishi, "Finite element beam propagation method for three dimensional optical waveguide structures," *IEEE J. Lightw. Technol*, 15(9), 1728, 1997.

[13] M. Koshiba and Y. Tsuji, "Curvilinear hybrid edge/nodal elements with triangular shape for guided wave problems," *IEEE J. Lightw. Technol*, 18(5), 737, 2000.

[14] Y. Tsuji and M. Koshiba, "Guided mode and leaky mode analysis by imaginary distance beam propagation method based on finite element scheme," *IEEE J. Lightw. Technol.*, 18(4), 618, 2000.

[15] F. Peterson, "Vector Finite Element Formulation for Scattering from Two Dimensional Heterogeneous Bodies," *IEEE Trans. Antennas and Propagat.*, 43(3), 357, 1994.

[16] Greenwood and J. Jin, "A Novel Efficient Algorithm for Scattering from a Complex BOR Using Mixed Finite Elements and Cylindrical PML," *IEEE Trans. Antennas and Propagat.,* 47(4), 620, 1999.

[17] J. F. Lee, M. Wilkins, and R. Mittra, "Finite element analysis of axisymmetric cavity resonator using a hybrid edge element technique," *IEEE Trans. on Microwave Theory and Techniques*, 41(11), 1981, 1993.

[18] J. C. Nédélec, "Mixed finite elements in R^3," *Numerische Mathematik*, 35, 315, 1980.

[19] J. Z. Huang, R. Scarmozzino, G. Nagy et al., "Realization of a compact and single mode optical passive polarization converter," *IEEE Photon. Technol. Lett.*, 12(3), 317, 2000.

[20] E. Yablonovitch, "Inhibited spontaneous emission in solid state physics and electronics," *Phys. Rev. Lett.,* 58, 2059, 1987.

[21] S. John, "Strong localization of photons in certain disordered dielectric superlattices," *Phys. Rev. Lett.,* 58, 2486, 1987.

[23] N. W. Ashcroft and N. D. Mermin, *Solid State Physics*, Philadelphia, Saunders College, 1976.

[22] E. Yablonovitch, "Photonic crystals: What's in a name?," *Opt. Photon. News,* 18, 12, 2007.

[24] K. M. Ho, C. T. Chan, and C. M. Soukoulis, "Existence of a photonic gap in periodic dielectric structures," *Phys. Rev. Lett.*, 65, 3152, 1990.

[25] R. D. Meade, A. M. Rappe, K. D. Brommer et al., "Accurate theoretical analysis of photonic band gap materials," *Phys. Rev. B,* 48, 8434, 1993.
[26] S. Johnson and J. D. Joannopoulous, "Block iterative frequency domain methods for Maxwell's equations in a planewave basis," *Opt. Express,* 8, 173, 2001.
[27] K. Sakoda, *Optical Properties of Photonic Crystals*, Springer, 2001.
[28] K. Busch and S. John, "Photonic band gap formation in certain self organizing systems," *Phys. Rev. E,* 58, 3896, 1998.
[29] G. J. Pearce, T. D. Hedley, and D. M. Bird, "Adaptive curvilinear coordinates in a plane wave solution of Maxwell's equations in photonic crystals," *Phys. Rev. B,* 71, 195108, 2005.
[30] J. A. West, C. M. Smith, N. F. Borrelli et al., "Surface modes in air core photonic band gap fibers," *Opt. Express,* 12, 1485, 2004.
[31] S. G. Johnson, P. R. Villeneuve, S. Fan, and J. D. Joannopoulos, "Linear waveguides in photonic crystal slabs," *Phys. Rev. B,* 62, 8212, 2000.
[32] M. J. Steel, "Reflection symmetry and mode transversality in microstructured fibers," *Opt. Express.,* 12, 1497, 2004.
[33] H. Kosaka et al., "Superprism phenomena in photonic crystals," *Phys. Rev. B,* 58, R10096, 1998.
[34] T. Baba and T. Matsumoto, "Resolution of photonic crystal superprism," *Appl. Phys. Lett.,* 81, 909, 2002.
[35] M. J. Steel et al., "Analytic properties of photonic crystal superprism parameters," *Phys. Rev. E,* 71, 056608, 2005.
[36] R. Petit, *Electromagnetic Theory of Gratings*, Berlin, Springer Verlag, 1980, p. 174.
[37] M. G. Moharam, T. K. Gaylord, "Rigorous coupled wave analysis of metallic surface relief gratings," *J. Opt. Soc. Am. A,* 3, 1780, 1986.
[38] Lifeng Li, "New formulation of the Fourier modal method for crossed surface relief gratings," *J. Opt. Soc. Am. A,* 14, 2758, 1997.
[39] Mingming Jiang, Theodor Tamir, and Shuzhang Zhang , "Modal theory of diffraction by multi layered gratings containing dielectric and metallic components," *J. Opt. Soc. Am. A,* 18, 807, 2001.
[40] Chung Hsiang Lin, K. Ming Leung, and Theodor Tamir, "Modal transmission line theory of three dimensional periodic structures with arbitrary lattice configurations," *J. Opt. Soc. Am. A,* 19, 2005, 2002.
[41] P. V. Mena, J. J. Morikuni, and K. W. Wyatt, "Compact Representations of Mode Overlap for Circuit Level VCSEL Models," in Proc. *IEEE/LEOS Annual Meeting Conf.*, 2000, p. 234.
[42] J. W. Scott, R. S. Geels, S. W. Corzine, and L. A. Coldren, "Modeling temperature effects and spatial hole burning to optimize vertical cavity surface emitting laser performance," *IEEE J. Quantum Electron.*, 29, 1295, 1993.
[43] N. Bewtra, D. A. Suda, G. L. Tan et al., "Modeling of quantum well lasers with electro opto thermal interaction," *IEEE J. Sel. Top. Quantum Electron.*, 1, 331, 1995.
[44] G. P. Agrawal and N. K. Dutta, *Semiconductor Lasers*, 2nd edition, New York, Van Nostrand Reinhold, 1993.
[45] M. X. Jungo, D. Erni, and W. Bächtold, "VISTAS: A comprehensive system oriented spatio temporal VCSEL model," *IEEE J. Sel. Top. in Quantum Electron.*, 9, 939, 2003.
[46] L. A. Coldren and S. W. Corzine, *Diode Lasers and Photonic Integrated Circuits*, New York, John Wiley and Sons, Inc., 1995.
[47] Matt Grupen and Karl Hess, "Simulation of carrier transport and nonlinearities in quantum well laser diodes," *IEEE J. Quantum Electron.*, 34(1), 120, 1998.
[48] B. Grote et al., "Quantum Well Laser Diodes: Temperature and Many Body Effects," in *Advanced Simulation and Analysis of Optoelectronic Devices* (J. Piprek ed.), 2004.
[49] B. Grote et al., "Integration of microscopic gain modeling into a commercial laser simulation environment," in *Physics and Simulation of Optoelectronic Devices XI Proc. SPIE*, (M. Osinski, H. Amano, and P. Blood, eds), 4986, 2003, p. 413.
[50] J. Piprek, *Semiconductor Optoelectronic Devices Introduction to Physics and Simulation*, New York, Academic Press, 2003.

[51] J. Piprek, *Optoelectronic Devices Advance Simulation and Analysis*, New York, Springer, 2005.
[52] Paul von Allman, "Derivation of the effective mass equation for a superlattice: A perturbational approach," *Phys. Rev. B*, 46(23), 15377, 1992 I.
[53] Paul von Allman, "Conduction subbands in GaAs/$Al_xGa_{1-x}As$ quantum well: Comparing differ ent kp models," *Phys. Rev. B*, 46(23), 15382, 1992 I.
[54] J. Hader, et al., "Quantitative prediction of semiconductor laser characteristics based on low intensity photoluminescence measurements," *IEEE Photon. Technol. Lett.*, 14(6), 762, 2002.
[55] J. Hader, J. V. Moloney, and S. W. Koch, "Microscopic theory of gain, absorption, and refractive index in semiconductor laser materials influence of conduction band nonparabolicity and coulomb induced intersubband coupling," *IEEE J. Quantum Electron.*, 35(12), 1878, 1999.
[56] W. W. Chow, S. W. Koch, *Semiconductor Laser fundamentals, Physics of the Gain Materials*, Berlin, Springer, 1999.
[57] W. W. Chow, S. W. Koch, and M. Sargent III, *Semiconductor Laser Physics*, Springer, Berlin (1994).
[58] G. P. Agrawal, *Nonlinear Fiber Optics*, 2nd edition, London, UK, Academic Press, 1995.
[59] Hasegawa and Y. Kodama, *Solitons in Optical Communications* Clarendon, Oxford, UK, 1995.
[60] R. Menyuk, "Application of multiple length scale methods to the study of optical fiber trans mission," *J. Eng. Math.*, 36, 113 136, 1999.
[61] G. J. Foschini and C. D. Poole, "Statistical theory of polarization dispersion in single mode fibers," *J. Lightw. Technol.*, 9(11), 1439 1456, 1991.
[62] F. Curti, B. Daino, G. De Marchis, and F. Matera, "Statistical treatment of the evolution of the principal states of polarization in single mode fiber," *J. Lightw. Technol.*, 8(8), 1162 1166, 1990.
[63] P. K. A. Wai and C. R. Menyuk, "Polarization mode dispersion, decorrelation, and diffusion in optical fibers with randomly varying birefringence", *J. Lightw. Technol.*, 14(2), 148 157, 1996.
[64] J. W. Cooley and J. W. Tukey, *Math. Comput.,* 19, 297, 1965.
[65] Oleg V. Sinkin, Ronald Holzlohner, John Zweck, and Curtis Menyuk, "Optimization of the split step Fourier method in modeling optical fiber communications systems," *J. Lightw. Technol.*, 21(1), January 2003.
[66] G. H. Weiss and A. A. Maradudin, *J. Math. Phys.*, 10, 129, 1976.
[67] Andrea Carena, Vittorio Curri, Roberto Gaudino et al., "A time domain optical transmission system simulation package accounting for nonlinear and polarization related effects in fiber," *J. Sel. Areas Commun.*, 15(4), May 1997.
[68] M. C. Jeruchim, P. Balaban, and K. S. Shanmugan, "*Simulation of Communication Systems*," New York: Plenum, 1992.
[69] G. Bosco, A. Carena, V. Curri et al., "Modulation formats suitable for ultra high spectral efficient WDM systems," *IEEE J. Sel. Top. Quantum Electron.*, 10(2), March/April 2004.
[70] IEEE Standard 802.3ae™ 2002 (Amendment to IEEE Std 802.3, 2002 Edition).
[71] D. Krumbholz, E. Brinkmeyer, and E. G. Neumann, "Core/cladding power distribution, propaga tion constant, and group delay: Simple relation for power law graded index fibers," *J. Opt. Soc. Am.*, 70(2), 179 183, 1980.
[72] D. Gloge and E. A. J. Marcatili, "Multimode theory of graded core fibers," *Bell Sys. Tech. J.*, 52(9), 1563 1579, 1973.
[73] M. J. Adams, Introduction to Optical Waveguides. New York, NY, John Wiley & Sons, Inc., 1981.
[74] J. Ritger and S. E. Golowich, "A simplified model of modal dispersion in multimode fiber," NIST Symposium on *Optical Fiber Measurements*, 2002, pp. 95 99.
[75] D. Marcuse, *Principles of Optical Fiber Measurements*, New York, NY, Academic Press, 1981.
[76] R. Mickelson, *Guided Wave Optics,* New York, NY, Van Nostrand Reinhold, 1993.
[77] J. B. Schlager and D. L. Franzen, NIST Symposium on *Optical Fiber Measurements*, September 1998, pp. 127 130.
[78] J. Morikuni, P. Mena, B. K. Whitlock, and R. Scarmozzino, "Simulation of Modal Delays for 10 Gb/s Multimode Fiber Applications," in Proc. *IEEE/LEOS Annual Meeting Conf.*, Glasgow, Scotland, 2002, pp. 903 904.

[79] R. Scarmozzino, A. Gopinath, R. Pregla, and S. Helfert, "Numerical techniques for modeling guided wave photonic devices," *IEEE J. Sel. Top. in Quantum Electron.*, 6(1), 150 162, 2000.
[80] Z. Huang, B. K. Whitlock, and R. Scarmozzino, "CAD optimizes component design at many levels," *WDM Solutions*, August 2000, pp. 41 48.
[81] D. Yevick and B. Hermansson, "New formulations of the matrix beam propagation method: Application to rib waveguides," *IEEE J. Quantum Electron.*, 25(2), 221 229, 1989.
[82] S. Jungling and J. C. Chen, "A study and optimization of eigenmode calculations using the imaginary distance beam propagation method," *IEEE J. Quantum Electron.*, 30(9), 2098 2105, 1994.
[83] G. R. Hadley and R. E. Smith, "Full vector waveguide modeling using an iterative finite difference method with transparent boundary conditions," *IEEE J. Lightw. Technol.*, 13(3), 465 469, 1995.
[84] J. Gowar, *Optical Communication Systems*, New York, NY, Prentice Hall, 1984.
[85] J. Morikuni, P. Mena, B. K. Whitlock, and R. Scarmozzino, "Multimode System Simulation as an Alternative to Spreadsheet Analysis for the Study of Gb/s Optical Communication Systems," in Proc. *IEEE/LEOS Annual Meeting Conf.*, paper MO4, Tucson, Arizona, October, 2003, p. 27.
[86] M. C. Jeruchim, "Techniques for estimating the bit error rate in the simulation of digital communication systems," *IEEE J. Sel. Areas in Commun.*, SAC 2, (1), January 1984.
[87] A. Papoulis, *Probability, Random Variables and Stochastic Processes*, New York, McGraw Hill, 1991.
[88] J. S. Lee and C. S. Shim, "Bit error rate analysis of optically preamplified receivers using an eigenfunction expansion method in optical frequency domain," *IEEE J. Lightw. Technol.*, 12, 1224 1229, 1994.
[89] A. H. Gnauck and P. J. Winzer, "Optical phase shift keyed transmission," *IEEE J. Lightw. Technol.*, 23(1), 115 130, January 2005.
[90] W. H. Press, S. A. Teukolsky, and W. T. Vetterling, *Numerical recipes in C*, Cambridge University Press, 1992.
[91] G. Bosco and P. Poggiolini, "On the joint effect of receiver impairments on direct detection DQPSK systems," *IEEE J. Lightw. Technol.*, 24(3), 1323 1333, 2006.
[92] C. W. Helstrom, "Distribution of the filtered output of a quadratic rectifier computed by numerical contour integration," *IEEE Trans. on Inform. Theory.*, IT 32(4), July 1986, 450 463.
[93] B. E. A. Saleh and M. C. Teich, *Fundamentals of Photonics*, New York, NY, John Wiley and Sons, 1991.
[94] M. C. Jeruchim, P. Balaban, and K. S. Shanmugan, *Simulation of Communication Systems*, New York, Plenum Publishing Corporation, 1992.
[95] J. Wang and K. Peterman, "Small signal analysis for dispersive optical fibers communication systems," *IEEE J. Lightw. Technol.*, 10(1), 96 100, January 1992.
[96] G. Bosco and R. Gaudino, "Towards New Semi Analytical Techniques for BER Estimation in Optical System Simulation," in Proc. *NFOEC 2000*, Denver (CO), Tuesday Sess. E1, USA, August, 2000.
[97] L. Kazovsky, S. Benedetto and A. Willner, *Optical Fiber Communication Systems*, Artech House, 1996.
[98] A. M. Mathai, S. B. Prevost, *Quadratic Forms in Random Variables*, New York, Marcel Dekker, 1992, Chapter 3.
[99] MetroWAND Ring user guide.
[100] MetroWAND Mesh user guide.
[101] V. Poudyal, R. H. Cardwell, O. J. Wasem et al., "The effects of demand levels and number of wavelengths on the economics of metropolitan WDM," in Proc. *NFOEC, 2001*, 2001, pp. 1133 1144.
[102] R. H. Cardwell, O. J. Wasem, V. Poudyal et al., "Planning for interoperable and reliable metropolitan DWDM ring networks to achieve minimum cost of ownership," in Proc. *NFOEC'99*, Chicago.

[103] M. Ajmone Marsan, A. Bianco, E. Leonardi et al., "All optical WDM multi rings with differ entiated QoS," *IEEE Commun. Mag.*, 37(2), 58 66, 1999.
[104] E. Modiano, "WDM based packet networks," *IEEE Commun. Mag.,* 37(3), 130 35, 1999.
[105] K. K. Ramakrishnan, G. Hjalmtysson, and J. E. Van der Merwe, "The role of signaling in quality of service enabled networks," *IEEE Commun. Mag.,* 37(6), 124 32, 1999.
[106] M. Ajmone Marsan et al., "SR3: A bandwidth reservation MAC protocol for multimedia applica tion over all optical WDM multi rings," in Proc. *INFOCOM 1997*, Kobe, Japan, pp. 761, April, 1997.
[107] C. K. Chan, L. K. Chen, and K. W. Cheung, "A fast channel tunable optical transmitter for ultrahigh speed all optical time division multiaccess networks," *IEE JSAC 1996*, 14(5), 1052 56, 1996.
[108] Cidon, and Y. Ofek, "MetaRing a full duplex ring with fairness and spatial reuse," *IEEE Trans. Commun.,* 41(1), 110 120, 1993.
[109] P. Labourdette, G. W. Hart, and A. S. Acampora, "Branch exchange sequences for reconfigura tion of lightwave networks," *IEEE Trans. Commun.*, 42(10), 2822 2832, October 1994.
[110] G. Ellinas and T. E. Stern, "Automatic protection switching for link failures in optical networks with bi directional links," in Proc. *GLOBECOM 1996*, London, UK, November 1996.
[111] M. Baldassari and G. Bruno, "PROTOB: An object oriented methodology for developing discrete dynamic systems," *Comput. Languages J.* 16(1), 39 63, 1991 (reprinted in *High level Petri Nets*, pp. 624 48, Springer Verlag, 1991).
[112] M. Baldassari and G. Bruno, "An environment for object oriented conceptual programming based on PROT nets," *Advances in Petri Nets*, Springer Verlag, 1988.
[113] *Artifex 4.2 Reference Manual*, by ARTIS Software Corporation, Torino, May 1999.
[114] *Artifex 4.2 Installation Guide & Getting Started*, by ARTIS Software Corporation, Torino, May 1999.
[115] *The Artifex Language*, by ARTIS Software Corporation, Torino, August 1997.
[116] T. Murata, "Petri Nets: Properties, Analysis and Applications," in Proc. *IEEE 1989*, 77(4), 1989, pp. 541 580.
[117] K. Jensen, *Colored Petri Nets, Volume 1: Basic Concepts*, Springer Verlag, Berlin and Heidelberg GmbH & Co. KG, 1992.
[118] K. Jensen, *Colored Petri Nets, Volume 2: Analysis Methods*, Springer Verlag, Berlin and Heidelberg GmbH & Co. KG, 1994.
[119] K. Jensen, *Colored Petri Nets, Volume 3: Practical Use*, Springer Verlag, Berlin and Heidelberg GmbH & Co. KG 1997.

This page intentionally left blank

Index to Volumes VA and VB

B

T

U

This page intentionally left blank